Oklahoma Geological Survey
Charles J. Mankin, *Director*

Circular 101
ISSN 0078-4397

Platform Carbonates in the Southern Midcontinent, 1996 Symposium

KENNETH S. JOHNSON, *Editor*

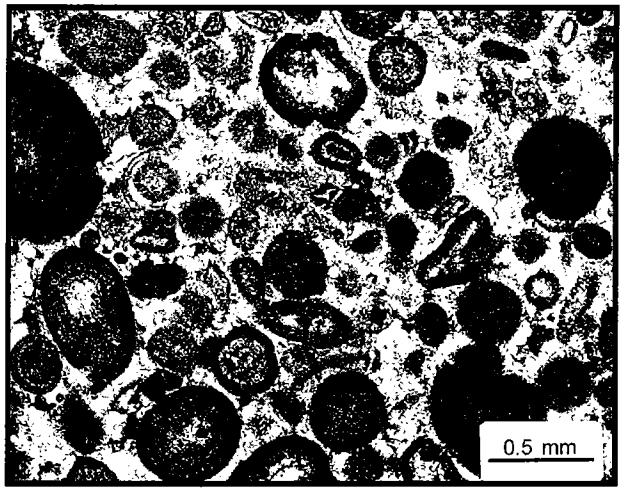

Proceedings of a symposium held March 26–27, 1996, in Oklahoma City.

Co-sponsored by:

Oklahoma Geological Survey

and

National Petroleum Technology Office,
U.S. Department of Energy

The University of Oklahoma
Norman

2000

OKLAHOMA GEOLOGICAL SURVEY

CHARLES J. MANKIN, *Director*
KENNETH S. JOHNSON, *Associate Director*

SURVEY STAFF

JAMES H. ANDERSON, *Cartographic Draftsperson III*
RICHARD D. ANDREWS, *Geologist III*
LARRY T. AUSTIN, *Core and Sample Library Assistant*
BETTY D. BELLIS, *Word-Processing Operator II/Technical Typist*
MITZI G. BLACKMON, *Clerk-Typist I*
RAYMON L. BROWN, *Geophysicist III*
RUTH E. BROWN, *Assistant to the Director*
JOCK A. CAMPBELL, *Geologist IV*
BRIAN J. CARDOTT, *Geologist IV*
JAMES R. CHAPLIN, *Geologist IV*
JANISE L. COLEMAN, *Office Assistant IV*
CHRISTIE L. COOPER, *Editor*
TAMMIE K. CREEL, *Secretary II*
CHARLES R. DYER III, *Drilling Technician*
WALTER C. ESRY, *Manager, Core and Sample Library*
ROBERT O. FAY, *Geologist IV*
AMIE R. FRIEND, *Research Specialist I*
T. WAYNE FURR, *Manager of Cartography*
PATRONALIA M. HANLEY, *Chemist*
PRISCILLA A. JOHNSON, *Office Assistant IV*
JAMES W. KING, *Research Specialist I*
JAMES E. LAWSON, JR., *Chief Geophysicist*
KENNETH V. LUZA, *Geologist IV*
TODD S. MCCORMICK, *Electronic Technician*
MICHAEL J. MERCER, *Manager, Log Library*
RICHARD G. MURRAY, *Copy Center Operator*
SUE M. PALMER, *Office Assistant II*
TRACY P. PEETERS, *Associate Editor*
DAVID O. PENNINGTON, *Operations Assistant II*
CONNIE G. SMITH, *Promotion and Information Specialist*
PAUL E. SMITH, *Supervisor, Offset Press Copy Center*
THOMAS M. STANLEY, *Geologist II*
LLOYD N. START, *Assistant Drilling Technician*
JOYCE A. STIEHLER, *Chief Clerk*
MICHELLE J. SUMMERS, *Technical Project Coordinator*
NEIL H. SUNESON, *Geologist IV*
JANE L. WEBER, *Coordinator, Departmental Computer Systems*
STEPHEN J. WEBER, *Chief Chemist*

Cover Photo

Ooid grainstone representing high-energy intertidal/upper subtidal facies (from p. 137 of this volume).

This publication, printed by the Oklahoma Geological Survey, is issued by the Oklahoma Geological Survey as authorized by Title 70, Oklahoma Statutes, 1981, Sections 231–238. 1,050 copies have been prepared for distribution at a cost of $12,334 to the taxpayers of the State of Oklahoma. Copies have been deposited with the Publications Clearinghouse of the Oklahoma Department of Libraries.

PREFACE

The transfer of technical information will aid in the search for, and production of, our oil and gas resources. To facilitate this technology transfer, the Oklahoma Geological Survey (OGS) and the U.S. Department of Energy, National Petroleum Technology Office (DOE–NPTO), in Tulsa, cosponsored a symposium dealing with the search for, and production of, oil and gas resources from platform carbonates in the southern Midcontinent. The symposium was held on March 26–27, 1996, in Oklahoma City. This volume contains the proceedings of that symposium.

Research reported upon at the symposium focused on limestones and dolomites deposited in shallow-marine, platform (shelf) environments. These carbonates are major sources of oil and gas in the southern Midcontinent, and they have great potential for additional recovery using advanced technologies. The research reports on geology, depositional settings, diagenetic history, reservoir characterization, exploration, petroleum production, and enhanced oil recovery. In describing these platform carbonates and their petroleum reservoirs, the researchers have increased our understanding of how the geologic history of an area can affect reservoir heterogeneity and our ability to efficiently recover the hydrocarbons they contain. We hope that the symposium and these proceedings will bring such research to the attention of the geoscience and energy-research community and will help foster exchange of information and increased research interest by industry, university, and government workers.

Thirty-two talks and posters presented at the symposium are printed here as full papers or extended abstracts. An additional five talks and posters are presented as abstracts at the end of the volume. About 275 persons attended the symposium. Stratigraphic nomenclature and age determinations used by the various authors in this volume do not necessarily agree with those of the OGS.

This is the ninth symposium in as many years dealing with topics of major interest to geologists and others involved in petroleum-resource development in Oklahoma and adjacent states. These symposia are intended to foster the exchange of information that will improve our ability to find and recover our nation's oil and gas resources. Earlier symposia covered: Anadarko Basin (published as OGS Circular 90); Late Cambrian–Ordovician Geology of the Southern Midcontinent (OGS Circular 92); Source Rocks in the Southern Midcontinent (OGS Circular 93); Petroleum-Reservoir Geology in the Southern Midcontinent (OGS Circular 95); Structural Styles in the Southern Midcontinent (OGS Circular 97); Fluvial-Dominated Deltaic Reservoirs in the Southern Midcontinent (OGS Circular 98); Simpson and Viola Groups in the Southern Midcontinent (OGS Circular 99); and Ames Structure in Northwest Oklahoma and Similar Features—Origin and Petroleum Production (OGS Circular 100).

Persons involved in the organization and planning of this symposium include: Kenneth Johnson and Charles Mankin of the OGS; and Tom Wesson and Chandra Nautiyal of DOE–NPTO. Other personnel who contributed include Michelle Summers and Tammie Creel, registration co-chairs; LeRoy Hemish, poster-session chair; Connie Smith, publicity chair; and Judy Schmidt, exhibits coordinator. Technical editing of this volume was done by William Rose, Frederick, Maryland; layout and production was done by Virginia Rose, Frederick, Maryland. Appreciation is expressed to each of them and to the many authors who worked toward a highly successful symposium.

KENNETH S. JOHNSON
General Chairman

CONTENTS

iii **Preface**

1 **Petroleum Production from Platform Carbonates of Oklahoma**
Kenneth S. Johnson, G. Carlyle Hinshaw, and Robert A. Northcutt

13 **Distribution and Geometries of Platform-Carbonate Reservoirs: Insight from Modern Counterparts in the Bahamas**
G. Michael Grammer and Robert N. Ginsburg

25 **Effects of Depth on Quality of Gas-Well Completions in Carbonate Reservoirs of the Anadarko Basin and Shelf Areas**
Paul W. Smith and Thomas J. Woods

47 **Initiation of the Arbuckle Platform—View from the Slick Hills, Oklahoma**
R. Nowell Donovan

57 **Initiation of a Carbonate Platform: A Comparison Between the Lower Jurassic Broadford Limestone, Isle of Skye, Scotland, and the Cambrian Honey Creek Limestone, Slick Hills, Oklahoma**
Andrea K. Bucheit and R. Nowell Donovan

65 **Unconformity in the Lower Part of the Cambrian Honey Creek Limestone, Slick Hills, Oklahoma: Candidate for a Grand Cycle Boundary**
Courtney McElmoyl and R. Nowell Donovan

79 **Boundary Between the Fort Sill and Signal Mountain Formations in the Lower Arbuckle Group, Slick Hills: Candidate for a Grand Cycle Boundary**
Randall M. Hosey and R. Nowell Donovan

89 **Four Hundred Feet of Core from the Cambrian Signal Mountain Formation, Slick Hills, Oklahoma**
Richard E. Whitehead and R. Nowell Donovan

97 **Preliminary Cyclic Stratigraphy of the Upper Arbuckle Group in the Richard's Spur Quarry, Slick Hills, Oklahoma**
Danielle Ayan, Andrea K. Bucheit, Matthew J. Kulow, and R. N. Donovan

103 **A Preliminary Reevaluation of the Stratigraphy of the Roubidoux Formation of Missouri and Correlative Lower Ordovician Units in the Southern Midcontinent**
John E. Repetski, James D. Loch, Raymond L. Ethington, and Russell I. Dresbach

107 **Depositional and Diagenetic Controls on Porosity Development in the Ordovician Viola Formation, South-Central Kansas**
K. David Newell

117 **Viola Group Reservoir Facies, Fitts Pool, Pontotoc County, Oklahoma**
Jim Puckette, Zuhair Al-Shaieb, and Michael Sykes

129 **Microbial Reservoir Characterization of Hobart Field, Kiowa County, Oklahoma**
Daniel C. Hitzman, James D. Tucker, and Brooks A. Rountree

131 **Sequence Stratigraphy of Hunton Group Ramp Facies, Arbuckle Mountains and Anadarko Basin, Oklahoma**
Zuhair Al-Shaieb and Jim Puckette

139 **Defining the Role of Woodford–Hunton Depositional Relationships in Hunton Stratigraphic Traps of Western Oklahoma**
Kurt Rottmann

147 **Production and Reservoir Characteristics of Selected Hunton Fields in the Anadarko Basin**
Paul W. Smith, Walter J. Hendrickson, and Craig M. Williams

157 **Depositional and Diagenetic History of Mississippian Chat Reservoirs, Northern Oklahoma**
Suzanne M. Rogers, James M. Forgotson, Jr., and Thomas A. Dewers

163 **Natural-Gas Production from the Boone Formation (Lower Mississippian), Northwestern Arkansas**
Walter L. Manger and Phillip R. Shelby

171 **PC-Based Reservoir Characterization and Simulation of Schaben Field, Ness County, Kansas**
Saibal Bhattacharya, Paul M. Gerlach, Tim R. Carr, Willard R. Guy, Scott Beaty, and Evan K. Franseen

183 **Biothem: A New Biostratigraphically Based Unit of Sequence Stratigraphy**
H. Richard Lane, Mark W. Frye, and Gary D. Couples

197 **Stratigraphic Relationships of Springer and Chester Groups within the Oklahoma Portion of the Anadarko Basin and Shelf: A Clarification**
Paul W. Smith, Walter J. Hendrickson, Craig M. Williams, and Ronald J. Woods

209 **Union Valley Limestone Bank (Pennsylvanian, Morrowan), Eastern Oklahoma**
James R. Derby, James E. O'Brien, J. Glenn Cole, and Dorothy L. Swindler

219 **Facies, Stratigraphic Relationships, and Fracturing in the Wapanucka and Spiro Formations (Pennsylvanian)**
Darrell L. Mauldin

223 **Integrated Analysis of Reservoir Petrofacies in Platform Carbonates of Kansas: Techniques and Case Studies**
John H. Doveton, W. Lynn Watney, and Willard J. Guy

227 **Sequence Stratigraphy and Reciprocal Sedimentation in Middle and Late Pennsylvanian Carbonate-Bank Systems, Eastern Shelf of the Midland Basin, North-Central Texas**
Arthur W. Cleaves

259 **Exploration- and Production-Scale Lateral Variability in Phylloid-Algal-Mound and Associated Reservoir Facies, Paradox Basin, Southeastern Utah**
G. Michael Grammer and Gregor P. Eberli

269 **Lithofacies Distribution and Reservoir Heterogeneity within Pennsylvanian Bioherms, Western Orogrande Basin, New Mexico**
Katherine A. Giles and Gerilyn S. Soreghan

275 **Outcrop-Based Sequence Stratigraphy of the Council Grove Group of the Midcontinent**
D. R. Boardman II and Merlynd K. Nestell

307 **Environments of Deposition for Clear Fork and Glorieta Formations, North Robertson Unit, Gaines County, Texas**
James Kamis, William Dixon, and Richard Vessell

319 **Improved Reservoir Characterization through Integrated Log and Core Data: Example from Permian San Andres Formation, Dawson County, Texas**
Gregory D. Hinterlong and Archie R. Taylor

327 **Seismic Estimation of Porosity in a Permian San Andres Carbonate Reservoir, Welch Field, Dawson County, Texas**
George P. Watts and Gregory D. Hinterlong

339 **Reservoir Characterization of the Upper Permian Grayburg Formation in Preparation for a Horizontal-Well CO_2 Flood, South Cowden Unit, West Texas**
Craig D. Caldwell, Ken J. Harpole, and Matt G. Gerard

355 **Carbonate Development and Potential Petroleum Productivity in the Southern Fort Worth Basin, Texas**
Deborah K. Sacrey and A. H. Wadsworth

356 **Sequence Stratigraphy and Reservoir Development, Marble Falls Limestone (Pennsylvanian), Central Texas**
Walter L. Manger and Patrick K. Sutherland

357 **Depositional Environments and Sequence-Stratigraphic Framework of the Subsurface Council Grove Group (Permian) of the Hugoton Embayment, Kansas**
Nicholas J. Pieracacos

358 **Characteristics of Cyclical, Mixed Carbonate/Siliciclastic Reservoirs: Early Permian Chase Group, Northern Oklahoma**
James R. Chaplin

359 **Sonic Velocity in Carbonates—A Product of Original Composition and Post-Depositional Porosity Evolution**
Flavio S. Anselmetti and Gregor P. Eberli

Petroleum Production from Platform Carbonates of Oklahoma

Kenneth S. Johnson
Oklahoma Geological Survey
Norman, Oklahoma

G. Carlyle Hinshaw
Consulting Geologist
Norman, Oklahoma

Robert A. Northcutt
Independent Geologist
Oklahoma City, Oklahoma

ABSTRACT.—Platform carbonates of Paleozoic age make up a significant part of the stratigraphic sequence in Oklahoma, and most of these limestones and dolomites are important sources of oil and gas production in some part of the State. Major carbonate reservoirs include the Arbuckle, Viola, and Hunton Group limestones and dolomites; the extensive and thick Mississippian limestones; and the numerous thinner limestones in the Pennsylvanian and Permian Systems. The abundance of platform carbonates results from various parts of Oklahoma having been the sites of shallow-water, normal-marine sedimentation during most of the Paleozoic Era.

Production data for leases in Oklahoma were retrieved from the Geo Information Systems data files by the geologic names of the producing intervals. The files contain 700 different geologic names for producing intervals, and, of these, 168 are carbonates. Nearly all Oklahoma carbonates are platform carbonates, so we list all 168 names in this paper. It is possible, through the mapping capabilities of SAS (an integrated system of software), to create a map showing oil and/or gas production for one or several (or all) producing intervals. Using these data, we prepared a series of eight maps to show production from carbonates by geologic age. The eight maps generated are for the following stratigraphic intervals: Upper Cambrian and Lower Ordovician, Middle and Upper Ordovician, Silurian and Devonian, Mississippian, Lower Pennsylvanian, Middle Pennsylvanian, Upper Pennsylvanian, and Permian.

INTRODUCTION

Oklahoma is one of the leading petroleum-producing states in the nation, and since 1979 a significant part of the State's oil and gas has been produced from Paleozoic platform carbonates. With petroleum exploration and production being of such great importance to the State, it is critical to understand the character and distribution of these prolific carbonate reservoirs. This paper provides an overview of the following: (1) the Paleozoic geologic setting and platform carbonates of Oklahoma, (2) the names and character of the principal carbonate reservoirs, and (3) the distribution of oil and gas production from the eight major groupings of Paleozoic carbonates. The discussion that follows under "Geologic Framework," and the general geologic characterization of each of the eight groups of Paleozoic carbonates, are largely modified from an earlier report by Johnson and Cardott (1992).

Production data for leases were retrieved from the GIS (Geo Information Systems, a research department of The University of Oklahoma) data files by the geologic names of the producing intervals. Oklahoma petroleum production is recorded by lease, *not by well,* by the Oklahoma Tax Commission. These data are public records and are marketed in several forms by commercial and governmental organizations. GIS provides the data 6 months in arrears, updated each 6 months. The database begins with 1979, with oil, condensate, associated gas, and nonassociated gas, recorded monthly. It is possible, through the mapping capabilities of SAS (an integrated system of software), to post a location map at almost any scale for one or several (or all) producing intervals by product or products. Also, individuals or companies can acquire the raw data and construct their own analyses.

GEOLOGIC FRAMEWORK

The geology of Oklahoma is complex, but it is remarkably well understood as a result of the extensive amount of drilling and seismic exploration in search of oil and gas. Great thicknesses of sedimentary rock are preserved in a series of major depositional and structural basins separated by orogenic uplifts that formed mainly during Pennsylvanian time (Fig. 1). The major sedimentary basins contain as much as 20,000–40,000 ft of sediments, most of which are Paleozoic and ma-

Johnson, K. S.; Hinshaw, G. C.; and Northcutt, R. A., 2000, Petroleum production from platform carbonates of Oklahoma, *in* Johnson, K. S. (ed.), Platform carbonates in the southern Midcontinent, 1996 symposium: Oklahoma Geological Survey Circular 101, p. 1–11.

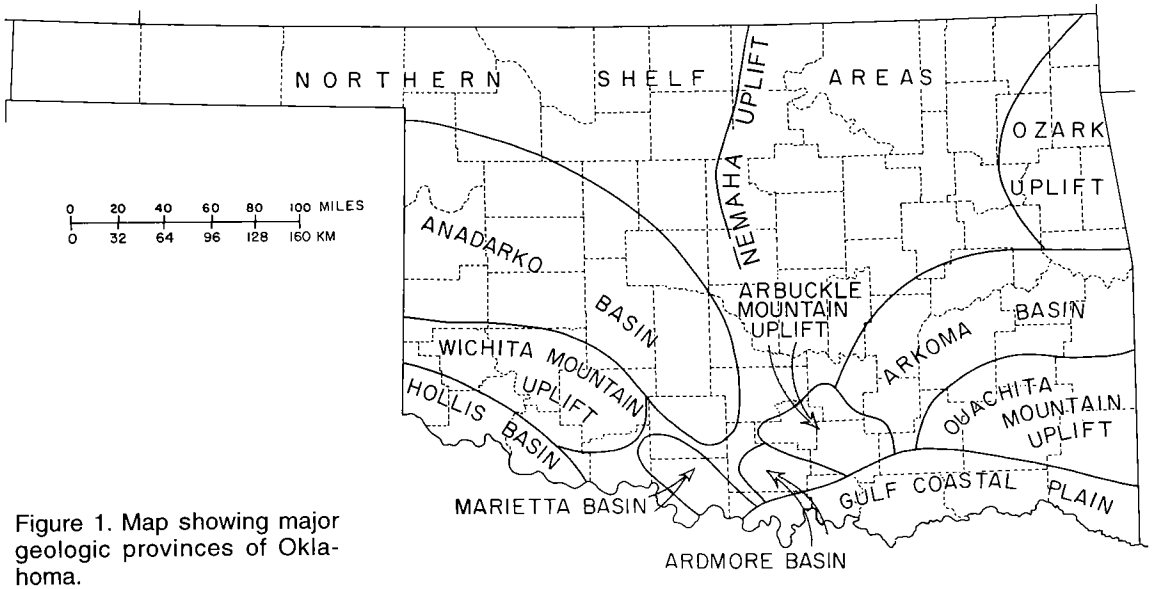

Figure 1. Map showing major geologic provinces of Oklahoma.

rine, resting upon a basement complex of igneous rocks and some low-rank metasedimentary rocks (Denison and others, 1984; Johnson and others, 1988). Basement rocks beneath most of Oklahoma are Precambrian granites and comagmatic rhyolites, but beneath the southern Oklahoma aulacogen they are Early and Middle Cambrian granites, rhyolites, gabbros, and basalts. Basement rocks beneath the Ouachita province have not been drilled and are unknown.

By early Paleozoic time, Oklahoma had three major tectonic/depositional provinces: the Oklahoma basin, the southern Oklahoma aulacogen, and the Ouachita trough (Fig. 2). The Oklahoma basin was a broad, shelflike area that received a sequence of remarkably thick and extensive shallow-marine carbonates interbedded with thinner marine shales and sandstones (Johnson and others, 1988). The southern Oklahoma aulacogen was the depocenter for the Oklahoma basin. It was a west-northwest-trending trough where sediments generally are similar to those elsewhere in the basin, but they are two to three times thicker. The aulacogen embraced the Anadarko, Ardmore, and Marietta protobasins, along with the present-day Arbuckle anticline and Wichita Mountain uplift. The Ouachita trough was the site of deep-water sedimentation along a rift at the southern margin of the North American craton; these sediments were thrust northward as much as 50 mi to their present position in the Ouachita Mountain uplift.

These three provinces persisted through the middle Paleozoic until Pennsylvanian time, when the Oklahoma basin and the aulacogen were divided into a series of well-defined marine basins by sharply uplifted crustal blocks (Johnson and others, 1988; McBee, 1995). The Ouachita trough was destroyed by Pennsylvanian uplift and northward thrusting. Orogenic activity throughout the State was limited to folding, faulting, and uplift, and was not accompanied by igneous or high-grade-metamorphic activity.

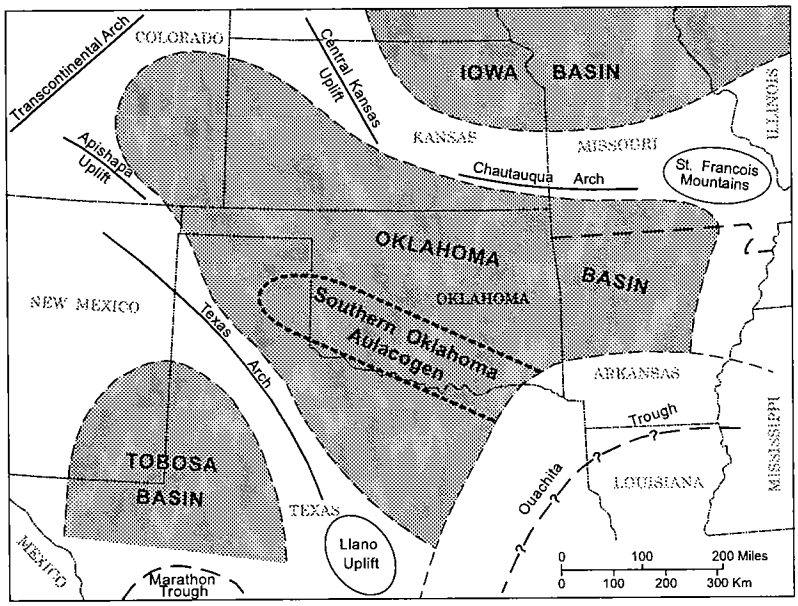

Figure 2. Map of southwestern United States, showing approximate boundary of the Oklahoma basin and other major features that existed in early and middle Paleozoic time (after Johnson and others, 1988).

PLATFORM CARBONATES AND PETROLEUM PRODUCTION

For purposes of this report, it is practical to discuss the carbonate geology and petroleum production by subdividing the Paleozoic Era into eight sequences: Upper Cambrian and Lower Ordovician, Middle and Upper Ordovician, Silurian and Devonian, Mississippian, Lower Pennsylvanian, Middle Pennsylvanian, Upper Pennsylvanian, and Permian (Fig. 3).

The stratigraphic names used to identify individual producing units in the GIS files are the specific names used by various geologists, producers, or drillers in reporting production data to the Oklahoma Tax Commission. Therefore, several names typically are given for the same unit, and a number of names in the database would not normally be published in the geologic literature. Of the total 700 names in the GIS

GEOLOGIC AGE	MAJOR PLATFORM CARBONATES THAT YIELD PETROLEUM
Permian	Chase Group
Upper Pennsylvanian	Topeka Checkerboard
Middle Pennsylvanian	Big Lime Oswego
Lower Pennsylvanian	Wapanucka
Mississippian	Chester Meramec Osage
Silurian and Devonian	Hunton Group
Middle and Upper Ordovician	Viola Group Simpson Gp. (carbs.)
Upper Cambrian and Lower Ordovician	Arbuckle Group

Figure 3. Eight stratigraphic sequences in the Paleozoic of Oklahoma that contain petroleum-producing platform carbonates.

files that represent producing units, 168 are names for carbonates; inasmuch as virtually all Oklahoma carbonates are platform carbonates, we list all 168 of them in this report (see Tables 1–8).

Cumulative-production figures presented for each of the eight sequences summarize data for production definitely assigned only to that sequence; they do not include commingled production, in which reservoirs in two or more sequences were coproduced on the same lease. Therefore, cumulative-production figures reported here are minimal for the time period January 1, 1979, through September 30, 1995.

Upper Cambrian and Lower Ordovician

Upper Cambrian and Lower Ordovician strata are a vast blanket of carbonate rocks deposited throughout the Oklahoma basin (Fig. 4). This unit, which consists mainly of the Arbuckle Group, is comparable to (though not precisely time-equivalent to) the Ellenburger Group of west Texas and the Knox Group of the eastern United States (Johnson, 1991a,b).

The Arbuckle Group is the thickest sequence of lower Paleozoic strata in Oklahoma. It is as much as 6,700 ft of limestone in the aulacogen, on the flank of the Arbuckle anticline (Fay, 1989), thinning to ~4,000 ft of dolomite in the eastern Arbuckle Mountains and about 1,000–4,000 ft of dolomite in most other shelf areas of the Oklahoma basin (Johnson and others, 1988). The transition from mainly limestone to mainly dolomite occurs near the boundary of the aulacogen (Fig. 4) and, in part, reflects differences in water depths and local restrictions in water circulation during deposition. Dolomite probably results from deposition and diagenesis of carbonates in shelf areas characterized by alternating shallow-marine and supratidal environments.

Table 1.—Names Used for Upper Cambrian and Lower Ordovician Carbonates That Produce Petroleum in Oklahoma

Lower Ordovician	Cotter
Arbuckle	Roubidoux
Canadian	Gasconade
Knox	
Arbuckle Group	**Upper Cambrian**
Turkey Mountain	Butterly
Bray zone	Fort Sill
Brown zone	Eminence
Kindblade	Honey Creek
Cumulative Production (1/1/79 through 9/30/95) Oil: 36,868,790 Bbl Gas: 413,151,805 Mcf	

Upper Cambrian and Lower Ordovician carbonates produce oil and gas at many widely scattered places in the State (Fig. 5), almost exclusively from dolomites of the Arbuckle Group. Shelf-dolomite reservoirs exhibit porosity and permeability controlled by dissolution and some collapse during subaerial exposure and karst cycles. In the southern Oklahoma aulacogen, tectonic dolomites also were altered by dissolution and karst development to form reservoir units. Notable fields are Cottonwood Creek and Healdton fields, producing oil and gas from tectonic-dolomite reservoirs in western Carter County in the southern Oklahoma aulacogen; the deep Wilburton field, a shelf-dolomite gas producer in the Arkoma basin in Latimer County; numerous shelf-dolomite fields that produce from structures formed over basement highs in Osage County; and the Ames structure, a suspected meteorite-impact crater in southeastern Major County. Other major producing fields are Oklahoma City (Oklahoma and Cleveland Counties) and Mayfield West (Beckham County).

Table 1 shows the producing-interval names and cumulative production for Upper Cambrian and Lower Ordovician reservoirs. Note that the West Spring Creek, Cool Creek, and McKenzie Hill Formations (Lower Ordovician) are not listed; all have been productive but are probably named *Arbuckle* in the files.

Middle and Upper Ordovician

Middle and Upper Ordovician strata include, in ascending order, the Simpson Group, Viola Group, and Sylvan Shale (Schramm, 1964, 1966; Johnson, 1997). The aggregate thickness of these units ranges from about 500 ft in the north and east to nearly 3,000 ft in the aulacogen (Fig. 4); platform carbonates are widespread in the Simpson and Viola Groups, and also are present as Sylvan-equivalent dolomite in a small area of northwestern Oklahoma.

Simpson Group strata in the Oklahoma basin are thick, cleanly washed quartzose sandstones interbedded with thick, shallow-water-marine limestones and thin to moderately thick greenish-gray shales; these lithologies are present in roughly equal amounts in the basin (Statler, 1965). The Viola Group is a marine-limestone sequence that is widespread in the Okla-

homa basin. It contains chert at several stratigraphic levels and commonly is highly fossiliferous. Terrigenous detritus, including some organic and graptolitic shale, is present in the lower Viola, particularly in the aulacogen; these components decrease upward, and the strata grade into clean-washed skeletal limestones (Johnson and others, 1988). This vertical change indicates an upward decrease in water depth and a corresponding increase in the energy level and aerobic activity of the depositional environment. Thus a significant part of the Viola is a platform carbonate, particularly the upper Viola within the aulacogen and all of the Viola in the shelf areas.

Most production from the Middle and Upper Ordovician is in the central and southern parts of the State (Fig. 6). Production is mainly from Viola Group limestones, although some Viola reservoirs are dolomites and dolomitic limestones. Fractures and cracking of the Viola have played an important role in the development of its reservoirs. Statewide, the Viola produces along, and either side of, the Nemaha uplift, mainly on "Midcontinent-type" structures. Many fields embraced within the Golden Trend are present in northwestern Garvin County and adjacent areas on the Pauls Valley uplift. In the Marietta basin of Jefferson and Love Counties, the Viola produces almost everywhere it is present. Here, the producing part of the Viola is not considered a platform carbonate by some workers in the area; instead, it is regarded as a basinal deposit consisting of material derived from the shelf. Other significant production is from the Earlsboro and St. Louis fields in Pottawatomie and Seminole Counties.

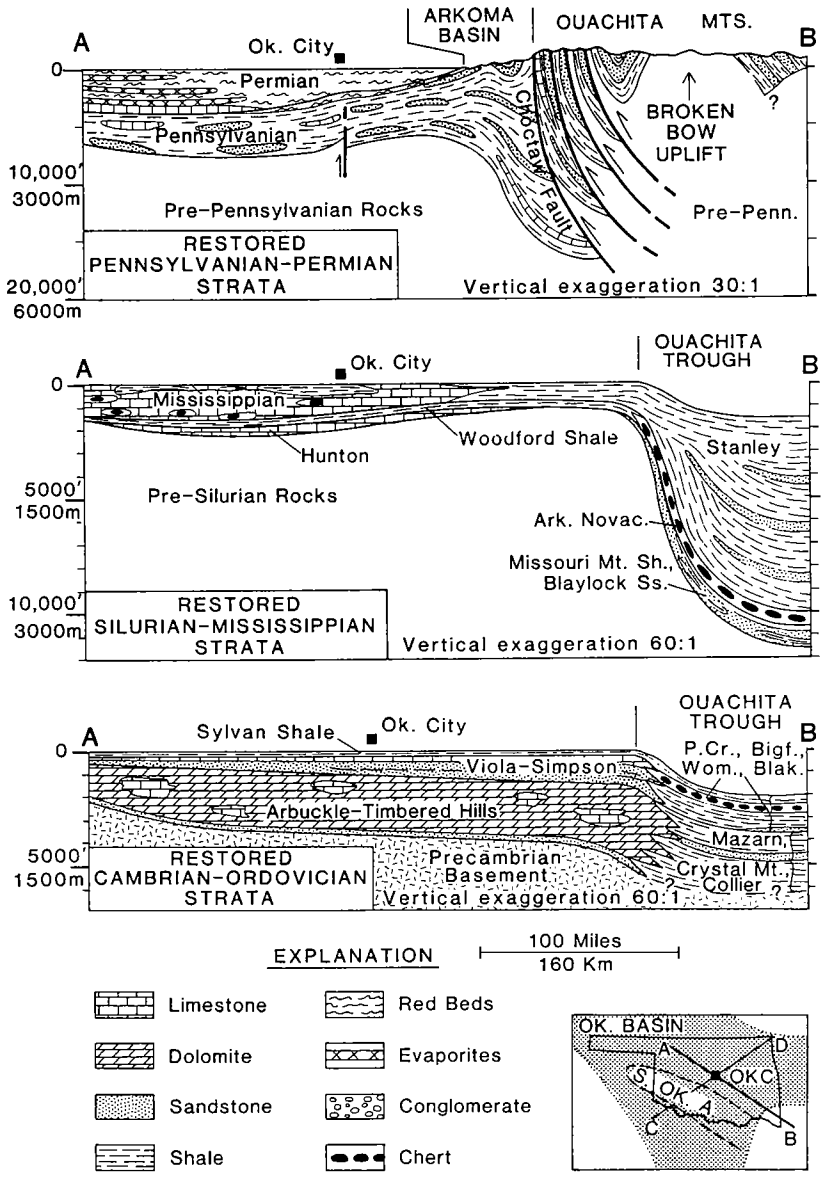

Figure 4 *(above and facing page).* Schematic cross sections showing restored thickness of strata in Oklahoma at the end of early, middle, and late Paleozoic times (Johnson and Cardott, 1992). Top cross sections (Pennsylvanian–Permian) have less vertical exaggeration than other cross sections.

Table 2 shows producing intervals and cumulative production in the Middle and Upper Ordovician. The Simpson Group is most productive from its sandstone units in most parts of Oklahoma, but it also contains important carbonate reservoirs that are highly productive locally (only the carbonate units are listed in Table 2, or are shown as producing reservoirs in Fig. 6). As a side note, the Birdseye lime generally is considered to be in the McLish Formation; there is, however, a Birdseye lime in the Oil Creek Formation that also has been productive.

Silurian and Devonian

Silurian and Devonian carbonate rocks in Oklahoma are all within the Hunton Group (Amsden, 1976, 1980, 1993; Johnson, 1993). The Hunton consists mainly of shallow-water, clean-washed skeletal limestones in the lower part (Chimneyhill Subgroup); argillaceous and silty carbonates in the middle (Henryhouse and Haragan–Bois d'Arc Formations); and clean-washed limestone at the top (Frisco Formation). Silt- and clay-sized detritus is largely restricted to the aulacogen area. Most of the Hunton carbonates are moderately to highly dolomitized on the northern shelf. The Hunton Group is as thick as 1,000 ft in the aulacogen; the upper surface is truncated toward the north, and the remaining parts of the unit are typically 100–400 ft thick on the northern shelf and in the Arkoma basin.

The Silurian–Devonian Hunton Group had a wide range of depositional environments and diagenetic changes that were conducive to reservoir development. Most of the fields are west of the Nemaha uplift, on the northeastern shelf of the Anadarko basin, although another major region of production is in central Oklahoma (Fig. 7). The productive interval contains a large number of stratigraphic traps. Typical depositional environments for reservoir units are low-relief skeletal

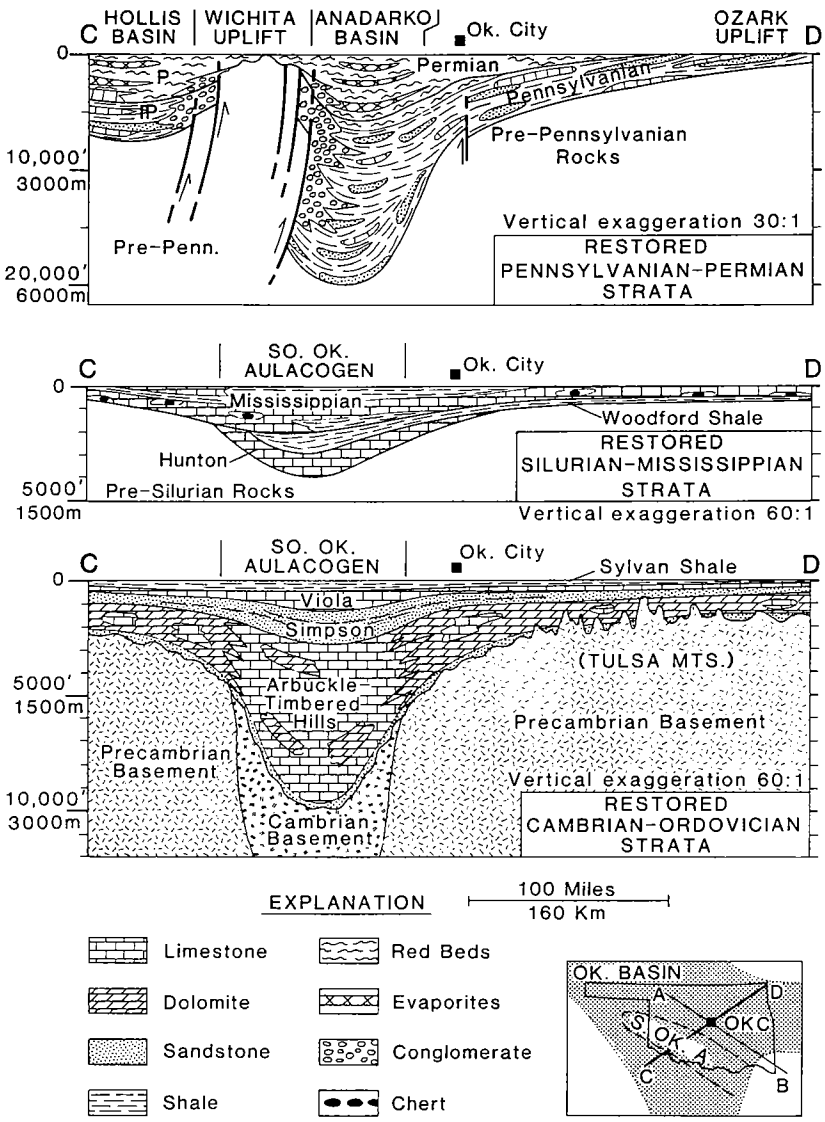

Figure 4 *(continued)*.

buildups and oolite shoals, both of which underwent some post-depositional dolomitization. Most structures containing Hunton rocks produce from the Hunton, but truncation traps are most common for this interval. The West Edmond field in northwestern Oklahoma County is a significant Hunton oil producer; at this site the Hunton is truncated on the west flank of the Nemaha uplift. An unusual structural–stratigraphic relationship is present in the Southeast Joiner City field of southwestern Carter County, where the Hunton is overturned and the Bois d'Arc and Chimneyhill units both produce from two repeated sections in the same borehole. Other major Hunton producing areas are on the north flank of the Anadarko basin and include the Golden Trend and the Sooner Trend, and the Ringwood, Aledo, and Custer City North fields. Table 3 shows that several names from the eastern United States have crept into the GIS files.

Mississippian

Mississippian strata are widespread over most of Oklahoma (Craig and others, 1979; Johnson and others, 1988). They consist of shallow-marine limestones and shales in most parts of the Oklahoma basin, but thick, dark-gray fissile shales (Caney, Goddard, and Springer Shales) predominate in the eastern part of the aulacogen. Cherty limestone was significant in the northern half of the State during Osagean and Meramecian time. The depositional environment for most Mississippian strata was well-aerated, warm, shallow seas that supported an abundance of benthic life forms. Stratigraphic thicknesses generally range from 200 to 2,000 ft in the northern shelf areas, but the dark-shale sequence in the aulacogen typically is 2,000–5,000 ft thick.

Mississippian carbonates (Table 4) have varied depositional and diagenetic histories that have led to reservoir development and hydrocarbon entrapment; diagenesis of the Osage rocks, fracturing of Meramec limestones, and deposition of Chester bioclastic packstones, wackestones, and oolitic grainstones are typical examples. Production from Mississippian carbonates, chiefly in the north half of Oklahoma (Fig. 8), extends over a larger area than all other carbonate production. Examples of field areas are (1) the Mississippi chat accumulations east of the Nemaha uplift, (2) the Chester limestones in the Mocane–Laverne field of Beaver and Harper Counties, and (3) the large number of fields (Sooner Trend, Ringwood, Enid Northeast, Okeene Northwest, Cedarvale Northeast, and others) that produce from the Chester and Mississippi lime on the northeast flank of the Anadarko basin.

Lower Pennsylvanian

Major changes took place in Oklahoma during Pennsylvanian time. Early and middle Paleozoic epeirogenic movements, accompanied by the deposition of relatively simple sequences of shelf carbonates (with some shales and sandstones) over vast regions of the Oklahoma basin, ended with a series of orogenic movements that subdivided the State into the tectonic provinces so easily recognized today (Figs. 1,4). First, an episode of Late Mississippian–Early Pennsylvanian epeirogenic uplift and erosion throughout most of the Oklahoma basin produced a widespread pre-Pennsylvanian unconformity, except where sedimentation apparently was continuous along the axis of the aulacogen (in the deep Anadarko and Ardmore basins). Then a series of orogenic pulses in the aulacogen and the Ouachita trough through Early, Middle, and Late Pennsylvanian time caused, or contributed to, the following: folding and thrusting of the Ouachita fold belt; raising of the Wichita, Criner, Arbuckle, Nemaha, and Ozark uplifts; and pronounced downwarping of the Anadarko, Ardmore, Marietta, Arkoma, and Hollis basins (Tomlinson and McBee, 1959; Ham and Wilson, 1967; Rascoe and Adler, 1983; Johnson and others, 1988; Sutherland, 1988; McBee, 1995).

Table 2.—Names Used for Middle and Upper Ordovician Carbonates That Produce Petroleum in Oklahoma

Upper Ordovician	Middle Ordovician
Sylvan[a]	Simpson Dolomite
Maquoketa[a]	Dolomite
Viola	Marshall
Trenton	Bromide Dense
Viola Upper	Dense Dolomite
Viola Lower	Plattin
Fernvale	Joachim
Viola Dolomite	Birdseye Lime
Trenton Dolomite	Everton
Kimmswick	Joins

Cumulative Production
(1/1/79 through 9/30/95)
Oil: 107,967,129 Bbl
Gas: 296,102,909 Mcf

[a] Refers to the dolomitic parts of these units.

Table 3.—Names Used for Silurian and Devonian Carbonates That Produce Petroleum in Oklahoma

Devonian	Silurian
Devonian	Silurian
Hunton	Hunton B
Hunton Group	Hunton Lower
Hunton Upper	Cayugan
Penters	Henryhouse
Bois D'Arc	Niagaran
Bois D'Arc Upper	St. Clair
Bois D'Arc Lower	Keel
Haragan	Chimneyhill
	Chimneyhill Lower
	Brassfield

Cumulative Production
(1/1/79 through 9/30/95)
Oil: 156,863,674 Bbl
Gas: 1,714,744,414 Mcf

Pennsylvanian strata in the State are sequences of marine and nonmarine shale, sandstone, conglomerate, and limestone that thicken markedly (to as much as 10,000–15,000 ft) into the rapidly subsiding basins (McKee and others, 1975). The thick wedges of terrigenous clastic sediments were shed from nearby uplifts, mainly in the south; thinner carbonates were deposited in shallow-water shelf areas distal to the uplifts. Successively younger Pennsylvanian strata commonly overlap older units at the margins of the basins and across some of the uplifts.

Lower Pennsylvanian carbonate units (Table 5) are thinner than those of the underlying four groups of rocks. Production from these carbonates is essentially restricted to the Arkoma basin and its nearby shelf area (Fig. 9), with notable production coming from the frontal fault zone in southern Pittsburg County. The Wapanucka lime produces in parts of Pittsburg and Latimer Counties in the Blanco South, Hartshorne South, and Pittsburg fields.

Middle Pennsylvanian

The major mountain systems of southern Oklahoma were uplifted and were shedding clastic debris during deposition of most Middle Pennsylvanian strata. This flood of clastics in the south restricted major carbonate sedimentation to the northern half of the State; therefore, petroleum production from carbonates also is restricted to the north (Fig. 10). Desmoinesian strata were the first Pennsylvanian units to be deposited across central and north-central Oklahoma.

Middle Pennsylvanian carbonates typically are thinner than those in the pre-Pennsylvanian strata. Middle Pennsylvanian limestones were deposited in cycles representing supratidal, intertidal, subtidal, shallow-marine, and shelf-break carbonate environments. A large number of named carbonate reservoirs in this sequence (Table 6) reflect the great thickness and the many facies changes of the Middle Pennsylvanian strata.

Most Middle Pennsylvanian production from carbonates

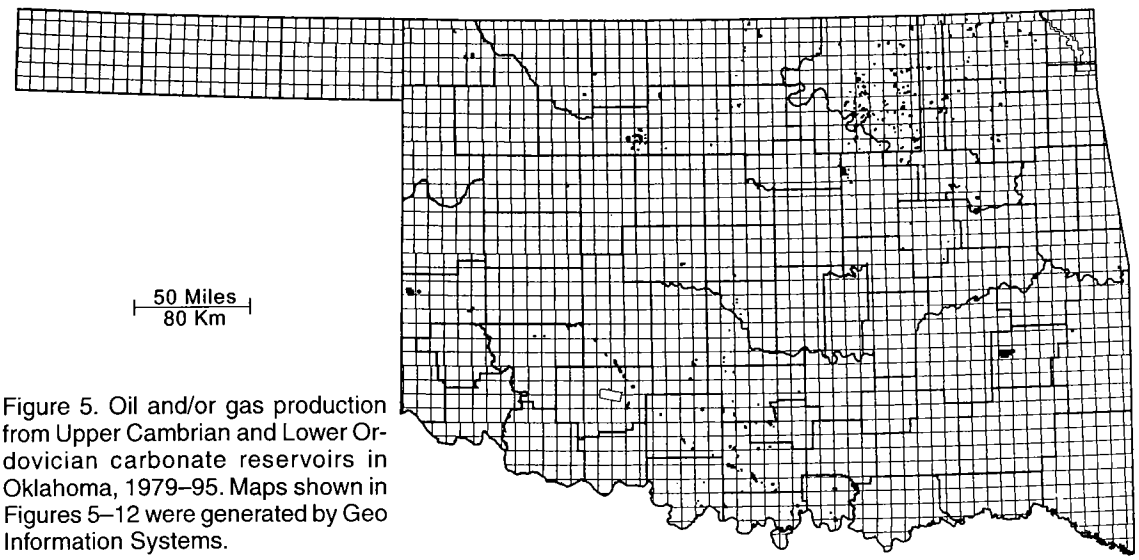

Figure 5. Oil and/or gas production from Upper Cambrian and Lower Ordovician carbonate reservoirs in Oklahoma, 1979–95. Maps shown in Figures 5–12 were generated by Geo Information Systems.

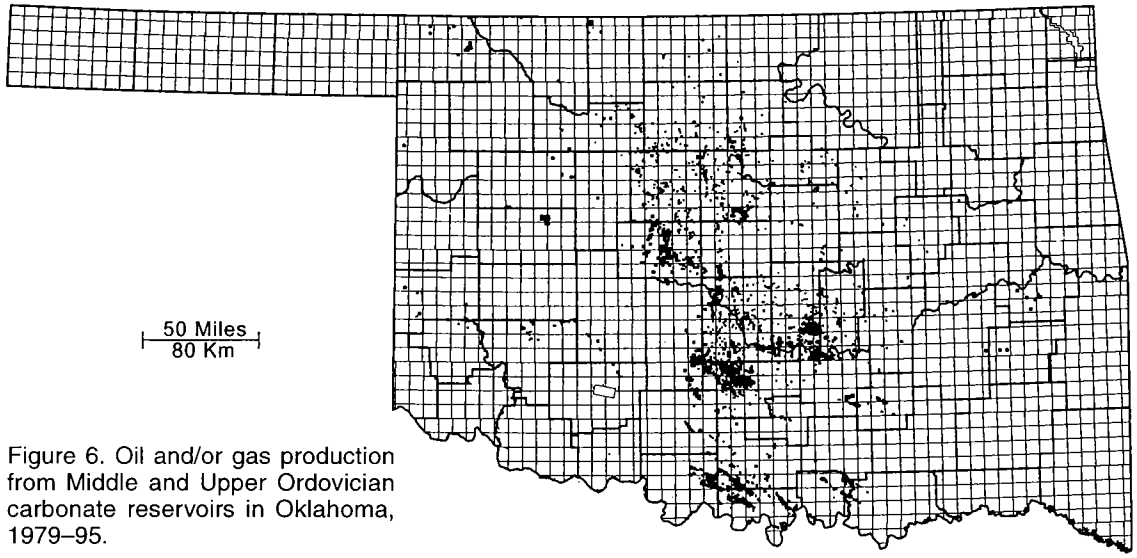

Figure 6. Oil and/or gas production from Middle and Upper Ordovician carbonate reservoirs in Oklahoma, 1979–95.

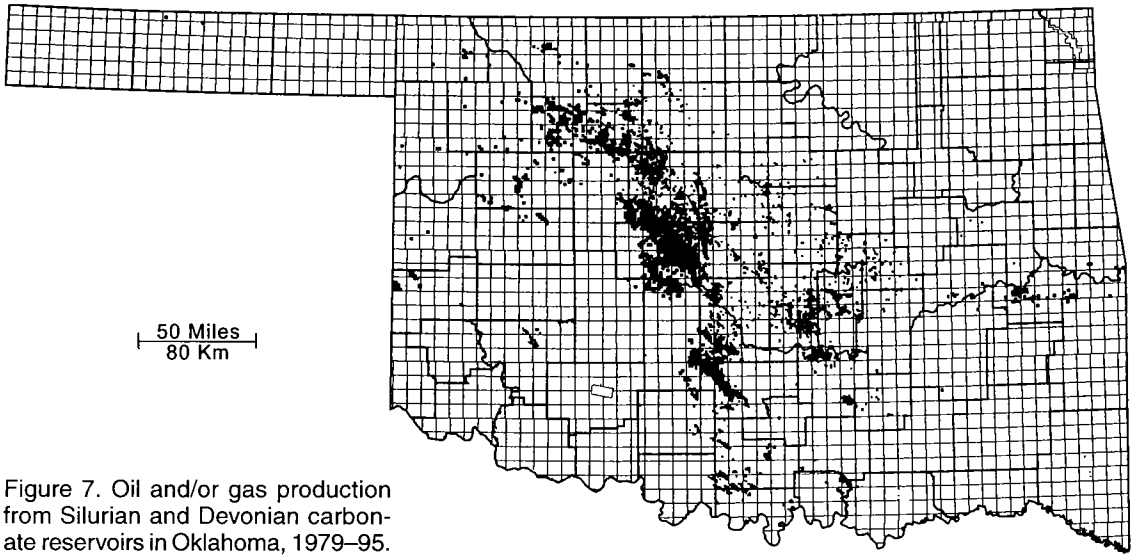

Figure 7. Oil and/or gas production from Silurian and Devonian carbonate reservoirs in Oklahoma, 1979–95.

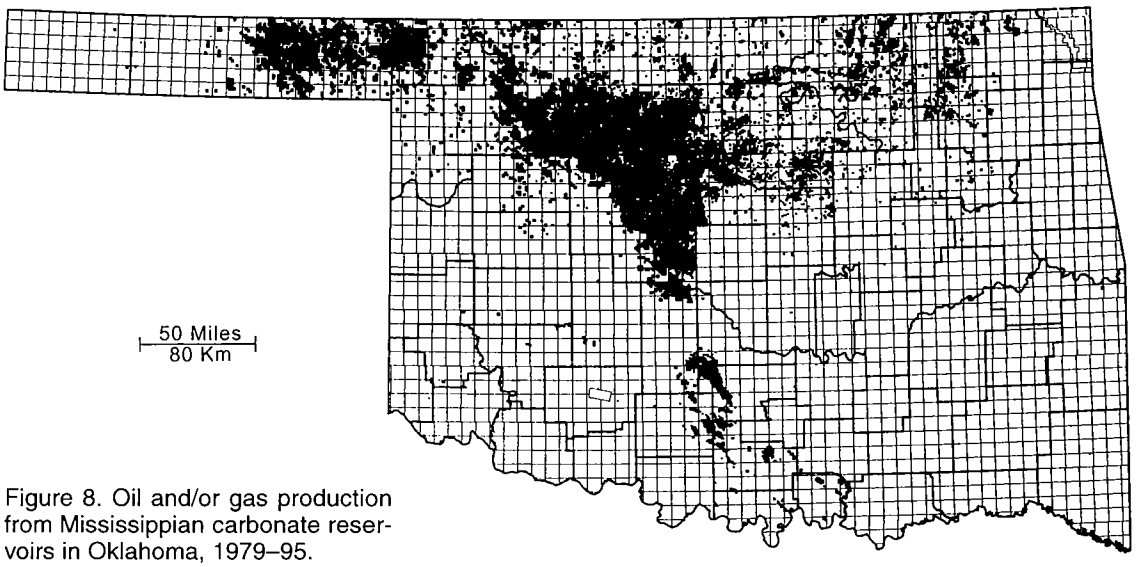

Figure 8. Oil and/or gas production from Mississippian carbonate reservoirs in Oklahoma, 1979–95.

Table 4.—Names Used for Mississippian Carbonates That Produce Petroleum in Oklahoma

Chesterian	St. Louis
Chester	Chappel
Miss:Chester	
Chester Upper Middle	**Osagean**
Chester Lower Middle	Osage
Chester Lower	Mississippi Chat
Chester Basal	Mississippi Lower
Manning	Mississippi Reef
Miss:Manning	Boone
Pitkin	Sycamore
Hindsville	Sycamore Upper
	Sycamore Middle
Meramecian	Sycamore Lower
Meramec	Keokuk
Mississippi Lime	Reeds Spring
Mississippi Upper	St. Joe
Mayes	
Moorefield	**Kinderhookian**
Black Lime	Kinderhook
Ste. Genevieve	

Cumulative Production
(1/1/79 through 9/30/95)
Oil: 308,753,749 Bbl
Gas: 3,677,013,699 Mcf

Table 5.—Names Used for Lower Pennsylvanian Carbonates That Produce Petroleum in Oklahoma

Atokan	**Morrowan**
Thirteen Finger	Wapanucka
	Wapanucka + Cromwell
	Union Valley Lime

Cumulative Production
(1/1/79 through 9/30/95)
Oil: 27,700,117 Bbl
Gas: 292,706,516 Mcf

is on the northwest shelf of the Anadarko basin and along the Nemaha uplift (Fig. 10). Production is concentrated in the Marmaton Group, which extends upward from the base of the Oswego to the top of the Lenapah. Putnam field in Dewey and Custer Counties is an Oswego algal-mound development along the shelf break, with porosity developed as fractures and vugs. Oswego production also comes from the following fields: Avard Northwest (Woods County), Oklahoma City (Oklahoma and Cleveland Counties), and Ringwood (Major, Alfalfa, and Garfield Counties).

Upper Pennsylvanian

Upper Pennsylvanian carbonates were a continuation of the relatively thin, cyclic sedimentation that started in the Middle Pennsylvanian. The distribution of carbonate production is scattered throughout central and western Oklahoma (Fig. 11). Important production comes from the Checkerboard lime in the Edmond Northeast field (Oklahoma County) and from the Topeka and Lovell limes in gas fields of the Oklahoma Panhandle. Owing to the cyclic nature of Upper Pennsylvanian limestones, there are many named carbonate reservoirs in the thick sequences of Missourian and Virgilian strata (Table 7).

Permian

Permian strata are limited to central and western Oklahoma. Clastics were eroded from the Ouachitas (reduced to low mountains by this time) on the east, the ancestral Rocky Mountains on the west, and the Wichita uplift in southwestern Oklahoma. Sediments accumulated mainly in the Anadarko basin, and also in the Hollis basin and the Panhandle region. Early Permian (Wolfcampian) carbonates and shales, both gray and red beds, are overlain by a major evaporite and red-bed sequence of Leonardian, Guadalupian, and Ochoan age. Evaporites (salt and gypsum/anhydrite) thicken into the basins that continued to subside more than the adjacent uplifts and arches. Permian strata are as thick as 7,000 ft in the Anadarko basin,

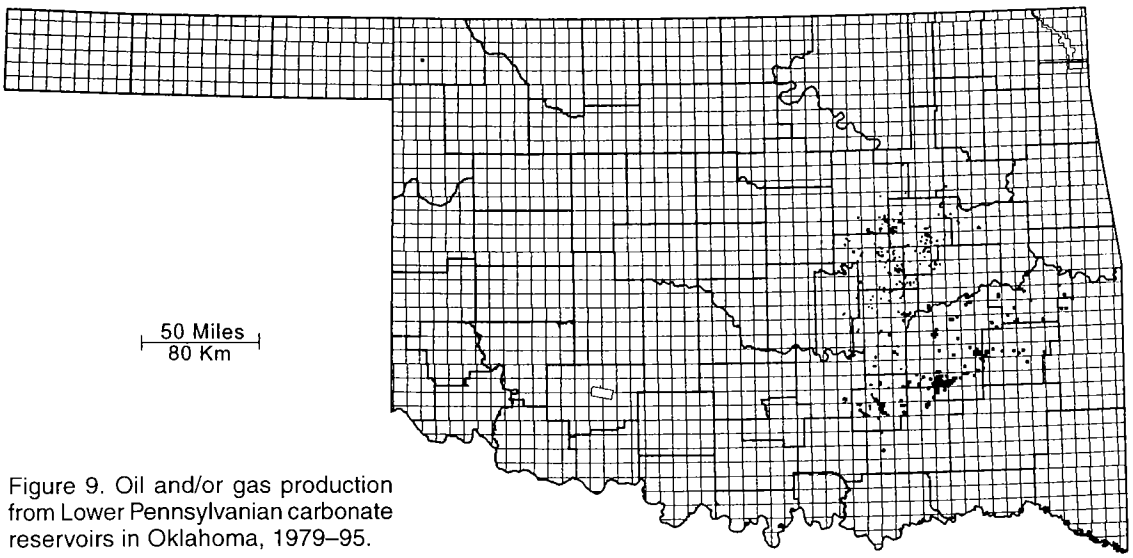

Figure 9. Oil and/or gas production from Lower Pennsylvanian carbonate reservoirs in Oklahoma, 1979–95.

Table 6.—Names Used for Middle Pennsylvanian Carbonates That Produce Petroleum in Oklahoma

Desmoinesian	Oswego 1st
Marmaton	Oswego 2nd
Lenapah	Oswego 3rd
Altamont	Oswego 4th
Oologah	Oswego Lower
Pawnee	Verdigris
Big Lime	Pink Lime
Big Lime–Oswego	Inola
Oswego	Spaniard
Oswego Upper	Frensley

Cumulative Production
(1/1/79 through 9/30/95)
Oil: 81,397,527 Bbl
Gas: 699,951,413 Mcf

4,000 ft in the Hollis basin, and 1,000–3,000 ft in nearby shelf or platform areas (McKee and others, 1967).

Permian carbonates are the youngest series of platform carbonates in Oklahoma (Table 8). The carbonates are thin, and production is almost exclusively gas. The Wolfcampian (Chase Group) is characterized by clastic–carbonate cycles, with the clastics being variegated marginal-marine or continental deposits; this contrasts with the Pennsylvanian basinal units that contain black phosphatic shales. A number of the Permian reservoirs are dolomites. Three producing areas are prominent (Fig. 12): the Guymon–Hugoton gas area in the Panhandle, one of the world's largest gas fields; the very shallow area on the Nemaha uplift in north-central Kay County; and the Brown dolomite production from the Erick area on the Wichita uplift in Greer and Beckham Counties.

SUMMARY

Oklahoma's platform carbonates, although not as productive as its clastics, yield oil and gas from most parts of the

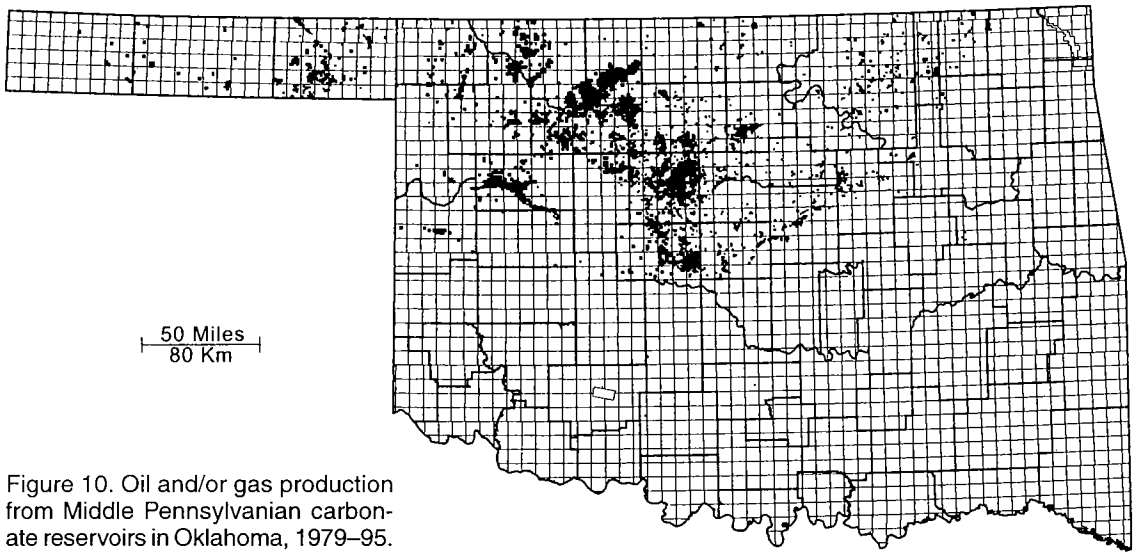

Figure 10. Oil and/or gas production from Middle Pennsylvanian carbonate reservoirs in Oklahoma, 1979–95.

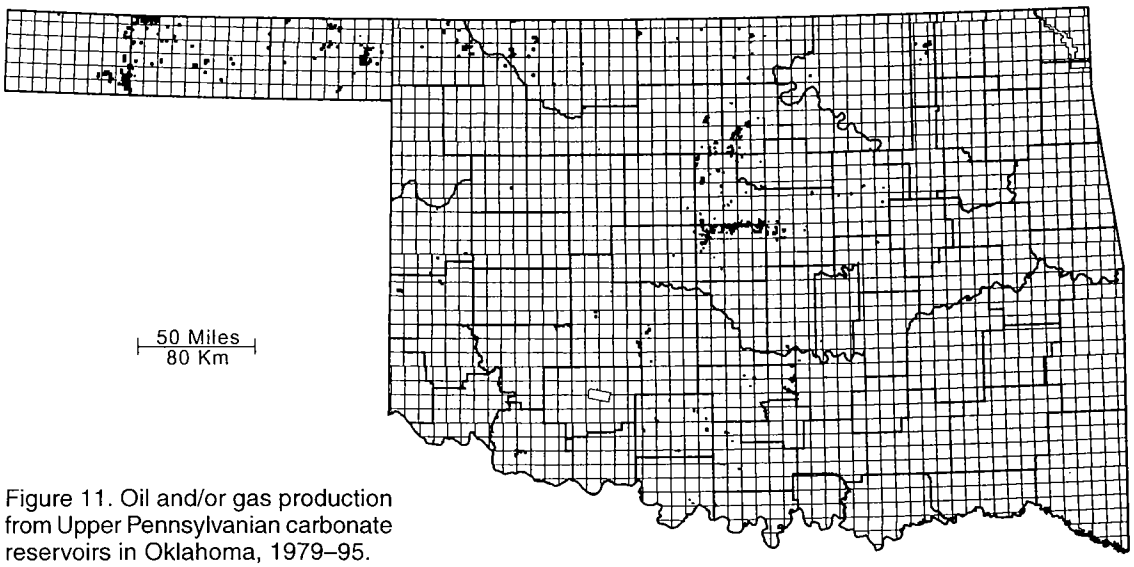

Figure 11. Oil and/or gas production from Upper Pennsylvanian carbonate reservoirs in Oklahoma, 1979–95.

Table 7.—Names Used for Upper Pennsylvanian Carbonates That Produce Petroleum in Oklahoma

Virgilian	County Line
Wabaunsee	Hoxbar Upper Oolitic
Brownville	Twin Lime
Stonebreaker	Ostracod
Ada	Anadarche
Emporia	Oolitic
Burlingame	Main Oolitic Lime
Topeka	Kansas City
Crinoidal	Avant
Pawhuska	Dewey
Deer Creek	Belle City
Oread	Canyon Lime
Toronto	Confederate
Lovell	Hogshooter
Pedee	Hertha
	Coffeyville
Missourian	Checkerboard
Lansing	Sasakwa
Zuckerman	Natsy
Daube	

Cumulative Production
(1/1/79 through 9/30/95)
Oil: 10,996,491 Bbl
Gas: 170,835,712 Mcf

Table 8.—Names Used for Permian Carbonates That Produce Petroleum in Oklahoma

Leonardian	Krider Upper
Cimarron	Krider Lower
	Winfield
Wolfcampian	Towanda
Wolfcamp	Fort Riley
Chase Group	Wreford
Guymon Hugoton Field	Council Grove
Herington	Crouse
Crystalline	Cottonwood
Brown Dolomite	Neva
Dolomite	Admire
Panhandle Dolomite	Foraker
Krider	

Cumulative Production
(1/1/79 through 9/30/95)
Oil: 8,472,525 Bbl
Gas: 1,304,481,791 Mcf

State. The geologic history of reservoir development and entrapment encompasses many depositional, orogenic, and tectonic environments. Significant carbonate discoveries, especially in lower Paleozoic strata, continue to appear. As a result, Oklahoma remains a fertile field for explorationists, developers, and operators seeking optimization of producing properties.

REFERENCES CITED

Amsden, T. W., 1976, Hunton Group (Late Ordovician, Silurian, and Early Devonian) in the Anadarko basin of Oklahoma: Oklahoma Geological Survey Bulletin 121, 214 p.

_____1980, Hunton Group (Late Ordovician, Silurian, and Early Devonian) in the Arkoma basin of Oklahoma: Oklahoma Geological Survey Bulletin 129, 136 p.

_____1993, Pre-Woodford subcrop map of the Anadarko basin, western Oklahoma and Texas Panhandle: Oklahoma Geological Survey Map GM-34, 2 sheets, scale 1:500,000, with text.

Craig, L. C.; and others, 1979, Paleotectonic investigations of the Mississippian System in the United States: U.S. Geological Survey Professional Paper 1010, pt. 1, p. 1–369; pt. 2, p. 371–559; pt. 3, 15 plates.

Denison, R. E.; Lidiak, E. G.; Bickford, M. E.; and Kisvarsanyi, E. B., 1984, Geology and geochronology of Precambrian rocks in the central interior region of the United States: U.S. Geological Survey Professional Paper 1241-C, 20 p.

Fay, R. O., 1989, Geology of the Arbuckle Mountains along Interstate 35, Carter and Murray Counties, Oklahoma: Oklahoma Geological Survey Guidebook 26, 50 p.

Ham, W. E.; and Wilson, J. L., 1967, Paleozoic epeirogeny and orogeny in the central United States: American Journal of

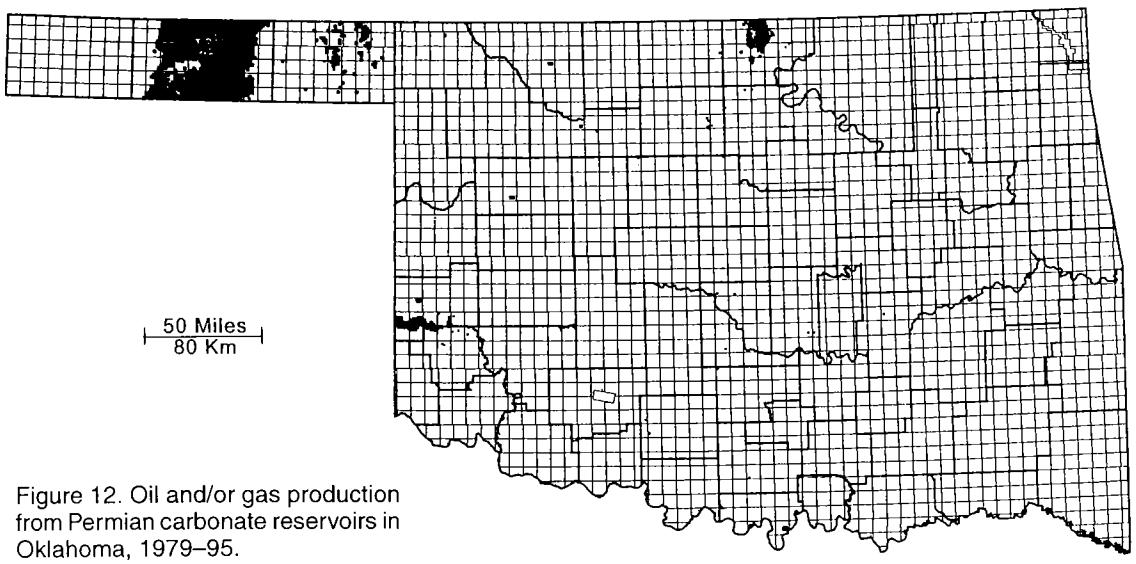

Figure 12. Oil and/or gas production from Permian carbonate reservoirs in Oklahoma, 1979–95.

Science, v. 265, p. 332–407.

Johnson, K. S., 1991a, Geologic overview and economic importance of Late Cambrian and Ordovician rocks in Oklahoma, *in* Johnson, K. S. (ed.), Late Cambrian–Ordovician geology of the southern Midcontinent, 1989 symposium: Oklahoma Geological Survey Circular 92, p. 3–14.

Johnson, K. S. (ed.), 1991b, Arbuckle Group core workshop and field trip: Oklahoma Geological Survey Special Publication 91-3, 266 p.

_____(ed.), 1993, Hunton Group core workshop and field trip: Oklahoma Geological Survey Special Publication 93-4, 212 p.

_____(ed.), 1997, Simpson and Viola Groups in the southern Midcontinent, 1994 symposium: Oklahoma Geological Survey Circular 99, 275 p.

Johnson, K. S.; and Cardott, B. J., 1992, Geologic framework and hydrocarbon source rocks of Oklahoma, *in* Johnson, K. S.; and Cardott, B. J. (eds.), Source rocks in the southern Midcontinent, 1990 symposium: Oklahoma Geological Survey Circular 93, p. 21–37.

Johnson, K. S.; Amsden, T. W.; Denison, R. E.; Dutton, S. P.; Goldstein, A. G.; Rascoe, Bailey, Jr.; Sutherland, P. K.; and Thompson, C. M., 1988, Southern Midcontinent region, *in* Sloss, L. L. (ed.), Sedimentary cover—North American craton, U.S.: Geological Society of America, The Geology of North America, v. D-2, p. 307–359. [Reprinted as Oklahoma Geological Survey Special Publication 89-2, 53 p.]

McBee, William, Jr., 1995, Tectonic and stratigraphic synthesis of events in the region of the intersection of the Arbuckle and Ouachita structural systems, Oklahoma, *in* Johnson, K. S. (ed.), Structural styles in the southern Midcontinent: Oklahoma Geological Survey Circular 97, p. 45–81.

McKee, E. D.; and others, 1967, Paleotectonic maps of the Permian System: U.S. Geological Survey Miscellaneous Geologic Investigations Map I-450, scale 1:5,000,000.

_____1975, Paleotectonic investigations of the Pennsylvanian System in the United States: U.S. Geological Survey Professional Paper 853, pt. 1, 349 p.; pt. 2, 192 p.; pt. 3, 17 plates.

Rascoe, Bailey, Jr.; and Adler, F. J., 1983, Permo–Carboniferous hydrocarbon accumulations, Mid-Continent, U.S.A.: American Association of Petroleum Geologists Bulletin, v. 67, p. 979–1001.

Schramm, M. W., Jr., 1964, Paleogeologic and quantitative lithofacies analysis, Simpson Group, Oklahoma: American Association of Petroleum Geologists Bulletin, v. 48, p. 1164–1195.

_____(ed.), 1966, Symposium on the Viola, Fernvale and Sylvan: Tulsa Geological Society Digest, v. 34, 151 p.

Statler, A. T., 1965, Stratigraphy of the Simpson Group in Oklahoma, *in* Herndon, Thomas (ed.), Symposium on the Simpson: Tulsa Geological Society Digest, v. 33, p. 162–211.

Sutherland, P. K., 1988, Late Mississippian and Pennsylvanian depositional history in the Arkoma basin area, Oklahoma and Arkansas: Geological Society of America Bulletin, v. 100, p. 1787–1802.

Tomlinson, C. W.; and McBee, William, Jr., 1959, Pennsylvanian sediments and orogenies of Ardmore district, Oklahoma, *in* Petroleum geology of southern Oklahoma: American Association of Petroleum Geologists, Tulsa, v. 2, p. 3–52.

Distribution and Geometries of Platform-Carbonate Reservoirs: Insight from Modern Counterparts in the Bahamas

G. Michael Grammer and Robert N. Ginsburg
University of Miami
Miami, Florida

ABSTRACT.—All shallow-water-carbonate facies have the potential ultimately to become reservoir rocks for hydrocarbons. Some, like the Jurassic lime sands of Saudi Arabia, qualified as reservoirs by retaining their originally high depositional or primary porosity. Other reservoir units, such as those found in the Ordovician of Texas and Oklahoma, required pervasive dolomitization and fracturing to provide an interconnected pore network. In between these two end-members is a spectrum of examples illustrating the synergism of depositional geometry, fabric, and diagenesis in the formation and evolution of reservoirs.

Geologists and engineers need to take advantage of the frequent coupling, or linkage, of deposition and diagenesis to be successful in the search for stratigraphic traps in carbonates. Patterns of deposition derived from the study of young carbonates provide a starting point, as they may yield a combination of details on the distribution or zonation of facies, their three-dimensional geometry, and potential for diagenetic modification. This information may then be utilized both to understand the distribution of carbonate reservoirs at an exploration scale and to develop carbonate fields at production and enhanced-production scales.

The study of Cenozoic carbonates in the Bahamas has provided significant insight into the distribution and early diagenetic modification of several potential carbonate reservoirs, including reef-margin, ooid-shoal, and off-platform marginal-slope deposits. These types of studies in young carbonates provide us with a better understanding of how, where, and why carbonate reservoirs form, and should aid in the successful search for, and development of, economic reservoirs in ancient carbonates.

INTRODUCTION

In the search for hydrocarbon reservoirs in carbonate rocks, concepts of deposition, especially facies distribution, play a key role in helping to select areas for exploration and in interpreting geophysical data. When reservoirs are discovered, interpretations of depositional facies and a search for applicable analogues become essential for both primary and enhanced field development. Among the conceptual models that have developed since World War II are reefs and reef mounds as reservoirs; facies zonation of carbonate platforms, shelves, and reefs; tidally controlled and oriented grainstone bars; and pinchout traps of interior platform cycles. Each of these models offers enhancement to both exploration strategy and development tactics, and many were developed from study of recent depositional environments in the Bahamas through the application of actualistic, or comparative, sedimentology.

In more recent times, sequence and seismic stratigraphy have been widely used new concepts for understanding depositional geometries that are widely applied to both exploration and development. Combined with advances in our understanding of the detailed internal architecture and diagenesis of carbonate depositional facies, conceptual models of the systems tracts that can be identified on seismic profiles and from outcrop and well data offer both predictability of the presence and probable distribution of potential reservoir facies as well as indications of their potential reservoir quality.

At present, we are seeing the birth of another critical era in the study of carbonates, as increasingly detailed information is needed on the three-dimensional distribution of facies for input into reservoir-characterization models being used both to maximize initial production in new fields and to aid in enhanced-recovery operations. The ability to construct realistic geologic-based reservoir models, and then to scale these models up into applicable engineering-based reservoir simulation models, depends in large degree upon the understanding of the lateral and vertical distribution of reservoir and associated facies, as well as their potential for diagenetic modification. The recent trend toward very high-resolution sequence-stratigraphic (cyclostratigraphic) studies, which provide the reservoir details necessary for modeling, relies heavily on both modern and ancient (outcrop) analogues.

As in earlier times, the depositional environments in the Bahamas continue to provide a wealth of information for application to hydrocarbon exploration and production as they are studied in increasing resolution. In this paper, we offer a brief and necessarily incomplete overview of some past and recent applications of comparative sedimentology, many of which share their genesis with the study of recent carbonates in the Bahamas.

Grammer, G. M.; and Ginsburg, R. N., 2000, Distribution and geometries of platform-carbonate reservoirs: insight from modern counterparts in the Bahamas, *in* Johnson, K. S. (ed.), Platform carbonates in the southern Midcontinent, 1996 symposium: Oklahoma Geological Survey Circular 101, p. 13–23.

REEF TRENDS

The post–World War II discovery of oil in ancient reef limestone—first in the Devonian of Western Canada (Link, 1949) and then in the Silurian of Illinois (Lowenstam, 1948)—sparked a major expansion of interest in depositional aspects of reefs, and it marked the beginning of expanded interest in all aspects of carbonates. It is difficult for us as geoscientists in the last half of the 1990s to fully appreciate the impact that these discoveries of isolated carbonate reservoirs had on explorationists who traditionally thought of linear accumulations of hydrocarbon-bearing strata as being either structurally controlled or as sand bodies. The interpretations of seismic profiles in carbonate terrains were now guided by mental images of Pacific atolls. Moreover, there was a need to consider where and how reefs were initiated, their internal facies anatomy, and what, if any, were the proximity indicators for reefs that might be found in their surrounding sediments. Interest in the basic lore of reefs was sufficient to inspire Seismograph Service Corp. to support the preparation of *Bibliography of Organic Reefs, Bioherms, and Biostromes* (Pugh, 1950), which contained some thousand entries.

The realization that ancient reefs, like their modern counterparts, have a potentially predictable zonation (Lowenstam, 1950) provided a powerful tactic to be applied to field development, and it spawned numerous studies of both modern and ancient reefs. Facies zonation in reefs has been used especially in the Devonian reefs of Western Canada. An example of this is shown in Figure 1 (from Walls, 1983), where the lateral distribution of diagenetically controlled porosity and permeability in the Golden Spike reef complex is tied back to the primary depositional facies. A great deal of our understanding of reef architecture, facies distribution, and oceanographic settings is the result of numerous studies of modern reefs in the Caribbean and other localities around the world (see, for example, the summary by James, 1983).

FACIES ZONATION

On the larger scale of carbonate platforms and shelves, facies zonation is also the key concept. In the post–World War II era, the simplest version of zonation was the undaform (shelf or platform), clinoform (slope), and fondoform (basin) first presented by Rich (1951). Later, in the 1960s, the influence of research on recent sediments of the Bahamas inspired an elaboration of this tripartite division and suggested an idealized pattern related to variations in degree of agitation and circulation (Shaw, 1964; Irwin, 1965; Wilson, 1970). Wilson (1975) is responsible for the full development of the general facies zonation that is now so widely applied to the interpretation of carbonate platforms and shelves.

One instructive example of how zonation in its simplest form was used to make significant discoveries of hydrocarbons was reviewed by LeMay (1972). In a figure from his paper (Fig. 2A), the pre-discovery situation for a Lower Permian reef trend along the margin of the Delaware basin in southeastern New Mexico is shown. In the early part of evaluating these reservoirs, little else was known other than the rapid and distinct lithologic change in facies from north to south. In wells to the north (Abo Formation), recovered facies included light-colored, shelf-type anhydritic dolomite and gray-green shales. In wells drilled to the south, toward the Delaware basin, rocks recovered from the correlative interval (Bone Springs Limestone) were characterized by black and brown cherty carbonates interbedded with fine-grained sandstones (LeMay, 1972). A single oil field, Lovington (Fig. 2A), was developed between these two contrasting lithologies. The concept of a barrier reef separating shelf and basin deposits was at the time well established from studies of the Permian Capitan reef, but it had not been applied to the Abo–Bone Springs interval. When this simple concept was combined with the occurrence of shelf and basinal deposits as illustrated in

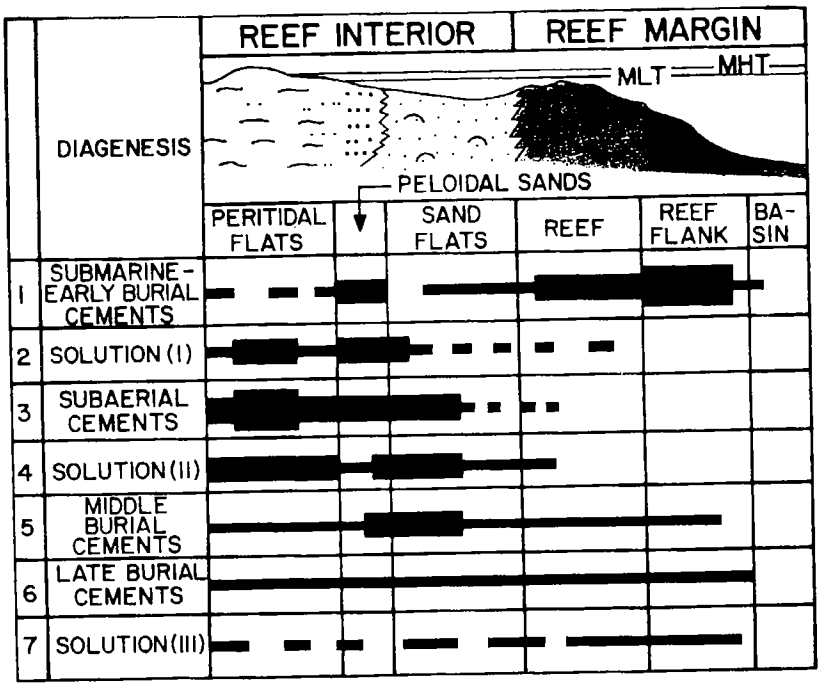

	POROSITY	PERMEABILITY (MD)
REEF MARGIN	MEAN 4-10% MODE 2-8%	MEAN 10-100 MODE 1-10
REEF INTERIOR	MEAN 7-12% MODE 6-10%	MEAN 50-60 MODE 10-20

Figure 1. Schematic summary of the facies distribution and diagenesis of Golden Spike reef complex, Upper Devonian of Alberta, Canada, including porosity and permeability data from Walls (1983). The porosity in the reef margin is variable but consistently lower than in the reef interior. In the reef margin, primary pores were occluded by internal sediment and early cement (see also discussion on rates of cement growth in Grammer and others, 1993b). In deposits of the reef interior, primary porosity of skeletal sands and peritidal laminites was retained and enhanced by solution. This example illustrates the selective effects of diagenesis that is related to depositional facies. From Walls (1983), reprinted by permission.

Figure 2A by geologists from Pan American Co. (Amoco), it provided the justification for initiating a search for a shelf-margin reef with seismic profiling, and led to the discovery of the Empire Abo field. Using the barrier-reef model to guide the seismic interpretation and exploratory drilling resulted in the discovery and development of a series of profitable oil fields in the Empire–Abo trend (Fig. 2B), which in 1972 had an estimated half-billion barrels of primary production.

Additional models, such as the one developed for carbonate ramps as an alternative to carbonate-shelf models (Ahr, 1973), or the summary work by Read (1984) on the variability of carbonate platforms and the concomitant changes in facies type and distribution, have provided increasing detail and flexibility needed for application to subsurface carbonate deposits. More recently, papers integrating studies of both modern and ancient deposits, such as the one by Handford and Loucks (1993), have incorporated the concept of sequence stratigraphy and the dynamic aspect of carbonate-platform sedimentation in response to changes in relative sea level to further refine exploration models.

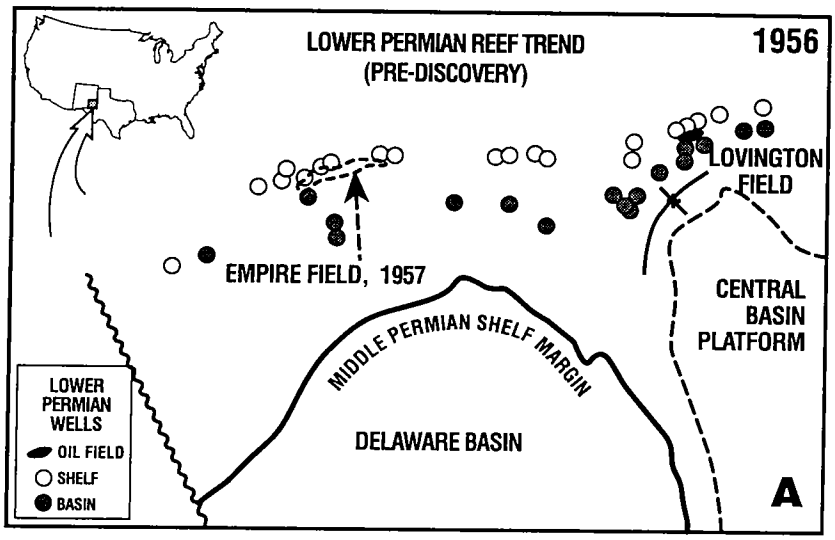

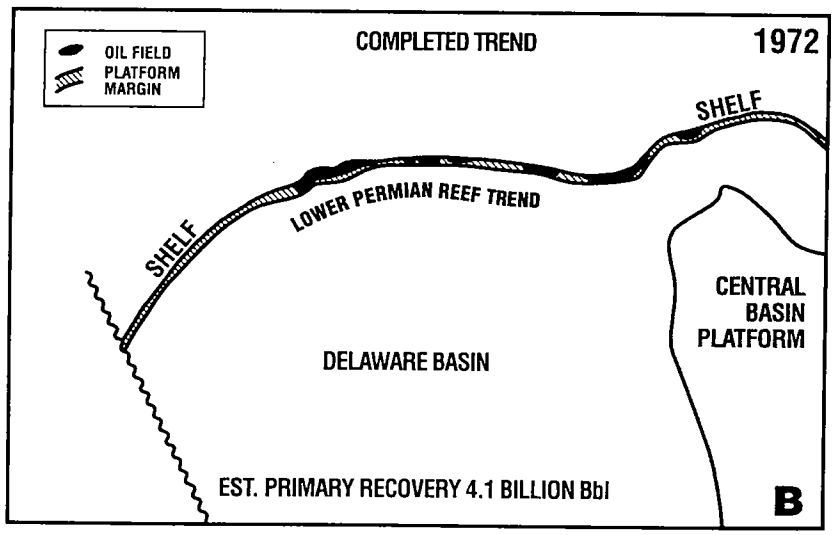

Figure 2. Pre- and post-discovery situations, Lower Permian Abo trend, New Mexico. (A) Pre-discovery situation, showing wells that recovered shelf deposits to the north and basinal sediments to the south. This pattern encouraged a seismic search for a reefal margin in between that resulted in the discovery of the Empire field. (B) Subsequent development of the trend to 1972, with an estimated half-billion barrels of primary production. From LeMay (1972), reprinted by permission.

Sequence-Stratigraphic Models

The major innovations of sequence stratigraphy over the zonal paradigm of Wilson (1975) have been to (1) make carbonate-platform models dynamic by introducing repeated cycles of sea-level fluctuations, each of which results in genetically related, time-equivalent facies realms (facies tracts) bounded by unconformities that can be mapped from seismic and/or subsurface data; (2) replace the nine lithofacies belts of Wilson (1975) with three systems tracts—highstand, transgressive, and lowstand—based on depositional geometries and their interrelationships as depicted in Figure 3, from James and Kendall (1992); (3) provide a hierarchy of rock successions recording relative changes in sea level, ranging from high-frequency, meter-scale parasequence (upward-shoaling or regressive cycles) units, through as many as four or five successively thicker successions (i.e., fifth to first order); and (4) provide a model that combines predictability of facies type, with inferences of lithology, gross depositional environment, and potential diagenetic modification (e.g., porosity development and/or occlusion related to exposure horizons). It is not necessary to subscribe to the global synchroneity of sea-level fluctuations to use sequence stratigraphy for the interpretation of a basin, nor is it required that one accept either a eustatic or tectonic explanation for the relative changes in sea level.

What contributions is sequence stratigraphy making to exploration strategies and development tactics? First and foremost, it has provided a new paradigm and method for exploration that translates seismic profiles into systems tracts whose idealized models include potential reservoir facies. For example, identifying a lowstand systems tract directs attention to the possibility of lenses of porous and permeable downslope gravity deposits and to increased porosity and permeability produced beneath the subaerial unconformity on the shelf or platform top, as depicted in Figure 4, from Sarg (1988). Similarly, the model predicts that for a period of rising sea level, potential exists for the development of an autochthonous carbonate bank or buildup that could be a potential reservoir (Fig. 5). During a highstand of sea level (Fig. 6), the model implies expanded development of shelf-margin, crestal deposits—reefs and winnowed grainstones—as well as the possibility of pinchouts of porosity in parasequences of the platform interior.

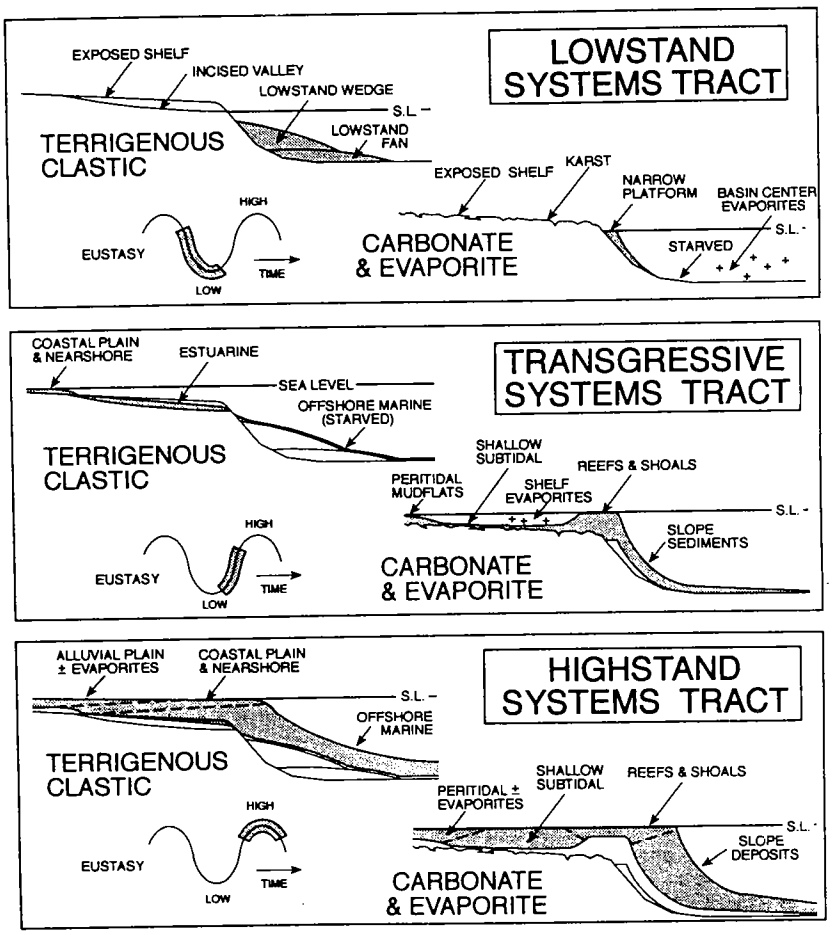

Figure 3. Schematic diagrams illustrating the significant differences expected between lowstand, transgressive, and highstand systems tracts of carbonate–evaporite settings and those of terrigenous clastics. From James and Kendall (1992), reprinted by permission.

CARBONATE-SAND RESERVOIRS

Some of the largest hydrocarbon reservoirs in the world occur in sparsely cemented grainstone deposits. The Jurassic Arab C and D Zones of Saudi Arabia were estimated by Wilson (1980) to contain a quarter of the world's total reserves. Although analysis of depositional facies played no role in the discovery of these reservoirs, it is now evident that diagenesis, controlled largely by the depositional succession, was responsible for the unusually high porosity and permeability found in these units. For both the Arab C and D Zones, high initial porosity and permeability in the grainstones were preserved as a result of capping anhydrites, which for the Arab D led to early dolomitization and for Arab C blocked any late, porosity-occluding diagenesis (Wilson, 1985). Why one sabkha-generated anhydrite led to the dolomitization of the underlying oolite, and the other did not, is unknown. The finer scale depositional anatomy of these reservoirs, and especially the presence of low-permeability zones resulting from seafloor cementation and/or lime mudstones, are critical in the management of the field and eventually in the secondary-recovery phase. Significant insight into reservoir development in units such as these, where depositionally and stratigraphically controlled diagenetic modifications are the primary factor in controlling reservoir deliverability, can be obtained through the study of young carbonates.

For example, in the ooid and peloid carbonate-sand complex of the late Pleistocene Miami Limestone, Evans and Ginsburg (1987) showed that the predominant theme in porosity development is the primary sediment fabric. They concluded that the primary fabric controls not only early cementation but also porosity development, both at the individual-grain scale as well as on larger scales such as those constrained by sedimentary structures. A significant conclusion of this study is that primary sedimentary fabric not only controls the early diagenetic modifications of ooid sand bodies but also may constrain late development of channel and cavernous porosity by creating preferential pathways for water movement through the rock unit.

In some cases, the distribution or geometry of carbonate grainstone reservoirs was determined through the application of known depositional processes. One example, illustrated in Figure 7, shows elongated skeletal grainstones with a northwest–southeast trend that are the principal reservoir facies in the Upper Permian Emma field in west Texas (Ruppel, 1990). Another example shows several linear ooid sand bodies with a similar type of orientation, in this case northeast–southwest, from the subsurface Mississippian of the Illinois basin shown in Figure 8, from Choquette and Steinen (1980). The depositional model for both of these examples of multiple, well-oriented grainstone bodies is the tidal bars of ooid sand described by Ball (1967) from Great Bahama Bank (Fig. 9). Recognition that a grainstone reservoir could be a tidal bar provides both a strategy for exploration and a tactic for field development. Tidal bars are almost invariably multiple; thus, finding one implies the probability of a series of regularly spaced bars, all with the same orientation. Development of a tidal-bar reservoir should be guided by their normally preferred orientation at high angles to sedimentary strike.

Not only are the exploration and development strategies of carbonate-sand bodies assisted by application of modern depositional and diagenetic models, but in many cases a modern analogue can help direct enhanced-production programs. For example, from modern studies we know that although tidally developed ooid shoals occur in a series of elongate bars oriented nearly perpendicular to depositional strike, deposits of these well-washed, relatively coarse-grained sand shoals are separated by units of finer grained material with higher mud content. The result is that even though the overall sand complex may extend for several kilometers in a strike direction along a carbonate-platform margin, the individual high-porosity and -permeability sand bodies that are oriented nearly perpendicular to strike are separated, at a scale of tens to hun-

dreds of meters, by lower porosity and permeability deposits that may form isolated flow units within the sand complex (see also Major and others, in press; Harris and others, 1993; Kerans and others, 1994). The distribution and geometries of these alternating higher and lower permeability units are clearly evident in satellite photographs of ooid shoal complexes from Joulters Cays and other areas in the Bahamas (e.g., Harris and Kowalik, 1994).

One example in which the rapid lateral variability of ooid sand bodies on a scale of tens of meters controls enhanced production is in the Pennsylvanian of the Paradox basin in southeastern Utah. In some fields, horizontal drilling of ooid reservoirs is being utilized to maximize recovery in mature reservoir intervals, but the reservoir-quality sands are interrupted laterally by low-permeability, fine-grained units (L. Amateis, personal communication). In a recent outcrop-based high-resolution sequence-stratigraphic study of reservoir and associated facies in the Paradox basin, Grammer and others (1996) and Eberli and others (1995) showed that ooid shoal facies occur in a series of overlapping sand waves of good-porosity grainstones, with muddier wackestones (lower energy facies between high-energy shoals) often found between. In addition, they found that the high-frequency cycles (5th order) containing the ooid shoal facies tend to stack vertically within a lower order sequence (4th order), with overall thickness of the grainstone facies, as well as porosity and permeability, increasing vertically within the 4th-order upward-shallowing sequence (Fig. 10).

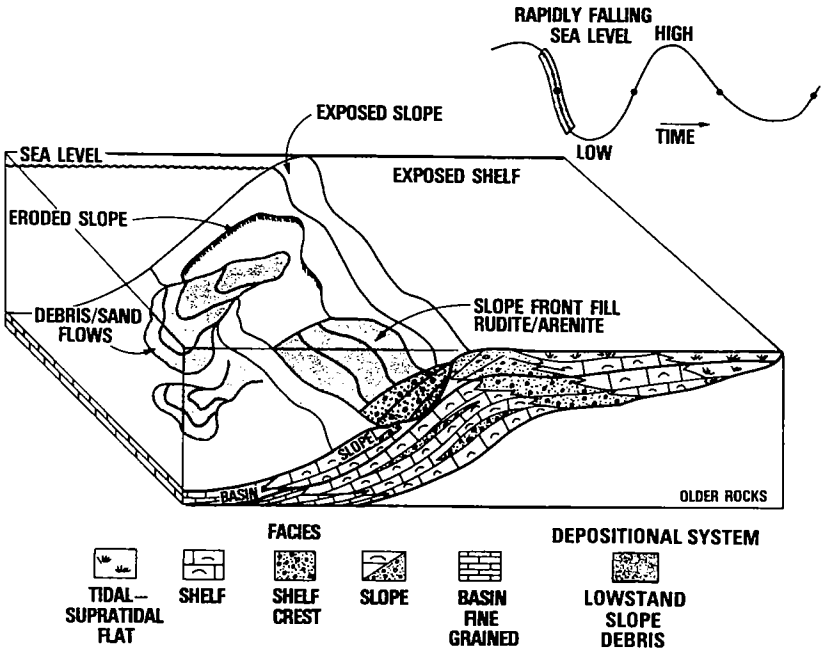

Figure 4. Schematic diagram showing the expected result of a rapid fall in sea level to below a carbonate-platform margin. Slope-front debris sheets and turbidites may be produced by subaerial erosion that can also increase porosity of the exposed shelf by dissolution. From Sarg (1988), reprinted by permission.

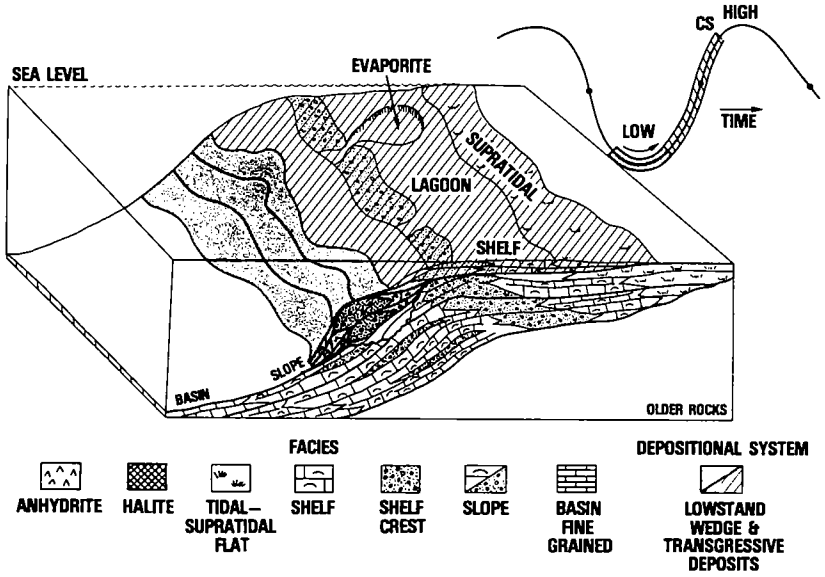

Figure 5. Schematic diagram showing the expected lowstand and transgressive systems tracts along a carbonate platform. An autochthonous bank may develop on the upper slope as sea level begins to rise, following the lowstand. When the shelf is flooded, both it and the bank become buried by transgressive deposits, while the starved area offshore develops a condensed section. From Sarg (1988), reprinted by permission.

PLATFORM-INTERIOR UPWARD-SHOALING CYCLES

Stratigraphic traps may be found in upward-shoaling cycles in the interior parts of carbonate platforms or shelves. For these reservoirs, an understanding of the lateral and vertical distribution of depositional facies provides both an exploration strategy and a guide for field development. Cyclic sedimentation that is characteristic of subsiding shelves and platforms is expressed in their interiors as upward-shallowing cycles that are generally a few to several meters thick (e.g., Roehl, 1967; Ginsburg, 1971; Lucia, 1972; Shinn, 1983; Goldhammer and others, 1987; Pratt and James, 1986). Each cycle consists of a succession of sedimentary structures, fossils, and traces that indicate an upward progression of environments from full marine (subtidal) through zones of intermittent exposure and flooding (intertidal) that are capped by beds indicative of only rare flooding (supratidal). In a humid climate, such as the Bahamas, the supratidal cap is a carbonate mudstone, but in arid climates, such as the present-day Arabian Gulf, the cap is anhydritic. These sabkha deposits (Evans and others, 1969; Shinn, 1983) provide an evaporitic seal and possibly a source of brines to dolomitize the underlying carbonates. The combination of

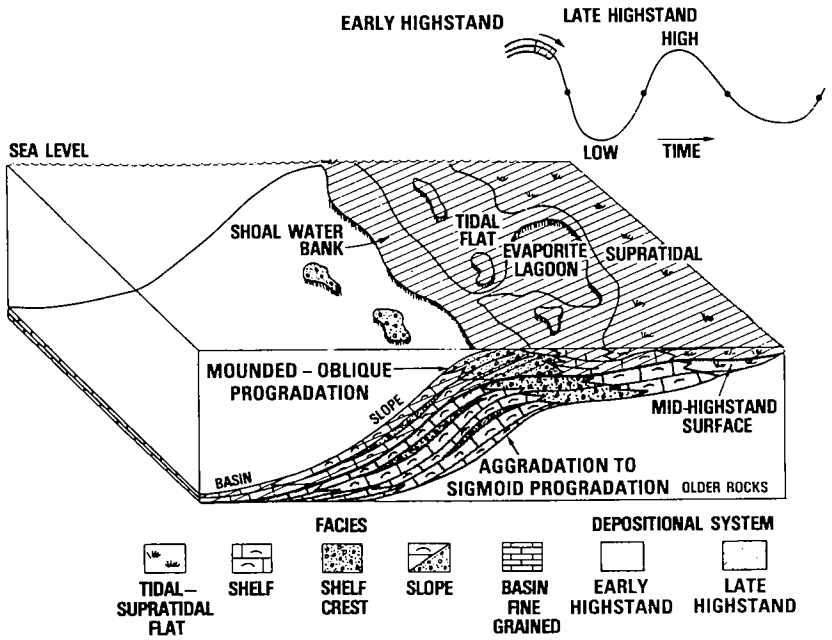

Figure 6. Schematic diagram showing the hypothetical early and late highstand deposits on a carbonate platform. Early highstand is characterized by aggradation to sigmoid progradation; late highstand deposition consists of mounded to oblique progradation. From Sarg (1988), reprinted by permission.

cyclic deposition and syndepositional dolomitization in an arid climate can produce a series of pinchouts of porous intertidal and subtidal dolomites sealed by evaporite caps, as illustrated in Figure 11, from Shinn (1983). This kind of stratigraphic–diagenetic reservoir is prominent in the oil-rich Permian carbonates of the Central Basin platform of west Texas and New Mexico (Wilson, 1980). The exploration strategy suggested by this model is a focus on the interiors of platforms or shelves that indicate accumulation in arid climates. The tactics for field development would be to seek stacked pinchouts of subtidal and intertidal dolomites and localized, coarser grained, sinuous tidal-channel deposits oriented at high angles to sedimentary strike.

MARGINAL-SLOPE DEPOSITS

Recent studies in the Bahamas and Caribbean have also provided much needed insight into the formation and evolution of platform-margin slope deposits, similar to those found in the Cretaceous of Mexico (e.g., Enos, 1977) or the Permian of west Texas (e.g., Brown and Loucks, 1993). The timing of deposition relative to sea level, and the paleogeographic position relative to wind direction (i.e., windward versus leeward), have been shown to be critical factors in controlling the composition, depositional fabric, and diagenetic potential of these downslope deposits (Grammer, 1991). For example, tremendous volumes of platform-top sediment are swept over the margin during highstands of sea level, especially along leeward margins of platforms, and form toe-of-slope sediment wedges (Wilber and others, 1990; Glaser and Droxler, 1991; Grammer and others, 1993a). In the Bahamas, these sediment wedges, which have formed only in the last 7,000–10,000 years following flooding of the platform (Grammer and Ginsburg, 1992), may be 70–90 m thick along open leeward margins (Wilber and others, 1990; Grammer and others, 1993a).

In addition, it has been found that the steep (35°–40°) slopes surrounding the Bahama platform consist of laterally heterogeneous lenses of coarse-grained skeletal material that were deposited during the transgressive phase of the latest sea-level rise (Grammer and others, 1993a). The high initial porosity and permeability of some of the foreslope deposits, however, were rapidly occluded by precipitation of marine pore-filling botryoidal aragonite and magnesium–calcite cements. The precipitation of these cements has been shown to have occurred within a few hundred years of deposition (Grammer and others, 1993a,b), and appears to have limited further diagenetic modification of these deposits. The sedimentary fabric, geometry, and scale documented in the lateral heterogeneity of foreslope deposits in the Bahamas, coupled with rapid occlusion of primary porosity and permeability, are significant findings for development of hydrocarbon reservoirs in these types of deposits, as the reservoirs may be characterized by discontinuous flow units of high porosity and permeability separated by low-permeability barriers.

FUTURE DIRECTIONS

Certainly the approaches now in practice that have been outlined above will continue to be used and modified; but what new directions are developing, and what is on the horizon? This brief review can provide only the outlines of an inventory of some of the promising new approaches that are being used for exploration, production, and enhanced production.

Reservoir Characterization

Reservoir characterization aimed at understanding the detailed anatomy of reservoirs is essential in field development and may also provide useful information for exploration. There is much current interest in developing basic data on facies anatomy or reservoirs that can be integrated with geophysics and petrophysics. Detailed mapping of outcrops is being used as one source of basic data (e.g., Kerans and others, 1994). A more direct approach is the use of inter-well tomography, which, if developed successfully, could allow construction of a three-dimensional anatomy of reservoir facies. Even porosity and permeability may soon be measured between boreholes. This need to understand the anatomy of sedimentary deposits on a scale of a few hundred meters mandates a whole new level of research both on modern sediments and their ancient counterparts.

Modeling

Modeling of various aspects of deposition at widely different scales continues to be widely practiced. Among those ap-

plications that seem most relevant to exploration and development are (1) basin-scale studies (e.g., Aigner and others, 1989; Kendall and others, 1991); (2) characterization of platform or shelf margins (e.g., Kendall and Lerche, 1988; Bond and others, 1989; Bosence and Waltham, 1990; Read and others, 1991); (3) parasequence development and stacking (e.g., Read and others, 1986; Goldhammer and others, 1993); (4) paleoclimate and source-rock distribution (e.g., Parrish, 1982; Barron, 1985); and (5) individual reservoir modeling (e.g., Tinker, 1996).

Three-Dimensional Geophysical Images

Three-dimensional geophysical images are on the way to becoming the standard prospect delineation. They can already provide remarkable views of the buried topography of individual horizons, and even greater refinement seems inevitable.

Integration of Deposition, Diagenesis, and Burial History

The integration of deposition, diagenesis, and burial history could provide a powerful new tool for analysis and prediction. Already, models relating diagenesis and systems tracts have been proposed, and if these kinds of relationships can be verified and codified, they would allow predictions of diagenesis to be made from seismic-stratigraphic analysis.

ACKNOWLEDGMENTS

This paper represents an updated and revised version of a paper published in a Special Publication of Technology Research Center of the Japanese National Oil Co. (JNOC) by R. N. Ginsburg in 1994. The authors gratefully acknowledge the help and advice of colleagues both in the Comparative Sedimentology Laboratory at the University of Miami (especially Flavio Anselmetti, Kevin Cunningham, Gregor Eberli, Leslie Melim, Don McNeill, and Peter

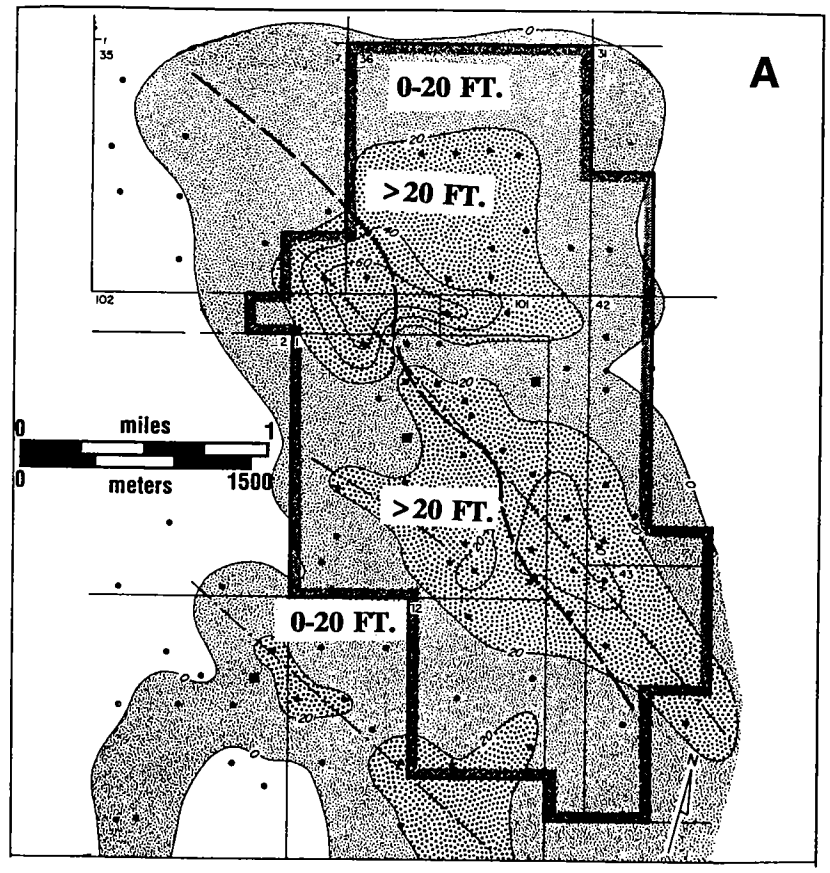

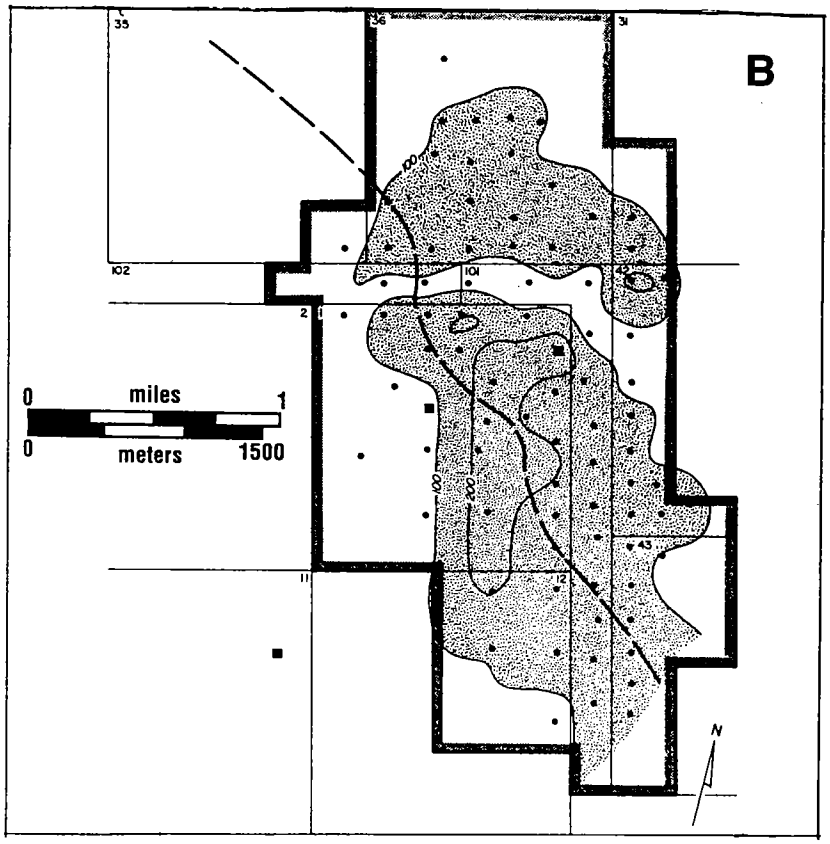

Figure 7 *(right column).* Reservoir facies and production from the Upper Permian Emma field, west Texas. (A) Isopach map of porous skeletal grainstones determined from porosity logs and core data. The northwest–southeast trend is at a high angle to the depositional strike. (B) Total production of the field from 1937 to 1965. Contours are in hundred-thousand barrels. An estimated 85% of the nearly 20 million barrels of oil produced came from the grainstone interval shown in Figure 7A. From Ruppel (1990), reprinted by permission.

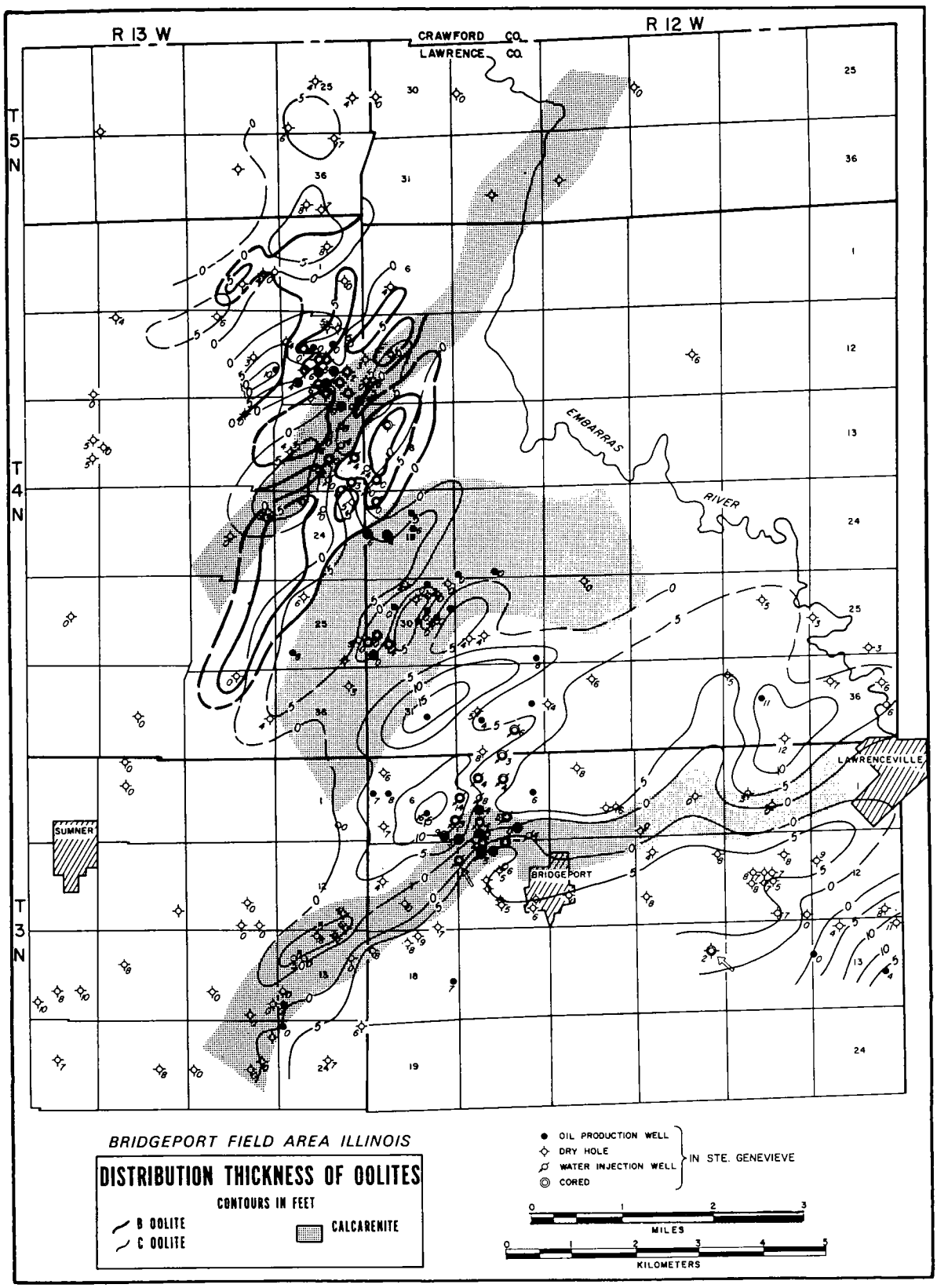

Figure 8. Isopach map of two middle Mississippian oolitic sand bodies in the Bridgeport field area of Illinois. The evidence that these bodies of ooid sands were formed by tidal currents includes their orientation nearly perpendicular to sedimentary strike and their similarity to oolitic limestones of the nearby outcrop belt that show bi-directional cross-bedding. The stippled areas outline channel-fill calcarenites that are probably also tidal deposits. From Choquette and Steinen (1980), reprinted by permission.

Swart), as well as from representatives of our past and present industrial sponsors (Amoco, ARCO, British Petroleum, Chevron, Conoco, Elf Aquitaine, Exxon, JNOC, Marathon, Mobil, Shell, Oryx, Texaco, Total, and Unocal). We thank the American Association of Petroleum Geologists, the Bureau of Economic Geology of Texas, the Geological Association of Canada, and the Society of Economic Paleontologists and Mineralogists (now the Society for Sedimentary Geology) for permission to reproduce illustrations from these publications.

REFERENCES CITED

Ahr, W. M., 1973, The carbonate ramp: an alternative to the shelf model: Gulf Coast Association of Geological Societies Transactions, v. 23, p. 221–225.

Aigner, T.; Doyle, M.; Lawrence, D.; Epting, M.; and Van Vliet, A., 1989, Quantitative modeling of carbonate platforms: some examples, *in* Crevello, P. D.; Wilson, J. L.; Sarg, J. F.; and Read, J. F. (eds.), Controls on carbonate platform and basin development: Society of Economic Paleontologists and Mineralogists Special Publication 44, p. 27–39.

Ball, M. M., 1967, Carbonate sand bodies of Florida and the Bahamas: Journal of Sedimentary Petrology, v. 37, p. 556–591.

Barron, E. J., 1985, Numerical climate modeling, a frontier in petroleum source rock prediction; results based on Cretaceous simulation: American Association of Petroleum Geologists Bulletin, v. 69, p. 448–459.

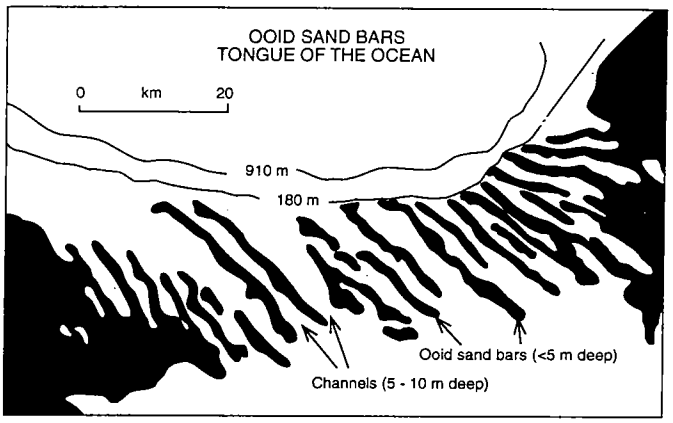

Figure 9. Active tidal bars of ooid sand at the southernmost end of the Tongue of the Ocean, Bahamas. The bars are ornamented with sand waves and ripples of various sizes that move twice daily with the reversing tidal currents; see Ball (1967) for further information. From Ball (1967), reprinted by permission.

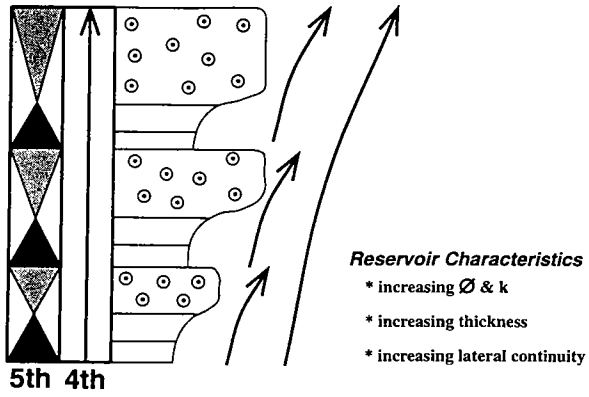

Figure 10. Diagram illustrating the 5th-order-cycle stacking pattern within a 4th-order upward-shoaling sequence in the Paradox basin, southeastern Utah (Grammer and others, in press). Recognizing the characteristics of cycle stacking patterns may aid in the development of production-scale strategies. Within the 4th-order sequences, 5th-order shoals become thicker and better washed (less mud, better porosity and permeability) moving upsection. In addition, the 5th-order shoals tend to be more laterally persistent. Understanding this pattern can help direct perforation strategies not only in vertically oriented wells but also in horizontal wells attempting to drain a sand body.

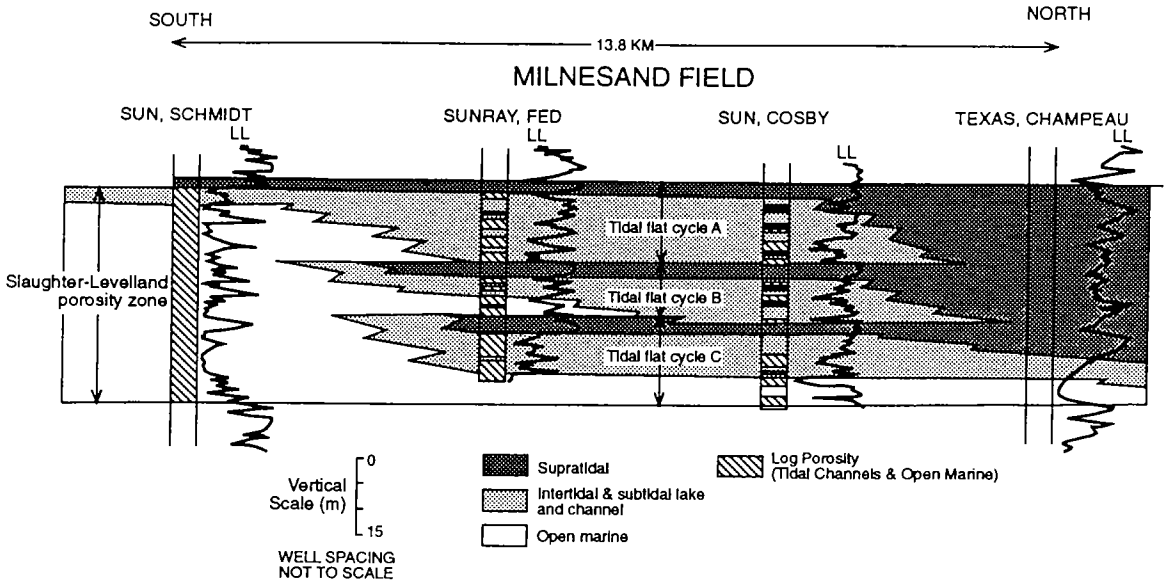

Figure 11. Cross section of a middle Permian oil field in New Mexico prepared by Fred Meissner (Shinn, 1983), showing supratidal (evaporitic) seals on top of the pinchouts of three cycles. Stratigraphic traps like these are a major contributor to the 10 billion barrels of oil produced from the middle Permian San Andres and Grayburg Formations (Ruppel, 1990). from Shinn (1983), reprinted by permission.

Bond, G.; Kominz, M. A.; Steckler, M. S.; and Grotzinger, J. P., 1989, *in* Crevello, P. D.; Wilson, J. L.; Sarg, J. F.; and Reed, J. F. (eds.), Controls on carbonate platform and basin development: Society of Economic Paleontologists and Mineralogists Special Publication 44, p. 39–63.

Bosence, D.; and Waltham, D., 1990, Computer modeling the internal architecture of carbonate platforms: Geology, v. 18, p. 26–30.

Brown, A. A.; and Loucks, R. G., 1993, Influence of sediment type and depositional processes on stratal patterns in the Permian basin–margin Lamar Limestone, McKittrick Canyon, Texas, *in* Loucks, R. G.; and Sarg, J. F. (eds.), Carbonate sequence stratigraphy, recent developments and applications: American Association of Petroleum Geologists Memoir 57, p. 133–156.

Choquette, P. W.; and Steinen, R., 1980, Mississippian non-supratidal dolomite, Ste. Genevieve Limestone, Illinois Basin: evidence for mixed-water dolomitization, *in* Zenger, D. H.; Dunham, J. B.; and Ethington, R. L. (eds.), Concepts and models of dolomitization: Society of Economic Paleontologists and Mineralogists Special Publication 28, p. 163–197.

Eberli, G. P.; Grammer, G. M.; and Homewood, P., 1995, Project summary: Mixed carbonate/siliciclastic system project—Miette and ancient wall buildups (Devonian), Alberta, Canada, and Paradox Basin (Pennsylvanian), Utah, U.S.A.: Elf Aquitaine, Pau, France, 70 p.

Enos, P., 1977, Tamabra Limestone of the Poza Rica Trend, Cretaceous, Mexico, *in* Cook, H. E.; and Enos, P. (eds.), Deep-water carbonate environments: Society of Economic Paleontologists and Mineralogists Special Publication 25, p. 273–314.

Evans, C. C.; and Ginsburg, R. N., 1987, Fabric-selective diagenesis in the Late Pleistocene Miami Limestone: Journal of Sedimentary Petrology, v. 57, p. 311–318.

Evans, G.; Schmidt, V.; Bush, P.; and Nelson, H., 1969, Stratigraphy and geologic history of the sabkha, Abu Dhabi, Persian Gulf: Sedimentology, v. 12, p. 145–159.

Ginsburg, R. N., 1971, Landward movement of carbonate mud—new model for regressive cycles in carbonates [abstract]: American Association of Petroleum Geologists Bulletin, v. 55, p. 340.

Glaser, K. S.; and Droxler, A. W., 1991, High production and highstand shedding from deeply submerged carbonate banks, northern Nicaragua Rise: Journal of Sedimentary Petrology, v. 61, p. 128–142.

Goldhammer, R. K.; Dunn, P. A.; and Hardie, L. A., 1987, High-frequency glacio-eustatic sea level oscillations with Milankovitch characteristics recorded in Middle Triassic platform carbonates in northern Italy: American Journal of Science, v. 287, p. 853–892.

Goldhammer, R. K.; Lehman, P. J.; and Dunn, P. A., 1993, The origin of high-frequency platform carbonate cycles and third-order sequences (Lower Ordovician El Paso Group, west Texas): constraints from outcrop data and stratigraphic modeling: Journal of Sedimentary Petrology, v. 63, p. 318–360.

Grammer, G. M., 1991, Formation and evolution of Quaternary carbonate foreslopes, Tongue of the Ocean, Bahamas: University of Miami unpublished Ph.D. dissertation, 375 p.

Grammer, G. M.; and Ginsburg, R. N., 1992, Highstand vs. lowstand deposition on carbonate platform margins: Insight from Quaternary foreslopes in the Bahamas: Marine Geology, v. 103, p. 125–136.

Grammer, G. M.; Ginsburg, R. N.; and Harris, P. M., 1993a, Timing of deposition, diagenesis, and failure of steep carbonate slopes in response to a high-amplitude/high-frequency fluctuation in sea level, Tongue of the Ocean, Bahamas, *in* Loucks, R. G.; and Sarg, J. F. (eds.), Carbonate sequence stratigraphy, recent developments and applications: American Association of Petroleum Geologists Memoir 57, p. 107–131.

Grammer, G. M.; Ginsburg, R. N.; Swart, P. K.; McNeill, D. F.; Jull, A. J. T.; and Prezbindowski, D. R., 1993b, Rapid growth rate of syndepositional marine aragonite cements in steep marginal slope deposits, Bahamas and Belize: Journal of Sedimentary Petrology, v. 63, p. 983–989.

Grammer, G. M.; Eberli, G. P.; van Buchem, F. S. P.; Stevenson, G. M.; and Homewood, P., 1996, Application of high-resolution sequence stratigraphy to evaluate lateral variability in outcrop and subsurface—Desert Creek and Ismay intervals, Paradox Basin, *in* Longman, M. W.; and Sonnenfeld, M. D. (eds.), Paleozoic systems of the Rocky Mountain Region: Rocky Mountain Section, SEPM (Society for Sedimentary Geology), p. 235–266.

Grammer, G. M.; Eberli, G. P.; van Buchem, F. S. P.; Stevenson, G. M.; and Homewood, P., in press, Application of high resolution sequence stratigraphy in developing an exploration and production strategy for a mixed carbonate/siliciclastic system (Carboniferous), Paradox Basin, U.S.A., *in* Homewood, P.; and Eberli, G. P., Genetic stratigraphy on the exploration and production scales: Case studies from the Upper Devonian of Alberta and the Pennsylvanian of the Paradox Basin: Elf Aquitaine Memoir.

Handford, C. R.; and Loucks, R. G., 1993, Carbonate depositional sequences and systems tracts—responses of carbonate platforms to relative sea-level changes, *in* Loucks, R. G.; and Sarg, J. F. (eds.), Carbonate sequence stratigraphy, recent developments and applications: American Association of Petroleum Geologists Memoir 57, p. 3–41.

Harris, P. M.; and Kowalik, W. S., 1994, Satellite images of carbonate depositional settings: Examples of reservoir- and exploration-scale geologic facies variation: American Association of Petroleum Geologists Methods in Exploration 11, 147 p.

Harris, P. M.; Kerans, C.; Bebout, D. G., 1993, Ancient outcrop and modern examples of platform carbonate cycles—implications for subsurface correlation and understanding reservoir heterogeneity, *in* Loucks, R. G.; and Sarg, J. F. (eds.), Carbonate sequence stratigraphy, recent developments and applications: American Association of Petroleum Geologists Memoir 57, p. 475–492.

Irwin, M. L., 1965, General theory of epeiric clear water sedimentation: American Association of Petroleum Geologists Bulletin, v. 49, p. 445–459.

James, N. P., 1983, Reef environment, *in* Scholle, P. A.; Bebout, D. G.; and Moore, C. H. (eds.), Carbonate depositional environments: American Association of Petroleum Geologists Memoir 33, p. 346–453.

James, N. P.; and Kendall, A. C., 1992, Introduction to carbonate and evaporite facies models, *in* Walker, R. G.; and James, N. P., Facies models: Response to sea level change: Geological Association of Canada, p. 265–277.

Kendall, C. G. St. C.; and Lerche, I., 1988, The rise and fall of eustasy, *in* Wilgus, C. K.; Posamentier, H.; Ross, C. A.; and Kendall, C. G. St. C. (eds.), Sea-level changes: An integrated approach: Society of Economic Paleontologists and Mineralogists Special Publication 42, p. 3–19.

Kendall, C. G. St. C.; Moore, P.; Strobel, J.; Cannon, R.; Perlmutter, M.; Bezdek, J.; and Biswas, G., 1991, Simulation of the sedimentary fill of basins, *in* Franseen, E. K.; Watney, W. L.; Kendall, C. G. St. C.; and Ross, C. A. (eds.), Sedimentary modeling: computer simulations and methods for improved parameter definition: Kansas Geological Survey Bulletin 233, p. 9–33.

Kerans, C.; Lucia, F. J.; and Senger, R. K., 1994, Integrated characterization of carbonate ramp reservoirs using Permian San Andres Formation outcrop analogs: American Association of Petroleum Geologists Bulletin, v. 78, p. 181–216.

LeMay, W. J., 1972, Empire Abo Field, Southeast New Mexico, *in* King, R. E. (ed.), Stratigraphic oil and gas fields—classification, exploration methods, and case histories: American Association of Petroleum Geologists Memoir 16, p. 472–481.

Link, T. A., 1949, Leduc oil field, Canada: Geological Society of America Bulletin, v. 60, p. 381–402.

Lowenstam, H. A., 1948, Marine pool, Madison County, Illinois, Silurian reef producer, *in* Structure of typical American oil fields: American Association of Petroleum Geologists, v. 3, p. 153–188.

_____1950, Niagaran reefs of the Great Lakes area: Journal of Geology, v. 58, p. 430–487.

Lucia, F. J., 1972, Recognition of evaporite–carbonate shoreline sedimentation, *in* Rigby, J. K.; and Hamblin, W. K. (eds.), Recognition of ancient sedimentary environments: Society of Economic Paleontologists and Mineralogists Special Publication 16, p. 160–192.

Major, R. P.; Bebout, D. G.; and Harris, P. M., in press, Facies heterogeneity in a modern ooid sand shoal—analogue for hydrocarbon reservoirs: Texas Bureau of Economic Geology, Geological Circular.

Parrish, J. T., 1982, Upwelling and petroleum source beds, with reference to the Paleozoic: American Association of Petroleum Geologists Bulletin, v. 66, p. 750–754.

Pratt, B. R.; and James, N. P., 1986, The St. George Group (Lower Ordovician) of western Newfoundland: tidal flat island model for carbonate sedimentation in shallow epeiric seas: Sedimentology, v. 33, p. 313–343.

Pugh, W. E. (ed.), 1950, Bibliography of organic reefs, bioherms, and biostromes: Seismograph Service Corp., Tulsa, 139 p.

Read, J. F., 1984, Carbonate platform facies models: American Association of Petroleum Geologists Bulletin, v. 69, p. 1–21.

Read, J. F.; Grotzinger, J. P.; Bova, J. A.; and Koerschner, W. F., 1986, Models for generation of carbonate cycles: Geology, v. 14, p. 107–110.

Read, J. F.; Osleger, D. A.; and Elrick, M. E., 1991, Two-dimensional modeling of carbonate ramp sequences and component cycles, *in* Franseen, E. K.; Watney, W. L.; Kendall, C. G. St. C.; and Ross, C. A. (eds.), Sedimentary modeling: computer simulations and methods for improved parameter definition: Kansas Geological Survey Bulletin 233, p. 473–488.

Rich, J. L., 1951, Three critical environments of deposition, and criteria for recognition of rocks deposited in each of them: Geological Society of America Bulletin, v. 62, p. 1–20.

Roehl, P. O., 1967, Stoney Mountain (Ordovician) and Interlake (Silurian) facies analogs of recent low-energy marine and subaerial carbonates, Bahamas: American Association of Petroleum Geologists Bulletin, v. 51, p. 1979–2032.

Ruppel, S. C., 1990, Facies control of porosity and permeability: Emma San Andres reservoir, Andrews County, Texas, *in* Bebout, D. G.; and Harris, P. M. (eds.), Geologic and engineering approaches in evaluation of San Andres/Grayburg hydrocarbon reservoirs—Permian Basin: Texas Bureau of Economic Geology, p. 145–175.

Sarg, J. F., 1988, Carbonate sequence stratigraphy, *in* Wilgus, C. K.; Posamentier, H.; Ross, C. A.; and Kendall, C. G. St. C. (eds.), Sea level changes: An integrated approach: Society of Economic Paleontologists and Mineralogists Special Publication 42, p. 155–181.

Shaw, A. B., 1964, Time in stratigraphy: McGraw-Hill, New York, 353 p.

Shinn, E. A., 1983, Tidal flat, *in* Scholle, P. A.; Bebout, D. G.; and Moore, C. H. (eds.), Carbonate depositional environments: American Association of Petroleum Geologists Memoir 33, p. 171–211.

Tinker, S. W., 1996, Building the 3-D jigsaw puzzle: Applications of sequence stratigraphy to 3-D reservoir characterization, Permian Basin: American Association of Petroleum Geologists Bulletin, v. 80, p. 460–485.

Walls, R. A., 1983, Golden Spike reef complex, Alberta, *in* Scholle, P. A.; Bebout, D. G.; and Moore, C. H. (eds.), Carbonate depositional environments: American Association of Petroleum Geologists Memoir 33, p. 445–453.

Wilber, R. J.; Milliman, J. P.; and Halley, R. B., 1990, Accumulation of bank-top sediments on the western slope of Great Bahama Bank, rapid progradation of a carbonate megabank: Geology, v. 18, p. 970–974.

Wilson, A. O., 1985, Depositional and diagenetic facies in the Jurassic Arab-C and -D reservoirs, Qatif Field, Saudi Arabia, *in* Roehl, P. O.; and Choquette, P. W. (eds.), Carbonate petroleum reservoirs: Springer-Verlag, New York, p. 319–341.

Wilson, J. L., 1970, Depositional facies across carbonate shelf margins: Gulf Coast Association of Geological Societies Transactions, v. 20, p. 229–233.

_____1975, Carbonate facies in geologic history: Springer-Verlag, New York, 471 p.

_____1980, Limestone and dolomite reservoirs, *in* Hobson, G. D. (ed.), Developments in petroleum geology: Applied Science, London, v. 2, p. 1–52.

Effects of Depth on Quality of Gas-Well Completions in Carbonate Reservoirs of the Anadarko Basin and Shelf Areas

Paul W. Smith
IHS Energy Group
Oklahoma City, Oklahoma

Thomas J. Woods
Gas Research Institute
Washington, D.C.

ABSTRACT.—Although most sediments below 10,000 ft in the contiguous United States can still be considered frontier exploration provinces, industry expectations for their productivity have been relatively modest. This reflects general expectations that the geological quality of reservoirs (and thus of gas prospects) deteriorates with depth. However, detailed evaluations of industry results with depth suggest that these expectations may be unduly pessimistic. Thus, deeper sediments may hold good prospects for new large gas discoveries. An analysis of trends in gas recovery with depth suggests that the increases observed in recovery per completion reflect the effects of gas compression with depth plus improved prospects for finding increasing reservoir volumes with depth.

INTRODUCTION

Although the contiguous United States is the most heavily explored and developed region in the world, over 90% of this exploration activity is shallower than 10,000 ft. As a result, most of the sediments in these 48 States can be considered frontier provinces for deep-gas exploration. However, during the course of typical exploration and exploitation endeavors, the gas industry makes decisions based on the premise that observed increased productivity with increased reservoir depth is primarily due to increased reservoir pressure. For example, most studies suggest that the sand/shale ratio deteriorates, porosity declines, and permeability is reduced with increased depth. In fact, most geological and engineering evaluations expect that aggregate reservoir quality deteriorates with depth. The critical issues are whether these deeper sediments could prove to be highly productive and whether reservoir quality and capacity do indeed decrease with depth.

Industry activity in particular regions and basins in the contiguous 48 States provides two observations, independent of those regions' geology and productivity. First, discoveries per cubic mile of sediment increase with depth. Second, they stop increasing only when industry activity has substantially decreased (Woods, 1993). This poses an interesting conundrum: are yields for deeper sediments poorer because they have not been adequately explored (frontier status), or does their limited exploration to date reflect poor prospective conditions (lack of encouraging success)? This report is the first phase of a research effort to address the prospects for deeper success and perhaps to answer the conundrum.

This phase of the project develops guidelines to indicate general trends in reservoir quality with depth in the Anadarko basin. These guidelines comprise ultimate recovery per completion in productive volume and the physically required reservoir volume to contain the ultimate recovery. Unlike oil, gas is highly compressible. As a result, even if reservoir quality does deteriorate with depth, the compressibility of gas, which allows for larger gas volumes to be contained in smaller pore-space volumes, could compensate for that decline in quality.

The Anadarko basin was selected for this project because it is one of the most productive gas basins in the country, and because its gas production extends to depths below 20,000 ft. Thus, a large amount of data is available to assess reservoir quality with depth. Because the basin has continuously dipping strata, whose production spans large depth ranges, reservoir quality can be evaluated by depth on a formation-specific basis, not just by an average of many formations within a completion-depth interval. In fact, several formations are amenable to evaluation through a wide range of depths. Furthermore, the basin is thought to have considerable undiscovered deep-gas potential.

An evaluation of the data quality for the Anadarko basin, however, indicated that the assignment of many well completions to a specific reservoir (e.g., Hunton, Springer) was incorrect. A productive reservoir (formation) may be incorrectly called various names within the same field. The converse is also a significant problem: a formation name is often incorrectly applied to numerous unique and differing zones within the same field. As a further complication to the understanding of the Anadarko basin's geology, few detailed regional cross sections are available (or even exist outside proprietary studies) that show the most up-to-date logs correlated

Smith, P. W.; and Woods, T. J., 2000, Effects of depth on quality of gas-well completions in carbonate reservoirs of the Anadarko basin and shelf areas, *in* Johnson, K. S. (ed.), Platform carbonates in the southern Midcontinent, 1996 symposium: Oklahoma Geological Survey Circular 101, p. 25–45.

Table 1.—Relative Gas Production between Study Area and Anadarko Basin

	Area (mi^2)	1994 annual Wells	1994 annual Prod. (TCF)	Historic Wells	Historic Prod. (TCF)
Study area	11,304	8,722	0.774	12,389	19.44
Anadarko basin	45,500	36,117	2.270	53,648	108.29

throughout the basin. Therefore, the completion data had to be reviewed well by well to ensure correct assignments. Because of the level of effort associated with this activity, only a part of the basin could be evaluated in this first phase.

Table 1 provides some general statistics for the study area and the Anadarko basin. The study area has a larger share of current gas production than it does of active well completions: the study area accounted for 24% of active gas-well completions in 1994 but provided 34% of the basin's gas production. Thus, the gas wells completed in the study area in 1994 are more productive than those completed in the rest of the basin that same year.

Gas-well volumes of ultimate gas equivalent (VUGE) in 1,000-ft depth categories were compared. The VUGE is the surface volume of the ultimate gas recovery of a well added to a computed volume of gas that would have been produced if the associated oil or condensate production had been gas (rather than a liquid) in the reservoir. The ultimate recoverable reservoir volume was determined by compressing the VUGE to its original reservoir temperature and pressure. The volume of gas at reservoir conditions is equal to the produced reservoir volume.

The results of this investigation suggest that formation characteristics (i.e., thickness, porosity, permeability) have a more pronounced effect on formation productivity than depth (pressure). The trend in ultimate recovery from the total population of gas wells suggests that gas wells have increased recoveries at rates that exceed compressibility owing to increased depth. Thus, the results of this project suggest that misconceptions may exist that significantly impact decision-making processes of those charged with the task of exploration and exploitation of the natural-gas resource. These results, therefore, can be used as an analogy to future resource potentials of other gas-producing basins.

Figure 1 presents a map of the Anadarko basin and indicates the study area, which encompasses Ts. 8–9 N., Rs. 10–15 W., and Ts. 10–29 N., Rs. 10–26 W.—about half the Oklahoma portion of the basin. The total study area is 11,304 mi^2, one-fourth the total basin area of 45,500 mi^2. It contains a disproportionate share of the deeper drilling in the basin.

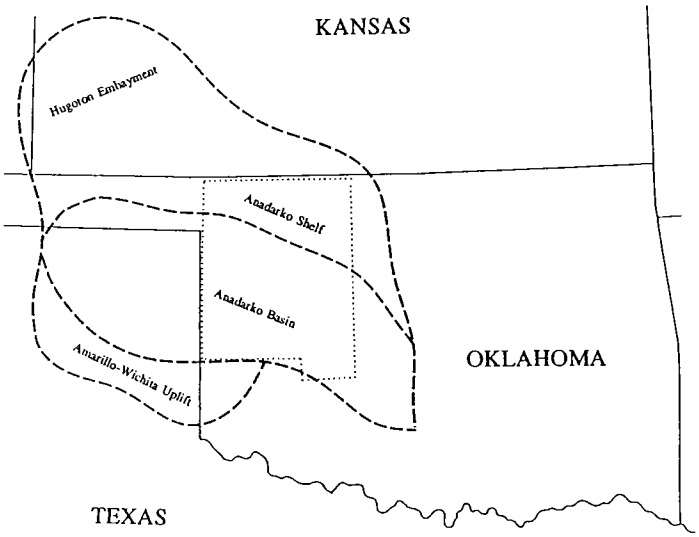

Figure 1. Map of Anadarko basin and surrounding region, showing study area (dotted outline).

DATA PREPARATION

The producing formation in a well is essentially defined by the operator of the well in the sense that operators are required to file completion reports (form 1002A) with the Oklahoma Corporation Commission (OCC), listing the perforated interval(s) and producing formation(s). The Oklahoma Tax Commission serves as the official source for all well-production data for the State of Oklahoma. The State enters producing depths into a database from these files. These data are also collected independently by the industry and are available for study.

In Oklahoma, it is the responsibility of each operator to designate the producing formation as correctly as possible. There are no standards to which operators are held to define the producing formation correctly, nor are there any mechanisms in place to ensure that the operator has correctly defined and named a producing formation. As a result of this practice, the nomenclature for the basin is erratic. This problem is not unique to Oklahoma, however.

IHS Energy Group generates regional geologic cross sections to demonstrate the stratigraphic sequences throughout the Anadarko basin. The OCC is the regulatory agency responsible for overseeing the oil and gas industry within the State of Oklahoma. The OCC currently utilizes IHS Energy Group's regional cross sections in an attempt to standardize the nomenclature used by operators in the basin.

As mentioned earlier, a detailed reservoir correlation and production reallocation effort was required prior to investigation of the relationships between depth and gas-well recovery.

The producing reservoir for each well was reviewed and corrected (if necessary) to conform to a standard system of nomenclature. This study also identified discrepancies in recovery–depth relationships on the basis of formation lithology. The lithologic relationships were further investigated by grouping the age of a formation and similar lithology. Figure 2 presents the stratigraphic section used in this study to designate reservoir and formation names.

To ensure nomenclatural consistency and accuracy, electric logs of nearly 18,000 oil and gas wells were reviewed for this study. A comparison was made between the perforated interval correlated on the log with the regional cross sections and the operator-defined producing formation. When the name of the correlated interval disagreed with the operator-defined producing formation, the correlated nomenclature, as indicated

SYS	SERIES	GROUP	UNIT	SANDSTONE	CARBONATE	EQUIVALENT
PENNSYLVANIAN	VIRGILIAN	Shawnee/Cisco	Topeka Ls Pawhuska Ls Hoover Ss Elgin Sd Oread Ls Heebner Sh Endicott Ss	Hoover Endicott	Pawhuska Oread Ls	
		Douglas/Cisco	Lovell Ls Haskell Ls Tonkawa Ss	Tonkawa	Douglas Group	
	MISSOURIAN	Lansing/Hoxbar	Avant Ls Cottage Grove Ss	Cottage Grove	Lansing Group	
		Kansas City/Hoxbar	Dewey Ls Hogshooter Ls Layton Ss Checkerboard Ls Cleveland Ss	Layton Cleveland Culp	Kansas City Group Melton	Marchand Upper Marchand Lower
	DES MOINESIAN	Marmaton	Big Lime Oswego		Big Lime Oswego	Marmaton Wash
		Cherokee	Cherokee Marker Prue Ss Verdigris Ls Skinner Ss Pink Ls Red Fork Ss Inola Ls Mona	Prue Skinner Red Fork Cherokee Wash Middle Cherokee Wash Lower/ Mona	Verdigris Inola	Prue Wash Skinner Wash Red Fork Wash Bartlesville, Tussy
	ATOKAN	Atoka	Atoka 13 Finger Ls	Atoka	Atoka 13 Finger	
	MORROWAN	Morrow	Morrow Primrose	Upper Morrow Morrow Lower Morrow Primrose		
	SPRINGERAN	Springer	Cunningham Britt Boatwright	Cunningham Britt Boatwright	Britt Boatwright	
MISSISSIPPIAN	CHESTERIAN	Chester	Chester Ls		Chester	
		Manning	Manning Ls		Manning	
	MERAMECIAN	Meramec	Meramec Chat Meramec Ls		Meramec Chat Meramec	
	OSAGEAN	Osage	Osage Ls			
	KINDERHOOKIAN	Kinderhook	Kinderhook Sh			
SIL./DEV.	CHATTANOOGIAN		Woodford Sh Misener Ss	Misener		
	ULSTERIAN	Hunton	Hunton Group		Hunton (Frisco) Hunton (Bois d'Arc) Hunton (Haragan) Hunton (Henryhouse) Hunton (Chimney Hill)	
	NIAGARAN ALEXANDRIAN					
ORDOVICIAN	CINCINNATIAN	Sylvan	Sylvan Sh Maquoketa		Maquoketa	
	CHAMPLANIAN	Viola	Viola Group		Viola (Fernvale) Viola (Trenton)	
		Simpson	Simpson Dense Bromide Ss Tulip Creek Ss McLish Ss Oil Creek Ss Joins	Bromide Tulip Creek McLish Oil Creek Joins		
	CANADIAN	Arbuckle	Arbuckle Group		Arbuckle	
CAMB.	CROIXAN					

Figure 2. Stratigraphic section used in this study for designating reservoir and formation names.

Table 2.—Effects of Production Reallocation by Lithology

Lithologic category	Original well count	Recovery (VUGE; BCFG)	New well count	Recovery (VUGE; BCFG)
Sandstone	6,978	16,815.8	7,291	17,668.7
Carbonate	3,743	5,873.6	4,006	6,062.7
"Wash"	156	426.8	400	955.1
Mixed	543	736.6	678	886.5
Blank	92	177.2	14	28.6
Vague	495	1,052.0	0	0
Total:	12,007	25,082.1	12,389	25,601.6

Note: Changes in new well counts include identified recompletions; changes in VUGE are partly due to 4 months of production (June to October, 1995).

Table 3.—Effects of Production Reallocation by Age

Age/group category	Original data Count	Original data (VUGE; BCFG)	Reallocated data Count	Reallocated data (VUGE; BCFG)
Carbonates	3,743	5,873.6	4,006	6,062.7
Desmoinesian[a]	368	307.3	542	761.7
Hunton[a]	384	2,011.0	399	2,036.4
Mississippian[a]	2,351	2,549.2	1,610	1,256.9
Missourian	41	22.2	36	21.9
Ordovician	53	199.0	62	216.6
Permian	1	0.0	1	0.0
Springeran[a]	0	0.0	746	1,205.2
Multi-aged carb.	545	307.3	610	523.4

[a]Age category further evaluated for trends in recovery and reservoir volume versus depth.

by the regional cross sections, was used. Almost 40% of the operator-defined producing formations either were too vague to use or were incorrect. Furthermore, about 15% of the perforated intervals required correction because of reporting or typographical errors, or because the perforation interval was simply absent from the production records.

Significant amounts of cumulative gas production were reallocated. Thus, some formations had a significant loss of cumulative production that was offset by a significant addition of cumulative production credited to other formations. Table 2 shows the effects of the reallocation effort by lithologic category. A total of 955 blank and vague completions and omitted recompletions were identified during the reallocation process. Reservoir names considered vague or blank included age names such as *Pennsylvanian* or *Desmoinesian,* which provide little insight as to the true producing reservoir. Furthermore, one could not place a "Pennsylvanian" well completion into any lithologic category. Figure 2 (stratigraphic section) shows the age and lithology of the reservoirs by formation name.

Once the proper producing reservoir was identified in a well, other characteristics could be established, such as the age and lithology, which could be determined from the formation name. Therefore, the trends in gas recovery could be investigated by total well-completion population, lithology, and age. When an age designation indicated an interesting trend, it could be further examined by constituent members (i.e., producing formations). First, the well population was split into four lithologic classifications: sandstone, carbonate, "wash," and mixed. This paper deals only with those wells that belong to the carbonate lithologic group.

Well completions in a carbonate reservoir of a specific age or series were assigned to their formations' series (age) name. For example, carbonates of Virgilian age were assigned to a category called *Virgilian.*

Table 3 illustrates the effect of production reallocation by age of the carbonate group. As a result of this effort, nearly 600 additional sandstone and carbonate completions representing more than 850 billion cubic feet of gas (BCFG) were identified. The four most significant age populations for the carbonate group were examined for trends in recovery versus depth. As shown in Table 3, the sum of the age populations was significantly altered. The redistribution of gas wells into different reservoirs also redistributed the producing depths in the different reservoir-name categories. Thus, the producing depths for each reservoir were dramatically altered.

Table 2 shows that sandstone reservoirs account for the major share of gas production in the study area, the average recovery from a sandstone reservoir being 60% higher than that from a carbonate reservoir. However, the Hunton, a carbonate reservoir shown in Table 3, has the highest average recovery per well of any formation in the study area.

Table 4 shows some of the reservoirs affected by the reallocation process and demonstrates the significance of the reallocation effort at the reservoir level. The individual reservoir (formation) is listed, showing the net gain and loss of wells with a brief description of the net effect of the reallocation process. The most significant changes occurred for the Morrow and the Mississippian (Chester), most of which reflected reallocations to the Springer (Smith and others, 1996).

Tables 2–4 show only the net changes in well count and recovery, but the VUGE (recovery) and depth are major elements of this study. However, the reallocation effort moved well-completion records from one age group into another, as well as from the "vague" or "blank" (missing) reservoir-name categories. Although many changes (trades) in and out of some of these groups were made, the net change in total well count and/or cumulative recovery may not seem significant; however, the changes did significantly affect the depths at which these groups are present. Thus, the errors contained in the data necessitated a significant data-preparation effort.

Table 2 shows that the operator identification of the completion lithology was fairly accurate, except for the "wash" category. Table 4 demonstrates that operator identification of the producing reservoir contained significant errors. Therefore, depending on the level of scrutiny, various degrees of error were present in the original data.

Relationships between VUGE, required reservoir volume, and depth were analyzed, in detail only, for the sandstone and

Table 4.—Examples of Redistribution of Production by Reservoir

Formation (group)	VUGE change (BCFG)	Percent change	Net wells change	Percent change	Probable reason
Morrow	–999	–15	–387	–14	To Springer
Springer sand	555	26	217	31	From Morrow
Springer carbonate	1,205	all	746	all	From Mississippian
Mississippian	–1,292	–103	–741	–46	To Springer
Mona (Bartlesville)	59	60	32	53	Vague names
Prue	–309	–4,414	–96	–600	To Skinner
Red Fork	373	9	173	10	Vague names
Skinner	416	53	152	44	From Prue
Atoka	–321	–164	–140	–141	To Morrow
"Wash"	528	55	244	61	Vague names
Cottage Grove	79	16	26	11	Wrong name
Oswego	–23	–5	–23	–3	Wrong name

Note: All percentages are relative to the correct value. Thus, a –16% change means that the original data would have overestimated the correct value by 16%; a +26% change means that the original data would have underestimated the correct value by 26%.

carbonate categories, which represent the largest percentage of gas-well completions and VUGE. Sandstone and carbonate reservoirs account for about 91% of the well population (11,297 of 12,389 well completions) and 93% of the ultimate gas-well recovery (23,731 of 25,602 BCFG). The "mixed" lithology refers to wells that have been perforated in two or more reservoirs with different lithologies: for example, a Hunton–Red Fork well producing from a carbonate unit (Hunton) and a sandstone unit (Red Fork). The "mixed" lithologic category accounted for 6% (678 of 12,389) of the total well population and about 4% (887 of 23,602) of the ultimate gas-well recovery. The "washes" accounted for 3% (400 of 12,389) of the well population and 4% (955 of 25,602) of the ultimate gas-well recovery. However, this paper presents only the results observed for the carbonate category.

METHODOLOGY

As the purpose of this project was to develop guidelines that could indicate general trends in reservoir quality with depth, estimates were developed for ultimate recovery for each gas-well completion. This recovery is the sum of the gas plus the condensate recovery. A framework was developed to reflect the effects of compression on the physical size of the drainage volume. The physical-drainage volumes reflect the sum of the volume occupied by the gas plus the volume occupied by the condensate.

The depth of a gas-well completion was taken to be the midpoint between the uppermost and lowermost perforations for that completion. Each completion was assigned to a 1,000-ft interval (i.e., 13,265 ft = 13,000-ft category). When the completion interval exceeded 1,000 ft, the completion was excluded from the analysis. About 625 completions were omitted because the perforated interval exceeded 1,000 ft. Where the perforation data were missing (and unobtainable), the completion was not included in the analysis. Less than 20 completions were omitted because of missing perforation-interval data. Of the 12,389 gas-well completions in the study, 11,751 could be used—95% of the total.

The recovery for each gas completion was calculated as the sum of the cumulative production plus the estimated remaining reserves. Remaining reserves were estimated as the product of the 1994 Oklahoma reserve-to-production (RP) ratio for nonassociated natural gas and condensate and 1994 production for each completion. In 1994, these RP ratios were 7.93 for nonassociated gas and 7.76 for condensate. The RP values were calculated from the Energy Information Administration's *U.S. Crude Oil, Natural Gas, and Natural Gas Liquid Reserves—1994 Annual Report* (DOE/EIA-0216, 1994).

Gas compressibility is calculated according to the Perfect Gas Law, which sets the product of pressure and volume divided by temperature (PV/T) equal to a constant. While actual gas compression deviates from this relationship, the deviations would work only to strengthen the observations drawn from the analysis. As the depth of a reservoir increases, reservoir pressure increases, owing to the weight of rock overburden and temperature. The geothermal gradient and pressure gradient can be estimated from observations within the Anadarko basin. With these estimates having been obtained, an equation to determine volume factor (vf) can be derived:

$$vf = \frac{VP}{T}$$

where vf = volume factor;
T = absolute temperature = [(0.0105° × depth) + 519.67° Rankine];
P = pressure = [(0.468 psi × depth) + 14.7 psi].

Thus, the volume factor in the Anadarko basin is:

$$vf = \frac{1{,}000 \times [(0.468 \times \text{depth}) + 14.7]}{[(0.0105 \times \text{depth}) + 519.67]}.$$

Using the volume factors developed, gas compressibility for a specific reservoir volume for the Anadarko basin can be examined as a function of depth, with the effects of temperature included. The effect of gas compressibility on reservoir capacity is significant and dramatic. A plot of gas compressibility as a function of depth is provided in Figure 3. This figure also shows the effect of gas compressibility on the reservoir volume required to contain a unit volume of gas. As shown, 1 BCFG occupies 1 BCF of reservoir volume at zero depth, but that same 1 BCFG requires a reservoir volume of only 0.00376 BCF at 10,000 ft of depth. Compression reduces the required reservoir volume by a factor of nearly 266 from 0 to 10,000 ft. Figure 3 demonstrates the effect of moving a surface unit volume of gas through a spectrum of depths.

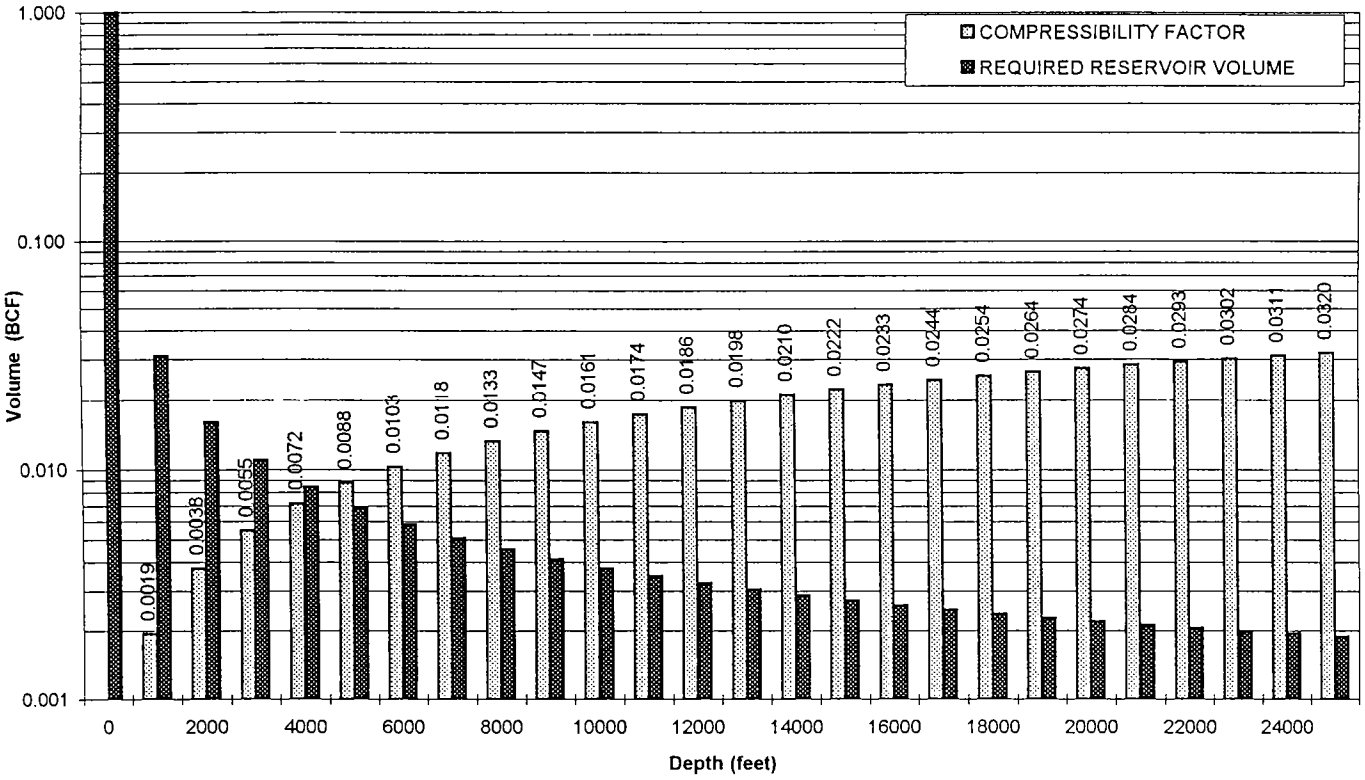

Figure 3. Gas compressibility as a function of depth, showing the effect of compressibility on the reservoir volume required to contain 1 BCFG.

Any liquid hydrocarbon (condensate or oil) produced from a gas well must be included in any depth–recovery comparison, because it occupies a portion of the produced reservoir volume in many gas wells. Therefore, the condensate volume was converted to a produced-gas volume equivalent to reflect the volume occupied by the condensate in the drainage volume. Whereas the condensate volume occupies a negligible share of the gas stream volume at surface temperature and pressure, its share grows with depth, because gas compresses much more rapidly than condensate. As a result, a barrel of condensate occupies a much larger gas-equivalent volume in a reservoir at 10,000 ft than it does at the surface. At 10,000 ft, a barrel of condensate occupies a reservoir volume that would expand to 1,939 CF at the surface, whereas at the surface this barrel of condensate would occupy only 5.6 CF. This provides a consistent basis for comparison of the required reservoir volumes between all gas wells, irrespective of the amount of oil or condensate produced. Thus, for this study, the VUGE recovery for each well represents ultimate gas recovery plus a gas-volume equivalent of the ultimate oil recovery.

The shrinkage factor for a barrel of condensate (or oil) varies, depending on the gravity of the oil and the molecular constituents involved. Because the molecular evaluations of the crude oils produced within the Anadarko basin were not available, an approximation was used consistently throughout the study area. The shrinkage factor used to convert stock-tank oil volume to reservoir volume is approximated at 1.3 bbl of reservoir oil to 1 bbl of stock-tank oil. The volume of produced oil is converted to a reservoir volume, and then, using compressibility ratios, a produced gas-equivalent volume is calculated for each well having a cumulative oil production.

Although the correction factor per barrel of condensate is relatively small compared to the volume of produced gas, it should be included to compare gas wells accurately, because some gas wells do produce liquid hydrocarbons. Figure 4 demonstrates the volume of gas equivalent of 1 bbl of condensate (or oil) with increased depth. As one would expect, the volume of gas contained in the same space occupied by a barrel of condensate increases with depth. Obviously, salt water also occupies a portion of the oil/gas reservoir space. However, salt water is not typically considered a commodity, because when the water-disposal costs exceed the produced commodity value, the well is abandoned. Records of produced salt water are not generally available; therefore, no attempt could be made to account for the volume of produced salt water.

RESULTS

Ultimate Recoveries and Reservoir Volumes of Total Population, Economic Population, and Historic Population

The average depth calculated from the uppermost perforation to the lowermost perforation was used to categorize each well into a 1,000-ft depth cell. Where the range of the perforated interval exceeded 1,000 ft, the well was excluded from the tabulations because the range exceeded the size of a depth cell and because of potential errors in using the geopressure gradient. Where the perforated interval was missing, the data were also excluded from analysis. Of the 12,389 gas wells in

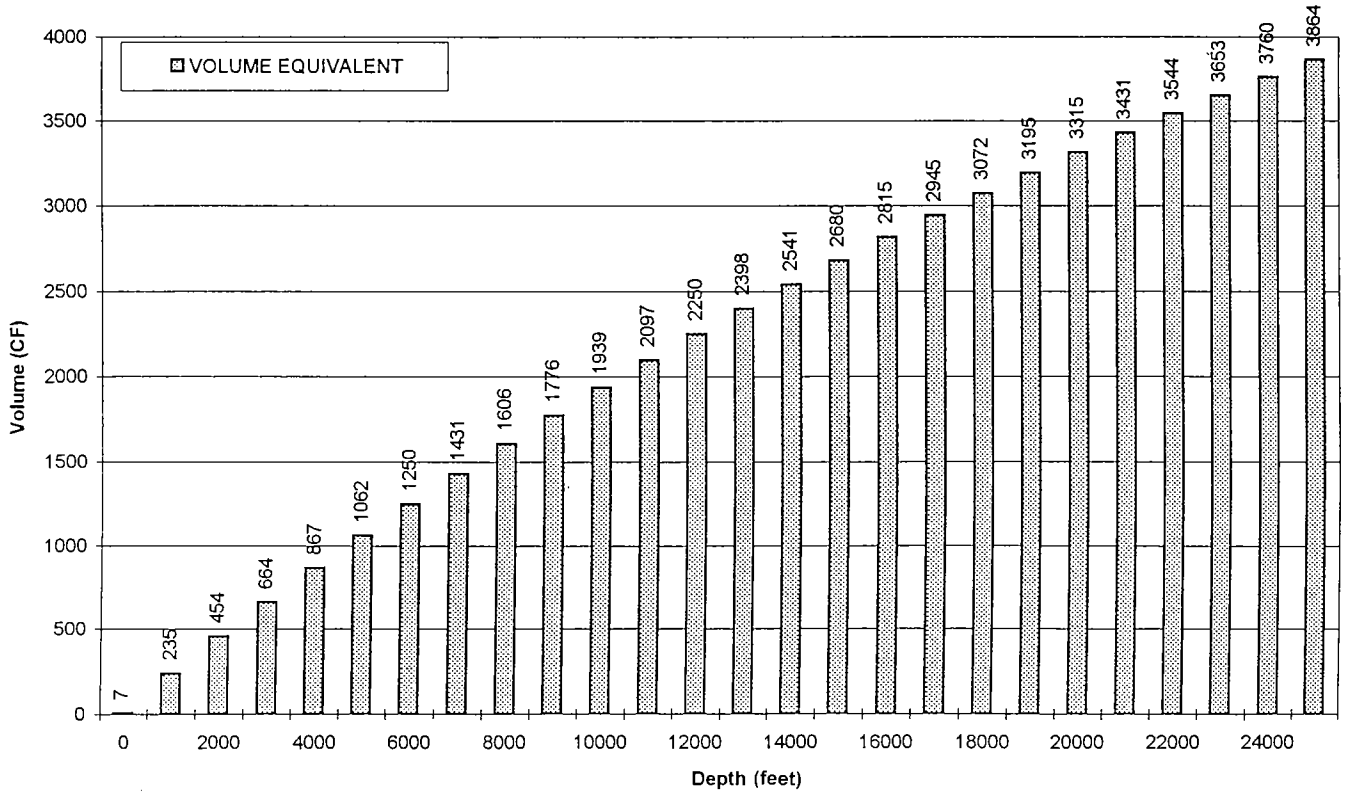

Figure 4. Volume of gas equivalent to 1 BO with increasing depth.

the study area, 11,751 (95%) were used in the depth evaluations. Consequently, the total gas-well population contains observations from 1,000 to 25,000 ft in depth. Every depth cell from 3,000 to 20,000 ft has more than five observations.

The recovery data were first analyzed for all completions in the data set. Because of greatly differing completion counts in depth intervals and lithologies, average recoveries used reflected the quality of the completion depth interval. Two subsequent methods were used to filter out "depletion" effects and "subeconomic" (bad-well) effects.

The first method used the basic premise of resource depletion, namely, that the best recoveries are disproportionately found first. Accordingly, these data included the first 145 completions for each 1,000-ft depth interval. Although this method included some low-recovery completions, it does reflect initial industry results for comparable levels of depletion. If the best recoveries are indeed found first, then the initial samples can indicate the relative well quality of the depth (formation) intervals. This method adequately represents a historical perspective of industry encouragement as wells were drilled to increased depths.

The second method removed well completions from the data that were little more than "completed dry holes." While these completions were a significant share of the activity, they were a very small share of the total recovery. As a result, the overwhelming impact of the subeconomic completions was to reduce the average recovery per completion; they added very little to the recovery of the sample. The minimum recovery for a well completion was designed to reflect the fact that drilling charges increase more rapidly than depth, particularly below about 10,000 ft. Therefore, the minimum recovery varied according to the following equation:

$$\text{Minimum recovery} = (\text{depth}^2/10{,}000) \times 50 \text{ MCFG}.$$

Thus, at 5,000 ft, recoveries with less than 0.125 BCFG were excluded from the analysis. At 10,000 ft, completions with recoveries less than 0.500 BCFG were excluded; at 15,000 ft, completions with recoveries less than 1.125 BCFG were excluded; and at 20,000 ft, completions with recoveries less than 2.00 BCFG were excluded.

The study area has 11,751 gas completions with an ultimate recovery of 24.8 trillion cubic feet of gas (TCFG). Table 5 summarizes the industry activity and recovery in the study area by 5,000-ft completion-depth intervals. The table shows that over 80% of the gas completions in the study area are in the 5,000–15,000-ft completion-depth interval, and that almost 60% are in the 5,000–10,000-ft interval. The table shows that almost as much gas has been discovered below 15,000 ft as has been discovered above 5,000 ft with less than a quarter of the well completions. The recovery per completion also shows a general upward trend with depth that accelerates below 15,000 ft. This suggests that a significant resource potential exists in the study area below 15,000 ft.

The low level of gas activity above 5,000 ft in the study area is interesting, because the 4,000–5,000-ft completion interval has the highest recovery per completion through 13,000 ft. This anomaly is due to the Pennsylvanian Hoover sandstone reservoir in Mocane–Laverne field in the northwest part of the study area. From this reservoir, 230 gas wells have pro-

Table 5.—Gas-Completion Activity, Anadarko Basin Study Area

Depth interval (feet)	Completions	Recovery (BCFE)	Average BCFE/comp.
0–5,000	333	1,192	3.58
5–10,000	7,050	10,027	1.42
10–15,000	3,718	9,482	2.55
15–20,000	633	3,682	5.82
>20,000	17	375	22.06
Total:	11,751	24,758	2.11

duced more than 1.06 TCFG, for an average of 4.6 BCFG per well to date. Despite the high yield of this interval, gas activity is low through 5,000 ft, even in the high-quality 4,000–5,000-ft interval.

Figure 5 presents the trends in gas recovery per completion for all completions in the study area, the average recovery of those that exceed the "economic" criteria for each depth interval, and for the first 145 completions. The "economic" filter removed 33% (3,922) of the total completions, but only 3% (751 billion cubic feet of gas equivalent, or BCFGE) of the total recovery. The average "uneconomic" completions have less than one-third (33%) of the minimum-recovery criteria. The curve for the first 145 historic completions has only a large enough population to span a range from the 4,000-ft interval through the 17,000–18,000-ft interval; the other depth intervals have too few completions to be included.

Excluding the Mocane–Laverne Hoover reservoir "anomaly," Figure 5 shows that the average recovery per completion increases with depth, particularly below 13,000 ft. The recovery per completion doubles between 4,000 and 11,000 ft and, interestingly, doubles again between 11,000 and 14,000 ft. The trend of the "economic" completions also shows an increase in recovery with depth, with a sharp incline at 14,000 ft.

The curve for the first 145 historic completions shows some interesting results. First, recovery per completion between 4,000 and 13,000 ft fluctuates significantly but shows no clear increase except for those below 13,000 ft. Furthermore, the two depth intervals between 10,000 and 12,000 ft have lower average recoveries than do all subsequent wells for these two intervals. The average recovery for subsequent completions in these two intervals exceeds the first 145 completions by more than 50%. At depth intervals below 10,000 ft, the average "economic" gas well recovered as much or significantly more gas than did the first 145 gas wells. Below 10,000 ft, the average economic well typically out-produces the average historic well by nearly 2.0 BCFG. At depths between 4,000 and 10,000 ft, the average historic well tended to out-produce the average "economic" well. Such improvements are contrary to what resource-depletion theories imply.

The amount of dollars risked in a shallow gas-well completion are not as large as the amount risked in a deep gas-well completion. Perhaps operators are not as likely to attempt completions in deep gas wells, which provide only a modest return on investment in comparison to shallow gas wells. Thus, for the shallow-depth ranges, the decrease in average well recovery from the initial 145 wells may be influenced by a high population of marginal but economic wells.

The unexpected observations for the trend of the first 145 historic completions suggest that as the industry drills deeper, the initial activity may not necessarily be a good indicator of the reservoir quality of the deeper interval. Many higher potential targets in a deeper interval may be held by shallower production and thus would not be developed until later in the development history of the interval. Therefore, initial results for deeper intervals may reflect something other than geologic factors.

A weakness of evaluating the first 145 wells is that they may tend to represent a few wildcat wells and many subsequent development wells. Thus, the geographic representation of the sample is likely to be limited. Furthermore, the historic well population does not adequately represent a continuum in either the carbonate or the sandstone population.

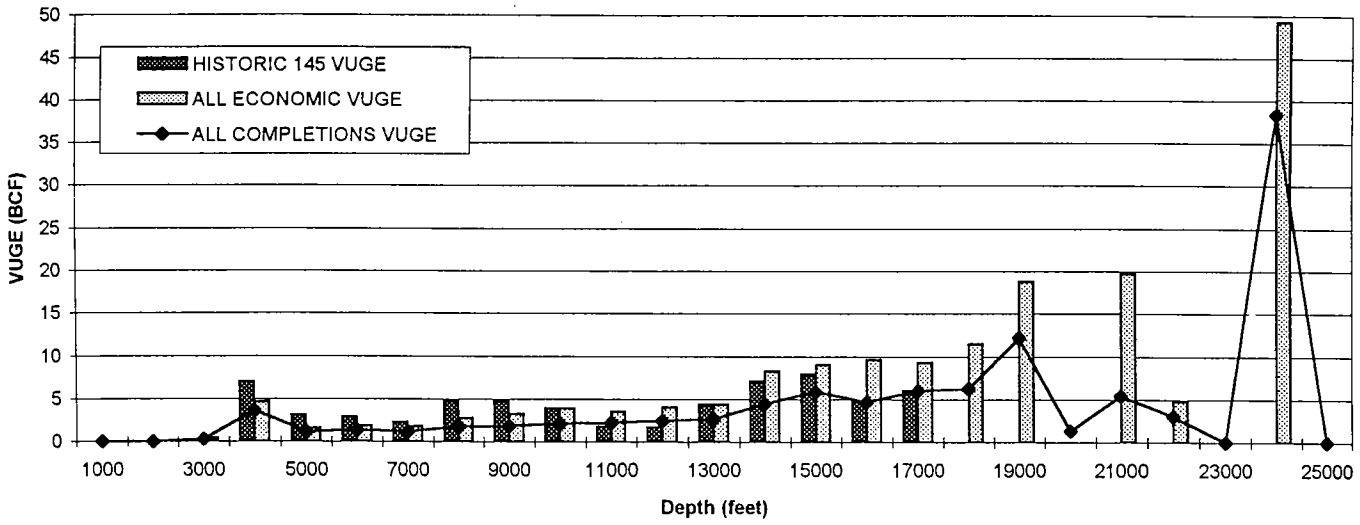

Figure 5. Gas recovery per completion. *VUGE* = volume of ultimate gas equivalent.

Therefore, the potential recovery from a future completion in any 10,000-ft or deeper interval should more closely follow the "economic" recovery trend rather than the historic recovery trend. On a gross scale, however, the historic well population agrees with the other data; as wells are drilled in increasingly deeper parts of the basin, they should yield increasingly larger recoveries.

Filtering out the "subeconomic" completions enhances the overall trend in recovery with depth. The average "economic" recovery tends to be about 50% larger than that of the total completion population for any given depth interval. From 5,000 to 13,000 ft, the average recovery is rather stable, but it does show an increasing trend. The significant increase in average reservoir recovery observed between the 13,000-ft and the 14,000-ft intervals results from a near doubling of the recovery (VUGE). Besides being significantly larger in size, the trend for average recovered reservoir volume between the depths of 14,000 and 18,000 ft suggests an increase in the reservoir volume. The assumption that reservoir capacity degrades with depth is not supported by the data.

The gas-well population and ultimate recoveries are categorized by lithology and by the "economic" filter. Because the sandstone and carbonate populations represent 91% of the total completion and recovery populations, they were examined further.

Ultimate Recovery and Reservoir Volume by Lithologic Group

The trends in gas-well-completion activity for the study area are very different for the three principal lithologic groups—sandstone, carbonate, and mixed. Table 6 presents gas-completion activity and average recovery per completion in the study area allocated to these lithologies plus "wash." Table 6 indicates that sandstone recoveries are noticeably better than carbonate completions above 10,000 ft, but that carbonate completions are much better below 10,000 ft. Figure 6 shows the trend in recovery of the total population of gas-well completions in 1,000-ft increments. As shown, recovery per completion specifically jumps at 13,000 ft for carbonate reservoirs and at 14,000 ft for sandstone reservoirs.

Table 6.—Gas-Completion Activity by Lithology, Anadarko Basin Study Area

Depth interval (feet)	Sandstone	Carbonate	"Wash"	Mixed
	Gas completions			
0–5,000	283	37	0	13
5–10,000	3,226	3,370	10	444
10–15,000	3,165	220	309	24
15–20,000	497	74	57	5
>20,000	6	11	0	0
Total:	7,177	3,712	376	486
	BCFE per completion			
0–5,000	4.13	0.43	–	0.68
5–10,000	1.69	1.20	0.40	1.23
10–15,000	2.53	3.08	2.36	2.24
15–20,000	5.58	9.42	3.32	4.08
>20,000	3.95	32.00	–	–
Average:	2.43	1.55	2.46	1.29

Above 10,000 ft, sandstone activity is somewhat greater than carbonate activity. Below 10,000 ft, activity is heavily concentrated in sandstone lithologies. In the 10,000- to 20,000-ft interval, there are 11 sandstone completions for each carbonate completion. Only below 20,000 ft do carbonate completions exceed sandstone completions. Completions in "wash" reservoirs account for only 3.2% of all gas completions in the study area; these completions are largely concentrated between 11,000 and 16,000 ft in depth. The recovery trends do not include completions that could not be assigned to a specific lithology; these mixed-lithology completions make up about 4.1% (486 wells) of the total well completions and 2.5% of the ultimate recovery in the study area. Mixed-lithology completions are typically shallower than 11,000 ft. Because

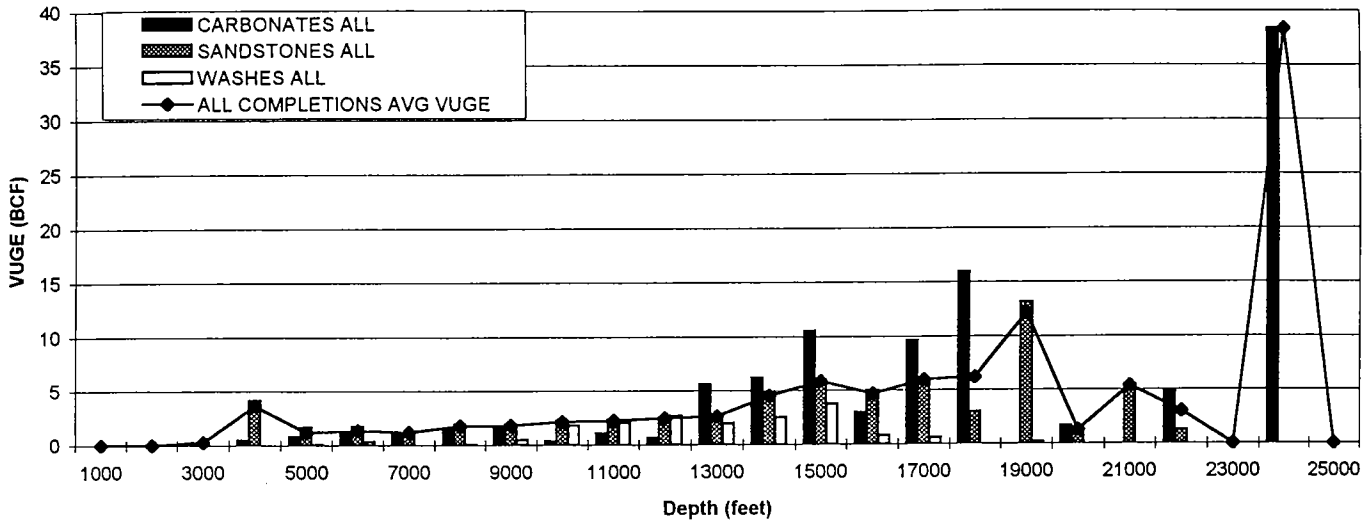

Figure 6. Average gas recovery by lithology versus depth.

the "wash" and mixed lithologies account for such small shares of the total activity, discussion of these groups is limited.

Figure 7 presents the number of "economic" gas completions in the study area by 1,000-ft depth intervals. Completions for each depth interval are allocated to sandstone, carbonate, and "wash" lithologies. As shown in Figure 6, average carbonate recoveries exceed average sandstone recoveries for depths below 13,000 ft. Even though carbonates are more productive below 13,000 ft, sandstone completions are significantly more common.

Carbonate Trends

The carbonate-lithology group includes 27.5% of all gas-well completions and 22.9% of the total ultimate recoveries in the study area. Sixty-four percent of all carbonate gas completions exceed the minimum economic filter. Figure 8A presents trends in the total carbonate population and the "economic" carbonate population. Because of limited populations, the historic trends were not calculated.

The carbonate population is bimodal, suggesting that some factor is influencing either carbonate-well drilling or carbonate completions. The first node (4,000 to 10,000 ft) may represent one population of carbonate wells, and the second node (13,000 ft and deeper) suggests an entirely different population.

As shown in Figure 8B, the average recovery (VUGE) from carbonates increases from the first observation through the 9,000-ft depth interval. For the 4,000–5,000-ft interval, 30 wells have an average ultimate recovery of 0.473 BCFG. For the 9,000–10,000-ft interval, the average ultimate recovery has increased to 1.762 BCFG. For 10,000–13,000 ft, there appears to be a "dead zone" in the trend of carbonate-well recoveries, the average recovery being only 0.673 BCFG. Drilling activity (Fig. 8A) corresponds to the "dead zone"; there exists a ninefold drop in drilling activity from the 9,000-ft interval in comparison to the 10,000-ft interval. With an average recovery of 5.601 BCFG per completion for the 13,000–14,000-ft interval, carbonate recoveries increase more than 300% over the 9,000–10,000-ft interval. The interest in this depth interval has also recovered, as more than twice the number of wells have been completed in the 13,000–14,000-ft interval than in the 10,000–11,000-ft interval ("dead zone"). Whereas recovery per completion continues to increase below 13,000 ft, the increase is somewhat erratic, reflecting the limited activity to date.

Filtering out the "subeconomic" carbonate population yields interesting results. Sixty-four percent of the carbonate completions are economic, but they account for more than 97% of the total ultimate recovery from carbonates. Typically, the average economic recoveries are 50% to 100% better than the total carbonate recoveries (see Fig. 8B). Interestingly, more than two-thirds of the wells in the "dead zone" are removed, yet these average economic recoveries are significantly poorer than those observed for the shallower and greater depths. Excluding the "dead-zone" anomaly, it is obvious that the trend in average recovery increases dramatically at the 13,000-ft interval. Below 13,000 ft, the carbonate population consists almost entirely of Hunton completions. Figure 8C presents the trend of increased reservoir volume with depth, corresponding to the increased average recovery.

The carbonate-lithology group was further defined by the age of the producing carbonates. Wells producing from a single zone were placed into the appropriate age category. Wells having perforations entirely within a single-age unit were placed within that unit (age). Wells having perforations in carbonates of two differing ages were omitted from the population. Wells producing from carbonates within a single-age unit accounted for 86% of the total defined carbonate population and 97% of the ultimate carbonate recovery. Thus, 14% of the carbonate completions were commingled with carbonates of differing ages, although these wells represent only 3% of the total carbonate recovery. In conjunction with the observations of the "economic" populations, the data suggest that carbonate wells from varying ages tend to be "subeconomic." Four of the eight ages of carbonate completions contributed 83% of the total defined carbonate-well population. These four carbonate ages are Desmoinesian, Springeran, Mississippian, and Hunton and account for 93% of the total

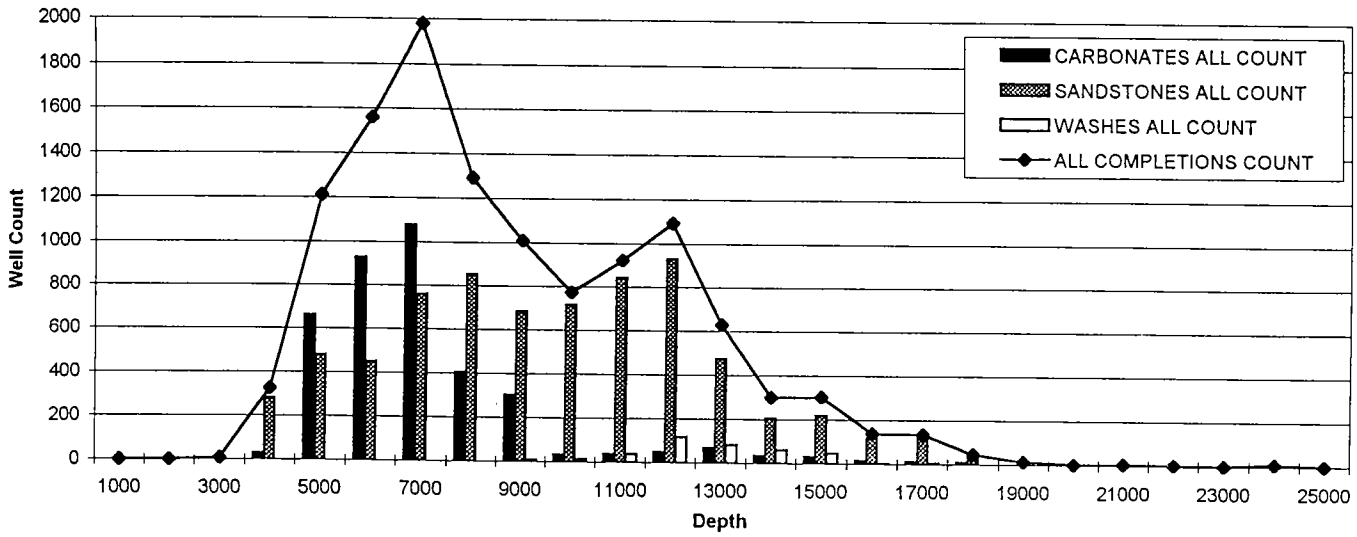

Figure 7. "Economic" gas completions by lithology versus depth.

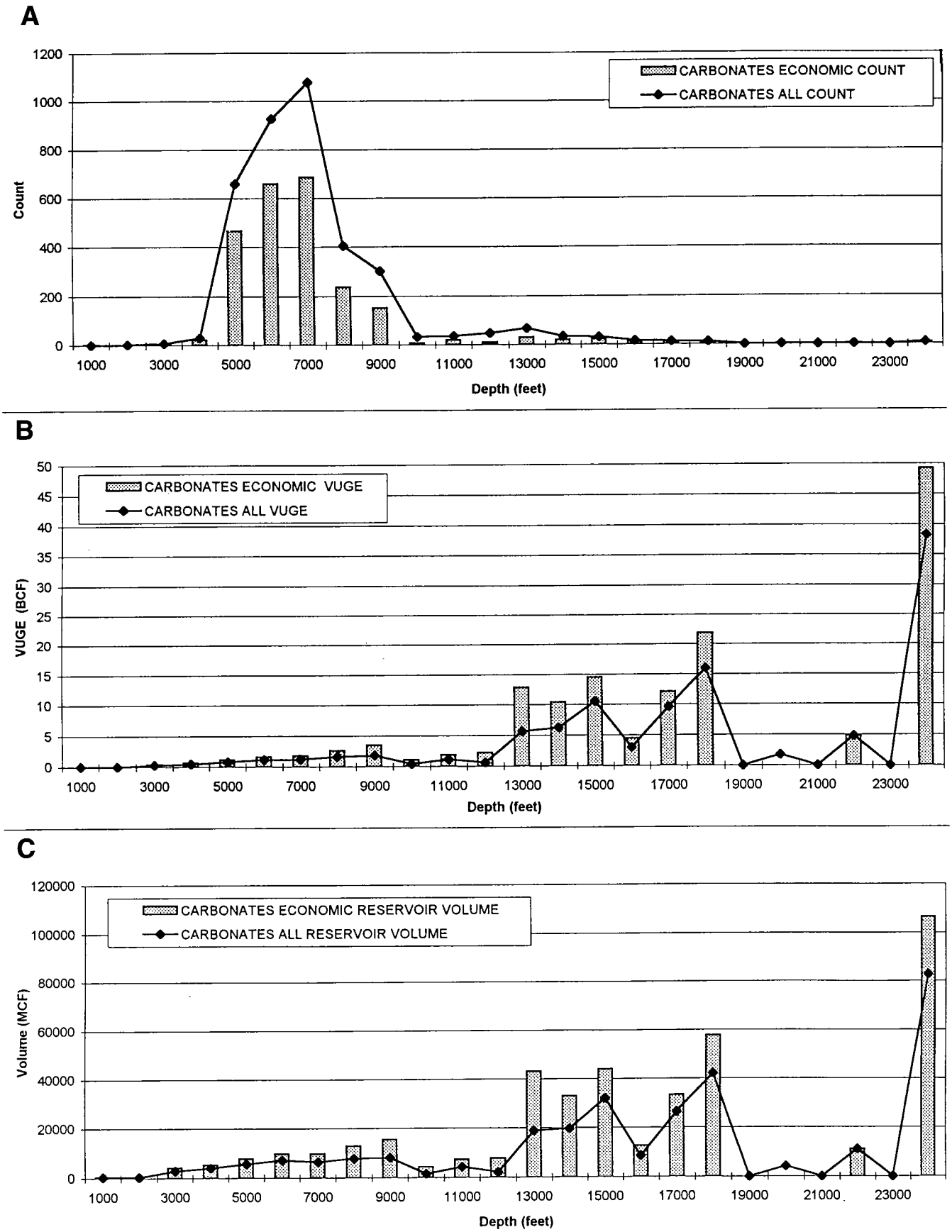

Figure 8. (A) "Economic" completions and total completions for carbonates versus depth. (B) "Economic" recovery (VUGE) and all recovery (VUGE) for carbonates versus depth. Although recovery per completion increases below 13,000 ft, this increase is erratic, reflecting the limited activity to date. (C) "Economic" carbonate-reservoir volume and total carbonate-reservoir volume versus depth.

ultimate carbonate recovery. Table 7 shows the primary producing reservoirs for each of the four most significant carbonate age groups.

Table 7.—Reservoir Names of the Four Most Significant Carbonate Age Groups

Desmoinesian	Big lime, Oswego, Inola
Springeran	Britt and Boatwright in specific areas
Mississippian	Chester, Manning, Meramecian, Meramec chat
Hunton	Hunton

Figure 9A shows the "economic" population relationships of the four major carbonate age groups and the total "economic" carbonate population. None of the trends in population of the individual carbonate ages appear similar to the overall carbonate-well population. The carbonate-well distribution thus does not represent a continuum. The ages show distributions of depths where a given age significantly influences the well population at certain depths, whereas at other depths the same age may be only a minor contributor to the total population. For example, from 6,000 to 8,000 ft, the carbonate facies of the Springer Group and the Mississippian carbonates contribute more than 75% of the total carbonate-well count; however, at depths greater than 13,000 ft, the Hunton population almost completely influences the carbonate population.

Not all the economic carbonate reservoirs are found throughout a wide range of depth intervals. Springer carbonates have been found economic only at depths between 5,000 and 10,000 ft (Smith, 1996; Smith and others, 1996). Hunton completions have proved to be "economic" at depths ranging from 6,000 to nearly 25,000 ft. Below 10,000 ft, 146 of the 176 "economic" carbonate completions are in the Hunton. Obviously, changes in dominant ages of reservoirs will necessarily influence the average recoveries observed.

The data suggest that the distribution of completion counts likely results from a common influence, indicating that prospective carbonate reservoirs are geographically present beneath shallower productive sandstone (or carbonate) reservoirs. Although this situation is also indicated for the sandstone group, the effects are much more apparent for the carbonate group. Consequently, the trends for deeper reservoirs may give a conservative picture of the actual condition of prospects in deeper sediments. For the prolific deep Hunton completions, a similar question might be asked about some of the shallower sediments held "behind pipe."

The trends observed in the average recovery per completion (VUGE) are controlled by the mix of producing ages, with the dominant age population significantly influencing the observed average recovery. Figure 9B shows the trends in "economic" recovery per completion (VUGE) of the four most significant carbonate ages (Desmoinesian, Springeran, Mississippian, and Hunton) in comparison to the average carbonate completion. Thus, the average carbonate recovery does not represent a continuum. Figure 9B illustrates this point; no trend of average recovery for any individual carbonate age fits the trend of the total carbonate average recovery. The total carbonate recovery is typically most similar only to parts of an individual carbonate age, which, by virtue of population, most influences the average.

The overall trend in average recoveries shows a dramatic increase (nearly 5 times) for depths below 13,000 ft. This jump is due to the dramatic increase in average recoveries observed for the Hunton. An anomalously low number of "economic" completions exist below 13,000 ft (5 of 139) for carbonate reservoirs other than Hunton.

Figure 9C presents the trends in recovered reservoir volumes for the four most significant ages of carbonates in comparison to all carbonate completions. Below 13,000 ft in depth, the average carbonate-reservoir well drains a volume that is nearly 5 times larger than the average well in the 4,000- to 10,000-ft depth range. As indicated by the distributions observed in the populations and recoveries for the individual carbonate ages, there exists a similar discontinuity in the trend of recovered reservoir volume. When averaged to represent the carbonate population, the discontinuities of the individual carbonate ages stack. The summation trend does indicate an increase in recovered reservoir volume with depth with an anomalous omnipresent "dead zone."

Although the reservoirs for the different carbonate ages appear to behave independently, they exhibit common trends. All the carbonate reservoirs have a pronounced drop in populations at 10,000 ft. All these reservoirs display a trend of increased recovery with depth down to 10,000 ft. The average recovery and recovered reservoir volume for completions between 10,000 and13,000 ft are significantly less than those observed for the 9,000-ft interval, although this trend is less obvious for Mississippian completions. The Hunton population, recovery, and reservoir volume are peculiarly bimodal (none of the other populations exhibit a similar trend); one population represents completions above 10,000 ft, and another population, completions below 13,000 ft. Except for Mississippian completions and the "dead zone," individual carbonate-reservoir volumes increase with depth. The population, recovery, and reservoir volume for all completions, and the "economic" completions for the four most significant carbonate reservoirs, are presented in Figures 10–13.

The carbonate reservoirs are known to have two distinctly different trapping mechanisms: structural and stratigraphic. For example, the Hunton produces primarily from stratigraphic traps above 10,000 ft and from structural traps below 13,000 ft. Interestingly, most of these structural trapping mechanisms are present in the overlying Mississippian carbonates. Thus, the Mississippian completions may prove to be more productive below 13,000 ft than presently indicated. It is unknown at this time if other carbonate reservoirs have a similar relationship.

A fivefold increase in reservoir volume between Hunton completions below 13,000 ft and above 10,000 ft was observed. Significant increases in reservoir volumes were also observed in carbonate reservoirs of other ages. For carbonate reservoirs, it is apparent that gas compression is not the most important factor that results in increased recovery as a function of depth. The second phase of this research effort will investigate physical parameters, such as thickness, porosity, pressure, and water saturation, to determine possible relationships of factors that cause the observed increases in average gas-well recovery and average recovered reservoir volume for carbonates by age.

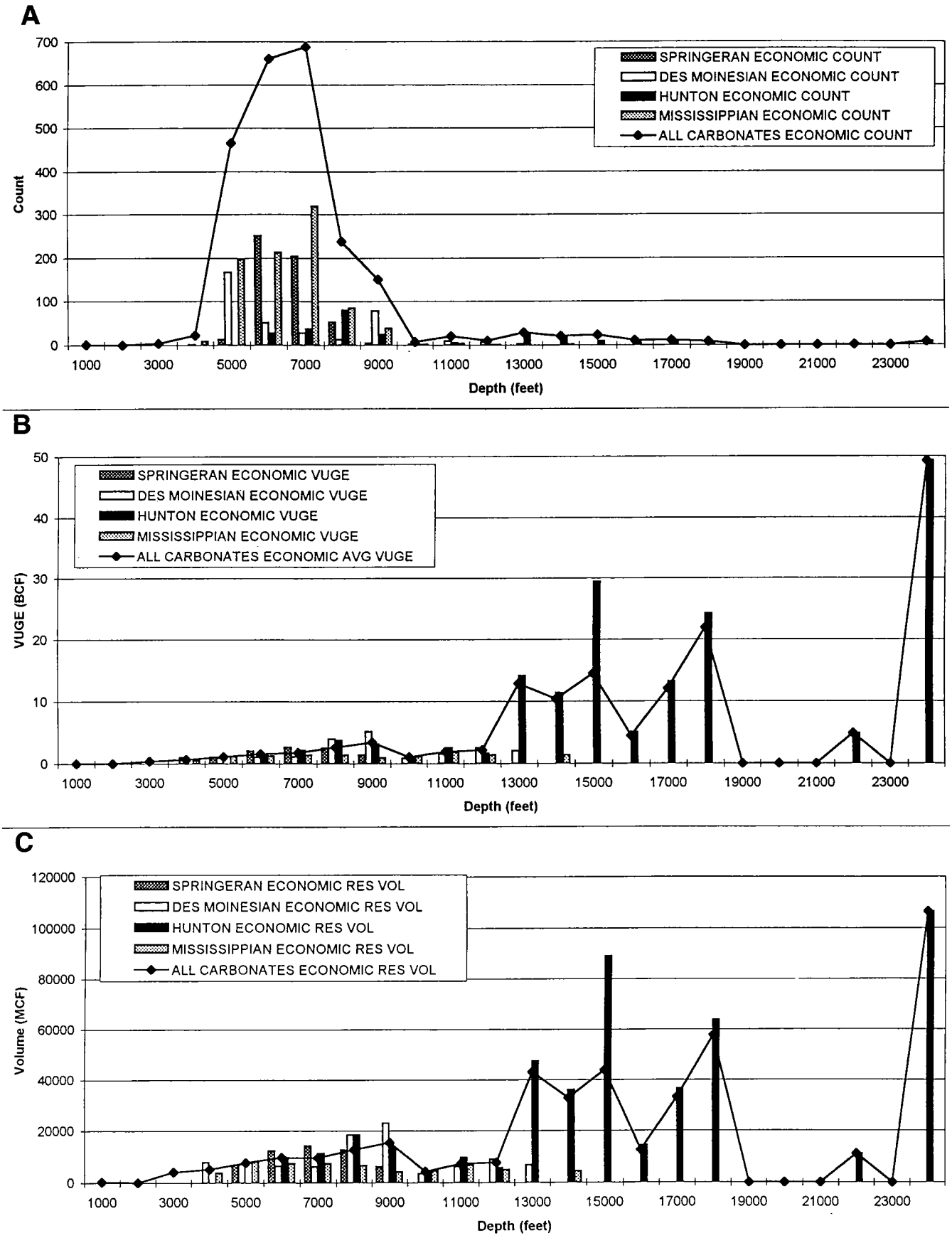

Figure 9. (A) Four "economic" carbonates by age, in comparison to all "economic" carbonates, versus depth. (B) Four "economic" carbonate recoveries (VUGE) by age, in comparison to all "economic" carbonate recoveries, versus depth. (C) Four "economic" carbonate-reservoir volumes by age, in comparison to all "economic" carbonate-reservoir volumes, versus depth.

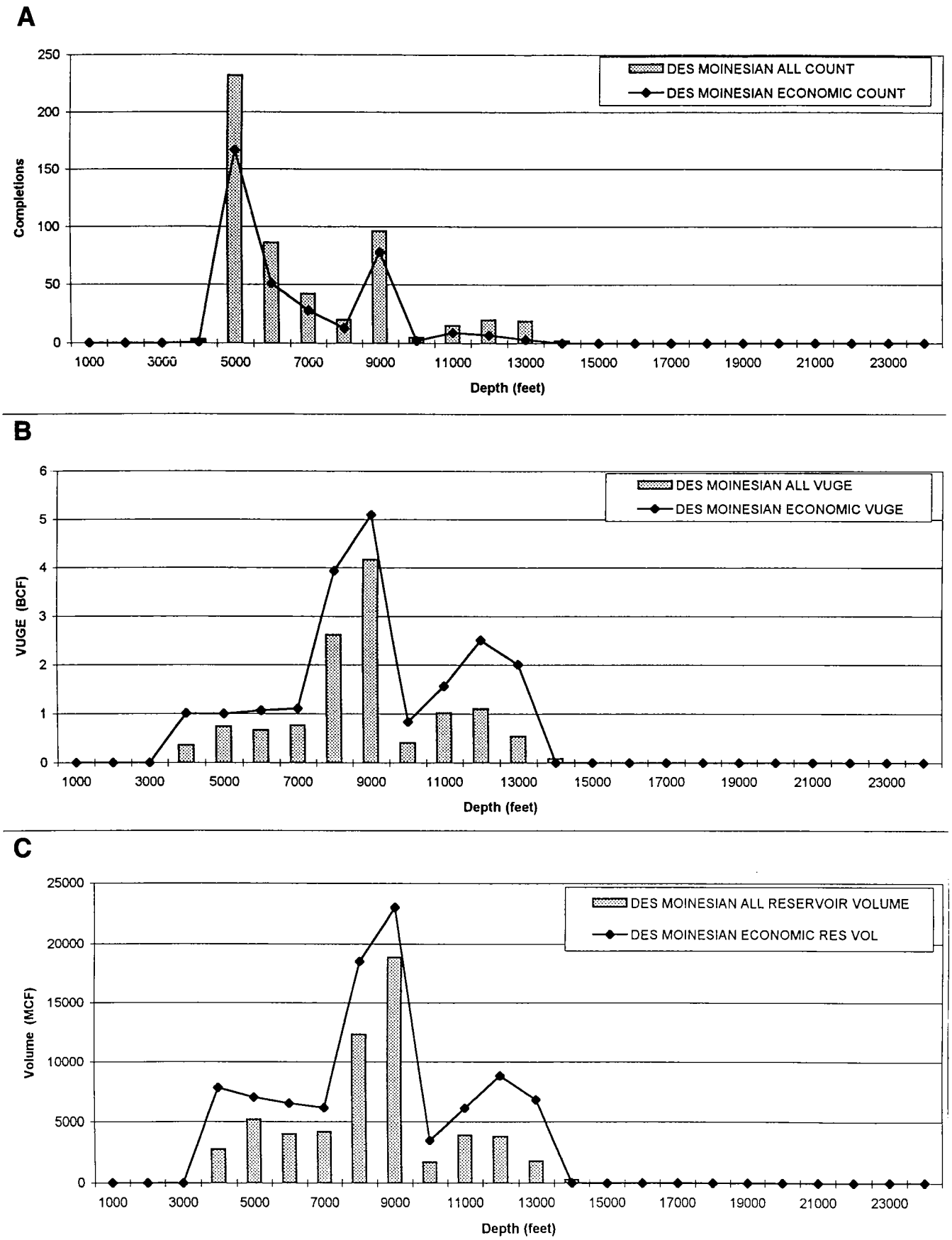

Figure 10. (A) Total completion count and "economic" completion count for Desmoinesian carbonate reservoirs versus depth. (B) Total recovery (VUGE) and "economic" recovery (VUGE) from Desmoinesian carbonate reservoirs versus depth. (C) Total Desmoinesian carbonate-reservoir volume and "economic" reservoir volume versus depth.

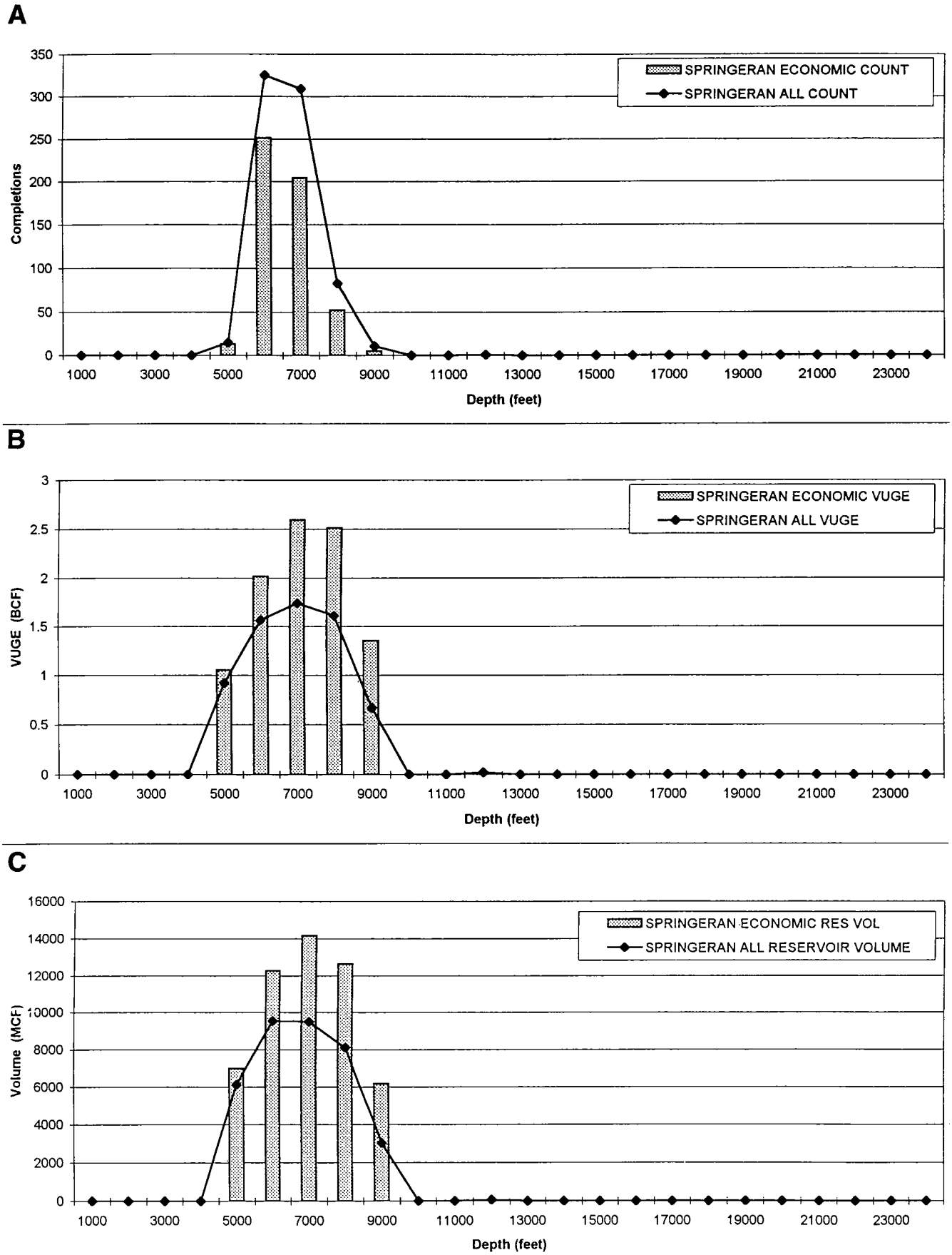

Figure 11. (A) "Economic" completion count and total completion count for Springeran carbonate reservoirs versus depth. (B) "Economic" recovery (VUGE) and total recovery (VUGE) from Springeran carbonate reservoirs versus depth. (C) "Economic" volume and total volume of Springeran carbonate reservoirs versus depth.

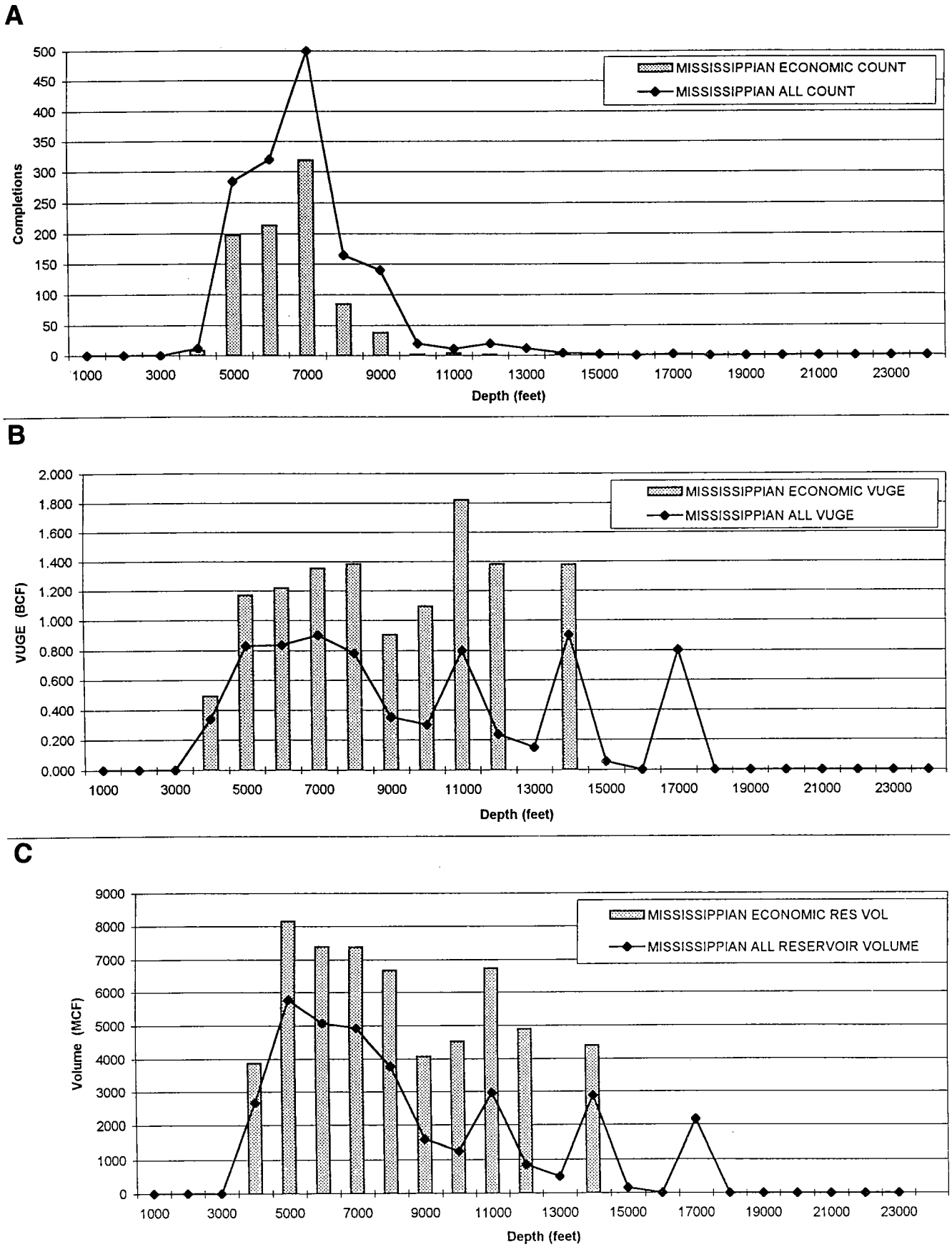

Figure 12. (A) "Economic" completion count and total completion count for Mississippian carbonate reservoirs versus depth. (B) "Economic" recovery (VUGE) and total recovery (VUGE) from Mississippian carbonate reservoirs versus depth. (C) "Economic" volume and total volume of Mississippian carbonate reservoirs versus depth.

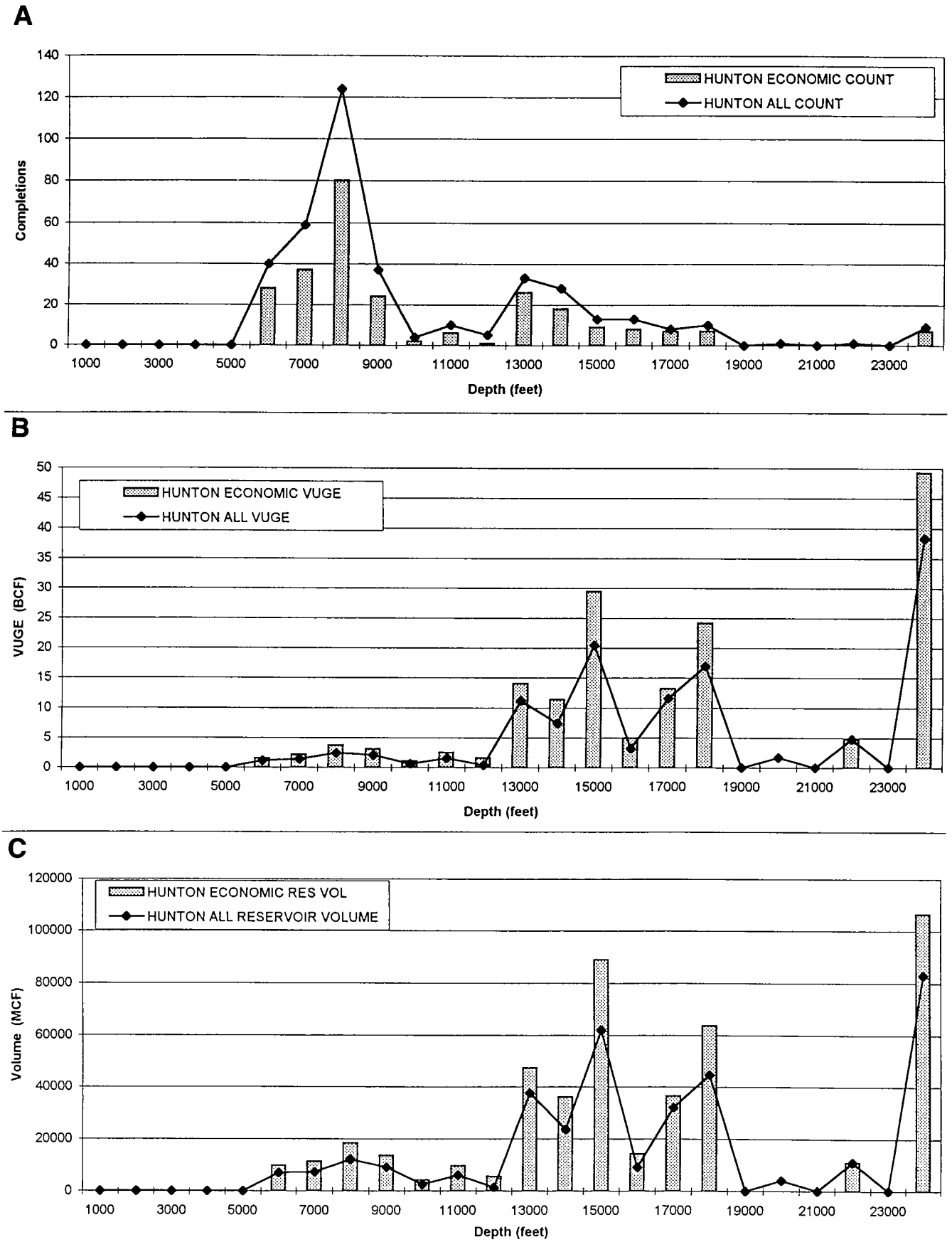

Figure 13. (A) "Economic" completion count and total completion count for Hunton carbonate reservoirs versus depth. (B) "Economic" recovery (VUGE) and total recovery (VUGE) from Hunton carbonate reservoirs versus depth. (C) "Economic" volume and total volume of Hunton carbonate reservoirs versus depth.

Final Observations

It is generally expected that the productive quality of reservoirs deteriorates with depth. Anomalies, such as the Hoover sandstone in Mocane–Laverne field, carbonate reservoirs in Hugoton field, and other unexplained aberrations (e.g., the carbonate "dead zone"), tend to support that expectation (Smith, 1996). However, the average recovery (VUGE) of the total gas-well population demonstrates that gas recovery increases with depth. The "economic" population strengthens the observation. Intuitively, one could conclude that increased pressure accounts for the increased recovery. The trend in recovered reservoir volume of "economic" completions demonstrates a near doubling of the reservoir volume from 5,000 to 13,000 ft. Below 13,000 ft, the average recovered reservoir volume doubles and then continues to increase at an accelerated rate.

In general, all the lithologies support the observation of increased reservoir volume and increased recovery with depth. Below 13,000–14,000 ft, the reservoir volumes drained by gas completions are substantially larger than they are above 13,000 ft. Whereas the increase is more pronounced in carbonate completions, it is indisputable for sandstone completions as well. This suggests that extrapolation of geological observations from huge (anomalous) fields may lead to underestimation of the prospects for deeper reservoirs.

The data indicate that historic trends in recovery per completion with depth may also understate the prospects for recovery from deeper reservoirs. Comparing the results for the "economic" filter and the "historic first 145" completions suggests that the best wells are not always drilled first. For depths below 10,000 ft, this certainly is the case. Although these data are not presented, we categorized the first 145 wells by reservoir lithology to determine if this trend is lithology-independent. The data indicated that the observation holds for all lithologies.

The more specific analysis of the sediments does not affect the general observations drawn for the sandstones and carbonates as a whole. In fact, the trends of the "economic" completions of individual carbonate ages display an overall increase in recovery and increased reservoir volume (excluding the "dead-zone" anomaly). All carbonates show poor recoveries and reservoir volumes through the "dead zone" (between 10,000 and 13,000 ft). The bimodal trends in the individual reservoir data (population and recovery) suggest the influence of geologic factors at the age and reservoir level.

Except for the Hunton, carbonate-completion activity has taken place almost totally above 10,000 ft. Exclusive of the Mississippian, carbonates show a stable increase in recovery and reservoir volume with depth through 10,000 ft. The analysis shows that the Mississippian carbonates are the poorest interval in the study area. Their low gas yields and high activity tend to reduce the aggregate quality markers (recovery and reservoir volume) for carbonates in the study area. Below 13,000 ft, the Hunton is the only carbonate reservoir with significant activity, which shows a significant jump (fivefold) in recovery and reservoir volume.

A geographic distribution of the four primary age groups of carbonates within the study area is presented in a series of production maps (Fig. 14). As suggested by the sandstone population, and as strongly indicated by the carbonate population, areas have been excluded from deep exploration because the lease rights were held by production. Figure 15A presents a composite well-spot map of the four individual maps presented in Figure 14. Figure 15B is a production map that shows the distribution of the four most significant sandstone groups. Figure 15A,B is provided to indicate lease areas that are likely to be held by shallow sandstone production. For example, areas showing producing sandstone wells would tend to hinder exploration efforts in the underlying carbonates. Furthermore, the Viola Limestone and the Arbuckle Group carbonates underlie the entire study area; proportionally, however, they are untested. Every spot on either the carbonate (Fig. 15A) or the sandstone (Fig. 15B) production map represents a well that is shallower than both the Viola and the Arbuckle. A vast majority of the shallow wells control the rights to deeper reservoirs. Consequently, no large areas remain with which to piece together a deep play without having to contend with rights that are held by production. Thus, the data indicate that deeper recoveries may reflect the effects of better prospects being held by shallower production as much as they reflect the intrinsic quality of deeper reservoirs. If this proves true, it would further strengthen the observation that increasing depth does not reduce the productive quality or capacity of deeper sediments.

SUMMARY AND CONCLUSIONS

The results of this study indicate that reservoir productivity does not decline with depth. The implication of this fact is contrary to industry expectations that reservoir quality degrades with depth, an expectation that has probably deterred interest in what appear to be highly productive reservoirs.

Gas compressibility is usually considered to be the most important factor leading to increased gas recovery with depth; the data indicate that it is not. In fact, by using the "economic" well group, average reservoir volumes are seen to increase 374% from 5,000 to 18,000 ft. Through the same interval, gas compression would increase the recovery by 183%. Increased reservoir volume has more than twice the impact on reservoir recovery than does gas compressibility. The average recovery actually increases by 635%, owing to a combination of increased volume and gas compressibility.

By using "economic" well populations, similar conclusions can be reached. From depths of 5,000 to 10,000 ft (above the "dead zone"), the average carbonate-reservoir volume increases by 151%, gas compressibility increases recovery by 81%, and thus gas recoveries increase by 214%. From 5,000 to 18,000 ft, the average carbonate-reservoir volume increases by 1,190%, gas compressibility increases recovery by 183%, and average recovery increases 1,881%. For carbonates, reservoir volume has more influence on recovery than does gas compression. For sandstones, reservoir volume is also as influential to more influential on recoveries as is gas compressibility.

None of the guidelines developed for the study area are consistent with a sustained deterioration in reservoir quality through a depth of 24,000 ft. Recovery increases faster than

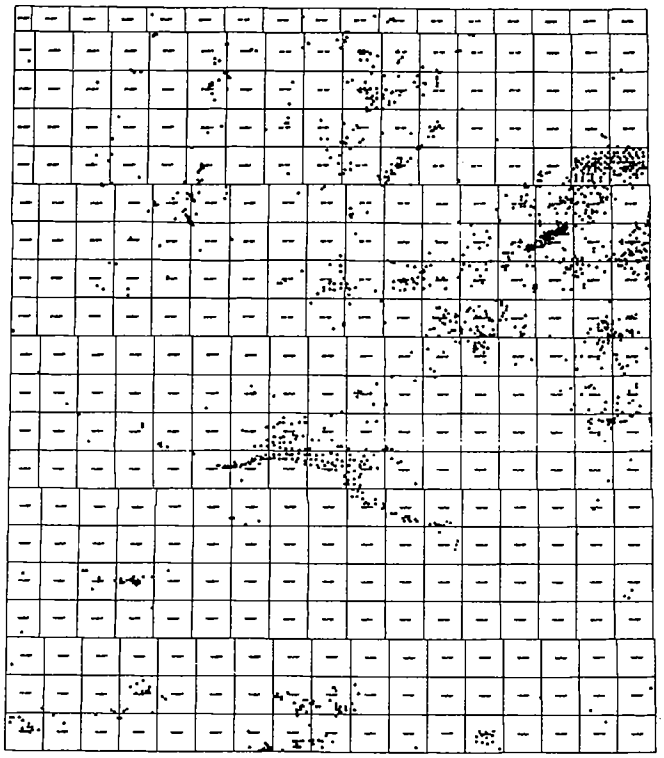

Desmoinesian carbonate production

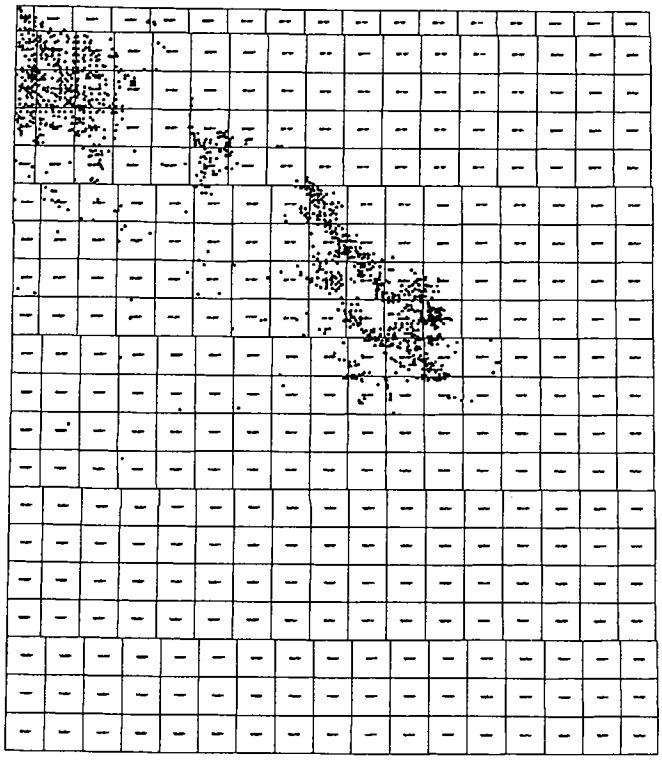

Springeran carbonate production

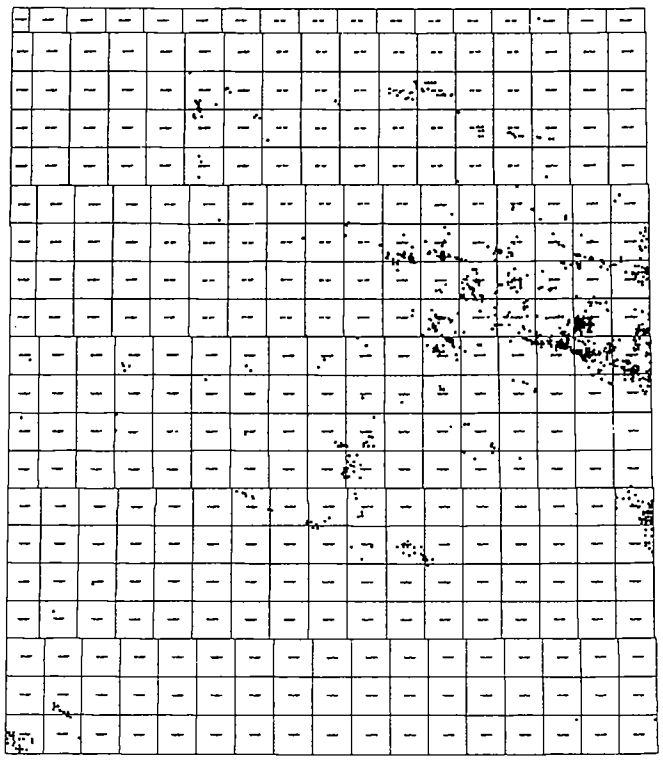

Hunton production

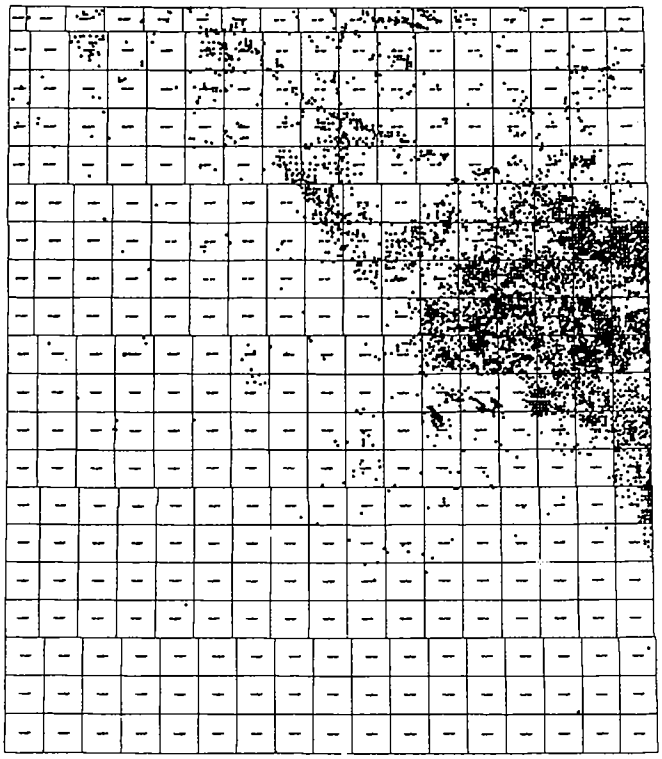

Mississippian production

Figure 14. Production maps for the four most significant carbonate groups. Each map covers an area encompassing Ts. 10–29 N., Rs. 10–26 W.

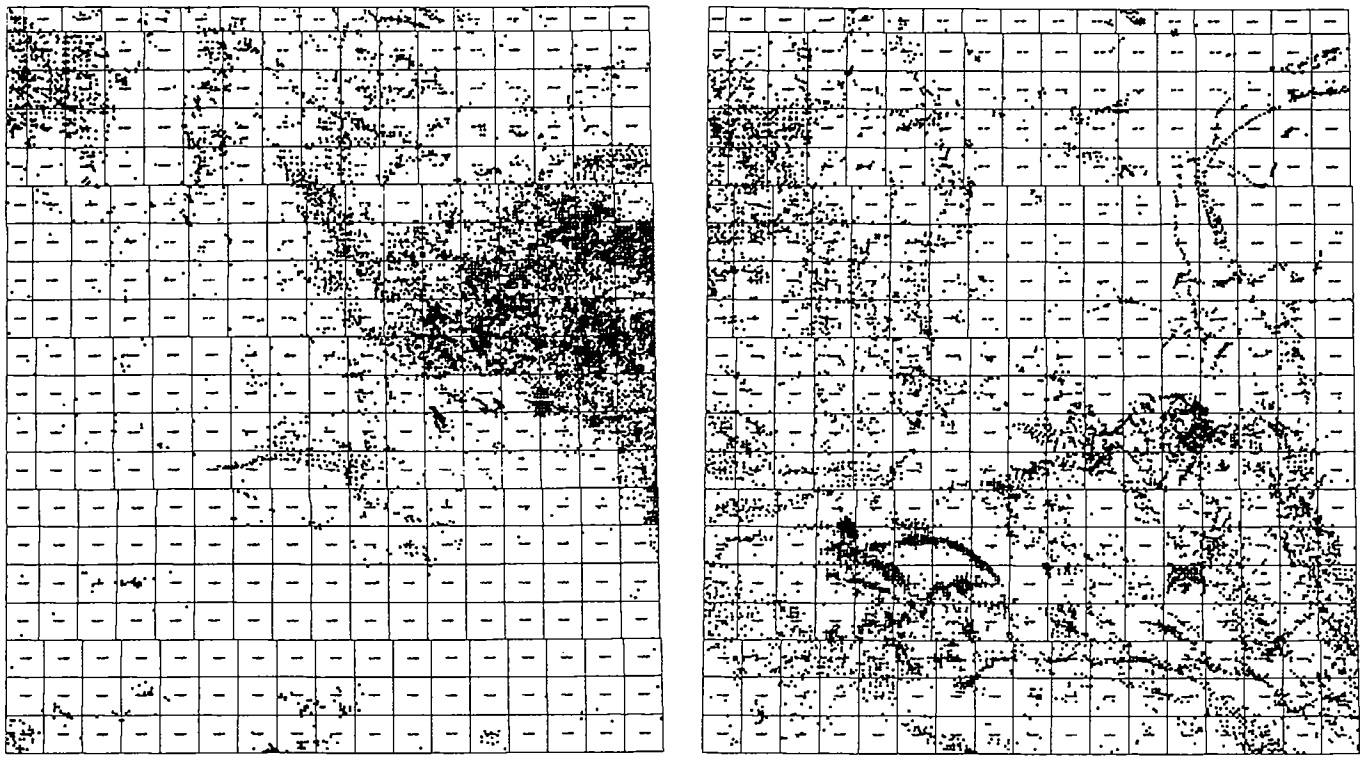

A Carbonate production
(Desmoinesian, Springeran, Mississippian, and Hunton)

B Sandstone production
(Cisco, Cherokee, Springer, and Morrow)

Figure 15. Combined production maps showing the four most significant carbonate reservoirs and the four most significant sandstone reservoirs. Each map covers an area encompassing Ts. 10–29 N., Rs. 10–26 W.

compression, thus indicating that the recovered reservoir volume of the produced hydrocarbons increases markedly with depth, particularly for carbonates. The regional geology indicates that producing intervals do not necessarily pinch out with depth, although their areal extent may shrink somewhat. Because areal extent versus depth is important in target discovery, this suggests that the pessimism toward drilling deeper targets may have reflected an expected risk for finding economic targets in deeper sediments more than their population. With the growing use of three-dimensional seismic methods, these risks have been substantially reduced.

Although these study results are different than industry expectations, they suggest that the difference reflects the extrapolation of industry activity through 13,000 ft of sediments. The pessimism may have been compounded by the severe deterioration (virtual collapse) in recoveries from carbonate reservoirs between 10,000 and 13,000 ft. Because 86% of industry activity in the study area is above 13,000 ft, these pessimistic expectations are understandable. Below 13,000 ft, recovery increases substantially for both sandstone and carbonate reservoirs at a rate far beyond what compression would imply.

Whereas carbonate recoveries virtually collapse between 10,000 and 13,000 ft, initial analysis of the data suggests that this collapse may be more institutional (i.e., the better carbonate prospects in this depth are held by shallower production) than geological. If further analysis supports this initial observation, it would suggest that areal location (where one drills) might be as important as "play" (target reservoir) for resource prospects. The critical question would be whether such an observation is more general or applicable only to specific geologic environments.

Although general trends in hydrocarbon recovery and macro geological guidelines, such as reservoir volume, indicate substantial prospects for deeper sediments, additional work needs to be done to tie the macro results developed in this study to more specific geological parameters. In addition, the study should be expanded to include the entire Anadarko basin. The second phase of this "Gas Recovery versus Depth Project" would investigate the geological and engineering characteristics of particular reservoirs across a wide range of depth intervals and for several specific reservoirs.

ACKNOWLEDGMENTS

We wish to acknowledge the assistance of Walter J. Hendrickson, Craig M. Williams, Ronald J. Woods, and Lindell Bridges of Dwight's Energydata (now a part of IHS Energy Group) for their assistance in assigning the gas-completion data to the proper formations and lithologies.

This paper addresses the carbonate reservoirs evaluated by a project jointly funded by the Gas Research Institute, Washington, D.C., and Dwight's Energydata, Inc., Oklahoma City. Dwight's Energydata, Inc., is now a part of IHS Energy Group. The project was a preliminary study to assess the pros-

pects for deeper reservoirs in the Anadarko basin. The full report discusses sandstone, carbonate, "wash," and mixed lithologic groups and is available from the Gas Research Institute as GRI Report GRI-96/0196 (Smith, 1996).

REFERENCES CITED

Smith, P. W., 1996, Anadarko Basin statistical study: gas well recovery -vs- depth in the Anadarko Basin of western Oklahoma: Gas Research Institute, Chicago, Report GRI-96/0196, 65 p.

Smith, P. W.; Hendrickson, W. J.; and Williams, C. M., 1996, Regional correlations and reservoir characterization studies of the Springer Group in the Anadarko Basin area of western Oklahoma: Tulsa Geological Society, Transactions of 1995 American Association of Petroleum Geologists, Mid-Continent Section Meeting, p. 116–126.

Woods, T. J., 1993, Exploring for the frontier in the US Lower-48: Oil and Gas Journal, September 27, p. 81–85.

Initiation of the Arbuckle Platform—View from the Slick Hills, Oklahoma

R. Nowell Donovan
Texas Christian University
Fort Worth, Texas

ABSTRACT.—A record of the Late Cambrian (Franconian) transgression across the Laurentian craton is preserved in the eastern Slick Hills of southwestern Oklahoma. Four factors that contributed to the character of the sequence are (1) the transgression, (2) the transgressed surface, (3) eustatic variations in sea level, and (4) tectonic adjustments associated with the development of the southern Oklahoma aulacogen.

Facies changes during the transgression provided the basic stratigraphic framework that constitutes the basal Reagan and Honey Creek Formations (together forming the Timbered Hills Group), which pass up into the Fort Sill Formation, the lowest division of the Arbuckle Group. The Reagan Formation consists of a basal alluvial sequence of red-brown sandstones and conglomerates. This is overlain by purple and tan quartz-rich sandstones that were deposited as tidally influenced sand bars. These sandstones are interbedded with green-shale heterolithics. The topmost Reagan is a glauconitic, tidally influenced green sandstone. The Honey Creek Formation consists of meter-scale alternations of quartz-rich sandstones and pelmatozoan-rich grainstones. The faunal-colonization sequence involved trace fossils (both vertical and horizontal), phosphatic brachiopods (*Lingula* sp.) that may be tied to glauconite peloid production, and finally carbonate organisms (principally pelmatozoans, but also including brachiopods and trilobites). The base of the Arbuckle Group is associated with the incoming of abundant lime mud. The changes that took place are a result of an expansion of the carbonate-producing environment into a platform, a resultant decrease in tidal energy (from macrotidal to microtidal), and a greater variety of colonizing organisms, particularly algae. The lower part of the Fort Sill Formation displays characteristic meter-scale shallowing-upward cycles; the top part of the formation (which locally is pervasively dolomitized) is built of massive algal boundstones. The succeeding Signal Mountain Formation, the base of which is marked by a disconformity, is dominated by "below-wave-base" facies.

The transgression inundated a hilly land surface of Cambrian Carlton Rhyolite; the resulting archipelago persisted until close to the end of the deposition of the Fort Sill Formation. Clear waters around the islands provided the initial environment for colonization by carbonate organisms. Much facies variation is related to the topography; wedges of breccia and conglomerate occur throughout the section, whereas leeward and windward carbonate facies are preserved in the carbonate formations.

Eustatic variations in sea level are recorded by meter-scale cycles in the Honey Creek and Fort Sill Formations. In addition, the sequence shows two "grand cycle" boundaries. One occurs low in the Honey Creek and is associated with a slight angular unconformity that is due to compactional draping around the rhyolite terrain. The other constitutes the Fort Sill–Signal Mountain formational boundary.

At the same time that the Franconian transgression was proceeding, tectonic definition of the southern Oklahoma aulacogen was taking place. This definition is recorded by aberrant variations in the size and type of siliciclastic grains, facies changes that record an increase in water depth and an increase in the thickness of grand-cycle packages.

INTRODUCTION

During the Late Cambrian Franconian Stage, a major transgression took place across the Laurentian craton. At this time, Laurentia was centered astride the equator between latitudes 30° N. and 30° S. (Scotese, 1984). The area that would become Oklahoma lay just south of the equator, between latitudes 8° and 10° S. Removal of the cumulative rotation of 70° that has taken place since the Cambrian places "Oklahoma" at the western margin of the continent. Assuming continuity of global meteorological patterns, the "Oklahoma" segment of the craton was subject to a maritime equatorial climate; specifically, it was on the lee side of the continent with respect to southeast trade winds.

At this time Laurentia was a modest-sized, tectonically stable continent, perhaps 30% smaller than the present North American plate and separated from the nearest cratonic masses, Baltica and Europe, by the Iapetus Ocean. This paper summarizes the geology of the Late Cambrian sedimentary record as it is displayed in the Slick Hills of southwestern Oklahoma. The sequence in this area is well exposed and offers perhaps the most complete record of Late Cambrian to Early Ordovician sedimentation in North America.

Donovan, R. N., 2000, Initiation of the Arbuckle platform—view from the Slick Hills, Oklahoma, *in* Johnson, K. S. (ed.), Platform carbonates in the southern Midcontinent, 1996 symposium: Oklahoma Geological Survey Circular 101, p. 47–56.

DISPOSITION OF OUTCROPS

The Slick Hills of southwestern Oklahoma are the exposed portion of the frontal fault zone, an area of intense Pennsylvanian tectonic deformation between the Wichita uplift and the Anadarko basin (Fig. 1). The Slick Hills are divided into eastern and western portions by the Blue Creek Canyon fault, a high-angle oblique back thrust with downthrow to the southwest of up to 8,000 ft (Donovan, 1995). In the eastern Slick Hills, the unconformable contact between igneous basement and the sedimentary section is exposed in a homoclinal section that dips northwest at 20°–50° over a length of approximately 10 mi (Fig. 2). The exposure quality is high, and facies variation can be adequately assessed. The basal part of the sedimentary section is not exposed in the western Slick Hills, an area of extravagant structural architecture.

STRATIGRAPHY

The formal lithostratigraphic division of the Upper Cambrian section in southern Oklahoma reflects a gradual upward passage from a siliciclastic to a carbonate depositional milieu. Although there has been a disputation over some of the details (summarized in McElmoyl and Donovan, 2000), the basic pattern of division can be equated over a large area of Texas, Oklahoma, Kansas, and Missouri. By the end of the Cambrian, a stable paleogeographic framework had developed that would persist well into the Ordovician.

Facies that record the transgression provide the basic stratigraphic framework (Fig. 3). The basal Reagan and Honey Creek Formations (which together form the Timbered Hills Group) pass upward into the Fort Sill Formation, the lowest division of the Arbuckle Group. Detailed changes in facies are particularly noteworthy in the Reagan. The base of this formation is constructed of a sequence of red-brown sandstones and conglomerates, interpreted as alluvium (Donovan, 1986). This alluvium is overlain by purple (hematite-cemented) and tan quartz-rich sandstones, deposited as tidally influenced sand bars. In places, a shoreline sandstone facies can be recognized. These sandstones are interbedded with poorly exposed green-shale heterolithics. The topmost Reagan is a distinctively glauconitic green sandstone, again deposited in a tidally influenced environment. The Honey Creek consists of meter-scale alternations of quartz sandstones and pelmatozoan grainstones. The faunal-colonization sequence involves trace fossils (both vertical and horizontal), phosphatic brachiopods (*Lingula* sp.) that appear to be tied to glauconite peloid production, and finally carbonate organisms (principally pelmatozoans, but also brachiopods and trilobites and minor amounts of other organisms). The lithological definition of the base of the Arbuckle Group, which involves the incoming of abundant lime mud, records expansion of the platform together with a diminution of tidal energy and an increased colonization by algae. The lower part of the Fort Sill displays meter-scale cycles (currently under investigation); the top part of the formation (which locally is pervasively dolomitized) is built of massive algal boundstones. The succeeding Signal Mountain Formation, which is marked by a disconformity, is dominated by "below-wave-base" facies.

FORM OF THE BASEMENT

The transgression that began in the Franconian was a worldwide event during which sea levels rose to an unprecedented height by the end of Early Ordovician time. Over most of Laurentia, this transgression inundated a terrain of various ages of Precambrian gneisses, schists, and various granitic rocks. However, in southern Oklahoma, the basement consists of Early and Middle Cambrian igneous rocks that were emplaced during the initial formation of the southern Oklahoma aulacogen. This aulacogen is a linear rift feature that has been conventionally interpreted as the failed arm of a triple junction associated with the opening of the "Ouachita Sea," a side arm of the Iapetus Ocean. At the present time the aulacogen is oriented N. 60° W. (i.e., 120°–300°). Given the rotation noted previously, the original orientation of the aulacogen was N. 10° E. (i.e., 010°–190°).

The topmost level of aulacogen-related igneous rocks within the Slick Hills is formed by the Carlton Rhyolite Group. Ham and others (1964) measured 3,600 ft of rhyolite and related rocks in their type section on Bally Mountain (Fig. 2), although the base of this section is not seen. Erosion prior to the Franconian transgression cut deeply into the sequence, sculpting a range of hills up to at least 750 ft high (Donovan and Stephenson, 1991). Slopes on these hills are generally gentle—no more than ~10°—except in Blue Creek Canyon, where a fault-related gorge apparently follows the line of an early fault. Marine transgression of this landscape gradually isolated summits as islands, forming the "southern Oklahoma archipelago." Along strike in the eastern Slick Hills, five distinct islands were present, the highest of which persisted until late in the deposition of the Fort Sill Formation.

FACIES

Alluvial Deposits

The initial deposits on the rhyolite topography were a series of red beds—conglomerates, sandstones, and shales—up to ~40 ft thick (Fig. 3). These deposits are essentially detritus derived from the rhyolite and were deposited as alluvium in hollows and valleys. Generally, the beds are cemented by hematite and silica cements, both of which may have been derived from weathering and devitrification of the rhyolite (Donovan, 1986).

Reagan Marine Facies

The beds that overlie the red beds mark the commencement of the Franconian transgression. They display abrupt facies changes that in part are due to the irregular nature of the transgressed topography. Thus the rhyolite islands themselves contributed detritus in the form of conglomerates composed of rhyolite pebbles that thin away from the adjacent topography. At higher levels, the conglomerates become less important and gradually pass into breccias, particularly in the Honey Creek and Fort Sill Formations. In addition, throughout their history the islands partitioned the marine environment into leeward and windward sub-environments (Donovan, 1986).

The general environment of deposition during formation of the Reagan was a strongly tidally influenced siliciclastic system in which several subfacies can be distinguished.

Shoreline Sandstones and Conglomerates

These sandstones differ from the underlying alluvium in being quartz rich, with grain size varying from fine to coarse. With the quartz are trace amounts of orthoclase and microcline; the grain populations are mineralogically mature and presumably were derived from the older parts of the craton, outside the aulacogen. In addition, up to 5% of ferruginous ooids may be present. Most of the ooids have been squashed against quartz and rhyolite grains during diagenesis: presumably they were reworked into the sandstones from the quieter environment in which they probably formed.

Lenticular Sandstones

Lenticular sandstone bodies show medium- and large-scale cross-bedding, reactivation surfaces, and colonization by the *Skolithos* ichnofacies (Donovan, 1986). Paleocurrents in these sandstones are bimodal and bipolar, with a northwest–southeast orientation. The frequency distribution of these cross-bed orientations is asymmetric; most cross-beds were deposited by currents flowing to the southeast. On the assumption that the transgression was to the northwest (today's coordinates), flood tides were evidently less effective than ebb tides in moving sediment. In other words, the adjacent craton was a net contributor of large volumes of siliciclastics to the transgressing seaway. This contribution continued throughout deposition of the Timbered Hills Group.

Heterolithic Sequences

Heterolithic sequences show a variety of forms of bipolar lenticular bedding and substantial colonization by horizontally crawling organisms. The shale component of these beds is grayish green: no organic carbon has been preserved. In places, this facies directly abuts rhyolite islands with no shoreline facies present.

Green Sandstones

In the uppermost parts of the Reagan, there is a widespread development of green sandstones that contain extraordinary amounts of glauconite peloids—as much as 60% in some samples. In some places, the green sands are characterized by bipolar cross-bedding in sets up to 5 ft thick; in others, the cross-bedding is more modest. In addition to glauconite peloids, these sands contain quartz, rhyolite fragments, some phosphatic nodules, and up to 10% phosphatic brachiopods, most if not all of which appear to be fragments of *Lingula* sp. The latter are the most likely culprits to be responsible for production of the glauconite peloids, perhaps aided and abetted by some of the horizontally crawling organisms.

Cementation of the Marine Reagan

The cementation history of the marine Reagan is complex; in the lower parts of the sequence, particulate coats of hematite are followed by secondary syntaxial quartz. Such sandstones are characteristically purple brown. In others, the hematite is not developed, and these sandstones are tan. In the upper parts of the sequence, the early phase of hematite precipitation is similarly absent, nor are the quartz overgrowths as well developed. In places a matrix of iron-rich illite is present (Donovan, 1986). As a result, the green sands weather more easily than the underlying purple and tan sandstones. Directly below the Honey Creek limestones, some calcite and ankerite cement are present, presumably recording infiltration from ambient seawater in the overlying formation.

Honey Creek Facies

There has been a lengthy dispute concerning the boundary between the Reagan and Honey Creek Formations (reviewed in McElmoyl and Donovan, 2000). Here, this boundary is taken as the lowest occurrence of grainstones in the section, following Donovan (1986); this boundary is clearly diachronous and must in part have been controlled by details of the archipelago.

Honey Creek limestones vary considerably in their composition, from more or less "pure" bioclastic grainstones to mixed-grain assemblages of carbonates, glauconite, quartz, rhyolite, and phosphatic shell debris. The variation is tied to the topography of the archipelago, with the purer carbonate accumulations having formed adjacent to islands. This relationship has led to the formulation of the "archipelago model" (Donovan, 1986) as a means of initiating carbonate production: simply put, the rocky rhyolite substrates were colonized by vast numbers of sessile organisms, principally pelmatozoans (examples of preserved in-situ holdfasts are described in Donovan and Stephenson, 1991, and McElmoyl and Donovan, 2000). Upon death, these organisms fragmented to very coarse sand and granule-sized grains that formed the bulk of the carbonate sands. Other organisms include thick-shelled trilobites and brachiopods (principally orthids).

In essence, the facies that developed involved the movement of carbonate and rhyolite sand away from the islands into places where they mingled with other grains. The grain-dispersal pattern was current-driven; there are few signs of significant bioherm buildup or stable-sea-bed relief around the islands. As a result, the Honey Creek limestones are comprehensively cross-bedded, displaying bipolar trends, and are punctuated by numerous reactivation surfaces. As is the case with the underlying Reagan, a tidal influence is apparent. However, the dimensions of the cross-beds are markedly different: cross-beds more than 6 in. thick are rarely seen in the Honey Creek, either in the siliciclastic- or carbonate-dominated facies. In areas of mixed petrography—i.e., distal to islands—a distinctive pattern of wavy bedding, involving an alternation of thin beds of carbonate and siliciclastic sandstone, is ubiquitous (Bucheit and Donovan, 2000). Both lithologies are characterized by small-scale cross-bedding. Evidently, the current power available was insufficient to mix the two varieties of sand. In part, this may have been due to the dis-

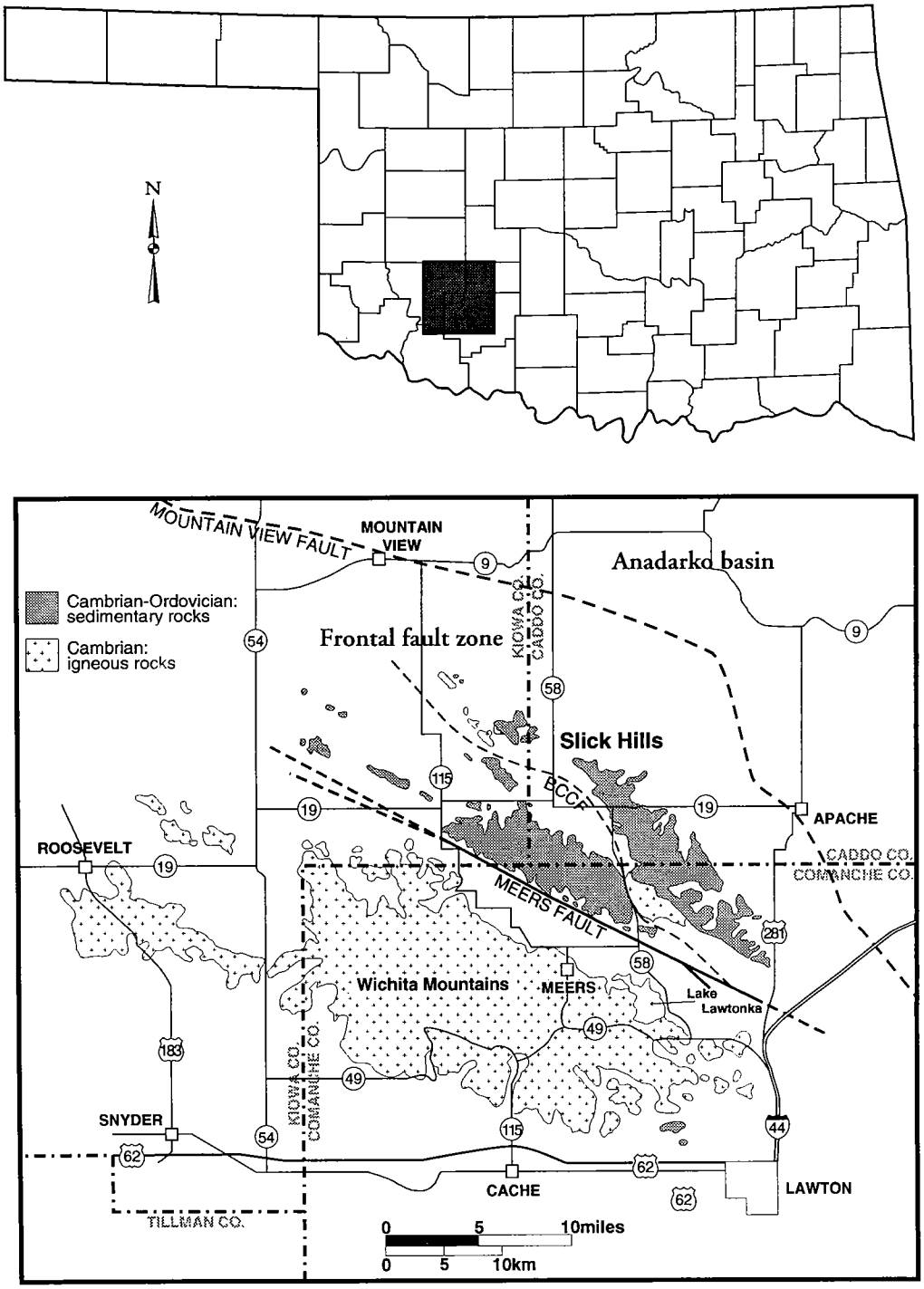

Figure 1. Map of southwestern Oklahoma, showing location of the Slick Hills and the Wichita Mountains.

crepancy in size of the particles—very coarse sand to granule-sized carbonate grains, as opposed to very fine to fine-sand siliciclastics. In addition, the carbonates appear to have cemented rapidly, principally through the growth of syntaxial overgrowths around pelmatozoan grains—so rapidly that there was little infiltration of the finer siliciclastics into the pores of the carbonate sands.

A caveat to the general facies patterns that are seen in the Honey Creek is provided by the sheltered lee-side environments identified by Donovan (1986) and by Donovan and Stephenson (1991). In these settings, lime mudstones, mechanical bafflestones, sponges, specific algae (*Renalcis* sp.), pelmatozoan holdfasts, ferruginous stromatolites, and glauconitic hardgrounds are preserved.

Transition to the Fort Sill Formation

The smaller size of the cross-beds in the Honey Creek probably resulted from a gradual diminution in tidal power, which

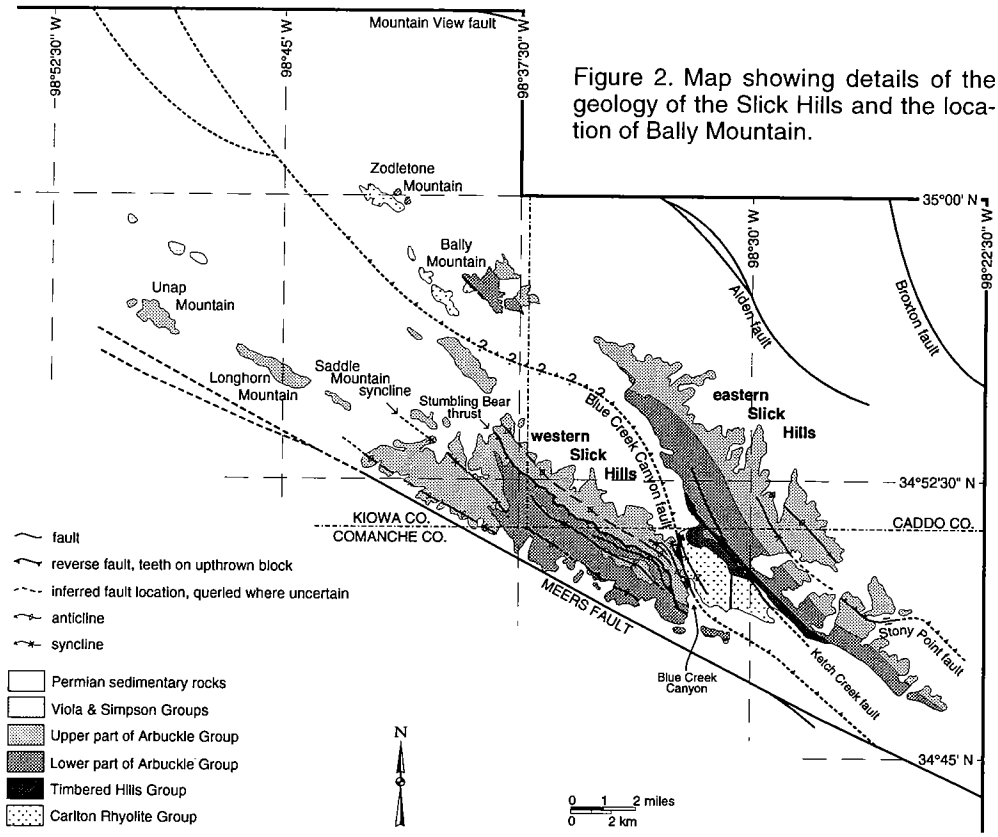

Figure 2. Map showing details of the geology of the Slick Hills and the location of Bally Mountain.

in turn was related to the increasing size of the platform. One of the constant motifs that can be tracked throughout the sequence is a diminution in the potency of sorting and tractive mechanisms. This inference can be explained by an increase in the area of the expanding platform and the resulting difficulty in moving large volumes of water on and off the platform by tidal power. The lessening influence of this major flushing process led ultimately to the preservation of large volumes of lime mud in the sequence, and to the creation of an environment where creatures that produced the lime mud were efficient.

In petrographic terms, the base of the Fort Sill is taken as the first limestone unit in the sequence that is dominantly mud based. Visually, this appears as the first of the persistent light-gray layers of "tombstone" lithology that are such a conspicuous feature of the Arbuckle Group. The choice of boundary would seem to be somewhat arbitrary, as the change from "typical" Honey Creek to "typical" Fort Sill takes place over a thickness of approximately 25 m. In practice, the choice can be surprisingly exact. For example, a 2-cm-thick hardground chosen as the boundary during the course of logging a single section on Bally Mountain can be traced along the entire width of outcrop—about 800 m. This hardground has acted as a substrate for pelmatozoan growth. Hardgrounds a little above this horizon have been phosphatized and glauconized.

The mud-supported lithologies of the Fort Sill are texturally diverse, involving a spectrum of lithologies from mudstones to packstones. Most allochems are fragments or complete specimens of a variety of fossils, which, in order of abundance, are trilobites (both thin and thick shelled), gastropods, pelmatozoans, brachiopods, sponges, calcispheres, and algae (*Renalcis* sp.). Other allochems include peloids and intraclasts; ooids are found higher in the section. Algal boundstones, generally of low relief and constant radius, are a persistent feature of the formation, although they are not common in the lowermost few meters of the sequence.

Lithological Subdivision of the Fort Sill Formation

The Fort Sill is a thick carbonate sequence that has been divided on lithostratigraphic criteria into three ad-hoc members. These are a lowermost sequence of light-gray limestones that appear to have a cyclic character; a very thinly bedded sequence of impure, quartz-silt-rich limestones that is a prominent cliff former; and an uppermost member that consists almost entirely of massive algal boundstones. All three members can be traced throughout the Slick Hills; they are currently under study and are not described further here.

Further lithostratigraphic complexity in the Fort Sill Formation is provided by the Bally Dolomite, an approximately 60-m-thick sequence of comprehensively dolomitized algal boundstones in the central part of the upper member of the formation. This dolomite is found only in the western part of the Slick Hills, at Bally and Zodletone Mountains; there is no trace of it in the Blue Creek Canyon area. Unfortunately, there are no intermediate exposures. Gao (1990) suggested that the dolomite formed early, a view supported by Hosey and Donovan (2000), who suggest that the dolomite was exposed in an area west of the present outcrop during the major nonconformity that preceded deposition of the Signal Mountain Formation. The Bally Dolomite finds a partial parallel in the Royer Dolomite of the Arbuckle Mountains, and the two units

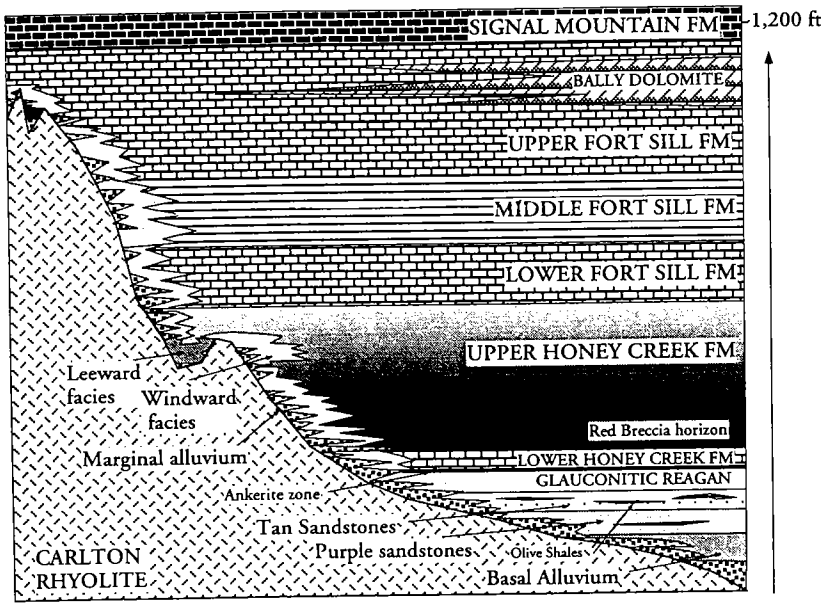

Figure 3. Schematic representation of the stratigraphic relationships described in the text.

have been equated (Gao, 1990). It is clear, however, that the Bally Dolomite replaced limestones that are older than those replaced by the Royer, an inference that has importance in any consideration of the tectonic stability of the opposing sides of the southern Oklahoma aulacogen.

Contact between the Signal Mountain and Fort Sill Formations

This contact is the most obvious visual discrepancy in the Arbuckle Group. A recent study by Hosey and Donovan (2000) has concluded that it records a period of significant exposure and some erosion. They further suggest that it correlates with a craton-wide regression. As has been noted previously, the topmost Fort Sill is built of massive algal boundstones; these are petrographically simple rocks with a sparse fauna of gastropods, trilobites, and algae. By contrast, the Signal Mountain preserves a fauna that is both more numerous and more diverse. Thin- and thick-shelled trilobites, pelmatozoans, brachiopods, gastropods, calcareous sponges, and calcispheres are abundant. In general, the fauna is similar to that seen in the lower, as opposed to the upper, Fort Sill.

The Signal Mountain contains more siliciclastic mud and silt detritus than any other formation in the Arbuckle Group. Textures and compositions throughout are a regular repetition of thin (millimeter to centimeter scale) but diverse lithologies, most of which were deposited below wave base (Whitehead and Donovan, 2000). The absence of algal boundstones, so common in the adjacent formations, suggests that the sea bed was below the photic zone. The absence of burrowing and the preservation of organic carbon in some layers led Whitehead and Donovan (2000) to suggest that anoxic conditions existed close to the sediment–water interface. The Signal Mountain is overlain by the McKenzie Hill Formation, the base of the latter being taken as the incoming of thick algal boundstones and associated lithologies. These boundstones form distinctive thrombolitic reefs up to 6 ft thick.

Summary of Petrographic Changes and Environmental Inferences That Mark the Section

The principal petrographic changes seen across the Timbered Hills–lower Arbuckle Group transition are as follows (Fig. 4):

- There is an upward diminution in the amount of rhyolite. This is related principally to distance above the basal unconformity and secondarily to lateral distance from an adjacent island. Basal alluvium consists of ~80–90% rhyolite plus its devitrification and weathering products. Rhyolite clasts occur up to the uppermost member of the Fort Sill Formation.
- Pebbles of rhyolite in the Reagan Formation are generally well rounded, whereas in the Honey Creek they are angular. This may reflect either a lesser capacity for abrasion in the carbonate-dominated Honey Creek and/or an increased rate of burial.
- Quartz is found in all members. Mineralogically, the quartz population is mature in consisting primarily of monocrystalline grains with straight extinction. This suggests that the quartz is the product of effective (i.e., long-lived and/or intense) weathering, an inference that is supported by the very small percentages of feldspar (almost all microcline) encountered. The presumed source of this quartz is the Laurentian craton, although a small percentage probably came from weathering of the Carlton Rhyolite. The rhyolite contains both quartz and potassium feldspar phenocrysts; the latter are found only in the basal Reagan and generally are heavily sericitized.
- The grain size of quartz generally decreased as the platform developed (an exception to this trend is noted below). In the lowermost parts of the Reagan, granules and very coarse sand grains of quartz are encountered, whereas in the Signal Mountain Formation the coarsest grains are very fine sand. The biggest change in grain size takes place across the boundary between the lower and upper members of the Honey Creek. Above this boundary, the largest quartz grains are medium to fine; below, more variety in size is encountered. McElmoyl and Donovan (2000) suggested that this boundary records a major, albeit temporary, regression. In general, the upward decrease in grain size is compatible with a gradual expansion of the platform and increasing distance to source.
- The percentage of quartz generally decreases when measured over the entire section. However, individual beds may contain as much as 90% quartz even quite high in the section. Donovan (1986) suggested that detrital siliciclastics in the Arbuckle Group are a signature of regression. In this context, it is noteworthy that the thickest quartz sandstone in the Honey Creek Formation occurs directly above the grand-cycle boundary described by McElmoyl and Donovan in 2000 (discussed below).
- The percentage of glauconite decreases upward from the greensand that marks the top of the Reagan Formation. The glauconite is seen in several forms: as peloids (by far the most abundant variety), as alteration of rhyolite clasts, as pore infillings of pelmatozoan grains, as matrix, and as joint coat-

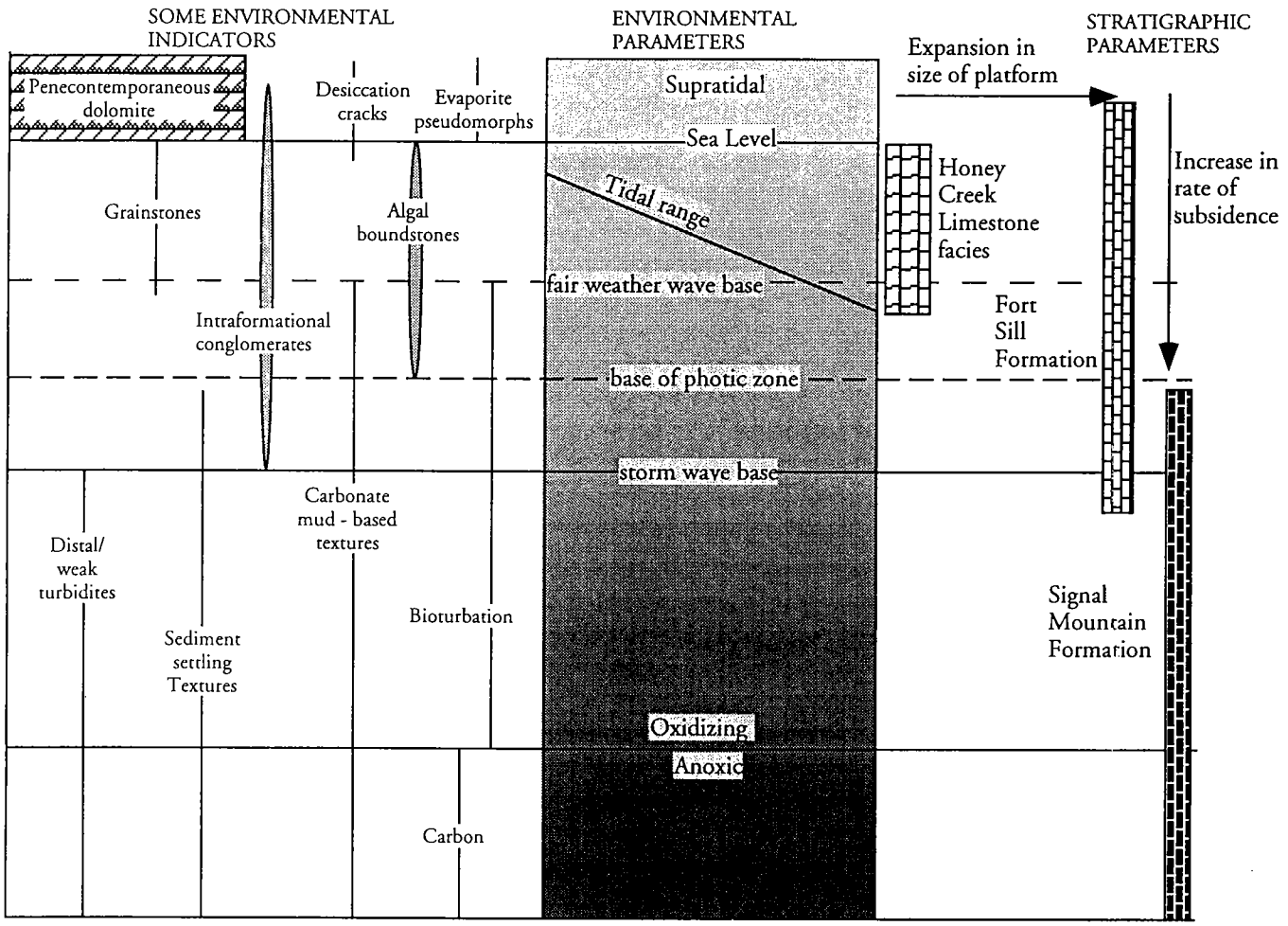

Figure 4. Synopsis of features that permit environmental discrimination of carbonate facies in the Timbered Hills and lower part of the Arbuckle Groups.

ings in the Carlton Rhyolite. Little glauconite is found in the Fort Sill Formation, and, although a spike of glauconite marks the base of the Signal Mountain Formation, it seems clear that the Arbuckle platform was not an environment conducive to glauconite formation.

• The occurrence of phosphate parallels that of glauconite, although the varieties differ. Most phosphate is seen as the broken shells of inarticulate brachiopods (*Lingula* sp.). In addition, some nodules and phosphatized rhyolite clasts are found. The inference seems to be that phosphatic brachiopods—which may or may not be responsible for glauconite peloid formation—were "at home" in the macrotidal environments that characterized the Timbered Hills Group but were not favored by the microtidal settings of the Arbuckle platform.

• Horizontal (i.e., burrowing) organisms are found in the finer grained facies of the Reagan and Honey Creek Formations and throughout the Fort Sill Formation. Vertical burrows are restricted to the siliciclastic sandstones of the Timbered Hills, being found principally in the purple and tan sandstones of the Reagan. The inference is that they were adapted to high-energy macrotidal settings.

• The calcareous biota seen in the section shows substantial, albeit gradational, changes. The initial fauna was dominated by organisms that were adapted to a macrotidal environment. Although environmental partitioning around some islands in the archipelago led to the development of a distinctive lee-side facies (Donovan, 1986; Donovan and Stephenson, 1991) in which mud-supported fabrics, mechanical bafflestones, and ferruginous stromatolites were deposited, the ecology of the Honey Creek Formation was dominated by sessile pelmatozoans and robust-shelled trilobites. By contrast, the ecology of the Fort Sill Formation was more complex, involving pelmatozoans (although in a less dominant role), thick- and thin-shelled trilobites, gastropods, brachiopods, calcareous sponges, algae (including *Renalcis* and *Girvanella*), stromatolites, and numerous horizontally burrowing organisms.

• As the Arbuckle platform expanded, mud-supported textures became increasingly dominant. A full range of textures from mudstone to various types of packstone and wackestone is present. The range of allochems includes intraclasts, peloids, and, less commonly, ooids—all rarely, if ever, seen in the Honey Creek Formation.

• Hardgrounds, some of which can be traced along strike for up to a mile, are characteristic of the Fort Sill (Fig. 5). Some phosphate and glauconite are associated with the hardgrounds, but most are simple erosional surfaces cemented by lime.



Figure 5. Photomicrograph of the lowest hardground in the Fort Sill Formation, showing a basal eroded hardground composed of quartz-rich carbonate mud and *Renalcis*. A pelmatozoan holdfast sits atop this hardground and is itself overlain by a coating of *Renalcis*. Field of view is ~3.5 mm in vertical dimension.

EUSTATIC CHANGES IN SEA LEVEL

The story summarized above is a record of apparently simple sequential changes that accompanied the Franconian transgression. At some point in this sequence of changes, conventionally at the boundary between the Honey Creek and Fort Sill Formations, it is semantically convenient to refer to the sequence as a platform sequence.

However, as noted previously, the transgression was interrupted by two major periods of regression, the lower of which is recorded by a distinctive suite of facies in the Honey Creek (McElmoyl and Donovan, 2000), and the upper by the complex boundary between the Fort Sill and Signal Mountain Formations. These two regressions are correlatable on a craton-wide scale (Chow and James, 1987) and clearly represent important breaks of considerable duration in the continuity of the sedimentary record (Fig. 6). In addition, smaller transgressive–regressive events are recorded in both the Honey Creek and Fort Sill Formations. The details in these smaller scale events vary sequentially, but cycle definition by the recognition of shallow water or emergence is generally possible.

As might be expected, the two larger regressive events have a more profound effect than the smaller ones on the general facies patterns that developed. The most notable of these changes is seen as an increase in the amount of siliciclastic detritus in the system. Additionally, glauconite peloids and phosphatic brachiopods either increase in abundance or reappear.

The lower regressive event is marked by a slight angular unconformity, a local reworking of island-related detritus and a thick (~15-ft) fine-grained quartz sandstone that can be traced throughout the Slick Hills. This bed, the lowest member of the upper Honey Creek, is remarkable as a record of the large amount of quartz sand that was transported into the area during the regression. The sand is generally one size grade less than that which is found in the underlying lower Honey Creek. Donovan (1986) and McElmoyl and Donovan (2000) suggested that this sand may be of eolian origin and that the dunes were reworked by marine processes following recommencement of the Franconian transgression.

The upper regressive event is more muted in its effects than the lower one. The surface of regression is sharp and apparently erosive, although without discernible relief. Although there is an increase in the amount of fine to very fine quartz sand in the basal Signal Mountain (as well as a reappearance of glauconite), the quartz is subordinate to carbonate and has no equivalent to the 15-ft sandstone seen above the lower regressive event. The difference between the two events may relate to the tectonic redefinition of the southern Oklahoma aulacogen, which approximately coincided with the development of the Arbuckle platform.

TECTONIC REDEFINITION OF THE SOUTHERN OKLAHOMA AULACOGEN

The simplicity of the record of the Franconian transgression was further complicated in the Slick Hills by the tectonic redefinition of the southern Oklahoma aulacogen as a major linear depocenter developed atop the initial igneous aulacogen (Fig. 7). This depocenter functioned as a site of sediment entrapment until the Mississippian. Typically, sediment thicknesses within the aulacogen are 3–4 times greater than those on the adjacent craton. The importance of this development to the present study is the recognition that thicknesses and facies in the Timbered Hills Group in the aulacogen area are generally comparable when traced south into Texas or north into northern Oklahoma and Missouri, but are dramatically thicker from the time of deposition of the Fort Sill Formation (Johnson and others, 1988). Recent work (Jusczuk and others, in press) suggests that the commencement of this redefinition is recorded in the uppermost part of the Honey Creek Formation.

During redefinition of the aulacogen, sediment-entrapment rates reached a maximum during deposition of the Signal Mountain Formation (Feinstein, 1981). As a result, this formation records a deeper water, below-wave-base suite of facies that was essentially restricted to the aulacogen (Whitehead and Donovan, 2000). For the first and only time in its history, the Arbuckle carbonate factory failed to keep pace adequately with subsidence. The overlying McKenzie Hill Formation records the restoration of the shallow, photic

"peritidal" environments that characterized the immense Laurentian carbonate platform and of which the southern Oklahoma area was just a small part.

SUMMARY AND CONCLUSIONS

This paper has examined the record of the Late Cambrian (Franconian) transgression across the Laurentian craton, as it is preserved in the eastern Slick Hills of southwestern Oklahoma. The following are the principal conclusions:

1. The transgressed surface of rhyolite was highly irregular and persisted for several million years as an archipelago of islands up to 800 ft high.

2. An initial siliciclastic petrography gradually gave way to a carbonate petrography. Specifically, lithic sandstones gave way to glauconite sandstones, which in turn gave way to mixed-lithology sandstones composed of carbonate, quartz, glauconite, rhyolite, and phosphate grains.

3. Subsequent definition of the Arbuckle Group, which semantically can be taken as the beginning of platform deposition, involved the incorporation of lime mud into the section and the development of numerous hardgrounds.

4. The initial faunal colonization involved *Skolithos, Lingula* sp. and horizontally burrowing organisms, pelmatozoans, and thick-shelled trilobites. As the platform evolved, a more diverse biota developed, including thin- and thick-shelled trilobites, pelmatozoans, gastropods, brachiopods, sponges, algae (e.g., *Renalcis*), and stromatolites.

5. Platform definition was accompanied by a lessening of tidal power from macrotidal to microtidal.

6. The transgression was interrupted by two major regressions, the lower of which divides the Honey Creek Formation into lower and upper members, the upper being the boundary between the Fort Sill and Signal Mountain Formations.

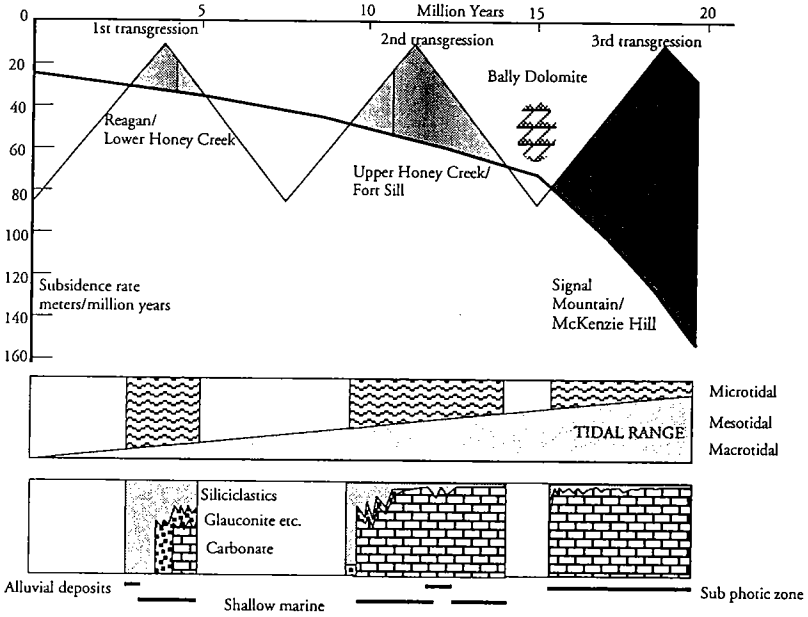

Figure 6. Summary of the impact of regressive events on the sequence under description. Important petrographic and environmental changes are also shown.

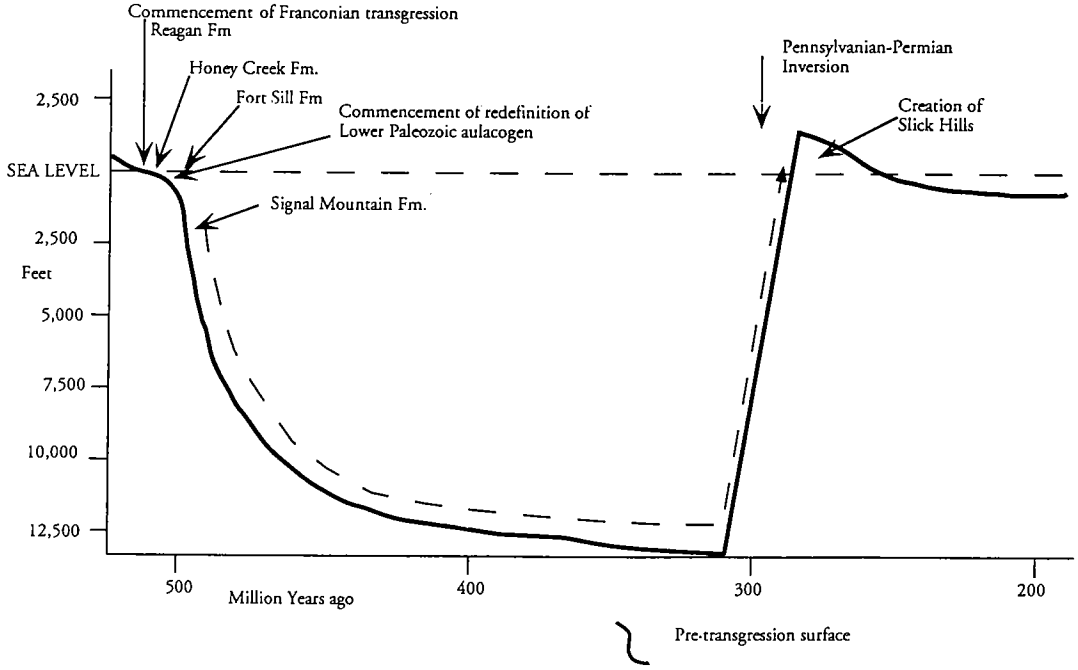

Figure 7. Time/sediment thickness graph, showing the redefinition of the southern Oklahoma aulacogen as a major depocenter, an event that roughly coincided with the beginning of expansion of the Arbuckle platform.

7. Basin redefinition of the southern Oklahoma aulacogen as a major linear depocenter atop the initial igneous aulacogen led to increasing rates of subsidence. As a result, the Signal Mountain Formation, which was deposited during the period of most rapid subsidence, is composed of distinctive facies that were deposited in subtidal- and subphotic-zone environments.

ACKNOWLEDGMENTS

I am grateful to the following landowners for permission to visit their property: the Kimbell family, Tommy Cavanagh, Doyle Leatherbury, Mrs. J. Kindblade, Earl Davis, and Ricky Clerk. The financial support of the Moncrief family is acknowledged.

REFERENCES CITED

Bucheit, A. K.; and Donovan, R. N., 2000, Initiation of a carbonate platform: a comparison between the Lower Jurassic Broadford Limestone, Isle of Skye, Scotland, and the Cambrian Honey Creek Limestone, Slick Hills, Oklahoma, *in* Johnson, K. S. (ed.), Platform carbonates in the southern Midcontinent, 1996 symposium: Oklahoma Geological Survey Circular 101 [this volume], p. 57–64.

Chow, N.; and James, N. P., 1987, Cambrian grand cycles: a northern Appalachian perspective: Geological Society of America Bulletin, v. 98, p. 418–429.

Donovan, R. N., 1986, Geology of the Slick Hills, *in* Donovan, R. N. (ed.), The Slick Hills of southwestern Oklahoma—fragments of an aulacogen?: Oklahoma Geological Survey Guidebook 24, p. 1–12.

_____1995, The Slick Hills of Oklahoma and their regional tectonic setting, *in* Johnson, K. S. (ed.), Structural styles in the southern Midcontinent, 1992 symposium: Oklahoma Geological Survey Circular 97, p. 178–186.

Donovan, R. N.; and Stephenson, M. D., 1991, A new island in the southern Oklahoma archipelago, *in* Johnson, K. S. (ed.), Late Cambrian–Ordovician geology of the southern Midcontinent, 1989 symposium: Oklahoma Geological Survey Circular 92, p. 118–121.

Feinstein, S., 1981, Subsidence and thermal history of southern Oklahoma aulacogen: implications for petroleum exploration: American Association of Petroleum Geologists Bulletin, v. 65, p. 2521–2533.

Gao, G., 1990, Geochemical and isotopic constraints on the diagenetic history of a massive stratal, Late Cambrian (Royer) dolomite, Lower Arbuckle Group, Slick Hills, SW Oklahoma, USA: Geochimica et Cosmochimica Acta, v. 54, p. 1979–1989.

Ham, W. E.; Denison, R. E.; and Merritt, C. A., 1964, Basement rocks and structural evolution of southern Oklahoma: Oklahoma Geological Survey Bulletin 95, 302 p.

Hosey, R. M.; and Donovan, R. N., 2000, Boundary between the Fort Sill and Signal Mountain Formations in the lower Arbuckle Group, Slick Hills: candidate for a grand cycle boundary, *in* Johnson, K. S. (ed.), Platform carbonates in the southern Midcontinent, 1996 symposium: Oklahoma Geological Survey Circular 101 [this volume], p. 79–88.

Johnson, K. S.; Amsden, T. W.; Denison, R. E.; Dutton, S. P.; Goldstein, A. G.; Rascoe, Bailey, Jr.; Sutherland, P. K.; and Thompson, C. M., 1988, Geology of the southern Midcontinent, *in* Sloss, L. L. (ed.), Sedimentary cover—North American craton, U.S.: Geological Society of America, The Geology of North America, v. D-2, p. 307–359. [Reprinted in 1989 as Oklahoma Geological Survey Special Publication 89-2, 53 p.]

Jusczuk, S. J.; Trice, D.; Walters, M. C.; and Donovan, R. N., in press, On granophyre fragments and variations in siliciclastic grain size—a possible Late Cambrian tectonic spike in the Slick Hills of southwestern Oklahoma: The Compass Journal of Earth Sciences, Sigma Gamma Epsilon.

McElmoyl, Courtney; and Donovan, R. N., 2000, Unconformity in the lower part of the Cambrian Honey Creek Limestone, Slick Hills, Oklahoma: candidate for a grand cycle boundary, *in* Johnson, K. S. (ed.), Platform carbonates in the southern Midcontinent, 1996 symposium: Oklahoma Geological Survey Circular 101 [this volume], p. 65–78.

Scotese, C. R., 1984, Paleozoic paleomagnetism and the assembly of Pangaea: American Geophysical Union Geodynamics Series, v. 12, p. 1–10.

Whitehead, R. E.; and Donovan, R. N., 2000, Four hundred feet of core from the Cambrian Signal Mountain Formation, Slick Hills, Oklahoma, *in* Johnson, K. S. (ed.), Platform carbonates in the southern Midcontinent, 1996 symposium: Oklahoma Geological Survey Circular 101 [this volume], p. 89–95.

Initiation of a Carbonate Platform: A Comparison Between the Lower Jurassic Broadford Limestone, Isle of Skye, Scotland, and the Cambrian Honey Creek Limestone, Slick Hills, Oklahoma

Andrea K. Bucheit and R. Nowell Donovan
Texas Christian University
Fort Worth, Texas

ABSTRACT.—The Lower Jurassic (Liassic–late Hettangian) Broadford Beds were deposited about 200 million years ago, during a period of crustal extension related to a connection between the Tethys and the Arctic. Outcrops on the Isle of Skye, northwestern Scotland, record rapid onlap across an eroded Caledonian orogene. A specific exposure at Allt nan Leac shows the marine inundation of a karsted hill built of steeply dipping Cambrian–Ordovician platform carbonates (Durness Group). This hill is an inundated fossil Triassic feature. Debris-filled fissures penetrate to 16 ft below the unconformity surface and contain both travertine coatings and rock borings by coelobitic organisms. The lowest part of the Broadford Beds is a shallow-water carbonate deposit—the Broadford Limestone. In the area under discussion, shelly faunas are dominated by *Gryphaea arcuata,* other mollusks, and the ammonite *Arnioceras semicostatum.*

The Honey Creek Limestone is the upper formation of the Timbered Hills Group, a unit in southwestern Oklahoma that records transgression across a hilly surface of rhyolite. Windward and leeward facies developed around rhyolite islands. Details of the unconformity show irregular fissures and rock pedestals. Carbonate sedimentation was dominated by bioclastic grainstones in which the chief architectural component was pelmatozoans, although brachiopods and thick-shelled trilobites are locally abundant. Siliciclastic grains, mostly derived from the craton to the north and west, are abundant—their relative proportion serving to differentiate meter-scale cycles that may record short-term fluctuations in sea level.

Both sequences display a superficially similar type of wavy bedding that is a result of the rapid alternation of carbonates and siliciclastic beds on a centimeter scale. In the Honey Creek, this wavy bedding records the differential compaction of small-scale cross-bedded ripples composed of grains derived from two separate sources: carbonate grains from island settings, siliciclastic grains from the craton. In the Broadford Limestone, shale and silt beds alternate with shelly limestones; again, two distinct sources are likely. However, significant differences between the two types of wavy bedding are evident. In the Honey Creek, the carbonate fraction is generally fragmented, well sorted, and intensively cemented, principally by syntaxial overgrowths around pelmatozoans. Subsequent diagenetic modification took place by grain-to-grain dissolution of carbonate at the boundaries of the carbonate beds. Conversely, the original carbonate textures in the Broadford were mud supported with well-preserved and poorly sorted grains; very little cement is present, and the entire sequence was subjected to early anaerobic diagenesis. In the absence of cement, significant grain rotation took place; as a result, fitted textures and dissolution seams are ubiquitous. The absence of cement led to a greater diagenetic enhancement of the waviness of bedding than in the Honey Creek examples.

Tectonic uplift of the hinterland led to the gradual encroachment of a clastic wedge that eventually terminated the short-lived Broadford carbonate platform. Continuing major transgression eventually cut off the siliciclastic source for the Honey Creek Limestone, leading to development of a full-blown carbonate platform on which the Arbuckle Group was deposited.

INTRODUCTION

This study compares two superficially similar examples of "wavy bedding" in mixed siliciclastic and carbonate sequences. Previous use has defined the term *wavy bedding* as an intermediate variety in the spectrum of lithologies defined as *flaser* and *lenticular bedding* that is developed in many mixed shale–sand siliciclastic sequences (Reineck and Singh, 1973; Collinson and Thompson, 1989).

We have expanded the use of the term as follows: *wavy bedding* is here defined as the weathered honeycombed pattern of a mixed thinly bedded carbonate–siliciclastic sequence (Fig. 1). This weathering texture, which is on a centimeter scale, is due to differential solution of the carbonates during weathering. The honeycomb pattern derives from the lenticular bedding that characterizes the mixed sequence: the origin of this lenticular bedding is a function of depositional setting and/or diagenetic modification.

Bucheit, A. K.; and Donovan, R. N., 2000, Initiation of a carbonate platform: a comparison between the Lower Jurassic Broadford Limestone, Isle of Skye, Scotland, and the Cambrian Honey Creek Limestone, Slick Hills, Oklahoma, *in* Johnson, K. S. (ed.), Platform carbonates in the southern Midcontinent, 1996 symposium: Oklahoma Geological Survey Circular 101, p. 57–64.



Figure 1. Wavy bedding in the Lower Jurassic Broadford Limestone, Loch Slapin, Isle of Skye, Scotland.

The two formations displaying wavy texture are, first, the Lower Jurassic Broadford Limestone as exposed at the mouth of the Allt nan Leac ("River of Leac") on the shores of Loch Slapin, Strath Peninsula, Isle of Skye, western Scotland (Fig. 2). The second occurrence is found in the Upper Cambrian Honey Creek Formation on the side of Ringtop Mountain in the Slick Hills area of Comanche County, Oklahoma, U.S.A. (Fig. 3).

The objectives of this study are to (1) provide a description and comparison of the formation of lenticular bedding in the two examples, and (2) analyze the depositional and diagenetic settings of the examples.

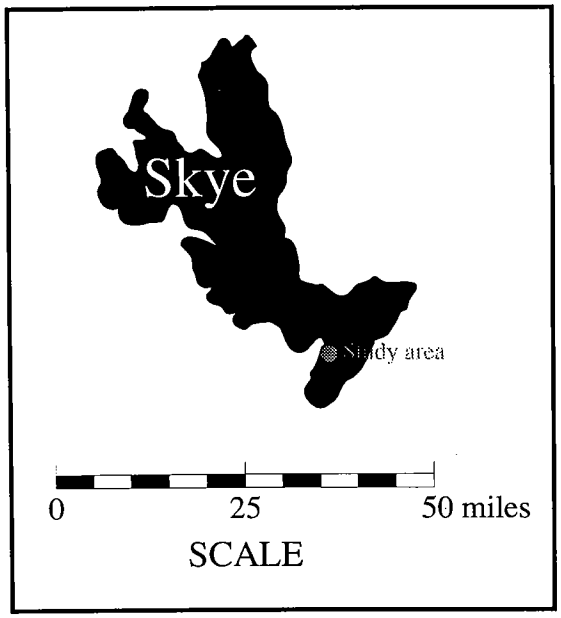

Figure 2. The Broadford Limestone was studied at an outcrop on the shores of Loch Slapin at the southern end of the Isle of Skye, northwestern Scotland.

DESCRIPTION: SKYE LOCATION

Geologic History

Precambrian gneisses and sandstones make up a Scottish basement that was marginal to the opening Proto Atlantic (Iapetus) Ocean during the early Paleozoic (Fig. 4). In the study area, this rifting resulted in the deposition of a Cambrian–Ordovician sequence characterized by basal siliciclastics that are overlain by the Durness Group, a carbonate-platform sequence up to 1,500 ft thick. Closure of the Proto Atlantic ~400 million years ago was accompanied by an intense orogenic imprint—the Caledonian Orogeny—that uplifted the area, which was followed by intense erosion. No significant upper Paleozoic record is preserved (Brown, 1991; Harris, 1991).

Renewed basin definition during the Mesozoic is recorded by Triassic conglomerates, Jurassic siliciclastics and limestones (including the Broadford Limestone), and Cretaceous sandstones (Fig. 5). Two distinctive periods of crustal extension can be recognized: the first provided linkage of the Tethys and the Arctic, and the second occurred as the central part of the North Atlantic began to develop (Lovell, 1991). Burial depths of Triassic and Lower Jurassic rocks were at least 1,200 ft.

A period of intense igneous activity began in the early Tertiary, when more than 3,000 ft of plateau basalts erupted (Emeleus, 1991); this was related to a third extensional period, which initiated development of the northernmost Atlantic Ocean. Since the Tertiary, uplift has raised the once deeply buried Triassic and Jurassic sedimentary rocks to the surface. In the part of the Isle of Skye described here, these rocks lie unconformably atop steeply dipping platform carbonates of the Cambrian–Ordovician Durness Group (Figs. 6,7).

Depositional Setting

The Lower Jurassic (late Hettangian) Broadford Beds were produced by a competition between a carbonate platform and prograding siliciclastics, with the latter eventually emerging victorious (Fig. 8). At Allt nan Leac, deposition of the bottom unit of the Broadford Beds, the Broadford Limestone, occurred unconformably atop a hillside of Cambrian–Ordovician Durness Group carbonates.

Two lines of evidence suggest that a carbonate hill existed at this site (Figs. 9,10). The first is recorded in the pebble composition of Triassic conglomerates near Allt nan Leac. Where the Triassic is unconformable on the Torridonian Sandstone (farthest east), the conglomerate consists of arkose, quartzite, and carbonate pebbles. Where it overlies Cambrian quartzite, only quartzite and carbonate pebbles are found. Farther west, where it lies above the Durness Group, the Triassic pebbles are all carbonate and related chert. In all three locations, carbonate content increases upward in the conglomerate (Donovan, 1966; Steel and others, 1975). This increase, plus the westward decrease in all other constituents, indicates the existence of a carbonate hill to the west. The second line

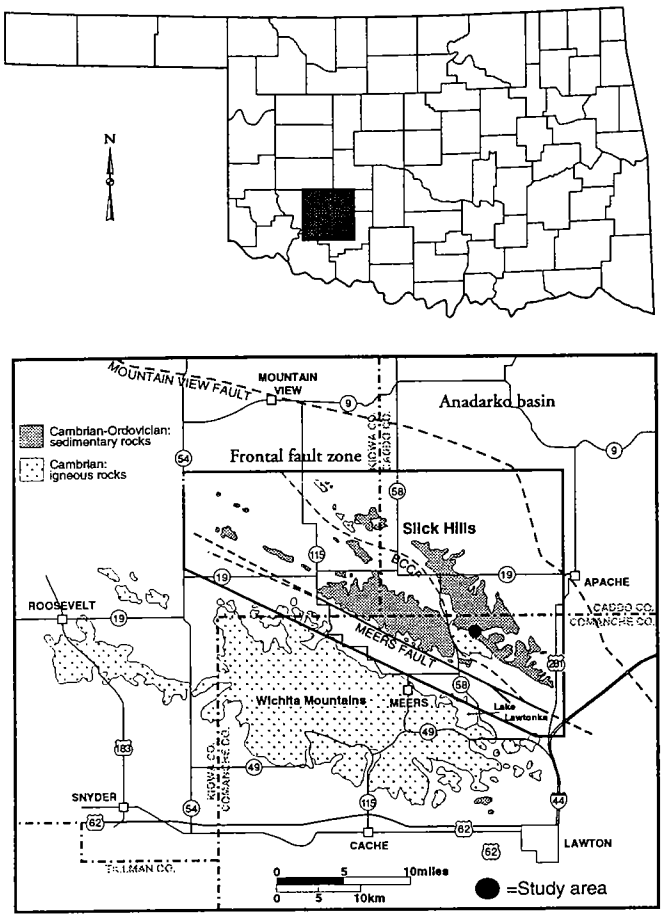

Figure 3. The upper Honey Creek Limestone was studied on the side of Ringtop Mountain in the Slick Hills of Comanche County, southwestern Oklahoma. *BCCF* = Blue Creek Canyon fault.

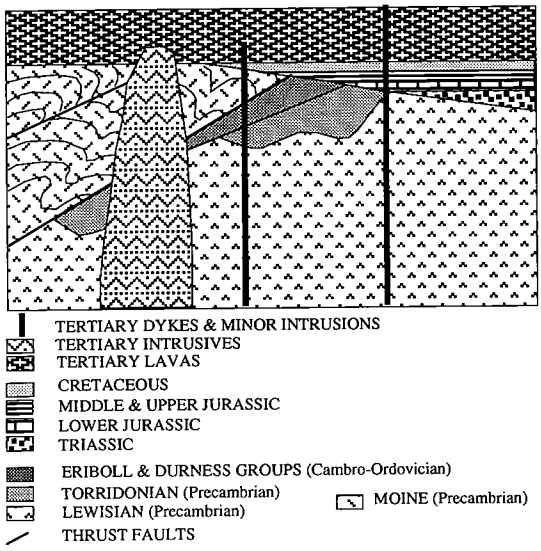

Figure 4. The geology of the Isle of Skye consists of Precambrian and lower Paleozoic rocks unconformably overlain by Mesozoic sedimentary rocks and Tertiary intrusive and extrusive igneous rocks.

of evidence is the onlap of the Liassic section to the west (Peach and others, 1910). The onlap is best quantified by a marker bed of the coral *Thecosmilia martini* within the lower Broadford Limestone. This coral band onlaps the Durness Group carbonate land surface just to the east of the study area, suggesting an existing slope upward in a westerly direction during deposition of the Jurassic sediments.

Lithologic Description

The carbonate hillside is cut by fissures of Jurassic age and is overlain by shell banks (Fig. 8). The fissures are narrow but penetrate as much as 16 ft into the carbonates. They are filled with cemented detritus (including Jurassic shell fragments), show some speleothem development (travertine), and locally display borings (i.e., examples of the *Trypanites* ichnofacies) up to half an inch deep. These borings resemble modern clam borings: their position suggests that the organisms involved were coelobitic (cave-dwelling). Although the fissures may have originated as karst features, it is clear that they were subsequently inundated during the Jurassic transgression. The lower section of the Broadford Beds, the Broadford Limestone, contains shell banks as well as the index fossil *Arnioceras semicostatum*. Two distinct lithologies occur: (1) a massively bedded light-gray wackestone with thin layers of *Gryphaea arcuata* (an oyster), and (2) mixed siliciclastic–carbonate beds characterized by wavy bedding (Fig. 11). The wackestone lithology locally displays a spaced tectonic cleavage.

The mixed lithology (2, above) of the Broadford Lime-

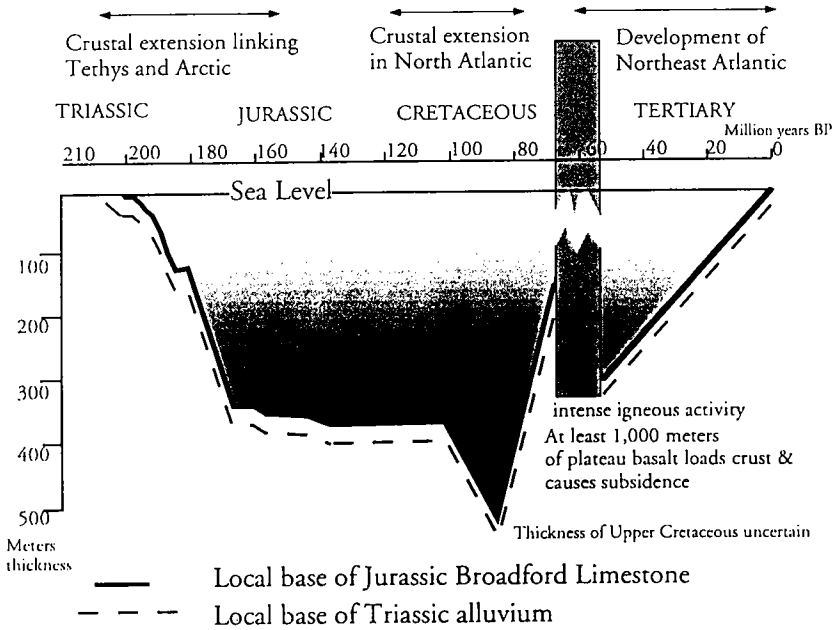

Figure 5. Three separate extensional events and intense igneous activity caused burial of the Broadford Limestone to depths of at least 1,200 ft. It is now exposed at the surface at Loch Slapin, Isle of Skye.

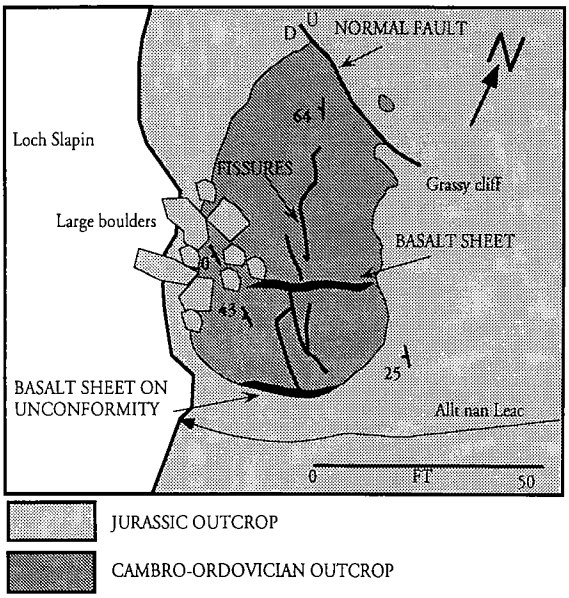

Figure 6. Map of the study area on the shores of Loch Slapin, Skye.

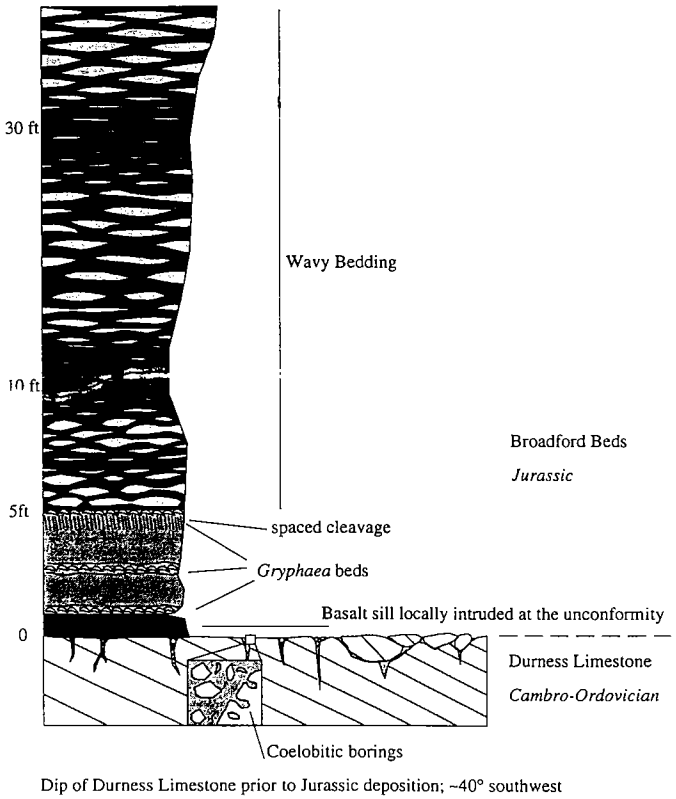

Figure 7. Log of the Cambrian–Ordovician/Jurassic section at Loch Slapin.

stone is composed of relatively continuous siliciclastic layers (siltstones and shales) with interspersed lenses of carbonate material, mostly wackestones. This mud-supported platform carbonate contains poorly sorted grains that were affected greatly during early diagenesis; substantial grain rotation took place during compaction: fitted fabrics, dissolution seams, and stylolites abound (Figs. 12,13). These processes were enhanced at contacts between the carbonate material and neighboring siliciclastic grains.

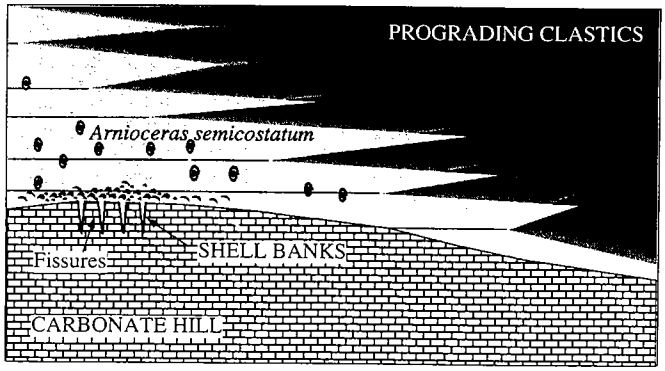

Figure 8. Dynamic facies relationships of the Broadford Beds on Skye. The lowest formation, the Broadford Limestone, contains shell banks of *Gryphaea arcuata*, the index fossil *Arnioceras semicostatum*, fissure-fills into the underlying Durness Group, and rock and shell borings by coelobitic organisms.

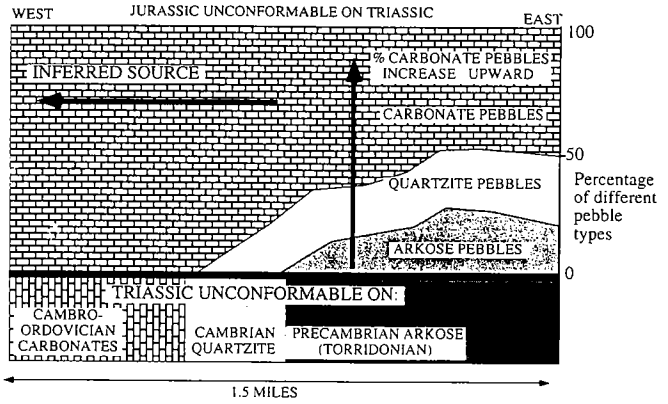

Figure 9. Evidence for the existence of a carbonate hill during Broadford Limestone deposition is found in the pebble composition of Triassic conglomerates in the valley of the Allt nan Leac, Skye. A total of 690 pebbles were identified. (Modified from Donovan, 1966.)

In 1987, Bathurst related the concepts of rotation, compaction, and dissolution in his "compaction index," a measure of the degree of grain rotation in a rock sample. The compaction index is the percentage of grains in a sample with long axes roughly parallel (within 30°) to bedding planes: Figure 14 shows a highly compacted sample of the mud-supported carbonate of the mixed unit. The compaction indices of seven samples of each Broadford Limestone lithology were analyzed and compared, and results indicated that the mud-supported mixed siliciclastic–carbonate unit underwent a significantly greater degree of rotation and compaction during diagenesis than did the massive limestone unit (Fig. 15).

DESCRIPTION: SLICK HILLS LOCATION

Geologic History

The Slick Hills of southwestern Oklahoma have been interpreted as the fragments of an aulacogen, a failed attempt at

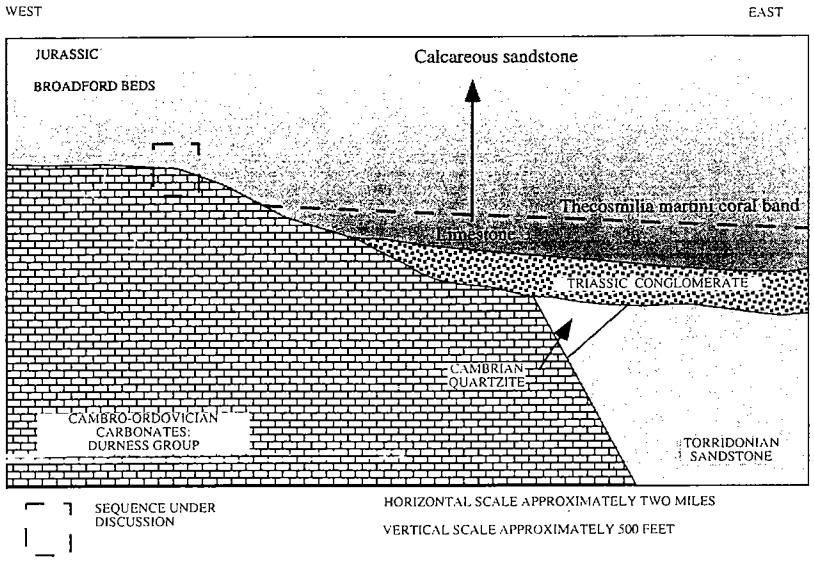

Figure 10. A coral band onlapping the Cambrian–Ordovician Durness Group near the study area provides evidence for the existence of a hill when Early Jurassic deposition commenced.



Figure 11. The two units of the Broadford Limestone are a massive gray limestone with spaced cleavage (bottom) and a mixed carbonate–siliciclastic sequence (top).

new ocean formation (see, e.g., Donovan, 1986). The development of the rift coincided with two heat-flux episodes in the late Precambrian and Cambrian that intruded and extruded ultrabasic, basic, and acidic rocks (see, e.g., Gilbert, 1986); only the uppermost igneous unit, the Carlton Rhyolite Group, is seen in the Slick Hills area. During Middle and Late Cambrian time, acidic volcanic rocks were eroded into a hilly region with at least 800 ft of discernible relief (Donovan and Stephenson, 1991). The second stage in the aulacogen evolution coincided with a major craton-wide transgression during the Late Cambrian (Franconian). The sediments deposited during this transgression are represented by the Timbered Hills and Arbuckle Groups. The general trends observed involve (1) the gradual burial of a hilly terrain—the southern Oklahoma archipelago—both by its own detritus and by entombment beneath siliciclastics derived from the adjacent craton; (2) an upward decrease in siliciclastic content as the transgressive shoreline migrated toward the northwest and local waters deepened; and (3) the gradual development of a major carbonate platform (see, e.g., Donovan, 2000). The honeycomb weathering (i.e., lenticular bedding) is developed at a stage when the supply of carbonates was approximately equal to the input of siliciclastics.

Following a long period of burial, during which the basal lower Paleozoic section was buried to a depth of approximately 12,000 ft, the basin partly inverted into a series of tectonically defined uplifts (e.g., the Wichita and Arbuckle uplifts) and basins (e.g., the Anadarko and Hollis basins) during the late Paleozoic. Extensive erosion on the uplifts eventually exhumed the Upper Cambrian section—as seen in the Slick Hills, for example. Little tectonic activity took place in the area during the Mesozoic and Cenozoic; as a result, the attitude of the outcrops is in essence a late Paleozoic inheritance (Donovan, 1986).

Depositional Setting

The Upper Cambrian (Franconian Stage) Honey Creek Limestone is the upper of two formations in the Timbered Hills Group (the lower is the Reagan Sandstone) and records the first incursion of carbonate material into a previously siliciclastic-dominated depositional system. The Honey Creek records a time during the transgression when the hills of Carlton Rhyolite had become a marine archipelago, surrounded by flanking deposits ("pelmatozoan aprons") of tide- and current-scoured bioclastic sands (Fig. 16). Distinct faunal assemblages developed in windward and leeward rocky-shoreline settings. Irregular fissures and rock pedestals formed at the unconformity between the rhyolite islands and their surrounding grainstones. The archipelago model was first introduced by Donovan in 1982 and modified in later publications (e.g., Donovan, 1986; Donovan and Stephenson, 1991).

Lithologic Description

The Honey Creek Limestone was subdivided into three ad hoc members by McElmoyl (1993): the "upper" and "lower" Honey Creek are bioclastic grainstones, containing significant amounts of siliciclastic detritus, that are separated by a discontinuous rudaceous packstone. This latter "red breccia" layer may record a continent-wide stratigraphic regression during the time represented by the *Elvinia* trilobite zone (McElmoyl, 1993; McElmoyl and Donovan, 1993, 2000). The

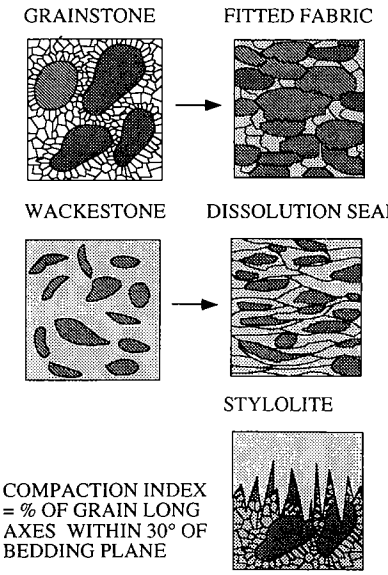

Figure 12. Pressure-dissolution features common to carbonate rocks. All can be found in the Broadford Limestone.



Figure 13. Photomicrograph of dissolution seams in the carbonate fraction of the mixed unit in the Broadford Limestone (plane light, 10×).

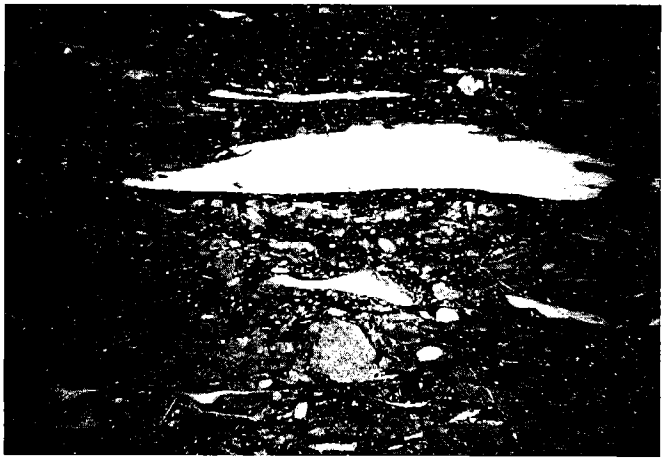

Figure 14. Photomicrograph of the Broadford mixed unit, which displays an exceptionally high compaction index (plane light, 10×).

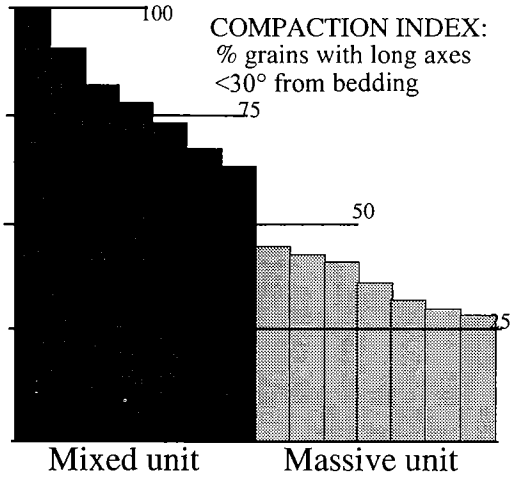

Figure 15. Compaction indices of 14 specimens from the Lower Jurassic Broadford Limestone.

upper grainstone commonly displays superb examples of wavy bedding.

The grainstone portion of the upper Honey Creek Limestone is made up of fragments of shallow-water invertebrates, dominantly pelmatozoans, although brachiopods and thick-shelled trilobites are locally abundant. These carbonate sands originated as aprons of detritus produced from the mechanical destruction of coastal communities that lived around the islands of the archipelago. Most of the siliciclastic detritus is very fine to fine quartz sand, presumably derived from the adjacent craton during lowstands and subsequently reworked into the marine environment. In addition, rhyolite fragments, broken phosphatic shells (probably *Lingula* sp.), and glauconite peloids are locally abundant. Accessory minerals include feldspar and zircon. Considerable facies variation is encountered: close to islands, more or less pure carbonate sandstones are developed; in more distal areas, the carbonate fraction drops to about 10%.

Although some mixing of the two grain assemblages has taken place, for the most part they have maintained a discrete identity. This suggests that the depositional setting lacked the energy to comprehensively mix the two types of sand. Both types of sandstone are characterized by small- to medium-scale cross-bedding, much of which is the product of reversing currents. Some of the individual beds are single ripple sets; in others, two or three sets of the same lithology are superposed. Some individual ripple marks "switch" lithologies, suggesting that either hydrodynamic and/or geographic partitioning was a finely tuned process. In essence, the general aspect of the lithology is reminiscent of the various varieties of siliciclastic "flaser" bedding; however, only a little fine-grained detritus of either the siliciclastic or carbonate type is present.

In addition, a vertical, or stratigraphic, meter-scale repetitive partial partitioning of carbonates and siliciclastics is a constant motif. Such larger scale variations in the relative proportions of siliciclastic and carbonate beds may relate to changes in the rate of supply of one or the other (or both)

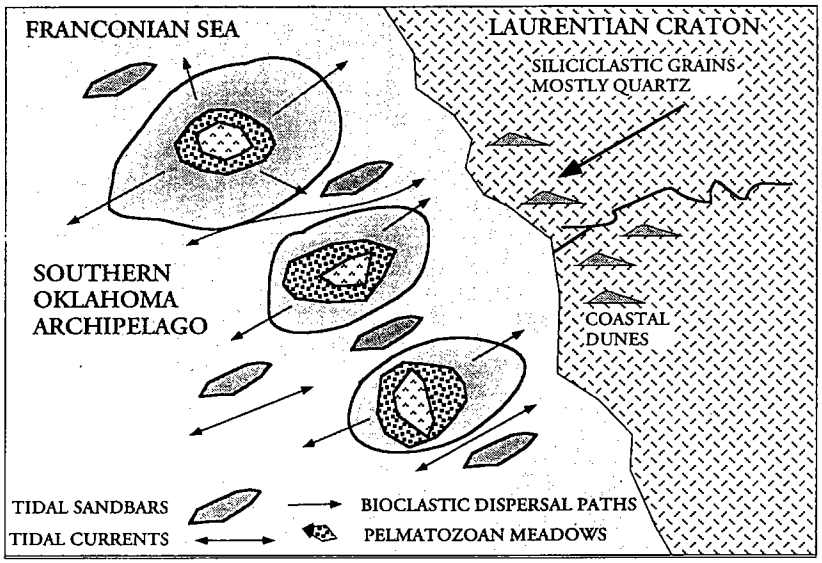

Figure 16. Archipelago model of southwestern Oklahoma (early Franconian), showing rhyolite islands, pelmatozoan aprons, tidal channels, and tidal bars.

types of detritus. Variations on this scale are laterally continuous and may be a response to cyclic fluctuations in sea level (detailed cataloging of these strata is ongoing).

In some parts of the Slick Hills, small amounts of angular clasts of rhyolite are a regularly occurring feature in this lithology, even in areas where there is no exposed source. The presence of these clasts, presumably derived from local islands, may also be a result of changes in shoreline base level.

The carbonate material is extremely well sorted and was cemented thoroughly and quickly by syntaxial overgrowths around the pelmatozoan grains. This rigid cement framework, along with the included siliciclastic grains, prevented compaction and rotation of the individual carbonate grains during deposition and initial lithification.

Diagenetic modification served only to dissolve carbonate materials at their boundaries with siliciclastics by way of grain-to-grain dissolution; more pervasive pressure-solution phenomena are absent in the Honey Creek. Instead, primary features, such as parallel laminae, small-scale cross-bedding, shelter porosity, and ripple marks, are well preserved (Figs. 17,18). These ripple marks, found both in outcrop scale and under the microscope, give the Honey Creek its wavy-bedded appearance.

CONCLUSIONS

Wavy bedding in both the examples described developed during a restricted time period when the depositional systems involved were changing character. In the Skye example, a topographic high on a carbonate platform was gradually overwhelmed by the distal detritus of an encroaching siliciclastic system. In the Oklahoma example, the reverse process took place. In both cases, wavy bedding developed in low-energy settings that did not significantly mix grain populations from two distinct sources.

Although the two examples show similar weathering features, significant differences are evident in the creation and modification of the wavy bedding in each. The lack of rigidity and the absence of an early phase of cementation in the mud-supported framework of the Broadford wackestone facilitated rotation and compaction of individual carbonate grains during early anaerobic diagenesis. Pressure-solution phenomena—fitted fabrics, dissolution seams, and stylolites—support the conclusion that sinuosity of the lenticular bedding was greatly enhanced during diagenesis. The carbonate lenses of the Honey Creek, on the other hand, appear to be primary ripple marks preserved in the rigid framework of the quickly cemented grainstone. Only minor grain-to-grain dissolution seems to have resulted from diagenetic modification.

A comparative study of the carbonate content and quartz-grain size of the two formations illustrates their differing evolutions (Fig. 19). As carbonate content decreased upward in the Broadford Formation, siliciclastic grain size increased as the carbonate source was overwhelmed. Exactly the reverse is true for the Honey Creek: as the carbonate platform came to dominate the area, quartz-grain size diminished upward as the percentage of carbonate escalated (Donovan and Ragland, 1986). Whereas the Broadford was a short-lived carbonate platform whose sedimentation was quickly overtaken by a tectonically uplifted continental source, the culmination of the Honey Creek coincided with the commencement of one of the world's great carbonate platforms, on which the Arbuckle Group was deposited.

ACKNOWLEDGMENTS

This work forms part of A.K.B.'s senior thesis. Financial support was provided by (1) the Mobil Foundation, (2) an Undergraduate Research Support Grant provided by Texas Christian University, and (3) the Moncrief family of Fort Worth. We are very grateful for this help and also wish to acknowledge support in the field by Erin, Corrie, and Jeanne Donovan.

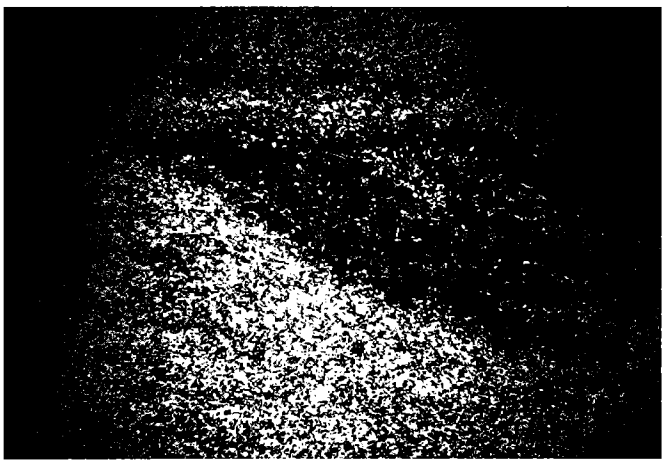

Figure 17. Photomicrograph of a preserved cross-bed (primary feature) in the Honey Creek; dark area is carbonate material, light is siliciclastic-rich (plane light, 10×).



Figure 18. Photomicrograph of preserved primary shelter porosity in the Honey Creek Limestone (plane light, 10×).

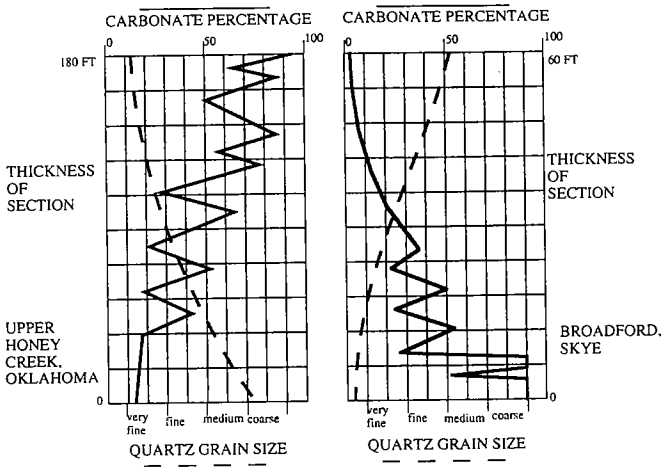

Figure 19. Comparison of carbonate content and quartz-grain size in the Honey Creek and Broadford Limestones. Whereas carbonates increase and quartz size decreases in the Honey Creek, the exact reverse occurs in the Broadford.

REFERENCES CITED

Bathurst, R. G. C., 1987, Diagenetically enhanced bedding in argillaceous platform limestones: stratified cementation and selective compaction: Sedimentology, v. 34, p. 749–778.

Brown, P. E., 1991, Caledonian and earlier magmatism, *in* Craig, G. Y. (ed.), Geology of Scotland: Geological Society [London], p. 229–295.

Collinson, J. D.; and Thompson, D. B., 1989, Sedimentary structures [2nd edition]: Unwin Hyman, London, 207 p.

Donovan, R. N., 1966, Field work carried out in the Strath area of the Isle of Skye July 23rd–September 30th, 1965: University of Newcastle Upon Tyne unpublished B.S. thesis, 81 p.

_____1982, Geology of Blue Creek Canyon, Wichita Mountains area, *in* Gilbert, M. C.; and Donovan, R. N. (eds.), Geology of the eastern Wichita Mountains, southwestern Oklahoma: Oklahoma Geological Survey Guidebook 21, p. 65–77.

_____1986, Geology of the Slick Hills, *in* Donovan, R. N. (ed.), The Slick Hills of southwestern Oklahoma—fragments of an aulacogen?: Oklahoma Geological Survey Guidebook 24, p. 1–12.

_____2000, Initiation of the Arbuckle platform—view from the Slick Hills, Oklahoma, *in* Johnson, K. S. (ed.), Platform carbonates in the southern Midcontinent, 1996 symposium: Oklahoma Geological Survey Circular 101 [this volume] p. 47–56.

Donovan, R. N.; and Ragland, D. A., 1986, Paleozoic stratigraphy of the Slick Hills, southwestern Oklahoma, *in* Donovan, R. N. (ed.), The Slick Hills of southwestern Oklahoma—fragments of an aulacogen?: Oklahoma Geological Survey Guidebook 24, p. 13–20.

Donovan, R. N.; and Stephenson, M. D., 1991, A new island in the southern Oklahoma archipelago, *in* Johnson, K. S. (ed.), Late Cambrian–Ordovician geology of the southern Midcontinent, 1989 symposium: Oklahoma Geological Survey Circular 92, p. 118–121.

Emeleus, H., 1991, Tertiary igneous activity, *in* Craig, G. Y. (ed.), Geology of Scotland: Geological Society [London], p. 455–492.

Harris, A. L., 1991, The growth and structure of Scotland, *in* Craig, G. Y. (ed.), Geology of Scotland: Geological Society [London], p. 1–23.

Lovell, J. P. B., 1991, Permian and Triassic, *in* Craig, G. Y. (ed.), Geology of Scotland: Geological Society [London], p. 421–434.

McElmoyl, C., 1993, Transgression and regression during the deposition of the Upper Cambrian Honey Creek Formation in the southern Oklahoma aulacogen: Unpublished M.S. thesis, Texas Christian University, Fort Worth, 62 p.

McElmoyl, C.; and Donovan, R. N., 1993, A transgression–regression event during the deposition of the Upper Cambrian Honey Creek Formation in the Southern Oklahoma aulacogen [abstract]: Geological Society of America, South Central Section Meeting, Fort Worth, Texas, Program with Abstracts, p. 38.

_____2000, Unconformity in the lower part of the Cambrian Honey Creek Limestone, Slick Hills, Oklahoma: candidate for a grand cycle boundary, *in* Johnson, K. S. (ed.), Platform carbonates in the southern Midcontinent, 1996 symposium: Oklahoma Geological Survey Circular 101 [this volume], p. 65–78.

Peach, B. N.; Horne, J.; Woodward, H. B.; Clough, C. T.; Harker, A.; and Wedd, C. B., 1910, The geology of Glenelg, Lochalsh and south-east part of Skye: Memoirs of the Geological Survey, Scotland, 206 p.

Reineck, H. E.; and Singh, I. B., 1973, Depositional sedimentary environments [1st edition]: Springer-Verlag, Berlin, 439 p.

Steel, R. J.; Nicholson, R.; and Kalander, L., 1975, Triassic sedimentation and paleogeography in Central Skye: Scottish Journal of Geology, v. 11, p. 1–13.

Unconformity in the Lower Part of the Cambrian Honey Creek Limestone, Slick Hills, Oklahoma: Candidate for a Grand Cycle Boundary

Courtney McElmoyl
Core Laboratories Inc.
Carrolton, Texas

R. Nowell Donovan
Texas Christian University
Fort Worth, Texas

ABSTRACT.—The transgression that inundated the southern Oklahoma aulacogen during the Late Cambrian (Franconian) flooded a landscape that consisted of hills of rhyolite up to 350 m in height. Initial deposits on and around this topography have been interpreted as alluvium. These deposits, together with overlying tidally influenced marine siliciclastics, form the Reagan Formation. The upward passage from the Reagan to the Honey Creek Formation is defined by the addition to the siliciclastics of carbonate detritus in the form of grainstones, mostly composed of pelmatozoan fragments. The passage from the Honey Creek to the overlying Fort Sill Formation of the Arbuckle Group is marked by the incoming of beds of lime mudstone. Grainstones and siliciclastics gradually disappear. Evidence of the continuing existence of rhyolite topography (i.e, an archipelago) can be detected to within 50 m of the top of the Fort Sill.

The overall facies pattern records a widespread transgression. However, a slight angular unconformity within the lower part of the Honey Creek is best interpreted as the record of a temporary regression. Three distinctive lithologies are involved at the unconformity: the lowest beds are light-gray, cross-bedded pelmatozoan grainstones with minor amounts of quartz and rhyolite grains. Syntaxial cements at the base of this unit are homogeneous under cathodoluminescence, whereas cements near the top display up to 27 zones of reflectance, interpreted as a fluctuating marine–meteoric-ground-water imprint. The overlying bed is a red-brown mud-supported limestone (ad hoc reference: "red limestone") that contains abundant angular rhyolite pebbles and a rich trilobite fauna. A few of the pebbles were substrates for pelmatozoan growth. This bed, which is 0–3 m thick, is interpreted as a locally derived regressive deposit from adjacent rhyolite-island shorelines. The variation in bed thickness may be due to compactional draping around the rhyolite topography. The uppermost beds are thinly bedded alternations of pelmatozoan grainstones and fine-grained quartz sandstones. These beds, which overstep the underlying units, are interpreted as the basal deposits of a succeeding transgression, incorporating siliciclastics that were transported into the area during the regression. The unconformity can be traced throughout the Slick Hills of southwestern Oklahoma; although it may reflect localized tectonism associated with the evolution of the southern Oklahoma aulacogen, the unconformity correlates with a craton-wide "sub-*Elvinia*" hiatus.

INTRODUCTION

This study examines the lower part of the Upper Cambrian Honey Creek Formation as it is exposed in Blue Creek Canyon in the Slick Hills of Comanche County, southwestern Oklahoma (Figs. 1,2). In particular, the study describes and evaluates a newly discovered angular unconformity within the Honey Creek. Recognition of this unconformity has led to the definition of ad hoc "lower" and "upper" stratigraphic members. A third, impersistent ad hoc member, the "red limestone," is recognized beneath this unconformity.

GEOLOGIC BACKGROUND

The Slick Hills are an eroded, tectonically disturbed fragment of rocks deposited in the southern Oklahoma aulacogen, a linear lower Paleozoic basin that presently trends N. 60° W. from southeastern Oklahoma into the Texas Panhandle (Schatski, 1946). The initial development of the aulacogen was marked by the intrusion and extrusion of a complex of ultrabasic, basic, and acidic rocks. This igneous activity ended in the Late Cambrian, leaving a surface covered by the Carlton Rhyolite Group, a thick sequence of acidic volcanics (Ham and others, 1964).

The Carlton Rhyolite surface was subsequently eroded to a range of small hills that have a maximum known relief of ~275 m (Donovan and Stephenson, 1991). This topography was gradually buried by Cambrian sediments, stratigraphically defined as the Timbered Hills Group and Fort Sill Formation (lowest unit of the Arbuckle Group). The two formations recognized in the Timbered Hills Group are the Reagan and over-

McElmoyl, Courtney; and Donovan, R. N., 2000, Unconformity in the lower part of the Cambrian Honey Creek Limestone, Slick Hills, Oklahoma: candidate for a grand cycle boundary, *in* Johnson, K. S. (ed.), Platform carbonates in the southern Midcontinent, 1996 symposium: Oklahoma Geological Survey Circular 101, p. 65–78.

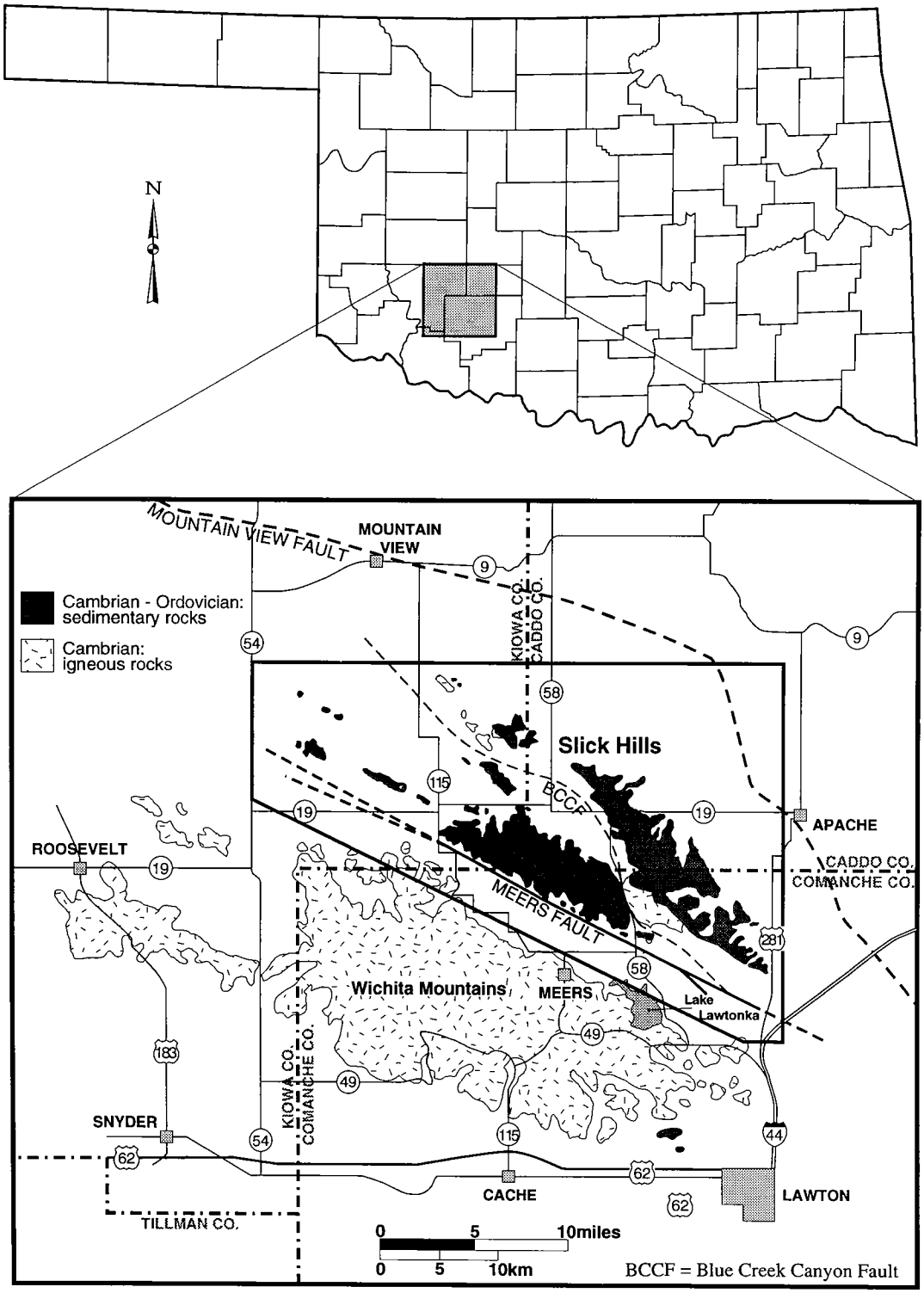

Figure 1. Location map of study area (modified from Hosey and Donovan, 1993).

lying Honey Creek Formations. The Reagan is a siliciclastic unit for which the lowermost deposits have been interpreted as alluvium; overlying deposits record a Franconian transgression (Donovan, 1986). The Honey Creek Formation records a period of mixed carbonate and siliciclastic sedimentation, during which increasing amounts of bioclastic limestones were deposited (Donovan and Ragland, 1986).

During this period, the hilly surface of the Carlton Rhyolite evolved into a marine archipelago (Fig. 3). Evidence for this archipelago can be found both in the Slick Hills of southwestern Oklahoma (Donovan, 1986, 2000), on the northern edge of the Arbuckle Mountains in south-central Oklahoma, and farther to the north beneath upper Paleozoic cover as the "Tulsa Mountains" (Ham and others, 1964). The presence of

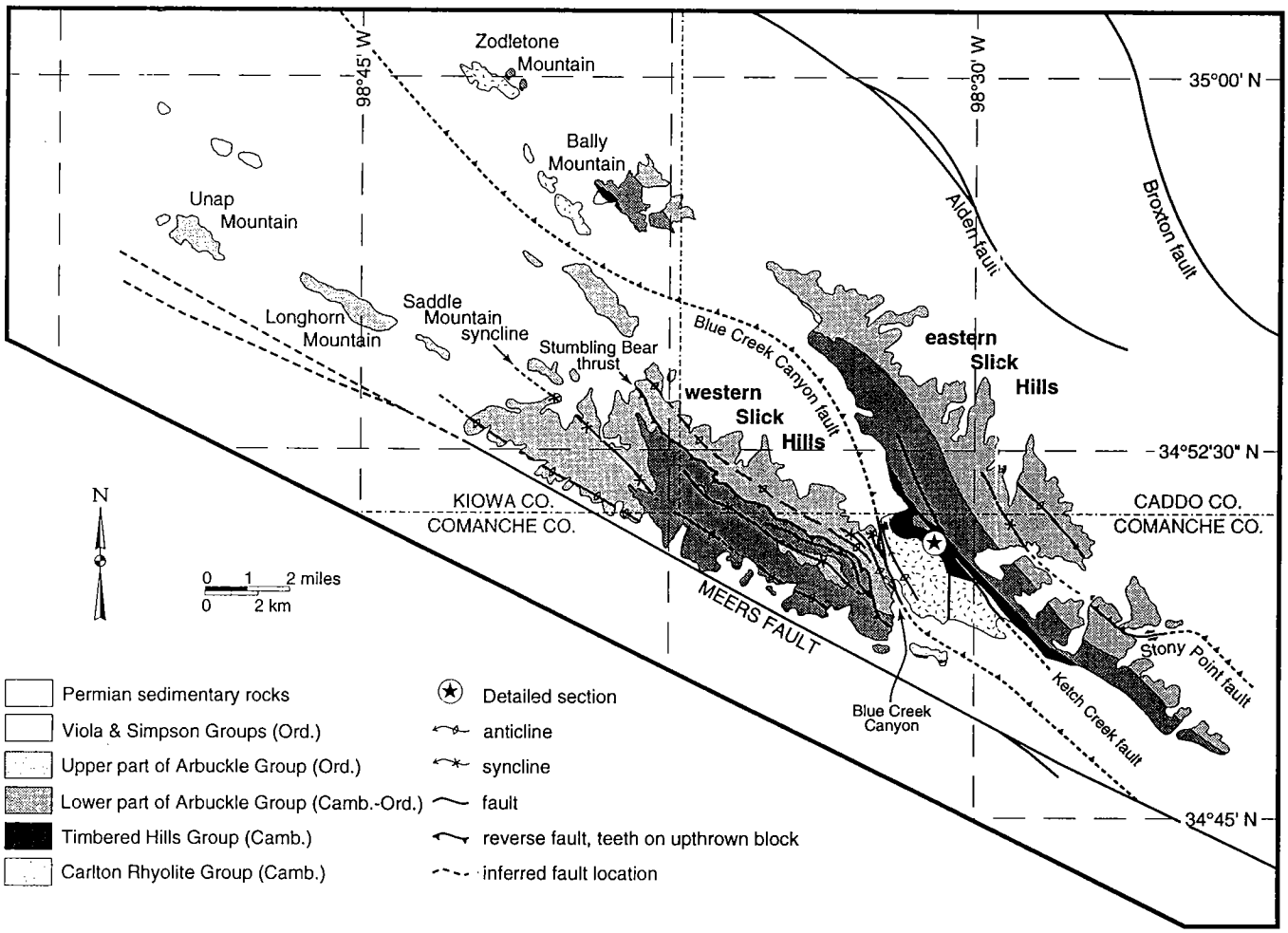

Figure 2. Map showing general geology of the Slick Hills, southwestern Oklahoma. The star marks the area of detailed study. Geology south of Meers fault is not shown. Modified from Hosey and Donovan (1993).

the archipelago resulted in considerable complexity in the lithostratigraphic architecture of the Timbered Hills Group (Donovan, 1986, 2000; Donovan and Stephenson, 1991). These complexities include (1) mixing of locally and distally derived detritus, (2) interpolation of impersistent wedges of conglomerate shed from the islands of the archipelago, (3) development of distinctive faunal assemblages that can be tied to leeward and windward rocky-shoreline communities, and (4) a high degree of detrital and diagenetic variability.

The Timbered Hills Group is overlain by the Arbuckle Group, a thick sequence of platform carbonates deposited across the area during a major Early Ordovician transgression (Figs. 4,5). The Fort Sill is the lowermost formation of the Arbuckle Group. The boundary between the Fort Sill and the underlying Honey Creek is defined by the widespread incoming of lime mud (Donovan, 2000).

PALEOLATITUDE AND PALEOCLIMATE

During the Late Cambrian, Laurentia (North America) was centered astride the equator between latitudes 20° N. and 30° S. (Scotese, 1984). The approximate location of southwestern Oklahoma was between latitudes 8° and 10° S. (Fig. 6). In addition to a cumulative northward drift of ~50°, a cumulative rotation of approximately 70° in a counterclockwise direction has taken place since the Late Cambrian. Assuming that present-day climatological circulation patterns were in effect, the rocks under discussion were deposited in a humid to subarid (tropical to subtropical) environment (Witzke, 1980).

STRATIGRAPHIC DEFINITION OF THE TIMBERED HILLS GROUP

The history of the stratigraphic definition of the Honey Creek Formation and related strata is confusing. In 1902, Taff first identified the Reagan Sandstone but did not recognize the Honey Creek. Instead, he thought that the Reagan was directly overlain by the Arbuckle Limestone. His Reagan included all the calcareous beds that would become the Honey Creek.

The Honey Creek Formation was first named by Ulrich in 1911, when he proposed that the calcareous layers in Taff's upper Reagan be separated into the Honey Creek Limestone Member of the Reagan. In 1932, Ulrich suggested that the Honey Creek Limestone Member be raised to the rank of formation. He designated a type section along Honey Creek on the south side of the East Timbered Hills in the Arbuckle Mountains in south-central Oklahoma (sec. 1, T. 2 S., R. 1 E.).

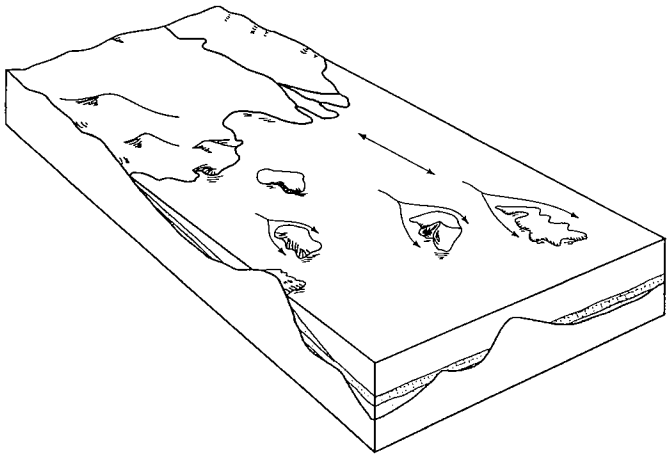

Figure 3. Southern Oklahoma archipelago. The islands are rhyolite, and the arrows show tidal-current motion. Note that the currents are dissipated around the islands, leaving the lee sides of the islands sheltered from high-energy currents. Redrawn from Donovan (1986).

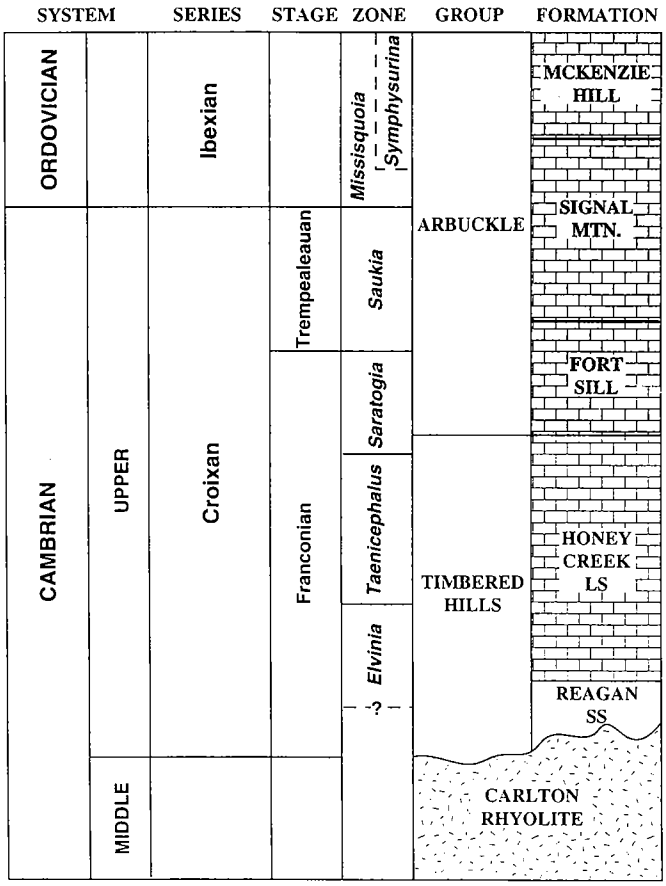

Figure 4. Stratigraphic column of the Carlton Rhyolite, Timbered Hills, and lower Arbuckle Groups (modified from Donovan and Ragland, 1986).

On the basis of his work in the Llano–Burnet area of central Texas, Ulrich suggested that he could correlate the Hickory Sandstone and Wilberns Formation of Texas with the Reagan and Honey Creek, respectively (Fig. 7). The basal Cambrian stratigraphy in central Texas, in ascending order, is the Hickory Sandstone, Cap Mountain Limestone, and Wilberns Formation. As he was unable to identify a Cap Mountain Limestone equivalent in the Wichita Mountains, Ulrich suggested that a disconformity must be present in the latter area. In consequence, he concluded that the Honey Creek should be distinguished as a separate formation from the Reagan (Ulrich, 1932).

Decker (1939) agreed that the Honey Creek should have formation status but suggested that there was no missing interval and that the Honey Creek was in fact Ulrich's Cap Mountain Limestone. Decker proposed that the Reagan and the Honey Creek be placed in the Timbered Hills Group, and he also recognized a "basal limestone" in the Reagan. In this context, the use of the term *basal* refers to the first occurrence of limestone in the section, not to the base of the Reagan Formation (Fig. 7).

In 1949, Frederickson argued that Ulrich's Cap Mountain and Decker's "basal limestone" should be included in the Honey Creek (Fig. 7). He chose the lowermost occurrence of trilobites in the *Elvinia* zone as the boundary between the Reagan and the Honey Creek. Following Frederickson, Fox (1958) chose the first occurrence of carbonates as his boundary.

In 1977, Stitt reverted to the stratigraphy of Ulrich (1932) and Decker (1939). He argued against Frederickson's divisions because his (Frederickson's) boundaries were based on biostratigraphy (Stitt, 1977). He also considered the limestones in the upper part of the Reagan to be laterally discontinuous and suggested that they were not significant in comparison to the siliciclastic units and therefore should only be considered members of the Reagan (Stitt, 1977) (Fig. 7).

However, Donovan (1986) suggested that the limestones that Stitt had placed in the Reagan were in fact traceable throughout the area of outcrop and that the boundary of the Honey Creek should be marked by the "first incoming of bioclastic grainstones." Donovan defined the top of the Reagan as a laterally continuous bed of richly glauconitic sandstone approximately 10 m thick. Donovan also recognized that the base of the Honey Creek is marked by an orange-weathering altered limestone layer. This layer is the result of diagenetic replacement of original calcite grains by ankerite (Cloyd and others, 1986). Although it is of variable thickness, the ankerite layer can be traced throughout the Slick Hills and therefore is an easily identifiable lithostratigraphic guide to the base of the Honey Creek. In this study, the stratigraphic usage of Donovan (1986) will be followed (Fig. 7).

With the exception of the pioneer work of Taff (1902), all workers have followed the stratigraphic practice of Ulrich (1911) in using the widespread incoming of lime mud to represent the boundary between the Honey Creek and the Fort Sill Formation, the lowermost unit of the Arbuckle Group.

In a broader context, the Honey Creek Formation correlates with the Davis Limestone in Missouri, the Welge and Morgan Creek Limestone Members of the Wilberns Formation in Texas, and the Franconia Formation in Wisconsin (Howell and others, 1944).

FIELD DESCRIPTION

In the field, the Honey Creek Formation can be divided into three ad hoc members: the "lower," the "red limestone," and the "upper" (Fig. 8). These units can be discriminated in

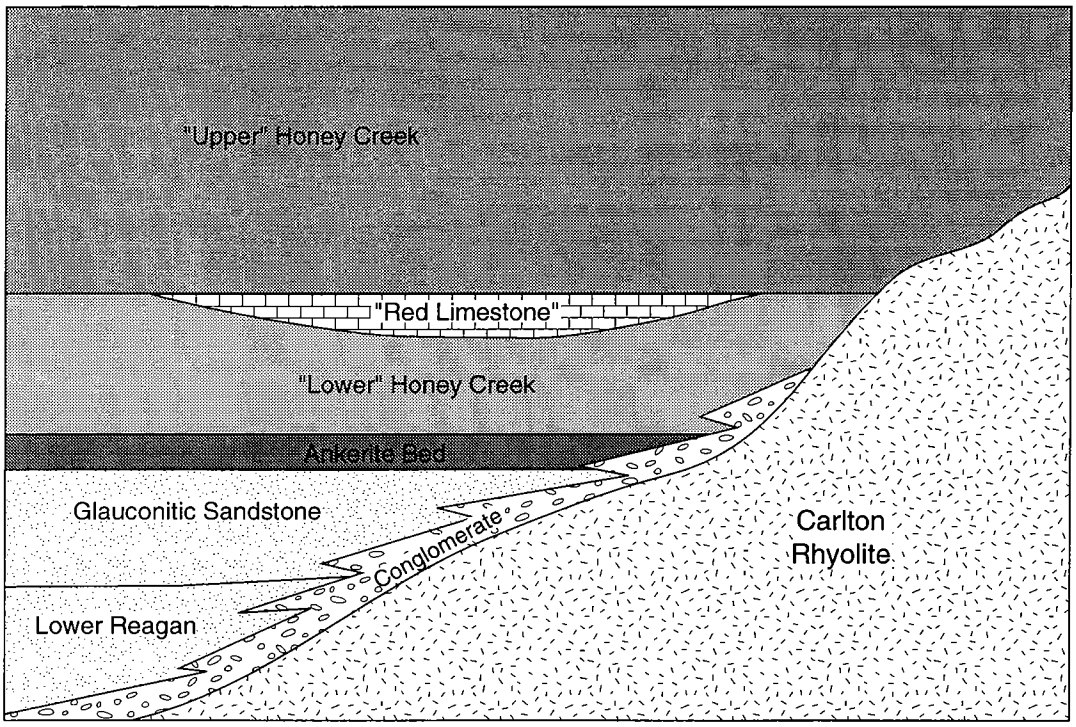

Figure 5. Stratigraphic relationships seen in the Slick Hills (modified from Donovan and Ragland, 1991).

the field on the basis of lithology, sedimentary structures, faunal and detrital content, and weathered appearance. We studied a section on the east side of Blue Creek Canyon as our type area: the exposure is good and extends laterally for 3 mi.

Lower Honey Creek Member

The lower Honey Creek is made up of light-gray, pelmatozoan-rich grainstones. In addition to the carbonate detritus, significant amounts of quartz, glauconite, and angular rhyolite pebbles are present (Fig. 9). North of the Blue Creek Canyon area, the percentages of these siliciclastic grains increase. Most fossils are broken and are variably abraded fragments of pelmatozoans, trilobites, and, less commonly, calcareous brachiopods. In addition, a few phosphatic brachiopods (*Lingula* sp.) are seen. Little lime mud is present, and most rocks are pervasively cemented by overgrowths of syntaxial calcite on pelmatozoans.

Most of the bedding in the member is defined by thin layers of detrital quartz that have acted as the sites of pressure solution. As a result, most bed boundaries are stylolitic. Crossbeds (in sets 2–10 cm thick) are found throughout the lower Honey Creek. Because of the character of exposures, very few of these sets yield precise cross-bedding directions, although some bimodal herringbone patterns are seen (Fig. 10). In general, it appears that a northwest–southeast flow pattern was operative (a similar pattern was observed by Donovan, 1986).

Orange-weathering patches of oxidized ankerite are observed throughout the lower Honey Creek, particularly near the base of the member. This lower ankerite zone marks the base of the Honey Creek Formation and is traceable throughout the Slick Hills (Donovan, 1986; Cloyd and others, 1986).

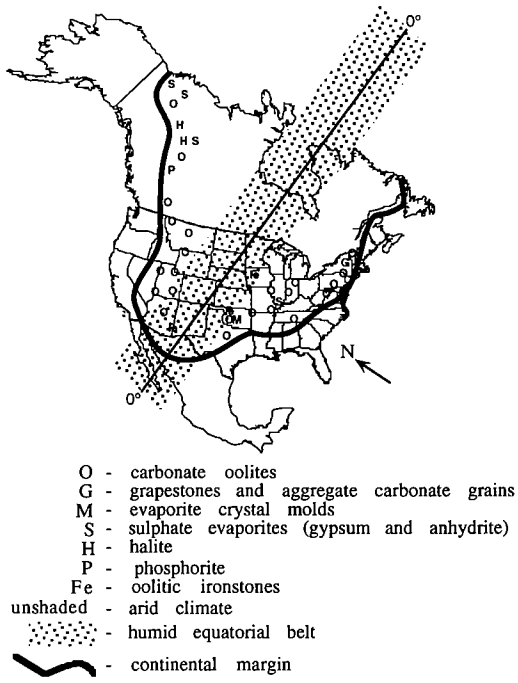

Figure 6. Late Cambrian paleogeography of North America (Laurentia) as inferred from lithic paleoclimate indicators (modified from Witzke, 1980).

Its thickness is variable, and in some areas (e.g., north of the section discussed here) it can be diffuse. The lower Honey Creek, as a unit, varies in thickness from 0 to 10 m. This variation is the result of either onlap against rhyolite islands or differential compaction in the underlying Reagan.

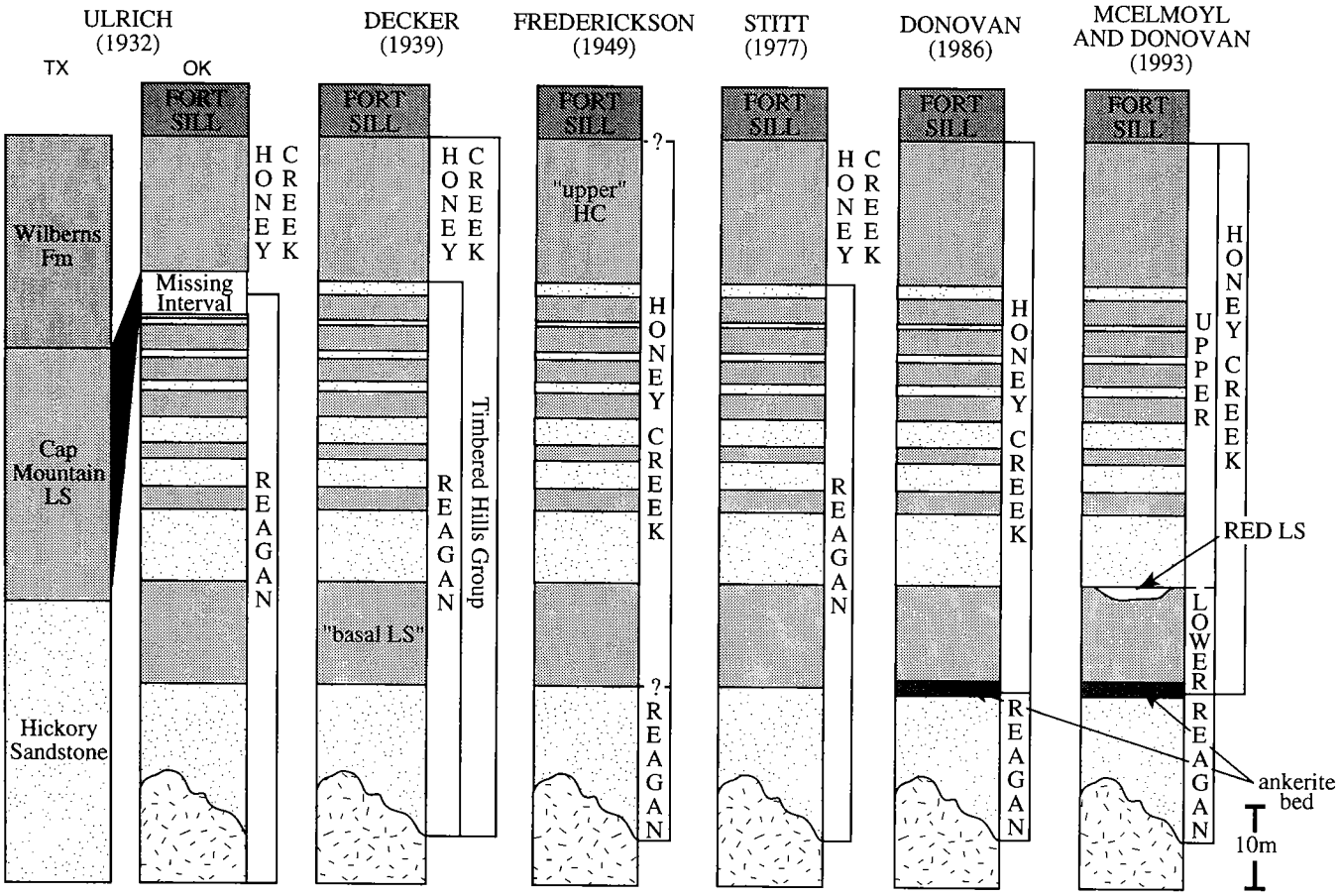

Figure 7. General history of the stratigraphic definition of the Honey Creek Formation.

Red Limestone Member

In the field, this member has a distinct pinkish-red to maroon color that is due to finely disseminated hematite. It is a poorly sorted, highly fossiliferous packstone, further characterized by parallel lamination, some hardgrounds, and a substantial percentage of angular rhyolite pebbles up to 10 cm in diameter. Fossils found in the member are similar in type and proportion to those occurring in the lower Honey Creek member; however, they are more complete and show far less abrasion. Some rhyolite pebbles have pelmatozoan holdfasts attached to them (Fig. 11).

At the contact between the red limestone and the lower Honey Creek members, there is evidence of erosion (Fig. 12). The red limestone member cannot be traced throughout the Slick Hills. For example, it is not found on Bally Mountain (Fig. 2), whereas in the eastern Slick Hills it varies in thickness from 0 to 3 m. There is a slight (2°–4°) angular discordance between the lower Honey Creek and red limestone and the upper Honey Creek in the Blue Creek Canyon section.

Upper Honey Creek Member

The upper Honey Creek member is a calcareous quartzarenite composed of alternating discrete beds of quartz and bioclastic sandstones 2–10 cm thick. Small- to medium-scale cross-beds (2–10 cm thick) and bioturbation are commonly seen. The member weathers to a characteristic honeycomb pattern (Bucheit and Donovan, 2000) and is a cliff-forming unit. The honeycomb pattern is the result of differential dissolution of carbonate-shell hash (Donovan, 1982). Variations in the proportions of quartz-rich and bioclastic layers characterize the entire upper part of the Honey Creek Formation. These variations range from 20% quartz-rich/80% bioclastic layers to 90% quartz-rich/10% bioclastic layers. We restricted our study to the lowermost 5 m of the member.

PETROGRAPHIC ANALYSIS

In general, the rocks of the Honey Creek Formation contain varying amounts of fossils (both calcareous and phosphatic), intraclasts, detrital quartz, rhyolite grains, lime mud, calcite cement, and other diagenetic components (principally replacement ankerite). The three ad hoc members of the formation can be discriminated by variations in the proportions of these constituents (Figs. 9,13).

The allochem content is mostly pelmatozoans, trilobites, calcareous and phosphatic brachiopods, and well-rounded mud intraclasts. Most of the pelmatozoans are surrounded by syntaxial calcite overgrowths. This cement has also occluded internal pores within the pelmatozoans. However, some pores were filled by glauconite and hematite prior to cementation. The trilobites are generally thick shelled and fragmented. Most of the trilobites appear to belong to the *Elvinia* biostratigraphic zone and have been preliminarily identified as *Cheilocephalus*

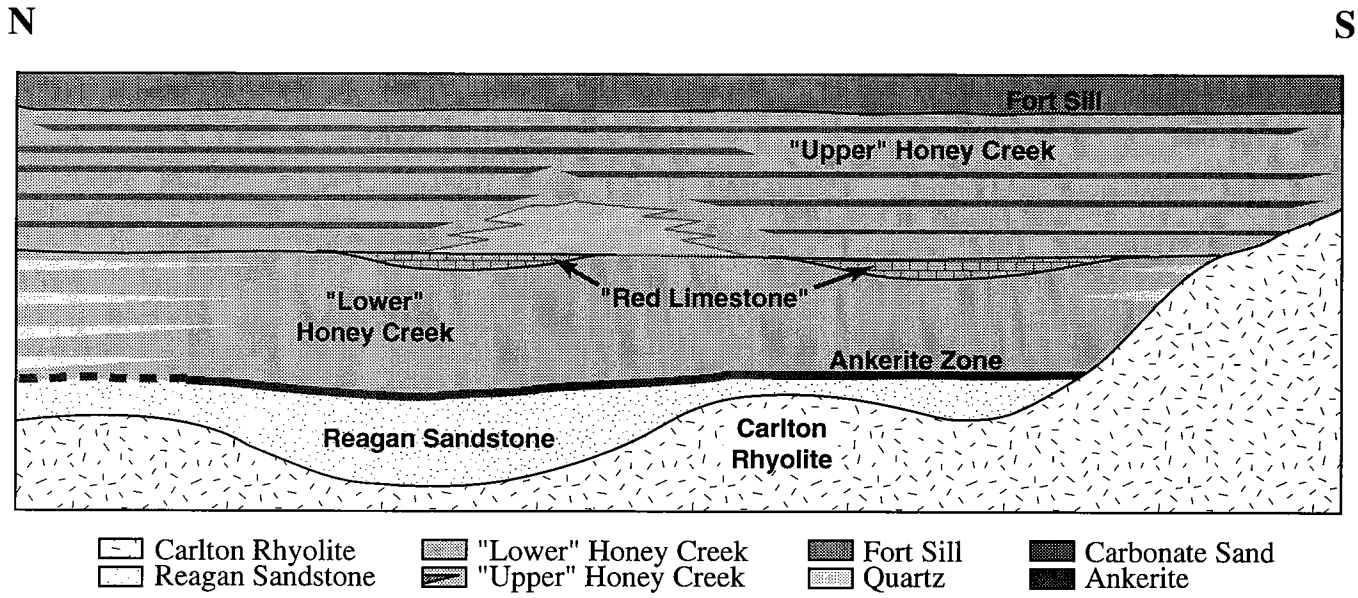

Figure 8. Field relationships in the area south of Ring Top Mountain in Blue Creek Canyon. The lower Honey Creek becomes more quartz rich to the north. Variation in thickness of the units presumably is due to differential compaction of the Reagan. The ankerite zone is diffuse in some areas, particularly to the north. Note the pronounced lateral variation in the percentage of carbonate sand in the lower part of the upper Honey Creek. It is suggested that variations of this type resulted from the complexity of facies patterns developed around islands of the archipelago.

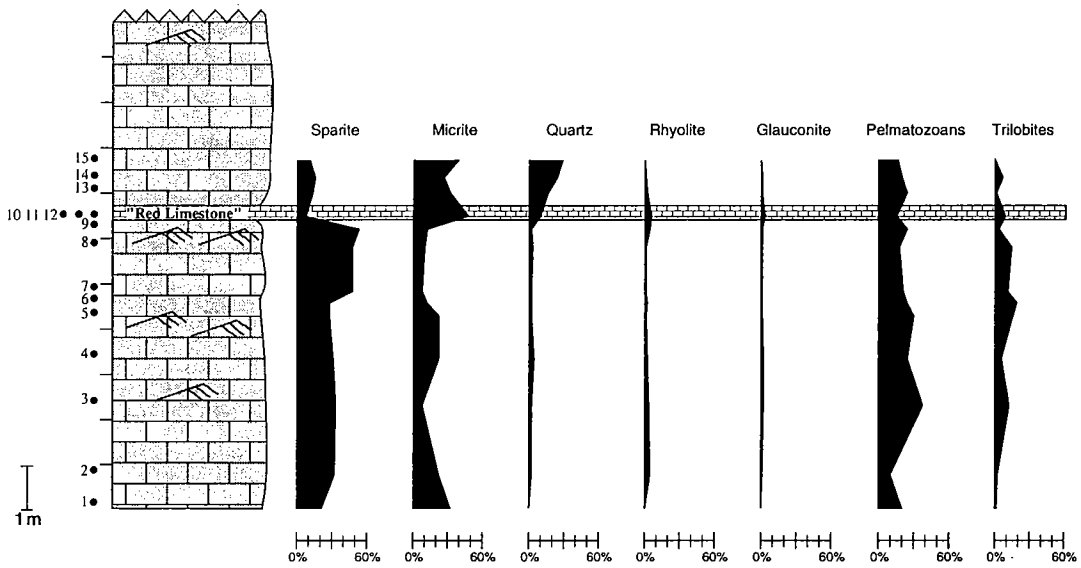

Figure 9. Petrographic variations within the Honey Creek Formation in Blue Creek Canyon. Notice the significant differences in quartz, micrite, and spar among the three members. The dots denote sample sites.

wichitaensis, C. librigina?, *Pseudosaratogia lata, Cliffia lataegenae*?, and *Saratogia americana* (A. B. Busbey, Texas Christian University, personal communication, 1993). The biostratigraphic studies of Stitt (1971, 1977), Frederickson (1948a,b), Wilson (1949, 1951), and Bauer (1985) were consulted in this identification.

The calcareous brachiopods (most of which are orthids) have fibrous, punctate internal shell structures; the phosphatic brachiopods are broken pieces of the genus *Lingula*. Rafalowski (1984) observed that some of the calcareous brachiopods were partly replaced by chalcedony and that the punctae had hematitic infillings. Other fossils, present in minor amounts, include the algae *Girvanella* and *Renalcis* and calcareous sponges.

The siliciclastic detritus includes quartz, glauconite, rhyolite fragments, feldspars, and muscovite. Most of the quartz is monocrystalline with non-undulose extinction; grains are well rounded to subrounded and vary from silt to medium-sand size. Quartz occurs both in thin beds and as debris in stylolites in the lower Honey Creek. In the red limestone, quartz grains, which are mostly very fine sand or silt, are disseminated throughout the rock. Quartz in the upper Honey Creek occurs

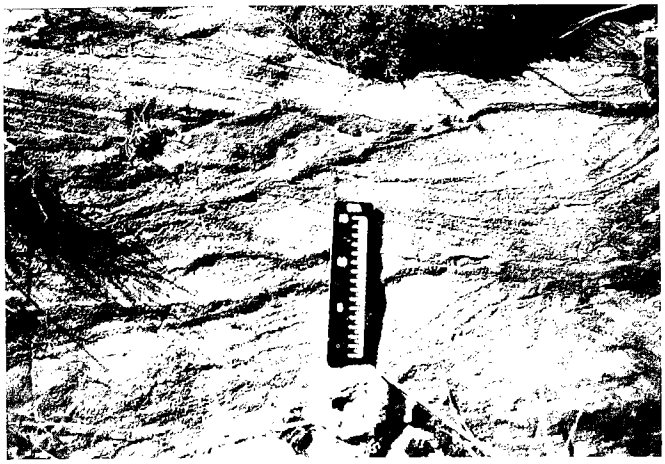

Figure 10. Characteristic cross-beds in the lower Honey Creek. Cross-set boundaries are defined by thin siliciclastic drapes.



Figure 11. Exposure of the red limestone, showing a pebble of Carlton Rhyolite that has acted as a holdfast for pelmatozoan colonization.

in lenticular beds characterized by small-scale cross-bedding (~10 cm). The amount of quartz varies throughout the section but is generally much greater in the upper Honey Creek.

Glauconite generally occurs as pellets, but some is seen as a replacement mineral in rhyolite fragments and as an infill of pelmatozoan pores. The glauconite is an apple-green color, in contrast to the darker green glauconite that is found in the overlying strata of the Arbuckle Group, at the base of the Signal Mountain Formation (Donovan, 2000; Hosey and Donovan, 2000).

Most of the rhyolite fragments are angular and are texturally similar to the underlying Carlton Rhyolite. They show a variety of devitrification textures. Rhyolite fragments are somewhat more common in the red limestone. In the lower Honey Creek, trace amounts of angular to subangular feldspar (potassium feldspar and some plagioclase) are present. Muscovite occurs in trace amounts throughout the section.

The red limestone is characterized by abundant lime mud. This mud is colored pink by trace amounts of fine hematite "dust."

Syntaxial overgrowths on pelmatozoan fragments dominate the cements of the Honey Creek, particularly the grainstones of the lower Honey Creek. Cathodoluminescence shows that the cements grew sequentially and were precipitated from waters of varying chemistry. Up to 27 distinct zones of luminescence are present (Fig. 14). Small amounts of later drusy cement are found. Ankerite is seen both as a late cement and as a replacement of existing calcite textures: it is usually heavily weathered to limonite.

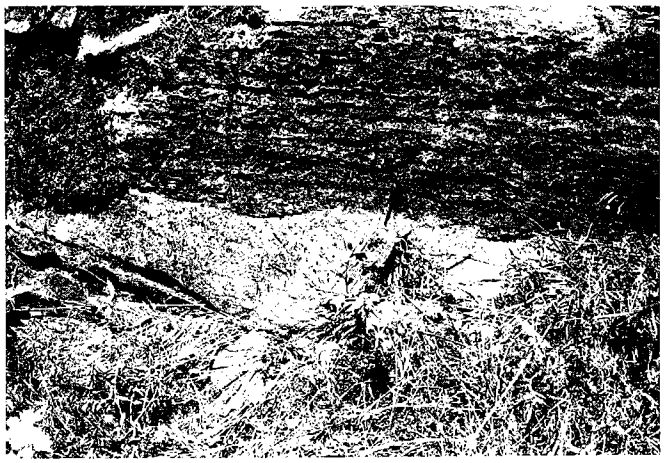

Figure 12. Contact between the lower Honey Creek and the red limestone, showing evidence of slight karst weathering.

DISCUSSION

Analysis of the stratigraphic and petrographic character of the Honey Creek Formation requires an understanding of both the depositional setting of the three members and the geometric relationships they exhibit. In a general context, the controlling parameters of depositional patterns during formation of the Timbered Hills Group, and specifically the Honey Creek Formation, were the unusual nature of the paleogeography, the Franconian transgression, and the development of the southern Oklahoma aulacogen.

Unusual Nature of the Paleogeography

During deposition of the Honey Creek, the area consisted of an archipelago, formed of Carlton Rhyolite and surrounded by shallow seas (Donovan and others, 1986) (Fig. 3). Although they were gradually onlapped, and hence diminished in size, the islands of the archipelago persisted throughout deposition of the Honey Creek. There is up to ~275 m of relief on the basement, and hill slopes up to ~10° are preserved (Donovan and Stephenson, 1991). Given the restrictions of the available exposure, it is possible that more relief may have existed than is presently apparent; this is certainly the case in the Arbuckle Mountain area (Ham and others, 1964).

Because of the topography, the stratigraphic architecture is complicated, and the problems of determining the environments of deposition are amplified. In particular, the existence of the archipelago may explain (1) the occurrence of detrital rhyolite clasts at all levels; (2) the variation of thickness in the preserved section from differential compaction, both around the rhyolite islands and around lenticular sandstone bodies in

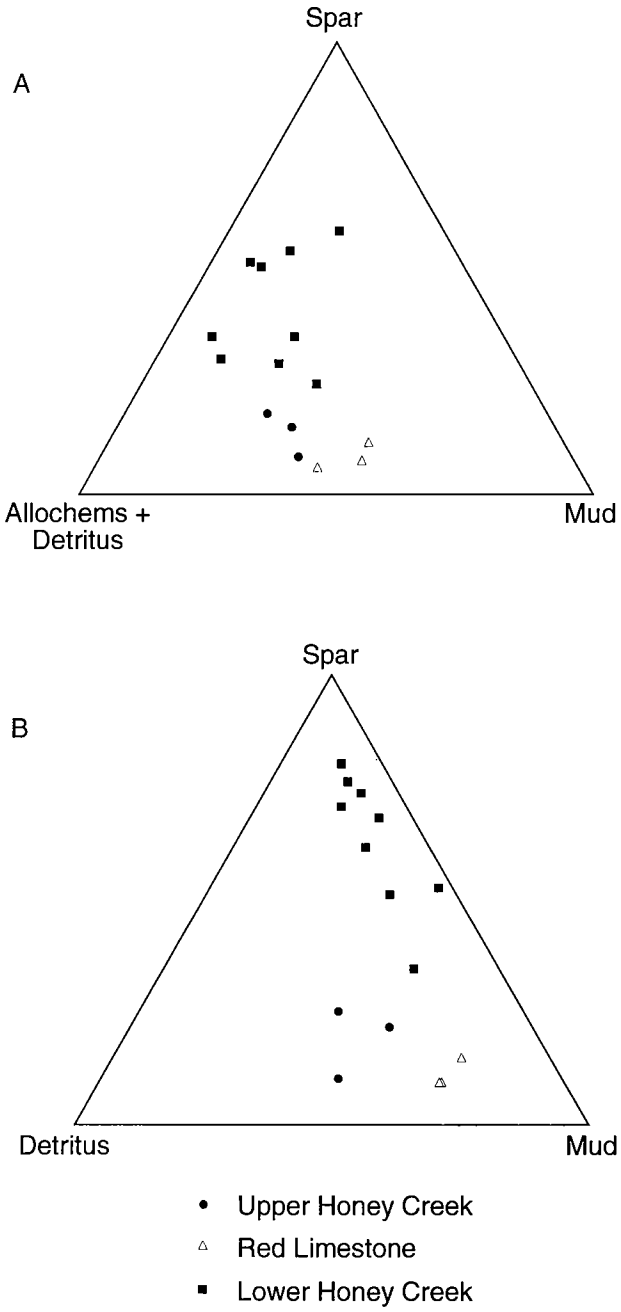

Figure 13. Ternary plots for the Honey Creek Formation. (A) Plot of spar, mud, and allochems plus detritus. Note how all three axes serve to discriminate the three members. (B) Plot of spar, mud, and detritus. Three distinct fields are discriminated.

the underlying Reagan (Donovan, 1986); (3) petrographic variations, for example, in the relative proportions of quartz and carbonate in the section; and (4) variations in the preserved fauna, interpreted as ecological partitioning (Donovan, 1986).

Franconian Transgression

During Franconian time, a major transgression affected the entire area that is now Oklahoma and the adjacent states to the north and south. This transgression apparently took place

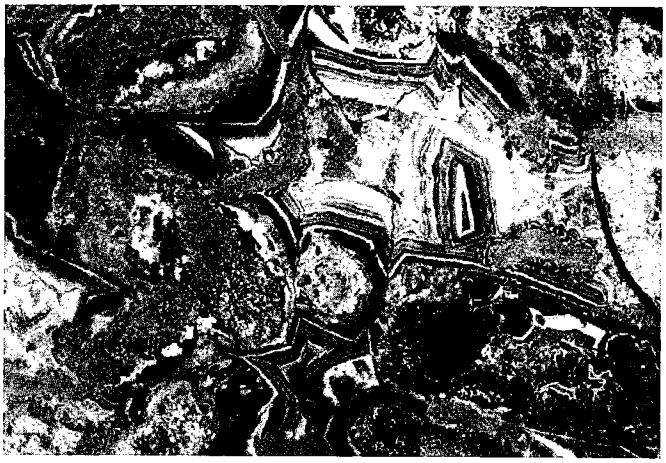

Figure 14. Cathodoluminescence patterns in the lower Honey Creek, showing rapid alternation in the composition of the syntaxial overgrowths that have developed around abraded pelmatozoan fragments. This speciman was collected just below the top of the member (site 9 in Fig. 9).

across a surface of deeply weathered iron-rich rhyolite; as a consequence, the Reagan and the Honey Creek contain an unusual abundance of "iron signatures" (Donovan, 1986, 2000; Donovan and others, 1986; Cloyd and others, 1986). These include (1) an abundance of glauconite (up to 50% in some sandstones in the Reagan); (2) ferruginous ooids (in the Reagan); (3) an abundance of hematite cement (up to 30% in some parts of the Reagan); (4) widespread ankerite in the Honey Creek Formation, both as a cement and as a replacement; (5) abundant iron-rich illite in the Reagan; and (6) diagenetic pyrite.

Whereas all the detritus of the initial deposits of the Reagan appears to be of local origin, the upper part of the Reagan, as well as the entire Honey Creek, contains abundant detrital quartz. Although some quartz may have been derived from the Carlton Rhyolite (which contains a small percentage of quartz phenocrysts), most must be of distal origin and was presumably incorporated into the sediments as the transgression advanced across the craton. The mixing of locally and distally derived detritus adds a further complexity to the character of these rocks.

Development of the Southern Oklahoma Aulacogen

The southern Oklahoma aulacogen is partly defined on the basis of the extraordinary thicknesses of lower Paleozoic sedimentary rocks that it contains. In general, thicknesses within the aulacogen are up to four times as great as those on the adjacent craton (Donovan and Ragland, 1991). Subsidence rates within the aulacogen were analyzed by Feinstein (1981), who took the regional unconformity of the Carlton Rhyolite with the overlying upper Cambrian sediments as the reference horizon for his subsidence curves. Following his usage, the curves originate at ~525 m.y. ± 25 m.y. (Rb/Sr age of youngest basement rocks as determined by Ham and others in 1964). Feinstein (1981) suggested that the initial subsidence rates for the basin (the first ~16 m.y.) were relatively slow and probably due to elastic flexure. However, the ±25-m.y.-

dating error bars create considerable problems of definition in deciding the precise rate of subsidence. The problem of precise timing is further complicated by the fact that the age of the lowest part of the Reagan Sandstone is poorly known. Nevertheless, it is clear that the initial rate of subsidence is much less than that which subsequently developed as a result of reactivation of the faults of the aulacogen that led to deposition of the Arbuckle Group.

INTERPRETATION

Developments of Stratigraphic Relationships Observed in the Honey Creek Formation

It was during the initial period of subsidence of the southern Oklahoma aulacogen that the sea first inundated the craton and the uppermost Reagan and Honey Creek Formations were deposited. As the transgression began, the rhyolite hills gradually evolved into islands that would eventually constitute the southern Oklahoma archipelago (Donovan and Stephenson, 1991). Initial deposits of the Reagan were alluvium, but, with deposition of the uppermost Reagan Sandstone, marine conditions were established throughout the area. The first evidence of life consists of trace fossils of the *Skolithos* and *Cruziana* ichnofacies. Subsequently, large numbers of phosphatic brachiopods established themselves in the area. As the transgression progressed, distinct faunal assemblages began to develop (Donovan, 1986). In the clear water around the islands, pelmatozoans flourished and dominated the preserved biomass. For the most part, the pelmatozoans are preserved as fragmentary remains, forming sand sheets that were constantly reworked by tidal currents. However, in some areas on the lee sides of islands, more diverse faunas, composed of pelmatozoans, trilobites, brachiopods, sponges, and varieties of algae, developed (Donovan and others, 1986; Donovan and Stephenson, 1991). Textures in deposits of this type are dominantly mud supported.

The stratigraphic architecture of the Honey Creek Formation was also influenced by the archipelago. As discussed previously, the lower Honey Creek varies laterally in thickness and detrital content (Fig. 8). Variations in thickness could be due to differential compaction in the Reagan Sandstone around the islands, and variations in the detrital content could be due to the location of the islands relative to the area of deposition. The petrography of the Honey Creek grainstones is consistent with their origin as winnowed sands subject to constant wave and current action. Zoning in the cements suggests that these sands were rapidly cemented by waters of varying ionic character.

There is evidence of erosion at the contact between the red limestone and the lower Honey Creek. We suggest that this contact records a regression, followed by limited subaerial erosion. The red limestone was deposited during the succeeding transgression and incorporates detritus (talus) from the adjacent archipelago.

The character of the red limestone—in particular the abundance of mud, the presence of a diverse and less abraded fauna, and the relative abundance of rhyolite clasts—suggests that the deposit is in some way related to a protected environment, perhaps the lee side of an island or a protected bay, as described by Donovan and others (1986). In such an area, the power of wave-generated currents would have been dissipated, leading to more complete preservation of faunal communities. The abundance of lime mud is consistent with the concept of a low-energy environment in which the sea bed was below normal wave base. The occurrence of hardgrounds is also consistent with such a setting. Thus the depositional model favored is one in which the relative depth at which wave power was effective depended more on proximity to the islands of the archipelago than on the depth of the sea.

One of the consequences that may have resulted from the existence of considerable relief on the basement is that faunal debris found in the red limestone may have been incorporated from the erosion of older (i.e., pre-red) beds that were spatially above the red limestone. If this is so, then the trilobite fauna in the red limestone may be partly or completely inherited, thus suggesting a somewhat older age for the red limestone than is in fact the case.

The red limestone is overlapped by the upper Honey Creek and is found only in two areas of the entire outcrop of the lower and upper Honey Creek boundary. Locally, a slight angular discordance is present at the contact, but over most of the outcrop the boundary between the two members is concordant. We consider that this relationship is best explained by differential compaction (i.e., supratenuous folding) related to the underlying and adjacent basement topography. This compaction can be tied to a period of nondeposition during the general period of regression that marks the boundary of the lower and upper members. Further evidence of a regression at this time is the heterogeneous character of cements developed in the lower and red limestones (as shown by cathodoluminescence). The numerous alterations in the character of sparry syntaxial overgrowths in these two members suggest that pores were filled by waters of varying chemistry, a condition more likely to have developed during a period of regression, when meteoric waters can mix with marine waters more easily than during a period of transgression.

One of the parameters that helps to define the upper Honey Creek, and which is also evident in the red limestone, is the incoming of substantial quantities of fine-grained quartz sand. As this sand could not have been generated by the weathering of the local basement, we suggest that it was derived from a more distal source, in all probability the "true" shoreline of the Franconian seaway, lying to the north and west (in modern coordinates). During the regression, the quartz (and other siliciclastic detritus) either may have been windblown or else transported by river systems into the general area of the archipelago. Subsequently, during the succeeding transgression, the quartz grains were incorporated into the sedimentary section. In essence, the facies tract that developed had its source from two distinct areas: carbonate sands were derived from a local source associated with the biological activity that developed around the islands of the archipelago, while quartz sands were derived by the reworking of the more distal cratonic source suggested above. The net result was a facies characterized by the interbedding of thin (centimeter-scale) beds of quartz-rich and carbonate-rich sandstones. Both types of sandstone are characterized by small- to medium-scale cross-beds (about 2–10 cm), suggesting a sea bed modified by currents

that were powerful enough to produce a comprehensively ripple-marked sea bed but not powerful enough to mix the two grain populations to a significant degree. Supporting evidence for a relatively quiet sea bed is the common occurrence of trace fossils whose form suggests crawling and perhaps grazing life styles.

The geometric relationships between the three ad hoc members (supratenuous folding, slight angular discordance) raise questions as to the original lateral extent of the red layer: was it essentially a local deposit that was spread over little more than the present area of outcrop, or was it originally deposited over the entire area and subsequently destroyed by the events associated with the incoming of the upper Honey Creek? The available exposures do not allow us to resolve this question.

The sequence of events that led to the stratigraphic relationships observed involved an initial transgression during which the upper part of the Reagan Sandstone was laid down as a series of tidally influenced sandstones and intervening heterolithic beds. Then the lower Honey Creek was deposited as tidally influenced sand shoals, which incorporated bioclastic debris that resulted from the successful colonization of the archipelago environment. Third, a regression occurred during which the lower Honey Creek was exposed and eroded, following which the red limestone was deposited. Subsequently, there was a further regression during which large quantities of quartz sand were either blown or transported by rivers into the area. During the subsequent transgression, these quartz sands were incorporated into the mixed carbonate and quartz sandstones of the upper Honey Creek (Figs. 15,16).

As the sequence was deposited, differential compaction occurred because the heterolithic beds in the Reagan compacted more readily than either the lenticular Reagan sandstones or the grainstones of the lower Honey Creek (thus producing slight variations in thickness of the lower Honey Creek and the red limestone). In addition, the entire sedimentary sequence was subject to compactional drape around the basement islands of rhyolite. This draping effect produced the slight angular discordances between the three recognized ad hoc units.

SUMMARY AND CONCLUSIONS

The stratigraphic definition of the Honey Creek Formation has long been in dispute. In this study, an attempt has been made to simplify and redefine the stratigraphy. In accordance with Donovan (1986), we suggest that the "first incoming of bioclastic grainstones"

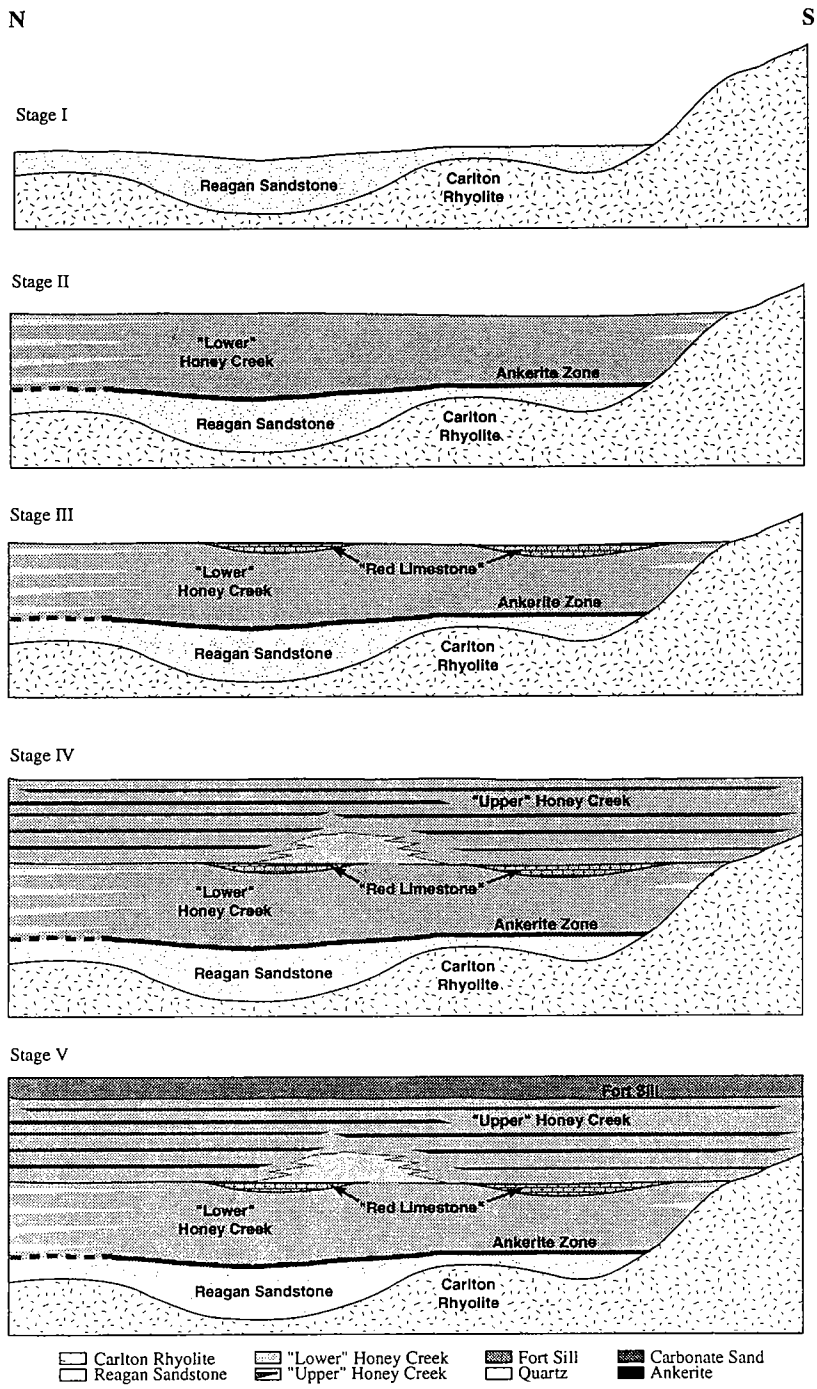

Figure 15. Five stages that led to the stratigraphic relationships found in the Honey Creek Formation. Stage I: Deposition of the Reagan Sandstone around the existing topography; gradual evolution of an archipelago of rhyolite islands. Stage II: Deposition of the limestones of the lower Honey Creek around the islands of the archipelago. Note the facies relationships in the limestone; these reflect the complexity of current flow around the islands. Stage III: Following slight regression, subaerial exposure, and compaction of the lower Honey Creek, the red limestone was deposited during the subsequent transgression. Stage IV: Following a further period of regression, the upper Honey Creek was deposited, initially exhibiting similar local facies changes to those seen in the lower Honey Creek. However, with time, the islands became less important geographic features, and the facies changes are less noticeable. Stage V: Continued transgression resulted in deposition of the Arbuckle Group, beginning with the Fort Sill Formation.

should be taken as the boundary between the Reagan Sandstone and the Honey Creek Formation. This boundary is distinct and traceable throughout the Slick Hills as the contact between the underlying, highly glauconitic sandstone of the Reagan and the overlying zone of ankerite in the lowermost Honey Creek (Cloyd and others, 1986). Three informal ad hoc members have been described and discriminated from each other on the basis of their petrographic characteristics: lower Honey Creek, red limestone, and upper Honey Creek.

The Honey Creek was deposited during a period of overall marine transgression that was punctuated by smaller scale regressions. Distinctive evidence for this cyclic pattern is preserved at outcrop level because of the unusual nature of the contemporary paleogeography (an archipelago of reasonably steep-sided islands). This evidence includes (1) complex geometric relationships between the three ad hoc members, (2) contemporary erosion at the contact between the three ad hoc members, and (3) a distinctive bed of local origin, the red limestone, which is best explained as a record of a major regression–transgression event.

The slight angular discordance of the lower units with the upper Honey Creek suggests a major regressive cycle during deposition of the Honey Creek Formation. What caused sea level to change? Two possible solutions are (1) that sea-level change was due to a craton-wide ("eustatic") withdrawal of the sea, or (2) that sea-level change was due to tectonic events—i.e., local and temporary uplift related to development of the southern Oklahoma aulacogen.

We suggest that the relationships observed are best interpreted by the hypothesis of a craton-wide regression. This interpretation follows from the work of Chow and James (1987), who identified "grand cycles" in the Cambrian rocks of Newfoundland (Fig. 17). Grand cycles are large-scale (tens to hundreds of meters) sedimentary cycles that are related to passive continental margins on which there was alternation of carbonate-dominated and siliciclastic-dominated sedimentation (Aitken, 1966; Holland, 1971). Chow and James (1987) argue that the cycle boundaries correlate with stratigraphic hiatuses that have been identified across North America. The timing of the regressive event described here corresponds to the *Elvinia* trilobite zone in which a considerable craton-wide break has been recognized. Because the lower Honey Creek and the red limestone are within the *Elvinia* zone, it is possible that the hiatus between these layers and the upper Honey Creek is related to this break.

The alternative interpretation—that the regression was related to local tectonic uplift within the southern Oklahoma aulacogen—is difficult to disprove. To date, we have not yet found field evidence to support the tectonic hypothesis, although some evidence of local fault adjustment exists in the upper part of the Honey Creek (Donovan, 2000). Our preference for the eustatic argument is based in part on the observation that the principal subsidence within the aulacogen did not begin until after initiation of the Arbuckle platform. Before this time, sediment thicknesses within the aulacogen were comparable to those found in Texas and northern Oklahoma.

ACKNOWLEDGMENTS

We would like to thank the Fort Worth Geological Society, the Adkins Fund, the Mobil Foundation, and the Moncrief family for their generous financial support. Sincere appreciation is expressed to the Kimbell family for their hospitality. Without their support, this project would not have been possible. We are grateful to Art Busbey for his help in fossil identification and to Randy Hosey for his help in drafting Figures

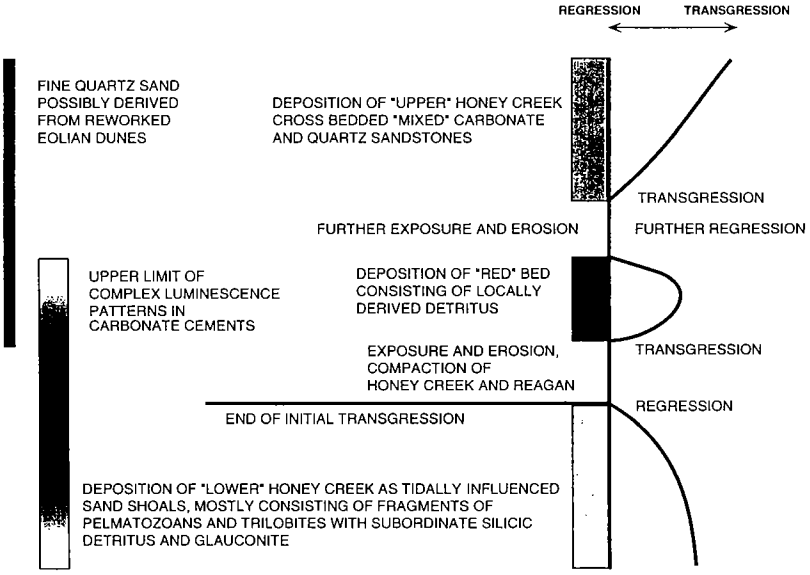

Figure 16. Synopsis of factors involved in the generation of the red limestone.

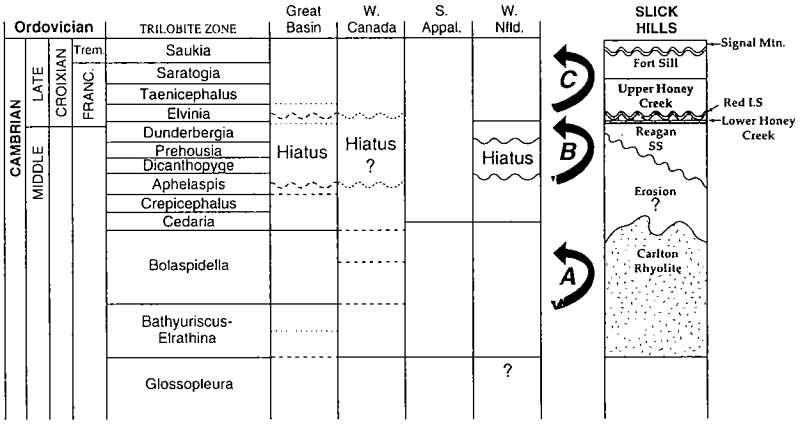

Figure 17. "Grand cycles" A, B, and C recognized in Newfoundland and how they correlate across North America. Note a regressive cycle in the *Elvinia* zone; this cycle could correlate with the contact between the upper Honey Creek and the lower strata. Modified from Chow and James (1987).

1 and 2. Sincere thanks also go to the Texas Christian University Department of Geology for use of their equipment and facilities.

REFERENCES CITED

Aitken, J. D., 1966, Middle Cambrian to Middle Ordovician cyclic sedimentation, southern Rocky Mountains of Alberta: Canadian Petroleum Geology Bulletin, v. 14, p. 405–441.

Bauer, D. A., 1985, Trilobites, biostratigraphy, lithostratigraphy, and environments of deposition of the Reagan Formation and Honey Creek Limestone, Kindblade Ranch area, Wichita Mountains, southern Oklahoma: University of Missouri unpublished M.S. thesis, 109 p.

Bucheit, A. K.; and Donovan, R. N., 2000, Initiation of a carbonate platform: a comparison between the Lower Jurassic Broadford Limestone, Isle of Skye, Scotland, and the Cambrian Honey Creek Limestone, Slick Hills, Oklahoma, *in* Johnson, K. S. (ed.), Platform carbonates in the southern Midcontinent, 1996 symposium: Oklahoma Geological Survey Circular 101 [this volume], p. 57–64.

Chow, N.; and James, N. P., 1987, Cambrian Grand Cycles: a northern Appalachian perspective: Geological Society of America Bulletin, v. 98, p. 418–429.

Cloyd, Kelly; Donovan, R. N.; and Rafalowski, M. B., 1986, Ankerite at the contact between the Reagan Sandstone and the Honey Creek Limestone (Timbered Hills Group), *in* Donovan, R. N. (ed.), The Slick Hills of southwestern Oklahoma—fragments of an aulacogen?: Oklahoma Geological Survey Guidebook 24, p. 17–20.

Decker, C. E., 1939, Contact of the Honey Creek and Reagan formations with igneous rocks in the Arbuckle and Wichita Mountains, Oklahoma: American Association of Petroleum Geologists Bulletin, v. 23, p. 1094–1098.

Donovan, R. N., 1982, Geology of Blue Creek Canyon, Wichita Mountains area, *in* Gilbert, M. C.; and Donovan, R. N. (eds.), Geology of the eastern Wichita Mountains, southwestern Oklahoma: Oklahoma Geological Survey Guidebook 21, p. 65–77.

_____1986, Geology of the Slick Hills, *in* Donovan, R. N. (ed.), The Slick Hills of southwestern Oklahoma—fragments of an aulacogen?: Oklahoma Geological Survey Guidebook 24, p. 1–12.

_____2000, Initiation of the Arbuckle platform—view from the Slick Hills, Oklahoma, *in* Johnson, K. S. (ed.), Platform carbonates in the southern Midcontinent, 1996 symposium: Oklahoma Geological Survey Circular 101 [this volume], p. 47–56.

Donovan, R. N.; and Rafalowski, M. B., 1984, The anatomy of an Early Ordovician shell bank in the Honey Creek Formation, southwestern Oklahoma [abstract]: Geological Society of America Abstracts with Programs, v. 16, no. 2, p. 82.

Donovan, R. N.; and Ragland, D. A., 1986, Paleozoic stratigraphy of the Slick Hills, southwestern Oklahoma, *in* Donovan, R. N. (ed.), The Slick Hills of southwestern Oklahoma—fragments of an aulacogen?: Oklahoma Geological Survey Guidebook 24, p. 13–16.

_____1991, Stop 10: The base of the Arbuckle Group at Bally Mountain, *in* Johnson, K. S. (ed.), Arbuckle Group core workshop and field trip: Oklahoma Geological Survey Special Publication 91-3, p. 244–246.

Donovan, R. N.; and Stephenson, M. D., 1991, A new island in the southern Oklahoma archipelago, *in* Johnson, K. S. (ed.), Late Cambrian–Ordovician geology of the southern Midcontinent, 1989 symposium: Oklahoma Geological Survey Circular 92, p. 118–121.

Donovan, R. N.; Ragland, D. A.; Cloyd, Kelly; Bridges, Steve; and Denison, R. E., 1986, Stop 2: Geological highlights of the Bally Mountain area, *in* Donovan, R. N. (ed.), The Slick Hills of southwestern Oklahoma—fragments of an aulacogen?: Oklahoma Geological Survey Guidebook 24, p. 92–95.

Feinstein, S., 1981, Subsidence and thermal history of southern Oklahoma aulacogen: implications for petroleum exploration: American Association of Petroleum Geologists Bulletin, v. 65, p. 2521–2533.

Folk, R. L., 1959, Practical petrographic classification of limestones: American Association of Petroleum Geologists Bulletin, v. 43, p. 1–39.

Fox, C. S., 1958, The Honey Creek formation of the Wichita Mountains, Oklahoma: University of Oklahoma unpublished M.S. thesis, 61 p.

Frederickson, E. A., 1948a, Upper Cambrian trilobites from Oklahoma: Journal of Paleontology, v. 22, p. 798–803.

_____1948b, Clarification of Upper Cambrian stratigraphy in Oklahoma: American Association of Petroleum Geologists Bulletin, v. 32, p. 1349–1355.

_____1949, Trilobite fauna of the Upper Cambrian Honey Creek formation [Oklahoma]: Journal of Paleontology, v. 23, p. 341–365.

Ham, W. E.; Denison, R. E.; and Merritt, C. A., 1964, Basement rocks and structural evolution of southern Oklahoma: Oklahoma Geological Survey Bulletin 95, 302 p.

Holland, C. H. (ed.), 1971, Cambrian of the New World: Wiley-Interscience, New York, 456 p.

Hosey, Randy; and Donovan, R. N., 1993, The geological significance of the boundary between the Fort Sill and Signal Mountain Formations in the lower Arbuckle Group (Cambrian) [abstract]: Geological Society of America Abstracts with Programs, v. 25, no. 1, p. 14–15.

_____2000, Boundary between the Fort Sill and Signal Mountain Formations in the lower Arbuckle Group, Slick Hills: candidate for a grand cycle boundary, *in* Johnson, K. S. (ed.), Platform carbonates in the southern Midcontinent, 1996 symposium: Oklahoma Geological Survey Circular 101 [this volume], p. 79–88.

Howell, B. F.; Bridges, J.; Deiss, C. F.; Edwards, I.; Lochman, C.; Raasch, C. E.; Duncan, D. C.; Mason, J. F.; and Denson, N. M., 1944, Correlation of the Cambrian formations of North America: Geological Society of America Bulletin, v. 55, p. 993–1004, chart 1.

McElmoyl, Courtney, 1993, Transgression and regression during the deposition of the upper Cambrian Honey Creek Formation in the southern Oklahoma aulacogen: Texas Christian University unpublished M.S. thesis, 64 p.

McElmoyl, Courtney; and Donovan, R. N., 1993, A transgression–regression event during the deposition of the Upper Cambrian Honey Creek Formation in the Southern Oklahoma aulacogen [abstract]: Geological Society of America Abstracts with Programs, v. 25, no. 1, p. 38.

Rafalowski, M. B., 1984, Sedimentary geology of the Late Cambrian Honey Creek and Fort Sill Formations as exposed in the Slick Hills of southwestern Oklahoma: Oklahoma State University unpublished M.S. thesis, 147 p.

Schatski, N. S., 1946, The Great Donets Basin and the Wichita system—comparative tectonics of ancient platforms: SSSR Akademiya Nauk Izvestia, Geology Series, no. 1, p. 5–62.

Scotese, C. R., 1984, An introduction to this volume: Paleozoic paleomagnetism and the assembly of Pangea, *in* Van der Voo, R.; Scotese, C. R.; and Bonhommet, N. (eds.), Plate reconstruction from Paleozoic paleomagnetism: American Geophysical Union Geodynamics Series, v. 12, p. 1–10.

Stitt, J. H., 1971, Late Cambrian and earliest Ordovician trilobites, Timbered Hills and lower Arbuckle Groups, western Arbuckle Mountains, Murray County, Oklahoma: Oklahoma Geological Survey Bulletin 110, 83 p.

_____1977, Late Cambrian and earliest Ordovician trilobites, Wichita Mountains area, Oklahoma: Oklahoma Geological Survey Bulletin 124, 79 p.

Taff, J. A., 1902, Description of the Atoka quadrangle [Indian Territory]: U.S. Geological Survey Geologic Atlas, folio 79, 8 p.

Tucker, M. E.; and Wright, V. P., 1990, Carbonate sedimentology:

Blackwell Scientific Publications, Oxford, 482 p.
Ulrich, E. O., 1911, Revision of the Paleozoic system: Geological Society of America Bulletin, v. 22, p. 622–627.
_____1932, Preliminary description of the Honey Creek, Fort Sill, Royer, and Signal Mountain formations of Oklahoma: Geological Society of America Bulletin, v. 43, p. 742–747.
Wilson, J. L., 1949, The trilobite fauna of the *Elvinia* zone in the basal Wilberns limestone of Texas: Journal of Paleontology, v. 23, p. 25–44, pls. 9–11.
_____1951, Franconian trilobites of the central Appalachians: Journal of Paleontology, v. 25, p. 617–654, pls. 89–95.
Witzke, B. J., 1980, Middle and Upper Ordovician paleogeography of the region bordering the Transcontinental arch, *in* Fouch, T. D.; and Magathan, E. R. (eds.), Paleozoic paleogeography of the west-central United States Rocky Mountain paleogeography [symposium no. 1]: Society of Economic Paleontologists and Mineralogists, Rocky Mountain Section, p. 1–18.

Boundary between the Fort Sill and Signal Mountain Formations in the Lower Arbuckle Group, Slick Hills: Candidate for a Grand Cycle Boundary

Randall M. Hosey
Cross Timbers Oil Company
Fort Worth, Texas

R. Nowell Donovan
Texas Christian University
Fort Worth, Texas

ABSTRACT.—During the Late Cambrian Epoch (Franconian), a marine transgression inundated southern Oklahoma, flooding a landscape that consisted of hills of Cambrian rhyolite up to 350 m in height. The oldest deposits on this topography, the Timbered Hills Group, initially were siliciclastics—the Reagan Formation. Subsequently, pelmatozoan-rich grainstones served to define the Honey Creek Formation. The passage from the Honey Creek to the overlying Fort Sill Formation of the Arbuckle Group was marked by incoming lime mudstones. Additionally, siliciclastics gradually disappeared upward through the section. The Fort Sill has been divided into three ad-hoc units, the topmost of which is an 80-m-thick complex of thick-bedded light-gray algal boundstones in which varieties of algal boundstone are common. This unit can be traced for more than 30 km in the Slick Hills of southwestern Oklahoma. In the western part of the area it has been extensively dolomitized; isotope data suggest that this dolomitization was initiated in the Late Cambrian or Early Ordovician.

The contact between the Fort Sill and the overlying thinly bedded dark-gray bioclastic limestones of the Signal Mountain Formation is one of the most distinctive horizons in the Arbuckle Group. The contact evidently marks a substantial change in depositional environment. Thus, (1) no boundstones are found in the Signal Mountain, (2) there is an abrupt upward increase in the amount of quartz silt and detrital clay, (3) up to 5% glauconite is found in the basal Signal Mountain, and none in the Fort Sill.

In detail, the contact is sharp and shows evidence of minor erosion, although no penetrative karst has been detected. Small pebbles of a dolomite similar in texture to that found in the underlying Fort Sill also suggest that local erosion of the Fort Sill has taken place, albeit outside the area of exposure.

We suggest that the contact surface records a regression, associated with dolomitization and some erosion. A regression is also indicated by the local occurrence of a laminated tidal-flat unit, with traces of evaporites, that crops out in the far west of the Slick Hills directly below the formation contact. We conclude that the Signal Mountain is a transgressive unit, incorporating siliciclastics transported into the area during the regression. In our view, the unconformity reflects localized tectonism associated with the evolution of the southern Oklahoma aulacogen. This suggestion is supported by subsidence curves indicating that the Signal Mountain marks the period of maximum subsidence in the evolution of the southern Oklahoma aulacogen. On the other hand, the surface appears to correlate with a craton-wide "Sauxian" hiatus and thus is a major sequence boundary. The dramatic difference between the two formations is due to the accelerating rate of subsidence in the aulacogen, whereas the sharp nature of the formational boundary is due to sea-level fluctuation.

INTRODUCTION

The Arbuckle Group, one of the world's thickest sequences of carbonates, has been broken into six formations, of which the Fort Sill and Signal Mountain are the two lowermost (Fig. 1). The contact between these formations is the most distinctive and easily recognizable within the Arbuckle Group. Our study was conducted to determine the geologic significance of this formation boundary.

The study area was confined to the Slick Hills of southwestern Oklahoma (Figs. 2,3). The Slick Hills are an eroded, tectonically disturbed fragment of rocks deposited in the southern Oklahoma aulacogen, a linear lower Paleozoic basin that presently trends N. 60° W. from southeastern Oklahoma into the Texas Panhandle (Schatski, 1946; Donovan, 1986, 1991). Within the parameters of Cambrian–Ordovician paleogeography, the Slick Hills are an inverted segment of a major carbonate platform that inundated a great part of the Laurentian craton (Fig. 4).

Most of the available sections pertinent to this study are in the eastern Slick Hills, where exposure quality is high. The upper 2.5 m of the Fort Sill and the lower 2.5 m of the Signal Mountain were examined in detail at selected sites.

Hosey, R. M.; and Donovan, R. N., 2000, Boundary between the Fort Sill and Signal Mountain Formations in the lower Arbuckle Group, Slick Hills: candidate for a grand cycle boundary, *in* Johnson, K. S. (ed.), Platform carbonates in the southern Midcontinent, 1996 symposium: Oklahoma Geological Survey Circular 101, p. 79–88.

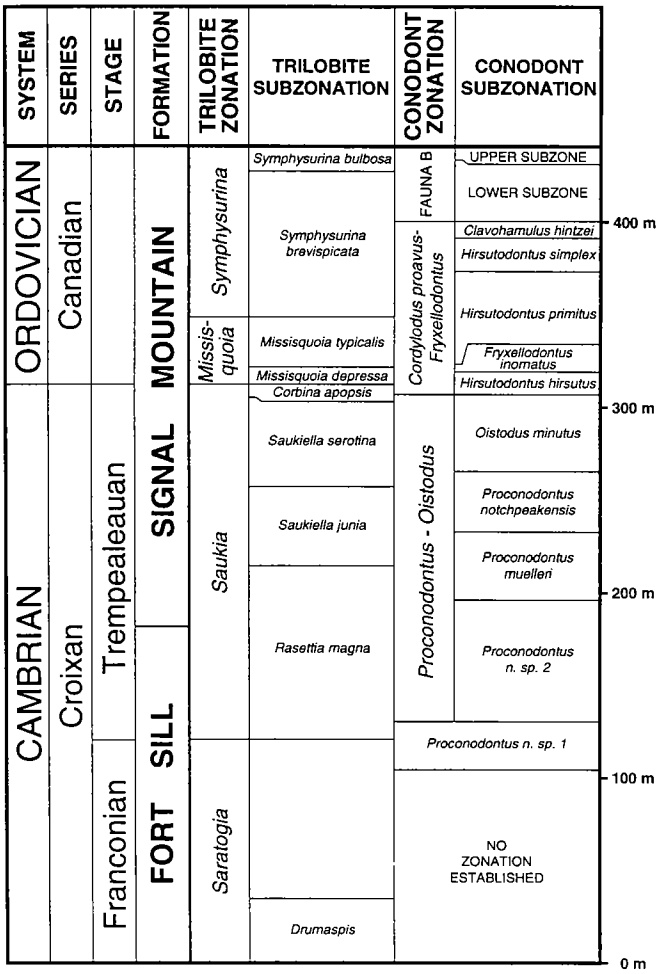

Figure 1. Lower Paleozoic stratigraphy of the Slick Hills. Data from Stitt (1971, 1977), Derby and others (1991).

PALEOLATITUDE AND PALEOCLIMATE

During the Late Cambrian Epoch, Laurentia (North America) was centered astride the equator between latitudes 30° N. and 30° S. (Scotese, 1984). The approximate location of southwestern Oklahoma was between latitudes 8° and 10° S. (Fig. 5). In addition to a cumulative northward drift of ~50°, a cumulative rotation of approximately 70° in a counterclockwise direction has taken place since the Late Cambrian. Assuming that present-day climatological circulation patterns were in effect, the rocks under discussion were deposited in a humid to subarid (tropical to subtropical, with temperatures greater than 20°C) environment (Witzke, 1980).

CHARACTER OF UPPERMOST FORT SILL FORMATION

The Fort Sill Formation is the most lithologically diverse of the Arbuckle Group formations (Taff, 1904; Decker, 1939; Nelms, 1958; Rafalowski, 1984; Donovan, 1986, 1991). Its contact with the underlying Honey Creek Formation of the Timbered Hills Group is taken as the first quantitatively significant incoming of abundant lime mud. Visually, this event marks the development of the monotonously persistent tombstone-weathering motif that characterizes all Arbuckle Group limestones. Whereas the formation contact is defined by the development of micritic limestones, a number of other changes take place at or about this horizon. Thus quartz silt, glauconite, phosphatic brachiopods, and rhyolite fragments are found less frequently, while algae and gastropods become more common. These changes are associated with three events: (1) expansion of the Franconian transgression across the Laurentian craton, (2) burial of the southern Oklahoma archipelago, and (3) a lessening of tidal impact on the platform.

Three ad-hoc members have been recognized in the Fort Sill Formation (Nelms, 1958; Donovan, 1986). The lowest member is a ~120-ft-thick sequence of thinly bedded light-gray cyclic limestones. The middle member displays a series of very thinly bedded dolomitic siltstones that form distinctive ledges at outcrop. The upper member consists of more thickly bedded algal (i.e., stromatolitic) limestones (Fig. 6). This tripartite division is complicated by a massive zone of complete dolomitization that is found in the central part of the upper member (Donovan 1986; Gao, 1990). This dolomite, the Bally Dolomite, is found only in the western Slick Hills, at Zodletone and Bally Mountains (Figs. 3,6). During the present study, a further lithostratigraphic complexity was added by the discovery of a thinly laminated dolomitic limestone unit close to the top of the formation that contains evaporite pseudomorphs and thin collapse breccias. This unit similarly is found only at Zodletone and Bally Mountains (Fig. 7).

With the exception of the aforementioned evaporite unit, the uppermost Fort Sill that was examined in this study is composed of light-gray, thickly bedded algal boundstones in which both stromatolites and thrombolites can be found. Early diagenetic, fabric-selective dolomite is commonly seen and often weathers orange.

Petrographic studies confirm that the uppermost Fort Sill is a lime mudstone–dominated sequence. The principal facies are massive mudstones, laminated algal boundstones, and intraclast-dominated wackestones and packstones. The intraclasts are of algal origin; other details include a few trilobite fragments, even fewer pelmatozoans and gastropods, a little quartz silt, and the alga *Renalcis*. The laminated dolomicrites of the aforementioned thinly laminated unit display evaporite pseudomorphs. Idiotopic dolomite rhombs and, more rarely, baroque (saddle) dolomite are scattered throughout the sections measured but are more common to the west, particularly on Zodletone Mountain.

CHARACTER OF LOWERMOST SIGNAL MOUNTAIN FORMATION

The lowermost Signal Mountain Formation is composed of thinly bedded, dark-gray limestones, similar to those characteristic of the formation as a whole (Whitehead and Donovan, 2000). In essence, the entire formation is constructed of very thin (~5–30-mm) beds in which numerous hardgrounds and abruptly varying facies are a distinctive signature. Individual facies include mudstones, bioclastic mudstones, mudstones with quartz silt, bioclastic wackestones, packstones, and grainstones and intraclast-rich grainstones, wackestones, and packstones as well as mixed allochem assemblages. Specific common fossils include pelmatozoans, trilobites, gastropods,

sponge spicules, and brachiopods; peloids are ubiquitous, quartz silt is locally abundant (as much as 10%), and a variety of intraclasts are present.

All these lithologies and allochems can be found throughout the Signal Mountain; however, there are some additions and deletions in the lowermost beds. For example, the basal beds contain fewer of the dark-gray (and more rarely gray-green) siliciclastic mudstones seen at higher levels in the formation (Whitehead and Donovan, 2000). However, they do contain ooid-rich packstones and grainstones, intraclasts of a dolomite that is similar in texture to the Bally Dolomite, and as much as 5% dark-green peloids of glauconite, all of which are uncommon or absent at higher levels.

A COMPARISON OF THE TWO FORMATIONS

As the preceding description has shown, the contrast between the two formations is stark, in terms of color, facies, and petrography (Fig. 8). In the field, color and bedding are the obvious differences. The Fort Sill is light gray and thickly bedded, whereas the Signal Mountain is brown to dark gray and thinly bedded. In a regional context, the Fort Sill varies somewhat when traced along strike. The principal change is due to the incoming of various types and ages of dolomite to the west. By contrast, the Signal Mountain shows little gross change from place to place.

The most striking petrographic difference is the absence of algal boundstones in the Signal Mountain. The appearance of glauconite and abundant quartz silt also distinguishes this formation. The uppermost Fort Sill contains a simpler fauna of algae, trilobites, and, more rarely, pelmatozoans and gastropods, whereas the Signal Mountain has a higher fossil diversity as well as a far greater total content of bioclasts.

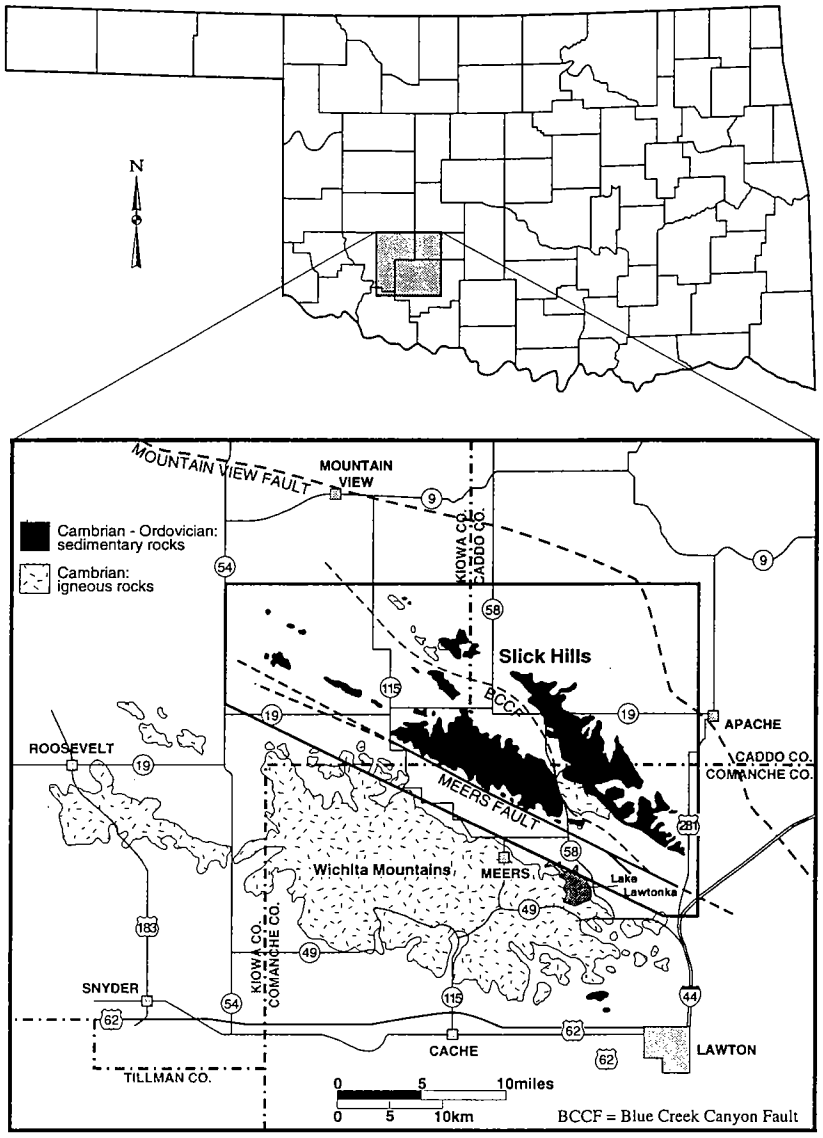

Figure 2. Location map showing relative positions of the Slick Hills and Wichita uplift.

These differences between the two formations occur along a boundary that is extremely sharp, has little erosional relief, and is the most easily recognizable formation contact in the Arbuckle Group (Fig. 9). Why is this, and what happened?

THE ARGUMENTS

Clearly, the differing petrographic characteristics of the two sequences indicate that a profound change in the environment of deposition took place. The initial impression is that the water depth on the Arbuckle platform increased by many meters; as a result, shallow peritidal and supratidal (in the west) conditions gave way to a deeper subtidal setting, below fair-weather wave base (Whitehead and Donovan, 2000). This deeper water supported a vigorous and rich fauna. At the same time, there was a definite increase in the entrapment of, and hence supply of, fine-grained siliciclastics. Mineralogically, the siliciclastics are mature, being dominated by quartz and clay. The source of these grains was almost certainly the Laurentian craton, although the pathways and mechanisms of delivery, whether eolian or fluvial, are unknown. Taken together, these interpretations lead to the conclusion that a major transgression took place at the same time that the catchment area for siliciclastics expanded. Such a scenario is compatible with the overall Late Cambrian history of major transgression across the Laurentian craton.

A closer, but still broad, focus has shown that this history of transgression was punctuated by significant regressive events. Several "grand cycles" were recognized across the craton by Chow and James (1987). Grand cycles are large-scale (tens to hundreds of meters) sedimentary cycles that are related to passive continental margins on which there was an alternation of carbonate-dominated and siliciclastic-dominated sedimentation as a result of sea-level fluctuation (Aitken, 1966, 1981). Chow and James (1987) argued that the cycle bound-

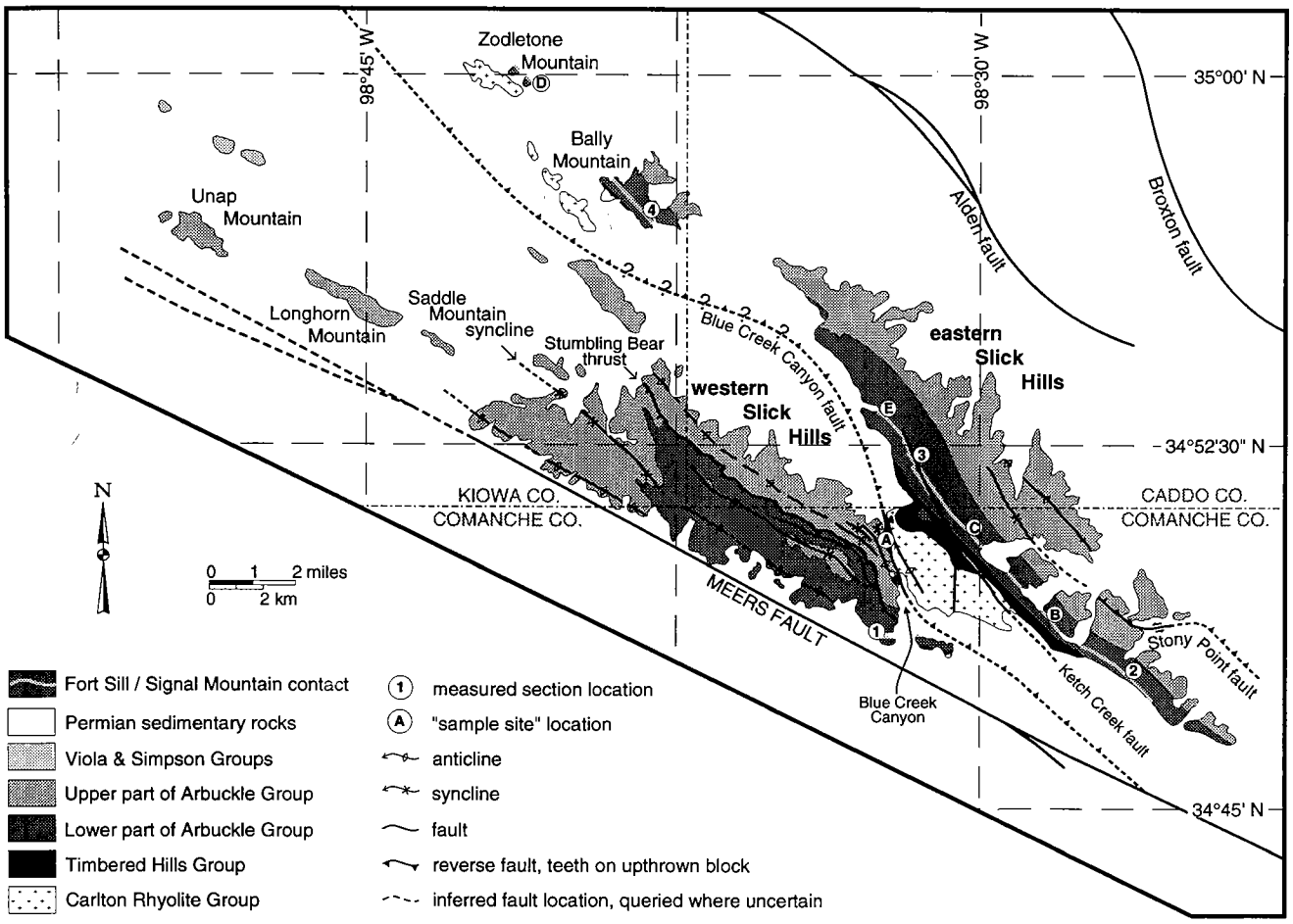

Figure 3. Geologic map of the Slick Hills, showing outcrop of Fort Sill–Signal Mountain boundary and locations of measured sections and sites sampled during this study.

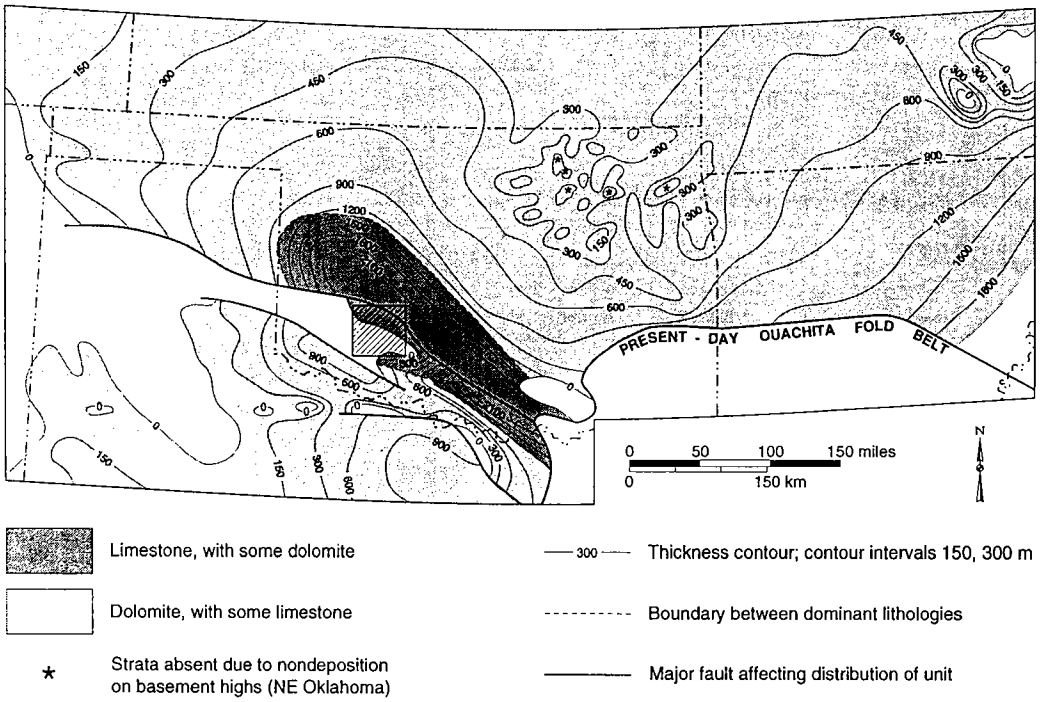

Figure 4. Isopach map of Cambrian–Ordovician carbonates in Oklahoma. Carbonates within the southern Oklahoma aulacogen are mostly limestones, whereas the surrounding craton is mostly dolomite. Box shows location of study area. Modified from Johnson (1991).

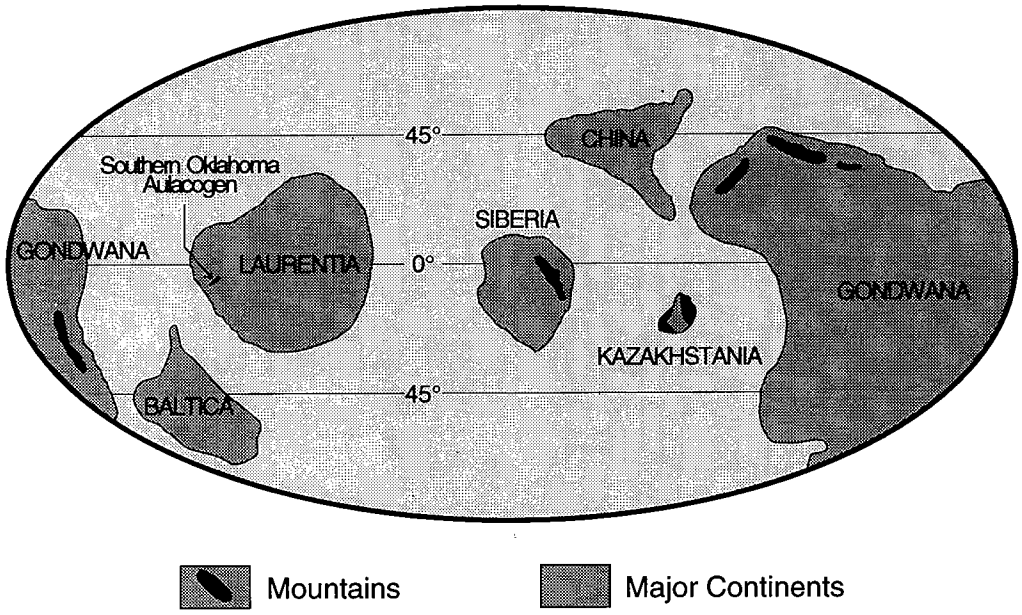

Figure 5. Global paleogeography during the Late Cambrian to Early Ordovician. Data from Witzke (1980) and Scotese (1984).

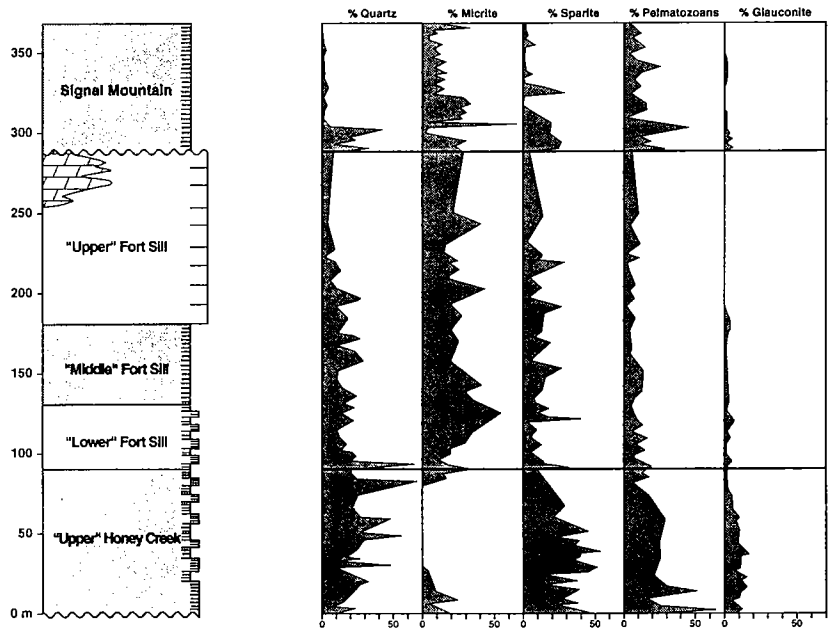

Figure 6. Illustration of the lithostratigraphic subdivision and principal petrographic differences between the upper Honey Creek, Fort Sill, and Signal Mountain Formations. Note position of Bally Dolomite near top of upper Fort Sill. Also note the increase in quartz, sparite, pelmatozoans, and glauconite in the Signal Mountain at the contact. Data from Ditzell (1982) and Rafalowski (1984).

aries correlate with stratigraphic hiatuses that have been identified across North America. In the present context, the Signal Mountain–Fort Sill boundary lies within the *Saukia* Trilobite Zone and the *Proconodontus–Oistodus* Conodont Zone (Fig. 10). This boundary may correlate with a Saukian grand-cycle top observed at numerous localities in North America (Hosey and Donovan, 1993).

Other grand-cycle boundaries have been identified within the Slick Hills, both above and below the boundary postulated here (McElmoyl and Donovan, 1993, 2000; Donovan, 2000), and the concept forms a useful framework for discussion. The base of the cycle during which the Fort Sill was deposited consists of the upper part of the Honey Creek Formation, a sequence comprising mixed siliciclastics and carbonates with abundant glauconite. This sequence records a sustained transgression that gradually inundated the basement and cut off the supply of siliciclastics. The passage from the Honey Creek into the "lower" and "middle" Fort Sill is dominated by meter-scale carbonate-mud-dominated cycles. These smaller cycles may record minor variations in sea level and/or vagaries of sediment organization on the expanding platform. The "upper" Fort Sill boundstones are aggradational and represent a period when the rate of sea-level rise slowed and eventually reversed. In this context, the supratidal deposit in the upper Fort Sill found in the west of the area represents the initial emergence of the carbonate platform during the developing regression. Further regression appears to have resulted in a period of emergence during which large-scale dolomitization, seen as the Bally Dolomite, took place as a result of ground-water mixing stemming from a relative fall in sea level. Chemical and isotopic studies by Gao and Land that indicate an early, though not penecontemporaneous, age for this dolomite, is in accord with the widespread occurrence of dolomite intraclasts in the lowermost Signal Mountain. These intraclasts are lithologically similar to the Bally Dolomite and permit the reasonable inference that somewhere adjacent to the present outcrop—probably to the west—this dolomite was eroded dur-

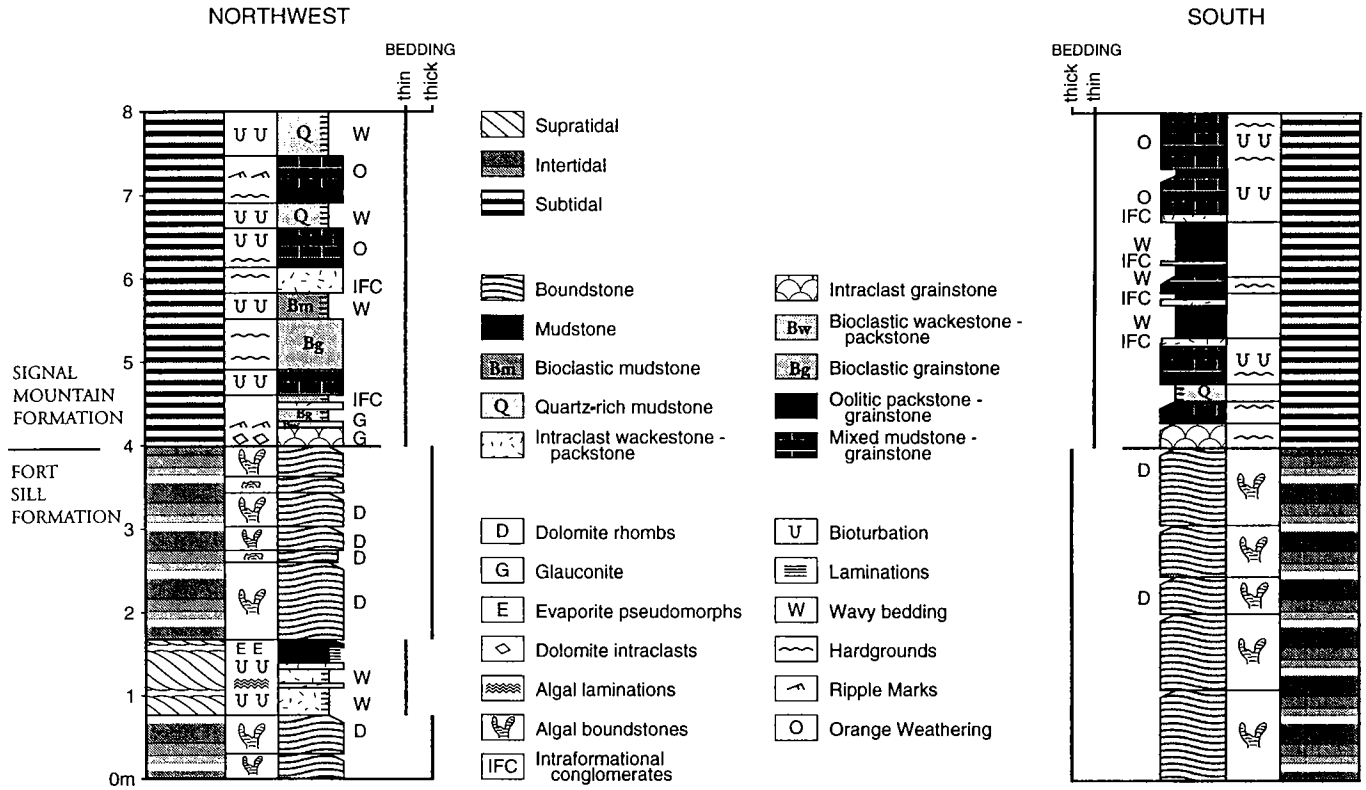

Figure 7. Measured sections of Fort Sill–Signal Mountain contact. The northwest section is from Bally Mountain and shows the supratidal deposit in the upper Fort Sill. The southeast section is from the south end of Blue Creek Canyon.

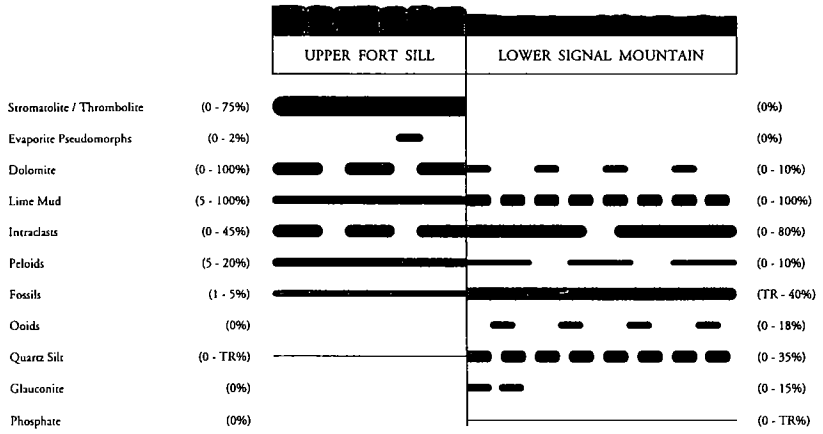

Figure 8. Synoptic comparison of the petrography of the uppermost part of the Fort Sill and lowermost part of the Signal Mountain Formations. A thickness of about 2 m of section is involved in the analysis, which is based on an amalgamation of four measured sections (1–4 in Fig. 3). Thickness of the bars represents relative abundance of the particular constituents. Note that no boundstones are present in the Signal Mountain, and no glauconite in the upper Fort Sill.

ing the hiatus recorded by the formation contact (Fig. 11).

The lowermost Signal Mountain records the beginning of another grand cycle. The appearance of glauconite and quartz silt suggests a transgression across an exposed surface, whereas the lack of penetrative karst and minimal erosion of the Fort Sill indicate that the relative rise in sea level probably involved the rapid flooding of a low-relief surface.

Thus far, the arguments advanced are general and could reasonably be applied to any Sauxian sequence. However, the facies seen in the Signal Mountain Formation suggests that water depth increased dramatically and rapidly. Only for a brief period were ooid-producing conditions developed, while the absence of stromatolites—uniquely within the Arbuckle Group—suggests that the sea bed stayed below the photic zone for a long time. Diagenetically, the formation is distinctive in being the only Arbuckle Group unit in which there was substantial early cementation under reducing conditions, as evidenced by ferroan calcite and dolomite cements.

The Signal Mountain Formation appears to be laterally restricted to the general area of the southern Oklahoma aulacogen (Donovan, 2000). Subsidence curves, both from wells in southern Oklahoma (Feinstein, 1981) and from surface logging in the Slick Hills (Donovan, 1986), indicate that subsidence rates increased dramatically during Signal Mountain deposition (Fig. 11). The increased subsidence may or may not be related to reactivation of basin-margin faults (Fig. 12). What can be inferred is that the aulacogen was redefining itself as a depocenter at the same time as the Sauxian transgression proceeded.

GENERAL CONCLUSIONS

Several factors influenced carbonate deposition within the southern Oklahoma aulacogen. These include (1) an initial irregular topography, (2) increasing size of the carbonate plat-

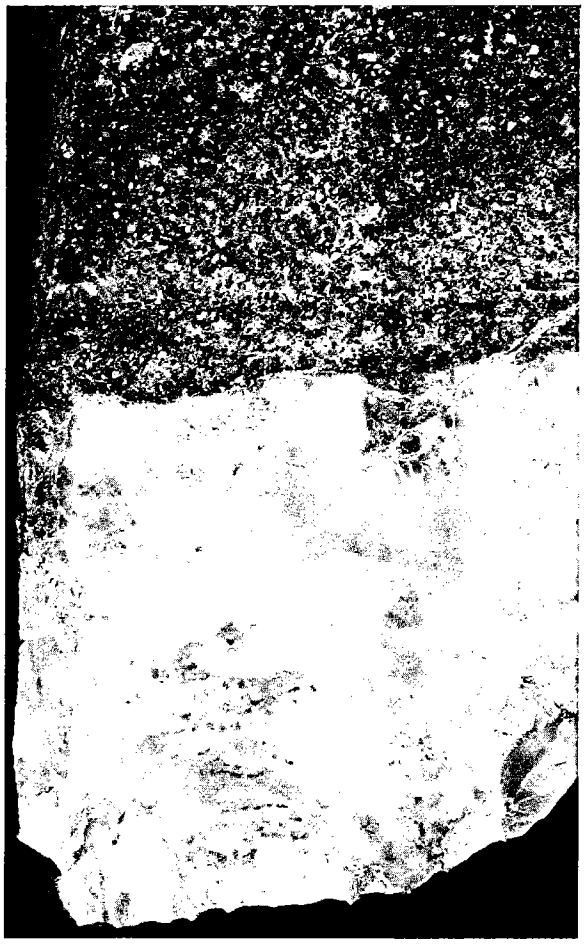

Figure 9. Photograph of a slab across the Fort Sill–Signal Mountain contact. The Fort Sill is light gray and stromatolitic. The Signal Mountain is coarse grained, with large fossil fragments visible. Vertical length of photo is about 10 cm.

form, (3) local tectonic development of the aulacogen, and (4) eustatic sea-level changes (Donovan, 2000).

The Timbered Hills Group and the lower and middle Fort Sill were deposited on a landscape that consisted of rhyolite hills. By the time that the Signal Mountain Formation was deposited, the irregular topography was probably buried and therefore did not influence the deposition of the upper Fort Sill or the Signal Mountain (Fig. 13).

The size and character of the platform subsequently were controlled both by development of the aulacogen and by sea-level changes. In this context, the Fort Sill–Signal Mountain contact is a record of regression, emergence, and transgression that coincides with an increased rate of basin subsidence associated with the definition of the southern Oklahoma aulacogen. As a result, water depth increased relatively rapidly. The regression appears to relate to a craton-wide event—the Saukian hiatus (Fig. 14).

ACKNOWLEDGMENTS

We are grateful to the following landowners for their support: Mr. and Mrs. D. Kimbell, Mr. D. Leatherbury, Mr. and Mrs. J. Worley, Mr. D. Farris, and Mrs. and the late Mr. J. Kindblade. We gratefully acknowledge financial and logistical support from the Mobil Foundation, the Adkins Fund, Texas Christian University, and the Moncrief family.

REFERENCES CITED

Aitken, J. D., 1966, Middle Cambrian to Middle Ordovician cyclic sedimentation, Southern Rocky Mountains of Alberta: Canadian Petroleum Geology Bulletin, v. 14, p. 405–441.

_____1981, Generalizations about grand cycles, *in* Taylor, M. E. (ed.), Short papers for the Second International Symposium on the Cambrian System: U.S. Geological Survey Open-File Report 81-743, p. 8–14.

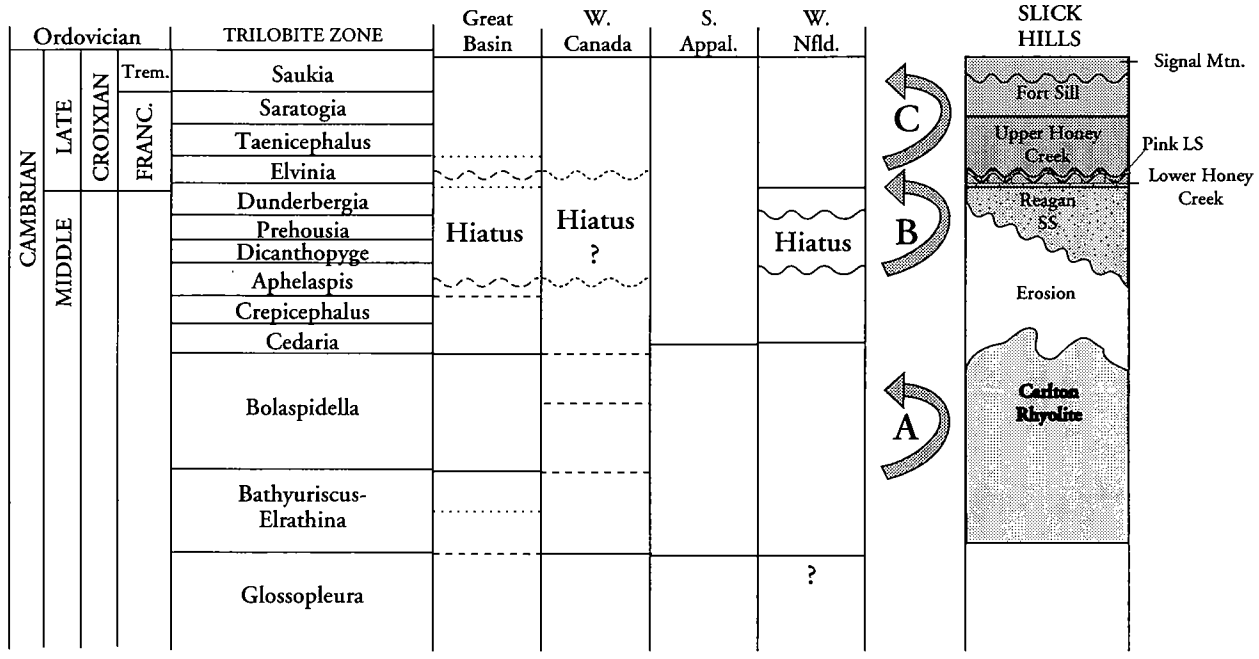

Figure 10. Integration of data from the Slick Hills into the concept of Laurentian grand cycles. Modified from Chow and James (1987).

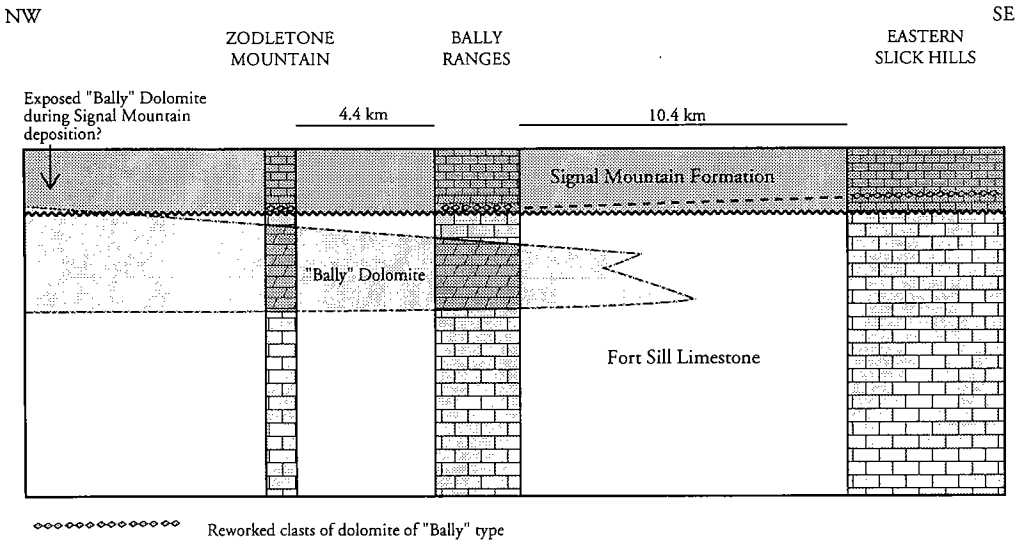

Figure 11. Cross section showing the relationship of the Bally Dolomite within the upper Fort Sill. To the northwest, the Bally Dolomite is a conspicuous development in the upper Fort Sill; dolomitization affects increasingly younger parts of the section to the northwest; dolomite clasts appear higher in the basal Signal Mountain to the southeast. We infer increasing erosion beneath the Signal Mountain hiatus to the northwest.

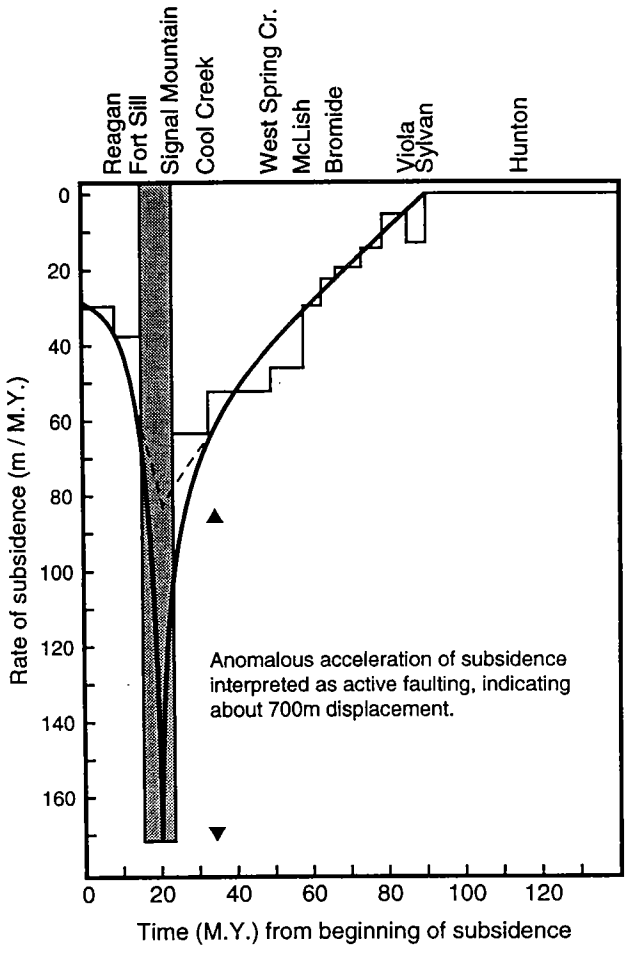

Figure 12. Subsidence rates for the southern Oklahoma aulacogen. The acceleration of subsidence during Signal Mountain deposition is anomalously high and may represent local tectonic adjustment of the aulacogen faults. Data from Feinstein (1981).

Chow, N.; and James, N. P., 1987, Cambrian grand cycles: a northern Appalachian perspective: Geological Society of America Bulletin, v. 98, p. 418–429.

Decker, C. E., 1939, Two lower Paleozoic groups, Arbuckle and Wichita Mountains, Oklahoma: Geological Society of America Bulletin, v. 50, p. 1311–1322.

Derby, J. R.; Bauer, J. A.; Creath, W. B.; Dresbach, R. I.; Ethington, R. L.; Loch, J. D.; Stitt, J. H.; McHargue, T. R.; Miller, J. F.; Miller, M. A.; Repetski, J. E.; Sweet, W. C.; Taylor, J. F.; and Williams, Mark, 1991, Biostratigraphy of the Timbered Hills, Arbuckle, and Simpson Groups, Cambrian and Ordovician, Oklahoma: a review of correlation tools and techniques available to the explorationist, *in* Johnson, K. S. (ed.), Late Cambrian–Ordovician geology of the southern Midcontinent, 1989 symposium: Oklahoma Geological Survey Circular 92, p. 15–41.

Ditzell, C. L., 1982, Sedimentary geology of the Cambro–Ordovician Signal Mountain Formation as exposed in the Wichita Mountains of southwestern Oklahoma: Oklahoma State University unpublished M.S. thesis, 165 p.

Donovan, R. N., 1986, The geology of the Slick Hills, *in* Donovan, R. N. (ed.), The Slick Hills of southwestern Oklahoma—fragments of an aulacogen?: Oklahoma Geological Survey Guidebook 24, p. 1–12.

_____1991, The Arbuckle Group—an *aide de mémoire, in* Johnson, K. S. (ed.), Arbuckle Group core workshop and field trip: Oklahoma Geological Survey Special Publication 91-3, p. 199–208.

_____2000, Initiation of the Arbuckle platform—view from the Slick Hills, Oklahoma, *in* Johnson, K. S. (ed.), Platform carbonates in the southern Midcontinent, 1996 symposium: Oklahoma Geological Survey Circular 101 [this volume], p. 47–56.

Donovan, R. N.; and Ragland, D. A., 1986, Paleozoic stratigraphy of the Slick Hills, southwestern Oklahoma, *in* Donovan, R. N. (ed.), The Slick Hills of southwestern Oklahoma—fragments of an aulacogen?: Oklahoma Geological Survey Guidebook 24, p. 13–16.

Feinstein, S., 1981, Subsidence and thermal history of southern Oklahoma aulacogen: implications for petroleum exploration: American Association of Petroleum Geologists Bulletin, v. 65, p. 2521–2533.

Gao, G., 1990, Geochemical and isotopic constraints on the diagenetic history of a massive stratal, Late Cambrian (Royer) dolo-

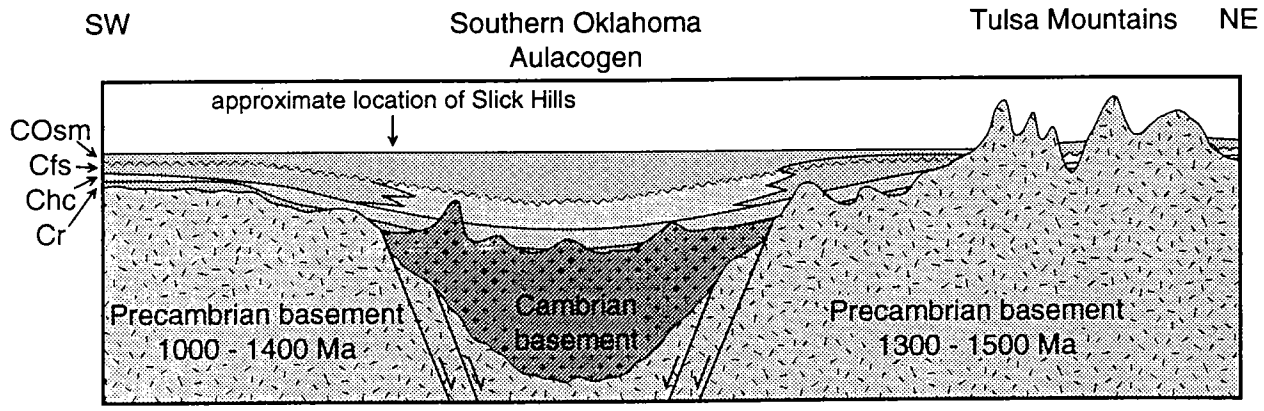

STAGE III - Reactivation of basin margin faults and deposition of Cambro-Ordovician Signal Mountain Formation in deeper waters? (Trempealeauan - Canadian)

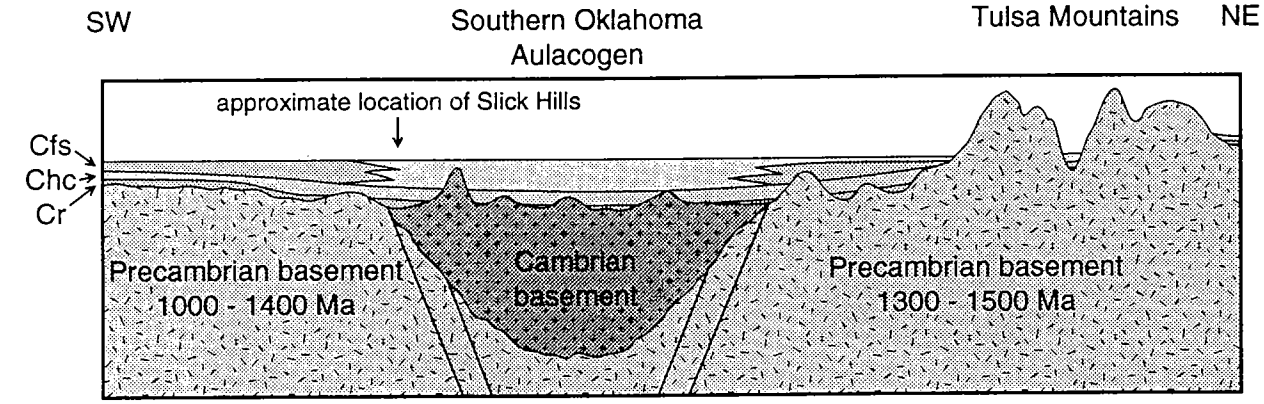

STAGE II - Deposition of Cambrian Timbered Hills Group and Cambrian Fort Sill Formation. (Franconian)

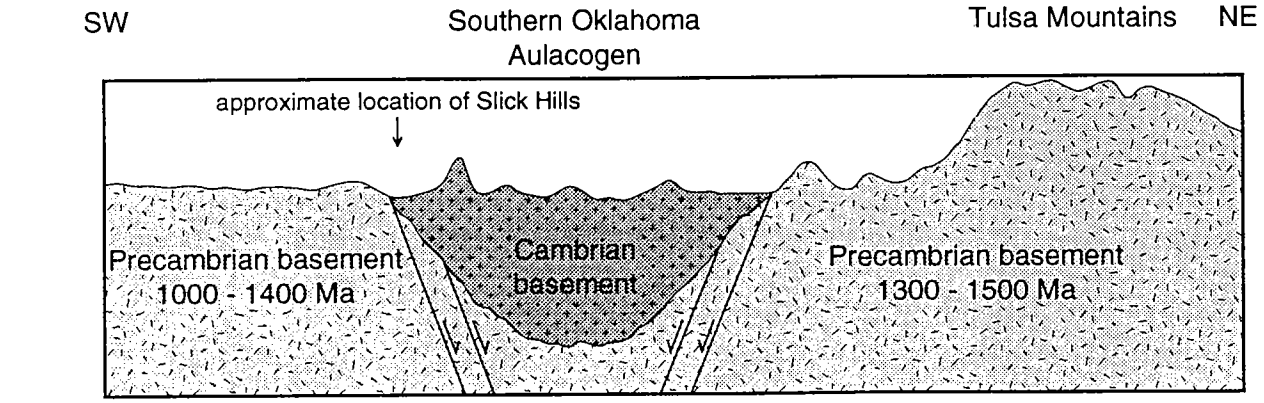

STAGE I - Development of rift basin. (Middle Cambrian)

Figure 13. Cross sections from southwest to northeast through the southern Oklahoma aulacogen. The sections show the interpreted stages of evolution of the aulacogen by reactivation of basin-margin faults during the Cambrian and Ordovician. *COsm* = Signal Mountain; *Cfs* = Fort Sill; *Chc* = Honey Creek; *Cr* = Reagan.

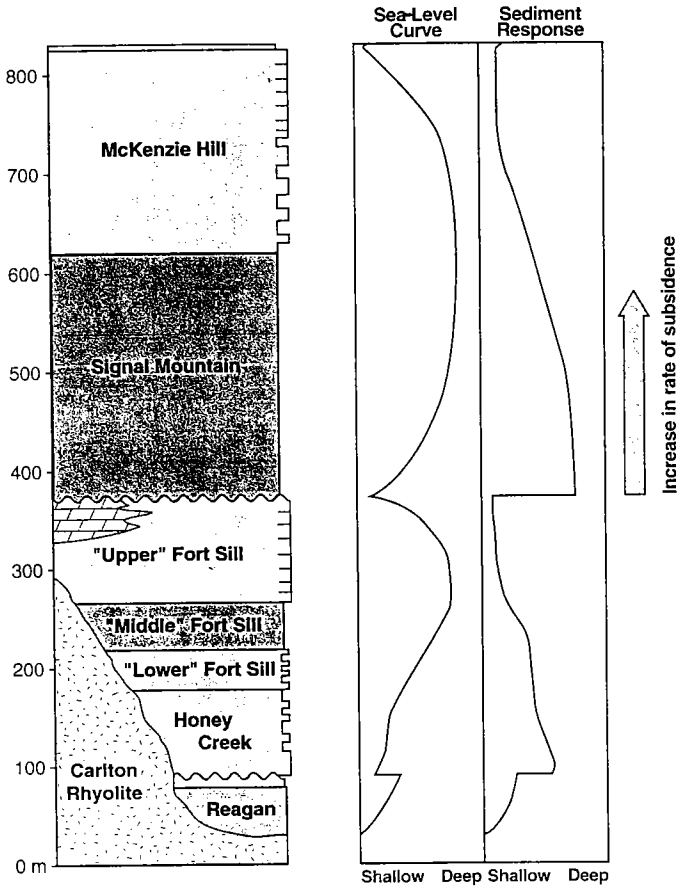

Figure 14. Interpreted sea-level curves for the Timbered Hills and lower Arbuckle Groups. Sediment response refers to the water depth at which sediments were deposited (intertidal, subtidal). Thicknesses from Donovan and Ragland (1986).

mite, Lower Arbuckle Group, Slick Hills, SW Oklahoma, USA: Geochimica et Cosmochimica Acta, v. 54, p. 1979–1989.

Hosey, R. M.; and Donovan, R. N., 1993, The geological significance of the boundary between the Fort Sill and Signal Mountain Formations in the lower Arbuckle Group (Cambrian) [abstract]: Geological Society of America Abstracts with Programs, v. 25, no. 1, p. 14–15.

Johnson, K. S., 1991, Geologic setting of the Arbuckle Group in Oklahoma, *in* Johnson, K. S. (ed.), Arbuckle Group core workshop and field trip: Oklahoma Geological Survey Special Publication 91-3, p. 3–7.

McElmoyl, Courtney, 1993, Transgression and regression during the deposition of the Upper Cambrian Honey Creek Formation in the southern Oklahoma aulacogen: Texas Christian University unpublished M.S. thesis, 64 p.

McElmoyl, Courtney; and Donovan, R. N., 1993, A regression–transgression event during the deposition of the Upper Cambrian Honey Creek Formation in the southern Oklahoma aulacogen [abstract]: Geological Society of America Abstracts with Programs, v. 25, no. 1, p. 38.

_____2000, Unconformity in the lower part of the Cambrian Honey Creek Limestone, Slick Hills, Oklahoma: candidate for a grand cycle boundary, *in* Johnson, K. S. (ed.), Platform carbonates in the southern Midcontinent, 1996 symposium: Oklahoma Geological Survey Circular 101 [this volume], p. 65–78.

Nelms, J. L., 1958, The Fort Sill formation of the Wichita Mountains, Oklahoma: University of Oklahoma unpublished M.S. thesis, 91 p.

Rafalowski, M. B., 1984, Sedimentary geology of the Late Cambrian Honey Creek and Fort Sill Formations as exposed in the Slick Hills of southwestern Oklahoma: Oklahoma State University unpublished M.S. thesis, 147 p.

Schatski, N. S., 1946, The great Donets basin and the Wichita system: comparative tectonics of ancient platforms: S.S.R. Akademiya Nauk Icvestichiya Geologia serie 6, no. 1, p. 5–62.

Scotese, C. R., 1984, An introduction to this volume: Paleozoic paleomagnetism and the assembly of Pangea, *in* Van der Voo, R.; Scotese, C. R.; and Bonhommet, N. (eds.), Plate reconstruction from Paleozoic paleomagnetism: American Geophysical Union Geodynamics Series, v. 12, p. 1–10.

Stitt, J. H., 1971, Late Cambrian and earliest Ordovician trilobites, Timbered Hills and lower Arbuckle Groups, western Arbuckle Mountains, Murray County, Oklahoma: Oklahoma Geological Survey Bulletin 110, 83 p.

_____1977, Late Cambrian and earliest Ordovician trilobites, Wichita Mountains area, Oklahoma: Oklahoma Geological Survey Bulletin 124, 79 p.

Taff, J. A., 1904, Preliminary report on the geology of the Arbuckle and Wichita Mountains: U.S. Geological Survey Professional Paper 31, 81 p.

Whitehead, R. E.; and Donovan, R. N., 2000, Four hundred feet of core from the Cambrian Signal Mountain Formation, Slick Hills, Oklahoma, *in* Johnson, K. S. (ed.), Platform carbonates in the southern Midcontinent, 1996 symposium: Oklahoma Geological Survey Circular 101 [this volume], p. 89–95.

Witzke, B. J., 1980, Middle and Upper Ordovician paleogeography of the region bordering the Transcontinental arch, *in* Fouch, T. D.; and Magathan, E. R. (eds.), Paleozoic paleogeography of the west-central United States, Paleogeography Symposium 1: Society of Economic Paleontologists and Mineralogists, Rocky Mountain Section, Denver, p. 1–18.

Four Hundred Feet of Core from the Cambrian Signal Mountain Formation, Slick Hills, Oklahoma

Richard E. Whitehead and R. Nowell Donovan
Texas Christian University
Fort Worth, Texas

ABSTRACT.—The Dolese Bros. Co. has kindly made available two core sections, each 200 ft thick, that penetrate the middle part of the Signal Mountain Formation, the second lowest division of the Arbuckle Group. The cores do not overlap; recovery is complete. They were obtained from the company's Richard's Spur property in the southern part of the eastern Slick Hills. The cores are important, as they partially cover a formation that is the most poorly exposed of all the Arbuckle units.

During our ongoing investigation of the core, we have noticed the following general features:

1. All beds are very thin, generally less than 3 cm.

2. Substantial diagenetic modification of the section has occurred, mostly seen as dissolution seams, stylolites, and lenticular (wavy) bedding. Where the percentage of shale is high, some limestone lenses were rotated and penecontemporaneously faulted. The net loss of carbonate is great, and the diagenetic impact so profound, that recognition of primary depositional features is not always possible.

3. The section contains much more siliciclastic detritus than is usually the case for the Arbuckle Group. Both black and, less commonly, olive-green (illitic) shales are present as numerous centimeter-thick interbeds with lenticular limestone.

4. Hydrodynamic sedimentary structures are rare and are restricted to small-scale cross-bedding and parallel lamination.

5. The most commonly seen carbonate textures are gradations of mudstones, wackestones, and packstones.

6. Sequences rich in grainstones are found at intervals throughout the section; hardgrounds are associated with this lithology.

7. We have recognized five distinct lithologies in the core. Although three of these lithologies are repeated on a frequent (<1-m) basis, the sequence does not show the compelling evidence of cyclicity that characterizes much of the rest of the Arbuckle Group.

The entire section is a relatively deep-water deposit. An absence of algal boundstones and stromatolites, etc., suggests that the bottom may have been not only below wave base but also below the photic zone. The Signal Mountain was deposited during the most rapid subsidence of the southern Oklahoma aulacogen; evidently, subsidence rates were great enough to challenge the potency of the Arbuckle carbonate factory.

Some tectonic features of interest include the preferential siting of tectonic fracturing and vein development in the grainstone lithologies. In addition, the green-shale-bearing lithology is a focus for tectonic disturbance. Assuming the widespread occurrence of this type of lithology, green-shale-rich sequences may have formed the décollement for the thrust and fold horizons that are such conspicuous features of the western Slick Hills.

INTRODUCTION

The Signal Mountain Formation is the most enigmatic of the six limestone formations that have been recognized in the Arbuckle Group. In common with the Fort Sill and McKenzie Hill Formations, the Signal Mountain was named by reference to topographic features in the Lawton area, where scattered outcrops of various parts of the Arbuckle Group peek out from beneath a veneer of Permian siliciclastics. A more complete sequence is exposed 20–30 mi northwest of Lawton, in the Slick Hills (Fig. 1; Donovan, 1986; Donovan and Ragland, 1986). In the eastern Slick Hills, an essentially homoclinal sequence of the lowest five formations of the Arbuckle Group dips to the northeast at 15°–70°. This sequence displays the finest available natural exposures of the lower Arbuckle Group, particularly the lowermost three formations. Detailed biostratigraphic work in this area has placed the Cambrian–Ordovician boundary in the central part of the Signal Mountain Formation (Stitt, 1977).

The enigmatic characteristics of the Signal Mountain Formation are threefold:

1. Although clearly a limestone formation, the Signal Mountain differs in lithological detail from all the other formations in the Arbuckle Group. The most obvious difference is in aver-

Whitehead, R. E.; and Donovan, R. N., 2000, Four hundred feet of core from the Cambrian Signal Mountain Formation, Slick Hills, Oklahoma, *in* Johnson, K. S. (ed.), Platform carbonates in the southern Midcontinent, 1996 symposium: Oklahoma Geological Survey Circular 101, p. 89–95.

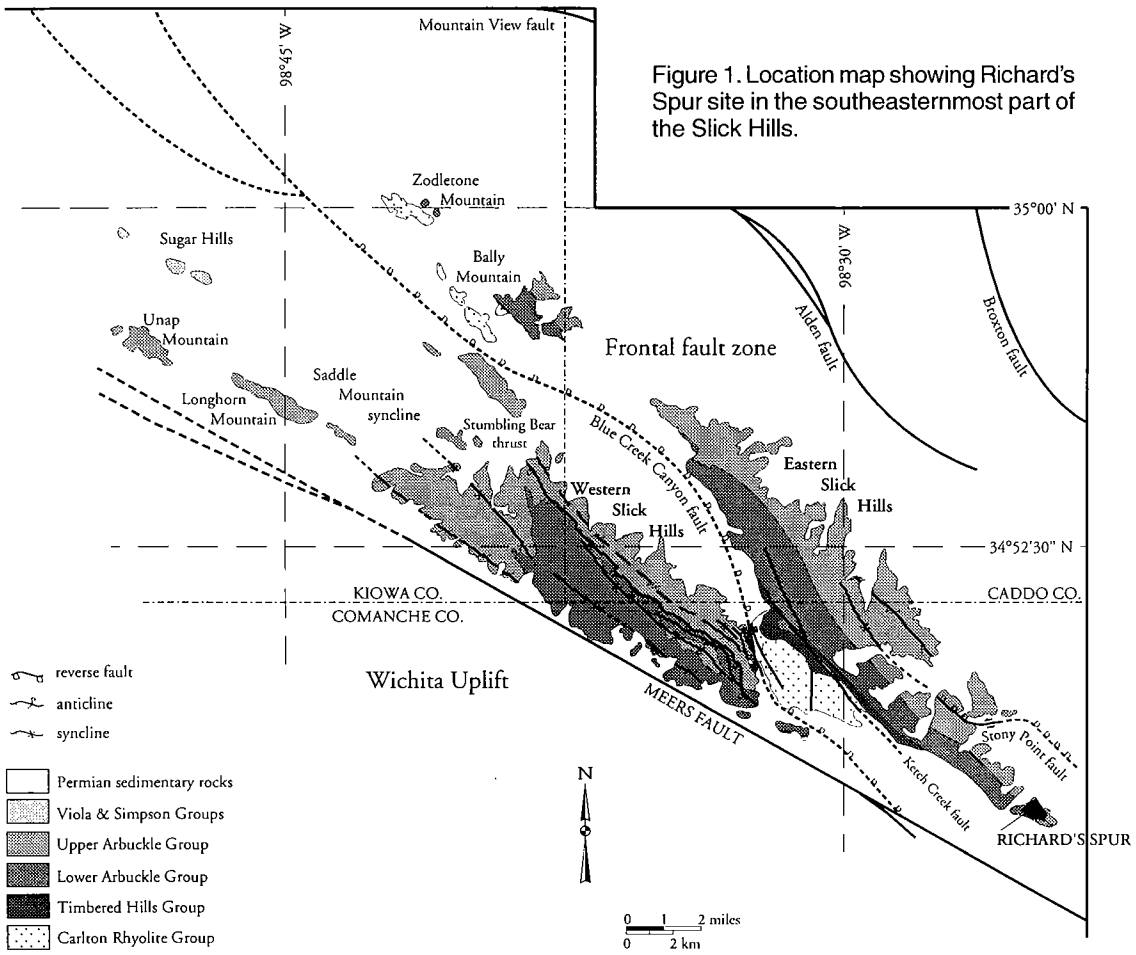

Figure 1. Location map showing Richard's Spur site in the southeasternmost part of the Slick Hills.

age bed thickness; whereas bed thickness in the other formations may reach 3 ft, it is unusual for a bed to be more than 3 in. thick in the Signal Mountain. One of the consequences of this is that Signal Mountain outcrops are not characterized by the well-known "tombstone" topography that characterizes the rest of the Arbuckle Group. As a result, the Signal Mountain is generally the most poorly exposed formation in the group.

2. The suite of limestone facies found, in varying proportions, in the rest of the Arbuckle Group—algal boundstones, oolitic and supratidal facies, etc.—is not found in the Signal Mountain. Clearly, within the general framework of the Arbuckle platform, the depositional environment in which this formation was laid down had unique features.

3. The thinly bedded character of the Signal Mountain has important structural consequences. During the Pennsylvanian deformation that created the structural dispositions in the Slick Hills, the formation was the preferred horizon of detachment in the Arbuckle Group. This function as a décollement, a consequence of the thinly bedded character of the formation, resulted in much bedding-parallel dislocation in many areas.

The Dolese Bros. Co. has kindly made available two core sections, each 200 ft thick, which penetrate the middle part of the formation. The cores do not overlap; recovery is complete. There is little tectonic disturbance of the cores. They were obtained from the company's Richard's Spur property in the southern part of the eastern Slick Hills, a few hundred yards north of the company's major quarry at Richard's Spur (Ayan and others, 2000). The dip in the immediate vicinity is 40°–50° to the northeast. Our purpose here is to provide a preliminary report on features observed in the cores, prior to a complete evaluation of the entire formation in the area.

DESCRIPTION OF THE CORE SEQUENCE

Our study of the core is conventional—slabbing, etching, staining, and insoluble-residue and thin-section analysis. During our ongoing investigation, we have noticed the following general features:

(a) The general characteristics of the core are typical of those seen at outcrop throughout the Slick Hills.

(b) All beds are very thin, generally <3 cm. Bed boundaries are generally clearly defined.

(c) The principal lithologies (Figs. 2–4) are as follows:

i. Lime mudstones with variable amounts of peloids, intraclasts, and fossils. The most common textures are gradations of mudstones, wackestones, and packstones.

ii. Grainstones, also with variable amounts of peloids, intraclasts, and fossils. Hardgrounds are associated with this lithology.

iii. Black to dark-gray shales, with variable amounts of quartz silt.

iv. Gray-green (illitic) shales.

(d) Abundant fossils in the Signal Mountain include trilo-



Figure 2. Small-scale penecontemporaneous compressional fault cutting a bioclastic grainstone that is overlain by quartz-silt-rich carbonate mudstone. Width of view, 12 mm.



Figure 3. Bioclast and intraclast mudstone with substantial quartz silt. In the center is the problematical trace fossil *Cylindrichnus concentricus*. This trace fossil may owe its distinctive appearance to passive or draft infilling rather than to activities of the burrowing animal. Width of view, 12 mm.



Figure 4. Laminated and bioturbated lime mudstone/quartz silt. Depth of view, 12 mm.

bites, brachiopods, echinoderms, and gastropods. Although some fossils are broken, many, including thin-shelled trilobites, are complete.

(e) Sorting of allochems, even in grainstones, is generally poor.

(f) The formation contains much insoluble residue—up to 25% angular quartz silt, clay, and organic material.

(g) Sedimentary structures indicative of current action are rare and are restricted to small-scale cross-bedding and parallel lamination. Strata characterized by grading suggest that gravity settling onto a motionless sea bed was commonplace.

(h) Bioturbation—generally horizontal burrowing—has disturbed a few of the mudstone textures (Figs. 3,4).

(i) Substantial diagenetic modification of the section has occurred, mostly seen as dissolution seams, stylolites, and the resulting development and enhancement of lenticular (wavy) bedding (Bucheit and Donovan, 2000). Where the percentage of shale was high, some limestone lenses were rotated and penecontemporaneously faulted (Figs. 5–7). The net loss of carbonate has been so great and the diagenetic impact so profound, that it is not always possible to recognize primary depositional features.

(j) In most grainstones, cements are zoned from non-ferroan to ferroan. In a few cases, late ferroan baroque dolomite is present. In many of the mud-supported textures, a proportion of the matrix is ferroan micrite (Fig. 8). In addition, rhombs of ferroan calcite are commonly seen in the siliciclastic shale layers.

We have recognized five lithological associations in the core (Fig. 9), all of which involve alternation of the four basic lithologies recognized above (c i–iv).

1. Black shales (c iii), alternating with lime mudstones and wackestones (c i) (Fig. 5).

2. Black shales (c iii), alternating with packstones and wackestones (c i). The difference between 1 and 2 is basically the proportions of allochems, particularly bioclasts in lithology (c i) (Fig. 6).

3. Lime mudstones, wackestones, and packstones (c i), confused by a comprehensive network of stylolites, some parallel to bedding, others subvertical (Fig. 7). This lithological association differs from 1 and 2 in containing less insoluble residue, i.e., shales.

4. Sequences of grainstones (c ii), with bed boundaries



Figure 5. Black to dark-gray shale interbedded with mudstone–wackestone textures (lithological association 1). Etched core slab shows convincing evidence of flowage and dissolution. Depth of view, 5 in.



Figure 6. Wackestones and packstones interbedded with black to dark-gray shales (lithological association 2). Etched slab shows evidence of near-contemporary faulting. Depth of view, 5 in.

defined by hardgrounds. This lithological association is rarely more than 1 ft thick; it is generally cut by thin calcite veins that are normal to bedding.

5. Gray-green shales (c iv) alternating with lime mudstones, wackestones, and packstones (c i). Only one thickness of this lithology has so far been encountered; it is the site of the greatest amount of tectonic deformation in the core.

Although three of these lithologies (1, 2, and 4) are repeated on a frequent (<1-m) basis in parts of the core, the sequence does not show the clear evidence of cyclicity that characterizes much of the rest of the Arbuckle Group.

DISCUSSION

Depositional Environment

The core is the record of a large number of frequently repeated small-scale events. The principal sources of sediment for these events appear to have been (1) an eolian or fluvial system that supplied silt and clay-sized siliciclastics on a regular basis; (2) a lively platform, subject to storms, colonized by a wide variety of organisms and capable of producing much lime mud; and (3) plankton.

The general environment of deposition was probably a low-energy subtidal carbonate platform, generally below the photic zone. As noted previously, the most commonly seen carbonate textures are gradations of mudstones, wackestones, and packstones. The absence of sorting in such deposits indicates that the sea bottom was generally below fair-weather wave base. Grading in some mud-supported textures suggests either a storm or density-flow origin for some beds. The abundance of lime-mud intraclasts is testimony to considerable reworking of a partially lithified sea bed, not necessarily at depth. The accumulation of these mud-supported facies was frequently interrupted by incursions of fine-grained siliciclastics deposited by gentle currents. The short (6–18-in.) sequences of grainstones with hardgrounds probably were generated by bottom currents strong enough to remove mud but not powerful enough to sort allochems effectively.

Greenish-gray clay beds may have been deposited at a time when the sea bottom was efficiently oxygenated. More usually, ferroan cements and the preservation of carbon suggest that the reduction–oxygenation boundary was near the sediment–water interface. Burrowing organisms were probably restricted to the top few inches of sediment.



Figure 7. Lime mudstone cut by numerous ramifying stylolites (lithological association 3). This lithology is the most impoverished with respect to both allochems and siliciclastic detritus. Depth of view, 5 in.



Figure 8. This photomicrograph illustrates the commonly observed partitioning effect of both vertical and bedding-parallel stylolites. The vertical stylolite in the center acted as a partition between ferroan (left) and non-ferroan cements. Depth of view, 3 mm.

Distinctiveness of the Signal Mountain Formation Facies

The Signal Mountain facies described above is distinctively different from facies found in the rest of the Arbuckle Group. A comparison of the Signal Mountain and Cool Creek Formations effectively illustrates this point.

One way of discriminating between the two formations is by variation in allochem type (Fig. 10). For example, whereas ooids are rarely seen in the Signal Mountain, except near its base, they are abundant in the Cool Creek, commonly forming sand shoals up to 1 m thick. On the other hand, fossils are plentiful in the Signal Mountain (trilobites, brachiopods, echinoderms, and gastropods all being abundant), whereas gastropods are the only common fossil in the Cool Creek.

Algal boundstones are a common feature of the Cool Creek but appear to be entirely absent from the Signal Mountain. Likewise, penecontemporaneous dolomite, chert, and evaporite traces are common in the Cool Creek but are rare or absent in the Signal Mountain. Although both formations contain siliciclastics, the Cool Creek is characterized by medium to coarse sand grains, whereas the coarsest grains in the Signal Mountain are silt size. Finally, the black-shale facies is unique to the Signal Mountain.

Basin Controls Operating During Deposition of the Signal Mountain Formation

The Arbuckle Group was deposited during a period of widespread transgression across the Laurentian craton. However, this overall scenario was interrupted on at least two occasions by widespread regression (McElmoyl and Donovan, 1993, 2000; Hosey and Donovan, 1993, 2000). In southern Oklahoma, the later of these regressions provides a clear demarcation of the base of the Signal Mountain Formation. In the Slick Hills, this regression resulted in a short-lived emergence of the platform.

At the same time that the "Signal Mountain" transgression recommenced, the definition of the lower Paleozoic southern Oklahoma aulacogen accelerated (Fig. 11). In essence, the Signal Mountain was deposited during the period of greatest basin subsidence in the developing aulacogen. The net result of renewed transgression, plus an increased rate of basin definition, was that the rate of sedimentation was stretched to keep pace with the increase in water depth. Hence, facies definition in the formation was poor: all lithologies appear to be

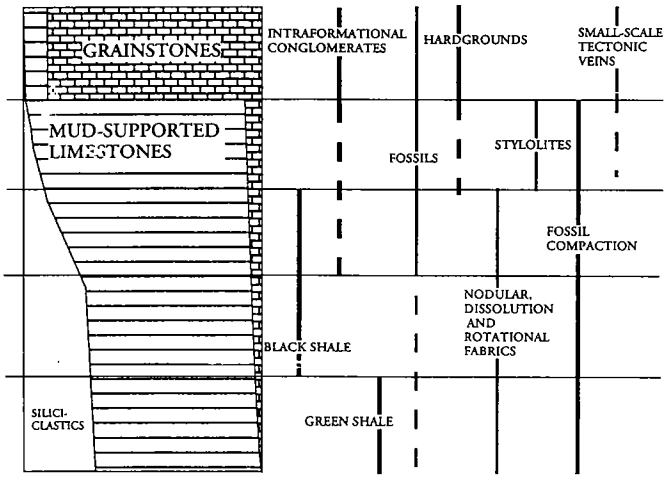

Figure 9. Generalized characteristics of lithological associations recognized in the core.

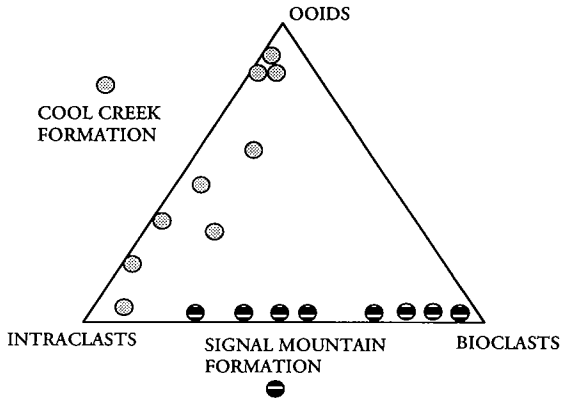

Figure 10. Triangular diagram discriminating allochem distributions typical of the Signal Mountain Formation from those typical of the Cool Creek Formation.

subtidal, and, to date, we have found no evidence of emergence.

The upper boundary of the Signal Mountain (with the McKenzie Hill Formation) is more difficult to place than the lower (Stitt, 1977; Donovan and Ragland, 1986). In essence, the thinly bedded Signal Mountain facies is increasingly interrupted by algal boundstones, a development that is compatible with a gradually slowing rate of subsidence and/or a decreasing rate of transgression, either or both of which would have led to a gradual decrease in water depth.

The Signal Mountain is likely to be a restricted facies, since it owes its definition in part to the tectonic evolution of the southern Oklahoma aulacogen. For example, Whiteside and McCommons (1991) found only 130 ft of the formation in the No. 1 Running High Ranch well in Montague County, north Texas. The organic-carbon content of the core at present is under investigation, and it may be quite high.

Tectonic Patterns

The cores are cut by a number of small faults and fractures at several levels, but particularly in greenish-gray shale/carbonate lithological association 5 (see above). This lithology is the weakest in the core and might be a major zone of décollement in other parts of the Slick Hills where intense parallel folding occurs (Donovan, 1995). As noted, the grainstone sequences (lithological association 4) are cut by calcite-filled veins perpendicular to bedding. Such veins probably formed early in the history of the sequence when the lithology formed a rigid, brittle element distinct from the rest of the sequence. Much of the rest of the sequence consists of diagenetically enhanced wavy and lenticular bedding. A common feature

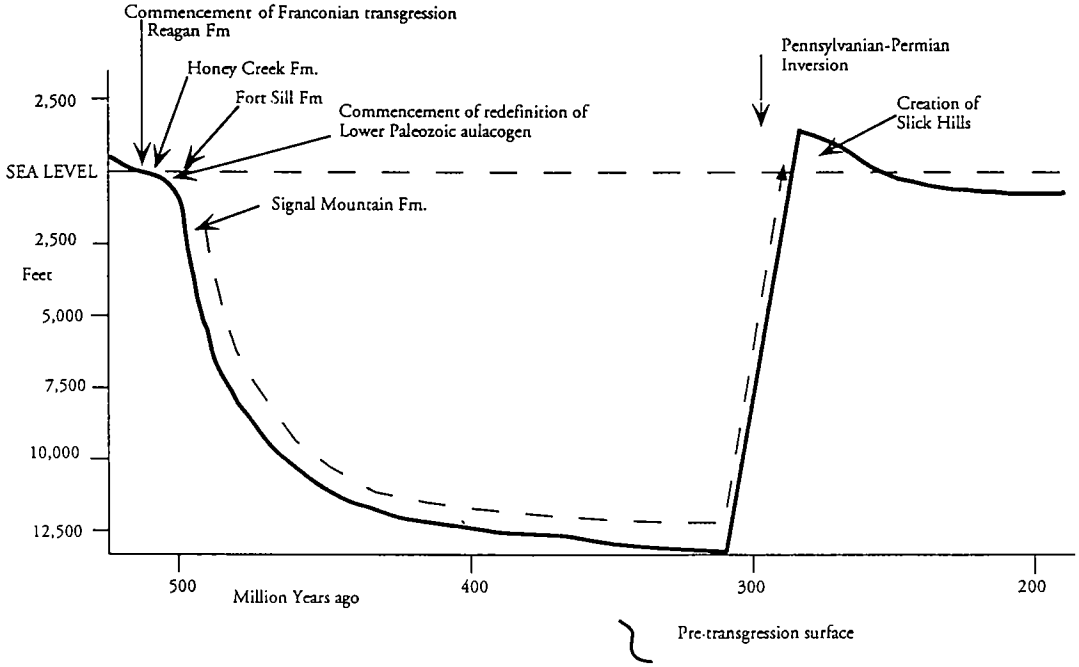

Figure 11. Burial-time curve illustrating tectono-stratigraphic history of the Signal Mountain Formation.

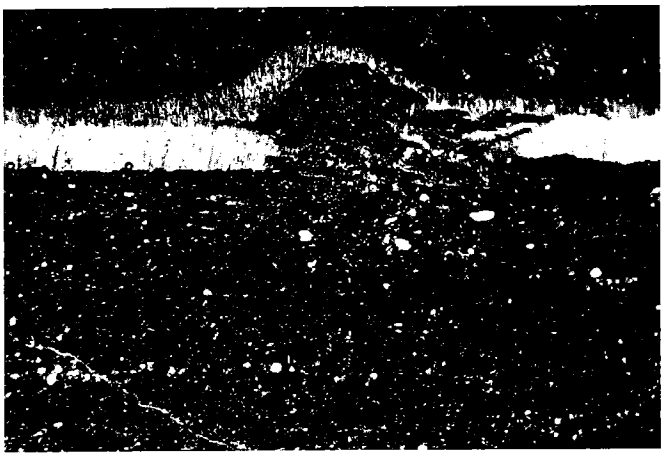

Figure 12. Calcite extension fibers perpendicular to bedding, developed along a shale–mudstone boundary. Two generations of calcite are present: the upper is ferroan, and the lower non-ferroan. Width of view, 3 mm.

seen throughout such beds is the separation of individual lenticles by thin rinds of fibrous ferroan calcite. In many examples, more than one generation of such calcite is present. The net effect of these rinds has been to dilate the entire section by about 3–5%, normal to bedding (Fig. 12). This dilation presumably took place during Pennsylvanian inversion of the area (Fig. 11).

ACKNOWLEDGMENTS

We are grateful to the Dolese Bros. Co. for permission to examine the core of the Signal Mountain Formation. Jim Allen, general manager, and Wayne Moran, superintendent, gave us enthusiastic support. The Moncrief family of Fort Worth are acknowledged for their financial support. We are grateful to Randy Hosey for his help in drafting Figure 1. The work was conducted as part of an undergraduate thesis by Whitehead.

REFERENCES CITED

Ayan, Danielle; Bucheit, A. K.; Kulow, M. J.; and Donovan, R. N., 2000, Preliminary cyclic stratigraphy of the upper Arbuckle Group in the Richard's Spur Quarry, Slick Hills, Oklahoma, *in* Johnson, K. S. (ed.), Platform carbonates in the southern Midcontinent, 1996 symposium: Oklahoma Geological Survey Circular 101 [this volume], p. 97–102.

Bucheit, A. K.; and Donovan, R. N., 2000, Initiation of a carbonate platform: a comparison between the Lower Jurassic Broadford Limestone, Isle of Skye, Scotland, and the Cambrian Honey Creek Limestone, Slick Hills, Oklahoma, *in* Johnson, K. S. (ed.), Platform carbonates in the southern Midcontinent, 1996 symposium: Oklahoma Geological Survey Circular 101 [this volume], p. 57–64.

Donovan, R. N., 1986, Geology of the Slick Hills, *in* Donovan, R. N. (ed.), The Slick Hills of southwestern Oklahoma—fragments of an aulacogen?: Oklahoma Geological Survey Guidebook 24, p. 1–12.

_____1995, The Slick Hills of Oklahoma and their regional tectonic setting, *in* Johnson, K. S. (ed.), Structural styles in the southern Midcontinent, 1992 symposium: Oklahoma Geological Survey Circular 97, p. 178–186.

Donovan, R. N.; and Ragland, D. A., 1986, Paleozoic stratigraphy of the Slick Hills, southwestern Oklahoma, *in* Donovan, R. N. (ed.), The Slick Hills of southwestern Oklahoma—fragments of an aulacogen?: Oklahoma Geological Survey Guidebook 24, p. 13–16.

Hosey, Randy; and Donovan, R. N., 1993, The geological significance of the boundary between the Fort Sill and Signal Mountain Formations in the lower Arbuckle Group (Cambrian) [abstract]: Geological Society of America Abstracts with Programs, v. 25, no. 1, p. 14–15.

_____2000, Boundary between the Fort Sill and Signal Mountain Formations in the lower Arbuckle Group, Slick Hills: candidate for a grand cycle boundary, *in* Johnson, K. S. (ed.), Platform carbonates in the southern Midcontinent, 1996 symposium: Oklahoma Geological Survey Circular 101 [this volume], p. 79–88.

McElmoyl, Courtney; and Donovan, R. N., 1993, A transgression–regression event during the deposition of the Upper Cambrian Honey Creek Formation in the southern Oklahoma aulacogen [abstract]: Geological Society of America Abstracts with Programs, v. 25, no. 1, p. 38.

_____2000, Unconformity in the lower part of the Cambrian Honey Creek Limestone, Slick Hills, Oklahoma: candidate for a grand cycle boundary, *in* Johnson, K. S. (ed.), Platform carbonates in the southern Midcontinent, 1996 symposium: Oklahoma Geological Survey Circular 101 [this volume], p. 65–78.

Stitt, J. H., 1977, Late Cambrian and earliest Ordovician trilobites, Wichita Mountains area, Oklahoma: Oklahoma Geological Survey Bulletin 124, 79 p.

Whiteside, J. R.; and McCommons, W. E., 1991, Results of a deep Cambro–Ordovician drilling program, northern Fort Worth basin, Texas, *in* Johnson, K. S. (ed.), Arbuckle Group core workshop and field trip: Oklahoma Geological Survey Special Publication 91-3, p. 157–162.

Preliminary Cyclic Stratigraphy of the Upper Arbuckle Group in the Richard's Spur Quarry, Slick Hills, Oklahoma

Danielle Ayan, Andrea K. Bucheit, Matthew J. Kulow, and R. N. Donovan
Texas Christian University
Fort Worth, Texas

ABSTRACT.—The Dolese Bros. Co.'s Richard's Spur Quarry in the southern part of the eastern Slick Hills is one of the largest quarries in the United States. The sequence that is being worked comprises the Lower Ordovician McKenzie Hill, Cool Creek, and Kindblade Formations of the Arbuckle Group, in ascending order. Our ultimate aim is the documentation of the entire sequence as it is worked by the owners. A total thickness of ~3,500 ft of rock has so far been worked by the company.

We have examined a short (~52-ft) section of the Cool Creek Formation. In common with previously described sections of this formation, an alternation of thin (<50-cm), shallow-water carbonate lithologies dominates the sequence. These lithologies include algal boundstones and stromatolites, a variety of mud-dominated lithologies, grainstones, intraformational conglomerates, and dolomitic mudstones (with idiotopic crystals and showing varying amounts of dedolomitization). Allochems, in order of abundance, are intraclasts > ooids > peloids >> fossils. We found very few fossils in the section (except for algal boundstones). Quartz grains up to 1 mm in diameter are abundant in several zones. One or two zones of mud cracks are present; evaporite pseudomorphs are further evidence of desiccation and indicate periodic salinity fluctuations. Nearly all cementing carbonate is nonferroan (as are vein fills). Secondary silica is present in the form of chert nodules and syntaxial overgrowths around detrital quartz grains. We interpret the section as a record of deposition in peritidal–supratidal environments. The regular repetition of particular lithologies is a function of sediment distribution on the Laurentian platform and fluctuations in sea level.

INTRODUCTION

This paper discusses and interprets the geology of a short section (~52 ft) of the Cool Creek Formation, part of a much lengthier section (~3,500 ft) exposed in Richard's Spur Quarry, southwestern Oklahoma. The Cool Creek is the fourth from the base of six formations that form the Arbuckle Group (reviewed in Donovan, 1991). The Arbuckle Group represents a generally transgressive carbonate sequence deposited on part of an immense platform that, at its maximum extent, formed approximately half of the Laurentian craton. Within the confines of the southern Oklahoma aulacogen, the group is more than 7,000 ft thick. Outside the aulacogen, thicknesses of approximately 2,000 ft are more typical.

The purpose of the paper is to add more detail to our knowledge of the Slick Hills section of the Arbuckle Group. It is part of an ongoing project to log and interpret the entire section in as much detail as is feasible.

NATURE OF THE EXPOSURE

The sequence at Richard's Spur Quarry, described here, was deposited within the southern Oklahoma aulacogen. Both the upper and lower boundaries of the section are covered by quarry debris; we estimate that the section is approximately 300 ft above the base of the Cool Creek Formation.

The quarry forms the southernmost extremity of the eastern Slick Hills, an exhumed Permian range that exposes a basically homoclinal sequence that dips to the northeast at angles of 15° to 75° (Fig. 1). Tectonic rotation took place during the Pennsylvanian Period, when the aulacogen sequence was partially inverted (Donovan, 1995).

In places, the top of the quarry coincides with an overlying Permian unconformity that is overlain by the Post Oak Conglomerate, a limestone boulder-and-pebble alluvial deposit. Numerous Permian karst fissures, coated by speleothems and containing Permian fossils and surface-derived detritus, cut through the entire quarry face.

The dip of the section is steep, approximately 60° to the northeast. The entire section is highly fractured; at least three generations of calcite-filled veins and small faults can be seen throughout the quarry. The latest of these veins (which predates the Permian unconformity) is associated with pyrite and hydrocarbon mineraloids. Veins of this generation postdate tilting of the section, for they utilize subvertical bedding planes. All rocks and thin sections examined in this study show evidence of great vein-compensated dilation—so much so that primary lithologies may be comprehensively dislocated, particularly where Permian karst features have overprinted the fractures. In addition, the rocks show much evidence of shearing, which is probably related to flexural slip during rotation.

Ayan, Danielle; Bucheit, A. K.; Kulow, M. J.; and Donovan, R. N., 2000, Preliminary cyclic stratigraphy of the upper Arbuckle Group in the Richard's Spur Quarry, Slick Hills, Oklahoma, *in* Johnson, K. S. (ed.), Platform carbonates in the southern Midcontinent, 1996 symposium: Oklahoma Geological Survey Circular 101, p. 97–102.

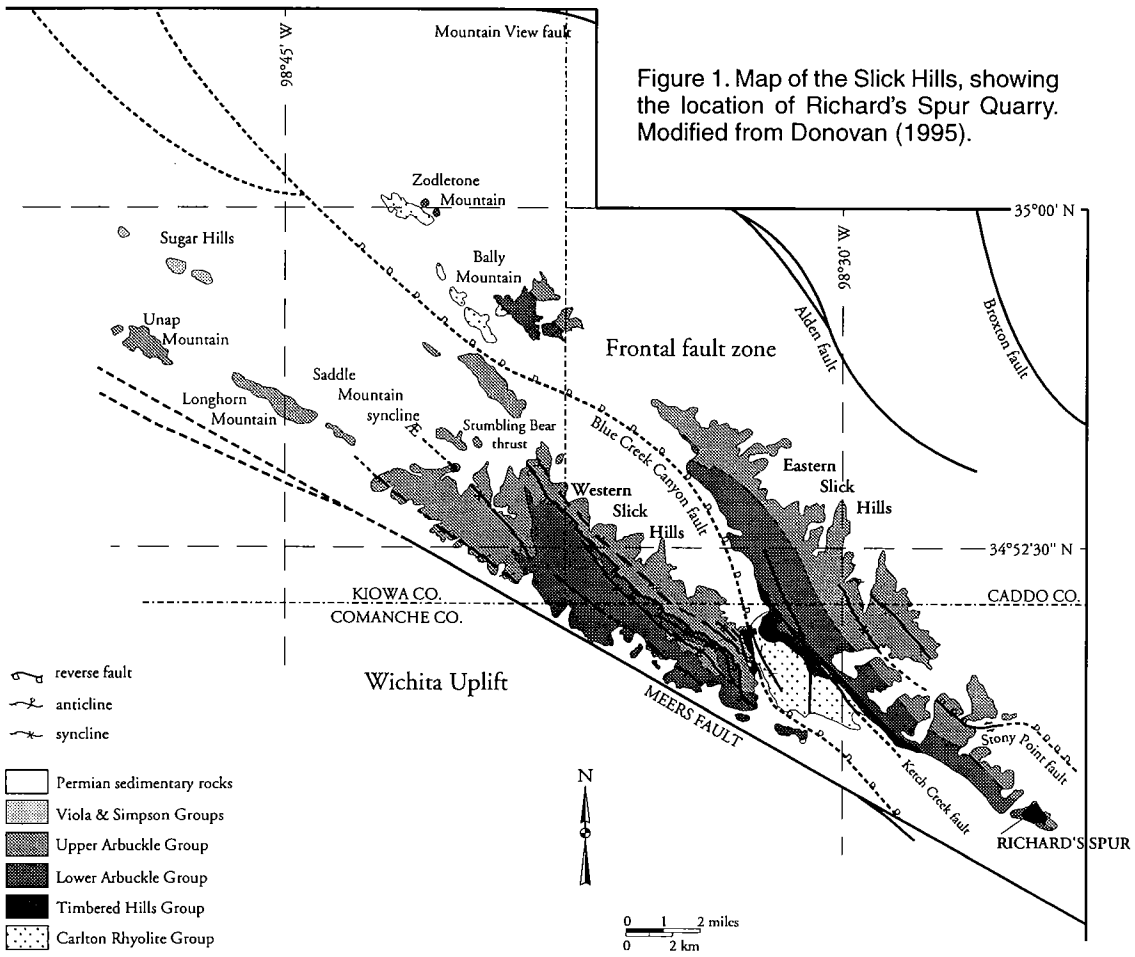

Figure 1. Map of the Slick Hills, showing the location of Richard's Spur Quarry. Modified from Donovan (1995).

SEDIMENTOLOGICAL DETAILS

A log of the section (Fig. 2) illustrates the basic similarity of this section to others found elsewhere in the Cool Creek Formation (e.g., Ragland and Donovan, 1985a,b, 1991a,b). The sequence is constructed of a large number of thin carbonate lithologies (generally <50 cm thick). Some boundaries between individual beds are unaltered, but many (~50%) bed boundaries are obscured by the development of bedding-parallel stylolites.

The primary lithologies that we recognized at the quarry face (Fig. 3) are described in the following paragraphs.

Algal Boundstones and Stromatolites (21.5% of Section)

Eleven distinct zones of algal boundstones, including algal mats and both domal and digitate stromatolites, occur in the section. The dome radius and amplitude vary considerably. Mostly, the character of the boundstone is distinctive for a particular zone. At one or two places, however, domal stromatolites have formed the substrate for colonization by digitate forms. The infill of the space between the stromatolites varies between coarse intraclast, ooid, and quartz-bearing grainstones and various mud-supported lithologies. We conclude that boundstone development took place in a spectrum of environments that involved variations in water depth and hydrodynamic energy. We could detect no obvious relationship between interarea infill and boundstone type.

Intraformational Conglomerates (18.7% of Section)

The eight zones of intraformational conglomerates in the section are composed of flat pebbles (up to 3 in. across) that represent all the mud-supported lithologies found in situ. Ooids and/or detrital quartz grains are an important component of the thicker conglomerates. Intraformational conglomerates indicate a degree of autocyclic reworking of the section, either by storms or by tidal-flat mechanics (see, e.g., Donovan, 1986). Limestone clasts generally testify to the efficiency of cementation close to or at the sediment–water interface on carbonate platforms. In this context, clasts of dolomitic limestone and chert in the conglomerates indicate that both silicification and dolomitization were at least partially penecontemporaneous.

Ooid-Bearing Lithologies (15.3% of Section)

Five ooid-bearing limestone zones were identified in the field. In addition, ooids are present in some of the undifferentiated limestones (see below). A variety of types of ooids—surficial, radial, and (more rarely) concentric—are nucleated upon both lime mud and detrital quartz.

Undifferentiated Limestones (51.8% of Section)

More than half the section consists of various shades of gray limestone, which is more usefully examined in the laboratory than in the field. In general, these limestones consist of thin beds (no more than 3 in. thick) of a variety of mud-supported lithologies and, less commonly, grainstones. The original bed boundaries are gradational, sharp, or hardground surfaces. However, about half of such boundaries have been obscured by the development of bedding-parallel stylolites. Thin-section and slab analyses (Fig. 4) provide the following data: (1) most allochems are ooids, peloids, and intraclasts (the last two were distinguished by angularity and sphericity); (2) such bioclasts as are present are dominantly gastropods plus minor thick-shelled trilobites; (3) little bioturbation was detected; (4) intraclasts generally represent the finer size fraction of the pebbles in intraformational conglomerates; (5) most samples contain trace amounts of silt-sized quartz; (6) grain populations are generally moderately to well sorted; (7) most textures are mud supported, if not wholly mudstone; (8) some packstones display irregular patches of cementing drusy sparite, and they may record rapid deposition and/or limited reworking of a subwave-base deposit; (9) grainstones are generally well sorted and cemented by simple drusy sparite that shows no variation in luminescence patterns; (10) except in late tectonic veins, all the carbonate (including dolomite) is nonferroan.

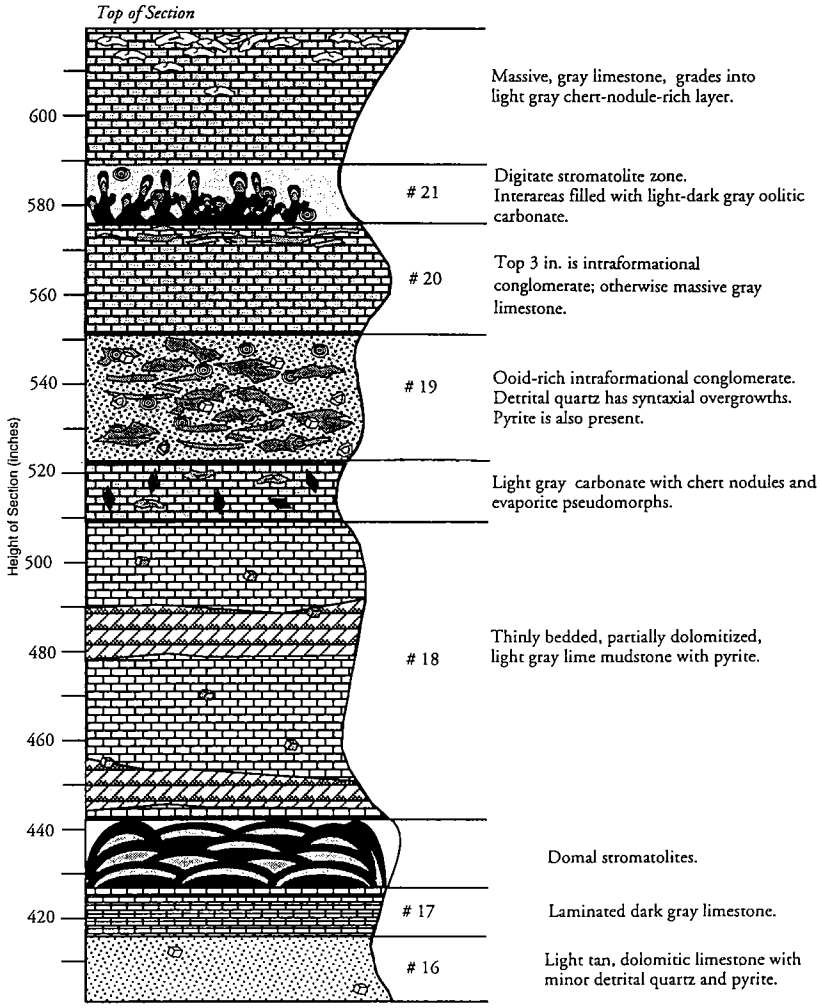

Figure 2 *(continued on pages 100 and 101).* Log of the Cool Creek Formation section examined in Richard's Spur Quarry.

Detrital Quartz (17.4% of Section)

As noted above, trace amounts of detrital quartz silt can be found throughout the section. More significant amounts of much coarser grained quartz—from medium to coarse sand grade—are concentrated in five zones in the section. Concentrations of this type are diagnostic of the upper formations of the Arbuckle Group (Ragland and Donovan, 1985a) and are particularly common in the Cool Creek Formation. Petrographically, these concentrations are monotonously similar; unless they have been diagenetically modified, the grains are well rounded. Compositionally, 99% of the grains are quartz, with trace amounts of microcline and orthoclase feldspar; most of the quartz grains are nonundulose.

DIAGENETIC IMPRINTS

Limestone Diagenesis

As noted previously, limestones are cemented by simple drusy sparite that shows no variation in luminescence patterns. The timing of cementation is ambiguous, however. Hardgrounds are common in the sequence (indicating penecontemporaneous cementation), and yet some grainstones show evidence of considerable compaction—in the form of indented ooids and grains—prior to cementation. Evidently the movement of saturated ground water was to some extent partitioned.

Dolomitization and Dedolomitization

Several thin zones of dolomitized limestone were identified in the field and constitute 11.5% of the section. This dolomite is fabric selective and consists of mosaics of small euhedral and subhedral idiotopic crystals. The percentage of dolomite present varies from 10% to 80%. The form of the dolomite is compatible with an early diagenetic origin, an interpretation supported by the aforementioned occurrence of dolomitic limestone clasts in some intraformational conglomerates. An understanding of the extent of this dolomitization is hampered by the common occurrence of dedolomitized fabrics. These fabrics were detected only under the microscope; thus it is probable that we have underestimated their significance. As clasts of dedolomitized fabric are found in intraformational conglomerates, it is reasonable to infer that both dolomitization and (at least in part) dedolomitization were penecontemporaneous processes.

Silicification

Further evidence of variation in the chemistry of waters on the Cool Creek platform is provided by two forms of silicification: nodules of cryptocrystalline chalcedony (four zones), and syntaxial overgrowths on detrital quartz grains. Not all quartz-bearing zones display overgrowths, however; grains in two zones have corroded margins, suggesting that they functioned as a source for silica in solution.

Evaporite Pseudomorphs

Two zones of calcite-spar pseudomorphs after a monoclinic salt (presumably gypsum) are further evidence of chemical fluctuation. In this context, two clasts of chert with "cauliflower" texture—thought to be pseudomorphs after anhydrite nodules (Ragland and Donovan, 1991a)—were found in an intraformational conglomerate.

DISCUSSION

Any discussion of the section must be prefaced by two caveats. First, the exposure is fresh and unweathered; we may have missed some details in consequence. Second, and inherently a greater problem, a considerable part of the section has been removed by dissolution along bedding-parallel stylolites.

Our analysis indicates that this section of the Cool Creek Formation is broadly similar to sections described by other authors (Ragland and Donovan, 1985a,b, 1991a,b) in that it consists of alternations of various lithologies that appear to have been deposited in peritidal–supratidal conditions. The diagenesis of the sequence also is comparable to others described for this formation.

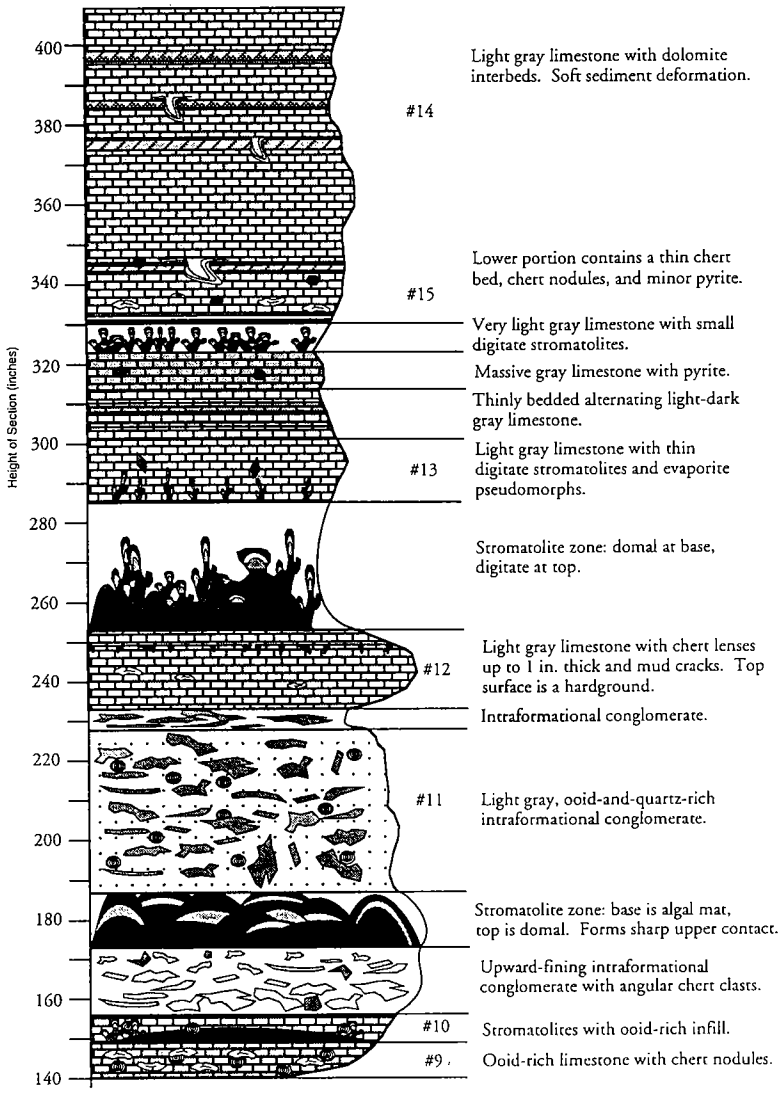

Figure 2 *(continued).*

Homotaxial problems bedevil lithologic correlation in the Arbuckle Group; the search for meaningful patterns has focused on meter-scale shallowing-upward cycles demarcated by an upward passage from peritidal to supratidal facies. Such cycles are widely recognized in the geological record, including sequences of comparable age to the Cool Creek (e.g., Read and Goldhammer, 1988). Furthermore, convincing cycles of this type have been recognized in the Cool Creek of the Arbuckle Mountains (e.g., Ragland and Donovan, 1991b, fig. 4). By conventional uniformitarian analogy, indicators of emergence—mud cracks, penecontemporaneous dolomitization, evaporite evidence, and quartz concentrations (see above)—are certainly present in the section, as are indicators of peritidal conditions.

As Ragland and Donovan (1991a) noted, however, a cyclic pattern is not easily identifiable throughout the Cool Creek Formation. The Richard's Spur Quarry section is similarly problematical in that, while all the required facies are present, it is difficult to demonstrate a cyclic control in their arrangement (Fig. 3). Part of the problem may be due to relatively minor diagenetic obfuscation—in particular, penecontemporaneous dedolomitization. As Donovan (1991) noted, however, there are inherent problems in the organization of sediment on the Arbuckle platform: (1) the immense size of the platform would have meant that the influx of tidal energy, particularly to distal parts of the platform, would have been small by comparison to modern day analogues; (2) the paleogeographic position of the platform—subtropical, south of the equator, and at the western edge of a craton—would have favored offshore winds, reversing tidal flow and further inhibiting the formation of systematic facies tracts; (3) the relatively high rate of subsidence (~400 ft/million years, Donovan, 1986) in the southern Oklahoma aulacogen, as compared to adjacent areas, would have further prevented systematic organization of the sediment: the sequence measured is the record of ~125,000 years.

In the context of facies definition, it is significant that Ragland and Donovan (1986) suggested that relief (i.e., "sabkha"-like islands) existed on the platform, whereas, in a related study of the Kindblade Formation in the Arbuckle Mountains, Donovan and others (1991) demonstrated the great

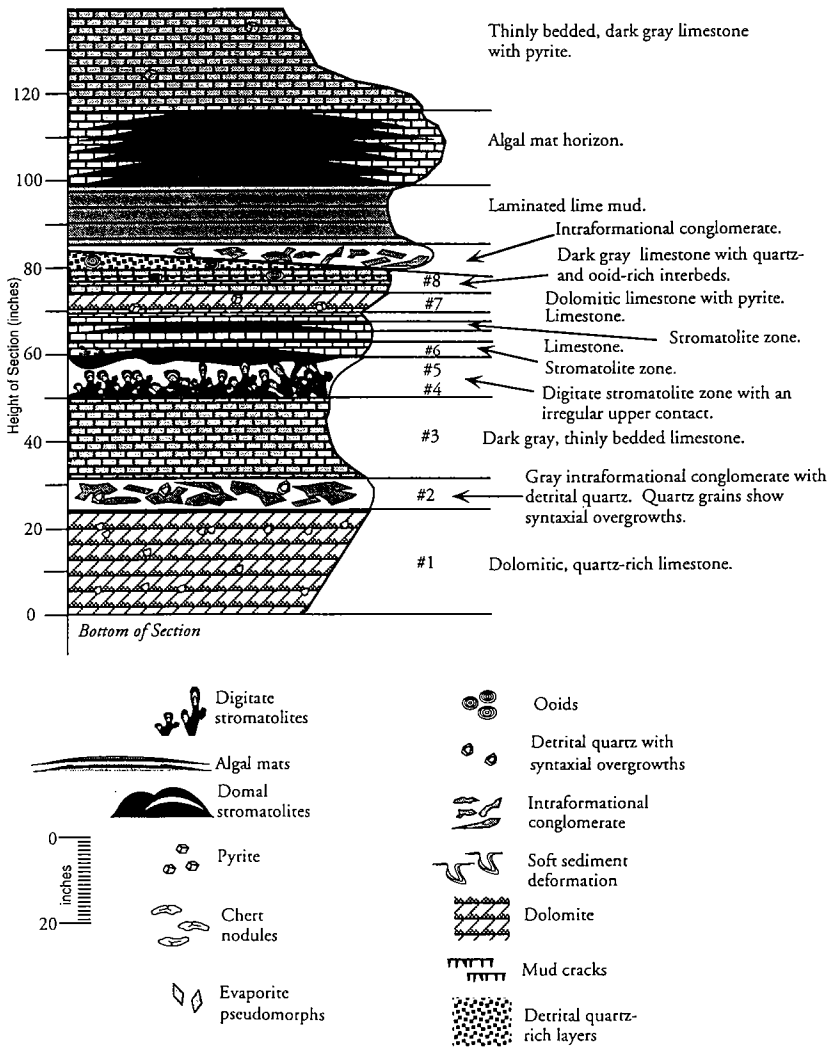

Figure 2 *(continued)*.

difficulty in correlating individual facies over as short a distance as 600 yards. Interestingly, these authors showed that the most satisfactory facies that can be correlated were siliciclastic and penecontemporaneous ("sabkha-style") dolomite zones, particularly where the two are in contact. Both of these facies were taken as evidence of lowstands in sea level.

Petrographically, the siliciclastics throughout the Cool Creek Formation are mineralogically and texturally mature. The mineralogical maturity of this population indicates prolonged and/or effective chemical weathering; the textural maturity indicates prolonged residence time in a depositional system that was effective in rounding and sorting grains prior to their arrival on the platform. The source of these grains was presumably the Laurentian craton; similar mature populations are found in the overlying Kindblade and West Spring Creek Formations of the Arbuckle Group. The implication is that the craton was essentially tectonically stable throughout this period; thus it is likely that the grain concentrations reflect periodic regressions, during which grains were transported into the area, to be reworked during succeeding transgressions (Donovan, 1991). The Richard's Spur Quarry sequence contains five siliciclastic concentrations, indicating a regression periodicity of ~25,000 years.

SUMMARY AND CONCLUSIONS

The sequence logged at Richard's Spur Quarry is a characteristic sequence of the Cool Creek Formation, displaying a suite of facies that record an interplay of peritidal and arid to semiarid supratidal environments. The thickness measured probably was deposited in ~125,000 years. Although there is little doubt that the platform was subject to frequent fluctuations in sea level, we could not convincingly discriminate the meter-scale shallowing-upward cycles that are recognized in contemporary sequences. The lack of a systematic facies pattern probably reflects the dynamics of the Arbuckle platform, particularly its large size, paleogeographic position, and relatively rapid burial rates.

ACKNOWLEDGMENTS

We are most grateful to the Dolese Bros. Co. for permission to work the site. Jim Allen, general manager, and Wayne Moran, superintendent, gave us enthusiastic support. The Moncrief family of Fort Worth are acknowledged for their financial support. We are grateful to Randy Hosey for his help in drafting Figure 1 and to Rick Whitehead for his help in sample collection.

REFERENCES CITED

Donovan, R. N., 1986, The geology of the Slick Hills, *in* Donovan, R. N. (ed.), The Slick Hills of southwestern Oklahoma—fragments of an aulacogen?: Oklahoma Geological Survey Guidebook 24, p. 1–12.

_____1991, The Arbuckle Group—An aide de mémoire, *in* Johnson, K. S. (ed.), Arbuckle Group core workshop and field trip: Oklahoma Geological Survey Special Publication 91-3, p. 199–208.

_____1995, The Slick Hills of Oklahoma and their regional tectonic setting, *in* Johnson, K. S. (ed.), Structural styles in the southern Midcontinent, 1992 symposium: Oklahoma Geological Survey Circular 97, p. 178–186.

Donovan, R. N.; Gallagher, M.; Hosey, R.; Phornpraphra, C.; Sith, A.; Smith, S. S.; and Templeton, J., 1991, Lateral variations in upper Arbuckle Group rocks—a comparison between sections on I-35 and US-77 in the Arbuckle Mountains, *in* Johnson, K. S. (ed.), Arbuckle Group core workshop and field trip: Oklahoma Geological Survey Special Publication 91-3, p. 225–232.

Ragland, D. A.; and Donovan, R. N., 1985a, The Thatcher Creek Member, basal unit of the Cool Creek Formation in southern Oklahoma: Oklahoma Geology Notes, v. 45, p. 83–96.

_____1985b, The Cool Creek Formation (Ordovician) at Turner Falls in the Arbuckle Mountains of southern Oklahoma: Oklahoma Geology Notes, v. 45, p. 132–148.

_____1986, An environmental analysis of the Early Ordovician Cool Creek Formation in southwestern Oklahoma, *in* Donovan,

R. N. (ed.), The Slick Hills of southwestern Oklahoma—fragments of an aulacogen?: Oklahoma Geological Survey Guidebook 24, p. 21–28.

_____1991a, Sedimentology and diagenesis of the Arbuckle Group in outcrops of southern Oklahoma, *in* Johnson, K. S. (ed.), Arbuckle Group core workshop and field trip: Oklahoma Geological Survey Special Publication 91-3, p. 9–29.

_____1991b, The Cool Creek Formation at Turner Falls Park—a platform compendium, *in* Johnson, K. S. (ed.), Arbuckle Group core workshop and field trip: Oklahoma Geological Survey Special Publication 91-3, p. 218–222.

Read, J. F.; and Goldhammer, R. K., 1988, Use of Fischer plots to define third-order sea-level curves in Ordovician peritidal cyclic carbonates: Geology, v. 16, p. 895–899.

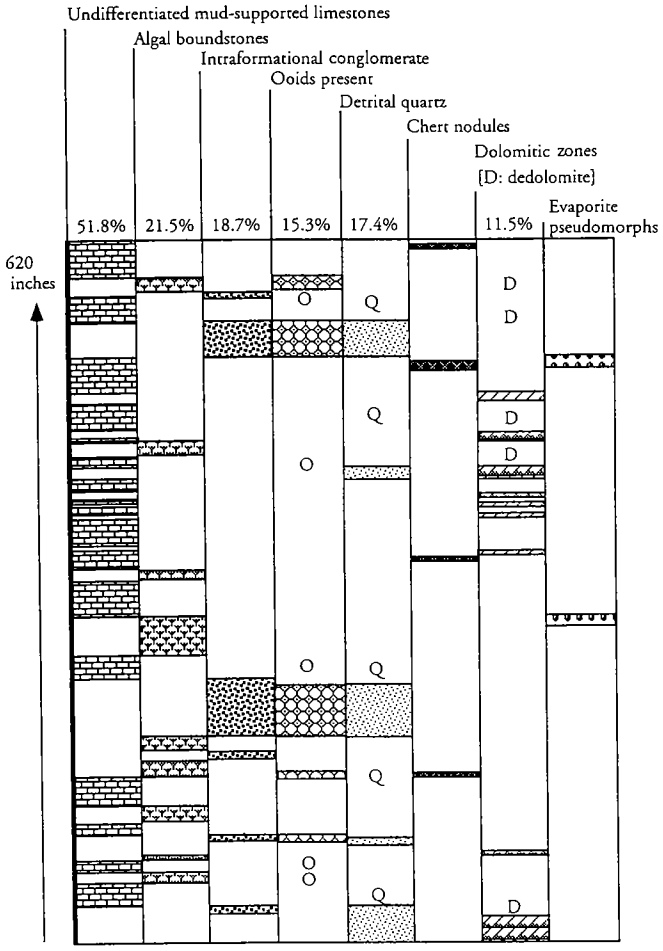

Figure 3. Synoptic log of Richard's Spur Quarry, showing breakout of petrographic characteristics recognized.

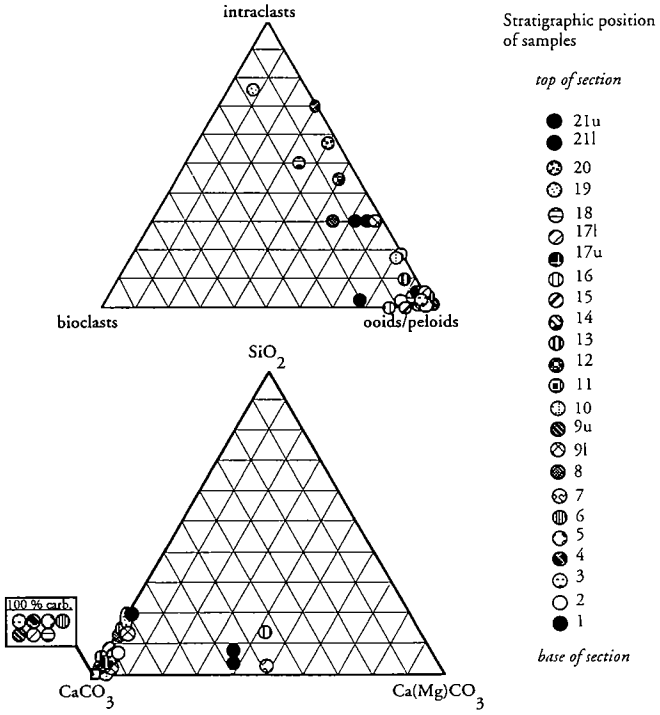

Figure 4. Triangular plots showing the petrographic and allochem breakdown of thin sections examined from the Richard's Spur Quarry section.

A Preliminary Reevaluation of the Stratigraphy of the Roubidoux Formation of Missouri and Correlative Lower Ordovician Units in the Southern Midcontinent

John E. Repetski
U.S. Geological Survey
Reston, Virginia

James D. Loch
Central Missouri State University
Warrensburg, Missouri

Raymond L. Ethington and Russell I. Dresbach
University of Missouri–Columbia
Columbia, Missouri

Earlier in the 20th century, the carbonate succession in the Ozarks was considered a standard for the Lower Ordovician in the United States, but relatively little stratigraphic work has been done on this predominantly dolomitic succession in the past 50 years. Recent focus on these regionally widespread carbonate strata for various socioeconomic reasons—e.g., availability and quality of through-flowing ground water—necessitates revision and refinement of this stratigraphic framework. Our studies use both conodonts and macrofossils for temporal and facies control. Preliminary efforts center on the Roubidoux Formation and directly subjacent and superjacent units, the Gasconade and Jefferson City Dolomites, respectively. A summary of the physical stratigraphy, lithologic descriptions, and nomenclatural histories of these units can be found in Thompson (1991).

We recovered conodonts from several sections of the Roubidoux Formation in south-central Missouri, including the type section designated by Heller (1954) along Roubidoux Creek, Texas County (Fig. 1); Heller's Ava section, in Douglas County (Fig. 2); and partial sections just west of Rolla, Phelps County (Thompson, 1991; Thompson and Robertson, 1993). The faunas comprise taxa typical of warm, shallow-marine conditions of the North American Midcontinent Faunal Realm. Numbers of both individual conodont elements and species per sample are low in these chiefly dolomitic strata. Sufficient data are available, however, to establish a preliminary conodont-based biostratigraphy and tentative regional correlations for this Ibexian interval (Fig. 3). Preliminary analysis indicates the following:

1. The upper part of the underlying Gasconade Dolomite in south-central Missouri extends from the *Rossodus manitouensis* Zone into the "Low Diversity Interval" of Ethington and others (1987), and as used in Ross and others (1997) and Repetski and others (1993). The "Low Diversity Interval" is equal to the lowest part of the range of conodont Fauna D of the Midcontinent Conodont Faunal Realm (Ethington and Clark, 1971). The lower limit of the "Low Diversity Interval" appears to be at least several meters below the top of the Gasconade.

2. At its type section, the Roubidoux ranges from within the "Low Diversity Interval" into or through the succeeding *Macerodus dianae* Zone (= middle of the range of Fauna D). *M. dianae* has not been recovered from the Roubidoux thus far, but the presence of *Histiodella donnae* indicates the *M. dianae* Zone. The conodont fauna recovered from the Roubidoux consists exclusively of species with coniform elements.

3. The Roubidoux–Jefferson City contact, at least in the area of the Roubidoux type section, lies either within the *M. dianae* Zone or very low in the succeeding (middle Ibexian) *Acodus deltatus–Oneotodus costatus* Zone (= upper part of the range of Fauna D). This formational boundary interval is difficult to clarify biostratigraphically owing to sparse recovery of faunas, occurrence of mostly long-ranging taxa, and rarity of continuously outcropping sections exposing the contact.

The base of the Roubidoux is equivalent to a level low in the Cool Creek Formation in the Arbuckle Mountains (Chapman Ranch section) and in the Wichita Mountains (Chandler Creek section) of southern Oklahoma (Ethington and others, 1987). Sparse conodont occurrence and low diversity in the lowest Cool Creek indicate assignment to the "Low Diversity Interval" (Dresbach and Ethington, 1991). *Macerodus dianae* is present approximately 130 m above the basal contact but still beneath the middle of the 400-m-thick Cool Creek. Trilobite biostratigraphic data demonstrate that the Roubidoux–Jefferson City contact correlates closely with the Cool Creek–Kindblade contact in Oklahoma, on the basis of the trilobite *Ranasasus brevicephalus* (Loch and others, 1993).

Repetski, J. E.; Loch, J. D.; Ethington, R. L.; and Dresbach, R. I., 2000, A preliminary reevaluation of the stratigraphy of the Roubidoux Formation of Missouri and correlative Lower Ordovician units in the southern Midcontinent, *in* Johnson, K. S. (ed.), Platform carbonates in the southern Midcontinent, 1996 symposium: Oklahoma Geological Survey Circular 101, p. 103–106.

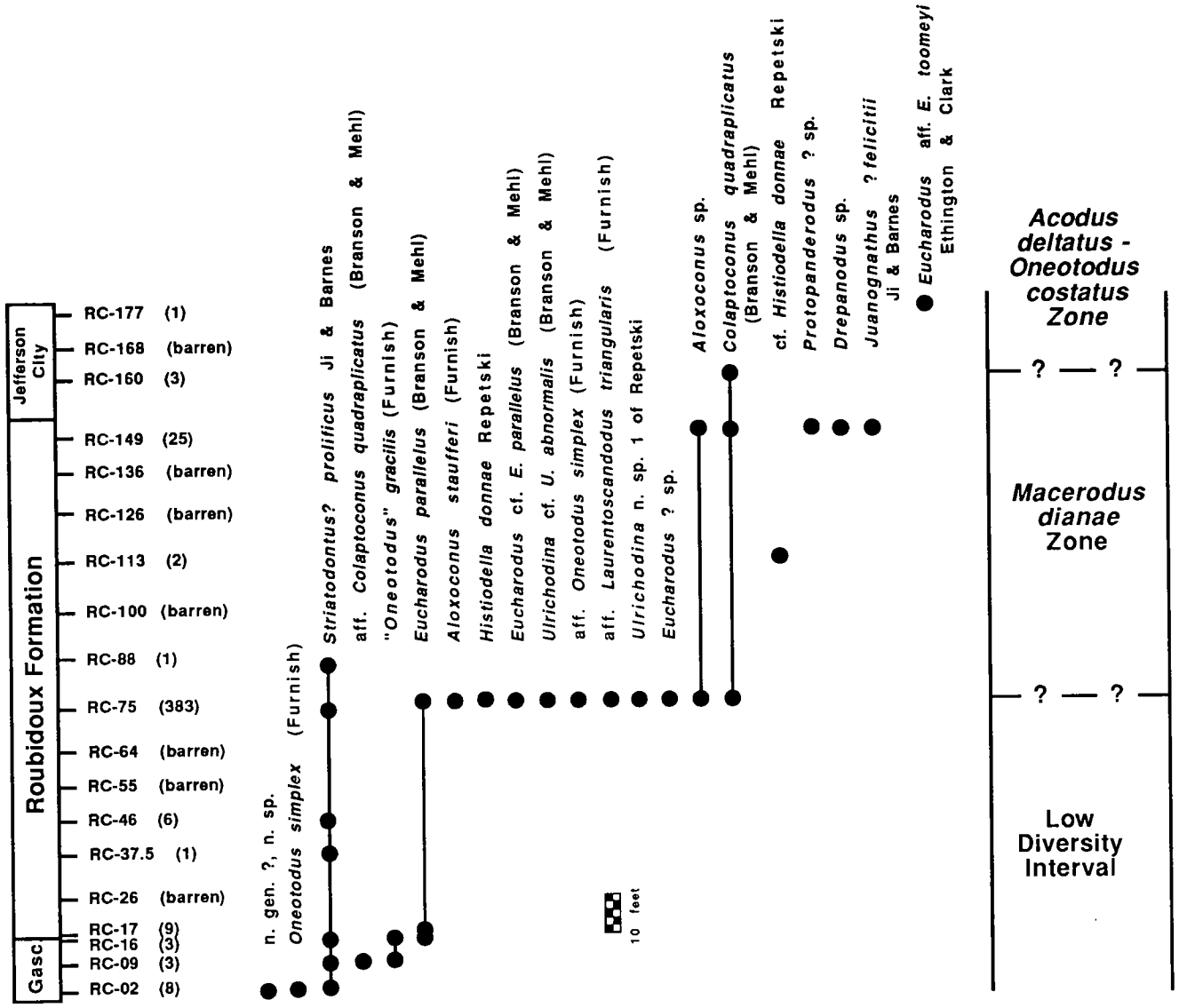

Figure 1. Conodont distribution from the type section (Roubidoux Creek section) of the Roubidoux Formation, including directly adjacent parts of the Gasconade and Jefferson City Dolomites. In both Figures 1 and 2, numbers in parentheses indicate numbers of individual identifiable conodont elements recovered. Each sample comprised approximately 2 kg of rock, except for sample RC-75, for which approximately 3 kg was processed.

The Manitou Formation of central Colorado ranges largely through the *Rossodus manitouensis* Zone at most places and thus is approximately correlative with the Gasconade Dolomite of Missouri (e.g., Seo and Ethington, 1993). At several localities, however, the upper part of the Manitou contains conodonts of the *M. dianae* Zone (undescribed collections of Ethington and USGS) and thereby is at least in part equivalent to the Roubidoux.

The Roubidoux interval in the Ouachita Mountains of west-central Arkansas is occupied approximately by the Crystal Mountain Sandstone. The Crystal Mountain is sparse in fossil data of any kind, but conodont collections indicate that at least some part of the formation is as old as the *R. manitouensis* Zone (undescribed collections of Ethington and Repetski). Collections from the lowest parts of the overlying Mazarn Shale are assignable to the *A. deltatus–O. costatus* Zone and only constrain the Crystal Mountain–Mazarn boundary to the lower or middle part of the range of Fauna D (Ethington and others, 1989).

REFERENCES CITED

Dresbach, R. I.; and Ethington, R. L., 1991, Conodont biostratigraphy of Lower Ordovician rocks, Arbuckle Group, southern Oklahoma, *in* Johnson, K. S. (ed.), Late Cambrian–Ordovician geology of the southern Midcontinent, 1989 symposium: Oklahoma Geological Survey Circular 92, p. 215–216.

Ethington, R. L.; and Clark, D. L., 1971, Lower Ordovician conodonts in North America, *in* Sweet, W. C.; and Bergström, S. M. (eds.), Symposium on conodont biostratigraphy: Geological Society of America Memoir 127, p. 63–82.

Ethington, R. L.; Engel, K. M.; and Elliott, K. L., 1987, An abrupt change in conodont faunas in the Lower Ordovician of the Midcontinent Province, *in* Aldridge, R. J. (ed.), Palaeobiology of conodonts: Ellis Horwood, Chichester, p. 111–127.

Ethington, R. L.; Finney, S. C.; and Repetski, J. E., 1989, Biostratig-

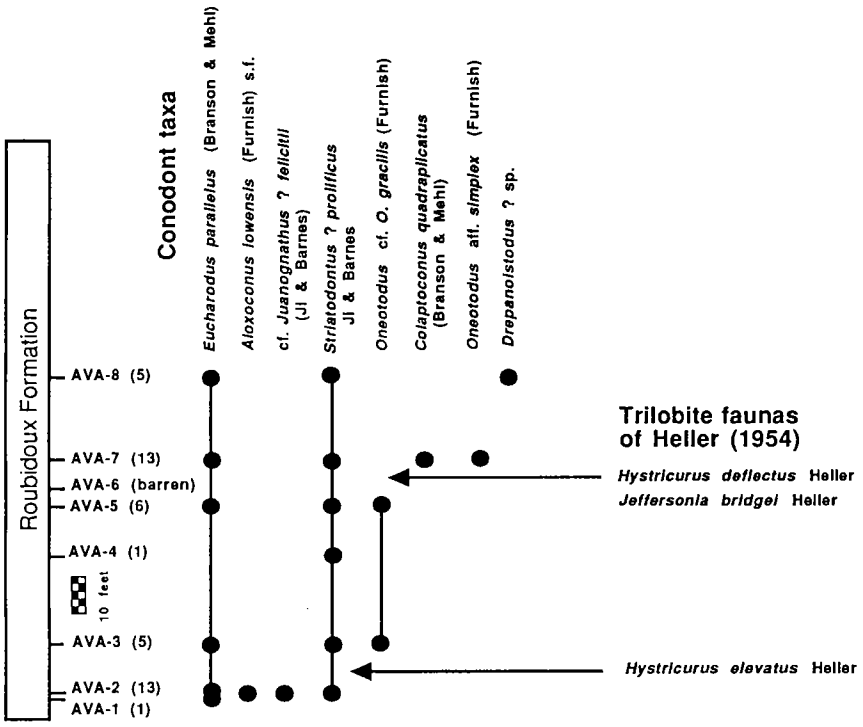

Figure 2. Conodont and trilobite distribution from the Ava section. Sample mass ranged from 2.5 to 3.3 kg.

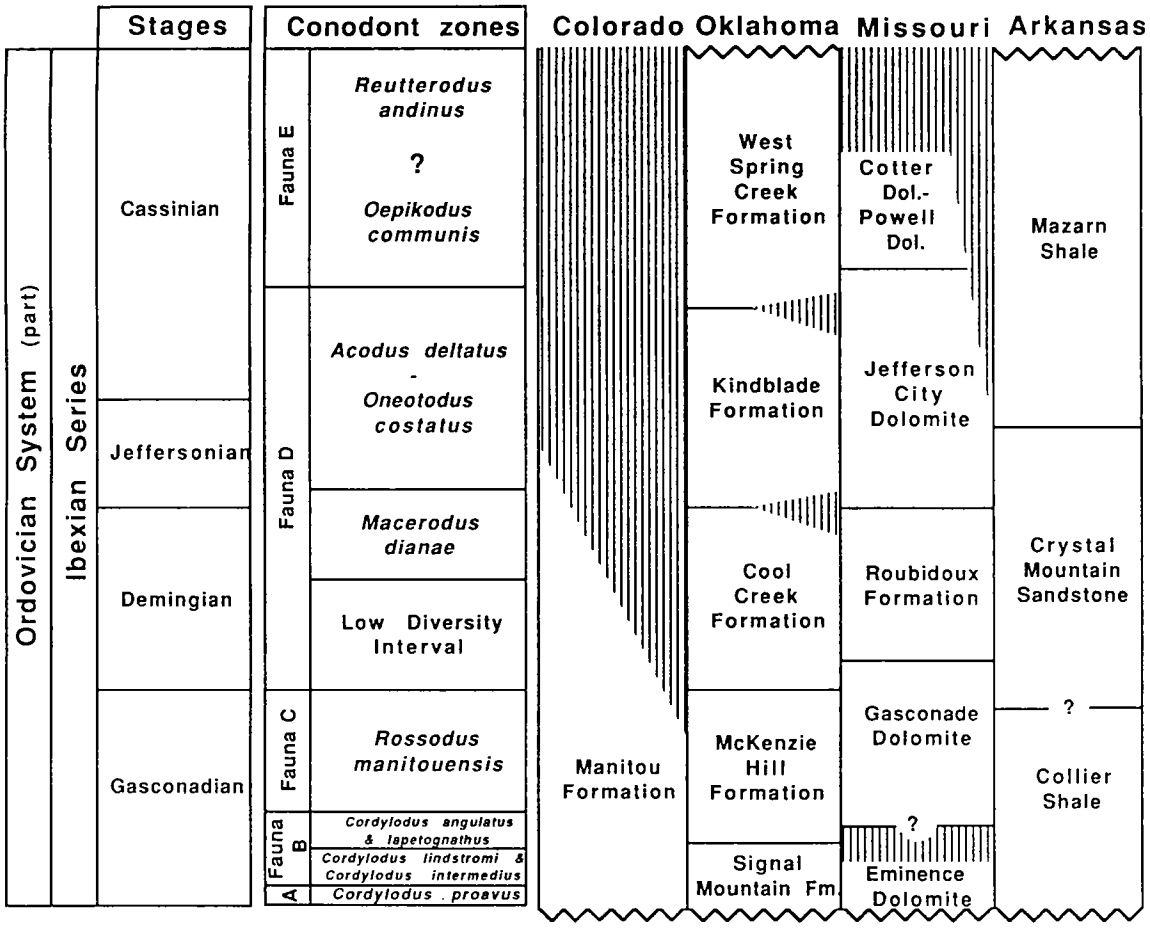

Figure 3. Biostratigraphic framework and correlation of the Ibexian Series sections in the southern Midcontinent discussed in text. Conodont zonation follows Ethington and Clark (1971; Faunas A–E) and Ross and others (1997).

raphy of the Paleozoic rocks of the Ouachita orogen, Arkansas, Oklahoma, and west Texas, *in* Hatcher, R. D., Jr.; Thomas, W. A.; and Viele, G. W., The geology of North America, v. F-2, The Appalachian–Ouachita orogen in the United States: Geological Society of America, p. 563–574.

Heller, R. L., 1954, Stratigraphy and paleontology of the Roubidoux formation of Missouri: Missouri Geological Survey and Water Resources, 2nd Series, v. 35, 118 p.

Loch, J. D.; Chludzinski, G. P.; and Spreng, A. C., 1993, Lower Ordovician faunas, correlation and bioherms in the Jefferson City near Rolla, Missouri [abstract]: Geological Society of America Abstracts with Programs, North-Central Section, v. 25, no. 3, p. 63.

Repetski, J. E.; Ethington, R. L.; Furnish, W. M.; and Kennedy, D. J., 1993, Conodonts from the Oneota and Gasconade Dolomites (Lower Ordovician) of the central midcontinent, U.S.A. [abstract]: Geological Society of America Abstracts with Programs, North-Central Section, v. 25, no. 3, p. 74–75.

Ross, R. J., Jr.; Hintze, L. F.; Ethington, R. L.; Miller, J. F.; Taylor, M. E.; and Repetski, J. E., 1997, The Ibexian, lowermost Series in the North American Ordovician, with a section on echinoderm biostratigraphy by James Sprinkle and T. E. Guensburg: U.S. Geological Survey Professional Paper 1579-A, 50 p.

Seo, K.-S.; and Ethington, R. L., 1993, Conodonts from the Manitou Formation, Colorado, U.S.A.: Journal of the Paleontological Society of Korea, v. 9, no. 1, p. 77–92.

Thompson, T. L., 1991, Paleozoic succession in Missouri, Part 2, Ordovician System: Missouri Department of Natural Resources Report of Investigations 70, 282 p.

Thompson, T. L.; and Robertson, C. E., 1993, Guidebook to the geology along Interstate Highway 44 (I-44) in Missouri: Missouri Department of Natural Resources Report of Investigations 71, Guidebook 23, 185 p.

Depositional and Diagenetic Controls on Porosity Development in the Ordovician Viola Formation, South-Central Kansas

K. David Newell
Kansas Geological Survey
Lawrence, Kansas

ABSTRACT.—The Upper Ordovician Viola Formation, an important petroleum reservoir in the Midcontinent, is a platform-carbonate unit present over much of the subsurface in Kansas. It is markedly thinner in south-central Kansas than in Oklahoma, averaging only about 100 ft in thickness. It is composed of two generally upward-fining sedimentary packages that are vertically separated from each other by a thin intraformational breccia. This breccia may represent a brief period of subaerial exposure. Each sedimentary package consists of an echinoderm-rich packstone unit overlain by a thicker unit composed of lime wackestones and mudstones. The echinoderm-rich packstones, with minor grainstones, were deposited in nearshore areas in agitated water. Overlying finer grained facies were deposited in deeper waters farther offshore. Subtidal environments dominate, with minor storm deposition represented by graded carbonate sands.

Original interparticle porosity in the echinoderm-rich packstones and grainstones was occluded early by syntaxial spar. Locally, some of the coarsest echinoderm grainstones have cement-reduced interparticle porosity that may be sufficient to make them viable petroleum reservoirs, but most grain-supported lithologies in the Viola are nonporous. Dolomitization also improved the porosity of the echinoderm-rich packstones and grainstones. The best porosity in the Viola is intercrystalline, moldic, and vuggy porosity, which is developed where the subtidal mudstones and wackestones have been dolomitized. The porosity in these dolomitized rocks averages 8% to 10% but may be as great as 23%. Approximately 6% porosity must occur before significant permeability is manifest in any Viola subunit.

The Viola was eroded down to its basal packstone subunit over the Central Kansas arch and was completely removed on the crest of the Chautauqua arch. Viola subunits on the flanks of these two early Paleozoic arches are dolomitized near their pinchouts. These subunits are generally undolomitized where they underlie outliers of the Upper Ordovician Maquoketa Shale. Breccia clasts of Viola dolomite below the unconformity at the base of the Upper Devonian–Lower Mississippian Chattanooga Shale, and strontium isotopes of Viola dolomite having values of approximately 0.709, indicate that the major episode of dolomitization occurred in Silurian time.

Existing petroleum-production trends in the Viola in south-central Kansas are in areas where dolomitized units are preserved on the crests of local anticlines. Possible stratigraphic traps may be present where porous Viola strata pinch out on the flanks of the northwest–southeast-trending Chautauqua and Central Kansas arches, and on the flanks of smaller anticlines. Local stratigraphic traps also may be present on the western flank of the south-plunging Pratt anticline, where westward-thickening wedges of dolomitized mudstones and wackestones are enclosed by nonporous packstone and grainstone beds.

INTRODUCTION

Dolomitization appears to be a major control of porosity in the Upper Ordovician Viola Formation in south-central Kansas (Fig. 1). In turn, the dolomitization is related to depositional texture and structural position of the Viola with respect to early Paleozoic arches. Geologic evidence points to most of the dolomitization having taken place during Silurian time.

GEOLOGIC BACKGROUND

The thick and regionally persistent carbonate unit above the Middle Ordovician Platteville (or Decorah) Formation, and below the Upper Ordovician Maquoketa Shale, is identified in Kansas as the Viola Formation (Goebel, 1968). The maximum thickness of the Viola Formation in Kansas is approximately 325 ft just south of the Nebraska state line in Jewell and Republic Counties (Cole, 1975). The Viola is markedly thinner in Kansas than it is in Oklahoma, where it is 935 ft thick in the subsurface north of the Wichita Mountains (Cram, 1930; Ireland, 1966). Various erosional events in the Paleozoic have removed the Viola from structural highs (Fig. 1).

St. Clair (1982, 1985) utilized cuttings, cores, and wireline logs to divide the Viola into four informal subunits on the western flank of the Sedgwick basin in Barber and Pratt Counties. From base to top, these units are (1) basal limestone, 5 to

Newell, K. D., 2000, Depositional and diagenetic controls on porosity development in the Ordovician Viola Formation, south-central Kansas, *in* Johnson, K. S. (ed.), Platform carbonates in the southern Midcontinent, 1996 symposium: Oklahoma Geological Survey Circular 101, p. 107–115.

25 ft thick; (2) lower cherty dolomitic limestone, 10 to 104 ft thick; (3) upper limestone, 4 to 32 ft thick; and (4) upper cherty dolomitic limestone, 4 to 48 ft thick (Fig. 2). The limestones are low-porosity crinoidal packstones and grainstones, whereas the cherty dolomites generally are mixed-skeletal dolomitized wackestones and mudstones with nodular chert (St. Clair, 1982, 1985). The subunits in the Viola can be mapped over much of southern Kansas, and they define two similar upward-deepening depositional cycles (Newell, 1996). The lower cycle is defined by the basal limestone subunit and lower cherty dolomitic limestone subunit; the upper cycle is defined by the upper limestone subunit and the upper cherty dolomitic limestone subunit (Fig. 2).

POROSITY DISTRIBUTION

Cross-plotted porosity and permeability data for the basal and upper limestone subunits from four cores (Fig. 3) indicate that these subunits generally have enhanced porosity where they are dolomitized. Permeability apparently is not significantly changed with dolomitization in the grain-supported lithologies. A breakdown of lithologies of these cores according to whether the sample analyzed is a mud-poor packstone/grainstone versus a wackestone (Fig. 3) also indicates that wackestones in the basal and upper limestone subunits have no more marked propensity to be dolomitized than the grain-supported carbonates.

A comparison of core-derived porosity and permeability data of the basal and upper limestones with those of the lower and upper cherty dolomitic limestones (Fig. 3) indicates that the basal and upper limestones are relatively nonporous and impermeable. Samples with less than 6% porosity generally have less than 1 md permeability. An inspection of cores indicates that these dolomitized mudstones and wackestones generally have significant porosity, either intercrystalline, vuggy, or moldic. Intercrystalline porosity is usually microscopic and is developed between dolomite rhombs. Molds are mostly megascopic, commonly after mollusk fragments.

VIOLA DOLOMITIZATION

A subcrop map of Viola subunits, based on over 1,700 wells, shows that the Viola Formation is eroded down to its lowermost informally identified subunit, the basal limestone, over the north-northwest–south-southeast-trending crest of the Central Kansas arch, which extends through southwestern Rice, northeastern Reno, and northwestern Sedgwick Counties (Newell 1996, 1997). Successively younger subunits are arrayed in a generally symmetric pattern along the flanks of the arch. Although uplift of the Chautauqua and Central Kansas arches continued into Late Mississippian time (Merriam, 1963), isopach maps of the Upper Devonian–Lower Mississippian Chattanooga Shale and its stratigraphic subdivisions in Lambert (1992, 1993) suggest that these arches were not active during deposition of the Chattanooga Shale.

A map of the limestone/dolomite ratio for the entire Viola Formation (Fig. 4) shows a heavily dolomitized area directly north and west of the Chautauqua arch. The spatial association

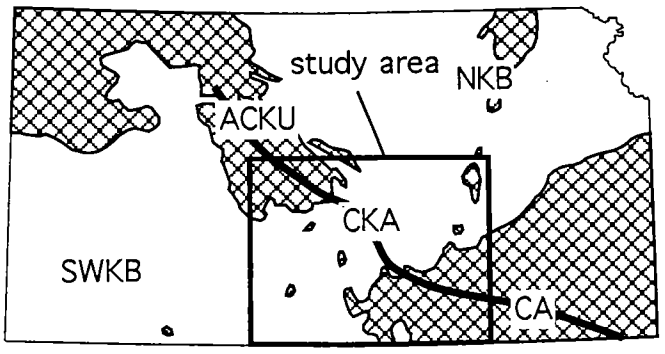

Figure 1. Location of study area and extent of Viola Formation in Kansas, and location of major early Paleozoic tectonic elements (from Merriam, 1963; Adkison, 1972). Cross-hatched areas are where Viola is now absent. *ACKU* = ancestral Central Kansas uplift; *CKA* = Central Kansas arch; *CA* = Chautauqua arch; *NKB* = North Kansas basin; *SWKB* = Southwest Kansas basin.

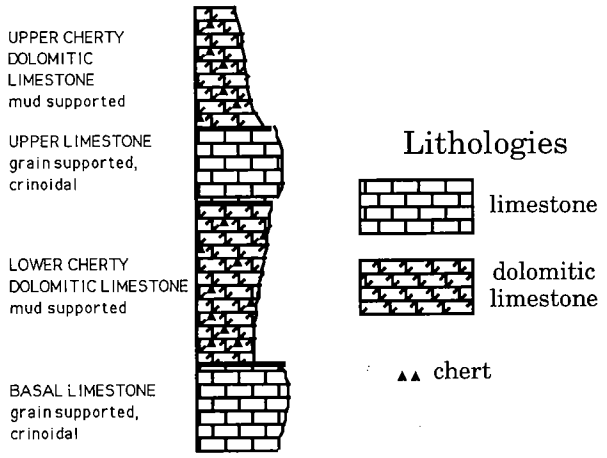

Figure 2. Subunits of the Viola Formation in south-central Kansas, according to St. Clair (1982, 1985).

of this dolomite with the Chautauqua arch implies that the arch exerted control in the genesis of much of the dolomite. The ancestral Central Kansas uplift does not have a similar halo of dolomite associated with it, therefore implying that it did not localize dolomitizing fluids and possibly was not a major uplift preceding or contemporaneous with Viola dolomitization.

In order to better understand the pattern of dolomitization within the Viola, the general lithology of the subunits was compiled from a series of well-sample logs commercially produced by J. D. Davies, which are on file in the Geoscience Data Library at the Kansas Geological Survey (Lawrence, Kansas). The use of a single genre of logs reduces possible inconsistencies inherent in utilizing observations by different well-site geologists. The lithologies of each of the Viola subunits were interpreted to be limestone, limestone with minor dolomite, dolomite with minor limestone, dolomite, or chert/chert breccia. Inasmuch as chert is a universal accessory in the lower and upper cherty dolomitic limestone subunits, its presence was not specifically noted unless it was the sole lithology.

Symbols signifying the respective lithologies are superimposed at the well locations on a worm's-eye-view map (Fig.

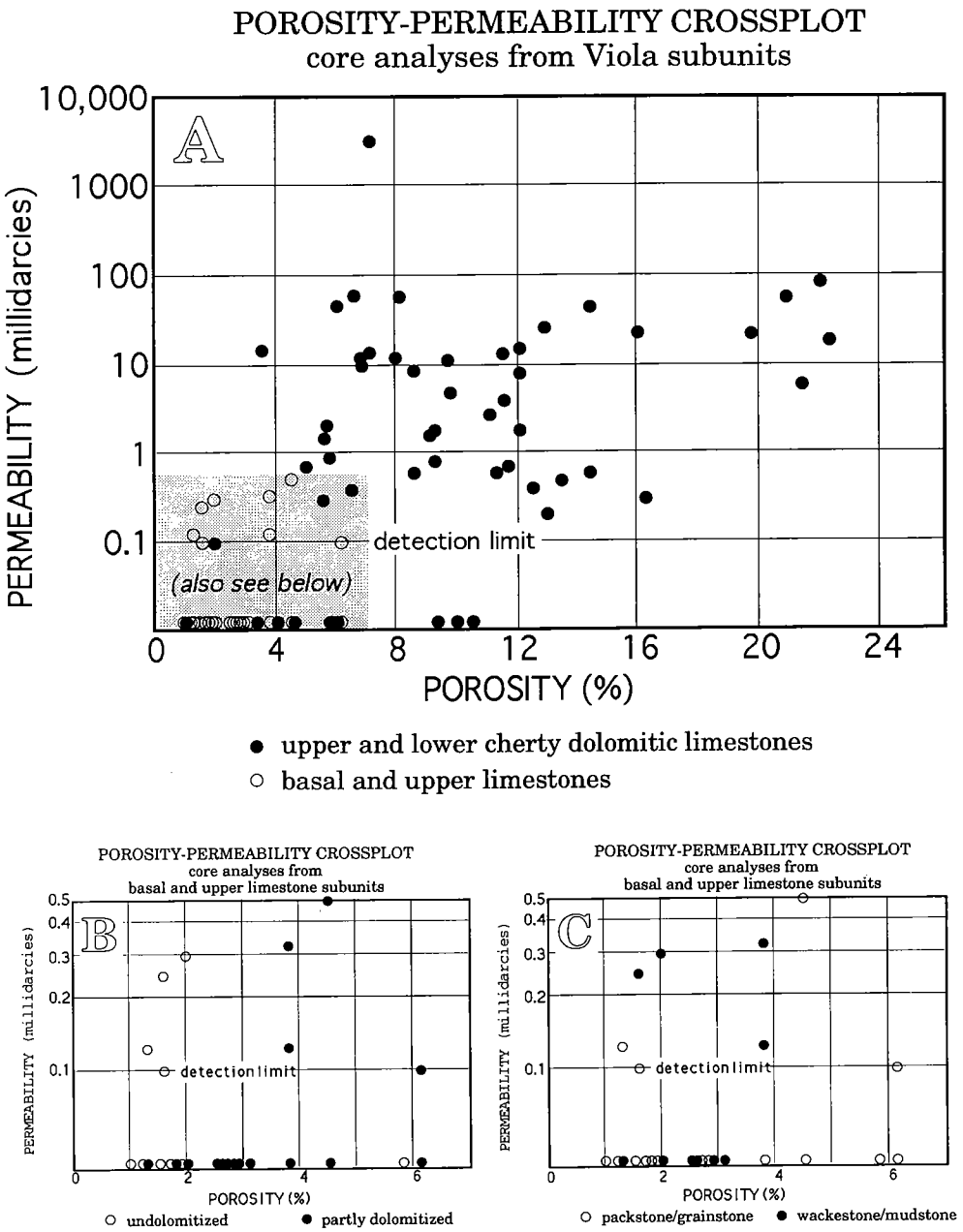

Figure 3. Permeability and porosity data from four Viola cores (Northern Natural Gas No. 1 Caldwell (sec. 2, T. 20 S., R. 8 W.), Braden-Zenith ZU-1 (sec. 11, T. 24 S., R. 11 W.), Braden-Zenith ZU-3 (sec. 11, T. 24 S., R. 11 W.), and Champlin No. 8 Speck (sec. 18, T. 20 S., R. 8 W.). In *A*, the Viola is differentiated according to subunit. The upper and lower cherty dolomitic limestone subunits are largely dolomitized, whereas the basal and upper limestone subunits are undolomitized or only slightly (<25%) dolomitized. In *B*, samples measured in the basal and upper limestone subunits are differentiated as to whether they are undolomitized or partly dolomitized. In *C*, they are differentiated as to depositional texture. Any sample below the detection limit of 0.1 md is displayed at the base of the graph. Better reservoir quality correlates with dolomitization. Petrophysical data were obtained by Core Laboratories, Inc. (Dallas, Texas) and are archived at the Kansas Geological Survey (Lawrence, Kansas).

5). (This type of map illustrates the geologic unit directly above the Viola Formation.) Although there is scatter to the data, wells recording "limestone" are more common beneath the Maquoketa Shale where it is preserved in off-arch positions, such as in southern Barber County and in Rice, Harvey, Reno, McPherson, and Marion Counties.

TIMING OF DOLOMITIZATION

The pattern of limestone being preferentially preserved under the Upper Ordovician Maquoketa Shale suggests that this unit was extant during dolomitization. Younger shales that directly overlie the Viola Formation, such as the Devo-

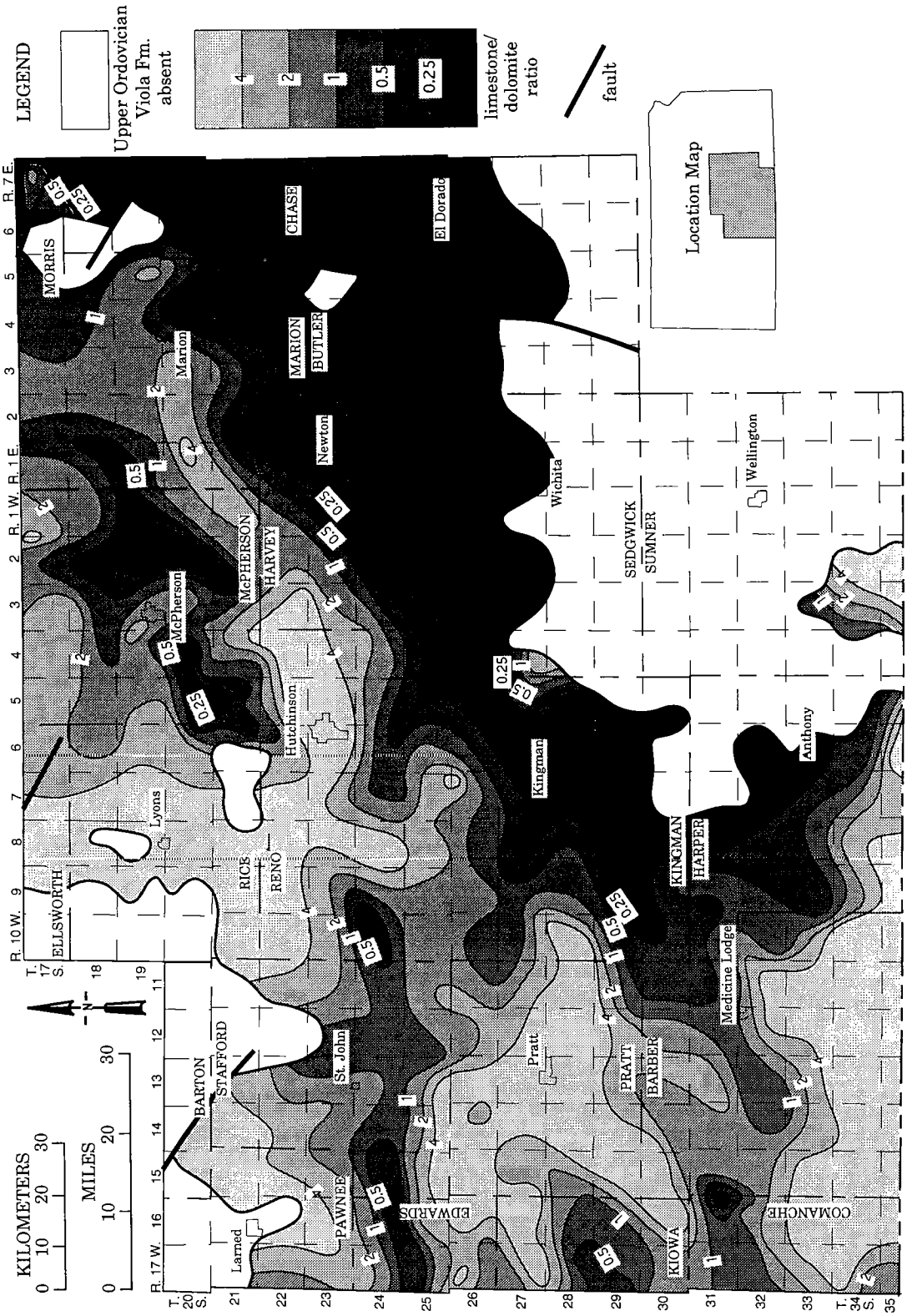

Figure 4. Limestone/dolomite ratio for entire Viola Formation (from Blair and Berendsen, 1988); based on a control of one well per township. Well-sample logs, supplemented with visual inspection of offsets of curves in neutron–density logs, provided an approximate stratigraphic determination of dolomite versus limestone.

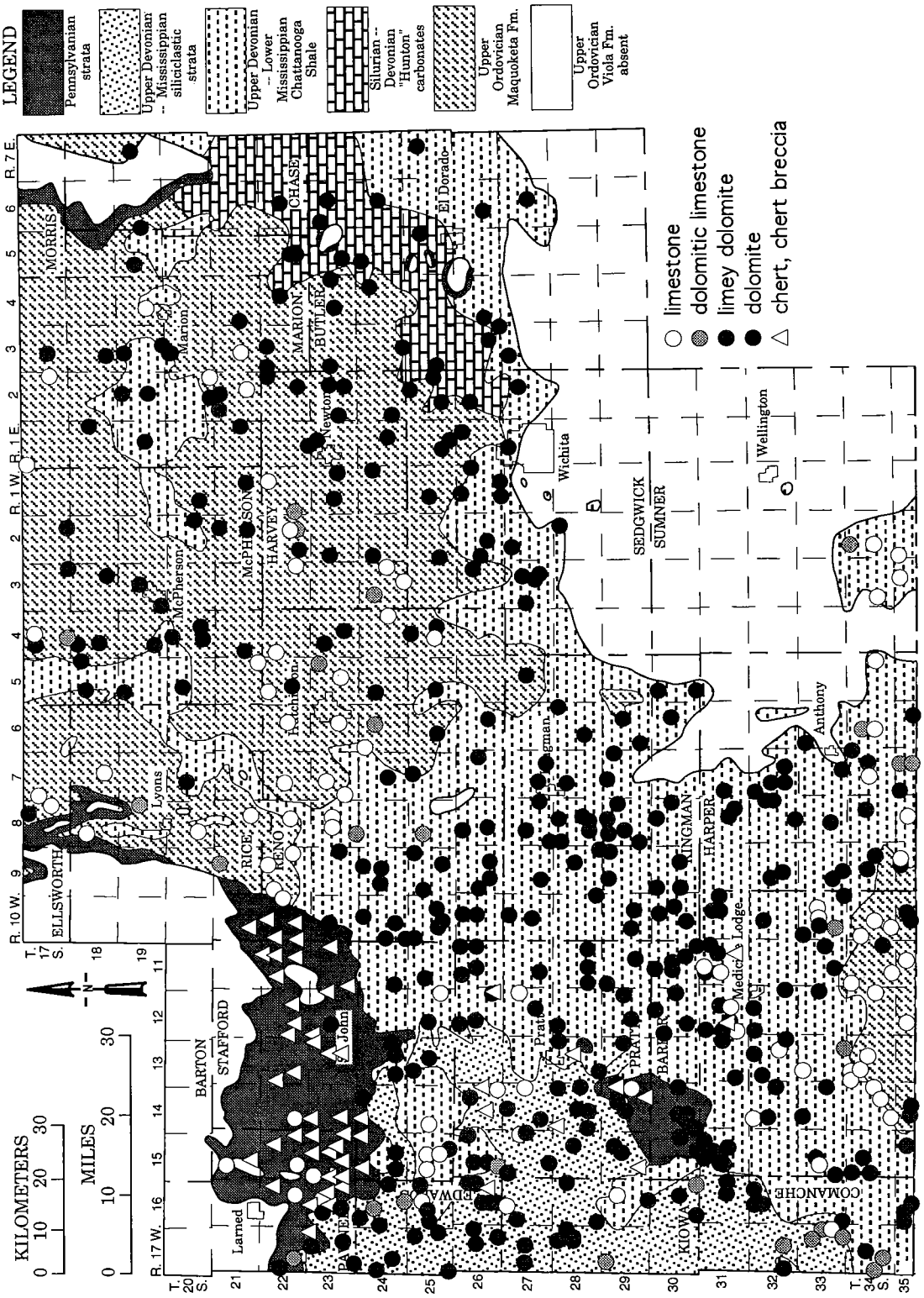

Figure 5. Dominant lithology at the top of the Viola Formation, from J. D. Davies' sample logs, superimposed on a worm's-eye-view map. Dolomite is dominant toward the pinchouts of the Viola subunits near the crest of the Chautauqua arch, and in the basal limestone subunit preserved atop this arch. Limestone may be preferentially preserved below the Maquoketa Shale.

nian–Mississippian Chattanooga Shale, apparently do not correlate with the pattern of dolomitization in the Viola; hence, they may have been deposited after dolomitization.

"Intraformational breccias" or "intrastratal karst" (see Mussman and Read, 1986; Kerans, 1988) is locally present in the upper cherty dolomitic limestone at the top of the Viola Formation. These breccias are the product of dissolution and generally consist of "fitted clasts" with interstitial coarsely crystalline calcite spar. An examination of the margins of the clasts in these intraformational breccias reveals key details regarding the timing of brecciation versus dolomitization. An intraformational breccia beneath the Chattanooga Shale at the Sinclair-Prairie No. 4 G. Oldfather well (4,328 ft depth) in Barber County (sec. 7, T. 31 S., R. 14 W.) is composed of clasts of dolomitic mudstone and chert set in a matrix of calcite. The margins of the dolomite clasts are sharp, and some dolomite rhombs are broken, indicating that dolomitization occurred before the brecciation. The brecciation, in turn, appears to be related to the unconformity at the base of the Chattanooga Shale.

Another clue to the timing of the dolomitization can be the strontium-isotope geochemistry of the dolomite. The $^{87}Sr/^{86}Sr$ ratio of a marine carbonate mineral is identical to the isotopic ratio of the water from which that mineral precipitated, because no significant isotopic fractionation in Sr occurs with precipitation (Veizer and Compston, 1974). A standard reference curve for secular variations of the $^{87}Sr/^{86}Sr$ ratio of seawater and associated marine carbonates over Phanerozoic time was documented by Burke and others (1982; Fig. 6). $^{87}Sr/^{86}Sr$ ratios for seawater changed drastically between Late Ordovician time (~0.708) and Late Silurian time (~0.709); therefore, the $^{87}Sr/^{86}Sr$ ratio of the dolomite in the Viola may ascertain its timing.

The results of isotopic analyses of Sr (Fig. 6) are consistent with major dolomitization of the Viola occurring from a fluid derived from Silurian seawater. Two samples of dolomitized basal limestone (1SH4042.2 and 1NH4132.7) from near the crest of the Chautauqua arch have Sr isotopic ratios corresponding to marine carbonates deposited during Early Silurian time. Two samples of dolomite (ZU13789.1 and 4GO4328) from the upper cherty dolomitic limestone have ratios consistent with Late Silurian marine waters. Two samples of dolomite, one from the basal limestone (D1W03.3) and one from the lower cherty dolomitic limestone (ZU33784.5), have relatively low isotopic ratios. These values are consistent with early dolomitization (possibly from fluids derived from Late Ordovician seawater), mixing of solutes derived from dissolved Ordovician carbonates and Silurian seawater, or mixing of Silurian seawater with Ordovician connate water. The process of dolomitizing fluids entering the Viola Formation from above is consistent with samples at the top of the Viola having a higher Sr isotopic ratio than those farther down within the formation.

POSSIBLE PETROLEUM TRAPS RELATED TO DOLOMITIZATION

A compilation of available literature on Viola oil and gas fields (Table 1) indicates that dolomites mostly compose the principal pay zones. Furthermore, Viola production trends in south-central Kansas (Newell, 1997) are spatially associated with broad synclines in which either the lower or upper dolomitic limestone subunits are preserved. Speculatively, stratigraphic traps may also occur partly as a result of the subcrop pattern of the Viola subunits—specifically, in areas where the basal and upper limestone subunits are present updip of either the lower or upper dolomitic limestones. Although this type of trap has yet to be documented, recognition of which Viola subunit is present within a given oil field may also aid in de-

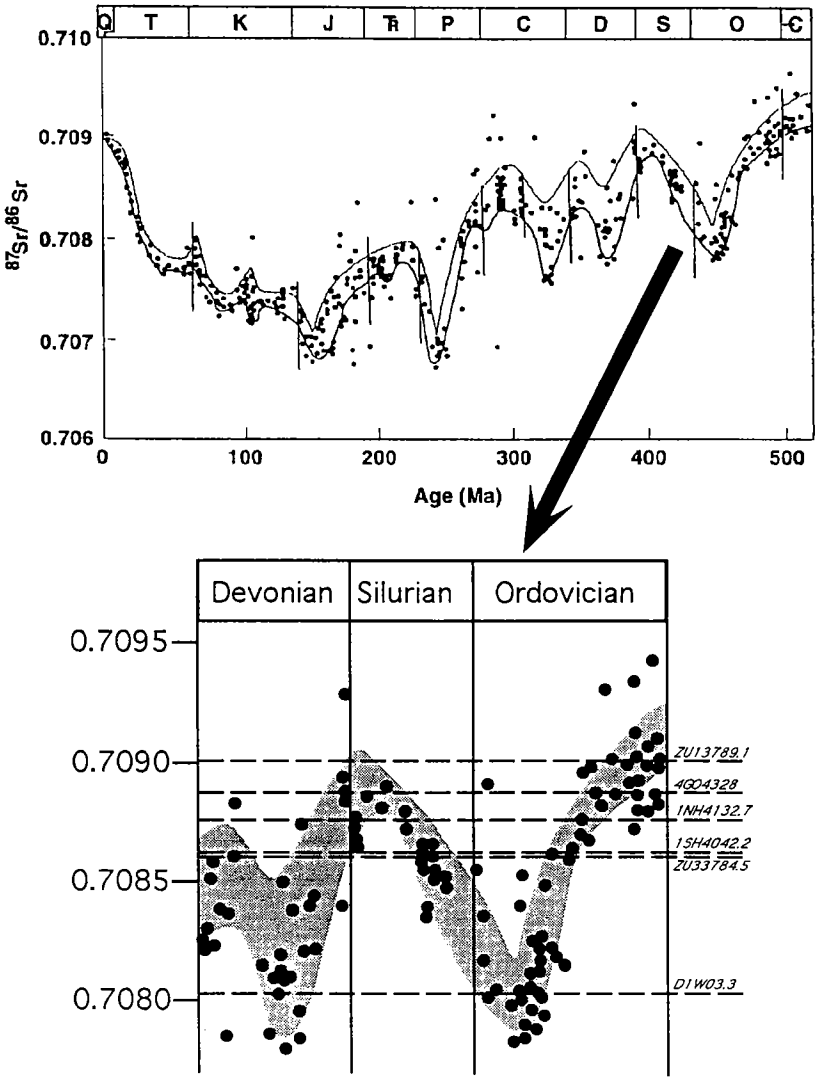

Figure 6. Secular variations (above) in strontium isotopes for marine carbonate rocks through Phanerozoic time, with results (below) from six dolomite samples from the study area. Upper part of figure from Burke and others (1982), reprinted in Allan and Wiggins (1993, p. 52); reprinted with permission of AAPG and GSA.

Table 1.—Survey of Literature on Oil and Gas Fields That Produce from the Viola Formation in South-Central Kansas

FIELD NAME	LOCATION (COUNTY)	TYPE of TRAP of PAY	TYPE	RESERVOIR LITHOLOGY	REFERENCE
Alameda	T.28S., R.7W. (Kingman)	structural	oil	med.-grained vuggy dolomite	King (1965a,b)
Albion, Albion North	T.26S., R.6W. (Reno)	stratigraphic	oil	fractured, vuggy dolomite	Oros (1965)
Cairo North	T.28S., R.11W. (Pratt)	stratigraphic	oil	med.-grained cherty dolomite	Thompson (1956)
Cunningham	T.27-28S., R.11-12W. (Kingman, Pratt)	struct./strat.	gas	porous dolomite	Rutledge and Bryant (1937) Page (1940) Skelly Oil Co. Geol. Dept. (1956)
Deerhead	T.32S., R.15W. (Barber)	stratigraphic	oil, gas	med.-grained dolomite, coarse-grained limestone	Tucker (1956)
El Dorado	T.25S., R.5E. (Butler)	structural	oil, gas	cherty dolomitic limestone	Reeves (1929) Biederman (1966)
Enlow	T.24S., R.16W. (Edwards)	structural	oil	vuggy med.-crystalline limestone	Sheats (1956)
Jem	T.30S., R.13W. (Barber)	stratigraphic	oil	chert breccia, dolomite	Brown and Banta (1993)
Lerado	T.26S., R.9W. (Reno)	structural	oil	med.-crystalline dolomite	McGinness (1956) Steincamp (1965)
Lerado Southwest	T.26S., R.9W. (Reno)	structural	oil	med.-crystalline dolomite	McGinness (1956)
Lindsborg	T.16-17S., R.3-4W. (McPherson, Saline)	struct./strat.	oil	coarse-crystalline limestone	Newell (1990)
Nescatunga	T.32S., R.18W. (Comanche)	structural	gas	vuggy cherty dolomite	Capps (1965)
Rhodes	T.33S., R.11W. (Comanche)	stratigraphic	oil	(not specified)	Clark (1956)
Skully	T.18S., R.1E. (Marion)	structural	oil	dolomite	Salgat (1983)
Sullivan	T.32S., R.8-9W. (Harper)	struct./strat.	oil show	sucrosic dolomite	Erlenwein (1985)
Valley Center	T.25-26S., R.1W., R.1E. (Sedgwick)	structural	oil	vuggy coarse-crystalline dolomite	Wright (1960)
Willowdale	T.21S., R.9W. (Kingman)	structural	oil	cherty med.-crystalline dolomite	Cruce (1956)
Zenith-Peace Creek	T.23S., R.10-11W. (Reno, Stafford)	stratigraphic	oil	cherty sucrosic dolomite	Imbt (1941) Paddleford (1941) Kornfeld (1943) Newell and others (1991)

termining flow patterns and oil deliverability within the field.

Another type of trap that has yet to be documented, but nevertheless may be a possible exploration play, is a stratigraphic trap created by the pinchout of porous beds by nonporous beds within the Viola. On the western flank of the Pratt anticline, the Viola is composed of alternations of porous dolomite with nonporous "crystalline" limestone beds (Fig. 7). The thinning of the Viola toward the crest of the Pratt anticline appears to be due to the convergence of the nonporous limestone beds at the expense of the intervening porous dolomite beds. The resulting pinchouts, or wedges of porous dolomite, may be potential stratigraphic traps within the Viola along the anticline.

CONCLUSIONS

Dolomitization is important in improving reservoir quality in the Viola Limestone in south-central Kansas, with most established production being derived from dolomitic pay zones. Mud-supported depositional textures are preferentially dolomitized, but on the broad crest of the early Paleozoic Chautauqua arch, even grain-supported textures in the Viola are dolomitized. Dolomitization in the early Paleozoic, most likely Silurian time, is indicated by (1) regional concentration of dolomite around and on the crests of early Paleozoic uplifts, (2) preferential preservation of limestone beneath outliers of Maquoketa Shale, (3) cross-cutting relationships of the dolomite with intraformational breccias associated with the unconformity at the base of the Chattanooga Shale, and (4) strontium-isotope ratios of the dolomite. Recognition of the stratigraphic and geographic characteristics of the dolomite allows speculation about possible stratigraphic traps in which additional oil may be found in the well-explored Sedgwick basin.

ACKNOWLEDGMENTS

I thank Robert Slamal and Michael Lambert for reviewing drafts of this manuscript. Paul Enos, Robert Goldstein, and John Doveton are also thanked for reviewing the dissertation on which much of this work is based. The Shell Research Fellowship granted by the University of Kansas Department of Geology helped defray expenses during research.

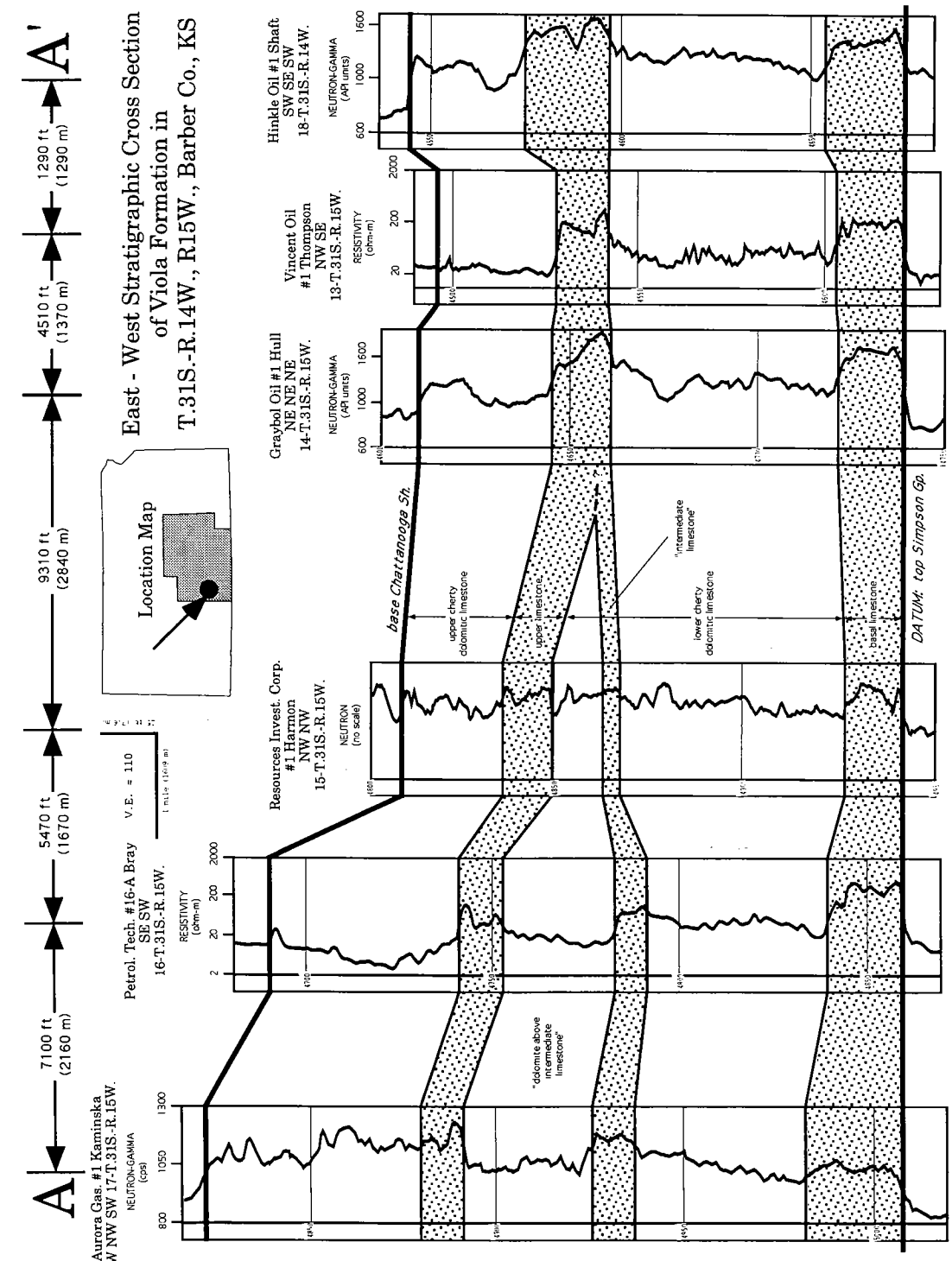

Figure 7. East–west stratigraphic cross section of the Viola Formation, extending off the western flank of the Pratt anticline; datum, top of Simpson Group. The basal, "intermediate," and upper limestones of the Viola Formation are relatively nonporous crinoidal packstones and grainstones that are interbedded with thicker cherty dolomitic limestones (primarily dolomitized mudstones and wackestones). Wedges of porous dolomite between nonporous limestone beds converging toward the crest (e.g., "dolomite above intermediate limestone") may be prospective stratigraphic traps.

REFERENCES CITED

Adkison, W. L., 1972, Stratigraphy and structure of Middle Ordovician rocks in the Sedgwick basin and adjacent areas, south-central Kansas: U.S. Geological Survey Professional Paper 702, 33 p.

Allan, J. R.; and Wiggins, W. D., 1993, Dolomite reservoirs; geochemical techniques for evaluating origin and distribution: American Association of Petroleum Geologists Course Notes Series, no. 36, 129 p.

Biederman, E. W., Jr., 1966, Petrology of the Viola formation, El Dorado field, Butler County, Kansas, *in* Schramm, M. W., Jr.; and Chenoweth, P. A. (eds.), Symposium on the Viola, Fernvale and Sylvan: Tulsa Geological Society Digest, v. 34, p. 41–60.

Blair, K. P.; and Berendsen, Pieter, 1988, Ordovician carbonate lithofacies: Kansas Geological Survey Open-File Report 88-51B, 1 sheet, scale 1:1,000,000.

Brown, H. A.; and Banta, A. D., 1993, Unusual occurrence of oil in the Viola Limestone, Pratt anticline, Kansas, *in* Johnson, K. S.; and Campbell, J. A. (eds.), Petroleum-reservoir geology in the southern Midcontinent, 1991 symposium: Oklahoma Geological Survey Circular 95, p. 104–112.

Burke, W. H.; Denison, R. E.; Hetherington, E. A.; Koepnick, R. B.; Nelson, H. K.; and Otto, J. B., 1982, Variation of seawater $^{87}Sr/^{86}Sr$ throughout Phanerozoic time: Geology, v. 10, p. 516–519.

Capps, W. M., 1965, Nestcatunga field, *in* Kansas oil and gas fields, v. 4: Kansas Geological Society, Wichita, p. 157–162.

Clark, W. R., 1956, The Rhodes field, *in* Kansas oil and gas fields, v. 1: Kansas Geological Society, Wichita, p. 77–81.

Cole, V. B., 1975, Subsurface Ordovician rocks in Kansas: Kansas Geological Survey Subsurface Geology Series 2, 18 p.

Cram, I. H., 1930, Early Paleozoic stratigraphy of the Wichita Mountain uplift, Oklahoma: American Association of Petroleum Geologists Bulletin, v. 14, p. 623–626.

Cruce, J. D., 1956, Willowdale field, *in* Kansas oil and gas fields, v. 1: Kansas Geological Society, Wichita, p. 95–97.

Erlenwein, S. D., 1985, Sullivan field, *in* Gerlach, P. M.; and Hansen, Thomas (eds.), Kansas oil and gas fields, v. 5: Kansas Geological Society, Wichita, p. 279–288.

Goebel, E. D., 1968, Ordovician System, *in* Zeller, D. E. (ed.), The stratigraphic succession in Kansas: Kansas Geological Survey Bulletin 189, p. 14–15.

Imbt, W. C., 1941, Zenith pool, Stafford County, Kansas, *in* Levorsen, A. I. (ed.), Stratigraphic type oil fields: American Association of Petroleum Geologists, Tulsa, p. 139–165.

Ireland, H. A., 1966, Resume and setting of Middle and Upper Ordovician stratigraphy, Midcontinent and adjacent regions, *in* Schramm, M. W., Jr.; and Chenoweth, P. A. (eds.), Symposium on the Viola, Fernvale and Sylvan: Tulsa Geological Society Digest, v. 34, p. 26–40.

Kerans, Charles, 1988, Karst-controlled reservoir heterogeneity in Ellenburger Group carbonates of west Texas: American Association of Petroleum Geologists Bulletin, v. 49, p. 1160–1183.

King, C. R., 1965a, Alameda field, *in* Kansas oil and gas fields, v. 4: Kansas Geological Society, Wichita, p. 1–17.

_____1965b, Alameda field, Sedgwick embayment "sleeper" [abstract]: American Association of Petroleum Geologists Bulletin, v. 49, p. 1562.

Kornfeld, J. A., 1943, Peace Creek field (Kansas), a stratigraphic trap: World Petroleum, v. 14, no. 13, p. 38–47.

Lambert, M. W., 1992, Lithology and geochemistry of shale members within the Devonian–Mississippian Chattanooga (Woodford) Shale, Midcontinent, USA: University of Kansas, Lawrence, unpublished Ph.D. dissertation, 163 p.

_____1993, Internal stratigraphy and organic facies of the Devonian–Mississippian Chattanooga (Woodford) Shale in Oklahoma and Kansas, *in* Katz, B., and Pratt, L. (eds.), Source rocks in a sequence stratigraphic framework: American Association of Petroleum Geologists Studies in Geology 37, p. 163–176.

McGinness, D. H., 1956, Lerado and Lerado Southwest fields, *in* Kansas oil and gas fields, v. 1: Kansas Geological Society, Wichita, p. 63–68.

Merriam, D. F., 1963, Geologic history of Kansas: Kansas Geological Survey Bulletin 162, 317 p.

Mussman, W. J.; and Read, J. F., 1986, Sedimentology and development of a passive- to convergent-margin unconformity; Middle Ordovician Knox unconformity, Virginia Appalachians: Geological Society of America Bulletin, v. 97, p. 282–295.

Newell, K. D., 1990, Lindsborg field—U.S.A., Salina basin, Kansas, *in* Beaumont, E. A.; and Foster, N. H. (eds.), Treatise of petroleum geology, atlas of oil and gas fields, structural trap IV: American Association of Petroleum Geologists, Tulsa, p. 347–382.

_____1996, Lithofacies and diagenesis of the Upper Ordovician Viola Formation on the Central Kansas arch and adjacent basins: University of Kansas, Lawrence, unpublished Ph.D. dissertation, 610 p.

_____1997, Correlation and distribution of reservoir and sealing facies within the Viola Formation, south-central Kansas, *in* Johnson, K. S. (ed.), Simpson and Viola Groups in the southern Midcontinent, 1994 symposium: Oklahoma Geological Survey Circular 99, p. 247–259.

Newell. K. D.; Cunningham, K. J.; Wong, J.-C.; Watney, W. L.; and Weatherbie, W. J., 1991, Large- and small-scale geological features of the Zenith field and their bearing on planning for enhanced oil recovery operations: 9th Tertiary Oil Recovery Conference Proceedings, Wichita; Tertiary Oil Recovery Project, University of Kansas, p. 99–130.

Oros, M. O., 1965, Albion and Albion North fields, Reno County, Kansas, *in* Kansas oil and gas fields, v. 4: Kansas Geological Society, Wichita, p. 18–35.

Paddleford, J. T., 1941, The Zenith pool of Stafford and Reno counties, Kansas: Mines Magazine, v. 31, p. 445–448, 454, 470, 472.

Page, J. H., 1940, Larger gas fields in Kansas: American Association of Petroleum Geologists Bulletin, v. 24, p. 1779–1797.

Reeves, J. R., 1929, El Dorado oil field, Butler County, Kansas, *in* Structure of typical American oil fields, v. 2: American Association of Petroleum Geologists, Tulsa, p. 160–167.

Rutledge, R. B.; and Bryant, H. S., 1937, Cunningham field, Kingman and Pratt counties, Kansas: American Association of Petroleum Geologists Bulletin, v. 21, p. 500–524.

St. Clair, P. N., 1982, Depositional history and diagenesis of the Viola Limestone in south-central Kansas: University of Kansas, Lawrence, unpublished M.S. thesis, 66 p.

_____1985, Core studies of the Viola Limestone in Barber and Pratt counties, *in* Watney, W. L.; Doveton, J. H.; and Walton, A. W. (compilers), Core studies in Kansas—sedimentology and diagenesis of economically important rock strata in Kansas: Kansas Geological Survey Subsurface Geology Series 6, p. 8–16.

Salgat, Brent, 1983, Scully field—Marion County, Kansas: American Association of Petroleum Geologists Bulletin, v. 67, p. 1327.

Sheats, Claude, Jr., 1956, Enlow pool, *in* Kansas oil and gas fields, v. 1: Kansas Geological Society, Wichita, p. 36–37.

Skelly Oil Company Geological Department, 1956, Cunningham field, *in* Kansas oil and gas fields, v. 1: Kansas Geological Society, Wichita, p. 25–28.

Steincamp, H. L., 1965, Lerado pool, *in* Kansas oil and gas fields, v. 4: Kansas Geological Society, Wichita, p. 114–122.

Thompson, J. W., 1956, Cairo North pool, *in* Kansas oil and gas pools, v. 1: Kansas Geological Society, Wichita, p. 16–17.

Tucker, V. M., 1956, Deerhead pool, *in* Kansas oil and gas pools, v. 1: Kansas Geological Society, Wichita, p. 29–31.

Veizer, Jan; and Compston, W., 1974, $^{87}Sr/^{86}Sr$ composition of seawater during the Phanerozoic: Geochimica et Cosmochimica Acta, v. 38, p. 1461–1484.

Wright, B. J., 1960, Valley Center field, *in* Curtis, G. R. (ed.), Kansas oil and gas fields, v. 3 (northeastern Kansas): Kansas Geological Society, Wichita, p. 149–156.

Viola Group Reservoir Facies, Fitts Pool, Pontotoc County, Oklahoma

Jim Puckette, Zuhair Al-Shaieb, and Michael Sykes
Oklahoma State University
Stillwater, Oklahoma

ABSTRACT.—Fitts pool is a 200-million-barrel oil field producing from the Franks graben, Pontotoc County, southern Oklahoma. Production is primarily from sandstones in the Simpson Group and carbonates in the Hunton and Viola Groups.

Detailed analysis of production, core, sample, and drilling data suggests that the Viola production is from shallow-water, grain-rich facies in the Viola Springs (Trenton) Formation. Higher porosity zones seen on wireline logs are related to moldic and vuggy porosity developed in packstone and grainstone lithofacies. Solution-enlarged fractures also enhanced porosity and permeability. Idiotopic dolomite occurs in mixed wackestone/packstone intervals and contributed to a certain extent to reservoir evolution by providing an avenue for fluid migration. On the other hand, the Welling (Fernvale), which is highly cemented grainstone with minimal porosity, is a nonproductive facies.

INTRODUCTION

The Fitts structure is a large fault-bounded anticlinal fold in the Franks graben, Pontotoc County, Oklahoma (Figs. 1,2). Fitts pool was discovered in 1933 and was developed rapidly in 1934 after oil was discovered in the Bromide Sandstone of the Simpson Group. By 1937, the field contained more than 300 wells that produced primarily from reservoirs in the Hunton, Viola, and Simpson Groups. In the main part of the field, the original oil–water contact in these reservoirs was relatively horizontal and crossed stratigraphic boundaries (Hyatt, 1936). As a result, progressively older rocks were petroleum bearing toward the crest of the structure (Fig. 3). The discovery and early development of Fitts pool are described in Dott and Swindell (1935), Hyatt (1936), and Teis and Teis (1937). The primary objective of this study was to analyze the Viola Group in Fitts pool and determine the stratigraphic position and character of its reservoir rocks.

STRATIGRAPHY

The Viola Limestone was first described by Taff (1902), who placed its age as Middle to Late Ordovician. Distinct differences in lithofacies subsequently led to the division of the Viola into two formations, Viola and Fernvale (Wengerd, 1948). These formations were later renamed the Viola Springs and Welling, respectively (Amsden and Sweet, 1983). In addition, the Viola has been interpreted as a single transitional unit (Grammer, 1983; Reid, 1980; Alberstadt, 1967; Glaser, 1965). In this paper, the terms *Viola Group, Viola Springs Formation,* and *Welling Formation* are used. The Viola Group formations correlate with Trenton and Fernvale, respectively. Traditionally, the industry utilizes this subsurface nomenclature (Fig. 4).

VIOLA LITHOFACIES

Cores and wireline logs of the Viola Group in Pontotoc County were examined to establish facies relationships in Fitts pool. Thin-section petrography and X-ray diffraction were used to augment whole-core analysis and determine rock constituents, textures, and diagenetic history. These results were supplemented with the findings of previous studies to develop a more comprehensive interpretation of lithofacies.

Four principal lithofacies were identified in the cores and named, using the Dunham (1962) classification: (1) pelmatozoan (crinoid)–bryozoan grainstone (facies A), (2) peloid–bioclast wackestone–packstone (facies B), (3) bioclastic (brachiopod–bryozoan) wackestone–packstone–grainstone (facies C), and (4) mudstone–wackestone (facies D).

Facies A: Pelmatozoan–Bryozoan Packstone–Grainstone

Facies A consists of disarticulated and abraded pelmatozoan (crinoid) and bryozoan bioclasts that are cemented by sparry calcite. This light-gray grain-rich facies forms sharp boundaries with facies D mudstone–wackestones (Fig. 5) and more gradational contacts with facies B and C.

The abraded skeletal grains and paucity of mud indicate a high-energy environment. Facies A likely represents shoal deposits within the shallow subtidal setting.

Facies B: Peloid–Bioclast Wackestone–Packstone

This facies is light to dark gray and brown, commonly burrowed, and consists of peloids and a variety of bioclasts in a mud-rich matrix or cemented by sparry calcite. Invertebrate allochems include brachiopods, trilobites, bryozoans, mollusks, ostracodes, and pelmatozoans. Bioclasts are smaller and

Puckette, Jim; Al-Shaieb, Zuhair; and Sykes, Michael, 2000, Viola Group reservoir facies, Fitts pool, Pontotoc County, Oklahoma, *in* Johnson, K. S. (ed.), Platform carbonates in the southern Midcontinent, 1996 symposium: Oklahoma Geological Survey Circular 101, p. 117–127.

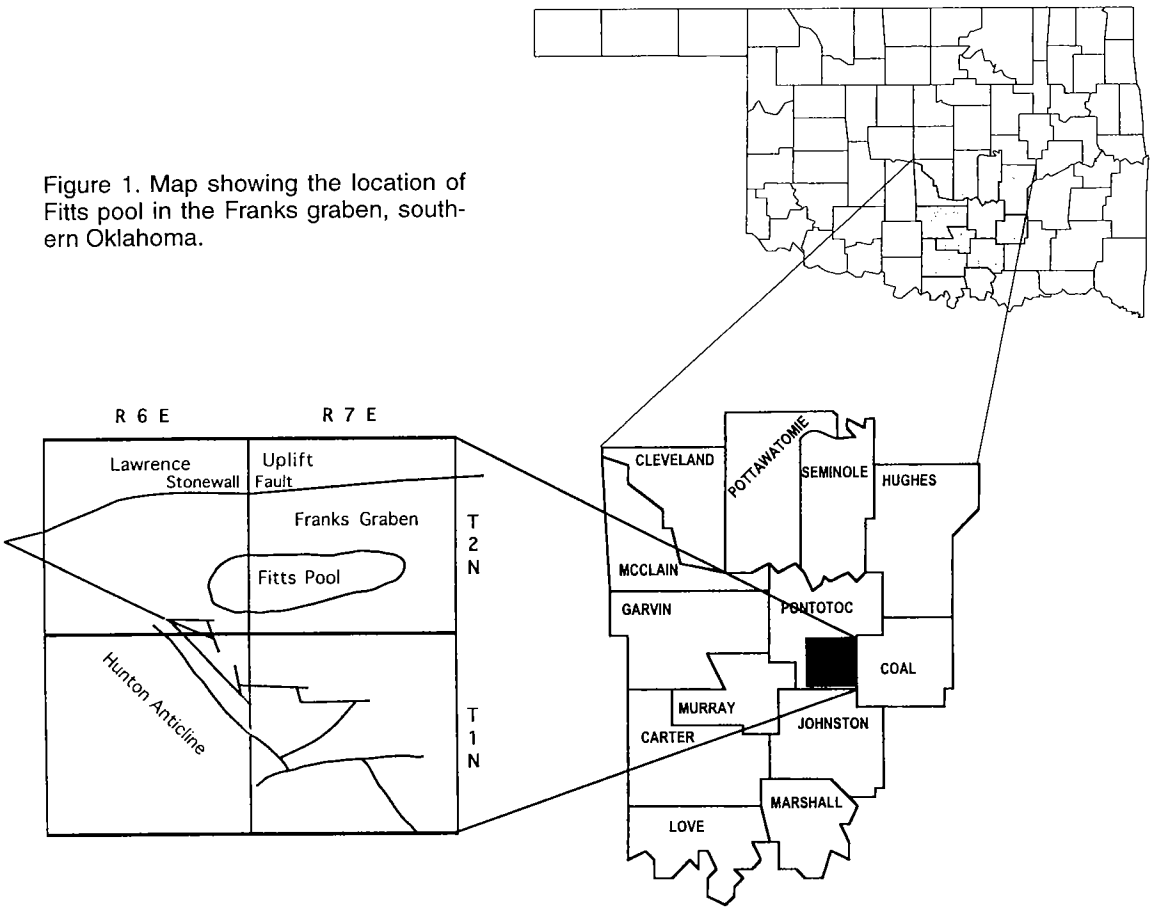

Figure 1. Map showing the location of Fitts pool in the Franks graben, southern Oklahoma.

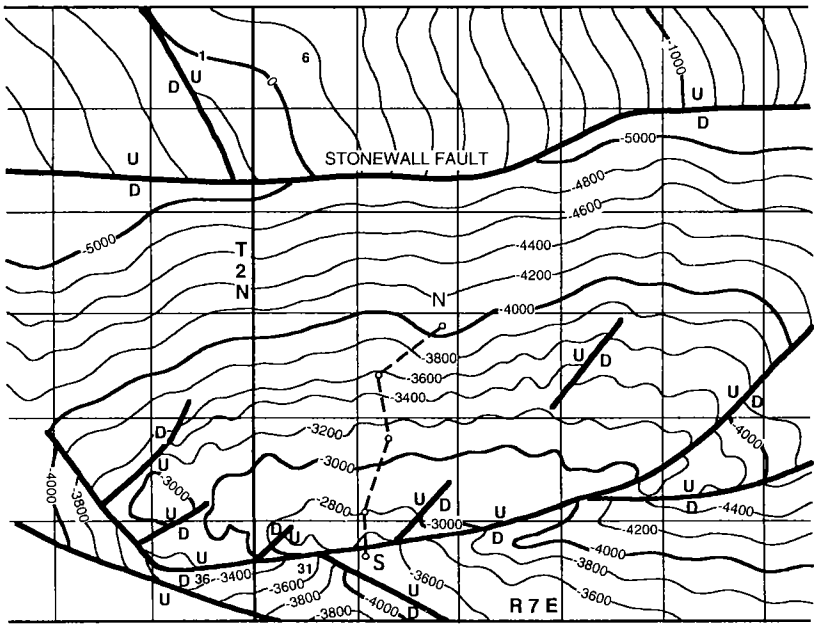

Figure 2. Structural-contour map showing the top of the Viola Group, Fitts pool. Contour interval south of the Stonewall fault is 200 ft; contour interval north of the fault is 100 ft. North–south cross section is shown in Figure 3.

more abraded in the sparry-cemented intervals. Peloids are variable in size and quantity and may compose up to 60% of the rock (Fig. 6).

The compositional and textural parameters described above suggest a possible lagoonal environment. Energy surges associated with storm cycles likely deposited coarser bioclastic debris. Gastropod- and ostracode-rich zones reflect more restricted conditions and water salinities that were unsuitable for supporting a diverse marine fauna.

Facies C: Bioclastic Wackestone–Packstone–Grainstone

This light-gray facies contains a more diverse fauna than facies A. Bioclasts are smaller and commonly aligned. Brachiopods are the dominant allochem, and bryozoans are numerous in selected intervals (Fig. 7). This facies is interbedded with mudstone that may be partially replaced by idiotopic dolomite and silicified.

Facies C represents a transition between high-energy pelmatozoan–grainstone facies A and lower energy wackestones–mudstones of facies D. The faunal diversity suggests a more stable environment than the pelmatozoan shoal (facies A) and a less restricted one than the mollusk–ostracode intervals of facies B. Bryozoan packstones may represent mound facies. The interbedded mudstone–packstone unit contains varying quantities of intact bioclasts and idiotopic dolomite. Episodic small-scale changes in energy and/or water depth are reflected in the mixed composition of this facies.

Facies D: Mudstone–Wackestone

The mudstone–wackestone facies (facies D) is present at the base of the Viola. This facies is in sharp contact with the underlying Bromide Formation and overlying grainstone (facies A). It contains stromatolitic, intraclastic microfacies (Reid, 1980) along its lower and upper boundaries and is dolomitized. Dark wackestone with graptolite debris (Fig. 8) and phosphate near the middle of the unit is indicative of deposition associated with maximum water depth. Increased invertebrate diversity toward the top suggests shallowing. Complete fossils indicate that most of the unit represents low-energy deposition below normal wave base.

A second dolomitized mudstone unit overlies the facies A grainstone near the base of the Viola. It has a sharp boundary with the underlying grainstone and a transitional one with the overlying facies C wackestone–packstones.

VERTICAL FACIES DISTRIBUTION

Core, outcrop, and wireline-log data document several depositional cycles in the Viola Group. Numerous small-scale depositional features were evident in the cores that were not reflected on wireline logs. While these features provide detailed insight into depositional history, their description is beyond the scope of this paper. Instead, the larger scale relationships are addressed that impact reservoir quality and petroleum accumulation.

Viola Springs Formation

The cored lithofacies document the flooding of the underlying Bromide Formation and subsequent sea-level fluctuations within the Viola Springs Formation. The flooding surface is represented by greenish-gray shale containing bioclastic debris. Mudstone (facies D) overlying this shale reflects continued marine transgression and deepening water. Graptolitic debris and phosphate represent the zone of maximum water depth. Increased faunal diversity and an intraclastic–stromatolitic microfacies (Reid, 1980) at the top of the unit suggest a marked decrease in water depth. A sharp (disconformable) contact separates facies D from the overlying crinoid–bryozoan grainstone of facies A. This abrupt juxtaposition of higher energy grainstones on mudstones–wackestones suggests a rapidly rising sea level and a shoreward shift of shallow intertidal facies.

Following deposition of facies A, sea level continued to rise, and carbonate mud (facies D) was deposited (Fig. 9). This unit shallows upward and forms a transitional contact with the bioclastic wackestone–packstones of facies C. The rich and diverse invertebrate fauna of facies C indicates shallow, well-circulated (open-marine) water..

The upper part of the Viola Springs (Fig. 9) is dominated by peloid-rich muddy carbonate (facies B) that likely was deposited in more restricted water (lagoons) behind pelmatozoan

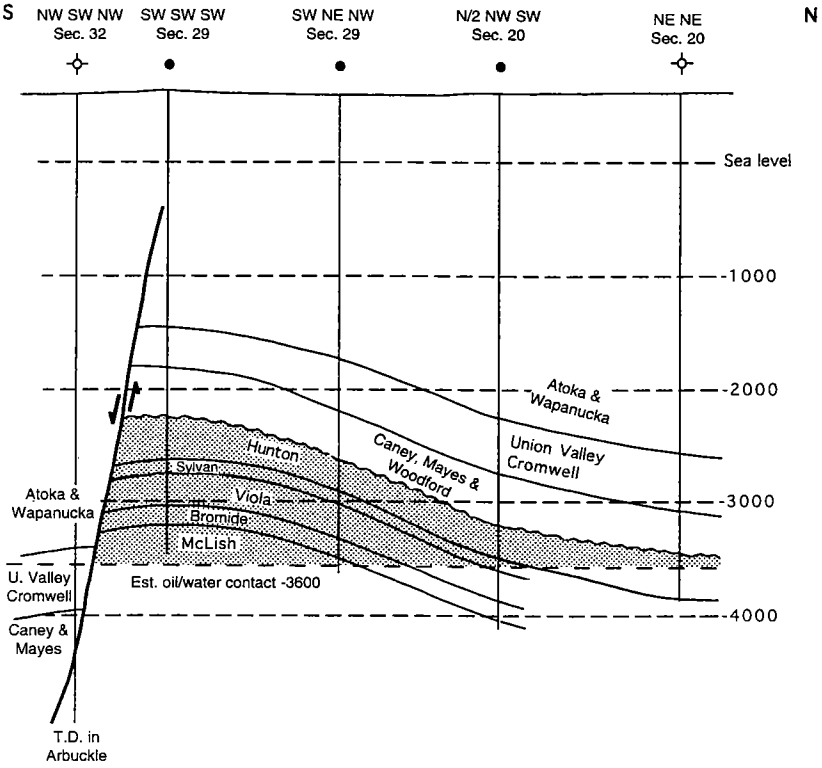

Figure 3. Structural north–south cross section through Fitts pool. The original oil–water contact (–3,600 ft) crosses stratigraphy, and progressively older rock units produce toward the crest of the structure. Depths shown in feet. Modified from Hyatt (1936).

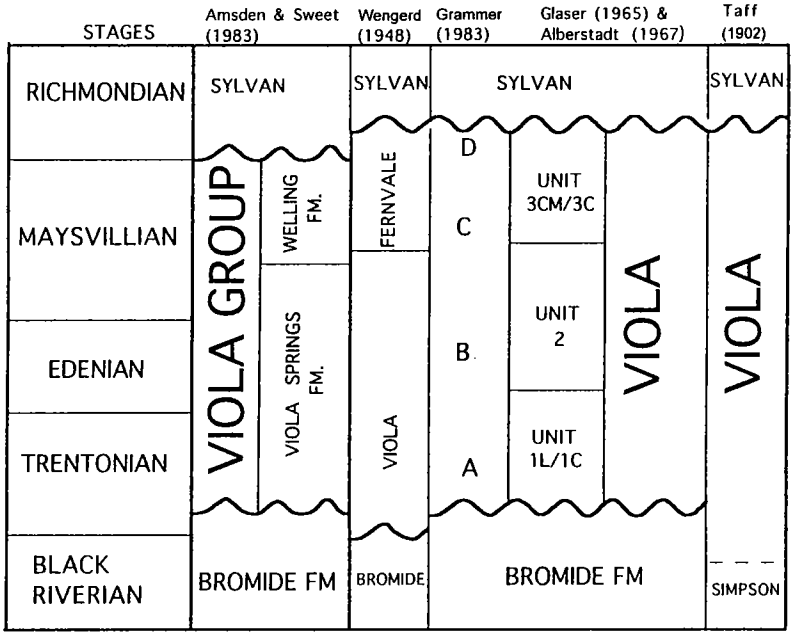

Figure 4. Generalized stratigraphic nomenclature of the Viola Group. Modified from Sykes and others (1997).

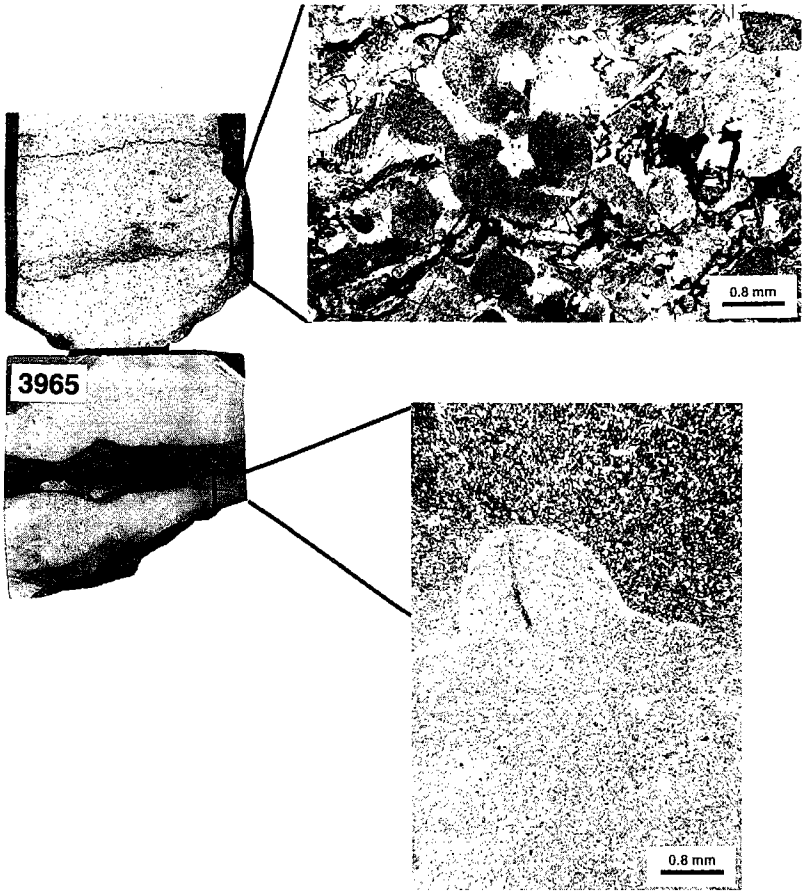

Figure 5. Core photograph and photomicrographs of grain-rich facies A (pelmatozoan grainstone) and underlying mud-rich facies D (mudstone–wackestone). Note sharp contact between the two facies and partial silicification (dark band) of facies D. Numeral on core slab indicates depth in feet.

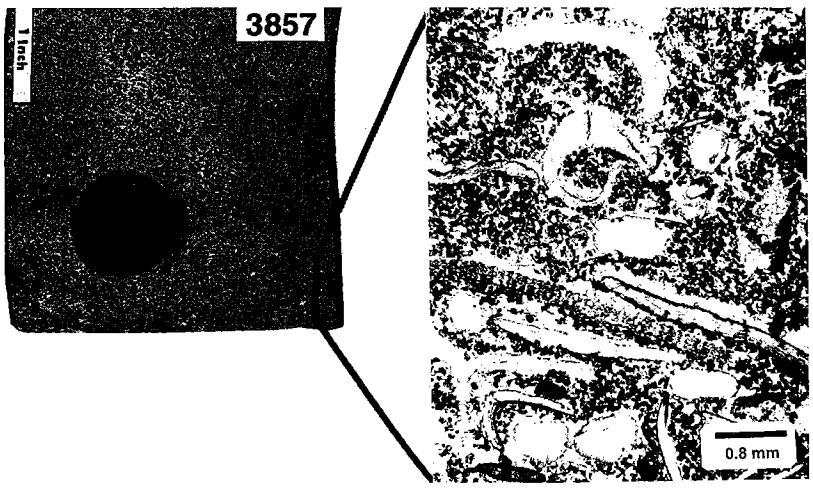

Figure 6. Facies B peloidal packstone. Much of the matrix is composed of small, dark peloids. Bioclastic allochems are primarily brachiopods, pelmatozoans, and trilobites. Darker spots in core photograph are moldic and vuggy pores. Depth, 3,857 ft.

shoals and/or bryozoan mounds. Grain-rich units within this low-energy subtidal interval contain disarticulated and abraded allochems that were likely transported into the lagoon during storm events.

Welling Formation

The Welling grainstone is cleaner than the underlying Viola Springs wackestone–packstone. Wireline-log signatures typically indicate decreasing radioactivity and porosity toward the top of the Viola that correlate with the Welling (Fig. 10).

DEPOSITIONAL MODEL

The Viola Group carbonates were deposited on a gentle southward-sloping carbonate ramp (Grammer, 1983; Smith, 1982; Galvin, 1982). The lithofacies in the Fitts area reflect those identified by Wilson (1975) as characteristic of shallow-marine settings.

Facies A pelmatozoan–bryozoan grainstone (abraded crinoid grainstone) represents high-energy subtidal shoal deposition. Facies B developed behind these shoals in a more restricted coastal lagoon. Peloids are a characteristic feature of this environment. Variations in faunal diversity and the volume of carbonate mud reflect a changing environment (restriction) and water depth in the lagoon. The high faunal diversity of facies C suggests a hospitable environment with significant water circulation. Facies C deposition occurred near the depth of normal wave base and basinward of the facies A grainstone shoals. Facies D mudstones are shallow-water open-marine subtidal rocks. The adaptation of these facies to the depositional models of Wilson (1975) and Burdette and Wright (1992) is shown in Figure 11.

DIAGENESIS

The Viola Group underwent multiple episodes of cementation and dissolution in response to sea-level fluctuation. Carbonates exposed during lowstands were dissolved by meteoric water. Liberated calcium carbonate precipitated as sparry calcite cement in the freshwater-saturated (phreatic) zone. This early cement formed syntaxial calcite overgrowths on pelmatozoan grains. Intergranular porosity developed when early sparry calcite cement and matrix were dissolved. Drusy calcite cement lined these pores.

Mixed-water idiotopic dolomite formed relatively early by the mixing of saline and meteoric waters when freshwater lenses migrated seaward in response to a drop in sea level. Dolomite formed in (1) burrows and (2) intergranular porosity in bryozoans, and (3) it replaced lime muds in the interbedded intervals. Silicification was also an early diagenetic product. Chert replaced mud matrix and allochems in interbedded/interlaminated intervals, generating brittle beds that were microfaulted during burial.

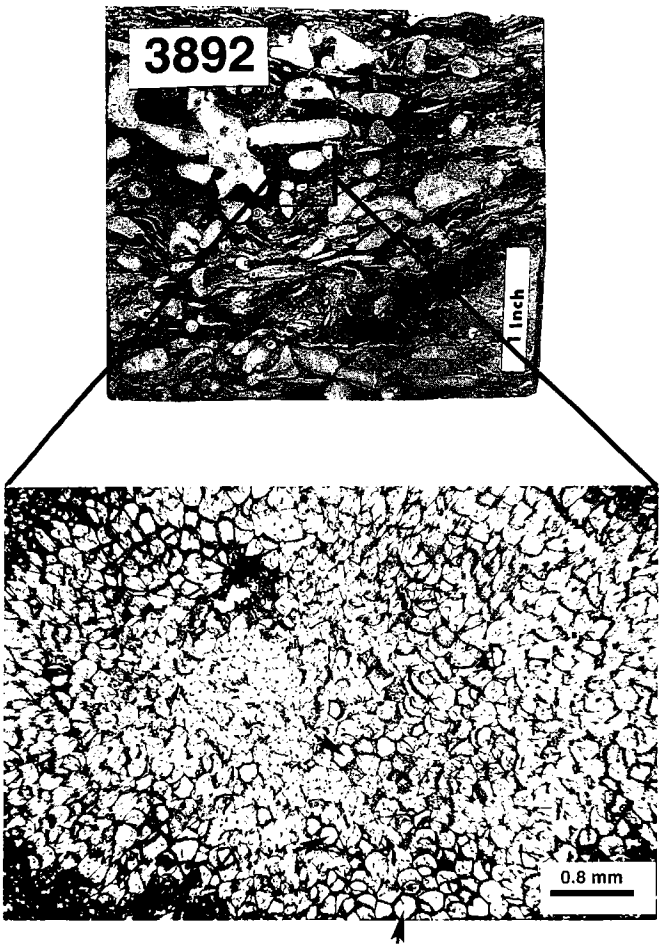

Figure 7. Facies C bioclastic packstone consisting of bryozoan and pelmatozoan fragments with a dolomudstone matrix. Bryozoans contain intragranular porosity (arrows), whereas the matrix is nonporous. Depth, 3,892 ft.

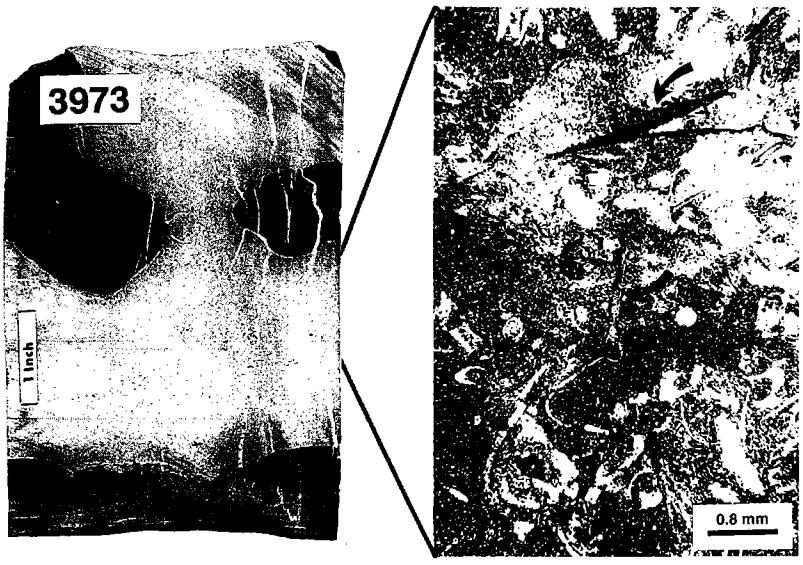

Figure 8. Abundant graptolitic debris (arrows) in wackestone of facies D. Cemented fractures (white) and silicification (dark nodules) are evident in the core photograph. Depth, 3,973 ft.

Burial and compaction partially collapsed pores in the zones with intergranular porosity. Post-compaction dissolution enlarged moldic pores and fractures, enhancing the porosity network. Fracture-filling sparry calcite and breccia-cementing carbonate matrix were dissolved during this episode. Late diagenetic products such as pyrite were associated with petroleum migration into the Viola porosity network.

RESERVOIR EVOLUTION

Vertical Distribution of Porosity

Porosity measurements recorded as wireline-log signatures indicate a similar vertical-porosity trend across the field. Porosity is very low (<4%) in the Welling and increases downward to a point 30–50 ft above the base of the Viola. From this point to the base, porosity is low (<5%) (Figs. 10,12).

Core-to-log calibrations indicate porosity increases in the grain-rich intervals of the Viola Springs Formation. Cores of the Welling–Fernvale from other fields in Pontotoc County contain solution-enlarged fractures and very little matrix porosity (Sykes and others, 1997). Wireline-log signatures across the Welling in Fitts pool measure similar low porosity (Figs. 10,12).

Porosity Types

Porosity in the Viola Springs is predominantly of five types: (1) moldic, (2) vuggy, (3) intergranular/intercrystalline, (4) intraparticle, and (5) solution-enlarged fracture.

Moldic porosity (Fig. 13) formed by the dissolution of bioclasts is the dominant type. Continued dissolution enlarged moldic pores to form vugs that cross-cut grains, cement, and matrix (Figs. 14,15). Bryozoan fragments were often preferentially dissolved, and their remnants remain in the pores (Fig. 14). Vuggy porosity is concentrated in the grainy intervals of facies B and C and correlates with the higher porosity evident in thin sections and wireline logs.

Intergranular porosity occurs primarily in grain-rich beds in facies B and C and results from the dissolution of early cement. These pores are often lined with grain-coating drusy calcite (Fig. 16).

Intercrystalline porosity is evident in thin dolomites of the interbedded/interlaminated wackestone–packstone intervals. Dolomite is concentrated in the muddier rocks and consists of limpid euhedral rhombs and cloudy rhombs with limpid rims (Fig. 17). These forms are characteristic of mixing-zone dolomite (Sears and Lucia, 1980). Intercrystalline porosity formed where the dolomite crystallized as clusters of rhombs in burrows or muddy layers. Dolomite also partially replaced calcite in bryozoan fragments, generating additional porosity. In Fitts pool, the volume of porosity attributed to dolomitization is relatively small. However, intercrystalline porosity may have been an important migration pathway for the corrosive fluids that formed moldic pores and vugs.

Intragranular porosity is common in bryozoan fragments (Fig. 7). Though volumetrically

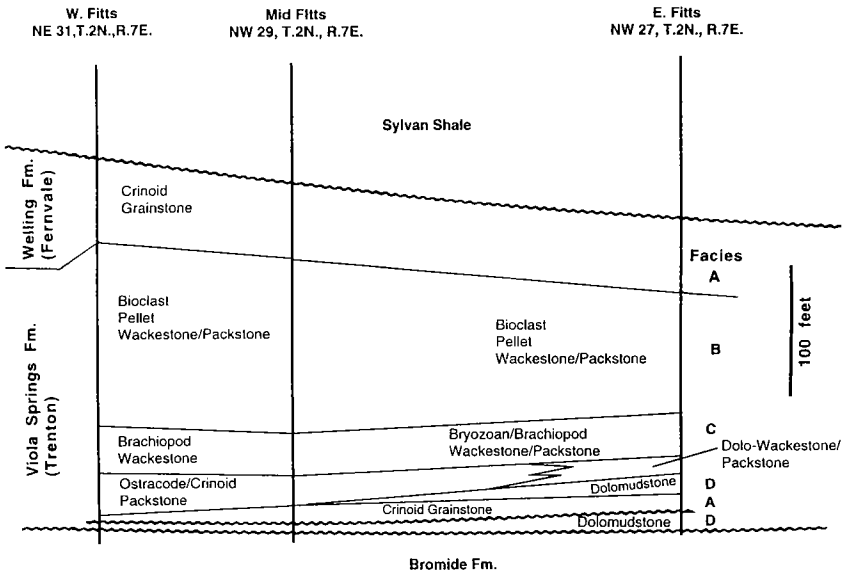

Figure 9. Stratigraphic cross section correlating Viola Springs lithofacies. Welling (Fernvale) lithofacies are inferred from log signature in the No. 21-29 East Fitts Unit well. Descriptions of the West Fitts and Mid Fitts cores are from Reid (1980).

small, this type of porosity also may have provided a pathway for fluids that dissolved grains and cement to form the reservoir facies.

Solution-enlarged fractures are present in several intervals. These fractures are partially cemented (Fig. 18) and are evidence of several stages of dissolution and cementation.

The original composition had a profound effect on reservoir evolution. Bioclast-rich zones with greater faunal diversity developed the highest porosity. Pelmatozoan-rich intervals with few other allochems were cemented extensively with syntaxial calcite overgrowths (Fig. 19). This cement occluded porosity and prevented porosity-forming corrosive fluids from migrating through the rock. This process accounts for the low porosity evident in the pelmatozoan grainstones (facies A) of the Welling and Viola Springs.

Bryozoans and mollusks were especially susceptible to dissolution. Consequently, facies B and C contain the most moldic and vuggy porosity. In addition, the non-pelmatozoan fauna did not form the extensive calcite overgrowths common to facies A. The absence of overgrowths allowed fluids to migrate through these rocks, dissolve early cements, and generate porosity (Figs. 14,15). Dolomite contributed to the dissolution process in facies B and C by providing additional pathways for fluid migration essential to dissolution and porosity generation. Facies D mudstones and wackestones lacked the abundant grains and early porosity network critical to the evolution of reservoir facies.

Porosity in the Welling consists of solution-enlarged fractures with scattered vugs (Fig. 20). These features reflect dissolution that likely occurred when the Viola was subaerially exposed prior to deposition of the Sylvan Shale (Sykes and others, 1997).

Paleokarstic Reservoir Models

The principal reservoirs in the Viola Group formed in the grainy beds of the Viola Springs Formation. During intra-Viola sea-level drops, these rocks were subjected to the diffuse flow (White, 1969) of ground water that dissolved grains and cement to form intergranular and moldic porosity. Matthews and Al-Shaieb (1993) identified similar reservoirs in the Hunton Group carbonates and called them type 2 paleokarstic reservoirs. These reservoirs accounted for most of the petroleum production from the Hunton Group.

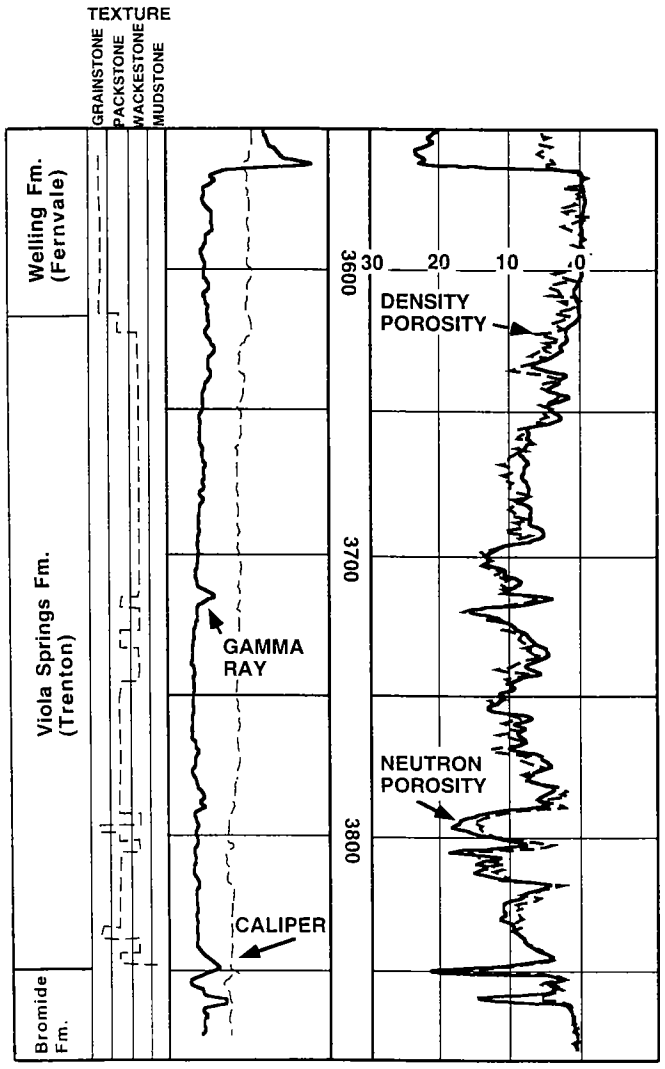

Figure 10 *(at left)*. Composite illustration of log signatures and lithofacies for the Viola Group, Sun Oil Co. West Fitts core, in the NE¼ sec. 31, T. 2 N., R. 7 E. Textural descriptions are from Reid (1980). Low porosity and a "clean" gamma-ray signature in the top 60 ft of the Viola are characteristic of Welling (Fernvale) pelmatozoan grainstones. The general increase in porosity with depth reflects the higher grain content of packstones and grainstones in the lower part of the Viola Springs (Trenton) Formation. Depths are in feet.

The second type of reservoir identified in the Viola Group resulted from conduit-flow dissolution (Kerans, 1989). These reservoirs consist primarily of collapse breccias and solution-enlarged fractures (Sykes and others, 1997). Porosity development in the Welling–Fernvale apparently depended on this mechanism. Therefore, this porosity is less prevalent and more difficult to predict. Similar reservoirs were identified in the Hunton Group by Matthews and Al-Shaieb (1993) and called type 1 paleokarstic reservoirs. Type 1 reservoirs are relatively insignificant producers of oil and gas in the Hunton (Matthews and Al-Shaieb, 1993) and Viola Groups.

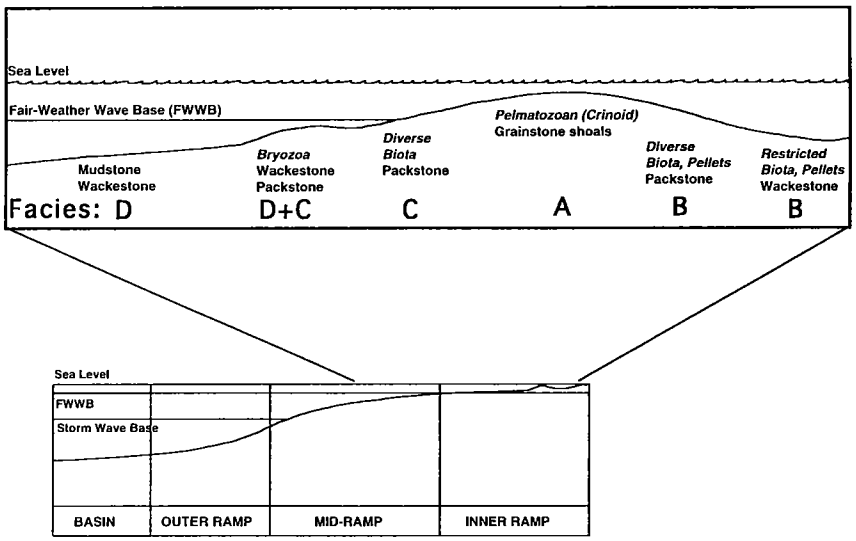

Figure 11. Generalized shallow carbonate-ramp model for the Viola Group. Facies A pelmatozoan grainstones represent high-energy, shallow shoal deposits. Facies B peloid-rich sediments were deposited in lagoons behind the shoals. Facies C bioclastic packstone–grainstones reflect more stable conditions seaward of the shoals or between them. Facies D mudstone–wackestones are open-marine subtidal deposits. Modified from Wilson (1975) and Burdette and Wright (1992).

CORRELATION OF SHOWS WITH CORE

The Viola Group was drilled with cable tools in many early wells in Fitts pool. As a result, detailed sample logs indicate the depth and type of petroleum shows encountered during drilling. Most early wells were cased into the Sylvan Shale and "open-hole" completed in the Viola. Some were later logged with gamma-ray tools, and many were subsequently twinned or offset by wells with resistivity- and porosity-log suites. By comparing these sets of data, it was possible to establish (1) the positions of permeable zones where fluid entered the hole during drilling, (2) points of fluid entry into a well while it produced, and (3) correlation of these producing reservoirs with core lithofacies.

All significant shows and production are from the Viola Springs section. Many wells flowed oil or filled with water after facies B and C rocks were drilled (Fig. 21). These reservoirs were encountered approximately 175–225 ft below the top of the Viola. In this interval, the amount of liquid production from facies A was difficult to determine because of the flow from the overlying beds. Significant indications of petroleum were also noted in the mixed mud- and grain-rich rocks in the upper part of facies B. These shows occurred 40–120 ft below the top of the Viola (Fig. 21). No significant shows of oil and gas were reported in the Welling.

Open-hole gamma-ray logs run in producing wells approximately 20–30 years after their completion confirm the positions of these reservoirs. High gamma readings in normally low-count rocks identify radioactive salts that precipitated at points of fluid entry into the wellbore. These "hot" gamma-ray signatures correlate with the position of the cored facies B and C packstone–grainstones (Fig. 22).

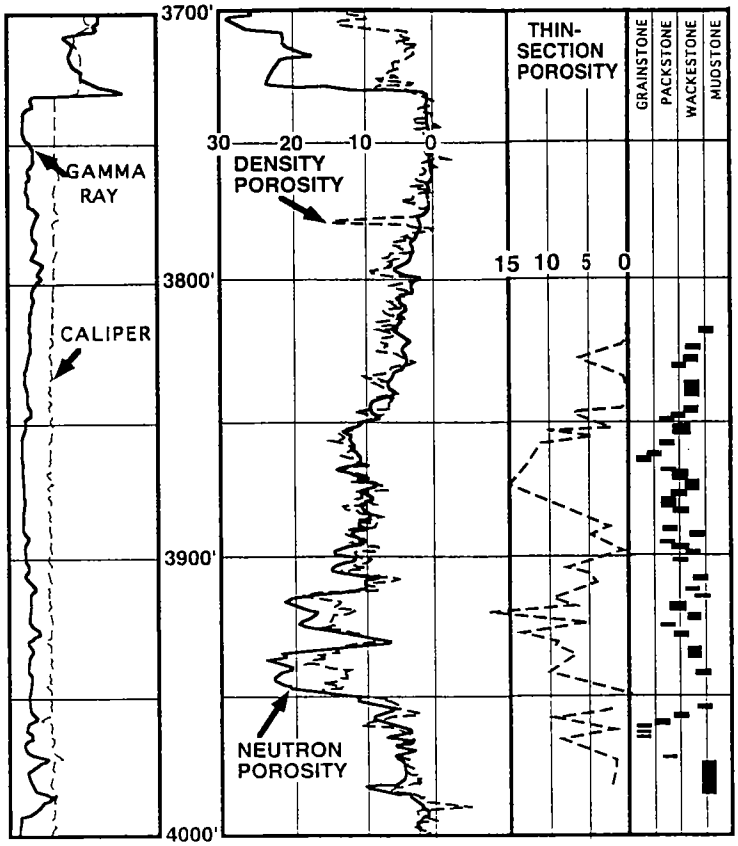

Figure 12. Correlation of wireline-log signatures, thin-section porosity, and lithofacies for the Viola Springs Formation in the Mobil Oil Corp. No. 21-19 East Fitts Unit well, NW¼ sec. 27, T. 2 N., R. 7 E. The Viola signatures and lithofacies are similar to those illustrated in Figure 10.

SUMMARY AND CONCLUSIONS

Most oil and gas reservoirs in the Viola developed in the Viola Springs Formation (Trenton). The loca-

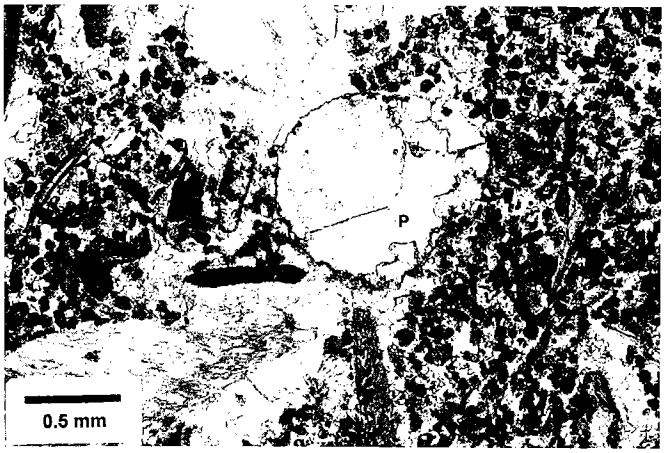

Figure 13. Crinoidal moldic porosity (*P*) in peloidal packstone (facies B). Mobil No. 21-19 East Fitts Unit. Depth, 3,851 ft.

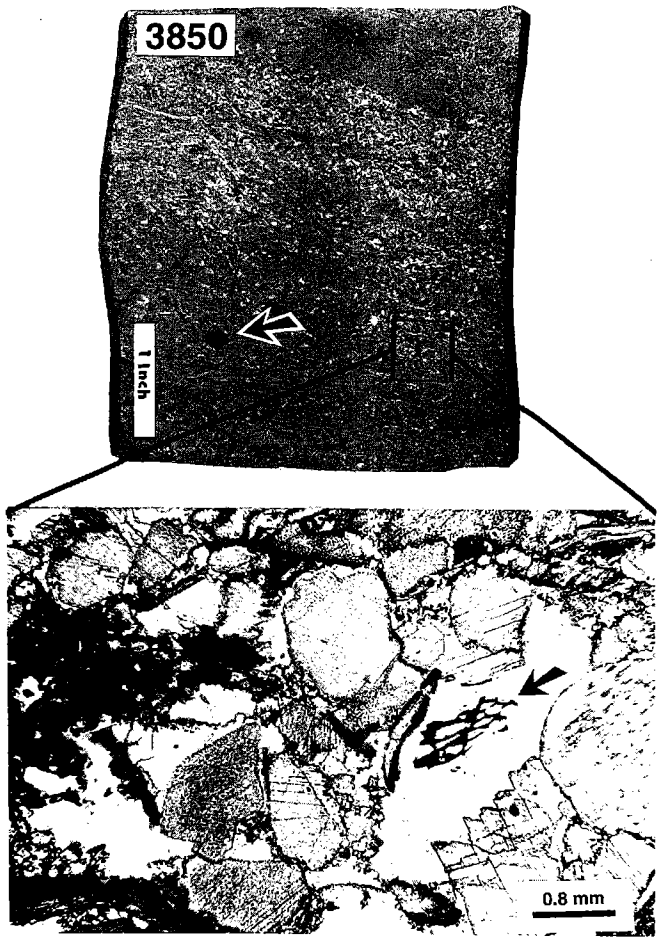

Figure 14. Remnant of bryozoan bioclast (arrow) in enlarged moldic pore. In pelmatozoan-rich intervals, vuggy porosity is commonly initiated by the dissolution of bryozoan grains. Vug in core photograph (arrow) is approximately 4.75 mm in diameter. Mobil No. 21-19 East Fitts Unit. Depth, 3,850 ft.

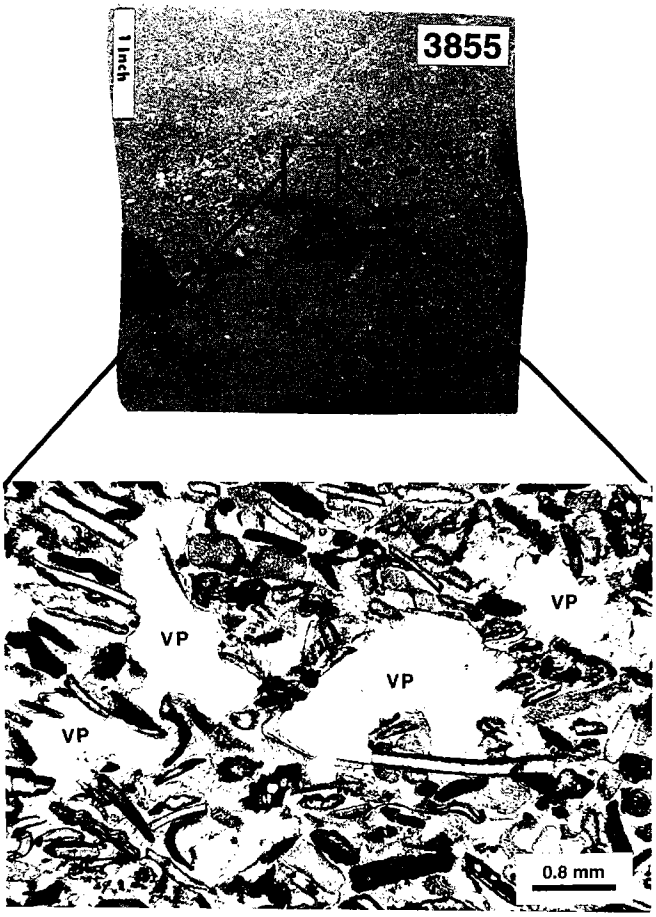

Figure 15. Vugs (*VP*) cross-cutting aligned grains in bioclastic packstone–grainstone (facies B). Vuggy porosity (dark spots on core piece) is concentrated in the grainy layers, whereas adjacent mud-rich wackestones are relatively low in porosity. Mobil No. 21-19 East Fitts Unit. Depth, 3,855 ft.



Figure 16. Intergranular porosity (arrows), lined with drusy calcite. Mobil No. 21-19 East Fitts Unit. Depth, 3,855 ft.

tion of the porosity fairway in the Viola Springs can be predicted by water depth on the Viola ramp. Reservoirs are associated with grainy, shallow subtidal carbonates of the inner ramp. Lagoonal muds and deeper ramp open-marine muds did not become reservoir rocks. The inner ramp was likely exposed during intra-Viola sea-level drops and subjected to meteoric dissolution. The locations of reservoirs are closely controlled by depositional facies. Sediments containing a diverse bioclastic-grain composition (facies B and C) formed rocks that



Figure 17. Intercrystalline porosity (*IP*) between limpid euhedral dolomite rhombs. Dolomites are not volumetrically important reservoirs in the Viola but provided critical avenues for migrating fluids that dissolved grains and generated moldic and vuggy porosity (*P*). Mobil No. 21-19 East Fitts Unit. Depth, 3,912 ft.



Figure 19. Pelmatozoan grainstone (facies A), cemented by syntaxial calcite overgrowths. Extensive cementing effectively blocked fluid movement and prevented the dissolution necessary to generate reservoir facies. Mobil No. 21-19 East Fitts Unit. Depth, 3,965 ft.

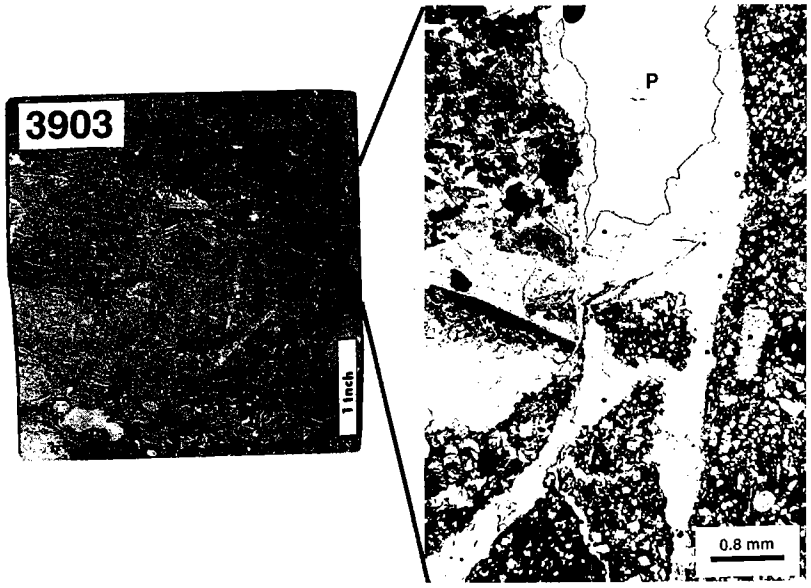

Figure 18. Solution-enlarged fractures that were partially cemented by calcite (white) and subsequently corroded, resulting in a large pore (*P*). These features indicate multiple stages of dissolution and cementation. Mobil No. 21-19 East Fitts Unit. Depth, 3,903 ft.

were susceptible to diffuse-flow dissolution and evolved into reservoir facies. These reservoirs contain intergranular, moldic, and vuggy porosity. On the other hand, the pelmatozoan grainstones of facies A are commonly cemented with calcite and are nonproductive. Porosity in the Welling is fracture and conduit-flow dependent and much less predictable than the porosity zones in the Viola Springs.

ACKNOWLEDGMENTS

The authors wish to express appreciation to Paul Blubaugh, Phebe Deyhim, Syed Mehdi, and Catherine Price of the School of Geology at Oklahoma State University for their efforts in finalizing this paper. We are also grateful to Walter Esry and the Oklahoma Geological Survey Core Library for providing core data essential to this research.

REFERENCES CITED

Alberstadt, L. P., 1967, Brachiopod biostratigraphy of the Viola and "Fernvale" Formations (Ordovician), Arbuckle Mountains, south-central Oklahoma: University of Oklahoma unpublished Ph.D. dissertation, 308 p.

Amsden, T. W.; and Sweet, W. C., 1983, Upper Bromide Formation and Viola Group (Middle and Upper Ordovician) in eastern Oklahoma: Oklahoma Geological Survey Bulletin 132, 76 p.

Burdette, T. P.; and Wright, V. P., 1992, Carbonate ramp depositional systems: Sedimentary Geology, v. 79, p. 3–57.

Dott, R. H.; and Swindell, F., 1935, Fitts pool is most important Oklahoma discovery in six years: Oil Weekly, v. 2, p. 16–18, 51–54.

Dunham, R. J., 1962, Classification of carbonate rocks according to depositional texture, *in* Ham, W. E. (ed.), Classification of carbonate rocks: American Association of Petroleum Geologists Memoir 1, p. 108–121.

Galvin, P. K., 1982, Deep-to-shallow ramp transition of the Viola Limestone (Ordovician), southwest Arbuckle Mountains, Oklahoma: Southern Methodist University unpublished M.S. thesis, 108 p.

Glaser, G. C., 1965, Lithostratigraphy and carbonate petrology of the Viola Group (Ordovician), Arbuckle Mountains, south-central Oklahoma: University of Oklahoma unpublished Ph.D. dissertation, 197 p.

Grammer, G. M., 1983, Diagenesis of the Viola Limestone (Middle and Upper Ordovician), southeastern Arbuckle Mountains, Oklahoma: Southern Methodist University unpublished M.S. thesis, 151 p.

Hyatt, D. L., 1936, Preliminary report on the Fitts pool, Pontotoc County, Oklahoma: American Association of Petroleum Geologists Bulletin, v. 20, p. 951–974.

Kerans, C., 1989, Karst-controlled reservoir heterogeneity and an example from the Ellenburger Group (Lower Ordovician) of West Texas: Texas Bureau of Economic Geology Report of Investigations 186, 40 p.

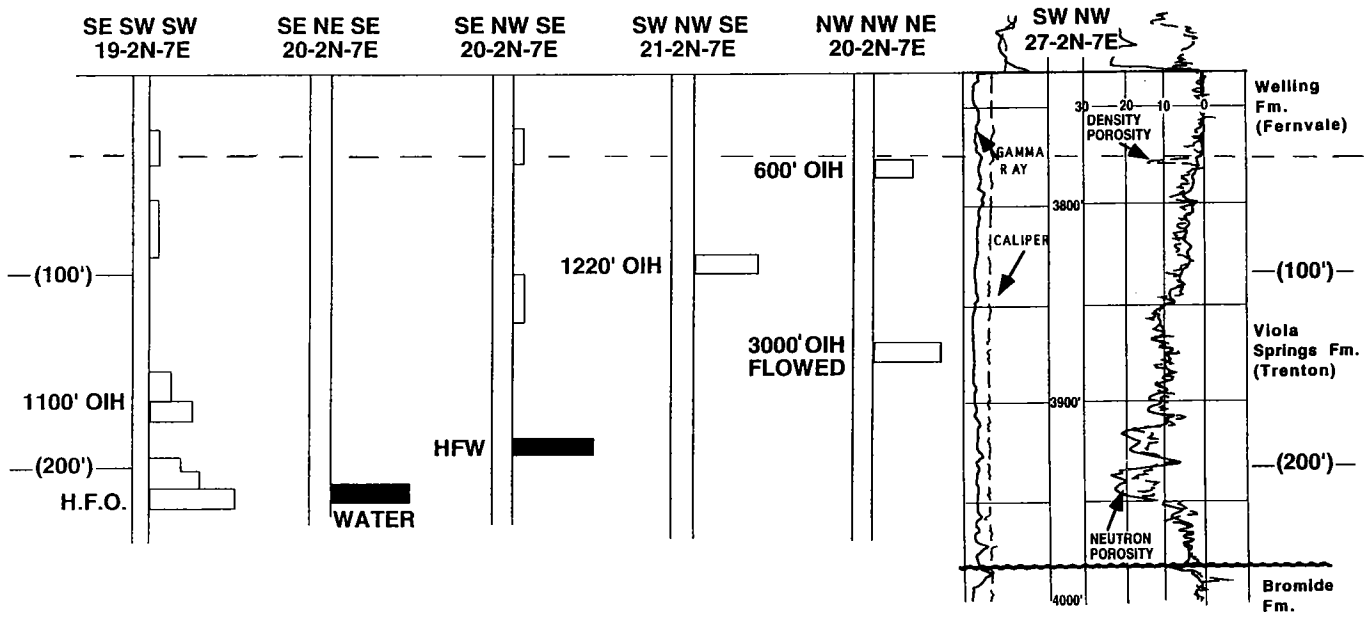

Figure 21. Schematic stratigraphic cross section showing depths where oil and water were encountered in cable-tool-drilled holes in the Viola Group. All significant shows were reported in the Viola Springs (Trenton), and many were encountered 175–225 ft below the top of the Viola Group. The wireline log relates porosity measurements and facies to reported shows. *OIH* = oil in hole; *HFO* = hole full of oil; *FLOWED* = flowed oil to surface; *WATER* = undetermined amount of water in hole; *HFW* = hole full of water.

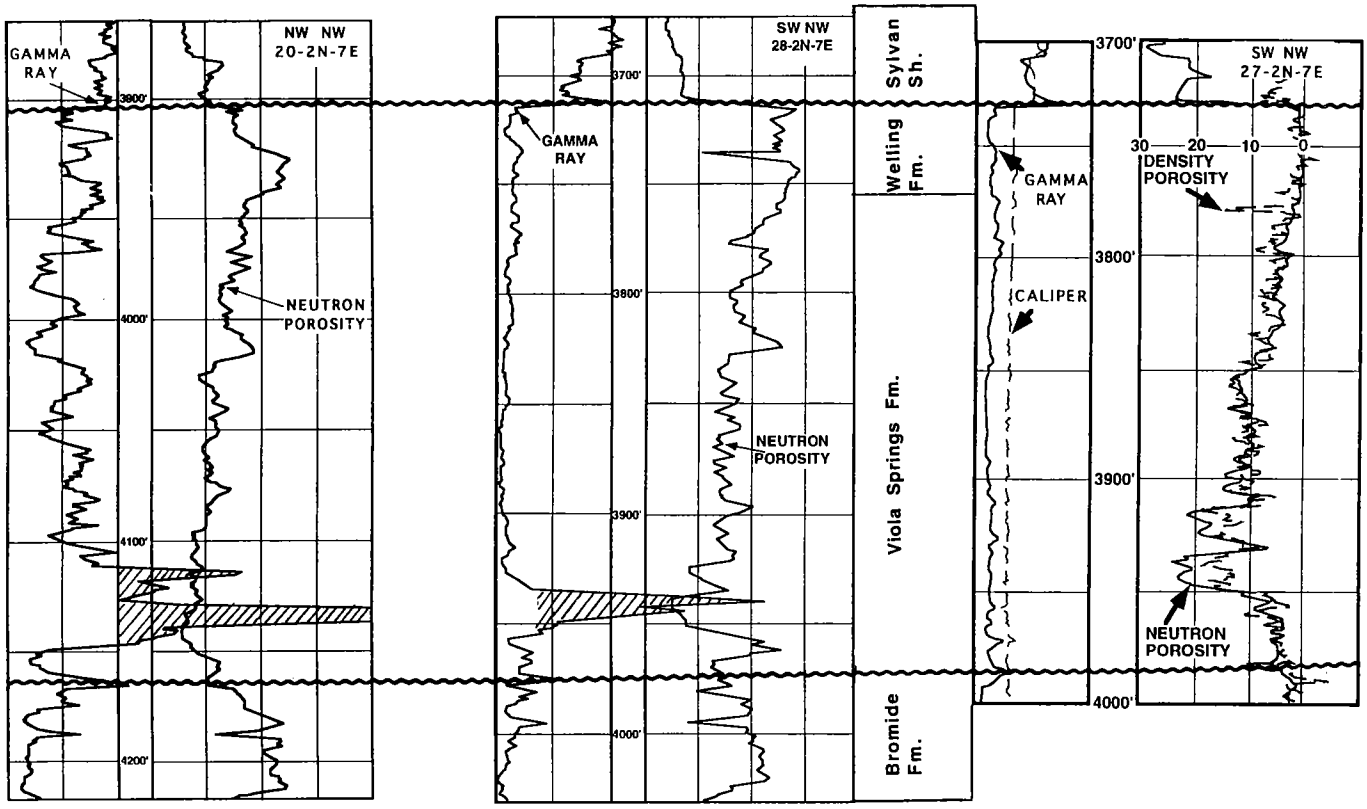

Figure 22. Correlation of zones of fluid movement (hatched "hot zones") in cable-tool holes with wireline-log porosity and stratigraphy. High gamma-ray readings in normally low-count rocks reflect 20–30 years of radioactive salt precipitation across intervals where fluids entered the borehole during production.

Microbial Reservoir Characterization of Hobart Field, Kiowa County, Oklahoma

Daniel C. Hitzman, James D. Tucker, and Brooks A. Rountree
Geo-Microbial Technologies, Inc.
Ochelata, Oklahoma

ABSTRACT.—Microbial reservoir characterization (MRC) integrates measurements of hydrocarbon microseepage escaping from petroleum reservoirs with developmental geologic and engineering data for an enhanced identification of the subsurface-reservoir fabric. Studies over producing fields demonstrate that MRC technology can monitor subsurface-fluid withdrawal patterns from microseepage patterns identified at the surface. Located in Kiowa County, Oklahoma, Hobart field produces from a carbonate reservoir recently tested by MRC for enhanced rehabilitation planning. Approximately 1.5 mi^2 was surveyed, and 239 microbial soil samples were collected. Maps generated from MRC data define areas of the reservoir showing contact between production and injection wells. Possible bypassed production, reservoir-heterogeneity characteristics, and potential offset-well locations were identified. Microbial microseepage signatures target the distribution of hydrocarbon traps, map the continuity (compartments) of a reservoir, and locate areas prone to higher quality reserves. Where the reservoir is in communication with producing wells, the upward buoyancy-driven force controlling the microseepage is altered along pressure pathways streaming to production wells.

INTRODUCTION

The microbial oil survey technique (MOST) is based on the presence of hydrocarbon microseeps above buried reservoirs. The microseeps are detected by observing the concentrations and distributions of hydrocarbon-indicating microorganisms found in shallow soils. There is a direct, positive relationship between the hydrocarbon concentrations in the soils and these microbial populations. This relationship between increased hydrocarbon concentrations and increased hydrocarbon-indicating microorganism populations is easily measurable and distinctly reproducible (Beghtel and others, 1987). High microbial-population distributions are therefore reliable indicators of hydrocarbon-gas migration (Pareja Lopez and others, 1993). A specific suite of microorganisms is measured from shallow soil samples collected from depths of 6–8 in.

A microbial reservoir characterization (MRC) interpretation of MOST data requires that samples be collected on a closely spaced grid pattern for effective evaluation of any subtle patterns within a reservoir. Clusters of elevated microbial values in a producing field indicate either pockets of hydrocarbons isolated from production wells or repressuring associated with injection fluids (Hitzman and others, 1994). Microbial low trends indicate areas in direct communication with producing wells. The MRC surveys are highly effective when used in conjunction with geological, geophysical, and production-history data.

The pattern of reduced microbial counts adjacent to oil and gas wells is common for mature producing areas. Over some well-drained gas reservoirs, the microbial values have been found even to be anomalously low. This phenomenon of apparent microseepage shutdown over producing fields is thought to be due to a change in the drive mechanism controlling microseepage. When a well is brought into production, the drive changes from a vertically migrating buoyancy force to horizontal gas streaming to pressure sinks created around producing wells. When this occurs, microseepage ends and microbial populations decline rapidly. This change in drive mechanism and microbial-population densities can be used to define reservoir-drainage direction, radius, and heterogeneities around existing wells in producing fields. Obviously, in *undrilled* areas, this phenomenon will not occur and there will be a direct relationship between high microbial populations, microseepage, and potential reservoirs.

HOBART UNIT GEOLOGY

Normal sedimentation occurred throughout southwestern Oklahoma in the Cambrian, Ordovician, Silurian, Devonian, and Mississippian Periods, with deposition of sands, shales, and limestones in relatively shallow water. At the close of the Mississippian, the Wichita orogeny began, which caused the deep Anadarko and southern Oklahoma basins to form. As the Anadarko basin began to subside, mountains began to rise to the south. The deep basins filled with the Mississippian Springer and Pennsylvanian Morrow shales, and the whole area was then covered with sands and shales. The Pennsylvanian was brought to a close by the Arbuckle orogeny, which caused major mountain building to the south and giant faults to the north. The Komalty area was faulted, uplifted, and peneplained, exposing steeply northward-dipping beds of Arbuckle, Simpson, Viola, Sylvan, and Hunton rocks. Per-

Hitzman, D. C.; Tucker, J. D.; and Rountree, B. A., 2000, Microbial reservoir characterization of Hobart field, Kiowa County, Oklahoma, *in* Johnson, K. S. (ed.), Platform carbonates in the southern Midcontinent, 1996 symposium: Oklahoma Geological Survey Circular 101, p. 129–130.

mian sands and shales were then deposited over the entire area.

HOBART UNIT PRODUCTION HISTORY

The Hobart Pontotoc–Viola unit encompasses 430 acres of Hobart field in Kiowa County, approximately 100 mi southwest of Oklahoma City. Hobart field was discovered in 1939, with production from the Pontotoc–Viola section at depths ranging from 1,100 to 1,400 ft. From its discovery until its initial abandonment in 1944, Hobart field yielded roughly 1,800,000 barrels of oil (BO) from primary production. The field's production-drive mechanism during this period is believed to have been solution-gas drive (depletion drive), which typically recovers between 15.5% and 21% of the original oil in place in this type of reservoir.

In 1987, Hobart field was unitized for the purpose of conducting secondary-recovery operations. Potential reserves targeted by the flood were estimated at 900,000 to 1,800,000 BO. The unit's original operator confirmed the field's primary drive mechanism and status by drilling the unit's initial redevelopment wells at both downdip and updip locations. The unit's initial redevelopment wells also identified isolated pockets of bypassed primary oil in what has now been labeled a "rubble zone" near the fault plane of the major thrust fault that established the relative structural relationships in the field. After the high production potential of this rubble zone was identified, developmental focus was shifted from conducting secondary-recovery operations to "chasing" potential production in additional rubble-zone completions. Records indicate that more than 50,000 barrels of primary oil was produced from rubble-zone completions high on structure prior to their apparent depletion. Following the decline of rubble-zone production, the unit's operations were redirected toward the waterflood project.

Broad Street Financial Co. acquired the operational rights to the unit in late 1994. This company, as unit operator, initiated activities to assess the status of the Pontotoc–Viola reservoir and to reactivate secondary-recovery operations. Unit re-injection and production were commenced in late 1995 and continue today.

SUMMARY AND CONCLUSIONS

1. A total of 239 MRC samples were collected across Hobart field to identify infill or stepout locations.
2. The microbial-distribution pattern and the low microbial average are typical for surveys conducted over producing fields.
3. According to MRC microseepage results, the productive zone has been in good communication with the primary-production wells.
4. There is little infill potential for unproduced pockets of hydrocarbons within the field.
5. There appears to be an east–west reservoir fabric that can be utilized to help determine the well spacing and pattern for future injection wells.
6. Several elevated microbial clusters on the edge of the survey area suggest that a potential for stepouts exists within this area.

ACKNOWLEDGMENT

The authors wish to thank Broad Street Financial Co. for its assistance with this project and permission to release data.

REFERENCES CITED

Beghtel, F. W.; Hitzman, D. O.; and Sundberg, K. R., 1987, Microbial Oil Survey Technique (MOST) evaluation of new field wildcat wells in Kansas: Association of Petroleum Geochemical Explorationists Bulletin, v. 3, no. 1, p. 1–14.

Hitzman, D. C.; Tucker, J. D.; and Rountree, B. A., 1994, Development drilling in correlation with hydrocarbon microseepage signatures: American Association of Petroleum Geologists, Annual Meeting Proceedings, Denver.

Pareja Lopez, J.; Tucker, J. D.; and Hitzman, D. C., 1993, Hydrocarbon microseepage signatures of seismic structures identified by microbial surveys, Sub-Andean region, Bolivia: American Association of Petroleum Geologists, Annual Meeting Proceedings, New Orleans.

Sequence Stratigraphy of Hunton Group Ramp Facies, Arbuckle Mountains and Anadarko Basin, Oklahoma

Zuhair Al-Shaieb and Jim Puckette
Oklahoma State University
Stillwater, Oklahoma

ABSTRACT.—The Henryhouse and Haragan/Bois d'Arc section in the Arbuckle Mountains and Anadarko basin represents a type 1 carbonate sequence within the Silurian–Devonian section of the Hunton Group. The lower boundary is the unconformity that separates the Henryhouse Formation from the underlying Clarita Limestone of the Chimneyhill Subgroup. The upper boundary is the unconformable Bois d'Arc–Woodford Shale contact. The retrogradational phase of the sequence (transgressive systems tract) was initiated with the flooding of the Clarita surface. Maximal flooding is recorded by graptolitic shale that represents the condensed section near the base of the Henryhouse. An increasing proportion of limestone in the upper Henryhouse and Haragan/Bois d'Arc Formations reflects the deposition of aggradational(?) and progradational units within the highstand systems tract.

The Henryhouse–Haragan/Bois d'Arc sequence contains seven to nine shallowing-upward shale–carbonate cycles or parasequences. A typical parasequence is composed of shale and argillaceous limestone at the base and cleaner fossiliferous limestones at the top. Beds are generally thicker near the top of each cycle. The succession of these parasequences forms the systems tracts that compose the Henryhouse–Haragan/Bois d'Arc sequence. The progradational phase of the sequence reflects regression during the Late Silurian and Early Devonian, which is evident on global sea-level curves.

Henryhouse–Haragan/Bois d'Arc facies in the Arbuckle Mountain section are notably different from those examined in cores from the Anadarko basin. The outcrop parasequences consist of only subtidal facies, whereas time-equivalent rocks in the western Anadarko basin include intertidal and supratidal facies. These additional facies and cycle thickening indicate a northwestward shallowing of the basin during the Late Silurian–Early Devonian.

INTRODUCTION

The Hunton Group was deposited in an epeiric sea with a gently inclined floor. In this ramp setting, facies belts developed subparallel to bathymetric contours. Distinguishable facies are subtidal, intertidal, and supratidal, which can be recognized in vertical successions in cores. Sea-level changes apparently caused extensive migration of facies and generated the lateral distribution and vertical succession evident in outcrop and cores. This paper examines these relationships in the context of sequence stratigraphy and presents a comparative analysis of the Henryhouse facies in outcrops in the Arbuckle Mountains, and of their subsurface equivalents in the Anadarko basin.

General stratigraphic divisions of the Hunton (Fig. 1) are the Chimneyhill Subgroup (Keel, Cochrane, and Clarita Formations), Henryhouse Formation, Haragan and Bois d'Arc Formations, and Frisco Formation (Amsden, 1980, 1989). Although the Hunton outcrops in the Arbuckle Mountains contain a nearly complete stratigraphic section, this paper focuses on the Henryhouse and Haragan/Bois d'Arc Formations and the impact their depositional settings and facies had on reservoir evolution.

OUTCROP DEPOSITIONAL FACIES

Henryhouse–Haragan/Bois d'Arc (HHB) depositional facies are drastically different from those of the underlying Clarita Formation and overlying Woodford Shale. The lower part of the Woodford Shale is dark-gray to black fissile shale that contrasts sharply with the light-colored Hunton shales and limestones. The Clarita and Cochrane are relatively clean pelmatozoan-rich packstones–grainstones that form a prominent ledge beneath the shales and "marly" limestones of the overlying Henryhouse Formation. Thin-bedded limestones in the HHB sequence are silty argillaceous mudstones and wackestones (Fig. 2), whereas thicker, more massively bedded limestones are wackestones to packstones (Fig. 3).

The vertical juxtaposition of Clarita and Woodford facies against distinctly different HHB facies identifies depositional breaks at the base and top of the interval. The upper surfaces of the Clarita and Haragan/Bois d'Arc are unconformities, owing to nondeposition and/or erosion.

In contrast, the vertical differences among facies within the HHB interval are results of shallowing-upward depositional cycles. These cycles, when considered together, suggest initial deepening and then subsequent shallowing of the epeiric sea.

Al-Shaieb, Zuhair; and Puckette, Jim, 2000, Sequence stratigraphy of Hunton Group ramp facies, Arbuckle Mountains and Anadarko basin, Oklahoma, *in* Johnson, K. S. (ed.), Platform carbonates in the southern Midcontinent, 1996 symposium: Oklahoma Geological Survey Circular 101, p. 131–137.

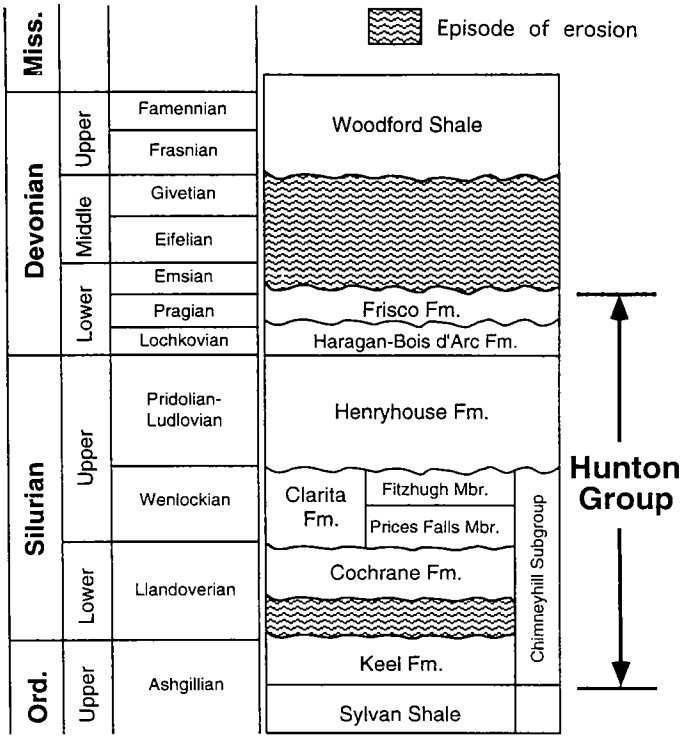

Figure 1. Stratigraphic nomenclature of the Hunton Group in Oklahoma. Modified from Barrick and others (1990), Amsden (1989).

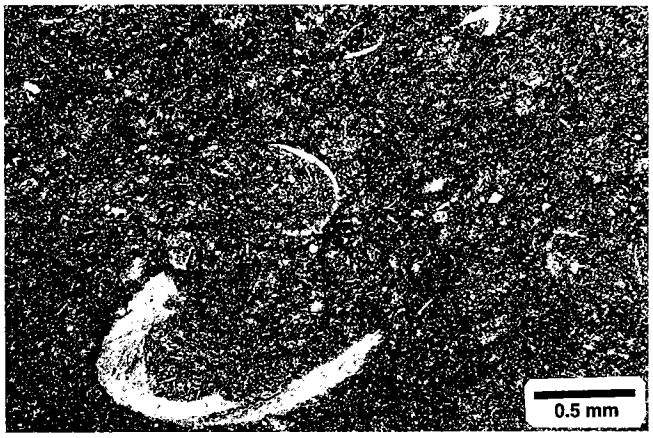

Figure 2. Photomicrograph of mudstone–wackestone within the Henryhouse Formation, an example of weakly indurated argillaceous limestone. Plane-polarized light.

HENRYHOUSE–HARAGAN/BOIS D'ARC SEQUENCE STRATIGRAPHY

Sequence Type and Boundaries

A depositional sequence is a conformable succession of genetically related sedimentary strata that is bounded at both its top and base by unconformities or their correlative conformities (Van Wagoner, 1985). The HHB interval is bounded by unconformities, and rock types above and below these unconformities are distinctly different. Erosion associated with the upper unconformity truncated the Hunton across northern Oklahoma; the Woodford Shale is disconformable on the eroded surface. Before deposition of the Henryhouse, the Clarita was thinned by erosion (Amsden, 1957).

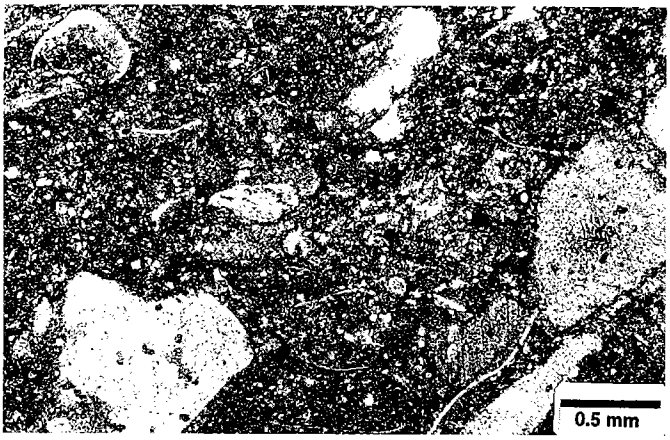

Figure 3. Photomicrograph of well-indurated bioclast-rich limestone (packstone). This facies forms hill-supporting ledges within outcrops of the Haragan/Bois d'Arc interval. Plane-polarized light.

Subaerial exposure of the ramp resulted in the extensive development of a variety of paleokarstic features. Most of these features lie below the pre-Woodford and pre-Henryhouse unconformities (Manni, 1985; Matthews, 1992). Subaerial exposure and erosion are characteristic of type 1 sequence boundaries (Sarg, 1988). Boundaries of this kind enclose the HHB sequence.

Cycles or Parasequences

The HHB sequence consists of a series of genetically related depositional cycles or parasequences. A parasequence is a relatively conformable succession of genetically related beds or bedsets bounded by marine-flooding surfaces and their correlative surfaces (Van Wagoner, 1985). The I-35 outcrop on the south flank of the Arbuckle Mountains contains seven to nine parasequences. A typical parasequence is composed of shale, argillaceous-limestone bedsets, and fossiliferous limestone, in ascending order (Fig. 4). Shale marks the flooding surfaces and cycle boundaries. As a result, the parasequences are shale rich toward the base and limestone rich at the top. The limestones in each cycle generally thicken toward the top and thin toward the base. The coarser grained (shallower, higher energy) carbonates are more resistant and form ridges. The finer grained (deeper, lower energy), shaly rocks form the soil-covered furrows (Fig. 5).

The upward increase in bioclastic debris and the corresponding decrease in mud indicate that transport energy increased with time. This shallowing-upward character occurs on several scales. Small-scale bedsets (0.5–1 ft thick) aggregate to form the thicker (5–20 ft thick) upward-shallowing parasequences. Each parasequence culminates with higher energy (cleaner) ledge-forming carbonate. Parasequences were terminated by a rapid sea-level rise and have deeper water facies in abrupt contact with underlying shallower water facies.

Systems Tracts

The HHB sequence is composed of two systems tracts (Fig. 6). The lower is the transgressive systems tract (TST) that was



A



B

Figure 4. (A) Aggregation of small-scale shale–limestone bedsets within a parasequence in the Haragan/Bois d'Arc interval. Scale bar equals 1 ft. (B) Shallowing-upward cycle in the Henryhouse Formation, consisting of thick-bedded limestones overlying thin-bedded limestones and shale. (Hammers for scale.)

initiated with the flooding of the Clarita surface during a rapid relative rise in sea level. This transgressive tract is the retrogradational phase of the sequence. Graptolitic shales near the base of the Henryhouse (Amsden, 1978, fig. 35) are a marine condensed section and indicate very slow deposition (Sarg, 1988). The maximum-flooding surface (MFS) occurs at the top of the transgressive systems tract and signifies the maximum extent of shoreline transgression. The upper systems tract is the highstand tract (HST; Fig. 6), which formed as sea-level rise slowed or sea level began to fall and may contain early aggradational and later progradational phases. Thin-bedded limestones near the middle of the Henryhouse may represent the aggradational phase, whereas thicker bedded limestones in the upper HHB characterize deposition during the progradational phase. During progradation, eustatic sea-level fall exceeds subsidence. Therefore, a basinward shift in coastal onlap results in deposition of "shallow-water" facies over "deeper water" facies. The upward increase in carbonate during the progradational phase of the Hunton sequence resembles the Silurian–Devonian shallowing trend shown on the global eustatic curve (Fig. 7).

Parasequences identified in the Hunton outcrop can be correlated to wireline logs (Fig. 8). The gamma-ray signatures of the various subsurface units reflect the outcrop lithofacies. Five coarsening-upward profiles are recognized in the sequence. Individual bedsets or thinner cycles are not well resolved by wireline tools. However, thicker carbonate-rich intervals or parasequence sets have a distinct gamma-ray deflection (lower gamma-ray readings) from the shale baseline. The shallowing during the progradational phase of the sequence is readily discerned by gamma-ray log signatures that exhibit a decrease in "shaliness" toward the top of the interval.

SURFACE AND SUBSURFACE LITHOFACIES RELATIONSHIP

The distribution of depositional facies for the Henryhouse Formation is shown in Figure 9. The Henryhouse is a major oil and gas reservoir in the Anadarko basin, and a detailed examination of Henryhouse cores was conducted by Al-Shaieb, Beardall, and others (1993). Sedimentary structures, lithology, fossil content, and fabric relationships were used to recognize various depositional facies bands that subparallel the paleoshoreline. Supratidal, intertidal, and subtidal facies can be readily distinguished, and their spatial relationships consistently indicate shallowing-upward cycles. Anhydrite is found at the tops of some cycles, suggesting that hypersaline conditions developed in supratidal environments (Al-Shaieb, Beardall, and others, 1993).

The subtidal facies (thin argillaceous limestones and shales) is the only one present in the Arbuckle Mountains. Equivalent rocks in the western and northern parts of the Anadarko basin contain additional intertidal and supratidal facies. Parasequences north and west of the Arbuckle Mountains are thicker and are composed mainly of carbonates. A general absence of shale and marly carbonates in these rocks is most evident as compared to the outcrops in the Arbuckle Mountains.

Several cores from northern and western Oklahoma show differences in facies from equivalent rocks in the Arbuckle Mountains. The Apexco Green core in sec. 31, T. 10 N., R. 26 W., Beckham County, illustrates the presence of shallow-water facies in the western part of the Anadarko basin. The cored interval consists largely of a single facies: light- to dark-gray dolomite, dolomitic and lime mudstone, and peloidal lime-wackestone. Fossils are rare or absent. Fenestral fabrics, algal laminations (Fig. 10), irregular carbonate laminations, and massive fabrics are common. These features are characteristic of supratidal facies (facies I of Al-Shaieb, Beardall, and others, 1993).

The Eason Van Curen core in sec. 3, T. 15 N., R. 5 W., Kingfisher County, contains subtidal, intertidal, and lagoonal (restricted-subtidal) facies. The open-subtidal facies (facies III of Al-Shaieb, Beardall, and others, 1993) is hummocky-bedded mudstone with abundant bioclasts. The intertidal facies is a cross-stratified ooid grainstone (Fig. 11) with scarce fossil debris (facies IIb of Al-Shaieb, Beardall, and others, 1993). The restricted-subtidal (lagoonal) facies (facies IIa of Al-Shaieb, Beardall, and others, 1993) is peloid dolomudstone. Fossils are rare, and faint burrows are evident even though dolomitization has obliterated many sedimentary features. Shale is not present, and the cycles are much thicker than their outcrop equivalents (Fig. 8). The transition from low-energy

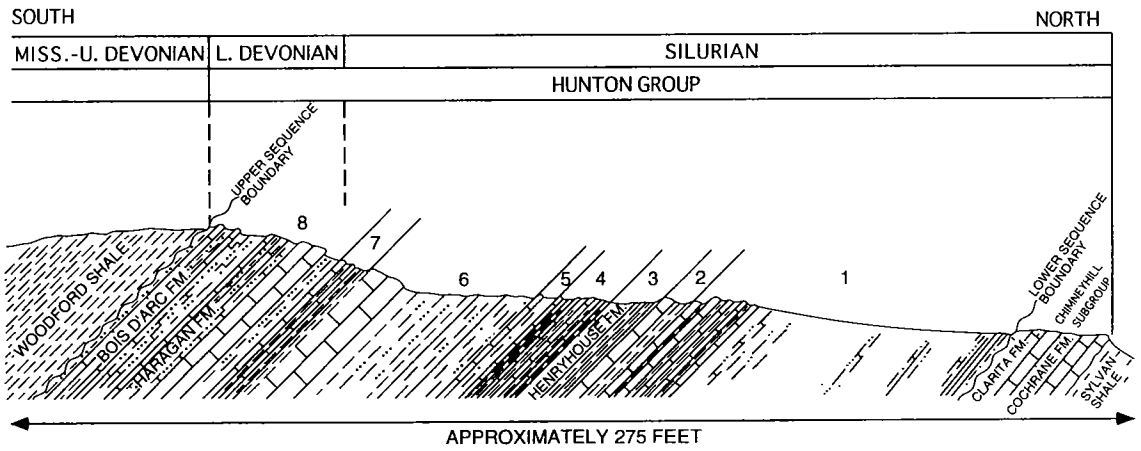

Figure 5. Proposed parasequence boundaries within the Henryhouse–Haragan/Bois d'Arc sequence. Hunton Group section on the south flank of the Arbuckle anticline; looking west from I-35. Modified from Fay (1989), Al-Shaieb, Fritz, and others (1993).

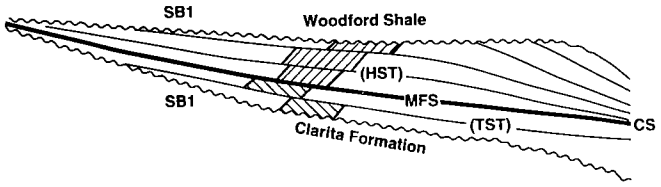

Figure 6. Schematic cross section of the systems tracts in the Henryhouse–Haragan/Bois d'Arc type 1 sequence. Modified from Vail (1987), Sarg (1988). *SB1* = type 1 sequence boundary; *HST* = highstand systems tract; *MFS* = maximum-flooding surface; *TST* = transgressive systems tract; *CS* = condensed section.

subtidal mudstones to high-energy intertidal grainstones and low-energy lagoonal mudstones represents a shallowing-upward sequence in a nearshore setting.

The Tenneco Jordan core in sec. 3, T. 21 N., R. 14 W., Major County, represents a subtidal- to intertidal-facies transition. The subtidal facies (facies III) is predominantly fossiliferous dolomudstone–wackestone that contains some vertical and horizontal burrows. Burrowing increases upward, and the overlying intertidal facies (facies II) is burrow-mottled at the top. Fossils are not abundant, but moldic porosity suggests that pelmatozoan fragments were dissolved. This core (120 ft) is apparently part of one parasequence (Fig. 8).

These cores illustrate the distinct differences between the Henryhouse facies in northern and western Oklahoma and those in the Arbuckle Mountains. Parasequences in both areas have shallowing-upward character, but those in outcrop are thinner and more argillaceous. The absence of shale, an increase in the percentage of carbonate relative to clay and silt, and thickening of the cycles represented in the cores indicate shallower water and more favorable conditions for carbonate precipitation. In this part of the basin, carbonate deposition kept pace with increasing accommodation space, and thicker parasequences were deposited. This apparent shallowing of the basin suggests a westward shoreline and a southeasterly dip of the Hunton ramp.

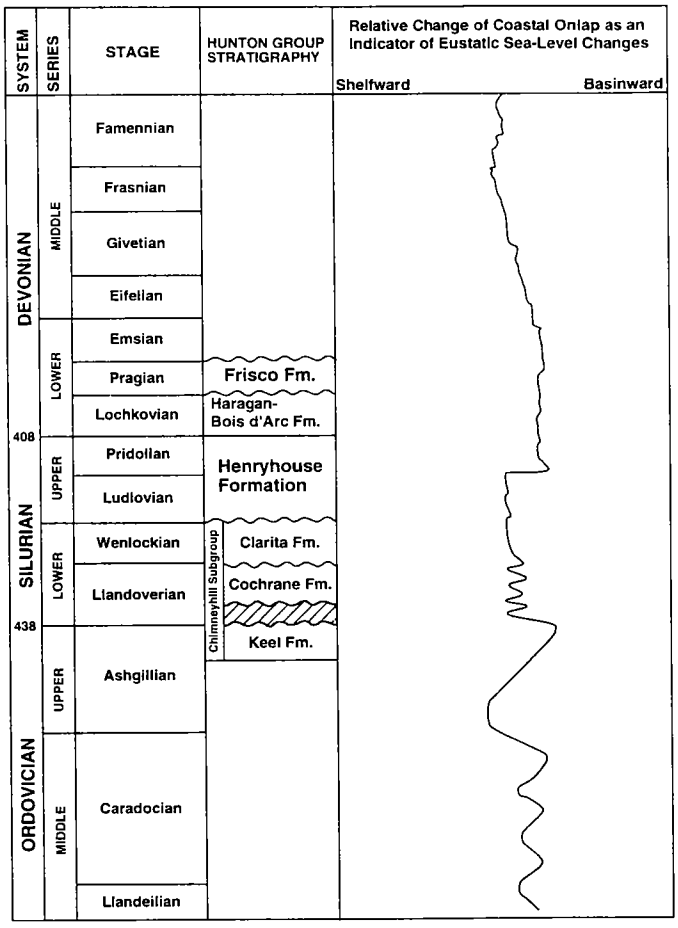

Figure 7. Global coastal-onlap/eustatic sea-level curve depicting a general shallowing trend through the Late Silurian–Early Devonian. Modified from Shelton and Gerken (1995), Boggs (1995). Numerals at systemic boundaries indicate age (Ma).

IMPLICATIONS

Sequence-stratigraphic concepts are directly applicable to exploration for oil and gas in the Hunton reservoirs. The two types of reservoirs that occur in the HHB sequence are found

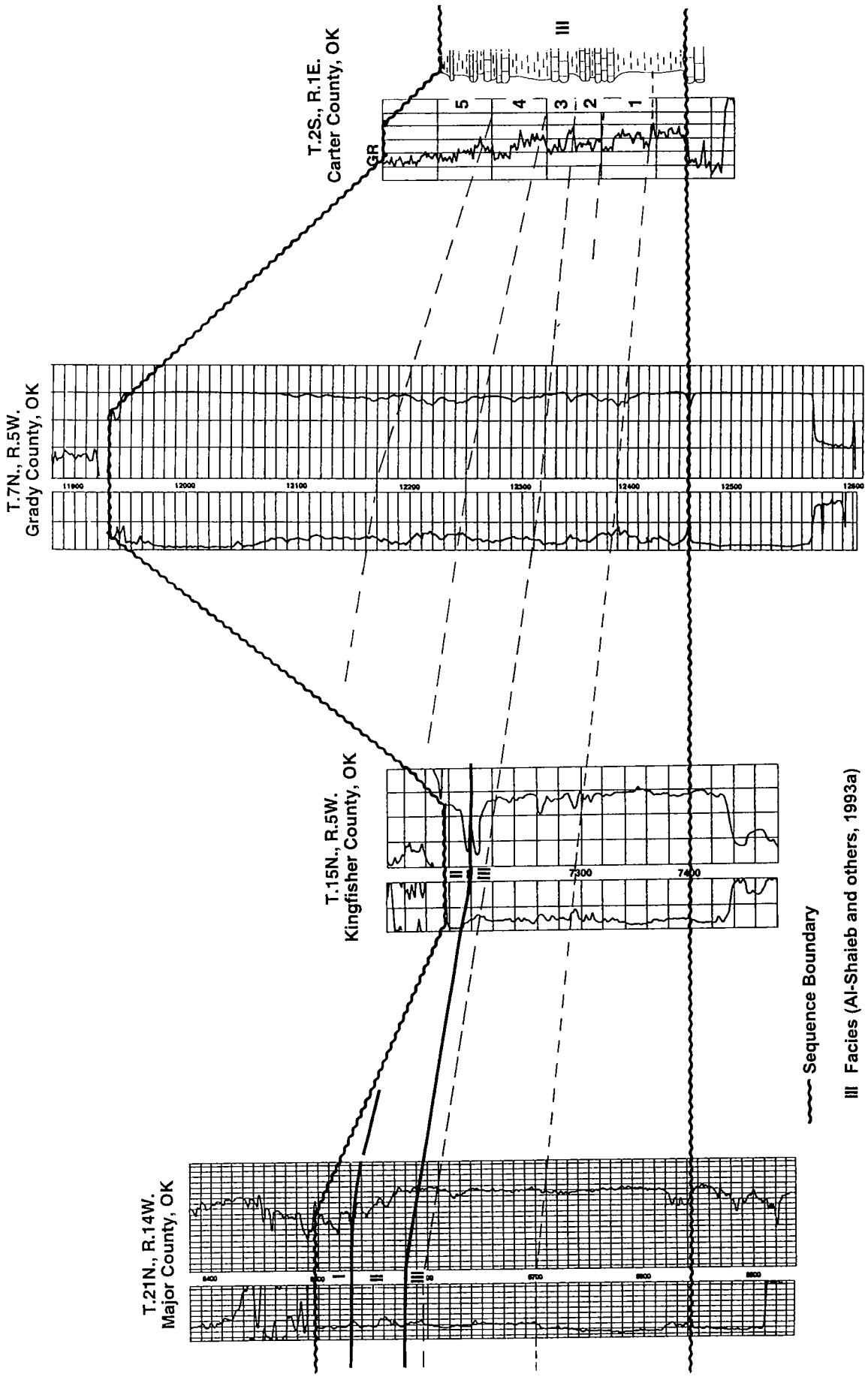

Figure 8. Cross section correlating outcrop and subsurface facies. North and west of the Arbuckle Mountains, parasequences are thicker and contain additional intertidal and supratidal facies. Location of section is shown in Figure 9. Five parasequences (shallowing-upward gamma-ray signatures) are indicated by Arabic numerals; facies (from Al-Shaieb, Beardall, and others, 1993) are indicated by Roman numerals.

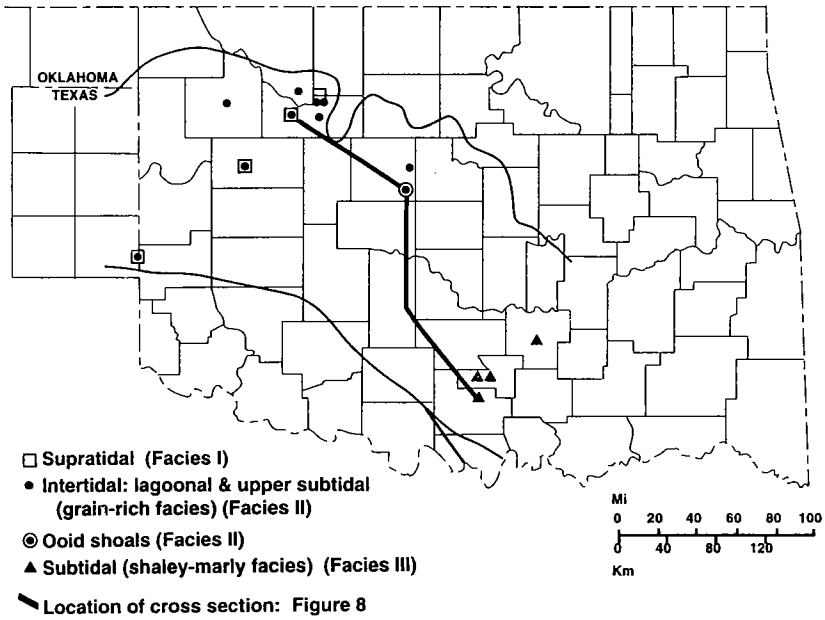

Figure 9. Distribution of subtidal, intertidal, and supratidal facies in the Henryhouse Formation. Facies designations are from Al-Shaieb, Beardall, and others (1993).

in the (1) dolomitized intertidal facies and (2) karstic zone below the upper unconformity.

The first type of reservoir forms during the highstand systems tract of the sequence. The characteristic features of intertidal facies that caused these reservoirs to develop porosity are burrowing and abundant grains (bioclasts or ooids). Burrowing enhanced porosity and permeability of the sediment, allowing dolomitizing fluids to permeate the carbonate. This dolomitization preserved porosity and permeability. Subsequent dissolving fluids were then able to attack the nondolomitized fossils, creating moldic porosity (Al-Shaieb, Beardall, and others, 1993).

If the reservoir is the second type, the spatial relationship of the reservoir to the unconformity is essential. Subaerial exposure associated with sequence boundaries may impact reservoir evolution through meteoric diagenesis (grain cementation or dissolution), dolomitization (Sarg, 1988), and karstification (Manni, 1985; Matthews, 1992; Fritz and Medlock, 1995).

Therefore, any exploration strategy should include a precise understanding of sequence stratigraphy and the identification of parasequences, facies analysis and distribution, dolomitization and other diagenetic overprints, and the positions of unconformities bounding the sequence.

ACKNOWLEDGMENTS

The authors wish to express their appreciation to Darwin Boardman, Paul Blubaugh, and Catherine Price for their helpful contributions. We thank Gary Stewart for his valuable suggested improvements.

REFERENCES CITED

Al-Shaieb, Zuhair; Beardall, G.; Medlock, P. L.; Lippert, K.; Matthews, F. D.; and Manni, F. M., 1993, Overview of Hunton facies and reservoirs in the Anadarko basin, *in* Johnson, K. S. (ed.), Hunton Group core workshop and field trip: Oklahoma Geolog-ical Survey Special Publication 93-4, p. 3–39.

Al-Shaieb, Zuhair; Fritz, R. D.; Barrick, J. E.; Medlock, P. L.; and Puckette, Jim, 1993, Hunton Group field trip to the Arbuckle Mountains, Oklahoma, *in* Johnson, K. S. (ed.), Hunton Group core workshop and field trip: Oklahoma Geological Survey Special Publication 93-4, p. 183–212.

Amsden, T. W., 1957, Part I. Introduction to stratigraphy, *in* Stratigraphy and paleontology of the Hunton group in the Arbuckle Mountain region: Oklahoma Geological Survey Circular 44, 57 p.

_____1978, Stop 3—Late Ordovician, Silurian, and Early Devonian strata, *in* Ham, W. E., Regional geology of the Arbuckle Mountains, Oklahoma: Oklahoma Geological Survey Special Publication 73-3, p. 39–43.

_____1980, Hunton Group (Late Ordovician, Silurian, and Early Devonian) in the Arkoma basin of Oklahoma: Oklahoma Geological Survey Bulletin 129, 136 p.

_____1989, Depositional and post-depositional history of middle Paleozoic (Late Ordovician through Early Devonian) strata in the ancestral Anadarko basin, *in* Johnson, K. S. (ed.), Anadarko basin symposium, 1988: Oklahoma Geological Survey Circular 90, p. 143–146.

Barrick, J. E.; Klapper, G.; and Amsden, T. W., 1990, Late Ordovician–Early Devonian conodont succession in the Hunton Group, Arbuckle Mountains and Anadarko basin, Oklahoma, *in* Ritter, S. M. (ed.), Early to middle Paleozoic conodont biostratigraphy of the Arbuckle Mountains, southern Oklahoma: Oklahoma Geological Survey Guidebook 27, p. 55–62.

Boggs, S., Jr., 1995, Principles of sedimentology and stratigraphy [2nd edition]: Prentice-Hall, Upper Saddle River, New Jersey, 774 p.

Fay, R. O., 1989, Geology of the Arbuckle Mountains along Interstate 35, Carter and Murray Counties, Oklahoma [revised edition]: Oklahoma Geological Survey Guidebook 26, 50 p.

Fritz, R. D.; and Medlock, P. L., 1995, Recognition of unconformities and sequences in Mid-Continent carbonates, *in* Hyne, N. J. (ed.), Sequence stratigraphy of the Mid-Continent: Tulsa Geological Society Special Publication 4, p. 49–80.

Manni, F. M., 1985, Depositional environment, diagenesis, and unconformity identification of the Chimneyhill Subgroup in the western Anadarko basin and northern shelf, Oklahoma: Oklahoma State University unpublished M.S. thesis, 133 p.

Matthews, F. D., 1992, Paleokarstic features and reservoir characteristics of the Hunton Group in the Anadarko basin, Oklahoma: Oklahoma State University unpublished M.S. thesis, 174 p.

Sarg, J. F., 1988, Carbonate sequence stratigraphy, *in* Sea-level changes—an integrated approach: Society of Economic Paleontologists and Mineralogists Special Publication 42, p. 155–181.

Shelton, John; and Gerken, L., 1995, Recognizing sequence surfaces in Mid-Continent siliciclastic strata, *in* Hyne, N. J. (ed.), Sequence stratigraphy of the Mid-Continent: Tulsa Geological Society Special Publication 4, p. 31–48.

Vail, P. R., 1987, Seismic stratigraphy interpretation using sequence stratigraphy. Part 1: Seismic stratigraphy interpretation procedure, *in* Bally, A. W. (ed.), Atlas of seismic stratigraphy, v. 1: American Association of Petroleum Geologists Studies in Geology 27, p. 1–10.

Van Wagoner, J. C., 1985, Reservoir facies distribution as controlled by sea-level change [abstract]: Abstract and Poster Session, Society of Economic Paleontologists and Mineralogists Midyear Meeting, Golden, Colorado, p. 91–92.

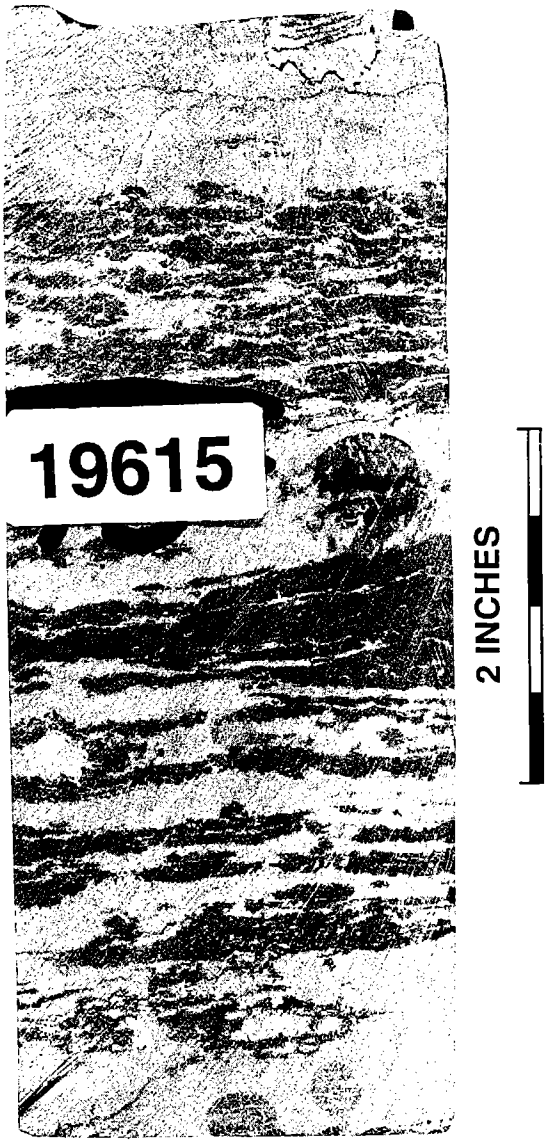

Figure 10. Dolomudstone with cryptalgal fabric. Supratidal facies I of Al-Shaieb, Beardall, and others (1993). Henryhouse Formation, Apexco Green core, Beckham County, Oklahoma. Depth, 19,620 ft.

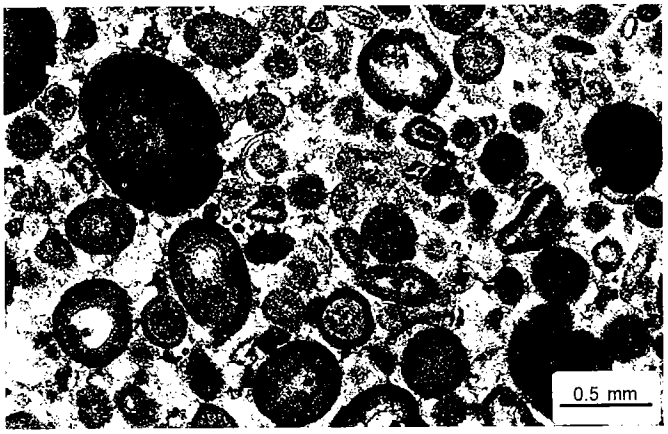

Figure 11. Photomicrograph of ooid grainstone representing high-energy intertidal/upper-subtidal facies. Facies IIb of Al-Shaieb, Beardall, and others (1993). Henryhouse Formation, Eason Van Curen core, Kingfisher County, Oklahoma. Depth, 7,149 ft. Plane-polarized light.

Defining the Role of Woodford–Hunton Depositional Relationships in Hunton Stratigraphic Traps of Western Oklahoma

Kurt Rottmann
Consultant Geologist
Oklahoma City, Oklahoma

ABSTRACT.—The Hunton Group is the principal hydrocarbon-producing carbonate reservoir in the western Oklahoma portion of the Anadarko basin. The following observations and conclusions result from a detailed original subsurface study of the Hunton Group in western Oklahoma.

The top of the Ordovician Sylvan Shale, after deposition, was a flat, featureless time-stratigraphic surface. Following deposition of the Hunton Group, subsequent regional uplift and erosion modified the Hunton, creating erosional features that were preserved by the Devonian Woodford Shale. This shale probably was deposited by the gradual inundation of the Devonian seas. The inundation was confined to the post-Hunton erosional channels, filling and preserving them. With a gradual rise in sea level, the Devonian seas eventually spread out over the non-channelized Hunton surface, depositing a regionally correlatable Woodford Shale facies. The top of the Woodford Shale prior to Kinderhook deposition was flat and featureless, indicating a time-stratigraphic surface. Assuming that structural activity on a local scale was minimal from post-Sylvan to post-Woodford time, the time-stratigraphic surfaces of the Sylvan and Woodford Shales would have been essentially parallel regardless of the stratigraphic irregularities or erosional modifications that occurred within the Hunton Group.

The organic sediments of the Woodford Shale probably contained at least 50% water, and on accumulation, they began to expel this water. With burial, the water would have been largely expelled, decreasing the thickness of the Woodford by approximately 50%. Thus, stratigraphic relationships between the Woodford and the Hunton, as seen from present-day thicknesses, cannot be correctly interpreted unless the Woodford Shale is restored to its original thickness.

Five primary processes could have caused the thickness of the Hunton Group to vary, as observed on the logs of two adjacent wells. Assuming that the Hunton interval penetrated by one well is unaffected, the Hunton in the second well, with respect to the first, could have changed in thickness by (1) post-Hunton–pre-Woodford erosion, (2) being in a post-Hunton–pre-Woodford horst block that was eroded to the level of the Hunton in the first well, (3) being in a post-Hunton–pre-Woodford graben that filled with detritus, (4) stratigraphic thickness changes within the Hunton as a result of penecontemporaneous faulting or folding, or (5) a fault that cut the Hunton section. Of these five thickness-change scenarios, (1) and possibly (5) would have a Woodford section of varying thickness between the two wells. Therefore, an analysis of the uncompacted thickness of the Woodford and the thickness of the Hunton can lead to an understanding of post-Hunton–pre-Woodford structural and stratigraphic relationships.

The geometries of Hunton stratigraphic traps that have been analyzed using present-day Hunton and Woodford thicknesses often change dramatically when the Woodford interval is restored to its original uncompacted thickness. Therefore, prospecting for Hunton stratigraphic traps that have been sealed by the Woodford Shale should be done only after the Woodford has been restored to its original depositional thickness.

INTRODUCTION

The Hunton Group is the principal hydrocarbon-producing carbonate reservoir in the western Oklahoma portion of the Anadarko basin. This report is an attempt to understand the relationship between Hunton erosional surfaces and the manner and method in which the Devonian Woodford Shale was deposited, with the resulting influence on Hunton stratigraphic traps. The report area covers approximately 4,000 mi² in western Oklahoma and includes Ts. 13–23 N., Rs. 15–26 W. Data for this paper were compiled primarily from electric logs from the Oklahoma City Geological Library. Where possible, the gamma-ray curve was the primary curve used for correlation, as this curve is seldom affected by fluid content. Figure 1 shows the geographic location of the report area. Although the cross sections used for this report may appear not to be in order, they were taken from a more in-depth study of the Woodford and Hunton by the author. Owing to the proprietary nature of some of the data, not all the cross sections or the prospect examples displayed and presented orally at the carbonate-platform symposium in March 1996 will be given in this report.

Rottmann, Kurt, 2000, Defining the role of Woodford–Hunton depositional relationships in Hunton stratigraphic traps of western Oklahoma, *in* Johnson, K. S. (ed.), Platform carbonates in the southern Midcontinent, 1996 symposium: Oklahoma Geological Survey Circular 101, p. 139–146.

A fence-diagram technique was employed in the stratigraphic correlations of the Woodford Shale and Hunton Group. This method involves subdividing a large surface such as a wall, large poster, or paper sheet into map divisions such as sections, townships, and ranges. The logs to be used are then copied, annotated, and trimmed to include enough of the zones above and below the formation in question to assure not only complete inclusion of the zones but also determination of any effects those zones might have on the zone in question. A stratigraphic datum is picked that is common to all logs used, and the logs are then secured to the fence diagram, with the stratigraphic datum serving as the spot location on the grid. Figure 2 is a photograph of the fence diagram used for this report, for which approximately 750 well logs were employed. The results of the correlations were compiled and calculated and were used to derive the principles and concepts that resulted in the stratigraphic cross sections incorporated in this report. Considerable research was done on the depositional environment and erosional history of the Hunton Group and is not discussed here. However, Amsden (1976) offers an excellent review of the depositional history and erosional modification of the Hunton Group.

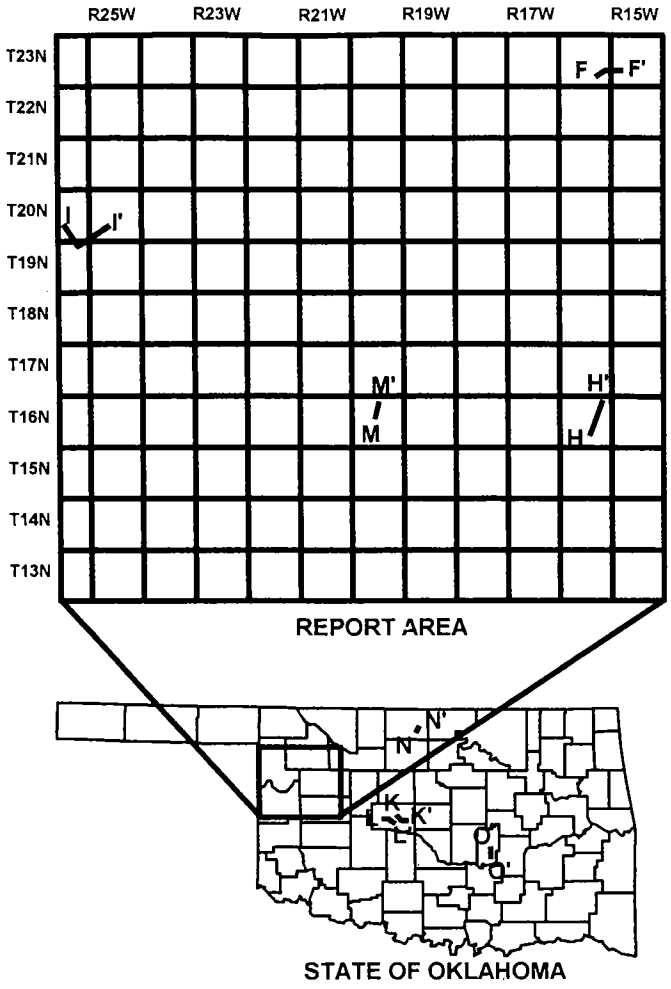

Figure 1. Location of report area and locations of cross sections used in this report.



Figure 2. Photograph of the fence diagram used for the current report.

Figure 3 is the geologic column used for the surface exposures of the Hunton in the Arbuckle Mountains and Criner Hills areas (Amsden, 1976). In the current report, the Chimneyhill Subgroup has not been subdivided into the Clarita, Cochrane, and Keel Formations, owing to the relative absence of paleontological data and the difficulty in correlating the zones by using electric logs. Unless otherwise noted, it can be assumed that the Clarita constitutes most of the Chimneyhill Subgroup and that the Cochrane and Keel Formations occupy a relatively short stratigraphic interval above the Sylvan Shale.

Figure 4 is the type log for the report area. Although the well represented by this log was drilled in Canadian County, east of the report area, the log is representative of the Hunton

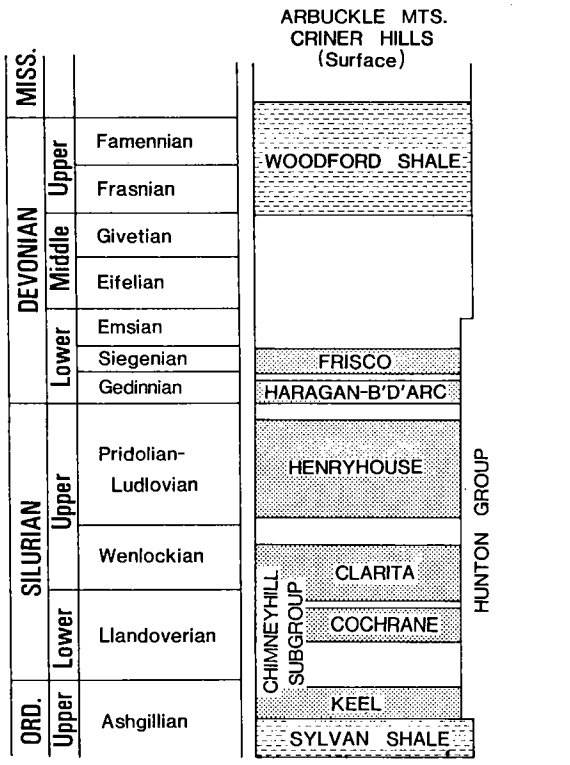

Figure 3. Geologic column of Ordovician, Silurian, and Devonian strata in Arbuckle Mountains and Criner Hills outcrops (modified from Amsden, 1976).

in the subsurface of western Oklahoma. The log was chosen as the type log for several reasons. First, thin shale lenses are present within the lower Henryhouse Formation that are regional in extent and easily correlated. As their thickness is uniform regionally, they can be considered time-stratigraphic markers within the Hunton. The second reason for the selection of this type log is the presence of all the major facies and formations of the Hunton section found in the report area. The third reason is the presence of an expanded section of the Chimneyhill Subgroup. Local thickness changes of this subgroup are common in Canadian County. This paper does not address the importance of the stratigraphic relationships of the various formations of the Hunton or their effect on porosity trends or development. (The author has available a more detailed study of the Hunton Group that addresses these issues.)

WOODFORD SHALE DEPOSITION

Figure 5 is a conceptual figure depicting two hypotheses for the way in which the Woodford Shale was deposited. Figure 5A represents a complete inundation of Woodford seas, with subsequent settling of clastic materials both in post-Hunton erosional channels and on adjacent non-channelized Hunton surfaces. This scenario would require almost similar facies both in the channels and on the high areas adjacent to the channels. Thus, in the right frame of Figure 5A, Woodford Shale facies should be present and correlatable both on the non-channelized Hunton surfaces as well as in the channels, although relative thicknesses of the Woodford may vary.

Figure 5B illustrates an alternative version of Woodford Shale deposition. This version implies a gradual initial inundation by transgressive Woodford seas being confined to post-Hunton erosional channels. Deposition was probably consistent with burial, resulting in the channels being filled and choked with clastic material. These Woodford channels were essentially filled with shale and clastic material prior to any regional Woodford deposition (Fig. 5B, middle frame). Ultimately, with the continuing rise in sea level, the Woodford seas would have emerged from the channels and inundated the remaining Hunton surface. The Woodford Shale, having been deposited regionally over both the paleotopographic highs and the choked erosional channels, is correlatable and basically uniform in thickness. This could have occurred only if the Woodford channels were filled with shale and the paleosurface of the channel fill was essentially flat to the Hunton surface adjacent to the channels at the time of regional Woodford Shale deposition. Thus, the facies of the Woodford Shale within the channel should not be present or correlatable with any facies deposited on non-channelized Hunton surfaces, as illustrated in the right frame of Figure 5B. For the purpose of this report, that portion of the Woodford Shale thought to have been deposited on the non-channelized Hunton surface is informally termed *regional Woodford Shale.* That portion of the Woodford Shale thought to have been deposited in and confined to the post-Hunton channels is informally termed *Woodford channel fill.*

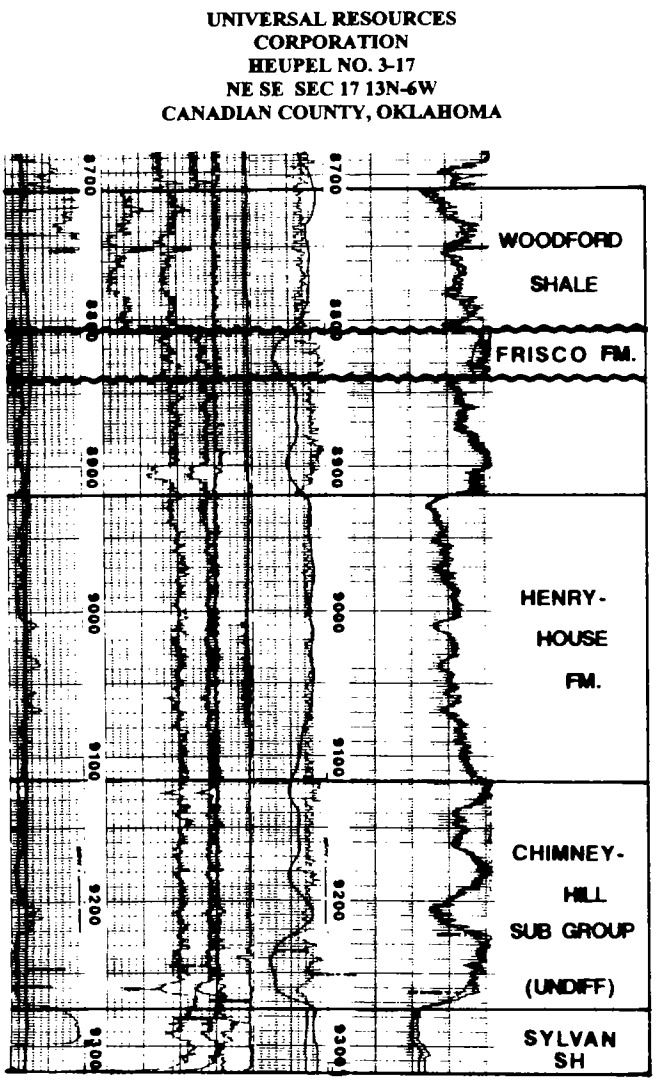

Figure 4. Type log illustrating the Woodford–Hunton–Sylvan section in central Oklahoma.

WOODFORD SHALE COMPACTION

Figure 6 is an illustration concerning the deposition and subsequent compaction of the Woodford Shale, which is one of the most important concepts of this report. Twenhofel (1950), when referring to the compaction of shales with high water contents, wrote: "This water from the moment of deposition begins to be expelled, and compaction results, which is thought gradually to increase as the sediments accumulate. After the sediments have been buried to depths of 1,000 feet or more, the water is thought to be largely expelled, and sediments originally with 50 per cent or more of water would decrease to half the original thickness" (p. 279). The Woodford Shale probably had a high water saturation at the time of deposition.

Before we discuss compaction, the concept of time-stratigraphic boundaries must be addressed. By definition, these are rock units with boundaries based on geologic time—i.e., with synchronous boundaries (Bates and Jackson, 1984, p. 527). The upper surface of the Sylvan Shale should fit this definition because the Sylvan and its various correlatable layers are uniform in thickness over wide areas. This lack of thick-

ness change within these layers over wide areas implies that the surface of the Sylvan Shale was flat and featureless. The upper layers of the Woodford Shale are identical in this characteristic to those of the Sylvan. Thus, the top of the Woodford also represents a topographic surface, prior to Mississippian deposition, that was flat and featureless. The surfaces at the tops of the Sylvan and Woodford Shales, therefore, are excellent examples of time-stratigraphic surfaces. If these formations were deposited in areas of minimal structural activity, then the two surfaces should be essentially parallel to each other prior to Mississippian deposition, as illustrated in the left frame of Figure 6.

The middle frame of Figure 6 illustrates the effect that compaction of the Woodford Shale, from deposition of Mississippian strata, exerted on the flat, featureless time-stratigraphic upper surface of the Woodford. With burial, this surface became distorted until the shale was squeezed to a thickness that is now approximately one-half its original thickness. The right frame of Figure 6 illustrates a major pitfall when attempting to reconstruct, by stratigraphic cross section, the original stratigraphic relationships of the Woodford and Hunton at the time of deposition. This pitfall occurs when the cross-section datum is the compacted and distorted top of the present-day Woodford (a time-stratigraphic surface), and the interpreter is unaware that flattening this distorted surface forces the surface of the Sylvan Shale to be artificially lifted. The artificial lifting of the Sylvan time-stratigraphic surface can lead to misinterpretation of post-Sylvan Shale–pre-Hunton Group structural activity.

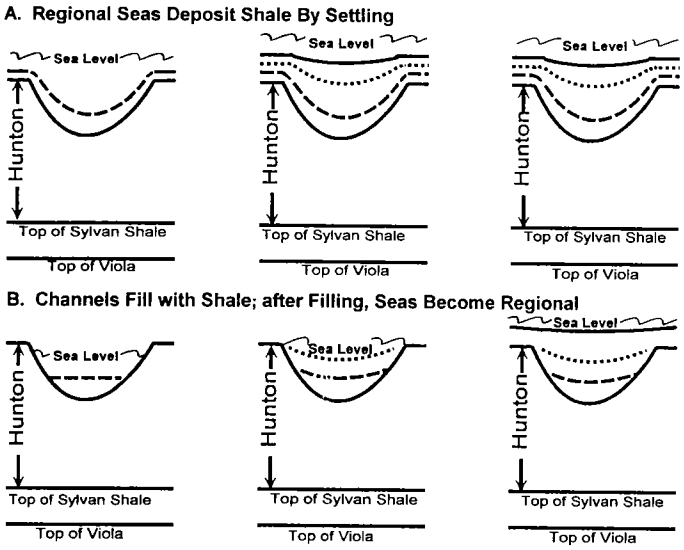

Figure 5. Two depositional hypotheses for Woodford Shale deposition. See text for explanation.

Figure 7 is an excellent example of the pitfalls of using the present-day thickness of the Woodford Shale in creating a stratigraphic cross section. This section (F–F′) was constructed to illustrate a major post-Hunton erosional channel that dissects West Campbell field in Major County. The stratigraphic datum is the top of the present-day Woodford Shale. Woodford channel-fill deposits can be seen in the lower part of the Woodford in the center well. Regional Woodford sediments were deposited at all three wells and are uniform in thickness and correlatable. As illustrated in the right frame of Figure 6, when a cross section is hung at the present-day time-stratigraphic surface at the top of the Woodford Shale, an artificial structure is created at the top of the Sylvan Shale (center well in Fig. 7). This feature is a false post-Sylvan structure.

Figure 8 is a revised stratigraphic cross section F–F′, which now incorporates the concept of compaction. The Woodford Shale has been reconstructed to pre-Mississippian stratigraphic conditions. The cross section is hung at the top of the Kinderhook Shale. The thicknesses of the Kinderhook and

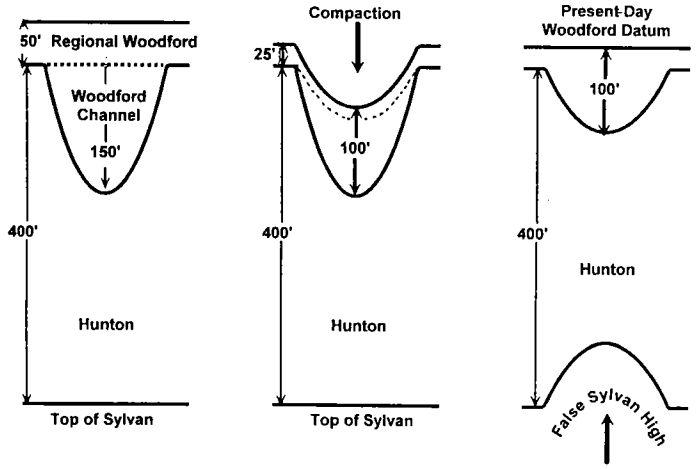

Figure 6. Interpretation of Woodford Shale compaction, and the pitfall of using a compacted Woodford section when considering the present-day Woodford surface as a stratigraphic datum. See text for further details.

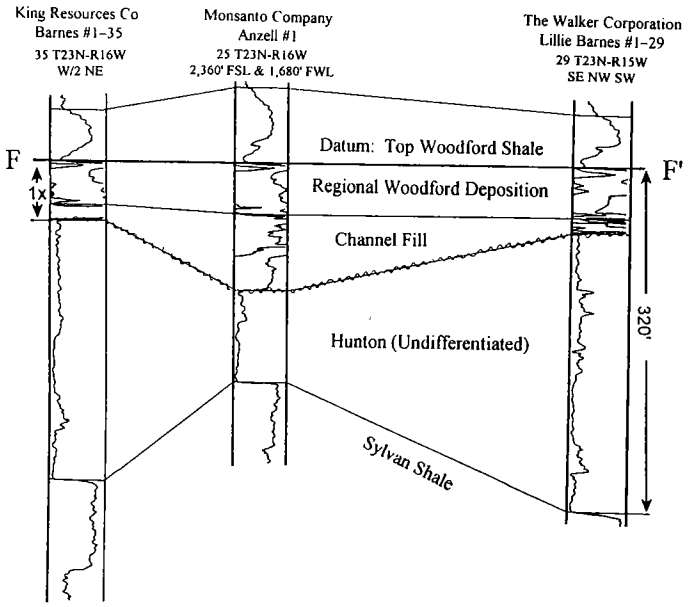

Figure 7. Cross section F–F′, constructed by using compacted present-day Woodford Shale thicknesses. Apparent structure is created in center well. Line of section shown in Figure 1.

Woodford Shales have been doubled to allow for the compaction. The regional Woodford Shale is correlatable and is the same thickness in all three wells. Notice that the time-stratigraphic surfaces of the Kinderhook, Woodford, and Sylvan Shales are essentially parallel. This indicates that the structure (other than regional dip) observed at the top of the Sylvan (Fig. 7) is an illusion. The porosity zone of the Hunton Group is sealed by the intersection of this zone and the Woodford Shale in the post-Hunton channel.

Figure 9 is a reconstruction of a stratigraphic cross section (N–N′, Garfield County), published by Kuykendall and Fritz (1993, p. 124). The thickness of the Woodford has been doubled to approximate its thickness prior to Mississippian deposition. The surface of the Viola is now essentially parallel to the surface of the Woodford. Of interest is the absence of Hunton strata. The post-Hunton channel removed the Hunton Group and incised into the Sylvan Shale. Note that the Sylvan Shale thickness has not been doubled to allow for its compaction. Compaction needs only to be considered for shales that have markedly varying thicknesses over short distances. Shales such as the Sylvan, which have a uniform thickness over broad areas, compact uniformly. Thus, the time-stratigraphic surface of the Sylvan remains flat because it has not been distorted. Geologists exploring the Midcontinent seldom take compaction of shales into consideration, because almost all of the geologic column in this region contains shale intervals that are relatively consistent in thickness over local areas.

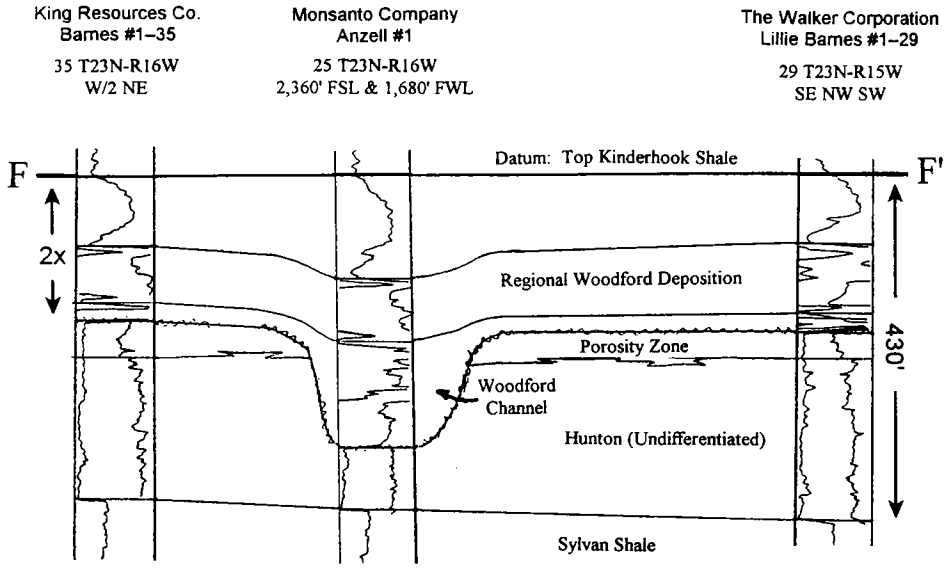

Figure 8. Revised cross section F–F′, constructed by using restored Woodford Shale thicknesses. The Woodford and Kinderhook Shales have been doubled in thickness to account for compaction.

Figure 10 is another example of a stratigraphic cross section (K–K′, Canadian County) that involves varying thicknesses of Woodford and Hunton strata. The section has been modified by doubling the Woodford to account for compaction, thus restoring it to its original thickness prior to compaction and deposition of Mississippian strata. The top of the Woodford Shale is parallel to the top of the Sylvan Shale and to the regional shales of the Henryhouse. This implies that

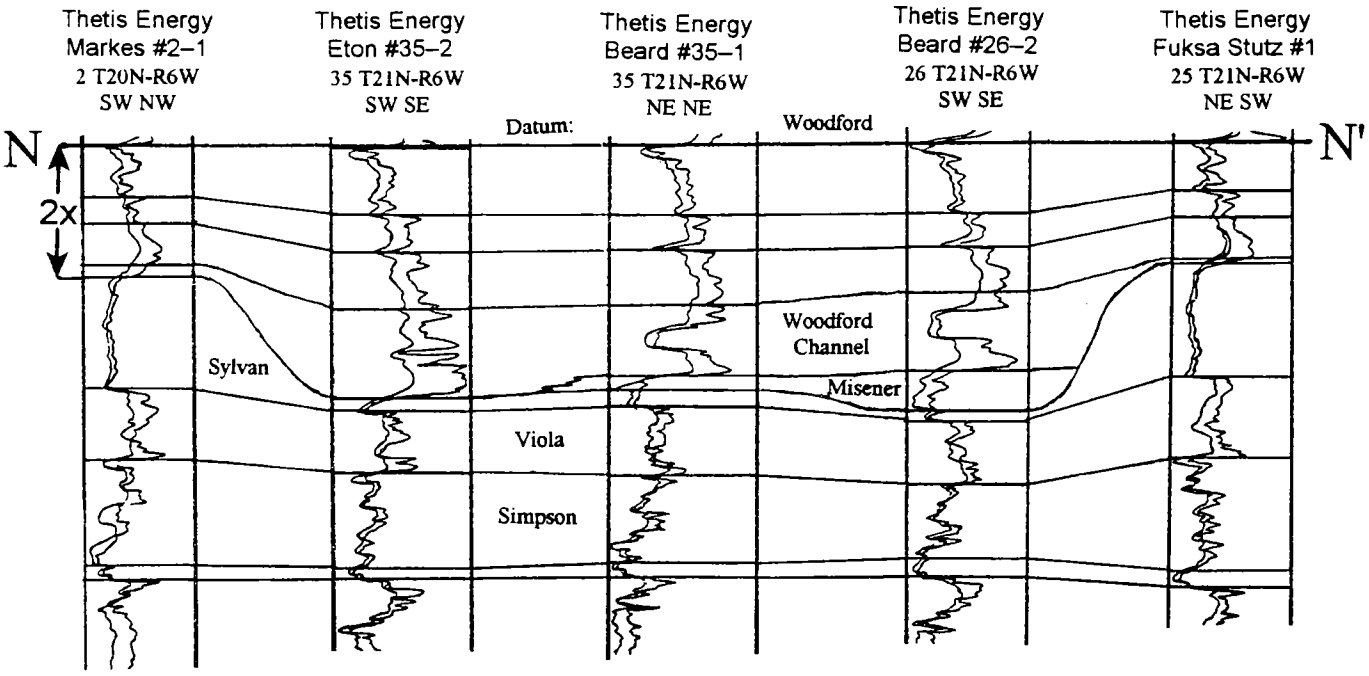

Figure 9. Stratigraphic cross section N–N′, illustrating a post-Hunton channel system incised into Sylvan Shale. Woodford Shale has been doubled in thickness to account for compaction. Modified from Kuykendall and Fritz (1993). Line of section shown in Figure 1.

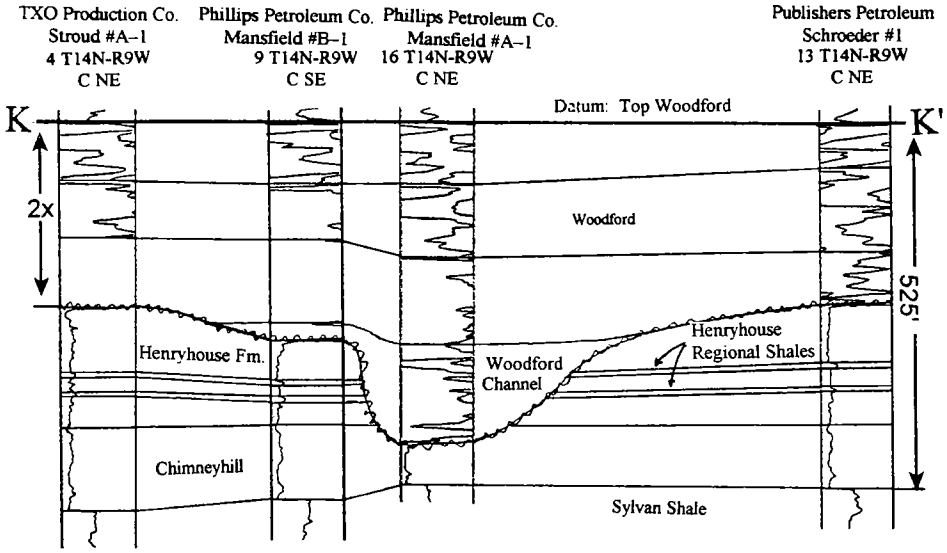

Figure 10. Stratigraphic cross section K–K′, illustrating the parallel time-stratigraphic surfaces of the Sylvan Shale and the top of the restored Woodford Shale. The Woodford Shale has been doubled in thickness to account for compaction. Line of section shown in Figure 1.

the thin Hunton section in sec. 16 did not result from post-Hunton structural uplift and erosion or faulting, but from post-Hunton erosion.

RESTORING WOODFORD–HUNTON STRATIGRAPHIC RELATIONSHIPS

The unconformity surface at the top of the Hunton Group is unique, because it is one of the few surfaces in the Mid-continent geologic column in which the erosional geometries include preserved deeply incised channel features. These channels were then filled with shale from the Woodford, resulting in dramatically varying shale thicknesses locally. On burial, and with the onset of compaction, connate water was expelled from the Woodford, and its thickness decreased until it was approximately 50% of its original thickness (as suggested by Twenhofel, 1950). Compaction of the shale distorts the original parallel surfaces of the Woodford in those areas where the shale is dramatically unequal in thickness.

The compaction factor for the Woodford must be determined, therefore, in order to restore the compacted shale section to its original thickness. This factor can be approximated simply by recreating stratigraphic cross sections using various compaction factors until the surfaces of the Woodford and the Sylvan are parallel. This can be accomplished only for those areas where deposition of the Woodford Shale and Hunton Group was unaffected by structure. As already noted, a compaction factor of 2, as suggested by Twenhofel (1950), was used in constructing the cross sections shown in Figures 8–10. A restored Woodford plus Hunton thickness can be created by adding the non-compacted Hunton to the restored Woodford thickness. This result reflects the thickness of the original Woodford plus the Hunton prior to Mississippian deposition. The thickness of the restored Woodford plus Hunton, therefore, should have parallel time-stratigraphic surfaces between the top of the Sylvan and the top of the Woodford except for thickening caused by regional dip in areas devoid of structural influences during deposition of these two units.

EXAMPLES OF STRUCTURAL RELATIONSHIPS OF THE WOODFORD–HUNTON

If the time-stratigraphic surface at the top of the Woodford Shale is parallel to the time-stratigraphic surface at the top of the Sylvan Shale on a stratigraphic cross section, it implies that deposition occurred during a lack of structural influences. However, if the two surfaces are not parallel, then an erosional or structural influence must have been active at the time of Woodford or Hunton deposition or post-deposition. The author has recognized the following five scenarios in which the restored Woodford plus Hunton would differ markedly in thickness between adjacent wells (Figs. 11–15; see Fig. 1 for cross-section locations).

Figure 11 is a structural north–south cross section (M–M′) through Leedy Hunton field in T. 16 N., R. 20 W., Dewey County. Notice that the thickness of the restored Woodford plus Hunton in sec. 16 is similar to that of the interval in the SW¼ sec. 10. However, the interval in the NW¼ sec. 10 is dramatically thinner. This well has been cut by a fault, which, incidentally, is the trapping fault for Leedy field. Thus, a dramatically thin restored Woodford plus Hunton interval could indicate the presence of a fault-cut section within the Woodford Shale or Hunton Group.

Figure 12 is cross section H–H′, in Dewey County. Notice that the Woodford is uniform in thickness in the three wells; however, the well in sec. 15 has cut a dramatically thicker Hunton section than the other two. Correlations indicate that the greater thickness in this well is in the upper Hunton section. This increase in thickness is due to a post-Hunton–pre-Woodford graben, determined by the author's regional correlations, that was filled with Hunton detritus prior to deposition of the Woodford Shale.

Figure 13 is cross section I–I′, in Ellis County. This section illustrates another example of markedly different restored Woodford plus Hunton thickness values caused by structural effects. Unpublished regional mapping by the author suggests that the well in the NE¼ sec. 2 penetrated a post-Hunton–pre-Woodford horst block. Although the thickness of the Woodford is similar to that of the other two wells, the restored Woodford plus Hunton interval is dramatically thinner in the center well owing to uplift and peneplanation of the horst block prior to Woodford deposition.

Figure 14 is a stratigraphic cross section (O–O′) across Little River Hunton field in Seminole County. Notice that the thickness of the Woodford Shale is similar in all three wells. However, the Hunton in the SW¼SE¼SE¼ sec. 19 is much

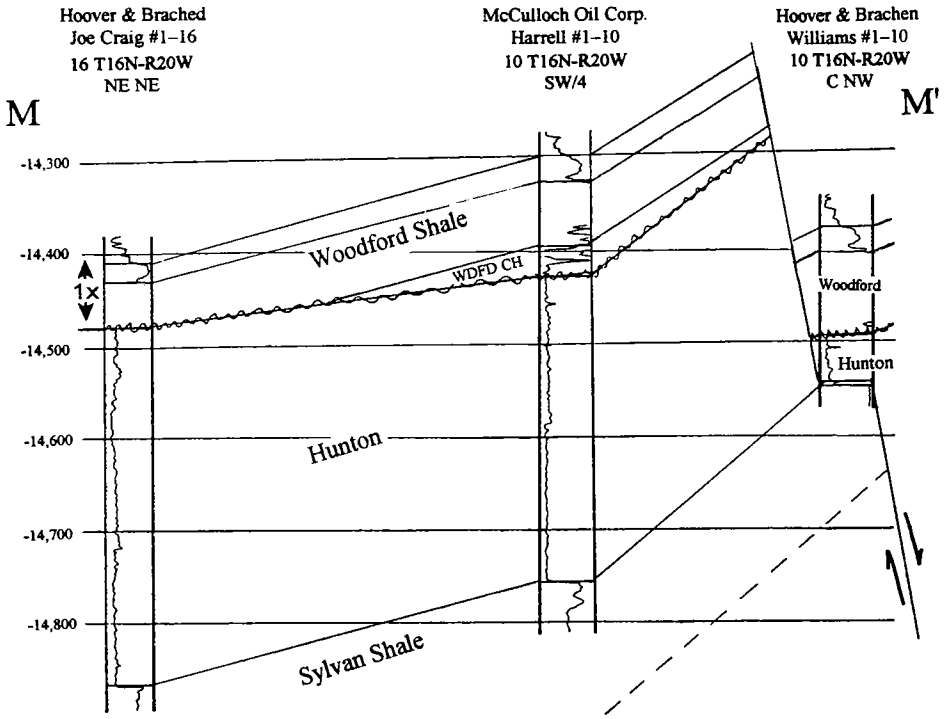

Figure 11. Example of a fault-cut Hunton section, which accounts for the unequal values for the top of restored Woodford plus Hunton thickness in the three wells. Line of section shown in Figure 1.

thicker than in the well in sec. 30. This is because the Sylvan Shale was incised prior to Hunton deposition, and the Hunton was deposited on this eroded surface. Thus, the Hunton was a fill deposit in the post-Sylvan erosional channel.

Figure 15, cross section L–L′ (Canadian County), also illustrates varying thicknesses for the restored Woodford Shale plus Hunton. All the Woodford thicknesses are uniform, but notice the dramatic changes that occur in the Chimneyhill. The top of the Chimneyhill Subgroup and the regional shales within the Henryhouse Formation are essentially parallel to the top of the Woodford. The thickness change occurs only within the Chimneyhill Subgroup. This suggests that the faulting or folding that occurred during or after Chimneyhill Subgroup deposition ceased prior to Henryhouse deposition. This thickness change thus represents penecontemporaneous faulting or folding during deposition of the Chimneyhill. During Henryhouse and Frisco deposition, however, structural movement was minimal or nonexistent except for regional dip.

WOODFORD CHANNEL HYDROCARBON SEALS

Figure 16 represents the ramifications of using present-day Woodford channel thicknesses when exploring for Hunton porosity-zone traps sealed by the Woodford channel shales. Suppose, as an example, that we recognize, by electric-log correlations, a Woodford channel sequence and that its present-day thickness is 150 ft (Fig. 16A1), but the regional Woodford thickness is 25 ft. A pitfall would exist by using the present-day thickness of 150 ft for the Woodford channel and by hanging the top of the present-day Woodford channel so that it is flat to the top of the adjacent nonchannelized Hunton. By using the compacted present-day thickness, the porous zone would not be sealed. By assuming that the compacted surface of the Woodford channel is flat, the distortion that occurred after compaction is not accounted for, as illustrated and explained in Figure 6. It would also appear that only 150 ft of the Hunton was eroded and that the base of the Woodford channel would cut and potentially seal only 150 ft of the 250-ft porous zone of the Hunton (Fig. 16A2).

The correct way to work with the Woodford channel is, first, to recognize that it is compacted and then to restore the thickness of the Woodford Shale to its original thickness at the time of deposition (Fig. 16B1). By multiplying the channel thickness by an approximate compaction factor of 2, the Woodford channel is restored to its original thickness of 300 ft. Now, the top of the Woodford channel surface can be hung at the top of the surface of the Hunton adjacent to the channel, as illustrated in Figure 16B2. Notice that the restored Woodford channel thickness of 300 ft indeed cuts the base of the porosity zone, creating a seal for a potential Hunton stratigraphic trap.

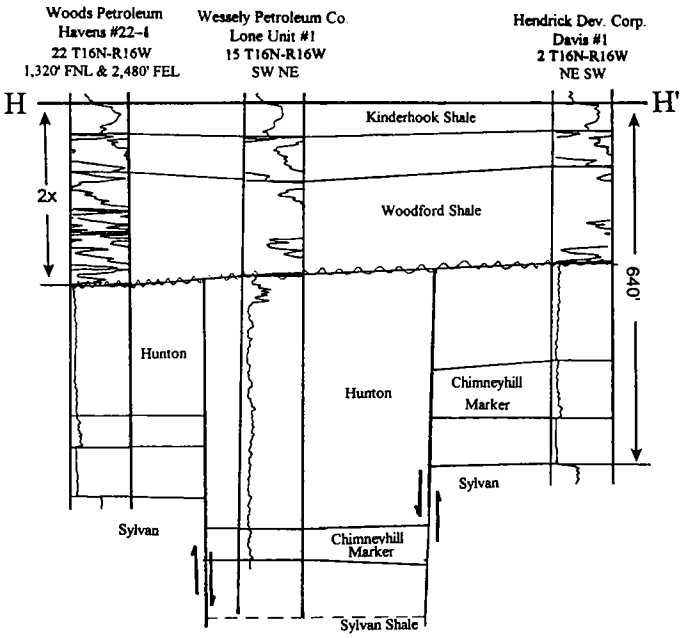

Figure 12. Example of a post-Hunton graben filled with detrital material prior to Woodford Shale deposition. The Woodford has been doubled in thickness to account for compaction. Line of section shown in Figure 1.

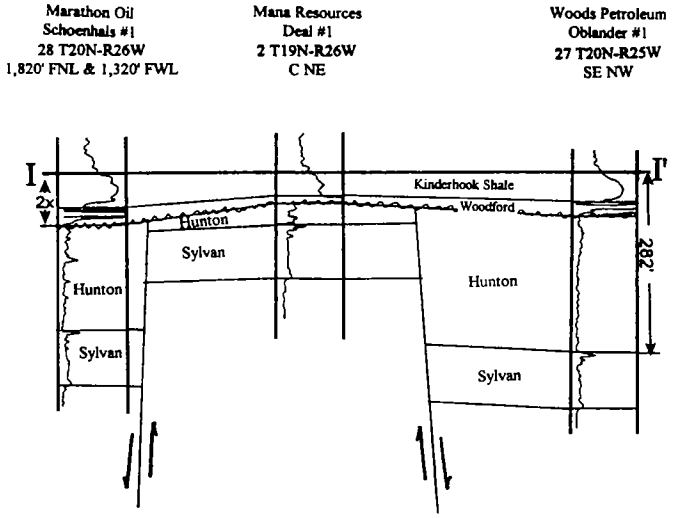

Figure 13. Example of a post-Hunton horst block that was peneplaned prior to Woodford Shale deposition. The Woodford has been doubled in thickness to account for compaction. Line of section shown in Figure 1.

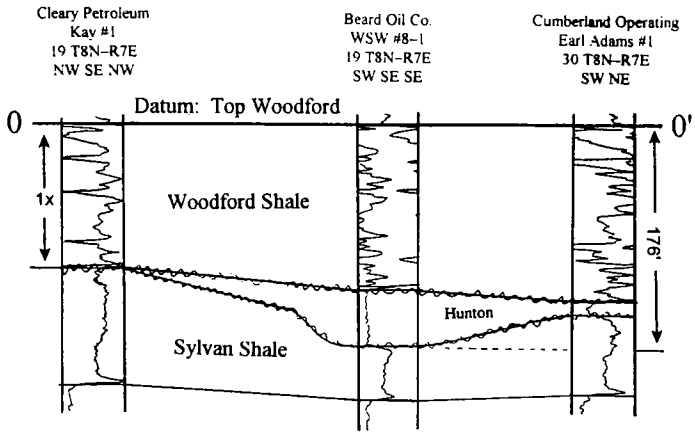

Figure 14. Example of Hunton sediments deposited on an eroded Sylvan surface as a fill deposit. Line of section shown in Figure 1.

SUMMARY AND CONCLUSIONS

The following points should be considered for determining Woodford Shale and Hunton Group stratigraphic relationships:

1. Compaction of the Woodford Shale must be accounted for when constructing stratigraphic cross sections that include wells containing post-Hunton channels.

2. Time-stratigraphic surfaces at the tops of the Sylvan and Woodford Shales are parallel in those areas devoid of structural movement.

3. Structural or erosional influences acting on the interval from the restored Woodford Shale thickness to the top of the Sylvan Shale could have caused unequal thicknesses between adjacent wells by one or more of the following influences: (a) faulted Woodford Shale or Hunton Group sections, (b) penecontemporaneous faulting or folding during Woodford Shale or Hunton Group deposition, (c) the Hunton Group deposited as fill on an eroded Sylvan Shale surface, (d) a Hunton Group section deposited on a post-Hunton–pre-Woodford peneplaned horst block, (e) a Hunton Group section deposited within a post-Hunton–pre-Woodford graben filled with detritus.

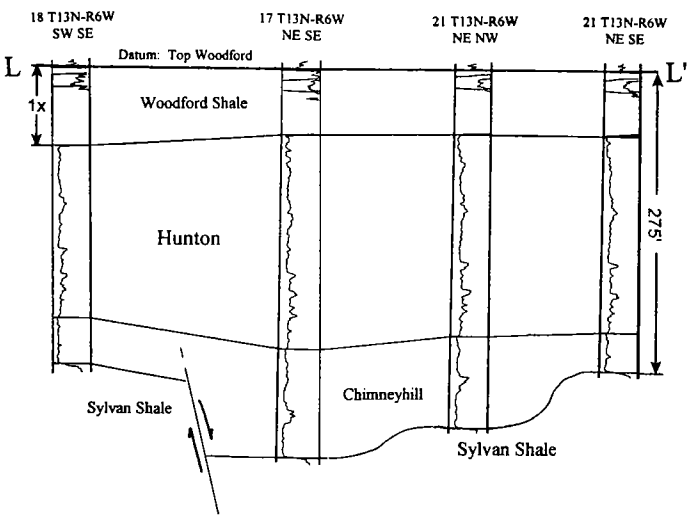

Figure 15. Example of thickening and thinning within the Chimney hill Subgroup, creating unequal restored Woodford plus Hunton thickness values. Line of section shown in Figure 1.

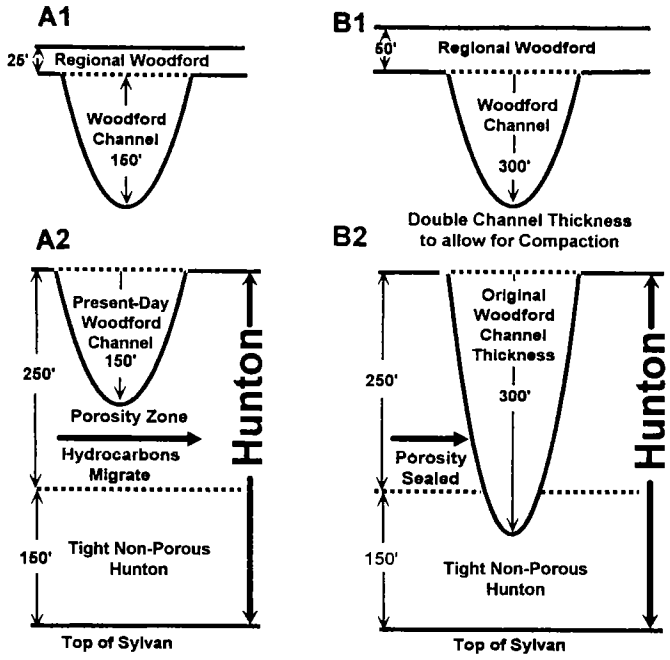

Figure 16. Incorrect method of using present-day Woodford Shale thicknesses (*A1* and *A2*), and correct method of using restored Woodford Shale thicknesses (*B1* and *B2*), when exploring for Hunton Group porosity seals from Woodford Shale channel deposits.

REFERENCES CITED

Amsden, T. W., 1976, Hunton Group (Late Ordovician, Silurian, and Early Devonian) in the Anadarko basin of Oklahoma: Oklahoma Geological Survey Bulletin 121, 214 p.

Bates, R. L.; and Jackson, J. A., 1984, Dictionary of geological terms [3rd edition]: Anchor Books, New York, 571 p.

Kuykendall, M. D.; and Fritz, R. D., 1993, Misener Sandstone: distribution and relationship to late post-Hunton unconformities, northern shelf, Anadarko basin, *in* Johnson, K. S. (ed.), Hunton Group core workshop and field trip: Oklahoma Geological Survey Special Publication 93-4, p. 117–134.

Twenhofel, W. H., 1950, Principles of sedimentation: McGraw-Hill, New York, 673 p.

Production and Reservoir Characteristics of Selected Hunton Fields in the Anadarko Basin

Paul W. Smith, Walter J. Hendrickson, and Craig M. Williams
IHS Energy Group
Oklahoma City, Oklahoma

INTRODUCTION

Wells completed in Hunton Group carbonates are the most prolific gas-producing wells in the Anadarko basin and are found throughout the basin and shelf areas. These completions represent a wide range of depths. Within the area studied—Ts. 10–29 N., Rs. 10–26 W.—the Hunton produces from depths of 5,000 to 25,000 ft. Of the 672 Hunton completions within the fields evaluated to date, the average well has produced more than 5 billion cubic feet of gas (BCFG). Within the Anadarko basin, cumulative production in some wells has exceeded 75 BCFG, with one well exceeding 112 BCFG.

This paper demonstrates that reservoir volume has more influence than does gas compressibility on increased gas recovery with depth. Preliminary evidence suggests that the thickness of the saturated interval has the most significant influence on recovery from Hunton wells and fields throughout the Anadarko basin and shelf. Figure 1 shows the area of the depth-versus-recovery study in relation to the Anadarko basin.

DATA PREPARATION

In Oklahoma, it is the responsibility of each operator to designate the producing formation as correctly as possible. There are no standards to which operators are held to define the producing formation correctly, nor are there any mechanisms in place to ensure that the operator has correctly defined and named a producing formation. As a result of this practice, the nomenclature for the basin is erratic. This problem is not unique to Oklahoma, however.

IHS Energy Group generates regional geologic cross sections to demonstrate the stratigraphic sequences throughout the Anadarko basin. The Oklahoma Corporation Commission (OCC) is the regulatory agency responsible for overseeing the oil and gas industry within the State of Oklahoma. The OCC currently utilizes IHS Energy Group's regional cross sections in an attempt to standardize the nomenclature used by operators in the basin.

To ensure nomenclatural consistency and accuracy, electric logs of nearly 18,000 oil and gas wells were reviewed for this study. A comparison was made between the perforated interval correlated on the log with the regional cross sections and the operator-defined producing formation. When the name of the correlated interval disagreed with the operator-defined producing formation, the correlated nomenclature, as indicated by the regional cross sections, was used. Almost 40% of the operator-defined producing formations either were too vague to use or were incorrect. Furthermore, about 15% of the perforated intervals required correction because of reporting errors or typographical errors, or because the perforation intervals were simply absent from the production records.

Significant amounts of cumulative gas production were reallocated. Thus, some formations had significant losses of cumulative production that were offset by significant additions of cumulative production credited to other formations. Typically, wells producing from the Hunton were correctly called; less than 5% were miscalled. However, we did observe errors, such as the Hunton being called the Red Fork (among other things).

METHODOLOGY

Depth versus Ultimate Recovery

As the purpose of this project was to develop guidelines that could indicate general trends in reservoir quality with depth, estimates were developed for ultimate recovery for each gas-well completion. The recovery is the sum of the gas plus the condensate recovery converted to a gas equivalent. For a discussion of the methodology used in this project, the reader is referred to the paper by Smith and Woods (2000) contained in this volume.

Reservoir Characteristics

Detailed reservoir studies were conducted for 42 producing Hunton fields in the Anadarko basin (Oklahoma and Texas). Reservoir characteristics were collected by log analysis to include porosity and thickness ranges and averages for the perforated, saturated, and gross-reservoir intervals. Many other parameters, such as reservoir pressure, water saturation, well spacing, and reservoir heterogeneity, were evaluated. The 42 fields comprise a total of 672 single Hunton completions and 458 commingled Hunton completions.

RESULTS

It is generally expected that the productive quality of reservoirs deteriorates with depth. Anomalies, such as Hugoton field and other unexplained aberrations (e.g., the carbonate

Smith, P. W.; Hendrickson, W. J.; and Williams, C. M., 2000, Production and reservoir characteristics of selected Hunton fields in the Anadarko basin, *in* Johnson, K. S. (ed.), Platform carbonates in the southern Midcontinent, 1996 symposium: Oklahoma Geological Survey Circular 101, p. 147–156.

"dead zone"), tend to support that expectation (Smith, 1996). However, the average recovery for the total gas-well population demonstrates that gas recovery increases with depth. The "economic" population strengthens the observation. The criteria for an "economic" well was defined by the following equation:

"Economic" required recovery = depth × depth/200.

Intuitively, one could conclude that increased pressure accounts for the increase in recovery. The trend in recovered reservoir volume of "economic" completions nearly doubles from 5,000 to 13,000 ft. At 13,000 ft, the average recovered reservoir volume again doubles, and then the trend increases at an accelerated rate.

In general, *all* the lithologies support the observation of increased reservoir volume and increased recovery with depth (Smith, 1996). Figure 2 shows the observed increasing trend in recovery versus depth for the study area. The more specific analysis of the sedimentary rocks does not affect the general observations drawn for the sandstones and carbonates as a whole. In fact, the trends of the "economic" completions of individual carbonate ages strengthen the observation (see Fig. 2). All carbonates show poor recoveries and reservoir volumes through a "dead zone" between 10,000 and 13,000 ft. The bimodal trends in the individual reservoir data (population and recovery) suggest the influence of geologic factors at the age and reservoir level.

Figure 3 shows the reservoir volumes required to contain those amounts of gas. Below 13,000 to 14,000 ft, the reservoir volumes drained by gas completions are substantially larger than those above 13,000 ft. Although the increase is more pronounced for carbonate completions, it is indisputable for sandstone completions as well. This suggests that extrapolation of geological observations from huge (anoma-

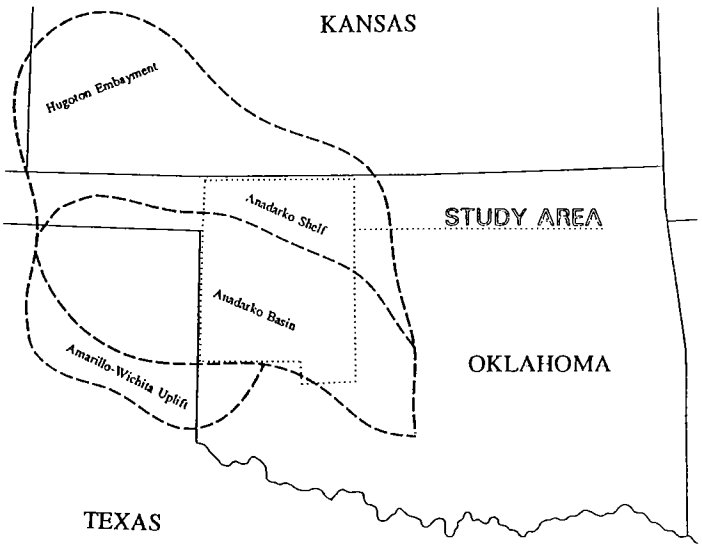

Figure 1. Map of Anadarko basin and surrounding region, showing study area (dotted outline).

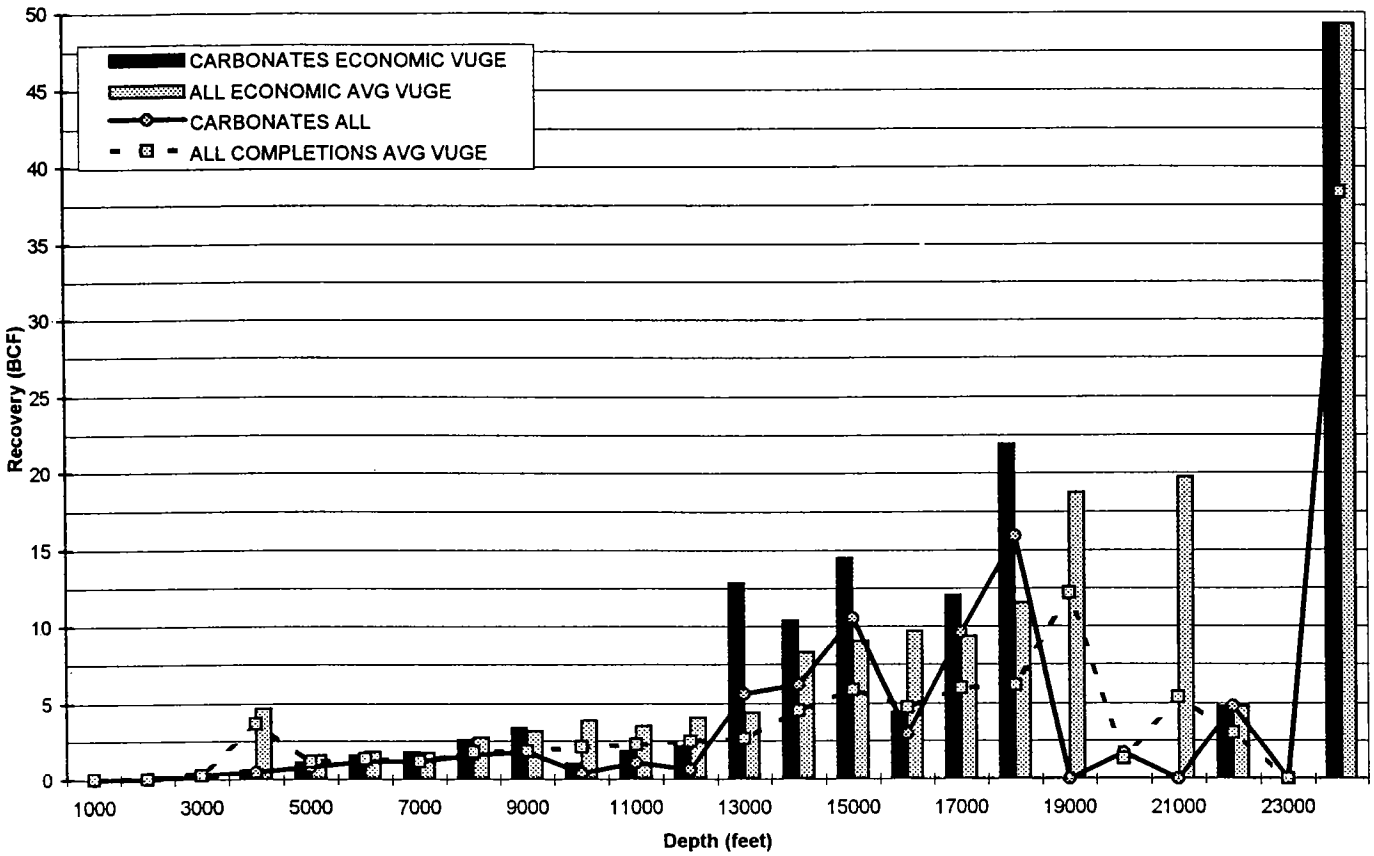

Figure 2. Trend showing increasing gas recoveries versus depth. *VUGE* = volume of ultimate gas equivalent.

lous) fields may lead to underestimation of the prospects for deeper reservoirs.

Except for the Hunton, carbonate activity has taken place almost totally above 10,000 ft. Below 13,000 ft, the Hunton is the only carbonate reservoir with significant activity, which shows a significant increase (fivefold) in recovery and reservoir volume. Figure 4A–C shows the distribution and trends observed in Hunton completion counts, ultimate recoveries, and reservoir volumes for the study area. Except for the carbonate "dead zone" from 10,000 to 13,000 ft, Hunton completions show increased recoveries with depth greater than what can be accounted for through compression. Most of the increase in recovery is due to increased reservoir volume.

The averages of detailed reservoir characterizations of Hunton producing fields were used to indicate the causes of increased recovery with increased depth. Some Hunton fields in the Texas Panhandle were used for collecting additional deep-reservoir characteristics outside the area investigated in the study by the Gas Research Institute (GRI) (Smith, 1996). Table 1 shows the cumulative production and well counts (sorted by depth) of the 42 Hunton fields used for this analysis. Figure 5 shows the distribution of average cumulative production with depth for these fields. Although oil production was not credited to these values (as was done in the GRI investigation), a high degree of similarity exists between Figure 5 (depth versus cumulative gas production) and Figure 4B (depth versus ultimate gas recovery). The observed increase in recovery from wells below 13,000 ft correlates with large increases in reservoir volume.

Within the fields evaluated, there are 436 single-zone Hunton completions above 13,000 ft in depth and 236 single-zone Hunton completions below 13,000 ft. Table 2 shows the physical characteristics of the Hunton (sorted by depth). Significantly more information on the reservoir characteristics for each well and field is available from IHS Energy Group.

As shown in Figure 6, perforated and saturated thicknesses increase with depth. For completions above 13,000 ft, the average Hunton well has 51.2 ft of saturated interval, of which an average of 24.5 ft was perforated (about half). Below 13,000 ft, typically less than one-third of the saturated interval is perforated. The average deep Hunton well has 265 ft of saturated interval, of which only 79 ft was perforated. With increased depth, operators typically perforate decreased proportions of the saturated interval. Figure 7 presents this trend.

As one might anticipate, trends in perforated and saturated porosities show a decrease with depth. As shown in Figure 8, however, increased depth does not necessitate decreased porosity. The average perforated zone above 13,000 ft has a porosity of 9.2%, and the average perforated zone below 13,000 ft has a porosity of 7.6%. Thus, the average perforated porosity below 13,000 ft is nearly 3 times greater than that above 13,000 ft (see Fig. 9).

Water saturation was observed typically to improve with depth (water concentration decreases). This improvement allows more of the available pore volume to be occupied by hydrocarbons (see Table 2). Well spacing does not appear to have a significant impact on recovery, because recovery ra-

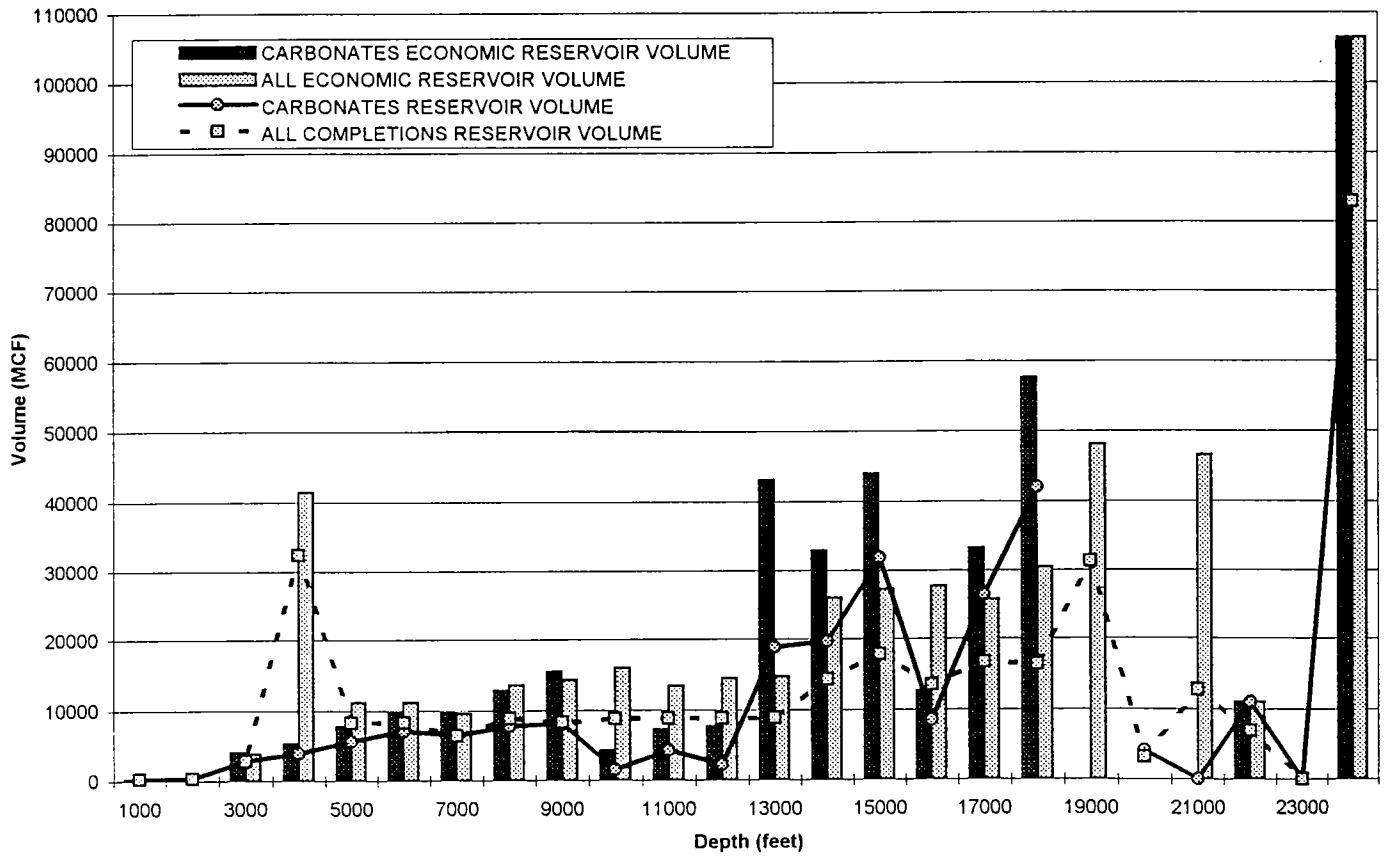

Figure 3. Required reservoir volumes versus depth.

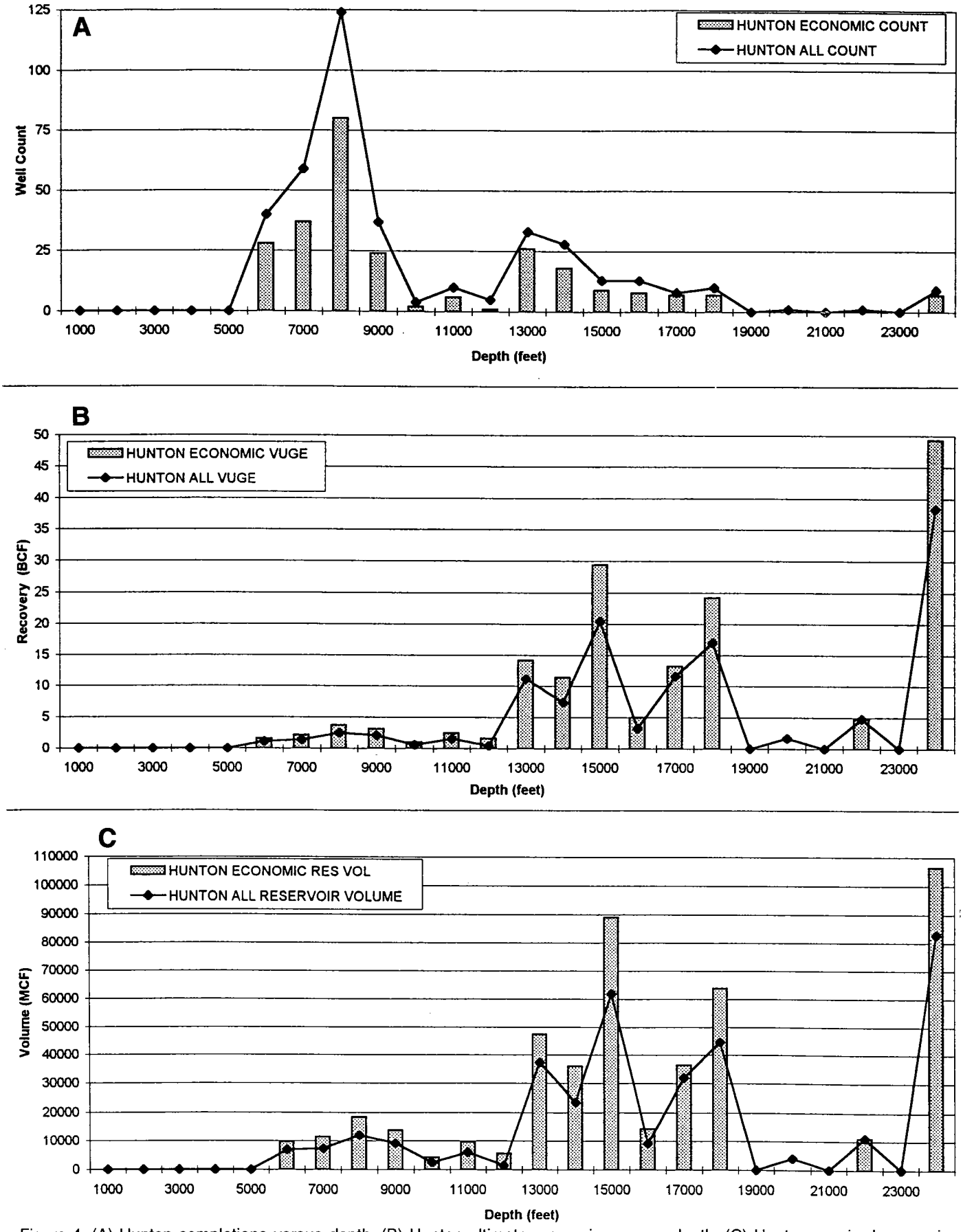

Figure 4. (A) Hunton completions versus depth. (B) Hunton ultimate recoveries versus depth. (C) Hunton required reservoir volumes versus depth.

Table 1.—Production Statistics of Selected Hunton Fields

	PRODUCTION					
	HUNTON			CMGLD		
FIELD	GAS(BCF)	OIL(MBO)	# WELLS	GAS(BCF)	OIL(MBO)	# WELLS
AVARD NW	19.5	3481	30	0	3	1
CHEROKEE WEST	6.9	40	10	4.2	19	2
HOPETON NORTH	17.6	42	7	0	0	0
LOVEDALE	5.7	129	13	2.8	129	7
LOVEDALE NW	4.9	17	3	0.2	40	3
OAKDALE	11.1	860	12	4.5	169	14
RINGWOOD	192.6	9000	166	56.1	5773	162
CAMPBELL	42.7	4044	43	6	137	12
CHEYENNE VALLEY	16.1	3036	32	39.6	3377	38
CEDARDALE NE	71.5	118	17	1.9	36	9
OKEENE NW	38.1	1851	52	37.2	2025	113
PHROSO NE	14.3	371	4	0	0	0
BADO EAST	1	53	2	2.5	38	2
SEILING NE	11.1	656	11	8.5	656	15
ORION SE	27	946	21	0.9	43	4
ALTONA	8.1	306	9	38.7	1000	65
OAKWOOD NORTH	7.4	82	4	1.6	24	2
ARNETT EAST	18.4	0	5	0	0	0
HARMON EAST	9.8	0	1	0	0	0
PUTNAM	329.2	57	36	4.6	8	5
CUSTER CITY NORTH	173.4	25	24	0.1	9	2
WHEELER-PAN (NW)	49.1	305	8	0	0	0
WHEELER-PAN	72.6	566	12	0	0	0
GAGEBY CREEK	136.7	203	10	0	0	0
ARNETT SE	3.3	0	1	0	0	0
ANTHON NE	4	0	1	0	0	0
ALEDO	230.2	9	8	16	1	1
FARRIS	10.9	81	3	0	0	0
LEEDEY	25.7	165	8	0	0	0
LEEDEY SE	24.8	3	2	0	0	0
MAYFIELD WEST	218.6	527	25	0	0	0
MATHERS RANCH	186.4	0	28	0	0	0
HOWE RANCH	36.2	0	7	0	0	0
TEXOLA	13	6	3	0	0	0
BUFFALO WALLOW	359.7	0	16	0	0	0
WASHITA CREEK	444.4	0	12	0	0	0
MILLS RANCH SOUTH	46.4	0	3	0	0	0
MILLS RANCH SE	30.8	0	2	0	0	0
MILLS RANCH	276.8	0	10	0	0	0
REYDON	4.8	0	1	0	0	0
NEW LIBERTY SW	7.6	0	1	0	0	0
MAYFIELD NE	181.9	0	9	2	0	1
totals	3389.1	26979	672	227.4	13487	468
Average	5.0	40.1		0.5	29.4	

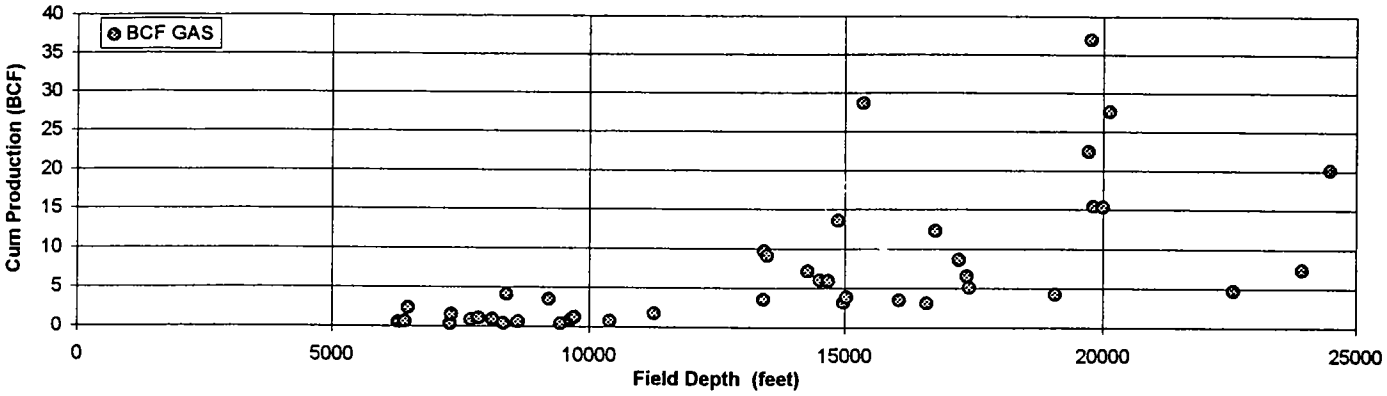

Figure 5. Average cumulative production versus depth for 42 Hunton fields. Field names and data are given in Tables 1–3.

tios appear to be influenced more by the relationship of perforated thickness to saturated thickness. However, most deep wells are spaced as 640-acre units. By using average saturated porosity, saturated thickness, water saturation, and well spacing, a hydrocarbon-saturated reservoir volume can be determined. Figure 9 shows the increase in hydrocarbon-saturated reservoir volume with increased depth. This volume shows trends similar to the required reservoir volume derived by recompressing the produced-gas volume to reservoir conditions (see Fig. 4C).

As suggested by the differences in porosities of the perforated intervals and saturated intervals, the Hunton is not a

Table 2.—Reservoir Characteristics of Selected Hunton Fields

Field	State	Disc Year	Trap Type	Specific Trap Type(s)	DEPTH	THICKNESS Average			POROSITY Average			Water Sat'n	ORIGINAL PRESSURE				Spacing
															Type		
					Avg	Perf'd	Gross	Sat'd	Perf'd	Gross	Sat'd	Avg	Average	High	Shut In	Btm	
AVARD NW	OK	1967	STRUCT STRAT	PORPERM NOSE FRACTUR UNCON	6300	10.0	25.9	24.5	7.1	5.6	5.8	27.80	2269	2613	SI		320
CHEROKEE WEST	OK	1965	STRAT	FACIES PORPERM	6433	6.8	10.1	9.6	12.0	10.2	10.1	33.50	2761	2840	SI		160
HOPETON NORTH	OK	1967	STRAT	PORPERM	6490	10.0	26.0	23.7	9.5	7.6	10.1	20.20	2641	2728		BH	640
LOVEDALE	OK	1960	STRAT	FACIES PORPERM	7314	41.4	57.8	57.8	4.4	4.8	4.8	46.50	2529	2901		BH	320
LOVEDALE NW	OK	1967	STRUCT STRAT	FACIES PORPERM FAULT	7338	32.0	62.6	52.0	5.5	5.1	5.1	49.00	2815	2960		BH	640
OAKDALE	OK	1952	STRAT	PORPERM CHEMALT	7708	7.5	171.3	15.4	15.1	5.1	14.9	27.70	2525	2600	SI		160
RINGWOOD	OK	1962	STRAT	FACIES PORPERM	7864	22.2	46.4	34.7	7.1	8.8	8.9	29.30	3350	4082		BH	160
CAMPBELL	OK	1960	STRUCT STRAT	PORPERM ANTICLN FAULT NOSE	8133	38.9	248.1	79.0	8.9	5.0	8.2	33.70	3178	3620		BH	160
CHEYENNE VALLEY	OK	1967	STRUCT STRAT	FACIES PORPERM HOMOCLN	8342	20.8	320.5	37.0	13.2	5.0	10.5	24.40	3495	3627	SI		160
CEDARDALE NE	OK	1959	STRAT	FACIES PORPERM NOSE	8400	33.2	52.3	43.2	9.1	9.2	8.7	38.30	3402	3687		BH	640
OKEENE NW	OK	1967	STRUCT STRAT	PORPERM MONOCLN CHEMALT	8627	11.5	393.9	70.1	13.1	3.5	7.0	32.60	2715	3778	SI		160
PHROSO NE	OK	1987	STRUCT STRAT	PORPERM ANTICLN FAULT	9217	50.5	380.0	73.0	12.2	5.6	10.9	26.50	3489	3539		BH	160
BADO EAST	OK	1979	STRUCT STRAT	PORPERM FAULT	9440	62.7	482.0	139.0	5.1	3.5	4.8	31.00	3345	3534		BH	640
SEILING NE	OK	1975	STRUCT STRAT	PORPERM FAULT CHEMALT	9643	22.8	431.6	52.5	13.0	4.2	10.6	28.80	3413	3566		BH	320
ORION SE	OK	1977	STRUCT STRAT	FACIES FAULT	9719	22.2	458.4	34.1	13.4	3.7	11.6	28.70	3684	3799		BH	80
ALTONA	OK	1970	STRAT	FACIES PORPERM	10405	134.6	350.5	350.5	4.1	3.4	3.4	18.60	3325	3650	SI		160
OAKWOOD NORTH	OK	1984	STRUCT STRAT	PORPERM ANTICLN FAULT	11274	19.0	506.7	132.3	8.5	3.6	5.0	21.50	4545	4869		BH	640
ARNETT EAST	OK	1965	STRUCT STRAT	PORPERM ANTICLN	13406	6.6	254.3	28.0	8.7	4.0	8.9	28.00	4649	5042		BH	640
HARMON EAST	OK	1970	STRUCT STRAT	PORPERM FAULT NOSE	13423	6.0	282.0	59.0	12.6	3.0	8.0	29.50	5638	5638	SI		640
PUTNAM	OK	1969	STRUCT STRAT	PORPERM ANTICLN FAULT	13475	35.6	380.0	163.0	8.4	2.3	3.7	21.50	6648	7577		BH	640
CUSTER CITY NORTH	OK	1958	STRUCT	ANTICLN FAULT	14274	52.2	534.0	176.4	5.1	1.7	3.0	20.80	6789	7379	SI		640
WHEELER-PAN (NW)	TX	1977	STRUCT STRAT	NOSE UNCON	14607	37.0	762.0	50.4	10.4	4.5	9.9	26.90	6627	7500		BH	640
WHEELER-PAN	TX	1974	STRUCT STRAT	NOSE UNCON	14678	25.2	722.7	51.4	13.0	5.3	9.4	29.40	6046	6180		BH	640
GAGEBY CREEK	TX	1964	STRUCT STRAT	ANTICLN FAULT CHEMALT	14863	67.8	332.6	267.8	10.6	7.0	7.2	18.00	6400	6400		BH	640
ARNETT SE	OK	1968	STRUCT	ANTICLN	14976	20.0	336.0	40.0	11.0	4.0	7.0	25.00	6303	6303		BH	640
ANTHON NE	OK	1980	STRUCT	ANTICLN	15033	26.0	346.0	102.0	8.8	2.9	5.0	30.00	6617	6617		BH	640
ALEDO	OK	1967	STRUCT	ANTICLN FAULT	15354	71.0	408.7	227.1	12.3	5.5	7.2	16.30	5303	5399	SI		640
FARRIS	TX	1975	STRUCT	ANTICLN FAULT	16057	48.5	678.2	597.5	7.2	4.0	4.2	17.60	6771	6771		BH	320
LEEDEY	OK	1970	STRUCT STRAT	PORPERM FAULT	16583	48.9	378.0	378.0	8.1	6.4	6.4	20.10	7466	7466	SI		640
LEEDEY SE	OK	1980	STRUCT STRAT	PORPERM	16750	32.5	401.0	401.0	12.3	6.2	6.2	23.70	2925	2925	FL		640
MAYFIELD WEST	OK	1976	STRUCT STRAT	FACIES PORPERM ANTICLN FAULT FRACTUR UNCON	17207	73.1	192.4	192.4	7.3	5.1	5.1	16.70	7950	8691		BH	320
MATHERS RANCH	TX	1970	STRUCT STRAT	PORPERM ANTICLN UNCON CHEMALT	17365	43.3	155.0	146.8	4.8	3.1	3.1	16.70	7941	8182		BH	640
HOWE RANCH	TX	1973	STRUCT STRAT	FACIES FAULT FRACTUR	17402	21.2	261.0	261.0	7.5	2.1	2.1	29.00	7233	7891		BH	640
TEXOLA	TX	1977	STRUCT	ANTICLN FAULT	19068	210.7	945.7	705.7	4.8	2.8	2.9	31.70	7460	8376	SI	BH	640
BUFFALO WALLOW	TX	1967	STRUCT	ANTICLN FAULT	19718	145.0	355.8	354.0	5.7	3.0	3.1	19.80	8765	9108		BH	640
WASHITA CREEK	TX	1966	STRUCT STRAT	ANTICLN CHEMALT	19772	110.7	475.3	475.3	8.6	3.3	3.3	15.80	9126	9155		BH	640
MILLS RANCH SOUTH	TX	1974	STRUCT STRAT	ANTICLN FAULT CHEMALT	19815	424.0	1031.0	999.0	4.0	3.6	3.7	24.00	7000	7000		BH	640
MILLS RANCH SE	TX	1975	STRUCT STRAT	ANTICLN FAULT CHEMALT	20007	83.0	825.0	825.0	5.7	4.7	4.7	23.80	9494	9494		BH	640
MILLS RANCH	TX	1972	STRUCT	ANTICLN FAULT	20136	183.0	959.0	855.7	6.3	4.3	4.4	24.80	9072	9072		BH	640
REYDON	OK	1974	STRUCT STRAT	PORPERM ANTICLN FAULT	22566	14.0	622.0	622.0	11.0	2.8	2.8	13.00	8579	8579		BH	640
NEW LIBERTY SW	OK	1979	STRUCT	ANTICLN	23920	1004.0	1274.0	1274.0	2.3	2.3	2.3	25.00	5143	5518		BH	
MAYFIELD NE	OK	1972	STRUCT	ANTICLN FRACTUR	24477	208.0	1081.0	208.0	6.9	5.0	6.9	9.00	8489	8489	SI		640

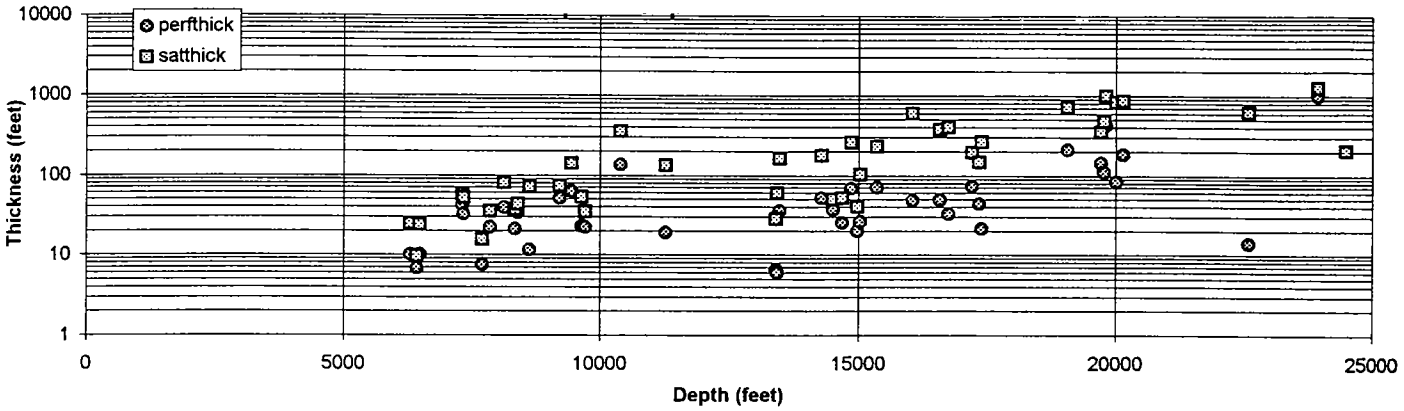

Figure 6. Perforated and saturated thicknesses versus depth for 42 Hunton fields. Thicknesses increase with depth.

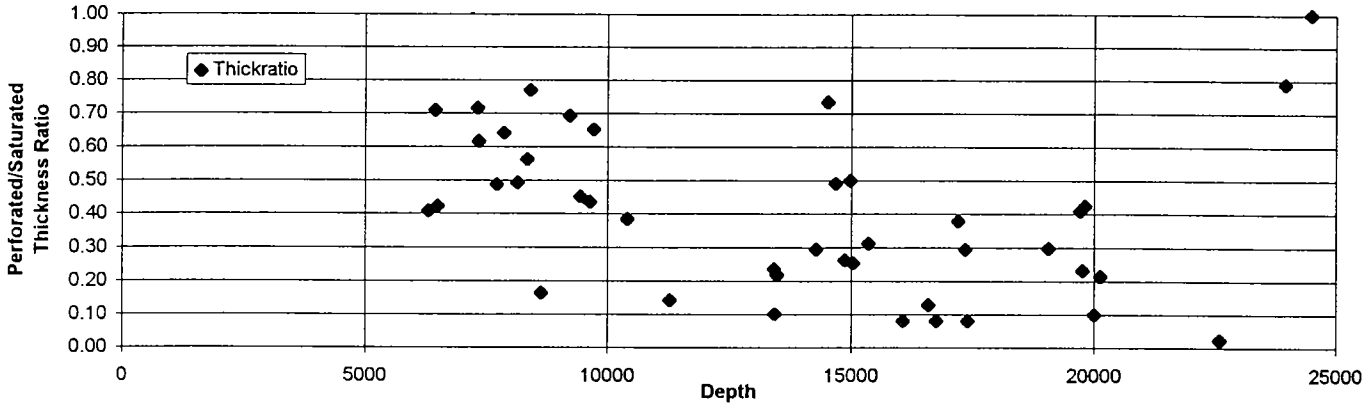

Figure 7. Ratios of perforated to saturated thicknesses versus depth for 42 Hunton fields. With increased depth, operators typically perforate decreased proportions of saturated interval.

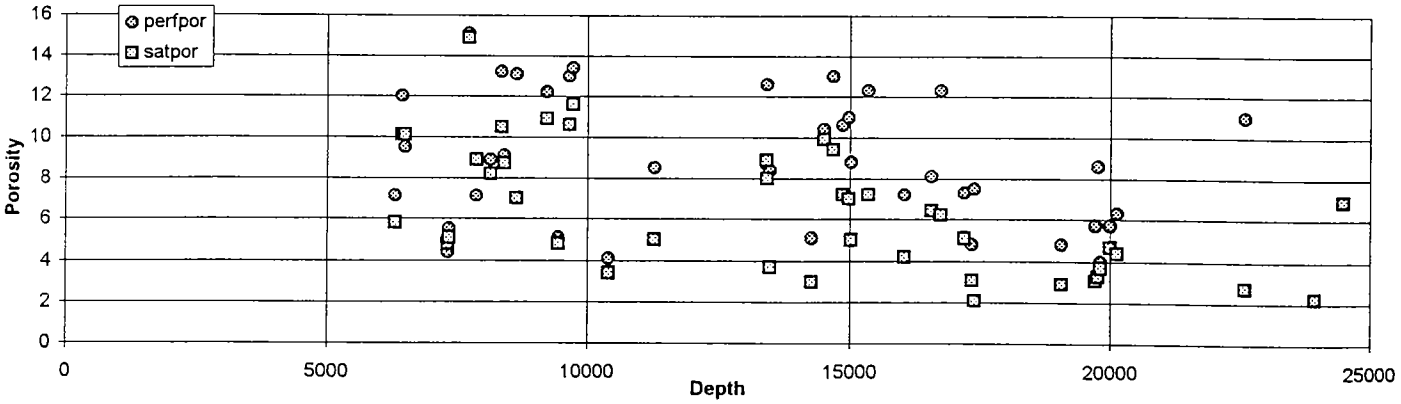

Figure 8. Perforated and saturated porosities versus depth for 42 Hunton fields. Porosity values are in percentages. As this graph shows, increased depth does not necessitate decreased porosity.

homogeneous reservoir. During the detailed reservoir-characterization efforts, reservoir heterogeneity was evaluated. The observed heterogeneities for each field are presented in Table 3. Typically, high levels of reservoir heterogeneity were observed, and the effects of this heterogeneity can be observed in well recovery. As higher proportions of the saturated interval are perforated, the effects of vertical reservoir heterogeneity are reduced. Figure 10 shows the trend in increased recoveries relative to increased perforated/saturated thickness ratios.

SUMMARY AND CONCLUSIONS

The results of this study indicate that reservoir productivity does not decline with depth. Even though gas compressibility is usually considered to be the most important factor leading to increased gas recovery with depth, the data indicate that it is not. In fact, using the "economic" Hunton well group, average reservoir volumes increase 551% from 6,000 to 18,000 ft. Through the same interval, gas compression would

Table 3.—Reservoir Heterogeneities of Selected Hunton Fields

FIELD	Observed Vertical Heterogeneities		Observed Horizontal Heterogeneities	
	Description	Degree	Descriptions	Degree
AVARD NW	Porosity Variations; Dolomitization;	HI	Porosity Variations; Dolomitization; Fractures	HI
CHEROKEE WEST	Porosity Variations; Dolomitization	MED	Erosional Surface; Dolomitization; Porosity Variations	HI
HOPETON NORTH	Porosity Variations; Dolomitization	HI	Erosional Surface; Porosity Variations; Dolomitization	HI
LOVEDALE	Porosity Variations; Dolomitization	HI	Porosity Variations; Dolomitization	HI
LOVEDALE NW	Porosity Variations; Dolomitization	HI	Porosity Variations; Dolomitization; Faults	HI
OAKDALE	Porosity Variations; Dolomitization	HI	Porosity Variations; Dolomitization	HI
RINGWOOD	Porosity Variations; Dolomitization	HI	Porosity Variations; Dolomitization	HI
CAMPBELL	Porosity Variations; Dolomitization;	HI	Porosity Variations; Dolomitization	HI
CHEYENNE VALLEY	Dolomitization	MED	Dolomitization	MED
CEDARDALE NE	Porosity Variations; Dolomitization	HI	Porosity Variations; Dolomitization	HI
OKEENE NW	Porosity Variations; Dolomitization	MED	Porosity Variations; Dolomitization	MED
PHROSO NE	Porosity Variations; Dolomitization	HI	Dolomitization; Porosity Variations	HI
BADO EAST	Porosity Variations; Dolomitization	HI	Porosity Variations; Dolomitization; Faults	HI
SEILING NE	Porosity Variations; Dolomitization	HI	Porosity Variations; Dolomitization; Faults	HI
ORION SE	Porosity Variations; Dolomitization	MED	Porosity Variations; Dolomitization; Faults	MED
ALTONA	Dolomitization; Fractures	MED	Dolomitization; Fractures	HI
OAKWOOD NORTH	Porosity Variations; Dolomitization	HI	Porosity Variations; Dolomitization; Faults	HI
ARNETT EAST	Porosity Variations; Dolomitization	HI	Porosity Variations; Dolomitization	MED
HARMON EAST	Porosity Variations	MED	Porosity Variations	LO
PUTNAM	Porosity Variations; Dolomitization	HI	Dolomitization; Porosity Variations; Faults	HI
CUSTER CITY NORTH	Porosity Variations; Dolomitization; Fractures	HI	Porosity Variations; Dolomitization; Fractures	HI
WHEELER-PAN (NW)	Porosity Variations; Dolomitization	HI	Dolomitization; Porosity Variations	MED
WHEELER-PAN	Porosity Variations; Dolomitization	HI	Porosity Variations; Dolomitization	MED
GAGEBY CREEK	Dolomitization; Porosity Variations; Fractures	LO	Dolomitization; Porosity Variations; Fractures	LO
ARNETT SE	Porosity Variations; Dolomitization; Fractures	MED	Porosity Variations; Dolomitization; Fractures	MED
ANTHON NE	Porosity Variations; Dolomitization; Fractures	MED	Porosity Variations; Dolomitization; Fractures	MED
ALEDO	Porosity Variations; Dolomitization	HI	Porosity Variations; Dolomitization	HI
FARRIS	Dolomitization; Porosity Variations	MED	Dolomitization; Porosity Variations	MED
LEEDEY	Porosity Variations; Dolomitization;	HI	Porosity Variations; Dolomitization	MED
LEEDEY SE	Porosity Variations; Dolomitization;	HI	Porosity Variations	MED
MAYFIELD WEST	Porosity Variations; Dolomitization	HI	Porosity Variations; Dolomitization; Faults	HI
MATHERS RANCH	Porosity Variations; Dolomitization	MED	Porosity Variations; Dolomitization; Erosional Surface	MED
HOWE RANCH	Fractures; Dolomitization; Porosity Variations	LO	Fractures; Dolomitization; Porosity Variations	LO
TEXOLA	Fractures; Dolomitization; Porosity Variations	LO	Fractures; Dolomitization; Porosity Variations	LO
BUFFALO WALLOW	Fractures; Porosity Variations; Dolomitization	LO	Fractures; Porosity Variations; Dolomitization	LO
WASHITA CREEK	Dolomitization;Porosity Variations	HI	Porosity Variations; Dolomitization	MED
MILLS RANCH SOUTH	Dolomitization; Porosity Variations; Fractures	LO	Dolomitization; Porosity Variations; Fractures	LO
MILLS RANCH SE	Dolomitization; Porosity Variations; Fractures	LO	Dolomitization; Porosity Variations; Fractures	LO
MILLS RANCH	Dolomitization; Porosity Variations; Fractures	LO	Dolomitization; Porosity Variations; Fractures	LO
REYDON	Porosity Variations; Dolomitization	HI	Porosity Variations; Dolomitization	MED
NEW LIBERTY SW	Porosity Variations; Dolomitization	HI	Porosity Variations; Dolomitization	HI
MAYFIELD NE	Porosity Variations	LO	Porosity Variations	LO

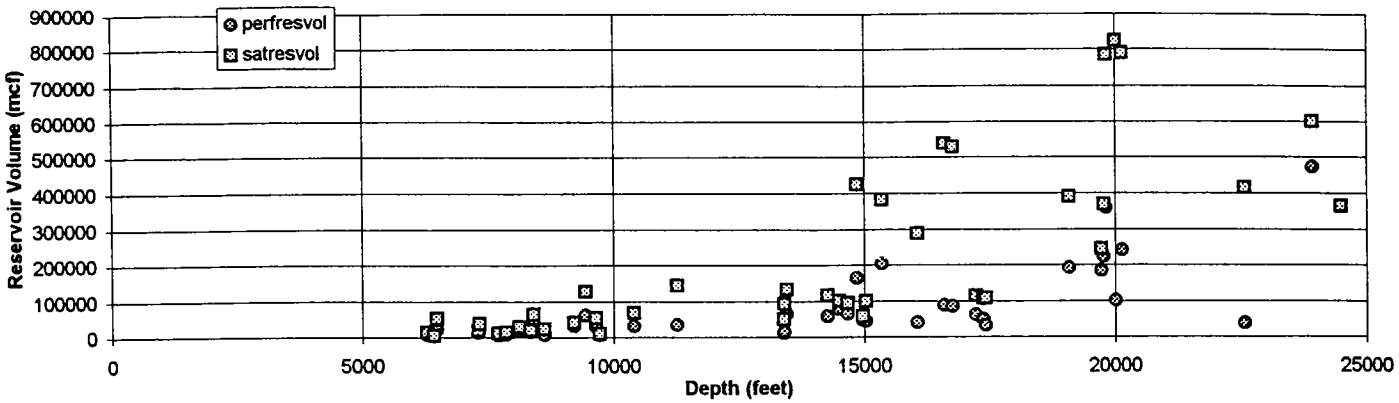

Figure 9. Perforated and saturated reservoir volumes versus depth for 42 Hunton fields. Hydrocarbon-saturated reservoir volume increases with depth.

increase the recovery by 146%. Increased reservoir volume has nearly four times the impact on reservoir recovery than does gas compressibility. Thus, the average recovery actually increases by 1,450%, owing to a combination of increased volume and gas compressibility.

The detailed reservoir-characterization studies indicate that reservoir porosity does not necessarily degrade with depth. The average perforated porosity in Hunton wells decreased by only 1.2 porosity units for completions below 13,000 ft in comparison to completions above 13,000 ft. The average porosity of the saturated interval decreased from 8.6% to 4.8% for the two depth groups. Saturated thicknesses and perforated thicknesses triple with depth. This more than compensates for any decreases in reservoir porosity. Increased reservoir thickness with depth

results in increased reservoir volumes. Consequently, the significant increases in recovery with depth are demonstrated to result from increased reservoir volumes, which are due primarily to increased thicknesses in saturated reservoirs.

Although the study results are different than industry expectations, they suggest that the difference reflects the extrapolation of industry activity through 13,000 ft of sediments. Using "economic" Hunton well populations, the original industry expectations can be substantiated. From 6,000 to 10,000 ft (above the "dead zone"), the average Hunton reservoir volume increases 40%, and gas compressibility increases recovery by 55%. Thus, gas recoveries are doubled, showing that increased recovery from shallow reservoirs is influenced more by gas compression than by increased reservoir volume. Industry pessimism for deep-gas exploration may have been compounded by the severe deterioration (virtual collapse) of recoveries from carbonate reservoirs between 10,000 and 13,000 ft (the "dead zone"). Because 86% of industry activity in the study area is above 13,000 ft, these pessimistic expectations are understandable. Below 13,000 ft, however, recovery increases substantially for Hunton reservoirs at a rate far beyond what compression would imply.

Although general trends in hydrocarbon recovery, and geological guidelines such as reservoir volume, indicate substantial prospects for deeper production, additional work needs to be done to tie the results developed in this study to more specific geological parameters. The reservoir characteristics used in this study represent the average observed values in 42 productive Hunton fields. A more accurate representation of the trends in reservoir characteristics with depth would incorporate individual well data rather than data aggregated to field level. However, the aggregated field data do provide valuable insights as to what one should anticipate. The second phase of this gas-recovery-versus-depth project will be conducted by using data collected from individual wells and will investigate several formations that are productive through a wide range of depths and with a large geographic distribution. In addition, the study should be expanded to include the entire Anadarko basin.

IMPLICATIONS

Hunton wells are prolific gas producers. Could they be better? The perforated-to-saturated-thickness ratio tends to decrease with increased saturated-reservoir thickness (see Fig. 11). Recovery increases relative to increased ratios of perforated to saturated thickness (see Fig. 10) because the effects of vertical heterogeneity are reduced. As shown in Figure 8, operators tend to perforate reduced proportions of the saturated interval with depth. Figure 12 demonstrates the results of this practice. Deeper completions encounter thicker intervals of saturated reservoir; as thicker intervals are encountered, reduced proportions of the saturated interval are perforated; as reduced proportions of a reservoir are perforated, lower recovery factors result. Would larger perforated intervals yield additional volumes of gas to the pipeline?

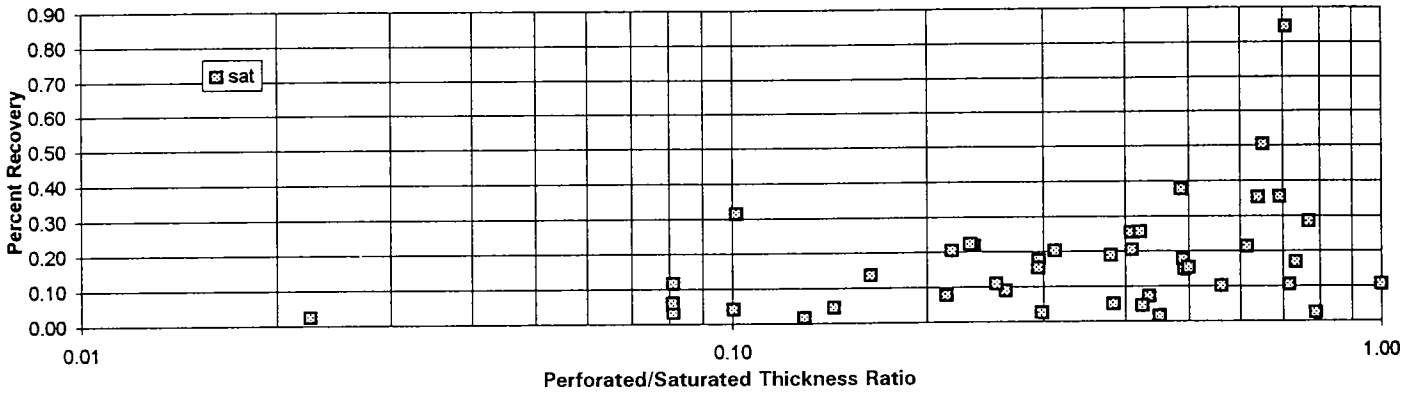

Figure 10. Trend in increased recoveries relative to increased perforated/saturated thickness ratios for 42 Hunton fields.

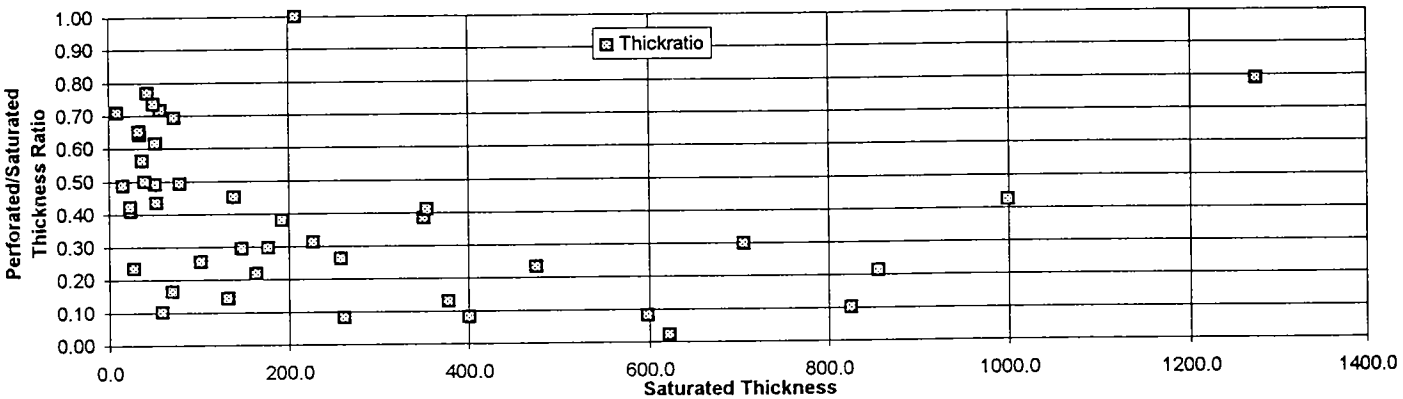

Figure 11. Trend showing decrease in perforated/saturated thickness ratios with increased saturated-reservoir thicknesses for 42 Hunton fields.

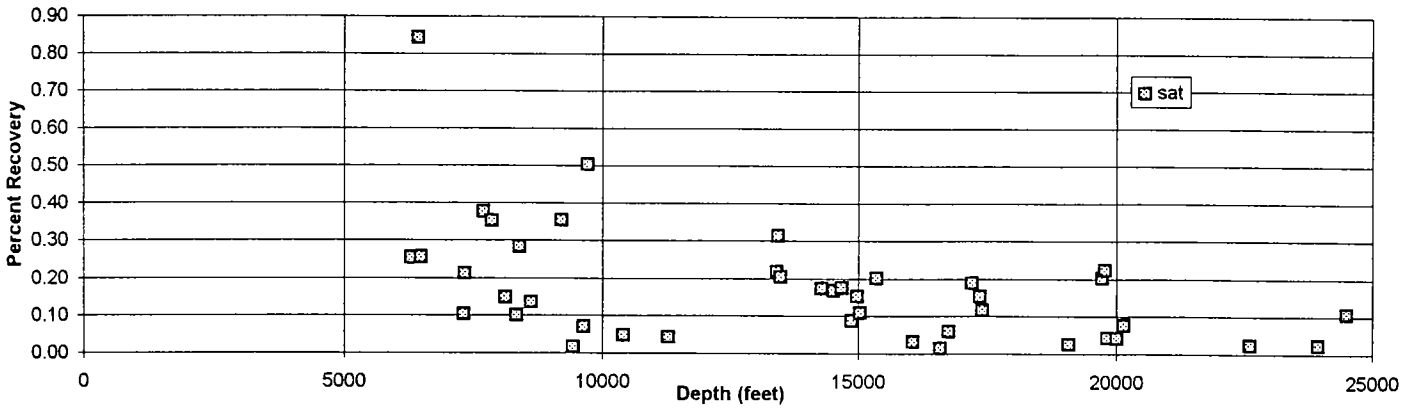

Figure 12. Trend showing effects of perforating reduced proportions of saturated interval with depth for 42 Hunton fields, resulting in lower percentages of recovery than might have been expected if larger proportions of the saturated interval had been perforated.

ACKNOWLEDGMENTS

This paper addresses the Hunton carbonate reservoirs evaluated by a project jointly funded by the Gas Research Institute, Washington, D.C., and Dwight's Energydata, Inc. (now a part of IHS Energy Group), Oklahoma City. The project was a preliminary study to assess the prospects for deeper reservoirs in the Anadarko basin. The full report discusses sandstone, carbonate, "wash," and mixed lithologic groups and is available from the Gas Research Institute as Report GRI-96/0196 (Smith, 1996).

REFERENCES CITED

Smith, P. W., 1996, Anadarko basin statistical study: gas well recovery -vs- depth in the Anadarko basin of western Oklahoma: Gas Research Institute, Chicago, GRI-96/0196, 65 p.

Smith, P. W.; and Woods, T. J., 2000, Effects of depth on quality of gas-well completions in carbonate reservoirs of the Anadarko basin and shelf areas, *in* Johnson, K. S. (ed.), Platform carbonates in the southern Midcontinent, 1996 symposium: Oklahoma Geological Survey Circular 101 [this volume], p. 25–45.

Depositional and Diagenetic History of Mississippian Chat Reservoirs, Northern Oklahoma

Suzanne M. Rogers, James M. Forgotson, Jr., and Thomas A. Dewers
University of Oklahoma
Norman, Oklahoma

ABSTRACT.—The Mississippian chat in northern Oklahoma is present at the unconformity between the Pennsylvanian and Mississippian Systems. Well logs and completion records from over 6,600 wells within Ts. 22–29 N. and Rs. 3 W.–5 E. indicate that the chat is widespread but not continuous. Because of uplift and subsequent erosion, the Mississippian in this area represents only the Osagean and locally the Kinderhookian Stages. The chat is found as a weathered and/or detrital, siliceous interval of tripolitic chat or more dense chert at the top of the Osagean sequence.

The depositional environment of the chat reflects uplift and both erosion and weathering in place of Osagean cherty limestone. From the size and variety of the unsorted clasts (0.5 to 3 in. across), the eroded fossiliferous clasts must have been in a high-energy environment such as that found above wave base in the shallow seas believed to have been present in northern Oklahoma during Mississippian time. These eroded clasts were transported by a debris flow into a lower energy environment and deposited with less fossiliferous material. Subsequently, either a limestone/siliceous cap or Pennsylvanian shales were deposited on top of the rubble.

The Osagean throughout northern Oklahoma is known to contain chert. Early diagenesis probably replaced some of the eroded limestone material with silica that was likely derived from siliceous sponge spicules. Examination of thin sections indicates later diagenesis that partially replaced calcite shells and cement with silica subsequent to the rockfall, and which dissolved the remaining calcitic fossils to create secondary porosity. Well-preserved original fossil structures indicate that force of crystallization was the method of calcite replacement by silica.

The chat can be a prolific reservoir rock that typically, after a rapid decline, has a long economic life. Production has been obtained from structural highs or where the chat pinches out on structural flanks. The chat appears on well logs as a low-resistivity zone with low density and high porosity, which by normal interpretation methods would appear to have a high water saturation. Oil and gas produced from such zones are almost always accompanied by salt water. Ultimate recovery from unitized fields ranges from 1 to 4 million barrels of oil (BO). Individual wells in good-quality chat reservoirs have produced over 150,000 BO.

Completion techniques in the chat should be designed for a siliceous zone containing detrital clays and no carbonate. A careful examination of samples should indicate whether the zone is tripolitic or cherty, with the former being preferable for a good-quality reservoir.

INTRODUCTION

The Mississippian chat was formed during Late Mississippian through Early Pennsylvanian time by the erosion and/or weathering of earlier Mississippian carbonates. It is a siliceous detrital or weathered zone that rests unconformably on top of Lower Mississippian Osagean limestone. This study encompasses Ts. 22–29 N. and Rs. 3 W.–5 E. in north-central Oklahoma. Geographically, all of Kay County and parts of Osage, Pawnee, Noble, Garfield, and Grant Counties are included in this area, as shown on the index map in Figure 1. The main structural feature in the area is the Nemaha uplift, which extends from south to north in the western half of the area.

Four of the five well cores examined are marked on the map. These include the No. 3 Charles, W½SE¼SE¼SE¼ sec. 31, T. 26 N., R. 5 E., Osage County; the No. 3 E. Davis, NE¼NW¼NW¼ sec. 8, T. 25 N., R. 3 E., Osage County; the No. 1 Williams, SW¼NE¼SW¼ sec. 3, T. 25 N., R. 4 E., Osage County; and the No. 1 Sowers, NE¼SE¼ sec. 20, T. 24 N., R. 3 W., Garfield County. The fifth core, from the No. 1 Hickok "A" Unit in the SE¼SW¼ sec. 3, T. 26 N., R. 8 W., is west of the study area in the Hawley field in Grant County. All these cores are from productive chat intervals except the one from the No. 1 Sowers (a dry hole) and are available at the Oklahoma Geological Survey Core and Sample Library. Thin sections from selected core intervals were prepared and examined. A well database of over 6,600 wells was compiled, and electric logs for most of these wells were examined. With the control

Rogers, S. M.; Forgotson, J. M., Jr.; and Dewers, T. A., 2000, Depositional and diagenetic history of Mississippian chat reservoirs, northern Oklahoma, *in* Johnson, K. S. (ed.), Platform carbonates in the southern Midcontinent, 1996 symposium: Oklahoma Geological Survey Circular 101, p. 157–161.

available from so many well logs, it was possible to map the Mississippian chat in detail and to illustrate the discontinuous nature of the formation.

The stratigraphic section used in this study is shown in Figure 2. Isopach and structure maps were made for intervals and formation tops between the base of the Oswego Limestone (Middle Pennsylvanian) and the top of the Woodford Shale (Lower Mississippian). These maps delineate areas of deposition that correlate with known reservoirs, potential reservoirs, and nonproductive areas.

DEPOSITIONAL HISTORY

Shallow seas favorable for carbonate deposition covered northern Oklahoma during Mississippian time. Uplift started in Late Mississippian time and continued into Early Pennsylvanian time. In the study area, erosion removed any Early Pennsylvanian deposits and all of the Mississippian younger than Osagean; in some areas on the crest of the Nemaha uplift, even the Osagean was removed. The unconformity at the top of the Mississippian separates the chat and/or limestone from Middle Pennsylvanian Desmoinesian sands and shales.

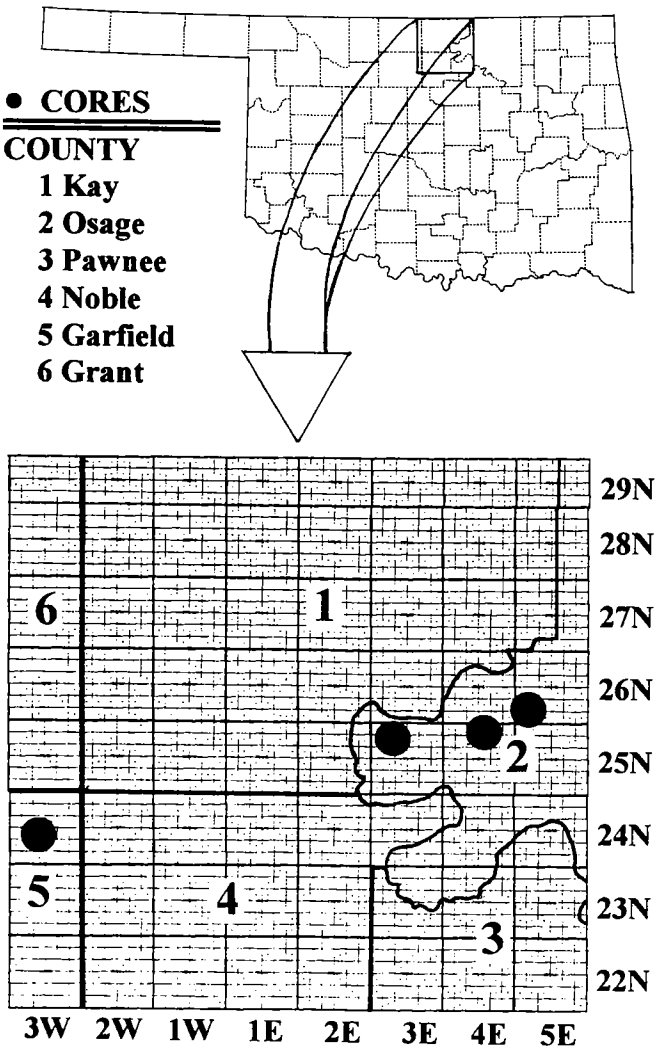

Figure 1. Index map of the study area.

Two processes, erosion and weathering, were involved in the development of the chat into tripoli or denser chert. During Late Mississippian tectonic activity, erosion of uplifted carbonates resulted in deposition of carbonate mud and fossiliferous clasts downslope from structural highs. The cores examined contain unsorted clasts suspended in a carbonate-mud matrix, a deposit generally described as a debris flow. The unsorted clasts, ranging from about 0.5 to 3 in. in diameter, appear as a darker tan color in a light-tan mud matrix. Crystallization is continuous across the clast–matrix interface, which is indicated in cores by a color change and in thin sections by a change in fabric. The general character of the clasts suggests that they were broken off in a high-energy marine environment above wave base. However, the lack of rounding or sorting indicates that the clasts became part of the debris flow very quickly. After deposition, this material was covered by a dense siliceous layer or by Pennsylvanian shales and sands.

An isopach map of the chat shows a thickness of over 200 ft in some areas on the downthrown side of faults. On the tops of some structures, principally at the crest of the Nemaha uplift, all the Mississippian section is missing. The tops of other structures comprise either productive chat intervals or only Mississippi lime with no chat present. The flanks of structures are characterized by some chat deposition. An isopach map of the Mississippi lime interval, together with a Woodford Shale structure map, provided data on paleotopography at the time of chat deposition. By comparing structure, the presence or absence of chat, and producing or nonproducing chat zones on these maps, one can determine likely areas for detailed study for development of future chat prospects.

The other process involved in the production of the chat was weathering. The cherty limestone from which the chat developed was susceptible to dissolution that created vugs and karst features on exposed structural highs and the resulting collapse breccias. The presence of siderite in the Williams and Charles wells suggests subaerial deposition and supports the weathering hypothesis (Andrews, 1995). Both processes are illustrated on the diagram in Figure 3.

DIAGENETIC HISTORY

The diagenetic history of the Mississippian chat can be described as a two-stage process: (1) force-of-crystallization-controlled replacement, and (2) dissolution of the remaining calcite by meteoric waters.

Force-of-crystallization-controlled replacement can be defined as a mechanism whereby nonhydrostatic stresses of growing silica crystals cause calcite dissolution (Maliva and Siever, 1988b). Replacement appears to be on a molecule-by-molecule basis, as evidenced by the preservation of minute fossil features. If calcite dissolution occurred prior to silica precipitation, one would not expect to see detailed features of fossils but perhaps only outlines of original fossil forms. If silica precipitation occurred prior to calcite dissolution, silica cement would fill the pore spaces between the fossil remains, and the pore spaces seen in thin sections today would appear to outline fossil forms. The conclusions to be drawn here are that the volumetric rate of silica precipitation is equal to the

volumetric rate of calcite dissolution, silica replaced calcite molecule by molecule (Maliva and Siever, 1989), and calcite-crystal dissolution was also caused by the incursion of meteoric waters. Sources of silica for the replacement include sponge spicules, which are present in a few thin sections, and possibly silica from the chert in Mississippian Osagean rocks or from surface waters.

Thin sections examined indicate that the replacement did not always result in complete substitution of the calcite by silica. Selective replacement can be attributed to several factors. First, the supply and location of sponge spicules, likely the major source of silica, would determine the areas of replacement where sufficient silica was present in solution. Second, the types of fossils and other carbonate material present could affect replacement. Some fossils are more susceptible to replacement than others (Maliva and Siever, 1988a). Meyers (1977) suggests an order of decreasing susceptibility to replacement of carbonates by silica in a study of the Mississippian Lake Valley Formation in New Mexico. He lists carbonate mud as more susceptible to replacement than such fossil fragments as thick-shelled brachiopods.

Other minerals in the rock, such as clays, could play a part in what is replaced and when. Hesse (1990) attributes selective replacement to factors such as pH, dissolved-silicon activity, and existing porosity and permeability of the rock material. Finally, a change in conditions, such as continued uplift and a resulting influx or increase in meteoric water flow, would result in a flushing of the rock and dissolution of remaining calcite by low-pH fluids without any silica precipitation.

The more dramatic dissolution of calcite by meteoric waters—the second stage in diagenesis—results when meteoric water, undersaturated with respect to calcite, flows through the zone. The important result of the second stage in the diagenetic process is the creation of secondary porosity and the chat reservoir.

Knauth (1979) suggests a meteoric–marine-mixing-zone model for silica replacement of carbonate. In this model, the quantity of silica increases as the water moves through the entire meteoric realm. If the mixing zone is narrow, silica is concentrated to the point at which complete or almost complete replacement can occur. In a later article, Knauth (1994) states that Maliva and Siever's (1988b) proposal that force of crystallization is the dominant mechanism for replacement ignores the geochemistry of the pore waters. Carbonate dissolution is affected by the pH and salinity of the water, the level of calcite saturation, and the anoxic–oxic state of the water. The question to be answered then is what condition takes precedence and under what circumstances.

The Maliva–Siever model of force-of-crystallization replacement seems reasonable on the basis of core and thin-section examination. The fine features of fossils are retained. However, for the massive amount (up to 200 ft thick) of chat to have been silicified, a huge amount of silica is required. Porosity within the chat indicates that complete replacement did not occur. It is not likely that a section of chat on the

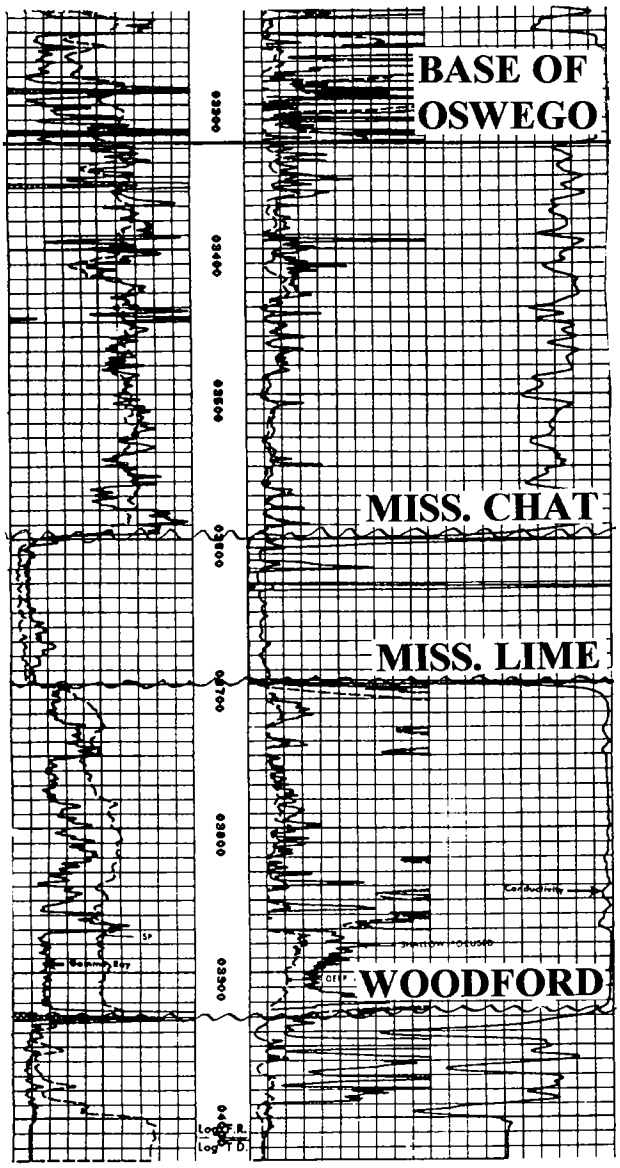

Figure 2. Stratigraphic section showing the position of the Mississippian chat unconformity in the rock column.

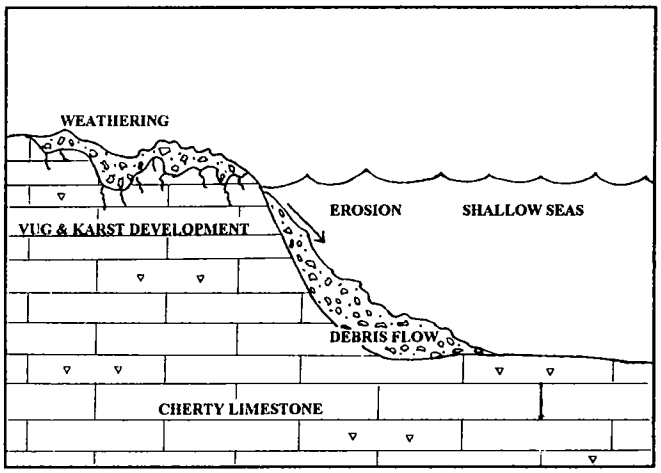

Figure 3. Illustration of the processes of erosion and weathering, which result in debris-flow deposits, vugs, and karst collapse-breccia deposits.

downthrown side of a fault could have been formed by continued uplift and intrusion of meteoric waters with resulting dissolution of the remaining carbonate if deposition is occurring on a continually dropping fault block. The same uplift and meteoric-water-intrusion theory would not apply to areas of chat deposition far from an obviously uplifted area. The evidence thus suggests a combination of factors, with force of crystallization being important and better reservoir quality having developed where exposure to meteoric-water flow enhanced secondary porosity.

The examination of thin sections from the small sample of well cores available in this area shows that silica replaced calcite slowly enough to preserve minute fossil features. The evidence shows partial replacement of individual fossils and dissolution of the remaining parts of the fossil fragments. Some fossil fragments are completely dissolved, and only the outlines remain in the mud matrix. The interface between fossiliferous clasts and the mud matrix of the debris flow is marked only by a color change. The visible continuation of silica crystallization across the change in fabric from matrix to fossil indicates that silicification occurred after deposition.

The literature (McCoy, 1978; Jordan and Rowland, 1959; McKnight and Fischer, 1970) indicates that the Mississippian Osagean contains widespread chert. These references suggest a possible three-stage process of diagenesis of the chat: (1) an initial stage of silicification, (2) force-of-crystallization-controlled replacement, and (3) dissolution of remaining calcite stages resulting from uplift, erosion, and/or weathering in Late Mississippian–Early Pennsylvanian time. The later stage of silicification probably would have obscured evidence of any earlier silicification.

HYDROCARBON POTENTIAL

The Mississippian chat can be a prolific oil-producing zone. Unitized fields such as the Ponca City Mississippi Chat Unit in T. 25 N., R. 2 E., have produced more than 4 million barrels of oil (BO). Single wells, such as the No. 1 Stalnaker in the SW¼ sec. 20, T. 29 N., R. 2 E., have produced over 150,000 BO. Two production characteristics are prevalent. First, water production is normal, so a disposal well is critical to economic production. Second, the decline curve flattens, indicating a long life for the well. Whether or not the well remains economically viable depends on other factors during this period of low but steady production. When prospecting for chat plays, one should look for appropriate well-log indicators and trapping mechanisms characteristic of the zone.

Standard logs run in the area are an induction log, a density–neutron log, and a microlog. Good-quality productive chat should have an R_t (true resistivity) of about 1–2 ohms on the resistivity curve of the induction log that coincides with an abrupt kick to the left on the spontaneous-potential (SP) curve. This low resistivity can be attributed to a high irreducible water saturation in a dual-porosity system comprising microporosity and vuggy porosity. For a productive zone, the density–neutron-log porosity curves should indicate good porosity, with a minimum of 15–20%, and 30% or higher for a good reservoir. The bulk-density curve should read less than 2.5 g/cm^3 and preferably close to 2.0 g/cm^3. The microlog should indicate good permeability in the zone. Figure 4 illustrates a productive chat interval on induction and density–neutron logs.

Log calculations using the Archie equation and a general value of $m = n = 2$, $a = 1$, and R_w (water resistivity) = 0.035 will result in a high water saturation. Although water is produced in almost all chat wells, using a value of $m = 2$ will result in a value of S_w (water saturation) that is too high. A lower value of m is more accurate for a quality chat reservoir—one that is tripolitic. The Pickett plot—values of R_t and porosity for a water zone plotted on log–log paper—can be used to determine a more reliable value for m. The slope of a straight line drawn through the plotted points equals $1/m$. Then, when the equation for m is solved, that value of m can be used in the Archie equation to approximate more closely the actual water saturation.

Typical trapping mechanisms for the chat include structural, stratigraphic, and diagenetic traps. Weathered chat is present on some structural highs. Vug and karst development, combined with collapse breccias, provide good reservoirs. In some areas where chat is not present on structural highs, reservoir-quality chat is present on the southwest flanks of such structures. The regional dip is to the southwest. Hydrocarbons can be trapped where the chat pinches out updip. Chat is usually present on the east side of structures, but these zones are of poor quality. Chat deposited on the downthrown side of a fault can be productive if there is a seal across the zone along the fault, if the chat pinches out before it reaches the fault, or if there is structural closure in the chat zone before it reaches the fault. A porosity or diagenetic trap is also possible.

All available information must be evaluated in determining the economic viability of a chat well. A proper suite of logs, together with a mud log, should provide the basics for adequate well evaluation before setting pipe. Other factors to evaluate in prospecting for chat include the results of drillstem tests and well-sample examination. A marginal show on a drillstem test, combined with poor permeability on the microlog and a porosity of 20% or less, would be a strong sign of a noncommercial well. A good gas indication on a mud log while drilling through the zone is a positive sign.

Completion techniques should be designed for a siliceous zone containing some clays. Huge water-fracture treatments might or might not be appropriate for an individual well. A large fracture treatment in one wellbore could result in a large increase in water production, but in another well such a treatment could be beneficial. Criteria for determining the size of a fracture treatment unfortunately are based mostly on trial and error. In general, a fracture treatment similar to one for a sandstone reservoir of comparable thickness would at least be expected not to do any damage.

SUMMARY

The Mississippian chat is a siliceous detrital or weathered deposit derived from Mississippian cherty limestone during Late Mississippian through Early Pennsylvanian time. The limestone was subjected to an erosional process that resulted in a debris-flow deposit and to a weathering process that created vugs, karst development, and collapse breccia. Diage-

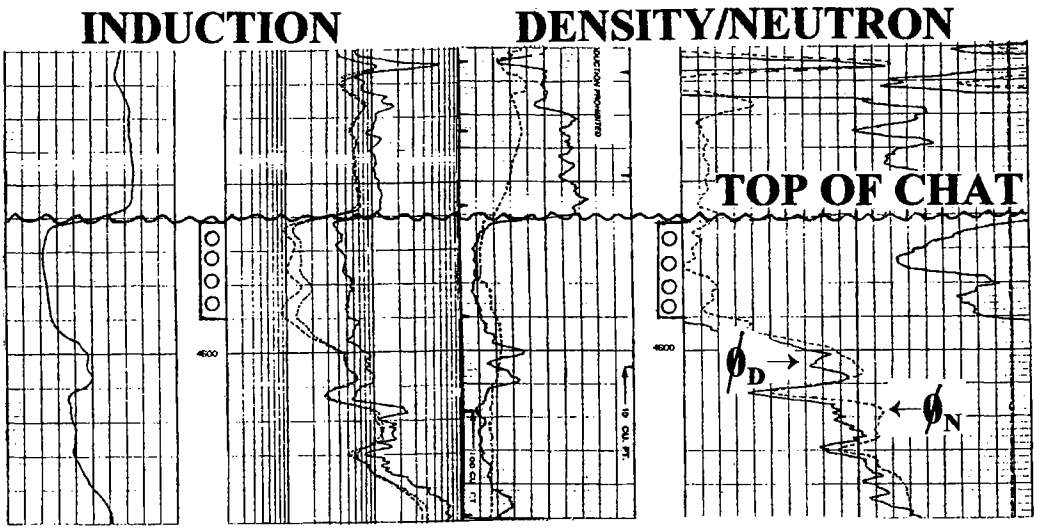

Figure 4. Induction and density–neutron porosity logs of a typical Mississippian chat producing interval. No. 1 Evans well, NE¼NE¼ sec. 31, T. 24 N., R. 2 W., Noble County, Oklahoma. Initial potential for the zone, perforated from 4,562 to 4,590 ft, was 69 BO per day and 1,226,000 cubic ft of gas per day.

netic processes include (1) force-of-crystallization replacement of calcite by silica below the meteoric zone, (2) supersaturation of silica in pore waters in a meteoric–marine mixing zone to create the potential for complete replacement of calcite by silica by means of force-of-crystallization replacement, and (3) continued uplift to expose some areas to an incursion of meteoric waters undersaturated with calcite to aid in dissolving any remaining carbonate material. Where the chat zone is present with good secondary-porosity development, it can be a good-quality oil reservoir if trapping conditions exist.

REFERENCES CITED

Andrews, R. D.; Campbell, J. A.; and Northcutt, R. A., 1995, Fluvial-dominated deltaic (FDD) oil reservoirs in Oklahoma, *in* Fluvial-dominated deltaic (FDD) oil reservoirs in Oklahoma: the Morrow play: Oklahoma Geological Survey Special Publication SP 95-1, p. 1–12.

Hesse, R., 1990, Silica diagenesis: origin of inorganic and replacement cherts, *in* McIlreath, I. A.; and Morrow, D. W. (eds.), Diagenesis: Geological Association of Canada Reprint Series 4, p. 253–275.

Jordan, L.; and Rowland, T. L., 1959, Mississippian rocks in northern Oklahoma: Tulsa Geological Society Digest, v. 27, p. 124–136.

Knauth, L. P., 1979, A model for the origin of chert in limestone: Geology, v. 7, p. 274–277.

_____1994, Petrogenesis of chert, *in* Heaney, P. J.; Prewitt, C. T.; and Gibbs, G. V. (eds.), Silica: Reviews in Mineralogy, v. 29, p. 233–258.

Maliva, R. G.; and Siever, R., 1988a, Mechanism and controls of silicification of fossils in limestone: Journal of Geology, v. 96, p. 387–398.

_____1988b, Diagenetic replacement controlled by force of crystallization: Geology, v. 16, p. 688–691.

_____1989, Nodular chert formation in carbonate rocks: Journal of Geology, v. 97, p. 421–433.

McCoy, J. R., 1978, Character of the Mississippian Formation in south central Kansas: Kansas Geological Survey Open File Report 78-9, 10 p.

McKnight, E. T.; and Fischer, R. P., 1970, Geology and ore deposits of the Picher field, Oklahoma and Kansas: U.S. Geological Survey Professional Paper 588, 165 p.

Meyers, W. J., 1977, Chertification in the Mississippian Lake Valley Formation, Sacramento Mountains, New Mexico: Sedimentology, v. 24, p. 75–105.

Natural-Gas Production from the Boone Formation (Lower Mississippian), Northwestern Arkansas

Walter L. Manger
University of Arkansas
Fayetteville, Arkansas

Phillip R. Shelby
Southwestern Energy Company
Fayetteville, Arkansas

ABSTRACT.—Sixty-one wells from 17 fields in northern Arkansas have produced 17.8 billion cubic feet of dry methane gas from the Lower Mississippian Boone Formation through January 1998. The porosity and permeability of the upper Boone carbonates are well below the industry productive window of 7% and 1 millidarcy, respectively, on the basis of outcrop studies. In contrast, fractured zones of high permeability in chert-bearing carbonates develop porosities of 15% or more through intervals averaging 48 ft in Batson field, Johnson County. Most of the natural gas formed in the Arkoma basin from Pennsylvanian source rocks, and migrated into the Boone reservoir within the Arkoma basin along east–west-trending normal faults that juxtapose the two intervals. Gas migrated into the Boone reservoir of a shallow gas province in Washington County, northwestern Arkansas, along major northeast-trending normal faults (i.e., Fayetteville fault system), where it joined gas produced locally by the Devonian–Mississippian Chattanooga Shale.

INTRODUCTION

Lower Mississippian chert-bearing carbonates are the thickest post–Lower Ordovician and pre-Atokan lithostratigraphic units in the southern Midcontinent of North America. They extend in an essentially unbroken belt from northeastern Illinois westward to southwestern Arizona and then northward to western Montana (Fig. 1). In northern Arkansas and northeastern Oklahoma, these thick limestones reflect transportation of crinozoan detritus and carbonate mud off the Burlington shelf, which occupied the continental interior to the north, and reflect deposition on a gently dipping ramp extending into the Ouachita–Marathon trough to the south (Fig. 1). In northern Arkansas, the Lower Mississippian sequence is referred to the St. Joe Limestone and the succeeding Boone Formation (Fig. 2). Deposition of the Boone Formation effectively ended recycling of clean, well-sorted terrigenous sediment eroded from the underlying strata, and it represents the last of the truly blanket stratal geometries that characterize the lower and middle Paleozoic record of the southern Ozark region.

Natural-gas production in northern Arkansas reflects a shallow gas province comprising 14 small fields occupying parts of Washington and Madison Counties (Ts. 13–16 N.), and the well-known Arkoma basin of western Arkansas and eastern Oklahoma (Fig. 3). There is or has been Boone production from 11 wells in 2 fields of the shallow gas province and from 50 wells in 15 fields in the Arkoma basin of Arkansas (Fig. 3). Collectively, these wells have produced 17.8 billion cubic feet of gas (BCFG) through January 1998 (Table 1), yet the Boone remains largely untested throughout most of northern Arkansas and the Arkoma basin.

LITHOSTRATIGRAPHY

Lower Mississippian carbonates in the southern Ozarks represent a single depositional sequence bounded by type 1 erosional unconformities (Fig. 2). The St. Joe Limestone forms the base of this transgressive carbonate sequence that began during middle Kinderhookian time (Handford and Manger, 1993). The basal unconformity is marked by a terrigenous clastic unit, the Bachelor Member, that reflects reworking of detritus derived by erosion from underlying units as young as the Late Devonian–Early Mississippian Chattanooga Shale and as old as the Early Ordovician Cotter Formation. The Bachelor is an orthoquartzitic sandstone, calcareous shale, or the two lithologies as a couplet. In southwestern Washington County, Arkansas, and northeastern Oklahoma, the Bachelor is not developed, and the Chattanooga Shale spans the Devonian–Mississippian boundary with no significant break (Kelly, 1997). Grainstones and packstones formed by crinozoan–bryozoan detritus lithified by carbonate mud and calcite spar began limestone deposition and are referred to the Compton and Pierson Members (Fig. 2). Those two carbonates are indistinguishable lithologically, but they can be differentiated by reference to the terrigenous clastic Northview Member (Fig. 2). The Northview was deposited as a small delta in its southwestern Missouri type area, but an extensive, thin, clay-rich siltstone representing the Northview interrupted limestone

Manger, W. L.; and Shelby, P. R., 2000, Natural-gas production from the Boone Formation (Lower Mississippian), northwestern Arkansas, *in* Johnson, K. S. (ed.), Platform carbonates in the southern Midcontinent, 1996 symposium: Oklahoma Geological Survey Circular 101, p. 163–169.

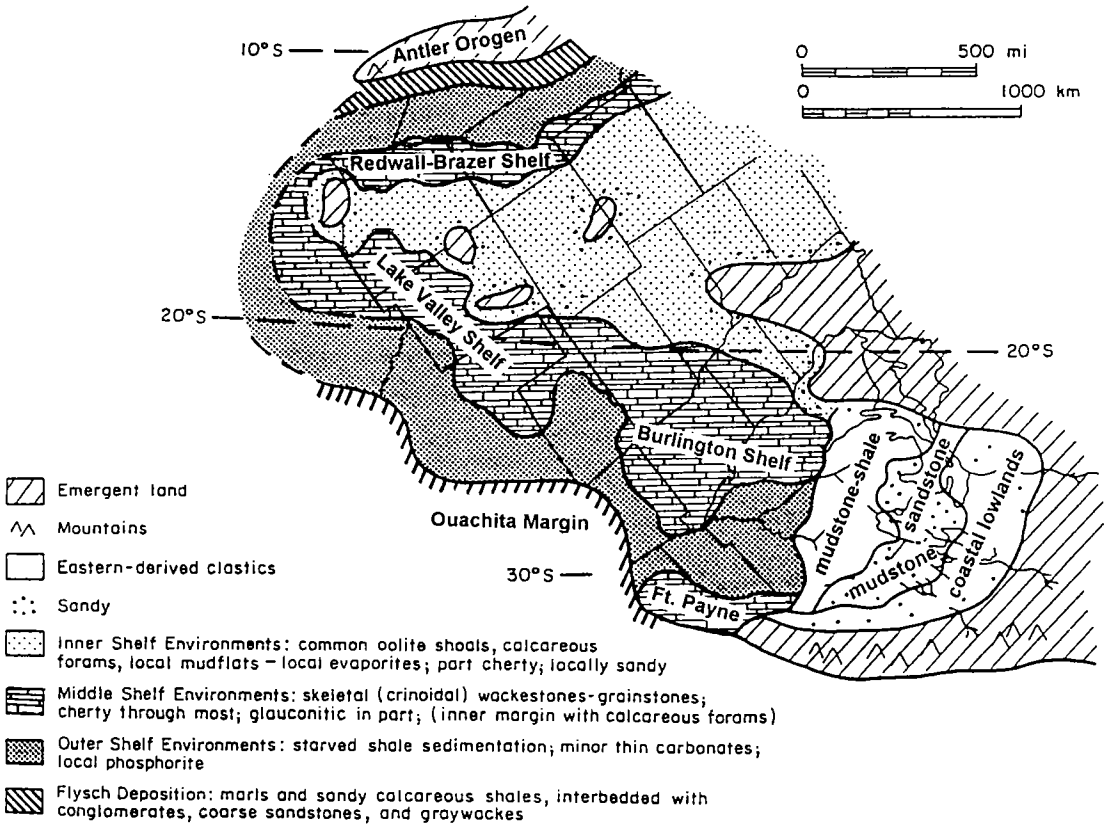

Figure 1. Regional paleogeography of the North American Midcontinent during the Early Mississippian. Note the shelf-to-basin transition across northern Arkansas. Modified from Witzke and others (1990).

deposition briefly across conterminous Oklahoma and Arkansas (Thompson, 1986) (Fig. 2). Away from the region of terrigenous influence, the Northview is not developed, and the Compton and Pierson Members are not differentiated (Fig. 2). The mud content of the carbonate section increases gradually from the Compton into the Pierson, reflecting deepening water conditions as the transgression continued across the southern Midcontinent. The members are described as noncherty, but scattered chert nodules can be found in both at some localities in Arkansas (Manger and others, 1988). The thickest St. Joe exposures exceed 100 ft in north-central Arkansas, although thicknesses of 20–40 ft are typical. The Kinderhookian–Osagean Series boundary occurs at the Northview–Pierson contact or within the first foot of the Pierson (Manger and others, 1988).

The contact between the St. Joe and the overlying Boone Formation is drawn at the change from grain-dominated to mud-dominated lithologies (Shelby, 1986). That change is also associated with the development of black penecontemporaneous chert and, at some localities, a thin calcareous shale. Penecontemporaneous chert formed as an early replacement of only partially lithified carbonate sediment just below the sediment–water interface in a deep-water setting that was established during maximum-flooding conditions. The occurrences of this chert are characterized by compaction phenomena and disruption of the bedding. The chert is spiculitic and may also preserve crinozoan and bryozoan detritus, although most of it lacks macrofossils. The chert character and carbonate lithology provide a basis for informal division of the Boone into lower and upper members.

Calcisiltites, crinozoan–bryozoan packstones and grainstones, all with pervasive anastomosing and nodular or crudely bedded black chert, characterize the lower Boone Formation, which represents the maximum-flooding interval of the Lower Mississippian carbonate sequence (Handford and Manger, 1993). Penecontemporaneous chert makes up typically 40–50% (and may reach as much as 65%) of the lower Boone interval in outcrop (Liner, 1979).

The upper Boone Formation is the highstand and regressive sequence of the Lower Mississippian carbonates in the southern Midcontinent (Fig. 2). This regression returned shallow-water, grain-dominated lithologies resembling those of the St. Joe to the region as aggradation and progradation accompanied retreat of the seas from the southern Midcontinent (Shelby, 1986). An oolite, formally named the Short Creek Member, is developed in the upper Boone (Fig. 2), but it lacks predictable persistency, is not mappable on a regional basis, and is not recognized in the subsurface beyond the immediate southern limit of exposures (Manger and others, 1988). Chert also characterizes the upper Boone interval, but in contrast to the lower Boone it is white and represents a later diagenetic event associated with ground-water movement through the carbonates. The chert replicates the texture of associated beds, and obvious silicification fronts bound the nodules and crude bedding. Later diagenetic chert is highly variable in its development, but in no case is the upper Boone entirely chert free.

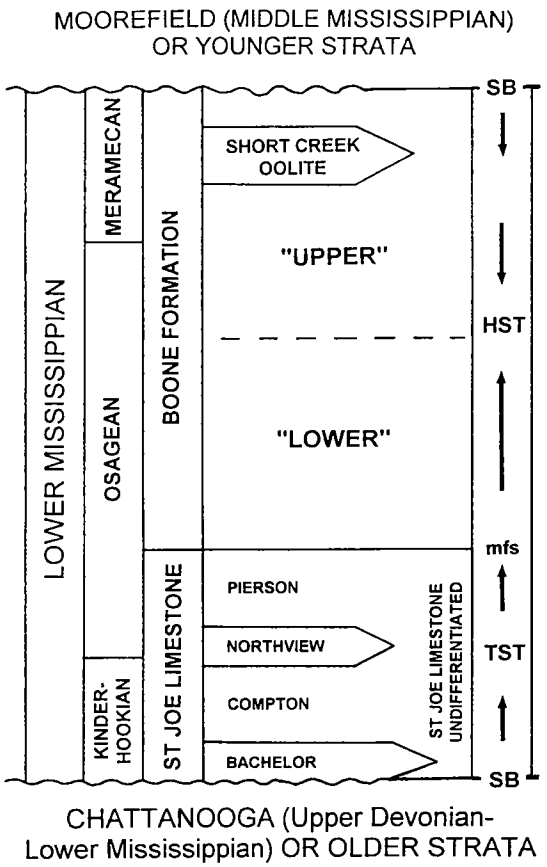

Figure 2. Lithostratigraphic succession and sequence-stratigraphic interpretation for the Lower Mississippian interval, southern Ozark region. *SB* = sequence boundary; *HST* = highstand systems tract; *TST* = transgressive systems tract; *mfs* = maximum-flooding surface.

Chert contribution to the upper Boone ranges from a low of approximately 30% of the interval to a high of >95% (Liner, 1979).

Boone thicknesses exceed 300 ft in the subsurface directly south of its surface exposures in the two tiers of counties constituting northwestern Arkansas.

The top of the Boone Formation is a regional unconformity across most of the southern Ozark region, and Chesterian (Upper Mississippian) strata rest on those of the Osagean Series. At most localities, the Boone is overlain by the Hindsville Limestone of Chesterian age. The Hindsville is an oolitic, crinozoan–bryozoan carbonate with a component of angular chert gravel derived from the underlying Boone Formation. In northeastern Arkansas, the Moorefield Shale intervenes above the Boone, and the Hindsville becomes the basal member of the succeeding Batesville Sandstone (Handford and Manger, 1993). There, the upper Boone may be of Meramecan age, and deposition may have been continuous across the Boone–Moorefield and the Meramecan–Chesterian boundaries (Handford and Manger, 1993) (Fig. 2). In the subsurface, these lithostratigraphic relations are mostly unrecognized. Industry practice usually places the top of the Boone on logs directly below the Fayetteville Shale, an interval easily seen using gamma-ray and neutron density tools, combining the Hindsville with the Boone. Where the Batesville or Moorefield is developed, the top of the Boone, as picked on logs, corresponds to the same level seen in outcrop. Figure 4 shows part of the log of the SEECO No. 2C Federal well, illustrating the characteristic gamma-ray, caliper, and compensated-neutron-density log signatures for the productive Boone interval in Batson field, Johnson County, Arkansas.

Pronounced changes take place in the Lower Mississippian carbonate sequence moving southward into the Arkoma basin in Arkansas and Oklahoma and eastward toward the Mississippi embayment (Fig. 1). The St. Joe Limestone, recognized as a non-chert-bearing interval above the Chattanooga Shale, does not occur in the subsurface south of the latitude of southern Washington and Madison Counties (T. 14 N.) in Arkansas. A similar distribution occurs in eastern Oklahoma, although the St. Joe forms a narrow, southwest-striking salient that extends into northern Sequoyah County but does not reach the Arkoma basin. Chert-bearing carbonates rest on the Chattanooga Shale across the northern Arkoma shelf. Whether the St. Joe is represented by those chert-bearing "Boone" carbonates, by black shale included in the Chattanooga, or by a nondepositional unconformity is not known. Eastward across the southern Ozarks, the St. Joe becomes a condensed interval in which the complete middle Kinderhookian–lower Osagean section is represented by 3 ft or less at the eastern limit of its exposure (Manger and others, 1988). Similar changes occur in the Boone interval. Lower Mississippian carbonates are not present in the southern Arkoma basin (generally south of T. 7 N.) or in the Mississippi embayment. Abrupt thinning of the Boone Formation occurs to the south and east, and the Lower Mississippian interval is represented by shale (Shelby, 1986; Manger and others, 1988).

THE BOONE RESERVOIR

Commercial natural-gas production has never been achieved from the St. Joe interval. Since the St. Joe is confined essentially to the outcrop belt, reservoir-quality carbonates are not associated or anticipated with that level anywhere in the southern Ozarks.

In contrast, the Boone Formation has produced significant natural gas in both the shallow gas province and the northern Arkoma basin of Arkansas. A study of Boone outcrops in northwestern Arkansas undertaken by Tenneco Oil Co. included permeability and porosity values determined for 122 samples (Van Den Heuvel, 1979). Twenty-three samples exhibited porosities of 0.01%, the minimum value measured, and an additional 36 samples had porosity values <1.0%. The highest recorded porosity was 20.3% from a microsparite near the top of the Boone exposed along Spavinaw Creek, western Benton County, Arkansas. The remaining 62 samples exhibited a porosity range of 1.0–17.9%, with an average of only 3.69%. This average porosity is significantly less than the productive minimum industry standard of 7% used throughout most of the Arkoma basin. Permeability for the exposed carbonates was also low. Eighty-five samples had permeability values <0.01 millidarcy (md). Only seven samples had permeability values above the productive minimum of 1 md. Ignoring the highest value of 25 md from the weathered base of an exposure along Sugar Creek, Benton County, the average

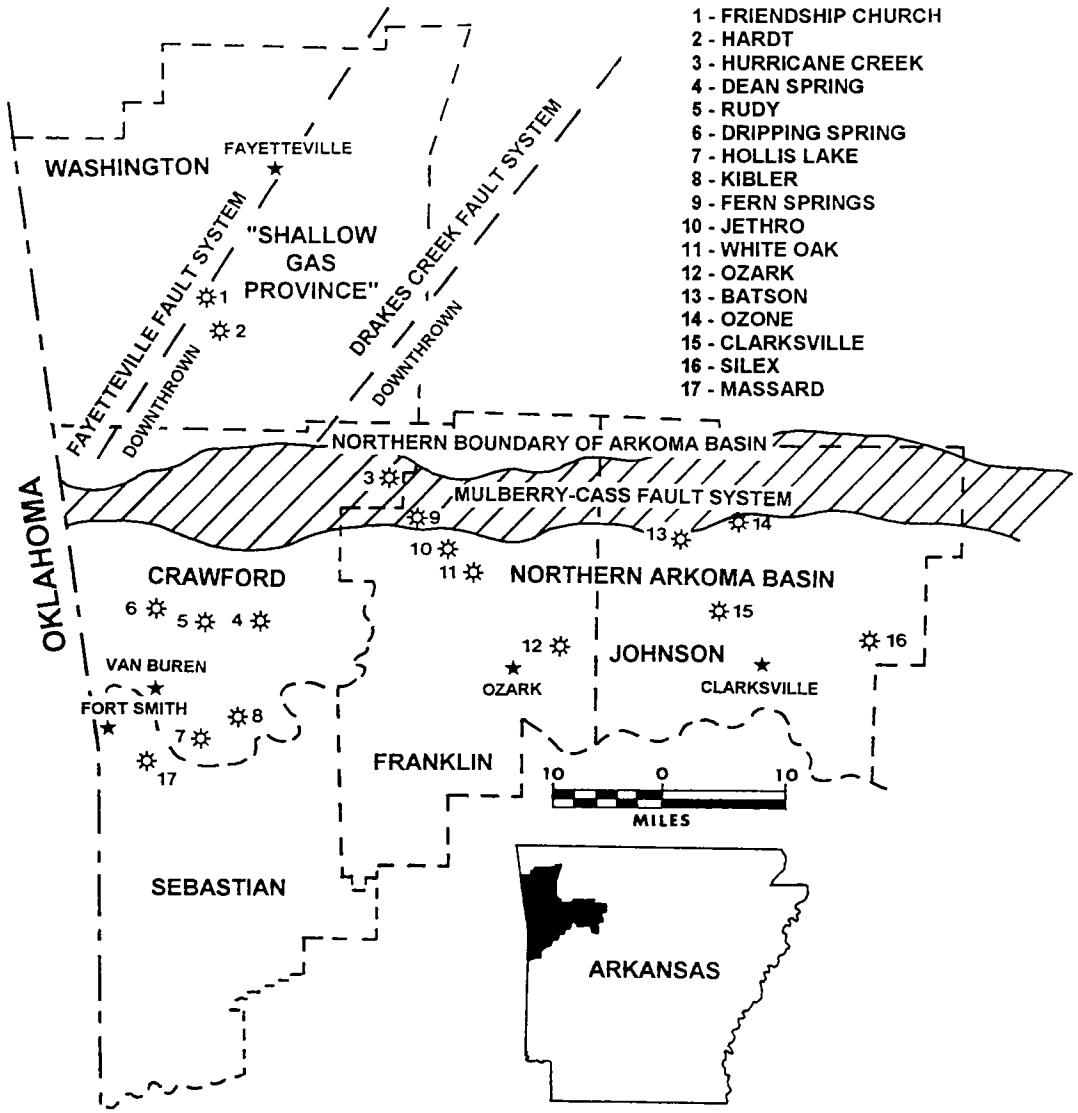

Figure 3. Distribution of fields with Boone production in the shallow gas province and northern Arkoma basin.

permeability for the remaining six Boone samples is 1.53 md.

From these data, it is obvious that carbonates of the Boone Formation develop little matrix porosity and permeability, even where some weathering and ground-water movement have occurred. Nevertheless, it is also important to recognize that these samples provide a biased view of porosity and permeability development within the Boone carbonate interval, because they do not take into account fracture porosity, particularly in chert-bearing intervals. It seems clear that subsurface Boone production reflects fractured reservoirs in both the shallow gas province and the Arkoma basin.

The Boone Formation encountered in subsurface penetrations has significantly greater values of permeability and porosity. Within its outcrop belt in northern Arkansas, the Boone is the principal unconfined aquifer for domestic and light-agricultural water supplies. Yields from these water wells are directly related to fracturing and dissolution along fractures. The concentration and upward propagation of fractures reflect carbonate-grain size and chert development, with the greatest number of fractures at high angles to bedding found in fine-grained carbonate lithologies with abundant chert. The chert typically has more fractures than the associated limestones. This situation controls natural-gas production from Friendship Church and Hardt fields, in the shallow gas province in Washington County, Arkansas. Natural gas in the upper member of the Boone Formation is produced from fractured intervals that lack matrix porosity. Stylolitization along chert–carbonate contacts also contributes to enhanced porosity and permeability. Log suites or cores have not been produced to establish permeability and porosity values, but neutron density logs exhibit a pattern of fluctuating values consistent with fractured intervals. Boone production from these fields also exhibits a steep decline curve, and wells encounter fresh ground water in this interval during drilling, or begin to produce ground water with the decline in production of natural gas. The carbonate lithologies composing the Boone in Friendship Church and Hardt fields are probably no different than those encountered in the outcrop belt 10–12 mi to the north.

Table 1.—Production Records for 61 Wells Penetrating the Boone Reservoir in Northern Arkansas[a]

	Tnshp/Rg	Sect.	Well Name	County	Field	1st Prd	Perfs	Reservoir	IP(mcf)	CP(bcf)	ISIP	PSIP	Status
1	08N-32W	09	Arco-Gordon #2	Sebastian	Massard	1-86	6055-6145	Boone	170	0.001	1765	5	p/a
2	08N-32W	34	Hanna-Airport 83 #1	Sebastian	Massard	5-89	6055-6186	Boone/Hunton/Penter	743	1.014	508	464	act
3	08N-32W	34	Hanna-Airport 83 #1-C	Sebastian	Massard		6066-6102	Boone		0.128			cmg
4	09N-30W	32	Stephens-Fontaine #1-C	Crawford	Kibler-Wil	11-62		Boone		0.045	2065	980	p/a
5	09N-31W	12	Sonat-Lovegrove #1-C	Crawford	Hollis Lake	12-82	3305-61	Boone	196	0.073	467	467	rec
6	09N-31W	23	Stephens-Greig Est #3-LT	Crawford	Hollis Lake	5-84	5844-53	Boone	363	0.001	175	175	ina
7	09N-31W	33	Samson-Edwards #2-T	Crawford	Hollis Lake	6-90	5096-6144	Boone/Orr	3677	0.111	783	305	cmg
8	10N-22W	25	Seeco-Leavell #1-T	Johnson	Silex	1-84	5422-50	Boone	123	0.007	1790	350	p/a
9	10N-24W	11	Sonat-King #1-T	Johnson	Clarksville	6-82	4733-72	Boone	303	0.508	331	216	ina
10	10N-26W	17	Hanna-Lee #1-T	Franklin	White Oak	7-80	5127-5256	Boone/Penters	106	0.203	1352	548	p/a
11	10N-26W	21	Hanna-Atha #1	Franklin	Ozark	6-88	2930-5436	Boone/Bynum/Penters	1353	0.296	550	345	act
12	10N-26W	21	Hanna-Atha #1-T	Franklin	Ozark	8-78	5306-5436	Boone/Penters	256	0.019	1535	461	cmg
13	10N-27W	16	Seeco-MaGruder #1-LT	Franklin	White Oak	11-93	4762-92	Boone/Penters	1882	0.069	1602	142	act
14	10N-30W	27	Seeco-Williams #1	Crawford	Dean Sprng		3832-4004	Boone/Hunton		0.001			p/a
15	10N-31W	30	Stephens-Hicks #2	Crawford	Rudy	2-88	2074-2384	Boone/Hale	454	0.246	745	325	act
16	10N-31W	30	Stephens-Hicks #2-T	Crawford	Rudy	8-84	2374-84	Boone	662	0.056	850	595	cmg
17	10N-31W	30	Lyons-Phillips #1-T	Crawford	Rudy	9-86	2509-32	Boone	774	0.004		1025	ina
18	10N-32W	12	Barfield-Massey #1-T	Crawford	Drpng Sprng	7-88	2263-69	Boone		0.001	647	647	ina
19	10N-32W	15	Barfield-Miller #1	Crawford	Drpng Sprng	8-87	2322-91	Boone	256	0.054	832	236	ina
20	10N-32W	21	JHS Energy-Brown #1-T	Crawford	Drpng Sprng	10-85	2310-63	Boone	117	0.218	612	460	act
21	10N-32W	22	JHS Energy-O'Roark #2-T	Crawford	Drpng Sprng	10-84	2295-2393	Boone	3532	0.34	814	624	act
22	11N-24W	01	Seeco-Taylor #1-T	Johnson	Ozone	12-75	2620-32	Boone	600	1.913	820	368	act
23	11N-24W	02	Seeco-Steele #1-LT	Johnson	Ozone	12-75	2603-68	Boone	340	0.075	695	350	act
24	11N-24W	07	Seeco-Tabor #1-LT	Johnson	Batson	10-76	2630-2705	Boone	473	0.018	767	457	ina
25	11N-24W	17	Seeco-Hunt #1-LT	Johnson	Batson	4-79	2844-2900	Boone	1100	0.202	805	516	act
26	11N-24W	18	Weis Br-Marshall #1-LT	Johnson	Batson	11-76	2660-2742	Boone	546	0.016	730	316	ina
27	11N-25W	01	Weis Br-Fed #1-T	Johnson	Batson	3-76	2376-90	Boone	2180	0.233	749	670	cmg
28	11N-25W	01	Weis Br-Fed #1-C	Johnson	Batson	8-76	2292-2390	Boone	8713	1.912	753	417	rec
29	11N-25W	02	Seeco-Phipps Lbr #1-T	Johnson	Batson	5-75	2481-2520	Boone	4100	1.272	754	413	p/a
30	11N-25W	03	Weis Br-Fed #1-T	Johnson	Batson	4-76	2521-48	Boone	1719	0.594	779	618	ina
31	11N-25W	04	Weis Br-USA #1-T	Johnson	Batson	8-78	2526-50	Boone	2621	0.548	652	519	ina
32	11N-25W	09	Weis Br-Sherrell #1-LT	Johnson	Batson	8-78	2598-2622	Boone	2727	0.349	742	283	ina
33	11N-25W	10	Seeco-Wooten/Fed #1-LT	Johnson	Batson	5-75	1922-40	Boone	2500	0.018	774	491	ina
34	11N-25W	11	Weis Br-Baskin #1-LT	Johnson	Batson	5-75	2540-97	Boone	5875	0.739	751	560	ina
35	11N-25W	12	Seeco-Fed #1-T	Johnson	Batson	4-74	2578-2686	Boone	9350	3.161	748	295	rec
36	11N-27W	20	Seeco-Moody #2-T	Franklin	Jethro		2962-74	Boone		0.002			ina
37	11N-27W	22	Seeco-Smith #1-LT	Franklin	Jethro		2992-3054	Boone		0.003			ina
38	11N-28W	04	Ranken-Fern Springs #1	Franklin	Fern Springs		2214-77	Boone		0.002			ina
39	11N-28W	24	Seeco-Hales #1-LT	Franklin	Jethro	12-76	2418-48	Boone	910	0.05	1023	298	cmg
40	11N-28W	24	Seeco-Hales #1-T	Franklin	Jethro	7-89	1674-2418	Boone/M. Hale	176	0.168	297	210	act
41	12N-23W	31	Tom Brown-Fed #1-T	Johnson	Ozone	5-77	2480-2511	Boone	6194	0.815	833	206	act
42	12N-23W	32	Seeco-Vause #1-T	Johnson	Ozone	1-96	2510-88	Boone	390	0.004			act
43	12N-24W	27	Seeco-Fed #1-C	Johnson	Batson	5-76	2308-18	Boone	1439	0.118	796	692	ina
44	12N-24W	28	Seeco-Fed #1	Johnson	Batson	4-74	2280-2339	Boone	2000	1.423	694	330	act
45	12N-24W	32	Seeco-Fed #2-C	Johnson	Batson	1-76	2316-82	Boone	5637	0.853	802	530	act
46	12N-24W	32	Seeco-Fed #2-T	Johnson	Batson	1-76	2410-20	Boone		0.001	711	40	ina
47	12N-24W	33	Seeco-Fed #1-T	Johnson	Batson	3-76	2250-55	Boone	527	0.247	462	138	act
48	12N-24W	36	Weis Br-Galloway #1-T	Johnson	Ozone	5-77	2437-60	Boone	4899	0.816	802	406	act
49	12N-28W	19	Ranken-Skunkaroma #2-T	Crawford	Hurricane Crk	12-90	1938-48	Boone	112	0.243	413	152	act
50	12N-29W	24	Ranken-Squirrelarama #1-T	Crawford	Hurricane Crk	12-90	1632-81	Boone	149	0.083	425	380	ina
51	14N-30W	06	Fossil Bay-Waterson #1	Washington	Friendship	8-87	405-797	Boone	34	0.002	52	54	ina
52	14N-30W	07	WF Gas-Rand #2	Washington	Friendship	4-90	350-715	Boone		0.006	54	34	ina
53	14N-30W	07	WF Gas-Winn #1-C	Washington	Friendship	4-89	468-830	Boone	61	0.014	53	34	ina
54	14N-30W	07	WF Gas-Rand #1	Washington	Friendship	8-87	350-715	Boone	261	0.065	95	40	act
55	14N-30W	29	WF Gas-Bowlin #1	Washington	Hardt	4-89	820-60	Boone		0.082	99	52	act
56	14N-30W	30	WF Gas-Irvin #1	Washington	Hardt	4-89	895-1000	Boone		0.015	97	52	ina
57	14N-31W	01	WF Gas-Yates #1	Washington	Friendship	8-89	788-90	Boone	79	0.013	53	36	ina
58	14N-31W	01	WF Gas-Reed #2	Washington	Friendship	10-89	416-65	Boone	77	0.007	53	36	ina
59	14N-31W	12	WF Gas-Fisher #8	Washington	Friendship	4-89	493-520	Boone	147	0.019	53	35	act
60	14N-31W	12	WF Gas-Fisher #6	Washington	Friendship	8-87	636-700	Boone	630	0.044	51	35	act
61	14N-31W	12	WF Gas-Fisher #5	Washington	Friendship	8-87	800-1217	Boone	92	0.003	48	54	ina

[a] In 17 fields occupying either the shallow gas province or the Arkansas basin (through January 1998). Abbreviations: *CP* = cumulative production; *ISIP* = initial shut-in pressure; *PSP* = present shut-in pressure; *p/a* = plugged and abandoned; *act* = active; *cmg* = commingled; *rec* = recompleted; *ina* = inactive.

Further insight into Boone porosity and permeability is provided by logs from producing wells in Batson and Ozone fields, northern Arkoma basin, Johnson County, Arkansas. These wells were logged with gamma-ray, caliper, and compensated-neutron-density tools (Fig. 4). The Boone exhibits a pattern of fluctuating porosity and permeability intervals identical to that seen in the shallow gas province (Fig. 3). Production from the upper Boone is within a range of 216–68 ft. A compilation of values from eight wells in the Batson field exhibits an average productive interval of 138 ft. The eight wells exhibit an average of 48 ft and a range of 15–74 ft of at least 7% porosity. All wells had intervals of at least 10% porosity, with a range of 4–30 ft, and an average of 17 ft. All wells also had intervals of at least 12% porosity, with a range of 2–17 ft, and an average of 9 ft. Four wells had intervals of at least 15% porosity, with a range of 2–6 ft, and an average of 5 ft. We believe that similar values probably occur in the Boone reservoir of the shallow gas province.

BOONE PRODUCTION

Production data through January 1998 are provided in Table 1 for 61 wells making up total Boone production from the shallow gas province and the Arkoma basin in Arkansas.

Shallow Gas Province

Eleven wells from two fields have a cumulative production of 0.27 BCFG. Only four wells, three in Friendship Church field and one in Hardt field, are currently active. These fields represent small domal structures with closures of approximately 40 ft that were identified by surface mapping in the late 1980s (Hairston, 1989). They lie east of the Fayetteville fault system, on its downthrown side, and the folding is probably a fault-induced strain. Both fields exhibit slight northeast–southwest elongation parallel to the Fayetteville fault system. Boone production is encountered at depths of 600–700 ft. The gas produced is dry methane with a heating value up to 1,400 Btu, but approximately 500 ppm hydrogen sulfide must be removed at the wellhead prior to sale (Hairston, 1989). We believe that the methane has two sources.

The bulk of the natural gas was formed in the Arkoma basin from Pennsylvanian source rocks and migrated northward along the Fayetteville fault system, where it eventually invaded the Boone reservoir along fracture systems generated by the fault and regional uplift of the Ozark dome. Some of the gas was generated from the Chattanooga Shale and migrated upward and laterally into the Boone reservoir along those same fracture systems. This gas contains hydrogen sulfide, and its concentration may indicate the contribution from the Chattanooga. Sulfur water is also commonly encountered in water wells penetrating the Boone in northern Arkansas.

Shut-in pressures are either just below 100 psi (Hardt field, and the WF Gas No. 1 Rand, Friendship Church field) or at approximately 53 psi (remainder of Friendship Church field). Both fields seem to operate as water-drive reservoirs. Field rules allow drilling on 40-acre spacing. Completions are typically open hole beneath a wireline packer. Wells have not been stimulated and are produced on chokes. Gas is scrubbed and compressed for transmission in an 8-in. Arkansas–Louisiana Natural Gas pipeline approximately 0.5 mi from the fields.

Arkoma Basin

A total of 50 wells from 15 fields have produced 17.53 BCFG through January 1998. Of these 50 wells, 17 produce in Batson field and 5 produce from the conterminous Ozone field, both in Johnson County, Arkansas. No other field in the basin contains more than 4 wells that produce Boone gas, and only 12 wells outside Batson and Ozone fields were actively producing Boone gas in January 1998. All wells produce dry methane that contains trace amounts of hydrogen sulfide. This natural gas was produced from a Pennsylvanian source and migrated into the Boone reservoir along faults that juxtapose the Mississippian and Pennsylvanian sections. A similar situation exists in other pre-Pennsylvanian Arkoma reservoirs that are only productive in settings where Pennsylvanian strata have been faulted against them. According to available well logs, the Chattanooga Shale is absent or very thin (2–3 ft) throughout the Batson and Ozone fields, and the low levels of hydrogen sulfide in the Arkoma natural gas compared with values from the shallow gas province confirm a Pennsylvanian source.

Batson field occupies parts of Ts. 11–12 N., Rs. 24–25 W., Johnson County. The smaller Ozone field lies directly to the

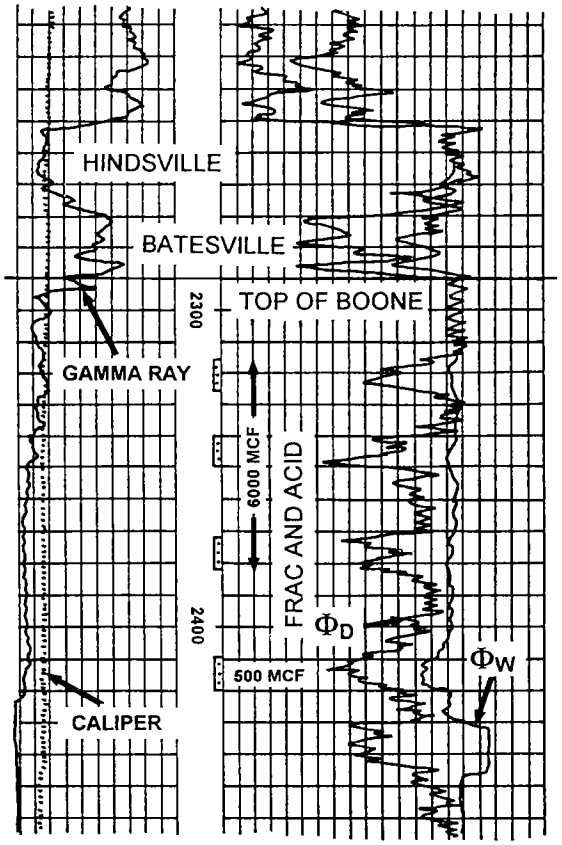

Figure 4. Characteristic log signatures for the SEECO No. 2C Federal well, sec. 32, T. 12 N., R. 24 W., Batson field, Johnson County, northern Arkansas. This well had an initial potential of 5,637 MCFGPD, a cumulative production of 0.853 BCFG through January 1998, and an estimated ultimate recovery of 1.7 BCFG.

east in the tiers of sections forming the corner of Ts. 11–12 N., Rs. 23–24 W., Johnson County. The discovery of both fields was the result of initial exploration of Pennsylvanian strata, but successful testing of the Boone interval soon followed. Boone production occurs from small anticlines on the upthrown sides of several east–west-trending, north-dipping normal faults. Structural closure is approximately 400 ft. The top of the Boone Formation is encountered between 2,200 and 2,300 ft, and most of the production comes from the upper 100–150 ft. Perforated intervals for eight producing wells range from 64 to 12 ft, with an average of 32 ft. Most of the wells were treated with 1,000–5,000 gallons of acid during completion. Ground-water protection is a concern in the fields, and consequently very few wells are fracture stimulated. The five Boone wells in Ozone field have produced 3.6 BCFG through January 1998, and all are currently active (Boone production began in 1975). The 17 Boone wells in Batson field have produced a total of 11.7 BCFG, averaging 0.69 BCFG per well, through January 1998. Seven of the Boone wells in Batson field are currently active, and most have been producing since the late 1970s.

SUMMARY AND CONCLUSIONS

The Boone Formation is a potential, but largely unexplored, reservoir for natural-gas production in both the shallow gas province and the Arkoma basin in northern Arkansas. There are 61 wells that have produced 17.8 BCFG from the interval in 17 fields. Porosity (up to 17%) and permeability (>1 md) are associated with fractured, chert-bearing parts of the upper 100–150 ft of the Boone Formation in both regions. In the shallow gas province, dry methane with its source from Pennsylvanian strata in the Arkoma basin "spilled" northward along the Fayetteville fault system, mingled with other natural gas produced by the Chattanooga Shale, and invaded Boone reservoirs in Washington County, Arkansas. Pennsylvanian strata were also the source for dry methane in Batson and Ozone fields, Johnson County, Arkansas. Fractured Boone reservoirs have collectively produced 15.3 BCFG through January 1998 from 22 wells in those two fields in the Arkoma basin. An essentially unexplored area of potential production lies between the shallow gas province and the boundary faults of the northern Arkoma basin (Fig. 3).

ACKNOWLEDGMENTS

This paper draws on theses prepared at the University of Arkansas by Jeffrey Liner and Paul Hairston under the direction of Manger, and a thesis by Peter Van Den Heuvel under the direction of Doy L. Zachry. We thank Gene Westover, exploration manager of the former Midcontinent Office of Tenneco Oil Corp., Oklahoma City, for funding an initial study of the Boone interval 20 years ago, including the porosity and permeability analyses discussed herein. We also thank Bill Winkelmann, Southwestern Energy Co., Fayetteville, Arkansas, for providing data on Batson and Ozone fields. Finally, we thank Kenneth Johnson, Oklahoma Geological Survey, for encouraging our participation in this project and for his infinite patience in seeing the manuscript into final form.

REFERENCES CITED

Hairston, P. R., 1989, Petroleum geology and exploration potential, shallow gas province, Washington and Madison Counties, Arkansas: University of Arkansas unpublished M.S. thesis, 94 p.

Handford, C. R.; and Manger, W. L., 1993, Sequence stratigraphy of a Mississippian carbonate ramp, north Arkansas and southwestern Missouri: New Orleans Geological Society Guidebook, 42 p.

Kelly, B. K., 1997, The age of the Chattanooga Shale in the southern Midcontinent, North America [abstract]: Geological Society of America Abstracts with Programs, v. 29, no. 2, p. A-17.

Liner, J. L., 1979, Lithostratigraphy of the Boone Formation (Lower Mississippian), northwest Arkansas: University of Arkansas unpublished M.S. thesis, 88 p.

Manger, W. L.; Shelby, P. R.; and Farris, S. G., 1988, Devonian–Lower Mississippian lithostratigraphy, northwestern Arkansas: Compass, v. 65, p. 223–231.

Shelby, P. R., 1986, Depositional history of the St. Joe and Boone Formations in northern Arkansas: Arkansas Academy of Science Proceedings, v. 40, p. 67–71.

Thompson, T. L., 1986, Paleozoic succession in Missouri; part 4, Mississippian System: Missouri Geological Survey Report of Investigations 70, 182 p.

Van Den Heuvel, Peter, 1979, Petrography of the Boone Formation, northwest Arkansas: University of Arkansas unpublished M.S. thesis, 75 p.

Witzke, B. J.; McKay, R. M.; Bunker, B. J.; and Woodson, F. J., 1990, Stratigraphy and paleoenvironments of Mississippian strata in Keokuk and Washington Counties, southeast Iowa: Geological Survey Bureau, Iowa Department of Natural Resources, Guidebook 10, 105 p.

PC-Based Reservoir Characterization and Simulation of Schaben Field, Ness County, Kansas

Saibal Bhattacharya, Paul M. Gerlach, Tim R. Carr, Willard R. Guy, Scott Beaty, and Evan K. Franseen
Kansas Geological Survey
Lawrence, Kansas

ABSTRACT.—The objective of this study was to characterize and simulate a typical oil field producing from a Mississippian reservoir by using tools that are modern and cost-effective for small independent producers. We used a PC-based simulator called BOAST 3, released by the U.S. Department of Energy, which is a three-dimensional, three-phase black-oil tool. The reservoir-simulation process is interactive and involves geologists and engineers working as a team. The entire project was performed by using a desktop computer and software that is either low cost or free.

The reservoir we studied in Schaben field produces from Meramecian and Osagean (Mississippian) cherty dolostones beneath the sub-Pennsylvanian unconformity on the western flank of the Central Kansas uplift. The field, discovered in 1963, was developed on 40-acre spacing.

Analysis of the reservoir began with detailed studies of core, log, and well data, which were integrated to develop a three-dimensional reservoir model. A volumetric study was completed on a grid-cell by grid-cell basis prior to the start of simulation for the purpose of verifying that various reservoir parameters, including effective porosity, net-pay thickness, and water saturation, were capable of supporting the historic production data.

A good match was obtained between the recorded and simulated daily oil- and water-production rates for the 34-year simulation period. Results indicate that significant additional oil production can be obtained from Schaben field if new wells are drilled in potential areas.

Implications of this study show that (1) practical application of cost-effective technologies in reservoir simulation enables the small independent producer to map remaining hydrocarbon reserves in marginal fields, (2) simulation studies can lead to proper field management by targeting infill drilling in areas of best potential, (3) PC-based reservoir simulation is a practical reality for producers with limited resources, (4) procedures demonstrated in this study provide a guide for geologic modeling, simulating, and managing similar reservoirs in Kansas and the Midcontinent.

INTRODUCTION

In today's competitive economic climate, cost-effective production technology is required by producers of marginal petroleum reservoirs to continue to survive and prosper. Field management based on reservoir characterization and simulation studies can aid the producer in efficient exploitation of remaining hydrocarbon reserves in marginal fields. In the past, reservoir simulation and management were restricted to "core assets" of large oil companies. Resources, such as mainframe computers or sophisticated workstations, that were required for reservoir-simulation study were not economically or technically feasible for the small independent producer.

In 1987, the U.S. Department of Energy released a PC-based reservoir simulator called BOAST (Black Oil Applied Simulation Tool). BOAST (Louisiana State University, 1997) is a three-dimensional (3D), three-phase black-oil applied simulation tool used for performing reservoir studies. The general application of desktop simulators, such as BOAST, to large-scale or full-field simulation has been hampered by hardware and/or software limitations. Recent advances in computational speed and in memory management have significantly reduced the time to run a desktop simulation. The availability of powerful and "user-friendly" spreadsheets, relational databases, gridding, and mapping software packages have provided the tools to efficiently assemble and manipulate simulation input data and to generate useful maps and charts from simulation output.

The objective of this study was to characterize and simulate a typical oil field producing from a Mississippian reservoir by using tools that are modern and cost-effective for small independent producers. As part of a U.S. Department of Energy Class 2 project, a number of producibility problems in Meramecian and Osagean dolostone reservoirs of Kansas have been addressed in this study. Schaben field, in Ness County, Kansas, was selected because it is representative of many Mississippian oil fields in the State (Fig. 1).

Reservoir simulation is an interactive process that involves geologists and engineers working as a team. The entire simulation study was performed by using a desktop computer and

Bhattacharya, Saibal; Gerlach, Paul M.; Carr, Tim R.; Guy, Willard R.; Beaty, Scott; and Franseen, Evan K., 2000, PC-based reservoir characterization and simulation of Schaben field, Ness County, Kansas, *in* Johnson, K. S. (ed.), Platform carbonates in the southern Midcontinent, 1996 symposium: Oklahoma Geological Survey Circular 101, p 171–182.

with software that is either low cost or is available in the public domain.

Reservoir simulation represents the final step in a process that begins with integrated reservoir characterization. Reservoir characterization forms the foundation for development of a descriptive reservoir model and provides the framework for simulation. Existing and newly acquired well data were integrated into a computerized three-dimensional geologic model. Reservoir parameters, such as effective porosity, net-pay thickness, and water saturation, were obtained from this geologic model. These parameters were used in a volumetric calculation to determine if the observed historical production could be supported by the petrophysical parameters. Following a successful volumetric calculation, the above reservoir parameters were input as grid-cell values and used to simulate the reservoir performance of Schaben field from its discovery to 1995. Analysis of the reservoir performance and the distribution of the remaining mobile oil in place (as predicted by the simulator) led to the identification of regions with potential for incremental oil recovery. The simulator was used to predict the performance of infill wells drilled in these potential areas.

Results from this study were used to design field-management and future infill-drilling plans in Schaben field. These infill-drilling plans will be demonstrated during phase 2 of the Schaben class project. It is hoped that this study will provide a model for improving field management of similar reservoirs in Kansas and in the Midcontinent.

BACKGROUND

The majority of Mississippian production in Kansas occurs at or near the top of the Mississippian System, beneath the regional pre-Pennsylvanian unconformity. These mature reservoirs are a major source of Kansas oil production, and they account for approximately 43% (21 million barrels in 1994) of total annual production (Carr and others, 1998). Cumulative production (as of 1994) from Mississippian reservoirs in Kansas exceeds 1 billion barrels. At present, small independent producers operate many of these Mississippian reservoirs. Extremely high water cuts and low recovery factors place continued operations at or near their economic limits.

Schaben field lies on the western flank of the Central Kansas uplift and produces from Mississippian Meramecian and Osagean cherty dolostones that are beneath the sub-Pennsylvanian

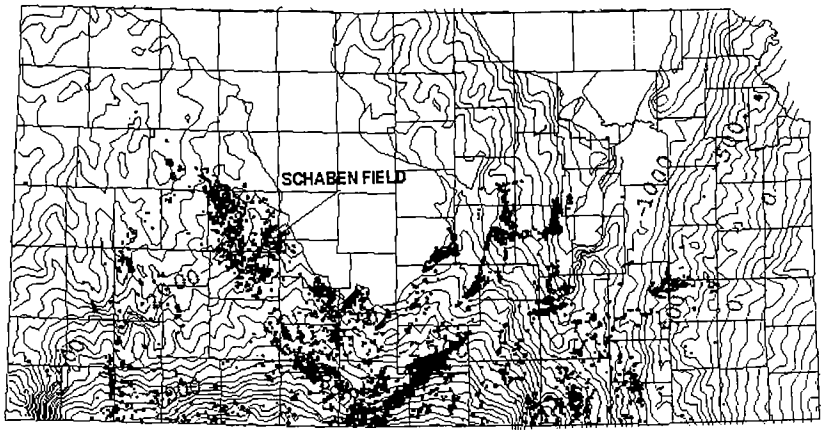

Figure 1. Mississippian structure map, showing fields producing from the Mississippian and the location of Schaben field. Datum, mean sea level; contour interval, 100 ft.

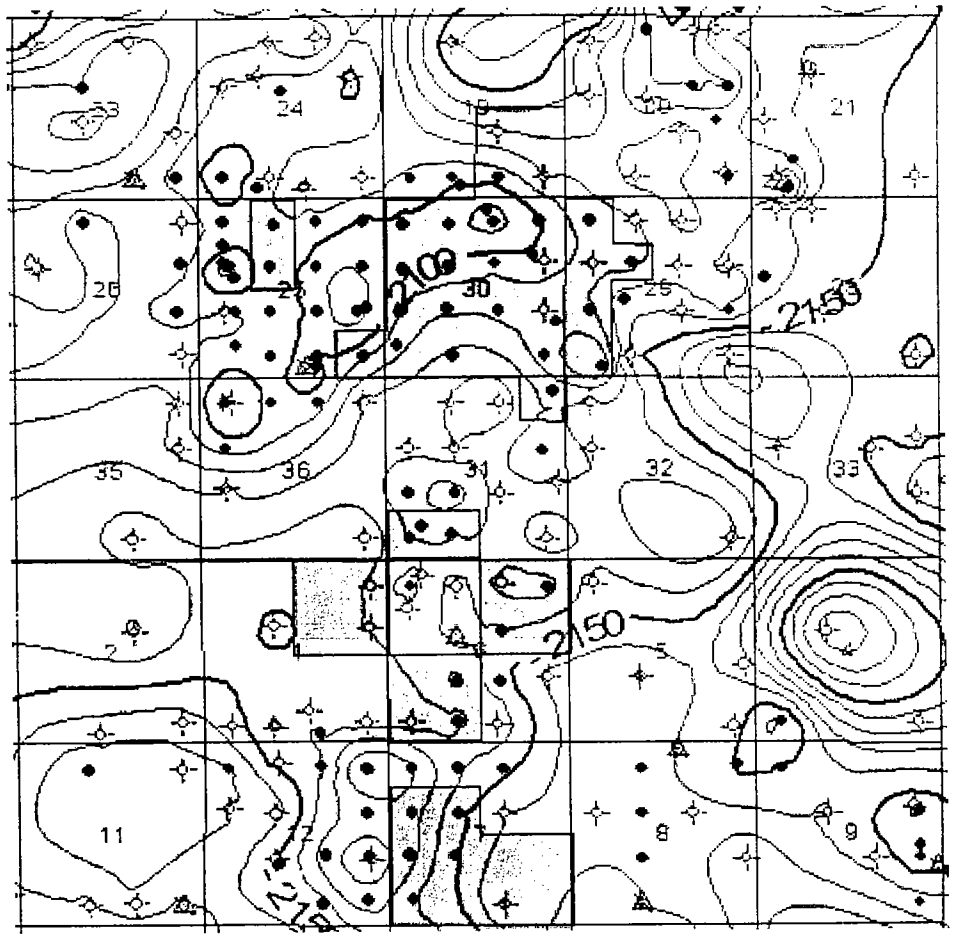

Figure 2 *(at right)*. Schaben field demonstration site, with structural contours showing the configuration of the top of the Mississippian limestone. The leases in the demonstration area are indicated in gray tone. Contour interval, 10 ft.

unconformity. Stratigraphically, it is situated at the western edge of the Osagean subcrop. The field produces oil at depths between 4,350 and 4,410 ft, from dolostones and limestones of the lower Meramecian Warsaw Limestone and Osagean Keokuk Limestone. The demonstration site consists of 1,720 contiguous acres within Schaben field in Ts. 19–20 S., Rs. 21–22 W., Ness County (Fig. 2). The leases constituting the demonstration site are shown in gray tone in the figure.

Schaben field was discovered in 1963 and consists of 78 completed oil wells that are spaced primarily on 40-acre locations. Cumulative field production as of May 1997 was 9.1 million barrels of oil (BO), and daily field production was 326 BOPD from 51 wells. Wells in the Schaben demonstration site have cumulatively produced 7,100,481 BO, and current (May 1997) daily production from 29 wells averaged 141 BOPD. The Schaben demonstration site contained 6 plugged and abandoned oil wells, 27 producing oil wells, and 2 water-disposal wells at the onset of this study.

Some of the common problems faced by the operators in designing optimum field-management plans include lack of production and geologic data, problems in drilling and completion design, inadequate reservoir-characterization studies, and lack of information about the current productive potential of the field. These problems caused the operators to realize a less than optimal primary recovery. The application of cost-effective reservoir-description and -management strategies can significantly extend the economic life of mature carbonate fields and result in the recovery of significant incremental reserves. Equally important is the innovative dissemination of data, methodologies, and results to promote a wider application of demonstrated technologies by the operators of numerous similar fields throughout the northern Midcontinent and the United States.

Descriptive reservoir characterization entailed creative integration of existing data with core studies from three new wells that were drilled through the reservoir interval. Core and log data from these three wells provided insight into fundamental reservoir parameters, such as the analysis of core plugs by nuclear magnetic resonance (NMR) to determine effective porosity. Descriptive core analysis, petrophysical and petrographic analysis, correlated log and core data, and existing well data were integrated to develop a computerized three-dimensional reservoir model for the Schaben site. All geologic, digital-log, and production data were entered into a database-management and analysis system. Data for 267 wells distributed over 36 sections in and around the Schaben project area were collected, edited, and loaded into a computer database. This database is publicly accessible through the Internet. The URL is as follows: http://www.kgs.ukans.edu/DPA/Schaben/schabenMain.html.

Log analyses, core analyses, and geologic maps provided a better understanding of the complexities existing in the heterogeneous reservoir of Schaben field. Determination of pore size, pore-throat size, irreducible water saturation, horizontal and vertical permeabilities, effective porosity, and mobile water saturations were part of the integrated reservoir-characterization study. Details of the study can be found in open-file reports and other publications (Carr and others, 1996; Carr and others, 1998; Guy and others, 1996).

Table 1.—Schaben Field Reservoir Model Parameters

General Data	
State:	Kansas
County:	Ness
Location:	T. 19 S., Rs. 21–22 W., T. 20 S., R. 21 W.
Discovery date:	September 4, 1963
Discovery well(s):	Cities Service Oil Co. #1 Moore "B," SE SE sec. 30, T. 19 S., R. 21 W., Mississippian oil, 4,494 ft RTD
Field size:	8,880 acres
Wells	Total: 90
	Operating (1996): 67
	Abandoned: 25
Reservoir Data	
Producing formation(s):	Mississippian (Osagean)
Lithology:	Dolostone, chert, limestone
Average depth:	4,400 ft (–2,100 ft subsea)
Original OWC	–2,145 ft subsea
Average porosity:	17.5%
Permeability, horizontal:	6.5 md to 167.0 md
Permeability, vertical:	0.15 times horizontal permeability
Archie equation parameters:	$a = 1$, $m = 2$, $n = 2$, $R_w = 0.13$
Temperature:	115°F
Original field pressure:	1,340 psi
Production Data	
Original oil in place:	40–50 MMBO
Cumulative oil prod.:	9.1 MMBO (Sept '96)
Est. recovery factor:	17%
Present oil production:	331 BOPD (Sept '96)
Present produced water:	2,541 BWPD (Sept '96)
Fluid Properties	
Crude Oil	
API gravity:	40°
Viscosity at PBP:	1.95 cp
Initial solution G/O ratio:	50 SCF/BBL
Bubble pnt. press. (PBP):	225 psia
Fm. vol. factor at PBP:	1.037 RB/STB
Gas	
Viscosity at PBP:	0.011 cp
Fm. vol. factor at PBP:	0.0123 RB/SCF
Produced Water	
Salinity:	15,000–20,000 ppm
Viscosity at 14.7 psi:	0.65 cp

RESERVOIR MODEL: PAY HEIGHT, POROSITY, AND SATURATION

Selected Schaben field input data and reservoir parameters are shown in Table 1. The first step in reservoir simulation is to establish a pattern of grid blocks that properly describes the reservoir. In this study, a commercial mapping and gridding package was used to generate the grid maps of porosity, satu-

ration, permeability, pressure, and pay thickness from the well data. The grid cells used in this study each measured 220 ft in the X and Y directions. This grid-cell dimension resulted in five grid blocks between most adjacent wells. The effects of numerical dispersion in reservoir simulators are reduced if there are more than two grid cells between adjacent wells (Mattax and Dalton, 1990a).

Subsurface petrophysical cross sections in Schaben field show that the original oil column had migrated across multiple correlated reservoir zones within the Mississippian. This suggests that reservoir units may be connected by a system of natural fractures. The presence of fractures in cores obtained from the three recently drilled wells confirmed the presence of a fracture system within the reservoir. The production history of most wells consists of water-free oil production for a few years, followed by a rapid drop in oil cut and decades of constant high water cuts (Fig. 3).

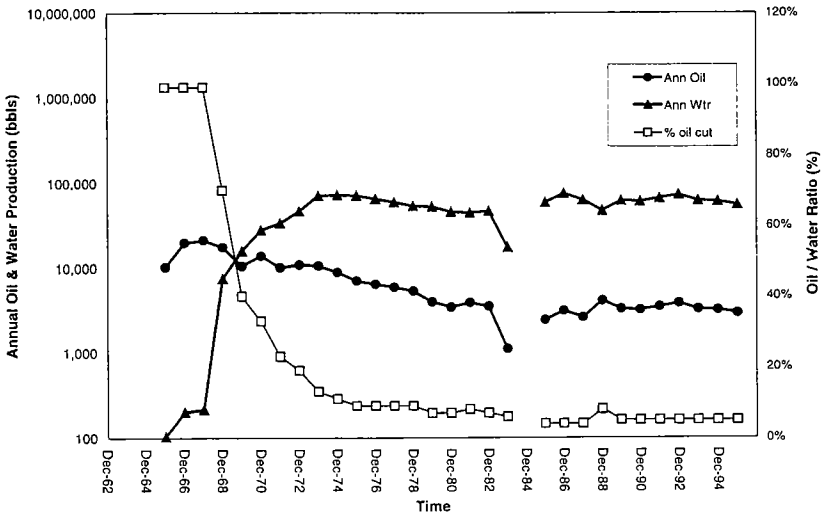

Figure 3. Rate-versus-time plot of annual oil and water production and oil/water ratio for the Moore D4 well, sec. 30, T. 19 S., R. 21 W.

Fluid-production data over the life of the field show a high water-production rate after the initial breakthrough. The fluid column in many producing wells indicates that the current reservoir pressure is close to the original reservoir pressure, suggesting a strong recharge of the reservoir by an underlying aquifer. Based on these observations, the Schaben field simulation was simplified as a two-layer model consisting of a reservoir layer with an underlying aquifer layer.

The grid-block dimensions are the same for both the reservoir layer and the aquifer layer. The gross- and net-pay thicknesses were assumed to be equal because it was difficult to distinguish productive and nonproductive zones by using petrophysical logs. The pay thickness was selected from petrophysical logs as the interval from the top of the reservoir to the oil–water contact (OWC). Geologic maps and DST data indicate the presence of a flat OWC at –2,145 ft subsea. Figure 4 shows the net-pay thickness of layer 1.

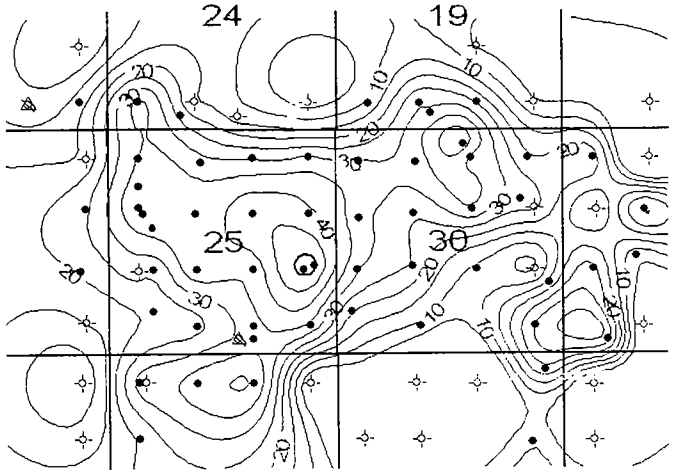

Figure 4. Map showing net-pay thickness of layer 1, Schaben field. Thickness interval, 5 ft.

A uniform aquifer thickness of 100 ft was assumed in this study on the basis of data from petrophysical logs from deep wells surrounding Schaben field. The regional dip of the Mississippian strata across the demonstration area is <0.25°. Given the negligible regional-dip angle, a zero dip angle was used in the simulation study.

"PfEFFER" (Doveton and others, 1996; Guy and others, 1996), a log-analysis software program, was used for petrophysical analyses in this study. The total reservoir porosity at each well was determined from petrophysical logs and was calculated as the average value obtained over the net-pay interval. Porosity values in Schaben field were obtained from a wide suite of logs, both old and new, that were run over a period of 35 years.

A review of the production data indicates that most of the wells initially produced less than 15% water for a period of 1 to 4 years, whereas average water saturations were calculated from logs to range between 65 and 75%. This contradiction indicates that not all of the water in the pore space is mobile. Analysis of the NMR data, at reservoir pressure, from core plugs indicates a significant difference at reservoir pressure between the total porosity (obtained from petrophysical logs) and the effective porosity. In addition to NMR data, thin-section and capillary-pressure studies reveal the presence of micropores (pore throat radii <0.5 mm; Guy and others, 1997; Guy and others, 1998; Doveton, 1996). It is assumed that the micropores are totally saturated with water and that at reservoir pressure this water is immobile. Conversely, macropores are assumed to contain both hydrocarbons and water.

In order to determine effective reservoir porosity, a correlation between the effective core-plug porosity and total core-plug porosity was developed from the NMR data (Fig. 5). This relationship was applied to the total porosity (obtained from petrophysical logs) to calculate the effective porosity of the reservoir interval. This effective porosity represents the pore volume where fluid flow can occur under reservoir conditions. Figure 6 is an effective-porosity map of Schaben field.

The field has not produced significant volumes of gas, and

thus the sum of water and oil saturations was assumed to be equal to 1.0. The initial total water saturation at individual wells was determined from petrophysical-log analysis. The total volume of oil present in each grid cell was obtained by multiplying the total grid volume by the grid-cell porosity and oil saturation.

The macropore volume of each grid cell was obtained by multiplying the grid volume by the effective porosity. The oil saturation in the effective porosity was obtained by dividing the total volume of oil present in the grid by the macropore volume of the grid.

The oil saturation in the effective porosity was used in the volumetric calculations. Mobile water saturation was obtained by subtracting the oil saturation in the effective pores from 1.0. Thus, the water saturation (Fig. 7) used in the volumetric calculations represents the water saturation in the effective pore volume of the reservoir (i.e., in the macropores).

RESERVOIR VOLUMETRIC CALCULATIONS

A volumetric study of the Schaben field demonstration area was completed on a grid-cell by grid-cell basis prior to the start of simulation. The volumetric calculations were performed to verify that the different reservoir parameters, such as effective porosity, net-pay thickness, and water saturation in the effective porosity, were capable of supporting the observed historic production data. A map of the original oil in place (OOIP) per grid cell (Fig. 8) was generated by using the effective porosity, effective oil saturation, and grid volume.

Monthly production data on a lease basis was available from 1963 to date. Also available were the results of annual productivity tests for each well during its operational history. The annual productivity-test data, a one-day test, included the total barrels of oil produced over a day and the water/oil ratio (WOR). The productivity-test data were used to allocate the annual lease oil production to the individual wells on the lease (i.e., annual oil production per well). The annual water production at individual wells was obtained by multiplying total annual oil production for the well by the corresponding WOR recorded during the annual productivity test.

Schaben field is spaced on a uniform 40-acre spacing, with each well near the center of the tract. A grid-cell dimension of 220 by 220 ft resulted in 36 grid cells in each 40-acre tract. A volumetric calculation on a grid-cell basis requires the cumu-

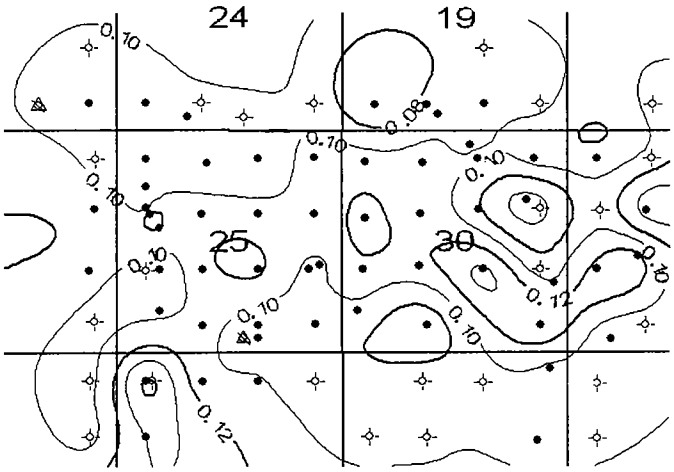

Figure 6. Effective-porosity map of Schaben field. Porosity indicated in hundredths (e.g., 0.10 = 10% porosity).

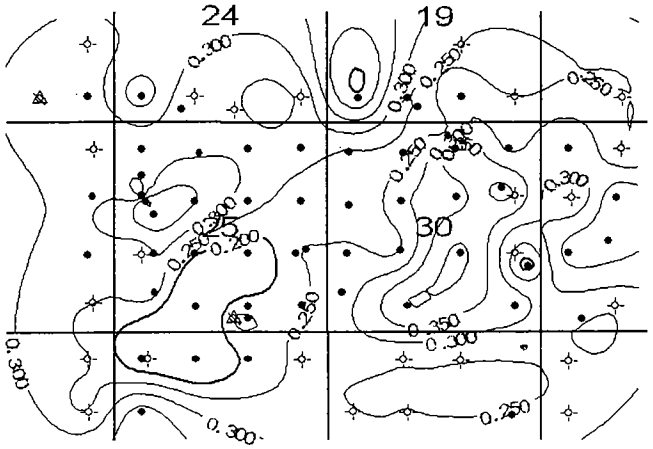

Figure 7. Map of effective water saturation in Schaben field. See text for explanation of contour values.

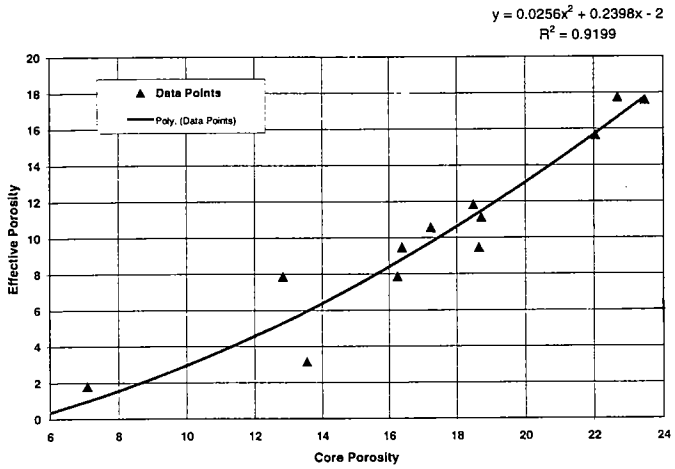

Figure 5. NMR-derived effective porosity versus core porosity for Schaben field. Porosity shown in percentages.

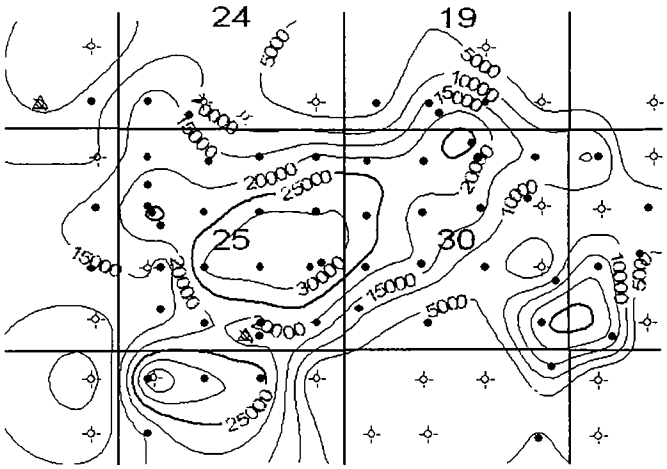

Figure 8. Map of original oil in place (in barrels) for Schaben field, based on values calculated per grid cell.

lative production of each well to be divided among the grid cells within the well-drainage area. Cumulative production for each well was divided by 36, and the resultant value was gridded to generate a map showing the volume of oil produced from each grid cell. A remaining-oil-in-place (ROIP) map was generated by subtracting the volume of oil produced from each grid cell from the volume of OOIP in each grid cell. The remaining oil saturation at each grid cell was multiplied by the pay thickness in the grid cell to obtain a residual-oil-saturation-thickness map as of 1996.

An irreducible oil saturation of 0.25 was assumed for the reservoir interval in Schaben field. The residual mobile oil saturation was calculated by subtracting 0.25 from the remaining oil saturations in each grid cell. To highlight the areas with remaining productive potential in the study area, a mobile-saturation-thickness map (Fig. 9) was generated by multiplying the mobile residual oil saturation in each grid cell by the pay thickness at the grid cell. The absence of negative oil-saturation values in any of the grid cells indicates that the combination of reservoir parameters, such as effective porosity, effective oil saturation, and pay thickness, is capable of supporting the observed historical production figures of the field.

RESERVOIR MODEL: PERMEABILITY, FLUID PROPERTIES, AND PRESSURE

A cross-plot of horizontal matrix permeability to effective porosity was generated from laboratory measurements of 104 core plugs that were collected from cores of different wells in Schaben field. The range of permeability values was 1.3–33.4 md in the cross-plot. An examination of permeability values obtained from DSTs in five wells indicates average values ranging between 73 and 246 md. Thus, matrix permeability as measured in core plugs appears to underestimate the effective permeability in the reservoir. Simulation runs using only the matrix permeability were unable to support the historical production rates of oil and water. History matching of field production by iterative simulation runs resulted in the use of effective-horizontal-permeability values that were 5 times the matrix-permeability values (Fig. 10). The permeability values that were finally used in the simulation ranged from 6.5 to 167.0 md.

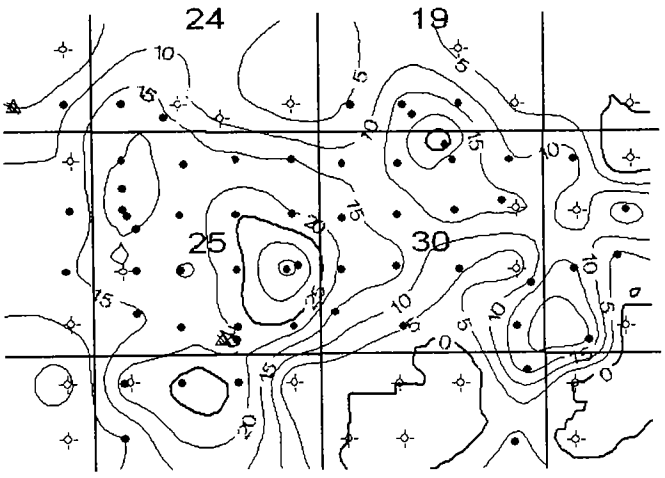

Figure 9. Map of remaining feet of oil saturation for Schaben field (time = 1996).

Maximum-horizontal-permeability and corresponding 90° permeability measurements were obtained from 48 whole cores taken from 7 different wells. A cross-plot of these values resulted in a slope approximately equal to 1.0 (Fig. 11). On the basis of this plot, it was assumed that horizontal-permeability values in the X and Y directions were equal.

A histogram plot of the ratio of vertical to horizontal permeability obtained from the 48 whole cores shows that the highest frequencies occur for permeability ratios ranging from 0.05 to 0.2, with a mean value of 0.15. History matching of field production by iterative simulation runs was used to adjust the vertical permeability to 0.15 times the horizontal permeability.

Relative-permeability ratios (K_{rw}/K_{ro}) at different water saturations were available from standard laboratory core-plug measurements from the No. 1 Moore D well (sec. 30, T. 19 S., R. 21 W.). This relative-permeability-ratio curve was used to generate relative-permeability curves (i.e., K_{ro} versus S_w and K_{rw} versus S_w). Initial simulation runs were carried out by using these relative-permeability curves. However, the end points and the shape of both curves were modified to match the historical field-production data.

Eighteen core plugs from the pay zones of three recently drilled wells were selected for capillary-pressure analysis. The

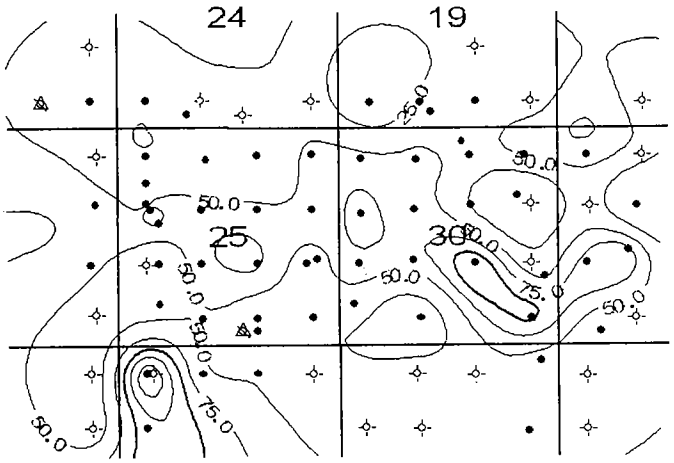

Figure 10. Map of effective horizontal permeability (in millidarcys) of layer 1 for Schaben field.

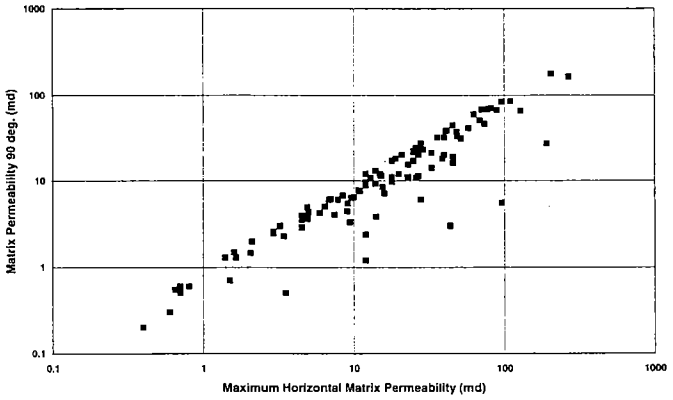

Figure 11. Maximum horizontal permeability versus 90° permeability for Schaben field.

irreducible water saturation was obtained from the relative-permeability data. From the series of 18 capillary-pressure curves, the curve showing an asymptotic rise in water saturation closest to the irreducible water saturation was selected as the capillary-pressure curve most representative of the field.

Historical production data from the Schaben demonstration site indicates that gas production was never significant during the history of the field. Thus, a solution-gas/oil ratio of 50 ft^3/bbl was assumed in this study. The gas gravity was assumed to be 0.7 (air = 1.0). Production records show that the average tank gravity of the oil is 40°API, and the average reservoir temperature, 115°F.

A bubble-point pressure of 225 psia was calculated from standard correlations (McCain, 1990). The subsea depth corresponding to this bubble-point pressure was –2,100 ft, the average subsea depth of the reservoir across the field. The oil viscosity above and below the bubble point was also calculated with the help of standard correlations (McCain, 1990). The viscosity of dead oil at reservoir temperature was determined to be 2.5 cp, and the slope of the oil viscosity above bubble point was calculated to be 0.000495 cp/psi (McCain, 1990).

The oil formation volume factor at the bubble point and above was also calculated by using standard correlations. This factor at the bubble point was determined to be 1.037 RB/STB with a slope above the bubble point of –0.000005 RB/(STB.psi) (McCain, 1990).

Water analyses from several wells in the Schaben demonstration area indicate that salinity in reservoir brine varied between 15,000 and 20,000 ppm. Correlations were used to calculate the water viscosity, corrected to average reservoir temperature and pressure (water viscosity = 0.65 cp; McCain, 1990). Standard correlations were also used to calculate the formation volume factor of water at pressures above the bubble point (McCain, 1990).

The calculated average reservoir porosity for all the grid blocks is 17.5%. This value was used to determine the total rock compressibility (3.8×10^{-6} psi^{-1}) from standard correlations (Amyx and others, 1960).

By using standard correlations, gas formation volume factor and gas viscosity were calculated at the bubble-point pressure and also at pressures above the bubble point (McCain, 1990). The gas viscosity at bubble point was determined to be 0.011 cp, and the gas formation volume factor at bubble point is 0.0123 RB/SCF. The stock-tank properties of oil, gas, and water used in the simulation were as follows: density of oil = 51.46 lb/ft^3; density of water = 64.55 lb/ft^3; density of gas = 0.0535 lb/ft^3.

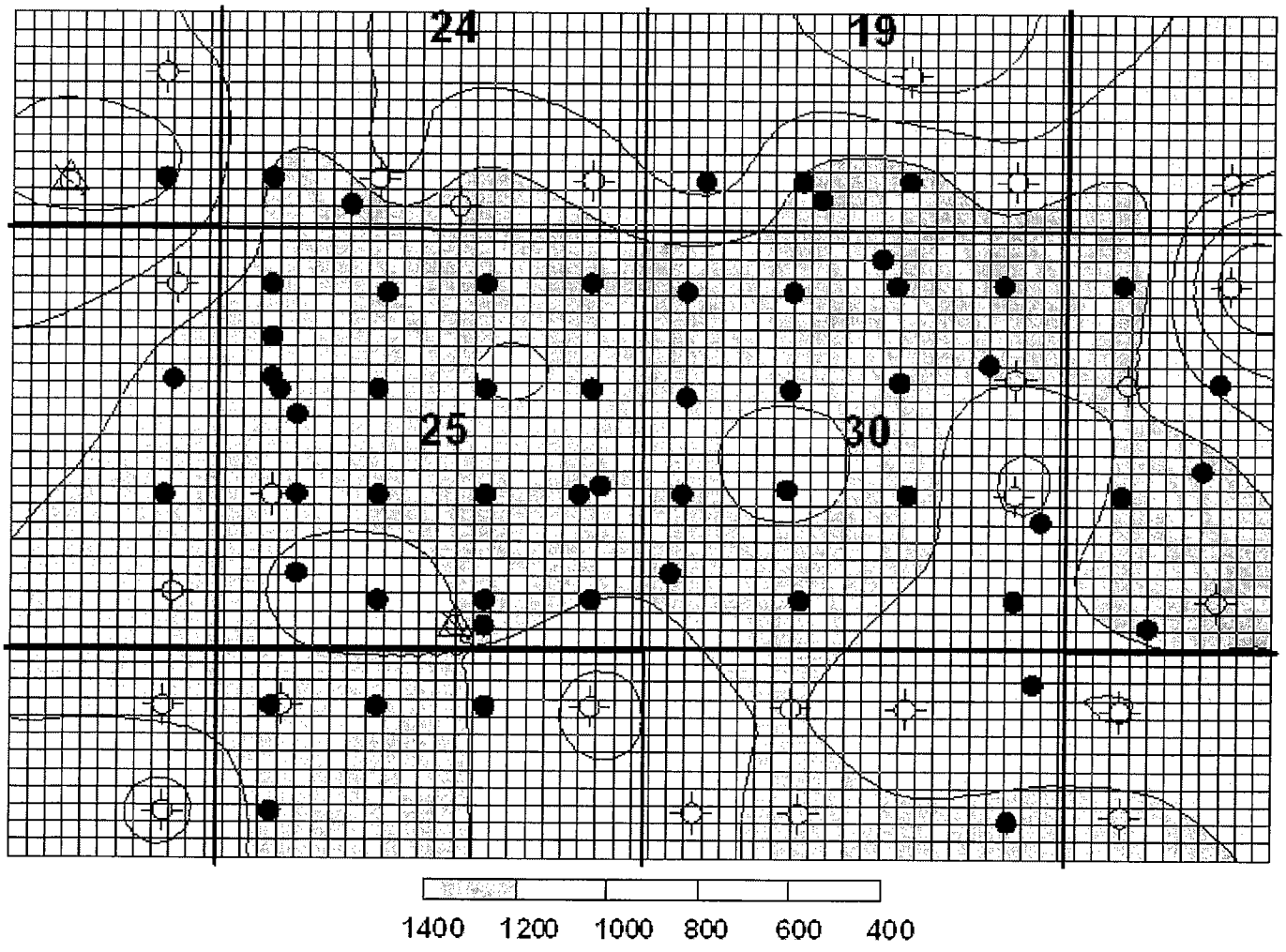

Figure 12. Map of reservoir pressure (psi) for Schaben field.

The average DST shut-in pressures in the Mississippian reservoir of Schaben field were used to generate an initial-reservoir-pressure map. As shown in Figure 12, most of the reservoir had pressures above 1,100 psi. However, two regions at the periphery of the field showed pressures near 400 psi. These anomalous low pressures were removed from the analysis, and the final map was normalized so that all the grid cells had at least a minimum pressure of 1,100 psi.

The aquifer in this simulation was designed solely to supply the necessary water required to recharge the reservoir layer and to maintain the reservoir pressure over time. A uniform porosity of 25% was used for the aquifer layer. Water saturation in the aquifer layer was set to 1.0. Vertical-permeability values assigned to the aquifer layer played a critical role in controlling the water production at the wells. A good fieldwide match was obtained (within 18% of what is believed to be the total water production in the field) when the horizontal permeability of the aquifer was set to 25 md and the vertical permeability of the aquifer ranged between 0.1 and 4.5 md. As in the reservoir layer, aquifer permeabilities in the X and Y directions were assumed to be equal. The aquifer pressure was assumed to be higher than the maximum pressure value in the reservoir, and was assigned a constant value of 1,400 psi.

BOAST 3 SIMULATION

BOAST 3 is an isothermal, 3D, three-phase black-oil simulator. Black-oil simulators are applicable for a large percentage of the world's oil and gas reservoirs. The BOAST 3 simulator has a wide range of applicability and can be used to simulate oil and gas recovery under different scenarios such as primary depletion, pressure maintenance by gas/water injection, and evaluation of secondary-recovery operations such as waterflooding. BOAST 3 is a finite-difference implicit-pressure/explicit-saturation (IMPES) numerical simulator. The well model in BOAST 3 allows the user to specify the well production rate or the well bottom-hole flowing pressure, and the user is free to add or recomplete wells during the course of the simulation. Multiple rock regions, and pressure, volume, and temperature (PVT) regions, can be defined; three aquifer models are available as options.

The primary design of this simulation study was to enter 11 years of historical data and to have the simulator predict and match the next 23 years of known field-production data. The historical data entered into the simulation input file consisted of the daily oil-production rate for each well. This rate was obtained by dividing annual cumulative oil production at each well by the number of days that the well operated during the year. For the first 11 years, the simulator calculated the bottom-hole flowing pressure at each well that was necessary to produce the given oil-production rate, and then used this bottom-hole pressure to calculate the water production at each well. As the simulator was able to predict the water-production rates during the first 11 years within a reasonable degree of accuracy, the corresponding bottom-hole flowing pressures at the end of 11 years were thought to be acceptable. The bottom-hole flowing pressure at each well at the end of the 11 years of simulation was noted. During the prediction phase, only the bottom-hole flowing pressure at each well was entered in the input file, and the simulator calculated both the oil- and water-production rates. The bottom-hole flowing pressure entered for each well during this prediction phase was based on the corresponding bottom-hole flowing pressure calculated by the simulator at the end of the 11th year. Production profiles show that the WOR at each well remained almost constant after 11 years. It was also assumed that as the well aged, the bottom-hole flowing pressure at each well would decline. Thus the pressure at each well during the prediction phase was entered as a percentage of the pressure calculated by the simulator at the end of the 11th year. This percentage value varied in a descending manner over the period of prediction (i.e., from the 13th to the 34th year).

For the entire field, a good match (Fig. 13A) was obtained between the simulated and the observed daily oil- and water-production rates for the 34-year simulation period.

Field-production records indicate that a large number of wells were shut in between 7,300 and 8,030 days for administrative and economic reasons. Because of technical problems during construction of the input file for BOAST 3, individual wells could not be shut off or reactivated after the first 11 years. Consequently, the simulation is unable to match the daily field-production rates during the 2-year period when many producing wells were idle.

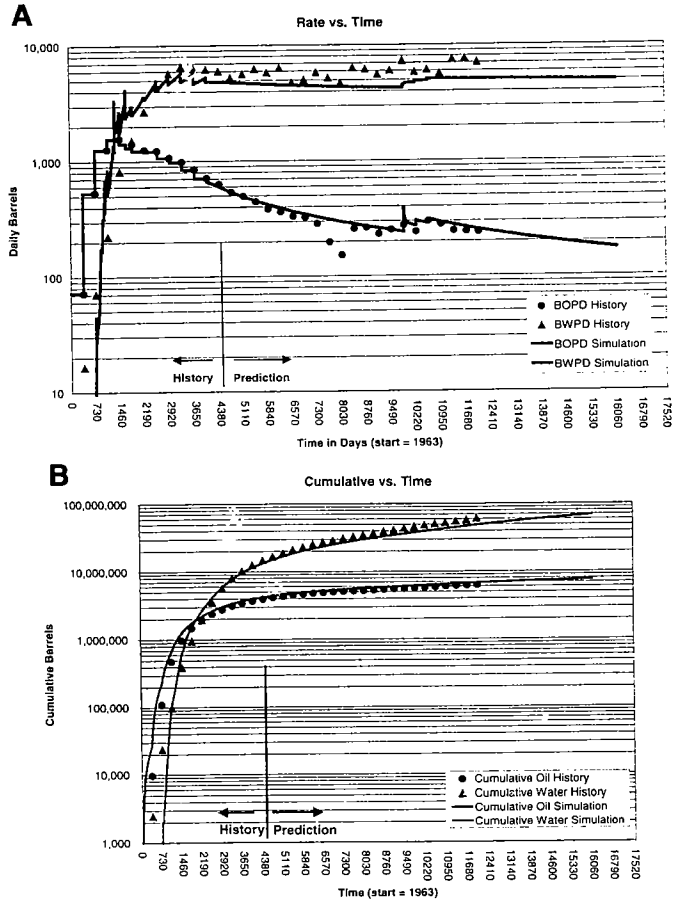

Figure 13. History match and performance prediction for Schaben field from BOAST 3 simulation. (A) Daily field-production rate versus time. (B) Cumulative field production versus time.

A good match within acceptable tolerances was obtained for the simulated and observed cumulative oil and water production for the field from 1963 to 1995 (Fig. 13B). Following these matches at a field scale, attention was focused on the performance of individual wells.

For individual wells, the degree of match achieved between simulated cumulative oil and water production and historical cumulative production was measured by a match ratio, which is defined as the ratio between historical cumulative production and predicted cumulative production for each well. A match ratio of 1.0 would indicate that simulated cumulative production is equal to the corresponding historical production. For cumulative oil production, most of the wells have a match ratio between 0.9 and 1.1, which indicates a good match on a well-by-well basis (Fig. 14).

In the case of water production, a majority of the wells had a match ratio varying from 0.8 to 1.2. However, several wells had a match-ratio value as high as 10 and some as low as 0.1 (this means that the simulator over- and under-predicted the water in some of the wells). The mismatch of water production from some of the wells may be due to inaccurate descriptions of the reservoir properties around these wells. As Schaben field has an active bottom-water drive, the vertical permeability in the reservoir, more specifically in the aquifer around the well, plays an important role in controlling water production at the well, especially if the reservoir is fractured. The vertical permeability in the aquifer and reservoir layers was

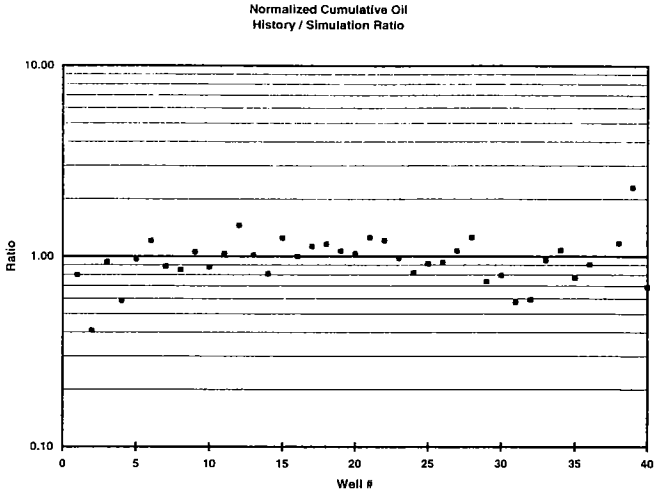

Figure 14. Ratio of historical oil production to simulated oil production for Schaben field.

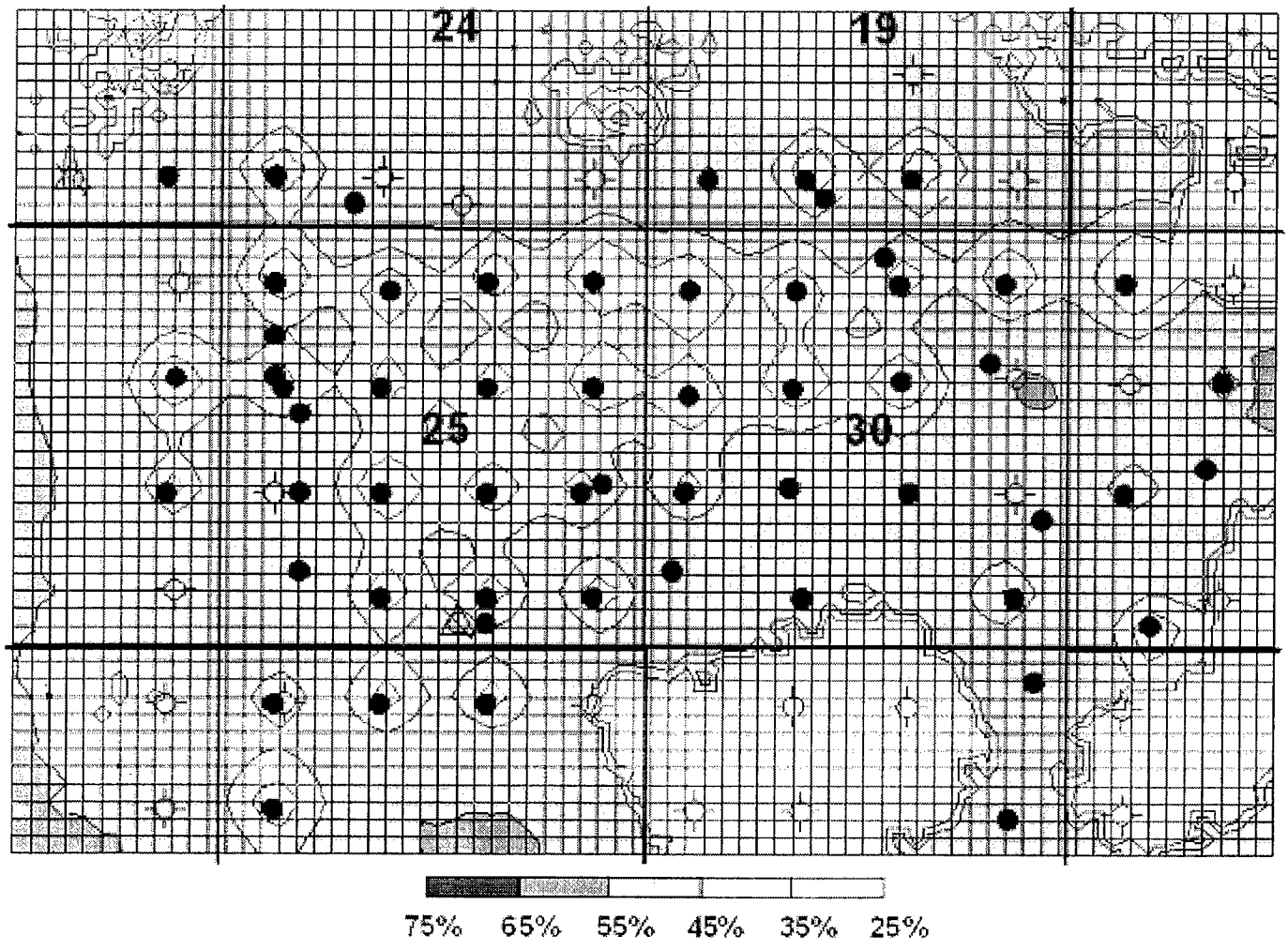

Figure 15. Map showing remaining oil saturation of layer 1 in Schaben field (time = 1973).

lowered for the grid cells surrounding the wells where the simulator predicted too much water production. This resulted in a significant reduction in water production from the affected wells.

Similarly, increasing the vertical permeability of the aquifer and reservoir layers around the wells with under-predicted water resulted in an increase of the simulated water production. This process of local adjustment of the vertical permeability was applied to every well to improve the match between the simulated results and the historical production volumes. Additionally, it is important to note that the historical water-production data for each well may not be accurate because it was derived from the reported oil-production volumes and the corresponding WORs from annual well tests. Each well was measured once a year, so the numbers may not represent well behavior throughout the entire year.

Oil-saturation maps generated from the simulation output at different time periods in the field history show a change in oil saturation across the field. The simulation indicates that by the end of 1973 (Fig. 15), areas of low oil saturation (S_o <45%) had started to develop around some wells, especially wells with a high production rate (e.g., NW¼ sec. 30).

Figure 16 shows that by the end of 1996, oil saturation around most wells had decreased to just above irreducible oil saturation (S_o <35%). However, significant pockets of high oil saturation (S_o >45%) are left unswept between the drainage areas of surrounding wells.

In today's economic climate, the efficient and cost-effective exploitation of remaining hydrocarbon reserves is a critical issue. Field management based on simulation studies allows an operator to "drill" "pseudo-wells" at a variety of locations and predict remaining recoverable reserves. The first step in choosing attractive infill locations is to determine which parts of the field contain the greatest remaining reserves. To accomplish this goal, a map of residual oil saturation–feet was generated by using cutoffs of pay height and oil saturation. As the relative-permeability curves used in the simulation indicate an irreducible oil saturation of 0.25, it will be difficult to produce oil from zones having an oil saturation that is near 0.30. A conservative oil-saturation cutoff of 0.40 was applied, along with a pay thickness cutoff >20 ft, to construct a map showing areas with the highest predicted infill potential (Fig. 17). All grid cells with a residual oil saturation <40% or with a net-pay thickness <20 ft were zeroed and left colorless on the map.

On the basis of the infill-potential map and consultation with one of the operators in Schaben field, three sites were

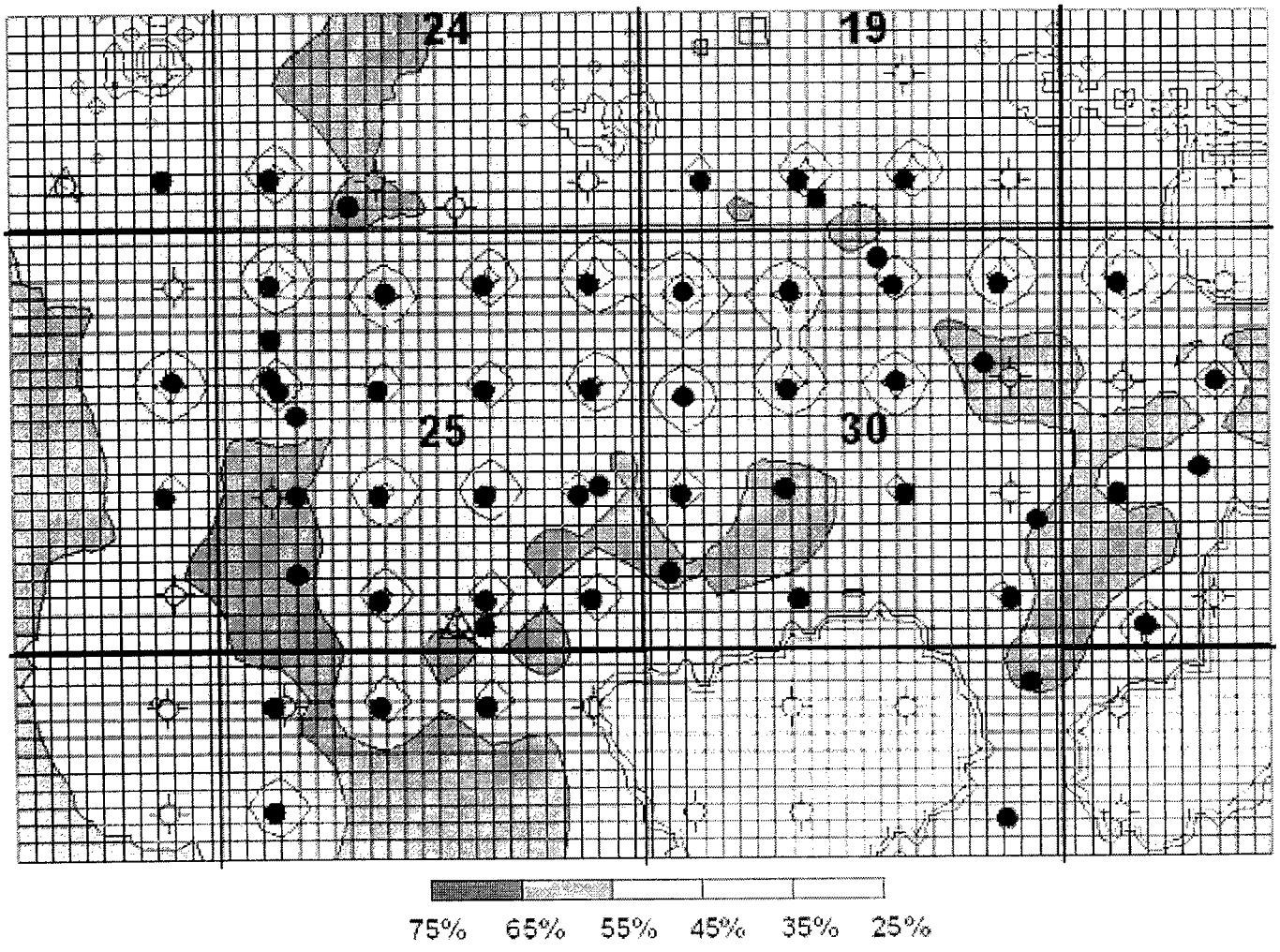

Figure 16. Map showing remaining oil saturation of layer 1 in Schaben field (time = 1996).

chosen to drill pseudo-wells. These sites are marked by white circles on the map in Figure 17. Subsequent simulation runs were carried out with these three pseudo-wells, with production starting in 1997. The simulation for the three pseudo-wells was run through the year 2006.

Daily field oil-production rates (Fig. 18), predicted by the simulator after the addition of the three pseudo-wells, indicate that significant additional oil production can be obtained from Schaben field if new wells are drilled in areas of greatest potential. Figure 19 is an oil-saturation map at the end of 2006 and includes the additional amount of oil expected to be recovered by three infill wells.

The three pseudo-wells were simulated to produce under a back pressure (i.e., a bottom-hole flowing pressure) equal to that of the nearest well at the end of the year 1995. The simulator predicted that the pseudo-well Moore BCP No. 3 (NE¼SW¼ sec. 30, T. 19 S., R. 21 W.) would produce a total of 47,200 BO and 227,600 BW over a period of 10 years. The simulator also predicted daily oil production above 10 bbl during the first 5 years.

IMPLICATIONS OF THIS STUDY

1. Practical application of cost-effective technologies in reservoir simulation enables the small independent producer to map remaining hydrocarbon reserves in marginal fields.

2. Simulation results allow proper field management by targeting infill drilling in areas of best potential.

3. PC-based reservoir simulation is a practical reality for small independent producers with limited resources.

4. Procedures demonstrated in this study provide a guide for geologic modeling, simulating, and managing similar reservoirs in Kansas and the Midcontinent.

ACKNOWLEDGMENTS

This paper is a part of the U.S. Department of Energy Kansas Class 2 Project (Cooperative Agreement DE-FC22-93BC14987). Work is in cooperation with Ritchie Exploration, Inc., of Wichita, Kansas. Geographix® provided access to mapping and gridding software.

REFERENCES CITED

Amyx, J. W.; Bass, D. M.; and Whiting, R. L., 1960, Petroleum reservoir engineering—physical properties: McGraw Hill, 610 p.

Carr, T. R.; Guy, W. R.; Franseen, E. K.; and Bhattacharya, Saibal, 1996, Enhanced carbonate reservoir model for an old reservoir utilizing new techniques: the Schaben Field (Mississippian), Ness County, Kansas [abstract]: American Association of Petroleum Geologists, Annual Meeting Abstracts, p. A23–A24.

Carr, T. R.; Green, D. W.; and Willhite, G. P., 1998, Improved oil recovery in Mississippian carbonate reservoirs of Kansas, Near

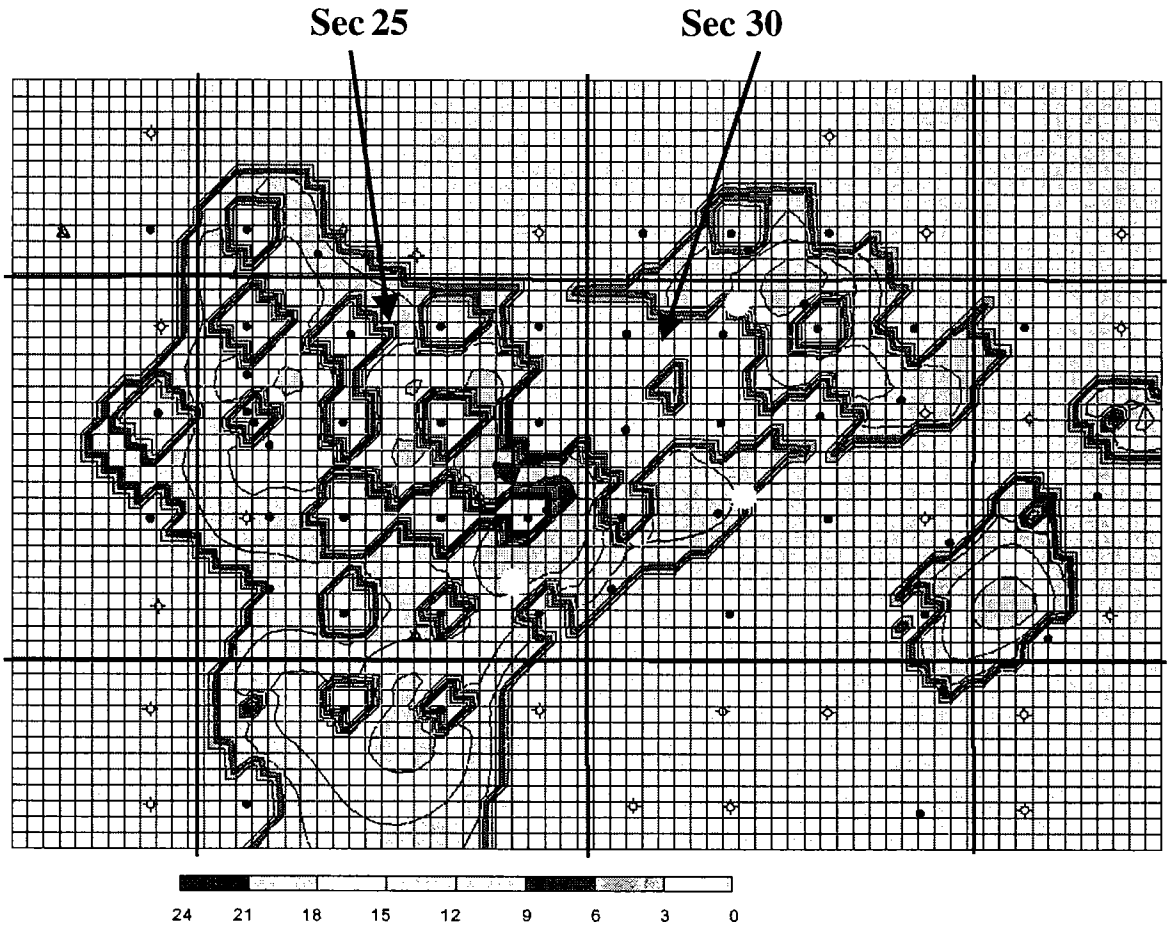

Figure 17. Map showing the vertical footage of oil satruation (in 5-ft increments), indicating the best infill potential, and the locations of three "pseudo-wells" (white circles) in Schaben field.

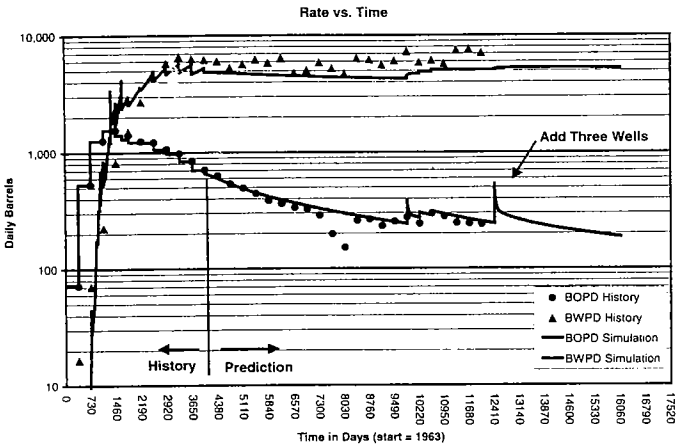

Figure 18. History match and performance prediction of Schaben field with three new "pseudo-wells" put on production from 1997.

Term, Class 2, annual report (September 18, 1994 to March 15, 1997): U.S. Department of Energy, Contract DE-FC22-93BC14987, 168 p.

Doveton, J. H., 1996, Wireline petrofacies analysis: Permian Basin Graduate Center, Course Manual, 98 p.

Doveton, J. H.; Guy, W. L.; Watney, W. L.; Bohling, G. C.; Ullah, S.; and Adkins-Heljeson, D., 1996, Log analysis of petrofacies and flow-units with microcomputer spreadsheet software: Tulsa Geological Society, Transactions of 1995 American Association of Petroleum Geologists, Mid-Continent Section Meeting, p. 224–233.

Guy, W. R.; Doveton, J. H.; Watney, W. L.; Carr, T. R.; and Bhattacharya, Saibal, 1996, Reservoir characterization utilizing a low cost resistivity–porosity crossplot and an interactive spreadsheet [abstract]: American Association of Petroleum Geologists, Annual Meeting Abstracts, p. A58.

Guy, W. R.; Carr; T. R.; Franseen, E. K.; Bhattacharya, Saibal; and Beaty, Scott, 1997, Combination of magnetic resonance and classic petrophysical techniques to determine pore geometry and characterization of a complex heterogeneous carbonate reservoir [abstract]: American Association of Petroleum Geologists, Annual Meeting Abstracts, Dallas, p. A45.

Guy, W. R.; Byrnes, A. P.; Doveton, J. H.; and Franseen, E. K., 1998, Influence of lithology and pore geometry on NMR prediction of permeability and effective porosity in Mississippian carbonates, Kansas [abstract]: American Association of Petroleum Geologists, Annual Meeting Abstracts, Salt Lake City, p. A264.

Louisiana State University, 1997, User's guide and documentation manual for BOAST 3 version 1.5: U.S. Department of Energy, Contract DE-AC22-91BC14831.

Mattax, C. C.; and Dalton, R. L., 1990, Reservoir simulation: Society of Petroleum Engineers Monograph Series, chapter 5, p. 46–51.

McCain, W. D., Jr., 1990, The properties of petroleum fluids: Pennwell Publishing Co., Tulsa, 548 p.

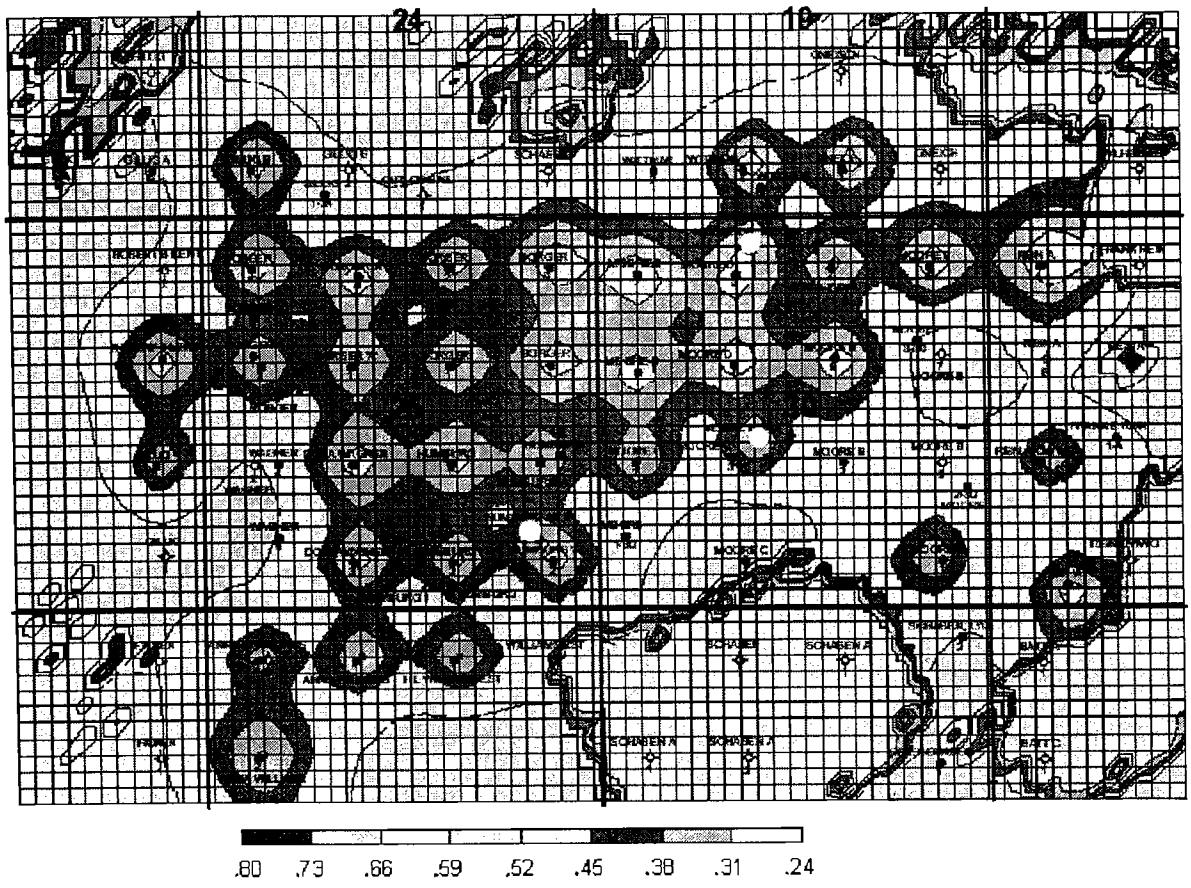

Figure 19. Map showing projected remaining oil saturation (fraction) in Schaben field (time = 2006), with three "pseudo-wells" (white circles) on production since 1997.

Biothem: A New Biostratigraphically Based Unit of Sequence Stratigraphy

H. Richard Lane
National Science Foundation
Arlington, Virginia

Mark W. Frye
KPMG LLP
San Antonio, Texas

Gary D. Couples
University of Glasgow
Glasgow, Scotland

ABSTRACT.—A biothem is a biostratigraphically based unit of sequence stratigraphy defined herein. Biothems are stratigraphic packages bounded by biostratigraphically recognized unconformities or their equivalent conformable counterparts. Biothem recognition is, therefore, critically dependent on zone-level or even on more detailed biostratigraphic data, which are commonly derived from the collection and interpretation of well-constrained vertical and lateral fossil assemblies that yield similarly meaningful zones. Because biothems are explicitly related to time, the lithofacies patterns revealed within them are, by definition, genetically related and represent rational vertical and lateral paleogeographic distributions. This makes biothems especially useful for creating detailed facies maps. Biothem morphology is predictable, especially in basins that were tectonically stable during biothem development.

The process by which biothems are identified and mapped is referred to herein as the Biothem Approach. Application of the Biothem Approach may yield more refined and time-stratigraphically accurate correlations in the same sequences than those previously derived solely from geophysical (seismic or wireline logging) or lithostratigraphic methods. This conclusion has proved valid for the thick cratonic carbonate-on-carbonate Paleozoic sequences of North America, and the resulting correlations significantly change the interpreted connectivity of rock sequences, altering scenarios of hydrocarbon migration and entrapment. It also has implications for other stratigraphically dependent fluids-based interests, such as mineralization and deep underground hazardous-waste isolation, which should be equally affected by improvements in correlation. The enhanced accuracy of time–space resolution made possible by the use of biothems may also provide details of basin development that are otherwise missed by the use of coarser resolution correlation techniques.

INTRODUCTION

Purpose of This Paper

We describe the Biothem Approach, a procedure that is especially applicable in subsurface areas where continuous core is available for biostratigraphic interpretation. We provide examples of how biothem use alters previous stratigraphic interpretations of some thick, cratonic, primarily carbonate middle Paleozoic sequences in North America. These revised interpretations have led us, for some areas, to create more meaningful facies maps, which in turn have enhanced our ability to predict prospective hydrocarbon migration and entrapment fairways where none were thought to exist. The enhanced time–space resolution made possible by the use of biothems as fundamental units of sequence stratigraphy has also permitted us to raise new questions regarding geodynamics and basin evolution. The enhanced accuracy of correlation afforded by use of the Biothem Approach may provide details of basin development that are otherwise missed by the use of coarser resolution correlation techniques. Such speculation has not been possible to date, because published models have not been tested by using such high-resolution, time-stratigraphically significant units as their foundation.

Current Practice

Sequences, as formally recognized lithostratigraphic units, were first utilized to describe North American cratonic-level stratigraphic packages (now termed *supersequences* by Mitchum and others, 1977) in a series of 1940s and 1950s publications by Sloss and a following of largely Northwestern University students and colleagues, culminating in the seminal paper on the cratonic sequences of the interior of North America by Sloss (1963). Since that time, a variety of se-

Lane, H. R.; Frye, M. W.; and Couples, G. D., 2000, Biothem: a new biostratigraphically based unit of sequence stratigraphy, *in* Johnson, K. S. (ed.), Platform carbonates in the southern Midcontinent, 1996 symposium: Oklahoma Geological Survey Circular 101, p. 183–196.

quence-stratigraphic units and accompanying terminologies have blossomed and are used widely by stratigraphers, all of whom are interested in achieving greater stratigraphic resolution and the ability to correlate rock units more accurately. The basis for many such units is the recognition of discontinuities in the stratigraphic record. Specialized sequence-stratigraphic units and terminologies have emerged, for example, for geophysicists (e.g., sensu seismic-stratigraphic terminology of Vail and others, 1977), sedimentologists (e.g., vertical facies profiles and sequences of Miall, 1986, 1990), and physical stratigraphers (e.g., the transgressive–regressive cycles of Grabau 1936, 1940, and Johnson and others, 1985, and the depositional systems of Fisher and McGowen, 1967, Brown and others, 1973, and Galloway, 1989a,b).

Sloss (1988) summarized "forty years of sequence stratigraphy" and provided his insights into the origins and practical applications and possible misapplications of sequence stratigraphy. Two key points Sloss made were that "(1) the stratigraphy of a cratonic region is divisible into rational and useful packages by reference to major regional unconformities, and (2) the history of such a region is divisible into tectonically characterized segments representing the times of accumulation of the succession of stratigraphic packages." In the same paper, Sloss further reflected that "the three-dimensional view of stratified rocks provided by subsurface exploration and the practical requirements of subsurface stratigraphic nomenclature in the service of industry and government produced an environment within which nonclassical approaches [to stratigraphy] were fostered and developed." We agree with Sloss's insights.

What sequence stratigraphy has lacked, in our opinion, is a unifying, biostratigraphically derived, relative-time-based architecture in which to relate the time-independent units recognized solely (especially in subsurface applications) by the use of other sequence-stratigraphic techniques. Our purpose in this paper is twofold: first, we wish to encourage the continued systematic collection and interpretation of the paleontologic data on which biothems are recognized. Second, we wish to encourage our colleagues to continuously challenge and improve subsurface correlations based solely on "stratigraphic imagery made available by multichannel, digitally recorded, and computer-massaged reflection seismography" (Sloss, 1988). As some of our examples demonstrate, a failure to challenge these correlations can lead to missed opportunities for resource exploration.

W. H. C. Ramsbottom (1977) proposed the first paleontologically based hierarchical classification of transgressive–regressive (T–R) cycles in the Namurian of Great Britain. He recognized three types of units based on the degree of resolution of their fossil content and called them, in descending order of magnitude: *synthem* (Chang, 1975), *mesothem,* and *cyclothem* (Wanless and Weller, 1932).

Since Ramsbottom's study, there have been a number of attempts to bridge biostratigraphic-based correlations with those based on other techniques. Our approach has focused on zonal or graphic correlation-based biostratigraphic units as the primary framework in which to evaluate correlations derived from other, more remote-sensing-based techniques (e.g., seismic and other geophysically based approaches, which typically consider biostratigraphic data only as a means of confirming major lithologic breaks). Our approach makes relative-time-stratigraphic relationships a forethought instead of an afterthought. The Biothem Approach has proved most useful for identifying the time-stratigraphic relationships of rock sequences in subsurface regimes for which nonbiostratigraphic approaches are of limited value.

DISCUSSION

Biothem Definition

Biothems are integrated regional wedge- or lens-shaped sequence-stratigraphic units. Their identification, however, is based solely on their fossil constituents. Biothem morphology is predictable but is dependent on basin size, physiography, and the lack of post-depositional tectonic disruption. Ideally, biothems are bounded at their cratonward extremities (their depositionally updip regions) by biostratigraphically recognizable unconformities (lacunae). Biothems tend to be relatively thinner in these regions than they are shelfward, where they are relatively thicker and more nearly conformable with underlying and overlying biothems. Farther basinward, but depending on both basin configuration and turbidite development, biothems are commonly thinner in comparison to their shelfward extents. In their most basinward extents, biothems may be bounded by biostratigraphically recognizable unconformities or may be conformable with underlying and overlying biothems. In some basins, the most basinward extents of biothems are extremely thin, having been deposited during conditions of starved sedimentation. These highstand, sedimentologically starved intervals commonly represent the bounding surfaces of thicker, more rapidly deposited lowstand biothems.

The primary constraint on biothem use, therefore, is that the rock successions being subdivided into biothems for correlation purposes must contain fossil assemblages that yield meaningful (ideally zonal-level) relative-age relationships or are sufficiently complete (datawise) to be successfully graphed against another succession/database (well or outcrop) of the same age using Shaw's (1964) graphic-correlation approach (see depositional sequences of Stein and others, 1995, for biothems defined through this approach).

As recognized to date, biothems have an internally consistent distribution of faunal and/or floral components (e.g., faunal and marine floral components exhibit a progression of shallow- to deeper water specific species and species groupings, as well as facies groupings that represent an internally consistent and logical sequence of depositional environments; floral components, when recovered, can be related to a natural progression of nonmarine environments). The use of biothems as primary sequence-stratigraphic units places the emphasis on relative time as the foundation on which units are recognized. The Biothem Approach provides a sequence-stratigraphic tool for use in applications in which the understanding of time-stratigraphic relationships is critical. It is hoped that biothem use will elevate relative time to a more prominent position in sequence stratigraphy.

Biothem Recognition and Approach

Biothems, herein, are recognized by following a standardized approach, the Biothem Approach, which is an outgrowth

of detailed biostratigraphic work conducted in the petroleum industry during the past two decades. The Biothem Approach was developed to enhance resource exploration and exploitation in carbonate-on-carbonate sequences, but it can be equally applied to fossiliferous clastic successions. The Biothem Approach is facilitated by access to large, integrated paleontologic databases such as those at major academic and industrial research centers.

The Biothem Approach leads to the recognition of biostratigraphically defined stratigraphic packages that are useful in resolving problems of basinal or regional correlation. A biothem framework also facilitates the recognition of depositional sequence boundaries that are not commonly resolvable by geophysical methods (e.g., carbonate-on-carbonate, sand-on-sand, and shale-on-shale sequences) or traditional lithostratigraphic evidence. The approach consists of a series of steps that center around recognizing significant vertical biostratigraphic changes (e.g., unconformities, zonal boundaries, graphic correlation, and composite standard terraces) that define upper and lower biothem boundaries.

In its application to hydrocarbon exploration, biothem identification proceeds by recovery, taxonomic identification, and biostratigraphic interpretation of paleontological collections from wellbore-derived cores and cuttings in a series of wells. Once biothems are identified, geophysical-well-log correlations are "recalibrated" to biothems rather than to sometimes distant and commonly irrelevant surface-defined lithostratigraphic formations, as is common petroleum-industry practice. This integration of biostratigraphic, lithostratigraphic, and geophysical-log data allows for the creation of cross sections that are based on biothems. This architecture then facilitates arrangement of lateral and vertical facies sequences to their proper distribution in relative time and space. The integrated dataset may in some cases lead to substantial refinement of seismically derived correlations, which, when viewed in a relative-time-stratigraphic sense, lead to enhanced overall data quality and the ability to meet play objectives.

To date, subsurface biothems have been readily recognized in cratonic Paleozoic carbonate-on-carbonate successions in which their boundaries cannot be recognized initially by some correlation tools (e.g., seismic stratigraphy or downhole geophysical logs). Although these successions can contain clastic constituents, the typical lack of discernible velocity contrast between carbonate units assignable to different biothems makes the use of continuous cores indispensable for biothem identification. Biothems are also readily recognized in fossiliferous siliciclastic turbidite successions. Because biothems are typically recognized by using high-resolution biostratigraphic-correlation techniques, even basinward strata that represent sedimentologically "starved" intervals usually can be assigned to the correct biothem if their fossil constituents can be recovered. Generally, these starved intervals form important bounding surfaces in the definition and recognition of lowstand biothems (e.g., North Sea Paleogene study of Stein and others, 1995) in basinal settings.

Key to the concepts presented herein is a refined understanding of both Mississippian conodont taxonomy and evolution. Conodonts are phosphatic, toothlike microfossils belonging to extinct organisms of uncertain biological affinity (Pander, 1856; Sweet, 1989), but because of their widespread occurrence, ease of recovery, and well-understood taxonomy, they are useful for refined time-stratigraphic correlation of Paleozoic units and for the recognition of biothems in our studies. The Mississippian conodont zonation used herein and its relationship to North American and European stages and series are shown in Figure 1. This zonation differs somewhat from that of the "standard" conodont zonation for rocks of this age as synthesized by Lane and others (1980), because it is one commonly used within Amoco Production Co. and the one within which data for this study have been synthesized. The numbers along the right margin of Figure 1 (modified

STAGES EUR.	SERIES N.A.	ZONES (of authors)	FU modified from LANE, 1974
NAMURIAN	CHESTERIAN	*muricatus* U	14
		muricatus L	13
		unicornis	12
		naviculus	11
VISEAN		*G. bilineatus - C.altus*	10
	MERAM.	*G. bilineatus C. charactus*	9
		A. scalenus Cavusgnathus	8 c b a
	OSAGEAN	*texanus*	7
			6
		anchoralis | *latus*	5 b a
			4U
TOURAISIAN		Upper *typicus*	4L
		Lower *typicus*	3 b a
	KINDERHOOKIAN	*isosticha* | Upper *crenulata*	2
			1F
		Lower *crenulata*	1E
		sandbergi	1D
		Upper *duplicata*	1C
		Lower *duplicata*	1B
		sulcata	1A

Figure 1. Mississippian conodont faunal-unit (FU) scheme, modified from Lane (1974, 1982).

from Lane, 1974, 1982) are a shorthand reference tool. Numbers equate to the zones, which are also referred to in this study as *faunal units*. The marine Mississippian System, as developed in North America, can be subdivided (as shown by the letters in the right-hand column of Fig. 1) into subzones, for a total of 24 paleontologically recognizable units. This scheme represents the most refined biostratigraphic control available for rocks of this age and represents the compilation of works of numerous authors. The relative precision of the conodont zonation, combined with the substantial Mississippian paleontologic database assembled at Amoco Production Co. during the past two decades, is the basis for our results.

Figure 2 illustrates a cross section of one complete and one partial biothem derived from the analysis of an integrated paleontological database, representing collections from the type Mississippian System of North America (Lane, 1978). The recognition of the Fern Glen/Burlington Biothem is based primarily on its faunal constituents and secondarily on its lithology and thickness. The numbers shown on the right and left of the figure show relative time control and equate to the conodont zonation shown in Figure 1. The maximum thickness of this biothem is approximately 500 ft. The cross section extends from southeastern Iowa to extreme southern Illinois (see map positions of localities and transect in Figure 5 and in Lane, 1982). It is important to note that the two biothems shown in Figure 2, as well as the other Mississippian examples referred to in this study, are composed almost entirely of carbonate-rock sequences. Unconformity recognition in these sequences is not always obvious when only lithologic data are evaluated.

Figure 3 depicts the same biothems as those in Figure 2 but includes their interpreted depositional environments as set within the temporal framework afforded by the Biothem Approach. Figure 3 demonstrates that biothems consist of both an internally consistent and logical sequence of depositional environments. Such consistencies are not always obvious until the relative ages of the facies are known. Lithofacies interpretation without a temporal framework can lead to erroneous paleogeographic interpretations, which in turn can lead to erroneous or "flawed" basin-evolution scenarios. The six most important characteristics of a biothem are as follows:

1. Wedge- or lens-shaped bodies of rock that are recognized solely by paleontologic methods.

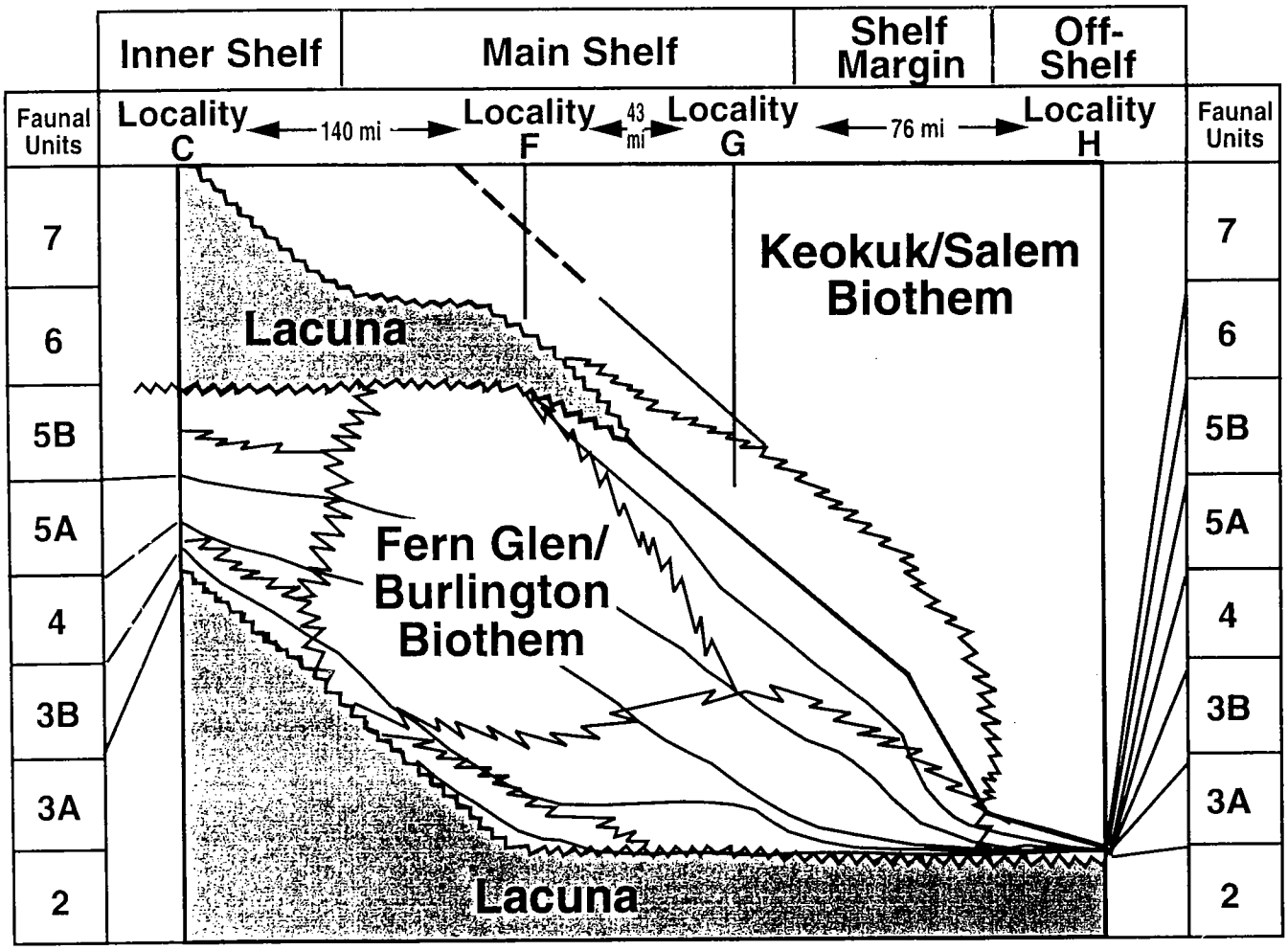

Figure 2. Cross section from southeastern Iowa to extreme southern Illinois (from Lane, 1978), illustrating the Fern Glen/Burlington Biothem overlain by the Keokuk/Salem Biothem. Numbered boxes on right and left represent a portion of the conodont faunal-unit scheme of Lane (1974, 1982) and Figure 1 herein. Vertical scale: 1 cm = approximately 2.5 m, or 1 in. = approximately 54 ft. Vertical lines represent missing faunas; wavy lines are unconformities; zigzag lines are lithofacies boundaries; straight lines are faunal boundaries. Localities and transect are shown in Figure 5.

2. Bounded updip by biostratigraphically defined unconformities (lacunae) in sea-level highstand settings.

3. Commonly conformable in near-shelf-edge or shelf-slope environments.

4. Commonly bounded downdip by sedimentologically starved intervals or biostratigraphically defined unconformities (hiatuses).

5. Internally consistent in their faunal and floral components.

6. Internally consistent in their sequence of depositional environments.

As a rule, a minimum of two wells or outcrops is necessary to identify biothem sequences. To date, we have informally named biothems on the basis of their established formational terminology; they could, however, be given new names in similar fashion to the rules set forth in the North American Stratigraphic Code (North American Commission on Stratigraphic Nomenclature, 1983).

The Biothem Approach has four major utilities:

1. Subdivision of stratigraphic successions into time-based, genetically related stratigraphic packages.

2. Construction of accurate relative-time-based paleogeographic maps.

3. Evaluation of subsurface correlations, which, in an exploration application, can lead to enhanced opportunities for resource exploration and exploitation.

4. Regional tectonic–stratigraphic analyses based on accurate time-stratigraphic interpretations.

Biothems Compared to Other Units of Sequence Stratigraphy

Figure 4, which we have modified from Busch and Rollins (1984), depicts possible relationships between biothems and some other units of stratigraphic analysis. No attempt has been made to include all such sequence-stratigraphic units that might be compared and contrasted to biothems. Our modifications of Busch and Rollins's original figure include the deletion of some less pertinent (for our purposes) studies they originally included; the addition of units described by Wheeler (1964), Johnson (1971), and Johnson and others (1985); and the addition of biothems. We interpret all of Ramsbottom's (1977) unit types to be biothems, because they are biostratigraphically defined in the same manner. Other units shown in Figure 4 are also recognized by discontinuities, but not those based solely on biostratigraphic evidence.

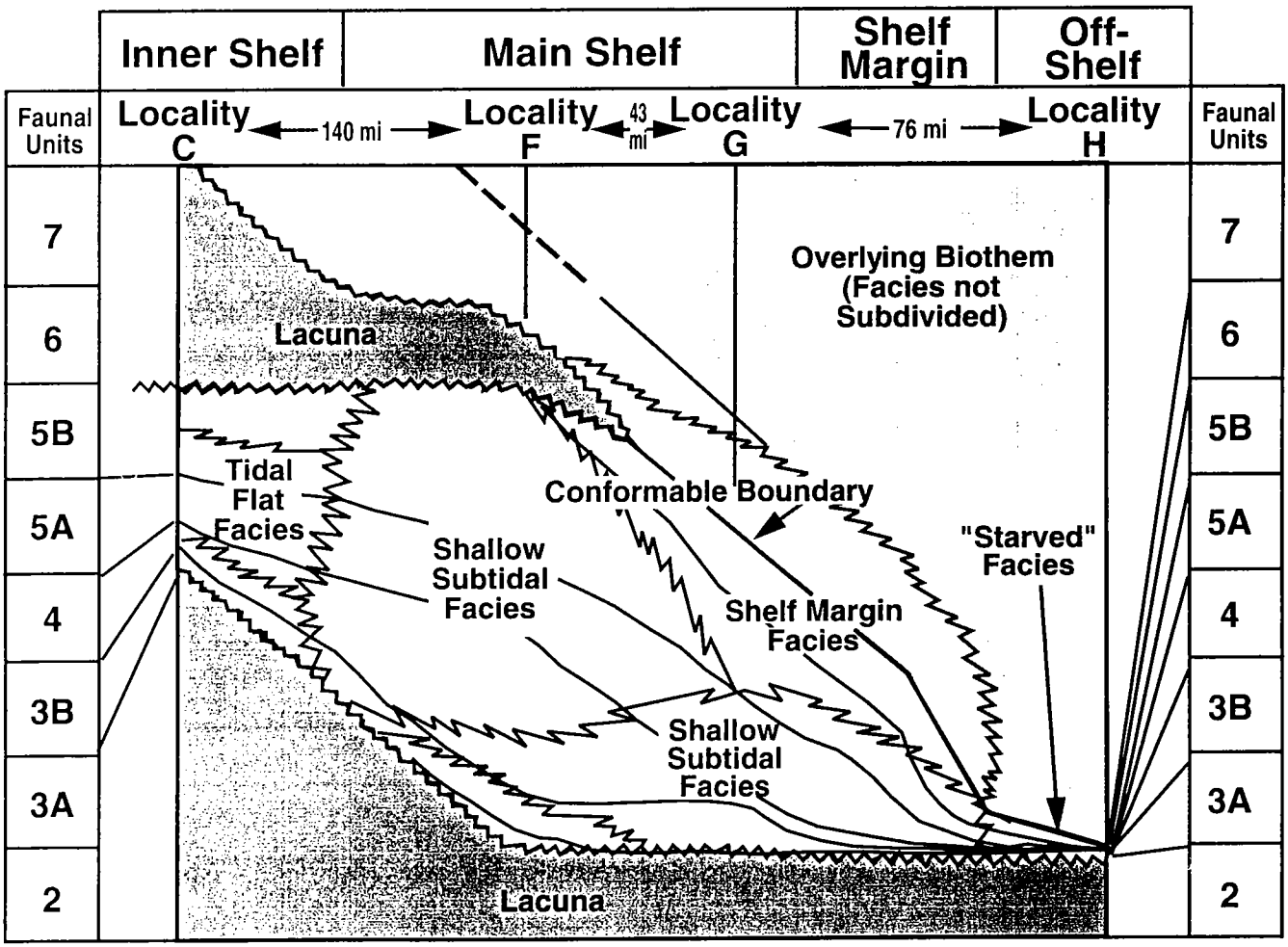

Figure 3. Modification of Figure 2, showing the natural progression of paleoenvironments when placed within the temporal framework afforded by the Biothem Approach. Localities and transect are shown in Figure 5.

Magnitude of Transgressive-Regressive Unit	Units of Stratigraphic Analysis				
	Vail et al., 1977	Ramsbottom 1977	Anderson and Goodwin, 1980 & 1982 and Goodwin & Anderson, 1985	Wheeler, 1964; Johnson, 1971; Johnson et al., 1985	Lane, Frye, & Couples (this study)
1st Order: 225 to 300 million years	1st Order Depositional Sequences				
2nd Order: 65 million years	2nd Order Depositional Sequences	Synthems		Depophases	
3rd Order: 8 to 10 million years	3rd Order Depositional Sequences				
4th Order: 0.8 to 1.5 million years		Mesothems		T-R Cycles	Biothems
5th Order: 400 to 500 thousand years		Cyclothems	Cyclothemic PAC Sequences		
6th Order: 100 to 225 thousand years			Punctuated Aggradational Cycles (PAC)	PACs	

Figure 4. Chart (modified from Busch and Rollins, 1984) comparing commonly used units of stratigraphic analysis with those of biothems as described herein. Note that biothem utility for construction of detailed, time-significant lithofacies maps diminishes above dashed line.

We do not attempt to promote biothems as "be-all" and "end-all" units of sequence-stratigraphic correlation. Rather, we believe that the examples provided in this study demonstrate that the Biothem Approach will provide more time-stratigraphically significant correlations in certain settings than will any other correlation technique. Busch and Rollins's use of absolute time values in the left-hand column of Figure 4 is perhaps one means of comparing the relative duration of time as represented by these units, although we are not certain that the original authors of the listed units would agree with the assignment of these or perhaps any time values to their units of stratigraphic analysis. The time interval represented by a biothem is completely dependent on the interval represented between its bounding surfaces. Biothems, as described herein, are units that may represent any useful (for the purpose of the sequence stratigrapher) biostratigraphically resolvable time-stratigraphic magnitude. The use of the Biothem Approach should be limited to areas in which biothem boundaries provide greater time-stratigraphic control than the use of other relative-time indicators.

Biothems also contrast in definition with seismic and physical stratigraphic units defined by Vail and others (1977), Brown and others (1973), Galloway (1989a,b), Miall (1986, 1990, 1991), and others by making time, as interpreted by the fossil record, their main element of definition. The biothem examples in this study generally represent time intervals of greater duration and magnitude than the punctuated aggradational cycles (PACs) of Anderson and Goodwin (1980, 1982) and Goodwin and Anderson (1985). Undoubtedly, the Biothem Approach may define units similar to PACs in areas where paleontological control is abundant and where the evolutionary successions are well known.

Biothems also differ fundamentally from both the allostratigraphic units defined in the 1983 North American Stratigraphic Code and the unconformity-bounded stratigraphic units of Salvador (1987). First, biothems are exclusively biostratigraphically defined. Both the Code and Salvador (1987, p. 234) clearly state that their allostratigraphic and unconformity-bounded stratigraphic units are not so defined. Second, biothems are not just restricted to that portion of their extent where they are bounded by unconformities, an important component of Salvador's unconformity-bounded stratigraphic units and the Code's allostratigraphic units. Although biothems are most easily identified in areas where they are bounded by biostratigraphically recognizable unconformities, they continue into and can be identified in areas of continuous deposition.

Benefits and Expected Benefits from Using the Biothem Approach

The Biothem Approach provides substantially more biostratigraphic—and thus more relative-time-stratigraphic—input into sequence stratigraphy by beginning with relative-time-based correlations rather than those based solely on lithostratigraphic or geophysical evidence. Previously, there has been a tendency to force-fit biostratigraphic evidence into units already defined by other means. As a consequence, biostratigraphic input into sequence stratigraphy has been underutilized, or worse, overlooked, ignored, or regarded as unnecessary duplication, especially in geographic areas where such input may be crucial to resolve long-standing correlation problems. There are no solely lithostratigraphic or geophysical data, or other practical procedures, that can adequately replace the fundamental time-stratigraphic architecture and temporal/spatial-based environmental information that the use of the Biothem Approach contributes to the sequence-stratigraphic process.

EXAMPLES

Biothems of the Illinois Basin: Fern Glen/Burlington Biothem

Definition and Paleogeographic Distribution

The Fern Glen/Burlington Biothem, originally defined and recognized in the Mississippi Valley (Lane, 1978), is shown in Figures 2 and 3 (modified from Lane, 1982) and is an example of the first utility of biothems discussed above (see earlier section, "Biothem Recognition and Approach"). In general, the thick Mississippian carbonate sequences surrounding the North American Transcontinental arch have been poorly understood from a time-stratigraphic perspective and typically have been treated as thick, monotonous successions with little internal complexities in a time-stratigraphic sense (see Rascoe and Adler, 1983). For example, distinguishing age relationships between "Burlington" and "Keokuk" carbonates in the western part of the Illinois basin cannot be easily achieved lithostratigraphically. In the area of St. Louis, Missouri, these two important formations, representing the contact between rocks of lower and middle Visean age in western Europe, are simply combined by local geologists to read *Burlington–Keokuk*. However, by using the

Biothem Approach, as described herein, this important contact and the significant faunal changes separating these two formations can be consistently distinguished regionally.

Figure 5 is an isopach and paleogeographic map of the rocks that represent the Fern Glen/Burlington Biothem in the Illinois basin and its equivalent interval of Mississippian time in adjacent areas surrounding the Transcontinental arch. This map represents sediment accumulations in central and western North America during a period lasting no more than 2 million years. During most of the Mississippian Period, the Transcontinental arch (TA; Eardley, 1962) was a major tectonically positive feature that extended in a northeast to southwest direction relative to present-day North America. Surrounding the TA were broad shelves on which carbonate-producing organisms thrived and produced tens of hundreds of meters of carbonate sediments, especially during Early and middle Mississippian time.

These carbonate areas typically thicken basinward and thin abruptly into "starved" sequences (Lineback, 1966, 1969; Rose, 1976; Lane, 1978, 1982; Lane and DeKeyser, 1980; Gutschick and Sandberg, 1983). Farther basinward, clastic sequences represented by the Borden delta (Lineback, 1966) to the northeast, the Stanley clastic tongue of the Ouachita trough (Graham and others, 1975), the Barnett and Tesnus Formations of Texas, and possibly the Chainman and Diamond Peak Formations of Nevada west of the TA (Rose, 1976) were shed from highlands in a cratonward direction. These clastic sequences smothered the Late Mississippian carbonate-producing organisms that lived on the shelves. Carbonate deposition was also affected by the gradual tectonic emergence of the TA, which is evidenced by the progressively more nonmarine sequences that were developed in the Early Pennsylvanian, as represented by the Morrowan Series. The Fern Glen/Burlington Biothem is an example of a unit that can be widely traced by using the Biothem Approach, thus permitting construction of the paleogeographic map (Fig. 5) for this interval.

Hugoton Embayment

Using the Biothem Approach for subsurface investigations of mature hydrocarbon provinces can lead to the identification of new exploration trends as well as a better understanding of the stratigraphic distribution of established reservoirs. For example, Mississippian hydrocarbon production has been established along the western side of the central Kansas uplift and Hugoton embayment for over 50 years, yet the reported reservoir intervals are generally referred to as *Mississippian carbonates, Osage,* or *Meramec*. Our work in this area, using the Biothem Approach, allowed us to recognize two main stratigraphically limited reservoir intervals: (1) the Keokuk/Salem Biothem trend along the western side of the central Kansas uplift, wrapping in an arcuate pattern westward to the Las Animas arch area in eastern Colorado, and (2) the St. Louis/Ste. Genevieve Biothem trend in a north–south direction in the central part of the Hugoton embayment.

Conventional Petroleum-Industry Correlations—Eastern Colorado and Western Kansas Subsurface

Figure 6 is a transect from the Las Animas arch in eastern Colorado (left) to the central Hugoton embayment of the Anadarko basin of southwestern Kansas. The transect illustrates Mississippian subsurface-formation-based correlations commonly used in the petroleum industry (see Rascoe and Adler, 1983). On the Las Animas arch, five conformable Mississippian formations, which are approximately 350 ft thick and bounded by the Ordovician–Mississippian and Mississippian–Pennsylvanian systemic unconformities, are recognized. Seven formations, approximately 1,000 ft thick and bounded by the same unconformities, are recognized from the subsurface of the Hugoton embayment. These formations bear names derived from the Mississippi Valley stratotypes. The conventional industry correlation made between the two areas suggests uniformly northwestward (TA-ward) thinning units. Dolomite-, chert-, and porosity-distribution maps based on these intervals suggest that porosity is relatively continuous within the same unit. These correlations are still commonly interpreted in the industry to have time-stratigraphic significance.

Biothem Correlations—Eastern Colorado and Western Kansas Subsurface

In contrast, Figure 7 illustrates correlations of the same transect after application of the Biothem Approach and is another example of utility 1 as discussed in the section "Biothem Recognition and Approach." Note that in addition to the Mississippian System bounding unconformities, three additional intra-Mississippian unconformities can be recognized.

If these relationships are displayed in the form of a time-stratigraphic transect, as shown in Figure 8, a series of four Mississippian biothems becomes obvious. The darker areas in the transect represent rocks containing conodont faunas from the associated numbered faunal unit (see Fig. 1). Unconformities were identified by analysis of conodont faunas above and below unconformities. The lighter areas in the figure represent the time intervals from which no conodont faunas were recovered. These biothems are bounded by unconformities that have been previously undetected using the wireline-log-based conventional correlation techniques. The correlations shown on the time-stratigraphic transect benefited also from a series of major cores taken by Amoco, which provided detailed paleontologic and lithostratigraphic control for this study. Note also that Figure 8 reveals a possible regional stratigraphic trap with the wedgeout of the porous Fern Glen/Burlington Biothem before reaching the Las Animas arch area, a relationship previously unrecognized. This interpretation is tied to the conodont zonation, as shown on the left and right. Sedimentologic studies at Amoco indicate these biothems to be largely intact, with little post-depositional removal of sediments in the updip areas. This is based on unpublished work by Jack Babcock, Mark Frye, and Robert Handford (all formerly or currently with Amoco), who have found facies representing progressively restricted environments of deposition in a stratigraphically updip direction, ultimately becoming tidal-flat facies near the Transcontinental arch.

Given a sufficiently dense biostratigraphic database, the subcrop of the youngest two biothems directly below the Pennsylvanian can be mapped (Fig. 9), illustrating that accurate relative-time-based paleogeographic maps can be constructed by using this approach (see utility 2 of biothems discussed earlier). For geographic reference, note the Colorado–Kansas

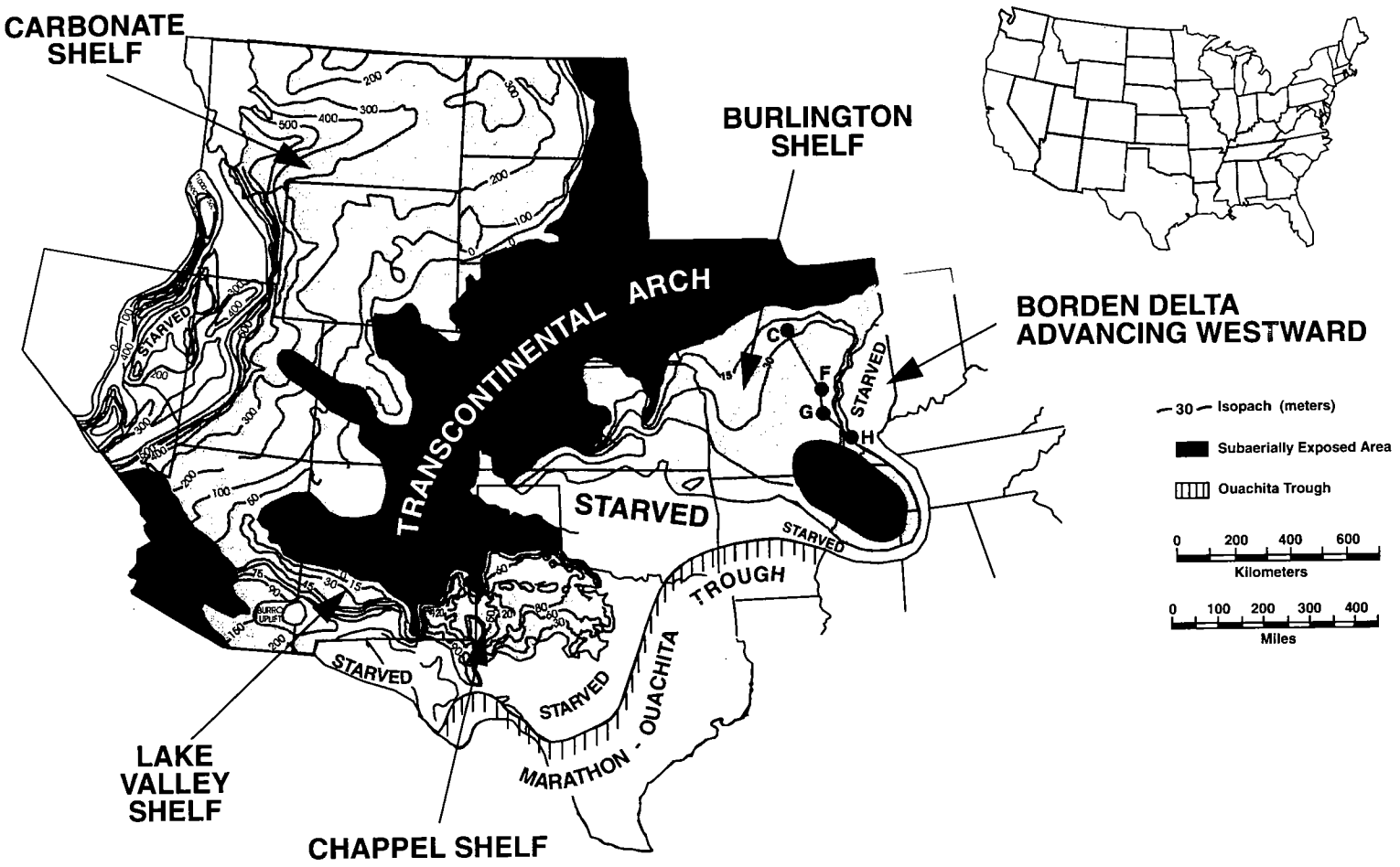

Figure 5. Map showing isopach of late Early Mississippian (faunal units 3–5; see Fig. 1) Fern Glen/Burlington Biothem and correlative biothems encircling the North American Transcontinental arch. Biothem boundaries and names do not necessarily coincide with formational contacts but are assigned to approximate the formational intervals of relative time most closely associated with the formation at its type locality. In this regional isopach map, other units besides the Fern Glen/ Burlington Biothem are shown. Localities and transect used in Figures 2 and 3 are shown.

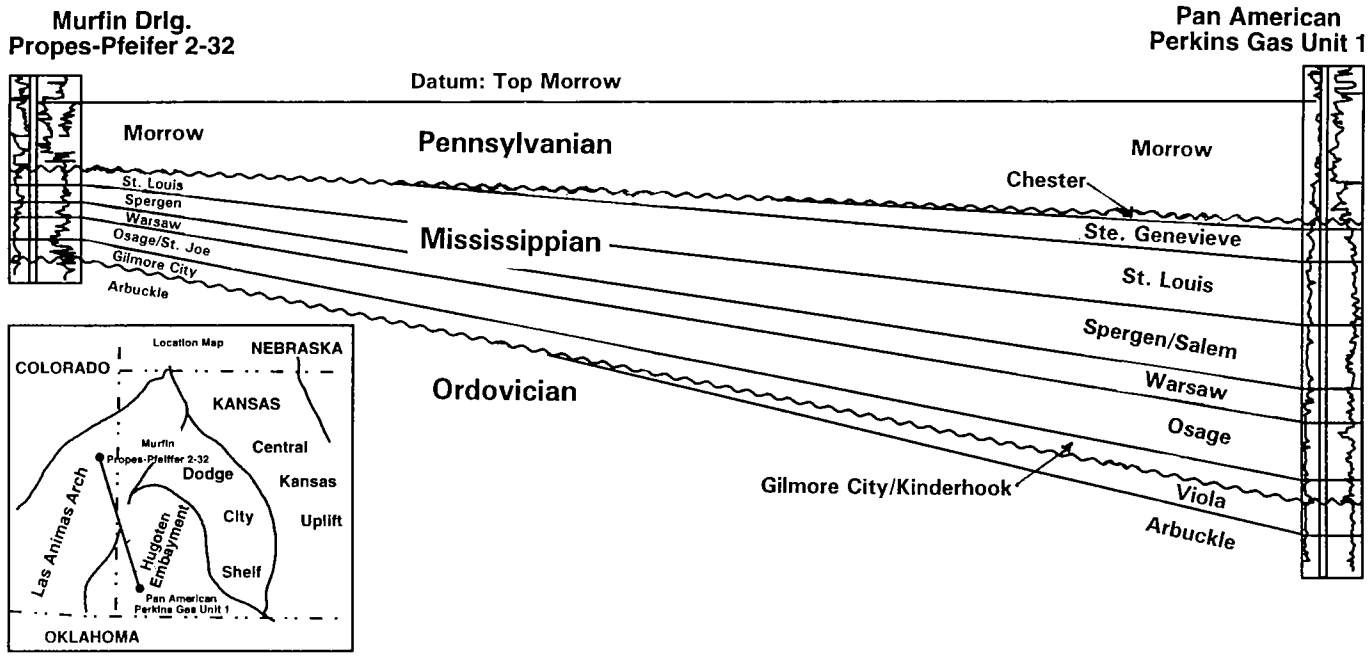

Figure 6. Conventional petroleum-industry subsurface correlations of Ordovician through Early Pennsylvanian rocks from the eastern Colorado Las Animas arch area to the central Hugoton embayment of southwestern Kansas, on the basis of wireline logs. Note that the only unconformities shown on this transect occur at the Ordovician–Mississippian and Mississippian–Pennsylvanian contacts. Geographic location of transect shown on map at lower left.

and Kansas–Oklahoma borders. The line extending from east-central Colorado into extreme southwestern Kansas indicates the position of the previously shown transects (Figs. 6–8). We emphasize that this subcrop map has been created on the distribution of biothems recognized by conodont faunas rather than on the basis of wireline-log-derived pseudo-lithostratigraphic units. The map illustrates the position of two major sub-Pennsylvanian subcrop bands (Keokuk/Salem and St. Louis/Ste. Genevieve Biothems). This approach has allowed more accurate mapping of the stratigraphic distribution of existing Mississippian hydrocarbon production at the Mississippian–Pennsylvanian unconformity.

Two major hydrocarbon-productive trends exist: (1) the subcrop of the Keokuk/Salem Biothem paralleling the central Kansas uplift, wrapping around to the Las Animas arch area, and (2) within the subcrop of the St. Louis/Ste. Genevieve Biothem in a general north–south trend in the central part of the Hugoton embayment.

Figure 10 illustrates the predicted subcrop of the Fern Glen/Burlington Biothem beneath the Keokuk/Salem Biothem. This subcrop, previously unrecognized (and undrilled), set up an entirely new play concept, which led to an extensive drilling and coring program by Amoco in the early and middle 1980s. The development of this play concept illustrates biothem utility 3, as discussed previously (see "Biothem Recognition and Approach"). The locations of the wells from which the following cores were acquired and used in this study are shown in Figure 10 and are as follows:

Champlin 558 No. 1 Amoco B, C SE¼SE¼ sec. 23, T. 13 S., R. 44 W., Cheyenne County, Colorado

Amoco No. 3 Max Cohen C, C SE¼NE¼ sec. 27, T. 25 S., R. 38 W., Kearny County, Kansas

Amoco No. 1 Puyear, C NW¼SW¼ sec. 23, T. 28 S., R. 40 W., Stanton County, Kansas

Amoco No. 1 Nordling, SW¼SE¼NE¼ sec. 30, T. 29 S., R. 39 W., Stanton County, Kansas

Amoco No. 1 Breeding Gas Unit F, sec. 34, T. 31 S., R. 33 W., Morton County, Kansas

Amoco No. 1 McPherson & Citizens State Bank, SW¼NE¼SW¼ sec. 28, T. 29 S., R. 39 W., Stanton County, Kansas

Murfin No. 2-32 Propes-Pfeiffer, SW¼SW¼ sec. 32, T. 12 S., R. 44 W., Cheyenne County, Colorado

Amoco No. 1 Ray Brian, sec. 7, T. 30 S., R. 33 W., Haskell County, Kansas

Amoco No. 1 I. L. King, sec. 13, T. 30 S., R. 33 W., Haskell County, Kansas

Amoco No. A-3 W. M. Wilson, SE¼NW¼ sec. 30, T. 30 N., R. 33 W., Haskell County, Kansas

Amoco No. 1 R. K. Bounds, SE¼NE¼ sec. 17, T. 18 S., R. 42 W., Greeley County, Kansas

Pan American No. 1 Perkins Gas Unit, NE¼SW¼ sec. 28, T. 31 S., R. 40 W., Morton County, Kansas

The results of the coring and consequent biostratigraphic analyses indicated that the updip extent of the Fern Glen/Burlington Biothem, as shown in Figure 10, had been overestimated and that the subcrop was actually much farther south and east in southern Kansas. These results did, however, set up other hydrocarbon-play possibilities that are still being evaluated. However, this restriction in the distribution of the Fern Glen/

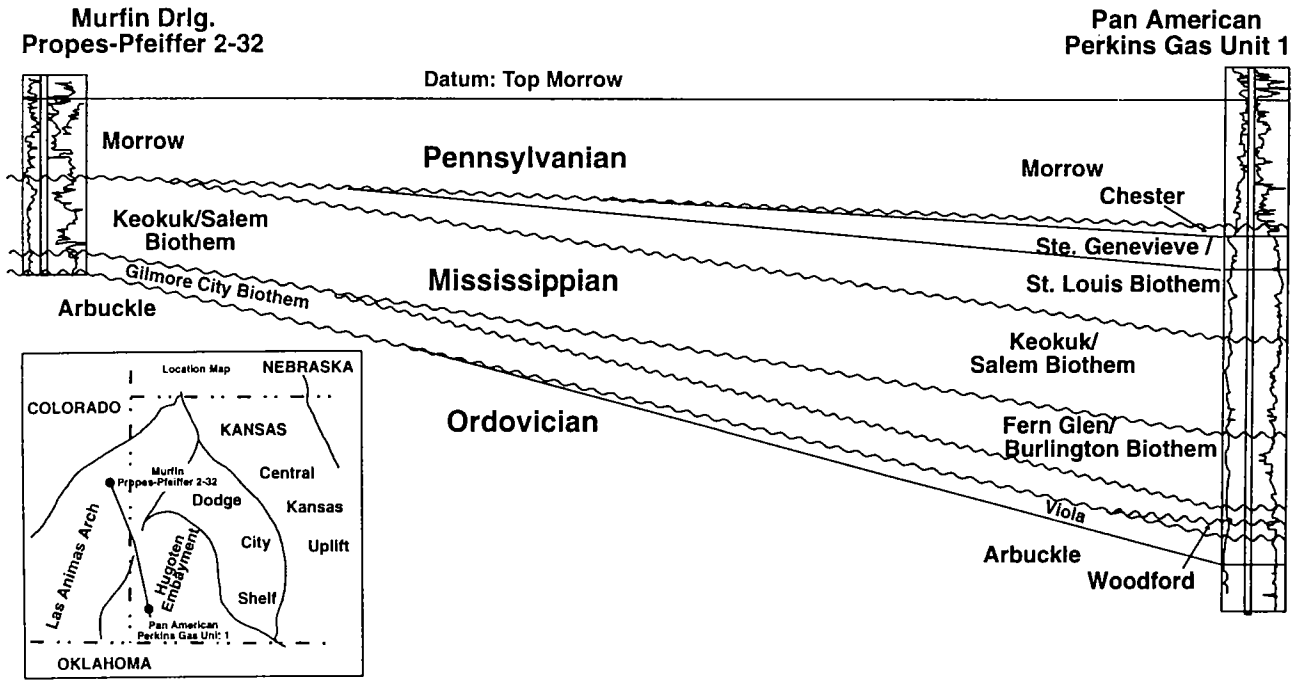

Figure 7. Revised biothem-based correlations of Ordovician–Early Pennsylvanian succession from the Las Animas arch in eastern Colorado to the central Hugoton embayment of southwestern Kansas, using the Biothem Approach and wireline-log correlations. Note the addition of three intra-Mississippian unconformities that were previously not recognized using the conventional industry correlations shown in Figure 6. Geographic location of transect shown on map at lower left.

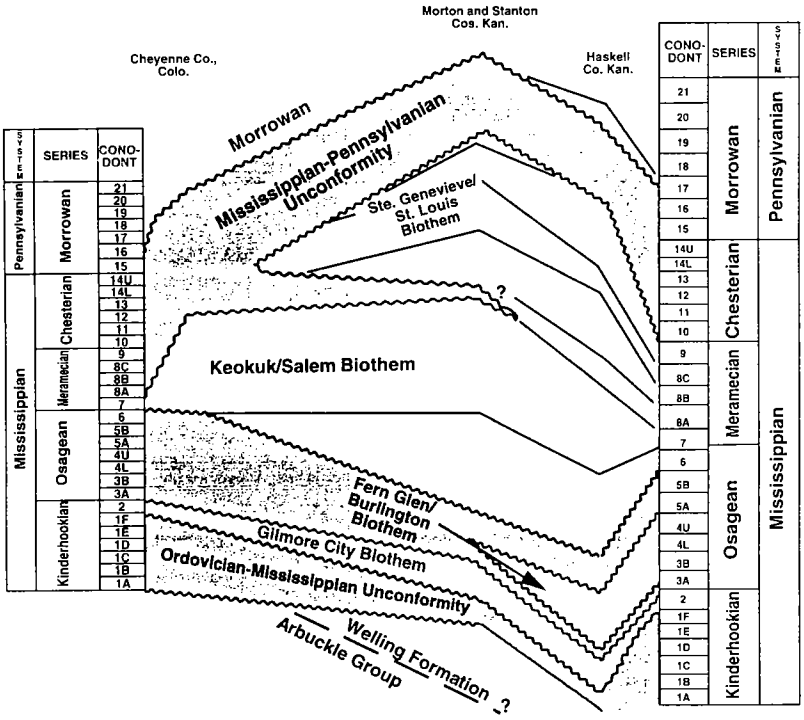

Figure 8. Relative-time-based correlation chart illustrating relationships among Mississippian and Early Pennsylvanian biothems and unconformities of the Las Animas arch and Hugoton embayment areas of eastern Colorado and southwestern Kansas. Intervals labeled as unconformities represent intervals of missing rock record as based on the absence of a fossil record. Solid areas between the unconformities are biothems named, for ease of reference, after the subsurface units commonly identified by use of conventional industry correlations. The boxes to the right and left of the diagram represent the conodont zonation illustrated in Figure 1. The diagram represents essentially the same transect illustrated in Figures 6 and 7 but is based on extensive subsurface coring to further refine the regional correlations suggested in Figures 6 and 7.

Burlington Biothem in the Hugoton embayment was an important discovery. In the Illinois basin, the same biothem is extensively developed well up onto the Transcontinental arch in much the same manner as the Keokuk/Salem Biothem in the Hugoton embayment–Las Animas arch area. These variations in the distribution of the same biothem from basin to basin along the Transcontinental arch have led to some important tectonic conclusions relating to utility 4 above, which, to date, we have summarized orally (Frye and others, 1991) and are the subject of a paper we are preparing for publication.

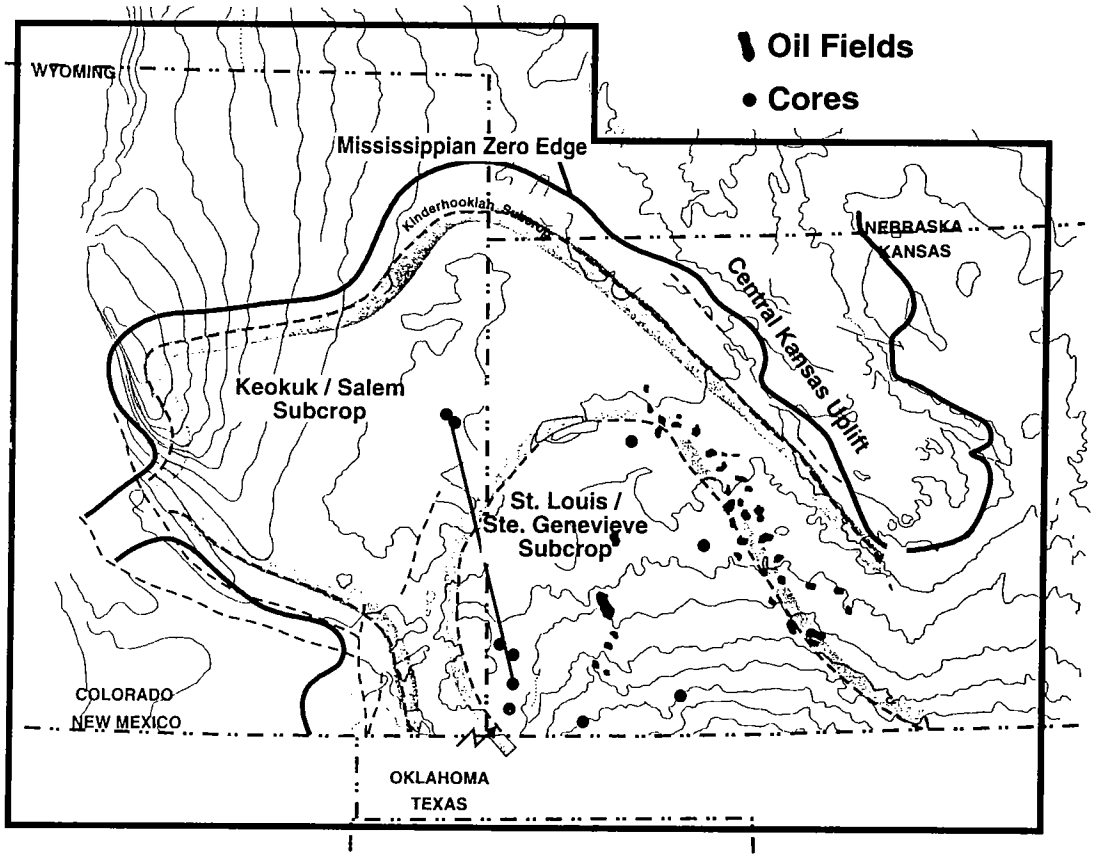

Figure 9. Subcrop map of Mississippian biothems beneath the base of the Pennsylvanian System in the Las Animas arch area of eastern Colorado and the Hugoton embayment of southwestern Kansas. Note that hydrocarbon production paralleling the southwestern side of the Central Kansas uplift comes from the Keokuk/Salem Biothem, whereas that in the central part of the Hugoton embayment is from the St. Louis/Ste. Genevieve Biothem. Although this map is based on conodont faunas from numerous Mississippian cores housed at the Kansas Geological Survey and at Amoco, the solid circles in Figures 9 and 10 represent only those cores taken by Amoco in the area during the early and middle 1980s in order to further refine regional subsurface biothem-based correlations.

Mississippian Biothems of New Mexico

The biothem concept has its origins in the work of Lane in the Mississippian of New Mexico. The long-standing controversy over the relationship between the shelfal Lake Valley Formation in the Sacramento Mountains near Alamogordo and the basinlike Rancheria/Helms Formations (Armstong, 1962, versus Laudon and Bowsher, 1949, and Pray, 1961; see Lane, 1974, for a full summary) to the south was resolved by using an early version of the Biothem Approach. The wedge-on-wedge relation noted by Lane (1974, fig. 4) between the Early Mississippian Lake Valley wedge in the Sacramento Mountains and the Late Mississippian Rancheria/Helms wedge represents what should now be termed a biothem contact as well as an erosional unconformity.

This rudimentary wedge-on-wedge relationship can be noted in the Mississippian all along the eastern flank of the Transcontinental arch (Lane, 1978, 1982; Lane and DeKeyser, 1980) and extending along the western flank of the TA (Rose, 1976; Lane, 1982; Gutschick and Sandberg, 1983). Lane (1982) and Lane and Ormiston (1982) were able to recognize four intervals defined by their biostratigraphic constituents that make up the Mississippian System of southern New Mexico. These intervals, originally termed *stratigraphic packages,* are biothems and can be seen in Figure 11, which is a cross section extending southward from Indian Wells Canyon in the central Sacramento Mountains of New Mexico to Vinton Canyon in the Franklin Mountains of Texas. This cross section illustrates some complex stratigraphic relationships, but the four biothems discerned are, in ascending order, the Caballero/Andrecito, the Alamogordo/Tierra Blanca, the Arcente/Dona Ana, and the Rancheria/Helms Biothems. These biothems correlate closely with counterpart biothems recognized to the north in the Hugoton embayment and the Illinois basin and also with unpublished biothems of similar ages on the western flank of the Transcontinental arch. Further details can be found in the above-referenced articles.

SUMMARY AND CONCLUSIONS

As defined herein, a biothem is a unit that is derived on the basis of its biostratigraphic constituents. Biothems can be used to provide a temporal framework in which to analyze lithofacies and other sequence components. Although restricted to use in fossiliferous portions of the crust, biothems can pro-

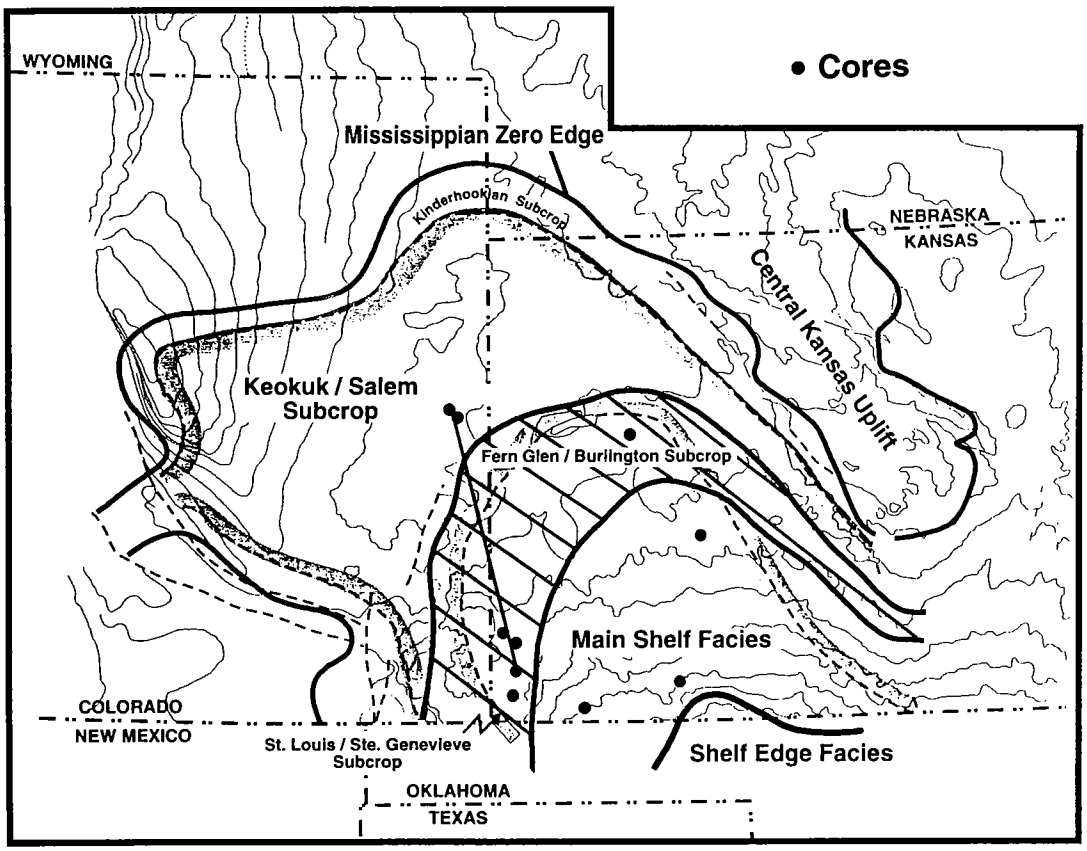

Figure 10. Comparison of the areal distribution of Mississippian subcrop patterns relative to biothem development in the Las Animas arch area of eastern Colorado and the Hugoton embayment area of southwestern Kansas. The hatched arcuate area in the lower part of the map represents the predicted subcrop of the Fern Glen/Burlington Biothem beneath the Keokuk/Salem Biothem. This map set up a play to test the feather edge of the Fern Glen/Burlington Biothem beneath the Keokuk/Salem Biothem for stratigraphic-trap possibilities.

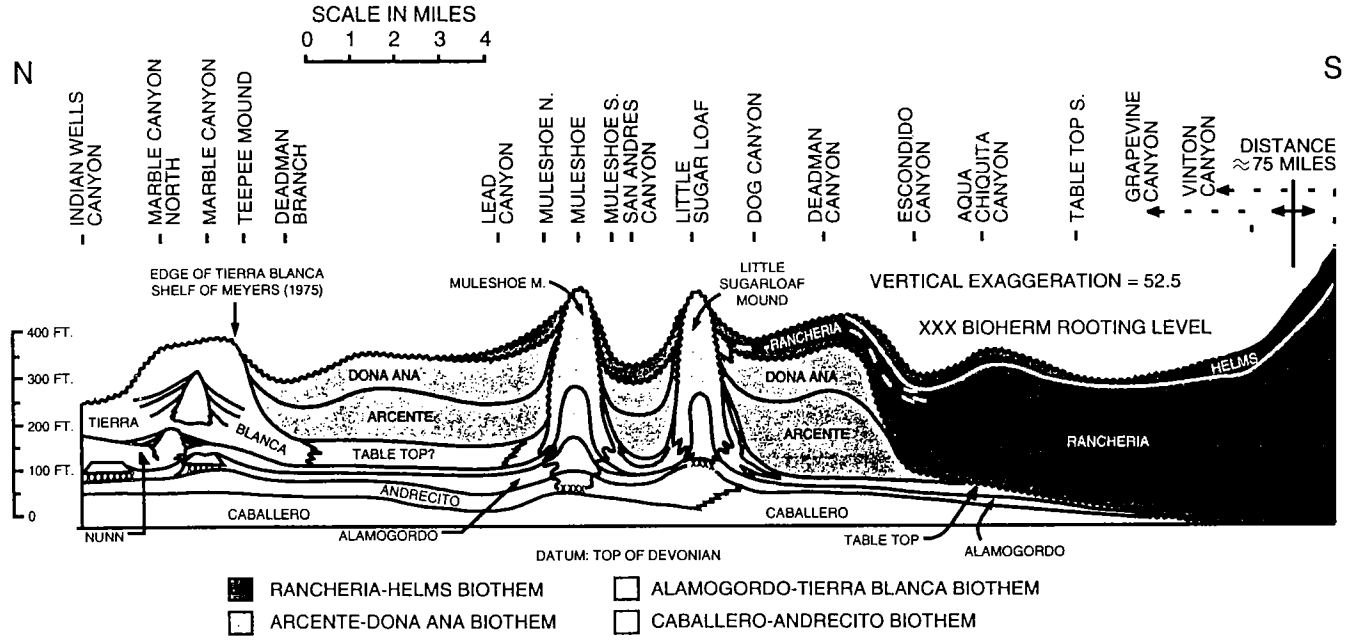

Figure 11. Four Mississippian biothems from Indian Wells Canyon, Sacramento Mountains, New Mexico, to Vinton Canyon in the Franklin Mountains, Texas. Note that the term *bioherm* refers to Waulsortian-type carbonate mounds typical of the Sacramento Mountains.

vide greater time-stratigraphic resolution to thick, lithologically homogeneous successions than can other sequence-stratigraphic correlation techniques.

The Biothem Approach, which consists of the recognition of biothems on the basis of biostratigraphic data collected and interpreted from a minimum of two outcrops or wellbores, has important applications in the analysis of hydrocarbon-bearing provinces, mineralization belts, hazardous-waste-isolation areas, and in the study of basinal and crustal geodynamics. The Biothem Approach has four major utilities, as follows:

1. Subdivision of stratigraphic successions into time-based, genetically related stratigraphic packages.

2. Construction of accurate, relative-time-based paleogeographic maps.

3. Evaluation of subsurface correlations, which, in an exploration application, can lead (and has led) to the generation of hydrocarbon-exploration plays.

4. Regional tectonic-stratigraphic analyses based on accurate time-stratigraphic interpretations.

ACKNOWLEDGMENTS

A number of people have contributed to the ideas and concepts presented in this study and the work behind their development. W. C. Sweet, Ohio State University, provided the Ordovician interpretation shown in Figure 8. Jeff Stein of Amoco Production Co.'s Paleontology Group reviewed a final draft of the manuscript. We also wish to thank Allen Ormiston and Jack Babcock of Amoco Research Center, Tulsa, for their contributions to the concepts presented here. Amoco Production Co. released the manuscript for publication. We also wish to thank MITRE Corp. and the University of Glasgow for their support.

REFERENCES CITED

Anderson, E. J.; and Goodwin, P. W., 1980, Application of the PAC hypothesis to limestones of the Helderberg Group: Society of Economic Paleontologists and Mineralogists, Eastern Section, Field-Trip Guidebook, 32 p.

_____1982, Application of the hypothesis of punctuated aggradational cycles—Allocyclicity in the Helderberg Group, New York: Proceedings, Belyea Conference on the Devonian System, Calgary, Alberta.

Armstrong, A. K., 1962, Stratigraphy and paleontology of the Mississippian System in southwestern New Mexico and adjacent southeastern Arizona: New Mexico Bureau of Mines and Mineral Resources Memoir 8, 99 p.

Baum, G. R.; and Vail, P. R., 1987, Sequence stratigraphic concepts applied to Paleogene outcrops, Gulf and Atlantic Basins, *in* Wilgus, C. K.; Hastings, B. S.; Kendall, C. G. St. C.; Posamentier, H. W.; Ross, C. A.; and Van Wagoner, J. C. (eds.), Sea-level research: An integrated approach: Society of Economic Paleontologists and Mineralogists Special Publication 42, p. 309–327.

Brown, L. F., Jr.; Cleaves, A. W., III; and Erxleben, A. W., 1973, Pennsylvanian depositional systems in north-central Texas: Texas Bureau of Economic Geology Guidebook 14, 122 p.

Busch, R.; and Rollins, H. B., 1984, Correlations of Carboniferous strata using a hierarchy of transgressive–regressive units: Geology, v. 12, p. 471–474.

Chang, K. H., 1975, Unconformity-bounded stratigraphic units: Geological Society of America Bulletin, v. 86, p. 1544–1552.

Eardley, A. J., 1962, Structural geology of North America [2nd edition]: Harper and Row, New York, 743 p.

Fisher, W. L.; and McGowen, J. H., 1967, Depositional systems in the Wilcox Group of Texas and their relationship to occurrence of oil and gas: Gulf Coast Association of Geological Societies Transactions, v. 17, p. 105–125.

Frye, M. W.; Lane, H. R.; and Couples, G. D., 1991, Biothem-based Mississippian transect from the Basin and Range Province to the Anadarko Basin [abstract]: American Association of Petroleum Geologists Program Abstracts, 1991 Convention, Dallas, p. 69.

Galloway, W. E., 1989a, Genetic stratigraphic sequences in basin analysis I: Architecture and genesis of flooding-surface bounded depositional units: American Association of Petroleum Geologists Bulletin, v. 73, p. 125–142.

_____1989b, Genetic stratigraphic sequences in basin analysis II: Application to Northwest Gulf of Mexico Cenozoic Basin: American Association of Petroleum Geologists Bulletin, v. 73, p. 143–154.

Goodwin, P. W.; and Anderson, E. J., 1985, Punctuated aggradational cycles: A general hypothesis of episodic stratigraphic accumulation: Journal of Geology, v. 93, p. 515–533.

Grabau, A. W., 1936, Oscillations or pulsations?: 16th International Geological Congress, Washington D.C., Report 1, p. 539–552.

_____1940. The rhythm of the ages: Henri Vetch, Peking, 561 p.

Graham, S. A.; Dickinson, W. R.; and Ingersol, R. V., 1975, Himalayan–Bengal model for flysch dispersal in the Appalachian–Ouachita System: Geological Society of America Bulletin, v. 86, p. 273–286.

Gutschick, R. C.; and Sandberg, C. A., 1983, Mississippian continental margins of the conterminous United States: Society of Economic Paleontologists and Mineralogists Special Paper 33, p. 79–96.

Johnson, J. G., 1971, Timing and coordination of orogenic and epeirogenic, and eustatic events: Geological Society of America Bulletin, v. 82, p. 3263–3298.

Johnson, J. G.; Klapper, G.; and Sandberg, C. A., 1985, Devonian eustatic fluctuations in Euramerica: Geological Society of America Bulletin, v. 96, p. 567–587.

Lane, H. R., 1974, Mississippian of southeastern New Mexico—A wedge-on-wedge relation: American Association of Petroleum Geologists Bulletin, v. 58, p. 269–282.

_____1978, The Burlington Shelf (Mississippian, north-central United States): Geologica et Palaeontologica, v. 12, p. 165–175.

_____1982, The distribution of the Waulsortian Facies in North America as exemplified in the Sacramento Mountains of New Mexico, *in* Bolton, K.; Lane, H. R.; and LeMone, D. V. (eds.), Symposium on the paleoenvironmental setting and distribution of the Waulsortian Facies: El Paso Geological Society and University of Texas at El Paso, International Field Seminar Guide, March 2–6, 1982, p. 96–114.

Lane, H. R.; and DeKeyser, T. L., 1980, Paleogeography of the late Early Mississippian (Tournaisian 3) in the central and southwestern United States, *in* Fouch, T. D.; and Magathan, E. R. (eds.), Paleogeography of west-central United States: Society of Economic Paleontologists and Mineralogists, Rocky Mountain Section, West-Central United States Paleogeography Symposium 1 Proceedings, p. 149–162.

Lane, H. R.; and Ormiston, A. R., 1982, Waulsortian Facies, Sacramento Mountains, New Mexico, *in* Bolton, K.; Lane, H. R.; and LeMone, D. V. (eds.), Symposium on the paleoenvironmental setting and distribution of the Waulsortian Facies: El Paso Geological Society and University of Texas at El Paso, International Field Seminar Guide, March 2–6, 1982, p. 115–182.

Lane, H. R.; Sandberg, C. A.; and Ziegler, W., 1980, Taxonomy and phylogeny of some Lower Carboniferous conodonts and preliminary post-*Siphonodella* zonation: Geologica et Palaeontologica, v. 14, p. 117–164.

Laudon, L. R.; and Bowsher, A. L., 1949, Mississippian formations of southwestern New Mexico: Geological Society of America

Bulletin, v. 25, p. 2107–2160.
Lineback, J. A., 1966, Deep-water sediments adjacent to the Borden Siltstone (Mississippian) delta in southern Illinois: Illinois State Geological Survey Circular 401, 48 p.
_____1969, Illinois basin—sediment starved during Mississippian: American Association of Petroleum Geologists Bulletin, v. 53, p. 112–126.
Meyers, W. J., 1975, Stratigraphy and diagenesis of the Lake Valley Formation, Sacramento Mountains, *in* Pray, L. C. (ed.), A guidebook to the Mississippian shelf-edge and basin facies carbonates, Sacramento Mountains and southern New Mexico: Dallas Geological Society, American Association of Petroleum Geologists and Society of Economic Paleontologists and Mineralogists Convention, Dallas, p. 45–65.
Miall, A. D., 1986, Eustatic sea level changes interpreted from the stratigraphic record: A critique of the methodology with particular reference to the North Sea Jurassic record: American Association of Petroleum Geologists Bulletin, v. 70, p. 131–137.
_____1990, Principles of sedimentary basin analysis [2nd edition]: Springer-Verlag, New York, 668 p.
_____1991, Stratigraphic sequences and their chronostratigraphic correlation: Journal of Sedimentary Petrology, v. 61, p. 497–505.
Mitchum, R. M., Jr.; Vail, P. R.; and Thompson, S., III, 1977, The depositional sequence as a basic unit for stratigraphic analysis, *pt. 2 of* Vail, P. R.; Mitchum, R. M., Jr.; Todd, R. G.; Widmier, J. M.; Thompson, S., III; Sangree, J. B.; Bubb, J. N.; and Hatlelid, W. G., Seismic stratigraphy and global changes of sea level, *in* Payton, C. E. (ed.), Seismic stratigraphy—applications to hydrocarbon exploration: American Association of Petroleum Geologists Memoir 26, p. 53–62.
North American Commission on Stratigraphic Nomenclature, 1983, North American Stratigraphic Code: American Association of Petroleum Geologists Bulletin, v. 67, p. 841–875.
Pander, C. H., 1856, Monographie der fossilen Fische des silurischen Systems der russisch-baltischen Gouvernements: Buchdruckerei der Kaiserlichen Adademie der Wissenschaften, St. Petersburg, 91 p.
Pray, L. C., 1961, Geology of the Sacramento Escarpment, Otero County, New Mexico: New Mexico Bureau of Mines and Mineral Resources Bulletin 35, 144 p.
Ramsbottom, W. H. C., 1977, Major cycles of transgression and regression (mesothems) in the Namurian: Yorkshire Geological Society Proceedings, v. 41, pt. 3, no. 24, p. 261–291.
Rascoe, Bailey, Jr.; and Adler, F. J., 1983, Permo-Carboniferous hydrocarbon accumulations, Mid-Continent, U.S.A.: American Association of Petroleum Geologists Bulletin, v. 67, p. 979–1001.
Rose, P. R., 1976, Mississippian carbonate shelf margins, Western United States: U.S. Geological Survey Journal of Research, v. 4, p. 449–466.
Salvador, A., 1987, Unconformity-bounded stratigraphic units: Geological Society of America Bulletin, v. 98, p. 232–237.
Shaw, A. B., 1964, Time in stratigraphy: McGraw-Hill, New York, International Series on the Earth Sciences, 365 p.
Sloss, L. L., 1963, Sequences in the cratonic interior of North America: Geological Society of America Bulletin, v. 74, p. 93–114.
_____1988, Forty years of sequence stratigraphy: Geological Society of America Bulletin, v. 100, p. 1661–1665.
Stein, J. A.; Gamber, J. H.; Krebs, W. N.; and Lacoe, M. K., 1995, A composite standard approach to biostratigraphic evaluation of the North Sea Paleogene, *in* Steele, R. J., and others (eds.), Sequence stratigraphy of the NW European Margin: Elsevier Norsk Petroleums Forening Special Publication 5, Amsterdam, p. 401–414.
Sweet, W. C., 1989, The Conodonta: Morphology, taxonomy, paleoecology, and evolutionary history of a long-extinct animal phylum: Oxford University Press, New York, 212 p.
Vail, P. R.; Mitchum, R. M., Jr.; Todd, R. G.; Widmier, J. M.; Thompson, S., III; Sangree, J. B.; Bubb, J. N.; and Hatlelid, W. G., 1977, Seismic stratigraphy and global changes of sea level, *in* Payton, C. E. (ed.), Seismic stratigraphy—applications to hydrocarbon exploration: American Association of Petroleum Geologists Memoir 26, p. 49–212.
Wanless, H. R.; and Weller, J. M., 1932, Correlation and extent of Pennsylvanian cyclothems: Geological Society of America Bulletin, v. 43, p. 1003–1016.
Wheeler, H. E., 1964, Baselevel, lithosphere surfaces, and time-stratigraphic concept: Geological Society of America Bulletin, v. 75, p. 599–609.

Stratigraphic Relationships of Springer and Chester Groups within the Oklahoma Portion of the Anadarko Basin and Shelf: A Clarification

Paul W. Smith, Walter J. Hendrickson, Craig M. Williams, and Ronald J. Woods
IHS Energy Group
Oklahoma City, Oklahoma

ABSTRACT.—It has long been apparent to those working the Anadarko basin and shelf areas of Oklahoma that the nomenclature used is typically erratic and the resulting production allocation less than precise. Correlative and equivalent formations may be called by various names, and there are many cases of nomenclature being vague, too broad, or incorrect altogether. Further complicating the understanding of the geology of the Anadarko basin and shelf is the fact that few detailed regional cross sections are available (or even exist outside of proprietary studies) that show the most up-to-date logs correlated throughout the basin and shelf areas.

As part of a regional study, logs from every producing well in a part of the Anadarko basin and shelf were reviewed to verify the actual producing reservoirs. Nearly 18,000 well logs in an area including Ts. 8–29 N. through Rs. 10–26 W. were examined. Regional cross sections were constructed and used to determine stratigraphic relationships and to develop a system of stratigraphic nomenclature that could be used across the area with accuracy, detail, and consistency.

The Springer Group (Upper Mississippian–Lower Pennsylvanian) is often misnamed as the overlying Pennsylvanian Morrow sandstone or the underlying Mississippian Chester limestone. Generally, the Springer Group consists of the Boatwright, Britt, and Cunningham stratigraphic units, in ascending order. Whereas the Cunningham was found always to be a sandstone, extensive correlations indicated that the Boatwright and/or Britt sandstone, in certain areas, developed a carbonate facies that was almost always referred to as *Chester limestone*. In these areas, the first carbonate below the Morrow and/or Cunningham clastic section has been called *Chester* by convention. Correlations from the deep Anadarko basin demonstrate that these carbonates are the shallow-marine-facies equivalent of the Boatwright and/or Britt sandstone members of the Springer Group. A highly conductive Boatwright shale directly above the true Chester limestone provides a reliable regional marker as the base of the Springer Group. This lateral facies change is illustrated by the included log cross sections. An estimated 1.2 trillion cubic feet of gas has been produced from the Boatwright and Britt carbonates, as herein defined.

PURPOSE

Smith and others (1996) reported that certain Springer sandstones within the Anadarko basin and shelf areas of Oklahoma were observed to undergo facies changes to carbonates. In the areas of Springer carbonate deposition, these carbonates had been identified as Mississippian Chester limestone. This paper provides condensed cross sections of those that were presented in a poster session at the Oklahoma Geological Survey's Platform Carbonate Symposium held in March of 1996. These cross sections demonstrate the relationships of the Springer sandstones, the Springer carbonates, and the Mississippian Chester limestones that have resulted in approximately 1.2 trillion cubic feet of gas being reallocated from what was originally indicated as Mississippian Chester carbonates to what more specifically is herein identified as Boatwright and Britt carbonates, which belong to the Springer Group. The included production maps indicate the areas of Boatwright and Britt production (specific as to sandstone and carbonate areas) as well as the areas of true Chester production.

Reservoir nomenclature was developed through regional correlations and was substantiated by a dense framework of contiguous and detailed cross sections. Hendrickson and others (1996), Williams and others (1996), and Smith and others (1996) previously discussed the correlation and allocation project, including some specific results.

STUDY AREA

Figure 1 presents a map of the Anadarko basin and shelf areas and indicates the original study area. At present, the study area encompasses Ts. 8–9 N., Rs. 10–15 W., and Ts. 10–29 N., Rs. 10–26 W. It occupies more than one-half of the Oklahoma portion of the Anadarko basin. The total study area is 11,304 mi^2, one-fourth of the total basin area of 45,500 mi^2, and is the locus of most of the deeper drilling in the basin. An extension of the study area is presently being completed to include the southeastern half of the Watonga–Chickasha trend, including Ts. 11–14 N., Rs. 8–9 W.; Ts. 8–10 N., Rs. 7–9 W.; T. 7 N., Rs. 6–9 W.; and T. 6 N., Rs. 6–8 W. A future exten-

Smith, P. W.; Hendrickson, W. J.; Williams, C. M.; and Woods, R. J., 2000, Stratigraphic relationships of Springer and Chester Groups within the Oklahoma portion of the Anadarko basin and shelf: a clarification, *in* Johnson, K. S. (ed.), Platform carbonates in the southern Midcontinent, 1996 symposium: Oklahoma Geological Survey Circular 101, p. 197–207.

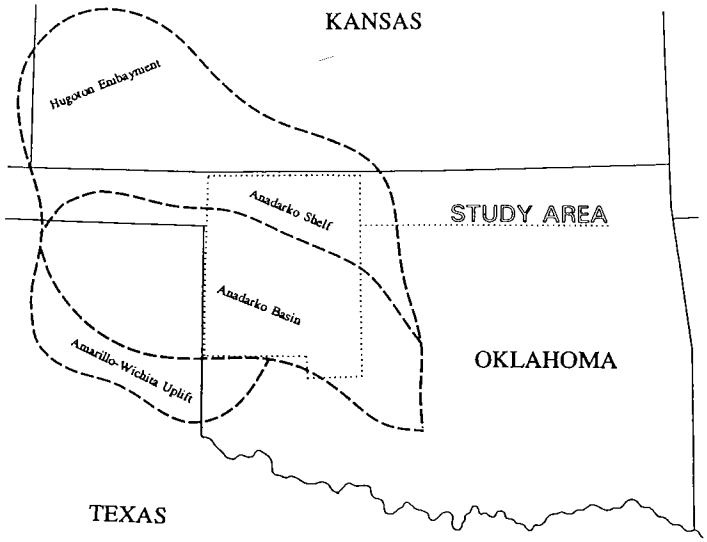

Figure 1. Map of Anadarko basin and surrounding region, showing study area (dotted outline).

sion is planned in the Oklahoma Panhandle to complete Mocane–Laverne field, of which approximately 36% lies within the original study area.

METHODOLOGY

The producing formation in a well is originally defined by the completion report (Form 1002A) filed with the Oklahoma Corporation Commission (OCC) in which both the perforated interval(s) and the producing formation(s) are listed. It is the operator's responsibility to see that the producing formation is identified as fully and correctly as possible, but there are no exacting standards for this process nor are there any mechanisms in place to ensure that the producing formation has been fully and correctly defined. As a result, much of the nomenclature for the basin and shelf areas is erratic and less than precise.

During a recent effort at IHS Energy Group to standardize reservoir nomenclature, the authors generated over 7,500 mi of geologic cross sections to demonstrate the stratigraphic sequences and relationships throughout the Anadarko basin and shelf areas. Figure 2 presents the stratigraphic section used in this study to designate reservoir and formation names. Figure 3 is a base map of the approximate study area, indicating the network of nearly 1,600 mi of cross sections, which are a small part of the total used in this project. Also indicated are the traces of the cross sections (A–A′ and B–B′) included in this paper and which demonstrate the facies change that has resulted in certain formations within the Springer Group, as herein defined, being identified as Mississippian Chester limestone.

To ensure nomenclatural consistency and accuracy, electric logs of nearly 18,000 wells were reviewed for this study. Regarding the perforated intervals (as indicated on completion cards and/or OCC Form 1002A), a comparison was made between formations as defined on IHS Energy Group's regional cross sections and formations as defined by operators. Where there was a difference between the two, the nomenclature defined on the regional cross sections was used. Almost 40% of the producing formations as originally defined on completion cards were either too vague or too broad to use or were incorrect, and were consequently reassigned a reservoir name to conform to the cross sections. Furthermore, about 15% of the perforated intervals required correction because of reporting or typographical errors, or because the perforated intervals were simply absent from the production records.

RESULTS

The overall results of this study have been twofold. First, a dense framework of regional cross sections was developed that demonstrates the stratigraphic sequences and relationships found within the Anadarko basin and shelf areas. Specifically, the relationships of the Springer and Chester Groups have been clarified. Second, a great improvement in the accuracy, detail, and consistency in the allocation of production, as reflected in IHS's Production Database, should be of great benefit to anyone using production data within the study area.

Regional correlations from the deep part of the Anadarko basin northwestward demonstrate that the Boatwright and Britt members of the Springer Group undergo a facies change from sandstone to carbonate. Previously, these carbonates were identified as Mississippian Chester by convention. However, they are distinct from the true Chester in that the intervening Boatwright shale is everywhere present and correlative, lying atop the true Chester and separating it from the overlying Boatwright and Britt. The Boatwright shale is present independently of the sandstone or carbonate facies of the Boatwright and Britt. The Cunningham sandstone was deposited over the south half of the study area; no carbonate facies was observed for this unit.

Cross-Section A–A′ (Fig. 4) is an approximate strike section. The southeast well of the section, the Arkla No. 1-21 Clancey Estate, was drilled in the Eakley–Weatherford trend (an area of notable Boatwright and Britt sandstone production) and produces from Boatwright sandstone between 16,115 and 16,220 ft. The massive Boatwright shale in this well occurs from 16,220 to 16,550 ft, at which depth the true Chester was encountered. Over the extent of this cross section, the Boatwright shale thins from 330 ft in the southeast to 225 ft in the northwest but is always present and lying atop the true Chester. From the Clancey well, the cross section progresses northwestward, where the Boatwright sandstone thins and then undergoes a facies change to thin carbonates. Northwestward, these thin carbonates coalesce with a massive carbonate section of more than 200 ft (T. 15 N., R. 21 W.), which in turn thins to a regionally persistent Boatwright carbonate bed approximately 40 ft thick, shown at the northwest end of the cross section. Similarly, the Britt sandstone, shown in the southeast part of the cross section, undergoes a facies change to a massive carbonate section (T. 16 N., R. 21 W.). This lithologic change takes place farther to the northwest than that of the Boatwright.

Cross section B–B′ (Fig. 5) is a dip section that intersects the strike section (A–A′) in T. 16 N., R. 21 W., toward its northwest end. From the southwest end of this section, the Boatwright and Britt carbonates can be correlated to the north-

SYS	SERIES	GROUP	UNIT	SANDSTONE	CARBONATE	EQUIVALENT
PENNSYLVANIAN	VIRGILIAN	Shawnee/Cisco	Topeka Ls Pawhuska Ls Hoover Ss Elgin Sd Oread Ls Heebner Sh Endicott Ss	Hoover Endicott	Pawhuska Oread Ls	
		Douglas/Cisco	Lovell Ls Haskell Ls Tonkawa Ss	 Tonkawa	Douglas Group	
	MISSOURIAN	Lansing/Hoxbar	Avant Ls Cottage Grove Ss	Cottage Grove	Lansing Group	
		Kansas City/Hoxbar	Dewey Ls Hogshooter Ls Layton Ss Checkerboard Ls Cleveland Ss	 Layton Cleveland Culp	Kansas City Group Melton	 Marchand Upper Marchand Lower
	DES MOINESIAN	Marmaton	Big Lime Oswego		Big Lime Oswego	Marmaton Wash
		Cherokee	Cherokee Marker Prue Ss Verdigris Ls Skinner Ss Pink Ls Red Fork Ss Inola Ls Mona	 Prue Skinner Red Fork Cherokee Wash Middle Cherokee Wash Lower/ Mona	 Verdigris Inola	 Prue Wash Skinner Wash Red Fork Wash Bartlesville, Tussy
	ATOKAN	Atoka	Atoka 13 Finger Ls	Atoka	Atoka 13 Finger	
	MORROWAN	Morrow	Morrow Primrose	Upper Morrow Morrow Lower Morrow Primrose		
MISSISSIPPIAN	SPRINGERAN	Springer	Cunningham Britt Boatwright	Cunningham Britt Boatwright	 Britt Boatwright	
	CHESTERIAN	Chester	Chester Ls		Chester	
		Manning	Manning Ls		Manning	
	MERAMECIAN	Meramec	Meramec Chat Meramec Ls		Meramec Chat Meramec	
	OSAGEAN	Osage	Osage Ls			
	KINDERHOOKIAN	Kinderhook	Kinderhook Sh			
SIL./DEV.	CHATTANOOGIAN		Woodford Sh Misener Ss	Misener		
	ULSTERIAN	Hunton	Hunton Group		Hunton (Frisco) Hunton (Bois d'Arc) Hunton (Haragan) Hunton (Henryhouse) Hunton (Chimney Hill)	
	NIAGARAN ALEXANDRIAN					
ORDOVICIAN	CINCINNATIAN	Sylvan	Sylvan Sh Maquoketa		Maquoketa	
	CHAMPLANIAN	Viola	Viola Group		Viola (Fernvale) Viola (Trenton)	
		Simpson	Simpson Dense Bromide Ss Tulip Creek Ss McLish Ss Oil Creek Ss Joins	 Bromide Tulip Creek McLish Oil Creek Joins		
	CANADIAN	Arbuckle	Arbuckle Group		Arbuckle	
CAMB.	CROIXAN					

Figure 2. Stratigraphic-correlation section for Anadarko basin region.

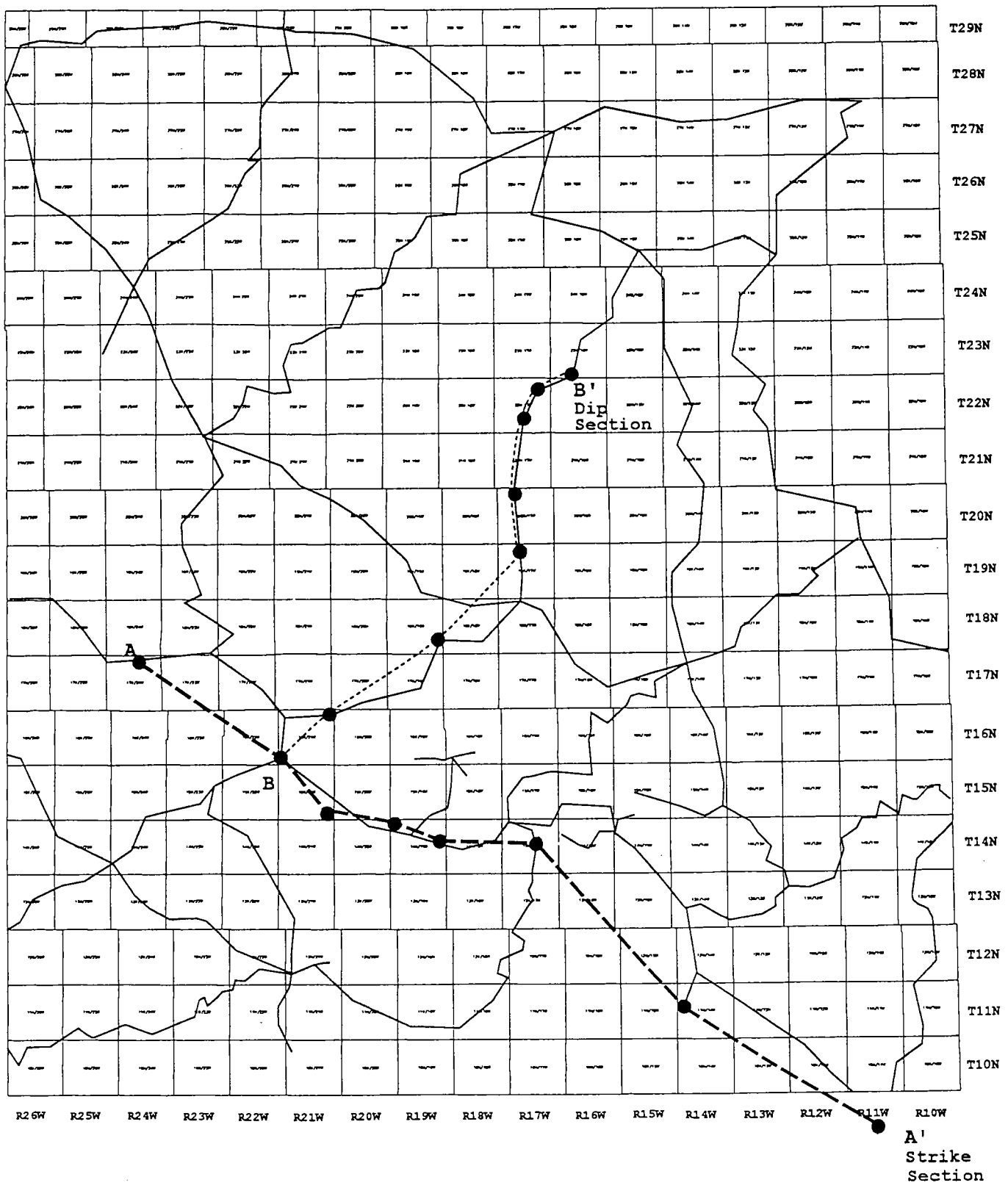

Figure 3. Map of approximate study area, indicating a network of nearly 1,600 mi of cross sections. Lines of cross sections A–A´ (Fig. 4) and B–B´ (Fig. 5) are also shown.

east to the points at which they are systematically truncated—first the Britt, and then the Boatwright. These units are carbonates on this cross-section, whose trace lies northwest of the points at which both units undergo a facies change from sandstone to carbonate. The Boatwright shale thins from 215 ft in the southwest to 60 ft toward the northeast, where an intervening limestone member that developed within the Boatwright shale unit accounts for 20 ft of the 60-ft gross thickness. As with the overlying Boatwright, Britt, and Cunningham members, the Boatwright shale is ultimately truncated (shown just to the left of the last log of the cross section). However, in the absence of truncation, the Boatwright shale is a regionally continuous and correlatable marker bed between the underlying true Chester and the overlying Boatwright and Britt carbonates and/or sandstones.

Owing to space constraints, the cross sections presented here have no horizontal scale, and the wells represented are widely spaced. These sections are a distillation of thousands of miles of cross sections that were constructed at IHS Energy Group. Logs included here were chosen to demonstrate specific points clearly. Although some correlations may not appear irrefutable, many additional logs between any two represented were used in the correlation process. Thus, the well-to-well correlation of individual sandstone members should not be taken literally, as they are only graphic in nature and are intended to illustrate lithologic variations.

Figure 6 is a map of the study area showing wells that have produced from the Springer Group, as herein defined. In general, Springer sandstone production—Boatwright, Britt, and Cunningham—is limited to the southeast quarter of the study area, with the exception of the Cunningham, which produces over the south half, having never developed a carbonate facies. Two northeast–southwest trend lines delineating the approximate location of the facies change from sandstone to carbonate observed for both the Boatwright and Britt are indicated, with sandstone deposition to the southeast and carbonate deposition to the northwest. As the Britt and Boatwright carbonates are successively truncated, the productive trends of these two units are indicated as they are found in subcrop.

Figure 7 is a map showing wells that have produced from true Mississippian Chester carbonates. In the southeast part of indicated Chester production, a full section of Chester is approximately 300 ft thick just before the beginning of its subcrop; at the northwest boundary of the study area, a full section is usually 150 ft thick. Productive Chester carbonates occur predominantly downdip from the ultimate truncation of the Chester. Hydrocarbon trapping occurs at and/or slightly downdip of the beginning of the Chester subcrop. This is because productive zones are generally limited to the upper Chester.

SUMMARY AND CONCLUSIONS

The stratigraphic and facies relationships of the Springer and Chester Groups have been demonstrated. In the case of the Boatwright and Britt carbonates, the definition of these individual units and their separation from the true Mississippian Chester limestone give additional, and heretofore unavailable, detail and insight into the reservoir-production data. Additionally, an understanding of these relationships is necessary for the proper mapping of these units within the study area.

Production within the study area has been allocated by IHS Energy Group to conform to a standardized system of nomenclature for the study area. For this effort, an extensive network of cross sections was generated to enhance the accuracy, detail, and consistency of the allocation process.

It is anticipated that the stratigraphic and facies relationships developed by this study, as well as the increased accuracy, detail, and consistency of the reallocated production, will aid in future exploration and exploitation endeavors.

ACKNOWLEDGMENTS

This paper addresses the regional correlations of the Springer and Chester Groups by a project jointly funded by the Gas Research Institute, Washington, D.C., and Dwight's Energydata, Inc. (now part of IHS Energy Group). The project was a preliminary study to assess the prospects for deeper reservoirs in the Anadarko basin. The full report discusses sandstone, carbonate, "wash," and mixed lithologic groups and is available from the Gas Research Institute as Report GRI-96/0196 (Smith, 1996).

REFERENCES CITED

Hendrickson, W. J.; Smith, P. W.; and Williams, C. M., 1996, Regional correlations and reservoir characterization studies of the Pennsylvanian System in the Anadarko basin area of western Oklahoma and the panhandle of Texas: Tulsa Geological Society, Transactions of 1995 American Association of Petroleum Geologists, Mid-Continent Section Meeting, p. 100–108.

Smith, P. W., 1996, Anadarko basin statistical study: gas well recovery -vs- depth in the Anadarko basin of western Oklahoma: Gas Research Institute, Chicago, Report GRI-96/0196, 65 p.

Smith, P. W.; Hendrickson, W. J.; and Williams, C. M., 1996, Regional correlations and reservoir characterization studies of the Springer Group in the Anadarko basin area of western Oklahoma: Tulsa Geological Society, Transactions of 1995 American Association of Petroleum Geologists, Mid-Continent Section Meeting, p. 116–126.

Williams, C. M.; Hendrickson, W. J.; and Smith, P. W., 1996, Regional correlation and reservoir characterization studies of the Morrow Group in the Anadarko basin area of western Oklahoma: Tulsa Geological Society, Transactions of 1995 American Association of Petroleum Geologists, Mid-Continent Section Meeting, p. 109–115.

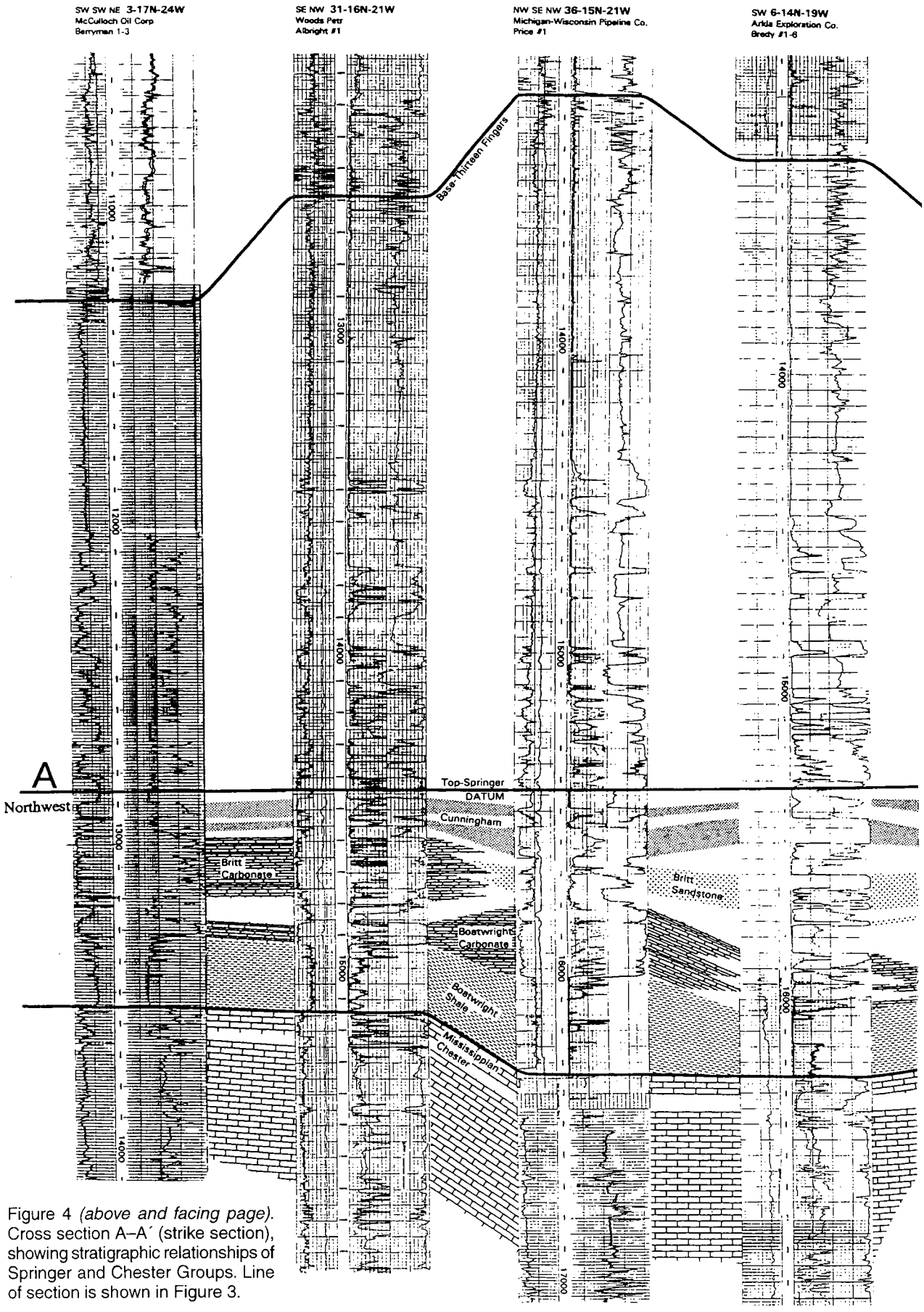

Figure 4 *(above and facing page).* Cross section A–A′ (strike section), showing stratigraphic relationships of Springer and Chester Groups. Line of section is shown in Figure 3.

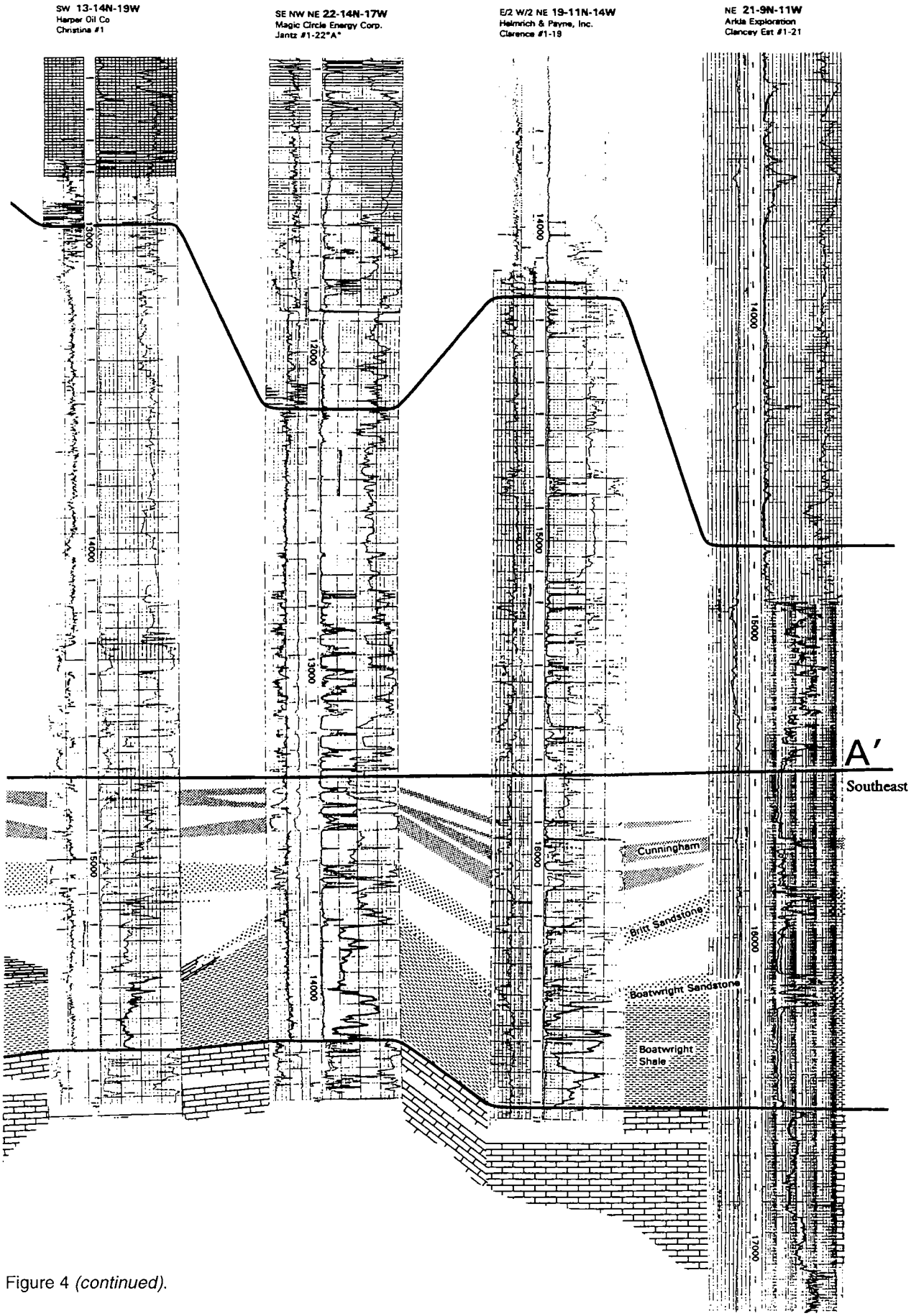

Figure 4 *(continued)*.

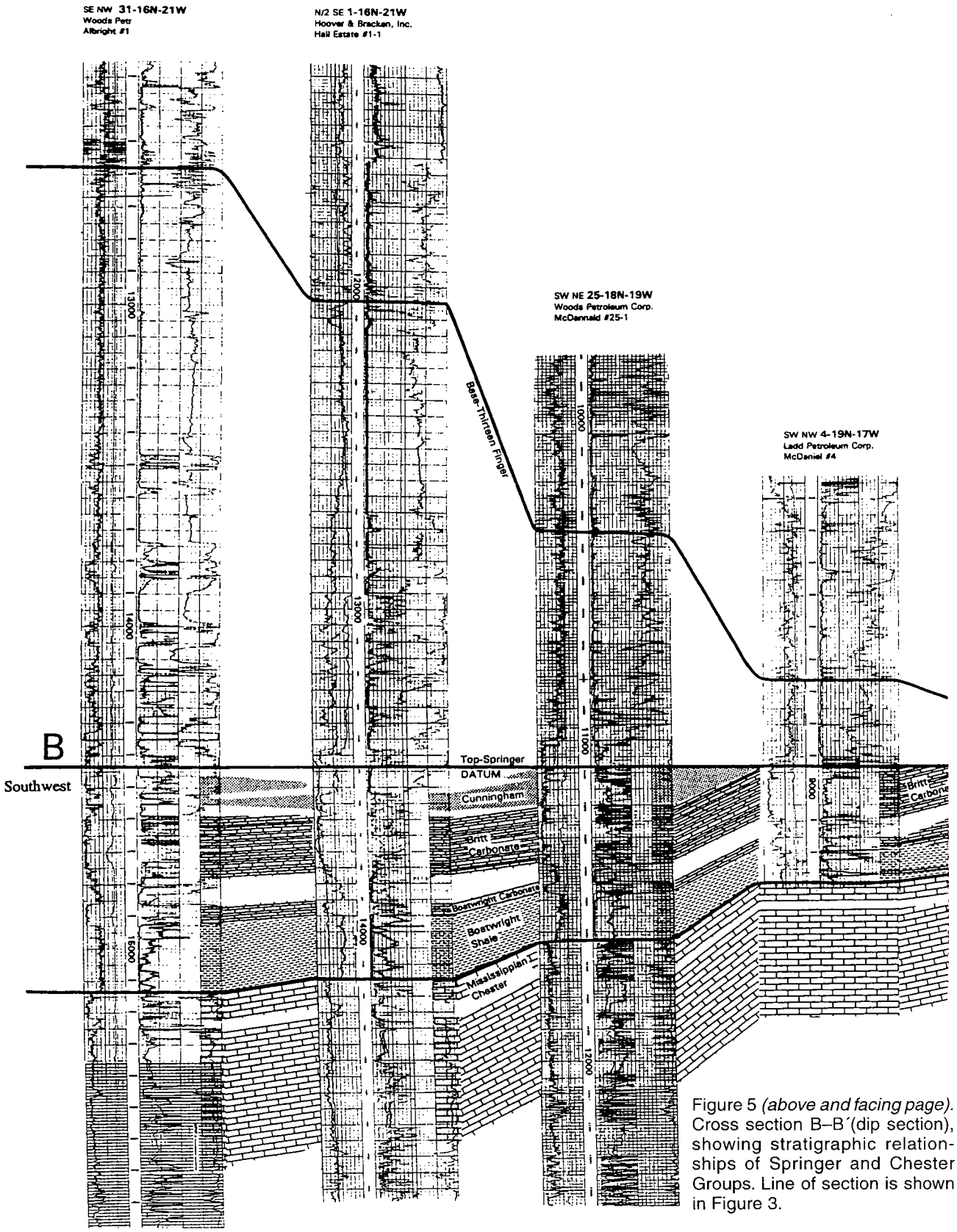

Figure 5 *(above and facing page).* Cross section B–B′(dip section), showing stratigraphic relationships of Springer and Chester Groups. Line of section is shown in Figure 3.

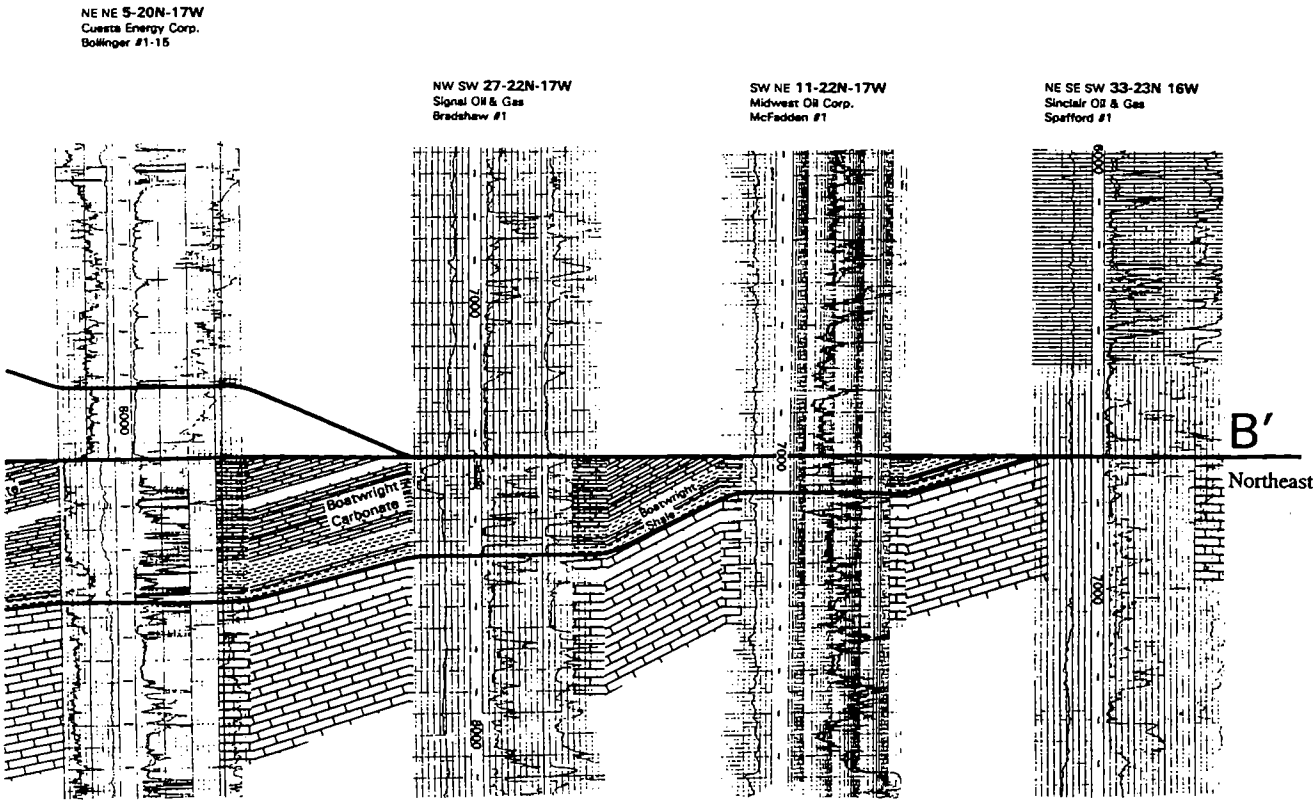

Figure 5 *(continued).*

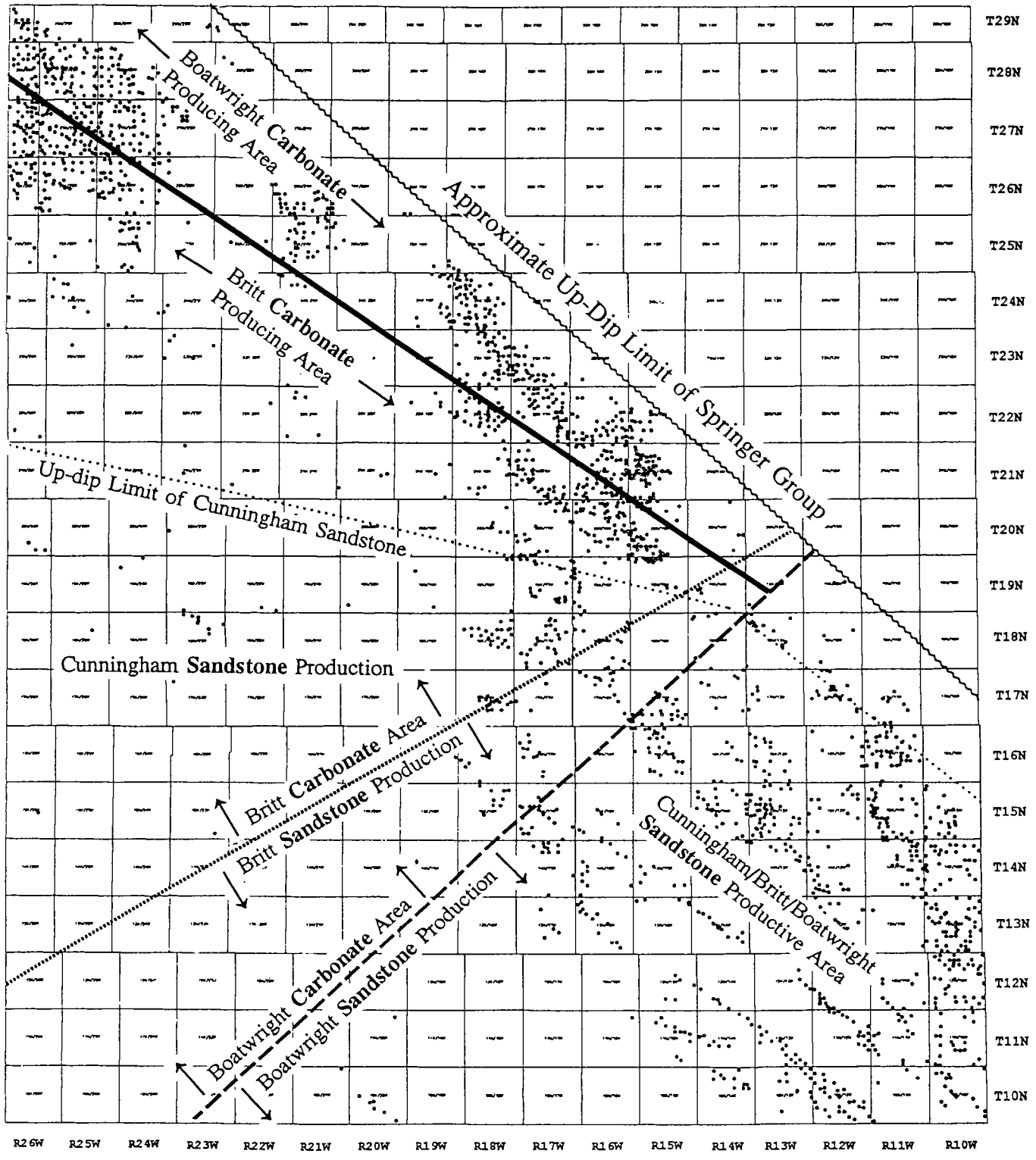

Figure 6. Map of study area, showing wells that have produced from members of Springer Group, with areas of lithologic facies indicated.

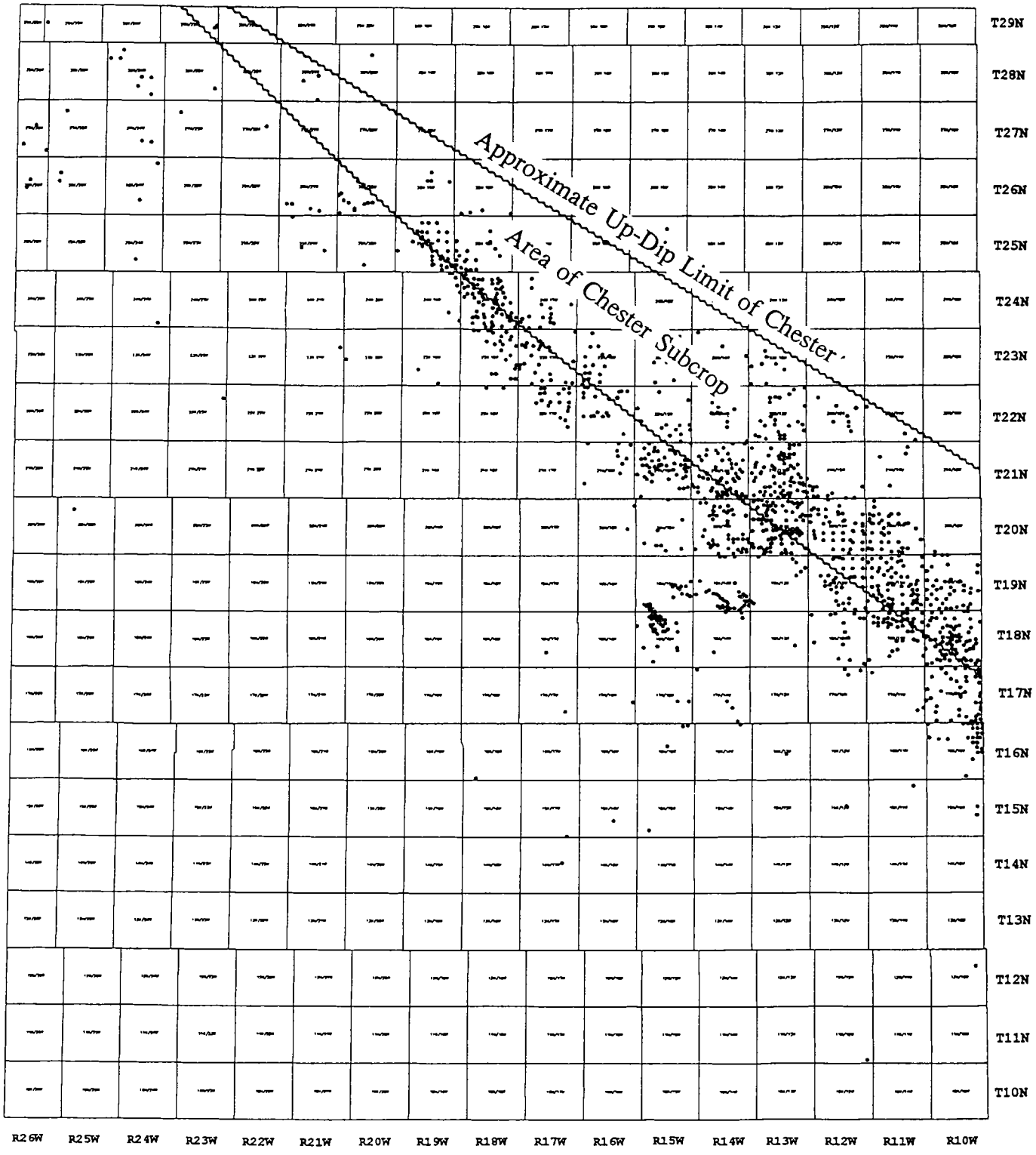

Figure 7. Map of study area, showing wells that have produced from Chester Group carbonates, with area of Chester subcrop indicated.

Union Valley Limestone Bank (Pennsylvanian, Morrowan), Eastern Oklahoma

James R. Derby, James E. O'Brien, J. Glenn Cole, and Dorothy L. Swindler
Independent Geologists
Tulsa, Oklahoma

INTRODUCTION

The subject of this paper is a Morrowan carbonate bank in the subsurface of Muskogee, Okmulgee, and McIntosh Counties, and along outcrops of eastern Oklahoma. This bank extends from outcrops in the east to a west-facing carbonate bank slope. The bank thins and is truncated by erosion northward, and it grades southward into calcareous sandstone. Various names have been applied to these rocks in the subsurface of eastern Oklahoma: *Union Valley limestone, Union Valley sandstone, Cromwell sandstone,* and *Union Valley–Cromwell.*

The work presented in this paper is part of an ongoing effort by the authors and the stratigraphic committee of the Tulsa Geological Society to understand the stratigraphic relationships between the Morrowan strata in the subsurface of eastern Oklahoma and Morrowan outcrops on the flanks of the Ozarks to the east, and in the Lawrence uplift, northeastern Arbuckle Mountains, to the southwest (Fig. 1).

AREA AND METHODS OF STUDY

An index map of the study area (Fig. 2) shows the locations of cores and well logs used in this study. Control wells shown in Figure 2 are part of a network of wireline-log and sample-log cross sections developed by O'Brien and Cole. O'Brien, as a well-site geologist, has prepared sample logs of dozens of wells in the area; his logs were supplemented by numerous sample logs in the Oklahoma Well Log Library. Cores from five wells in the area were examined by the authors (Fig. 2). Descriptions of three of the cores (numbered in Fig. 2), which were studied in detail, are included in the Appendix.

STRATIGRAPHIC NOMENCLATURE

Figure 3 shows the Morrowan nomenclature used in this paper. A representative log from the study area is shown in Figure 4. The name *Union Valley Sandstone Member* was given by Hollingsworth (1933, 1934) to a thick sandstone and overlying thinner limestone of the Wapanucka Formation (Morrowan) in the Lawrence uplift area of the northeastern Arbuckle Mountains (Fig. 2). Hyatt (1936), in a paper on the Fitts pool, refers to the Union Valley *Formation* with two members, the Union Valley Sandstone and Union Valley Limestone. Barker (1951) described the Union Valley Formation in the Lawrence uplift area as 125–260 ft of sandstone overlain by 12–25 ft of sandy limestone. The shale below the Union Valley was called *"Springer"* (Barker's quotation marks), thereby restricting the Wapanucka Formation to the shale and limestone above the Union Valley Formation in the northeastern Arbuckle area (Fig. 3). In the frontal Ouachitas, the Wapanucka Formation includes the interval from the top of the "Springer" shale to the base of the Atoka Formation (Sutherland and Manger, 1979).

The Morrowan rocks at the surface in northeastern Oklahoma and northwestern Arkansas (Ozark uplift area) were assigned to the Hale and Bloyd Formations (Moore, 1947; Huffman, 1958). The terms *Hale* and *Bloyd* have also been used for the subsurface, especially near the Ozark outcrops (e.g., Laudon, 1958). Based in part on differences in lithology between the Morrowan rocks in Oklahoma and the lithology of the Hale and Bloyd type sections in Arkansas, which have much more sand and shale, Sutherland and Henry (1977) defined two new formations for the Morrowan rocks in the Oklahoma Ozark outcrops, the McCully and Sausbee Formations. We correlate the subsurface Union Valley limestone, Wapanucka shale, and Wapanucka limestone with the McCully and Sausbee Formations of the Oklahoma Ozark outcrop and with the Union Valley and Wapanucka Formations in the Lawrence uplift area (Fig. 3).

LIMESTONE-BANK FACIES

The thick carbonate-bank limestone was studied in the core of the Saket Petroleum No. 1 Noble well, Okmulgee County (Fig. 2, core 1). This core contains 112 ft of the Union Valley Formation and 36 ft of oolitic Pitkin Limestone (Mississippian). Wireline logs and the core lithology are shown in Figure 5; a detailed core description is included in the Appendix. The core consists largely of coarse to medium skeletal grainstone and packstone with abundant pelmatozoans, corals, bryozoans, molluscs, brachiopods, and foraminifers. A sandy siltstone 13 ft thick interrupts the carbonate sequence, as do 3 thin sandstones and 3 shaly intervals. Hardgrounds (1,949.8 and 1,969.1 ft) and corrosion surfaces (2,004.9 ft), as well as shale beds and other features, suggest periodic interruptions in sedimentation, possibly from drowning. Dissolution features and intraclastic conglomerates suggest periodic subaerial exposure. The fact that the core consists dominantly of coarse fossiliferous grainstones and packstones led us to interpret a shoal—a high-energy environment of deposition. The shaly

Derby, J. R.; O'Brien, J. E.; Cole, J. G.; and Swindler, D. L., 2000, Union Valley Limestone bank (Pennsylvanian, Morrowan), eastern Oklahoma, *in* Johnson, K. S. (ed.), Platform carbonates in the southern Midcontinent, 1996 symposium: Oklahoma Geological Survey Circular 101, p. 209–217.

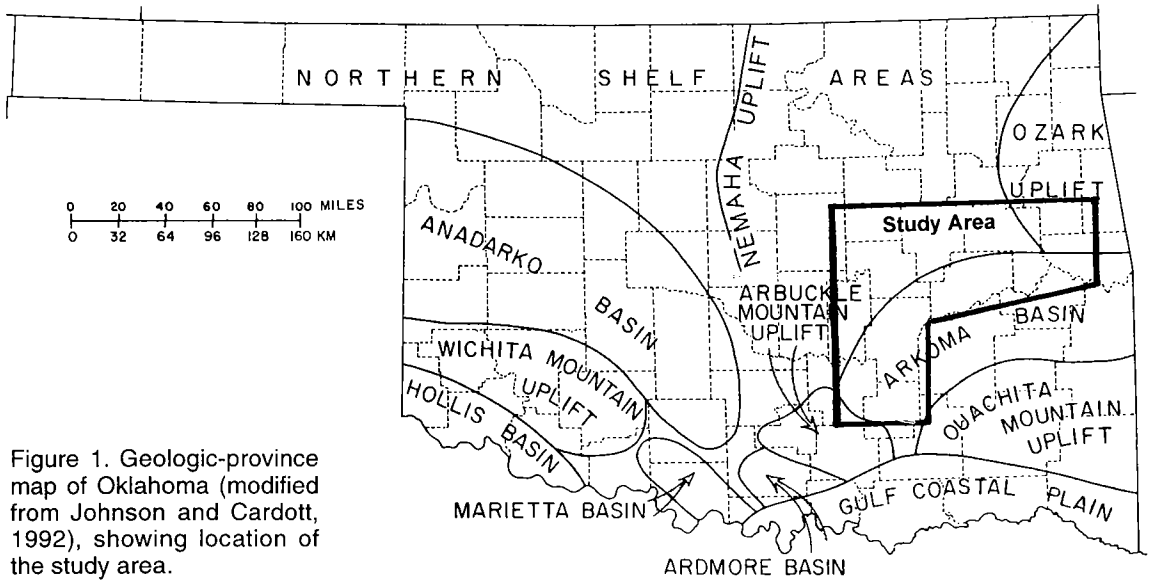

Figure 1. Geologic-province map of Oklahoma (modified from Johnson and Cardott, 1992), showing location of the study area.

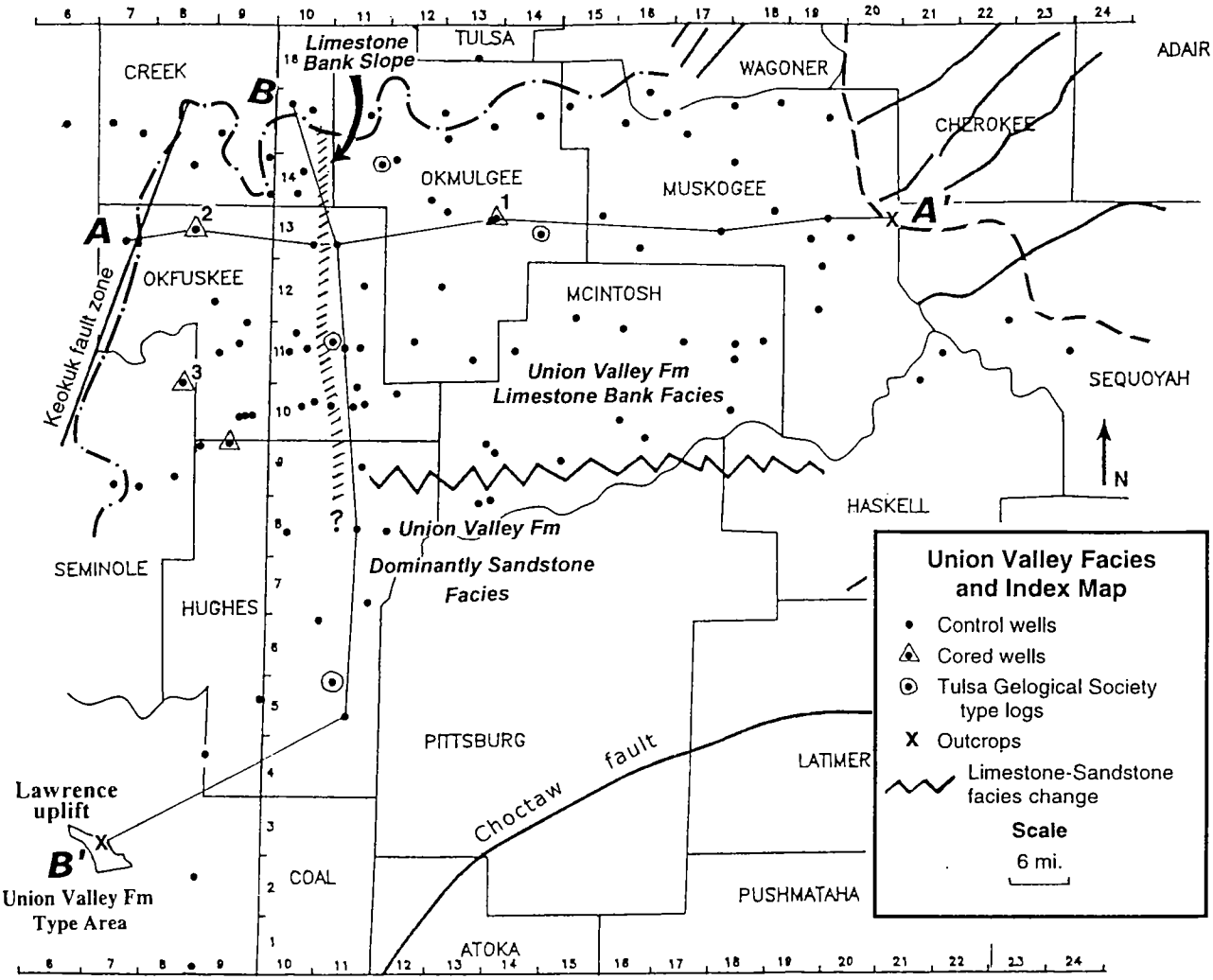

Figure 2. Union Valley facies and index map. The Union Valley limestone bank extends westward from Morrowan outcrops on the southwest flank of the Ozark uplift (dashed line) to the west-facing bank slope (north–south-trending hatched line). The Choctaw fault, the subsurface Keokuk fault zone, and major surface faults radiating from the Ozark uplift are shown by heavy solid lines. The dash–dot line shows the northern erosional limit of Morrowan rocks in the subsurface (modified from Karnchanakphan, 1979). Cross sections A–A´ and B–B´are shown in Figures 6 and 7, respectively.

Lawrence Uplift, Northeastern Arbuckle Mountains		Eastern Oklahoma Subsurface (this paper)	Ozark Uplift Oklahoma		Arkansas
Wapanucka Formation		Wapanucka limestone Wapanucka shale	Greenleaf Lake Limestone Shale "A" Member Chisum Quarry Limestone	McCully Formation	Bloyd Shale
Union Valley Formation	Union Valley Limestone Member Union Valley Sandstone Member	Union Valley limestone Union Valley sandstone	Brewer Bend Limestone Mbr Braggs Member	Sausbee Formation	Hale Fm

Figure 3. Morrowan stratigraphic nomenclature for the subsurface in eastern Oklahoma and outcrops in the northeastern Arbuckle Mountains and the Oklahoma Ozarks. In the left column (Lawrence uplift), nomenclature is from Barker (1951). In the right column (Ozark uplift), a shale above the Greenleaf Lake Limestone Member, originally designated the Shale B Member of the McCully Formation (Sutherland and Henry, 1977), was later assigned to the overlying Atoka Formation (Sutherland and Manger, 1979).

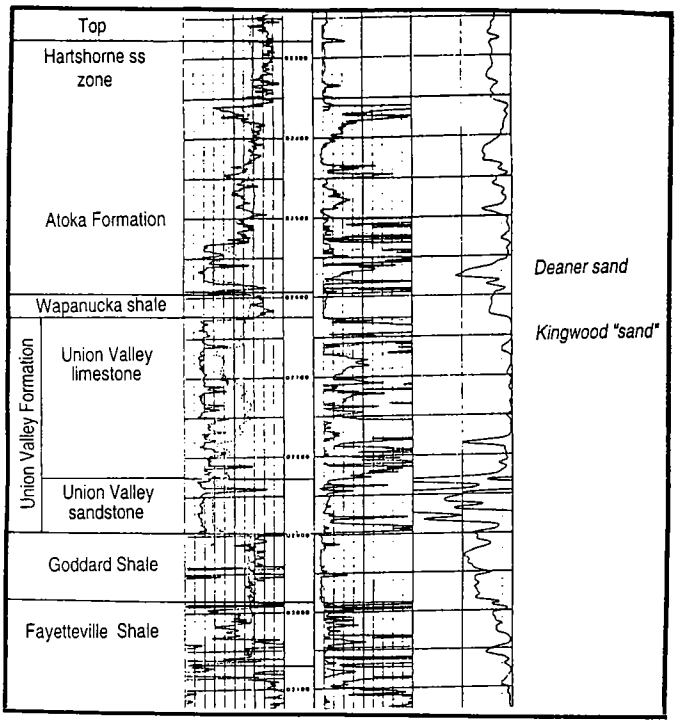

Figure 4. Representative log from the Union Valley limestone bank area: R. B. French Exploration No. 1 Hilderbrandt (SE¼SW¼NE¼ sec. 16, T. 11 N., R. 11 E.) in Deaner field. The upper part of the Union Valley limestone produced oil in Deaner field and was called *Kingwood sand* by drillers in the early 1920s. The "sand," however, is porous Union Valley limestone.

units may represent local lagoonal conditions on the shoal carbonate bank or possibly brief periods of drowning caused by relative sea-level rise.

The limestone-bank facies extends westward from the Morrowan outcrops of the Ozark uplift to R. 10 E. in a belt from Ts. 9 to 15 N. (Fig. 2). The limestone bank ranges in thickness from about 125 to about 250 ft and thins abruptly in R. 10 E. (Fig. 6). The abrupt thinning in R. 10 E. is also documented by a Union Valley limestone isopach map published by Busby (1986, fig. 2, p. 139). We interpret this abrupt thinning as a west-facing bank slope beyond which the Union Valley Formation is much thinner and sandier. West of the limestone bank, the "off-bank facies" contains 0–15 ft of sandy limestone and as much as 50 ft of calcareous sandstone (Fig. 6).

Cross section A–A′ also shows the correlation of the Union Valley limestone and the overlying Wapanucka shale and Wapanucka limestone to the Morrowan outcrop on the west flank of the Ozark uplift. North–south cross section B–B′ near the western edge of the bank is shown in Figure 7. The bank thins northward from about 250 ft in T. 11 N., R. 11 E., to about 50 ft in T. 14 N., R. 11 E. Farther north, the Union Valley limestone and overlying shale are truncated by the unconformity at the base of the Atoka Formation (Figs. 2,7).

OFF-BANK FACIES

West of the limestone-bank slope, extending to the western boundary of the study area, the off-bank facies contains ~15 ft of sandy limestone and as much as 50 ft of calcareous sandstone (Fig. 6).

Three cores from the off-bank facies were also studied (Fig. 2). Complete descriptions of cores from the Sunray D-X No. WI-5 North Cromwell Unit (sec. 4, T. 10 N., R. 8 E.) (core 3, Fig. 2) and the Gulf Oil Corp. No. 1 Droppleman (sec. 23, T. 13 N., R. 8 E.) (core 2, Fig. 2) are included in the Appendix. Wireline-log and core lithology for the Sunray well are shown in Figure 8. The off-bank cores are dominantly calcareous, fossiliferous sandstone with subordinate amounts of sandy limestone. The off-bank facies is dominated by small fossil fragments that are easily transported—largely fine fragments of bryozoans of the same types that are abundant in the limestone-bank facies.

Depositional features and burrow types (*Thalassinoides*) indicate offshore deposition in waters shallow enough to be well within the effective depth of currents and above wave base. The relief of the upper surface of the limestone bank (Fig. 6) suggests that the off-bank facies was deposited in water 100–200 ft deep, which is too deep for rapid carbonate production but is within the range of current and wave activity. The relationship of this facies to the thick carbonate bank suggests that the area west of the bank was unable to sustain in-situ carbonate production and received only carbonate material swept off the shallower water carbonate bank.

DOMINANTLY SANDSTONE FACIES

Southward from T. 11 N., R. 11 E., in the western part of the study area, the thickness of the Union Valley Formation (Union Valley limestone plus Union Valley sandstone) changes very little, except that the Union Valley

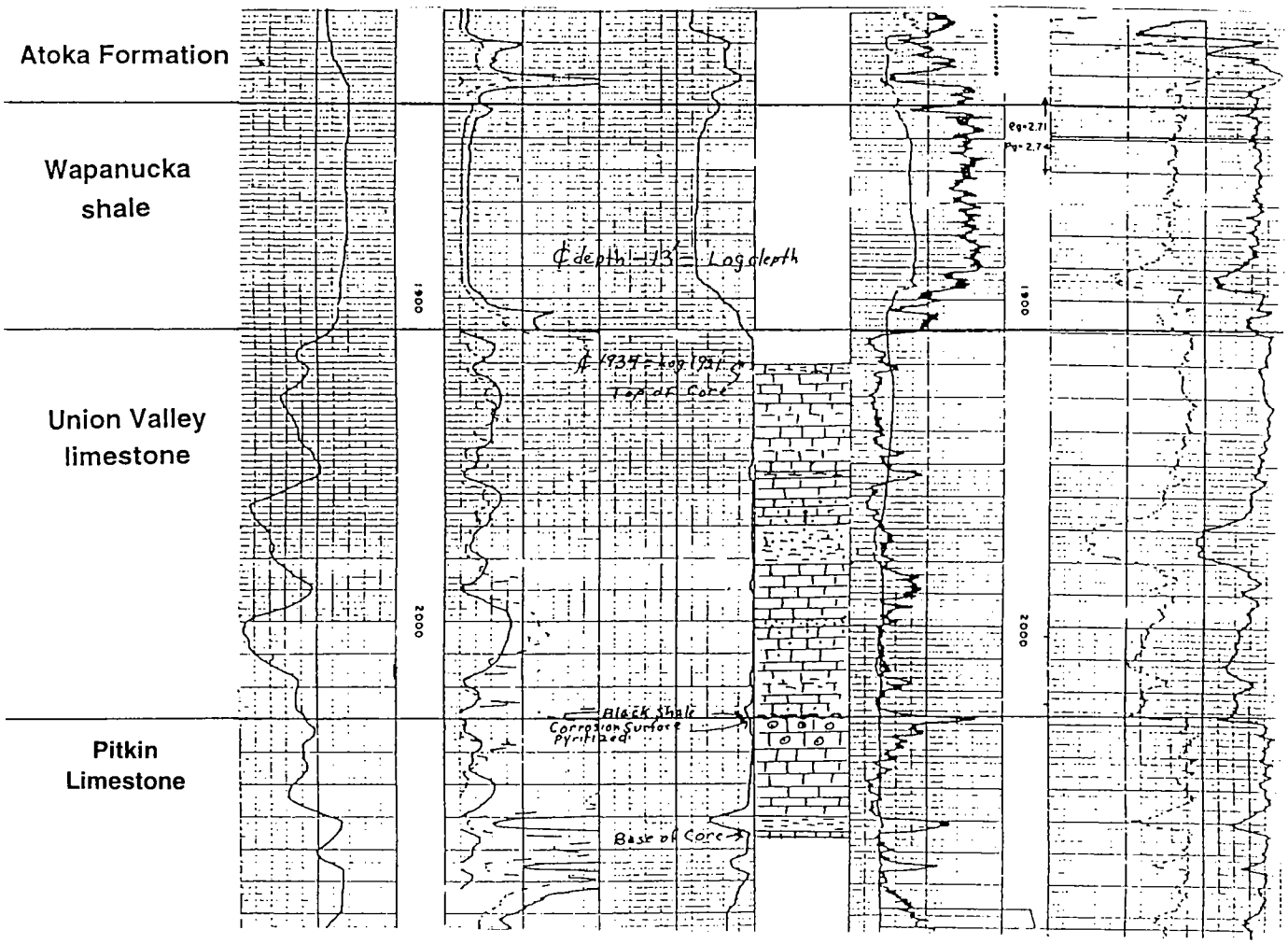

Figure 5. Wireline log and core lithology from Saket Petroleum No. 1 Noble (core 1, Fig. 2), sec. 12, T. 13 N., R. 13 E., Okmulgee County. The Union Valley limestone in this core is from the limestone-bank facies. See Appendix for core description.

sandstone thickens at the expense of the Union Valley limestone (Fig. 7). In the southwestern part of the study area, sample descriptions indicate a considerable amount of carbonate as fossil fragments and cement in a section composed dominantly of quartzose sandstone. The authors interpret the change from dominantly limestone to dominantly sandstone as a gradual facies change (Figs. 2,7). In the southernmost well in cross section B–B′ (sec. 21, T. 5 N., R. 11 E.), about 210 ft of Union Valley sandstone is overlain by about 20 ft of Union Valley limestone (Fig. 7). On the basis of similarity in thickness and lithology, the subsurface Union Valley in the southwestern part of the study area was correlated to the Union Valley Formation outcrop in the type area (Fig. 2), which was described by Barker (1951) as consisting of 150–260 ft of sandstone overlain by 12–25 ft of sandy limestone.

OIL PRODUCTION FROM THE UNION VALLEY LIMESTONE BANK

Reports of oil production from the Union Valley limestone are limited, owing to production being attributed to a variety of named units, one of which is the *Kingwood sand*. In the early 1920s, initial-production rates of 800 to 1,200 barrels of oil per day from the "Kingwood sand" were reported for wells in Deaner field (T. 11 N., R. 11 E.). This "sand" was later found to be porous limestone in the upper part of what is now known as the Union Valley limestone (Jordan, 1957). A log from Deaner field (Fig. 4) shows the upper part of the Union Valley limestone and the porous Kingwood "sand." The terms *Kingwood sand* and *Kingwood lime* were used to some extent in nearby fields and for other porous zones in the Union Valley limestone (Jordan, 1957). Although thin sandstone beds are present within the Union Valley limestone, in the areas where the name *Kingwood sand* has been used the production is actually from porous limestone, as determined by J. E. O'Brien.

DISCLAIMER AND FUTURE PLANS

This study is a work in progress, many phases of which remain incomplete. The senior author has taken the liberty of presenting his interpretation of the work of the study team; therefore, not all co-authors agree with, or should be held responsible for, all the interpretations and correla-

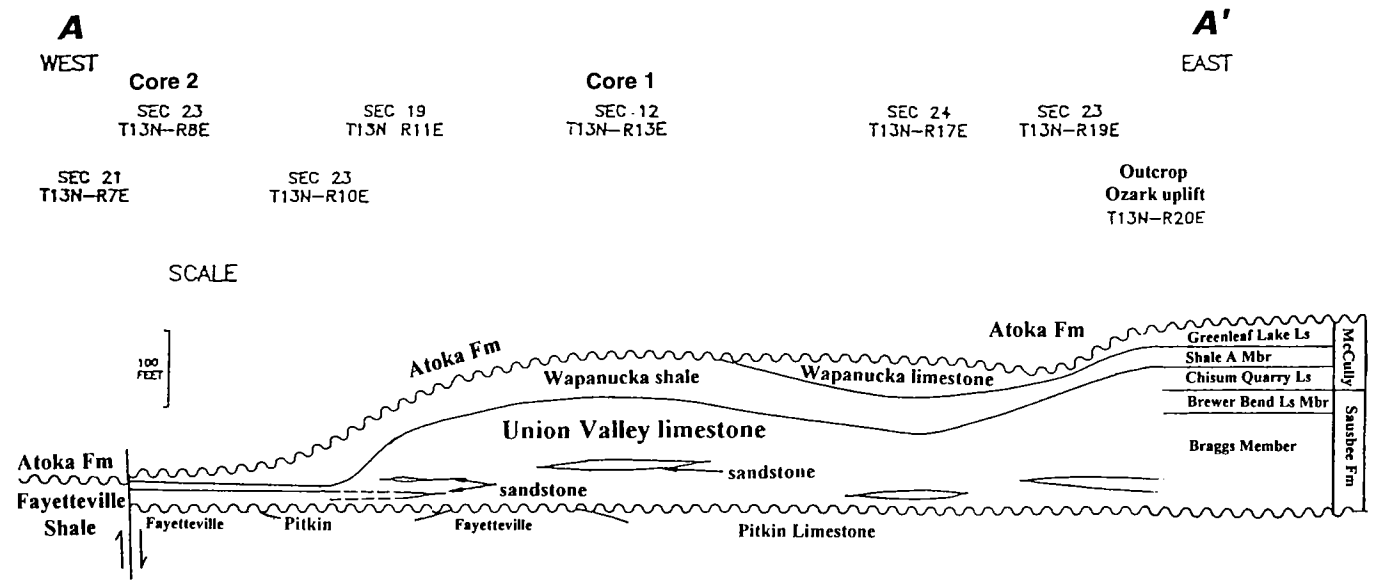

Figure 6. Schematic west–east cross section A–A′ across the Union Valley limestone bank. The section is based on wireline logs correlated to the McCully and Sausbee measured outcrop section published in Sutherland and Henry (1977). See Figure 2 for locations of wells and outcrop.

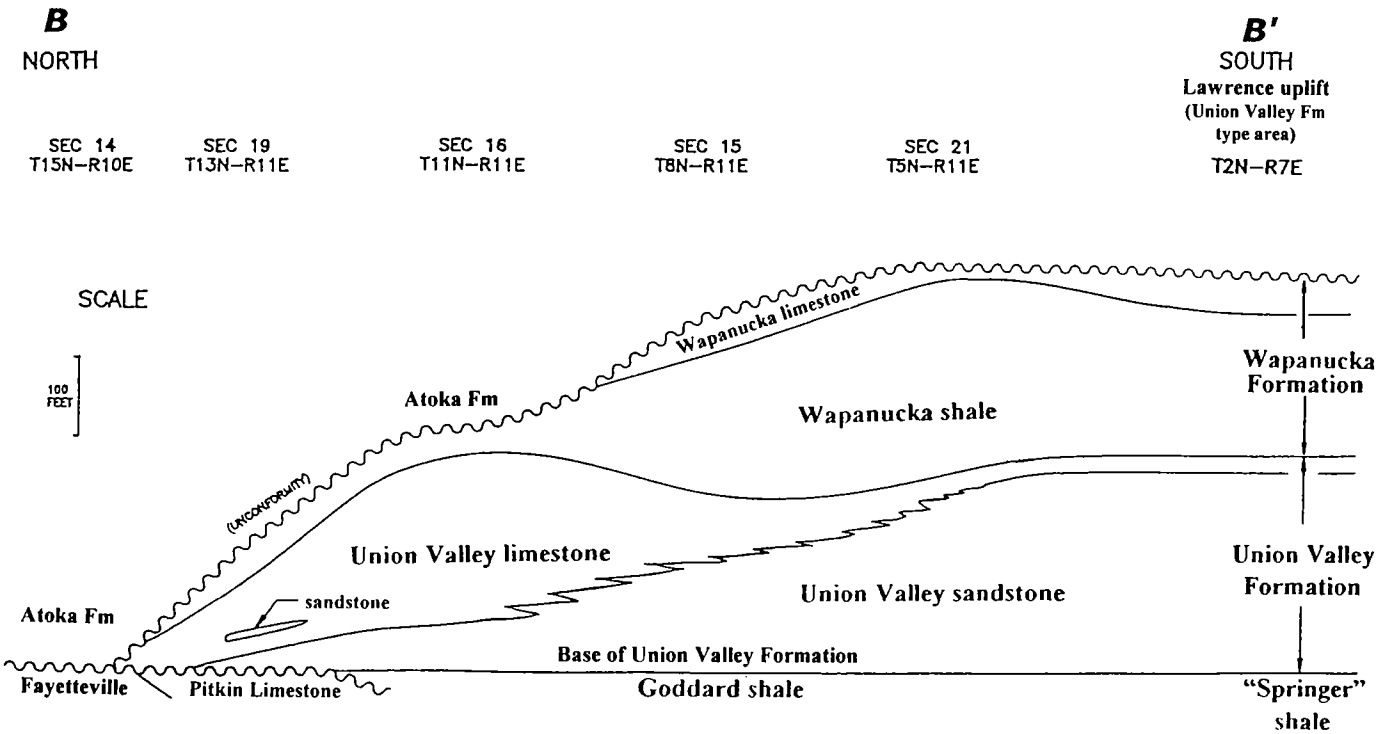

Figure 7. Schematic north–south cross section B–B′ across the Union Valley limestone bank and the Union Valley "dominantly sandstone" facies to the south. The section is based on wireline logs and on the lithology and thickness of the Union Valley and Wapanucka Formations in the Lawrence uplift area reported by Barker (1951). The contact between the Union Valley sandstone and the Union Valley limestone is a gradual lateral change in the ratio of carbonate to sandstone and is neither as sharp or as precisely located as suggested by the schematic cross section. See Figure 2 for locations of wells and outcrop.

tions presented herein. Especially incomplete at this time is the correlation of the carbonate bank into the southern sandstone facies, and detailed correlation across southern Seminole and western Hughes Counties to the Union Valley Formation type section in Pontotoc County. The intent of this paper is to document the thick Union Valley limestone bank and its relationship to the Morrowan outcrops on the eastern flank of the Ozark uplift and to the thinner off-bank facies to the west. In the future, we hope to document the age relationship of the thick limestone bank with the thin off-bank limestone and with the Union Valley Limestone Member of the Union Valley Formation at the type locality.

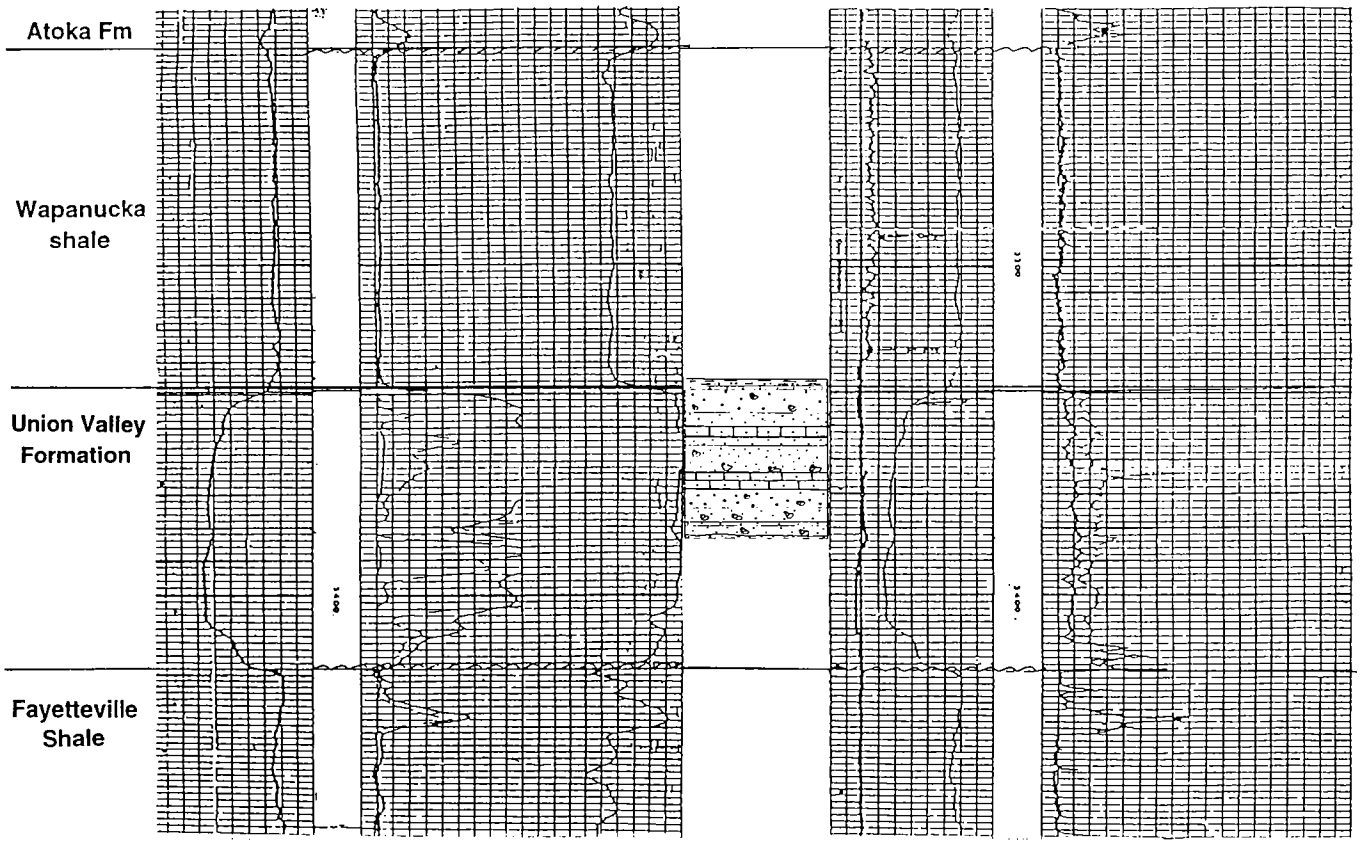

Figure 8. Wireline-log and core lithology from Sunray D-X No. WI-5 North Cromwell Unit (core 3, Fig. 2) in sec. 4, T. 10 N., R. 8 E. The Union Valley Formation in this core is from the off-bank facies. See Appendix for core description.

ACKNOWLEDGMENTS

The authors wish to thank the Oklahoma Geological Survey Core and Sample Library for use of the cores studied; Dr. Roderick Tillman of Tulsa, who examined some of the sandstone intervals in the cores and offered helpful suggestions; Mr. Peter L. Schultz, Geologist with A & M Engineering and Environmental Services, Inc., who prepared CAD drawings for Figures 2, 6, and 7; and Mrs. Jeanne Holcombe, also of A & M Engineering and Environmental Services, Inc.

REFERENCES CITED

Barker, J. C., 1951, The geology of a portion of the Lawrence uplift, Pontotoc County, Oklahoma: Tulsa Geological Society Digest, v. 19, p. 169–191.

Busby, J. M., 1983, Cromwell–Union Valley (Lower Pennsylvanian) relations in eastern Oklahoma: Oklahoma Geology Notes, v. 43, p. 4–9.

_____1986, Further notes on Union Valley–Cromwell (Lower Pennsylvanian) stratigraphic relationships in eastern Oklahoma: Oklahoma Geology Notes, v. 46, p. 135–139.

Hollingsworth, R. V., 1933, The Union Valley sandstone member of the Wapanucka formation: University of Oklahoma unpublished M.S. thesis, 118 p.

_____1934, Union Valley sandstone [abstract]: Proceedings of Geological Society of America, 1933, p. 364–365.

Huffman, G. G., 1958, Geology of the [south and west] flanks of the Ozark uplift, northeastern Oklahoma: Oklahoma Geological Survey Bulletin 77, 281 p.

Hyatt, D. L., 1936, Preliminary report on the Fitts pool, Pontotoc County, Oklahoma: American Association of Petroleum Geologists Bulletin, v. 20, p. 951–974.

Johnson, K. S.; and Cardott, B. J., 1992, Geologic framework and hydrocarbon source rocks of Oklahoma, *in* Johnson, K. S., and Cardott, B. J. (eds.), Source rocks in the southern Midcontinent, 1990 Symposium: Oklahoma Geological Survey Circular 93, p. 21–37.

Jordan, Louise, 1957, Subsurface stratigraphic names of Oklahoma: Oklahoma Geological Survey Guidebook 6, 220 p.

Karnchanakphan, Teerakun, 1979, Effects of shoreline movements and Mississippian paleotopography on Morrowan, Atokan, and Lower Desmoinesian depositional patterns in northeastern Oklahoma: University of Tulsa unpublished M.S. thesis, 71 p.

Laudon, R. B., 1958, Chesterian and Morrowan rocks in the McAlester basin of Oklahoma: Oklahoma Geological Survey Circular 46, 30 p.

Moore, C. A., 1947, The Morrow series of northeastern Oklahoma: Oklahoma Geological Survey Bulletin 66, 151 p.

Sutherland, P. K.; and Henry, T. W., 1977, Carbonate platform facies and new stratigraphic nomenclature of the Morrowan Series (Lower and Middle Pennsylvanian), northeastern Oklahoma: Geological Society of America Bulletin, v. 88, p. 425–440.

Sutherland, P. K.; and Manger, W. L., 1979, Comparison of Ozark shelf and Ouachita basin facies for Upper Mississippian and Lower Pennsylvanian Series in eastern Oklahoma and western Arkansas, *in* Sutherland, P. K.; and Manger, W. L. (eds.), Mississippian–Pennsylvanian shelf-to-basin transition, Ozark and Ouachita regions, Oklahoma and Arkansas: Oklahoma Geological Survey Guidebook 19, p. 1–13.

Tulsa Geological Society, Stratigraphic Committee, 1984–89, Type logs of Oklahoma: Riley's Electric Log, Inc., Oklahoma City.

APPENDIX
Core Descriptions

Core 1: Saket Petroleum No. 1 Noble
Sec. 12, T. 13 N., R. 13 E.
Okmulgee County, Oklahoma

Core depth (in feet) = log depth + 13 ft

Described by J. R. Derby, D. L. Swindler, and J. G. Cole

Union Valley Limestone:

1,934.0–1,936.1 Shaly limestone, nodular lime mudstone, and skeletal wackestone nodules in dark-greenish-gray (5 GY 4/1) lime mudstone, burrow-mottled; contains fragile bryozoans. Grades into unit below.

1,936.1–1,947.9 Limestone, coarse skeletal grainstone, mostly pelmatozoans; a few large (2-cm-diameter) colonial corals; locally abundant encrusting algae. Stylolites at 0.5–1-ft intervals, major clayey stylolites at 1,945.5 and 1,944.6.

1,947.9–1,951.1 Limestone, light-olive-gray (5 Y 6/1), fine–medium skeletal packstone contains large brachiopods, corals, and abundant small pelmatozoan fragments. Shaly intervals at 1,948.3, 1,949.4, 1,950.1, and 1,951.1. Corals encrust hardground surfaces between 1,949.8 and 1,950.3. Abrupt, sharp contact with unit below.

1,951.2–1,954.2 Limestone, light-olive-gray (5 Y 6/1), coarse skeletal wackestone and packstone; locally fossiliferous mudstone. Shaly interval (1,953.6–1,954.0) contains intraclasts of lime mud and lime-mud-filled brachiopods.

1,954.2–1,960.3 Limestone, light-olive-gray (5 Y 6/1), coarse skeletal grainstone and packstone with diverse fauna (solitary and small colonial corals, small bryozoans, brachiopods, and pelmatozoans); local lime-mud intraclasts and locally abundant glauconite.

1,960.3–1,961.2 Shaly limestone, coarse skeletal grainstone interbedded with dark-greenish-gray (5 GY 4/1) and greenish-black (5 GY 2/1) shale. Diverse fauna (pelmatozoans, brachiopods, fusulinids, bryozoans). Abrupt lower contact.

1,961.2–1,966.9 Limestone, medium-gray (N5), coarse skeletal grainstone and packstone with diverse fauna (pelmatozoans, brachiopods, fusulinids, bryozoans, and others) with scattered glauconite and sparse quartz sand. Basal 0.2 ft is shaly limestone with evidence of dissolution, compaction, and breakage of shells in shale matrix, which grades up into overlying clean limestone. Scattered zones within clean limestone are similar to, but less shaly than, basal 0.2 ft. Contains several thin stylolitic, slightly argillaceous zones. Abrupt base.

1,966.9–1,968.5 Shaly sandstone, very fine grained, silty, calcareous, dark-gray (N3). Rippled and wavy laminae of very fine quartz sand and fine skeletal debris are separated by black silty-shale laminae. Local small, horizontal to subhorizontal burrows. Base is sharp and stylolitic; top of underlying limestone is a corrosion surface. Top is a sharp, truncated surface.

1,968.5–1,969.1 Limestone, dark-gray (N3), oolitic molluscan wackestone to grainstone. Large molluscs (cephalopods and gastropods) in a matrix of sparry, oolitic grainstone gradationally interbedded with oolitic wackestone. Molluscan shells commonly contain geopetal void-filling spar. Top and base are sharp; top is a corrosion surface with truncated grains.

1,969.1–1,970.0 Limestone, light-olive-gray (5 Y 6/1); skeletal grainstone grades upward into oolitic skeletal grainstone. Diverse fauna, dominantly pelmatozoans, molluscs with trilobites, foraminifers, and dasyclad algae. Top 0.1 ft is a cemented hardground with evidence of dissolution, compaction, shell breakage, and grains with truncated upper surfaces.

1,970.0–1,983.4 Limestone, coarse skeletal packstone–grainstone, with 10% tan, very fine grained, glauconitic sandstone in very thin contorted lenses. Tops of some sandstone laminae sets appear to be iron-cemented hardgrounds.

1,983.4–1,996.0 Sandy siltstone, pale-yellowish-brown (10 YR 6/2), with light-gray (N7) carbonate-cemented burrow mottles. Unit becomes slightly coarser downward, grading into very fine sandstone with medium-sized fossil fragments and fossil-moldic porosity in lower 3 ft. Grades into unit below.

1,996.0–2,002.4 Limestone, light-olive-gray (5 Y 6/1), fine–medium skeletal packstone–grainstone, with thin fine-sandstone and sandy-limestone beds. Mostly tight, with local dissolution porosity in grainstones.

2,002.4–2,004.9 Sandstone with interlaminated black shale (10%). Sandstone is gray (N5), mostly fine grained, and contains glauconite and fine carbonate grains. Sandstone beds 1–3 cm thick separated by black-shale laminae differ in grain size and percentage of carbonate grains and glauconite; grain size ranges from very fine and silty to fine. Carbonate grains are very fine and range from 3 to 10%. Sandstone–shale contacts are very sharp; discrete sand-filled horizontal burrows are present at some contacts (no vertical mixing of sandstone and shale). Internal structure includes very faint horizontal burrow mottles, gently undulose laminae, and some cross-laminae. Contact with underlying limestone (at base of lowermost shale laminae) is sharp.

2,004.9–2,007.0 Limestone, light-olive-gray (5 Y 6/1), is interbedded with skeletal grainstone, packstone, and wackestone, mostly tightly cemented. Contains 2 laminated wackestone beds 1–3 cm thick. Diverse fauna is dominantly pelmatozoans with trilobites, brachiopods, foraminifers, molluscs (partly pyritized), corals, dasyclad algae, and bryozoans. Bryozoan in growth and near-growth position (2,005.7–2,006.3) is supported and filled with sandy grainstone. The same interval also contains a large cephalopod with geopetal void-filling spar. Large void at 2,006.3, partially filled with coarsely crystalline calcite (dogtooth spar) and saddle dolomite. Very fine quartz sand increases upward from <1% near base to 10% in upper 0.2 ft; horizontal burrows in upper 0.2 ft contain up to 30% sand. Top is probably a corrosion surface—upper 1 cm is faintly iron stained and has fairly open packing, with fossil fragments truncated at upper contact.

2,007.0–2,007.9 Sandstone, medium-gray (N5), fine-grained, very well sorted, with sparse fossil clasts, 1 colonial coral (*Chaetetes*?), calcite cement, horizontal-burrow mottles, and about 3% glauconite.

2,007.9–2,013.5 Limestone, light-olive-gray (5 Y 6/1), fine to coarse skeletal packstone with a few coarse pelmatozoans and corals (*Chaetetes*?), mostly tightly cemented. A few zones of dissolution porosity are present near top. Top 2 cm is argillaceous, stylolitic, and slightly iron stained. Unit is conformable with unit below.

2,013.5–2,030.8 Limestone, pale-yellowish-brown (10 YR 6/2), coarse skeletal packstone and grainstone with abundant fusulinids and pelmatozoans, sparse corals, and 5–10% dissolution porosity (grains and sparry cement). Unit is cross-bedded with foresets up to 30°. Base is gradational.

2,030.8–2,031.4 Limestone intraclast conglomerate, containing

lime-mudstone intraclasts, sandy-shale intraclasts, and very large fossil fragments in sandy matrix. Matrix is quartz sand (30%), fine carbonate, 3% glauconite, with sparry cement. Limonitic stain is common. Sharp base; top is gradational.

2,031.4–2,031.7 Shale, grayish-black (N2) and fissile, with sparse fine carbonate grains, grades downward, mainly by an increase in number and size of carbonate grains, to shaly, stylolitic, pyritic, coarse-grained limestone in basal 1 cm; contact with underlying unit is stylolitic, probably conformable.

2,031.7–2,041.9 Limestone, skeletal grainstone with medium to coarse skeletal grains (dominantly pelmatozoans with fewer brachiopods, bryozoans, and foraminifers), glauconite (common), and minor amounts of fine to medium quartz sand, and 5–10% dissolution porosity after grains and sparry matrix, and low-angle cross-bedding. Base is sharp, irregular, with load structures and soft-sediment deformation.

2,041.9–2,042.2 Shale, grayish-black (N2), fissile, organic-rich, and pyritic near base. Bedding, especially near base, is irregular, contorted by compaction over irregular top of underlying limestone. Base is sharp.

Pitkin Limestone:

2,042.2–2,045.7 Limestone, medium-gray to olive-gray, oolitic, fine skeletal grainstone interbedded with coarse skeletal packstone–grainstone and sparse darker, argillaceous thin laminae. Trace amounts of fine pyrite and glauconite are disseminated throughout. Base is sharp. Top is very irregular (1 cm relief), an apparent dissolution surface. Base is sharp.

2,045.7–2,046.1 Limestone, fine to coarse skeletal packstone grades upward to dark-greenish-gray limy shale, 1 cm thick.

2,046.1–2,057.8 Limestone, dark-gray to olive-gray (5 Y 4/1), peloidal mudstone and wackestone. Locally abundant skeletal debris and sparse thin skeletal packstone layers. Upper part contains interbedded fine skeletal wackestone.

2,057.8–2,058.0 Shale, grayish-black (N2), mostly nonfossiliferous. Upper 1 cm contains sparse skeletal debris (brachiopods and pelmatozoans) in discrete laminae.

2,058.0–2,073.0 Limestone, medium-gray (N5), mixed very fine skeletal grainstone with sparse cement and very fine skeletal, ooid, and coated-grain grainstone–packstone. Contacts between lithologies are gradational. Centimeter–decimeter-scale beds have faint cross-laminae. Trace of glauconite. Skeletal debris includes pelmatozoans, brachiopods, foraminifers, bryozoans, and sparse large cephalopods. Grades abruptly upward to shale.

2,073.0–2,076.0 Shale, grayish-black (N2), limy; sand-sized skeletal debris (foraminifers and pelmatozoans) and sparse chonetid brachiopods.

2,077.0–2,078.5 Limestone, olive-gray (5 Y 4/1), fine to medium skeletal packstone and wackestone interbedded in centimeter-scale beds. Traces of glauconite and pyrite.

Core 2: Gulf Oil Corp. No. 1 John Droppleman

Sec. 23, T. 13 N., R. 8 E.
Okfuskee County, Oklahoma

Depths in feet

Described by J. R. Derby, D. L. Swindler, and J. G. Cole

Core 1: 3,437–3,447 ft (8 ft recovered)

Union Valley Limestone:

3,437–3,439.5 Limestone, coarse sparry grainstone, dominantly pelmatozoan fragments with common fusulinids, cephalopods, corals, and sparse bryozoans. Thin zones contain sparse coarse quartz sand and glauconite grains. Unit becomes sandier downward. Lower 0.4 ft contains 10% medium quartz sand, contorted greenish-gray clay-rich laminae, and abundant stylolites. Clear spar cement, partly chalky; same fossils as in upper part plus large encrusting bryozoans and algae. Estimated porosity is 5%, most from dissolution of bryozoans and foraminifers. Slight chalky matrix porosity. Base not preserved.

3,439.5–3,441 Sandy limestone, coarse fossiliferous grainstone, with 20–40% medium to coarse quartz sand. Large fossil fragments, mainly pelmatozoans with minor brachiopods; about 3% coarse sand-sized and pebble-sized phosphatic grains. Chalky porosity in fine microspar cement. Base is sharp and stylolitic.

Cromwell sandstone (top from scout ticket is 3,440):

3,441–3,442 Fine sandstone (~150 mm), very well sorted, very calcareous in upper part, slightly calcareous below. Sparse (~2%) medium-sand-sized fossil fragments (bryozoans, mostly dissolved, and pelmatozoans); 2–4% glauconite.

3,442–3,446 Fossiliferous sandstone, medium quartz sand (60%), well sorted, calcite microspar cement, about 2% glauconite. Fossils are coarse-sand-sized pelmatozoans and bryozoans. Porosity ranges from 5 to 15% and is largely from dissolution of bryozoans.

Core 2: 3,447–3,452 ft (5 ft recovered)

3,447–3,451 Sandstone, fine–medium-grained, with scattered coarse pelmatozoans and large bryozoan fragments (mostly dissolved).

3,451–3,452 Sandstone, coarse to medium quartz sand with about 30% coarse sand and pebble-sized fossil fragments (mostly pelmatozoans and bryozoans), about 5% phosphatic black pebbles, and ~2% glauconite; 15% porosity after dissolution of carbonate grains.

Core 3: Sunray D-X No. WI-5 North Cromwell Unit

Sec. 4, T. 10 N., R. 8 E.
Seminole County, Oklahoma

Core depth (in feet) = log depth

Described by D. L. Swindler, J. R. Derby, and J. G. Cole

Union Valley Formation:

3,335.5–3,336.0 Shale, black, fissile, well-laminated, with a 2-cm-thick sideritic bed. Sharp base.

3,336.0–3,336.8 Muddy siltstone, medium and dark gray, with glauconite and scattered (~3%) coarse-sand-sized fossil fragments. Medium-gray siltstone laminae with 5% glauconite, intercalated with dark-gray muddy siltstone to silty-shale laminae with <2% glauconite. Beds 0.1–0.2 ft thick differ in relative abundance of clean and muddy laminae. Fossil fragments are mostly pelmatozoans. Bedding in lower 0.2 ft is distorted by compaction over irregular top of limestone below. Base is very sharp, irregular, and conformable.

3,336.8–3,338.1 Fossiliferous fine sandstone, pale-yellowish-brown, upper fine (Mz ~250 μm) quartz sand with about 35% coarse-sand-sized fossil fragments (1–3 mm), sand-sized phosphatic grains, and glauconite. Well cemented (sparry carbonate). Overall, well sorted; sandstone laminae are very well sorted. Carbonate grains are rounded, mostly pelmatozoans with some brachiopods, cephalopods, and bryozoans. Faint low-angle (5°–10°) lamination. Contact with unit below is abrupt, conformable, and is marked by a color change and difference in cementation.

3,338.1–3,345.5 Fossiliferous medium sandstone, yellowish-brown, moderately well-sorted, 55% medium (~300 μm) quartz sand, 15% coarse carbonate grains (~1 mm, 2–3 mm in some laminae), 15% sparry calcite cement. Porosity (15%, estimated) is from dissolution of fossils and cement. Pale brown clay (drilling mud?) lines some fossil molds and occupies some intergranular spaces. Fragments of fenestrate bryozoans parallel to bedding. Overall, coarsens upward slightly, and percentage of carbonate grains increases upward.

3,345.5–3,349.4 Fine sandstone (~200 μm), pale-yellowish-brown, oil-stained, very well sorted. Sandstone with sparse to no carbonate grains and ~5% scattered sand-sized, soft, dark grains is interbedded with sandstone that contains up to 20% scattered fossil fragments. Carbonate grains are mostly altered pelmatozoans with fewer brachiopods and bryozoans. Low-angle laminae. Porosity is ~8% (estimated). Base not preserved.

3,349.7–3,352.9 Sandy grainstone, pale-yellowish-brown. Coarse-sand-sized (Mz ~1 mm), well-sorted carbonate grains are mostly pelmatozoans and foraminifers (many are leached) with 10% fine quartz sand (Mz ~250 μm); 1–2% glauconite and 1–2% pyrite. Inclined beds 0.1–0.3 ft thick are separated by millimeter-scale sandy beds that contain 30–70% fine quartz sand. Base is sharp and irregular.

3,352.9–3,355.6 Fine sandstone, pale-yellowish-brown, fine-grained (Mz 177 μm), very well sorted; contains 15% coarse-sand-sized carbonate grains, small bryozoans, pelmatozoans, elongate and coiled foraminifers, trace of glauconite, and ~1% sand-sized dark grains. Estimated porosity is 7–8% and is mostly intergranular with some after dissolution of carbonate grains and cement. Sharp base. In top few centimeters, bedding is interrupted by near-vertical linear patches of very well oriented quartz grains (long axes are vertical) interpreted to be biogenic traces.

3,355.6–3,363.6 Sandstone, very fine-grained (Mz 125 μm), with 20% coarse-sand-sized carbonate grains; small bryozoans, pelmatozoans, elongate and coiled foraminifers, goniatites, and brachiopod fragments; colonial coral (*Chaetetes*?) at 3,359 ft. Estimated porosity is 7–8% and is mostly intergranular, with some dissolution porosity after carbonate grains and cement. Faint parallel–subparallel low-angle laminae; bedding is indistinct, evident as differences in sand- to carbonate-grain ratios, carbonate grain size, and amount of carbonate cement (most of which is clear spar). Bryozoans concentrated on bedding surfaces.

3,363.6–3,369.7 Sandy grainstone, pale-yellowish-brown; carbonate grain size ranges from fine sand to granules. Fine and medium grains are dominantly foraminifers and bryozoans; coarse grains and granules are dominantly pelmatozoans with some brachiopods and cephalopods. Estimated porosity, about 12%, is largely from dissolution of foraminifers, bryozoans, and microspar. Base is sharp.

3,369.7–3,377.9 Fossiliferous sandstone, pebbly; 20% fine-pebble-sized pelmatozoans and phosphatic intraclasts interbedded with fine-grained calcareous sandstone, pale yellowish brown, with sparse fossils that are coarse sand–pebble sized (mostly pelmatozoans and brachiopods) and fragments of degraded (partly dissolved) bryozoans. Estimated porosity, 8–11%, mostly dissolution porosity. Local sideritic shale and black-shale rip-up clasts; more common in lower 1 ft. Base not preserved.

3,377.9–3,379.6 Sandstone, fine-grained (~150 μm), medium-gray, well-sorted, very slightly calcareous, with faint, wispy mottles, possibly biogenic, and one 4-cm-wide lined *Thalassinoides*-type burrow filled with very light-gray clean sandstone. Estimated porosity is 5%. A 1–2-mm-thick black organic-rich shale lamination is present, and fine-sand-sized, round, argillaceous, black grains are scattered throughout (~2%). Base not preserved.

3,379.6–3,382.0 Fossiliferous sandstone, pale- to medium-yellowish-brown. Coarse sand- to granule-sized carbonate grains, with upper fine to medium quartz sand interbedded with medium-grained sandy grainstone. Abundant small bryozoan fragments are partially dissolved; large carbonate grains are dominantly pelmatozoans. Up to 3% dark phosphatic grains and black shale rip-up clasts. Estimated porosity is ~12%. Base is sharp.

3,382.0–3,383 Sandstone, pale-yellowish-brown, fine-grained, well-sorted, somewhat friable. About 20% bryozoans and foraminifers. Estimated porosity ~15% after dissolution of bryozoans and foraminifers. Core spacers with sample numbers indicate that core from 3,382 to 3,383 was recovered and tested; only about 0.3 ft remains.

Facies, Stratigraphic Relationships, and Fracturing in the Wapanucka and Spiro Formations (Pennsylvanian)

Darrell L. Mauldin
Geological Consultant
Abilene, Texas

Although gas production in the frontal Ouachita Mountains has been primarily from the Spiro Sandstone, limestone of the underlying Wapanucka Formation is locally a gas reservoir and thus is a secondary objective. An outcrop study of imbricate thrust sheets forms a basis for predicting the character of rocks in the subsurface.

The Wapanucka limestone crops out in the frontal Ouachita thrust system along the Choctaw fault (Fig. 1). The study area includes approximately 150 mi^2 along the northern margin of the Ouachita Mountains. Here, the Wapanucka–Spiro crops out as repeated thrust ridges in a narrow belt approximately 50 mi long and 5 mi wide just south of the Choctaw fault in Pittsburg, Atoka, and Latimer Counties in southeastern Oklahoma.

This paper is derived from the work done on a Master of Science thesis at Baylor University (Mauldin, 1996). The purpose of this Wapanucka study was to determine (1) detailed classifications by hand-sample and thin-section examination; (2) facies relationships; (3) distribution and geometry of each facies, particularly to define more precisely the location of the Wapanucka shelf margin; and (4) depositional environments. In addition, fractures were studied to determine their orientation, extent and intensity, and relationship to each lithofacies in the Wapanucka and Spiro. Five cross sections (see Mauldin, 1996) were constructed to demonstrate the vertical and lateral relationships of the Wapanucka, a middle shale (sub-Spiro), and the Spiro (Figs. 2,3).

Seven lithofacies were recognized in the Wapanucka out-

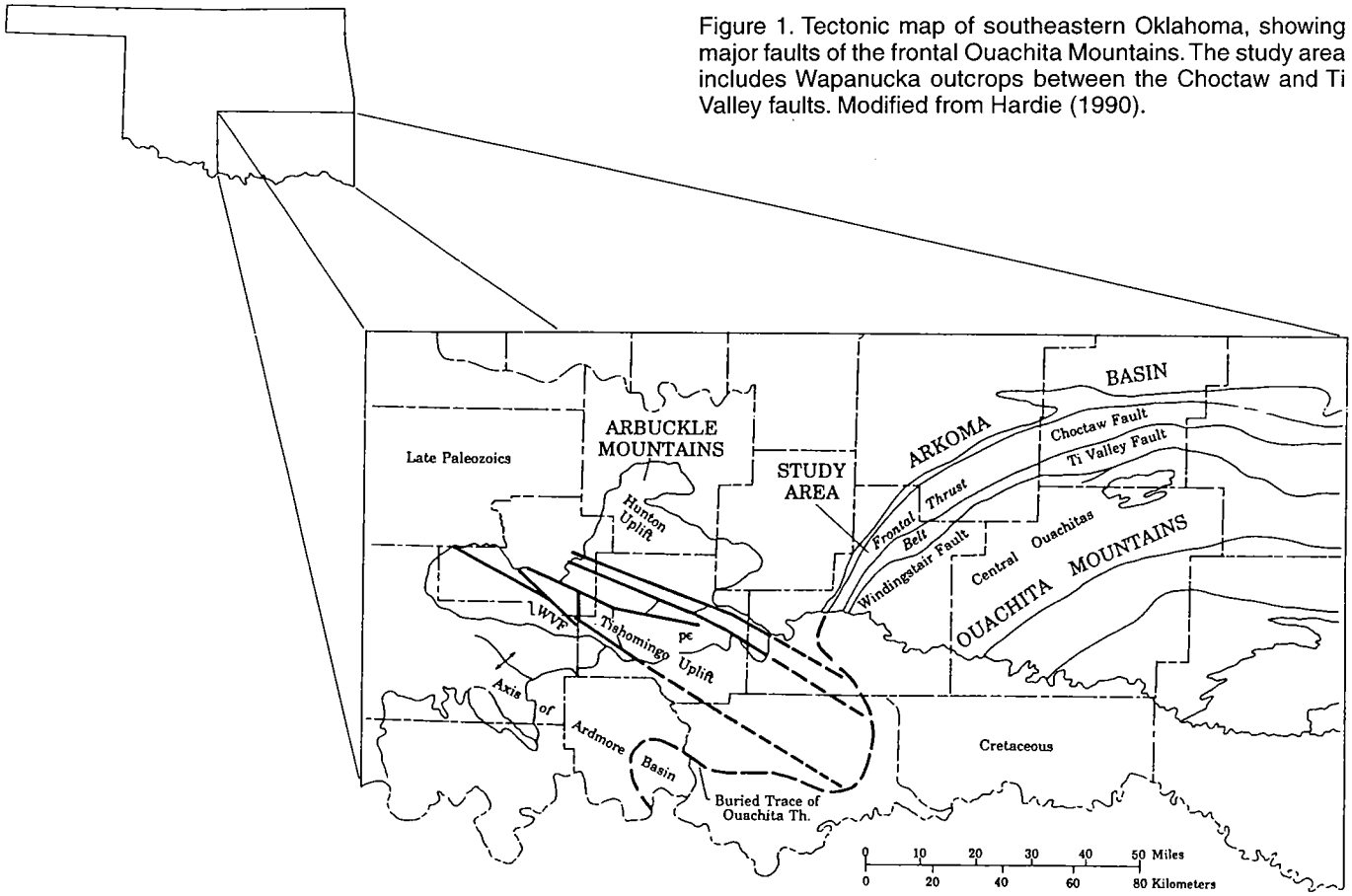

Figure 1. Tectonic map of southeastern Oklahoma, showing major faults of the frontal Ouachita Mountains. The study area includes Wapanucka outcrops between the Choctaw and Ti Valley faults. Modified from Hardie (1990).

Mauldin, D. L., 2000, Facies, stratigraphic relationships, and fracturing in the Wapanucka and Spiro Formations (Pennsylvanian), *in* Johnson, K. S. (ed.), Platform carbonates in the southern Midcontinent, 1996 symposium: Oklahoma Geological Survey Circular 101, p. 219–222.

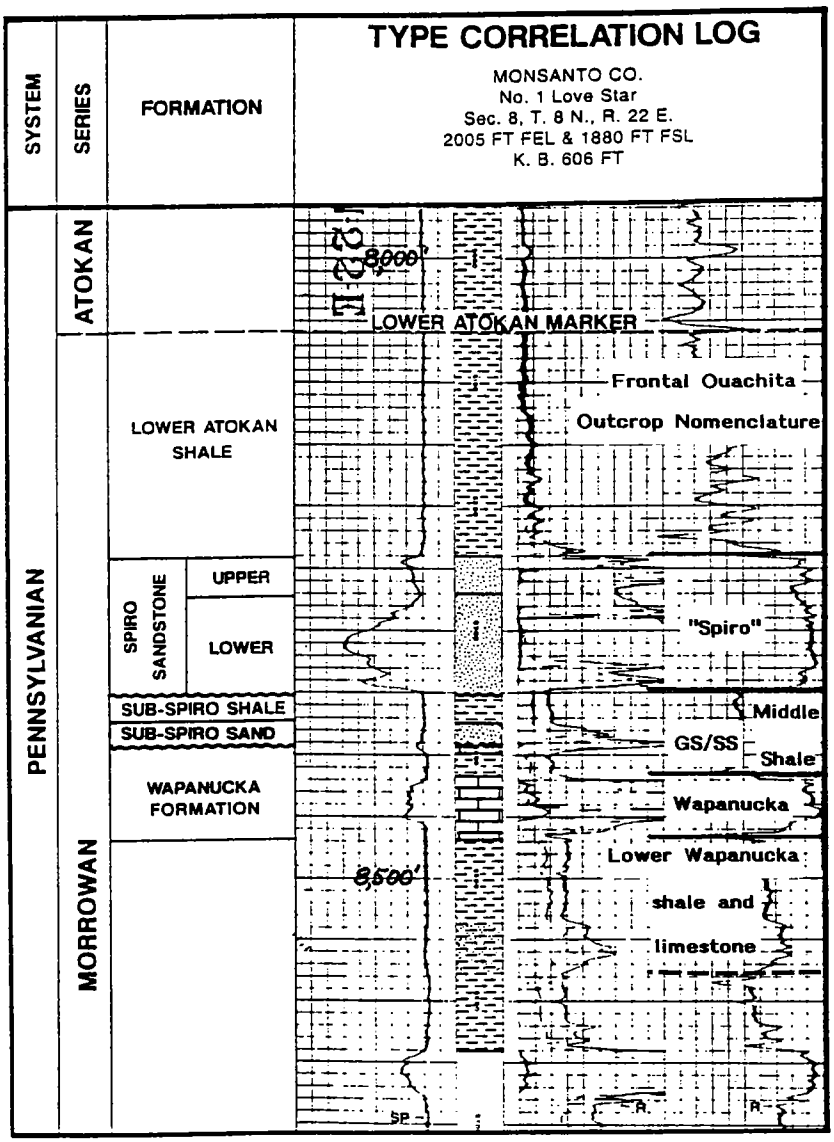

Figure 2. Frontal Ouachita outcrop nomenclature compared with a type correlation log for the Wapanucka and Spiro units. The right column shows the divisions and nomenclature for outcrops in this paper. The rest of the figure shows the subsurface nomenclature, age relations, lithologic character, and log character of upper Morrowan and lower Atokan units in the Arkoma basin and northern Ouachita Mountains (from Fritz and Hooker, 1994). Notice that the sub-Spiro sand of the subsurface is equivalent to the middle shale grainstone/sandstone (*GS/SS*) found at many outcrops. Also, the Wapanucka sequence in outcrop does not include any of the shale above the Wapanucka limestone, which has been included with the Wapanucka Formation for the subsurface. In addition to inclusion of the outcrop nomenclature with this figure, the Morrowan–Atokan series boundary has been moved up because the Atokan foraminifer *Profusinella* was not found in the Spiro either in outcrop (Groves and Grayson, 1984) or subsurface (Robert C. Grayson, Jr., personal communication, 1993).

crops. With the exception of the shale facies, deposition is generally a function of water energy and depth. From what are interpreted as roughly the shallowest to deepest water deposits, these facies are, in order: (1) "beach and near-beach," (2) oolitic calcarenite, (3) bioclastic grainstone/packstone, (4) foraminifer peloid packstone, (5) spiculitic limestone and sponge boundstone, (6) algal micritic limestone, and (7) shale.

The Wapanucka limestone is commonly characterized by upward-shoaling sequences. At the shelf margin (Fig. 4), these subtidal cycles are capped by shoaling carbonate sand bodies such as bioclastic and oolitic grainstones. In areas of paleotopographic highs, these shoal deposits can build up above sea level and form island beaches. Subaerial exposure is evidenced by the abundance of trees that grew on the islands, which are now preserved as large carbonaceous plant fragments that occur in the beach deposits. Foraminifer peloid packstones occasionally were formed as moderately agitated deposits on the flanks of the grainstone shoals.

Sponge boundstones and spiculitic limestones formed adjacent to the shelf margin, while phylloid algal bioherms formed in slightly deeper water (Fig. 5). Isolated sponges and sheetlike mats of sponge bioherms grew in fairly shallow water. Encrusting phylloid algae were abundant in localized areas. They formed in growth position in open-marine waters with tubular algae, and some of the phylloid-algal plates were found as higher energy bioclastic debris. Tubular algal (*Donezella*) boundstones were abundant in the deeper open-marine waters and occasionally formed small banks. Sponge spicules and fine clastics were transported to the lower shelf slope and deposited as spiculites and shale in the Chickachoc Chert (Fig. 4).

To gain a more thorough understanding of lithologic characteristics, lateral and basinward facies relationships, and the nature of depositional sequences is important, because well control and seismic data do not provide this kind of information. The detailed surface work performed in this study, however, has led to more complete information. These data could be used in association with subsurface geology to aid in hydrocarbon exploration.

The Wapanucka limestone contains several facies that are potential hydrocarbon-reservoir rocks. Therefore, a significant contribution of the study was identification of lithologies that might preserve primary porosity or those that might preserve fracture porosity and thus constitute possible reservoir facies.

The Wapanucka contains several facies associated with grainstone-shelf bars and phylloid-algal deposits that are possible reservoirs. These might contain primary or diagenetic porosity in the subsurface. Spiculitic limestones are highly fractured in outcrop, so they may contain fracture porosity in the subsurface.

Fracturing is believed to be of major importance to the reservoir potential of the Wapanucka limestone (Mauldin and Grayson, 1995). Studying the characteristics of fractures in imbricate-thrust outcrops of the Wapanucka allows the prediction of subsurface fractures. Numerous fractures in the frontal Ouachitas cut through bedding, and most of these are oriented perpendicular and/or parallel to strike.

This study proposes a new theory for depositional settings for spiculitic and algal limestones. Previous studies of the Wapanucka and other Paleozoic limestones of the Midcontinent usually assume that algal limestones are produced in very shallow water in lagoonal environments and that sponge and spiculitic limestones are deposited in deeper water, possibly even in a basinal environment. In the Wapanucka limestone, algal boundstones, wackestones, and mudstones were the deepest in-situ carbonate deposits, and the sponge boundstones and the spiculitic-limestone facies were deposited in shallow water, mostly near the shelf margin (Fig. 5).

An understanding of the stratigraphic boundaries and lithofacies of the Wapanucka, the middle shale (termed *sub-Spiro shale* for the subsurface), and the Spiro will lead to a better prediction of the location of potential petroleum reservoirs. Although the Spiro rests uncon-

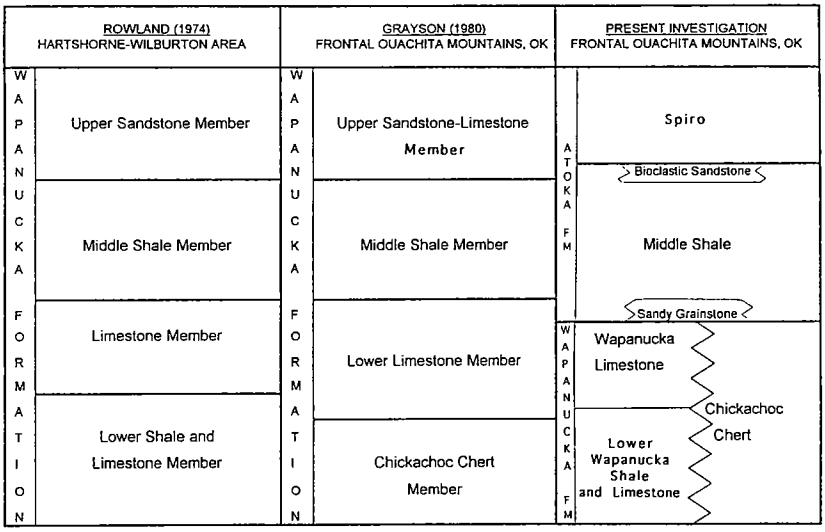

Figure 3. Stratigraphic divisions of this study and previous studies. Earlier informal stratigraphic subdivisions of the Wapanucka, middle shale, and Spiro are compared with those recognized in this study (at right). Modified from Grayson (1980).

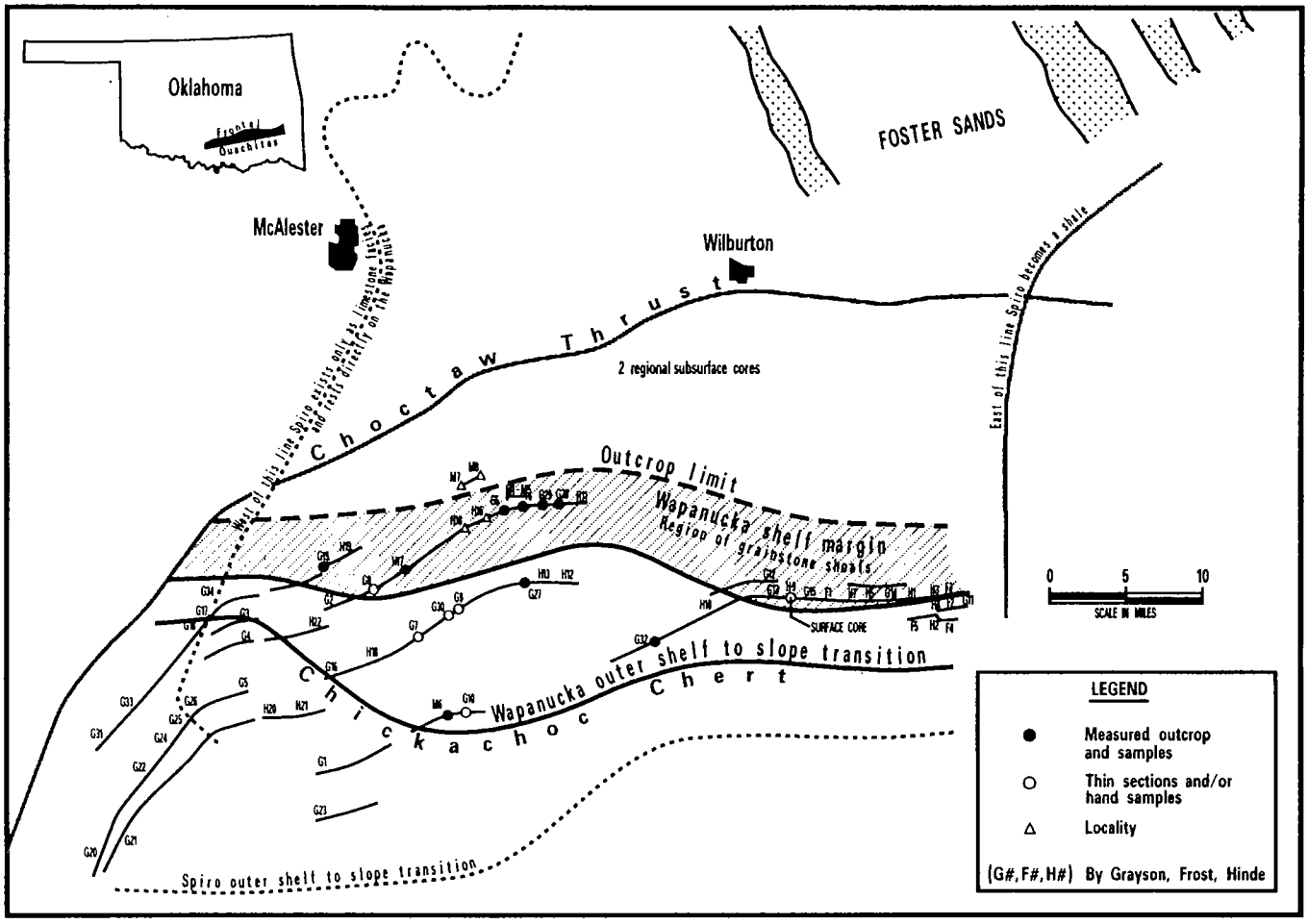

Figure 4. Palinspastic restoration of the Wapanucka shelf and outcrop locations in the frontal Ouachitas, southeastern Oklahoma. (Sample sites and outcrops are shifted 5–20 mi south of present position owing to palinspastic restoration.) The Wapanucka limestone contains grainstone shoals that were deposited as shelf bars on the outer part of a broad platform. Sponge-boundstone and algal-boundstone facies were deposited basinward of the shelf margin. The Chickachoc Chert was deposited on the lower shelf slope (adapted from Hinde, 1992). Locality number prefixes: *M* numbers denote localities described in this study; *H* numbers are from Hinde (1992); *F* numbers are from Frost (1981); *G* numbers are from Grayson (1980).

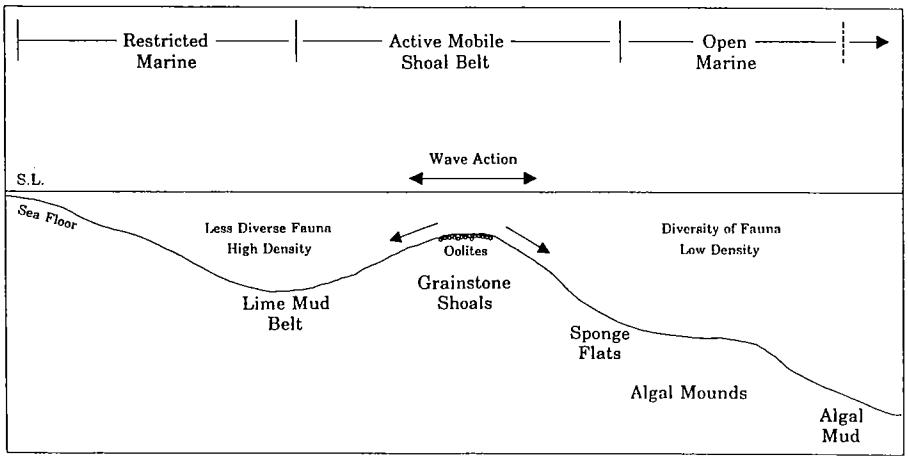

Figure 5. Generalized depositional model for Wapanucka limestones. *S.L.* = sea level. Grainstone shoals and basinward deposits of the Wapanucka crop out in the frontal Ouachitas of southeastern Oklahoma.

formably on the Wapanucka in some parts of the Arkoma basin, the base of the Spiro and the top of the Wapanucka are conformable surfaces throughout the frontal Ouachita outcrops. Small, discontinuous deposits of cross-bedded sandy calcarenites and bioclastic sandstones commonly occur within the middle shale sequence (Fig. 3). These are commonly referred to as the *sub-Spiro sand* for the subsurface (Fig. 2) and can make distinguishing the base of the Spiro and the top of the Wapanucka difficult.

REFERENCES CITED

Fritz, R. D.; and Hooker, E. O., 1994, Stop 10, Spiro sandstone, *in* Suneson, N. H.; and Hemish, L. A. (eds.), Geology and resources of the eastern Ouachita Mountains frontal belt and southeastern Arkoma Basin, Oklahoma: Oklahoma Geological Survey Guidebook 29, p. 64–67.

Frost, R. W., 1981, The stratigraphy and distribution of the Wapanucka Formation in the Red Oak/Wilburton area of eastern Latimer County, Oklahoma: Baylor University, Waco, Texas, unpublished senior thesis, 83 p.

Grayson, R. C., Jr., 1980, The stratigraphy of the Wapanucka Formation (Lower Pennsylvanian) along the frontal margin of the Ouachita Mountains, Oklahoma: University of Oklahoma unpublished Ph.D. dissertation, 319 p.

Groves, J. R.; and Grayson, R. C., Jr., 1984, Calcareous foraminifers and conodonts from the Wapanucka Formation (Lower–Middle Pennsylvanian), frontal Ouachita Mountains, southeastern Oklahoma, *in* Sutherland, P. K.; and Manger, W. L. (eds.), The Atokan Series (Pennsylvanian) and its boundaries—a symposium: Oklahoma Geological Survey Bulletin 136, p. 81–89.

Hardie, W. E., 1990, Subsurface structural study of the buried Ouachita Thrust front, southeastern Oklahoma: Baylor University, Waco Texas, unpublished M.S. thesis, 156 p.

Hinde, L. K., 1992, Stratigraphy and structural styles of the Spiro Formation, frontal Ouachita Mountains, southeastern Oklahoma: Baylor University, Waco, Texas, unpublished M.S. thesis, 100 p.

Mauldin, D. L., 1996, Lithofacies, regional depositional relationships, and fracturing in the Wapanucka limestone, frontal Ouachita Mountains, southeastern Oklahoma: Baylor University, Waco, Texas, unpublished M.S. thesis, 303 p.

Mauldin, D. L.; and Grayson, R. C., Jr., 1995, Wapanucka Formation (Morrowan): facies and fractures, frontal Ouachita Mountains, *in* Johnson, K. S. (ed.), Structural styles in the southern Midcontinent, 1992 symposium: Oklahoma Geological Survey Circular 97, p. 249–258.

Rowland, T. L., 1974, Depositional facies in the Wapanucka Formation (Lower Pennsylvanian) in the Hartshorne–Wilburton area, Oklahoma, *in* Shelton, J. W.; and Rowland, T. L., Guidebook to the depositional environment of selected Pennsylvanian sandstones and carbonates of Oklahoma: Oklahoma Geological Survey Special Publication 74-1, p. 46–51, 53–56. (Published in cooperation with Oklahoma State University for Field Trip 3, Geological Society of America, South-Central Section, 1974 annual meeting.)

Integrated Analysis of Reservoir Petrofacies in Platform Carbonates of Kansas: Techniques and Case Studies

John H. Doveton, W. Lynn Watney, and Willard J. Guy
Kansas Geological Survey
Lawrence, Kansas

Besides providing production information, wireline logs are typically the only data that are common to wells in an improved recovery effort, and it is imperative that they be calibrated with reservoir properties to provide substantive information for reservoir-management decisions and operations. The use of either rules-of-thumb procedures or simple petrophysical models may prove to be too rigid in the satisfactory resolution of complex platform-carbonate oil and gas fields. Heterogeneities in rock texture and pore geometry, coupled with layered reservoir structure, can cause perplexing log characteristics that require thoughtful analysis.

These problems and uncertainties have been known for many years and have been a factor in the continuing popularity of cross-plot methods. These methods provide the medium for pattern recognition, so that trends and discriminations within data clouds can be related to pay-zone evaluation and reservoir structure. Cross-plots are readily displayed on computer-monitor screens, while interactive spreadsheet programs allow real-time interaction and experimentation with parameters to provide optimal solutions (Doveton and others, 1996). Collectively, data clusters and trends reflect "petrofacies": associations of common attributes of rock textures, pore types, and related properties that control fluid saturations and permeabilities.

A cross-plot of log values of resistivity and porosity (the "Pickett plot") can be a fundamental tool in reservoir analysis. The disposition of points (Fig. 1, upper) gives general indications of reservoir character, which are made explicit when contour lines of water saturation and bulk-volume water (*BVW*) are added (Fig. 1, lower). The parameters of these lines are set by the classic Archie equations (Archie, 1942), and their location and orientation are found by the graphical procedure devised by Pickett (1973). The idealized Pickett plot (Fig.1) shows points from a water leg located along a fully water-saturated "water line" (*G–J*), a ragged trend of more resistive points from an overlying transition zone (*D–F*), which terminates in a steeply trending reservoir section where zones appear to be at "irreducible water saturation" (*A–C*). Low values of irreducible BVW reflect large average pore sizes; high values are linked with finer pores. The distinction is important, because it determines which zones should produce water-free oil or gas, and which should produce water or water-cut hydrocarbons.

The pattern-recognition approach is particularly valuable, because data can be compared directly and easily to production results rather than indirectly through results of model equations. As an illustration of this concept, Pickett plots are shown for Lansing–Kansas City (Pennsylvanian) zones in a single Kansas well that were all drillstem tested (Fig. 2). The DST production results (90 min measured or estimated cumulative flow period) were:

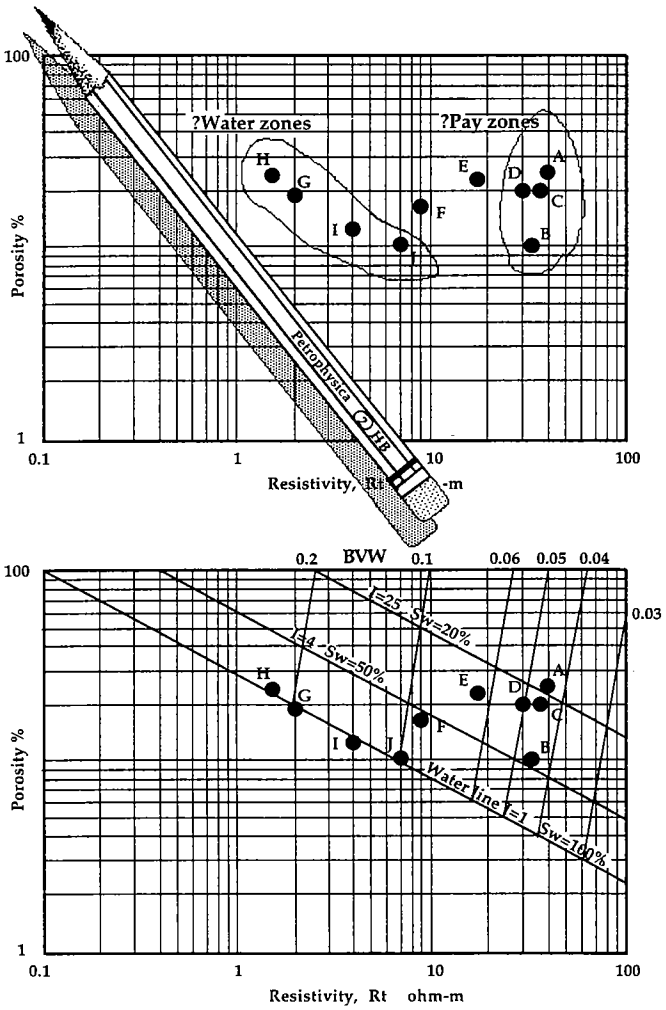

Figure 1. Schematic "Pickett plot" of a hypothetical reservoir, with cross-plotted zones (above) and the addition of water-saturation (S_w) and bulk-volume-water (*BVW*) contours (below).

Doveton, J. H.; Watney, W. L.; and Guy, W. J., 2000, Integrated analysis of reservoir petrofacies in platform carbonates of Kansas: techniques and case studies, *in* Johnson, K. S. (ed.), Platform carbonates in the southern Midcontinent, 1996 symposium: Oklahoma Geological Survey Circular 101, p. 223–225.

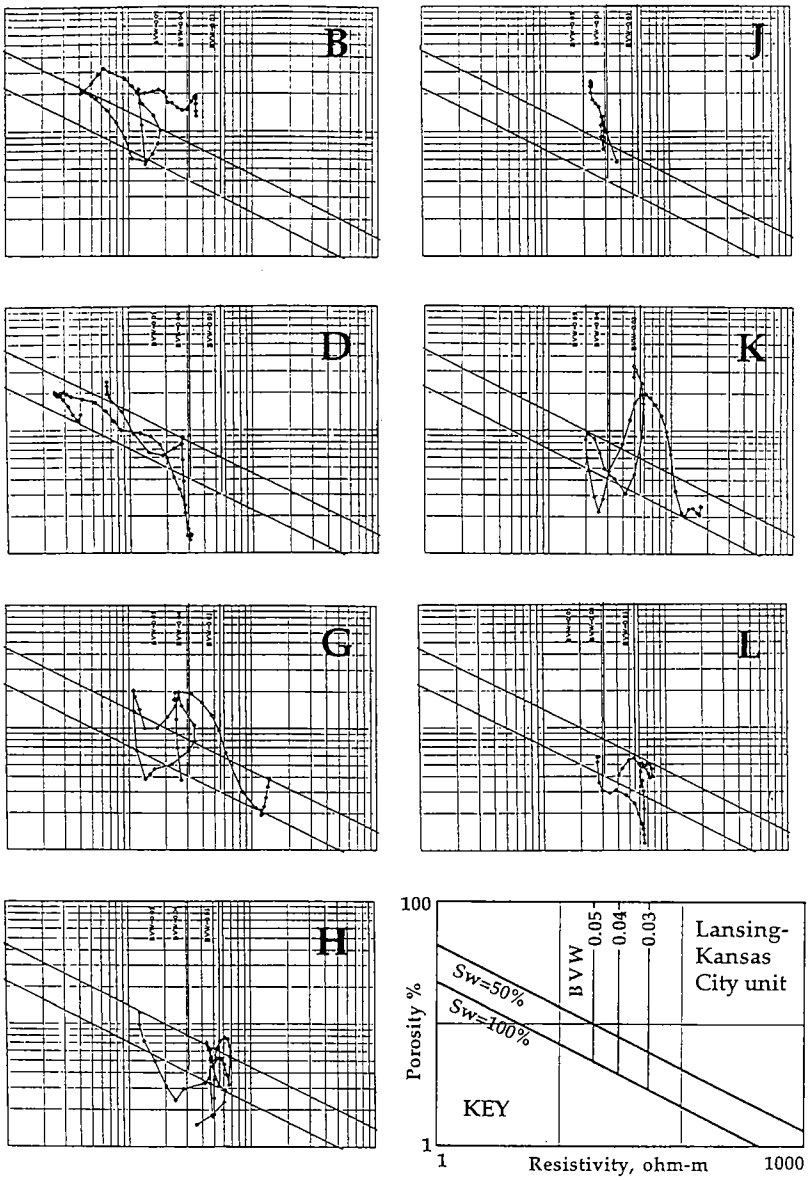

Figure 2. Pickett plots of Pennsylvanian Lansing–Kansas City intervals from a single Kansas well. All intervals were drillstem tested (see text for results).

Lansing B: 600 ft gas; 480 ft oil; 180 ft gas-cut muddy oil;
Lansing D: 747 ft mud-cut water;
Lansing G: 405 ft gas; 285 ft oil; 120 ft highly oil-cut mud;
Lansing H: 8 ft oil; 15 ft highly oil-cut mud;
Lansing J: 155 ft gas-cut oil; 135 ft highly oil-cut mud;
Lansing K: 630 ft gas-cut oil; 90 ft highly oil- and gas-cut mud;
Lansing L: 1,650 ft water.

Examination of the graphical patterns gives reservoir-specific keys to zone fluid content and producibility when viewed simultaneously in terms of porosity, water saturation, BVW (for effective pore size), and depth (for height of oil column). Intervals whose cross-plotted data show steep legs, low BVW values, and porosity development greater than 15% reflect limestones with well-developed oomoldic porosity and are close to irreducible water saturation (zones G, J, K). Similar patterns, but with porosities below 10%, indicate poorly developed oomoldic porosity, with either water production (zone L) or limited oil (zone H). Intervals with intermediate values of BVW signify smaller, intercrystalline porosity, with hydrocarbon production where water saturations are less than 50% (zone B) but water production where water saturations exceed 50% (zone D).

The file-handling and graphic capabilities of even small computers can also be used in the mapping of parameters observed from logs or computed from log analysis across fields or leases (Doveton and others, 1996). Maps can be displayed in plane or three-dimensional view that can be integrated with the tabular data from the spreadsheet or transferred into a text document. In the initial stages of an evaluation, simple maps are effective as quality-control devices to monitor log-data integrity and highlight potential inconsistencies in log analysis between wells. At a more mature stage, the maps can be used to view and interpret the spatial variation of structural, stratigraphic, and petrophysical variables. A map of the minimum BVW from each well section is a useful guide to locations with optimal reservoir conditions, because lower BVW values reflect larger pores and/or higher elevation above the hydrocarbon–water contact. In the example shown in Figure 3, a clear association exists between low values of minimum BVW and productive wells (nos. 4, 5, and 7).

The integrated strategy of iterative well-log analysis and spatial mapping with spreadsheet software offers a cost-effective tool to enhance the characterization of complex carbonate reservoirs. The approach can help the user in making improved decisions for reservoir management.

REFERENCES CITED

Archie, G. E., 1942, The electrical resistivity log as an aid in determining some reservoir characteristics: Transactions of American Institute of Mechanical Engineers, v. 146, no. 1, p. 54–62.

Doveton, J. H.; Guy, W. J.; Watney, W. L.; Bohling, G. C.; Ullah, S.; and Adkins-Heljeson, D., 1996, Log analysis of petrofacies and flow-units with microcomputer spreadsheet software: Tulsa Geological Society, Transactions of 1995 American Association of Petroleum Geologists, Mid-Continent Section Meeting, p. 224–233.

Pickett, G. R., 1973, Pattern recognition as a means of formation evaluation: Log Analyst, v. 14, no. 4, p. 3–11.

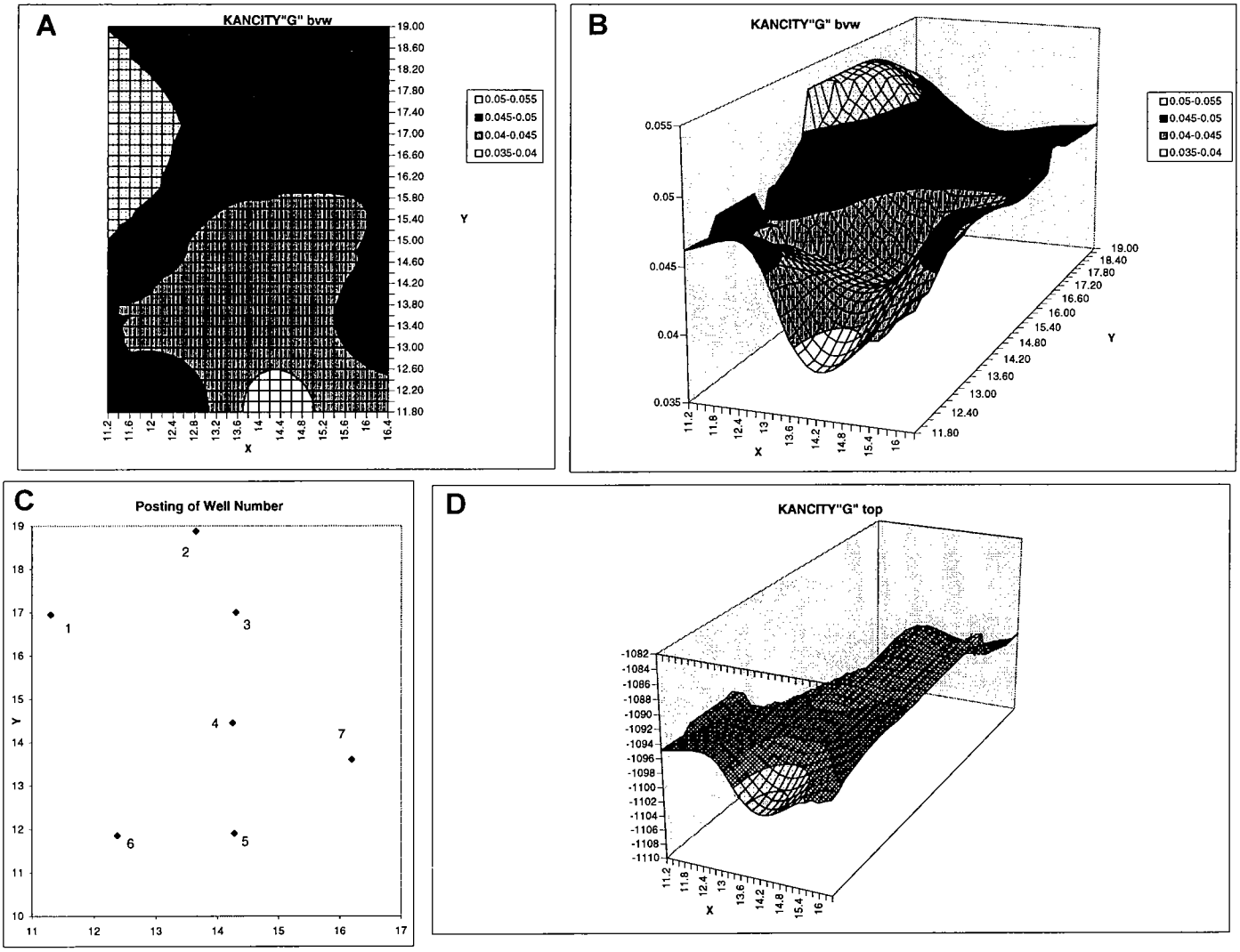

G ZONE			VALUES AT MINIMUM BVW			P-FACTOR	
Well	Subsea (feet)	Thickness (ft)	Sw	Porosity	BVW	phi/Sw	P-factor x h
1	-1109.00	6.00	38.00	14	0.0532	0.37	2.21
2	-1104.00	4.00	41.00	11	0.0451	0.27	1.07
3	-1092.00	5.00	28.00	17	0.0476	0.61	3.04
4	-1093.00	3.00	40.00	10	0.04	0.25	0.75
5	-1101.00	9.00	24.00	16	0.0384	0.67	6.00
6	-1094.00	8.00	43.00	11	0.0473	0.26	2.05
7	-1094.00	5.00	25.00	19	0.0475	0.76	3.80

Well	DST recovery (feet)	Total fluid rec. (feet)	Final flow pressure (psi)	Swab test (BFPD)	%oil	Lithology	Initial IP (BOPD)	Initial IP (BWDP)	Prod. zones
1									
2	276gip+306go+376gwco+184ocw	1142	298			microxln.			
3	230gip+140gco+90smwco+360somcw	820	259			dol. interxln vug			
4	345gip+305gco+185hogm	835	245	19.17	68	dol. sucrosic	67	7	c+g+h
5	185gip+295smgo+90gocm	570	176	13.92	95	pel. fos vug	55		g
6	120hgco+80ogcm	200	114			dol. sucros fine			
7	405gip+285fo+120hocm	810	137	5.88	9	dol. fine sucrosic	121	31	b+g+j+k

Figure 3. Map (A) and block diagram (B) of minimum BVW for G zone, map (C) of well locations, block diagram (D) of subsea elevation at the top of the G zone reservoir, and table (bottom) of reservoir parameters and test data. Graphic and tabular output can be compiled at one location to facilitate interpretation.

Sequence Stratigraphy and Reciprocal Sedimentation in Middle and Late Pennsylvanian Carbonate-Bank Systems, Eastern Shelf of the Midland Basin, North-Central Texas

Arthur W. Cleaves
Oklahoma State University
Stillwater, Oklahoma

ABSTRACT.—The Middle to Late Pennsylvanian Concho platform/Eastern shelf (of the Midland basin) and adjacent structural elements of north-central Texas illustrate a variety of settings for carbonate accumulation and reservoir development. With virtually all these carbonate buildups, the dominant mechanism for porosity formation involved meteoric diagenesis during eustatic sea-level lowstands when the carbonate facies were fully or partially exposed above sea level and contained a freshwater lens in pore spaces. Dolomitization, either from supratidal-flat brine concentration or from the impounding of water in evaporitic-shelf basins, played no role in porosity enhancement. Isolated buildups such as the Scurry atoll, Spur platform, Red River uplift, and Seymour pinnacle were subjected to minimal influx of terrigenous clastic detritus and underwent relatively lengthy histories of vertical accretion. Multiple episodes of eustatic lowstand gave rise to the formation of numerous zones of dissolution porosity, particularly in association with phylloid-algal-mound facies.

Carbonate deposition on the Concho platform/Eastern shelf during the late Desmoinesian through Virgilian Epochs evidenced several distinct patterns of reciprocal sedimentation owing to the presence of a major terrigenous clastic source area to the east (Ouachita Mountains). Carbonate-bank sedimentation in the late Atokan–early Desmoinesian Caddo and Odom systems was little affected by siliciclastics, because this material was trapped in the actively subsiding Fort Worth basin. The Odom banks developed on an early Desmoinesian (lower Strawn) ramp system that bordered the Midland basin, whereas the Caddo system accreted on the opposite side of the Concho platform facing the Fort Worth basin. However, beginning with the middle Desmoinesian Buck Creek cycle, deltaic systems prograded onto the platform. Reciprocal sedimentation was manifested by an alternation of carbonate-bank and -shelf accretion during eustatic sea-level transgressions and early highstands and deltaic progradation to the shelf edge or outer-ramp margin during lowstands. Hence, the growth of potential carbonate-reservoir facies was restricted to transgressive and highstand systems tracts.

Late Desmoinesian carbonate reservoirs on the Concho platform involved largely isolated phylloid-algal and *Chaetetes* buildups associated with marine transgressions across the lower and middle Strawn ramps adjacent to the Midland basin. Pinnacle reefs also became established on the outer margins of the ramps and occupied positions beyond the later formed shelf margin. By the latest Desmoinesian, subsidence in the Midland basin was sufficient to allow for the growth of the Anson shelf-margin bank system. Subsequently, during the Missourian, an accreting double bank formed (Palo Pinto–Winchell system) where the outer, shelf-edge bank grew only during lowstands (with the absence of deltaic facies) and the shelf-interior bank grew during the highstands, especially during the early phase when siliciclastics were being trapped in estuaries. Virgilian carbonate-bank deposition took place on a single shelf-margin bank complex in association with the transgressive and highstand systems tracts but was suppressed during lowstands. Highstand accretion was probably restricted to the early stage, when sea level was still rising. Subsurface evidence indicates that most of the Virgilian shelf-edge banks were drowned and became dormant when maximum flooding was attained. Active lowstand deltaic sedimentation prograded the shelf margin basinward and fed submarine fans.

All the major types of carbonate buildups, except perhaps the Missourian shelf–interor banks, represent important exploration targets and have yielded significant quantities of oil and gas production in north-central and west-central Texas. The Horseshoe isolated platform constitutes the most prolific hydrocarbon-bearing depositional system in the region, with more than 2 billion barrels in reserves credited to its various fields. Pinnacle buildups that developed basinward from (but parallel to) upper Strawn and Canyon shelf edges constructed smaller stratigraphic traps but have also contributed significantly to hydrocarbon reserves of the Eastern shelf. Shelf-margin, barrier banks of the uppermost Strawn and Canyon Groups, despite the large volume of potential reservoir rock contained within them, have provided fewer exploration successes. Strawn ramp–interior patch reefs containing phylloid algae and the sponge *Chaetetes* represent the most recent carbonate exploration play in the region. Three-dimensional seismic surveys can be exceedingly successful in pinpointing the location of these small reservoir-rock bodies.

Cleaves, A. W., 2000, Sequence stratigraphy and reciprocal sedimentation in Middle and Late Pennsylvanian carbonate-bank systems, Eastern shelf of the Midland basin, north-central Texas, *in* Johnson, K. S. (ed.), Platform carbonates in the southern Midcontinent, 1996 symposium: Oklahoma Geological Survey Circular 101, p. 227–257.

INTRODUCTION

During the Middle and Late Pennsylvanian, the Concho platform/Eastern shelf north of the Llano uplift comprised a region of mixed carbonate and siliciclastic sedimentation (Fig. 1). Terrigenous clastic sediment was derived principally as a result of uplift associated with collisional orogenesis in the Ouachita fold belt to the east. Carbonates accumulated as shelf and bank depositional systems in settings isolated from progradational fluvial–deltaic sedimentation. This isolation resulted either from physical barriers such as intervening basinal sumps between the terrigenous clastic source area and the sites of carbonate generation or from the effects of eustatic highstands of sea level, which caused the siliciclastic sediment to be trapped at the shoreline. Additionally, regional tectonism in the source area influenced the temporal distribution of carbonate facies. Carbonate sedimentation on the Eastern shelf was most prominent and widespread during the Missourian Stage (Canyon Group). At that time, uplift in the Ouachita trend of Texas was limited to areally restricted point sources near the present-day Red River.

With the exception of the Scurry atoll, carbonate depositional systems have proved to be less prolific hydrocarbon reservoirs than have siliciclastic delta, fan-delta, and submarine-fan systems. Individual pools have tended to encompass small geographic areas and thin stratigraphic intervals. Nevertheless, since the discovery of the Jameson reef (Coke County) in 1946, a moderate number of successful carbonate stratigraphic-trap plays have been carried out in north-central Texas. Interestingly enough, the two most active exploration plays pursued in the region during the middle 1990s involved the search for "Goen" patch reefs (Strawn Group) and Chappel (Mississippian) Waulsortian mounds.

Exploring for Pennsylvanian carbonate stratigraphic traps in north-central Texas is a considerably more difficult undertaking than the search for traps in siliciclastic facies. For example, electrofacies analysis of spontaneous-potential (SP) or natural-gamma-ray curves is an effective tool for facies interpretation within sandstone–shale sequences. Both the porosity/permeability characteristics and shale content of the sandstone reservoir commonly reflect the primary depositional environments where the sediment accumulated. Discrete parasequences, flooding surfaces, and parasequence stacking patterns, all of which enter into the sequence-stratigraphic interpretation of lithologic units, can be inferred from well logs without the use of outcrop or core descriptions. On the other hand, carbonate porosity and permeability are largely the product of post-depositional, diagenetic modifications that may have little to do with the original depositional environment. Electrofacies analysis of carbonates rarely provides diagnostic curve shapes or other indicators for characterizing unaltered primary depositional facies. Core studies involving cut slabs and thin sections are absolutely necessary for facies interpretation of subsurface carbonate reservoirs. Identification of porosity-enhancement mechanisms in carbonates often requires instrumental analysis of rock samples to obtain diagnostic isotopic signatures. Similarly, carbonate sequence-stratigraphic interpretation is directly dependent on "lithologic truth" for delineating facies successions, disconformity surfaces, and rapid changes of inferred water depth. Given the greater complexity of methodology necessary for evaluating carbonate reservoirs, it is not difficult to understand why the majority of explorationists working in north-central Texas have avoided getting involved with systematic searches for carbonate stratigraphic traps.

This paper discusses the Pennsylvanian subsurface stratigraphy of carbonate buildups in terms of the interaction between facies development, regional tectonics, and effects of cyclic eustatic sea-level changes. The presentation has four specific goals. The *first* of these is to furnish a province-wide overview as to the types of carbonate depositional systems present throughout north-central and west-central Texas. *Second,* the historical context for the accumulation of these systems will be considered in terms of the tectonic evolution of the Concho platform/Eastern shelf and its surrounding basins. Of critical importance here are the nature of the shelf margin (ramp or rimmed platform) and the stacking patterns seen for individual carbonate buildups at the shelf edge. A *third* goal

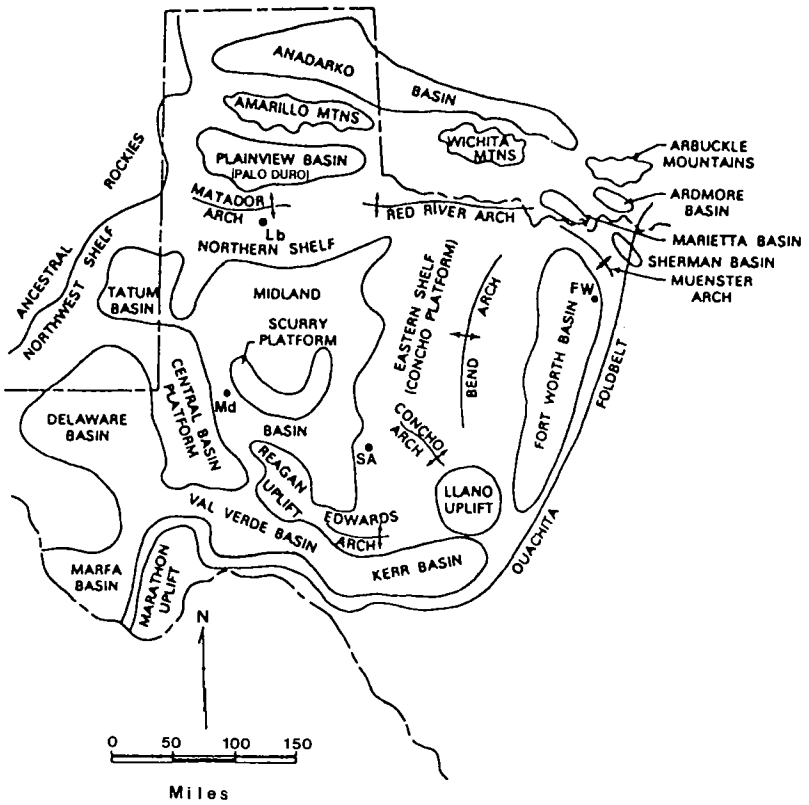

Figure 1. Structural elements of north-central and west Texas during the Pennsylvanian Period. Locations of Forth Worth (*FW*), San Angelo (*SA*), Midland (*Md*), and Lubbock (*Lb*) are indicated by dots. Modified from Wermund and Jenkins (1970).

involves demonstrating how sequence-stratigraphic concepts can explain the paleogeographic positioning, growth, and porosity/permeability development for the principal types of carbonate "reefal" buildups. The *fourth* and final goal is to outline an exploration approach useful for locating stratigraphic traps in Pennsylvanian carbonates across the Eastern shelf. Special attention will be devoted to delineating the most important carbonate exploration plays in the region.

CARBONATE DEPOSITIONAL SETTINGS AND REGIONAL STRATIGRAPHY

The distribution of carbonate depositional systems in mixed carbonate–siliciclastic settings is influenced by controls very different from those acting on terrigenous clastic systems such as deltas, barrier bars, or submarine fans. Carbonate sedimentation depends directly on the health and vigorous productivity of an organic calcium carbonate production factory to construct bank systems and accrete shelf platforms. Sediment generation occurs almost entirely within the ultimate environment of deposition. Carbonate particles thus undergo little, if any, transport. Consequently, it is not necessary for one to evaluate grain provenance or reconstruct sediment-dispersal pathways to explain the geometry and areal distribution of carbonate-rock bodies. Local environmental influences play the dominant role in determining primary sediment composition, texture, and initial (primary) porosity. Ecologic factors such as warm marine waters, shallow water depth (<80 ft), good circulation, absence of turbidity, and the presence of local or regionally elevated substrates taken together constitute necessary conditions for the active growth of carbonate systems. Heckel's reconstruction of the Late Pennsylvanian paleogeography for Texas and the Midcontinent region (Fig. 2) clearly shows that the Eastern shelf of the Midland basin was situated within the tropics less than 10° from the equator (Heckel, 1980). Hence, the climate was hot, humid, and perhaps monsoonal in nature (Fig. 2).

On the basis of extensive research during the last 30 years, exploration geologists have delineated five principal types of stratigraphic-trapping styles that give rise to prolific production in carbonate reservoirs (North, 1985). It is meaningful to review these situations, as several of them are well exemplified by oil and gas fields in north-central and west-central Texas.

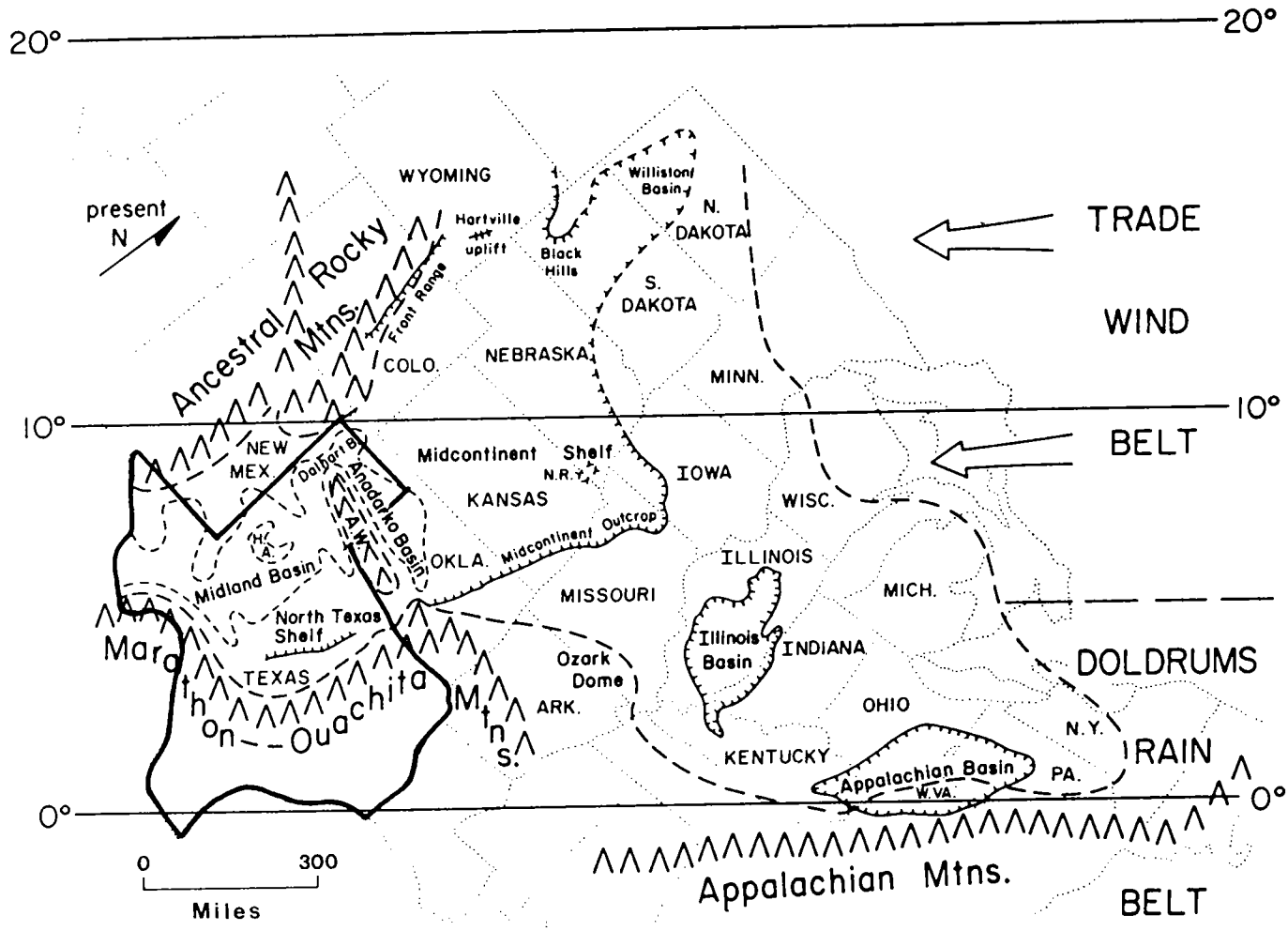

Figure 2. Late Pennsylvanian paleogeography of the Midcontinent and east-central United States, showing the paleotectonic and paleodepositional settings for the region. Note that the Midland basin and adjacent shelf regions to the east lay at approximately 5° N. latitude. *N.R.* = Nemaha ridge; *H.A.* = Horseshoe atoll; *A.W.* = Amarillo–Wichita Mountains. Modified from Heckel (1980).

The *first* of these trap scenarios involves subtidal and intertidal lagoonal-facies assemblages that undergo updip lithologic changes. Evaporite sedimentation associated with either isolated (barred) marine-water bodies or arid-area supratidal flats (sabkhas) plays an important role in generating the porosity/permeability contrasts needed for stratigraphic traps.

With the lagoon or barred basin, hypersaline brines accompanying evaporite precipitation dolomitize the various subtidal facies to produce intercrystalline and dolomoldic porosity. Massive gypsum, anhydrite, or halite may be interbedded with more typical open-marine facies. The middle–Late Permian evaporites of the Midland basin and the Middle Silurian deposits in the Michigan basin both exemplify large, silled basins containing thick intervals of sulfate or halide minerals. Smaller, lagoonal, hypersaline water bodies may form in isolated lows on carbonate platforms during marine regressions that bring the shoreline out to the shelf edge. Such stranded, high-salinity salinas caused extensive dolomitization of subtidal facies on the Permian western shelf of the Delaware basin (Guadalupe Mountains region).

Cyclic sabkha deposits represent another type of evaporite setting that demonstrates updip facies change. Dolomitization generates reservoir rock because precipitation of calcium phosphate (gypsum or anhydrite) in the supratidal facies gives rise to brines that are enriched in magnesium and depleted in calcium. These brines flow basinward in the local ground-water column because of their greater density. Porosity is formed in the intertidal and subtidal facies owing to the dissolution of calcite or aragonite and its replacement with rhombic dolomite crystals. In the supratidal facies, the evaporite minerals occlude porosity and serve as the seal. Sabkhas are important reservoirs in the San Andres Formation (Upper Permian) of the Central Basin platform and the northwestern shelf of the Midland basin.

Evaporite basin and sabkha carbonate systems constitute sedimentologic responses to arid climatic conditions. As noted previously, paleogeographic reconstructions place the Middle and Late Pennsylvanian Concho platform/Eastern shelf in the humid tropical belt near the paleoequator. Consequently, no major evaporite accumulations have been noted either in outcrop or in the subsurface for the rock units under consideration. Tidal-flat facies are present in the outcrop zones of the Strawn, Canyon, and Cisco Groups of north-central Texas but invariably are preserved as laminated siliciclastics and not as a carbonate–evaporite suite of minerals. True carbonate sabkha facies first appeared in late Paleozoic sediments of north-central Texas near the end of the Wolfcampian (Early Permian).

The *second* significant setting for carbonate reservoirs emphasizes the importance of organic buildups as sites for hydrocarbon entrapment. Primary porosity in Paleozoic stratigraphic reefs has largely been lost, but later dolomitization by hypersaline brines or leaching by downward-circulating fresh water may generate significant secondary porosity. Without doubt, organic buildups constitute the predominant carbonate reservoir sought by explorationists in north-central and west-central Texas. These buildups take the form of linear, elongate shelf-margin banks, banks on isolated platforms or block-fault horsts, and non-shelf-rim features of small size (patch reefs) or more regional extent (interior banks). Rather surprisingly, the larger bank systems lack rigid, framework-constructing organsims in the core of the buildup, such as colonial corals. Instead, these banks can often be described as being phylloid-algal bafflestones. Smaller patch reefs, which are encountered on Strawn and Cisco carbonate shelves, contain *Chaetetes* (probable sponge), *Caninia* (coral), *Komia* (a stromatoporoid), and bryozoans (Toomey and Winland, 1973; Mazzullo, 1985). Dolomitization by means of surface or shallow-subsurface hypersaline brines did not take place with the Pennsylvanian reefs of the Eastern shelf and adjacent areas for the climatic reasons already discussed. The leaching of carbonate-bank facies by meteoric fresh water was the dominant mechanism for porosity enhancement. Episodes of leaching were associated with cycles of eustatic sea-level change during the Pennsylvanian. This correlation of reservoir development with eustasy is considered in greater detail later in the paper.

Settings *three* and *four* regarding the formation of carbonate reservoirs include talus accumulations at the base of carbonate buildups and lime sands at the shelf margin or across the shelf interior. The Cretaceous Tamabra Limestone talus accumulation at the base of the Golden Lane platform near Vera Cruz, Mexico, is the best example of a deep-water carbonate conglomerate (Enos, 1985). Oolitic or pelloidal lime-sand bodies, if leached or incompletely cemented, can also form highly productive reservoir-rock bodies. The Jurassic Arab D unit of Saudi Arabia and the Smackover of the U.S. Gulf Coast represent this reservoir type. Unfortunately, neither of these settings furnishes useful insights for purposes of identifying exploration fairways in the carbonate rocks of the Eastern shelf.

Mazzullo (1982) and Mazzullo and Reid (1989) report that resedimented periplatform-debris deposits at the base of pinnacle reefs and isolated platforms constitute potential hydrocarbon reservoirs along the Missourian and Virgilian margins of the Eastern shelf. These deposits, however, are volumetrically insignificant in comparison with other productive facies in the region and should not be sought as a distinct exploration play. Similarly, shelf-margin and shelf-interior lime-sand bodies occur as locally distributed component facies of much larger carbonate depositional systems. Oolitic-sand bodies are not numerous or widespread in Pennsylvanian rocks of north-central Texas but can form fringing calcarenite shoals around emergent carbonate islands (Mazzullo and Mazzullo, 1983). The outcropping Chico Ridge Limestone of Wise County (equivalent to the Canyon Winchell Limestone of the Brazos River Valley) represents the only extensive oolitic-sand body on the Pennsylvanian Eastern shelf (Erxleben, 1975).

The *fifth* major setting for carbonate reservoirs discussed here involves altered carbonate zones directly beneath regionally distributed unconformity surfaces. Lengthy periods of subaerial exposure can bring about extensive freshwater leaching of carbonate terrains. Residual soils, fracturing, and the development of porous karst zones (vuggy or cavernous porosity) within the carbonate bedrock commonly result. Disconformity surfaces at the top of the Devonian carbonate section in northwest Texas and the top of the Ordovician Ellenburger Group in Eastland County, Texas, represent two examples of such karst reservoirs.

Despite the development of numerous paleosol zones in Strawn, Canyon, and Cisco rocks associated with episodes of eustatic lowstand, there is no evidence that extensive karst surfaces were formed when the shelf was exposed. During most of the individual cycles, the inner shelf, which would have been above sea level for the greatest length of time, was dominated by siliciclastic sedimentation and thus could not give rise to karst terrains. Carbonates were thickest and most widespread near the shelf margin. However, the distal shelf was exposed for the least amount of time during a given transgressive–regressive cycle. Brown (1982), Harrison (1973, 1991), and Yancey and McLerran (1988) have all described paleosols and other freshwater diagenetic effects in outcrops of shelf-limestone facies. They failed to document the development of extensive karst zones in any of the shelf-limestone facies, even where a thick carbonate section is present. It is likely that the Middle and Late Pennsylvanian eustatic cycles gave rise to lowstands too brief to allow for extensive cavern formation in the exposed shelf carbonates.

Figure 3 illustrates the distribution of carbonate depositional systems on the Concho platform/Eastern shelf and surrounding areas during the Pennsylvanian Period. The specific types of structural settings where these carbonate buildups accreted, as well as the age range for the principal carbonate accumulations, are summarized in Table 1. Carbonate systems formed on local or regional structural highs that were overlain by shallow water; they subsided gradually and were isolated from terrigenous clastic source areas by a basin or narrow trough. Favored settings included isolated atolls within starved basins, fault-block horsts, and the broad platform region between the Fort Worth foreland basin and the Midland epicratonic basin. Isolated elements such as the Horseshoe atoll and the Seymour pinnacle grew on local structural highs surrounded by deep water. The Red River uplift and Matador arch accreted shallow-water carbonates on block-faulted horsts that had been eroded and planed off during the Atokan. The King County (Spur) platform represents a southward extension of one of the Matador horst blocks.

Carbonate buildups were also prominent on the shelf margins and shelf interior of the Concho platform/Eastern shelf. Ramp systems developed on the western margin of the Concho platform during the early and middle Desmoinesian. The oldest Pennsylvanian shelf-margin banks in north-central Texas (Caddo system) accreted along the eastern boundary of the Concho platform (Weber, 1995) during the latest Atokan and earliest Desmoinesian (Fig. 4). A much more extensive shelf-margin bank system became established along the western periphery of the platform near the end of the Desmoinesian. The Palo Pinto–Winchell bank and successor banks of the Virgilian–Wolfcampian Sylvester system served to define the eastern shelf edge for the Midland basin (Fig. 5). Shelf-interior bank systems characterize the Missourian-age Eastern shelf but not the younger versions of this shelf. Patch

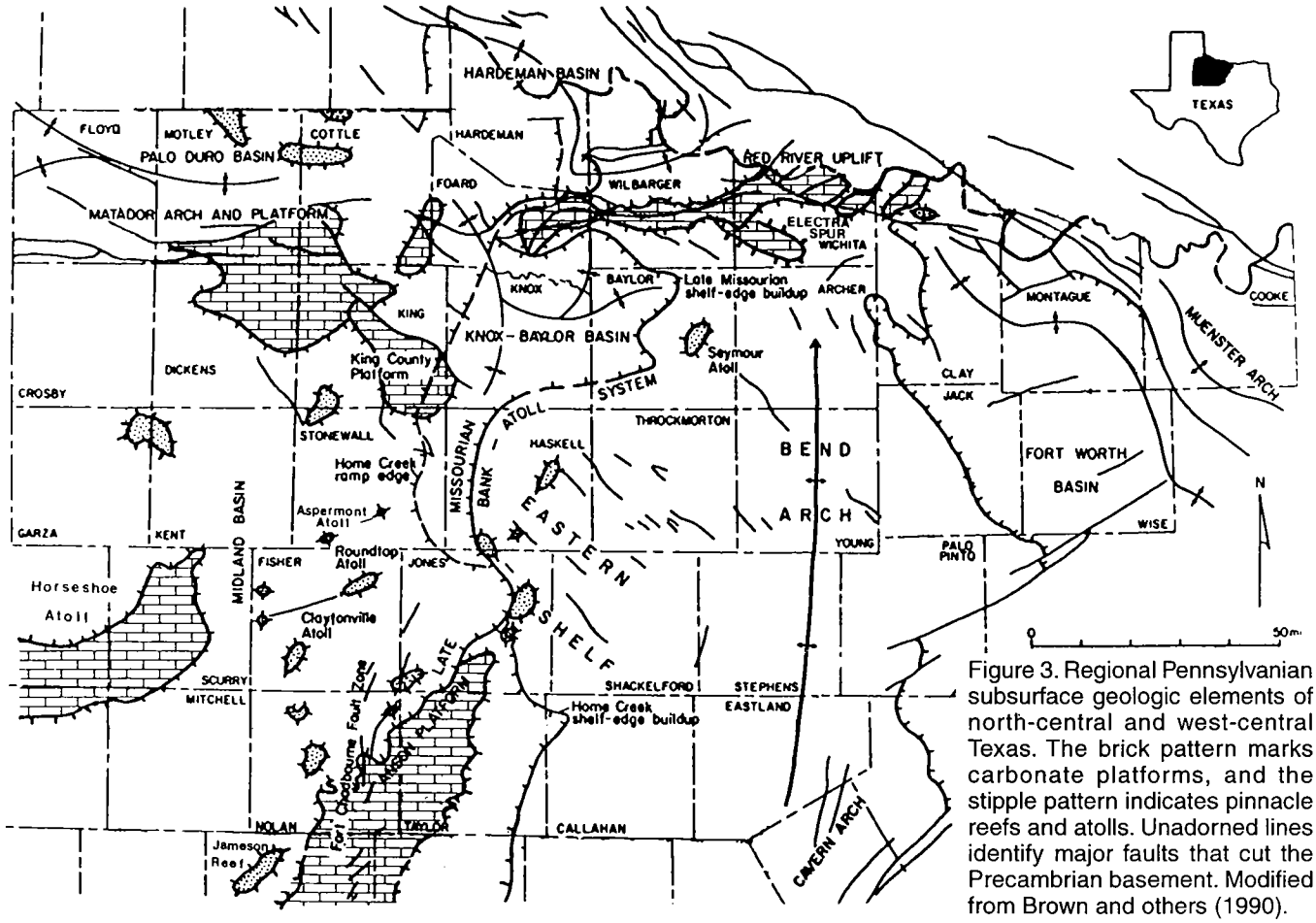

Figure 3. Regional Pennsylvanian subsurface geologic elements of north-central and west-central Texas. The brick pattern marks carbonate platforms, and the stipple pattern indicates pinnacle reefs and atolls. Unadorned lines identify major faults that cut the Precambrian basement. Modified from Brown and others (1990).

reefs were present in both the ramp and rimmed-platform settings for several stratigraphic intervals during the Middle and Late Pennsylvanian.

EVOLUTION OF THE EASTERN SHELF AND NEARBY CARBONATE BUILDUPS

A more detailed discussion of the structural and sedimentologic evolution of the Concho platform and Eastern shelf is undertaken now for the sake of identifying the most important carbonate-reservoir systems in the region and placing them within their proper historical context. During the middle Paleozoic, the Concho arch was the dominant structural element throughout most of north-central and west-central Texas (Fig. 4). This broad, slightly positive structural feature extended northwestward from the Llano uplift to the vicinity of Lubbock. Silurian, Devonian, and basal Mississippian rocks are largely absent from this trend in north-central Texas. The Lower Mississippian (Osagean) Chappel Limestone commonly rests directly on Ordovician Ellenburger carbonates (Cheney and Goss, 1952). Before the Late Mississippian, the region incorporating the Fort Worth basin was tectonically quiescent and accumulated shallow-water carbonates. However, near the end of the Mississippian, active downwarping was initiated in the developing foreland basin as the North American craton margin began undergoing subduction beneath the Ouachita fold belt (Walper, 1982). This subsidence defined the eastern boundary of the Concho platform.

Shallow-water, platform carbonate facies of the Comyn, Marble Falls, Big Saline, and Caddo Formations were deposited successively westward as the axis of the Fort Worth basin migrated in the same direction (Hogden and Martin, 1974). The Comyn through Big Saline units comprise shallow subtidal carbonates that lack large-scale carbonate-bank buildups. Higher in the section, with the late Atokan Caddo, carbonate-ramp and platform-margin bank systems formed on the side of the Concho platform directly facing the Fort Worth basin (Weber, 1995). A broad shelf containing interior-platform carbonate buildups was present behind the rimmed-platform margin. Terrigenous clastic detritus, with its sources from the Ouachita fold belt to the east and from the Muenster arch and Red River uplift to the north of the platform, was largely trapped in the Knox–Baylor trough and in the foreland basin itself. This entrapment of siliciclastics in basins adjacent to the Concho platform enabled the Caddo to stack vertically to a maximum thickness greater than 700 ft (Weber, 1995). Farther west, the incipient Midland basin was present as a shallow structural depression whose eastern margin had not yet become differentiated into a distinct hinge line.

During the Desmoinesian, subsidence in the central and southern Fort Worth basin decelerated, but uplift in the Ouachita fold belt continued to shed sediment toward the west. These factors allowed terrigenous clastic, fluvial–deltaic de-

Table 1.—Structural Settings for Pennsylvanian Carbonate Buildups, North-Central and West-Central Texas

CARBONATE RAMPS
- **1. Lower Caddo ramp (Atokan)**
  - *Location:* Eastern margin of Concho platform facing Ft. Worth basin
- **2. Lower Strawn ramp (early Desmoinesian)**
  - *Location:* Western margin of Concho platform facing Midland basin
- **3. Middle Strawn ramp (middle Desmoinesian)**
  - *Location:* Western margin of Concho platform facing Midland basin
  - *Includes:* Shelf-interior banks (Odom) and patch reefs (Goen)

RIMMED SHELF (Eastern shelf)
- **1. Shelf-margin bank systems**
  - **a) Anson shelf-margin bank (latest Desmoinesian)**
    - Accretionary shelf margin only
  - **b) Missourian shelf-margin bank complex**
    - Well-defined Palo Pinto and Winchell banks
    - Less accretion on Ranger and Home Creek banks
    - Accretionary shelf margin only
  - **c) Sylvester shelf-margin banks (Virgilian)**
    - Accretionary and progradational shelf margin
- **2. Shelf-interior bank systems (middle Missourian)**
  - **a) Palo Pinto shelf-interior bank**
  - **b) Winchell shelf-interior bank**

ISOLATED PLATFORM (Midland basin)
- **1. Horseshoe atoll**
  - Desmoinesian platform-carbonate accretion
  - Missourian, Virgilian, and Wolfcampian platform rim and pinnacle growth

BLOCK-FAULTED STRUCTURAL HIGHS
- **1. Red River uplift–Matador arch**
  - Desmoinesian through Wolfcampian carbonate wackestone deposition
- **2. King County (Spur) platform**
  - Southward extension of Matador horst block
  - Desmoinesian and Missourian platform accretion
- **3. Electra spur**
  - *Location:* Southern Wichita County
  - *Deposits:* Middle and late Desmoinesian oolitic shoals

PERI-PLATFORM PINNACLE REEFS AND ATOLLS
- **1. Seymour pinnacle**
  - *Location:* Eastern Baylor County
  - *Deposits:* Missourian phylloid-algal(?) accretion
- **2. Strawn–Canyon pinnacles**
  - *Location:* Shallow basin, paralleling trend of eastern shelf
  - *Deposits:* Small atolls containing phylloid-algal and *Chaetetes* buildups; ooid and bioclastic beach grainstones

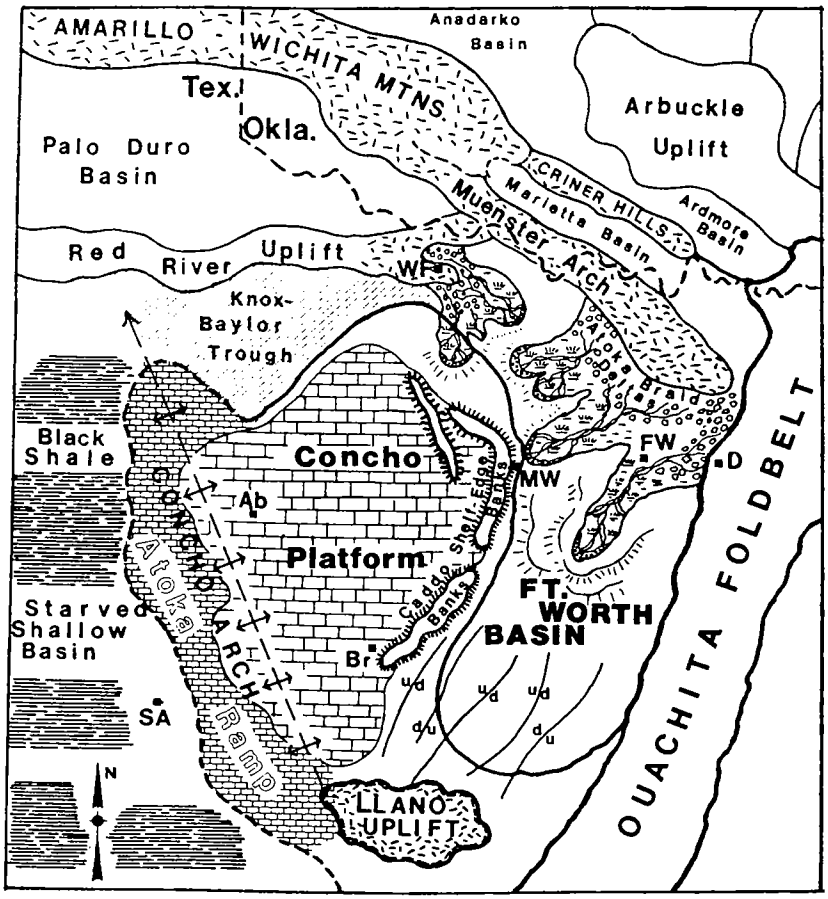

Figure 4. Atokan (Early Pennsylvanian) paleogeography, structural elements, and carbonate depositional systems of north-central and west-central Texas. Note that siliciclastic braid-delta deposits were trapped in the Fort Worth basin and failed to prograde onto the Concho platform. Caddo shelf-edge carbonate banks formed the eastern margin of the Concho platform, whereas a ramp system was present along the platform's transitional border with the Midland basin. Cities noted: *WF* = Wichita Falls; *FW* = Fort Worth; *D* = Dallas; *MW* = Mineral Wells; *AB* = Abilene; *SA* = San Angelo; *Br* = Brownwood. Modified from Cleaves (1996).

tritus, beginning with the Strawn Buck Creek transgressive–regressive cycle, to prograde across the filled basin and onto the previously carbonate-dominated Concho platform. As a result, carbonate-shelf and platform-interior bank systems were displaced toward the western side of the Concho platform (Strawn Caddo and Odom limestone units). At approximately the same time, a north–south hinge line began to form along the platform's western margin. The hinge line served as the western boundary for accumulation of a middle Desmoinesian Strawn ramp system and the latest Desmoinesian Anson bank (Fig. 5). At the beginning of the Missourian, a new shelf-edge carbonate-bank complex (outer Palo Pinto bank) accumulated directly on top of the underlying Anson bank. This new bank defined the eastern rim of the Midland basin, within which subsidence had begun to accelerate. The outer Palo Pinto bank system demarcated the boundary for the Eastern shelf.

During the time interval between deposition of the Brannon Bridge Limestone (Strawn Group, middle Desmoinesian) and the Saddle Creek Limestone (Cisco Group, end of Virgilian), the Eastern shelf evolved through four distinct stages. Excluding the Horseshoe atoll feature and the Caddo Limestone, the location and stratigraphic distribution of the principal carbonate reservoirs in north-central and west-central Texas can be explained in terms of the evolution of the Eastern shelf.

With the first stage of its evolution, the outer margin of the Eastern shelf began as a poorly defined carbonate ramp that graded westward into basinal black shale. After deposition of the Buck Creek and Dobbs Valley deltas across the entire shelf and ramp, *Chaetetes* (sponge) patch-reef growth proliferated on the southern third of the Concho platform (south and southwest of Abilene) and adjacent ramp. Goen patch-reef growth took place because fluvial–delatic sedimentation of the Ada cycle of deltation was restricted to the region of the platform north of Mineral Wells. Subsequently, Brazos River Formation fluvial–deltaic sedimentation blanketed the entire shelf as far south as the Llano uplift. This extensive episode of siliciclastic deposition suppressed the growth and accumulation of carbonate systems for the one cycle (Cleaves, 1975).

Shelf-margin carbonate-bank growth first became established on the Eastern shelf as the late Desmoinesian Anson bank system (Figs. 3,6). The Anson bank accreted vertically without basinward progradation during the Hog Mountain and Lake Pinto cycles of the Strawn Group (Fig. 7). Such accretion came about because the age-equivalent delta systems failed to prograde onto the outer one-third of the shelf. A similar pattern characterized the stratigraphically higher outer Palo Pinto bank system. Deltation was more extensive with the Strawn Devil's Den and Turkey Creek cycles, but these delta systems, too, failed to prograde the shelf margin westward. Also, no shelf-interior bank system was laid down at this time.

The third stage in the development of the Eastern shelf is seen with the middle Missourian Palo Pinto and Winchell carbonate units and, to a lesser extent, with the Ranger and Home Creek Limestones (Figs. 8,9). Aggradation without basinward progradation of the platform edge continued as before. However, during this stage a shelf-interior bank developed that exactly paralleled the trend of the outer bank over much of its length (Fig. 10). The western boundary of the interior bank is approximately 26 mi east of the shelf edge.

The existence of two parallel banks on the same shelf during the middle Missourian constitutes strong evidence for a type of reciprocal sedimentation brought about by large-scale eustatic changes of sea level (Cleaves, 1993). Both banks could not have been active, simultaneous sites of sedimentation without significantly modifying shelf-interior water circulation and perhaps even bringing about inner-shelf or sabkha evaporite precipitation (Fig. 11). The upbuilding of the shelf-margin bank, unimpeded by any deltaic sedimentation in the region, occurred only during sea-level lowstands (Fig. 12A). This

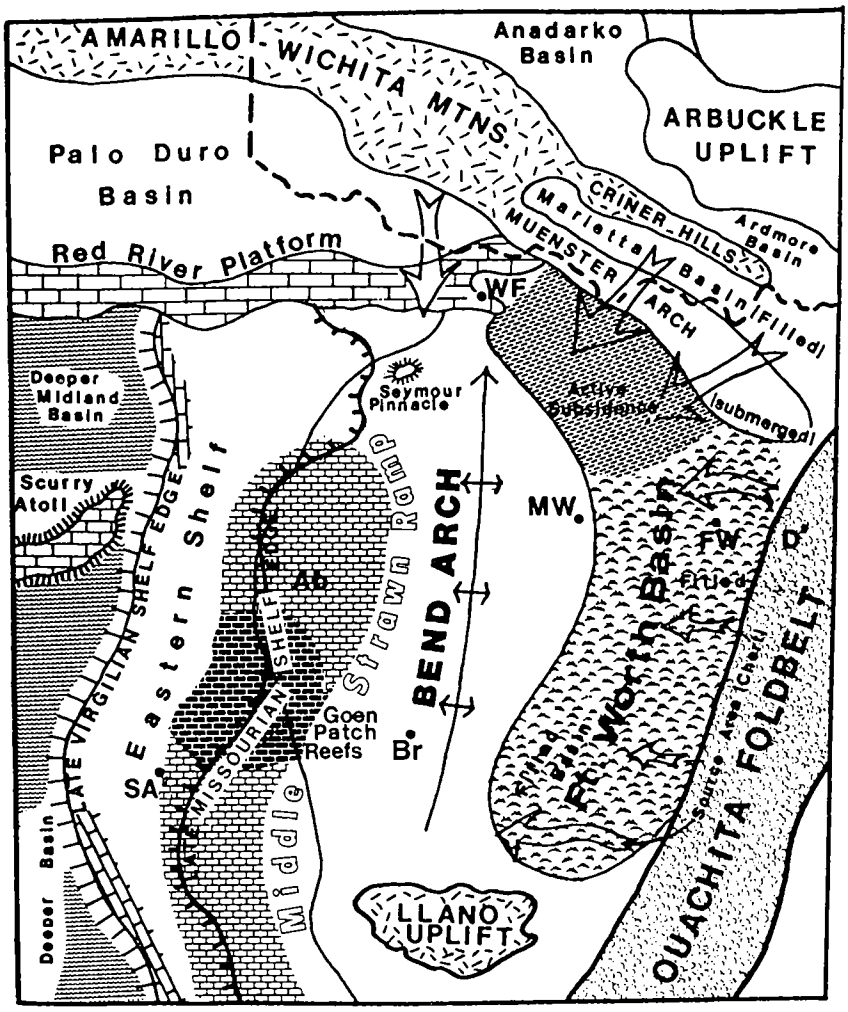

Figure 5. Middle and Late Pennsylvanian paleogeography, structural elements, terrigenous clastic-sediment-dispersal pathways, and carbonate depositional systems for north-central and west-central Texas. The Bend arch is a residual structural high that evolved from Late Mississippian and Early Pennsylvanian downwarping in the Fort Worth basin, followed by Middle Pennsylvanian subsidence, to form the Midland basin. The Desmoinesian middle Strawn ramp (open brick pattern) and accompanying Goen patch-reef complex (shaded bricks) formed before and directly underlie the middle Missourian Palo Pinto–Winchell shelf-margin carbonate-bank system. Abbreviations for cities are the same as in Figure 4.

bank, constructed largely of phylloid-algal wackestone, grew in moderately shallow water (20–60 ft), and its trend along strike reflects a bathymetric water-depth contour and not the actual lowstand shoreline. The growth of the inner bank took place during highstands, particularly during the early phase when siliciclastic sediment was being trapped in coastal estuaries (Fig. 12B). The outer bank was submerged below the photic zone throughout a given highstand and thus was dormant. Four Canyon Group cycles of alternating growth on the sites of the lowstand (shelf-margin) bank and highstand (shelf-interior) bank document this unique pattern of carbonate deposition. Carbonate growth returned to the same exact bank trend three times, owing to the propensity of organic-carbonate-manufacturing factories to favor the shallower water on top of the preexisting bank system.

The fourth stage in the evolution of the Eastern shelf of the Midland basin includes the shelf edges associated with the Cisco Group (Virgilian). Cisco shelf-edge carbonate banks have been termed the Sylvester bank system (Galloway and Brown, 1973; Brown, 1990; Brown and others, 1990). No shelf-interior banks formed during this time interval, because siliciclastic deposition largely covered the shelf for each of the 11 Virgilian transgressive–regressive cycles (Yancey and Cleaves, 1990; Brown and others, 1990). A more or less continuous period of uplift in the Ouachita fold belt during the entire Virgilian supplied abundant terrigenous clastic sediment sufficient for both vertical accretion and westward progradation of the shelf margin (Fig. 13).

Cisco fluvial–deltaic systems enlarged the shelf by means of forced regression that brought siliciclastics to the shelf edge during sea-level lowstands. This detritus prograded the shelf margin by covering and killing the preexisting shelf-edge bank (middle and late phases of the lowstand) or by diverting sediment through low areas between actively upbuilding segments of the bank trend (early phase of the lowstand). Lowstand siliciclastic accumulation beyond the shelf margin generated a coalescent submarine-fan wedge that ultimately served as the substrate for younger carbonate sediment. A new shelf-edge bank would then establish itself in a more basinward position from the previous bank on top of the inner part of the submarine fan or distal delta-front facies. This younger bank would subsequently undergo vertical accretion during the transgressive and early highstand phases of the next eustatic cycle (Fig. 14). Renewed shelf-edge progradation would take place when forced regression again brought deltas to the shelf margin.

Although evolution of the Eastern shelf has received the greatest attention, several other sites in north-central and west-central Texas also merit some discussion. The Horseshoe atoll developed independently from the Concho platform/Eastern shelf in west-central Texas (Fig. 1) and was not affected by Ouachita-derived siliciclastics until late Wolfcampian (Permian) time. The atoll became established on a structural high within the Midland basin during the early Desmoinesian (Odom equivalent). Strawn carbonate sedimentation produced an aggradational isolated platform roughly 80 mi across that lacked well-defined buildups around its periphery. The actual upbuilding of the platform margins to form a U-shaped atoll began during the Missourian and ended during the early Wolfcampian (Myers and others, 1956; Stafford, 1959). The highest points on the rim crest are elevated as much as 3,000 ft above the basin floor (Galloway and others, 1983).

The Red River uplift and Matador arch involve carbonate platforms constructed on top of block-faulted horsts. Vertical

movement that constructed the platforms occurred during the late Morrowan and Atokan. Arkosic sediment in the form of fan deltas and braid deltas was shed southward from the uplifted horsts into the Knox–Baylor trough and northwestern arm of the Fort Worth basin. These elevated blocks were planed off to sea level from subaerial erosion by the earliest Desmoinesian and then began to subside gradually. Shallow-water carbonate sedimentation became established on the structural highs and accreted to keep pace with the subsidence. Ultimately, the carbonate-platform facies on the individual fault blocks coalesced to build a continuous bank trend across north Texas. Vertical accretion along the Red River–Matador trend lasted until mid-Virgilian time.

Carbonate deposition on the block-faulted King County (Spur) platform, a southward extension of the Matador arch, also began during the early Desmoinesian. It supported thick, superposed Desmoinesian through Wolfcampian shelf-edge limestones. Ultimately, the King County platform became the eastern extremity for the Northern shelf of the Midland basin (Brown and others, 1990).

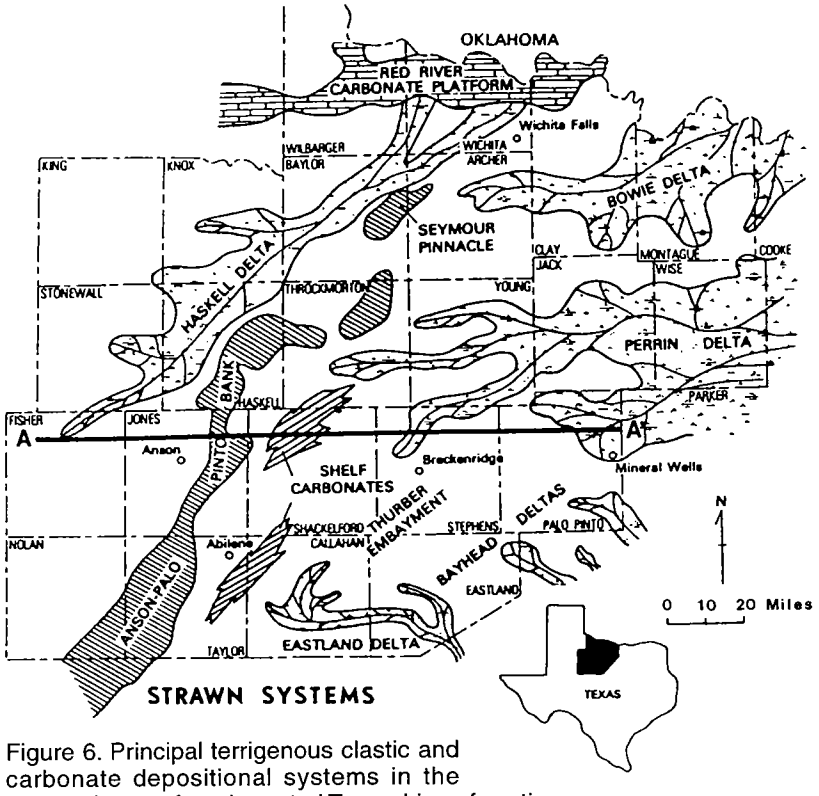

Figure 6. Principal terrigenous clastic and carbonate depositional systems in the Strawn Group of north-central Texas. Line of section A–A′ indicates the line of cross section in Figure 7.

The Seymour pinnacle reef of eastern Baylor County (Figs. 10,15) represents the largest of a number of isolated carbonate buildups that formed around the basin-facing periphery of the Concho platform/Eastern shelf. Vertical accretion to form the pinnacle was delayed until the beginning of the Missourian, owing to siliciclastic sedimentation in the Knox–Baylor trough (Gunn, 1979). Upbuilding was relatively rapid, and an edifice more than 1,300 ft tall was constructed (Fig. 15). Renewed uplift in the Ouachita fold belt at the beginning of the Virgilian brought fluvial–deltaic facies back into the trough, thus permanently ending carbonate deposition on the pinnacle.

To summarize, the structural evolution of the Concho platform/Eastern shelf and its surrounding basins and platforms constitutes the dominant factor controlling the regional positioning of carbonate shelves, isolated platforms, and reefal buildups. Active subsidence in the Fort Worth basin not only prevented siliciclastics from blanketing the Concho platform but also allowed for the formation of a Caddo carbonate-bank complex along the basin's western border. This bank was soon covered by middle Desmoinesian (Strawn) fluvial–deltaic siliciclastics from the rising Ouachita Mountains. Later, the western margin of the Concho platform evolved from a ramp to a rimmed-shelf margin when subsidence accelerated in the Midland basin. During the Missourian, the outer-shelf-margin bank accreted vertically but did not prograde westward into the adjacent basin. An absence of terrigenous clastic deposition on the shelf interior allowed for development of a pattern of reciprocal sedimentation that involved alternating carbonate accumulation on the shelf margin and on a parallel shelf-interior bank without any net progradation of the shelf margin. Later, with the Virgilian, active deltation across the entire Eastern shelf suppressed growth of an interior-bank complex. Submarine fans and perched delta lobes of the lowstand wedge prograded the shelf edge basinward and participated in building up the shelf margin. A carbonate bank capped each cycle of lowstand wedge deposition and formed the new shelf edge. Carbonate accretion at the shelf margin took place largely during the ensuing transgression until the complete drowning of the shelf edge was accomplished. The combination of basinal subsidence and carbonate upbuilding gave rise to several Virgilian platform margins that developed a shelf-to-basin relief of up to 1,600 ft (Galloway and Brown, 1973).

Carbonate accretion on the Horseshoe atoll and Red River–Matador horst blocks was favored during the lengthy period of time when the structures were undergoing gradual subsidence and siliciclastic deposition was absent from the area. The life span of the Seymour pinnacle was much briefer than the other isolated carbonate buildups, owing to its position at the head of the Knox–Baylor trough. Vertical accretion of this pinnacle, though, was more rapid.

SEQUENCE STRATIGRAPHY

Introduction

Sequence-stratigraphic analysis of Pennsylvanian carbonate buildups in north-central and west-central Texas is an essential tool for carbonate stratigraphic-trap exploration. High-frequency, eustatic changes of sea level averaging about 600 ft per cycle exerted two strong controls on the distribution of reservoir rock capable of entrapping hydrocarbons. First, the positions of stable highstand and lowstand coastlines deter-

mined the location and strike-oriented trend of local or regional buildups on the platform. Inasmuch as most of the Pennsylvanian carbonate-generating buildups involved shallow subtidal facies within the photic zone, such conditions developed in bands parallel to the paleocoastline and not simultaneously across the entire shelf. Water depths exceeding 80 ft would be unfavorable for the active accretion of chaetetid or phylloid-algal banks (Wermund, 1975; Heckel, 1972).

The second strong control imposed by eustatic sea-level changes on the formation of reservoirs relates to the formation of porosity within the banks. Much of the effective porosity identified in producing Pennsylvanian reservoirs of the region is not primary porosity associated with deposition of the carbonate particles. Although Toomey and Winland (1973) reported that primary shelter porosity (provided by phylloid-algal fronds) and fine intercrystalline porosity are major contributors to the overall porosity in Nena Lucia field of Nolan County (Fig. 16), later workers state that secondary, dissolution porosity predominates in most "reefal" buildups. Mazzullo (1982) and Reid and Mazzullo (1988) observe that secondary porosity brought about by the leaching of meteoric (fresh) water within vadose and shallow phreatic diagenetic settings typifies virtually all these carbonate reservoirs. Extensive freshwater diagenesis occurs when the reservoir facies is subaerially exposed for a period of time and a freshwater lens develops within it (Fig. 17). Cyclic, eustatic drops of sea level brought about such exposure numerous times during the Middle and Late Pennsylvanian. Hence, multiple zones of high porosity and permeability have been preserved in many of the longer lived carbonate edifices.

Sequence Types

Any regional consideration of sequence stratigraphy pertinent to a depositional basin must consider the fundamental types of sequences present within the stratigraphic section (type 1 versus type 2) as well as the distribution of systems tracts within each of the sequences. The distinction between type 1 and type 2 sequences is most easily made on mixed carbonate–siliciclastic shelves that contain fluvial and deltaic facies.

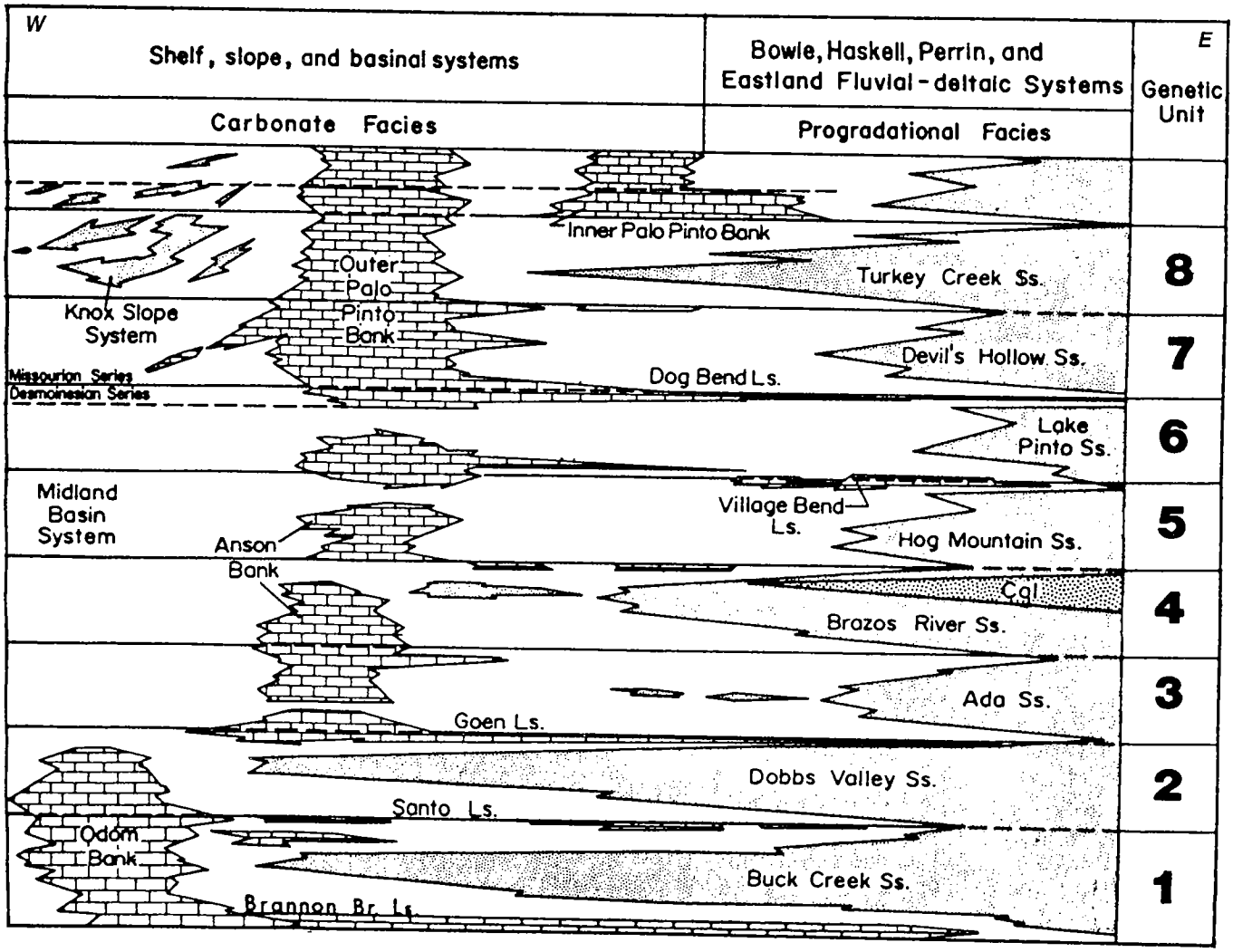

Figure 7. Schematic dip cross section of middle and upper Strawn genetic units (formats), Concho platform of north-central Texas. Sandstone names are derived from formal outcrop nomenclature in the Brazos River Valley rather than from informal subsurface designations of the reservoir units. Carbonate names for the cycle-bounding limestones are also surface terms. See Figure 6 for line of section. Modified from Cleaves (1975).

Sarg (1988) furnishes useful criteria for their distinction in wholly carbonate depositional settings, but these are difficult to apply without numerous cores and extensive seismic data.

Type 1 sequence boundaries (disconformities) form when a eustatic decline in sea level brings the regional coastline out to or beyond the shelf margin of the basin. The resulting increase in stream gradients on the parts of the shelf where fluvial–deltaic depositional systems are active gives rise to incised valleys that funnel sediment to perched deltas at the shelf margin (Fig. 18). The base of individual channels typically downcuts through the underlying marine shale and into transgressive limestone facies of the previous cycle. In fluvial-divide areas away from the eroded channels, the disconformity is preserved as a soil zone developed in marine shale or carbonate facies.

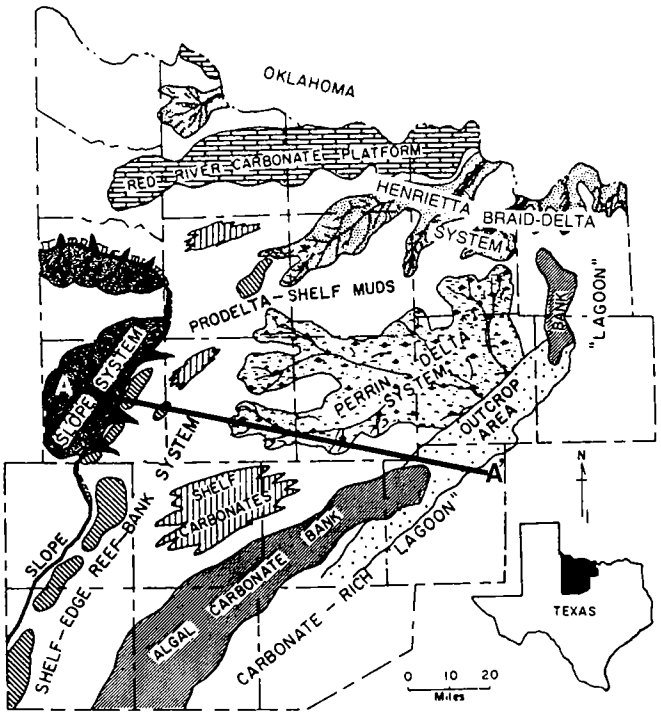

Figure 8. Canyon Group siliciclastic and carbonate depositional systems of north-central Texas. Line of section A–A′ applies to Figure 9. Modified from Erxleben (1975).

Type 2 sequence boundaries form when the drop in sea level fails to bring the lowstand shoreline out to the shelf margin. The overall rate of eustatic sea-level fall is less than or equal to the rate of shelf-margin subsidence (Van Wagoner and others, 1990). Fluvial systems under this circumstance do not incise subjacent marine facies. Regionally widespread, thick soil zones are rarely created, because a portion of the shelf was never exposed. Type 2 sequences typically develop at ramp platform margins, when tectonic subsidence to form a basin-margin hinge line is at a maximum. The sequence boundary occurs at the position in the carbonate interval where the parasequence stacking pattern abruptly changes from progradational to aggradational (Van Wagoner and others, 1990).

Type 2 sequences are almost completely absent from the surface and subsurface stratigraphic section of north-central Texas. Outcrop evidence from the middle Strawn Group (first cycle above the Brannon Bridge Limestone) to the top of the Cisco Group in the Brazos River Valley indicates that terrigenous clastic incised-valley-fill units appear in virtually all the transgressive–regressive units. Carbonate-ramp sedimentation occurred during most of the Desmoinesian along the western margin of the Concho platform in the subsurface, but outcrop evidence from the same cycles contains chert-conglomerate incised-valley fills laid down as part of the Eastland and/or Perrin delta systems. Hence, the tectonic and shelf-margin conditions most conducive to the formation of type 2 sequences did not generate them during the middle and late Desmoinesian for the region under consideration. The Atokan

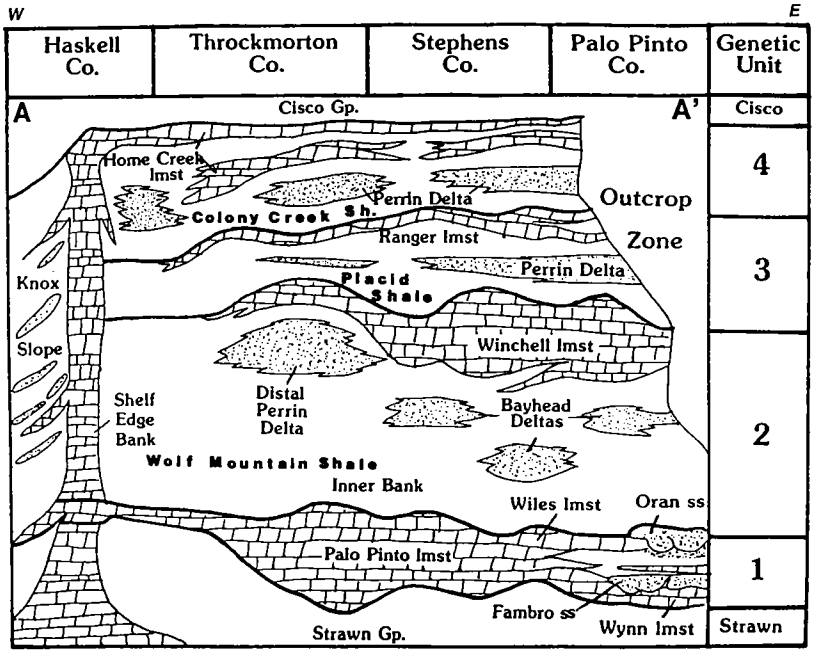

Figure 9. East–west schematic cross section illustrating Canyon Group siliciclastic and carbonate depositional systems on the northern side of the Bend arch. The Canyon Group has been subdivided into four principal transgressive–regressive units. Names for the cycle-bounding limestones are surface terms. The sandstone units have not been given names either in the subsurface or on the surface but are contained within shale intervals that have been given formation names. The inner-bank systems of the Palo Pinto and Winchell Limestones are clearly expressed in this section. Line of section illustrated in Figure 8. Modified from Erxleben (1975).

and the lower Strawn Caddo Limestone, as well as the age-equivalent fluvial–deltaic facies, do not crop out in the Brazos River Valley. Extrapolation from the lower Strawn outcrop siliciclastic section in the Colorado River Valley of central Texas as mapped by Kier (1972) and Kier and others (1976) suggests that type 1 sequences also predominated during the early Desmoinesian across the Concho platform. Unfortunately, the distribution of the subsurface Caddo Limestone has not been mapped on a regional basis, and one can only speculate about its depositional settings. Based on regional subsurface cross sections by Cleaves (1975), it appears that the Caddo formed a homoclinal ramp along the eastern margin of the incipient Midland basin, but it may have accreted to form a rimmed margin along the western periphery of the actively subsiding Fort Worth basin (Fig. 4).

Reciprocal Sedimentation

Reciprocal sedimentation is the dominant depositional pattern on the mixed carbonate–siliciclastic Desmoinesian through Virgilian Concho platform and Eastern shelf of the Midland basin. In order to interpret the sequence stratigraphy of the region, it is necessary to understand the variations in this pattern seen in Pennsylvanian rocks of north-central and

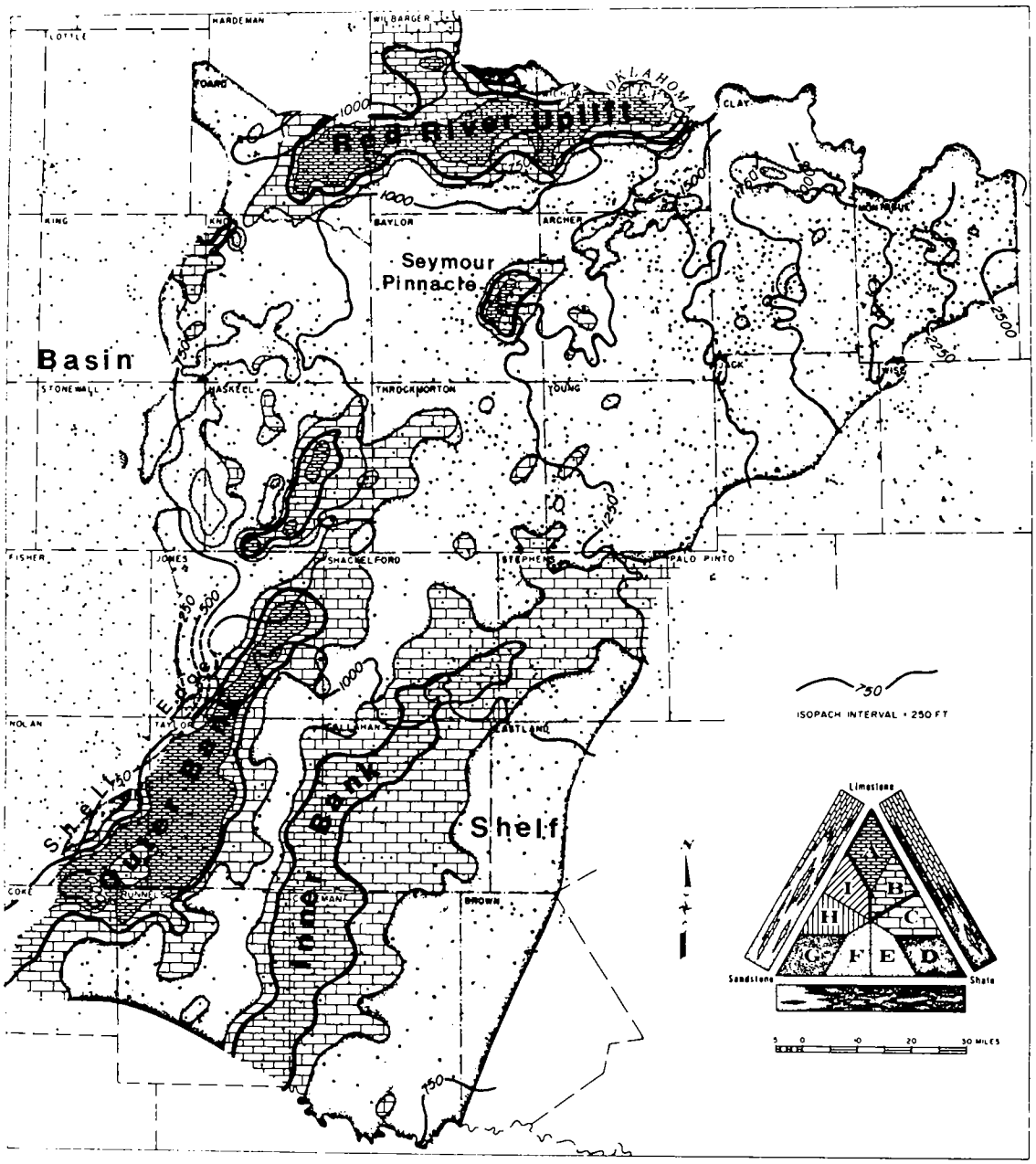

Figure 10. Lithofacies and interval isopach map of the Missourian Stage in north-central Texas. Isopach contours indicate thickness of the interval between the top of the Dog Bend Limestone and the top of the Home Creek Limestone. The inner bank, shelf-margin bank, Red River uplift, and Seymour pinnacle have been labeled. Modified from Wermund and Jenkins (1969).

west-central Texas. Reciprocal sedimentation explains the distribution of carbonate reservoirs and depositional systems in type 1 lowstand, transgressive, and highstand systems tracts associated with ramps and rimmed platforms. For certain periods of the shelf's history, especially in the area south of Mineral Wells and Abilene (Fig. 16), carbonate accretion occurred without interference from fluvial–deltaic depositional systems. At such times, siliciclastics were laid down only on the northern one-third of the shelf and in the adjacent northwestern arm of the Fort Worth basin. At other times, the complete shelf was blanketed with terrigenous clastic deposits fed by two or more discrete fluvial–deltaic systems. Progradational regression, brought about by extensive high-constructive (river-dominated) deltaic sedimentation during stable highstands, prevented thick carbonate buildups from developing on the middle and inner Eastern shelf for parts of the late Desmoinesian and

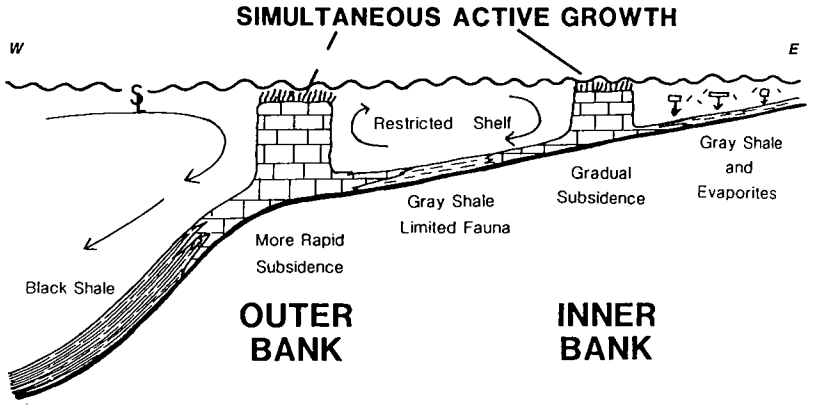

Figure 11. Diagrammatic dip-oriented cross section of hypothetical Missourian double-bank deposition on the Eastern shelf without reciprocal sedimentation. One must assume that the outer bank is subsiding more rapidly and is accreting at a greater rate than the inner bank. Under these conditions, evaporites would likely accumulate on the innermost shelf and make conditions inhospitable for inner-shelf carbonate-bank growth. Documented major episodes of eustatic sea-level change, as well as the absence of shelf evaporites, render the nonreciprocal-deposition scenario highly unlikely for the Late Pennsylvanian of north-central Texas.

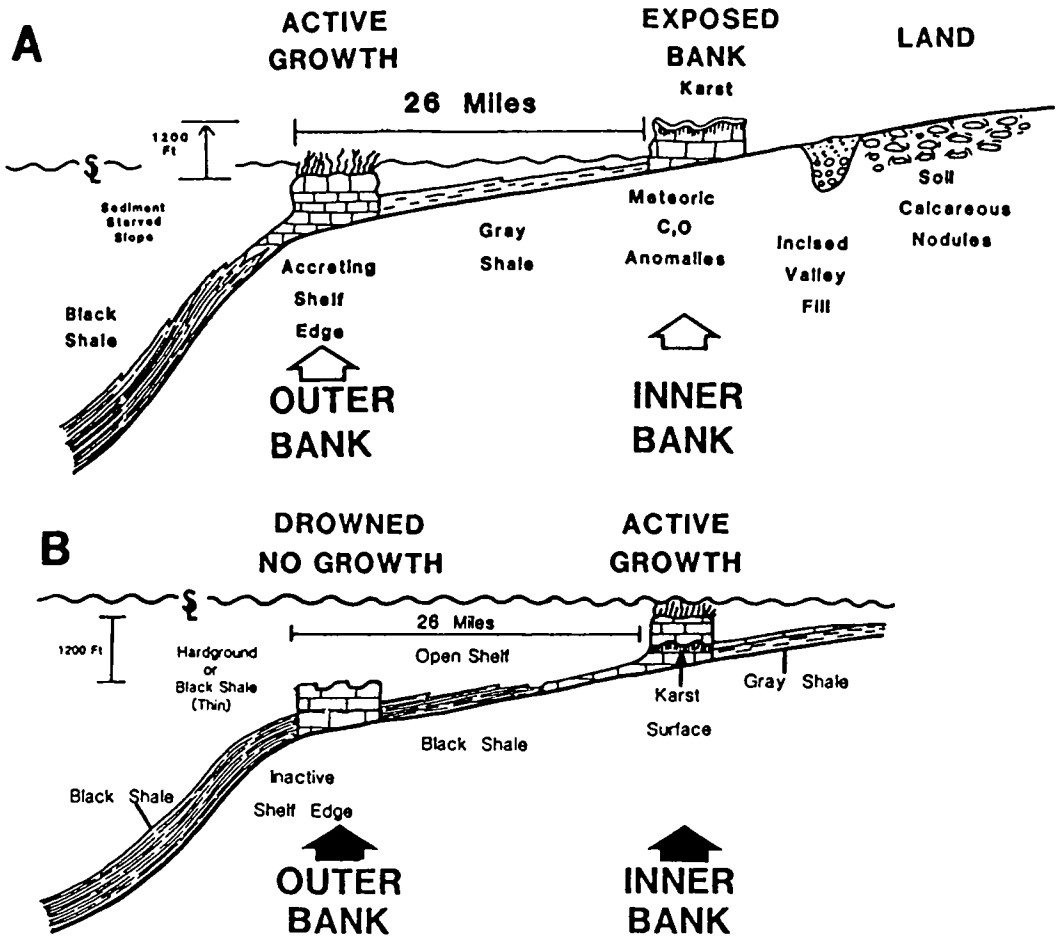

Figure 12. Missourian reciprocal sedimentation and double-bank carbonate complex on the Eastern shelf of the Midland basin. (A) Lowstand of sea level enables accretion of outer bank, while inner bank is subaerially exposed and subjected to meteoric diagensis. (B) With a sea-level highstand, the inner bank is shallowly submerged and undergoes active upbuilding, but the outer bank is drowned below the photic zone and stops building upward. From Yancey and Cleaves (1990).

all of the Virgilian. Thick prodeltaic-shale intervals ranging from 60 to 250 ft characterize this type of siliciclastic-dominated shelf. Forced regressions, brought about by major eustatic drops in sea level, led to the accumulation of much thinner prodelta-shale sequences (Cleaves, 1996). In addition, the shale was incised by fluvial systems following trends that proceeded directly downdip from active highstand delta lobes.

The pattern of carbonate-systems distribution across the

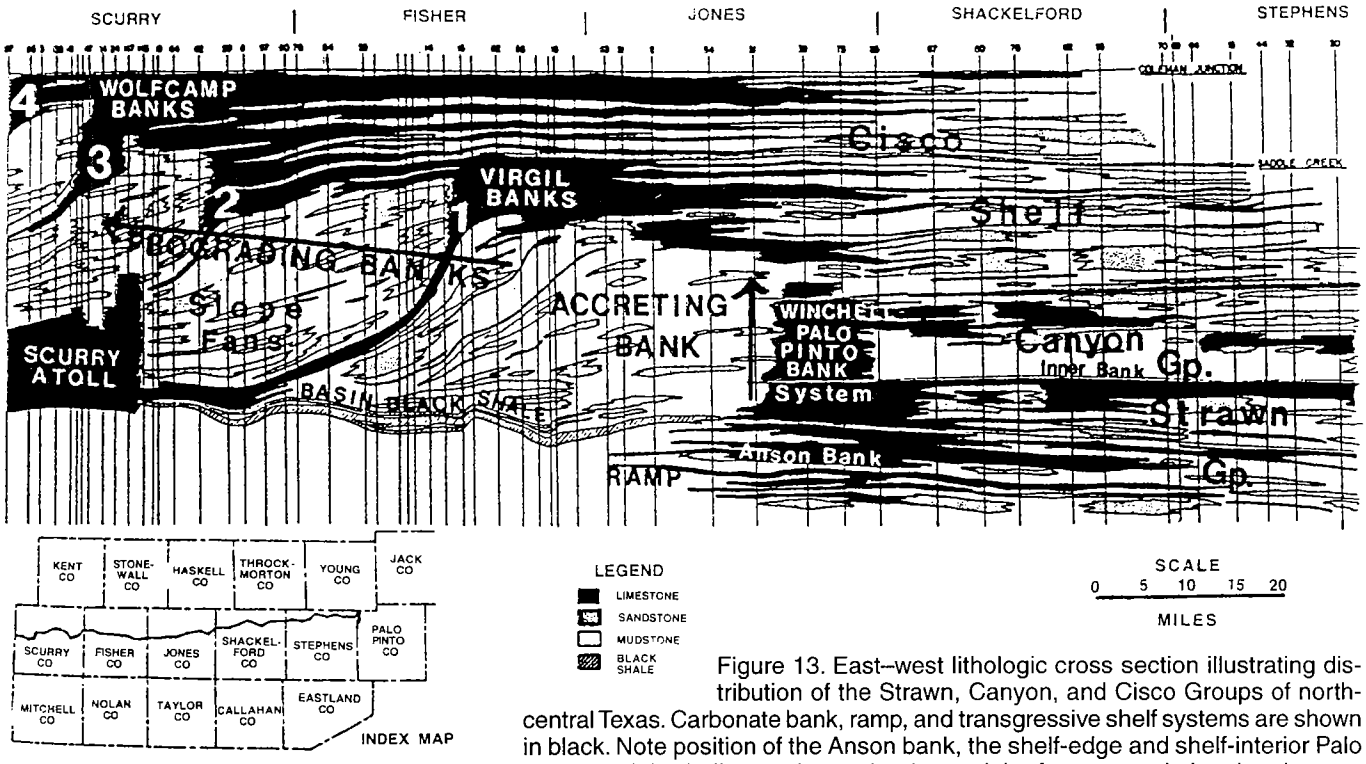

Figure 13. East–west lithologic cross section illustrating distribution of the Strawn, Canyon, and Cisco Groups of north-central Texas. Carbonate bank, ramp, and transgressive shelf systems are shown in black. Note position of the Anson bank, the shelf-edge and shelf-interior Palo Pinto and Winchell accretionary banks, and the four progradational and accretionary shelf-edge banks of the Cisco Group. Modified from Wermund (1975).

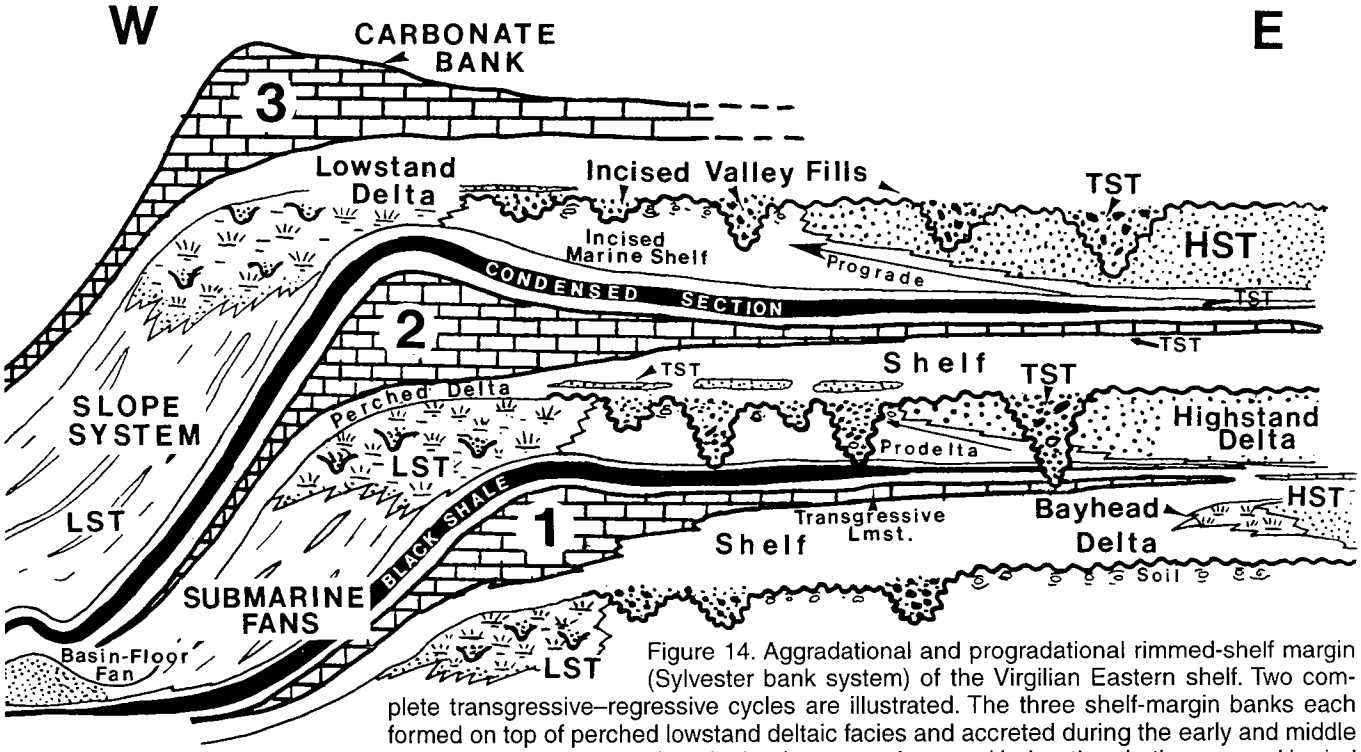

Figure 14. Aggradational and progradational rimmed-shelf margin (Sylvester bank system) of the Virgilian Eastern shelf. Two complete transgressive–regressive cycles are illustrated. The three shelf-margin banks each formed on top of perched lowstand deltaic facies and accreted during the early and middle parts of the eustatic transgression. With maximum transgression, the banks were submerged below the photic zone and buried beneath deep-water black shale. *LST, TST,* and *HST* refer to lowstand, transgressive, and highstand systems tract facies, respectively. Each cycle on the shelf is approximately 150 ft thick.

Concho platform/Eastern shelf during the Middle and Late Pennsylvanian was directly related to both the shelf-margin evolution and the availability of terrigenous clastic sediment. Carbonate-ramp settings for the middle Strawn Buck Creek and Dobbs Valley cycles (Figs. 7,13) lacked large-scale carbonate buildups at the hinge line bordering the Midland basin. Lowstand delta lobes accumulated on the outer ramp and interfingered with basinal black shale. All the platform as far south as the San Angelo area accumulated siliciclastics during the progradational highstand and forced regressive phases of the eustatic cycle for these two sequences. Only during eustatic transgression were carbonates deposited in any significant quantity. These rock bodies included localized, ramp-interior buildups (Odom Limestone), smaller patch reefs (Goen and Capps Limestones), and mud-rich marine-transgressive limestones (outcrop Santo, Goen, and Dog Bend) at the top of each cycle (Fig. 7). Deep-water, condensed-section black shales overlie each of the transgressive limestone units. Productive Odom banks developed in the transgression following progradation of Buck Creek deltas; *Chaetetes* patch reefs grew on the shelf interior during the Goen transgression.

For the latest Desmoinesian, as well as for all the Virgilian, the overall pattern of reciprocal sedimentation involved a single shelf-margin bank system and no widespread linear trend of interior banks. The Desmoinesian Anson platform-margin bank first appeared with the lowstand of the Ada cycle, having become established at the distal end of coarse-grained Dobbs Valley deltaic facies (Fig. 7). This bank underwent sporadic upbuilding during the ensuing two cycles, culminating with the Capps Limestone. Lowstand/transgressive growth returned to the same shelf-margin position for each cycle. The upbuilding of this shelf rim took place during the part of the lowstand when the bank accreted to sea level, and during the early phase of the following transgression. Vadose diagenesis to form reservoir-quality porosity took place later during the same lowstand, after accretion to sea level had been completed.

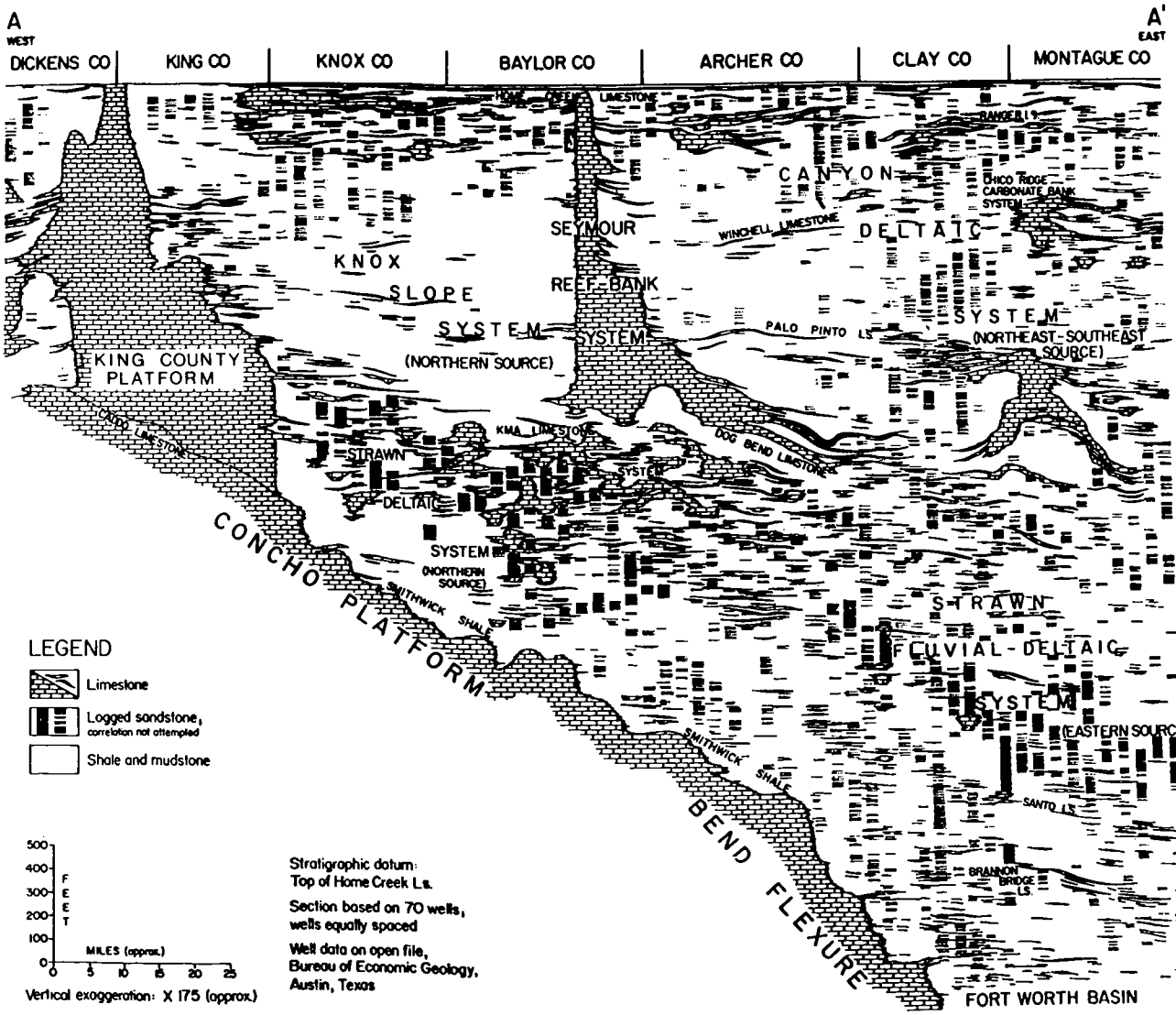

Figure 15. East–west lithologic cross section illustrating distribution of the Strawn and Canyon Groups in north Texas. The carbonate lithologies are represented by a laterally correlated brick pattern, and sandstone is indicated by a vertically stacked stipple pattern. The principal carbonate systems noted beyond the northern end of the Bend arch include the Seymour reef-bank (pinnacle) system, King County platform, and Red River uplift. Section A–A′ is shown in Figure 16.

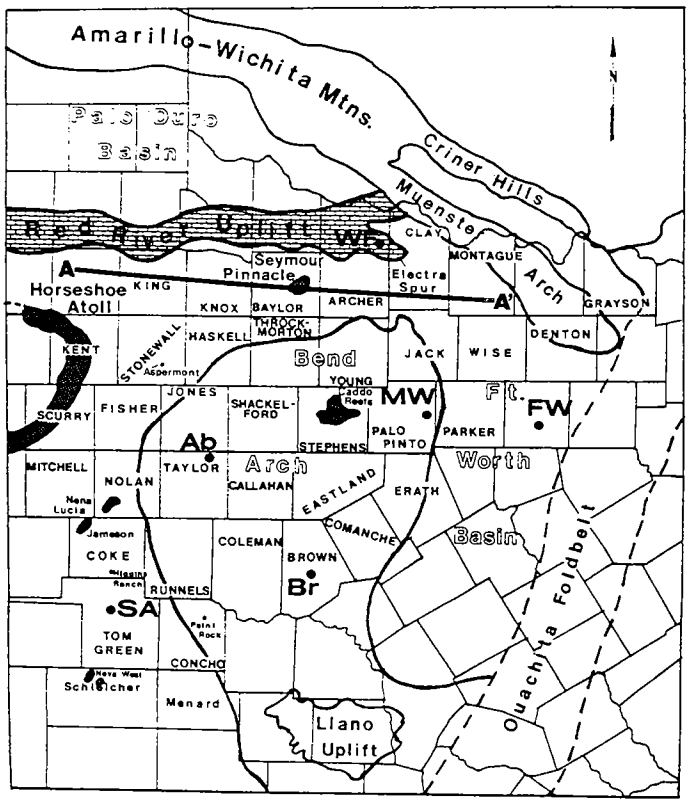

Figure 16 *(at left)*. Location of carbonate depositional features discussed in text. Section A–A′ is seen in Figure 15. Abbreviations for cities are shown in Figure 4.

Additional vadose diagenesis involving the same bank (now shallowly buried) may also have occurred during the early phase of the subsequent lowstand. No progradation of the late Desmoinesian shelf margin took place, because differential tectonic subsidence at this hinge was proceeding at a relatively rapid rate. Furthermore, no lowstand deltas reached the Anson platform rim south of Young and Throckmorton Counties. Hence, no slope submarine apron could form basinward from the carbonate bank. Such aprons served as the substrate for the shelf-margin bank of the subsequent cycle during the Virgilian. Platform-interior banks and patch reefs were absent from the siliciclastic-dominated Thurber embayment for the Brazos River and Hog Mountain cycles. Widely scattered shelf-interior phylloid-algal buildups are seen with the more carbonate-dominated Thurber embayment of the Capps interval (Figs. 6,7).

Carbonate systems associated with Virgilian reciprocal sedimentation on the Eastern shelf were also dominated by a single shelf-margin bank system. The Virgilian pattern, however, differs from that of the late Desmoinesian pattern in one important aspect. The Virgilian platform margin (Sylvester

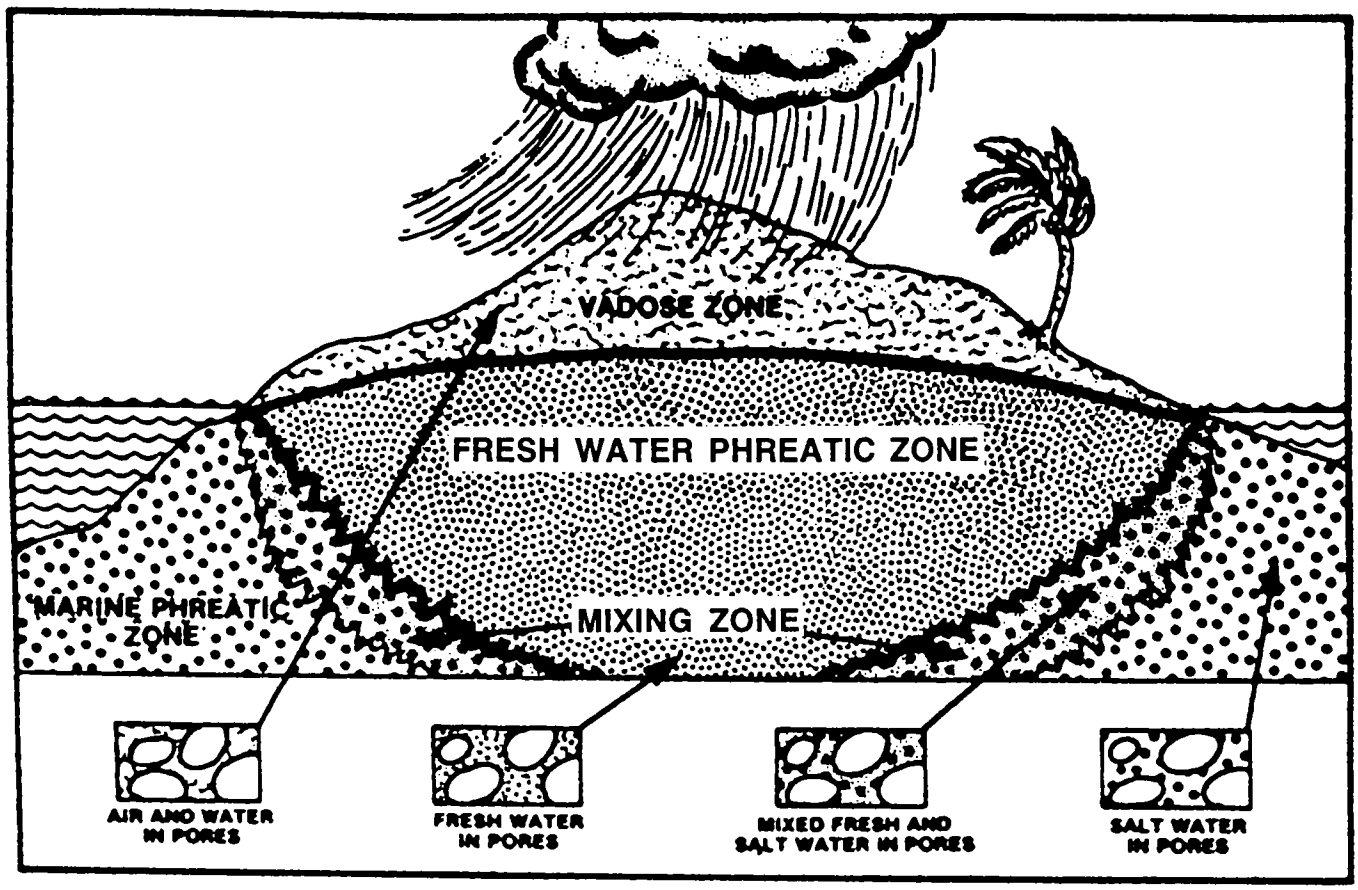

Figure 17. Distribution of principal diagenetic environments in the shallow subsurface of an idealized porous and permeable carbonate-sand island. No scale is provided, but the vertical thickness would typically be 20–30 ft, and the horizontal distance 2–3 mi. From Longman (1982).

bank system) was both aggradational and progradational, whereas the Desmoinesian (Anson bank system) showed only aggradation (Fig. 14). Virgilian (Cisco) fluvial–deltaic sediment covered the entire Eastern shelf during both the highstand progradational regression and lowstand forced regression for each cycle. Lowstand perched deltas were present along the entire shelf margin, thus suppressing the formation of lowstand, platform-margin carbonate banks. These deltas rested on top of the drowned shelf-margin banks of the previous eustatic cycle and supplied sediment to a slope submarine-fan apron (Sweetwater slope system) that paralleled the platform edge (Fig. 18). At the beginning of the next transgression, carbonate sedimentation became established on top of the distal delta front and proximal slope facies and accreted a new shelf-edge bank as sea level began to rise. Ultimately, the rise in sea level outpaced the ability of the bank to keep its upper surface in the photic zone. Thus, each of the Sylvester banks, similar to their Anson predecessors, was drowned and covered by a thin interval of deeper water black shale associated with the maximum transgression. Vadose diagenesis later generated reservoir-quality porosity during the next lowstand, when deltas occupied the shelf edge directly above the previous bank. Forced regression brought the meteoric groundwater lens to the shelf edge. This enabled fresh water to move downward and dissolve metastable constituents in the underlying carbonate buildup.

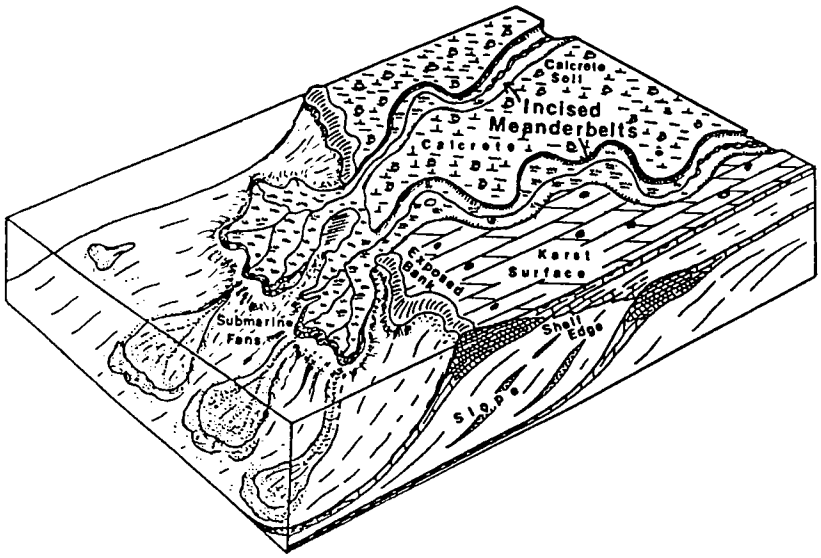

Figure 18. Lowstand systems tract for a typical Cisco fluvial–deltaic complex associated with a type 1 sequence. Incised-valley-fill fluvial systems feed river-dominated lobate deltas perched at the Eastern shelf margin. The deltas, in turn, supply sediment to a shelf-margin submarine-fan apron. Modified from Cleaves (1993, 1996).

During the middle and late Missourian, reciprocal sedimentation on the Eastern shelf manifested itself as two accretionary carbonate banks, one at the platform edge and the second approximately 26 mi inward on the shelf interior (Fig. 12). Lowstand terrigenous clastics of the Perrin and Bowie deltaic systems and the Henrietta braid-delta system were laid down around the northern periphery of the Eastern shelf in the northwestern Fort Worth basin and in the Knox–Baylor trough (Fig. 8). These siliciclastic systems also supplied sediment to Knox slope-system submarine fans that were active at this time in the Knox–Baylor trough of Knox and Haskell Counties. Owing to the lack of active middle to late Missourian fluvial–deltaic systems on the Eastern shelf south and southwest of Jack County, a carbonate-dominated shelf setting prevailed over the remainder of the platform for the entire transgressive and highstand systems tracts. With the lowstand systems tract, though, the entire platform out to the shelf edge was emergent and thus subject to soil formation and freshwater diagenesis.

As noted earlier in this paper, the Palo Pinto, Winchell, Ranger, and Home Creek shelf-edge carbonate banks were superimposed on top of one another without bringing about significant progradation of the shelf margin (Fig. 13). For this accretionary pattern to have taken place, there had to have been insufficient deposition of carbonate-platform talus and siliciclastic sediment basinward of the shelf edge during the lowstands to form a peri-platform apron. Perched deltas and submarine fans funished such an apron for Virgilian reciprocal sedimentation. With the Missourian pattern, upward growth of the shelf-margin bank began as soon as glacio-eustatic transgression covered the previously exposed, subjacent carbonate buildup with normal-salinity marine waters. Accretion continued until the rise in sea level exceeded the capability of the carbonate-generating organisms to catch up. Ultimately, the shelf-edge bank became submerged below the photic zone, the carbonate-manufacturing factory shut down, and condensed-section black shale accumulated on the dormant bank. With the next cycle of transgression after a lowstand, bank accretion resumed in exactly the same position as before. The carbonate-secreting organisms favored the slightly elevated, partially cemented substrate provided by the older bank.

The highstand systems tracts of the middle and late Missourian Eastern shelf contain open-shelf nodular limestone and shelf-interior banks. This inner-bank complex parallels the platform margin in a north-northeasterly direction through Runnels, Callahan, and Shackelford Counties (Wermund, 1969). Its trend and position are consistent with a backstepping of the photic zone onto the shelf interior, accompanied by a gradual but constant rate of subsidence across the platform. Accretion and progradation of the inner bank for each cycle occur, once a stable highstand has become established. This represents the only circumstance with Missourian reciprocal sedimentation in which widespread regression of carbonate-bank facies could take place.

In Jones and Shackelford Counties, the trends of the two bank systems diverge sharply. For the Winchell unit, the outer-bank system ends and is replaced by a disconnected set of isolated pinnacles that continues northward to the Red River uplift (Fig. 19). The inner bank, on the other hand, swings eastward and enters the outcrop zone. With the underlying Palo Pinto inner bank, a similar trend is seen, where the bank first extends eastward and then to the northeast to form a broad

arc that reaches as far as southwestern Montague County (Fig. 20). This entire northern segment of the Palo Pinto shelf-interior bank is directly underlain by coarse-grained fluvial–deltaic facies of the Strawn Turkey Creek Sandstone (Cleaves, 1975). Carbonate accretion in the northern arm of the bank complex was restricted to the earlier portion of the highstand for both the Palo Pinto and Winchell depositional intervals. Late highstand progradational facies of the Perrin and Bowie delta systems suppressed carbonate deposition during accumulation of siliciclastics of the Wolf Mountain and Placid Formations (Canyon Group; Fig. 9).

To summarize, the Desmoinesian, Missourian, and Virgilian deposits on the Concho platform/Eastern shelf of north-central and west-central Texas demonstrate four basic patterns of reciprocal sedimentation that are associated with an overall regime of mixed carbonate–siliciclastic deposition. Critical variables controlling the specific patterns include (1) the type of shelf margin (ramp versus rimmed platform); (2) rates of subsidence in the Midland basin, at its shelf margin, and in the shelf interior; (3) subsidence patterns for the Knox–Baylor trough and the northwestern Fort Worth basin; (4) siliciclastic-sediment supply; and (5) cycles of glacio-eustatic sea-level change.

The first pattern is illustrated by the early and middle

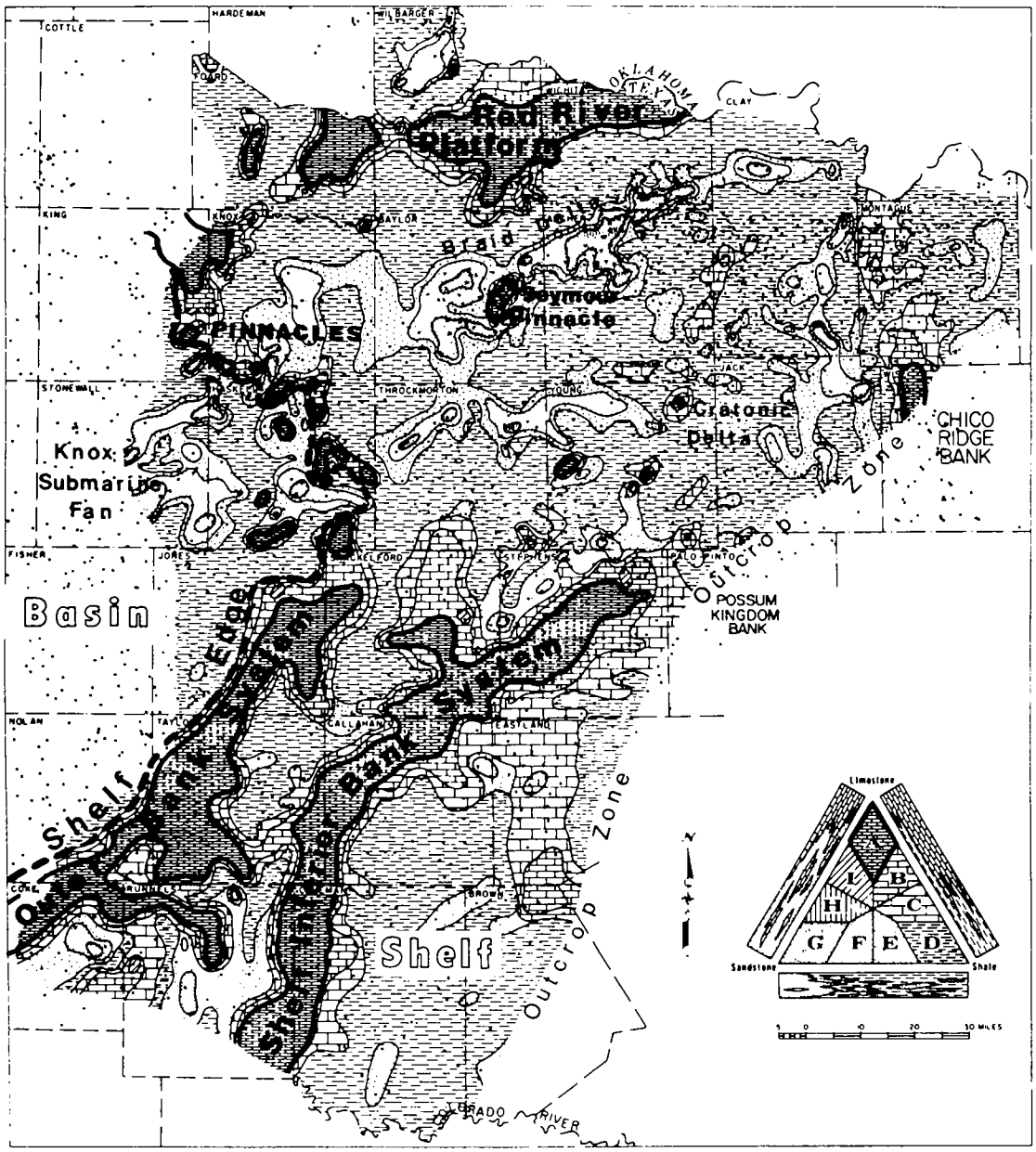

Figure 19. Lithofacies map of upper Winchell Limestone in north-central Texas. Note the isolated pinnacles north of the outer, shelf-edge bank trend. The shelf-interior bank system is present in outcrop as the Possum Kingdom and Chico Ridge banks. Presumably, these banks were once connected, but subsequent uplift and erosion have removed the Canyon carbonates and exposed the underlying Strawn Group in the area between them. Modified from Wermund (1975).

Desmoinesian accretionary carbonate-ramp margin that separated the Concho platform from the incipient Midland basin. Transgressive and highstand deposits accumulated on a carbonate-dominated shelf and contained patch reefs and shelf-interior banks. Late highstand involved regressive-bank parasequences for the lower Strawn (to the top of the Brannon Bridge interval) and deltaic progradation across a siliciclastic-dominated shelf with the middle Strawn (Buck Creek and Dobbs Valley cycles). The lowstand systems tract was restricted to discontinuous carbonate buildups on the outer ramp during accumulation of the earlier cycles but contained deltaic facies that directly interfingered with basinal black shale for the later cycles. The entire shelf was exposed at maximum lowstand.

A single, shelf-margin carbonate bank characterizes both the late Desmoinesian and Virgilian eastern margin of the Midland basin. The second (Desmoinesian) pattern of reciprocal sedimentation involved bank accretion without extensive progradation. Inasmuch as no active delta systems were present across most of the Concho platform, lowstand conditions did not bring about the accumulation of perched delta lobes at the shelf edge or a submarine-fan apron distal to the carbonate rim. Accretion of the shelf-edge bank with minimal basinward progradation took place during the late lowstand and continued through deposition of most of the transgressive systems tract. The pinnacle reefs of the shelf margin and adjacent slope aggraded to sea level and were subject to meteoric diagenesis during maximum lowstand. These carbonate buildups tracked the rise in sea level for most of the transgression but gave up and were drowned below the photic zone before maximum transgression was attained.

With the third, or Virgilian, pattern of reciprocal sedimentation, the Sylvester rimmed margin underwent both accretion and progradation. For each major-cycle lowstand, shelf-edge deltas directly fed a siliciclastic submarine-fan apron that paralleled the the shelf edge and provided a stable substrate for later carbonate-bank growth. As with the Anson banks, most of the upbuilding of the Sylvester banks occurred during the early and middle stages of deposition of the transgressive systems tract. No shelf-interior bank complex formed throughout the Virgilian, as siliciclastic sedimentation dominated the flooded shelf until transgression brought about depo-

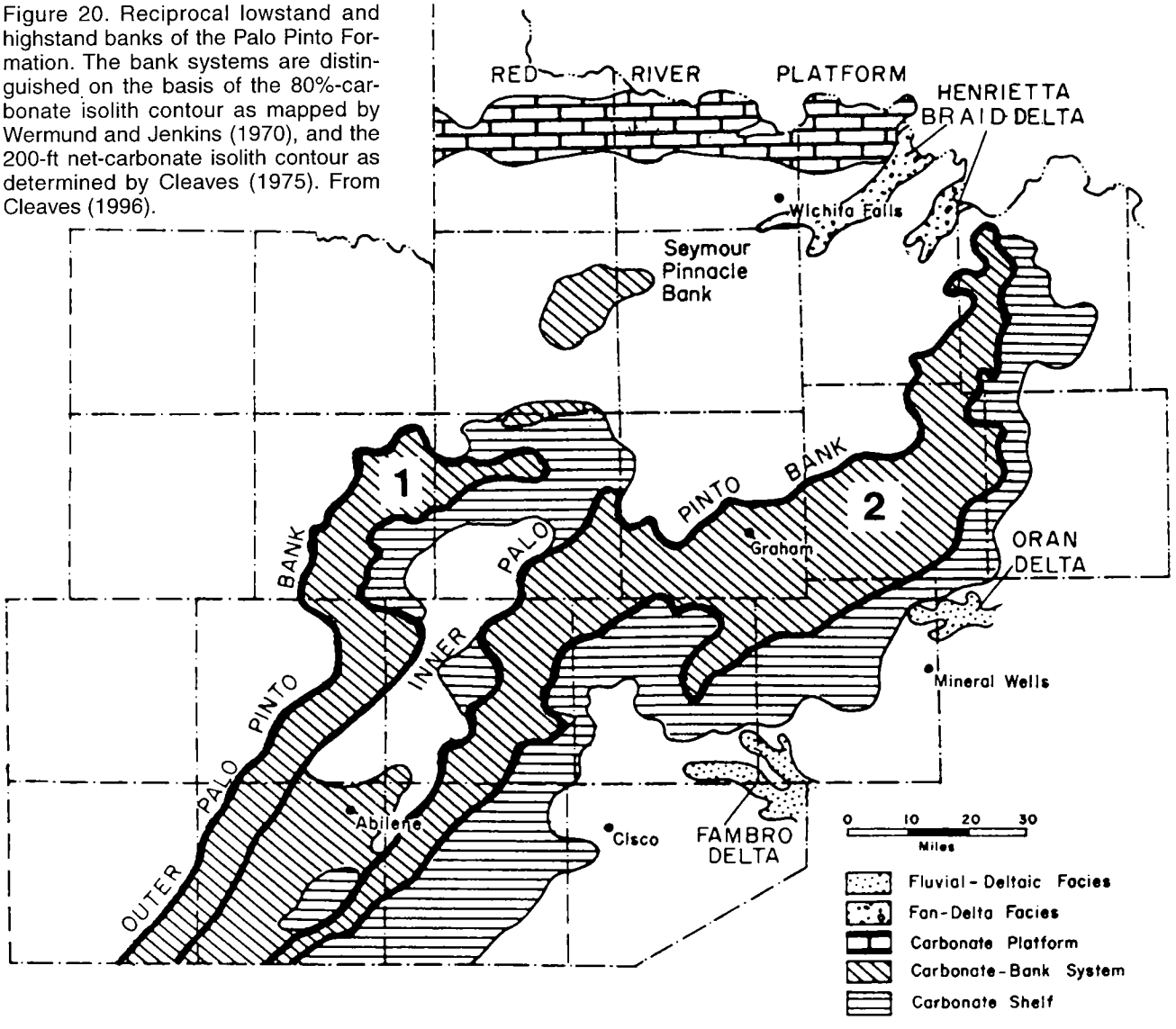

Figure 20. Reciprocal lowstand and highstand banks of the Palo Pinto Formation. The bank systems are distinguished on the basis of the 80%-carbonate isolith contour as mapped by Wermund and Jenkins (1970), and the 200-ft net-carbonate isolith contour as determined by Cleaves (1975). From Cleaves (1996).

sition of the format-bounding limestone and condensed-interval black shale.

The fourth pattern of reciprocal sedimentation is seen with the Missourian Eastern shelf. Parallel accretionary-shelf-margin and shelf-interior banks were laid down during an extended period when carbonate deposition dominated all phases of the platform's eustatic cycle. Elements of the Palo Pinto shelf-margin bank system aggraded directly on top of the older Anson bank system. This shelf edge did not prograde basinward owing to the absence of lowstand siliciclastics. Accretion took place during accumulation of late lowstand and transgressive-systems-tract parasequences. As with all the shelf-margin banks of the Anson and Sylvester systems, the Palo Pinto shelf-rim banks could not keep pace with sea-level rise and were drowned. Growth of the shelf-interior bank occurred during the stable sea-level phase of the highstand; it involved both upbuilding and some progradation. Inner-bank growth was brought to an end with subaerial exposure at the beginning of the ensuing lowstand.

CARBONATE PLAYS AND EXPLORATION APPROACHES

Introduction

Productive carbonate depositional systems of the Middle and Upper Pennsylvanian rocks of north-central and west-central Texas lack surface expression in the predominantly terrigenous clastic outcrop zones of the Brazos and Colorado river valleys. As a consequence, a strictly subsurface approach must be utilized to identify shelf and ramp carbonate buildups that contain economic oil and gas accumulations. This situation contrasts greatly with that seen for many of the productive siliciclastic depositional systems throughout the region. Fluvial and deltaic facies of several different systems are well exposed on the surface. They have served as the basis for depositional models applicable to subsurface producing units (Brown, 1979; Cleaves, 1993, 1996). Only the Midland basin submarine fans of the Canyon Knox slope system and Cisco Sweetwater slope system do not have time-equivalent analogues in the Pennsylvanian outcrop zone.

Regional subsurface mapping of carbonate depositional systems within the context of genetic units delineated by sequence-stratigraphic principles is a necessary first step toward locating productive carbonate facies. Format-bounding, marine-transgressive, shelf limestones such as the Santo, Goen, and Dog Bend Limestones of the Strawn Group (Fig. 7) have most commonly served as the boundaries for mapping the distribution and internal lithologic content of transgressive–regressive cycles. Unfortunately, these inner-shelf limestones (which are present on the surface as well as in the subsurface) become thicker, more massive carbonate-rock bodies downdip and cannot be correlated as discrete units out to or beyond the shelf edge. On the other hand, the condensed-section black-shale unit directly overlying each of the shelf-interior transgressive limestone units does not become significantly thicker toward the shelf edge or lose its identity among other units of similar lithology. The bottom of each black-shale unit represents the surface of maximum flooding and serves as a boundary for a Galloway-type sequence (Fig. 21). Such Galloway sequences, once accurately correlated out to or beyond the shelf margin by means of stratigraphic cross sections that utilize gamma-ray well logs, represent the intervals from which net-carbonate isolith maps and total-interval isopach maps can be constructed for each genetic sequence.

Subsurface exploration during the last 50 years has demonstrated that a variety of different carbonate-exploration plays can be pursued throughout north-central and west-central Texas. The plays can be subdivided on the basis of the large-scale carbonate depositional system in which the individual plays are situated. These include (1) carbonate patch reefs on carbonate ramps, (2) pinnacle reefs, (3) shelf-margin banks of rimmed carbonate platforms, (4) shelf-interior banks and patch reefs of rimmed carbonate platforms, and (5) isolated platform banks. As has been indicated by earlier discussion, it is important to note that the regional distribution of these play types was controlled by the tectonic behavior of the Concho platform/Eastern shelf and adjacent basins as well as by patterns of reciprocal sedimentation on the platform.

Carbonate-Ramp Patch Reefs

Carbonate-ramp deposition occurred on the Concho platform during the early and middle Desmoinesian. Goen-equivalent *Chaetetes* patch reefs and phylloid-algal buildups associated with the Odom Limestone constitute the most widespread carbonate reservoir rocks deposited on the Strawn ramp (Fig. 7). Goen patch reefs of the middle ramp have become a major exploration target over the last 10 years among independent geologists and continue to be an active play. Discoveries in the Odom Limestone have been much more sporadic and have not resulted from the application of play concepts. Up to the present time, no predictive concepts have been developed that simplify exploration for either type of reef.

Goen patch reefs formed within the context of a glacio-eustatic marine transgression that progressively drowned the entire middle Desmoinesian (Strawn) ramp and interior Concho platform. Patch-reef growth on the middle ramp, none of which evidences a distinct linear trend, was favored by the absence of large-scale fluvial–deltaic sedimentation on the platform south of Palo Pinto, Stephens, and Shackelford Counties during accumulation of the post–Dobbs Valley (Ada) genetic interval (Figs. 7,22). Exploration in Coke, Runnels, and Concho Counties (Figs. 5,16) has led to the discovery of several small Goen reef fields. New fields will likely be found within the same stratigraphic interval and in the same platform setting in Tom Green, Schleicher, and Menard Counties.

Marquis (1987) and Marquis and Laury (1989) describe the subsurface distribution and petrographic characteristics of one set of Goen patch reefs that produces both oil and gas in southeastern Runnels and northeastern Coke Counties (Fig. 23). Detailed descriptions of six cores demonstrated the presence of five facies associated with the patch reefs. Facies 1 (lower ramp mudstone) and facies 5 (terrigenous clastic sandstone on the middle ramp) are unproductive, but the mudstone serves as a seal for the more porous lithologic elements. Potential reservoir facies in the regressive reefs include (1) an upper ramp (lagoonal), back-mound, bryozoan–coral wackestone reservoir (facies 4); (2) a middle-ramp, shallow-subtidal,

phylloid-algal wackestone (facies 3); (3) a middle-ramp, shallow-subtidal, foraminiferal wackestone (facies 2); and (4) middle-ramp, subtidal to intertidal *Chaetetes* groves (facies 3A). Of the specific reefs studied, Marquis and Laury (1989) determined from thin-section analysis that facies 2 and 4 contain reservoir-quality porosity. Meteoric vadose leaching of fragmental phylloid-algal fronds and invertebrate skeletal debris in the two facies gave rise to this porosity. On the other hand, the phylloid-algal mounds and *Chaetetes* reefal elements were largely responsible for the elongate, moundlike geometry and accretion of the reef structures. In other Goen patch reefs, the *Chaetetes* reefal mass or the phylloid-algal wackestone-mound accumulations contain the productive porosity.

Regional exploration for the small reservoirs formed by these localized reef complexes on the middle Strawn ramp requires accurate identification and correlation of the Goen Limestone and its associated condensed-section black shale. Numerous closely spaced electric-log cross sections, including several gamma-ray curves illustrating the stratigraphic position of the black shale, are a necessary starting point. A net-carbonate isolith map of the Goen Limestone rock body itself (not the total thickness of limestone within the complete format unit between the Goen and Santo Limestones) will serve to identify sites of local thickening of the limestone unit.

Once one or more areas of local thickening have been selected for further study, the explorationist should drill a test well and core the complete Goen interval. Coring is an absolute necessity for reef prospecting, because only direct rock description can confirm the presence or absence of various reservoir facies. Low-magnification binocular-microscope classification of porosity types is a bonus that can be obtained from slabbed cores. Thin sections should then be cut from selected core slabs to document petrographically the mechanisms of porosity formation and determine the specific lithologic constituents that were removed during formation of secondary porosity. A detailed petrographic description of the textural and diagenetic features of the reservoir and non-reservoir facies should also be undertaken before additional wells are drilled. Porosity-sensitive wireline logs are effective for demonstrating the presence of porosity but cannot be used as a substitute for the lithologic truth of core descriptions. Three-dimensional seismic surveys can document the overall geom-

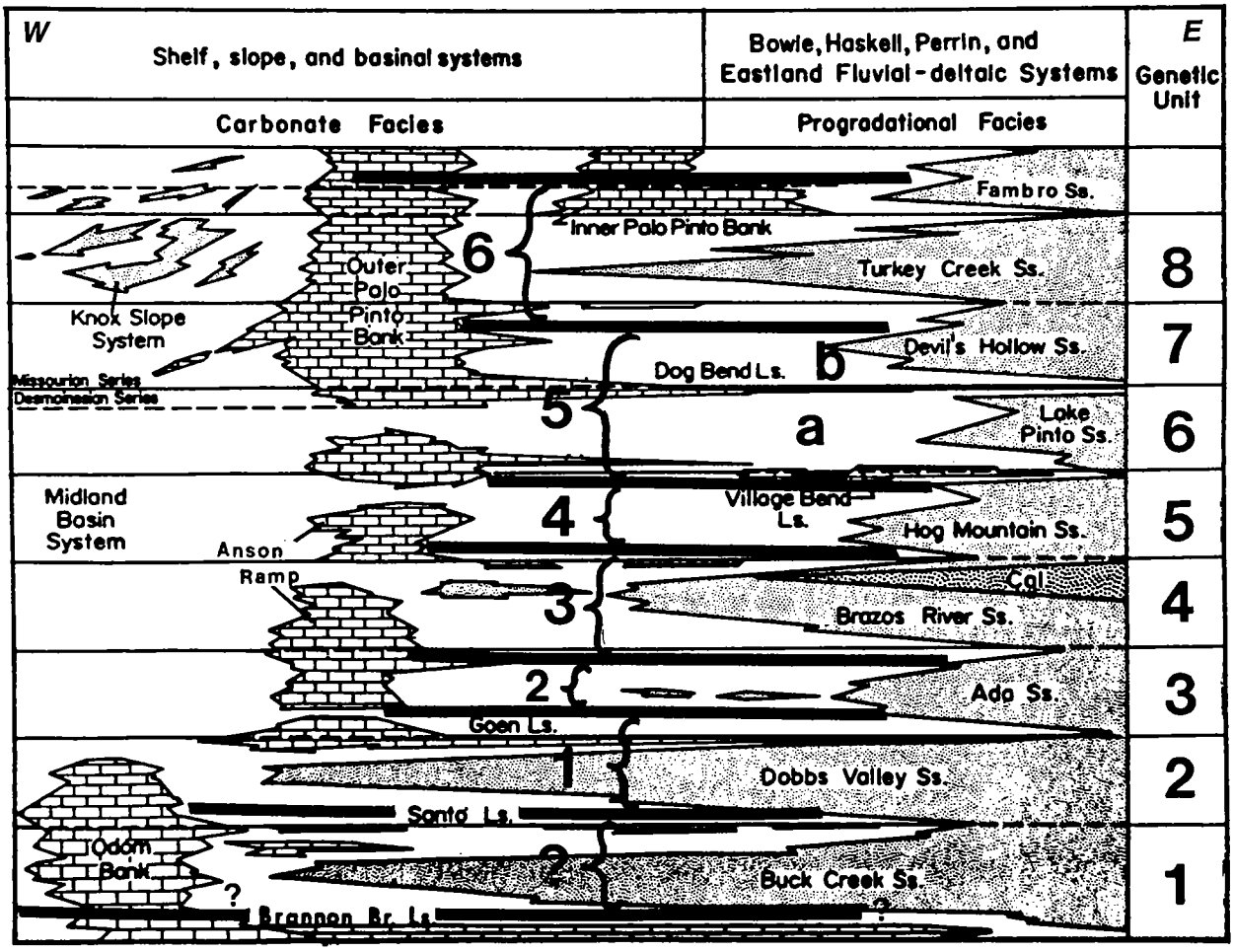

Figure 21. East–west schematic dip-oriented cross section for the Strawn Group above the Brannon Bridge Limestone. Galloway genetic-sequence subdivisions (numbers in interior of diagram) for the upper Strawn are based on the presence of outcrop black-shale units that likely continue into the subsurface as far as the shelf edge. Numbers on the side of the diagram indicate transgressive–regressive (format) units, as illustrated in Figure 7. Line of section is the same as for Figure 7.

etry of a carbonate buildup that is encased in shale or mudstone. They cannot, however, delineate the detailed geometry of reservoir facies within the reef. Such expensive surveys probably should not be run until an initial test well identifies reservoir-quality porosity and (hopefully) commercial quantities of hydrocarbons. At this point, defining the geometry of the carbonate-rock body becomes of critical importance for determining the location of future wells. The previously completed thin-section work would validate the speculation that eustatically induced meteoric diagenesis could have produced hydrocarbon reservoirs in any significant biogenic-carbonate buildup.

Pinnacle Reefs

Pennsylvanian pinnacle reefs of north-central and west-central Texas formed in several distinct depositional settings. These settings include both independent structures developed on the slope basinward from a rimmed platform margin and small, areally restricted "fingers" that accreted upward from the main mass of a shelf-edge bank system. For purposes of play development, the slope-situated pinnacles have attracted the most attention. The greatest success for discovering production has occurred with pinnacles that grew downdip but parallel to the Strawn Anson bank and the Canyon shelf-margin bank system. The Canyon bank system accreted directly on top of the Anson bank without undergoing basinward progradation. According to Bloomer (1990), most of the productive pinnacles paralleling the Eastern shelf first became established on top of the Odom Limestone.

Mazzullo and Reid (1989) describe several examples of Strawn and Canyon pinnacle reefs adjacent to the Eastern shelf that formed in response to cyclic, eustatic sea-level changes.

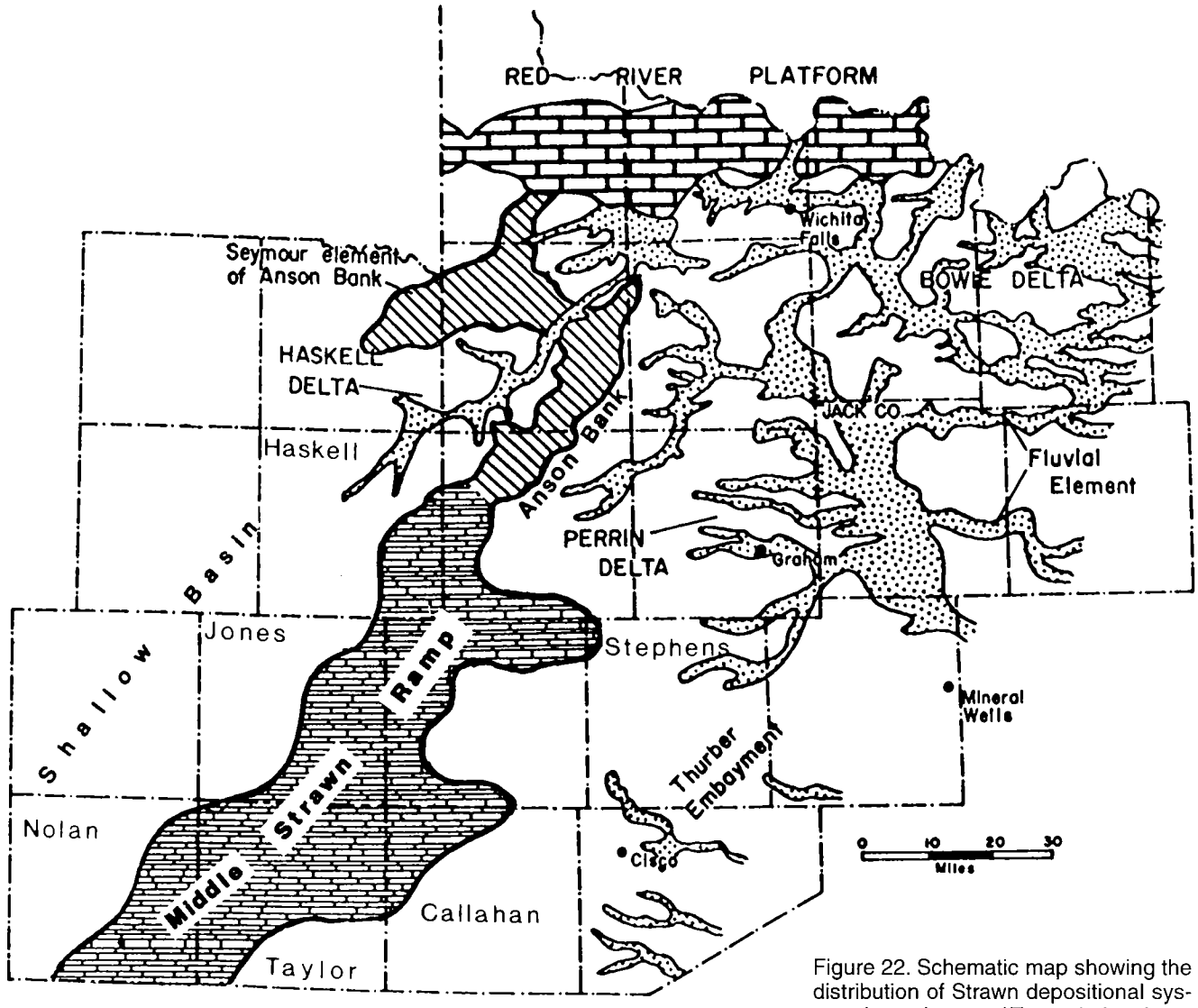

Figure 22. Schematic map showing the distribution of Strawn depositional systems in north-central Texas during deposition of transgressive–regressive genetic unit 3 (Ada sandstone interval). Stippled zones indicate fluvial–deltaic facies containing a minimum of 20 ft of net sandstone. The irregular brick pattern represents an area containing 20–80 ft of net limestone that has been interpreted as being a carbonate-ramp system with minimal shelf-to-basin relief. The diagonal pattern denotes carbonate-bank facies greater than 80 ft thick, where significant bank-to-basin relief has developed. Modified from Cleaves and Erxleben (1985).

Higgins Ranch field of Coke County (Figs. 16,24) produces hydrocarbons from a small highstand atoll that built upward to sea level during the large-scale marine transgression associated with deposition of the Palo Pinto Limestone. The productive intervals are within a 200-ft-thick pinnacle that is roughly 1 mi by 1 mi in plan view. These reservoirs include lagoonal phylloid-algal wackestone and atoll-margin, intertidal (beach) biograinstones whose porosity was enhanced by subaerial exposure and freshwater vadose diagenesis (Mazzullo and Mazzullo, 1983). Multiple episodes of island formation and lagoonal upward shoaling during the highstand gave rise to local freshwater lenses that created a stacked set of porous zones. Onlapping basinal black shale and argillaceous limestone formed both the seal and the source rock for the field's hydrocarbons.

Lowstand pinnacle reefs produce oil and gas from Neva West (Fig. 16) and Carlsbad fields in Schleicher County (Reid and others, 1992). These reefs grew in slope environments directly seaward of the Eastern shelf in narrow bands of shallow-water deposition. Pinnacles of this setting have an equant shape in map view and show high depositional relief. Their cores are phylloid-algal mounds. Porosity is generated by the sheltering effect of platy algal fronds as well as from the presence of interparticle, moldic, and vuggy void spaces (Mazzullo and Reid, 1989). Meteoric diagenesis induced by the next lowstand cycle created most of the moldic and vuggy pores.

The Seymour pinnacle of northeastern Baylor County is the largest of the pinnacle buildups throughout north-central and west-central Texas (Figs. 6,10,15). It started growing upward at the beginning of the Missourian (Dog Bend interval) and accreted vertically more than 1,300 ft during that complete age (Haeberle, 1956). Interestingly enough, the pinnacle carbonates produce hydrocarbons from only the highest 15 ft of the edifice. This zone undoubtedly originated from meteoric diagenesis linked to subaerial exposure of the reef top. The porous zone correlates stratigraphically with the lowstand of sea level that gave rise to the Kisinger incised-valley channel-fill complex of southeastern Young County (Cleaves, 1996; Lee, 1938).

Pinnacle reefs can also form oil and gas fields by means of compactional subsidence. Reefal carbonate undergoes less compaction than surrounding and overlying siliciclastic sediment. If fluvial-deltaic or turbidite sands cover the top of the pinnacle, the greater subsidence of the off-reef shale and mudstone will form a compactional anticline. At Aspermont field of Stonewall County (Fig. 16), deltaic-sandstone facies occupying a structurally high position overlie a Strawn pinnacle buildup and form a highly productive reservoir (Richards, 1952). Similarly, compactional draping of Wolfcampian turbidite sands above elevated nodes on the southwestern rim of the Horseshoe atoll has also formed anticlinal traps (Fig. 25A,B). Careful structural-contour mapping of an overlying marker limestone or of the most continuous of the reservoir sandstone bodies should serve to locate and characterize the anticline.

Shelf-Margin Banks

Important shelf-margin banks for the purposes of regional hydrocarbon exploration include the accretionary Upper Strawn (Anson)–Canyon bank system and the four principal Virgilian–Wolfcampian banks of the Cisco Group (Fig. 13). Productive reservoir facies have been discovered in all these bank trends, but the greatest success has been achieved with the oldest of the shelf margins.

Conselman (1960), Mazzullo and Reid (1989), Galloway and others (1983), and Kosters and others (1989) all summarize aspects of the distribution and production characteristics of hydrocarbon-bearing bank systems of the Eastern shelf. They clearly demonstrate that Strawn and Canyon Group carbonates dominate both in terms of total production and in total number of different fields. A possible explanation for the greater drilling success obtained in the upper Strawn–Canyon bank system may reside with the facts that this one bank complex was much longer lived than the others and that it incorporates a greater number of eustatic cycles. With numerous cycles recorded in a single, areally restricted lithologic section, a greater number of meteoric vadose diagenetic zones formed in the one carbonate buildup. Such zones are most likely to contain reservoir-quality porosity and permeability. A single drilled well could potentially tap into more than one producing zone.

It should also be apparent from studying Figure 13 that the upper Strawn–Canyon shelf-margin bank complex directly abuts a very thick interval of slope and basinal shale (up to 1,700 ft) that greatly exceeds the thickness (and total volume) of the same facies adjacent to the higher Cisco shelf edges (see also the dip-oriented cross

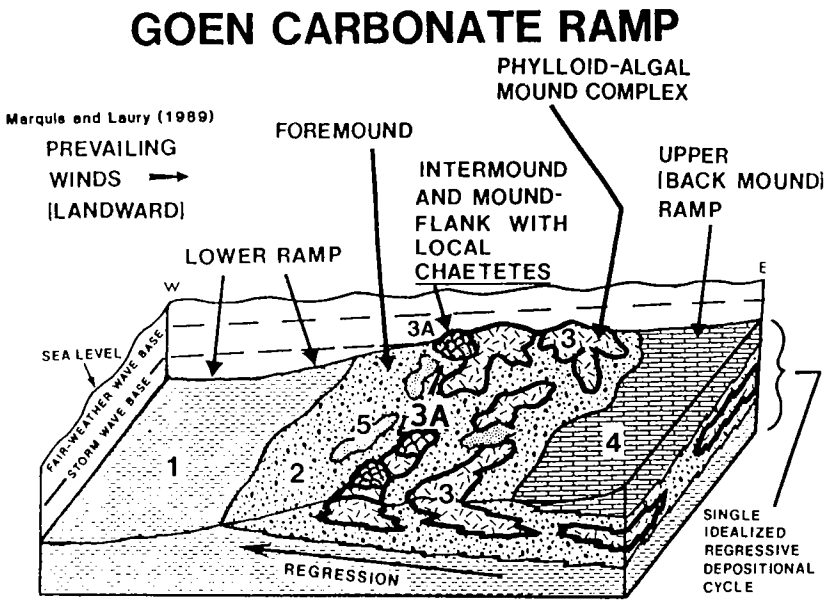

Figure 23. Goen patch reefs on the Strawn ramp of west-central Texas. Such patch reefs typically produce from diagenetically altered phylloid-algal and *Chaetetes* buildups. With the specific example provided by Marquis and Laury (1989), however, the phylloid-algal and sponge-reef entities (facies 3 and 3A) do not give rise to the best reservoir porosity. Modified from Marquis and Laury (1989).

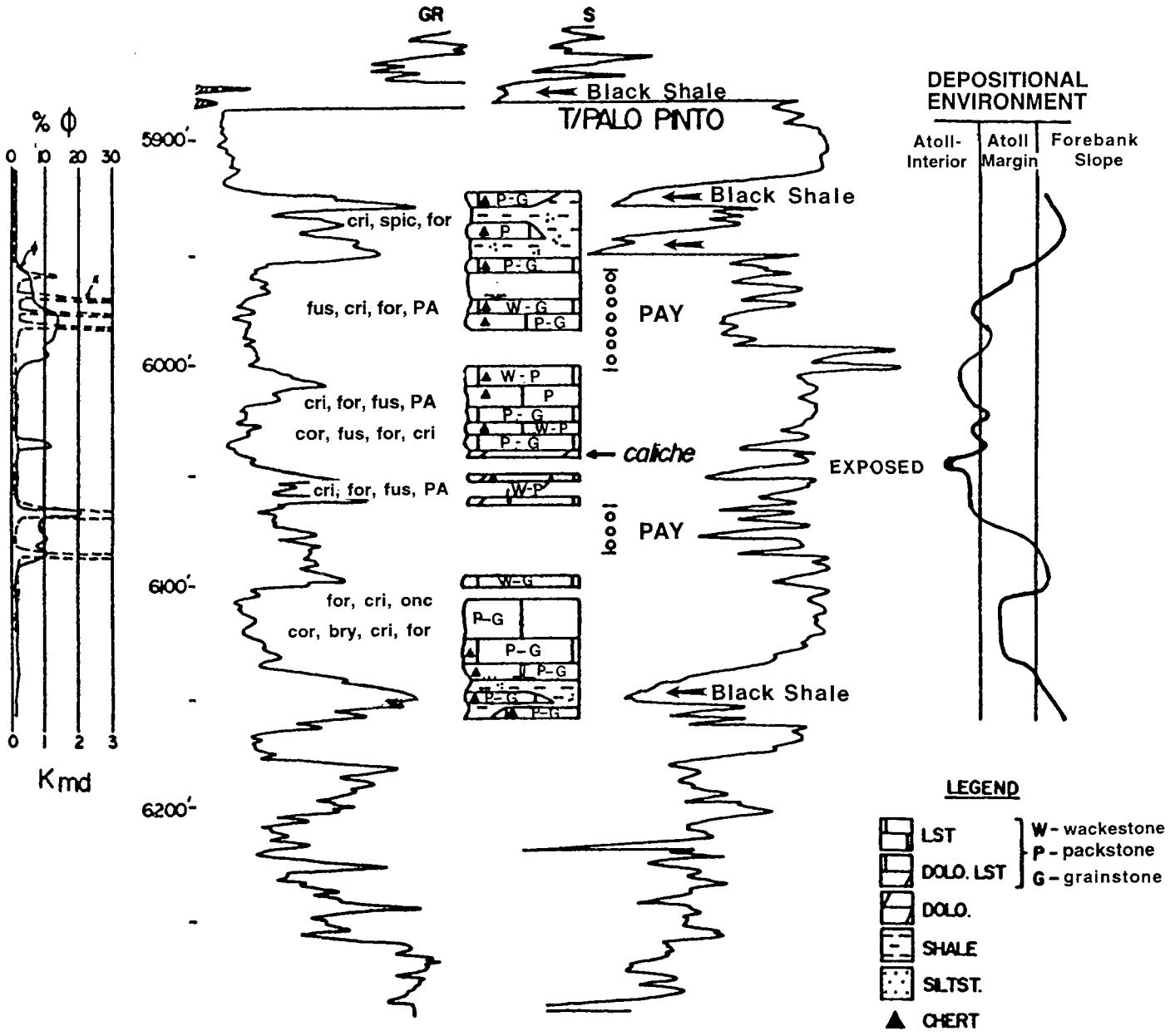

Figure 24. Log of a productive oil well in a Palo Pinto pinnacle buildup along the Eastern shelf margin (Higgins Ranch field of Coke County). Natural-gamma-ray and sonic wireline-log curves, as well as a core lithologic summary, are shown in the figure. Lagoonal phylloid-algal wackestone and atoll-margin biograinstone facies that have been leached during subaerial exposure by fresh water constitute the dominant reservoirs. The column on the left of the well-log curves indicates porosity percentages (solid curve) and permeability in millidarcys (dashed curve). The column on the right shows inferred changes of depositional environment. Modified from Mazzullo and Mazzullo (1983).

sections of Brown and others, 1990). Slope and basin black shale is the principal source rock for the oil and gas entrapped in all the carbonate reefal structures. Consequently, the Strawn basinal shales, the Canyon Knox slope system, and the lowest part of the Cisco Sylvester slope system all generated large quantities of hydrocarbons that initially migrated directly into porous shelf-edge bank facies. The higher Cisco shelf-margin bank systems drained thinner columns of source rocks and accumulated hydrocarbons over much briefer periods of time.

One good example of a productive shelf-margin bank is seen in Nena Lucia field of southwestern Nolan County (Toomey and Winland, 1973). The field is 1–3 mi wide, 11 mi long, and trends in a northeast–southwest direction that reflects the overall trend of the upper Strawn shelf rim in the area. Production is obtained solely from a porous algal-plate reservoir (reef core) that has a maximum thickness of 100 ft (Figs. 16,26). As noted by Wermund (1969, 1975), such algal bafflestone and packstone buildups grew in low-energy, micrite-rich environments within the photic zone. An absence of abraded algal fronds and grainstone textures from within the reservoir of this specific field suggests that water depths greater than 20 ft were present during the growth of the algal organisms. Thin seams of red iron-staining in the reef core indicate several episodes of brief subaerial exposure. The po-

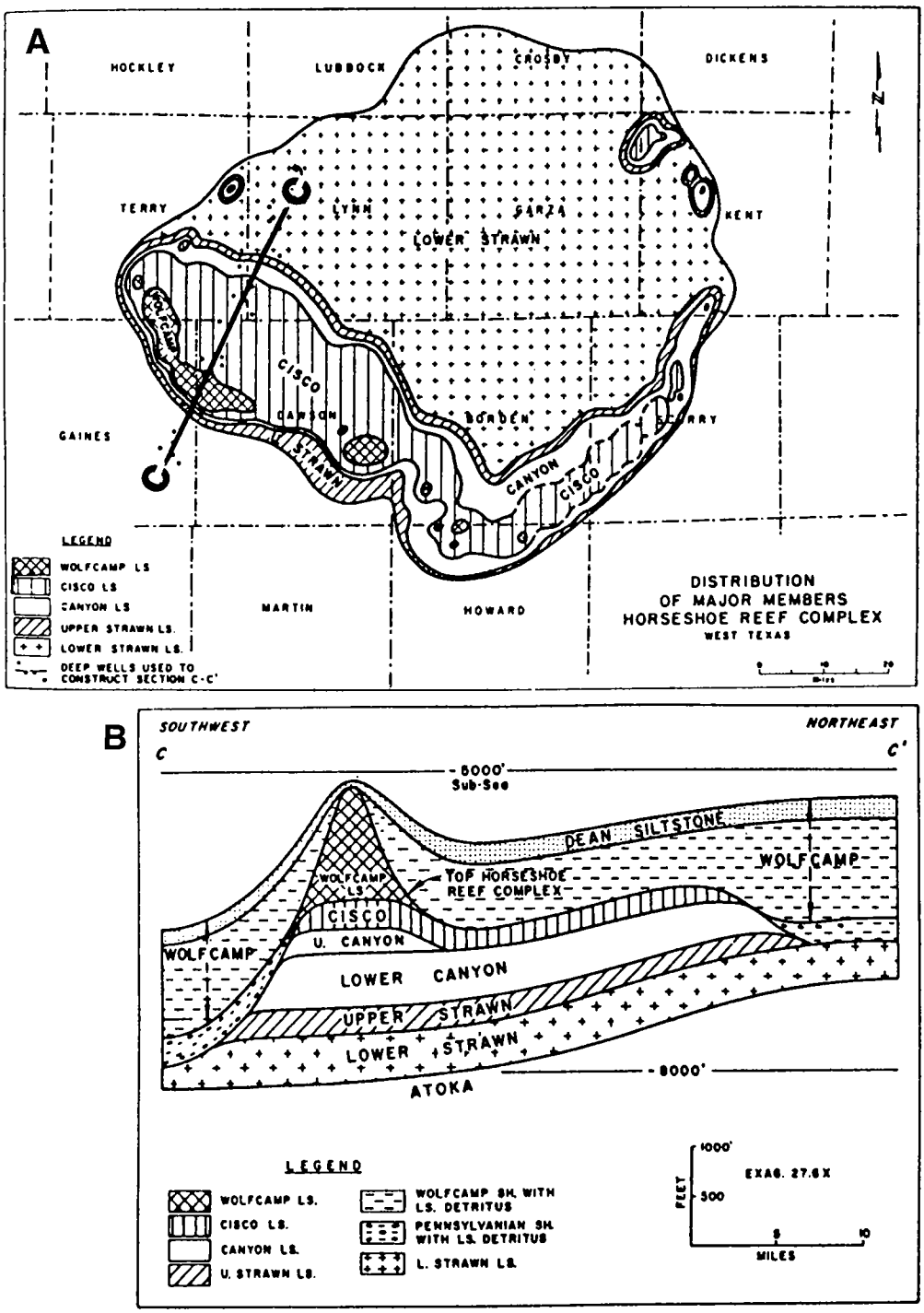

Figure 25. Horseshoe atoll of west Texas. (A) Map view illustrating the distribution of chronostratigraphic carbonate units in the atoll buildup. Line of section (C–C') for Figure 25B is indicated. (B) North–south cross section through the thickest part of the atoll. The Dean siltstone is compactionally draped over the highest pinnacles on the southwest margin of the isolated carbonate platform. Modified from Vest (1970).

rosity resulted from both the dissolution of algal fronds (meteoric diagenesis) and the formation of intercrystalline pores from neomorphism of micrite matrix (also likely as the consequence of subaerial exposure).

Shelf-margin carbonate banks are highly sought-after exploration objectives on the Concho platform/Eastern shelf owing to their commonly great thicknesses, widespread lateral continuity along strike, and large hydrocarbon reserves. They are relatively easy to locate by means of subsurface geologic mapping as well as by two-dimensional seismic identification of reef-core and talus facies (in dip sections).

Bloomer (1990) lists and describes a series of subsurface-exploration steps by which geologists can explore for shelf-margin carbonate reservoirs in west-central Texas. These ideas are equally applicable to the Strawn–Canyon and Cisco shelf-edge carbonate buildups and can be applied in somewhat modified form to all the shelf-edge barrier complexes. Numerous east–west regional stratigraphic cross sections constitute a necessary starting point for an exploration program. As noted earlier, the cross sections should illustrate both the correlation of format-bounding limestone units across the Concho platform/Eastern shelf and condensed-section black shales that

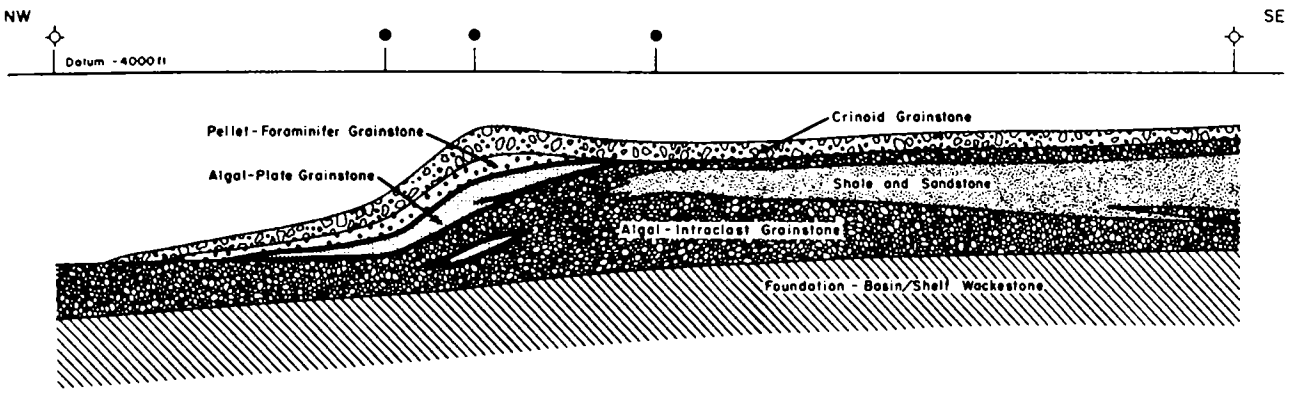

Figure 26. Lithologic cross section of facies in middle Strawn reef of Nena Lucia field, Nolan County. Production is obtained from the algal-plate grainstone facies. Modified from Toomey and Winland (1973).

can be correlated beyond the shelf edge into the basin. Specific regional carbonate markers—such as the Odom, Santo, Goen, Capps/Village Bend, Dog Bend, Palo Pinto, Winchell, Ranger, and Home Creek Limestones—should be identified on the shelf segment of each cross section. The bottoms (or tops) of successive transgressive carbonate markers define the boundaries for isopach- and isolith-mapping intervals. The positions of the shelf-interior facies assemblage and the shelf-margin carbonate-bank system are also well demarcated by regional cross sections. This is especially true if carbonate lithologic continuity (as indicated by a brick pattern) rather than well-log curves is shown on some of the cross sections (Fig. 15). Wherever possible, seismic evidence that documents the same or nearly the same line of section as the lithologic cross sections should be included with the study.

The second step in Bloomer's (1990) suggested protocol for reef prospecting involves construction of whole-interval isopach and net-lithology isolith maps. All the map types should be prepared for single genetic units (Galloway sequences or format units) that are most likely to contain reefal buildups at the shelf edge. Within a single interval, the shelf-interior, shelf-margin, slope, and basinal deposits each show a characteristic thickness pattern that is easily identified on an isopach map. Net-sandstone isolith mapping of the same interval delineates the facies belts of interior-shelf fluvial–deltaic siliciclastics and the exceedingly thick slope submarine-fan complex beyond the shelf edge. Of course, for the Strawn Group, there is no slope system beyond the carbonate ramp; the starved-basin black shale of the basin system does not exceed 40 ft per genetic interval. Net-carbonate isolith maps indicate a maximum thickness of limestone at the shelf edge, a dramatic thinning of carbonate on the slope, and a much more gradual thinning toward the shelf interior. The exact position and trend of the shelf margin are the most important features illustrated on this map. Regional limestone isolith maps can also pinpoint large pinnacle reefs on the slope as well as interior carbonate buildups on the shelf. More detailed, larger scale maps covering specific areas of interest can then be constructed that determine the geographic extent and total interval of section contained within prospective shelf-edge reefal buildups.

Once individual buildups have been delineated along a shelf margin, additional maps should be prepared to locate specific prospects. A structural-contour map showing the top of the reefal buildup for a given genetic interval will demonstrate its elevation above the surrounding non-reef facies and delimit the area of most likely hydrocarbon entrapment. Transgressive black shales within the accretionary upper Strawn–Canyon shelf-margin reef for each of the principal genetic sequences help prevent migration of hydrocarbons out of the individual components of the total stacked reefal edifice. Thus, one need not restrict exploration efforts only to the highest parts of the complete upper Strawn–Canyon reef complex. A structural-contour map showing the top of the Odom Limestone, the effective base for post-Caddo reefing, might also be meaningful. This map would help identify basement structural highs on which later reefing took place.

For the Cisco shelf margins, it would also be desirable to prepare structural-contour maps of carbonate markers that overlie the buildups. Because Cisco lowstand deltas of the superjacent cycle prograde out on top of and beyond the older shelf edge, these supra-reef contour maps will delineate closure caused by differential compaction. Similarly, complete-sequence isopach maps between two marker beds above shelf-edge reef zones act to quantify the amount of thinning that takes place there. This is another indicator of possible differential compaction. Production will be obtained from fluvial–deltaic facies draped over the shelf-edge reef.

The final step of the initial exploration effort is achieved by drilling a well into the reef buildup as high on the structure as possible. A three-dimensional seismic survey, if carried out preceding the drilling of this well, can be used to pinpoint the site for this well and supply a better visualization of the overall reef geometry. On the other hand, the explorationist may wait until after drilling the first well to conduct the seismic survey. Under this circumstance, he will seek confirmation of reservoir porosity and the presence of hydrocarbons from a detailed analysis of well cuttings, porosity logs, and mud logs. With subsequent development wells, cores should be taken from all the identified reservoir-quality reefal-porosity zones.

Shelf-Interior Carbonate Banks

Middle and Late Pennsylvanian carbonate banks that accumulated on the interior of rimmed shelves can be subdivided into two basic types. The first type comprises Missourian bank complexes that formed during accumulation of the highstand systems tract of the Palo Pinto, Winchell, Ranger, and Home Creek depositional cycles. These non-shelf-edge banks parallel the trend of the shelf-edge bank system on the Eastern shelf and reflect the position of a shallow, subtidal bathymetric contour on the inner shelf. The inner Palo Pinto bank, which enters the outcrop zone in northwestern Palo Pinto County, is composed almost entirely of offshore subtidal phylloid-algal wackestone. Grainstones are thin and not numerous in the large exposed section near Morris Sheppard Dam (Wermund, 1969, 1975).

Within the subsurface, these four bank systems have proved to be nonproducing features throughout the area where they have been accurately mapped (Wermund, 1975; Wermund and others, 1962). South of Runnels County, the inner-bank trend has not been mapped in an isolith- or isopach-map format. Its production potential is unknown in that region. This absence of hydrocarbons is somewhat surprising, because one would expect thick, meteorically generated porous intervals within the banks and even karst development on the lowstand tops of the bank buildups for each cycle. After all, these inner banks were exposed and above sea level for the deposition of the complete lowstand systems tract. On the other hand, shelf-interior banks are adjacent to and interbedded with a much thinner interval of shale source rocks than are the outer banks.

The second type of a Pennsylvanian interior carbonate-bank system is illustrated by the Capps Limestone, which contains a group of shelf-interior buildups that did not give rise to a distinct strike-elongate bank system that paralleled the shelf margin (Fig. 7). This unit is present at the top of the Hog Bend genetic interval of the Strawn Group. The buildups involve irregularly distributed chaetetid and phylloid-algal patch reefs that produce from small fields in Runnels and adjacent counties. This area was a carbonate-dominated segment of the Concho platform/Eastern shelf, inasmuch as no major fluvial–deltaic systems were active across the southern two-thirds of the shelf during the latest Desmoinesian. A similar depositional scenario occurred for the more aggressively explored Goen patch-reef interval. Although the Capps is commonly used as a local marker for structural-contour mapping, no published regional carbonate isolith map has ever been presented for the unit.

Isolated Platforms

Isolated Pennsylvanian carbonate platforms of north-central and west-central Texas formed on top of uplifted basement segments that underwent tectonic upwarping and faulting during the late Morrowan and Atokan. The Red River–Matador arch involves a parallel trend of horst blocks that were elevated above sea level during the Atokan. Individual blocks shed arkosic braid-delta sediment into the Knox–Baylor trough and northern Fort Worth basin but were planed off to sea level by the late early Desmoinesian (Ammentorp and Cleaves, 1990). From that time onward to the end of the Pennsylvanian, subtidal carbonate accumulated on the fault-bounded blocks and generated a continuous carbonate platform. Significant hydrocarbon production is seen only along the southern periphery of the platform. On the Electra spur in southern Wichita County (Fig. 16), upper Strawn oolitic grainstones (KMA limestone of the Brazos River and Hog Mountain genetic sequences) are highly prolific reservoirs. They produce oil from anticlinal traps in the giant KMA field (Dobyns and others, 1952). Farther to the west, small-scale reefal buildups on the King County platform entrapped minor quantities of hydrocarbons.

The Horseshoe atoll of west Texas is unarguably the largest and most petroliferous assemblage of carbonate stratigraphic traps in Pennsylvanian rocks of the southwest. Stacked Desmoinesian through Wolfcampian peritidal and shallow subtidal carbonates aggraded from a subdued intrabasinal platform within the Midland basin. All the producing intervals occur within the raised outer margin of the isolated platform. The atoll has a U-shaped configuration, with the rim opening to the north (Fig. 25A). It has a maximum dimension of 90 mi in an east–west direction and covers parts of 12 counties (Stafford, 1959; Myers and others, 1956). Owing to the prevailing Pennsylvanian wind- and water-circulation patterns, the greatest vertical relief in the reef complex (exceeding 3,000 ft) is along the southwest segment of the atoll rim. Subsidence and sediment starvation in the Midland basin enabled distinct pinnacles to build upward from the laterally continuous Desmoinesian carbonate-platform foundation. The largest oil fields are in the structurally updip southeastern part of the atoll.

Kelly–Snyder represents the most important and most extensively described of the Horseshoe atoll carbonate fields. Oil is trapped in the topographically higher crests of atoll pinnacles and reef ridges, giving rise to a maximum oil column of 700 ft (Galloway and others, 1983). Oil migrated from adjacent black-shale source rocks of the basin center. The complete buildup was subsequently sealed by burial beneath progradational, mud-dominated slope siliciclastics derived from advancing Wolfcampian shelf margins. With more than 1 billion cumulative barrels already produced, Kelly–Snyder qualifies as a giant oil field. The ultimate recovery from all the atoll-related fields is expected to exceed 2.5 billion barrels. This contrasts with an expected total recovery of approximately 1.5 billion barrels for all carbonate buildups on the Eastern shelf (Galloway and others, 1983).

The Kelly–Snyder field produces predominantly from nine discrete reservoirs in the Missourian (Canyon) portion of the buildup, although four Desmoinesian (Strawn) porosity zones also contribute to the overall total. Prominent reservoir lithofacies include (1) sponge–algal–bryozoan and phylloid-algal-mound bafflestone, boundstone, and wackestone; (2) tidal-flat and peritidal wackestone on pinnacle crests; (3) shoal and shoreface grainstones; and (4) subaqueous-debris-flow lithoclast packstone and wackestone of the reefal slope (Schatzinger, 1983; Waite, 1993). These lithofacies are schematically illustrated in Figure 27. The greatest porosity occurs within grainstone and algal-mound packstone and wackestone facies. Meteoric diagenesis caused by periodic exposure of the reef crest during eustatic lowstands was the

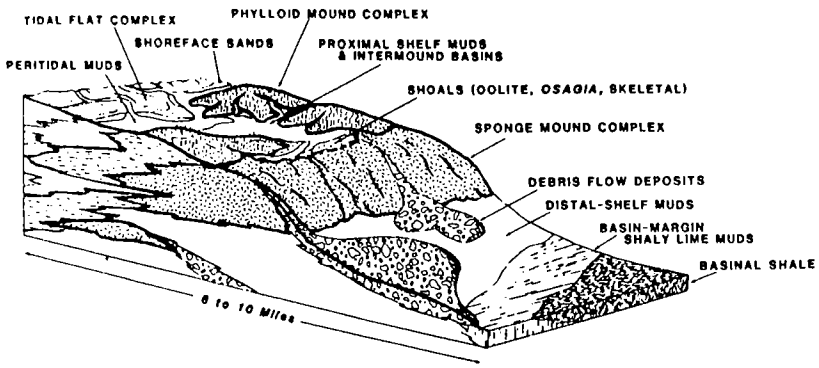

Figure 27. Model for carbonate reefal facies in the Kelly–Snyder field of the Horseshoe atoll. From Schatzinger (1983).

principal mechanism for porosity creation in these facies. Although the porosity zones have been extensively correlated across the one isolated platform, they have not been linked to the previously described eustatic cycles on the Eastern shelf.

Regrettably, the Horseshoe atoll is a one-of-a-kind feature for the Midland basin and surrounding Pennsylvanian epicratonic basins. The geologic conditions controlling oil accumulation in carbonate facies on isolated platforms, central basin platforms, and shelf edges are well understood and have been intensively prospected for in west Texas. Two-dimensional seismic surveys furnish excellent imaging of carbonate buildups that have been covered by thick mudstone intervals. Consequently, recent drilling in the Horseshoe atoll area has largely been restricted to infill development wells and tertiary-recovery projects. More extensive drilling in the less explored parts of the Midland basin next to the Matador arch might, however, locate small platform or pinnacle elements that have been overlooked by earlier exploration efforts.

SUMMARY AND CONCLUSIONS

Five major types of carbonate depositional systems are present in subsurface Pennsylvanian sedimentary rocks of north-central and west-central Texas: (1) isolated platforms, (2) carbonate ramps, (3) shelf-margin barrier banks, (4) basin-margin pinnacles, and (5) shelf-interior banks. The Horseshoe atoll, King County (Spur) platform, and Red River uplift carbonates are all examples of carbonate buildups that became established on structural highs. Carbonate-ramp deposition was restricted to the eastern margin of the Midland basin and occurred during the Early and Middle Pennsylvanian. Ramp interior banks associated with the Odom Limestone and Goen patch reefs consisting of sponge and phylloid-algal accumulations were the predominant reefal-rock bodies. A rimmed-shelf margin first developed with the late Atokan Caddo bank system, which formed on the eastern side of the Concho platform facing the Fort Worth basin. Later shelf-edge banks include the Anson, Palo Pinto–Winchell, and Sylvester systems, all of which faced the Midland basin. Pinnacle reefs and small atolls formed in proximal basin settings that paralleled the Anson and Palo Pinto–Winchell shelf margins. One larger, more long-lived buildup, the Seymour pinnacle, accreted at the eastern end of the Knox–Baylor trough throughout the Missourian. Shelf-interior banks were most prominent and widespread on the Eastern shelf during the Missourian but also developed during the middle and late Desmoinesian on the ramp interior.

The location, lateral extent, and degree of vertical accretion for carbonate buildups that form reservoirs can best be explained in terms of the interactions between three controlling factors: type of carbonate depositional system, local and regional tectonic setting, and cyclic eustatic changes of sea level.

The interplay of tectonics and sedimentation patterns in determining the positioning of carbonate systems is best illustrated by the western margin of the Concho platform/Eastern shelf, which evolved through several distinct stages. From the early Atokan to the late Desmoinesian, a homoclinal ramp system separated the platform from the sediment-starved Midland basin. Near the end of the Desmoinesian, accelerated subsidence in the Midland basin created sufficient shelf-to-basin relief to allow for the growth of the Anson shelf-margin bank system. Siliciclastic sedimentation, however, still predominated on the shelf interior, and no large-scale bank system accumulated there. During the middle and late Missourian, deltaic sedimentation was restricted to the northernmost part of the Eastern shelf. The remainder of the shelf became a broad area of carbonate-dominated deposition, where eustatically induced reciprocal sedimentation generated both a platform-margin and a platform-interior bank system. Owing to the relatively rapid subsidence in the Midland basin, as well as the absence of a submarine-fan apron bordering the shelf edge, accretion without shelf-margin progradation was the norm for both the Anson and Missourian shelf-edge bank systems. Later, during the Virgilian, active fluvial–deltaic sedimentation across the entire north–south length of the Eastern shelf brought a return to predominantly siliciclastic sedimentation on the shelf interior. Thus, no bank systems could develop there. Deposition of lowstand wedges consisting of perched deltas and a submarine-fan apron both prograded and aggraded the shelf margin.

Cycles of eustatic sea-level change fine tuned the location, overall timing of accretion, and pattern of growth for Pennsylvanian carbonate-platform buildups throughout north-central and west-central Texas. Virtually all the middle and late Pennsylvanian eustatic cycles involved type 1 sequences. Under such conditions, the lowstand coastline was present below the shelf break, and incised-valley-fill fluvial systems became entrenched on the shelf. The middle Strawn ramp system contained shelf-interior banks such as the Odom system and localized Goen patch reefs constructed by phylloid algae and chaetetid sponges. Eustatic lowstands exposed these buildups above sea level, and meteoric diagenesis gave rise to reservoir-quality porosity zones. The Goen reefs accreted during deposition of the transgressive systems tract. With the patch reefs described by Marquis and Laury (1989), there was also a regressive phase of reefal sedimentation that took place during a stillstand that came after completion of the transgression. Vertical upbuilding of the Anson and outer (shelf-mar-

gin) Missourian banks was initiated only after a stable lowstand of sea level was established. The shelf-edge banks, as well as localized basin-margin pinnacles, then accreted to sea level. Some of the pinnacles formed atolls that contained biograinstone beach facies, tidal flats, and oolitic shoals. These facies, where present adjacent to emergent islands, were subjected to freshwater, vadose diagenesis. The large banks had a reef core made up of *Chaetetes* and phylloid-algal bafflestone. Additional, more extensive upbuilding of the pinnacles and banks took place during the ensuing transgression. Ultimately, for each major transgressive phase, the pinnacles and shelf-margin carbonate features failed to keep pace with sea-level rise and were drowned. With the beginning of the next lowstand, the transgressive carbonates also underwent freshwater leaching.

The Missourian shelf-interior banks formed on a carbonate-dominated part of the Eastern shelf where no major deltaic depositional systems were active. Growth began in relatively shallow water, once stable highstand conditions became established and accretion tracked the gradual rate of subsidence across the shelf interior. When forced regression brought about the next drop in sea level, the complete inner bank was exposed above sea level. Subsequent highstands reinitiated vertical growth along the same bank trend owing to the tendency for organic carbonates to accumulate on elevated, cemented substrates.

Virgilian carbonate banks accumulated under conditions significantly different from those seen with the Anson and Missourian bank complexes. Inasmuch as the Virgilian shelf interior was dominated by siliciclastics, no shelf-interior bank could be laid down. Furthermore, because lowstands of sea level brought perched deltas to the shelf margin along the entire western periphery of the Eastern shelf, bank growth could not begin again on top of the older bank of the previous cycle. During each lowstand, no carbonate bank growth took place, and a siliciclastic wedge consisting of submarine fans and deltaic facies prograded the shelf edge basinward. At the beginning of the next transgression, a new carbonate-bank complex became established on top of the new delta-floored shelf edge. Terrigenous clastic sediment could not reach the shelf edge during the transgressive phase of the eustatic cycle and was trapped within inner-shelf estuaries until after sea level stopped rising. Virtually all accretion for Virgilian banks took place during the transgression, as these banks were ultimately drowned before maximum flooding was attained. Porosity formation occurred during the next lowstand cycle, when deltas again reached the shelf edge.

Hydrocarbon production from carbonate systems in north-central and west-central Texas has been, with the exception of the Horseshoe atoll, far less significant than production obtained from terrigenous clastic depositional systems in the same regions. Not only are potential drilling targets more widely scattered, but successful exploration strategies are more complex and difficult to implement. Reservoir-quality porosity and permeability are typically developed in transgressive-systems-tract limestone buildups that have been exposed and subjected to meteoric diagenesis during sea-level lowstands. Desmoinesian and Missourian shelf-margin banks and proximal basin pinnacles, associated with the accretionary phase in the evolution of the Eastern rimmed-shelf margin, present the best opportunities for multiple pay zones and economic accumulations of oil and gas. These shelf-margin buildups grew directly adjacent to a thick column of basinal source rocks during multiple episodes of eustatic sea-level change. Technological innovations such as three-dimensional seismic surveys cannot serve as an economical substitute for older, more conventional methods of subsurface exploration. Most importantly, to be successful in the long term, the explorationist must have a comprehensive understanding of the regional tectonics, the history of eustatic sea-level change, and the chronologic evolution of depositional systems for the area under consideration.

REFERENCES CITED

Ammentorp, Alan; and Cleaves, A. W., II, 1990, Depositional systems, diagenesis, and hydrocarbon entrapment in the upper Atokan "Caddo clastic interval" of the northwestern Fort Worth basin, *in* Gibbs, C. M.; Reynolds, C. R.; Tucker, Will; and Ritchie, Jeff (eds.), Transactions, American Association of Petroleum Geologists, Southwest Section, 1990 regional meeting: North Texas Geological Society, Wichita Falls, p. 121–130.

Bloomer, R. R., 1990, Jameson Field, *in* Beaumont, E. A.; and Foster, N. H. (eds.), Treatise of petroleum geology, Atlas of oil and gas fields, stratigraphic traps I: American Association of Petroleum Geologists, p. 137–153.

Brown, Alton, 1982, Intraformational subaerial exposure of carbonates in the Canyon Group (Pennsylvanian), north-central Texas: evidence for eustatic control of facies distribution on the Eastern shelf of the Midland basin, *in* Cromwell, D. (ed.), Middle and Upper Pennsylvanian System of north-central and west Texas, symposium and field conference guidebook: Society of Economic Paleontologists and Mineralogists, Permian Basin Section, Midland, Publication 82-21, p. 201–214.

Brown, L. F., Jr., 1979, Deltaic sandstone facies of the Mid-Continent, *in* Hyne, N. D. (ed.), Pennsylvanian sandstones of the Mid-Continent: Tulsa Geological Society Special Publication 1, p. 35–63.

_____1990, Use of sequence stratigraphy to define stratigraphic plays in Upper Pennsylvanian and Lower Permian lowstand systems tracts, north-central Texas, *in* Linsay, D.; Ross, J. R.; and Swartz, B. (eds.), Transactions, American Association of Petroleum Geologists, Southwest Section, 1989 regional meeting: San Angelo Geological Society, p. 1–21.

Brown, L. F., Jr.; Solis-Iriarte, R. F.; and Johns, D. A., 1990, Regional depositional systems tracts, paleogeography, and sequence stratigraphy, Upper Pennsylvanian and Lower Permian strata, north- and west-central Texas: Texas Bureau of Economic Geology Report of Investigations 107, 116 p.

Cheney, M. G.; and Goss, L. F., 1952, Tectonics of central Texas: American Association of Petroleum Geologists Bulletin, v. 36, p. 2237–2265.

Cleaves, A. W., II, 1975, Upper Desmoinesian–Lower Missourian depositional systems (Pennsylvanian), north-central Texas: University of Texas at Austin unpublished Ph.D. dissertation, 256 p.

_____1993, Sequence stratigraphy, systems tracts, and mapping strategies for the subsurface Middle and Upper Pennsylvanian of the Eastern shelf, *in* Crick, R. E. (ed.), Transactions, American Association of Petroleum Geologists, Southwest Section, 1993 regional meeting: Fort Worth Geological Society, p. 26–42.

_____1996, Sequence stratigraphy, delta models, and fluvial–deltaic sediment-dispersal systems in the Pennsylvanian cyclic deposits of north-central Texas, *in* Johnson, K. S. (ed.), Deltaic reservoirs in the southern Midcontinent, 1993 symposium: Oklahoma Geological Survey Circular 98, p. 143–167.

Cleaves, A. W.; and Erxleben, A. W., 1985, Upper Strawn and Canyon cratonic deposition of the Bend arch, north-central Texas, *in* McNulty, C. I..; and McPherson, J. C. (eds.), Transactions of the American Association of Petroleum Geologists, Southwest Section, 1985 regional meeting: Fort Worth Geological Society, p. 27–46.

Conselman, F. B., 1960, Pennsylvanian reef patterns in west-central Texas, *in* Aspects of the geology of Texas, a symposium: University of Texas at Austin Publication 6017, p. 1–13.

Dobyns, R. P.; and others, 1952, Petroleum engineering study of the K. M. A. reservoir, southwestern part of K. M. A. oil field, Wichita and Archer Counties, Texas: U.S. Bureau of Mines Report of Investigations 4892, 88 p.

Enos, Paul, 1985, Cretaceous debris reservoirs, Poza Rica Field, Vera Cruz, Mexico, *in* Roehl, P. O.; and Choquette, P. W. (eds.), Carbonate petroleum reservoirs: Springer-Verlag, New York, p. 455–471.

Erxleben, A. W., 1975, Depositional systems in the Pennsylvanian Canyon Group of north-central Texas: Texas Bureau of Economic Geology Report of Investigations 82, 76 p.

Galloway, W. E.; and Brown, L. F., Jr., 1973, Depositional systems and shelf–slope relations on cratonic basin margin, uppermost Pennsylvanian of north-central Texas: American Association of Petroleum Geologists Bulletin, v. 57, p. 1185–1218.

Galloway, W. E.; and others, 1983, Atlas of major Texas oil reservoirs: Texas Bureau of Economic Geology, 134 p.

Gunn, R. D., 1979, Desmoinesian depositional systems in the Knox–Baylor trough, *in* Hyne, N. J. (ed.), Pennsylvanian sandstones of the Mid-Continent: Tulsa Geological Society Special Publication 1, p. 221–234.

Haeberle, F. R., 1956, Seymour Strawn and Caddo fields, Baylor County, Texas: American Association of Petroleum Geologists Bulletin, v. 40, p. 879–889.

Harrison, E. P., 1973, Depositional history of Cisco–Wolfcamp strata, Bend Arch, north-central Texas: Texas Technological University (Lubbock) unpublished Ph.D. dissertation, 256 p.

_____1991, Cyclic deposition on the Eastern shelf, *in* Cyclic deposition of Pennsylvanian and Permian sediments on the Eastern shelf, Texas: Guidebook, American Association of Petroleum Geologists, Southwest Section, 1991 regional meeting, Abilene Geological Society, p. 1–6.

Heckel, P. H., 1972, Recognition of ancient shallow marine environments, *in* Rigby, J. K.; and Hamblin, W. K. (eds), Recognition of ancient sedimentary environments: Society of Economic Paleontologists and Mineralogists Special Publication 16, p. 226–286.

_____1980, Paleogeography of eustatic model for deposition of Midcontinent Upper Pennsylvanian cyclothems, *in* Fouch, T. D.; and Magathan, E. R. (eds.), Rocky Mountain paleogeography, Symposium 1: Paleozoic paleogeography of the west-central United States: Society of Economic Paleontologists and Mineralogists, Rocky Mountain Section, Denver, p. 197–215.

Hogden, J.; and Martin, C. A., 1974, Fort Worth basin very busy again: Oil and Gas Journal, Nov. 11, p. 244–251.

Kier, R. S., 1972, Carboniferous stratigraphy of eastern San Saba County and western Lampasas County, Texas: University of Texas at Austin unpublished Ph.D. dissertation, 437 p.

Kier, R. S.; Harwood, P.; Brown, L. F., Jr.; and Goodson, J. L., 1976, Brownwood Sheet, *in* Barnes, V. E. (project director), Geologic atlas of Texas: Texas Bureau of Economic Geology, scale 1:250,000.

Kosters, E. C.; and others, 1989, Atlas of major Texas gas reservoirs: Texas Bureau of Economic Geology, 181 p.

Lee, Wallace, 1938, Stratigraphy of the Cisco group of the Brazos basin, *in* Stratigraphic and paleontologic studies of the Pennsylvanian and Permian rocks in north-central Texas: University of Texas at Austin Publication 3801, p. 11–90.

Longman, M. W., 1982, Carbonate diagenesis as a control on stratigraphic traps: American Association of Petroleum Geologists Education Course Notes 21, 159 p.

Marquis, S. A., Jr., 1987, Facies and diagenesis of the Goen Limestone cyclothem (early late Desmoinesian), Concho and Runnels Counties, central Texas: Southern Methodist University, Dallas, unpublished M.S. thesis, 165 p.

Marquis, S. A., Jr.; and Laury, R. I., 1989, Glacio-eustasy, depositional environments, and reservoir character of Goen Limestone cyclothem (Desmoinesian), Concho platform, central Texas: American Association of Petroleum Geologists Bulletin, v. 73, p. 166–181.

Mazzullo, S. J., 1982, Types and controls of Permo-Pennsylvanian carbonate stratigraphic traps of shallow marine origin in Permian basin: exploration models: Oil and Gas Journal, Oct. 4, p. 124–141.

_____1985, Pennsylvanian facies-diagenetic reservoir, Lower Strawn Formation, Seminole Southeast field, Midland basin, West Texas, *in* Roehl, P. O.; and Choquette, P. W. (eds.), Carbonate petroleum reservoirs: Springer-Verlag, New York, p. 227–238.

Mazzullo, S. J.; and Mazzullo, L. J., 1983, Atoll reservoir facies in Pennsylvanian limestone, Higgins Ranch field, Coke County, Texas, *in* Harris, P. M. (ed.), Carbonate buildups—a core workshop: Society of Economic Paleontologists and Mineralogists Core Workshop 4, p. 223–243.

Mazzullo, S. J.; and Reid, A. M., 1989, Subtle traps in Ordovician to Permian carbonate petroleum reservoirs, Permian basin: an overview, *in* Flis, J. E.; Price, R. C.; and Sarg, J. F. (eds.), Search for the subtle trap: hydrocarbon exploration in mature basins: West Texas Geological Society Publication 89-85, p. 155–190.

Myers, D. A.; Stafford, P. T.; and Burnside, R. J., 1956, Geology of the late Paleozoic Horseshoe atoll in west Texas: University of Texas at Austin Publication 5607, 113 p.

North, F. K., 1985, Petroleum geology: Allen and Unwin, Boston, 607 p.

Reid, A. M.; and Mazzullo, S. J., 1988, Paint Rock and Paint Rock Southwest fields, Concho County, Texas: Strawn analogues of modern shelf island systems: West Texas Geological Society Bulletin, v. 27, p. 5–10.

Reid, A. M.; Modley, M. A.; and Reid, S. A., 1992, Shelf edges, reefs, and associated stratigraphic traps on the Eastern shelf, *in* Mruk, D. H.; and Curran, B. C. (eds.), Permian basin exploration and production strategies: application of sequence stratigraphic and reservoir characterization concepts: West Texas Geological Society Publication 92-91, p. 51–63.

Richards, O. H., 1952, Aspermont Lake field, Stonewall County, Texas: Abilene Geological Society Geological Contributions, p. 1–14.

Sarg, J. F., 1988, Carbonate sequence stratigraphy, *in* Wilgus, C. K.; and others (eds.), Sea level changes: an integrated approach: Society of Economic Paleontologists and Mineralogists Special Publication 42, p. 155–181.

Schatzinger, R. A., 1983, Phylloid algal and sponge–bryozoan mound-to-basin transition: a late Paleozoic facies tract from the Kelly–Snyder field, west Texas, *in* Harris, P. M. (ed.), Carbonate buildups—a core workshop: Society of Economic Paleontologists and Mineralogists Core Workshop 4, p. 244–303.

Stafford, P. T., 1959, Geology of part of the Horseshoe atoll in Scurry and Kent Counties, Texas: U.S. Geological Survey Professional Paper 315-A, 18 p.

Toomey, D. F.; and Winland, H. D., 1973, Rock and biotic facies associated with Middle Pennsylvanian (Desmoinesian) algal buildup, Nena Lucia field, Nolan County, Texas: American Association of Petroleum Geologists Bulletin, v. 57, p. 1053–1074.

Van Wagoner, J. C.; Mitchum, R. M.; Campion, K. M.; and Rahamian, V. D., 1990, Siliciclastic sequence stratigraphy in well logs, cores, and outcrops: concepts for high-resolution correlation of time and facies: American Association of Petroleum Geologists Methods in Exploration 7, 55 p.

Vest, E. L., 1970, Oil fields of Pennsylvanian–Permian Horseshoe Atoll, west Texas, *in* Halbouty, M. T. (ed.), Geology of giant

petroleum fields: American Association of Petroleum Geologists Memoir 14, p. 185–203.

Waite, L. E., 1993, Upper Pennsylvanian seismic sequences and facies of the eastern and southern Horseshoe Atoll, Midland basin, west Texas, *in* Loucks, R. G.; and Sarg, J. F. (eds.), Carbonate sequence stratigraphy: recent developments and applications: American Association of Petroleum Geologists Memoir 57, p. 213–240.

Walper, J. L., 1982, Plate tectonics evolution of the Fort Worth basin, *in* Martin, C. A. (ed.), Petroleum geology of the Fort Worth basin and Bend arch area: Dallas Geological Society, p. 237–252.

Weber, L. J., 1995, Depositional and diagenetic control of reservoir quality and continuity of the Pennsylvanian Caddo Limestone, *in* Pausé, P. H.; and Candelaria, M. P. (eds.), Carbonate facies and sequence stratigraphy: practical applications of carbonate models: SEPM (Society for Sedimentary Geology), Permian Basin Section, Midland, Publication 95-36, p. 257–286.

Wermund, E. G., 1969, Late Pennsylvanian limestone banks: a résumé, *in* Brown, L. F., Jr.; and Wermund, E. G. (eds.), A guidebook to Late Pennsylvanian shelf sediments, north-central Texas: Dallas Geological Society, p. 12–20.

_____1975, Upper Pennsylvanian limestone banks, north-central Texas: Texas Bureau of Economic Geology Geologic Circular 75-3, 34 p.

Wermund, E. G.; and Jenkins, W. A., Jr., 1969, Late Pennsylvanian Series in north-central Texas, *in* Brown, L. F. Jr.; and Wermund, E. G. (eds.), A guidebook to Late Pennsylvanian shelf sediments, north-central Texas: Dallas Geological Society, p. 1–11.

Wermund, E. G.; and Jenkins, W. A., Jr., 1970, Recognition of deltas by fitting trend surfaces to Upper Pennsylvanian sandstones in north-central Texas, *in* Morgan, J. P. (ed.), Deltaic sedimentation: modern and ancient: Society of Economic Paleontologists and Mineralogists Special Publication 15, p. 256–259.

Wermund, E. G.; Jenkins, W. A.; and Ohlen, H., 1962, The distribution of sedimentary facies on a model shelf, Upper Pennsylvanian of north-central Texas: Mobil Research Lab, Exploration Research Division Report R62.10, 3 p., 32 pls.

Yancey, T. E.; and Cleaves, A. W., II, 1990, Carbonate and siliciclastic sedimentation in Late Pennsylvanian cycles, north-central Texas, *in* Guidebook for Field Trip 7, Geological Society of America, 1990 annual meeting: Dallas Geological Society, p. 1–20.

Yancey, T. E.; and McLerran, R. D., 1988, Cycle stratigraphy of the Late Pennsylvanian of north-central Texas, *in* Cunningham, B. K. (ed.), Permian and Pennsylvanian stratigraphy, Midland basin, west Texas: studies to aid hydrocarbon exploration: Society of Economic Paleontologists and Mineralogists, Permian Basin Section, Midland, Research Seminar 1, p. 65–77.

Exploration- and Production-Scale Lateral Variability in Phylloid-Algal-Mound and Associated Reservoir Facies, Paradox Basin, Southeastern Utah

G. Michael Grammer and Gregor P. Eberli
University of Miami
Miami, Florida

ABSTRACT.—Hydrocarbon production from Late Carboniferous (Pennsylvanian) phylloid-algal-mound reservoirs in the Paradox basin of the southwestern United States has exceeded 400 million barrels of oil over the last 40 years, and estimates suggest that a similar amount of recoverable reserves is still in place within the basin. The exploration and development history of the basin indicates that the cycles containing prolific algal-mound reservoirs are characterized by extreme lateral variability, resulting in close step-out dry holes or, conversely, reservoirs encountered with virgin pressures. An outcrop-based study combining detailed facies analysis and cyclostratigraphy from equivalent facies on the exposed Paradox shelf has provided insight into the three-dimensional architecture and distribution of both the algal-mound reservoirs and their associated facies as well as the timing of mound growth and porosity development relative to sea-level change.

Lateral variability within the shelfal cycles is observed in both the distribution and thickness of facies. This variability in reservoir and associated facies occurs within tens or a few hundreds of meters, as well as on a kilometer scale, and is a function of antecedent topography, facies types, exposure, unfilled accommodation space, and the amplitude and frequency of relative sea-level change. Landward and seaward shifting of facies belts across the shelf by tens of kilometers, for example, occurs in response to 4th-order (100–400 k.y.) relative sea-level changes. An awareness of facies shifts at this scale can help direct and refine exploration efforts. In addition, abrupt lateral variability in the thickness of algal-mound reservoirs and associated facies observed in 4th- and 5th-order (<100 k.y.) depositional cycles may influence both exploration- and production-scale efforts in the basin. These results, coupled with facies analysis indicating that many of the cycles did not fill all available accommodation space, suggest that cyclostratigraphic correlations across the basin based on a limited amount of vertical data must be applied with caution.

INTRODUCTION

Cyclic sedimentation has been documented in numerous sedimentary basins of Pennsylvanian age, which was a time of extensive glaciation in the Southern Hemisphere (Crowell, 1978). This characteristic cyclicity might therefore be related to short-term (Milankovitch band) glacio-eustatic pulses that dominated the sedimentary record, especially in North America (e.g., Goldhammer and others, 1991; Heckel, 1980, 1986; Wanless, 1972; Wanless and Shepard, 1936). On the Paradox shelf, cyclicity is recorded in a mixed system of carbonates and siliciclastics, with an additional component of basin-centered evaporites (Choquette and Traut, 1963; Pray and Wray, 1963; Peterson and Hite, 1969; Hite and Buckner, 1981; Hite, 1970).

Goldhammer and others (1991) showed that the Desert Creek and the Lower and Upper Ismay sequences exhibited a distinct cyclicity that was characterized by a hierarchical stacking pattern within which 5th-order upward-shallowing cycles are grouped into 4th-order sequences, which in turn stack vertically into part of a 3rd-order accommodation trend. They concluded that the 4th- and 5th-order cyclical patterns are primarily controlled by high-frequency glacio-eustatic changes in response to waxing and waning of glaciers on the Gondwana supercontinent (Crowell, 1978), whereas the lower frequency 3rd-order sequences were probably driven by long-term patterns in subsidence.

A major focus of this study was to further evaluate the lateral continuity of the vertical stacking patterns established by Goldhammer and others (1991) to see if there was a recognizable pattern in outcrop that would help explain the established lateral variability in subsurface exploration and production trends. For example, the temporal and spatial positioning of algal-buildup facies in the subsurface in the lower and upper Desert Creek, as well as in the Lower and Upper Ismay, should be predictable through the analysis of facies patterns exposed in outcrop. In addition, although Goldhammer and others (1991) correlated the 4th-order sequences in their vertical section at Honaker Trail with subsurface core and wireline-log sections as far away as 80 km, the exploration and production history of the basin is one that documents abrupt lateral variability in economic reservoirs at both exploration (0.8–16 km) and development scales (<0.8 km).

Building on the previous study of Goldhammer and others

Grammer, G. M.; and Eberli, G. P., 2000, Exploration- and production-scale lateral variability in phylloid-algal-mound and associated reservoir facies, Paradox basin, southeastern Utah, *in* Johnson, K. S. (ed.), Platform carbonates in the southern Midcontinent, 1996 symposium: Oklahoma Geological Survey Circular 101, p. 259–267.

(1991) and the more recent work of Weber and others (1994, 1995a,b), we performed a high-resolution, outcrop-based sequence-stratigraphic and cyclostratigraphic analysis of the Desert Creek and Ismay intervals of the Paradox Formation, focusing on both the vertical and lateral variability of reservoir and associated facies. The primary goals of this study were (1) to determine the causal mechanisms and scale of lateral variability found in the sedimentary cycles and to assess the consequences of such variability to the application of cyclostratigraphy, and (2) to evaluate the efficacy of high-resolution outcrop studies to high-grade the evaluation and prediction of subsurface economic reservoir facies at both exploration and production scales.

GEOLOGIC SETTING

The Paradox basin is an elongate, northwest–southeast-trending intracratonic evaporitic basin that extends from the northwestern part of New Mexico into east-central Utah (Fig. 1) and covers an area of approximately 27,000 km^2 in southwestern Colorado and southeastern Utah (Stevenson and Baars, 1988). Although the basin was most actively subsiding and accumulating sediments during the Late Carboniferous (Pennsylvanian), the basin's structural framework developed by late Precambrian time (Baars and Stevenson, 1981). Recurrent tectonic movement throughout the Paleozoic resulted in vertical movements along basement fractures (Baars and Stevenson, 1982). In the basin center, shale, anhydrite, salt, and potash were deposited, whereas along the northern Uncompahgre uplift, thick siliciclastic wedges accumulated. Deposition on the Paradox shelf farther to the south and west was characterized primarily by cyclical carbonates, with subordinate shales and siliciclastics.

The Paradox Formation is defined as an evaporite facies in the basin, but carbonates and siliciclastics were deposited coevally on the shelf farther to the southwest. The Desert Creek and Ismay intervals form the top of the shelfal equivalent of the Paradox Formation. The Desert Creek and Ismay intervals of the Paradox Formation (Desmoinesian) exposed along the San Juan River in southeastern Utah are characterized by high-frequency cyclic repetition of carbonate and siliciclastic facies controlled primarily by 4th- and 5th-order changes in relative sea level. These cycles are typically mixed and are characterized by a basal sandstone unit, with black shales and sapropelic carbonate mudstones recording a subsequent major flooding event. A well-defined upward-shallowing trend in carbonates at the top of the cycle is interpreted as deposition during the relative highstand and early stages of the next fall.

The shelfal cycles are correlated with basinal evaporite cycles in the subsurface through the use of these black-shale and dark-carbonate-mudstone markers, which appear to be time-stratigraphic units (Choquette and Traut, 1963). The cycle-bounding shales include the Chimney Rock Shale (base of Desert Creek), the Gothic Shale (base of Lower Ismay), and the Hovenweep Shale at the base of the Upper Ismay. Both the Desert Creek and the Lower and Upper Ismay are characterized by extensive development of phylloid algal buildups in the subsurface and are important hydrocarbon reservoirs in different regions throughout the Paradox basin.

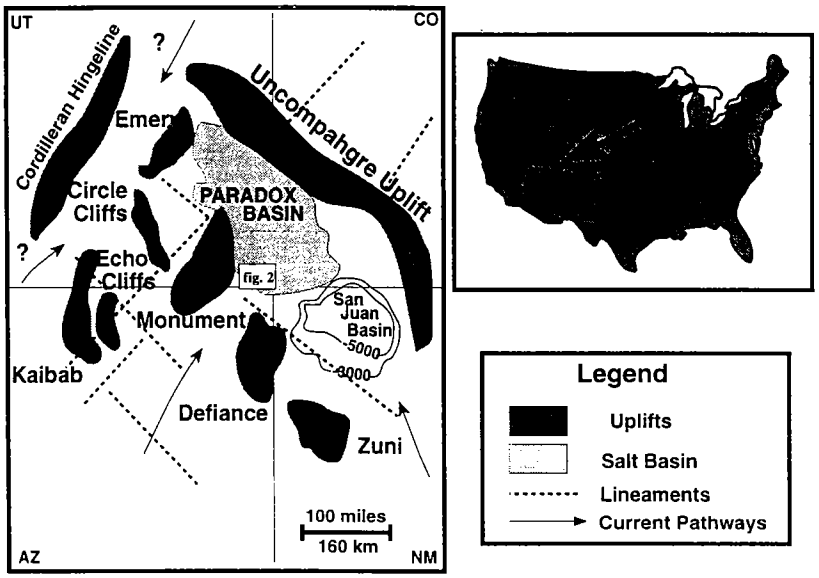

Figure 1. Regional map showing the extent of Paradox salt basin, Pennsylvanian uplifts, and major basement lineaments. Arrows in south and southwest show possible flow directions of marine waters into the Paradox basin region from the open ocean, which was farther to the southwest. Arrow in the north shows projected southward path of siliciclastic eolian dunes into the region (Driese and Dott, 1984). Uplifts were areas of positive topographic relief during Pennsylvanian time, providing local sources of terrigenous clastics and also restricting the flow of marine waters into the Paradox salt basin. Details of the study area are shown in Figure 2. Modified from Baars and Stevenson (1982).

METHODS

Four primary outcrop locations were chosen along the San Juan River (Honaker Trail, Navajo Goosenecks, Raplee Anticline, and Eight-Foot Rapids) to establish benchmarks for the vertical pattern of cyclicity and to evaluate exploration-scale lateral variability of the Desert Creek and the Lower and Upper Ismay sequences (Fig. 2). The outcrop sections are oriented slightly oblique to the strike of the shelf (northwest–southeast), with the evaporite basin situated to the northeast. The total distance covered between these four locations is approximately 16 km, with distances between individual locations varying from 3 to 13 km. The primary sections were measured at vertical intervals ranging from a decimeter to 0.5 m.

In addition to the 4 primary sections, 15 other infill sections (Honaker Trail–2; Navajo Goosenecks–2; Raplee Anticline–4; Eight-Foot Rapids–7) were measured to establish the lateral variability at a production scale. The spacing between these sections ranges from approximately 500 to less than 50 m. Key beds from these sections were then traced laterally between

sections for hundreds of meters (up to 1 km) to evaluate the lateral variability in facies character and/or thickness.

In addition to the outcrop sections, 372 m of slabbed core and 141 thin sections were evaluated from the three zones of interest from seven cored wells to evaluate the consistency of facies types and vertical stacking patterns observed in outcrop to the subsurface. The cored wells were 25–50 km from the outcrop sections (Fig. 2).

RESERVOIR-EQUIVALENT PHYLLOID-ALGAL MOUNDS

The phylloid-algal facies consists of phylloid-algal bioherms that vary in morphology from biostromal (flat and elongate) to moundlike with flat bases. The internal fabric of the algal facies varies from grain-supported algal bafflestones to algal wackestones and packstones with an associated normal-marine faunal assemblage (Fig. 3). The porosity is generally fair to excellent (5%–18%), with the highest porosity values in the moundlike buildups. Primary interparticle and shelter porosity, combined with secondary, dissolution-enhanced porosity, represents the bulk of the pore types.

The term *phylloid algae* was first used by Pray and Wray (1963) to describe a growth form of leaflike algae that includes both calcareous red algae and codiacean green algae. The genus *Ivanovia,* a codiacean green alga, is the most abundant type of phylloid algae in the Paradox basin (Pray and Wray, 1963). *Ivanovia* is thought to have grown in warm, shallow-marine environments with low tidal ranges at depths of 1–10 m (Wray, 1968; Toomey and others 1977).

Algal mounds are typically made up of individual plates forming either a bafflestone fabric or a packstone fabric, indicating that mounds may have been constructed by aggradational growth of phylloid-algal-dominated mounds similar to modern *Halimeda* mounds (e.g., Hine and others, 1988) and/or as accumulations of individual plates by currents and/or wave action. Well-developed moundlike morphologies of algal buildups are exposed at the Eight-Foot Rapids locality (Fig. 4). The mounds are approximately 8–14 m high, with spacing between individual mounds varying from 33 to 58 m. In addition, spacing between groups of coalesced mounds varies from about 350 to 500 m. These coalesced mounds are characterized by a series of closely spaced individual mounds as described above, but with lateral termination, or pinchout, of the algal facies within a few hundred meters.

The algal mounds are interpreted to have been deposited in moderate-energy, open-platform environments of varying depth. The best developed algal mounds combine hydrodynamic accumulation of plates with aggradational growth characterized by a bafflestone fabric. Abundant fibrous and botryoidal marine cements were likely fast growing and syndepositional, on the basis of modern examples (Grammer and others 1993), and would have provided a rigid framework for the mounds to continue their aggradational growth (Roylance, 1990). These mounds may have kept pace with sea-level rise and grown into waters only 1–2 m deep, as indicated by the presence of intertidal *Chaetetes*-bearing facies (Connolly and others, 1989) or high-energy, well-washed shoals that cap the mounds. Some of the mounds at Eight-Foot Rapids exhibit evidence of having been subaerially exposed, with microkarst filled with internal breccia at the tops. Many of the mounds were subsequently capped by tidal sandstones.

The biostromal, algal-rich beds are interpreted to have formed primarily through the hydrodynamic accumulation of phylloid-algal plates in response to currents and wave action in water depths of 5–10 m. The biostromal beds are characterized by a wackestone to packstone fabric with more interstitial mud and a lack of an interlocking fabric of algal plates (i.e., bafflestone) characteristic of algal mounds.

SEQUENCE-STRATIGRAPHIC MODEL

The concept of sequence stratigraphy divides sedimentary sequences into genetically related units and thus into predictable facies patterns (Posamentier and others, 1988; Sarg, 1988). For this concept, the relative change of sea level (i.e., the combination of eustasy and subsidence) is the determining control for the sedimentary stratal pattern. Although the concept is controversial in its stratigraphic application (e.g., Pitman and Golovchenko, 1991; Miall, 1994), and there may be other factors that influence the facies distribution, the sequence-stratigraphic approach of analyzing sedimentary sequences has proved to be a valuable concept that is applicable in both subsurface and outcrop.

A generalized model for facies evolution within a 4th-order, mound-bearing sequence is summarized in Figure 5. This model is based on lithofacies relationships observed both in the field and in the subsurface.

During the early highstand systems tract, mound growth that initiated during the latest transgressive system tract continued, and deposition of mound-flanking skeletal wackestones started to fill in areas between the mounds (Fig. 5–1). Mound

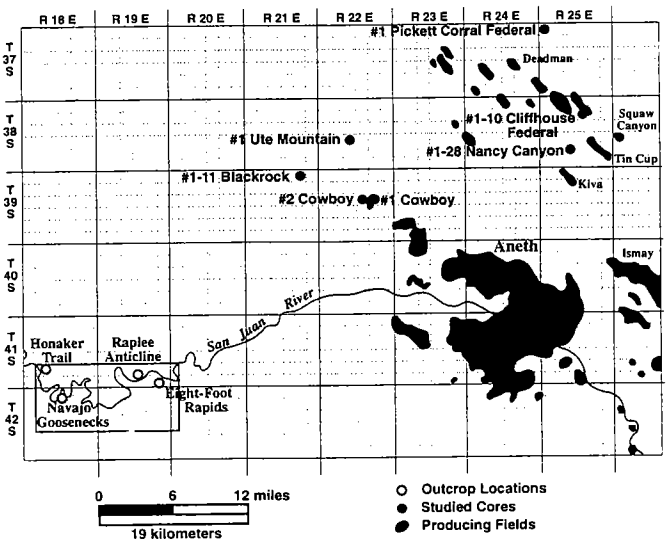

Figure 2. Map showing location of the four primary outcrops (box at lower left) on the Paradox shelf and the cored wells studied through the same interval in the basin. Total distance between outcrop sections is approximately 16 km. The studied wells range from 50 to 75 km basinward of the outcrop sections.

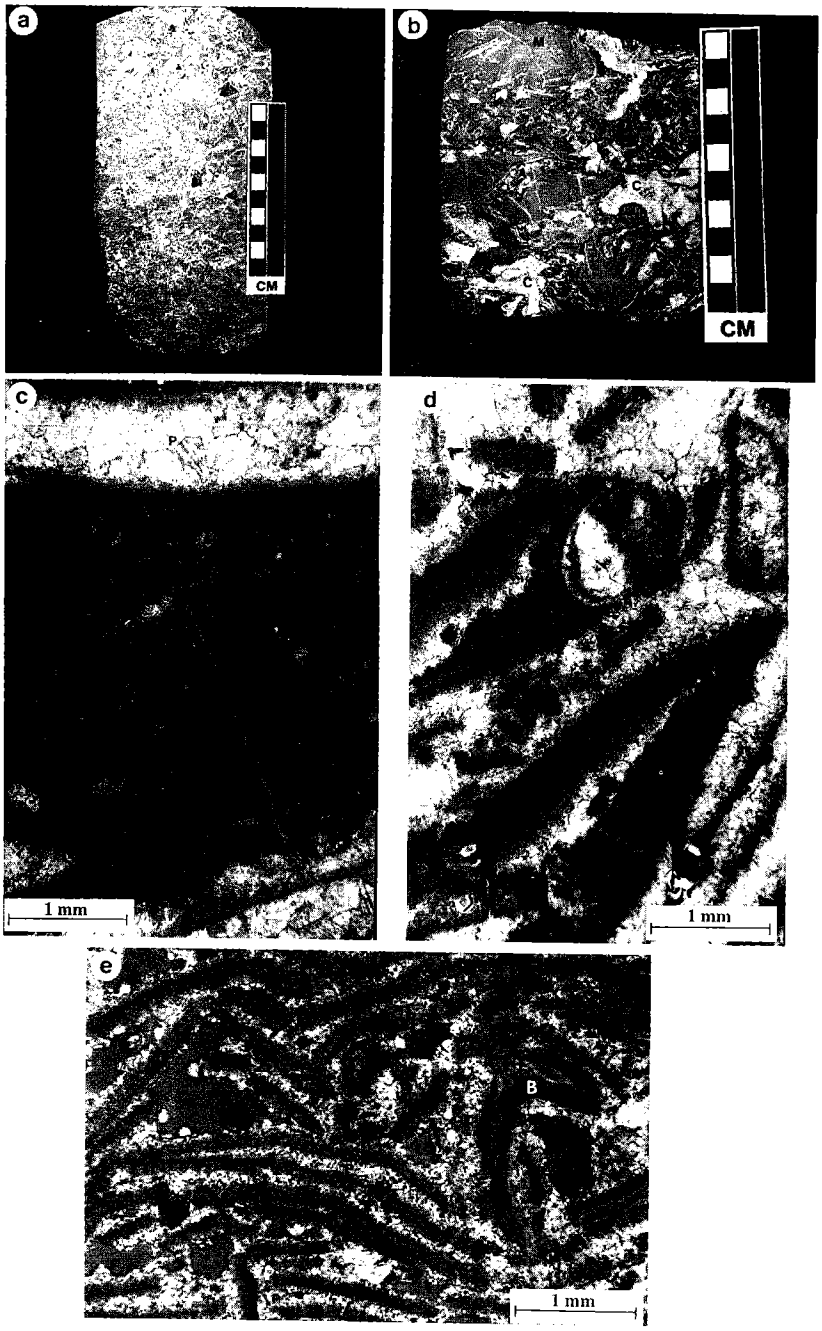

Figure 3 *(at left).* (a,b) Core slabs of phylloid-algal wackestone to packstone with minor interparticle and vuggy porosity. Most pores are partially to fully occluded by blocky calcite-spar cement (*C*). Some pores are filled with late-stage anhydrite (*A*). Lower Ismay; Mountain Fuel NW Bluff No. 1 Cowboy well. (c) Thin-section photomicrograph of phylloid-algal (*p*) mudstone typical of some of the mound flanking beds. Lower Ismay; Eight-Foot Rapids. (d) Thin-section photomicrograph of phylloid-algal bafflestone with abundant internal sediment (arrows). Fibrous marine cements along the micritized rims of the algal plates were followed with blocky calcite spar that occludes the remaining porosity. Lower Ismay; Eight-Foot Rapids. (e) Thin-section photomicrograph of phylloid-algal (*p*) bafflestone with good interparticle and moldic porosity. Note admixed brachiopod fragment (*B*). Lower Ismay; Honaker Trail.

growth and flanking-bed deposition continued during highstand. Aggradational growth of the mounds with increased accommodation space led to mounds (or stacked mounds) with up to 10–12 m of relief. Capping skeletal or ooid grainstones were deposited as water depth decreased, owing to aggradational growth of the mounds and/or fall of sea level. The nondolomitized algal-mound reservoirs typically exhibit primary shelter and secondary moldic porosity, with minor amounts of fracture-enhanced porosity (see also Weber and others, 1995a). Moldic porosity in the algal mounds, as well as within the cycle-capping ooid grainstones, developed during subsequent subaerial exposure of the platform during sea-level lowstands and dissolution of unstable carbonate by meteoric waters. In the subsurface, evaporites in some cycles are found both onlapping the mounds and capping the mounds, indicating that evaporite deposition began in shallow, restricted lagoons between mounds during latest highstand or early lowstand.

During the early phases of relative lowstand (Fig. 5–2), the proximal portions of the shelf were subaerially exposed. During this time (T-1), no sediment was deposited on the proximal portions of the shelf, and when subaerial exposure lasted long enough, dissolution took place in underlying carbonates. Evaporite precipitation continued in the restricted lagoons on the shelf and also started in the basin. During the later phases of lowstand (T-2), siliciclastics were transported out onto the shelf by eolian processes. Some of these sandstones made it all the way into the basin, where they were intercalated with the thick evaporite packages.

The transgressive systems tracts are characterized by marine reworking of eolian sandstones followed by basinwide deposition of black "shales" and spiculitic mudstones (Fig. 5–3). During the earliest phases of transgression, evaporites continued to precipitate in the basin. With initial flooding of the shelf, the eolian siltstones and sandstones were reworked in a marine environment (T-3). This was followed by deposition of black "shales" during the peak of the transgression. As reported by Goldhammer and others (1991), the Chimney Rock, Gothic, and Hovenweep "shales" are interpreted to represent the major transgressive phases of the Desert Creek and the Lower and Upper Ismay 4th-order sequences. These black "shales" are sapropelic dolomites composed of two types of organic material: (1) oxidized, transported type III kerogen; and (2) mature, marine type II kerogen (van Buchem and Houzay, in press). Total-organic-carbon values of up to 5% have been measured in outcrop, with values as high as 15% reported from the subsurface (Hite, 1970). Following deposition of the black "shales," circulation and oxygenation of marine waters

gradually increased on the platform, enabling the normal-marine carbonate factory to become established. During this period, mound growth began during the latest transgressive systems tract in the more seaward parts of the shelf and continued as the shelf underwent progressive flooding.

LATERAL VARIABILITY IN SEQUENCES AND CYCLES

Although the vertical pattern of cyclicity is relatively consistent in both outcrop and subsurface, we have observed significant lateral variability in the lithology, thickness, and geometries of facies in both 4th-order sequences and 5th-order cycles. The thickness of some of the 4th-order sequences in outcrop may vary from 20% to 40% on a kilometer scale, depending on the proximal or distal position on the shelf as a result of both depositional and structural controls (i.e., differential subsidence). The Lower Ismay sequence, for example, which is capped by a regionally extensive (and presumably long-lived) subaerial-exposure surface, thins from approximately 31 m at the more distal Eight-Foot Rapids to less than 20 m at Honaker Trail, a thickness reduction of approximately 37% over a distance of 16 km (Fig. 6).

In addition, we observed landward and seaward shifts of tens of kilometers in facies along the shelf between 4th-order depositional sequences. For example, the lower half of the Desert Creek sequence in outcrop is dominated by deposits of relatively shallow, inimical-water, low-diversity mudstones with abundant intercalated quartz silt and sand stringers. In contrast, the upper Desert Creek is characterized by normal-marine subtidal deposits shallowing to shoals. This facies succession suggests that the lower Desert Creek is more seaward stepped (relative to the Paradox basin to the northeast) than the upper Desert Creek. The overall landward stepping (i.e., transgressive) pattern from the lower to the upper Desert Creek is continued through much of the Lower Ismay. As a result, algal mounds developed progressively farther to the southwest, where they are exposed in outcrop. The system turns around abruptly (i.e., becomes more regressive) in the Upper Ismay, where approximately 70% of the section was deposited in near-tidal to tidal conditions, indicating that the system had prograded seaward tens of kilometers relative to the underlying Lower Ismay. This landward–seaward pattern of deposition observed in outcrop is responsible for large-scale facies variability throughout the basin, which is readily apparent in the shifting pattern of producing algal-mound belts for the four sequences observed in the subsurface (Grammer and others, 1996, fig. 19).

Small-scale lateral variations in the higher frequency (5th- and 6th-order) cycles are primarily facies controlled. Differential sediment accumulation and production rates between algal-mound facies, shoals, and subtidal platform carbonates probably result in significant lateral variability in thickness within a single cycle. For example, high-frequency cycles containing phylloid-algal buildups may vary in thickness by 25%–30% within tens of meters, depending on whether the algal facies accumulates as a relatively thin biostrome or whether well-developed mounds form. The aggradational growth of some mounds, owing either to more favorable environmental conditions or perhaps to initiation on a low-relief antecedent high, resulted in the near-filling of available accommodation space, whereas adjacent platform carbonates were unable to keep up with the relative sea-level rise. The resulting depositional record in both outcrop and subsurface is one of rapid lateral variability in the thickness of a single cycle.

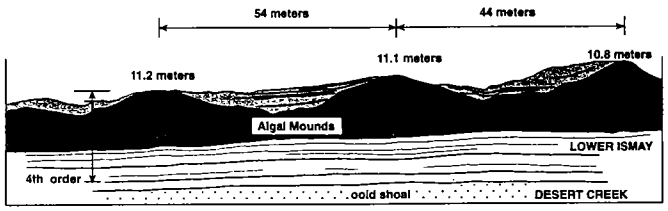

Figure 4. Line drawing of phylloid-algal mounds exposed along the San Juan River in southeastern Utah. Note abrupt lateral variability in mound thickness within a single 4th-order cycle.

DEVELOPMENT OF ALGAL MOUNDS

Although the processes and controls of algal-mound field development are still poorly understood and widely debated, there are at least five generally recognized, regionally pervasive trends in the Paradox basin. First, most of the individual fields are oriented with their long dimensions in a strike-parallel (northwest–southeast) direction; and with the exception of the giant Aneth field, a majority of the fields are 1.5–3 km wide in dip direction by 1.5–11 km long in strike direction (see Fig. 2). Second, individual mound fields typically develop on a regional thickness of underlying "shale" (Peterson and Hite, 1969; Wilson, 1975). Third, there is a regional shift in the proximal and distal distribution and limits of productive algal-mound belts in the subsurface (Grammer and others, 1996). Fourth, regional evaporites generally thin over the crests of the mound fields. Fifth, a strong component of lateral variability within mound fields is indicated from field-development histories (e.g., Petroleum Frontiers, 1984; Herrod and Gardner, 1988; Weber and others, 1995a).

These trends indicate some kind of depositional or structural control on the regional alignment of many of the mound fields as well as the landward and seaward stepping of major facies belts across the basin. In addition, the pattern of individual mound fields developing on shale thicknesses, also aligned in a strike-parallel direction, suggests a concomitant control mechanism. It is also clear that, by the end of algal-mound growth, areas of positive topographic relief were documented by the thinning of overlying evaporites, suggesting that the mounds accreted vertically.

We conclude, following many previous workers, that the major control on the regional distribution of mound fields was the change in relative sea level through time. We also propose, as have others, that the primary mechanism for relative sea-level change across the basin is most likely glacio-eustatic in origin. We suggest, however, that the general distribution of individual mound fields, as well as the observed smaller scale variability, may be a result of a combination of both structural and depositional controls (Fig. 7). Baars and

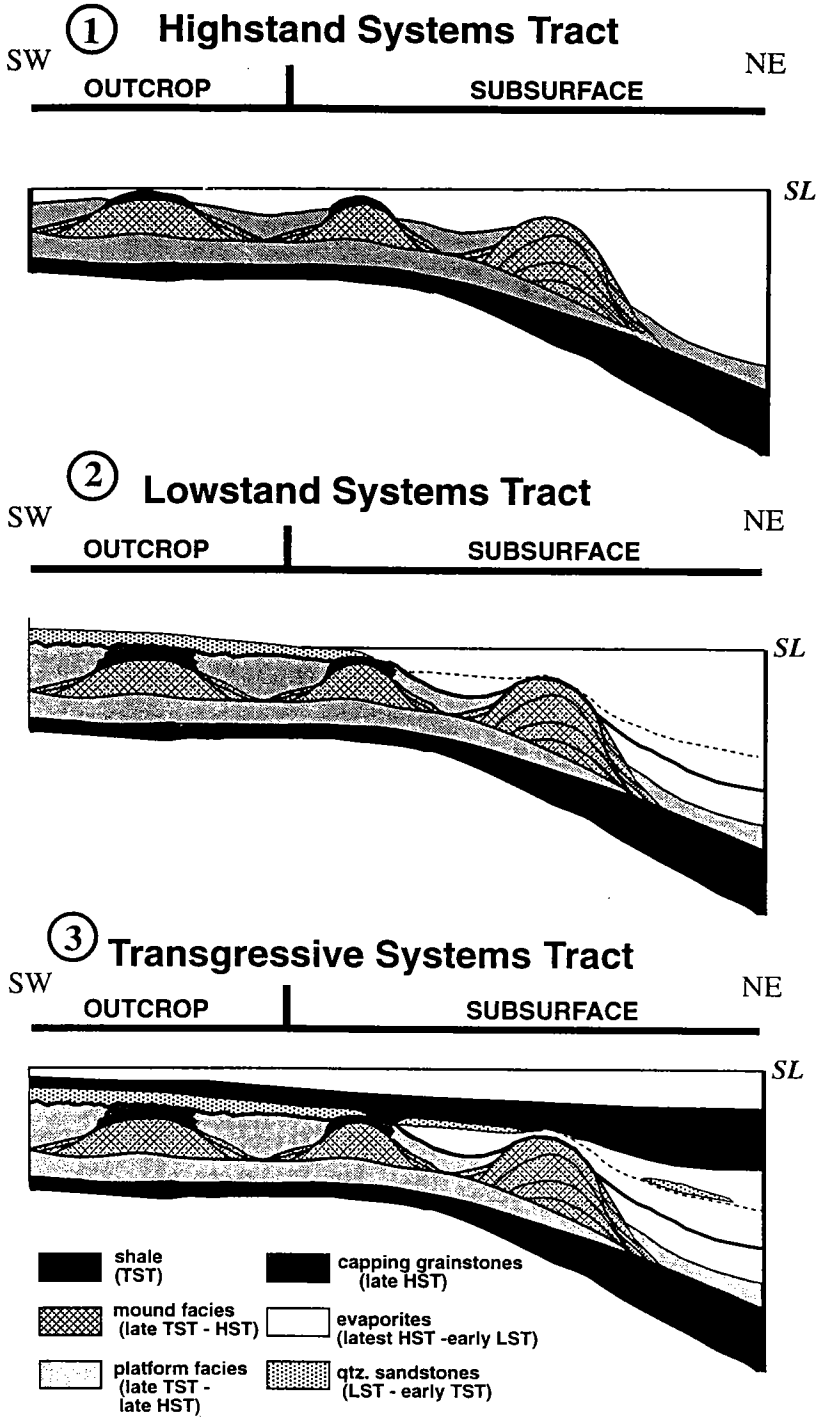

Figure 5. Schematic diagram illustrating the general model for cycle development in the studied intervals. This model is based on both outcrop and subsurface relationships and illustrates the evolution of a 4th-order, mound-bearing sequence (i.e., with laterally coalesced mounds. See text for discussion.

Stevenson (1982) and Stevenson and Baars (1986, 1988) argued persuasively for a series of deep-seated northwest–southeast-trending faults that remained active through Pennsylvanian time. The strong correlation between algal-mound-field orientation and these regional faults is strong circumstantial evidence that the two are interrelated. One possibility is that the algal-mound fields developed on a series of slightly downthrown blocks associated with these regional faults. This would explain both the regional trend of the mound fields as well as the underlying "shale" thicknesses. Differential and increased subsidence in the area of mound development would create increased accommodation space for the mounds to grow vertically and would explain the propensity for the mounds to stack in some fields. Another possibility is that the "shale" thicknesses formed in response to current and/or wave action that resulted in strike-parallel mud banks, similar to those found today off the coast of South America (e.g., Rine and Ginsburg, 1985).

Accretionary algal-mound growth would have been able to outpace the relative rise in sea level in response to the combination of tectonic and eustatic mechanisms (Schlager, 1981; Goldhammer and others, 1991). That the mounds are accretionary features, and not purely sediment dumps, is indicated by the bafflestone fabric, with little internal sediment, that is typically present in the core of well-developed mounds. The growth of mounds vertically into shallow water is indicated by the general decrease in mud toward the tops of mounds, the extensive brecciation that likely is due to wave action, and the evidence of subaerial exposure on some of the mounds. The regional thinning of overlying evaporites confirms that the mounds were positive topographic features.

The lateral variability within the mound fields is a function of the distribution of individual mounds within the field. In outcrop at least, lateral variability of the mounds is observed on two scales. Well-developed, high-amplitude algal mounds with good porosity and permeability occur in coalesced units that are typically 300–400 m in long dimension and that pinch out laterally into muddy facies (Grammer and others, 1996). The individual mounds that make up the coalesced units typically are spaced at intervals of 45–60 m. These individual mounds, in general, have the best porosity and permeability values near the core of the mound, with an increase in mud and an overall decrease in porosity and permeability toward the flanks.

One possibility for the occurrence of these coalesced units is formation on local areas of slightly higher relief, either on the regional-scale mud banks or within structurally controlled lows. Low-relief antecedent highs could then have formed through the accumulation of smaller scale mud banks in both strike- and dip-parallel orientations, also similar to that described in modern time by Rine and Ginsburg (1985). In this scenario, the distribution of individual mounds would be controlled by current and/or wave action, as suggested by the near-sinusoidal distribution of algal mounds in outcrop (Fig. 4).

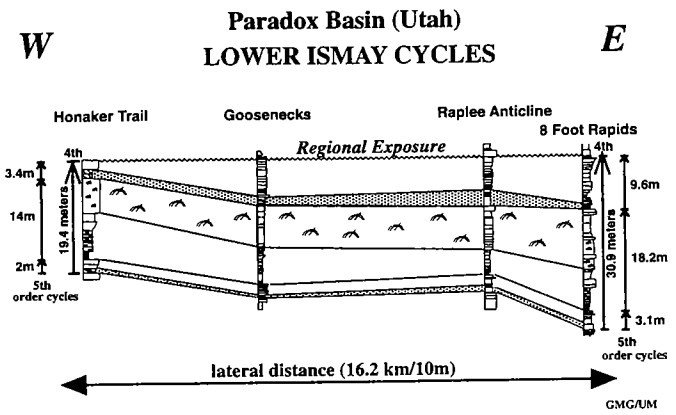

Figure 6. Regional cross section of the 4th-order Lower Ismay sequence, which is capped by a 3rd-order sequence boundary, illustrating how 4th- and 5th-order-cycle thickness may vary from 20% to 40% on a kilometer scale in response to both the proximal versus distal position on the shelf as well as the character of the higher frequency cycles that make up the 4th-order sequence. In this figure, the more distal Eight-Foot Rapids section is approximately 37% thicker than the Honaker Trail section, approximately 16 km farther shelfward. This variability is due both to the relative positions of the sections on the shelf (i.e., longer duration of sedimentation in the more distal positions) and to the internal makeup of higher frequency cycles. In outcrop, the Lower Ismay sequence consists of mound-bearing 5th-order cycles, which result in significant lateral thickness variations within single cycles. See Grammer and others (1996) for further discussion.

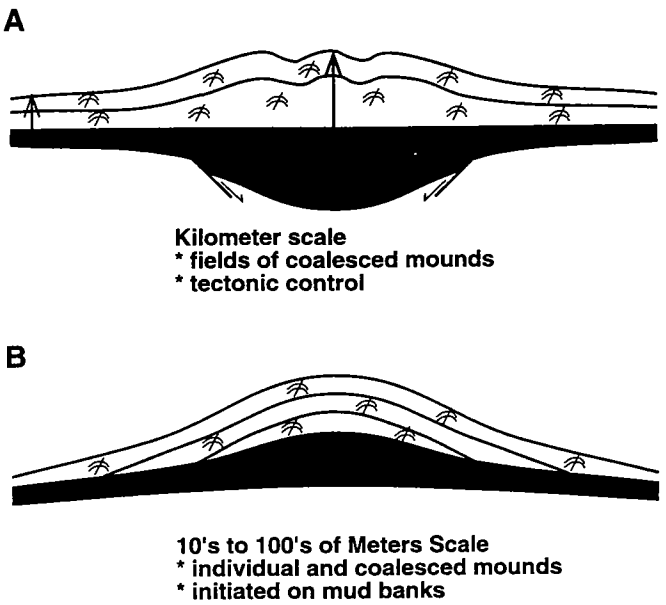

Figure 7. Diagrams illustrating possible mechanisms to explain the distribution of both kilometer-scale algal-mound fields (A) and smaller scale individual and coalesced mounds (B). Field-scale mound complexes typically grow on thick shale sequences that may be the result of differential subsidence rates, whereas smaller scale mound complexes may result from deposition on mud banks. See text for discussion.

SUMMARY AND IMPLICATIONS FOR HYDROCARBON EXPLORATION

In this study, we have confirmed that the general vertical stacking patterns originally defined by Goldhammer and others (1991) are consistent in both outcrop and subsurface, but we found that there is significant lateral variability in the thickness and distribution of facies within the high-frequency cycles. This variability occurs at both kilometer and tens-of-meters scales; it is a function of both regional-scale landward and seaward stepping of facies belts in response to 4th-order relative sea-level fluctuations as well as facies-controlled variability within the higher frequency (5th- and 6th-order) cycles. This lateral variability suggests that cyclostratigraphic correlations across the Paradox basin, or other sedimentary basins, on the basis of limited vertical data, must be applied with caution.

The high-resolution sequence-stratigraphic analysis of outcrop and subsurface sections has shown that the Pennsylvanian mixed carbonate–siliciclastic system in the Paradox basin exhibits three levels of lateral variability of significance to petroleum exploration and production. These three levels are a function of the lateral variability observed in the 4th- and 5th-order cycles. The predictability of the three levels of lateral variability (rank-wildcat, exploration, and production scale) of phylloid-algal reservoir facies is, therefore, greatly enhanced through the detailed understanding of cycle stacking patterns and the regional sequence stratigraphy.

General exploration trends at the rank-wildcat level (tens of kilometers) are indicated by the landward- and seaward-stepping patterns of the 4th-order Desert Creek, Lower Ismay, and Upper Ismay sequences. For example, the proved general trends of upper Desert Creek and Lower Ismay production in more proximal positions on the Paradox shelf relative to the Upper Ismay would have been predicted by the lithofacies characteristics of each sequence, which show the Upper Ismay interval seaward-stepped by tens of kilometers relative to the upper Desert Creek and Lower Ismay intervals (Grammer and others, 1996). The realization that 4th-order relative sea-level changes may result in this basinal-scale landward or seaward shifting of facies belts can help direct and refine exploration efforts.

Exploration-scale prediction (0.8–16 km) is enhanced by the knowledge that most of the individual fields are oriented with their long dimensions in a strike-parallel (northwest–southeast) direction. With the exception of the giant Aneth field, a majority of the fields are 1.5–3 km wide in dip direction by 1.5–11 km in strike direction. Lateral variability in phylloid-algal mounds at this scale is clearly shown in outcrop where well-developed mounds 9–14 m thick gradually thin to muddier algal bioherms that are less than 4.5 m thick over a distance of 3 km or less.

At the production scale (<0.8 km), lateral variability is again observed on two scales. In outcrop, well-developed high-amplitude mounds with good porosity and permeability occur in coalesced units that are 300–400 m in long dimension, suggesting a well spacing of approximately 40 acres to access individual mound complexes (Grammer and others, 1996). This scale of variability is also observed within ooid shoal facies, which are secondary reservoir targets within the basin. Compartmentalized algal-mound reservoirs at this scale have been shown to occur within Aneth field, where original 160–

80-acre-spaced wells were infilled to 40 acres for waterflooding; yet, reservoirs with virgin pressures were encountered.

Detailed outcrop work also indicates, however, that individual flow units within both the mound complexes and the ooid shoals may vary within 45–60 m. High-porosity and -permeability algal bafflestones at the core of individual mounds may thin laterally by 30%–70% within 40–50 m (Grammer and others, 1996). The thinner, laterally equivalent facies are typically muddier, with lower porosity and permeability values. Likewise, the ooid-shoal facies occur in a series of overlapping sand waves (good-porosity grainstones), with muddier wackestones (lower energy facies between high-energy shoals) often found between. Anticipating this abrupt lateral variability in both algal-mound reservoirs and associated facies in 5th-order depositional cycles should help to maximize initial development as well as enhanced-recovery operations.

ACKNOWLEDGMENTS

This report is a condensation of an earlier paper by Grammer and others (1996). The Paradox basin project at the University of Miami was part of an applied-research project funded by the French COPREP Consortium (Elf Aquitaine, Institut Français du Pétrole, Total, and Gaz de France). We gratefully acknowledge the field and laboratory support, and the scientific input of numerous individuals from both the supporting companies and the University of Miami. This report is a contribution of the University of Miami's Comparative Sedimentology Laboratory.

REFERENCES CITED

Baars, D. L.; and Stevenson, G. M., 1981, Tectonic evolution of the Paradox Basin, *in* Wiegand, D. L. (ed.), Geology of the Paradox Basin: Rocky Mountain Association of Geologists, 1981 Field Conference, p. 23–31.

_____1982, Subtle stratigraphic traps in Paleozoic rocks of Paradox Basin, *in* Halbouty, M. T. (ed.), The deliberate search for the subtle trap: American Association of Petroleum Geologists Memoir 32, p. 131–158.

Choquette, P. W.; and Traut, J. D., 1963, Pennsylvanian carbonate reservoirs, Ismay field, Utah and Colorado, *in* Bass, R. O. (ed.), Shelf carbonates of the Paradox basin: Four Corners Geological Society, 4th Field Conference Guidebook, p. 157–184.

Connolly, W. M.; Lambert, L. L.; and Stanton, R. J., 1989, Paleoecology of Lower and Middle Pennsylvanian (Middle Carboniferous) *Chaetetes* in North America: Facies, v. 20, p. 139–168.

Crowell, J. C., 1978, Gondwana glaciation, cyclothems, continental positioning, and climate change: American Journal of Science, v. 278, p. 1345–1372.

Driese, S. G.; and Dott, R. H., Jr., 1984, Model for sandstone–carbonate "cyclothems" based on upper member of Morgan Formation (Middle Pennsylvanian) of northern Utah and Colorado: American Association of Petroleum Geologists Bulletin, v. 68, p. 574–597.

Goldhammer, R. K.; Oswald, E. J.; and Dunn, P. A., 1991, Hierarchy of stratigraphic forcing: Example from Middle Pennsylvanian shelf carbonates of the Paradox basin, *in* Franseen, E. K.; Watney, W. L.; Kendall, C. G. St. C.; and Ross, W. (eds.), Sedimentary modeling: Kansas Geological Survey Bulletin 233, p. 361–413.

Grammer, G. M.; Ginsburg, R. N.; Swart, P. K.; McNeill, D. F.; Jull, A. J. T.; and Prezbindowski, D. R., 1993, Rapid growth rate of syndepositional marine aragonite cements in steep marginal slope deposits, Bahamas and Belize: Journal of Sedimentary Petrology, v. 63, p. 983–989.

Grammer, G. M.; Eberli, G. P.; van Buchem, F. S. P.; Stevenson, G. M.; and Homewood, P., 1996, Application of high-resolution sequence stratigraphy to evaluate lateral variability in outcrop and subsurface—Desert Creek and Ismay intervals, Paradox Basin, *in* Longman, M. W.; and Sonnenfeld, M. D. (eds.), Paleozoic systems of the Rocky Mountain region: Rocky Mountain Section, SEPM (Society for Sedimentary Geology), p. 235–266.

Heckel, P. H., 1980, Paleogeography of eustatic model for deposition of Midcontinent Upper Pennsylvanian cyclothems, *in* Fouch, T. D.; and Magathan, E. R. (eds.), Paleozoic paleogeography of the west-central United States: Rocky Mountain Section, Society of Economic Paleontologists and Mineralogists, Symposium 1, p. 197–215.

_____1986, Sea-level curve for Pennsylvanian eustatic marine transgressive–regressive depositional cycles along mid-continent outcrop belt, North America: Geology, v. 14, p. 330–334.

Herrod, W. H.; and Gardner, P. S., 1988, Upper Ismay reservoir at Tin Cup Mesa field, *in* Goolsby, S. M.; and Longman, M. W. (eds.), Carbonate symposium: Rocky Mountain Association of Geologists, p. 175–192.

Hine, A. C.; Hallock, P.; Harris, M. W.; Mullins, H. T.; Belknap, D. F.; and Jaap, W. C., 1988, *Halimeda* bioherms along an open seaway: Bawihka Channel, Nicaraguan Rise, SW Caribbean Sea: Coral Reefs, v. 6, p. 173–178.

Hite, R. J., 1970, Shelf carbonate sedimentation controlled by salinity in the Paradox basin, southeast Utah, *in* Ron, J. L.; and Dellwig, L. F. (eds.), Third symposium on salt: Northern Ohio Geological Society, v. 1, p. 48–66.

Hite, R. J.; and Buckner, D. H., 1981, Stratigraphic correlation, facies concepts, and cyclicity in Pennsylvanian rocks of the Paradox basin, *in* Wiegand, D. L. (ed.), Geology of the Paradox Basin: Rocky Mountain Association of Geologists, 1981 Field Conference, p. 147–159.

Miall, A. D., 1994, Sequence stratigraphy and chronostratigraphy: Problems of definition and precision in correlation, and their implications for global eustasy: Geoscience Canada, v. 21, p. 1–27.

Peterson, J. A.; and Hite, R. J., 1969, Pennsylvanian evaporite–carbonate cycles and their relation to petroleum occurrence, southern Rocky Mountains: American Association of Petroleum Geologists Bulletin, v. 53, p. 884–908.

Petroleum Frontiers, 1984, Paradox Basin: Unraveling the mystery: IHS Energy Group, Denver, 54 p.

Pitman, W. C.; and Golovchenko, Xenia, 1991, Modelling sedimentary sequences, *in* Muller, D. W.; McKenzie, J. A.; and Weissert, H. (eds.), Controversies in modern geology: Academic Press, New York, p. 279–309.

Posamentier, H. W.; Jervey, M. T.; and Vail, P. R., 1988, Eustatic controls on clastic deposition I—conceptual framework, *in* Wilgus, C. K.; Posamentier, H.; Ross, C. A.; and Kendall, C. G. St. C. (eds.), Sea level changes: An integrated approach: Society of Economic Paleontologists and Mineralogists Special Publication 42, p. 109–124.

Pray, L. C.; and Wray, J. L., 1963, Porous algal facies (Pennsylvanian), Honaker Trail, San Juan Canyon, Utah, *in* Bass, R. O. (ed.), Shelf carbonates of the Paradox basin: Four Corners Geological Society, 4th Field Conference Guidebook, p. 204–234.

Rine, J. M.; and Ginsburg, R. N., 1985, Depositional facies of a mud shoreface in Suriname, South America—A mud analogue to sandy, shallow-marine deposits: Journal of Sedimentary Petrology, v. 55, p. 633–652.

Roylance, M. H., 1990, Depositional and diagenetic history of a Pennsylvanian algal-mound complex: Bug and Papoose Canyon fields, Paradox Basin, Utah and Colorado: American Association of

Petroleum Geologists Bulletin, v. 74, p. 1087–1099.

Sarg, J. F., 1988, Carbonate sequence stratigraphy, *in* Wilgus, C. K.; Posamentier, H.; Ross, C. A.; and Kendall, C. G. St. C. (eds.), Sea level changes: An integrated approach: Society of Economic Paleontologists and Mineralogists Special Publication 42, p. 155–181.

Schlager, Wolfgang, 1981, The paradox of drowned reefs and carbonate platforms: Geological Society of America Bulletin, v. 92, p. 197–211.

Stevenson, G. M.; and Baars, D. L., 1986, The Paradox: A pull-apart basin of Pennsylvanian age, *in* Peterson, J. A. (ed.), Paleotectonics and sedimentation in the Rocky Mountain region: American Association of Petroleum Geologists Memoir 41, p. 513–539.

_____1988, Overview: Carbonate reservoirs of the Paradox Basin, *in* Goolsby, S. M.; and Longman, M. W. (eds.), Carbonate symposium: Rocky Mountain Association of Geologists, p. 149–162.

Toomey, D. F.; Wilson, J. L.; and Rezak, R., 1977, Evolution of Yucca mound complex, Late Pennsylvanian phylloid algal buildup, Sacramento Mountains, New Mexico: American Association of Petroleum Geologists Bulletin, v. 61, p. 2115–2133.

van Buchem, F. S. P.; and Houzay, J.-P., in press, Stratigraphic context of organic geochemical characteristics of the black laminated shales in the Desert Creek and Ismay intervals, *in* Homewood, P.; and Eberli, G. P. (eds.), Genetic stratigraphy on the exploration and production scales: Case studies from the Upper Devonian of Alberta and the Pennsylvanian of the Paradox Basin: Elf Aquitaine Memoir.

Wanless, H. R., 1972, Eustatic shifts in sea level during the deposition of late Paleozoic sediments in the central United States, *in* Elam, J. G.; and Chuber, S. (eds.), Cyclic sedimentation in the Permian basin [2nd edition]: West Texas Geological Society Publication 72-60, Midland, p. 41–54.

Wanless, H. R.; and Shepard, F. P., 1936, Sea level and climatic changes related to late Paleozoic cycles: Geological Society of America Bulletin, v. 47, p. 1177–1206.

Weber, L. J.; Sarg, J. F.; Wright, F. M.; and Huffman, A. C., 1994, High resolution sequence stratigraphy: Reservoir description and geologic setting of the giant Aneth oil field, SE Utah—a field guide to exposures along the San Juan River canyon: American Association of Petroleum Geologists/Rocky Mountain Association of Geologists Field-Trip Guidebook, 179 p.

Weber, L. J.; Wright, F. M.; Sarg, J. F.; Shaw, E.; Harman, L. P.; Vanderhill, J. B.; and Best, D. A., 1995a, Reservoir delineation and performance: Application of sequence stratigraphy and integration of petrophysics and engineering data, Aneth field, southeast Utah, U.S.A., *in* Stoudt, E. L.; and Harris, P. M. (eds.), Hydrocarbon reservoir characterization: Geologic framework and flow unit modeling: Society for Sedimentary Geology (SEPM), Short Course 34, p. 1–30.

Weber, L. J.; Sarg, J. F.; and Wright, F. M., 1995b, Sequence stratigraphy and reservoir delineation of the Middle Pennsylvanian (Desmoinesian), Paradox basin and Aneth field, *in* Read, J. F.; Kerans, C.; and Weber, L. J. (organizers), Milankovitch sea-level changes, cycles, and reservoirs on carbonate platforms in greenhouse and ice-house worlds: Society for Sedimentary Geology (SEPM), Short Course 35, p. 1–81.

Wilson, J. L., 1975, Carbonate facies in geologic history: Springer-Verlag, New York, 471 p.

Wray, J. L., 1968, Late Paleozoic phylloid algal limestones in the United States: 23rd International Geological Congress Proceedings, Prague, v. 8, p. 113–119.

Lithofacies Distribution and Reservoir Heterogeneity within Pennsylvanian Bioherms, Western Orogrande Basin, New Mexico

Katherine A. Giles
New Mexico State University
Las Cruces, New Mexico

Gerilyn S. Soreghan
University of Oklahoma
Norman, Oklahoma

ABSTRACT.—Pennsylvanian strata within the San Andres Mountains (western Orogrande basin) contain very well-developed phylloid-algal bioherms, but these bioherms remain unstudied owing to their location within the bounds of the U.S. Army White Sands Missile Range. The exposed Upper Pennsylvanian section within Hembrillo Canyon affords a three-dimensional view of mound structure, and therefore an excellent opportunity for characterizing lithofacies distribution and reservoir heterogeneity that may prove useful for exploration/exploitation efforts in analogous petroliferous mound systems.

The mounds are vertically stacked within a mixed carbonate–siliciclastic shallow-marine sequence punctuated by upward-shallowing cycles. Each mound site comprises a stack of individual biohermal growth events characterized by a subtidal initiation phase, a core boundstone phase, and a peritidal to subaerially exposed packstone–grainstone phase. Individual biohermal-growth events range up to 30 m in thickness; vertical stacking of these bioherms has produced aggregate mounds reaching up to 120 m in stratigraphic thickness and 200–300 m in diameter. Individual biohermal thickness decreases abruptly and markedly away from mound sites, and silty, calcareous mudstone dominates intermound regions.

Potential reservoir facies within this system are highly compartmentalized. However, unlike standard algal-mound reservoir models wherein core facies exhibit the highest porosity–permeability, the western Orogrande mound core facies are tight. High-porosity and -permeability zones are associated with dolomitized flank facies adjacent to sequence boundaries. Recognition of the scale, character, and probable controls on these lateral and vertical changes is important for effective exploration and exploitation in phylloid-algal-mound systems.

INTRODUCTION

This paper presents preliminary depositional and diagenetic facies descriptions and interpretations of an Upper Pennsylvanian phylloid-algal-mound complex within the San Andres Mountains, New Mexico (Figs. 1,2). The mound complex trends roughly northeast–southwest, and it formed along the western shelf margin of the late Paleozoic Orogrande basin. Fusulinid dating constrains the age of the algal mounds as middle to late Virgilian and coeval with phylloid-algal mounds exposed in the Sacramento Mountains that formed on the eastern margin of the Orogrande basin.

FACIES DESCRIPTIONS AND INTERPRETATIONS

Two stratigraphic sections were measured and described for this study that correspond to the proximal-flank and distal-flank portions of the mound complex (Fig. 3). These two stratigraphic sections were correlated to a third previously measured section in Hembrillo Canyon (Soreghan, 1992) that traverses the Upper Pennsylvanian section in a backmound (shoreward) position.

Figure 4 summarizes facies descriptions and interpretations based on macroscopic and petrographic analysis of over 50 samples. Depositional facies include shallow subtidal–peritidal carbonates and subtidal clastics; many peritidal carbonate facies have undergone pedogenesis.

Facies Cyclicity

The depositional facies are arranged vertically into a series of upward-shallowing carbonate cycles punctuated by siliciclastic-rich facies. Cycles are thicker in the proximal-flank section (10 to 30 m) than in the distal-flank section (2 to 5 m) and contain a distinctly different vertical facies progression (Fig. 5). The proximal-flank vertical succession initiates with open-marine, subtidal skeletal wackestone grading upward into massive beds of phylloid-algal bafflestone and is capped by high-energy intertidal packstone to grainstone facies that commonly display evidence of subaerial exposure. The distal-flank vertical succession initiates with high-energy intertidal grain-rich peloidal facies, abruptly overlain by peritidal algal laminite that grades into thick zones of pedogenically altered, intraclastic packstone that contains evaporite pseudomorphs.

Giles, K. A.; and Soreghan, G. S., 2000, Lithofacies distribution and reservoir heterogeneity within Pennsylvanian bioherms, western Orogrande basin, New Mexico, *in* Johnson, K. S. (ed.), Platform carbonates in the southern Midcontinent, 1996 symposium: Oklahoma Geological Survey Circular 101, p. 269–274.

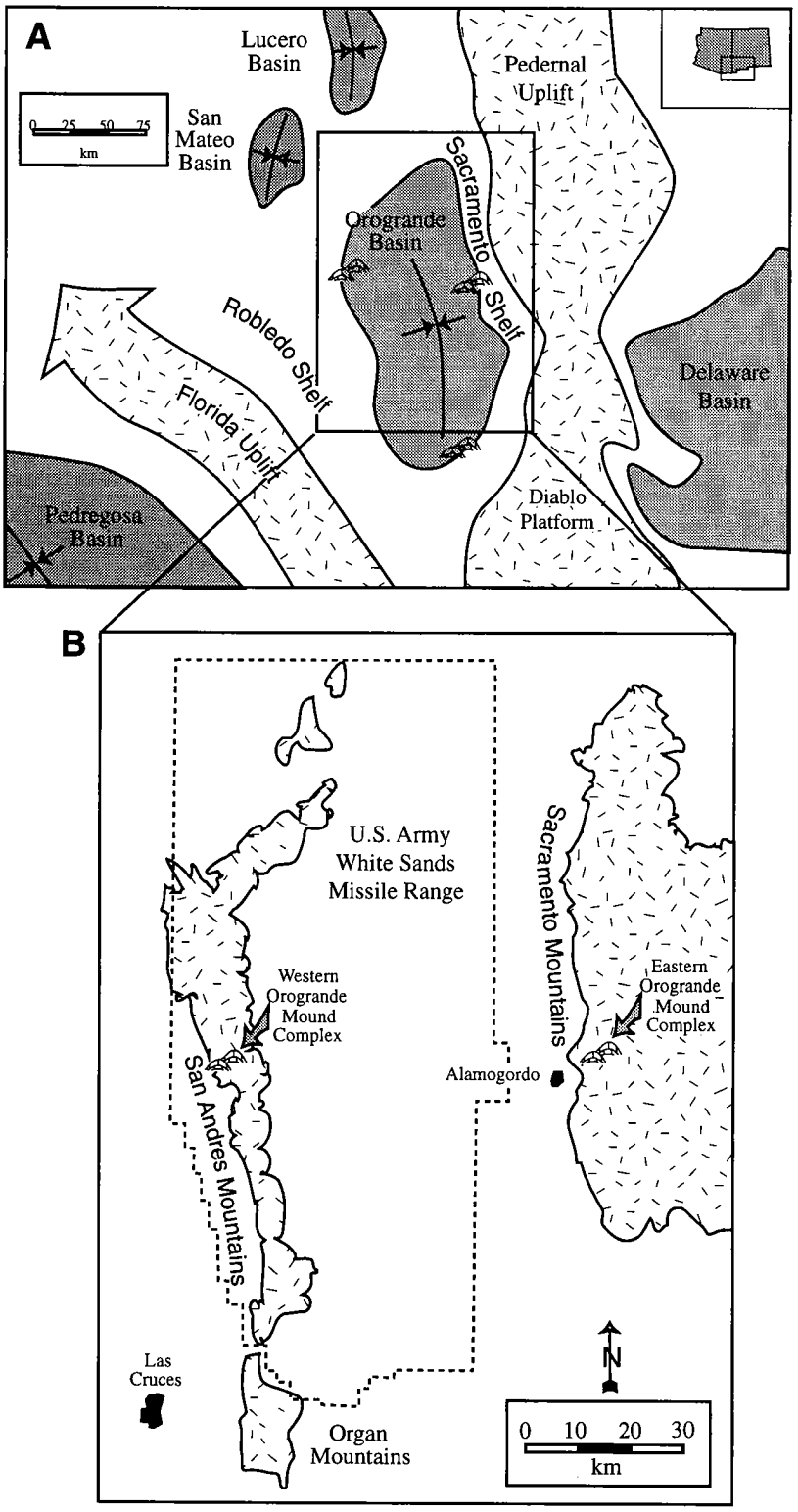

Figure 1. Paleogeographic (A) and location (B) maps for the Orogrande basin region. Locations of Upper Pennsylvanian phylloid-algal-mound complexes are shown schematically. Modified from Algeo and others (1991).

The proximal-flank and distal-flank facies were not deposited simultaneously but were generated at different points on a sea-level-transit cycle. The dominantly subtidal facies of the proximal flank were deposited during the transgressive to highstand portion of the sea-level-transit cycle. As regression ensued, the topographically high algal mounds became subaerially exposed. Deposition then initiated at the distal-flank position under shallow-subtidal to intertidal conditions. At the most regressive point of the sea-level-transit cycle, the entire shelf was subaerially exposed. Soils formed in the topographically low areas (distal flanks). The following sea-level-transit cycle initiated with restricted flooding of topographically low areas. Local brine pools formed on the leeward side of the topographically high algal mounds, which induced a shadow effect and resulted in precipitation of dolomitic mudstone.

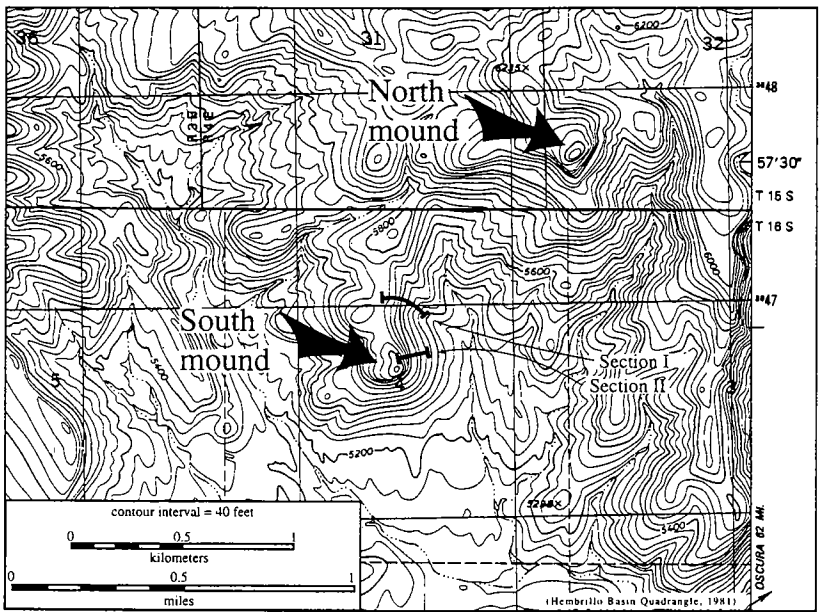

Figure 2. Topographic map of study area in Hembrillo Canyon, San Andres Mountains, showing locations of measured sections.

POROSITY TRENDS

Porosity was characterized in accord with the classification scheme of Choquette and Pray (1970) and was visually estimated for all thin sections (Fig. 4). Backscatter-imaging estimates of porosity were performed on representative samples of each facies and are listed in Figure 4. Porosity is dominantly intercrystalline and is associated with secondary dolomitization. Unlike standard algal-mound reservoir models wherein core facies (containing leached phylloid-algal blades) exhibit the highest porosity–permeability, the western Orogrande mound core facies are tightly cemented. The highest porosity facies in these mounds comprise flanking dolomitic mudstone and dolomitized intraclastic packstone. These two facies are vertically adjacent and are associated with sequence boundaries.

Our preliminary model of dolomitization entails precipitation of the dolomitic-mudstone facies by early transgressive lagoonal brines generated directly shoreward of the emergent phylloid-algal mounds. Subsequently, these brines seeped into the underlying porous and permeable soil facies, inducing dolomitization.

CONCLUSIONS

1. Phylloid-algal mounds of the western Orogrande basin exhibit pronounced lateral and vertical heterogeneity of porosity–permeability, controlling depositional and diagenetic facies on a production (10–100-m) scale.

2. Unlike "standard" algal-mound-reservoir models wherein algal (mound core) facies exhibit the highest porosity–permeability trends owing to leaching of algal plates (e.g., Schatzinger, 1983), high-porosity zones in this system are associated with dolomitization largely within peritidal facies.

3. Dolomite abundance decreases downward from paleosubaerial-exposure surfaces, suggesting a genetic link between porosity–permeability-creating dolomitization and cycle-boundary development.

ACKNOWLEDGMENTS

G. Morgan of The University of Oklahoma performed SEM (backscatter electron imaging) analyses on selected samples. We thank the U.S. Army for permission to access White Sands Missile Range and R. G. Myers for on-base assistance.

REFERENCES CITED

Algeo, T. J.; Wilson, J. L.; and Lohmann, K. C., 1991, Eustatic and tectonic controls on cyclic sediment accumulation patterns in Lower–Middle Pennsylvanian strata of the Orogrande basin, New Mexico: New Mexico Geological Society, 42nd Field Conference Guidebook, p. 203–212.

Choquette, P. W.; and Pray, L. C., 1970, Geologic nomenclature and classification of porosity in sedimentary carbonates: American Association of Petroleum Geologists Bulletin, v. 54, p. 207–250.

Schatzinger, R. A., 1983, Phylloid algal and sponge-bryozoan mound-to-basin transition: a late Paleozoic facies tract from the Kelly–Snyder field, West Texas, *in* Harris, P. M. (ed.), Carbonate build-ups—a core workshop: Society of Economic Paleontologists and Mineralogists Core Workshop 4, p. 244–303.

Soreghan, G. S., 1992, Sedimentology and process stratigraphy of the Upper Pennsylvanian, Pedregosa (Arizona) and Orogrande (New Mexico) basins: University of Arizona, Tucson, unpublished Ph.D. dissertation, 278 p.

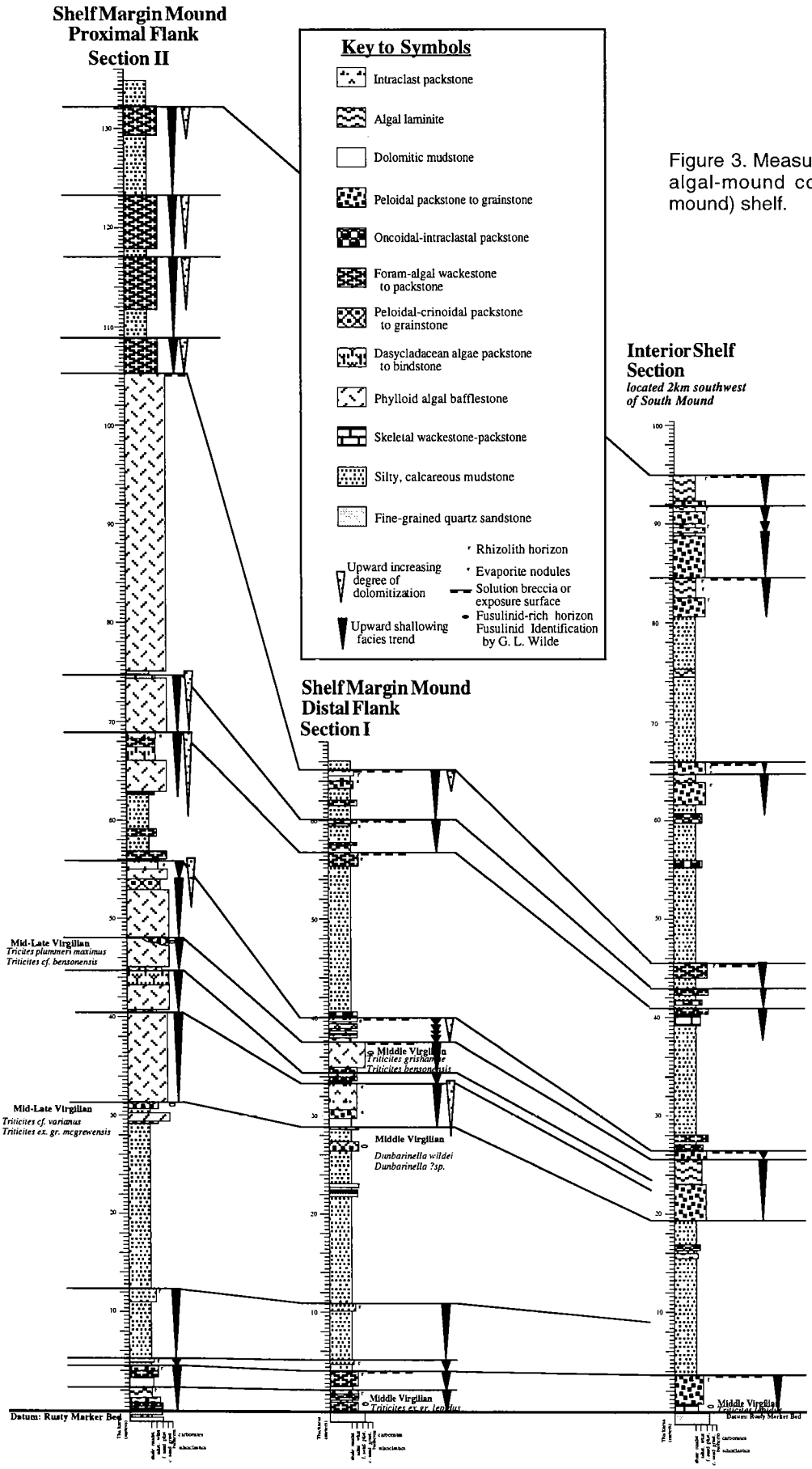

Figure 3. Measured sections of the southern algal-mound complex and interior (back-mound) shelf.

Lithofacies	Symbol	Bedding Characteristics & Sedimentary Structures	Grain Types: primary / secondary	Depositional Setting	Common Diagenetic Fabrics	Average Porosity Percentage and Types
Intraclast packstone		Thick to massive Pedoturbation Fitted intraclast fabric	Micrite intraclasts Leached dasyclad algae	Supratidal soil	Pervasive dolomitization Poikalotopic low Mg calcite cement	**20%** Intercrystalline Intergranular Vuggy
Algal laminite		Thin Algal laminae Fenestral fabric Mudcracks Rhizolith tubules	Algal mat Peloids Intraclasts,calcispheres, ostracods quartz silt	High intertidal to supratidal	Dolomitized laminae Coarse, blocky calcite cement in fenestrae Microstylolites	**1.5%** Intercrystalline
Peloidal packstone -grainstone		Thin to thick Bioturbation Local current lamination	Peloids Intraclasts Forams, quartz silt, algal coated grains	Wave winnowed intertidal to shallow subtidal	Dolomitized peloids Coarse. blocky calcite cement	**4%** Intercrystalline
Dolomitic mudstone		Thin to thick Homogeneous	Local ghost peloidal fabric Ostracods, quartz silt	Lower intertidal to shallow subtidal, restricted, low energy lagoon	Dolomitization pervasive	**8%** Intercrystalline
Oncoidal -intraclastal wackestone to packstone		Med to thick Current lamination Clast imbrication	Micrite intraclasts Oncoids Abraded skel. Peloids, calcispheres ostracods, forams, gastropods, echinoids	Tempestites in intertidal to shallow subtidal	Local matrix dolomitization Leached skel. Microstylolites Hematite replacement	**<1%** Intercrystalline
Foram-algal packstone -bindstone		Thick to massive Highly burrowed	Forams Algal coating & clots Peloids Ostracods, intraclasts calcispheres, worm tubes, marine skeletal debris	Shallow subtidal	Local matrix dolomitization Overcompacted Microstylolites Rare syntaxial overgrowths	**<1%** Intercrystalline
Peloidal-crinoidal packstone -grainstone		Thick Burrowed	Echinoderm Peloids	Shallow subtidal	Local matrix dolomitization Rim cements Coarse, blocky calcite spar Microstylolites	**3%** Intercrystalline
Dasycladacean packstone /bindstone		Thick to massive Burrowed	Encrusting algae Dasycladacean algae Peloids, red algae, ostracods, quartz silt marine skel., algal coats	Shallow subtidal	Local matrix dolomitization Coarse, blocky calcite spar Recrystal. of Dasyclads	**<1%** Intercrystalline Isolated vugs as high as 20%
Phylloid algal bafflestone		Thick to massive Burrowed	Phylloid algae Dasycladacean algae Brachiopods, forams Bryozoans, calcisphere	Subtidal	Local matrix dolomitization Coarse, blocky calcite spar Leached algal grains	**<1.5%** Intercrystalline Isolated vuggy
Skeletal wackestone -packstone		Thin to thick wavy Burrowed	Brachiopods, bryozoan, phylloid algae, intraclasts Gastropods, echinoderms, forams, dasyclads, trilobites, skeletal debris	Subtidal Sub-fair weather wave base	Local coarse, blocky calcite spar Overcompaction Microstylolites	**<<1%** Intragranular
Silty, carbonate mudstone		Thin Laminated Local rhizolith tubules	Angular quartz silt	Variable lower shoreface to coastal plain	Local matrix dolomitization	**1.3%** Intercrystalline
Fine-grained quartz sandstone		Medium to thick Tangential cross sets Planar bedded Ripple cross laminae	Fine-grained, subrounded to angular, mod. sorted quartz Muscovite, feldspar Chert & limestone frags. Fossil fragments	Upper shoreface to foreshore		

Figure 4. Lithofacies characteristics, depositional setting, diagenesis, and porosity of the phylloid-algal mounds studied. Based on macroscopic and petrographic analysis of over 50 samples.

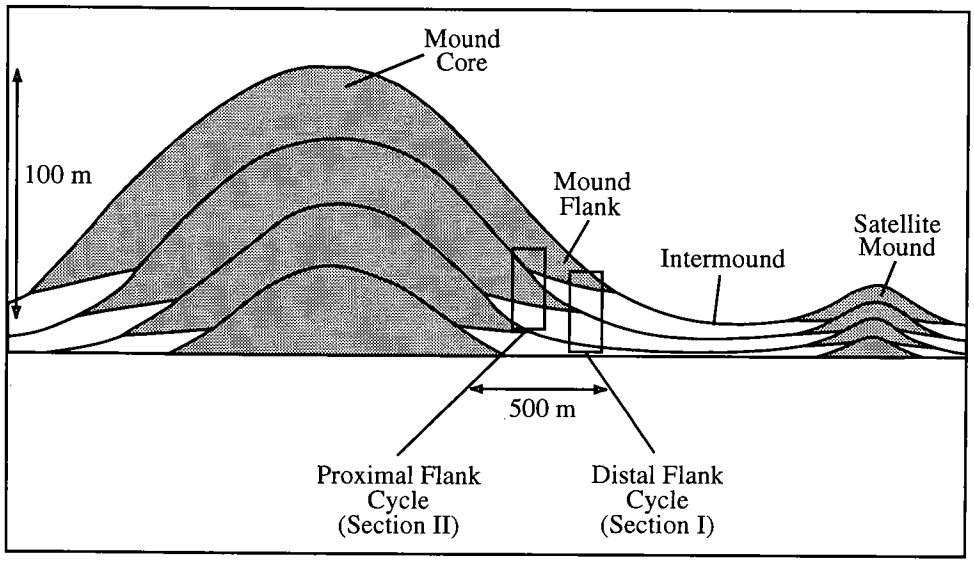

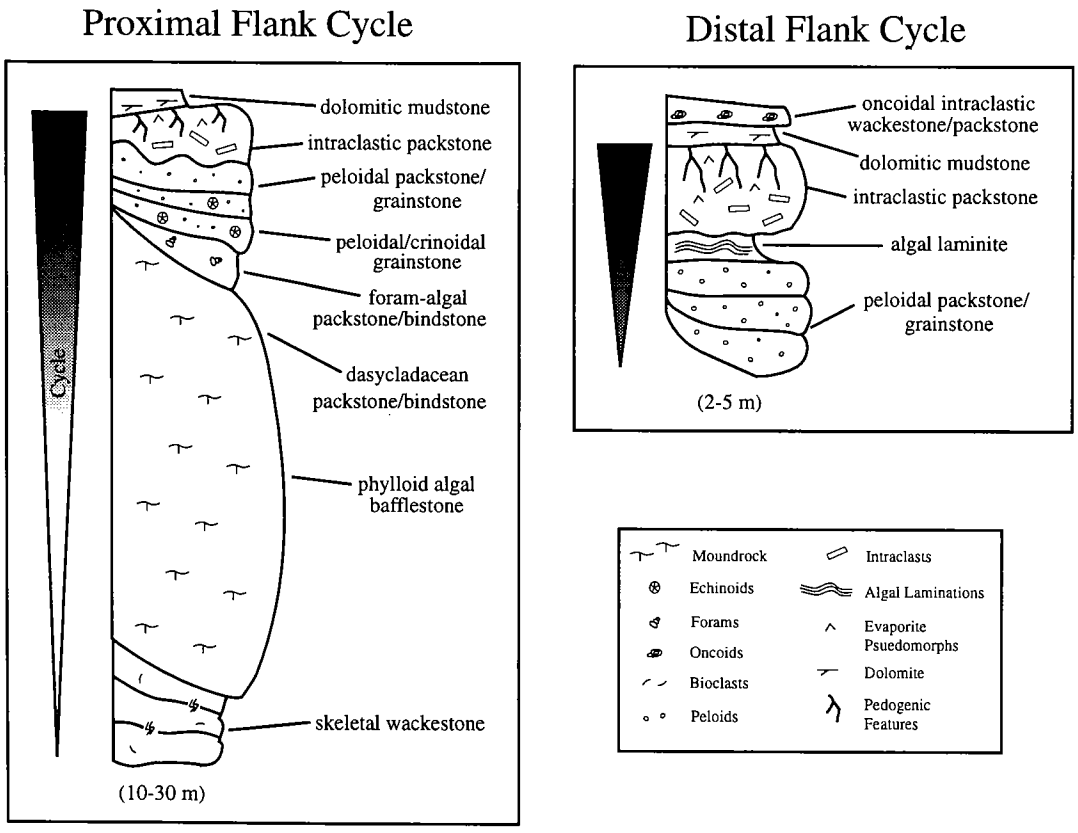

Figure 5. Generalized upward-shallowing vertical facies progression observed within a single cycle of the proximal-flank (section II) and distal-flank (section I) regions. Dolomitization preferentially affects the upper parts of cycles.

Outcrop-Based Sequence Stratigraphy of the Council Grove Group of the Midcontinent

D. R. Boardman II
Oklahoma State University
Stillwater, Oklahoma

Merlynd K. Nestell
University of Texas at Arlington
Arlington, Texas

ABSTRACT.—Sequence-stratigraphic analysis of outcropping uppermost Carboniferous and Lower Permian Council Grove Group strata of the North American Midcontinent strongly suggests a distinctive hierarchy of stratigraphic forcing. The Council Grove Group represents one composite third-order depositional sequence (1–10 m.y.) and is divisible into nine fourth-order depositional sequences (0.1–1 m.y.). Each fourth-order depositional sequence contains between two and eight high-frequency fifth-order depositional cycles (0.01–0.1 m.y.) that form the parasequences that stack into the retrogradational transgressive systems tract and the aggradational to progradational highstand/forced regressive systems tracts. In total, 38 widely correlatable fifth-order depositional sequences are present in the Council Grove Group. On the basis of this study, we suggest that this type of analysis should lead to a basinwide three-dimensional sequence-stratigraphic analysis that should aid in the search for facies-related stratigraphic traps.

INTRODUCTION

A number of carbonates constitute the lower Wolfcampian Council Grove unit and serve as significant gas reservoirs in the Hugoton embayment and northern Oklahoma platform. This paper focuses on the sequence-stratigraphic framework of the Council Grove Group, based on detailed outcrop analysis (Figs. 1,2). This outcrop analysis will serve as the focal point for further study, integrating surface, subsurface, and seismic data.

REGIONAL GEOLOGY AND GENERAL STRATIGRAPHIC OVERVIEW

Outcropping uppermost Carboniferous and lowermost Permian (Council Grove) cyclothemic strata of this study lie on a broad northern shelf region of the Anadarko basin (Fig. 3). Outcrops in Nebraska through central Kansas straddle the Nemaha ridge along with the westernmost Forest City basin and the easternmost terminus of the Salina basin. Outcrops in southern Kansas and northern Oklahoma are on the eastern edge of the Sedgwick basin along with the Cherokee platform. Because of the inferred paleogeographic position of the land–sea interface, a north–south transect from Kansas through northern Oklahoma represents a dip section that demonstrates the successive pinchouts of marine into nonmarine red-bed deposits (Figs. 4,5).

A number of paleotopographic features, including structurally positive and negative features as well as faults, are present in the broad shelf area from Oklahoma to Nebraska. These features exerted considerable effect on the thickness and lithologic nature of each of the depositional sequences. Additionally, changes in the rates of subsidence of the Anadarko basin had a dramatic effect on the nature of the depositional sequences from Pennsylvanian to Permian time. The maximum areal extent of the starved basinal facies of the Anadarko basin occurred during Missourian time (Rascoe, 1962). This time period also corresponds to maximum subsidence rates of the basin. A gradual trend of reduced subsidence rates and concomitant restriction of the Anadarko basin through sediment infilling occurred from Virgilian through Wolfcampian time (Figs. 6–11). Admire and Council Grove basinal facies were restricted to six counties in the Panhandle areas of Texas and Oklahoma, whereas no basinal facies are present in the Chase Group (Fig. 11).

Major changes in climate from the Virgilian to the Wolfcampian have been suggested on the basis of changing lithofacies and mineralogy, including an increase in dolomite and celestite along with the evaporitic minerals gypsum, anhydrite, and halite. A number of late highstand peritidal carbonates of the Council Grove Group contain abundant celestite and dolomite as well as anhydrite molds. Additionally, gypsum and halite occur in some of the siliciclastic intervals. This increase in evaporitic minerals probably represents a major climatic change from a wetter to a generally drier climate (Miller and West, 1993). This change probably represents movement of the present-day Midcontinent region into drier latitudes during Early Permian time (Scotese, 1986).

Council Grove strata are characterized by a complex shelf-

Boardman, D. R., II; and Nestell, M. K., 2000, Outcrop-based sequence stratigraphy of the Council Grove Group of the Midcontinent, *in* Johnson, K. S. (ed.), Platform carbonates in the southern Midcontinent, 1996 symposium: Oklahoma Geological Survey Circular 101, p. 275–306.

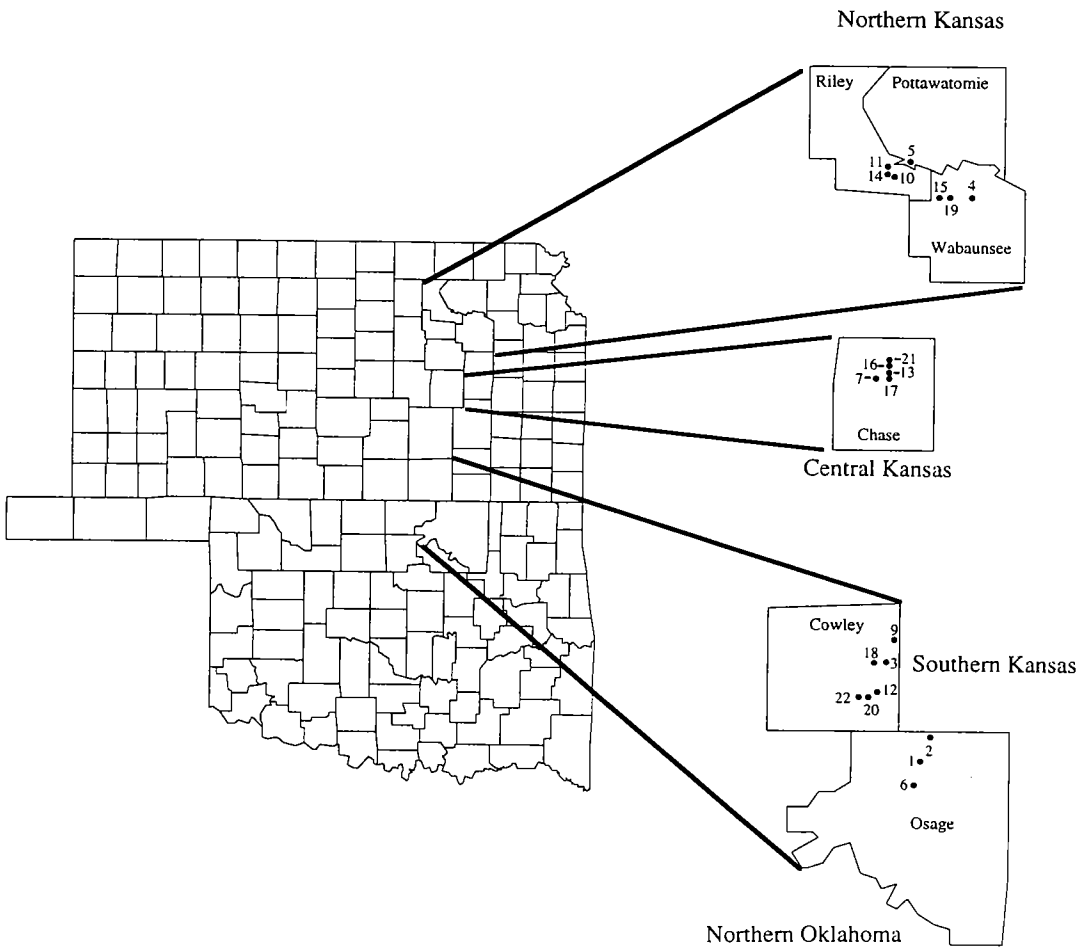

Figure 1. Map of Kansas and Oklahoma showing localities used in this study.

wide mixed siliciclastic–carbonate system that records a hierarchy of stratigraphic forcing similar to that described by Goldhammer and others (1991) for the carbonate-dominated Desmoinesian cyclothemic strata of the Paradox basin. Cyclothemic-scale depositional sequences in the Council Grove Group generally exhibit a two-component (hemicycle) system, one being carbonate dominated and the other siliciclastic dominated. The carbonate-dominated parts of the depositional sequence generally are thick (5–25 m) and generally represent more dominantly marine conditions. The thick carbonates are overlain by relatively thick (5–15 m) red and green caliche-bearing blocky, silty mudstones and siltstones that commonly contain well-defined pedogenic features (Miller and West, 1993). These red and green deposits are generally thought to have formed during late stages of sea-level fall, lowstand, and perhaps earliest transgression. A close examination of both the dominantly marine carbonate hemicycle as well as the dominantly nonmarine siliciclastic hemicycle reveals a much more complicated scenario for their origin.

Within the carbonate hemicycle, fossiliferous wackestones and packstones are dominant along with foraminiferal grainstones that cap the hemicycle. Additionally, three basic types of siliciclastic lithofacies are present within the carbonate hemicycle including (1) gray to black, fissile to blocky, commonly silty, poorly fossiliferous shales and mudstones (BSFI); (2) gray to black, fissile to blocky, commonly silty, highly fossiliferous shales and mudstones with abundant *Streptognathodus* conodonts, *Ammodiscus* foraminifers, orbiculoid brachiopods, abundant fish debris, and ammonoids (BSFII); and (3) light-gray, green, or tan, blocky to fissile, poorly fossiliferous silty mudstones and shales (MMFI).

Black shale facies I (BSFI) occurs directly above maximum-marine-flooding levels in a number of Council Grove depositional sequences including, in ascending order: above the lower Americus Limestone, in the basal Legion Shale above the Sallyards Limestone, above the lower Burr Limestone, above a limestone in the Salem Point Shale, above an unnamed limestone in the middle Stearns Shale, above the lower Middleburg Limestone, above the lower Crouse Limestone, and above the lower Funston Limestone. These shales contain a limited ostracode fauna and encrusting-foraminifer assemblage with no conodonts of any biofacies, and also locally contain evaporite minerals. Additionally, they grade laterally into poorly fossiliferous silty carbonates with shallow-water indicators such as *Ottonosia* algal colonies as well as a local abundance of low-diversity bivalves including pectinid clams. We view this facies as representing a marginal-marine lagoonal environment caused by extremely rapid sea-level fall after maximum marine flooding. This sea-level fall caused low-oxygen and perhaps high-salinity lagoonal conditions to form locally on the proximal or high shelf.

Black shale facies II (BSFII) occurs, in ascending order: in

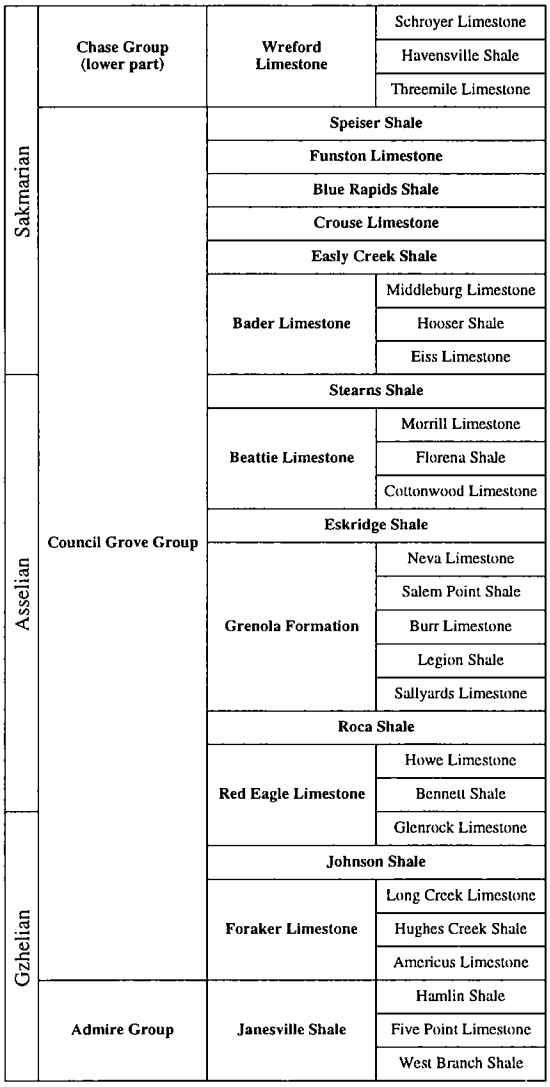

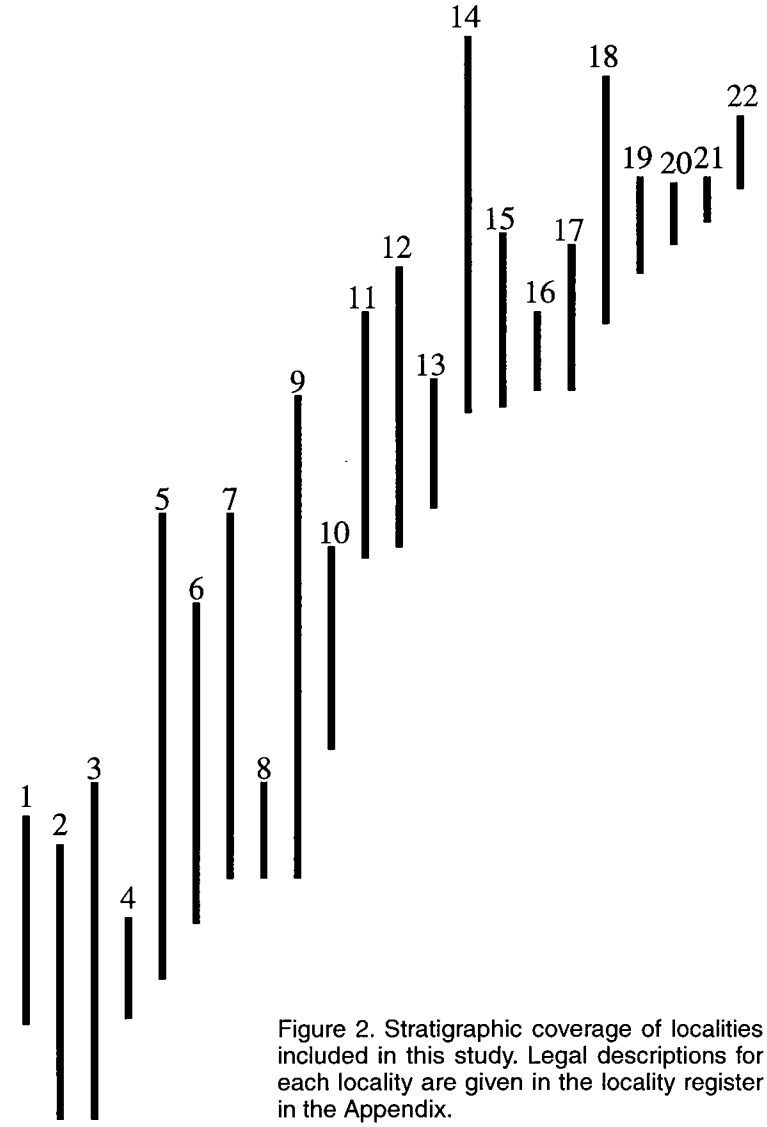

Figure 2. Stratigraphic coverage of localities included in this study. Legal descriptions for each locality are given in the locality register in the Appendix.

the upper Americus Limestone, the middle Hughes Creek Shale, the upper Hughes Creek Shale, the Bennett Shale, and in a shale parting within the lower Neva Limestone. These black shales are best developed in northern Kansas and Nebraska but also have been documented in the Hugoton embayment (Puckette and others, 1995). This facies contains the offshore *Streptognathodus* conodont biofacies, the offshore *Ammodiscus* foraminifer biofacies, ammonoids, and orbiculoid brachiopods. Additionally, this facies shows evidence of condensed sedimentation (100–1,000 platform conodonts/kg). Laterally, in southern Kansas and northern Oklahoma, this facies changes into highly fossiliferous, shaly glauconitic wackestone with the same conodont biofacies plus evidence of condensed sedimentation along with phosphatized molluscs. We interpret the BSFII facies, along with the equivalent shaly glauconitic carbonate facies, to represent maximum marine flooding of condensed sections. These facies are restricted to the lower Council Grove Group. The lower Council Grove marine condensed sections differ from those of the Desmoinesian–middle Virgilian strata in lacking nonskeletal radiolarian-bearing phosphate nodules. The phosphate nodules likely formed in response to a regional thermocline augmented by upwelling of nutrient-rich waters from the starved intracratonic basin across the broad shelf during or near maximum transgression (Schenk, 1967; Heckel, 1977). Progressive restriction of the Anadarko basin from infilling and concomitant reduced subsidence during the Late Carboniferous through the Early Permian served to shut off upwelling, cool nutrient waters onto the shelf. In strata of the upper Council Grove Group, maximum transgression is represented by highly fossiliferous, shaly glauconitic carbonates with moderately abundant conodonts but with noticeably less condensation than in strata of the lower Council Grove Group.

Marginal-marine facies I (MMFI) occurs in numerous carbonate-dominated hemicycles within the Council Grove Group. This lithofacies commonly overlies the BSFI lithofacies or may directly overlie and separate carbonates within the hemicycle. This lithofacies is poorly fossiliferous, usually containing a low-diversity ostracode and foraminifer assemblage, and grades laterally into poorly fossiliferous shallow- to restricted-marine carbonates. This facies is interpreted to represent a marginal-marine condition created by rapid forced

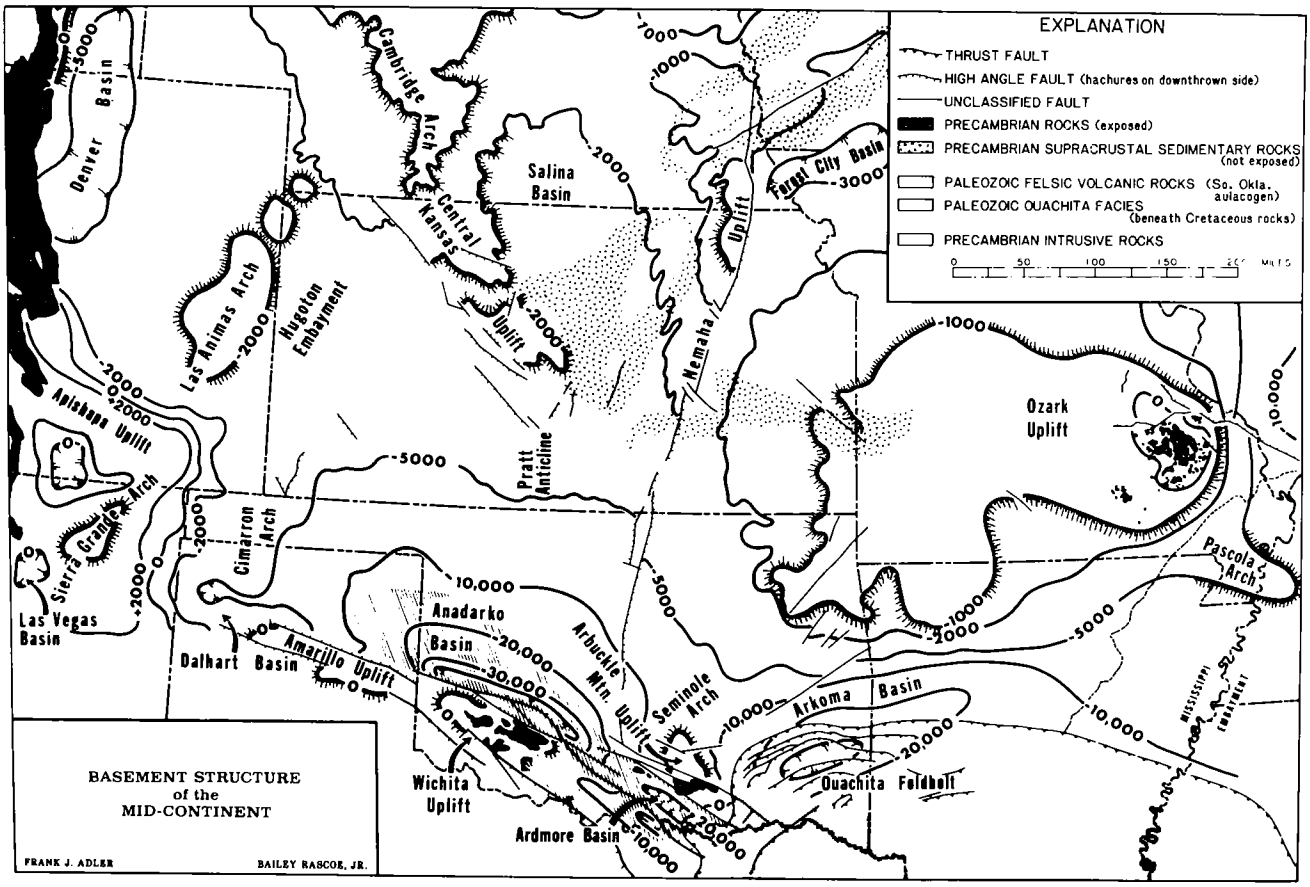

Figure 3. Map showing basement structure of the Midcontinent (modified from Adler and others, 1971).

regression that resulted in an increase in siliciclastic sedimentation on the shelf. This facies commonly separates high-frequency fifth-order cycles within the overall thicker carbonate hemicycle.

The thick (5–15-m) red and green mudstone intervals are also highly complex. Within these intervals, extensive evidence of pedogenesis is present, including columnar peds, blocky peds, pseudo-anticlines, root traces, desiccation cracks, carbonate nodules, and rhizocretions (Miller and West, 1993; Miller, 1994). These thick siliciclastic intervals are commonly punctuated by thin (<1-m) carbonates and mudstones that indicate marine-influenced deposition. The thin marine or marginal-marine deposits commonly contain a low-diversity foraminifer and ostracode microfaunal assemblage along with a low-diversity molluscan-dominated or rarely brachiopod macrofossil assemblage. Commonly, the 5–15-m siliciclastic intervals contain up to two of these minor marine bands. Each of the bands is separated by red to green, blocky to crumbly mudstones that demonstrate clear evidence of pedogenic features. During subaerial exposure, many of the underlying siliciclastic inner-shelf deposits were oxidized and subjected to pedogenesis, resulting in the development of numerous paleosol indicators within the formerly inner-shelf sediments. Siliciclastics that make up the paleosol parts of these intervals are thought to have been eolian in origin in central Kansas through Nebraska (Joeckel, 1989), whereas, in southernmost Kansas and Oklahoma, fluvial siliciclastics clearly are also present. In stark contrast to Virgilian depositional sequences that indicate well-developed incised-valley fills (Archer and Feldman, 1995), such valley fills are rare to absent in the Council Grove outcrop belt from northernmost Oklahoma to Nebraska.

IDENTIFICATION OF DEPTH TRENDS WITHIN DEPOSITIONAL SEQUENCES

Depth-trend analysis used in this research is based on textural trends of carbonates and siliciclastic facies combined with detailed paleoecologic analysis, using both macro-invertebrates as well as microfossils. Paleoecologic analysis used in this report for delineating paleodepth trends within the depositional sequence, as well as for identifying flooding surfaces and maximum-marine-flooding condensed sections, is based on the models presented by Elias (1937) and Boardman and others (1984) for macro-invertebrates and by Boardman and others (1995) for microfossil taxa. Distinctive microfaunal biofacies are present in Upper Carboniferous and Lower Permian strata of the North American Midcontinent (Fig. 12). Marginal-marine deposits are characterized by a very low-diversity microfaunal assemblage consisting of *Geisina* ostracodes, *Thurammina* foraminifers, and no conodonts. These deposits usually occur as green, gray to black, clayey to silty mudstones. Nearshore, shallow, normal-marine deposits contain a low-diversity microfaunal assemblage consisting of the *Cavellina* ostracode biofacies, encrusting foraminifers with agglutinated foraminifers including *Ammodiscus* cf.

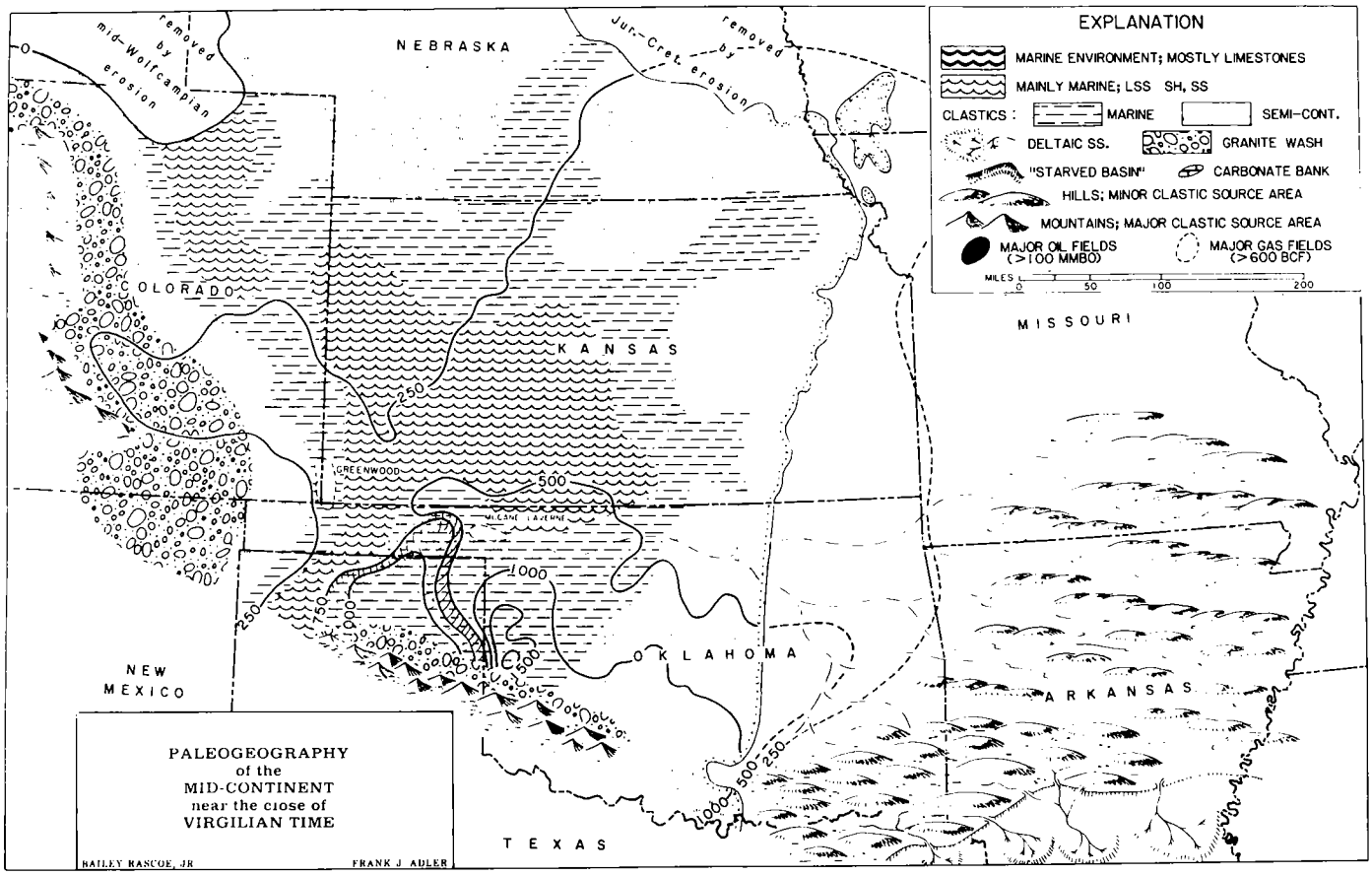

Figure 4. Map showing lithofacies and paleogeography of the late Virgilian in the Midcontinent (modified from Rascoe and Adler, 1983).

A. semiconstrictus var. *regularis*, and the *Adetognathus–Sweetognathus* conodont biofacies. The moderate-depth, open-shelf microfaunal assemblage consists of a high-diversity *Amphissites* ostracode biofacies; a high-diversity benthic-foraminifer biofacies including *Tetrataxis, Globivalvulina, Climacammina, Deckerella, Endothyra, Endothyranella, Ammobaculites,* and fusulinaceans; and the *Streptognathodus* conodont biofacies. Deep-shelf marine deposits contain a reduced-diversity benthic assemblage including inarticulate brachiopods (e.g., *Orbiculoidea*) and the *Ammodiscus* foraminifer biofacies, along with a pelagic component consisting of rare ammonoids, fish debris, and the *Streptognathodus* conodont biofacies. This deep-shelf assemblage is well represented in maximum-marine-flooding condensed sections of the BSFII facies but is restricted to the lower Council Grove Group.

SEQUENCE-STRATIGRAPHIC NOMENCLATURE, IDENTIFICATION OF FOURTH-ORDER SEQUENCE BOUNDARIES, AND DELINEATION OF SYSTEMS TRACTS

Late Carboniferous and Early Permian fourth-order depositional sequences demonstrate a plexus of superimposed orders of cyclicity (frequency) as well as amplitudes. Similar hierarchies with superposed cycles were described in Pennsylvanian carbonate strata of the Paradox basin (Goldhammer and others, 1990), Triassic carbonate strata of northern Italy (Goldhammer and others, 1987), and Cenozoic siliciclastic strata of the Gulf Coast of Mexico (Mitchum and Van Wagoner, 1991). Documentation of various orders of cyclicity within the Midcontinent cyclothemic succession was illustrated by Busch and West (1987), Miller and others (1992), Miller and West (1993), Boardman and Nestell (1993), and Youle and others (1994).

The fundamental unit for sequence-stratigraphic analysis of Upper Carboniferous and Lower Permian strata of the Midcontinent region is the cyclothemic-scale depositional sequence that has been referred to as a fifth-order depositional sequence by some authors (e.g., Watney and others, 1989) or as a fourth-order depositional sequence by others (e.g., Goldhammer and others, 1990; Youle and others, 1994).

Little agreement exists on the hierarchical ordinal scheme of depositional sequences. Posamentier, Allen, and James (1992, p. 311) argue that "sequence stratigraphic principles are scale and time independent." Furthermore, Mitchum and Van Wagoner (1991, p. 134) define a *sequence* as "a genetically related succession of strata with no apparent internal unconformities, composed of parasequences and parasequence sets arranged in systems tracts, and bounded by unconformities or their relative conformities. A stratal package conforming to this definition is properly called a sequence, no matter what its frequency." They further state that "a stratal package

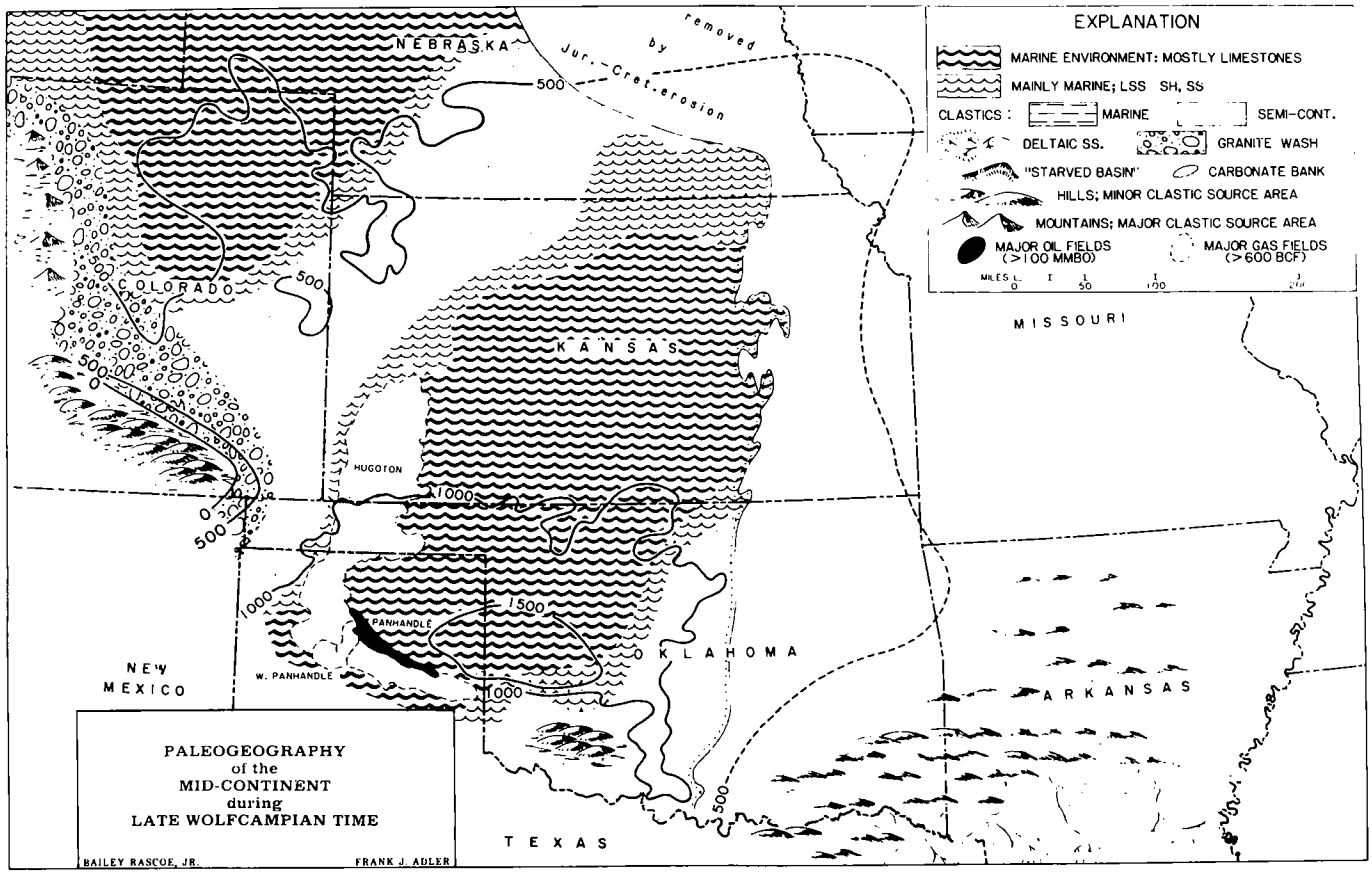

Figure 5. Map showing lithofacies and paleogeography of the late Wolfcampian in the Midcontinent (modified from Rascoe and Adler, 1983).

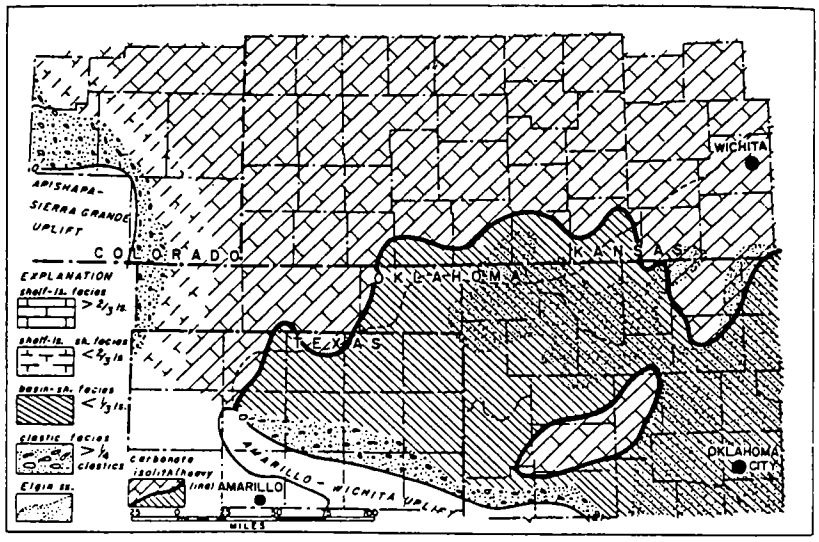

Figure 6. Lithofacies map of the Shawnee Group (modified from Rascoe, 1962).

bounded by unconformities but internally composed of high-frequency sequences, cannot itself be properly called a sequence." They proposed the term *composite sequence* for a succession of genetically related sequences that stack into lowstand, transgressive, and highstand sequence sets.

In contrast to the objective definition of *depositional sequence* advocated by Mitchum and Van Wagoner (1991) and Posamentier, Allen, and James (1992), Vail and others (1991) argue that a depositional sequence is formed only during a third-order cycle that ranges from 0.5 to 3 m.y. in duration. This narrow definition precludes application of the term *depositional sequences* for unconformity-bounded stratal packages that form within the Milankovitch-band periodicities (20,000, 40,000, 100,000, and 400,000 years). However, in strata that were deposited during major glacial episodes such as in the Pliocene–Pleistocene (Carter and others, 1991), Miocene (Moore and others, 1982), and Carboniferous–Permian (Heckel, 1986; Boardman and Heckel, 1989; Boardman and Nestell, 1993; Youle and others, 1994), third-order cyclicity is secondary and is derived from analysis of the stacking patterns of cyclothemic-scale (fourth-order) depositional sequences. The amplitudes of Pliocene–Pleistocene sequences (Carter and others, 1991), as well as Late Carboniferous–Early Permian sequences (Heckel, 1986; Boardman and Heckel, 1989; Boardman and Nestell, 1993; Boardman and others, 1995), are of similar magnitude to third-order Mesozoic and early Cenozoic tectono-eustatic events

(Mitchum and Van Wagoner, 1991). Moreover, it is apparent that the order of cyclicity (frequency) may have little bearing on the amplitude of sea-level change during times of major glaciation. High-amplitude Late Carboniferous sea-level changes are apparently related to the 400,000 orbital eccentricity cycle (Heckel, 1986), whereas late Pleistocene high-amplitude sea-level changes are controlled by 100,000-year orbital eccentricity cycles (Denton and Hughes, 1983). Therefore, the figure demonstrating a reduction in amplitude of sea-level change with increasing order of eustatic cycle presented by Mitchum and Van Wagoner (1991, fig. 7, p. 140) is misleading and possibly incorrect for times of Earth history in which there were major glacial episodes. Because the accommodation space created by glacio-eustatic rises in sea level can be identical to that created by tectono-eustasy, it seems untenable to demand that only third-order sea-level changes produce true depositional sequences. Therefore, we view depositional sequences as being scale and time independent, following Posamentier, Allen, and James (1992). For purposes of this report, we follow the hierarchical sequence-stratigraphic nomenclature proposed by Goldhammer and others (1990) and Youle and others (1994).

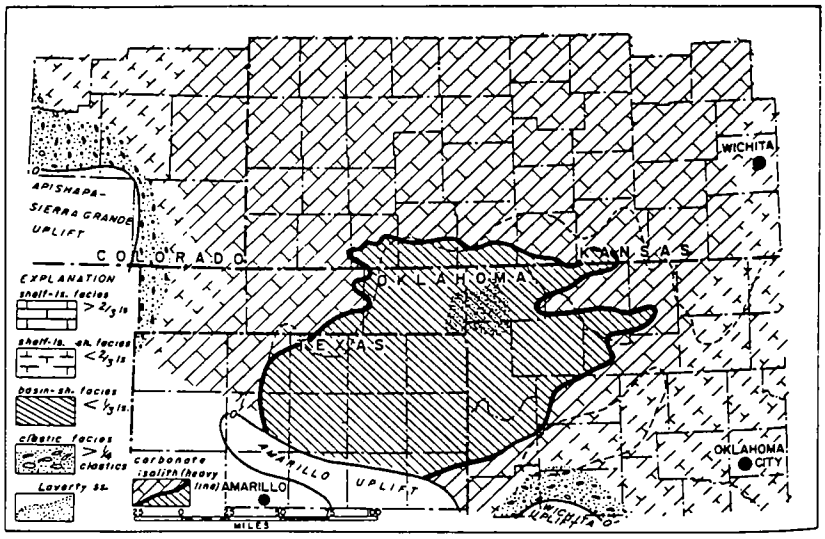

Figure 7. Lithofacies map of the Sac Fox Subgroup of the Wabaunsee Group (modified from Rascoe, 1962).

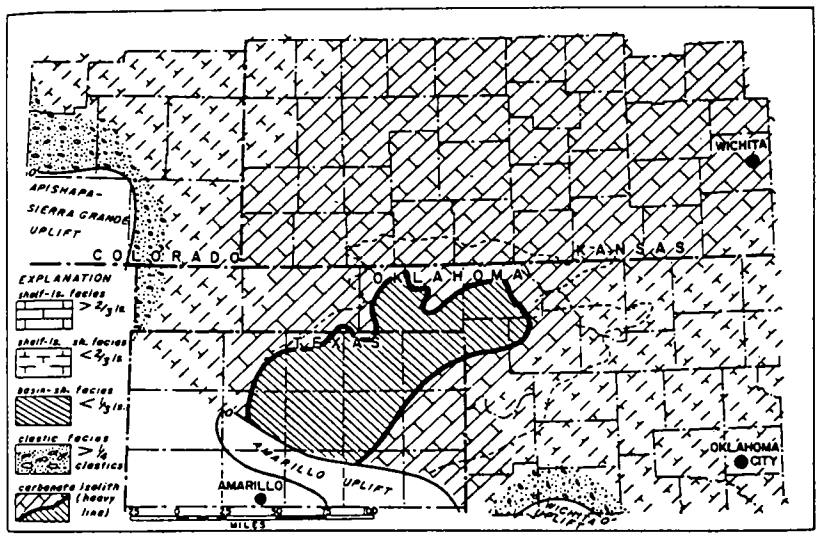

Figure 8. Lithofacies map of the Nemaha Subgroup of the Wabaunsee Group (modified from Rascoe, 1962).

On the basis of observed stacking patterns, fourth-order sequences can be objectively grouped into composite third-order depositional sequences, following Mitchum and Van Wagoner (1991). A similar methodology was utilized by Youle and others (1994), who proposed composite third-order sequences for Middle Pennsylvanian strata of the Anadarko basin on the basis of stacking patterns of fourth-order cyclothemic-scale depositional sequences. In contrast to the derivation of third-order cyclicity on the basis of stacking patterns, Ross and Ross (1985, 1987) presented charts demonstrating coastal-onlap curves and defined third-order depositional sequences for Carboniferous and Lower Permian strata of the North American Midcontinent largely on the basis of faunal criteria. For purposes of this report, we follow the methodology of Youle and others (1994).

The Council Grove Group comprises one third-order sequence (Council Grove third-order sequence), with the base of the Americus Limestone representing the transgressive surface. The Bennett Shale Member of the Red Eagle Limestone contains the most widespread maximum-marine-flooding condensed section of the Council Grove Group and thus corresponds also to maximum transgression of the composite third-order sequence. Additionally, the Red Eagle Limestone extends farther paleo-landward into Oklahoma than any other unit of the Council Grove Group. The Foraker and Red Eagle sequences form a retrogradational stacking pattern of sequences and constitute the transgressive systems tract of the third-order sequence. The highstand systems tract includes sequences that stack into aggradational (lower and upper Grenola sequences) and progradational stacking patterns (Beattie through Funston sequences) with a major type 1 unconformity in the Speiser Shale at the top of the Council Grove Group. The Wreford and Barneston sequences of the overlying Chase Group belong to the retrogradational transgressive systems tract of the Chase third-order sequence.

In addition to the cyclothemic-scale fourth-order sequences, many high-frequency fifth-order sequences are evident within the fourth-order packages. Within the dominantly marine part of many latest Carboniferous and Early Permian Midcontinent cyclothemic depositional sequences (e.g., Foraker and Grenola sequences), widely correlatable, subsequence-scale divisions (higher order sequences) on the order of 2–5 m thick are

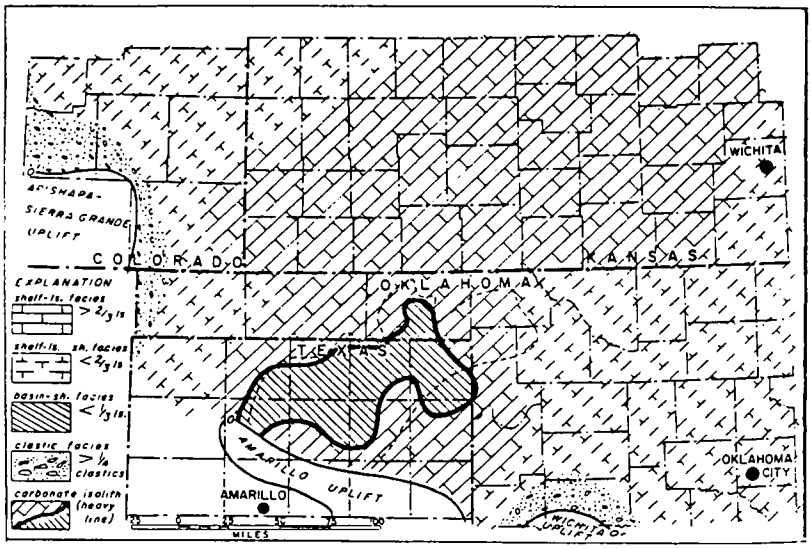

Figure 9. Lithofacies map of the Richardson Subgroup of the Wabaunsee Group (modified from Rascoe, 1962).

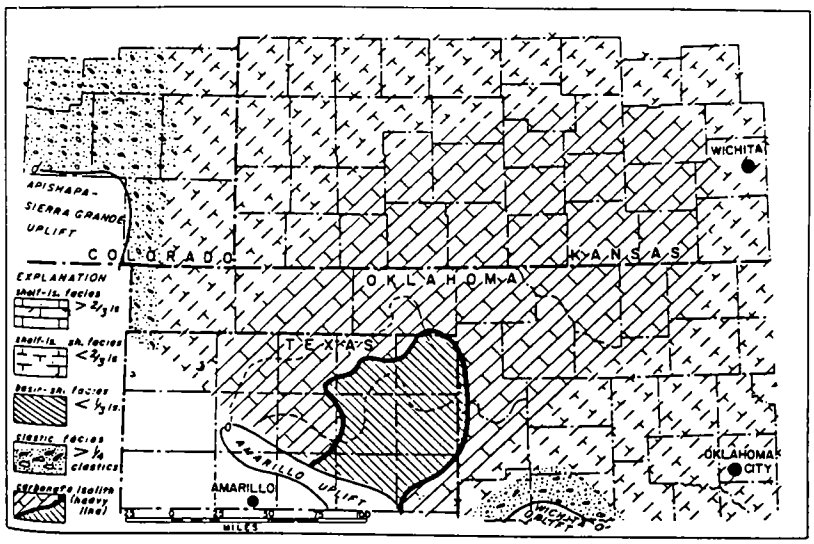

Figure 10. Lithofacies map of the Admire and Council Grove Groups (modified from Rascoe, 1962).

present. These higher order sequences form the parasequences and parasequence sets that clearly stack into the systems tracts that subdivide the fourth-order depositional sequences.

A basinward shift in facies is clearly evident where the fifth-order sequences were not terminated by subaerial exposure. In addition to fifth-order cyclicity in the dominantly marine part of the fourth-order depositional sequence, the minor transgressive–regressive marine bands with distinctive transgressive and highstand systems tracts that are commonly present within the thick siliciclastic-dominanted intervals that overlie the thick carbonate-dominated part of the sequence (Miller and West, 1993) also represent high-frequency fifth-order depositional sequences. These higher order sequences are referred to as *fifth-order transgressive–regressive cycles,* following the terminology of Goldhammer and others (1991). The fifth-order cycles that are terminated by subaerial exposure are referred to as *exposure cycles,* whereas fifth-order cycles that are terminated without subaerial exposure are referred to as *subtidal cycles* after the nomenclature proposed by Goldhammer and others (1991).

Type 1 depositional sequences (as defined by Van Wagoner and others, 1988), such as those in this study, have been subdivided into lowstand systems tract, transgressive systems tract, highstand systems tract, and forced regressive systems tract (Posamentier, Allen, James, and Tesson, 1992; Hunt and Tucker, 1992, 1995; and the equivalent falling sea-level systems tract of Nummedal, 1992; Nummedal and Molenaar, 1995). Historically, the lowstand systems tract comprises basin-floor fans, slope fans, and prograding coastal wedges. The only lowstand deposits thought to have accumulated on the shelf form the prograding wedge deposited during late sea-level fall or early sea-level rise. The shelfal expression of the prograding wedge consists largely of incised-valley-fill deposits formed during late sea-level fall or earliest eustatic rise.

Incised-valley fills have thus far not been documented in Council Grove strata of the Midcontinent. During Council Grove time, arid conditions predominated, and sea-level fall resulted in subaerial exposure of most of the shelf, resulting in meteoric diagenesis of the highstand/forced regressive carbonates. A small number of the tops of the highstand/forced regressive carbonates (Long Creek, Eiss, and Middleburg Limestones) demonstrate direct subaerial exposure, as evidenced by red internal-sediment infilling of solution vugs and brecciation associated with regolith development, whereas the rest are evidently capped by nearshore to marginal-marine siliciclastics. Therefore, sequence boundaries generally lie within the thick (5–15 m) red- to green-mudstone intervals of siliciclastic deposits that separate the dominantly carbonate facies. Thick siliciclastic intervals contain zones that exhibit a plethora of pedogenic structures indicative of extensive paleosol development (Miller and West, 1993). The thick siliciclastic packages dramatically thicken to the south of Osage County, Oklahoma. The predominant percentage of the thick package is composed of fluvial depositional systems with distinctly lesser amounts of paleosols.

Because minor marine bands (higher order cycles) punctuate the complex of paleosols, several unconformities typically are present within each thick siliciclastic section. This makes identification of the shelfal expression of the fourth-order master depositional-sequence boundary difficult. The following stratigraphic surfaces could be utilized as the master sequence boundary: (1) the stratigraphic position that corresponds to the surface above which the first sediments were

deposited during a sea-level fall (Posamentier, Allen, James, and Tesson, 1992); (2) the basal unconformity corresponding to the first evidence of a major basinward shift in facies and the first evidence of subaerial exposure (Van Wagoner, 1990); (3) the top of the paleosol interval that is coincident with the easily identifiable transgressive surface (ravinement) (Watney and others, 1989; French and Watney, 1993); (4) the subaerial-exposure surface that corresponds to maximum sea-level lowstand (Hunt and Tucker, 1995); (5) the maximum flooding surface (marine condensed section) (Galloway, 1989a,b).

Placing the sequence boundary at the first indication of forced regression would result in the maximum lowstand erosional surface lying above the sequence boundary. The basal unconformity surface would also yield a sequence boundary lying below the maximum sea-level lowstand but would provide an easier surface to identify in the field as well as in the subsurface. The use of the top of the paleosol interval that is coincident with the transgressive surface would provide an easy surface to identify in the field as well as in the subsurface but would likely represent a diachronous surface from the distal to the proximal shelf setting. It is for this reason that this level is not coincident with the true sequence boundary. Theoretically, the best option is to place the sequence boundary at the unconformity surface that corresponds to the maximum lowstand, following Hunt and Tucker (1995). However, this procedure also presents a serious challenge in identifying which part of the paleosol interval corresponds to maximum lowstand. The unconformity surface that extends farthest basinward corresponds to this master-sequence boundary. In order to delineate master-sequence boundaries for these Late Carboniferous–Early Permian depositional sequences, a number of dip cores would have to be analyzed from the proximal shelf to the distal shelf and into the Anadarko basin. Unfortunately, the availability of cores from this stratigraphic interval is largely restricted to the proximal shelf region and the Hugoton embayment. Therefore, in the absence of these crucial data, we recognize a master-sequence-boundary zone that includes the true master-sequence boundary. This zone is bounded at the base by the first evidence of significant subaerial exposure and at the top by the highest subaerial exposure surface that is also coincident with the transgressive surface of the succeeding depositional sequence.

On the basis of the glacio-eustatic model for sea-level fluctuation, it is likely that the master-sequence boundary lies near the top of the paleosol interval. As a result of our utilization of a sequence-boundary zone, we do not recognize a lowstand systems tract but include the sequence-boundary zone within the forced regressive systems tract. If and when the precise position of the master-sequence boundary is picked, then a lowstand systems tract, including strata above the sequence boundary and below the transgressive systems tract, could be recognized. Because the initial surface of forced regression lies directly above the marine condensed section, and the marine condensed section represents the latest transgressive systems tract and the earliest highstand systems tract, the stratigraphic thickness of the highstand systems tract as utilized in this study is limited to the upper part of the marine condensed section. The transgressive systems tract includes strata from the base of the transgressive surface to the marine condensed section (downlap surface). These deposits form a retrogradational-parasequence-set stacking pattern. The highstand systems tract historically encompasses the upper part of the marine condensed section along with the thick dominantly marine part of the depositional sequence that includes aggradational to progradational parasequence sets formed during late stages of sea-level rise, eustatic stillstand, and early sea-level fall (Van Wagoner and others, 1988).

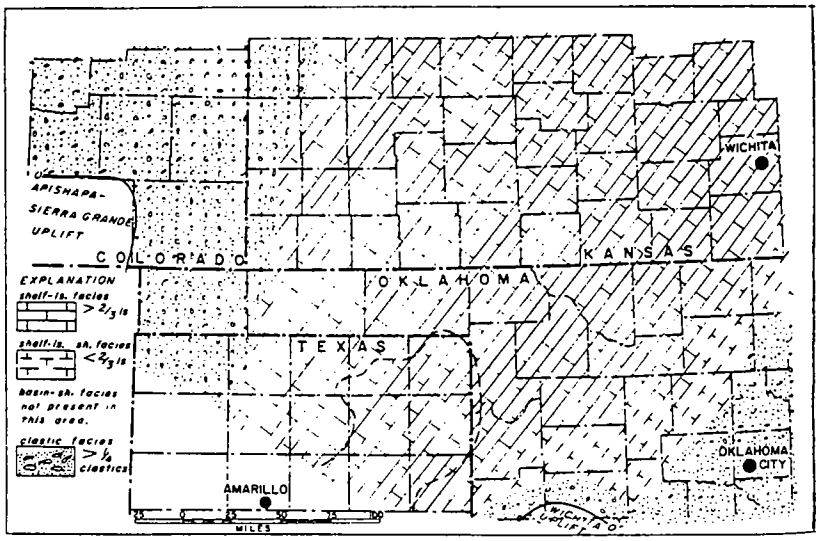

Figure 11. Lithofacies map of the Chase Group (modified from Rascoe, 1962).

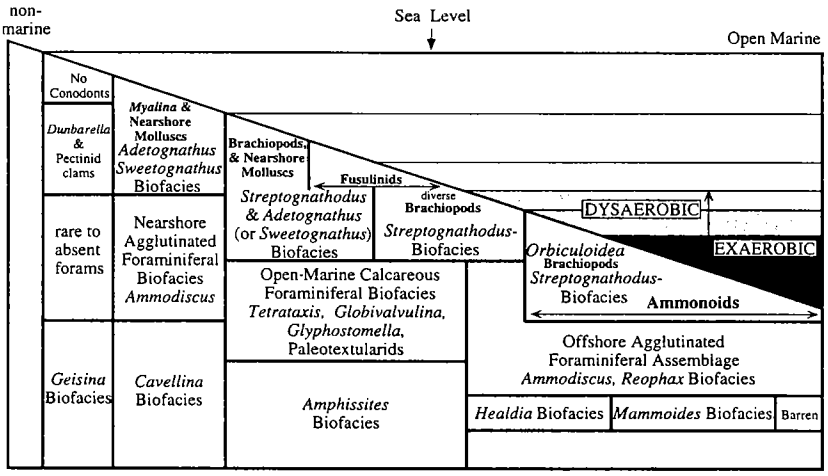

Figure 12. Onshore–offshore model for uppermost Carboniferous and Lower Permian depth- and oxygen-related biofacies (modified from Boardman and others, 1984; Boardman and Nestell, 1993; Boardman and others, 1995).

Sinusoidal sea-level-fluctuation curves, such as those presented by Jervey (1988) and Posamentier and others (1988), have served as the paradigm for modeling depositional sequences. This model has been used to demonstrate that most of the highstand systems tract is associated with aggradation and progradation that occurred during maximum eustatic stillstand and early sea-level fall. The idealized symmetrical sinusoidal sea-level-fluctuation curve contrasts starkly with actual observed highly asymmetric sea-level curves produced by glacial buildup and decay documented for late Pleistocene, Holocene, and Pennsylvanian time.

On the basis of oxygen-isotope data from Imbrie and others (1984), Collier and others (1990) illustrated a late Pleistocene sea-level curve for the last 400,000 years and demonstrated exceptionally rapid sea-level rises associated with deglaciations, followed by episodic, generally gradual sea-level falls caused by slow glacial buildups. Additionally, they showed that the sea-level falls were punctuated by sea-level rises that represented episodic reversals in the trend toward glacial buildups. Maximum lowstands occurred immediately before the major sea-level rises associated with major deglaciations.

In terms of specific rates, Broecker and van Donk (1970) documented that late Pleistocene glacial buildups were slow, lasting as long as 90,000 years, whereas deglaciations are exceedingly rapid, lasting no more than 10,000 years. Carter and others (1986, p. 640) determined that glacial advances and retreats were episodic in addition to being asymmetrical, thereby resulting in rapid episodic transgressions associated with slow episodic regressions. The pattern of exceptionally rapid episodic transgressions, with slow episodic regressions associated with glaciation and deglaciation of the Pleistocene, is virtually identical with observations of Pennsylvanian and Early Permian depositional sequences by Heckel (1977, 1986), French and Watney (1993), and Boardman and Nestell (1993), as well as with the patterns we report (Fig. 13). Although the overall time for ice-sheet buildup is much slower than sea-level melt, resulting in rapid transgressions and slow regressions, minor drops in sea level as part of the episodic regressions may be rapid, resulting in a rapid basinward shift in shallow-marine facies. This is demonstrated as part of our research presented herein.

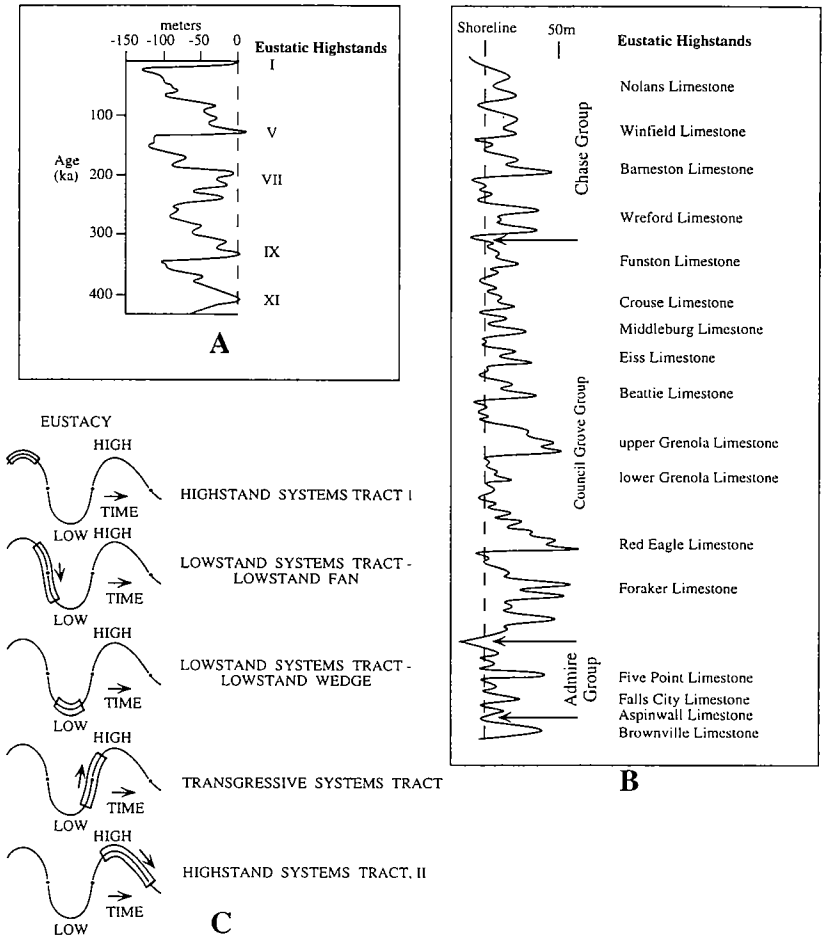

Figure 13. (A) Sea-level curve for the late Quaternary, based on oxygen-isotope data (from Imbrie and others, 1984). (B) Sea-level curve for the uppermost Carboniferous to Lower Permian (modified from Boardman and Nestell, 1993; Boardman and others, 1995). (C) Sinusoidal sea-level-curve model with superimposed systems tracts (modified from Jervey, 1988; Posamentier and others, 1988).

The asymmetrical sea-level curve allows little time during maximum stillstand in contrast to the symmetrical sinusoidal sea-level model. The asymmetrical model suggests that the thick aggradational to progradational sedimentary package that has been placed traditionally in the highstand systems tract is deposited during times of falling sea level. Evidence for falling sea level includes widespread subaerial exposure of subtidal carbonates, as documented by Watney and others (1989) as well as in this report, along with evidence of rapid basinward shift in facies, resulting in facies dislocation. This suggests that during times in Earth history that were dominated by major glaciation, the forced regressive systems tract or the equivalent falling-sea-level systems tract best describes the thick aggradational to progradational parasequence sets historically relegated to the highstand systems tract.

We follow the definition of *forced regressive systems tract* by Hunt and Tucker (1995), which "includes all sediments deposited during times of falling relative sea-level regardless of the depositional environment." The lower systems tract boundary is placed at the horizon that shows evidence of forced regression, and the top at the master-sequence boundary. Even though our forced regressive systems tract is very close to the usage of the traditional highstand systems tract of the Exxon model, we suggest that it is a better conceptual approach.

Maximum-flooding surfaces also have been proposed as sequence boundaries for genetic stratigraphic sequences (Galloway, 1989a,b), a conceptual alternative to depositional sequences. The genetic stratigraphic sequences are supposedly easier to define and correlate because the sequence boundaries are placed at maximum flooding surfaces (marine con-

densed sections). This is ideal where marine condensed sections are represented by highly radioactive shales ("hot" shales) that carry a distinctive high gamma-ray–neutron response, or likewise where downlap surfaces that equate to maximum flooding surfaces are easily identified on seismic profiles. These hot shales make three-dimensional sequence-stratigraphic analysis easier because the sequences are easier to correlate in the subsurface. This approach provides much easier definition and correlation in sequences where radioactive black fissile shales represent the marine condensed sections. However, in this study, radioactive black shales are restricted to the lower Council Grove Group (Puckette and others, 1995). Additionally, the black shales are discontinuous in the subsurface and in surface outcrops. These black-shale marine condensed sections grade laterally into shaly, glauconitic, and phosphatic fossiliferous wackestones (carbonate marine condensed sections) and typically lose their high distinctive gamma-ray signatures.

Watney and others (1989) demonstrated that marine condensed sections that lack phosphatic, black fissile shales in Missourian depositional sequences (e.g., the Quindaro and Hickory Creek Shales) also lack high gamma-ray responses, based on scintillation analysis of surface outcrops. Because of the scarcity of easily identifiable radioactive shales, three-dimensional sequence-stratigraphic analysis, including subsurface well data, must include thin-section as well as paleoecological analysis from cores in order to document maximum-flooding surfaces that define the genetic stratigraphic sequences. It is for this reason that we do not consider this approach to be superior to the traditional approach toward depositional sequences defined on the basis of widespread unconformities.

Because the Late Carboniferous and Early Permian global chronostratigraphic framework is not formally established, we provisionally use the marine cyclothem names as names for the fourth-order depositional sequences. Owing to the current lack of reliable absolute dates for this time interval, we recognize different orders of depositional sequences but do not attempt to correlate a particular order to an absolute time duration, nor do we attempt to identify particular Milankovitch cycles.

COUNCIL GROVE GROUP SEQUENCES

Foraker Fourth-Order Depositional Sequence

The Foraker depositional sequence comprises the Americus Limestone, Hughes Creek Shale, Long Creek Limestone, and the lower two-thirds of the Johnson Shale (Figs. 14,15). The transgressive surface of the Foraker sequence occurs at the base of the Americus Limestone and consists of a regionally extensive, transgressive lag and ravinement surface characterized by an ostracode-rich conglomeratic shale or carbonate. The Foraker sequence is composed of eight fifth-order sequences that are correlatable across the entire outcrop area. The lower six fifth-order sequences are capped by nearshore-marine to marginal-marine deposits consisting of poorly fossiliferous silty shales, whereas the upper two are capped by green to red, blocky, caliche-bearing mudstones indicative of paleosols. The fifth-order depositional sequences that are capped by marginal-marine deposits are analogous to the fifth-order subtidal cycles of Goldhammer and others (1991) for the Desmoinesian of the Paradox basin, whereas those capped by subaerial-exposure surfaces are similar to their fifth-order exposure cycles. The exposure cycles occur at the top of the Foraker fourth-order sequence in a similar fashion to those of the Paradox basin. The base of each fifth-order sequence is defined by a major flooding surface characterized by a highly fossiliferous wackestone with ubiquitous horizontal boxworks of the trace fossil *Thalassinoides* and an abundant open-marine fauna that includes bryozoans, brachiopods, and fusulinaceans.

Chaplin (1996) interpreted the occurrences of horizontal boxworks of *Thalassinoides* to represent transgressive surfaces in analogous Chase Group strata (Lower Permian) of the Midcontinent. Maximum-marine-flooding surfaces are represented by highly fossiliferous wackestones without evidence of condensed sedimentation in cases of minor to intermediate sea-level rises. Highly fossiliferous glauconitic and phosphatic wackestones or dark-gray to black shales give evidence of condensed sedimentation for greater sea-level rises. Three of the fifth-order sequences contain marine condensed sections, including the upper Americus Limestone (fifth-order sequence B), the middle Hughes Creek (fifth-order sequence D), and the upper Hughes Creek (fifth-order sequence E). These maximum-marine-flooding-surface condensed sections contain an abundant *Streptognathodus*-dominated conodont fauna with major evidence of condensed sedimentation, including abundant glauconite and phosphatized molluscs in addition to the conodonts that range from 100 to 1,000 platforms/kg.

In northern Kansas and Nebraska, these marine condensed sections contain well-developed black shales, whereas in central and southern Kansas they occur as shaly, glauconitic, and phosphatic wackestones. Maximum-marine-flooding surfaces of the lower Americus (fifth-order sequence A), the lowermost Hughes Creek (fifth-order sequence C), the top of the Hughes Creek–Long Creek (fifth-order sequence F), and the Long Creek (fifth-order sequence G) are characterized by a mixed *Adetognathus–Streptognathodus* biofacies with no evidence of condensed sedimentation. Maximum marine flooding of the lower Johnson (Foraker fifth-order sequence H) is characterized by only a sparse assemblage of ostracodes and encrusting foraminifers without conodonts.

Maximum marine flooding for the Foraker fourth-order depositional sequence is placed at the condensed section of the upper Hughes Creek Shale (Foraker fifth-order sequence E), as it corresponds to the most widespread black-shale bed and greatest condensed interval in the sequence. Fifth-order sequences above this level demonstrate progressively shallower water facies developed at maximum marine flooding, coupled with termination of the cycles by subaerial exposure. The transgressive systems tract of the Foraker fourth-order sequence encompasses the Americus Limestone and the lower two-thirds of the Hughes Creek Shale, whereas the forced regressive systems tract encompasses the top of the Hughes Creek Shale, the Long Creek Limestone, and the lower two-thirds of the Johnson Shale.

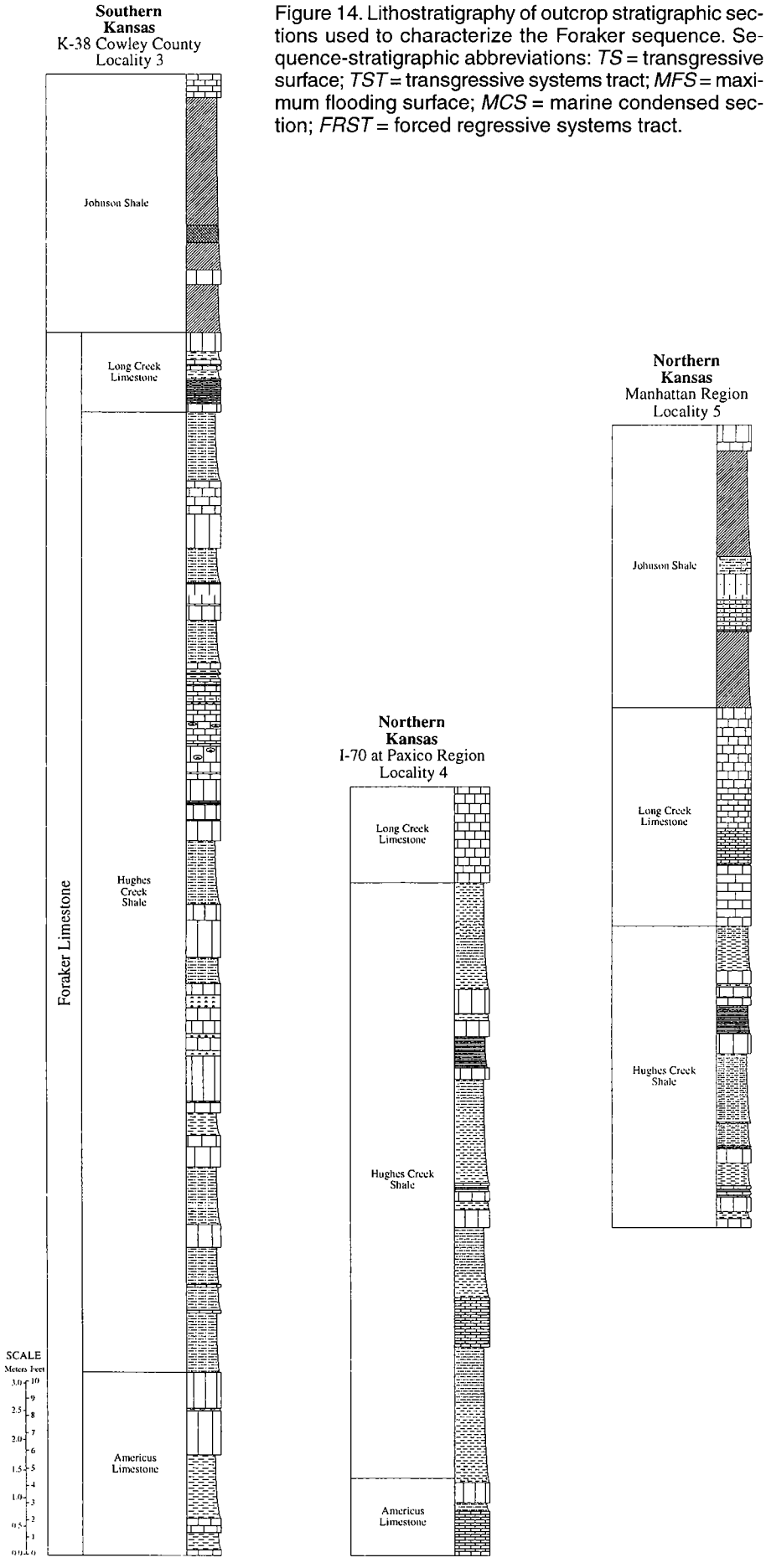

Figure 14. Lithostratigraphy of outcrop stratigraphic sections used to characterize the Foraker sequence. Sequence-stratigraphic abbreviations: *TS* = transgressive surface; *TST* = transgressive systems tract; *MFS* = maximum flooding surface; *MCS* = marine condensed section; *FRST* = forced regressive systems tract.

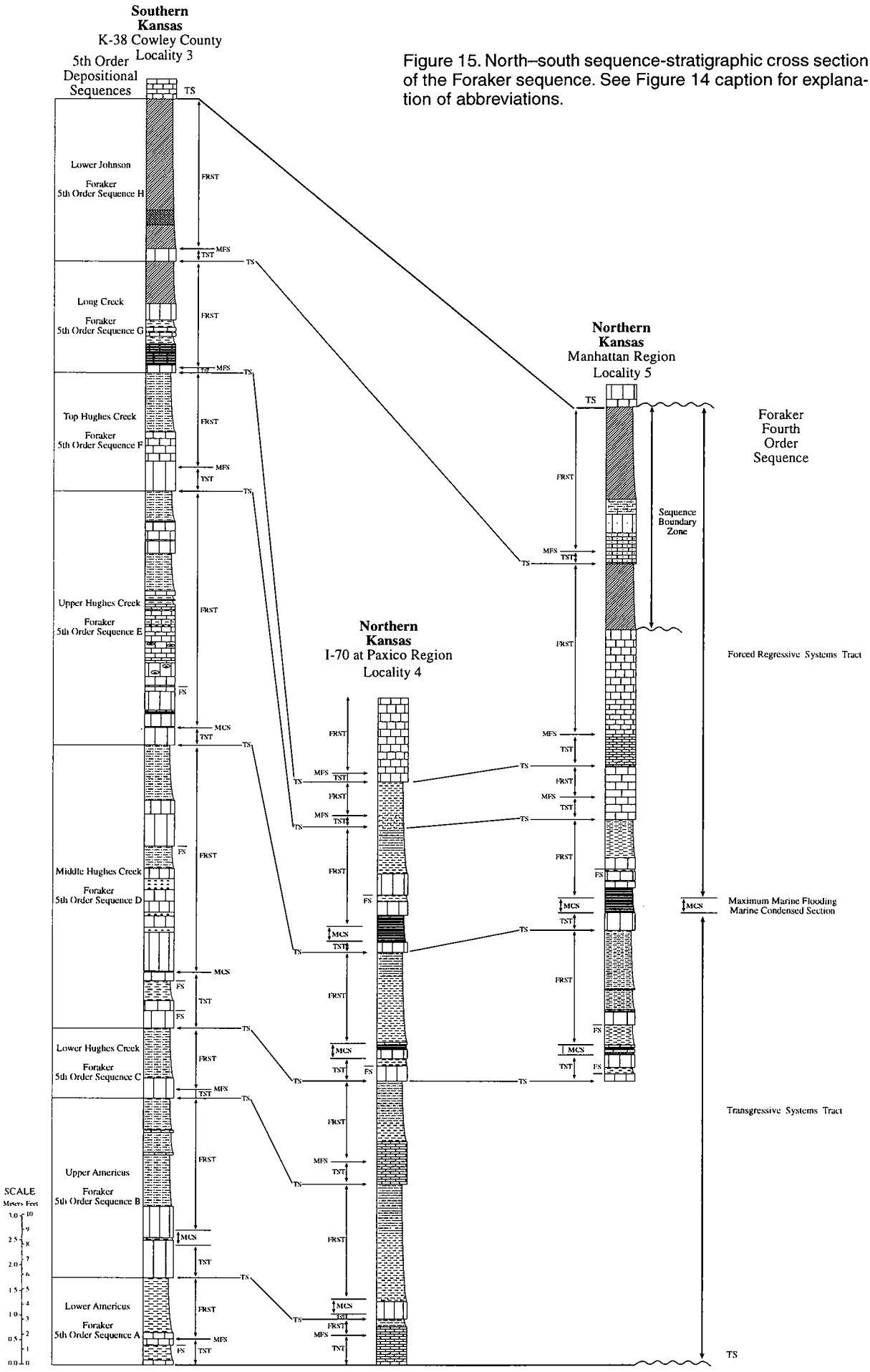

Figure 15. North–south sequence-stratigraphic cross section of the Foraker sequence. See Figure 14 caption for explanation of abbreviations.

Red Eagle Fourth-Order Depositional Sequence

The Red Eagle depositional sequence comprises the upper Johnson Shale, Glenrock Limestone, Howe Limestone, and Roca Shale (Figs. 16,17). The maximum marine flooding of this sequence corresponds to the provisional correlated position of the base of the Permian in North America on the basis of the appearance of *Streptognathodus isolatus* (Chernykh and others, 1997). The Red Eagle sequence consists of seven regionally correlative fifth-order depositional sequences. The transgressive surface of the Red Eagle sequence occurs in the upper part of the Johnson Shale and is represented typically by a thin intraclastic packstone developed as a transgressive lag and ravinement. The lowermost Red Eagle sequence is developed entirely within the top of the Johnson Shale and contains abundant ostracodes and rare conodonts of a mixed *Streptognathodus–Adetognathus* assemblage, along with locally abundant molluscs and brachiopods including *Juresania, Linoproductus,* and *Derbyia*. This fifth-order sequence is terminated by silty, dark mudstones and shales locally exhibiting silty rhythmites, which are indicative of tidally influenced deposition.

The next two fifth-order sequences (Red Eagle B and C) contain marine condensed sections at maximum marine flooding. Maximum marine flooding of sequence B occurs at the base of the Bennett Shale and is represented by abundant *Streptognathodus* conodonts, orbiculoid brachiopods, ammonoids, and fish debris. In northern Kansas through Nebraska, this condensed section occurs at the base of black fissile shale of the Bennett Shale in contrast to central Kansas to Oklahoma, where this condensed section occurs as a highly fossiliferous, shaly, glauconitic, phosphatic wackestone. This cycle is terminated by poorly fossiliferous siltstone within the Bennett Shale in Nebraska, by an upper black-shale facies with no evidence of condensation of the Bennett in northern Kansas, and by a phylloid-algal, brachiopod-rich wackestone in central Kansas to northern Oklahoma. The maximum-marine-flooding, condensed-section sequence C is represented by a black fissile shale above the poorly fossiliferous siltstone in Nebraska; by a calcite-cemented black mudstone with horizontal boxworks of *Thalassinoides*, orbiculoid brachiopods, and abundant fish debris in the upper Bennett Shale in northern Kansas; and by either a highly fossiliferous shaly, glauconitic, phosphatic wackestone or a thin gray, highly fossiliferous, phosphatic shale parting (<3 cm) in central Kansas to northern Oklahoma. In all regions, *Streptognathodus* conodonts from 500 to 1,000 platforms/kg are noted from this condensed section.

In northern Oklahoma and southern Kansas, the top three fifth-order sequences of the Red Eagle sequence demonstrate a progressive shallowing of lithofacies and corresponding biofacies developed at maximum transgression. The top fifth-order sequence is capped by paleosols of the Roca Shale. In central Kansas through Nebraska, only fifth-order sequence D is well developed in what is mapped as the Red Eagle Limestone. However, in those regions, the Roca Shale is considerably thicker and contains two well-developed marine-flooding surfaces within the lower part of the shale (Miller and West, 1993).

We interpret these additional marine-flooding surfaces that are not present in southern Kansas or northern Oklahoma to represent maximum marine flooding of fifth-order sequences E and F. This implies that northern Kansas and southern Nebraska were topographically higher on the shelf during deposition of the Red Eagle sequence. According to this interpretation, while silty nearshore marine shales and carbonates were being deposited in southern Kansas and northern Oklahoma during terminations of fifth-order sequences D and E, paleosols were forming in northern Kansas and Nebraska. Marine flooding associated with fifth-order sequences E and F then resulted in deposition of thin marine carbonates with the paleosol intervals.

The transgressive systems tract of the Red Eagle fourth-order depositional sequence includes the interval from the transgressive lag deposit in the upper Johnson Shale to the maximum-marine-flooding-surface condensed section in the upper Bennett Shale (sequence C). The forced regressive systems tract includes the interval from the upper condensed section to the base of the Sallyards Limestone, which marks the base of the lower Grenola fourth-order depositional sequence.

Lower Grenola Fourth-Order Depositional Sequence

The lower Grenola sequence comprises the Sallyards Limestone, Legion Shale, Burr Limestone, and Salem Point Shale, in ascending order (Figs. 18,19). The lower Grenola sequence comprises four fifth-order depositional sequences. A transgressive lag (ravinement) surface marks the base of the Grenola sequence. This lag surface generally coincides with the basal bed of the Sallyards Limestone, except in central Kansas, where it occurs in the top part of the Roca Shale.

The Sallyards (fifth-order sequence A) includes the Sallyards Limestone and the Legion Shale. Maximum flooding at the top of the Sallyards Limestone is characterized by abundant pectinid and myalinid clams that are locally abundant at the top of the unit. No conodonts have been recovered from this fifth-order sequence. The lower part of the Legion Shale is typically gray to black silty mudstone with an abundant low-diversity ostracode assemblage. This unit is interpreted as having been deposited in a shallow, perhaps lagoonal, marginal-marine environment. The abrupt contact between the maximum-flooding surface at the top of the Sallyards Limestone and the base of the Legion Shale, with no transitional lithofacies or biofacies, suggests a basinward shift of facies associated with rapidly falling sea level.

In northern Kansas, a thin conglomeratic ostracode-bearing carbonate is present near the top of the Legion Shale, which represents the transgressive surface of the lower Burr fifth-order sequence (sequence B). In other regions, including northern Oklahoma, southern Kansas, central Kansas, and Nebraska, the base of the Burr Limestone contains the transgressive surface of the lower Burr fifth-order sequence. Throughout the outcrop belt, the top of the lower Burr Limestone is locally developed as a hardground with abundant brachiopods (*Juresania, Composita,* and *Linoproductus*) along with a variety of molluscs, crinoids, and abundant phosphatic skeletal debris including fish and conodonts. This unit is interpreted to represent relatively minor condensation and maximum flooding.

In northern Kansas, the top of the lower Burr is directly overlain by a gray to black, silty, locally gypsiferous mudstone and shale characterized by a sparse fauna of *Promytilus* clams and rare ostracodes. This zone is interpreted to represent a marginal-marine, possibly hypersaline environment. The abrupt contact between diversely fossiliferous wackestone, which marks the maximum-flooding surface, and overlying poorly fossiliferous, black mudstone is indicative of a basinward shift in facies and forced regression.

In central Kansas, this interval is represented by thin-bedded, poorly fossiliferous, ostracode-bearing mudstone to wackestone, whereas poorly fossiliferous silty mudstones are present in southern Kansas and northern Oklahoma.

The base of the upper Burr across the entire study area is characterized by a transgressive lag deposit with locally abundant skeletal fish debris. It is interpreted to represent the transgressive surface of the upper Burr fifth-order sequence (lower Grenola fifth-order sequence C). The upper part of the Burr Limestone contains abundant clams and locally abundant evaporite molds and is interpreted to represent a shoal sabkha environment.

The lower part of the overlying Salem Point Shale from Nebraska to southern Kansas consists of poorly fossiliferous, silty, blocky mudstones. Within the middle part of the Salem Point Shale, a thin pectinid- and myalinid-bearing carbonate is present from southern Nebraska to northern Oklahoma. This bed is interpreted to represent the base of the Salem Point fifth-order sequence (lower Grenola fifth-order sequence D). It is overlain by gray to black silty mudstones and shales with a low-diversity ostracode assemblage. The upper Salem Point Shale across the outcrop belt consists of green to red, blocky mudstones with locally developed columnar peds, blocky peds, slickensides, and other indications of paleosol development. This paleosol is well developed throughout the outcrop region.

The transgressive systems tract of the lower Grenola fourth-order sequence includes the interval from the base of the Sallyards Limestone to the maximum-marine-flooding surface at the top of the lower Burr Limestone. The forced regressive systems tract includes the interval from the maximum-marine-flooding surface to the Neva Limestone, which marks the base of the upper Grenola fourth-order sequence.

Upper Grenola (Neva) Fourth-Order Depositional Sequence

The upper Grenola (Neva) sequence includes the Neva Limestone and Eskridge Shale, in ascending order (Figs. 18,19). The upper Grenola (Neva) sequence comprises five regionally correlative fifth-order sequences, the basal two of which contain maximum-marine-flooding condensed sections. The base of this sequence is characterized by a regional transgressive lag deposit that marks the base of the Neva Limestone and represents initial marine flooding.

Maximum marine flooding of the lower Neva fifth-order sequence (sequence A) is exhibited in a tan, dark-gray, or black mudstone with ubiquitous skeletal phosphate composed of conodonts, orbiculoid brachiopods, and fish debris. It is present above the basal Neva Limestone in Nebraska, throughout Kansas, and in northern Oklahoma. This condensed section contains 100–1,000 *Streptognathodus* platforms/kg throughout the outcrop belt. This fifth-order sequence is terminated by a phylloid-algal-rich wackestone to packstone throughout the outcrop belt. This unit is sharply overlain by a thin transgressive interval below a regionally developed maximum-marine-flooding condensed section of the upper Neva fifth-order sequence (sequence B), which contains 100–300 *Streptognathodus* platforms/kg. This fifth-order sequence is also terminated by a phylloid-algal-rich wackestone to packstone. The top three fifth-order sequences are exposure cycles, as they are capped by subaerial-exposure surfaces developed as red to green, blocky-mudstone paleosols.

The upper Grenola sequence is significant in containing the last well-developed maximum-marine-flooding condensed section and offshore-black-shale facies in the Council Grove Group. Although maximum-marine-flooding condensed sections are present in the lower Chase Group (Threemile, Schroyer, and basal Florence), no offshore black shales are present.

The maximum-marine-flooding surface of the upper Grenola (Neva) fourth-order sequence occurs coincident with the lower Neva fifth-order-sequence marine condensed section. Therefore, the transgressive systems tract includes the interval from the transgressive lag deposit at the base of the Neva Limestone to the marine condensed section. The forced regressive systems tract includes the interval from the condensed section to the base of the Cottonwood Limestone, which marks the base of the Beattie fourth-order depositional sequence.

Beattie Fourth-Order Depositional Sequence

The Beattie sequence comprises the Cottonwood Limestone, Florena Shale, Morrill Limestone, and lower Stearns Shale, in ascending order (Figs. 20,21). This sequence is composed of two fifth-order depositional sequences. The base of the Cottonwood Limestone consists of a well-developed transgressive lag deposit with abundant ostracodes in Nebraska through central Kansas. In southern Kansas, the lower Cottonwood Limestone changes facies from a massive, cherty, highly fossiliferous wackestone to packstone into highly fossiliferous shales and interbedded shaly wackestones. The transgressive surface occurs as a transgressive lag deposit in the first fossiliferous thin carbonate bed, which has been mapped previously with the Eskridge Shale. Maximum marine flooding of the Cottonwood (Beattie fifth-order sequence A) is reflected near the center of the Cottonwood in Nebraska through central Kansas and is associated with fusulinaceans, a diverse brachiopod assemblage, corals, and some *Streptognathodus* platforms (10–30 platforms/kg). In southern Kansas, the Cottonwood Limestone and Florena Shale have a gradational contact, and maximum marine flooding is exhibited in a highly fossiliferous, glauconitic wackestone about 0.5 m below the top of a limestone that has been mapped as the top of the Cottonwood in that region. In southern Kansas, maximum flooding is represented by a rich brachiopod assemblage of *Juresania, Reticulatia, Meekella, Neochonetes, Composita, Punctospirifer, Beecheria, Wellerella, Hustedia, Orbiculoidea,* and *Petrocrania,* along with bryozoans, corals, trilobites, a rich and diverse foraminifer and ostracode assemblage, and a mod-

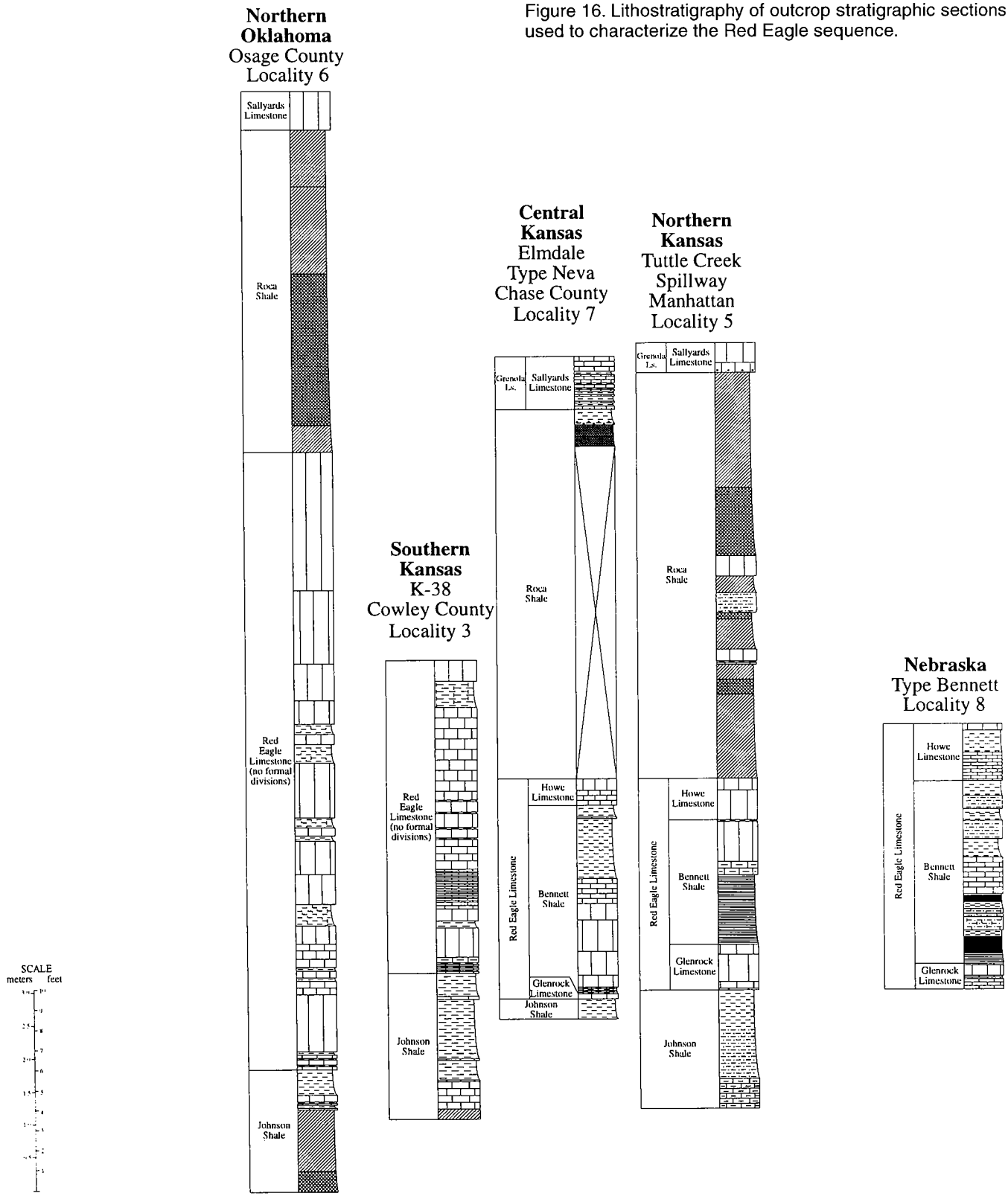

Figure 16. Lithostratigraphy of outcrop stratigraphic sections used to characterize the Red Eagle sequence.

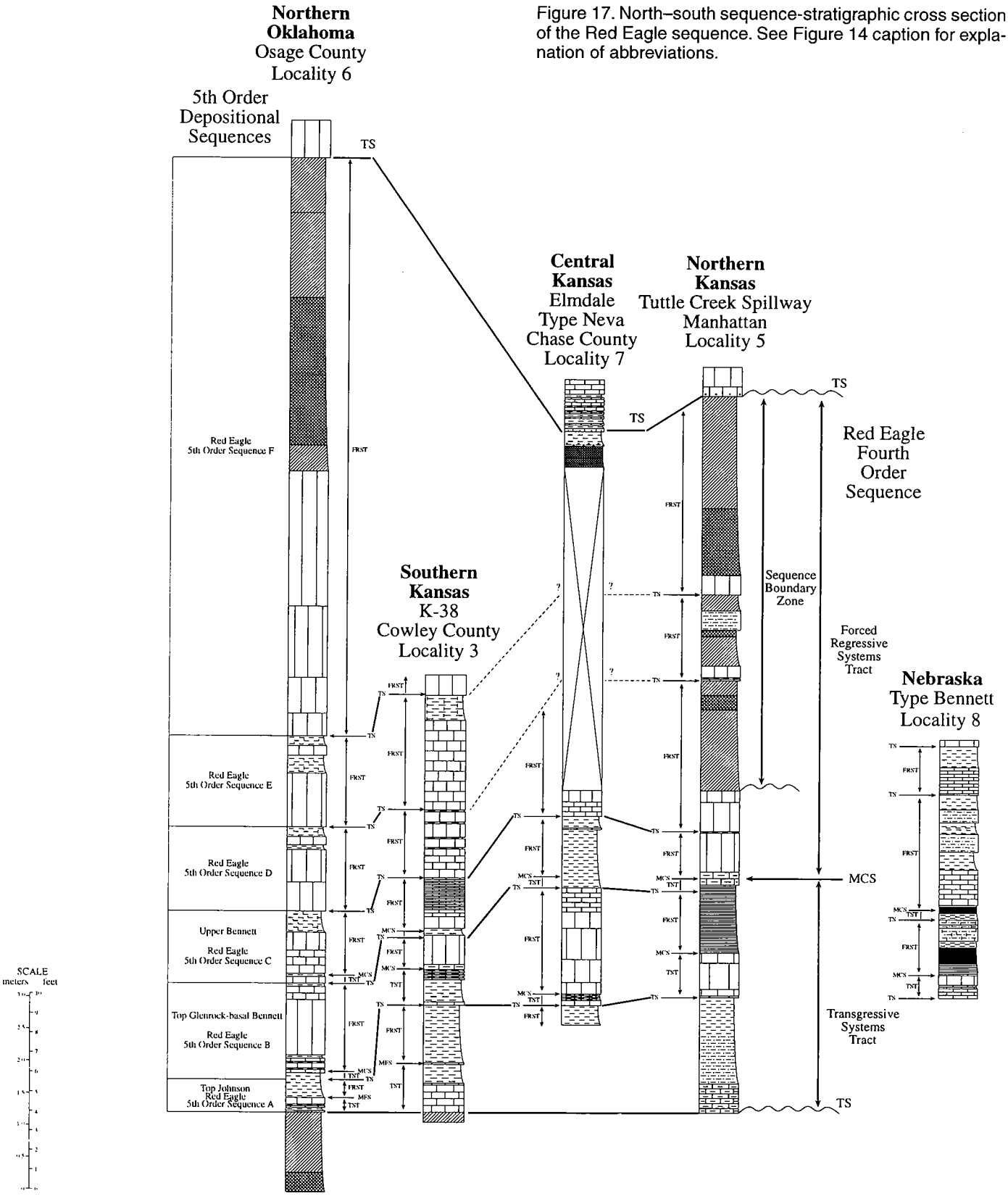

Figure 17. North–south sequence-stratigraphic cross section of the Red Eagle sequence. See Figure 14 caption for explanation of abbreviations.

Figure 18. Lithostratigraphy of outcrop stratigraphic sections used to characterize the lower and upper Grenola sequences.

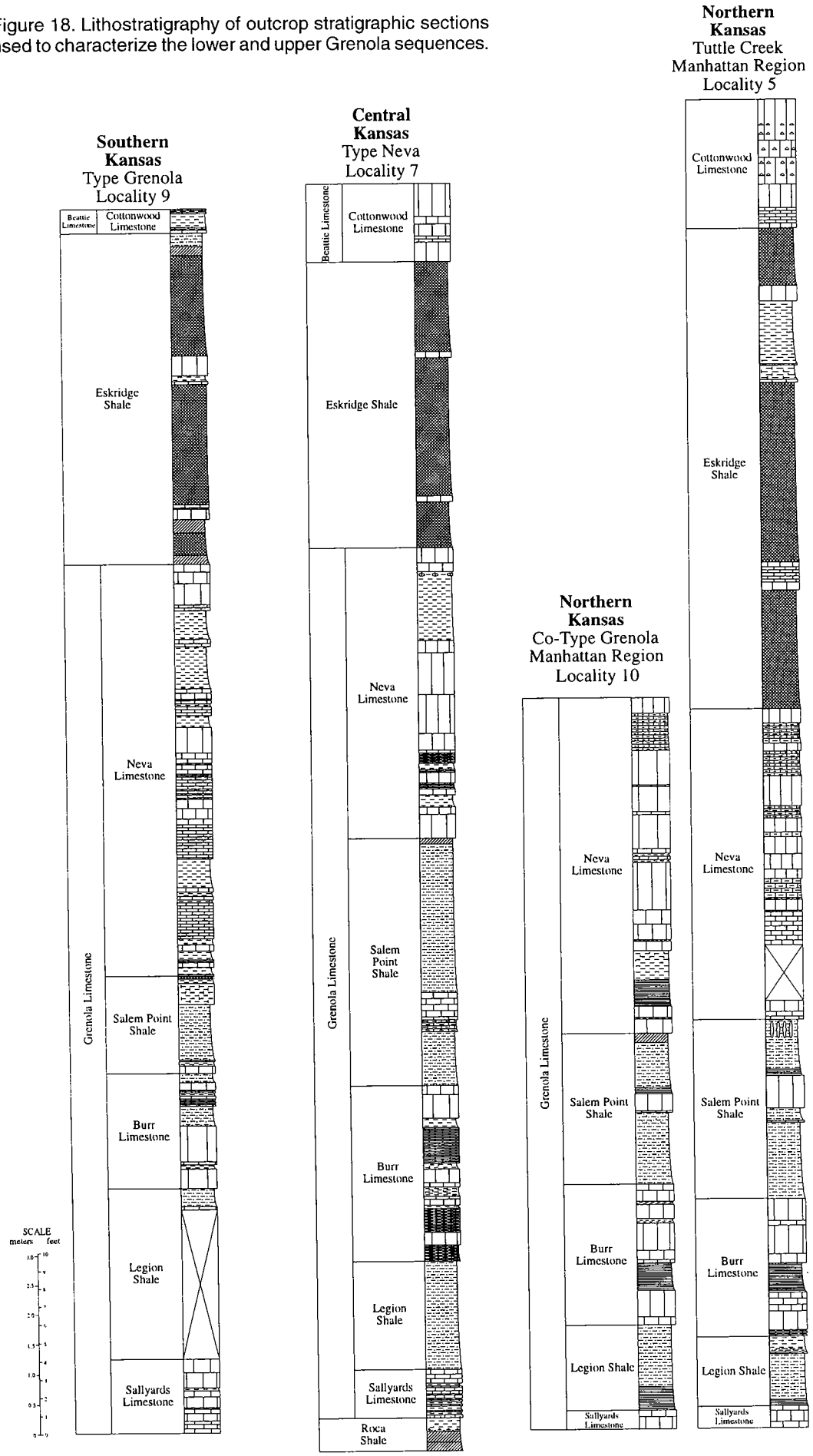

Figure 19. North–south sequence-stratigraphic cross section of the lower and upper Grenola sequences. See Figure 14 caption for explanation of abbreviations.

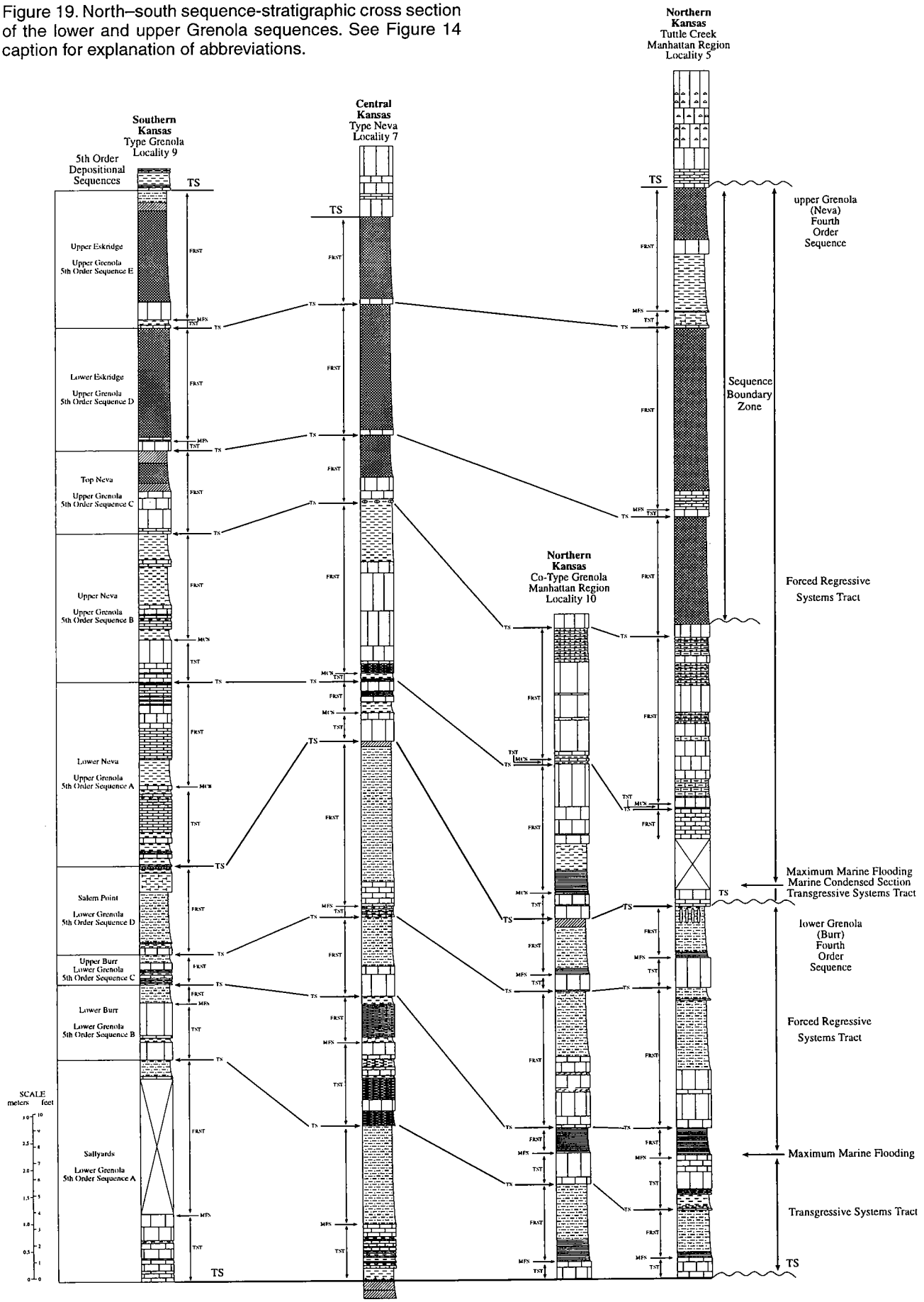

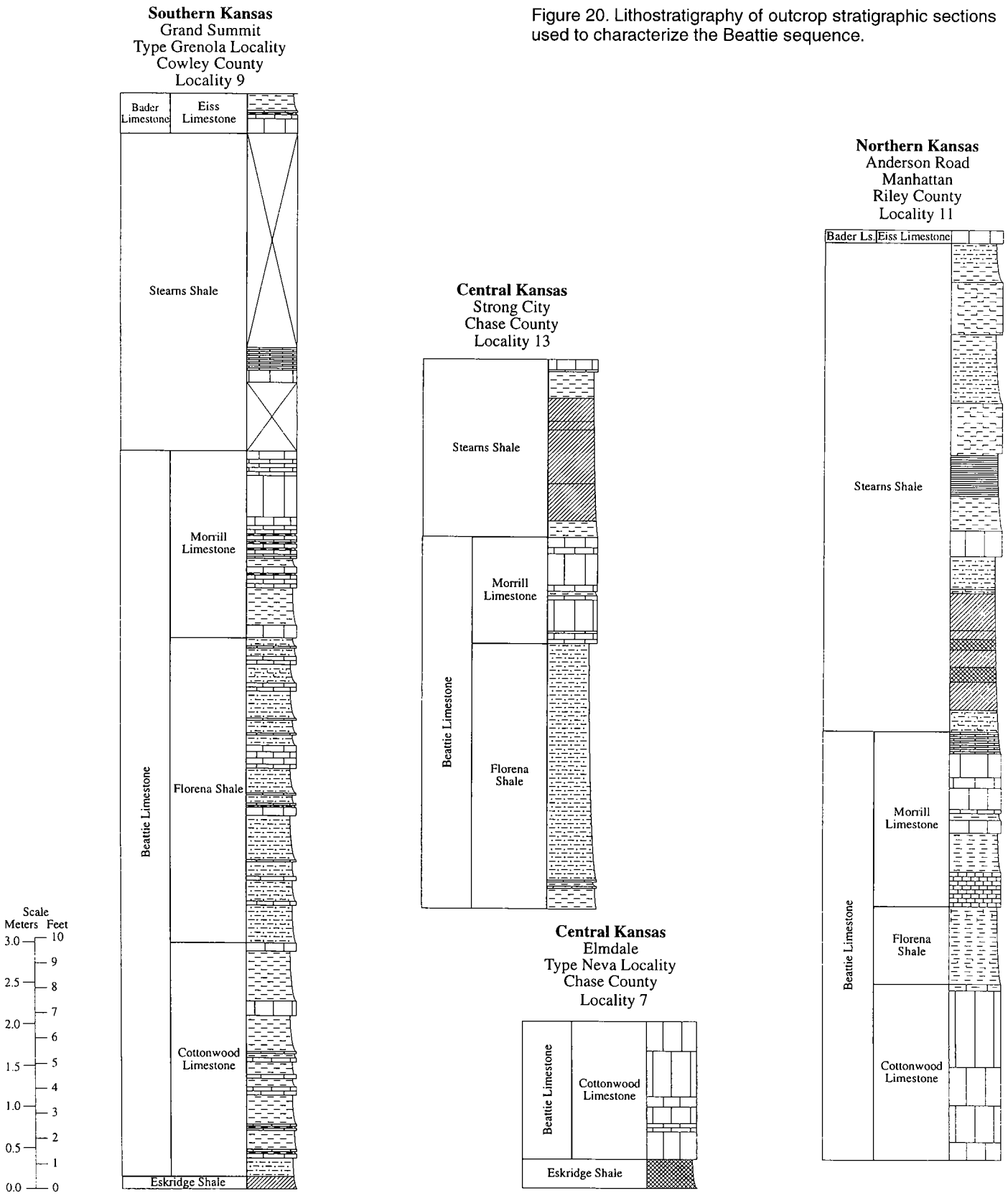

Figure 20. Lithostratigraphy of outcrop stratigraphic sections used to characterize the Beattie sequence.

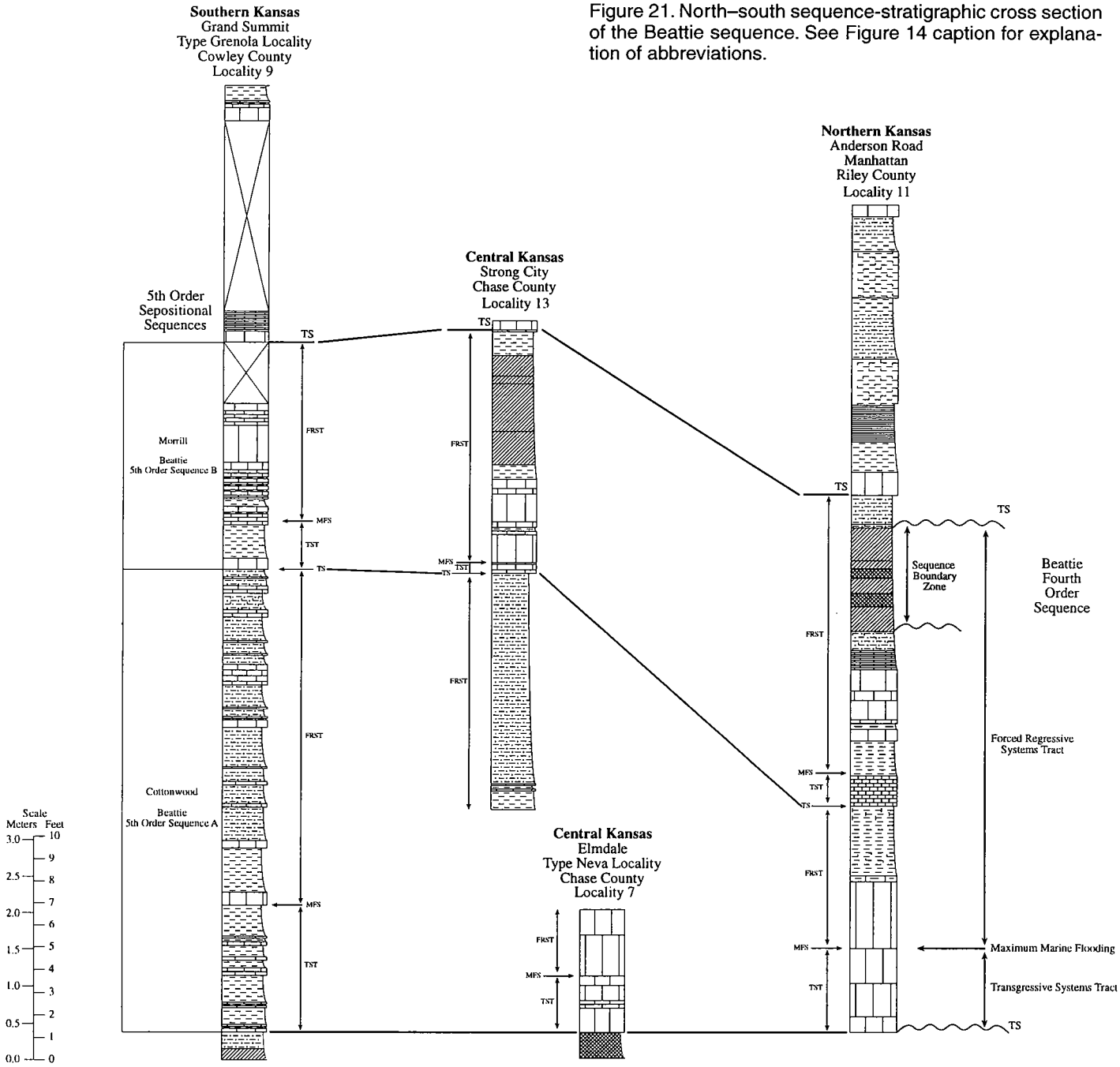

Figure 21. North–south sequence-stratigraphic cross section of the Beattie sequence. See Figure 14 caption for explanation of abbreviations.

erate amount of *Streptognathodus*. This fifth-order sequence is terminated by poorly fossiliferous, silty, locally dolomitic shale and mudstones of the upper Florena Shale.

The Morrill (Beattie fifth-order sequence B) is characterized by a flooding surface at its base throughout the outcrop belt. Maximum marine flooding is reflected in a *Derbyia*-rich brachiopod interval in northern exposures and fossiliferous, fusulinacean-rich shaly wackestone in central and southern exposures. This fifth-order sequence is terminated by a regionally correlative paleosol in the lower Stearns Shale. This paleosol is represented for the most part by green to red, blocky, caliche-bearing mudstones and silty mudstones, and marks the sequence boundary between the Beattie fourth-order sequence and the Eiss fourth-order sequence.

Eiss Fourth-Order Depositional Sequence

The lower Bader (Eiss) sequence comprises the upper Stearns Shale, Eiss Limestone, and lower Hooser Shale, in ascending order (Figs. 22,23). This sequence is characterized by three fifth-order sequences, one of which is developed in the upper Stearns Shale and the other two in the Eiss Limestone. The transgressive surface of the lower Bader (Eiss) sequence is present in the slightly fossiliferous silty mudstones that overlie the paleosol interval. Maximum flooding of the Stearns fifth-order sequence (sequence A) is reflected in gray shale above a thin fossiliferous wackestone in northern Kansas and in a thin fossiliferous carbonate in central and southern Kansas. This shale contains an abundant fauna of ostra-

codes and foraminifers and a low-diversity fauna of brachiopods and molluscs. No evidence of condensed sedimentation or the presence of conodonts is noted in this sequence, which is terminated by poorly fossiliferous silty shales and mudstones of the uppermost Stearns Shale.

In southern and central Kansas, the base of the Eiss Limestone marks the base of the lower Eiss fifth-order sequence and consists of a lower, algal-rich carbonate with *Aviculopinna* clams and *Meekella* brachiopods that represents the initial marine flooding, whereas in northern Kansas a slightly fossiliferous silty shale denotes initial transgression of the sequence. Maximum flooding throughout the outcrop area is evidenced in an abundantly and diversely fossiliferous shale or shaly wackestone with moderately abundant *Streptognathodus* that also contains trilobites, crinoids, bryozoans, and brachiopods including *Composita, Meekella, Juresania, Neochonetes,* and *Reticulatia*. This cycle is regionally terminated by poorly fossiliferous, marginal-marine silty mudstones.

The upper Eiss fifth-order sequence is characterized regionally by locally abundant gastropods and bivalves along with *Sweetognathus* conodonts. The top part of the upper Eiss shows direct evidence of subaerial exposure, with regolith and red internal sediment infilling a massive vug network along with a brecciated regolith developed at the very top. Regionally, the overlying basal Hooser Shale is a red to variegated blocky mudstone with numerous paleosol features.

The maximum-marine-flooding surface of the lower Bader (Eiss) fourth-order sequence is coincident with the maximum-flooding surface of the lower Eiss fifth-order sequence. The transgressive systems tract includes strata from the transgressive surface in the Stearns Shale to the maximum-marine-flooding surface, and the forced regressive systems tract includes strata from the maximum flooding surface to the next transgressive surface in the Hooser Shale.

Middleburg Fourth-Order Depositional Sequence

The Middleburg fourth-order sequence comprises the Middleburg Limestone and the Easly Creek Shale, in ascending order (Figs. 22,23). Two fifth-order sequences constitute this Middleburg sequence, the base of which is highly complex. In northern Kansas, the transgressive surface is coincident with a limestone in the middle of the Hooser Shale. In central Kansas, the transgressive surface occurs in shale near the top of the Hooser Shale, whereas in southern Kansas it occurs at the base of the Middleburg Limestone. Apparently, the middle and upper Hooser of the northern outcrop belt are stratigraphic equivalents of the basal Middleburg of southern Kansas.

The lower Middleburg fifth-order sequence includes strata from the transgressive surface to the base of the upper Middleburg ledge, and the upper Middleburg fifth-order sequence includes strata from the upper Middleburg ledge to the base of the Crouse Limestone. In northern Kansas, the Middleburg Limestone contains abundant gastropods near the base, and sparse brachiopods, crinoids, and *Streptognathodus* conodonts near the center. In central and southern Kansas, the lower part of the lower Middleburg Limestone contains abundant pectinid bivalves, local phylloid algae, and gastropods. The upper part of the lower Middleburg contains an abundant and diverse open-marine fauna including corals, bryozoans, brachiopods, crinoids, and trilobites, with some *Streptognathodus*. The brachiopod interval is interpreted as the maximum marine flooding of the lower Middleburg fifth-order sequence. Directly overlying this interval is a thin-bedded, shaly, dark-gray, poorly fossiliferous mudstone to wackestone in northern Kansas; a black, fissile, somewhat silty, poorly fossiliferous shale in central Kansas; and a calcareous and silty, poorly fossiliferous shale in southern Kansas. This interval represents rapid shallowing, a basinward shift in facies, and forced regression; it is sharply overlain by a fossiliferous wackestone to packstone with gastropods, encrusting foraminifers, and algal-coated grains that mark the base of the upper Middleburg fifth-order sequence. The base of the limestone also marks maximum flooding of the upper Middleburg sequence. This fifth-order sequence is apparently devoid of conodonts and is capped by green and red, blocky, silty mudstones interpreted to represent paleosols within the Easly Creek Shale.

Maximum marine flooding of the Middleburg fourth-order sequence is reflected by the brachiopod facies at the top of the lower Middleburg ledge. In northern Kansas, the transgressive systems tract includes strata from the base of the limestone in the middle Hooser Shale to the top of the lower Middleburg. In central Kansas, the transgressive systems tract includes strata from the uppermost Hooser Shale to the top of the lower Middleburg, and in southern Kansas it includes strata from the base of the Middleburg Limestone to the top of the lower Middleburg ledge. The forced regressive systems tract includes strata from the top of the lower Middleburg to the base of the Crouse Limestone.

Crouse Fourth-Order Depositional Sequence

The Crouse fourth-order sequence comprises the Crouse Limestone and Blue Rapids Shale, in ascending order (Figs. 24,25). Four fifth-order sequences constitute the Crouse sequence, three of which are developed within the Crouse Limestone and one within the Blue Rapids Shale. The base of the Crouse throughout the outcrop area constitutes the transgressive surface of the sequence and locally exhibits a well-developed transgressive lag deposit.

The lower Crouse fifth-order sequence contains a moderately diverse fauna of brachiopods, bryozoans, and crinoids throughout the outcrop area that includes abundant *Ottonosia* algal colonies in central and southern Kansas. Commonly, the *Ottonosia* colonies contain silicified specimens of *Composita* in the nucleus of the algal masses. Evidence of maximum marine flooding in northern and central Kansas is present at the top of the lower Crouse limestone ledge in a fossiliferous shaly wackestone with bryozoans, crinoids, and *Neochonetes* brachiopods. In southern Kansas, only one limestone ledge is present in the Crouse, and maximum flooding is reflected in a fossiliferous wackestone above the *Ottonosia*-bearing interval. Sparse numbers of *Streptognathodus* mark the maximum marine flooding, but this genus is more abundant in central and southern Kansas. In central and northern Kansas, the lower Crouse fifth-order sequence is terminated by black, poorly

fossiliferous shales that are overlain by increasing amounts of silt upward in the section. In southern Kansas, the cycle is capped by a poorly fossiliferous packstone.

The base of the middle Crouse fifth-order sequence coincides with the base of the middle limestone ledge of the Crouse Limestone in northern Kansas. Maximum marine flooding of that cycle is evident near the top of the middle ledge in that region and is represented by ostracodes and bivalves with moderate numbers of the conodont *Sweetognathus*. The base of this sequence coincides with the base of the upper Crouse ledge in central Kansas. There, *Sweetognathus*, pectinid bivalves, and ostracodes dominate the fauna. In southern Kansas, the middle Crouse fifth-order sequence lies above a small shale break above the packstone that terminates the lower Crouse fifth-order sequence. A more open-marine fauna is present, including brachiopods, bryozoans, bivalves, and rare specimens of *Sweetognathus* and *Streptognathodus*.

The top Crouse fifth-order sequence, along with the lower Blue Rapids Shale fifth-order sequence, are exposure cycles that contain an assemblage of shallow-water ostracodes and encrusting foraminifers throughout the outcrop belt.

Evidence of maximum marine flooding of the Crouse fourth-order sequence is coincident with the maximum-flooding surface of the lower Crouse fifth-order sequence. The transgressive systems tract includes strata from the base of the Crouse to the maximum-marine-flooding surface. The forced regressive systems tract includes strata from the maximum-flooding surface to the sequence boundary in the upper Blue Rapids Shale.

Funston Fourth-Order Depositional Sequence

The Funston fourth-order sequence comprises the upper Blue Rapids Shale, Funston Limestone, and most of the Speiser Shale, in ascending order (Figs. 26,27). Four fifth-order sequences make up the Funston sequence, one of which is developed in the top part of the Blue Rapids Shale and three of which are developed in the Funston Limestone. The transgressive surface of the Funston sequence occurs at the base of a regionally correlative limestone in the upper Blue Rapids Shale. This limestone marks the base of the upper Blue Rapids fifth-order sequence and is best developed in southern Kansas. It gradually thins into central and northern Kansas. In southern and central Kansas, this carbonate contains algae, bivalves, and encrusting foraminifers at its base, interpreted to represent maximum marine flooding. In northern Kansas, the unit contains mainly ostracodes and encrusting foraminifers. Conodonts in this fifth-order sequence are restricted to southern Kansas, where they include only rare specimens of *Sweetognathus*. This cycle is terminated by silty, poorly fossiliferous mudstones in central and northern Kansas and by poorly fossiliferous, dark-gray shales in southern Kansas.

The base of the lower Funston fifth-order sequence coincides with the base of the Funston in all areas except along Kansas Highway K-38, where it occurs a few centimeters below the base of the Funston. Maximum marine flooding is marked at the base of the cycle, where a moderately diverse assemblage of crinoids, bryozoans, bivalves, and brachiopods, including *Juresania* and *Derbyia,* is present. Moderate numbers of *Streptognathodus* and *Sweetognathus* typify this horizon. This cycle is terminated by silty, poorly fossiliferous shales in all outcrop regions except southernmost Kansas, where it is denoted by a shaly, poorly fosssiliferous carbonate. In central Kansas, northward to I-70 in northern Kansas, a poorly fossiliferous black shale sharply overlies the lower Funston limestone.

The top two fifth-order sequences contain largely bivalves and gastropods and lack conodonts. The top fifth-order sequence is an exposure cycle overlain by red and green silty mudstones of the Speiser Shale.

Maximum marine flooding of the Funston fourth-order sequence corresponds to the top of the lower Funston fifth-order-sequence maximum-marine-flooding surface. The transgressive systems tract includes strata from the transgressive surface in the upper Blue Rapids Shale to the maximum-marine-flooding surface, and the forced regressive systems tract includes strata from the maximum-flooding surface to the transgressive surface near the top of the Speiser Shale, which marks the base of the Wreford fourth-order sequence.

DISCUSSION AND CONCLUSIONS

Sequence-stratigraphic analysis of outcropping strata of the uppermost Carboniferous and Lower Permian Council Grove Group of the North American Midcontinent strongly suggests a distinctive hierarchy of stratigraphic forcing (Fig. 28). The Council Grove Group represents one composite third-order depositional sequence (1–10 m.y.) and is divisible into nine fourth-order depositional sequences (0.1–1 m.y.). Each fourth-order depositional sequence contains between two to eight high-frequency fifth-order depositional cycles (0.01–0.1 m.y.) that form the parasequences that stack into the retrogradational transgressive systems tract and the aggradational to progradational highstand/forced regressive systems tracts. In total, 38 widely correlatable fifth-order depositional sequences are present in the Council Grove Group.

Several significant trends are noted in this study. Maximum-marine-flooding condensed sections are restricted to sequences of the lower Council Grove Group. These sequences contain the greatest faunal diversity, contain a greater number of high-frequency fifth-order sequences, have a greater stratigraphic thickness, and extend farther landward into Oklahoma. Maximum-marine-flooding surfaces within upper Council Grove Group sequences show much less evidence of condensation and demonstrate deposition in significantly shallower water regimes on the basis of their contained biofacies. Additionally, these sequences contain fewer higher frequency fifth-order sequences, are stratigraphically thinner, and pinch out into terrestrial facies slightly south of the Oklahoma border.

Sea-level-fluctuation curves derived from this study (Fig. 28), combined with the biostratigraphic data obtained through the course of paleoecological investigations, can be used for correlation of these sequences on an interbasinal or a potentially global scale. On the basis of this preliminary outcrop study, we suggest that this type of analysis should lead to a basinwide three-dimensional sequence-stratigraphic analysis that should aid in the search for facies-related stratigraphic traps.

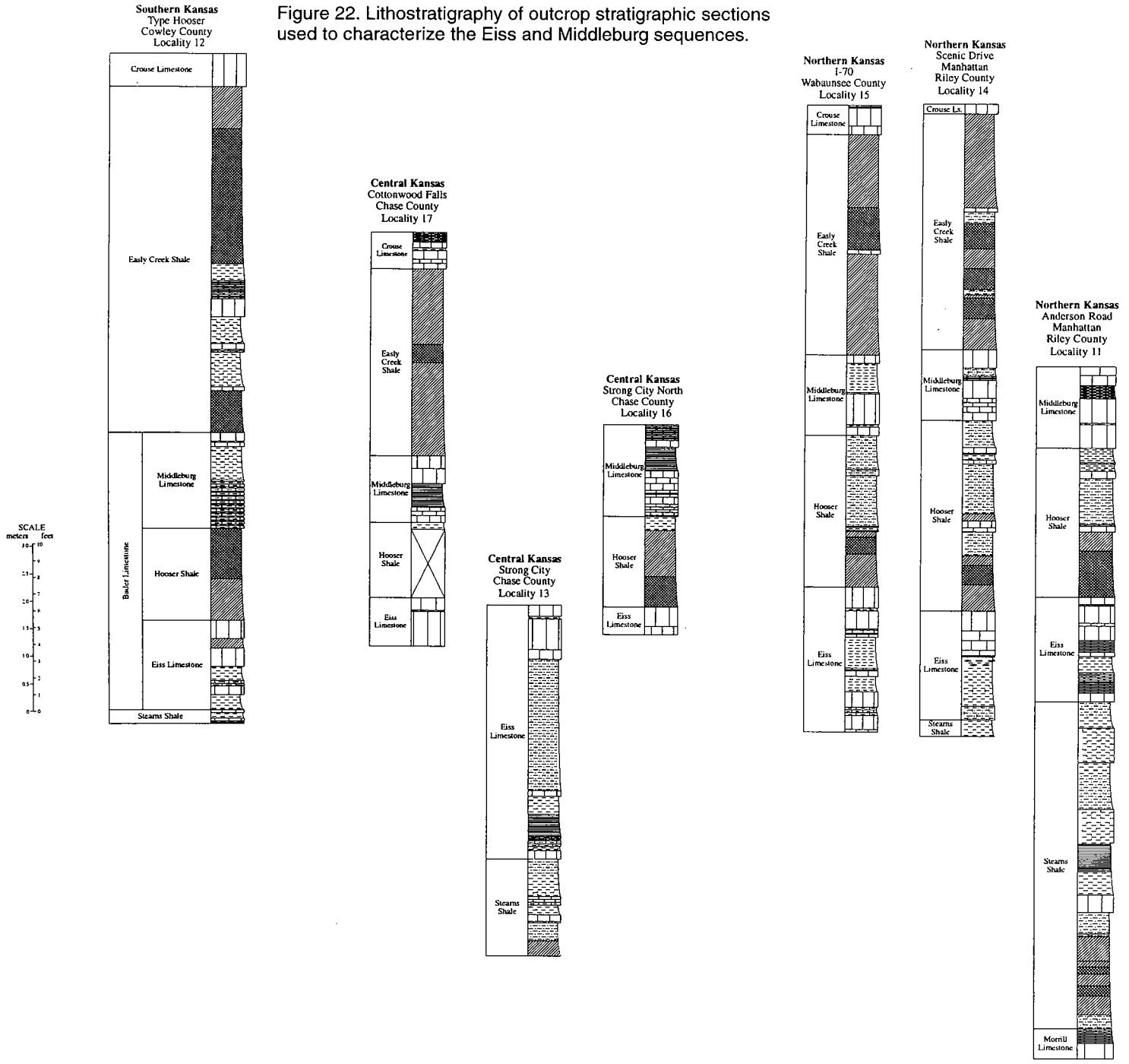

Figure 22. Lithostratigraphy of outcrop stratigraphic sections used to characterize the Eiss and Middleburg sequences.

REFERENCES CITED

Adler, F. J.; Caplan, W. M.; Carlson, M. P.; Goebel, E. D.; Henslee, H. T.; Hicks, I. C.; Larson, T. G.; McCracken, M. H.; Parker, M. C.; Rascoe, Bailey, Jr.; Schramm, M. W.; and Wells, J. S., 1971, Future petroleum provinces of the Mid-Continent, region 7, *in* Cram, I. H. (ed.), Future petroleum provinces of the United States—their geology and potential: American Association of Petroleum Geologists Memoir 15, v. 2, p. 985–1120.

Archer, A. W.; and Feldman, H. R., 1995, Incised valleys and estuarine facies of the Douglas Group (Virgilian): implications for similar Pennsylvanian sequences in the U.S. Mid-Continent, *in* Hyne, N. J. (ed.), Sequence stratigraphy of the Mid-Continent: Tulsa Geological Society Special Publication 4, p. 119–140.

Baars, D. L.; Maples, C. G.; Ritter, S. M.; and Ross, C. A., 1992, Redefinition of the Pennsylvanian–Permian boundary in Kansas, Mid-continent USA: International Geology Review, v. 34, p. 1021–1025.

Boardman, D. R., II; and Heckel, P. H., 1989, Glacial-eustatic sea-level curve for early Late Pennsylvanian sequence in north-central Texas and biostratigraphic correlation with curve for Mid-Continent North America: Geology, v. 17, p. 802–805.

Boardman, D. R., II; and Nestell, M. K., 1993, Glacial-eustatic sea-level fluctuation curve for Carboniferous–Permian boundary strata based on outcrops in the North American Mid-Continent and north-central Texas, *in* Crick, R. (ed.), American Association of Petroleum Geologists, Southwest Section, Transactions and Abstracts, p. 15–25.



Figure 23. North–south sequence-stratigraphic cross section of the Eiss and Middleburg sequences. See Figure 14 caption for explanation of abbreviations.

Figure 24. Lithostratigraphy of outcrop stratigraphic sections used to characterize the Crouse sequence.

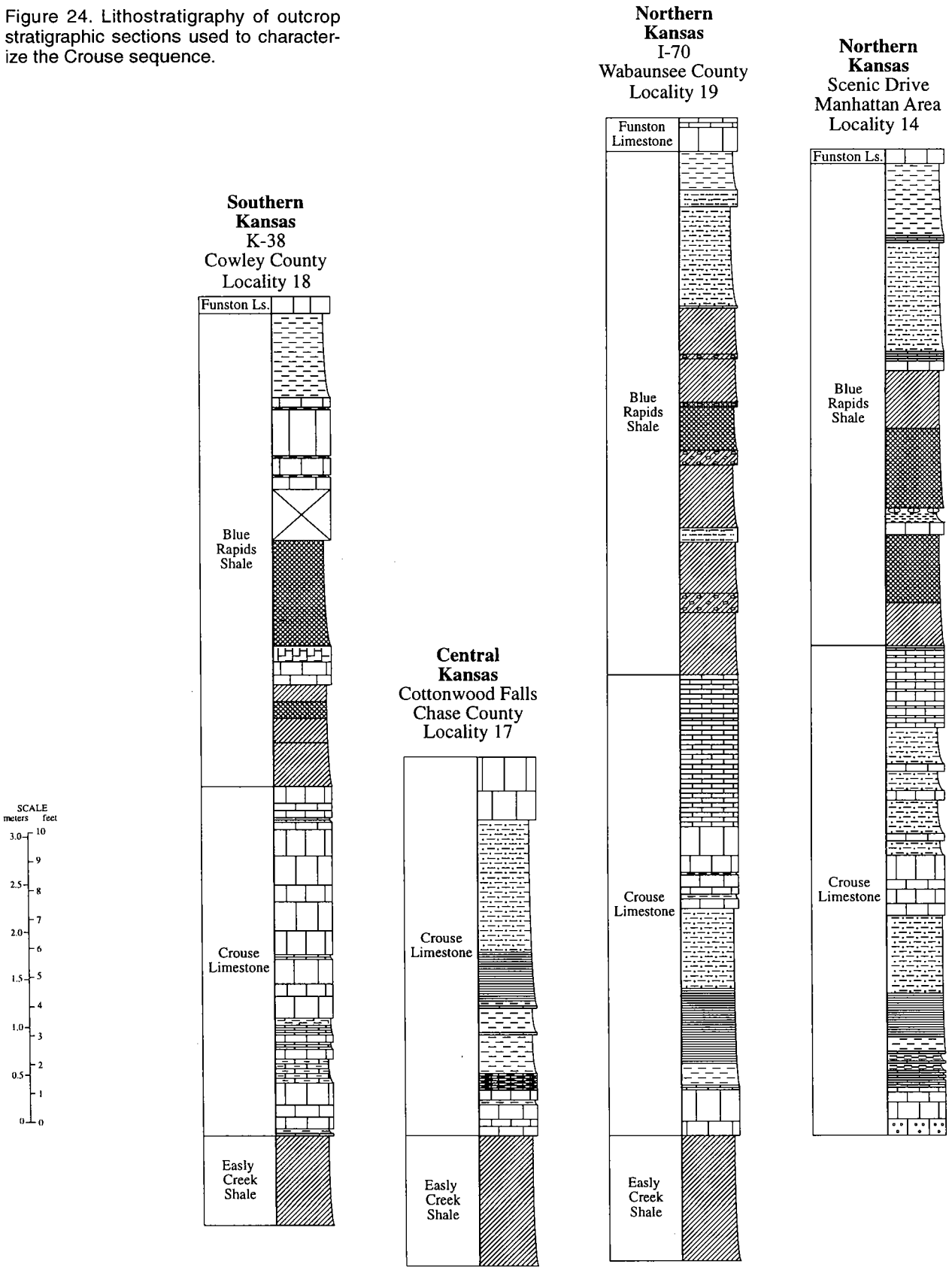

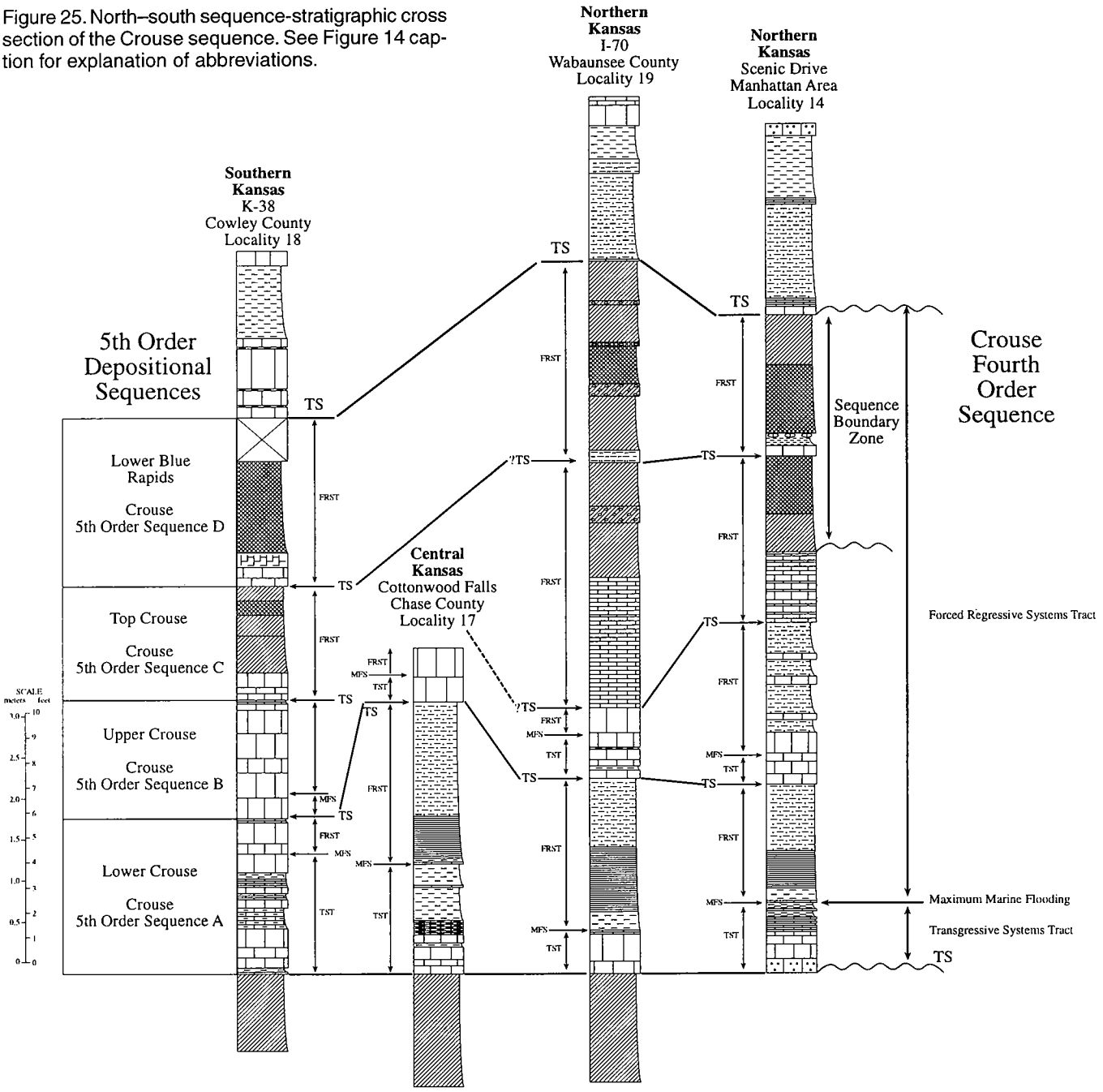

Figure 25. North–south sequence-stratigraphic cross section of the Crouse sequence. See Figure 14 caption for explanation of abbreviations.

Boardman, D. R., II; Mapes, R. H.; Yancey, T. E.; and Malinky, J. M., 1984, A new model for the depth-related allogenic community succession within North American Pennsylvanian cyclothems and implications on the black shale problem, *in* Hyne, N. J. (ed.), Limestones of the Mid-Continent: Tulsa Geological Society Special Publication 2, p. 141–182.

Boardman, D. R., II; Nestell, M. K.; and Knox, L. W., 1995, Depth-related microfaunal biofacies model for Late Carboniferous and Early Permian cyclothemic sedimentary sequences in Mid-Continent North America, *in* Hyne, N. J. (ed.), Sequence stratigraphy of the Mid-Continent: Tulsa Geological Society Special Publication 4, p. 93–118.

Broecker, W. S.; and van Donk, J., 1970, Insolation changes, ice volumes and the O18 record in deep-sea cores: Reviews of Geophysics and Space Physics, v. 8, p. 169–188.

Busch, R. M.; and West, R. R., 1987, Hierarchical genetic stratigraphy—a framework for paleoceanography: Paleoceanography, v. 2, p. 141–164.

Carter, R. M.; Carter, L.; and Johnson, D. P., 1986, Submergent shorelines in the SW Pacific: evidence for an episodic post-glacial transgression: Sedimentology, v. 33, p. 629–649.

Carter, R. M.; Abbott, S. T.; Fulthorpe, D. W.; Haywick, D.W.; and Henderson, R. A., 1991, Application of global sea-level and sequence-stratigraphic models in Southern Hemisphere Neogene strata from New Zealand, *in* Macdonald, D. I. M. (ed.), Sedimentation, tectonics and eustasy-sea-level changes at active margins: International Association of Sedimentologists Special Publication 12, Blackwell Scientific Publications, Oxford, p. 41–68.

Chaplin, J. R., 1996, Ichnology of transgressive–regressive surfaces in mixed carbonate–siliciclastic sequences, Early Permian Chase Group, Oklahoma, *in* Witzke, B. J.; Ludvigson, G. A.; and Day, J. (eds.), Paleozoic sequence stratigraphy: views from the North

American craton: Geological Society of America Special Paper 306, p. 399–418.
Chernykh, V. V.; Ritter, S. M.; and Wardlaw, B. W., 1997, *Streptognathodus isolatus* new species (Conodonta): proposed index for the Carboniferous–Permian boundary: Journal of Paleontology, v. 71, p. 162–164.
Collier, R. E. Ll.; Leeder, M. R.; and Maynard, J. R., 1990, Transgressions and regressions: a model for the influence of tectonic subsidence, deposition and eustasy, with application to Quaternary and Carboniferous examples: Geological Magazine, v. 127, p. 117–128.
Denton, G. H.; and Hughes, T. J., 1983, Milankovitch theory of ice ages: hypothesis of ice-sheet linkage between regional insolation and global climate: Quaternary Research, v. 20, p. 125–144.
Elias, M. K., 1937, Depth of deposition of the Big Blue (late Paleozoic) sediments in Kansas: Geological Society of America Bulletin, v. 48, p. 403–432.
French, J. A.; and Watney, W. L., 1993, Stratigraphy and depositional setting of the lower Missourian (Pennsylvanian) Bethany Falls and Mound Valley limestones, analogues for age-equivalent ooid-grainstone reservoirs, Kansas: Current Research on Kansas Geology, Kansas Geological Survey Bulletin 235, p. 27–39.
Galloway, W. E., 1989a, Genetic stratigraphic sequences in basin analysis I: Architecture and genesis of flooding-surface bounded depositional units: American Association of Petroleum Geologists Bulletin, v. 73, p. 125–142.
_____1989b, Genetic stratigraphic sequences in basin analysis II: Application to northwest Gulf of Mexico Cenozoic basin: American Association of Petroleum Geologists Bulletin, v. 73, p. 143–154.
Goldhammer, R. K.; Dunn, P. A.; and Hardie, L. A., 1987, High frequency glacio-eustatic sea level oscillations with Milankovitch characteristics recorded in Middle Triassic platform carbonates in northern Italy: American Journal of Science, v. 287, p. 853–892.
_____1990, Depositional cycles, composite sea level changes, cycle stacking patterns, and the hierarchy of stratigraphic forcing—examples from platform carbonates of the Alpine Triassic: Geological Society of America Bulletin, v. 102, p. 535–562.
Goldhammer, R. K.; Oswald, E. J.; and Dunn, P. A., 1991, Hierarchy of stratigraphic forcing: Example from Middle Pennsylvanian shelf carbonates of the Paradox basin, *in* Franseen, E. K.; Watney, W. L.; Kendall, C.; and Ross, W., Sedimentary modeling: computer simulations and methods for improved parameter definition: Kansas Geological Survey Bulletin 233, p. 415–430.
_____1994, High-frequency, glacio-eustatic cyclicity in the Middle Pennsylvanian of the Paradox basin: an evaluation of Milankovitch forcing, *in* de Boer, P. L.; and Smith, D. G. (eds.), Orbital forcing and cyclic sequences: International Association of Sedimentologists Special Publication 19, Blackwell Scientific Publications, Oxford, p. 243–284.

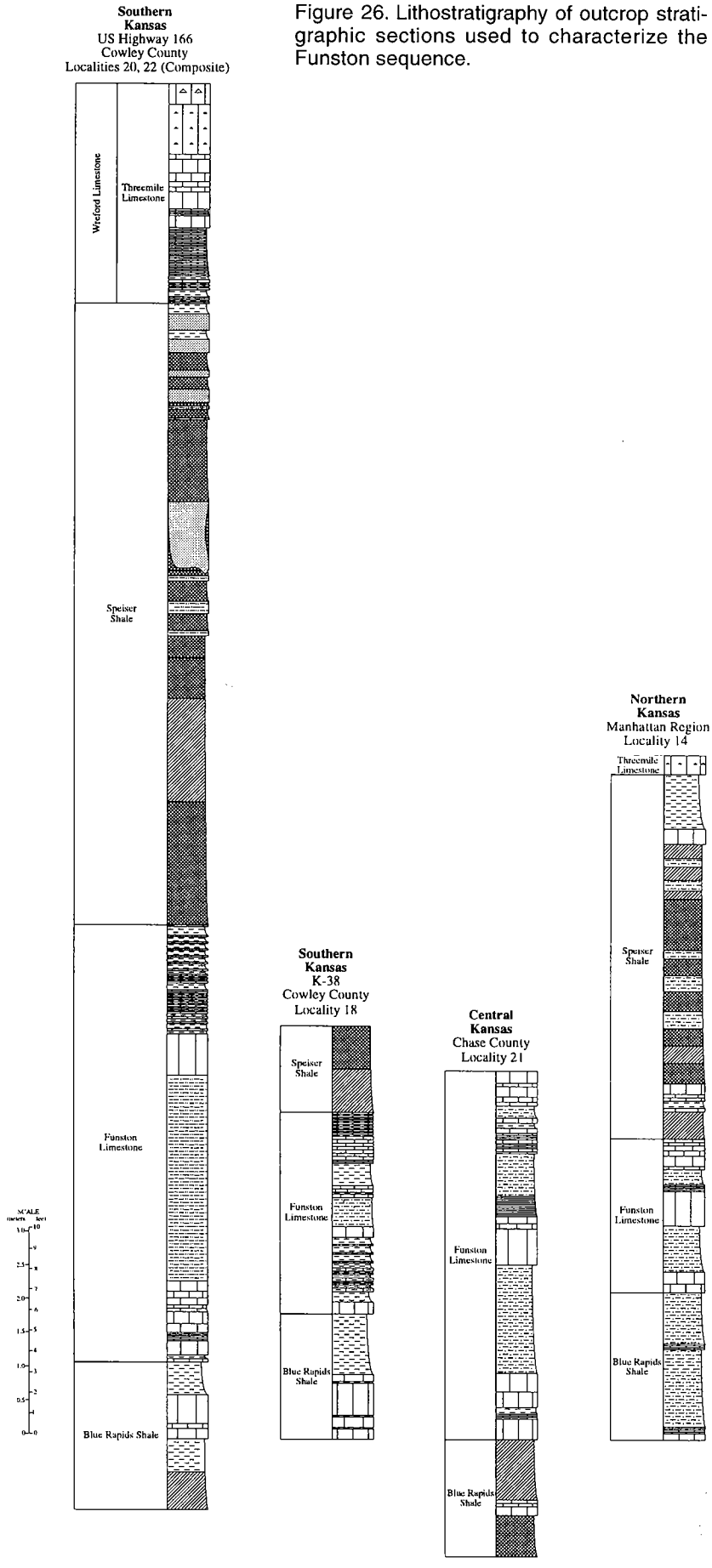

Figure 26. Lithostratigraphy of outcrop stratigraphic sections used to characterize the Funston sequence.

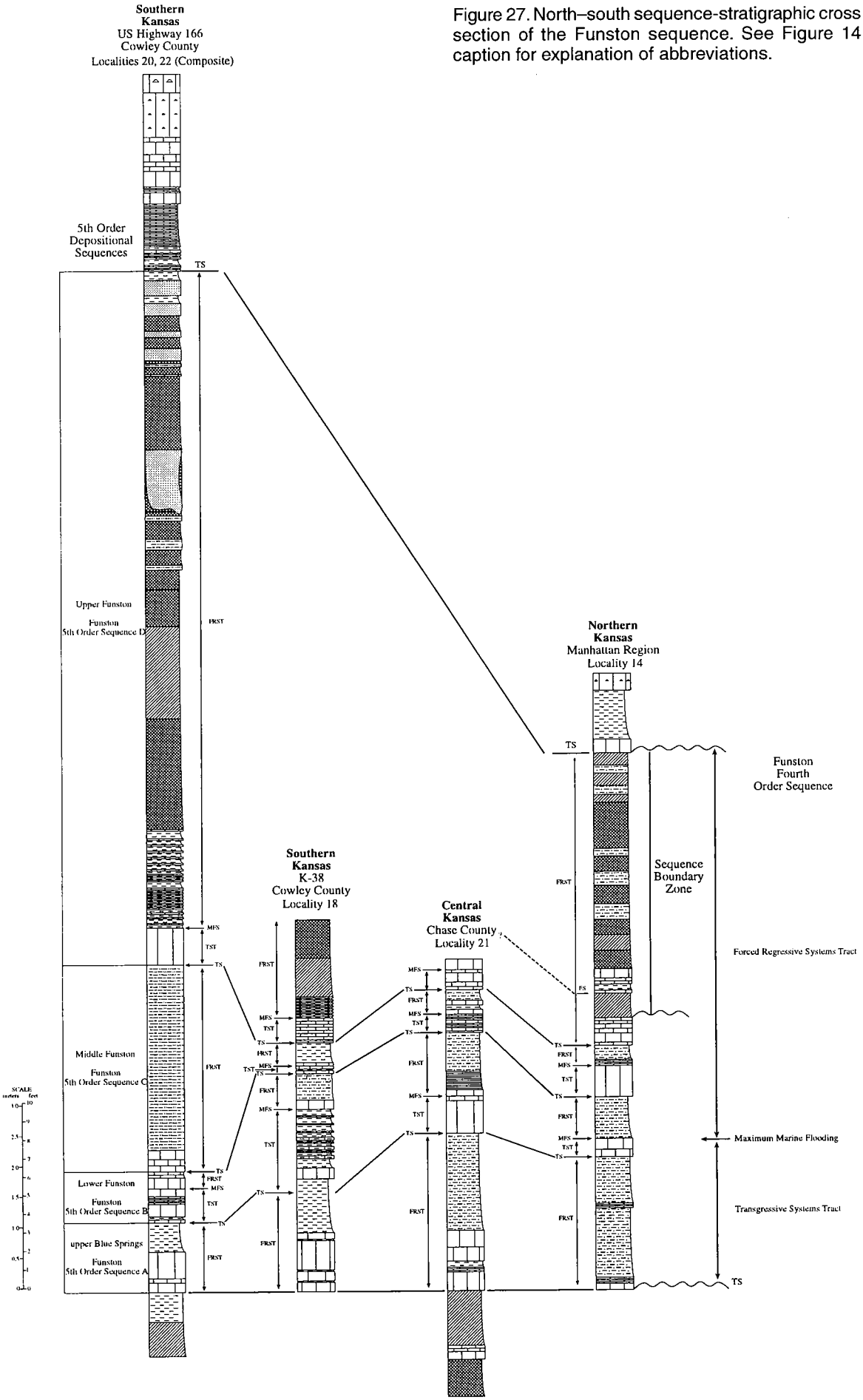

Figure 27. North–south sequence-stratigraphic cross section of the Funston sequence. See Figure 14 caption for explanation of abbreviations.

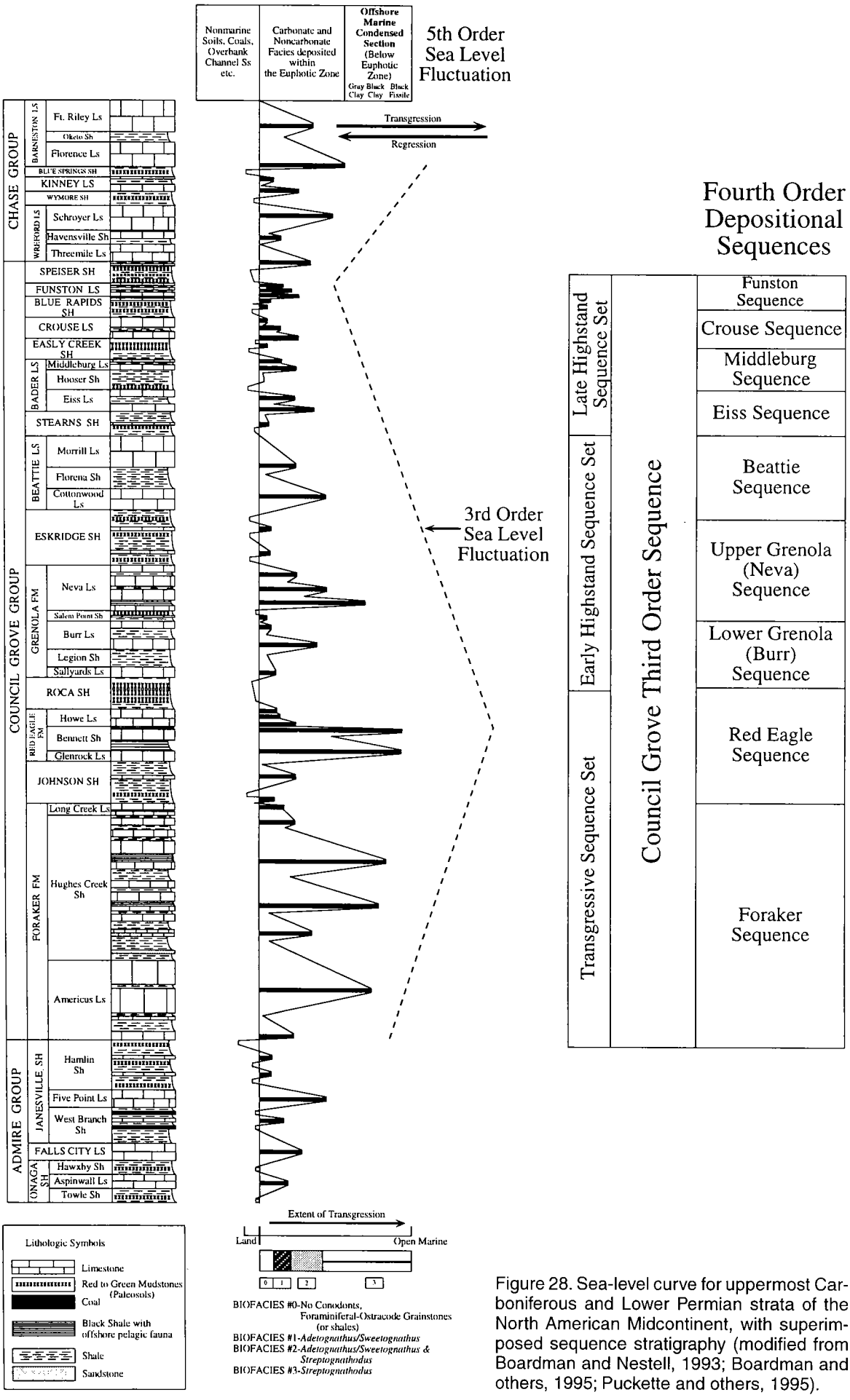

Figure 28. Sea-level curve for uppermost Carboniferous and Lower Permian strata of the North American Midcontinent, with superimposed sequence stratigraphy (modified from Boardman and Nestell, 1993; Boardman and others, 1995; Puckette and others, 1995).

Heckel, P. H., 1977, Origin of phosphatic black shale facies in Pennsylvanian cyclothems of Mid-Continent North America: American Association of Petroleum Geologists Bulletin, v. 61, p. 1045–1068.

_____1986, Sea-level curve for Pennsylvanian eustatic marine transgressive–regressive depositional cycles along Mid-Continent belt, North America: Geology, v. 14, p. 330–335.

Hunt, D.; and Tucker, M. E., 1992, Stranded parasequences and the forced regressive wedge systems tract: deposition during base-level fall—reply: Sedimentary Geology, v. 81, p. 1–9.

_____1995, Stranded parasequences and the forced regressive wedge systems tract: deposition during base-level fall—reply: Sedimentary Geology, v. 95, p. 147–160.

Imbrie, J.; Hays, J. D.; Martinson, D. G.; McIntyre, A.; Mix, A. C.; Morley, J. J.; Pisias, N. G.; Prell, W. L.; and Shackleton, N. J., 1984, The orbital theory of Pleistocene climate: support from a revised chronology of the marine $\delta^{18}O$ record, *in* Berger, A. L.; Imbrie, J.; Hays, J.; Kukla, G.; and Saltzman, B. (eds.), Milankovitch and climate, Part I: D. Reidel, Dordrecht, p. 269–305.

Jervey, M. T., 1988, Quantitative geological modeling of siliciclastic rock sequences and their seismic expression, *in* Wilgus, C. K.; Hastings, B. S.; Kendall, C. G. St. C.; Posamentier, H. W.; Ross, C. A.; and Van Wagoner, J. C. (eds.), Sea-level changes—an integrated approach: Society of Economic Paleontologists and Mineralogists Special Publication 42, p. 47–70.

Joeckel, R. M., 1989, Paleosol stratigraphy of the Eskridge Formation—Early Permian pedogenesis and climate in southeastern Nebraska: Journal of Sedimentary Petrology, v. 61, p. 234–255.

Miller, K. B., 1994, Tuttle Creek Lake spillway exposure: cycle patterns and paleosol profiles: Kansas Geological Survey Open-File Report 94-23, 26 p.

Miller, K. B.; and West, R. R., 1993, Reevaluation of Wolfcampian cyclothems in northeastern Kansas: significance of subaerial exposure and flooding surfaces: Current Research on Kansas Geology, Kansas Geological Survey Bulletin 235, p. 1–26.

Miller, K. B.; McCahon, T. J.; and West, R. R., 1992, Introduction to Lower Permian (Wolfcampian) cycles of Kansas, *in* Project Pangea workshop field-trip guidebook: Lawrence, Kansas, Global Sedimentary Geology Program, International Union of Geological Sciences, p. I1–I47.

Mitchum, R. M., Jr.; and Van Wagoner, J. C., 1991, High-frequency sequences and their stacking patterns: sequence-stratigraphic evidence of high-frequency eustatic cycles: Sedimentary Geology, v. 70, p. 131–160.

Moore, T. C., Jr.; Pisias, N. G.; and Dunn, D. A., 1982, Carbonate time series of the Quaternary and late Miocene sediments in the Pacific Ocean—a spectral comparison: Marine Geology, v. 46, p. 217–233.

Nummedal, D., 1992, The falling sea level systems tract in ramp settings [abstract], *in* Mesozoic of the Western Interior: Society of Economic Paleontologists and Mineralogists Theme Meeting, Fort Collins, Colorado, p. 50.

Nummedal, D.; and Molenaar, C. M., 1995, Sequence stratigraphy of ramp-setting strand plain successions: the Gallup Sandstone, New Mexico, *in* Van Wagoner, J. C.; and Bertram, G. T. (eds.), Sequence stratigraphy of foreland basin deposits—outcrop and subsurface examples from the Cretaceous of North America: American Association of Petroleum Geologists Memoir 64, p. 277–310.

Posamentier, H. W.; Jervey, M. T.; and Vail, P. R., 1988, Eustatic controls on clastic deposition. I.—conceptual framework, *in* Wilgus, C. K.; Hastings, B. S.; Kendall, C. G. St. C.; Posamentier, H. W.; Ross, C. A.; and Van Wagoner, J. C. (eds.), Sea-level changes—an integrated approach: Society of Economic Paleontologists and Mineralogists Special Publication 42, p. 109–124.

Posamentier, H. W.; James, D. P.; and Allen, G. P., 1990, Aspects of sequence stratigraphy: recent and ancient examples of forced regression: American Association of Petroleum Geologists Bulletin, v. 74, p. 742.

Posamentier, H. W.; Allen, G. P.; and James, D. P., 1992, High resolution sequence stratigraphy—the East Coulee Delta, Alberta: Journal of Sedimentary Petrology, v. 62, p. 310–317.

Posamentier, H. W.; Allen, G. P.; James, D. P.; and Tesson, M., 1992, Forced regressions in a sequence stratigraphic framework: concepts, examples, and exploration significance: American Association of Petroleum Geologists Bulletin, v. 76, p. 1687–1709.

Puckette, Jim; Boardman, D. R., II; and Al-Shaieb, Zuhair, 1995, Evidence for sea-level fluctuation and stratigraphic sequences in the Council Grove Group (Lower Permian), Hugoton embayment, southern Mid-Continent, *in* Hyne, N. J. (ed.), Sequence stratigraphy of the Mid-Continent: Tulsa Geological Society Special Publication 4, p. 269–290.

Rascoe, Bailey, 1962, Regional stratigraphic analysis of Pennsylvanian and Permian rocks in the western Mid-Continent (Colorado, Kansas, Oklahoma, Texas): American Association of Petroleum Geologists Bulletin, v. 46, p. 1345–1370.

Rascoe, Bailey; and Adler, F. J., 1983, Permo-Carboniferous hydrocarbon accumulations, Mid-Continent, U.S.A.: American Association of Petroleum Geologists Bulletin, v. 67, p. 979–1001.

Ross, C. A.; and Ross, J. R. P., 1985, Late Paleozoic depositional sequences are synchronous and worldwide: Geology, v. 13, p. 194–197.

_____1987, Late Paleozoic sea levels and depositional sequences, *in* Ross, C. A.; and Haman, D. (eds.), Timing and depositional history of eustatic sequences: constraints on seismic stratigraphy: Cushman Foundation for Foraminiferal Research Special Publication 24, p. 137–149.

Schenk, P. E., 1967, Facies and phases of the Altamont Limestone and megacyclothem (Pennsylvanian), Iowa to Oklahoma: Geological Society of America Bulletin, v. 78, p. 1369–1384.

Scotese, C., 1986, Atlas of Paleozoic base maps—paleoceanographic mapping project: University of Texas, Institute for Geophysics, Technical Report 66, 23 p.

Vail, P. R.; Audemard, F.; Bowman, S. A.; Eisner, P. N.; and Perez-Cruz, C., 1991, The stratigraphic signatures of tectonics, eustasy, and sedimentology—an overview, *in* Einsele, G.; Ricken, W.; and Seilacher, A. (eds.), Cycles and events in stratigraphy: Springer-Verlag, New York, p. 617–659.

Van Wagoner, J. C., 1990, Sequence boundaries in siliciclastic strata on the shelf; physical expression and recognition criteria [abstract]: American Association of Petroleum Geologists Bulletin, v. 74, p. 1774–1775.

Van Wagoner, J. C.; Posamentier, H. W.; Mitchum, R. M., Jr.; Vail, P. R.; Sarg, J. F.; Loutit, T. S.; and Hardenbol, J., 1988, An overview of the fundamentals of sequence stratigraphy and key definitions, *in* Wilgus, C. K.; Hastings, B. S.; Kendall, C. G. St. C.; Posamentier, H. W.; Ross, C. A.; and Van Wagoner, J. C. (eds.), Sea-level changes—an integrated approach: Society of Economic Paleontologists and Mineralogists Special Publication 42, p. 39–46.

Watney, W. L.; French, J. A.; and Franseen, E. K., 1989, Sequence-stratigraphic interpretations and modeling of cyclothems: Kansas Geological Survey and Kansas Geological Society, Guidebook for 41st Annual Field Trip, 211 p.

Youle, J. C.; Watney, W. L.; and Lambert, L. L., 1994, Stratal hierarchy and sequence stratigraphy—Middle Pennsylvanian, southwestern Kansas, U.S.A.: Geological Society of America Special Paper 288, p. 267–285.

APPENDIX
Locality Register

Locality 1. Spillway exposure for Shidler Lake (formerly called Phillips Lake) and adjacent road cut on Oklahoma Highway 18, N½ sec. 10, T. 26 N., R. 6 E., Osage County, Oklahoma.

Locality 2. Road cut on unimproved road north of Foraker, SW¼ sec. 16, T. 29 N., R. 8 E., type locality for Foraker Formation, Osage County, Oklahoma. (Type locality for Foraker Limestone.)

Locality 3. Road cut on Kansas Highway K-38, south line of sec. 21, T. 32 S., R. 8 E., Cowley County, Kansas.

Locality 4. Road cut on north side of Interstate Highway I-70 southwest of Paxico, SW¼SE¼ sec. 27, T. 11 S., R. 11 E., Wabaunsee County, Kansas.

Locality 5. Spillway cut for Tuttle Creek Dam, NE¼ sec. 19, SE¼ sec. 18, T. 9 S., R. 8 E., Pottawatomie County, Kansas.

Locality 6. Quarries on the east side of Burbank, SE¼ and NE¼ sec. 25, T. 26 N., R. 5 E., Osage County, Oklahoma. (Principal reference section for Red Eagle Limestone.)

Locality 7. Road cuts on north side of road from Elmdale to Cottonwood Falls, SE¼SW¼NW¼ sec. 26, T. 19 S., R. 7 E., Chase County, Kansas. (Type locality for Neva Limestone.)

Locality 8. Stream-bank cut just south of Bennet, Nebraska, east of center line of NW¼SW¼NE¼ sec. 10, T. 8 N., R. 8 E., Lancaster County, Nebraska. (Type locality for Bennett Shale.)

Locality 9. Railroad cuts, stream cut bank, and hillside exposures, SE¼SW¼SW¼ sec. 4, T. 31 S., R. 8 E., Cowley County, Kansas. (Type locality for Grenola Limestone.)

Locality 10. Road cut on north side of Kansas Highway 18 (Fort Riley Boulevard) west of Manhattan, SW¼ sec. 23, T. 10 S., R. 7 E., Riley County, Kansas. (Co-type locality for Grenola Limestone.)

Locality 11. Road cut on both west and east sides of Anderson Road in Manhattan, Kansas, W½ sec. 10, T. 10 S., R. 7 E., Riley County, Kansas.

Locality 12. Stream-bank cut directly east of Cowley County Road 7 near Hooser, Kansas, NW¼NW¼ sec. 36, T. 33 S., R. 7 E., Cowley County, Kansas.

Locality 13. Road cut on east side of Highway 177 on northeast side of Strong City, 200 m south of its intersection with U.S. Highway 50, S½NW¼ sec. 17, T. 17 S., R. 8 E., Chase County, Kansas.

Locality 14. Road cut on east side of Scenic Drive in Manhattan, Kansas, NW¼ sec. 22, NE¼ sec. 21, T. 10 S., R. 7 E., Riley County, Kansas.

Locality 15. Road cut on north side of Interstate 70, center of north line of SE¼ sec. 30, T. 11 S., R. 10 W., Wabaunsee County, Kansas.

Locality 16. Road cut on west side of U.S. Highway 177 at a point 2.9 mi north of its intersection with U.S. Highway 50, center of east line of sec. 31 (long section), T. 18 S., R. 8 E., Chase County, Kansas.

Locality 17. Road cut on south side of road from Elmdale to Cottonwood Falls, 1.8 mi west of its intersection with U.S. highway 177, NE¼ sec. 30, T. 19 S., R. 8 E., Chase County, Kansas.

Locality 18. Road cut on both sides of Kansas Highway K-38, NW¼ sec. 30 (long section), T. 32 S., R. 8 E., Cowley County, Kansas.

Locality 19. Road cut on north side of Interstate 70, center of north line of SW¼ sec. 29, T. 11 S., R. 10 W., Wabaunsee County, Kansas.

Locality 20. Road cut on eastbound lane of U.S. Highway 166, NW¼ sec. 11, T. 34 S., R. 7 E., Cowley County, Kansas.

Locality 21. Road cut on east side of U.S. Highway 177 at a point 5.3–5.5 mi north of its intersection with U.S. Highway 50, NW¼ sec. 20, T. 18 S., R. 8 E., Chase County, Kansas.

Locality 22. Road cut on north side of westbound lane of U.S. Highway 166, NE¼ sec. 11, T. 34 S., R. 7 E., Cowley County, Kansas.

Environments of Deposition for Clear Fork and Glorieta Formations, North Robertson Unit, Gaines County, Texas

James Kamis
Texaco, Inc.
Midland, Texas

William Dixon
Fina Oil and Chemical Company
Houston, Texas

Richard Vessell
David K. Davies & Associates, Inc.
Kingwood, Texas

ABSTRACT.—This paper documents depositional environments of the Permian Clear Fork and Glorieta Formations in the North Robertson Unit (NRU) in Gaines County, Texas. The NRU has a project area of 5,633 acres, and contained a total of 270 wells as of October 1996. This includes 156 active producing wells, 113 active injection wells, and 1 water-supply well. Production is from the Glorieta and Clear Fork Formations, which are Permian carbonates. The hydrocarbon-bearing interval extends from the base of the Glorieta to the base of the lower Clear Fork, between correlative depths of approximately 6,160–7,200 ft. The trapping mechanism is primarily structural and lies along the northern part of the Robertson field anticline; however, significant variations in stratigraphic and rock quality across the unit influence the sites of hydrocarbon accumulations.

NRU Clear Fork and Glorieta rocks were deposited in a broad, shallow carbonate bank, developed along the northwestern part of a regionally extensive platform, the Central Basin platform (CBP). Paleostructures on the CBP, such as the Pennsylvanian Robertson anticline, and frequent sea-level fluctuations during Permian time, were both important factors in shaping a complex and diverse network of depositional environments at the NRU. These environments included continental, supratidal, tidal flat, restricted lagoon, island, open lagoon, bioherm, reef, shoal, intershoal, and open shelf.

INTRODUCTION

This work is part of an extensive multidisciplinary reservoir-characterization study (Davis & Associates, 1996a,b) funded in part by the U.S. Department of Energy (DOE) as a Class II—Shallow-Shelf Carbonate Study. It is the combined effort of many people from different companies and disciplines.

The work led to the discovery of an extremely interesting aspect of the paleoclimatic conditions at the time of deposition. Several previous articles (Silver and Todd, 1969; Handford and Fredericks, 1980; Handford, 1981; Mazzullo, 1982), and all the companies contacted during the course of this study, indicated that the NRU Clear Fork and Glorieta paleoclimate was either semiarid or arid, representative of a sabkha-like setting, with little or no fresh water, and nearly void of plant growth.

In contrast, current work strongly suggests that this was a humid and hot time period, during which the presence of abundant fresh water supported dense plant growth and helped create extensive dissolution/diagenetic features. These conclusions are based on core information, such as abundant fine to coarse plant debris of varying species throughout most of the 1,200-ft pay section, several 2-in. coal beds, root traces, large intact fern leaves, large palm leaves, erosion-surface lag gravels on top of open solution fractures, and 40-ft-thick alteration and/or collapse breccias.

PROJECT PURPOSE

The overall thrust of the project was that "geologically targeted" infill drilling could optimize economics for each new well in an infill-drilling program. Blanket drilling in shallow-shelf, heterogeneous, low-permeability carbonate reservoirs of west Texas is not always prudent or warranted because of the highly variable reservoir quality. Performing a pre-drilling detailed reservoir-characterization study is the key to designing and implementing an economic infill-drilling program. Understanding the types of depositional environments, their distribution in time and space, and their relationship to engineering parameters and productivity is an important aspect of the detailed reservoir-characterization study.

Kamis, James; Dixon, William; and Vessell, Richard, 2000, Environments of deposition for Clear Fork and Glorieta Formations, North Robertson Unit, Gaines County, Texas, *in* Johnson, K. S. (ed.), Platform carbonates in the southern Midcontinent, 1996 symposium: Oklahoma Geological Survey Circular 101, p. 307–317.

HISTORICAL PERFORMANCE—UNIT PRODUCTION AND INJECTION

Production from the North Robertson field area (Fig. 1) began in the early 1950s with 40-acre primary well development. This 40-acre primary development resulted in 141 wells producing from the Permian Clear Fork and Glorieta Formations by 1965 (Fig. 2). The NRU was formed effective March 1987 for the purpose of implementing waterflood and infill-drilling operations, and nominal well spacing was reduced from 40 to 20 acres. At the time of unitization, oil production from the unit area was approximately 670 stock-tank barrels per day (STB/D), with a gas/oil ratio (GOR) of 1,550 standard cubic feet per stock-tank barrel (SCF/STB), and water production of 500 barrels of water per day (BW/D). Secondary-recovery operations were initiated after unitization and in conjunction with infill drilling. Most of the 20-acre infill drilling was completed between unitization and the end of 1991. The cumulative produced and injected fluid volumes are summarized in Table 1 and illustrated in Figure 3, which shows the production and injection history of the unit from development in 1956 through the initiation of a targeted 10-acre well-infill program in April 1996.

At the time of unitization, the estimated ultimate recovery (EUR) for primary production was 20.5 STB, and the secondary- to primary-recovery ratio was estimated to be approximately 1:1. The current waterflood utilizes an east–west staggered line drive (regular five-spot) pattern with 20-acre nominal well spacing. Unit production rates in April 1996 were 2,757 STBO/D, 1,130 MCF/D, and 12,700 BW/D. Unit oil production after the recent infill program is approximately 3,600 STBO/D. Water-injection volumes are approximately 19,000 BWI/D, with injection water composed of produced water and fresh water obtained from a water-supply well within the unit.

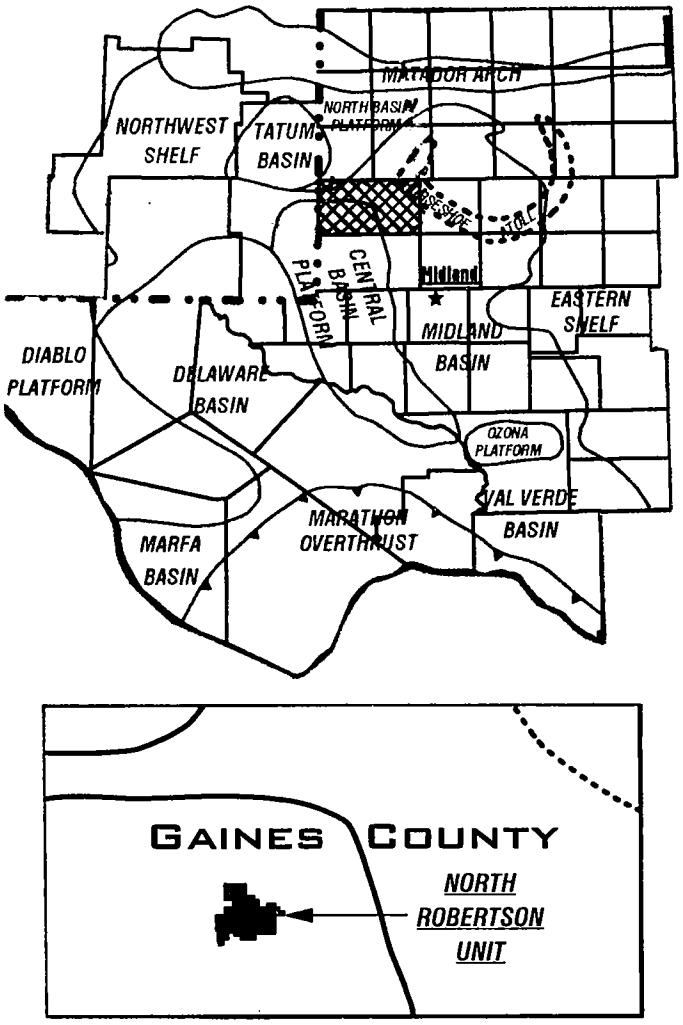

Figure 1. Location of North Robertson Unit in Gaines County, Texas.

CORING PROCEDURE

During the course of this work, we acquired and described 2,730 ft of new core, described 7,918 ft of existing core, and analyzed a total of 300 thin sections. Fina geologists obtained high-quality data from the new core by following these procedures:

1. To prevent the usual caustic flood and wettability change caused by high-pH drilling fluids, the mud was conditioned prior to reaching core point to a pH of 7.0, with low water loss, and a viscosity of 45.

2. The core bit was rotated at 60–80 RPM, with weight on the bit of 7,000–10,000 lb.

3. Only 58 ft was cut on 60-ft barrels to reduce jamming and compaction damage to the core and to facilitate extraction from the barrel.

4. The core was removed from the inner barrel by Fina personnel and immediately loaded into 5-in. PVC tubes open on one end. Approximately 2 quarts of degassed lease crude oil was added to the tubes, and then they were sealed with rubber end caps.

5. After transport to the laboratory, the core was carefully laid out by Fina personnel, one tube at a time, ensuring that care was taken to accurately fit the core back together, mark depths, and record lost intervals. The marking and sampling procedures are shown in Figure 4.

6. It was imperative to open and work on only one tube at a time. When warranted, a 1.5- by 3-in. special core-analysis (SCAL) plug was taken by Fina personnel across potential reservoir intervals and important rock types. The SCAL plugs were cut in degassed reservoir oil. These plugs were stored in sealed containers filled with degassed lease crude to preserve the native state of the rock characteristics and fluid content. Trimmed ends were measured by Core Laboratories, Inc., for porosity, air permeability, and grain density. Selected trimmed ends were made into thin sections to assist in the study of the relationship between pore geometry and relative permeability.

7. Plugs 1 by 0.75 in. were taken *every* foot, exactly 0.1 in. below the foot mark. Core Laboratories, Inc., measured porosity, air permeability, and grain density from these plugs using quick-turnaround techniques (typically 24–48-hour processing). This technique was most useful in providing timely and reasonably accurate data for monitoring reservoir quality and stratigraphic position. These data were loaded into the

Table 1.—North Robertson Unit Historical Production and Injection

Time frame	Oil produced (MMSTB)	Water produced (MMBW)	Water injected (MMBW)
As of 1987	17.5	8.2	0.0
1987–96	9.2	27.6	63.4

Terrasciences workstation (Terrasciences, 1994), depth-corrected to the logs, and used principally to normalize the porosity tools and to refine porosity–permeability algorithms.

8. Samples for whole-core analysis were selected by Fina personnel from the reservoir intervals. These samples provide porosity and permeability data from a larger and potentially more representative part of the reservoir. The samples were nicked with the rock saw to ensure that the core piece could be reoriented with the rest of the core after the core analysis.

9. Samples for crushed fluid analysis must be taken with a saw cut only partway through the core in order to preserve the slab side, as shown in Figure 4.

10. General descriptions were made at Core Laboratories, Inc., by Fina geologists of oil staining; bleeding of oil, gas, or water; reservoir quality; and lithology.

11. Fina personnel slabbed all core at their own facility to ensure that core pieces were not out of place, upside down, marked incorrectly, or with lost intervals. Experience has shown that these are common problems associated with production slabbing by vendors as opposed to slabbing by the end user. The result of these problems is often an inaccurate or incomplete core description.

12. Fina geologists completed core descriptions of the slabs, frequently utilizing thin-section descriptions completed by geologists at David K. Davies & Associates, Inc.

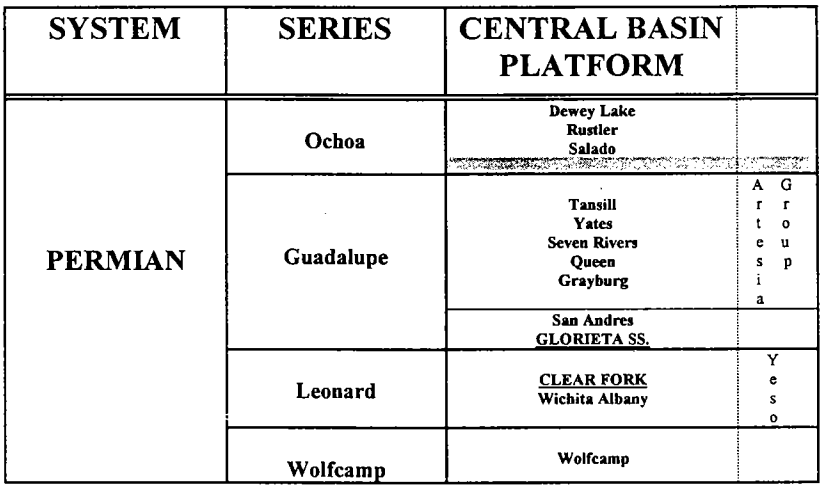

Figure 2. Stratigraphic chart for Permian rocks on the Central Basin platform.

This rock work formed the basis for generating our initial depositional model. At this point, it was important to use all other available geologic and engineering data in an attempt to refine and test the rock-based depositional model.

Such information and activities included the petrophysical analysis of 106 wells with modern log data (David K. Davies & Associates, Inc.) and picking tops for 20 fifth-order upward-shallowing carbonate cycles in all wells. This work also included the correlation of historical performance with environment of deposition and reservoir-rock type, and the generation of conformance cross sections, including injection profiles, after-fracture tracer logs, and cased-

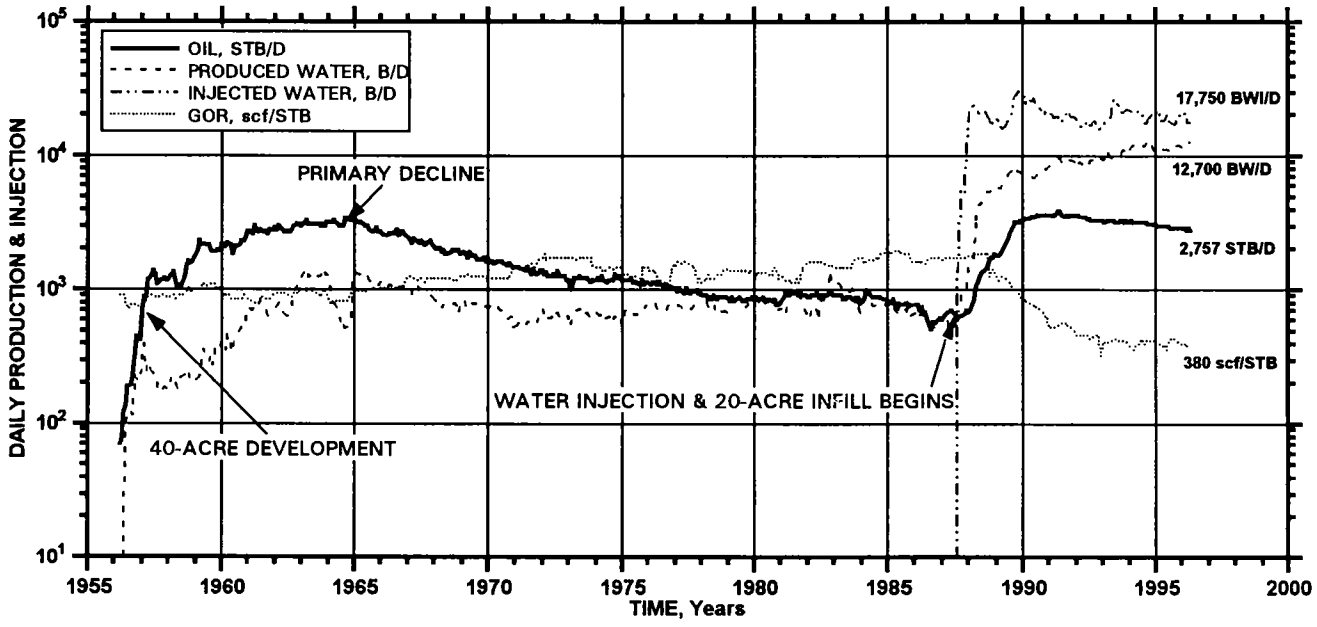

Figure 3. North Robertson Unit historical production and injection data, 1956 to May 1996.

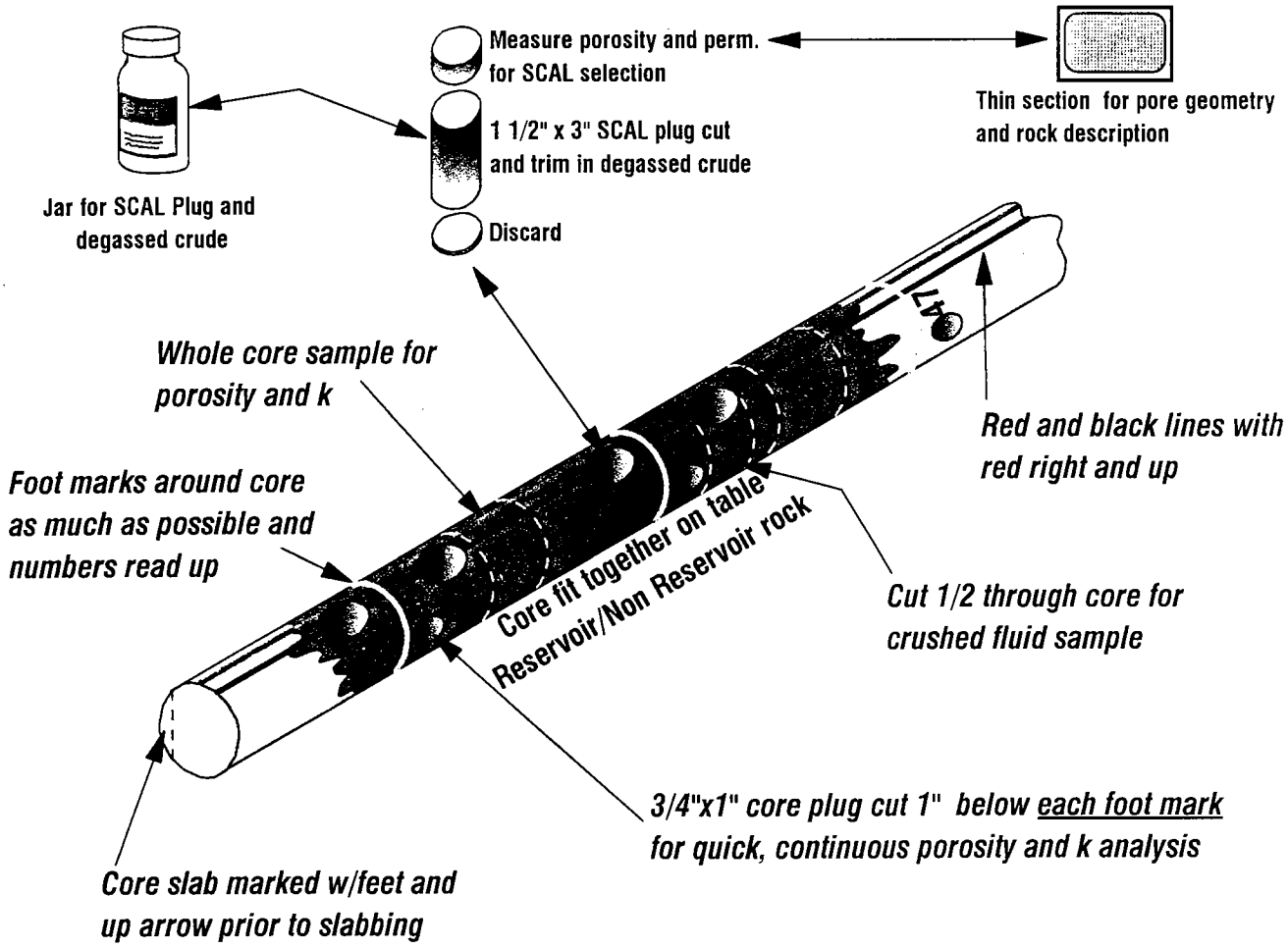

Figure 4. Procedures for marking and sampling of cores delivered to laboratory; k = permeability.

hole pulsed neutron logs. In addition, the comparison of minipermeameter permeability and porosity readings on slabbed sections of the core with quick-plug and whole-core data, and the creation of hundreds of cross sections and thousands of maps, were part of the overall effort to refine the model.

It is remarkable, given the vast array of modern logs from new wells at the NRU (Table 2), that we have not been able to predict depositional facies from open-hole logs. Detailed rock work remains the single most important means of establishing a three-dimensional (3-D) picture of depositional environments. This fact is important because it became apparent during the course of this project that geologists from many companies have abandoned rock examination in determining depositional environments. An approach that employs a cursory check of the rock data, and an assumed or preconceived environment of deposition, followed by exhaustive open-hole log and 3-D seismic studies, generally results in an inaccurate and/or poorly defined depositional model.

ENVIRONMENTS OF DEPOSITION

Individual depositional environments are discussed below, and their unique spatial interrelationship is illustrated in Figure 5. Comments concerning the typical reservoir quality for each depositional environment are included in these discussions. It is important to note that reservoir quality of the NRU Clear Fork and Glorieta rocks is a function of both depositional environment and post-depositional diagenesis. Even though the two are commonly interrelated, this is not always the case. The reader is directed to published reports by David K. Davies & Associates, Inc., listed in the references, for a more in-depth discussion of pore-family types, diagenetic history, and reservoir quality.

Open Shelf

Grainstone–wackestone sediments that are bioturbated to burrowed, having varied types of allochems, and are interpreted to have been deposited seaward (east) of reefs and bioherms, have been classified as open shelf.

Shoal

Grainstone deposits with allochems composed primarily of fusulinids, bryozoans, unrecognizable skeletal constituents, peloids, and rare oncolites occur throughout the Clear Fork and Glorieta section (Fig. 6A). They are typically void of sedimentary structures, owing in part to dolomitization, which has obscured or obliterated original features. Even so, scattered burrows, scour and fill features, abundant graded bedding, and basal rip-up clasts were observed. Only rare individual

beds contained all the aforementioned sedimentary structures. A lack of significant depositional anhydrite in either the nodular or finely distributed parts implies that these grainstones were deposited in more open-marine conditions. A lack of carbonate mud implies a higher energy environment. The most likely interpretation for this broad category of rocks is a shoal environment. These rocks typically contain abundant and uniformly distributed biomoldic and intercrystalline porosity, and as a result are typically the best reservoir rocks, except where they are found proximal to reefs or bioherms. Shoals are most abundant and best developed within the lower Clear Fork along the eastern side of the NRU. This is in an area thought to have been influenced by strong waves and currents, perhaps in a seaway between the NRU and the more distinctly shelf-edge carbonates of Seminole field.

Table 2.—Logs Run at North Robertson Unit

Development wells	20-acre infill wells	10-acre infill wells
Old electric logs and micrologs	Compensated neutron	Compensated neutron
Gamma-ray–neutron logs	Litho-density	Litho-density
Sonic Δt	Dual laterolog	Dual laterolog
Gamma ray	Gamma ray	Micro-SFL, Microlaterolog
		Sonic Δt, full waveforms
		Spectral gamma ray
		Dielectric (Western Atlas)
		NMR (Numar)
		CBIL (Western Atlas)
		EMI (HLS)

Fusulinid Shoal

Grainstone shoal deposits, with fusulinids (*Parafusulina*) as the dominant allochem, have been given a separate name for two reasons: they have a distinctly different appearance (Fig. 6B), and they typically have a strong bimodal distribution of porosity. This is due to the presence of both fusumoldic and intercrystalline porosity. Permeability varies greatly. Fusulinid shoals with variable size and a high density of test solution pores (Fig. 6C) are best developed on the eastern, more open-marine side of reefs and bioherms. More uniform, smaller size fusulinids (*Schubertella* type) are found in the sheltered area behind the reef areas.

Intershoal

Intershoal regions exist laterally to grainstone shoals and contain greater amounts of muddy carbonate material and correspondingly lesser amounts of allochem material. Oncoids that are 2–5 mm in diameter occur in this environment, possibly as a result of the gentle rolling action of allochems in protected areas between topographically higher carbonate sand waves (shoals). Typically, these sediments are darker, reflecting a higher mud content (Fig. 6D). Distinguishing the difference between shoal and intershoal rocks is difficult because of the subtle gradational nature of these two environments.

Reef Center

Striking in their appearance were portions of the core that contained abundant amounts of large, well-preserved bryozoans and rugose corals encased in a dark carbonate-mud matrix (Fig. 6E,F). The bryozoans and corals were not rounded or significantly abraded, implying that they had not been transported any great distance. In close association with this interval, we observed a variety of clams, brachiopods, gastropods, crinoids, and fusulinids. All these species were larger and more numerous than we observed in any other part of the core. This sequence is interpreted as wave-resistant framestone reef centers. Reefs are best developed in the lower Clear Fork and best preserved in the limestone portion of the section. Similar reefs occur in the rest of the Clear Fork but are not as well developed and are referred to as *bioherms* in this paper. Reservoir quality is poor to nonexistent in all the reefs observed.

Reef Talus

Directly adjacent to the reef (on the lagoonal side), grainstones were deposited that exhibit prominent bedding planes dipping steeply away from the reef at up to 30° (Fig. 7A). It is not uncommon to find rounded clasts (2–4 in. diameter) of consolidated reef debris incorporated into these grainstones (Fig. 7B). Some of the clasts have undergone several periods of rolling, based on the occurrence of multiple coated layers that covered irregular parts of the clasts. A few of the clasts were covered on one side by unidentified encrusting algae. This sequence is interpreted as a reef talus, deposited primarily during storms. The reservoir quality is variable, increasing away from the reef core, but typically poor.

Reef-Debris Apron

Complexly interbedded with the reef talus and encircling the reefs, largely around the lagoonal side, are deposits of grainstones. Allochems from these grainstones are typically composed of reef-building animals; however, they also contain significant amounts of fusulinids and unidentifiable skeletal constituents. Internal sedimentary structures, such as burrowing and bedding, are conspicously absent within these deposits (Fig. 7C). We interpret these deposits as reef-debris aprons. For a few selected upward-shallowing sequences, the debris aprons from separate reefs appear to have coalesced with one another, forming areally extensive blankets of grainstone debris (Fig. 5). These debris aprons are typically excellent reservoirs, except in proximal position to the reef center.

Open Lagoon

Wackestone–packstone rocks that are typically bioturbated to burrowed, lack finely distributed anhydrite, and occur stratigraphically landward of the debris aprons but seaward of the restricted-lagoon rocks have been classified as open lagoon (Fig. 5). Open-lagoonal dolostones are an important

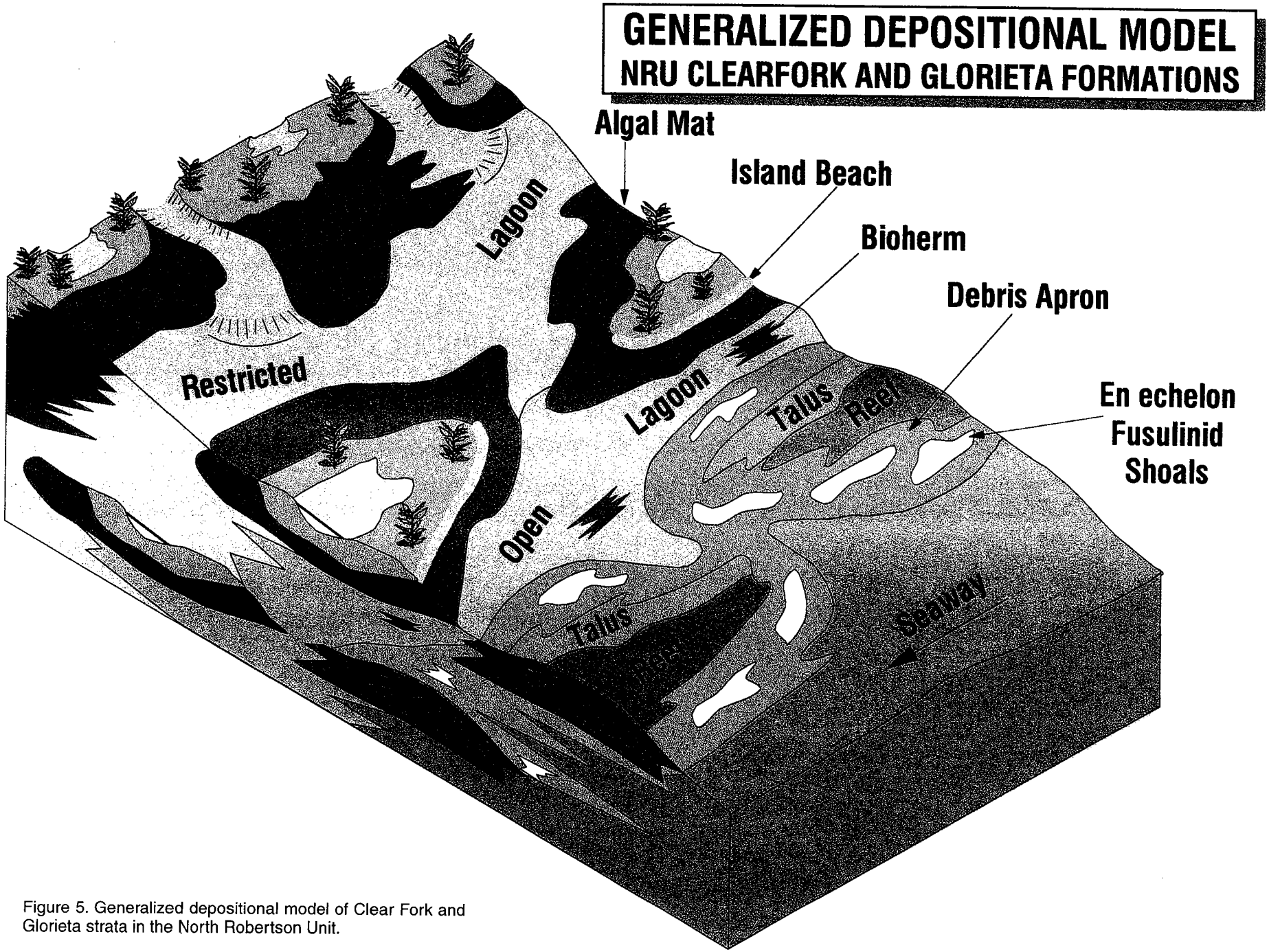

Figure 5. Generalized depositional model of Clear Fork and Glorieta strata in the North Robertson Unit.

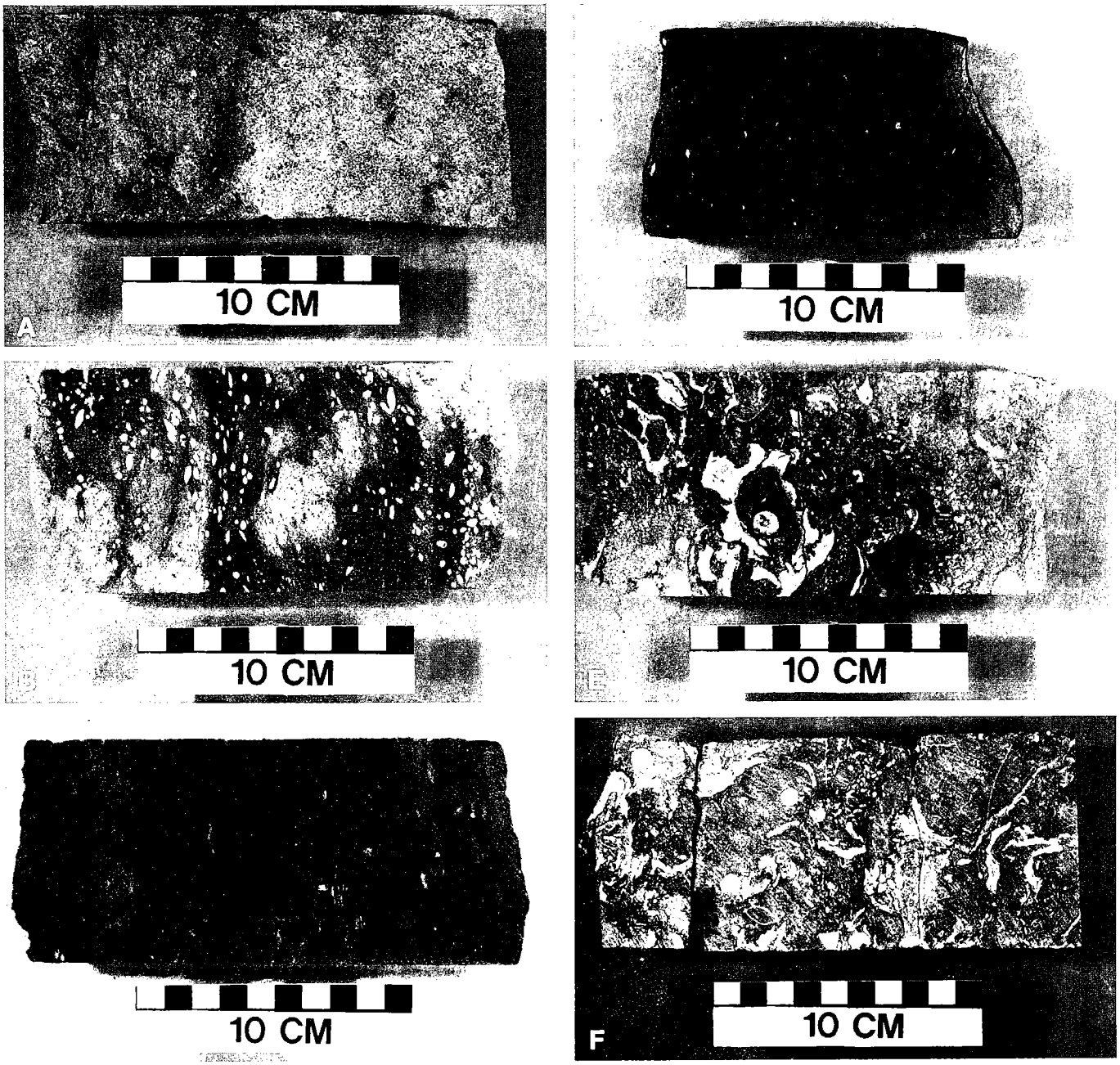

Figure 6. (A) Shoal grainstone of pellets and numerous fossil allochems. NRU 3319 (7,209.3–7,209.7 ft). (B) Fusulinid shoal composed of pellets and fusulinids (*Parafusulina* spp.). NRU 1509 (7,252.2–7,252.8 ft). (C) Fusulinid shoal with test solution pores, some filled with anhydrite. NRU 1509 (7,212.9–7,213.6 ft). (D) Intershoal wackestone–packstone with pellets and fossil fragments and varying amounts of lime mud. NRU 3319 (7,210.9–7,211.3 ft). (E) Reef robust to laterally expanded cyclostome bryozoans (*Dybowskiella* spp.) with thin-shelled brachiopods. NRU 1509 (7,279.8–7,280.1 ft). (F) Reef with rugose coral (upper left) and dense white bryozoan (*Cyclotrypa* spp.) in near-growth position. NRU 1509 (7,281.9–7,282.5 ft).

portion of the reservoir interval. They have moderate porosity and permeability values, are thick and widespread, and represent a significant part of the total rock volume.

Bioherm

Less striking in appearance than the reef, but still uniquely different from all other sequences, especially with regard to fossil content, are the bioherms. They contain *Archimedes* bryozoans and small, poorly developed bryozoans, crinoids, and fusulinids. These rocks have a mottled appearance owing to the color difference between binding carbonate mud and the fossils. Unlike the reefs, these bioherms are not associated with talus; however, they are typically associated with debris aprons. These aprons are thinner and less well developed than the reef aprons. These bioherms were not wave resistant, and, as such, developed in protected marine conditions.

Restricted Lagoon

Wackestone–packstone sequences containing significant amounts of finely distributed early(?) anhydrite, abundant

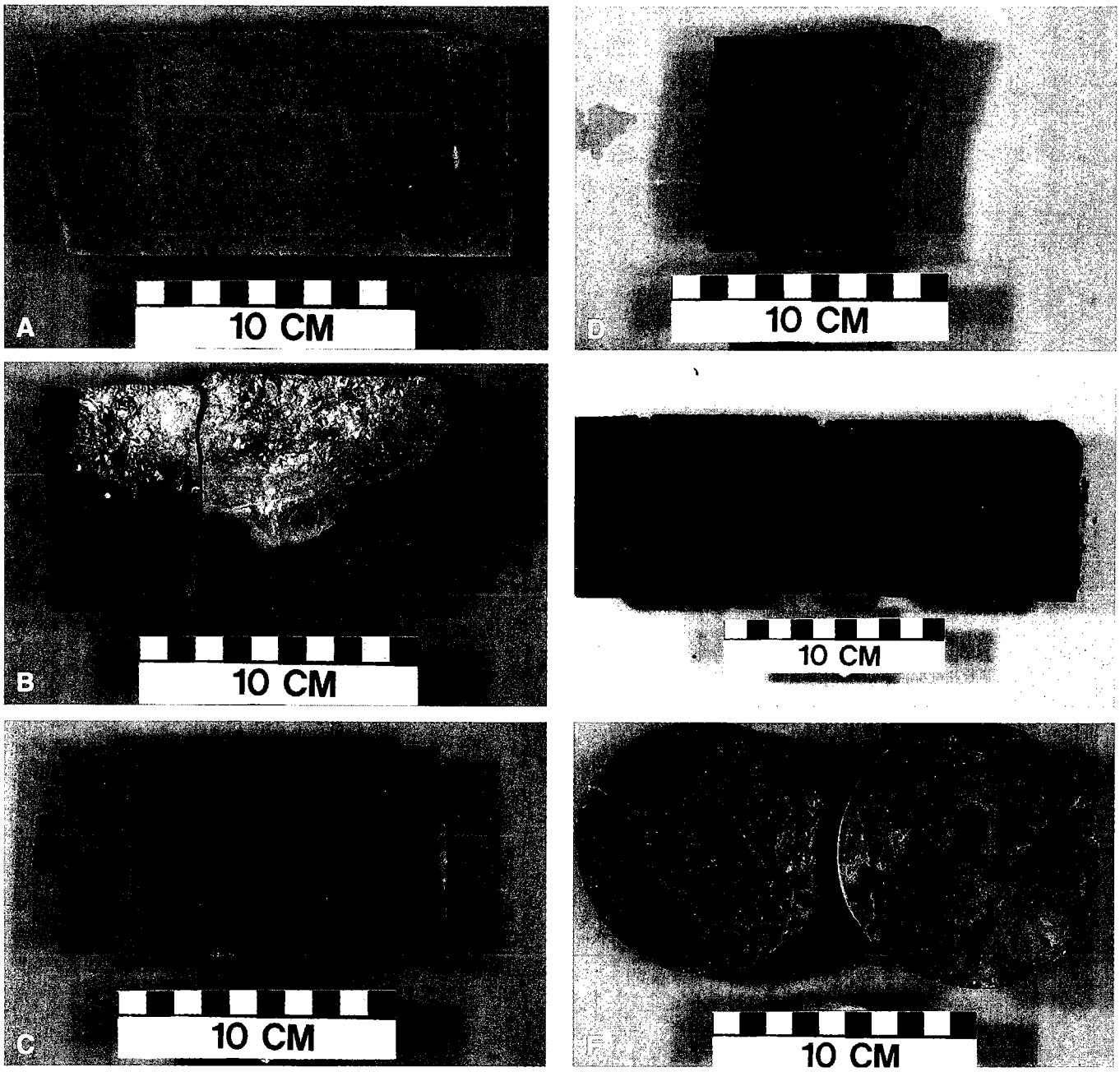

Figure 7. (A) Reef-talus grainstone with prominent bedding. NRU 1509 (7,227.0–7,227.5 ft). (B) Clast of reef talus, probably deposited by storm-wave action. NRU 1509 (7,219.7–7,220.1 ft). (C) Reef-debris-apron grainstone of numerous allochems. NRU 1510 (7,173.3–7,176.6 ft). (D) Probable root traces in dolostone. NRU 3533 (6,638.1–6,638.3 ft) (E) Island sequence of carbonaceous unit overlying algal mat. NRU 3319 (7,084.8–7,086.3 ft). (F) Abundant plant fragments in island sequence. NRU 3533 (6,636.7 ft).

burrowing, wispy laminations, scattered nodular anhydrite, scattered rip-up layers, and faint graded bedding have been interpreted as restricted lagoon. Reservoir quality is very poor, and as a result these sequences have been identified as potential flow barriers in the reservoir.

Island Complex

Wackestone–packstone sediments displaying root casts (Fig. 7D), drying cracks, abundant whole-plant fragments, no burrowing, and rounded allochems have been interpreted as island complex (Fig. 7E,F). The massive to burrowed gray units associated with these deposits are interpreted to be island centers. These are probably the higher salinity ponds that form in similar settings in recent times (Fig. 8A).

Near-Island Beach

Rimming the island on all sides but more prominent in the open lagoon (east side) were packstone–grainstone sediments that have rounded allochems, inclined bedding, lack of burrowing, and fine plant debris. We interpret these sediments to have been deposited as beaches during storms and associated wave processes (Fig. 5).

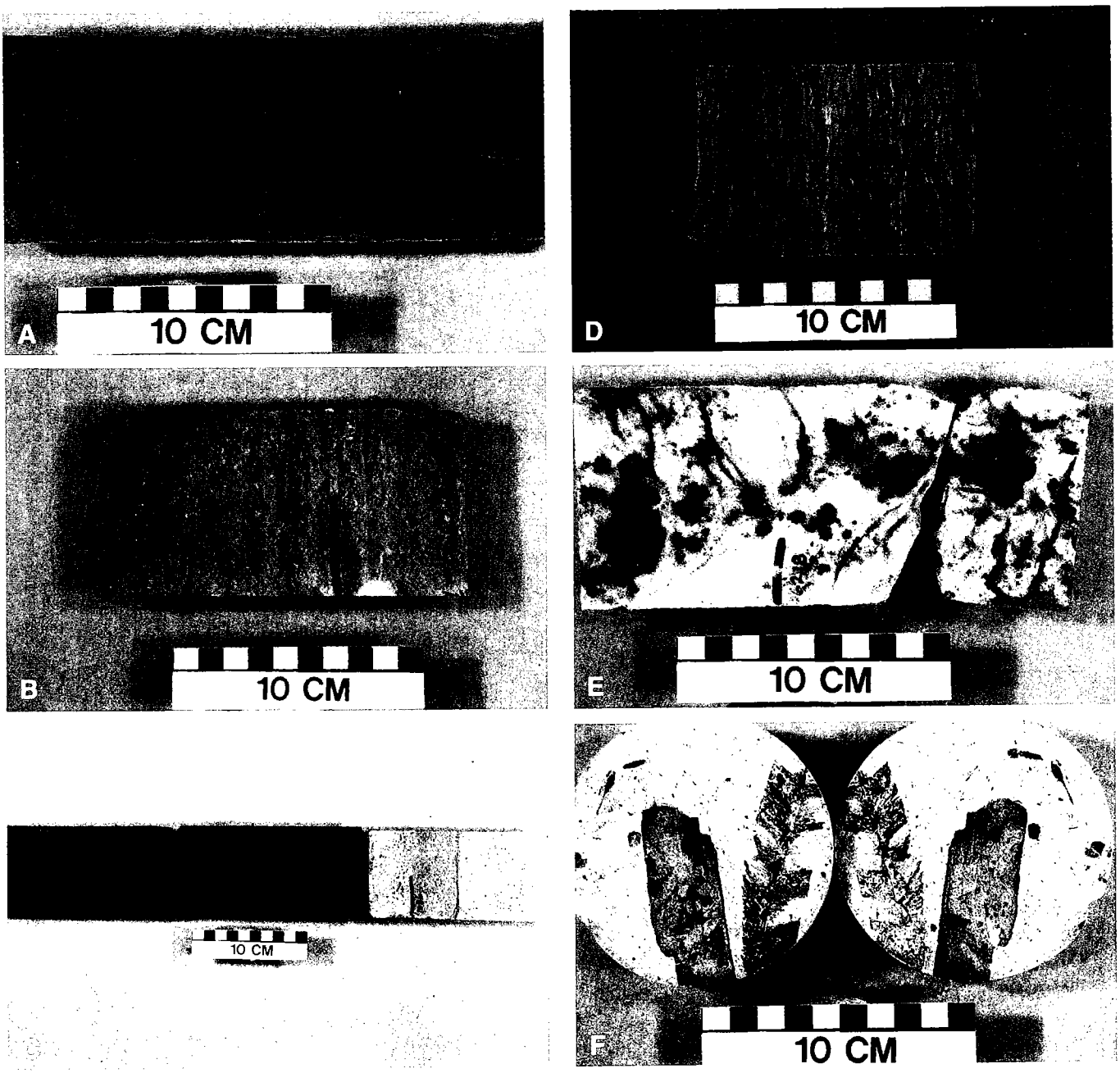

Figure 8. (A) Dense, light-gray burrowed island center. NRU 3319 (7,103.3–7,104.0 ft). (B) Tidal-flat algal mat. NRU 3319 (7,130.7–7,131.1 ft). (C) Tidal channel with burrowed top and abundant carbonaceous plant fragments on top of algal mat. NRU 3319 (7,084.7–7,086.5 ft). (D) Supratidal mud cracks and silty dolostone. NRU 1509 (6,245.3–6,245.7 ft). (E) Collapse breccia with oil staining outlining broken fragments. NRU 3533 (6,217.8–6,218.3 ft). (F) Palm-frond fragments(?). NRU 1509 (6,232.8 ft).

Island Algal Mat

Typically interbedded with the near-island beach sediments are thinly bedded, light-gray algal-mat sediments that display fenestral texture (Fig. 8B). These algal mats were deposited during fair-weather times in shallow flats circumventing the islands.

Outer-Island Beach

Interbedded with (and on the lagoon side) the algal mats for a few of the island complexes, we observed a second "outer"-beach facies. These sediments are the fair-weather equivalent of the inner beach (Fig. 5).

Tidal Flat—General

Mudstone–packstone carbonate sediments observed to have rare drying cracks, graded bedding, wispy carbonate-mud laminations, large amounts of fine anhydrite, a lack of burrowing, very low species diversity, a general lack of fossils, a typical 2–6-in. bedding thickness, and typically light gray to light tan are interpreted as having been deposited in a general tidal-flat environment (Fig. 5). Tidal-flat sequences are very thinly bedded and display numerous changes in rock type and sedimentary structure. Probably this is because the very low relief of the tidal-flat environment was dramatically affected by small

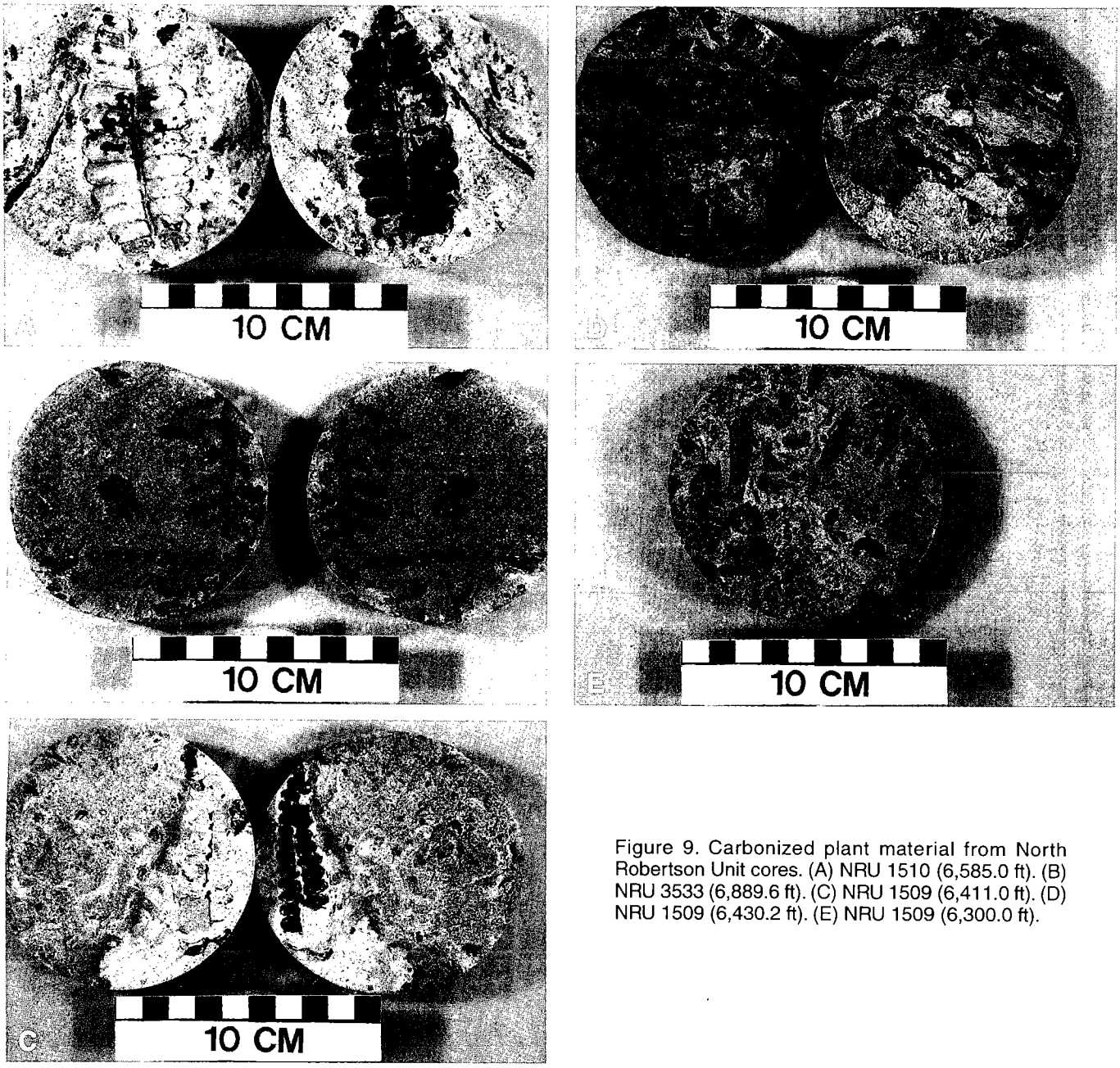

Figure 9. Carbonized plant material from North Robertson Unit cores. (A) NRU 1510 (6,585.0 ft). (B) NRU 3533 (6,889.6 ft). (C) NRU 1509 (6,411.0 ft). (D) NRU 1509 (6,430.2 ft). (E) NRU 1509 (6,300.0 ft).

changes in relative sea level or sediment supply. Notable subenvironments of the tidal flat are reviewed below.

Tidal-Flat Algal Mat

Light-gray sediments displaying fenestral texture that are finely laminated and void of fossils are thought to have been deposited as algal mats in the tidal-flat environment (Fig. 8B).

Tidal-Flat Channel

Mudstone–packstone sediments displaying prominent graded bedding, typically high-angle planar and festoon cross-bedding, rare lag gravels, abundant scoured surfaces, high-angle 2–3-in. mudstone beds, abundant fine plant debris, finely distributed anhydrite, and are commonly bioturbated are interpreted to be tidal channel in origin (Fig. 8C).

Shallow Subtidal Silty Dolostone

Wackestone sediments with abundant silt, graded bedding, large burrows, scour surfaces, inclined bedding, and finely distributed anhydrite have been interpreted as shallow subtidal dolostones. The interpretation of these sediments is complicated by the fact that they were typically reworked as sea level rose during maximum-flooding events.

Supratidal

Wackestone–mudstone intervals containing, in part, bedded anhydrite, shrinkage cracks, rip-up clasts, algal mats, graded bedding, ripple laminations, cross-bedding, abundant silt, and abundant plant fragments were interpreted to be supratidal (Fig. 8D). Permeability is very poor. Porosity is varied, however, and where it occurs, it is fenestral.

Solution-Collapse Breccias

These features were caused by dissolution of carbonate beneath extensive exposure surfaces. The presence of these surfaces is supported by coal beds, abundant "freshwater"-plant-debris zones, erosion lag soils, and some root casts. Parts of the unit were only partially exposed, most probably as a series of small islands and associated carbonate-sand beaches (Fig. 8E). This information is of important economic significance, because there is more natural fracturing in the Clear Fork zone than previously thought. Further analyses will determine the interconnection and influence of this fracturing from solution-collapse breccias.

PALEOCLIMATE

This work also led to the discovery of an extremely interesting aspect of paleoclimatic conditions at the time of deposition. Silver and Todd (1969), Handford and Fredericks (1980), Handford (1981), and Mazzullo (1982), and all the company representatives we spoke with during the course of this study believed that the paleoclimate during deposition of the Clear Fork and Glorieta was semiarid to arid. Our work strongly suggests that this is not true; in fact, we believe that this was a humid and hot time period. Almost all the core we described was filled with abundant plant debris of varying species. Several coal beds were identified, and rarely preserved root traces, lag gravels, and large numbers of varying types of whole plant leaves, including numerous ferns, were identified in the core (Figs. 8F,9A–E).

The implications of this new interpretation are significant. With abundant fresh water percolating down through carbonate rocks exposed during lowstands of sea level, one would expect extensive weathering and dissolution. This is, in fact, typical of many of the Clear Fork and Glorieta sequences at the NRU. Forty-foot sections of solution-collapse breccias with some type of alteration were identified. These zones are characterized by large amounts of secondary porosity, typically good permeability, and open fractures; however, they are not laterally continuous in all directions. Typically, they act as water-injection thief zones in injection wells and may contribute disproportionately to oil production. We theorize that the presence of large amounts of fresh water could also set up exploration plays around the flanks of the NRU in zones selectively enhanced by this process.

ACKNOWLEDGMENTS

The authors would like to acknowledge the work of Mike Clark, former Fina project geologist, and the assistance of Fred Behnken of FBH Stratigraphic Services, Midland, Texas, who helped identify the fossils. Thanks to Louis Doublet, Texas A&M University, for editing the manuscript.

REFERENCES CITED

David K. Davies & Associates, Inc., 1996a, Reservoir characterization to optimize infill drilling and enhanced recovery: Presented at North Robertson Unit/U.S. Department of Energy internal meeting, Jan. 3, Tulsa.

_____1996b, Geological–petrophysical reservoir characterization: Presented at North Robertson Unit internal meeting, July 13, Midland, Texas.

Handford, C. R., 1981, Coastal sabkha and salt pan deposition of the lower Clearfork Formation (Permian), Texas: Journal of Sedimentary Petrology, v. 51, p. 761–778.

Handford, C. R.; and Fredericks, P. E., 1980, Facies patterns and depositional history of a Permian sabkha complex, Red Cave Formation, Texas Panhandle: Texas Bureau of Economic Geology Geological Circular 80-9, 138 p.

Mazzullo, S. J., 1982, Stratigraphy and depositional mosaics of lower Clearfork and Wichita Groups (Permian), northern Midland basin, Texas: American Association of Petroleum Geologists Bulletin, v. 66, p. 210–227.

Silver, B. A.; and Todd, R. G., 1969, Permian cyclic strata: American Association of Petroleum Geologists Bulletin, v. 53, p. 2244.

Terrasciences, Inc., 1994, Terrasciences reservoir analysis package (version 5.4): Littleton, Colorado.

Improved Reservoir Characterization through Integrated Log and Core Data: Example from Permian San Andres Formation, Dawson County, Texas

Gregory D. Hinterlong and Archie R. Taylor
OXY USA Inc.
Midland, Texas

ABSTRACT.—The characterization of reservoir rocks is often restricted to interpretation of log response by the lack of available core data. These interpretations by necessity require assumptions on the interpreter's part that, although reasonable, may not reflect actual reservoir conditions. Through the judicious utilization of special core analysis, many of the assumptions can be improved for a better understanding of reservoir performance and consequently better reservoir predictions. The results presented in this paper cover the integration process and geologic implications, which may be of use in similar studies elsewhere.

The Permian San Andres Formation in the West Welch Unit (Welch field) is currently being characterized for numerical simulation as part of a U.S. Department of Energy Class II project (DE-FC22-93BC14990). The goal of the study is to determine the feasibility of an economic tertiary carbon dioxide (CO_2) flood in a heterogeneous, low-permeability shelf-carbonate reservoir. A detailed reservoir description is required, because the high costs of injecting and recycling CO_2 dictate a very efficient flood design. Identification of reservoir barriers, flow units, and permeability, and the prediction of continuity, present the greatest challenges to the description. The pay interval is mineralogically simple, being composed dominantly of dolomite and common anhydrite with minor amounts of chert and illitic clay. The diagenesis of these shallow shelf deposits has created a highly complex pore system that crosses depositional facies boundaries at some points. As is often the case, the bulk of the reservoir data is derived from logs of varying quality and vintage. Rock and fluid interaction further complicate the descriptive process by affecting the log responses. These effects were not recognized until the log data were integrated with the special core analysis. The resulting log interpretations were much more consistent with core data.

INTRODUCTION

Patterns of the San Andres depositional environments and facies distribution have been extensively documented in the literature. These reservoirs were typically deposited in a sequence of upward-shallowing cycles. The regional dip of the shelf was very low, creating broad bands of similar facies. Low-energy facies dominate the sequences, with carbonate muds forming most of the resulting rocks. Equivalent rocks can be traced for hundreds of miles throughout the Permian basin and beyond in both outcrop and subsurface. Reservoirs in the formation have produced billions of barrels of oil since the early 1920s and continue to do so under both primary recovery and waterflooding. As these waterfloods reach their economic limits, the opportunity exists for further recovery by carbon dioxide (CO_2) floods. The expense of the injected CO_2 fluid and recycling requires a thorough understanding of the reservoir prior to initiating the flood. The description begins at the pore level and gradually expands to the field scale.

WEST WELCH UNIT GEOLOGY

The Welch field is in the northwest corner of Dawson County, Texas, on the northern shelf of the Midland basin (Fig. 1). The field produces from dolomite of the Permian (Guadalupian) San Andres Formation (Fig. 2) at an average measured depth of 4,825 ft. The producing interval is approximately 400 ft below the top of the formation. The reservoir section thins to the north, toward the paleoshoreline, and is overlain by impermeable evaporites and anhydritic dolomites. The permeability decreases to the east and west. The southern limits of the field are determined by downdip high water saturations. The current structure (Fig. 3) reflects post-depositional movement of deeper fault blocks. A three-dimensional seismic survey of the field confirms that these faults do not reach the San Andres interval.

The average porosity for the unit is 9.5%, with a geometric mean permeability of 1 md. Within the project area, the average porosity is 12%, and the average permeability is 2.2 md. As of December 1995, the West Welch Unit had produced 67 million barrels of oil (MMBO), 11 billion cubic feet of gas (BCFG), and 129 million barrels of water (MMBW). Since waterflood operations began in 1960, 254 MMBW has been injected. The West Welch Unit currently has 340 active producers and 207 active injection wells and covers over 12,000 surface acres. Current monthly production is 2,837 BO, 518 MCFG, and 22,896 BW. The average water cut for the entire unit is 89%. The U.S. Department of Energy (DOE) project area covers 564 acres in the south-central part of the West

Hinterlong, G. D.; and Taylor, A. R., 2000, Improved reservoir characterization through integrated log and core data: example from Permian San Andres Formation, Dawson County, Texas, *in* Johnson, K. S. (ed.), Platform carbonates in the southern Midcontinent, 1996 symposium: Oklahoma Geological Survey Circular 101, p. 319–326.

Welch Unit. This area alone has produced 7.7 MMBO. The project area currently has 38 producing wells, 23 injection wells, 2 observation wells, and 1 water-supply well. Within the project area, 11 of the wells have been cored.

Depositional fabrics from whole-core description range from supratidal mudstones and evaporites to oolitic grainstones, commonly within the same cored well (Fig. 4). Reservoir description by facies sometimes provides a means for extrapolating the vertical sequence to the lateral interwell area. The crux of an effective extrapolation is a reliable correlation of facies to reservoir parameters. Depositional facies from the West Welch Unit have not proved to exhibit these uniform characteristics. Good-quality reservoir rock can be found as likely in mudstones as in grainstones. Diagenesis has produced a highly complex system of pores that crosses depositional boundaries. Thus, the simple mineralogy of the reservoir has been offset by the complexity of the pore geometry and interconnections.

The thin-section examination of core produced eight visually distinct rock types on the basis of the pore geometry. However, these rock types were not readily definable by wireline-log responses. As reflected in the work of Wardlaw and Taylor (1976), the pore geometry has a more profound effect on the resulting permeability than on the total porosity. Lucia (1995) proposed a classification based on the particle size and porosity types (vuggy and nonvuggy). This classification produced rock types with narrower ranges of permeability for any given porosity.

The interior surface area of the pores has proved to be a significant consideration for the descriptive process. As the interior surface area increases, the friction within the pore increases and the permeability decreases. Log-analysis equations have attempted to compensate for increased surface area and tortuosity with changes to the m and n exponents in the Archie equation. In pore systems with high internal surface areas, the irreducible water saturation will be higher than other rocks of equivalent porosity.

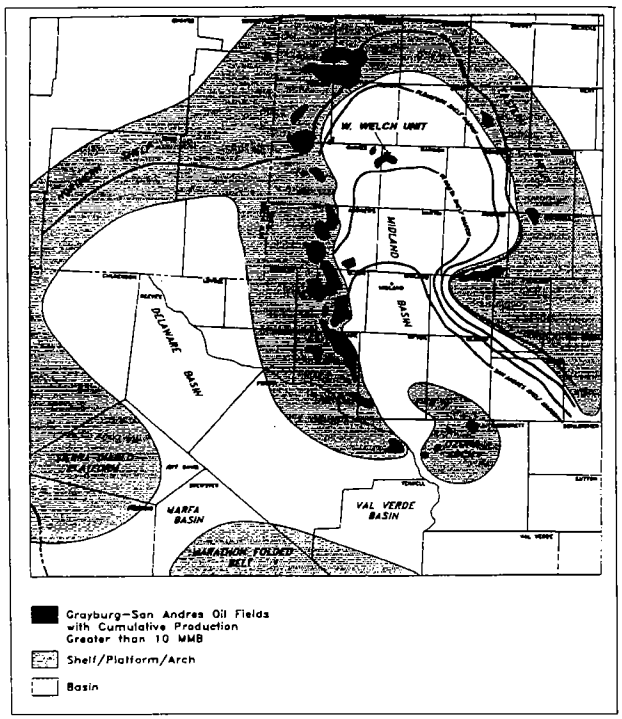

Figure 1. Paleogeography of the Permian basin, showing location of Welch field.

POROSITY AND PERMEABILITY RELATIONS

As is the case with most carbonates, the relationship of total porosity to permeability is weak, displaying the typical "shotgun" appearance in a semilog cross plot (Fig. 5). The comparison of maximum permeability with the permeability at 90° indicates no matrix preferential flow direction (Fig. 6). Many of the samples that exhibited a spread in the values between the maximum permeability and the permeability in the same sample at 90° to the maximum permeability had fractures reported in the "remarks" section of the analysis. On visual examination of the samples, these fractures appear related to the coring process and would not be open in the subsurface under normal conditions.

For reservoir modeling, a reservoir description as complete as possible is necessary to predict the performance of a CO_2 flood. Paramount to the description is the distribution of the permeability and porosity. Through comparisons of log with core (Fig. 7), a close agreement on the total pore volume is readily obtainable; however, for reasons mentioned earlier, this value alone will not provide an acceptable estimation of permeability. A comparison of two observation wells (WWU7916 and WWU4852, 2,700 ft apart) illustrates the

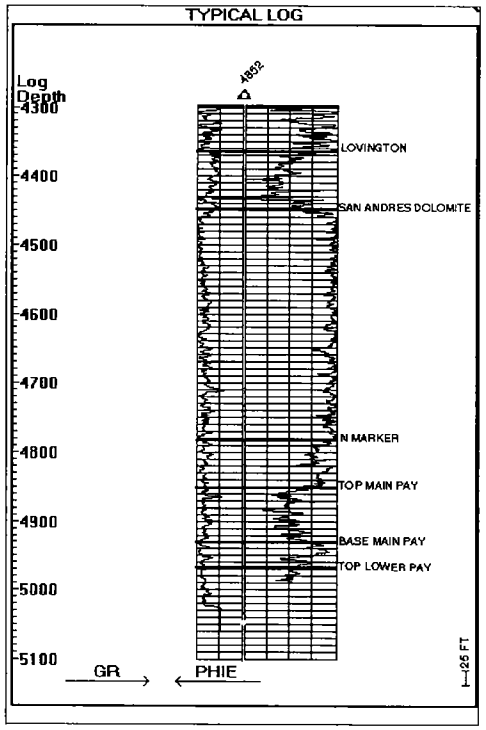

Figure 2. Type log of the reservoir interval and overlying cap rock. Depths in feet. The producing interval lies approximately 400 ft below the top of the San Andres Formation. The gamma-ray curve (*GR*) is scaled from 0 to 100 API units, and the porosity curve (*PHIE*) is scaled from 30% to 0%.

disparity of using a total pore-volume cutoff alone for determination of net pay:

	WWU7916	WWU4852
Gross thickness	78.0 ft	79.0 ft
6%-porosity cutoff	67.0 ft	78.0 ft
1-md-permeability cutoff	27.0 ft	64.0 ft

The change in net to gross ratios is significantly greater when a permeability cutoff is employed in this reservoir than when using a total-porosity value. Early in the screening process, a determination of the tertiary-recovery target must be made to evaluate the economic viability of the project. Both of these observation wells were cored through the entire pay interval, and the measured core values used in the net-pay determination.

CAPILLARY-PRESSURE MEASUREMENT

The mercury-injection, capillary-pressure (MICP) method has proved a useful tool in defining fluid saturations within reservoirs. Recently, significant work has been referenced in the literature on the use of MICP data in a quantitative descriptive process of pore systems (rock typing) for understanding the performance of stratified reservoirs (Wardlaw and Cassan,1978; McCreesh and others, 1991; Pittman, 1992; Salem, 1993; Kopaska-Merkel, 1994; and others).

Initially, 10 samples of reservoir-quality rock were selected for MICP analysis. The results indicated that a further subdivision of the better quality rock was needed. Most of the samples had a single pore-throat size dominating the interconnection of the pores in the rock. The heterogeneity of these carbonate rocks required a larger sample to make the dominance apparent, which was difficult to identify in thin section.

From the capillary-pressure data, the dominant pore-throat size was determined by the histogram of the entry pressure. To relate this parameter to rock type, the calculated mean radius was entered into the following equation:

$$PRG = \frac{\phi \cdot r^2}{4}$$

where ϕ = porosity of sample in percent, r = radius of dominant pore throat in microns, and PRG = pore radius group.

The following equation relates the PRG to the permeability by the $K_o\tau$constants:

$$k = \frac{1}{K_o\tau}(PRG)$$

where k = permeability (md), K_o = Kozeny constant, τ = tortuosity, and PRG = pore radius group.

The resulting PRG values for each sample were cross-plotted on linear axes against the laboratory-measured air permeability of the sample. The slope of a line passing through each group and the origin is equivalent to $1/K_o\tau$ from the Carman-

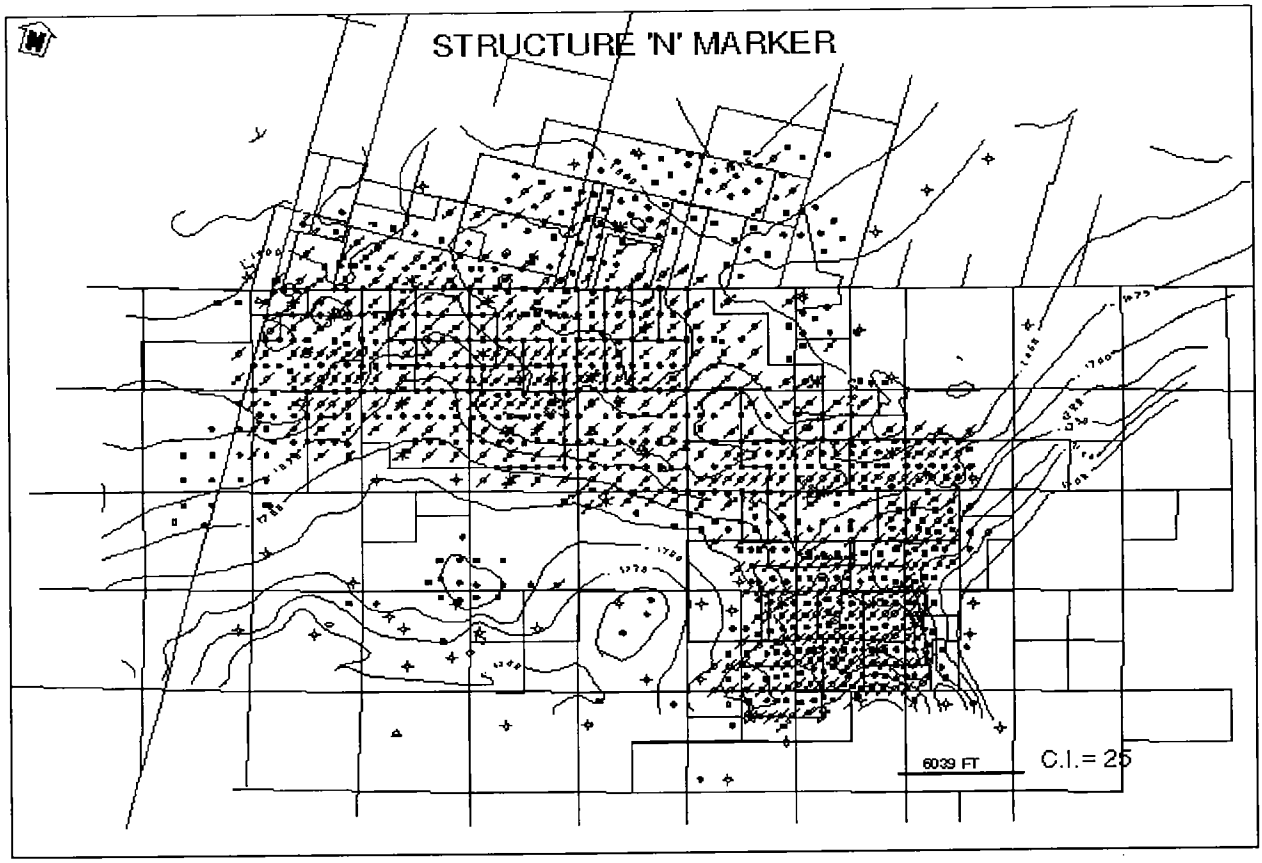

Figure 3. Structure map of Welch field, depicting the base of the "N" marker; contour interval, 25 ft. Most of the structural configuration is post-depositional, created by movement of deeper fault blocks. No fault displacement occurs within the San Andres; however, the deeper faults locally affect the stress fields within the reservoir interval.

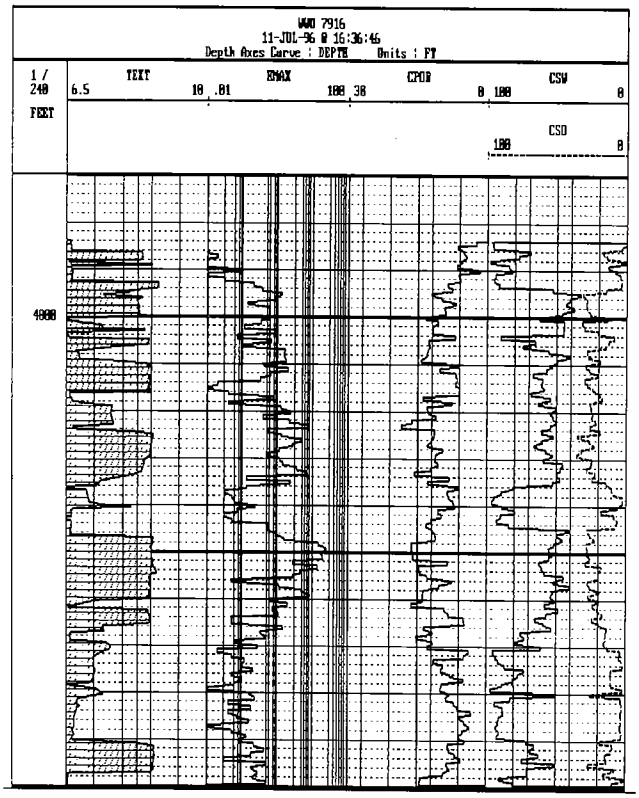

Figure 4. Comparison of core-measured parameters with depositional textures. The first track displays the depositional texture with increases in the percentage of grains to the right (relative scale). The second track is the logarithm of the maximum permeability (0.01 to 100 md). The third track is core porosity (30% to 0%). The fourth track contains the core water saturation (solid line) and core oil saturation (dashed line) scaled 100% to 0%. Reservoir parameters do not reliably equate to depositional texture.

Kozeny equation (Kozeny, 1927; Carman, 1937). The significance of the τ value is its reflection of the length of the flow path in the interconnected pore system. The higher the slope, the straighter the flow path. The data fell into three distinct groupings. An additional 11 samples were selected with a wider range of porosity and permeability values for MICP treatment. These additional samples fell within the boundaries of the three groups defined by the first set of samples (Fig. 8).

Thin sections of the 21 samples were examined to identify petrophysical characteristics that would account for the separation of the groups (Fig. 9). Group 3 (lowest slope) has oversize pores with rough interiors and a fine-grained matrix. Group 2 (intermediate slope) has a more uniform pore size, but the interiors are smoother. Group 1 (high slope) has larger pores with smooth interiors and coarser grain (or crystal) size. Group 4 is the nonreservoir group. The increase in roughness (internal surface area) of the pores increases the friction of the fluids passing through the pores, decreasing the permeability. This relates to the K_o constant.

RELATIVE-PERMEABILITY EXPERIMENTS AND WETTABILITY

Along with the 21 MICP samples, seven steady-state, relative-permeability experiments were conducted on samples from the two observation wells. The results (Fig. 10) indicated that both water-wet and intermediate-oil-wet rocks are present in the same reservoir section. The differing wettabilities have a profound effect on log response (Pinzon and Asquith, 1994) as well as on tertiary recovery (Anderson, 1984a,b; Craig, 1971). The resulting effects can be identified on the open-hole log response and used to identify the intervals of differing wettability.

INTEGRATION OF LABORATORY AND LOG DATA

The laboratory data have indicated four basic rock types within the reservoir section and each rock type having the potential of being either water wet or intermediate oil wet. The problem then becomes how to identify these parameters throughout the reservoir where laboratory data are unavailable.

The interpretation of the PRG indicated a weighting on the internal surface area (roughness) of the dominant pore system. Laboratory measurement of the internal surface area is difficult and at times questionable. Monicard (1980) proposed an equation based on the Carman-Kozeny equation to relate the properties of porosity and permeability to the internal surface area of the pores. During routine core analysis, these parameters are independently measured and can be incorporated reliably into the equation:

$$k = \frac{\phi^3}{5S_g^2(1-\phi)^2}$$

where ϕ = decimal porosity, k = permeability in darcys, and S_g = internal surface area.

A continuous curve was calculated by using the above equation to compute the surface area. The resulting curve showed a strong similarity to the borehole gamma-ray log (Fig. 11). The lack of exact correspondence with the computed curve can be attributed to the fact that the computed surface values are discrete samples of rock and the gamma-ray curve is a statistical running average of the section. By normalizing the

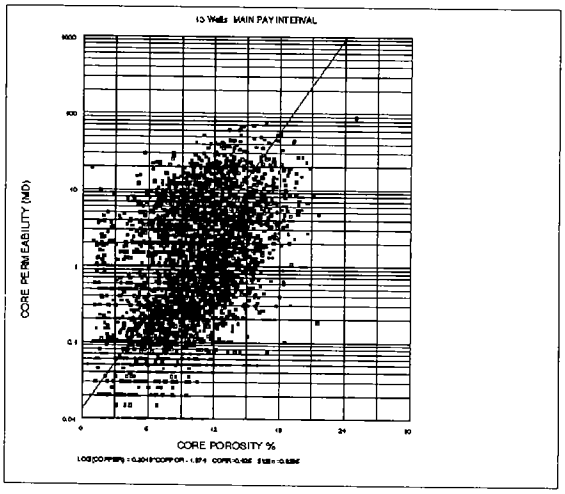

Figure 5. Semilog cross plot of core porosity (in percent) against core permeability (in millidarcys) for 13 cored wells in the study area. This "shotgun" scatter is a common occurrence in carbonate rocks, making estimation of permeability from total porosity unreliable.

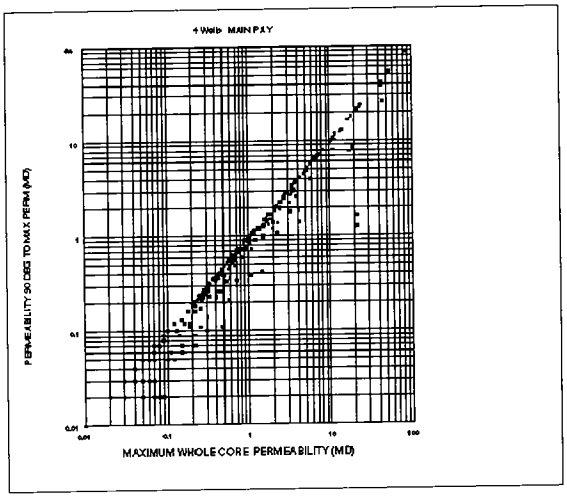

Figure 6. Logarithmic cross plot of the maximum permeability and the permeability measured at 90° to the maximum direction in four wells in the study area. Most of the separation of the measurements occurs at values below 1 md, which are difficult to measure in the laboratory. The differences above the 1-md level were reported to contain fractures. The reservoir does not have a directional bias on the core-sample-size level.

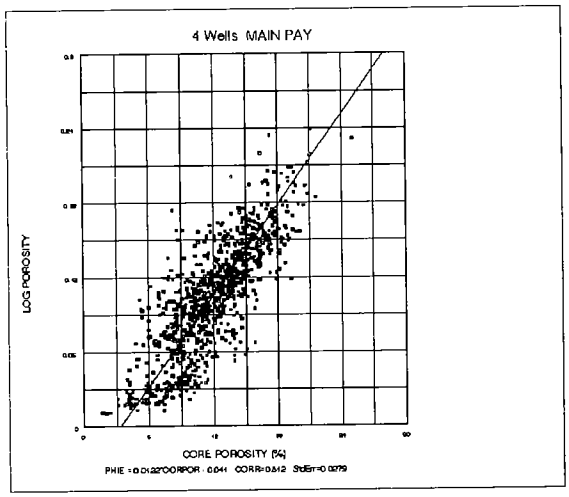

Figure 7. Cross plot of core measured porosity and log-derived porosity from four wells in the study area. The values agree well above 6% porosity; however, core analysis tends to run higher than log-derived porosity below this value. In this range, surface irregularities can produce optimistic values in core analysis.

gamma-ray-log response to values ranging from 0 to 0.1 within the reservoir interval, reasonable approximations for the value of the internal surface area could be generated. Diederix (1982) demonstrated experimentally effects of pore interior roughness by using etched-glass-bead packs. As a result, the simple increase in surface roughness caused the saturation exponent to change from a straight-line relation to a curved relation in the laboratory-determined resistivity index and the water saturation.

Lake (1992), in a discussion of permeability, stated that the Carman-Kozeny equation in its fundamental form theoretically relates the porosity, the internal surface area of the pores, and the length of the flow path through the rock (τ) to the permeability of the medium. Accurate estimations of the

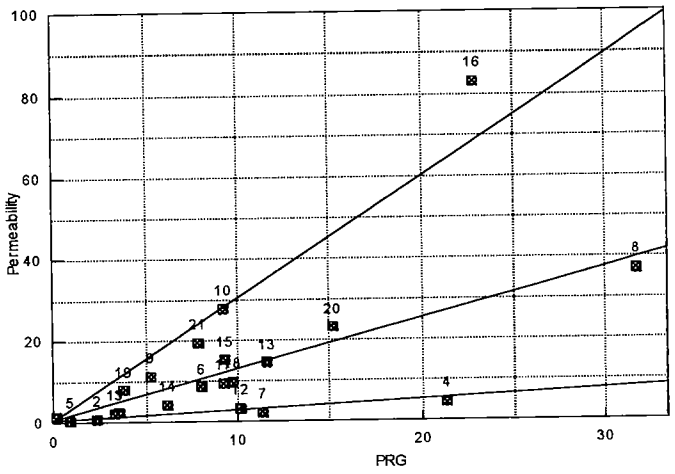

Figure 8. Cross plot of the pore radius group (*PRG*) against the permeability for the 21 mercury-injection, capillary-pressure samples. The slope of each line is equal to the reciprocal of $K_o\tau$, and must pass through the origin.

permeability should be possible if each of these parameters can be arrived at independently.

The tau (τ) function has been related to the formation factor used in log analysis in differing ways by Wyllie and Rose (1950), Pirson (1958, 1963), and others. They relate the change in electrical resistivity to the total pore volume. For this study, the resistivity-derived porosity from the shallow-resistivity tool, when compared with the total porosity of the rock, provides an indication of τ. The formula used in the relationship is a modification of Nugent's (1984) equation

$$m = \frac{2\log\phi_A}{\log\phi_T}$$

where ϕ_A = acoustic porosity, ϕ_T = total porosity, and m = cementation exponent, and which is used to calculate a variable, m, in log analysis when vuggy rocks are anticipated. In this paper, a resistivity-derived porosity from the shallow-reading resistivity tool is substituted for the acoustic porosity in the above equation, resulting in a comparison of the water-filled porosity with the total porosity of the rock (Nugent R). The shallow-resistivity tool was selected because of the finer bed resolution and the uncertainty of the value for formation-water resistivity. The resistivity of the mud filtrate, which usually is more accurately known, substitutes for the formation-water resistivity in the porosity equation.

In water-wet reservoirs, the Nugent R (modified cementation exponent) values reflect the electrical-flow-path length through the interconnected pore system. This function deviates from earlier work by incorporating an independent measure of the water-filled volume of pore space in relation to the total porosity of the rock. A change in the wettability changes the distribution of the water in the pore system: the water is now located in the center of the pore instead of lining the pores. Before applying the Nugent R calculation in permeability estimations, the wettability must be distinguished.

The resistivity curves and relative-permeability experiments were instrumental in determining the intervals of differing wettabilities. Cross-plotting the shallow-resistivity curve

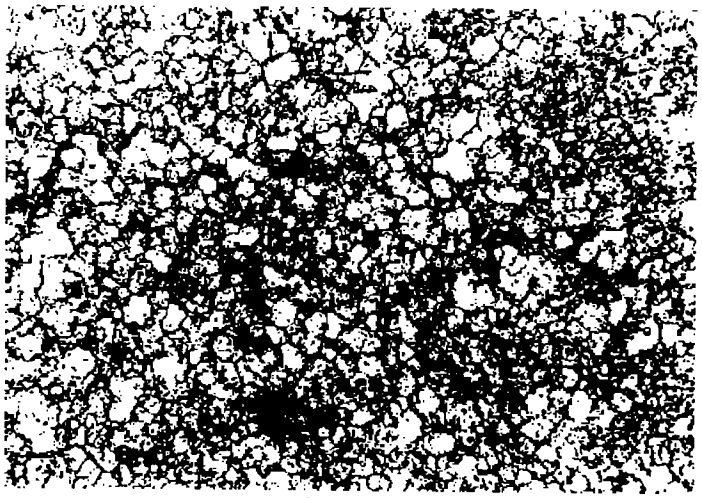

Group 1

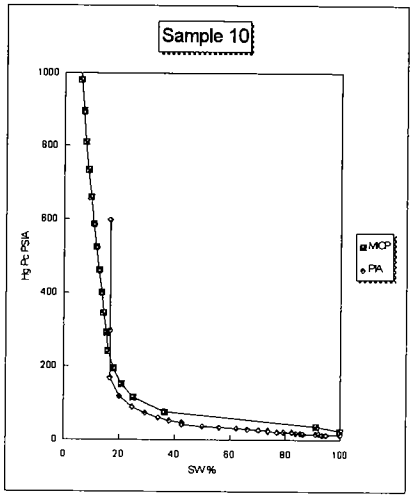

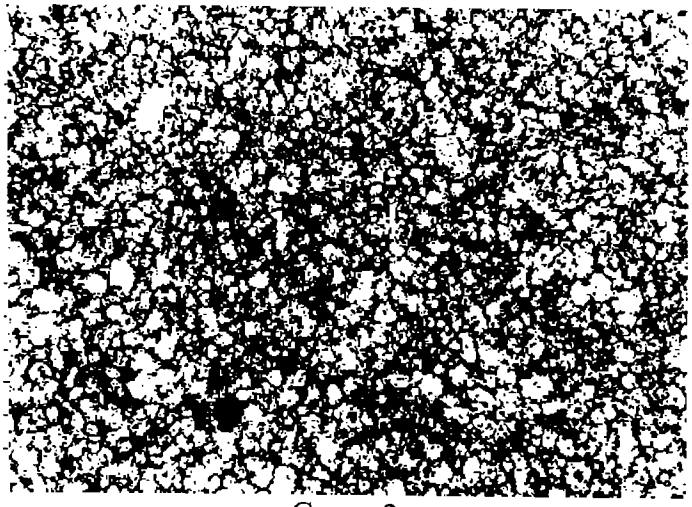

Group 2

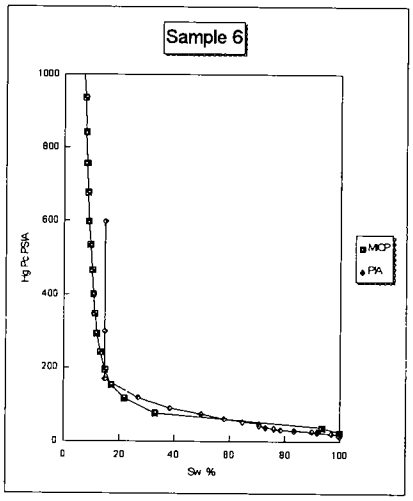

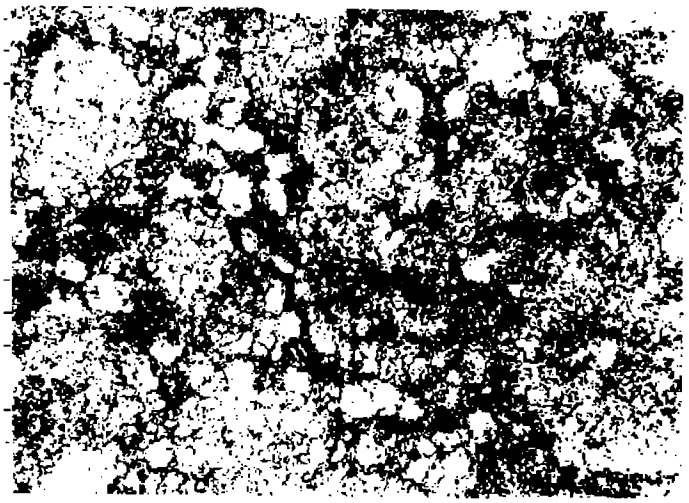

Group 3

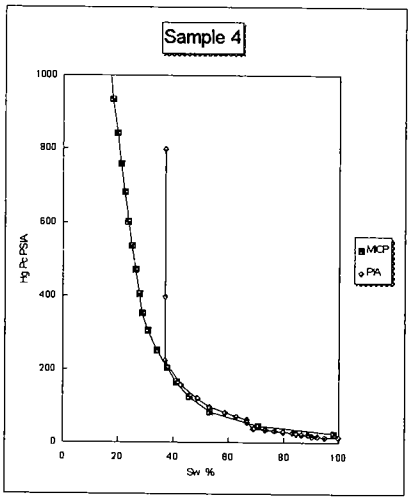

Figure 9. Thin-section photomicrographs of representative examples of each pore radius group (PRG). All three photographs are at the same magnification and taken under plane-polarized light. The width of the photograph represents 4.2 mm. The black areas are pore spaces injected with blue epoxy. Also displayed are the capillary-pressure measurements for the thin section.

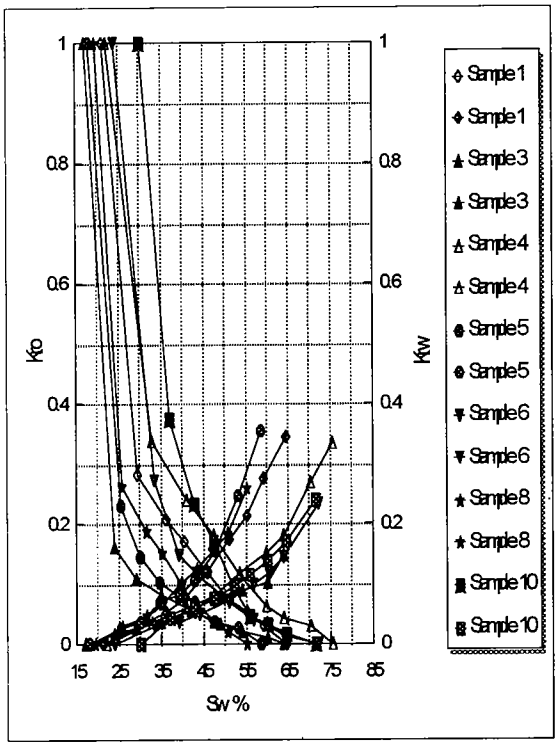

Figure 10. Results of relative-permeability experiments for seven samples from the study area. The curves break into two groups, one with a midpoint indicating more oil wet, and the other indicating water wet.

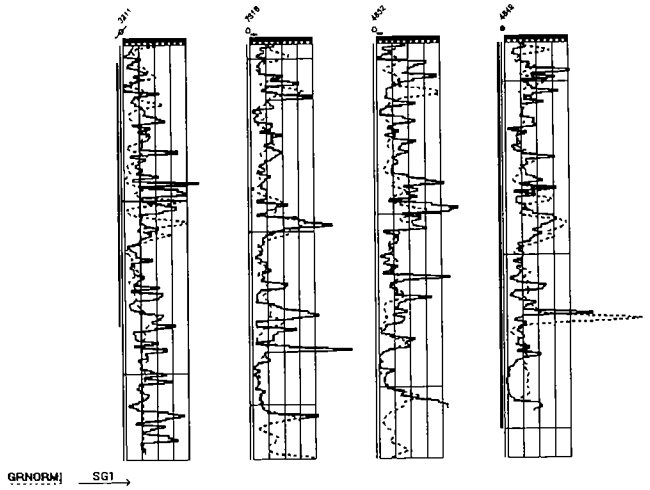

Figure 11. Comparison of the computed surface area per grain volume (S_g) in the solid line with the normalized gamma ray (*GRNORM*) in the dashed line for four wells in the study area.

against the deep-resistivity curve on logarithmic axes should form a linear cloud of data points (Fig. 12). The length of the cloud will reflect changes in the pore types, and the slope of the cloud axis will be controlled by the ratio of the mud-filtrate resistivity and the formation-water resistivity. When the samples from the relative-permeability experiments were plotted on the resistivity-curve cross plots, the seven samples all fell within the same part of the data cloud. The water-wet

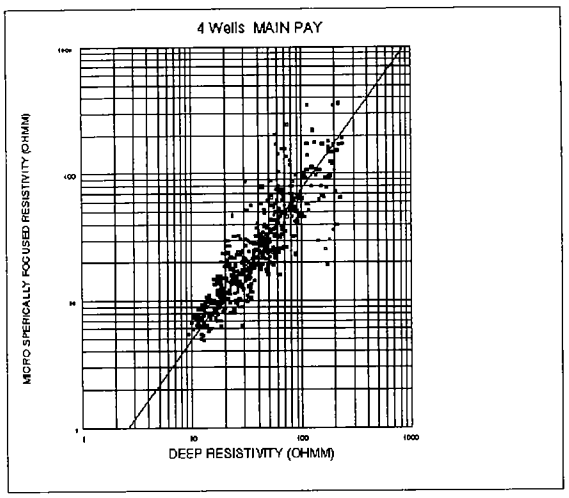

Figure 12. Logarithmic cross plot of the shallow resistivity (R_{xo}) against the deep resistivity (R_t). The scatter observed in the higher resistivities is induced by the changes in wettability in the pore system.

samples formed a plot along the central axis of the data cloud below 50-ohm deep-resistivity values. The intermediate oil-wet samples formed a plot above the 50-ohm values where the data cloud begins to diffuse. The points remaining above the 50-ohm values, clustering around the central axis, were of low porosity (<4%), which increased the resistivity of the rock. By combining the limiting factors of porosity and deep resistivity, a reasonable distinction between the wettabilities resulted. No attempt was made to quantify the degree of wettability.

Taking into account the rock types and rock–fluid interactions as determined from well logs, and substituting a modified Carman-Kozeny equation (Hinterlong and Taylor, 1996), enabled us to generate an improved estimate of reservoir permeability (Fig. 13).

SUMMARY AND CONCLUSIONS

For the interpretation of well logs, certain assumptions about the reservoir have to be made by the interpreter. By the integration of laboratory data from both the physical makeup of the rock (porosity, permeability, mineralogy, and pore geometry) and the rock–fluid interaction (capillary pressure, relative permeability) into theoretical relations, the quantitative use and interpretation of well-log responses improved.

The sample-selection process for special testing should begin after the basic reservoir description has been completed to optimize the utility of laboratory data. In this instance, subtleties of wettability changes were not obvious until after attempts were made to identify rock types from well logs. The gamma-ray curve was used to predict the internal surface area of the pores. Petrophysical rock types do not always coincide with visual core facies. In low-permeability reservoirs such as the West Welch Unit, the accuracy of permeability prediction in uncored wells plays a major role in the viability of the tertiary-recovery project. The final permeability-prediction model was significantly improved by the incorporation of the well-log data and core analysis.

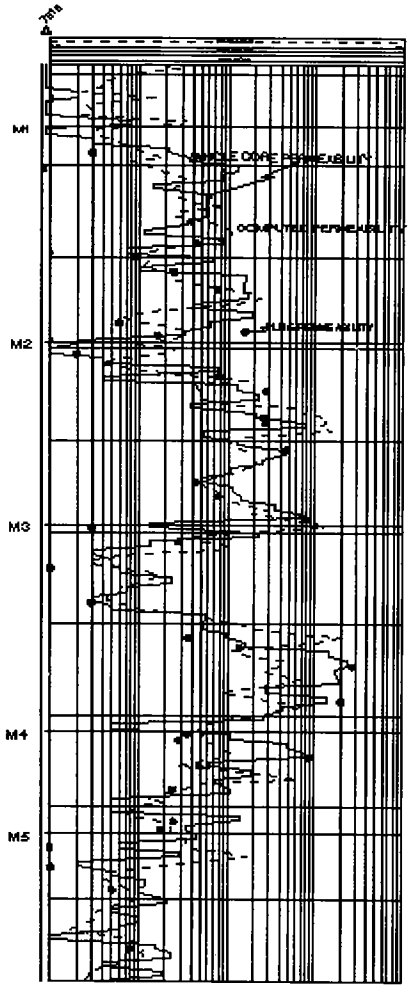

Figure 13. Vertical profile of the whole-core permeability (solid curve), the computed permeability (dashed curve), and the plug permeabilities (small solid squares). The overall fit of the measured and computed curves is excellent and well within the range of plug to whole-core measurements. For the few intervals where the agreement is not as good, the logging tools probably measured a different volume of rock than the core analysis did.

ACKNOWLEDGMENTS

The information presented is from a portion of the Class II Oil Program Cooperative Agreement with OXY USA Inc. and the U.S. Department of Energy (DE-FC22-93BC14990). The authors would like to thank the Department of Energy and OXY USA Inc. for support and permission to publish the results.

REFERENCES CITED

Anderson, W. G., 1984a, Wettability literature survey—Part 2: Wettability measurement: Society of Petroleum Engineers of AIME Paper SPE 13933, Dallas, 34 p.

_____1984b, Wettability literature survey—Part 4: The effects of wettability on capillary pressure: Society of Petroleum Engineers of AIME Paper SPE 15271, Dallas, 38 p.

Carman, P. C., 1937, Fluid flow through granular beds: Institute of Chemical Engineers Transactions, v. 15, p. 154–155.

Craig, F. F., 1971, The reservoir engineering aspects of waterflooding: Society of Petroleum Engineers of AIME Monograph 3, Dallas, 134 p.

Diederix, K. M., 1982, Anomalous relationships between resistivity index and water saturations in the Rotliegend Sandstone (The Netherlands): Society of Professional Well Log Analysts 23rd Annual Logging Symposium, Corpus Christi, Texas, Paper X, 16 p.

Hinterlong, G. D.; and Taylor, A. R., 1996, Characterization of rock types with mixed wettability using log and core data—DOE Project, Welch Field, Dawson County, Texas: Society of Petroleum Engineers of AIME Paper SPE 35160, Permian Basin Oil and Gas Recovery Conference, Midland, Texas, p. 139–147.

Kopaska-Merkel, D. C., 1994, Pore-throat morphology in the Upper Jurassic Smackover Formation of Alabama: Journal of Sedimentary Research, v. A64, p. 524–534.

Kozeny, J., 1927, On capillary movement of water in soil: Wein. Akad. Wiss. Sitz. Berichte (IIA), v. 136, p. 271–306.

Lake, L. W., 1992, Reservoir characterization: From the laboratory to the field: Short Course Notes presented to OXY USA, Midland, Texas.

Lucia, F. J., 1995, Rock-fabric/petrophysical classification of carbonate pore space for reservoir characterization: American Association of Petroleum Geologists Bulletin., v. 79, p. 1275–1300.

McCreesh, C. A.; Ehrlich, R.; and Crabtree, S. J., 1991, Petrography and reservoir physics II: Relating thin section porosity to capillary pressure, the association between pore types and throat size: American Association of Petroleum Geologists Bulletin, v. 75, p. 1563–1578.

Monicard, R. P., 1980, Properties of reservoir rocks: Core analysis: Gulf Publishing, Houston, 168 p.

Nugent, W. H., 1984, Letters to the editor: Log Analyst, v. 25, no. 2, p. 2–3.

Pinzon, I. D.; and Asquith, G. B., 1994, The application of dielectric logs to the recognition of oil versus water-wet reservoirs and in the determination of relative permeabilities, *in* Gibbs, J. F. (ed.), Synergy equals energy—teams, tools, and techniques: West Texas Geological Society 1994 Fall Symposium, p. 93–100.

Pirson, S. J., 1958, Oil reservoir engineering [2nd edition]: McGraw-Hill, New York, 735 p.

_____1963, Handbook of well log analysis for oil and gas formation evaluation: Prentice-Hall, Englewood Cliffs, New Jersey, 326 p.

Pittman, E. D., 1992, Relationship of porosity and permeability derived from mercury injection–capillary pressure curves for sandstones: American Association of Petroleum Geologists Bulletin, v. 76, p. 191–198.

Salem, H. S., 1993, Derivation of the cementation factor (Archie's exponent) and the Kozeny–Carman constant from well log data, and their dependence on lithology and other physical parameters: Society of Petroleum Engineers of AIME Unsolicited Paper SPE 26309, 26 p.

Varva, C. L.; Kaldi, J. G.; and Sneider, R. M., 1992, Geological applications of capillary pressure: A review: American Association of Petroleum Geologists Bulletin, v. 76, p. 840–850.

Wardlaw, N. C.; and Cassan, J. P., 1978, Estimation of reservoir efficiency by visual observation of pore systems in reservoir rocks: Bulletin of Canadian Petroleum Geology, v. 26, p. 572–585.

Wardlaw, N. C.; and Taylor, R. P., 1976, Mercury capillary pressure curves and the interpretation of pore structure and capillary behavior in reservoir rocks: Bulletin of Canadian Petroleum Geology, v. 24, p. 225–262.

Wyllie, M. R. J.; and Rose, W. D., 1950, Some theoretical considerations related to quantitative evaluation of physical characteristics of reservoir rocks from electrical log data: AIME Transactions, v. 189, p. 105–118.

Seismic Estimation of Porosity in a Permian San Andres Carbonate Reservoir, Welch Field, Dawson County, Texas

George P. Watts and Gregory D. Hinterlong
OXY USA Inc.
Midland, Texas

ABSTRACT.—OXY USA Inc. and the U.S. Department of Energy are partners in an advanced-technology demonstration project (DE-FC22-93BC14990) at OXY's West Welch Unit in Welch field in Dawson County, Texas. The project requires detailed reservoir characterization of porosity, utilizing modern well logs integrated with core data, which is to be extended into the interwell space with a three-dimensional (3-D) seismic volume. Oil production at the West Welch Unit is from a stratigraphic trap in a low-permeability San Andres reservoir of Permian age similar to many shallow-shelf carbonate reservoirs in the Permian basin. Porosity was determined from compensated neutron/density logs and integrated with laboratory measurements of porosity on core samples. Three seismic attributes—structure, amplitude, and phase—were found to have high correlation to the porosity. A multiple variable transform equation was developed, and porosity values were estimated at each seismic-bin location. The seismic-guided porosity estimates were mapped and compared to the porosity map from the well data only. The seismic-guided porosity map ties the well data accurately, provides all the detailed variation in the interwell space expressed by the 3-D seismic data, and reveals extensions of the reservoir beyond the well control. The seismic-guided porosity estimates are also in a form ready for input to a geological model for the reservoir simulator.

INTRODUCTION

In August 1994, a grant was awarded to OXY USA Inc.'s Western Region in Midland, Texas, by the U.S. Department of Energy for an advanced-technology demonstration project. The demonstration site is within OXY's West Welch Unit in Welch field, Dawson County, Texas. The project's primary objective is aimed at proving that the remaining oil reserves in lower quality, shallow-shelf carbonate reservoirs can be economically produced by applying reservoir characterization and a combination of carbon dioxide (CO_2) flooding and cyclic CO_2 stimulation. The project combines the latest technology for reservoir characterization with reservoir simulation to improve production forecasting, production economics, and recovery in a DOE Class II reservoir. The reservoir characterization will include data from cores, modern well logs, a 3-D seismic volume, and 15 cross-wellbore seismic-tomography lines. Only the contribution of the 3-D seismic data to the reservoir-characterization effort will be discussed here.

The rock data within a reservoir-simulation model require the following pieces of data for each reservoir pay zone at each grid node: (1) elevation (structural depth), (2) thickness (isopach), (3) average porosity, (4) average permeability, (5) average fluid saturations, (6) average compressibility, (7) relative permeability, and (8) capillary pressure (Crichlow, 1977). The greatest challenge to the reservoir characterization is describing the rock data in the areas between and outside the well control. The overall objective of the 3-D seismic evaluation is to translate as many of these rock data as possible to the concentration of 3-D seismic data points via the measurable seismic attributes within the seismic volume.

One of the initial seismic objectives was to develop a software capability to convert seismic-attribute data to log properties. This was accomplished by using a non-geostatistical, data-driven method suited for 3-D seismic-data volumes where data points are uniform, closely spaced, and extensive (Schultz and others, 1994a). The data input are reservoir properties derived from well logs and attributes transformed from 3-D seismic volumes. Every log property is cross-plotted with each seismic attribute. A significance measure is applied to each cross-plot to determine how well each seismic attribute relates to a property. Underlying physical relationships between the seismic attributes and log properties are important, but not necessary, in this method. A calibration function is sought to best convert one or more attributes to a property. The coefficients for the fit of an over-determined linear-regression solution are applied to the seismic-attribute data to estimate the log property. A residual correction is added to the converted property values to ensure good ties with the well data. Confidence estimates are made by leaving selected wells out of the procedure and comparing the seismic-attribute converted values to the log-projected values at the missing well locations (Schultz and others, 1994b).

By design, OXY's proprietary geological-workstation software for the personal computer called the Stacked Curves System (SCPC) allows the management, manipulation, integration, and mapping of data from cores, well logs, seismic lines and volumes, tomography lines, and other sources (Srivastava, 1994). The SCPC system was upgraded to ex-

Watts, G. P.; and Hinterlong, G. D., 2000, Seismic estimation of porosity in a Permian San Andres carbonate reservoir, Welch field, Dawson County, Texas, *in* Johnson, K. S. (ed.), Platform carbonates in the southern Midcontinent, 1996 symposium: Oklahoma Geological Survey Circular 101, p. 327–338.

tract representative samples from grid files across selected areas, to cross-plot and determine probability of relationship for a pair of variables, and to perform multiple variable-linear-regression analysis. With this new SCPC capability, all components necessary for converting seismic attributes to log properties are in place.

WEST WELCH UNIT

The San Andres Formation in Welch field is representative of DOE Class II reservoirs. The field is in the northwest corner of Dawson County, Texas, on the northern shelf of the Midland basin (Fig. 1) and produces from dolomite of Permian age (Guadalupian) in the San Andres Formation (Fig. 2) at an average measured depth of 4,825 ft. The producing interval is approximately 400 ft below the top of the formation. The reservoir thins to the north, toward the paleoshoreline, and is overlain by impermeable evaporites and anhydritic dolomites. Permeability decreases to the east and west. The southern limits of the field are determined by downdip high water saturations.

The average porosity for the unit is 9.5%, with a geometric average permeability of 1 md. As of December 1995, the West Welch Unit had produced 67 MMBO, 11 BCFG, and 129 MMBW. Since waterflood operations began in 1960, 254 MMBW has been injected. The West Welch Unit currently has 340 active producing wells, with 207 active injection wells, and covers more than 12,000 surface acres. Current monthly production is 2,837 BO, 518 MCFG, and 22,896 BW. The unit-wide average water cut is 89%. The DOE project area covers 564 acres in the south-central part of the West Welch Unit (Fig. 3). Within the DOE project area, the average porosity is 12%, and the average permeability is 2.2 md. This area alone has produced 7.7 MMBO. The project area currently has 38 producing wells, 23 injection wells, two observation wells, and one water-supply well. Eleven of the wells within the project area have been cored.

GEOLOGY AND PETROPHYSICS

The San Andres reservoir in the West Welch Unit is composed of shallowing-upward carbonate cycles. The main pay in the southern part of the West Welch Unit includes four distinct shallowing-upward cycles: two major cycles with subtidal facies capped by thick supratidal deposits, and two minor cycles with relatively deep subtidal deposits consisting of mudstones and wackestones shallowing upward into tight packstones and grainstones deposited in a high-energy subtidal environment or intertidal environment. This sequence and the corresponding porosity and permeability relationships are illustrated on the type log in Figure 4.

The M1 log pick marks the top and the M5 pick marks the base of the main-pay interval. The M3 log pick is the boundary separating the two major cycles within the main-pay interval. The other log picks—M2S, M2S2, M4S, M4T, and M4S2—define the four minor cycles within the two major cycles. Northward in the unit, the minor cycles become more pronounced and are also capped by supratidal facies. In the northernmost part of the unit, the subtidal rocks are very thin and are capped by the thick supratidal rocks, creating the trap for oil and gas, as demonstrated on north–south cross section A–A′ (Figs. 3,5) across the West Welch Unit.

Available core and log data have been used to define the depositional cycles and to map flow units; however, the continuity of the individual porosity layers in the interwell area cannot be accurately determined with the current data set. The 3-D seismic volume will help to map interwell pay continuity and thus create a more accurate simulation, which we can use to better design, implement, and monitor the CO_2 flood.

As is the case with many older reservoirs, the distribution of data is sporadic. In order to maximize the number of control points, both the core and the log data had to be integrated

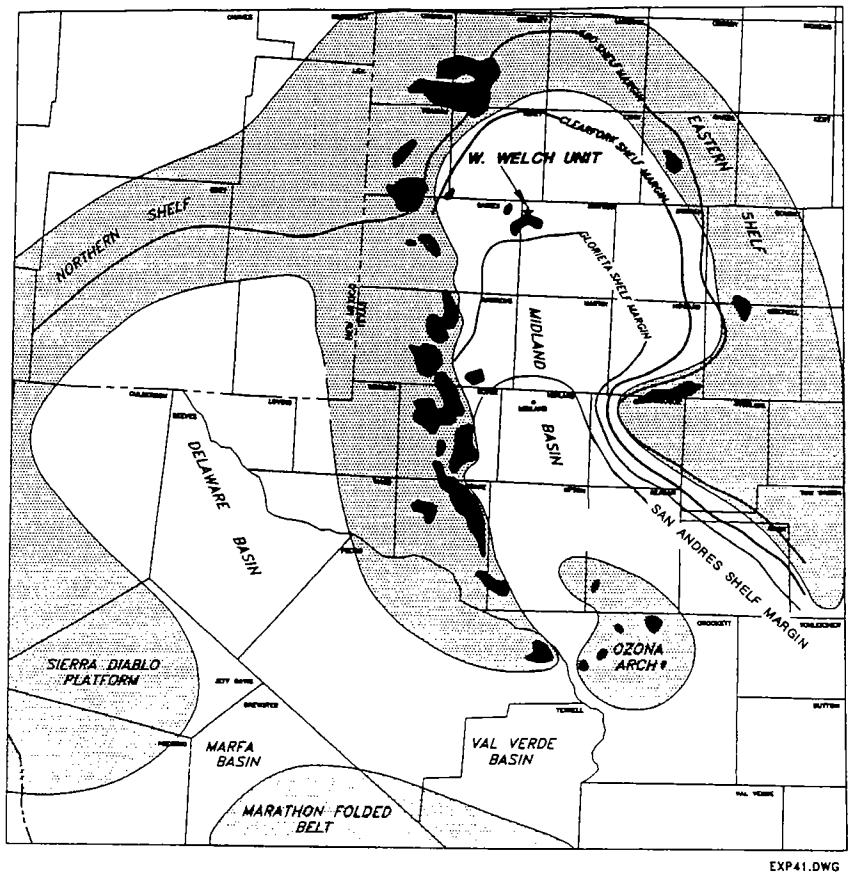

Figure 1. Simplified map of Permian basin, showing location of West Welch Unit with respect to other, similar DOE Class II San Andres reservoirs.

into a single data set. Only the modern logs (density/compensated neutron) were used to determine average porosity (PHIA). Wells with core data alone were used only if the entire interval had been cored and analyzed, thus avoiding bias. Wells for which both log and core data were available were used for quality control.

Porosity was determined from the compensated neutron/density logs after correcting for lithologic variations. Although additional wells were logged with older neutron logs, scaled in counts per second, the error in converting those logs to a porosity measurement introduces additional unreliable porosity values. Therefore, those logs were not used for porosity determination. Once satisfactory porosity measurements were determined, an arithmetic average (PHIA) was determined for the M1–M5 interval, without using a porosity cutoff, to better reflect the rock volumes sampled by the seismic data.

Age	Geologic Epoch		Delaware Basin		Central Basin Platform		Midland Basin
PERMIAN	Ochoan		Dewey Lake				
			Rustler				
			Salado				
			Castile				
	Guadalupian	Late	Bell Canyon	Capitan Reef	Tansill		
					Yates		
					Seven Rivers		
		Middle	Cherry Canyon	Goat Seep and Getaway	Queen		
					Grayburg		
			Cherry Canyon Tongue		San Andres	Upper	
						Lower	San Andres
		Early	Brushy Canyon				
	Leonardian		Bone Spring		Glorieta		Clear Fork
					Clear Fork (Yeso)		Spraberry
					Tubb-Drinkard		Dean

Figure 2. Geologic correlation chart for Permian formations in the Permian basin.

The average-porosity map (Pl. 1) shows a trend of increasing porosity to the south and southeast. The increase in porosity coincides with the increasing volume of subtidally deposited rocks. As a general rule, these rocks tend to have better preservation of porosity. Subsequent diagenesis creates most of the variation seen in this map, as anhydrite fills in the pores.

THREE-DIMENSIONAL SEISMIC DATABASE

The 3-D seismic data were acquired across Welch field from December 1992 through February 1993. The acquisition parameters and the seismic-data-processing sequence are summarized in Tables 1 and 2. The seismic area (Fig. 3) covers 36 mi^2, and the 3-D seismic data dedicated to the DOE project is a 5.9-mi^2 area. The seismic-bin locations are spaced 110 ft north–south by 165 ft east–west. There are a minimum of 24 seismic data points in the interwell spaces (Pl. 2), and the seismic volume also supplies approximately 150 additional control points for every well with log- and/or core-porosity determinations to help provide a more complete description of the reservoir continuity.

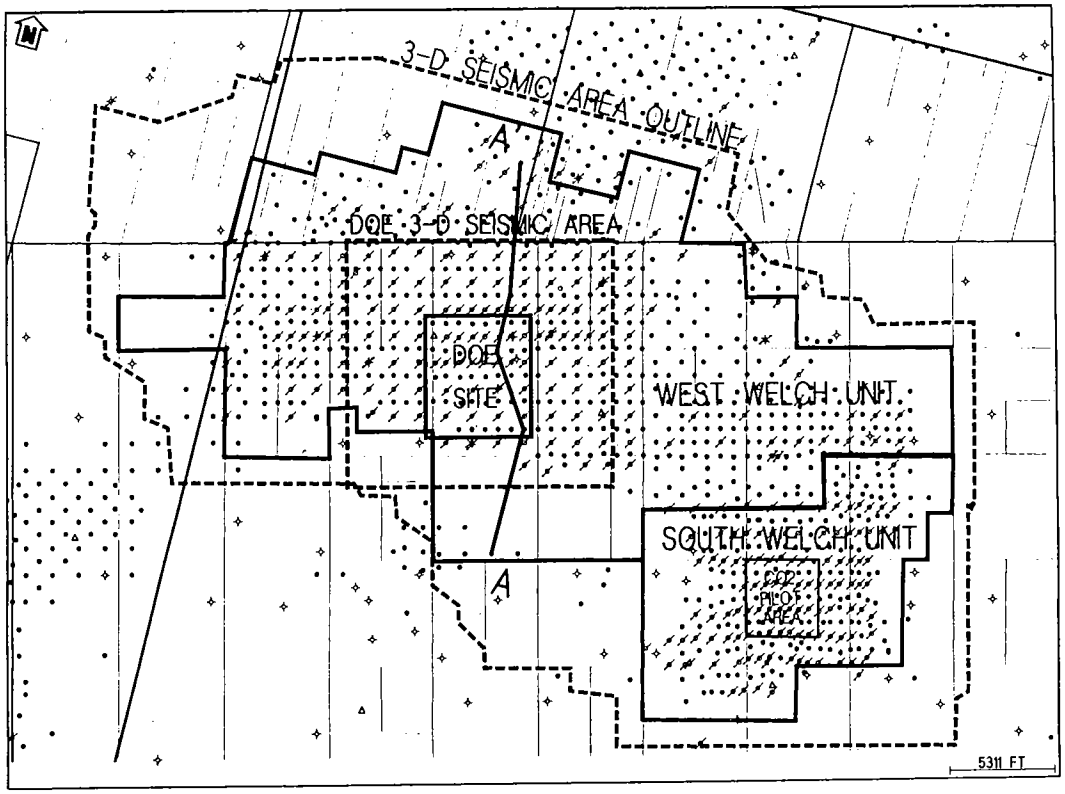

Figure 3. Location plat of Welch field, showing outlines of the producing units, the DOE demonstration site, and the 3-D seismic-data areas.

Table 1.—Seismic-Data-Acquisition Parameters, Welch Field, Dawson County, Texas

Recording Parameters	
Recording equipment:	Input/output two system
Channels:	480 with roll along
Receiver lines:	8
Groups per line:	60
Geophones per group:	12 (buried)
Sample rate:	2 milliseconds
Record length:	4 seconds
Low-cut filter:	3 hertz
High-cut filter:	120 hertz
Notch filter:	Out
Pre-amplifier setting:	48 decibels
Receiver Line and Group Parameters	
Receiver line interval:	1,320 ft aligned north–south
Receiver group interval:	220 ft
Geophone spacing:	Approximately 9 ft
Geophones per group:	12 in 100-ft linear array
Geophone type:	Mark Products L200 10 hertz
Energy-Source Parameters	
Vibroseis equipment:	4 Failing Y2400 vibrators on Pelton Advance II electronics on line at all times
Sweep length:	8 seconds
Sweeps per point:	8
Sweep frequency:	8–120 hertz, nonlinear, 6 decibels/octave
Source line interval:	1,320 ft aligned east–west
Source point interval:	330 ft, staggered between lines
Sampling Effort	
Variable bin spacing:	110 ft N–S by 165 ft E–W or 110 ft N–S by 82.5 ft E–W
Fold at 4,500-ft level:	8–9 for 110-ft × 165-ft bins and 5–6 for 110-ft × 82.5-ft bins
Total survey size:	36 mi^2
DOE 3-D seismic area:	5.9 mi^2

Synthetic seismograms were produced from nine sonic logs within the DOE seismic area to obtain correspondence between the well data and the seismic data. The synthetic wavelet that best matches the seismic data is produced from an 8/12–80/90 hertz bandpass filter. The seismic volume was found to be 90° out of phase with the sonic data. The best fit occurs when the seismic volume is rotated by 270° and the synthetic seismogram is rotated by 180° (Figs. 6,7). The M1 horizon (top of main pay) ties to a seismic peak-to-trough crossover, and the M5 horizon (base of main pay) ties to a seismic trough-to-peak crossover. Therefore, the San Andres main-pay interval corresponds to a relatively low-amplitude seismic trough (Fig. 7). The seismic trough correlates to the M3 log pick, which is the boundary separating the two major depositional cycles within the main-pay interval. Although both of these major depositional cycles were mapped for the study, only the total main-pay interval (M1–M5) is discussed in this paper.

Table 2.—Seismic-Data-Processing Sequence, Welch Field, Dawson County, Texas

1. Geometries	6. Velocity analysis
2. Preprocessing steps Spherical divergence Binary-gain removal Linear-noise removal	7. Residual statics 8. Normal moveout 9. Final stack
3. Trace deconvolution	10. Time-variant filter
4. Brute stack	11. Single-pass 3-D migration
5. Refraction statics	

The M1 and M5 horizons were correlated throughout the DOE 3-D volume, using the Vest 3DSEIS workstation software, which is designed for the personal computer. The seismic expression of the San Andres main-pay interval is dominantly a seismic trough of varying low amplitudes throughout the volume. There are places where isolated seismic peaks are scattered within this trough. These scattered peaks are more concentrated in the northern half of the DOE seismic area, which are exhibited on trace 115 (Fig. 7), a typical north–south seismic section from the middle of the seismic volume. A seismic-trough reflection disrupted with sporadic seismic peaks would produce variations in certain seismic attributes (amplitude and phase in particular) that are extracted across the seismic trough. The pay zones in the northern part of the study area thin, become tight owing to diagenesis, and pinch out in places. Mapping the variations in seismic attributes can help identify and delineate these kinds of changes within the reservoir (Watts and others, 1995b).

SEISMIC-ATTRIBUTE DATA

Seismic-attribute data are commonly associated with the amplitude, frequency, and phase information within the seismic record. More recently, data requiring specialized data processing—i.e., acoustic impedance, spectral ratio, and dozens of other measurements—are referred to as *seismic attributes*. And for purposes of seismic-guided estimation of log-derived properties, the term is even broader. Seismic-attribute data are all measurable quantities extracted from the seismic volume at the reservoir level and also include time or depth structure and isochron or isopach values.

Average velocity gradients were established from the seismic datum to each of the M1 and M5 horizons, using the well data for depth values and the seismic data for time values. The velocity gradients were applied to the seismic time picks to create subsea-depth structure values. The difference between the two depth structure values provides the isopach or reservoir-thickness value. The structural surfaces (Pls. 3,4) dip at approximately 1° to the south-southeast. A terrace feature is in the center of the map, with a low area in the form of a broad trough to the northwest. Notice the increased level of detail in the seismic map (Pl. 4), even though there are a large number of control points for the well-data map (Pl. 3).

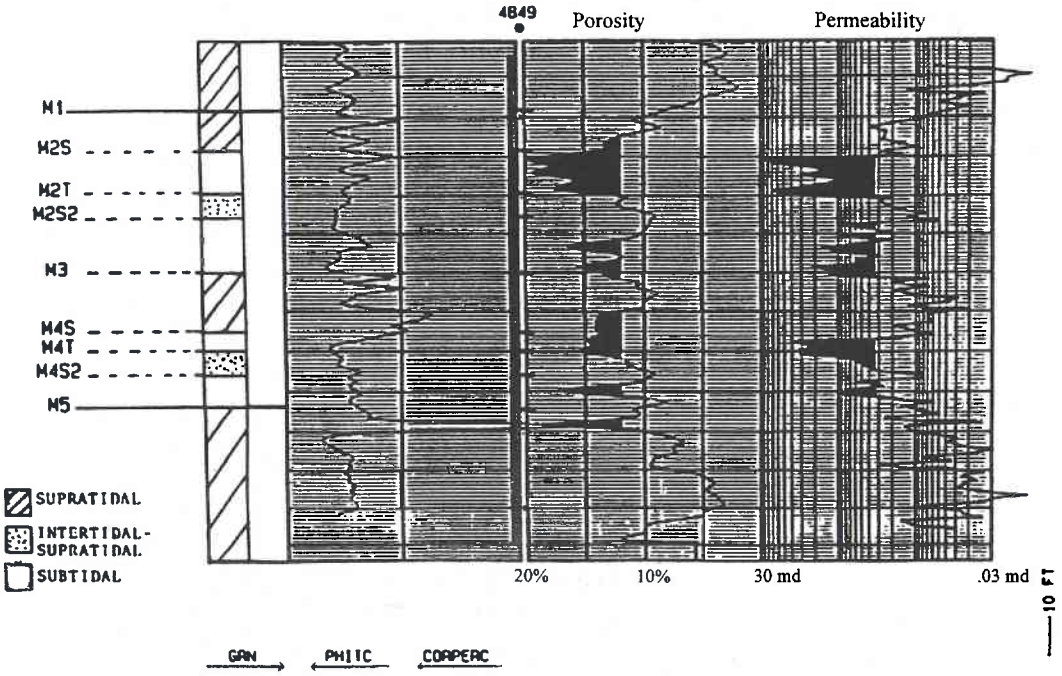

Figure 4. Type log for the West Welch Unit across the San Andres main-pay interval.

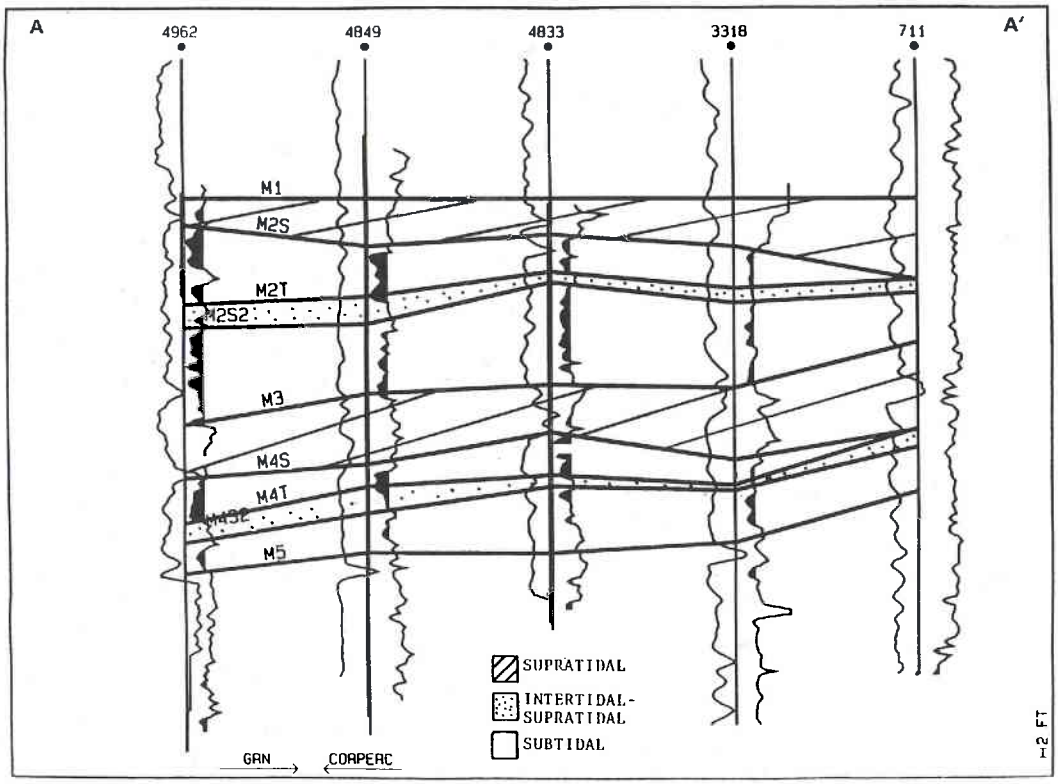

Figure 5. North–south cross section through the DOE demonstration site.

The Hilbert transform capability within Vest 3DSEIS was used to create seismic-attribute values of instantaneous amplitude, instantaneous frequency, and instantaneous phase. The 3DSEIS system was also used to average all three seismic attributes between the M1 and M5 horizons to create reservoir-amplitude, reservoir-frequency, and reservoir-phase files. The amplitude and phase maps (Pls. 5,6) both contain positive and negative values across the area. The negative amplitudes represent the main-pay seismic trough and increase in negative value to the south. The isolated areas of positive amplitudes across the northern half of the map represent the sporadic seismic peaks within the main-pay seismic trough. The seismic volume is phase rotated by 270°, which is the same as –90°. The mapped phase values are from the –90° rotation. Therefore, the negative- and positive-phase values coincide with the negative- and positive-amplitude distribution.

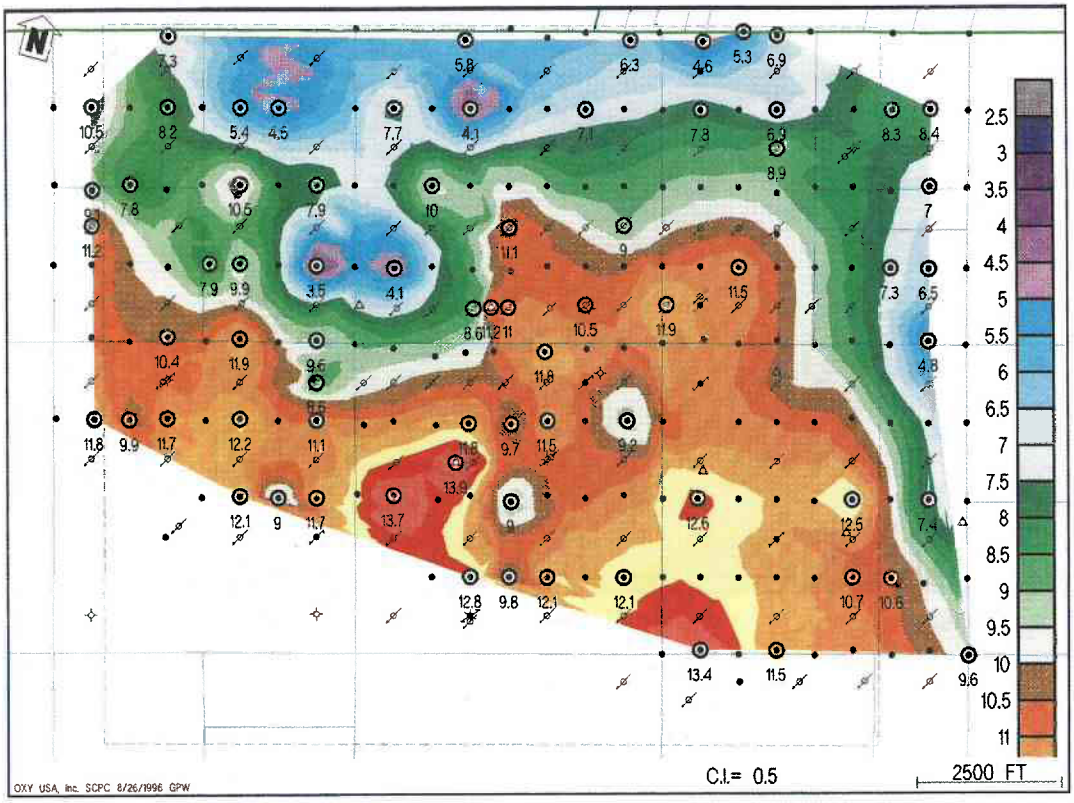

Plate 1. Gridded-map distribution of the average-porosity values derived from the modern well-log data combined with core measurements.

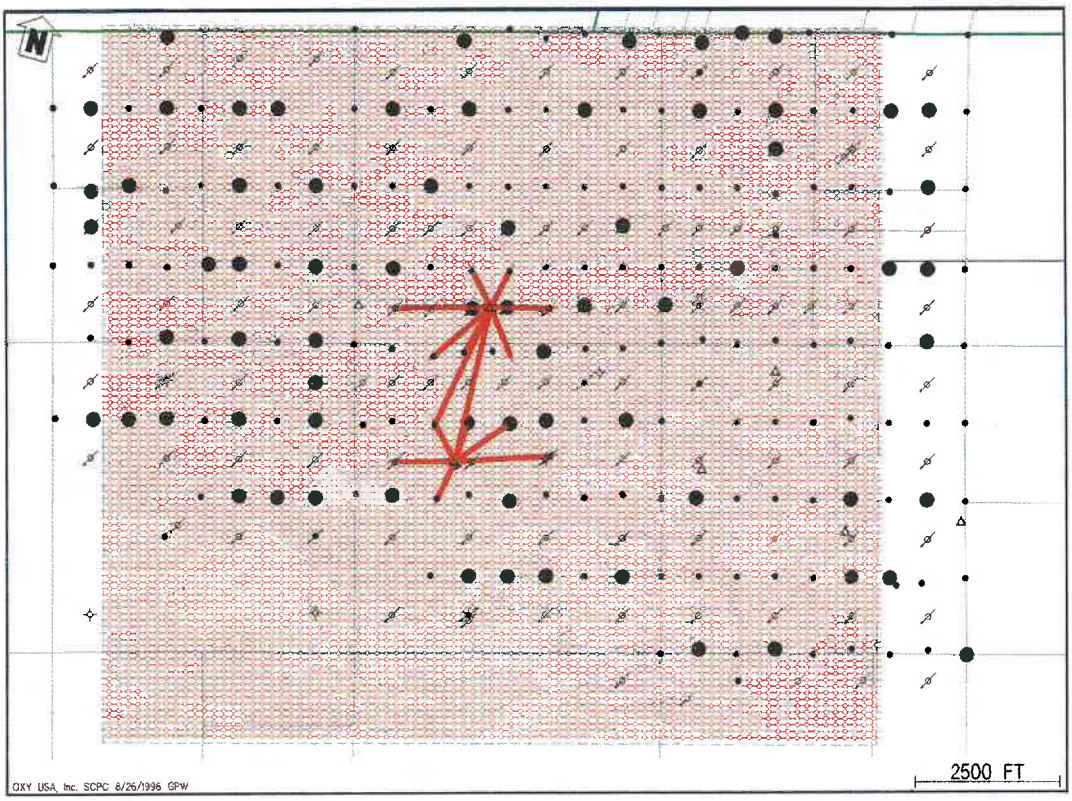

Plate 2. Base map showing the spatial relationships of the wells, wells with porosity measurements, cross-well seismic-tomography lines, and 3-D seismic bins.

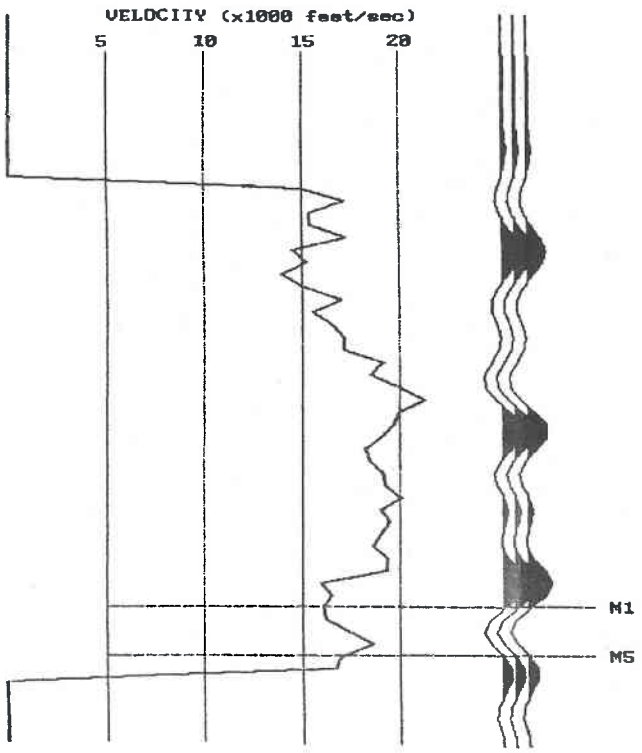

Figure 6. Sonic-log curve from West Welch Unit well 4852 with synthetic seismic waveform derived from sonic-generated reflection coefficients. M1 and M5 log picks are correlated to the synthetic seismogram.

CORRELATION OF SEISMIC ATTRIBUTES TO POROSITY

The five seismic attributes from above—reservoir structure (M1 horizon), reservoir thickness (M1–M5 isopach), reservoir amplitude, reservoir frequency, and reservoir phase—were all sampled to the well locations. The average porosity (PHIA) values were cross-plotted with each seismic attribute. All five cross-plots have considerable scatter, and each was evaluated with a significance measure derived from the slopes of the data points called Kendall's tau indicator (Schultz and others, 1994a). The tau indicator is a measure of the probability of relationship for both linear and nonlinear distributions, and it is posted above each cross-plot in the SCPC system. The tau indicator for each seismic attribute evaluated with the porosity is summarized in a quality matrix as follows:

PHIA Quality Matrix—Kendall's Tau Indicator (%)

Seismic attribute	M1 structure	M1–M5 isopach	M1–M5 amplitude	M1–M5 frequency	M1–M5 phase
Tau indicator	98.7	20.3	95.7	49.2	97.6

The tau indicator is required to be greater than 70% to be considered in the development of a calibration equation. The quality matrix shows that the cross-plotted distributions for the structure (SUBC), amplitude (AMPS), and phase (PHAZ) meet this requirement.

The multiple variable-linear-regression-analysis capability within OXY's SCPC software is used to produce regres-

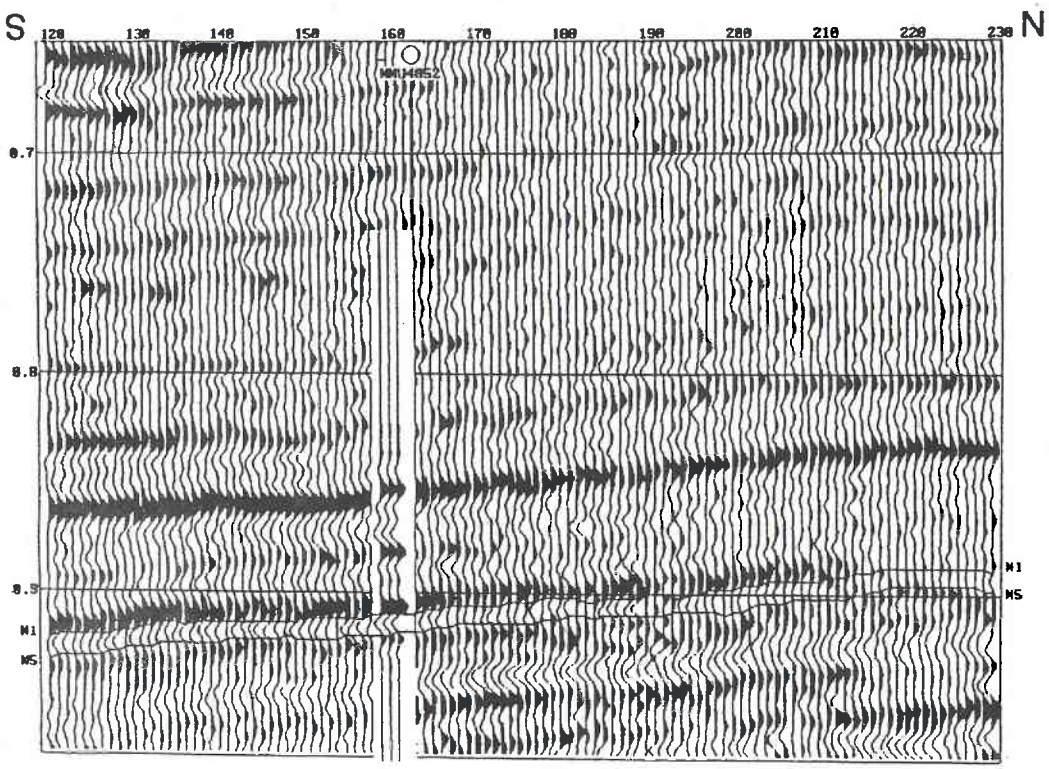

Figure 7. North–south seismic section, trace 115, from the 3-D volume inlaid with the synthetic seismogram from WWU well 4852, showing the correspondence between the sonic and seismic reflectivity. Seismic section courtesy of Geotrace Technologies, Inc.

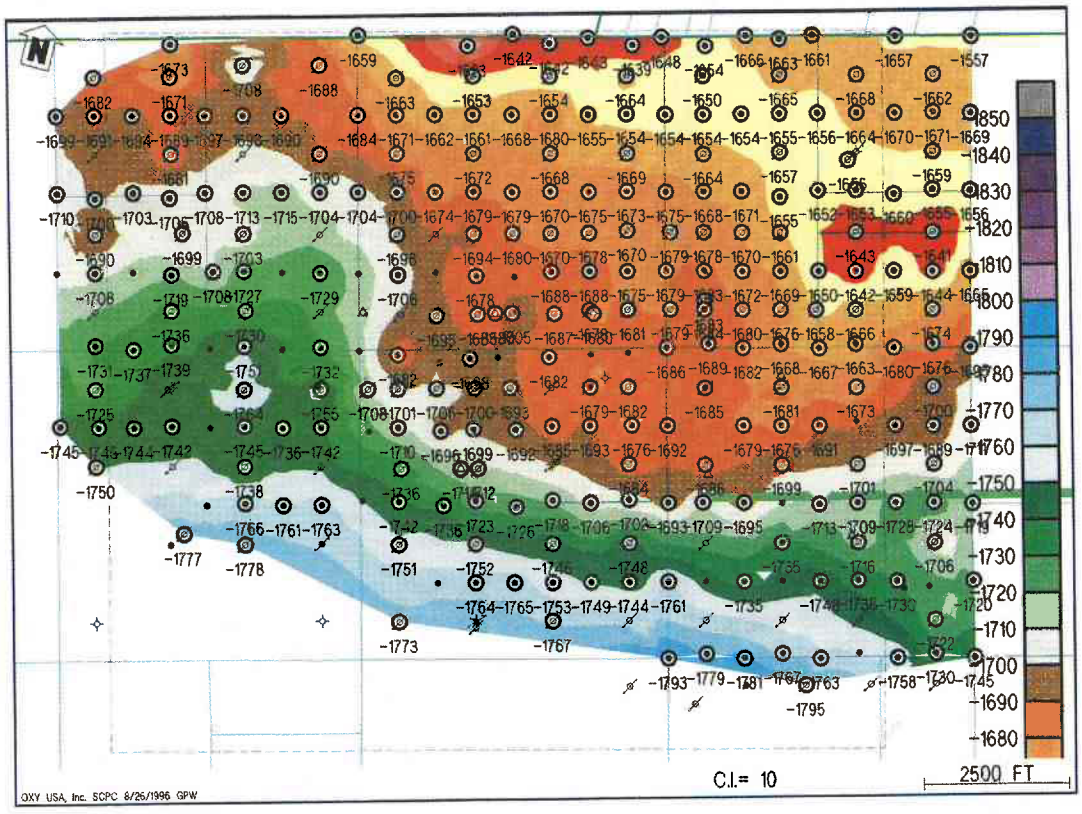

Plate 3. Gridded structure map of the top of the M1 well-log picks.

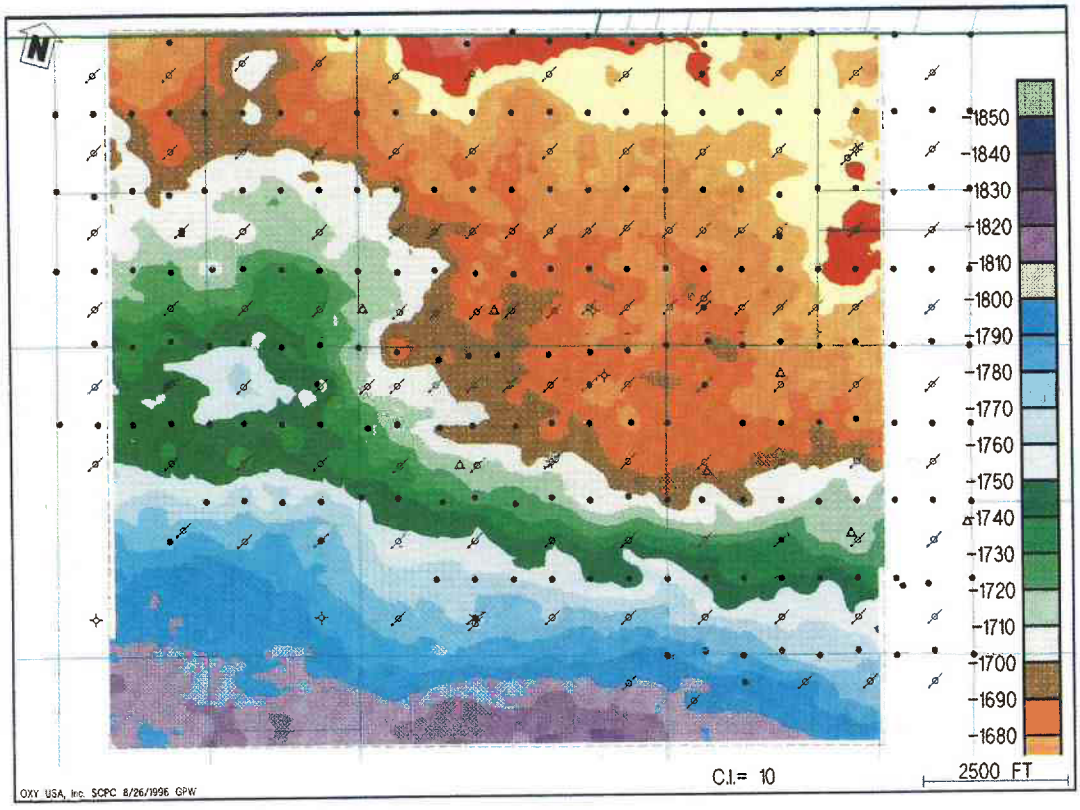

Plate 4. Seismic-structure map of the M1 horizon tied to the top of the M1 well-log picks.

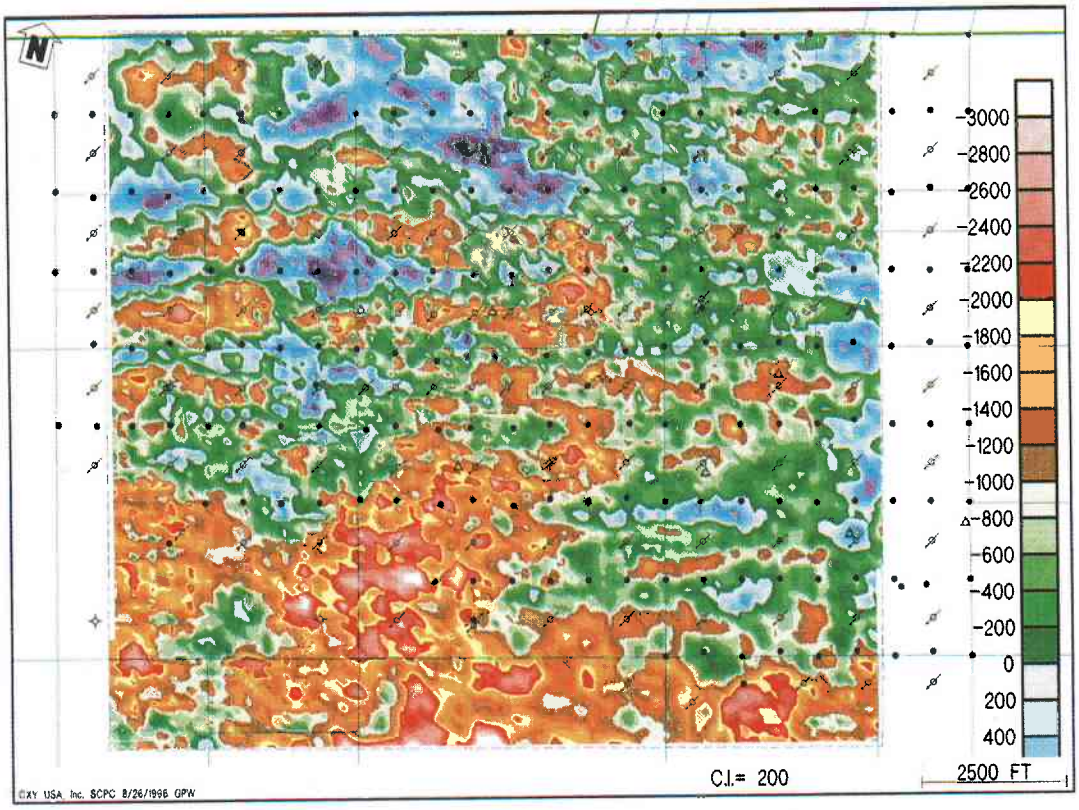

Plate 5. Map of the seismic-amplitude distribution between the M1 and M5 horizons.

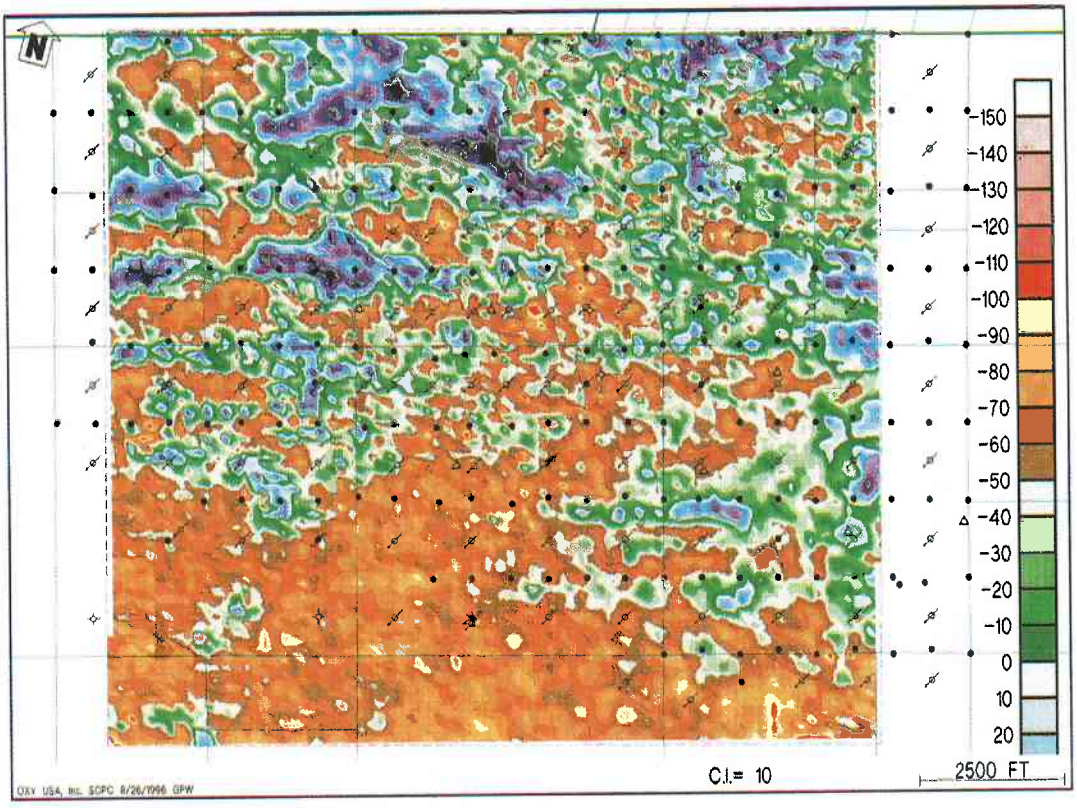

Plate 6. Map of the seismic-phase distribution between the M1 and M5 horizons.

sion coefficients. The average porosity (PHIA) was entered as the dependent variable, and the three qualifying seismic attributes (SUBC, AMPS, and PHAZ) were input as independent variables. The regression coefficients were generated and used in the equation

$$PHIA = -38.1103 - (0.0274\ SUBC) - (0.0006\ AMPS) - (1.0168\ PHAZ)$$

to calculate a predicted PHIA value at each seismic-bin location. The map of the seismic PHIA predictions (Pl. 7) gives estimates of the log- and core-determined PHIA that do not exactly tie the well data. The cross-plot of the seismic-predicted PHIA versus the well-data PHIA (Fig. 8) illustrates the discrepancy. If the points are distributed along a diagonal, the seismic-predicted porosity values would agree exactly with the log- and core-derived PHIA values. Because it is desirable in reservoir simulation for the predictions to agree at the wells, a residual correction is necessary (Jones and others, 1986).

SEISMIC-GUIDED MAPPING

The seismic PHIA predictions at the well locations were subtracted from the actual PHIA computations from the well data to create a PHIA differences (residuals) file. The PHIA residuals were gridded, sampled to the seismic-bin-location files, and added to the seismic-PHIA-prediction values to create a seismic-guided PHIA file. The cross-plot of the seismic-guided PHIA with the log-derived PHIA (Fig. 9) is greatly improved over the cross-plot involving the seismic-predicted PHIA (Fig. 8). All 59 seismic-guided PHIA values agree with the well PHIA to within 1%.

The seismic-guided PHIA map (Pl. 8) has significantly greater detail than the original PHIA distribution displayed on the map from the well data (Pl. 1). A comparison of the two maps reveals that the seismic-guided PHIA has higher porosity values in the east-central part of the study area. The areas of low porosity to the north are certainly delineated with greater definition in the seismic-guided distribution. And the seismic-guided map provides extension of the reservoir to the southern part of the study area. The seismic-guided-mapping method has used seismic measurements to shape the interwell geologic variability and to map beyond the well control with reliability (Watts and others, 1995a).

SUMMARY AND CONCLUSIONS

The most common distance between wells with modern log suites and/or core data is 957 ft with a non-uniform distribution. Therefore, much lateral interpolation is needed to produce a reservoir-simulation model at a grid-node spacing of 100 by 100 ft. The current interpretation of depositional cycles subdivides the main-pay interval into an eight-layer model. This interpretation provides bed thicknesses to as little as 6 in. The 3-D seismic data are able to resolve bed thickness to 35 ft, and the two major cycles of deposition within the main-pay interval are the smallest mappable seismic units. The 3-D seismic-data evaluation has provided reservoir-elevation values (structure grids), reservoir-thickness values (isopach grids), and average-porosity estimates across the reservoir intervals (seismic-guided PHIA grids) at a uniform spacing of 110 ft north–south by 165 ft east–west across the DOE 3-D seismic area. The lateral interpolation to a 100- by 100-ft grid will be minimal.

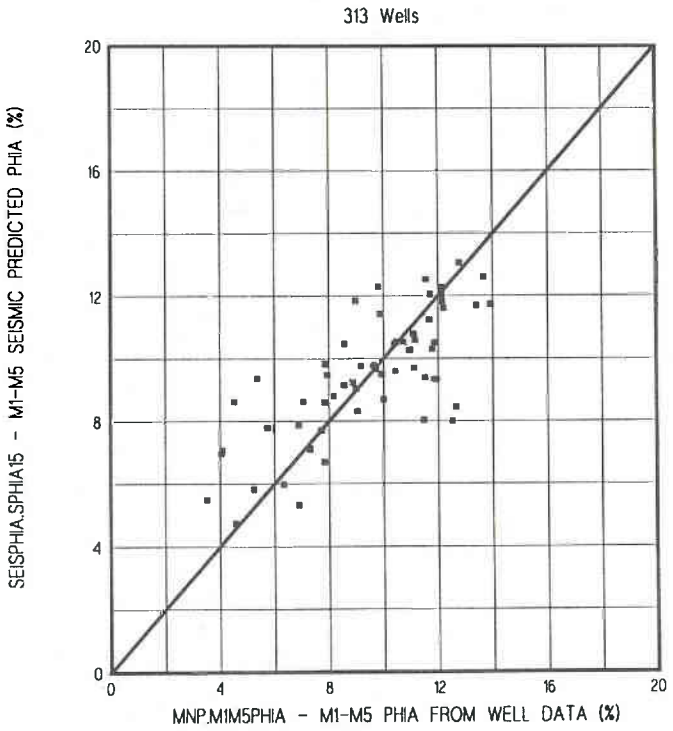

Figure 8. Cross-plot of the average porosity from the well data with the seismic-predicted porosity. Probability of relationship using Kendall's tau indicator = 99.6%.

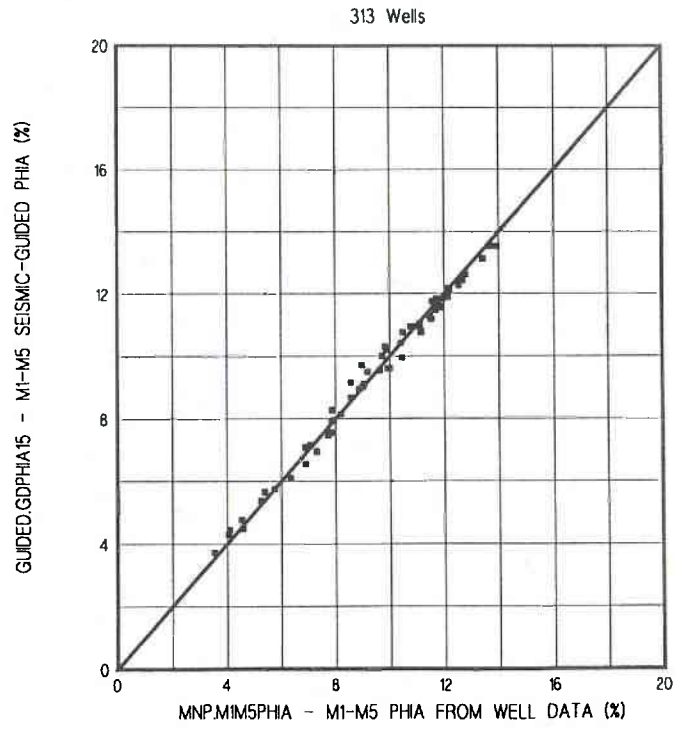

Figure 9. Cross-plot of the average porosity from the well data with the seismic-guided porosity. Probability of relationship using Kendall's tau indicator = 100.0%.

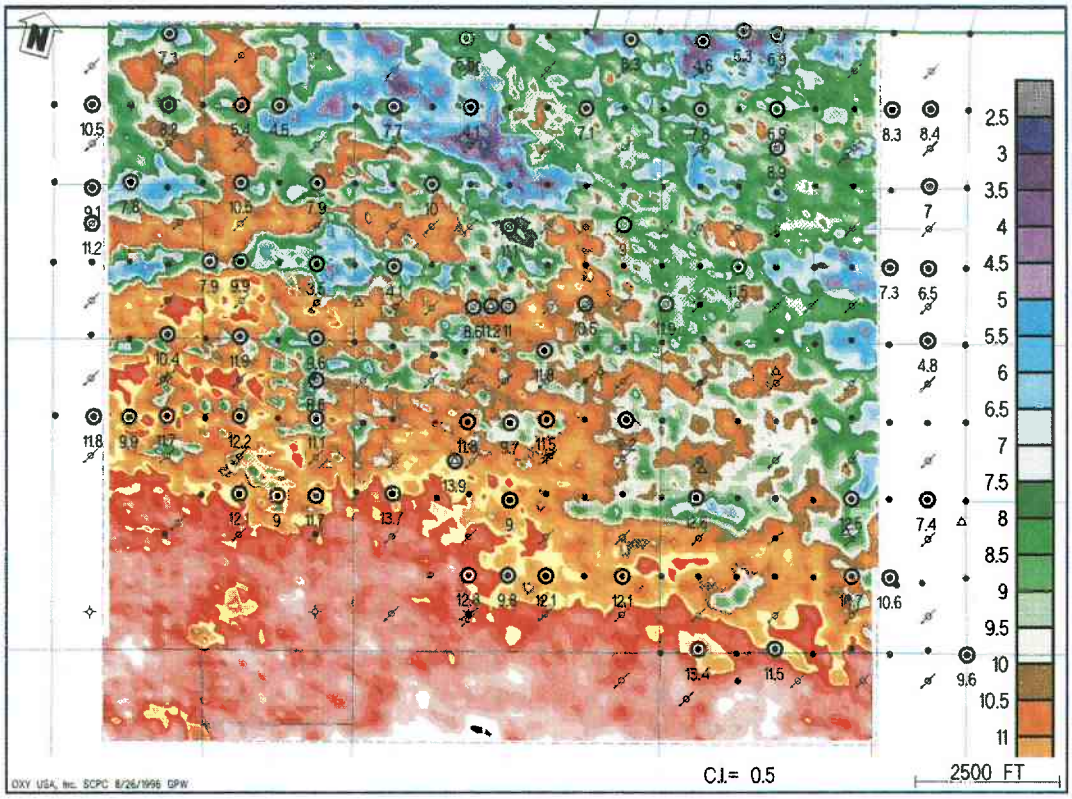

Plate 7. Seismic-predicted average-porosity distribution within the M1 to M5 interval.

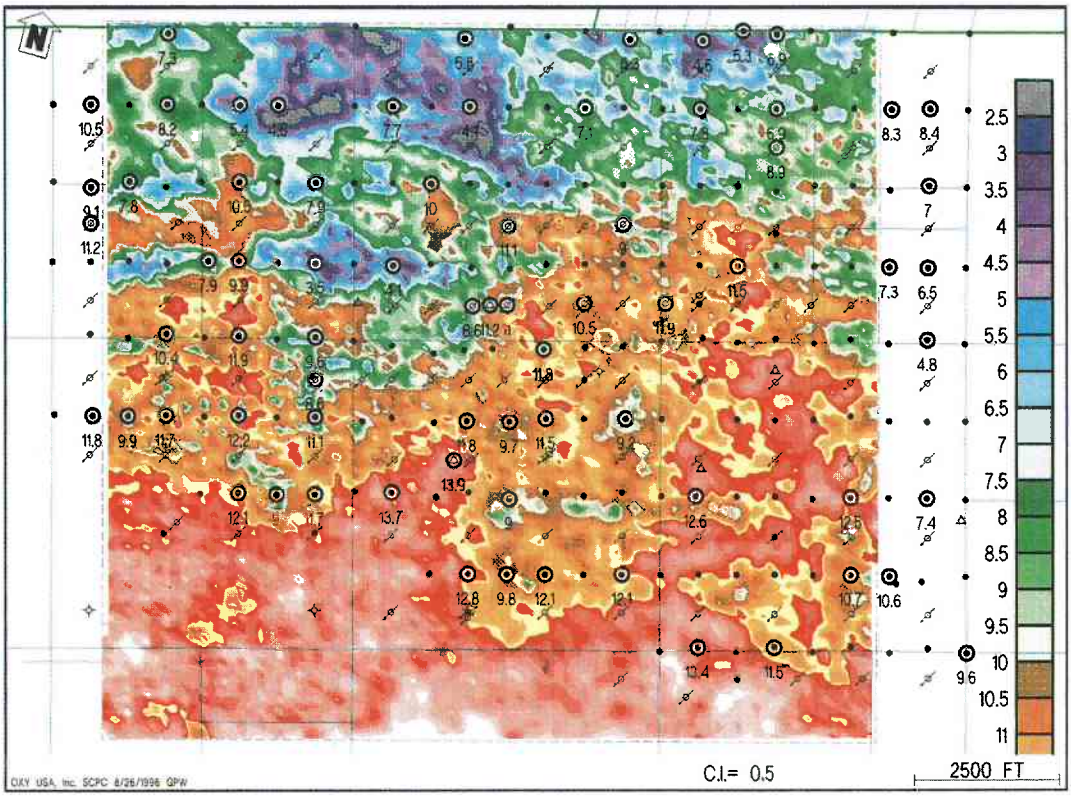

Plate 8. Seismic-guided average-porosity distribution within the M1 to M5 interval.

Several benefits are gained by using the 3-D seismic data in the reservoir-simulation model. All the detailed areal variation in the interwell space expressed by the seismic-attribute information is contained in the structure, isopach, and porosity interpretations. The seismic interpretations are accurately tied to the well data. The seismic interpretation reveals extensions of the reservoir outside the well control in the southern part of the DOE 3-D seismic area.

The seismic-bin spacing (110 by 165 ft) supplies approximately 150 additional control points for every well with porosity measurements to provide a more complete description of reservoir continuity. The porosity profile from the well data can be proportioned to match the seismic-guided porosity values at each bin location. This will effectively extend the vertical resolution of the well control to the seismic-data volume within the constraints of the seismic-guided porosity values. The final reservoir-porosity volume will be consistent with the core, the well-log, and the seismic data.

ACKNOWLEDGMENTS

This paper is part of an effort to transfer to industry technological methods learned from the U.S. Department of Energy–sponsored project (DE-FC22-93BC149900) at the West Welch Unit. We are indebted to both the Department of Energy and OXY USA Inc. for allowing us to use the West Welch Unit as a case-history study for the seismic-guided estimation of log-properties methodology. We also thank GeoStrat for granting permission to illustrate and discuss their seismic data in this paper. And much gratitude is extended to Francis Herzog for graphic-arts support and to Erma Galindo for finalizing the manuscript.

REFERENCES CITED

Crichlow, H. B., 1977, Modern reservoir engineering—a simulation approach: Prentice-Hall, Englewood Cliffs, New Jersey, 354 p.

Jones, T. A.; Hamilton, D. E.; and Johnson, C. R., 1986, Contouring geologic surfaces with the computer: Van Nostrand Reinhold, New York, 314 p.

Schultz, P. S.; Ronen, Shuki; Hattori, Masomi; and Corbit, Chip, 1994a, Seismic-guided estimation of log properties, Part 1: A data-driven interpretation methodology: Leading Edge (May), Society of Exploration Geophysicists, Tulsa, p. 305–310, 315.

Schultz, P. S.; Ronen, Shuki; Hattori, Masomi; Mantran, Pascal; and Corbit, Chip, 1994b, Seismic-guided estimation of log properties, Part 3: A controlled study: Leading Edge (July), Society of Exploration Geophysicists, Tulsa, p. 770–776.

Srivastava, G. S., 1994, Interactive software integrates geological and engineering data: Oil and Gas Journal, v. 92, no. 36, p. 85–91.

Watts, G. P.; Lyons, T. D.; and Taylor, A. R., 1995a, 3-D seismic prediction of reservoir properties, West Moose Field, Ector County, Texas: High-Definition Seismic Guidebook, Rocky Mountain Association of Geologists, Denver, p. 185–195.

Watts, G. P.; Hinterlong, G. D.; Taylor, A. R.; Justice, J. H.; and Underwood, G. E., 1995b, DOE Class II Project Technical Report: 3-D seismic evaluation for reservoir description, West Welch Unit, Dawson County, Texas: Presentation to Petroleum Industry Alliance at Center for Energy and Economic Diversification, Midland, Texas, 60 p.

Reservoir Characterization of the Upper Permian Grayburg Formation in Preparation for a Horizontal-Well CO_2 Flood, South Cowden Unit, West Texas

Craig D. Caldwell, Ken J. Harpole, and Matt G. Gerard
Phillips Petroleum Company
Bartlesville, Oklahoma

ABSTRACT.—Since initial development in the late 1940s, South Cowden Unit (SCU), on the eastern margin of the Central Basin platform of the Permian basin, has produced 35 million barrels of oil from the Upper Permian Grayburg Formation. Under waterflood since 1965, SCU is approaching the economic limit of waterflood operation, and a carbon dioxide (CO_2) flood employing horizontal injection wells has been proposed. A detailed geologic description of the reservoir interval was prepared for integration into a reservoir-simulation model used to predict CO_2-flood performance.

The reservoir interval at SCU has a gross thickness of approximately 150 ft and is composed mainly of burrow-mottled dolopackstones. These dolostones are characterized by a distinctive gray/tan mottling reflecting variations in porosity and oil staining. Tan oil-stained areas, interpreted to be carbonate-sand-filled burrows, are dolograinstones, dolopackstones, and washed dolopackstones. Porosity in these areas typically ranges from 10% to 32% and is intergranular, intercrystalline, and moldic. Permeability generally varies from 2 to 400 md. Gray interburrow areas, lacking oil staining, are dolopackstones and dolowackestones with 2–9% moldic and intercrystalline porosity and 0.002–2-md permeability. The relative amounts of tan and gray dolomite, determined by the degree of bioturbation, can profoundly affect reservoir porosity and permeability.

Reservoir porosity and permeability are also a function of anhydrite content. An inverse relationship exists between porosity and permeability and the amount of poikilotopic anhydrite cement in the tan-dolomite areas. Limited core data suggest that the decrease in porosity in the northwestern (paleolandward) part of SCU is related, at least in part, to an increase in anhydrite content.

Reservoir permeability is a function of bioturbation, anhydrite content, and pore size in the tan-dolomite areas. Pore size is related to depositional texture, diagenesis, and consequent crystal size. Very finely to finely crystalline tan dolomites, most likely reflecting dolomitization of muddy burrow-filling sediments, are characterized by very small intercrystalline pores and permeabilities generally ranging from <1 to 16 md. Finely to medium-crystalline tan dolograinstones and washed dolopackstones, reflecting dolomitization of carbonate-sand-filled burrows with relatively minor mud-size material, are characterized by larger intergranular pores and significantly better permeabilities typically ranging from 100 to 500 md. Tan dolomites with similar porosities may have markedly different permeabilities because of differences in pore size, and thus more than one porosity/permeability transform is necessary to characterize rocks of the SCU reservoir interval.

The vertically oriented character of the porous and permeable tan-dolomite burrow structures, characterizing rocks of the SCU reservoir interval, provides a favorable condition for the application of horizontal injection wells. The vertical movement of fluids and gases through the reservoir interval may be partially restricted, however, by rare, laterally continuous, relatively low-permeability sandy dolopackstone layers. It is critical to determine the stratigraphic positions of these low-permeability layers relative to those of the proposed horizontal, CO_2-injection wells.

INTRODUCTION

More than 10 billion barrels of oil has been produced from the San Andres and Grayburg Formations of the Permian basin, west Texas and southeast New Mexico (Bebout and others, 1987). The San Andres and Grayburg fields, discovered mainly in the 1920s, 1930s, and 1940s, have cumulative productions ranging from <1 million to >750 million barrels of oil (Ward and others, 1986). Major Permian basin San Andres and Grayburg fields, including South Cowden Unit, the focus of this study, are shown in Figure 1.

San Andres and Grayburg reservoirs exhibit low recovery efficiencies, generally <30%, in response to conventional primary- and secondary-recovery practices. Galloway and others (1983), Tyler and others (1984), Ruppel and Cander (1988), and Fogg and Lucia (1990) stated that the low recovery effi-

Caldwell, C. D.; Harpole, K. J.; and Gerard, M. G., 2000, Reservoir characterization of the Upper Permian Grayburg Formation in preparation for a horizontal-well CO_2 flood, South Cowden Unit, west Texas, *in* Johnson, K. S. (ed.), Platform carbonates in the southern Midcontinent, 1996 symposium: Oklahoma Geological Survey Circular 101, p. 339–353.

ciencies of these reservoirs are a function of inefficient sweep of the reservoirs related to an incomplete understanding of reservoir heterogeneities. The aforementioned authors suggested that a significant amount of the remaining mobile oil can be produced through a better understanding of the reservoir architecture and the integration of geologic and engineering data to develop and improve infill-drilling programs, carbon dioxide (CO_2) and waterflood programs, and selective completion procedures. This study provides a detailed petrographic description of the South Cowden Unit reservoir interval for integration into a reservoir-simulation model for a proposed CO_2 flood using horizontal injection wells.

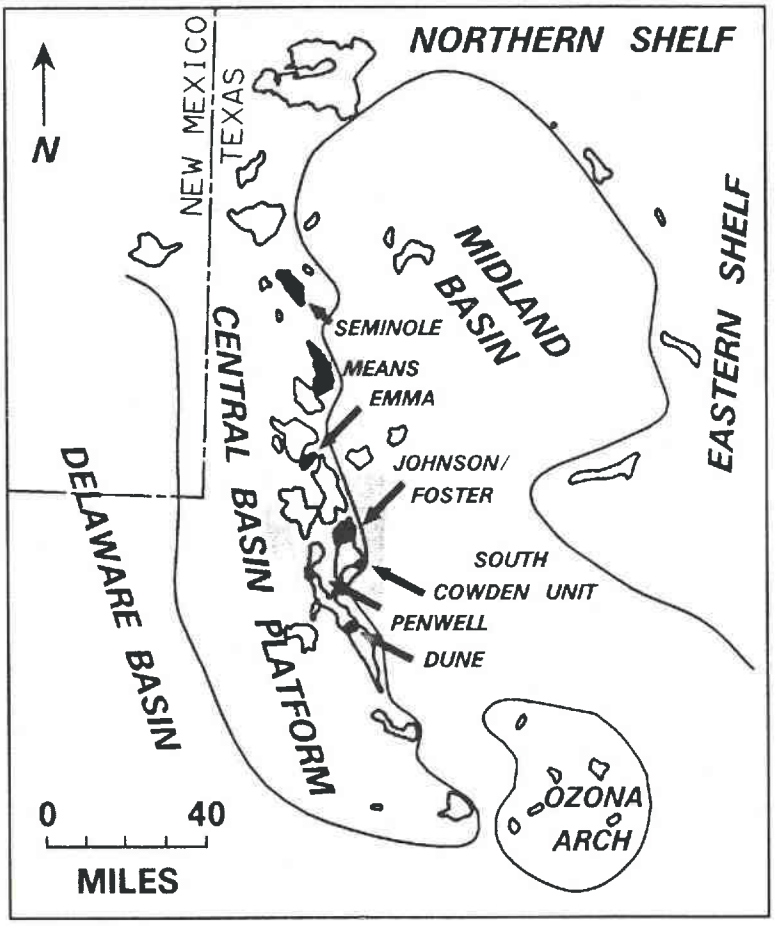

SYSTEM	SERIES	STRATIGRAPHIC UNIT
UPPER PERMIAN	GUADALUPIAN	CAPITAN FM. / TANSILL FM. / YATES FM. / SEVEN RIVERS FM.
		GOAT SEEP / QUEEN FM.
		GRAYBURG FM.
		SAN ANDRES FM.
LOWER PERMIAN	LEONARDIAN	GLORIETA FM.
		CLEAR FORK GP.

Figure 1. Paleogeographic map of the Permian basin, west Texas and southeast New Mexico, and the Leonardian and Guadalupian stratigraphic column for this region. The paleogeographic map shows those San Andres and Grayburg fields that have produced >10 MMBO. Named fields (black) are referred to in the text. The square shaded area on the map is Ector County, Texas. (Modified from Bebout and Harris, 1986.)

FIELD/UNIT HISTORY

South Cowden field, discovered in 1932, is in Ector County, Texas, on the eastern margin of the Central Basin platform (Fig. 1). The field is part of a nearly continuous trend of Upper Permian Grayburg production extending northward into Foster and Johnson fields. As of January 1994, South Cowden field had produced 154 million barrels of oil from the Grayburg Formation (Ruppel and Bebout, 1995). The number of producing wells in the field reached 516 in 1980 (Ward and others, 1986).

South Cowden field is divided into several units. The most productive units are, from north to south: the Unocal Moss Unit, the Fina Emmons Unit, and the Phillips Petroleum South Cowden Unit (Fig. 2). South Cowden Unit (SCU), the focus of this study, produces from an anticlinal structure formed by the drape of Grayburg strata over a lobe-shaped San Andres depositional "thick" (Ruppel and Bebout, 1995). The gross thickness of the Grayburg reservoir interval at SCU is approximately 150 ft, with the top of the interval occurring at drilling depths of approximately 4,500–4,700 ft.

Hydrocarbon production from the area that is now South Cowden Unit began in 1948. Since then, approximately 100 producing wells were drilled in the area on 20-acre spacing. The area was unitized for secondary waterflood operations in 1965 with initial water injection from peripheral wells around the edge of the anticlinal structure. Leaseline cooperative water injection along the northern unit boundary was added in the early 1970s, and several additional water-injection wells were drilled in the interior of the unit in the late 1970s and early 1980s. In early 1995, SCU, nearing its economic limit for waterflood operations, was producing just over 400 BOPD at a water cut greater than 95% from 39 producers and 11 water injectors (Fig. 3). The cumulative primary and secondary recovery from SCU is estimated to be 35 million STB of oil, or approximately 20% of the original oil in place.

CO_2 feasibility studies conducted in the early 1990s indicated that SCU was a good technical candidate for a conventional CO_2 flood, but the project did not meet economic criteria. Harpole and others (1996) suggested that most of the wells

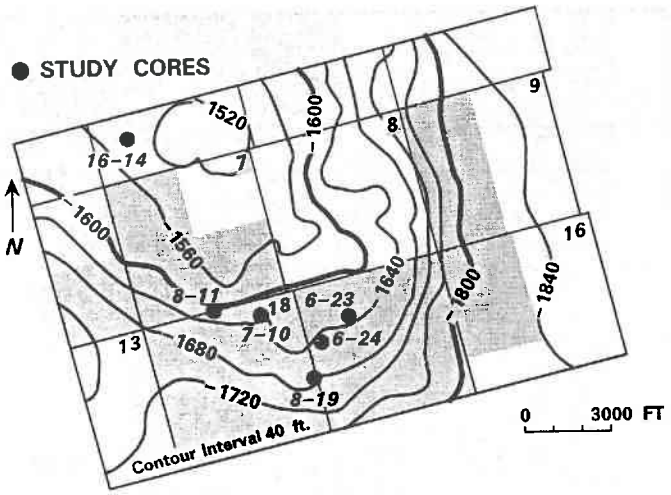

Figure 2. Map showing structure at top of Grayburg Formation. South Cowden Unit (SCU) is shaded. Fina Emmons Unit is sec. 8, blk. 42, directly north of SCU. The remaining area to the north and northwest is the Unocal Moss Unit. Wells from which cores were studied are shown.

in the unit were not suited for conversion to a CO_2 water and gas (WAG) injection because of mechanical or completion problems, and the cost for new injection wells and related facilities for a conventional CO_2 flood was too high relative to the recoverable oil. Thus, a CO_2 flood was proposed using two horizontal injection wells drilled from a centralized facility, thereby reducing upfront capital costs. Engineering studies and a detailed reservoir description, the latter of which is summarized in this paper, will be integrated into a reservoir-simulation model for a CO_2 flood using horizontal injection wells. This project was selected as a demonstration project under the U.S. Department of Energy (DOE), Class II Oil Program, for shallow-shelf carbonate reservoirs and is financially supported in part by the DOE.

METHODS OF INVESTIGATION

Approximately 1,300 ft of core was described from five SCU wells (SCU 8-19, 470 ft; SCU 7-10, 249 ft; SCU 8-11, 170 ft; SCU 6-23, 237 ft; and SCU 6-24, 180 ft). An additional 120 ft of core was reviewed from the Unocal No. 16-14 Moss Unit well. Locations of the cored study wells are shown in Figure 2. Cored intervals are primarily from the Grayburg Formation; the lower 120 ft and 35 ft of the overlying Queen Formation were cored in the SCU 8-19 and 6-23 wells. In addition to macroscopic descriptions, 211 thin sections were described and point counted (SCU 8-19, 97 t.s.; 7-10, 63 t.s.; 8-11, 12 t.s.; 6-23, 15 t.s.; 6-24, 13 t.s.; and Moss Unit 16-14, 11 t.s.). Most of these thin sections are from the Grayburg reservoir interval. A total of 53 samples from the SCU 8-19, 7-10, and 8-11 wells were analyzed by X-ray diffraction. The most complete Grayburg–Queen section was recovered from the SCU 8-19; thus, this well serves as the type well for much of the following discussion (Fig. 4). The Grayburg Formation at SCU is divided into seven stratigraphic intervals, designated zones A–G (Fig. 4). The basis for this division is discussed later in this report.

LITHOFACIES DESCRIPTIONS

Eleven rock types defined from the SCU Grayburg and Queen core studies are grouped into five dolostone lithofacies (Fig. 4, key), as follows: (1) fusulinid dolowackestone, (2) ooid-peloid dolograinstone, (3) sandy dolopackstone, (4) burrow-mottled dolopackstone, and (5) fenestral dolopackstone.

Fusulinid dolowackestones and ooid-peloid dolograinstones make up the lower part of the cored Grayburg Formation at SCU (zone A, Fig. 4). The middle part of the Grayburg (zones B, C, and the lower part of zone D, Fig. 4) is interbedded sandy dolopackstone, ooid-peloid dolograinstone, fusulinid dolowackestone, and burrow-mottled dolopackstone. The upper Grayburg (zones E, F, G, and the upper part of zone D) is dominated by burrow-mottled dolopackstone. Sandy dolopackstones and fenestral dolopackstones make up the cored portion of the Queen Formation. The SCU reservoir interval, zones C through F, is composed mainly of burrow-mottled dolopackstones.

Although most Grayburg dolostones at SCU contain <2% anhydrite, some Grayburg intervals contain as much as 15–20% anhydrite. Anhydrite occurs as replacement nodules and cements intercrystalline, intergranular, moldic, and fracture porosity. In the SCU 8-19, the lower 50 ft of the Queen Formation is 1–10% anhydrite, and the overlying 70 ft of cored Queen is 15–45% anhydrite. Gypsum is rare in the Grayburg–Queen cored interval and is generally restricted to white alteration rims on anhydrite nodules.

Siliciclastics, mainly very fine- to fine-grained detrital quartz and feldspar, are <5% in all Grayburg–Queen lithofacies with the exception of the sandy dolopackstone lithofacies. Sandy dolopackstones of the Grayburg and Queen Formations are 10–20% and 10–40% siliciclastics, respectively. Gypsum and calcite are generally absent or occur in trace amounts in the Grayburg and Queen Formations. Depositional textures are difficult to distinguish in all lithofacies owing to diagenesis, in particular dolomitization.

Fusulinid-Dolowackestone Lithofacies

Much of the lower Grayburg Formation at South Cowden Unit is composed of fusulinid dolowackestones and dolopack-

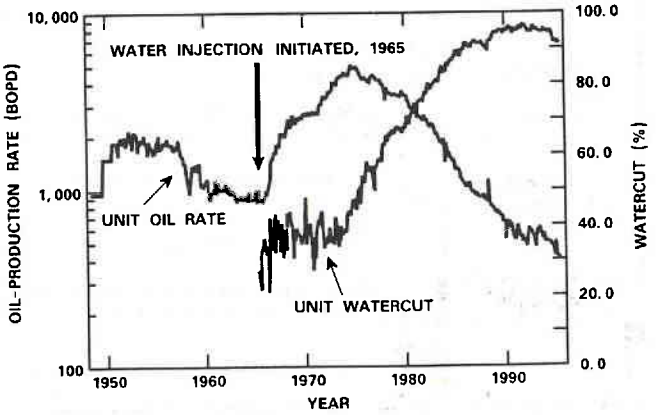

Figure 3. Graph showing production history of South Cowden Unit, Ector County, Texas

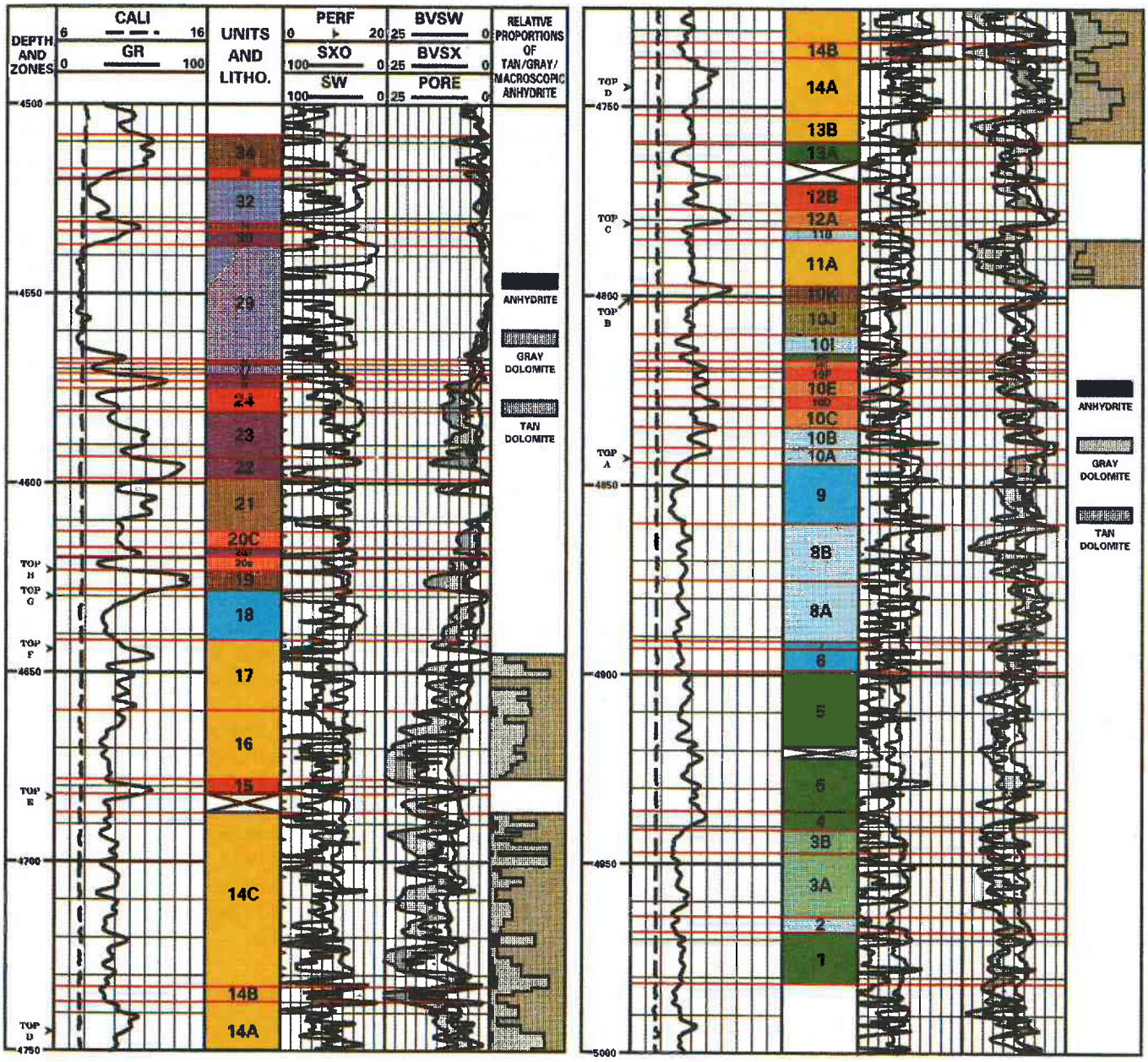

CORE LITHOLOGIES

Fusulinid Dolowackestone Lithofacies

- Fusulinid–peloid dolowackestone & dolopackstone
- Mottled, fusulinid–peloid dolowackestone, dolopackstone & washed dolopackstone

Ooid–Peloid Dolograinstone Lithofacies

- Ooid dolograinstone & washed dolopackstone
- Medium–grained (ooid?), washed dolopackstone & dolograinstone

Burrowed–Mottled Dolopackstone Lithofacies

- Mottled, peloid dolowackestone, dolopackstone & washed dolopackstone – chaotic
- Peloid dolopackstone & washed dolopackstone

Sandy Dolopackstone Lithofacies

- Sandy (<20% qtz sand), peloid washed dolopackstone with varying amounts of fusulinids, ooids, and intraclasts
- Sandy (<20% qtz sand), peloid dolopackstone & washed dolopackstone
- Sandy (>20% qtz sand), peloid washed dolopackstone with common ooids and intraclasts
- Dolomitic sandstone & anhydritic sandstone

Fenestral Dolopackstone Lithofacies

- Fenestral dolopackstone & washed dolopackstone

Figure 4. Wireline log/core graph of the Phillips Petroleum Co. No. 8-19 SCU well, sec. 18, blk. 42, T. 3 S., T. and P. RR. Co. Survey, Ector County, Texas.

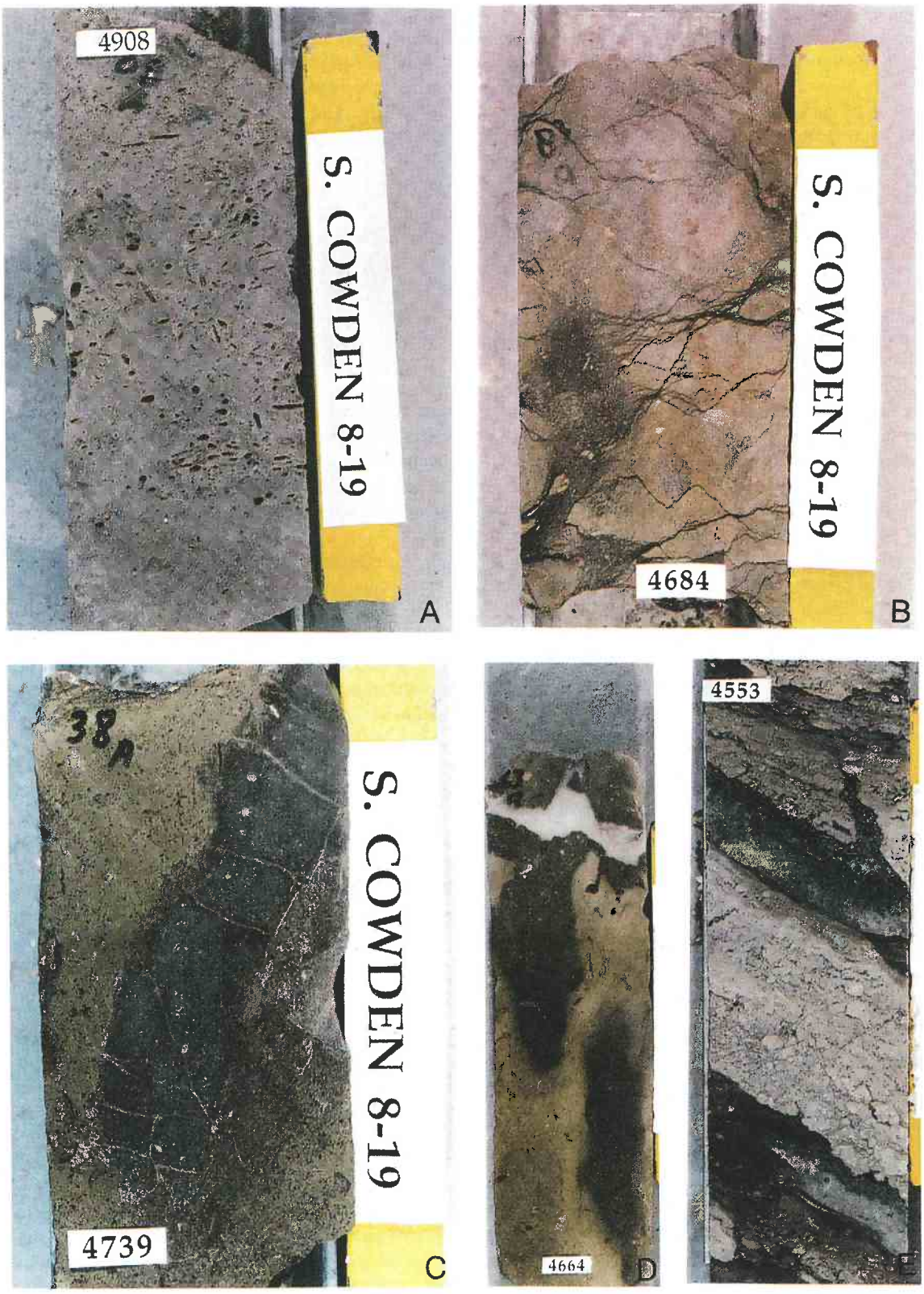

Figure 5. Core photographs of Grayburg and Queen lithofacies, South Cowden Unit. Numbers indicate depths in feet. (A) Fusulinid dolowackestone with moldic porosity (SCU 8-19, core unit 5). (B) Sandy dolopackstone with common stylolites (SCU 8-19, core unit 15). (C,D) Burrow-mottled dolopackstone lithofacies showing characteristic vertically oriented gray/tan mottling. Tan areas are oil stained and have significantly better porosity and permeability than adjacent gray-dolomite areas (SCU 8-19, core units 14A and 16). (E) Fenestral-dolopackstone lithofacies, displaying inclined bedding typical of tepee structures. The large, anhydrite-cemented desiccation structure (layer) in the upper part of the slab contains internal sediment visible along the right side of the core (SCU 8-19, unit 29).

stones (Figs. 4, 5A). Fusulinid dolostones are rare in the middle part of the Grayburg Formation and absent in the upper Grayburg and overlying lower part of the Queen Formation. Fusulinids are scarce to common, and echinoderm debris is rare in rocks of this lithofacies; no other bioclasts are distinguishable. Intergranular areas are generally dolomitized carbonate mud, which in places appears pelleted. Very fine- to fine-sand-size detrital quartz is <3%, and coarsely to very coarsely crystalline anhydrite, typically cementing or partially cementing biomoldic pores, varies from 3% to 14%. Small anhydrite nodules are rare.

Carbonaceous and argillaceous stylolitic seams and laminae are numerous in some fusulinid dolowackestone/dolopackstone intervals, e.g., core units 4 and 5, SCU 8-19, resulting in slightly higher gamma-ray-log values for these intervals (Fig. 4). The "hotter" gamma-ray log signature associated with core units 4 and 5 is observed at this stratigraphic level throughout SCU.

Burrow mottling significantly affects porosity and permeability in rocks of this lithofacies. Fusulinid dolostones lacking burrow mottling have core-analysis porosities of 5–17% and maximum-permeability (K_{max}) values of 0.4–2.5 md. Burrow-mottled, oil-stained fusulinid dolostones have core-analysis porosities ranging from 15% to 20% and K_{max} values from 280 to 880 md. The better porosity and permeability in burrow-mottled dolostones are related to the presence of intergranular porosity within bioturbated areas. In areas lacking bioturbation, porosity is mainly biomoldic and intercrystalline (Fig. 6A). Biomolds are typically leached or partially leached fusulinids. As stated above, biomolds are commonly cemented or partially cemented by anhydrite.

The normal-marine biota, bioturbation, and generally muddy character of fusulinid dolowackestones and dolopackstones suggest deposition in an open-marine outer-platform setting in waters generally below normal wave base, perhaps 10–20 m or less in depth. Rare fusulinid intraclast dolograinstones and washed dolopackstones interbedded with the muddy fusulinid rocks suggest times or areas of higher energy traction deposition. Numerous authors have proposed a similar outer-platform or outer-ramp depositional setting for San Andres and Grayburg fusulinid wackestones and packstones of the Permian basin (Bebout and others, 1987; Ruppel and Cander, 1988; Tyler and others, 1991; Kerans and others, 1994). Sonnenfeld's (1991) study of San Andres–age rocks of the Permian basin suggests that the optimal depth for fusulinids was approximately 10 m. Fusulinids may have been transported downslope, however, to depths of 60 m (Kerans and others, 1994).

Ooid-Peloid Dolograinstone Lithofacies

Ooid-peloid dolograinstones and washed dolopackstones occur mainly in the lower and middle parts of the Grayburg Formation (zone B and the upper part of zone A, Fig. 4). Rocks of this lithofacies are mottled or display small- to medium-scale trough cross-stratification. In places, mottling appears to be related to bioturbation. Burrowed areas are commonly oil stained. Framework grains are mainly medium- to coarse-sand-size ooids and peloids. Echinoderm debris, peloidal intraclasts, and grapestone grains are rare. Detrital quartz is generally absent. Owing to dolomitization, ooid nuclei and oolitic coats (cortices) are difficult to distinguish (Fig. 6B).

Porosity in rocks of this lithofacies is intergranular and, relatively rare, moldic (Fig. 6B). Core-analysis porosity is typically 6–16%, and K_{max} generally varies from 3 to 40 md, with some dolograinstone intervals having permeabilities of 100–300 md. Intergranular porosity has been partially occluded by finely to medium-crystalline dolomite cement and small amounts (<1% to 3%) of coarsely crystalline calcite cement. The ooid-dolograinstone interval that occurs at the top of the Grayburg Formation throughout SCU (core unit 18, Fig. 4) is partially cemented by coarsely to very coarsely crystalline anhydrite. Cored dolograinstones elsewhere in the Grayburg Formation are generally <1% anhydrite.

Cross-stratified and bioturbated ooid-peloid dolograinstones and washed dolopackstones record deposition on moderate- to high-energy shoals and in near-shoal areas. Water depths in this setting were a few meters or less. Wave and current energy on shoal crests winnowed mud-size material and produced oolitically coated grains. Carbonate sands washed into off-shoal areas were bioturbated in places.

Sandy-Dolopackstone Lithofacies

Thin, areally extensive sandy-dolopackstone and dolomitic-sandstone beds are used to establish the internal stratigraphy of the Grayburg reservoir interval at SCU (see Stratigraphy and Depositional Cycles section). Sandy dolopackstones and dolomitic sandstones are relatively scarce in the Grayburg Formation but dominate the cored portion of the overlying Queen Formation (Fig. 4). Sandy dolopackstones in the two formations display some noteworthy differences addressed below.

Angular to subangular, very fine- to fine-sand-size siliciclastic material typically varies from 10% to 20% in sandy dolopackstones of the Grayburg Formation and from 10% to 40% in sandy dolopackstones/dolomitic sandstones of the Queen Formation. Siliciclastic material in both formations is approximately 85–90% quartz and 10–15% alkali feldspar, as determined by X-ray-diffraction (XRD) analysis. Carbonaceous and argillaceous stylolitic seams and laminae are locally common in rocks of this lithofacies (Fig. 5B), and some beds contain small amounts of sand-size opaque material resembling detrital carbonaceous debris. The clay-mineral content, determined by XRD analysis, varies from 1% to 7%. The relatively "hot" gamma-ray-log character of sandy dolopackstones and dolomitic sandstones (Fig. 4) is related to the presence of clay minerals, carbonaceous debris, and detrital alkali (potassium-bearing) feldspars. Anhydrite is generally <1% in sandy dolopackstones of the Grayburg Formation and varies from 1% to 45% in sandy dolostones of the Queen Formation.

Carbonate grains in sandy dolopackstones of the Grayburg Formation are predominantly fine-sand-size peloids (Fig. 6C). These grains are most likely fecal pellets and micritized bioclasts. Medium- to coarse-sand-size ooids and less numerous peloidal intraclasts and grapestone grains are rare to common in Grayburg sandy dolopackstones (Fig. 6D), and fusulinids and echinoderm debris, though generally absent, are present in some beds. Sandy washed dolopackstones of the Queen Formation contain common peloids, ooids, and intraclasts (Fig. 7A).

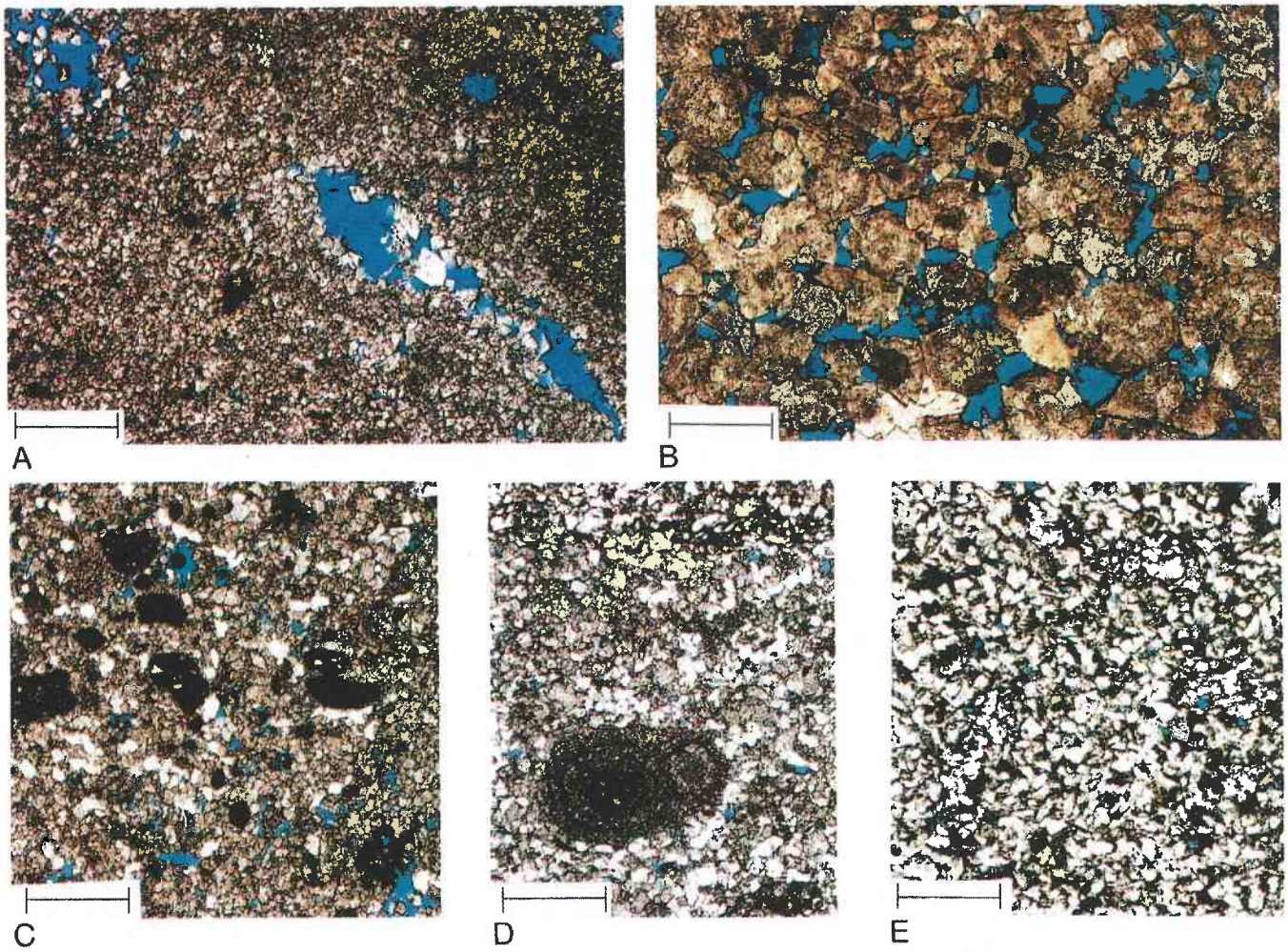

Figure 6. Thin-section photomicrographs of the Grayburg Formation, South Cowden Unit. (A) Moldic and intercrystalline porosity characteristic of the fusulinid-dolowackestone lithofacies. Large molds are leached fusulinids (SCU 8-19, core unit 5, 30×). (B) Ooid-peloid-dolograinstone lithofacies, displaying good intergranular porosity (SCU 8-19, core unit 9, 30×). (C–E) Sandy dolostone (C,D) and dolomitic sandstone (E) of the sandy-dolopackstone lithofacies. Siliciclastics are very fine sand. Fine- to medium-sand-size peloids of uncertain affinity are shown in photo C. Photo D shows a coarse-sand-size coated grain (grapestone). Pores in the photo C sample are intercrystalline, moldic (leached carbonate grains), and leached feldspars (C, SCU 8-19, core unit 10E, 30×; D, SCU 8-19, core unit 12A, 30×; E, SCU 8-19, core unit 15, 30×). All scale bars are 0.5 mm in length.

Sandy dolostones of the Grayburg Formation are commonly mottled and display small burrows that are elliptical on the slabbed-core surfaces. By contrast, sandy washed dolopackstones of the Queen Formation display horizontal and low-angle stratification, ripple cross-stratification, and, less commonly, burrows.

Porosity in these rocks is intergranular, intercrystalline, and leached grain (Fig. 6C). Carbonate grains and detrital feldspars display evidence of dissolution. Core-analysis porosity is typically 10–13%, and K_{max} is 0.1–9 md. The effect of relatively low-permeability sandy dolostones and dolomitic-sandstone layers on Grayburg production is discussed in the Reservoir Character section.

Low-angle and ripple stratification and common ooids and intraclasts in sandy washed dolopackstones of the Queen Formation indicate deposition in moderate- to relatively high-energy marine waters a few meters or less in depth. The amount of siliciclastic sand, typically >20%, suggests an inner-platform nearshore or shoreline setting and differentiates these oolitic rocks from ooid-peloid dolograinstones of the lower and middle Grayburg. Sandy dolopackstones of the Grayburg Formation typically contain <20% siliciclastic sand, are burrow mottled, and have relatively scarce ooids, intraclasts, fusulinids, and echinoderms, suggesting lower energy deposition in a more seaward setting.

Ruppel and Bebout (1995) suggested that the well-sorted, very fine- to fine-grained Grayburg siliciclastic units at South Cowden field record the subaqueous reworking of lowstand eolian sediments during sea-level rise and marine transgression. A similar depositional process was proposed by Fischer and Sarntheim (1988) for numerous Permian siliciclastic units in the Delaware basin.

Burrow-Mottled Dolopackstone Lithofacies

Rocks of the burrow-mottled dolopackstone lithofacies display a distinctive, vertically oriented gray/tan mottling re-

flecting variations in porosity and oil staining (Fig. 5C,D). Tan oil-stained areas are typically 2–8 cm in width, up to a few tens of centimeters in length, and are dolograinstones, dolopackstones, and washed dolopackstones. Gray, lower porosity areas, lacking oil staining, are generally dolopackstones and dolowackestones and commonly display short (<2-cm) anhydrite-cemented fractures. These fractures do not extend into the adjacent tan-dolomite areas.

Owing to diagenesis, in particular dolomitization and dissolution, grains are generally difficult to distinguish in both the tan- and gray-dolomite areas. Distinguishable grains are typically classified as peloids. Coated grains are recognizable in some tan dolomites, and fusulinids and echinoderms are visible in burrow-mottled dolopackstones in the middle part of the Grayburg Formation (zones C and D). Bryozoans, green algae, and intraclasts are rare. Quartz sand is generally absent.

The distinctive gray/tan mottling that characterizes rocks of this lithofacies was observed at Rhodes Cowden Unit, just north of Johnson/Foster field, by C. D. Caldwell and described by numerous other authors working San Andres/Grayburg fields of the Permian basin (e.g., Longacre, 1980; Bebout and others, 1987, Dune field; Ruppel and Cander, 1988, Emma field; Major and others, 1990, East Penwell Unit; and Leary and Vogt, 1990, Seminole field). Most of these papers relate this mottling to bioturbation and consequent variations in porosity and oil staining. This lithofacies makes up the bulk of the reservoir interval at South Cowden Unit and is the major reservoir lithofacies at East Penwell and Rhodes Cowden Units.

Gray areas are a very finely to medium-crystalline anhedral-dolomite mosaic (Fig. 7B). Dolomite crystals in these areas are typically 0.01–0.1 mm in length, as determined from thin-section study, with most crystals occurring in the coarser part of this size range, i.e., 0.03–0.1 mm.

Tan-dolomite areas fall into one of three categories on the basis of crystal size. Category I tan dolomites are very finely to medium crystalline with crystals typically 0.01–0.1 mm in length (Figs. 7C,D; 8A,C). Crystals are evenly distributed throughout this size range, or in some samples occur mainly in the coarser end of the size range (Fig. 8C). Category II dolomite crystals also range from 0.01 to 0.1 mm, but crystals in this category occur mainly in the finer part of the size range, i.e., 0.01–0.03 mm (Fig. 8D). Tan dolomites of category III are very finely to finely crystalline with crystals typically <0.01 to 0.03 mm in length (Fig. 8B). Pore size and permeability are directly related to crystal size in most tan-dolomite samples. The relationship of crystal size to permeability is discussed in the Reservoir Character section.

Thin-section study suggests that tan dolomites have significantly better porosity than gray dolomites in rocks of this lithofacies (compare Fig. 7B, gray dolomite, and Fig. 7C,D, tan dolomite). In an effort to quantify this relationship, 79 core plugs were taken specifically from the tan and gray areas to determine the petrophysical properties of these two dolomites. Plugs were taken from the SCU 8-19, 7-10, 6-23, and 8-11 cores.

Core plugs from the gray-dolomite areas generally have 2–9% porosity and 0.002–2-md permeability (Fig. 9). Porosity in the gray areas is moldic and intercrystalline (Fig. 7B).

Table 1.—Average Porosity and Anhydrite Content of Tan Dolomites, Burrow-Mottled Dolopackstone Lithofacies, by Well

Well	Average porosity (%), tan dolomites (core analysis)	Percentage of anhydrite, tan dolomites (thin section)
6-23	21.0	1.0
7-10	21.0	5.5
8-19	24.0	1.0
6-24	N.A.	10.7
8-11	14.5	11.5
16-14	about 5.5–7	15.5

By contrast, tan-dolomite plugs have porosities typically ranging from 10% to 32% and permeabilities ranging from 2 to 400 md (Fig. 9). Porosity in the tan areas is intergranular, intercrystalline, and, less commonly, moldic. Intergranular porosity is significantly better in the tan dolomites than in the lower porosity gray dolomites. This intergranular porosity may have acted as a conduit for the movement of diagenetic fluids, some of which may have partially leached carbonate grains and matrix-enhancing porosity in the tan dolomites. Tan-dolomite areas are interpreted to be carbonate-sand-filled burrows, and gray, lower porosity dolomites are muddy interburrow areas.

Core-plug data indicate that the relative amounts of gray and tan dolomite, which are largely a function of bioturbation, can markedly affect porosity and permeability in rocks of the burrow-mottled dolopackstone lithofacies. Mottled dolopackstone porosity is also related to the amount of intergranular and intercrystalline anhydrite cement. An inverse relationship exists between porosity and anhydrite content (Table 1). The possible role of late-stage anhydrite (or gypsum?) dissolution in porosity development is discussed later in this report.

An average porosity and permeability were calculated, in each of the five SCU study wells, for rocks of the burrow-mottled dolopackstone lithofacies. These calculations were derived from whole-core data. Thus, core pieces used in these analyses typically contain both tan and gray dolomites. The average porosities from the five wells range from 12.8% to 15.5%, and the average maximum permeabilities vary from 4.9 to 30 md.

The variability of carbonate-grain types, including fusulinids and coated grains; the presence of vertical, relatively large carbonate-sand-filled burrows; and the general absence of siliciclastics in rocks of this lithofacies suggest subtidal marine deposition generally below or near normal wave base in a mid-platform setting. Coated grains, formed on higher energy shoals in this setting, were washed into quieter water, muddy near-shoal areas. An open, subtidal-platform setting has been proposed by numerous authors for similar burrow-mottled peloid packstones and grainstones on the Central Basin platform (Ruppel and Cander, 1988; Leary and Vogt, 1990; Major and others, 1990).

Leary and Vogt (1986, 1990) studied the isotopic compo-

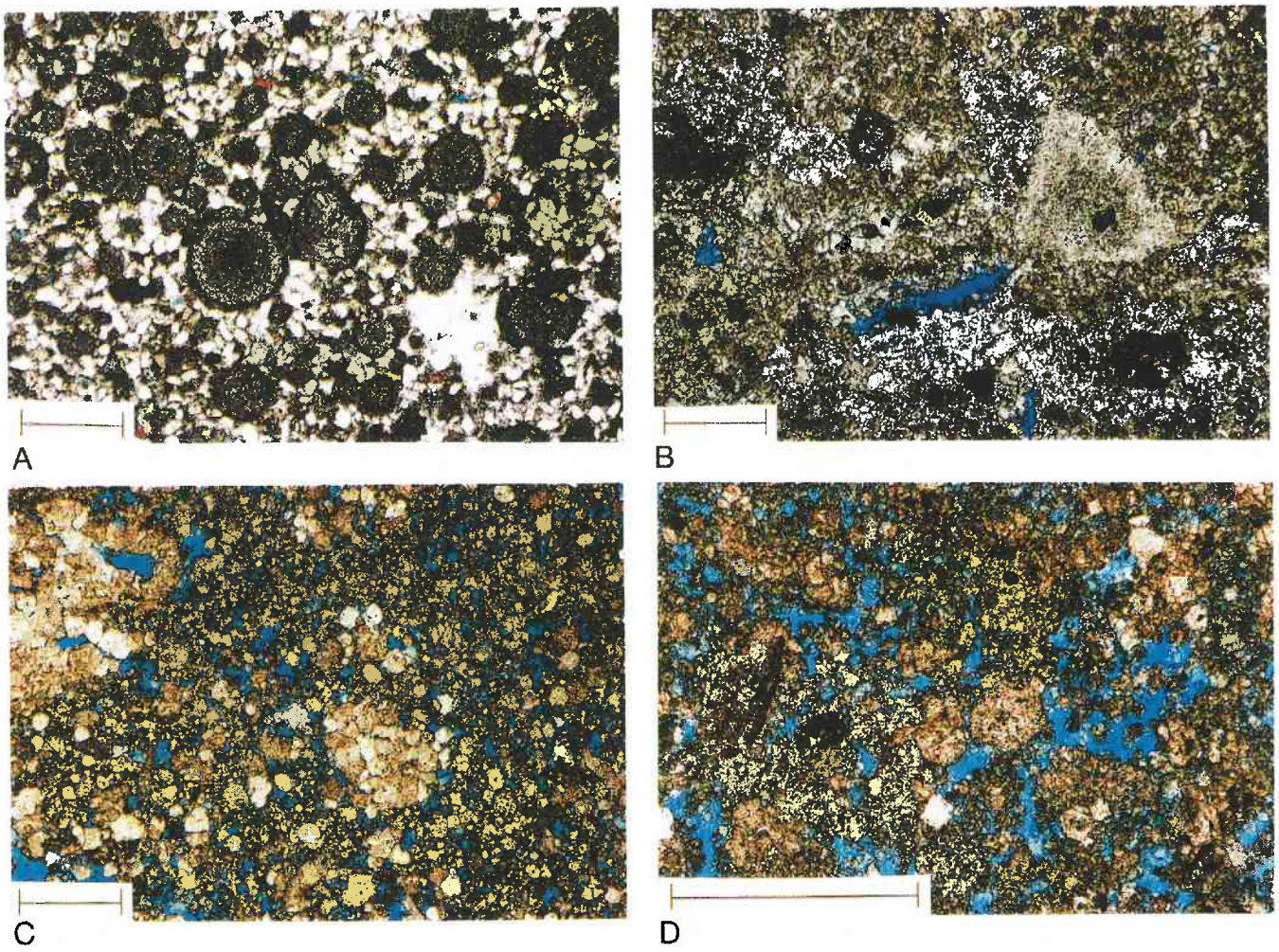

Figure 7. Thin-section photomicrographs of the Queen and Grayburg Formations, South Cowden Unit. (A) Sandy-dolopackstone lithofacies of the Queen Formation, displaying common medium-sand-size ooids and abundant very fine-grained siliciclastic sand (SCU 8-19, core unit 26, 30×). (B) Gray dolomite of the burrow-mottled dolopackstone lithofacies. This sample displays moldic porosity and at right center an echinoderm fragment (SCU 8-19, core unit 14C, 30×). (C,D) Porous category I tan dolomite of the burrow-mottled dolopackstone lithofacies. Porosity is mainly intergranular (C, SCU 8-19, core unit 14C, 30×; D, SCU 8-19, core unit 16, 80×). All scale bars are 0.5 mm in length.

sition of gray/tan-mottled San Andres dolostones from five fields along the eastern margin of the Central Basin platform (Seminole, Foster, Means, Hanford, and North Robertson). Gray and tan dolomites studied by Leary and Vogt have $\delta^{18}O$ values of 4.6‰ and 3.1‰, respectively. In paired gray and tan samples, in which the tan and gray samples were taken within 10 cm of each other, tan dolomites were depleted by as much as 3.5‰. Leary and Vogt suggested a diagenetic sequence for the mottled dolostones that consists of an early selective dolomitization of more permeable bioturbated areas by mixed marine/meteoric fluids; a large-scale replacement dolomitization by seawater evaporated to gypsum saturation, responsible for the gray dolomite of the interburrow areas; and a final phase of dolomitization or dolomite stabilization of the more permeable, bioturbated tan areas by an isotopically lighter fluid.

Major and others (1990) presented an alternative diagenetic model to explain similar isotopic compositions of gray and tan dolomites at East Penwell Unit. In their model, a late-stage leaching increased permeability in the tan areas by widening intercrystalline pore throats and preferentially removing the early isotopically enriched centers of dolomite rhombs, thus resulting in the depleted oxygen-isotopic compositions of the tan areas.

Isotopic data are not available for gray and tan dolomites of the burrow-mottled dolopackstone lithofacies at SCU. It is speculated, however, that these dolostones are isotopically similar to those discussed in the aforementioned studies. It is noteworthy that the dissolution of the central parts of dolomite rhombs, described by Major and his coauthors, is relatively rare in the South Cowden Unit burrow-mottled dolopackstones, and in most samples this dissolution had very little effect on porosity, permeability, and presumably isotopic composition of the tan areas.

Fenestral Dolopackstone Lithofacies

Rocks of the fenestral dolopackstone lithofacies are restricted to the Queen Formation in the five SCU study wells.

Anhydrite layers and lenses, a few millimeters to several centimeters thick, are associated with fenestral dolopackstones and dolowackestones composing this lithofacies (Fig. 5E). Bedding is rarely inclined with dips up to 30° (Fig. 5E).

Carbonate grains in this lithofacies are fine-sand-size peloids; less numerous medium- to coarse-sand-size peloidal intraclasts and coated grains; and rare granule-size broken and coated grains, some resembling vadose pisolites. Mollusk debris, though generally rare, is common in some beds. Quartz sand is <1%.

Anhydrite occludes most of the intergranular and fenestral porosity in dolopackstones and dolowackestones of this lithofacies and in places replaces grains and matrix. Fenestral dolopackstones are typically 20–25% anhydrite. Core-analysis porosity and permeability data are not available for rocks of this lithofacies, but wireline-log studies indicate porosities of <4%.

Anhydrite layers and lenses described above record the cementation of desiccation cracks by coarsely to very coarsely crystalline, blocky to bladed anhydrite. Finely textured internal sediment lines the floor of some of the larger desiccation structures. These desiccation structures, the aforementioned fenestral fabric, and the relatively rare and restricted marine biota that characterize this lithofacies suggest upper-intertidal to supratidal deposition marked by periods of subaerial exposure. The aforementioned inclined beds are most likely the limbs of tepee structures.

DEPOSITIONAL MODEL

Grayburg/Queen lithofacies defined in this study are similar to San Andres and Grayburg lithofacies recognized by other authors working in the Permian basin (Bebout and others, 1987; Rupple and Cander, 1988; Garber and Harris, 1990; Leary and Vogt, 1990; Ruppel and Bebout, 1995). Fusulinid dolowackestones, which compose most of the lower Grayburg Formation at SCU, record outer-platform open-marine deposition below normal wave base in waters 10–20 m or less in depth. Published reports suggest that fusulinid wackestones and packstones generally record maximum water depths in San Andres–Grayburg deposits of the Permian basin. This outer-platform setting passed landward (westward) into high-energy carbonate shoals and intershoal areas characterized by cross-stratified and burrow-mottled ooid-peloid dolograinstones. Where high-energy carbonate shoals did not develop, outer-platform, muddy fusulinid-rich sediments passed westward into a mid- or inner-platform setting characterized by burrow-mottled dolopackstones. Ruppel and Bebout (1995), in their depositional model for South Cowden field, placed peloid wackestones/packstones, analogous to rocks of the burrow-mottled dolopackstone lithofacies, in an inner-ramp setting behind high-energy ramp-crest shoals, and Leary and Vogt (1990) showed burrow-mottled pellet grainstones on a shallow subtidal platform landward of open-marine fusulinid wackestones and packstones. The inner-platform setting at SCU is represented by sandy and fenestral dolopackstones of the Queen Formation. Sandy, oolitic and intraclastic washed dolopackstones record moderate- to high-energy shoreline deposition, and interbedded fenestral dolopackstones and thin anhydrites record upper-intertidal to supratidal deposition.

The Grayburg–Queen carbonate platform faced prevailing winds from the northeast (Walker and others, 1995) and open-marine waters of the Midland basin. Cyclicity of the outer-platform, mid-platform, and inner-platform deposits is discussed below.

STRATIGRAPHY AND DEPOSITIONAL CYCLES

Laterally extensive sandy-dolostone layers, characterized by relatively "hot" gamma-ray-log signatures, were used to establish the Grayburg reservoir stratigraphy at South Cowden Unit. These sandy dolopackstones and dolomitic sandstones form the basal units of zones C, D, and F of the Grayburg Formation (Fig. 4). The relatively "hot" gamma-ray interval at the base of zone E reflects the concentration of carbonaceous and argillaceous material along locally common stylolites.

Bebout and others (1987) used similar, laterally extensive dolomitic-siltstone layers to establish the Grayburg stratigraphy at Dune field, and Ruppel and Cander (1988) stated that thin siliciclastic units form readily traceable marker beds at Emma San Andres field. Bebout and his coauthors wrote that the dolomitic-siltstone beds at Dune field represent geologic-time lines and thus can be used to establish a time-stratigraphic framework.

As discussed in the lithofacies descriptions, sandy dolopackstones and dolomitic sandstones of the Grayburg Formation at SCU may record marine reworking of lowstand eolian sands during a sea-level rise or marine transgression (Kerans and others, 1995; Ruppel and Bebout, 1995). In this model, thin, sandy dolomite beds are the initial deposits of high-frequency cycles (HFC) that make up the Grayburg Formation. Kerans and his coworkers stated that these cycles are equivalent to parasequences defined by Vail (1987) and Van Wagoner and others (1988).

Sandy dolopackstones and dolomitic sandstones composing core units 10K (base of C zone), 12A (base of D zone), and 15 (base of F zone) in the SCU 8-19 (Fig. 4) correlate with the basal transgressive units of three HFCs recognized by Ruppel and Bebout (1995) at South Cowden field. A typical Grayburg HFC at SCU consists of a basal transgressive sandy dolopackstone/dolomitic sandstone, recording marine reworking of lowstand siliciclastics, overlain by outer-platform fusulinid dolowackestone and/or mid-platform burrow-mottled dolopackstone, and, capping the cycle, a regressive ooid-peloid dolograinstone. Tidal-flat deposits, capping high-frequency Grayburg cycles in the updip platform interior of South Cowden field (Ruppel and Bebout, 1995), were not recognized in the five SCU study wells. Inner-platform tidal-flat deposits, represented by rocks of the fenestral-dolopackstone lithofacies, are restricted to the Queen Formation in the study wells.

In an alternative depositional model, sandy dolopackstones and dolomitic sandstones of the Grayburg Formation may reflect deposition in subtidal marine waters landward of the platform-crest oolite shoals. In this model, fusulinid dolowackestones and/or burrow-mottled dolopackstones record the initial phases of marine transgression. These rocks are overlain by regressive ooid-peloid dolograinstones, and capping the sequence are back-shoal sandy dolopackstones. This model

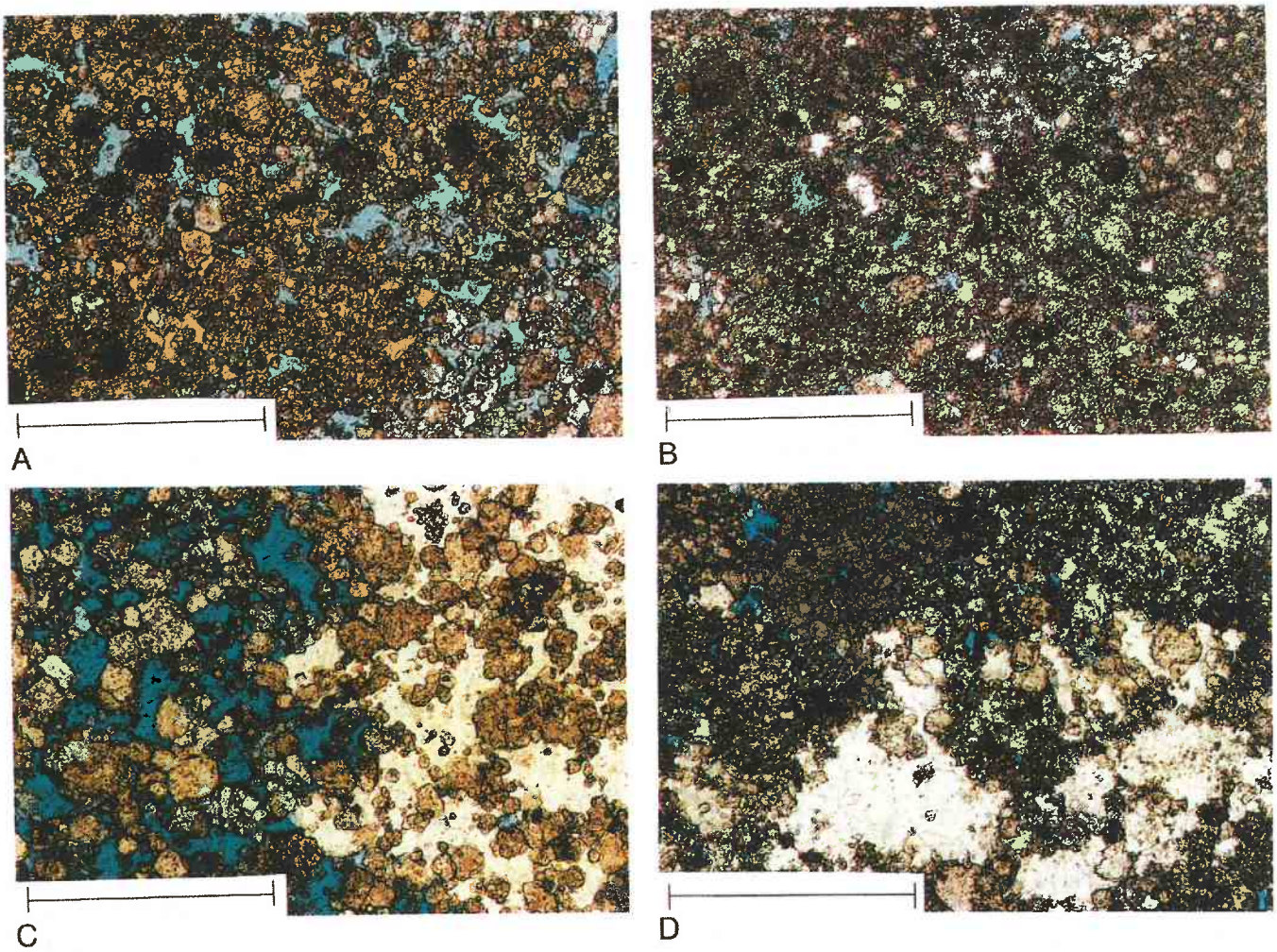

Figure 8. Thin-section photomicrographs of the burrow-mottled dolopackstone lithofacies, Grayburg Formation, South Cowden Unit. (A) Finely to medium-crystalline category I tan dolomite with 20% porosity and 190-md permeability. This sample appears to be a peloid dolograinstone or washed dolopackstone (SCU 6-23, 80×). (B) Very finely crystalline category III tan dolomite, peloid dolopackstone, with 19% porosity and 4-md permeability (SCU 7-10, 80×). This sample and the photo A sample have similar porosities but markedly different permeabilities. (C) Category I tan dolomite with 23% porosity and 137-md permeability. The right half of the photomicrograph shows an area cemented by anhydrite. The left half of the photo shows an area where anhydrite cement was not precipitated or was precipitated and subsequently leached (SCU 8-19, core unit 14C, 80×). (D) Category II tan dolomite with 16% porosity and 6.9-md peremeability. Anhydrite replaces dolomite and cements porosity. Anhydrite dissolution would create pores markedly larger than those characterizing this sample (SCU 8-11, 80×). All scale bars are 0.5 mm in length.

lacks the regional insights of the work of Kerans and others and of Ruppel, and at present is considered the least attractive of the two models.

RESERVOIR CHARACTER

Porosity and Bioturbation

Grayburg porosity and permeability at SCU are a function of original depositional texture and diagenesis, reflected in the lithofacies classification. Biomoldic and intercrystalline porosity, characterizing rocks of the fusulinid-dolowackestone lithofacies, lower Grayburg, records secondary dissolution of carbonate grains and intergranular carbonate mud. Bioturbated areas in some fusulinid dolostones display intergranular porosity. By contrast, the main pore type associated with ooid-peloid dolograinstones in the lower and middle parts of the Grayburg Formation is intergranular. Rocks of the fusulinid-dolowackestone and ooid-peloid-dolograinstone lithofacies in places display good porosity and permeability, but, in general, these rocks occur below the SCU oil–water contact (approximately –1,800 ft) and thus are not hydrocarbon productive. Sandy dolopackstones are generally finely textured and have relatively poor permeabilities, and anhydrite cement occludes most of the primary and secondary porosity in sandy dolopackstones and fenestral dolopackstones of the Queen Formation.

Reservoir rocks at SCU are predominantly burrow-mottled dolopackstones. Porosity in these rocks is mainly a function of bioturbation and anhydrite cementation. As discussed in the lithofacies descriptions, tan-carbonate-sand-filled burrows have porosities generally ranging from 10% to 32%, and gray, muddier interburrow areas have porosities ranging from 2%

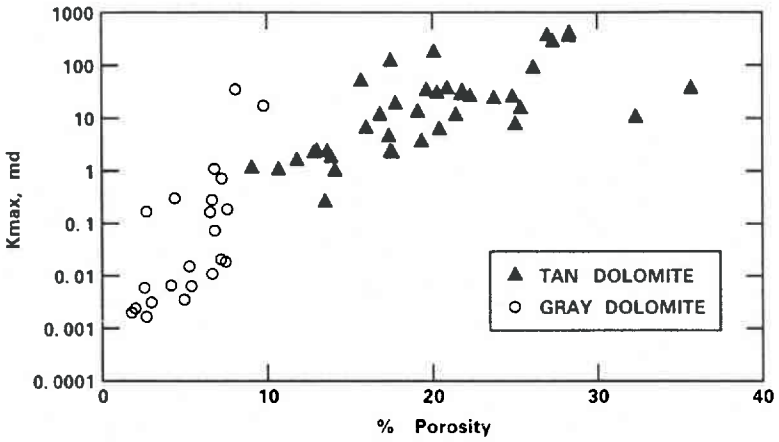

Figure 9. Cross-plot of porosity and permeability data for gray and tan dolomites of the burrow-mottled dolopackstone lithofacies, SCU 8-19, 7-10, 6-23, and 8-11 cores.

to 9%. Porosity in the tan areas is mainly intergranular and intercrystalline and, less commonly, moldic.

A clear mylar sheet with a 1-in.^{2} grid pattern was used to estimate the relative amounts of gray and tan dolomite and nodular anhydrite for each 1-ft interval of burrow-mottled dolopackstone in the five SCU study wells. Percentages of tan and gray dolomite and megascopic anhydrite were calculated and plotted on wireline-log/core graphs (Fig. 4). Those intervals dominated by gray dolomite typically have relatively low wireline-log porosities; intervals dominated by tan dolomite typically have relatively good wireline-log porosities. A comparison of the gray/tan plot and wireline-log porosity in the SCU 8-19 reservoir interval shows that porosity variation in this interval is largely a function of the varying amounts of gray and tan dolomite related to the extent of bioturbation.

Some of the low-porosity gray-dolomite layers appear to be correlative in the five SCU study wells. Laterally continuous gray-dolomite layers may reflect times or areas where conditions were less conducive to bioturbation. Some tan-dolomite layers also appear to be correlative on a local scale.

Porosity and Anhydrite Cementation

An inverse relationship exists between anhydrite content and porosity in tan dolomites of the burrow-mottled dolopackstone lithofacies—i.e., as the amount of anhydrite increases, porosity decreases (Table 1). Poikilotopic anhydrite, the main form of anhydrite in the reservoir interval, is generally restricted to tan-dolomite areas and is typically difficult to distinguish without the aid of thin sections. Poikilotopic anhydrite cements intergranular, intercrystalline, and moldic pores and replaces dolomite (Fig. 8C,D).

On the basis of limited data, there appears to be a general increase in anhydrite, and a corresponding decrease in reservoir porosity, in the northwestern part of the study area. For example, compare the anhydrite content and porosity in the SCU 8-19 and 6-23 to those in the more westward SCU 8-11 and Moss Unit 16-14 (Table 1). This regional variation may be related to a northwestward (paleolandward) source of anhydrite-precipitating fluids. Alternatively, this variation may be related to regional variations in anhydrite dissolution discussed in the following paragraph. Contrary to this general trend are significant local variations in anhydrite content (e.g., tan dolomites in the SCU 6-24 contain significantly more anhydrite than tan dolomites in the nearby 8-19 or 6-23). Determining the cause of these local variations requires additional study.

Sulfate dissolution and consequent porosity enhancement have been reported from numerous San Andres and Grayburg reservoirs in the Permian basin (Bebout and others, 1987; Ruppel and Cander, 1988; Longacre, 1980; Siemers and others, 1995), and Ruppel and Bebout (1995) suggested that sulfate dissolution was critical to porosity development in mottled dolostones of South Cowden field. By contrast, anhydrite crystals showing evidence of dissolution are rare or absent in most burrow-mottled dolopackstone samples studied for this report. Additionally, anhydrite in the category II and III tan dolomites typically occurs in small patches a few tenths of a millimeter across, the dissolution of which would result in pores significantly larger than those observed in these rocks (Fig. 8D). By contrast, the dolomite fabric of some category I, anhydrite-cemented tan-dolomite areas is similar to that of directly adjacent porous areas lacking anhydrite cement (Fig. 8C). This similarity suggests that porosity development in some category I tan dolomites may be related in part to sulfate dissolution, resulting in the relatively open dolomite framework that characterizes these rocks. Ruppel and Bebout wrote that the fluids responsible for sulfate dissolution at South Cowden field may have been derived from the basin during a pre-oil-migration phase of diagenesis. This basinal source of sulfate-leaching fluids would be consistent with the general westward increase in anhydrite observed at SCU.

Porosity/Permeability Relationships

Burrow-mottled dolopackstone permeability is a function of bioturbation and anhydrite content, as described above, and pore size. Pore size is related to depositional texture and diagenesis and consequent crystal size in the tan-dolomite areas. As previously discussed, tan dolomites can be placed in one of three categories on the basis of crystal size. Categories I, II, and III are characterized by progressively smaller crystal size. Decreases in crystal size are accompanied by decreases in pore-body and pore-throat size and lower permeabilities (Fig. 10).

Markedly different permeabilities characterizing tan dolomites of the burrow-mottled dolopackstone lithofacies are not necessarily related to significantly different porosities. For example, the average porosity of tan-dolomite plugs from the SCU 6-23 and 7-10 wells is 21%, but the average permeability of plugs from the 6-23 and 7-10 is 90 and 10 md, respectively (Table 2). Whole-core-analysis data for burrow-mottled dolopackstones from the 6-23 and 7-10 also show this relationship, suggesting that a single porosity/permeability transform does not adequately describe the varying porosity/permeability relationships at South Cowden Unit (Fig. 11).

Relatively low permeabilities that characterize tan dolomites of the SCU 7-10 are a function of comparatively small pore-body and pore-throat sizes (Table 3). Tan dolomites of the 7-10 are predominantly those of category III (Fig. 8B), whereas tan dolomites of the SCU 6-23 are predominantly those of category I (Fig. 8A). The very finely to finely crystalline tan dolomites that characterize burrow-mottled dolopackstones of the 7-10 suggest that burrow-filling sediments in the area of the 7-10 were generally finer grained and muddier than burrow-filling sediments in the area of the 6-23. Tan dolomites of the 7-10 are mainly dolopackstones with intercrystalline porosity. By contrast, tan burrow-filling sediments of the 6-23 are dolopackstones, washed dolopackstones, and dolograinstones, and pores in these rocks are predominantly intergranular. Core data are limited, but muddier burrow-filling sediments that resulted in categories II and III tan dolomites, characterizing much of the SCU 7-10 and 8-11 reservoir intervals, may dominate burrow fillings in more protected, quieter water interior parts of the platform. Category I dolograinstones and washed dolopackstones, which characterize tan dolomites of the SCU 6-23 and 8-19, may reflect deposition and bioturbation in higher energy, more seaward parts of the platform.

Table 2.—Average Porosity and Permeability of Tan Dolomites, Burrow-Mottled Dolopackstone Lithofacies, by Well

Well	Average porosity, tan dolomites (%)	Average permeability, tan dolomites (md)	% Samples, tan dolomites, categories I	II	III
6-23	21.0	90	50	30	20
7-10	21.0	10	0	33	67
8-19	24.0	175	83	17	0
8-11	14.5	8	0	100	0

Table 3.—Porosities, Permeabilities, and Pore-Throat Radii of Tan Dolomites (Categories I, II, and III) of the Burrow-Mottled Dolopackstone Lithofacies

Well	Sample depth (ft)	Core porosity (%)	Core permeability (md)	Pore-throat radius[a] (μm)	Tan-dolomite category
8-19	4,709.0	26.1	338	6.80	I
	4,723.6	26.7	374	6.03	I
	4,724.3	19.4	100	6.80	I
	4,736.0	24.3	514	8.50	I
7-10	4,639.6	25.0	8.14	4.27	II
	4,672.0	25.3	16.2	0.76	III
	4,679.0	20.4	6.6	0.34	III
	4,682.3	17.5	2.5	1.09	III
8-11	4,613.0	21.6	29.1	1.69	II
	4,670.0	16.8	12.3	0.43	II
6-23	4,652.8	35.7	38.7	1.68	III
	4,702.8	19.1	14	0.84	II
	4,640.7	20.1	190	5.34	I

[a]James Howard, personal communication (1996).

Low-Permeability Sandy-Dolopackstone Layers

Areally extensive sandy-dolopackstone/dolomitic-sandstone layers, used to establish the internal stratigraphy of the Grayburg reservoir interval at SCU (Fig. 4, zones C–F), may in some cases partially restrict the vertical movement of fluids and gases within the reservoir. For example, the sandy-dolopackstone layer at the base of zone D (core unit 12A, Figs. 4, 6D), "separating" zone D from underlying zone C, has an average K_{max} of <0.1 to 0.55 md and an average porosity of approximately 10% in the five SCU study wells. This low-permeability layer, and a thin, anhydrite-cemented fusulinid-dolowackestone layer near the middle of zone D (core unit 13A, K_{max} 0.2–2.8 md in the SCU study wells), may partially restrict vertical flow between reservoir rocks in zone C and the upper part of zone D. Data from the repeat formation tester (RFT) tool from the SCU 8-19 and 6-23 suggest that vertical communication between zones C and D is partially restricted. By contrast, the relatively "hot" gamma-ray interval at the base of zone E is not associated with a sandy dolostone layer, and the average K_{max} over this interval varies from 0.37 to 15 md for the five study wells. Core-analysis and RFT data suggest that reservoir rocks of zone E and the upper part of zone D should be in communication in most wells. Finally, the average K_{max} of the sandy-dolostone layer at the base of zone F (core unit 15, Fig. 4), "separating" zones E and F, varies from 0.02 to 0.6 md in the SCU 8-19, 7-10, 6-23, and 6-24 but is significantly

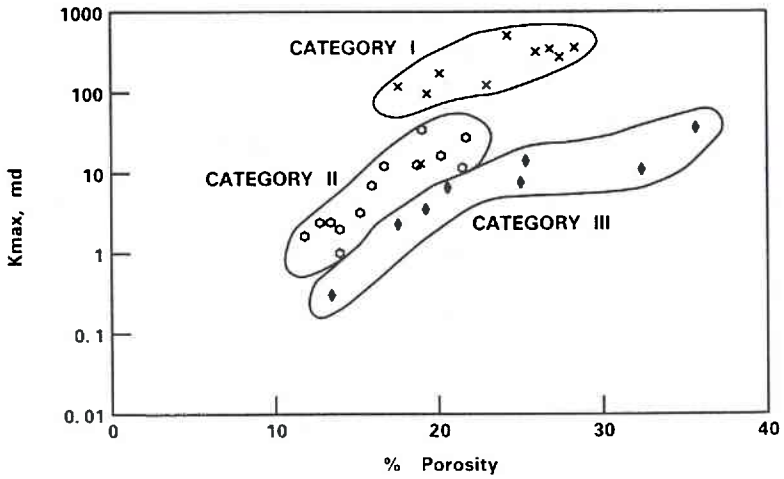

Figure 10. Cross-plot of porosity and permeability data for tan dolomites of the burrow-mottled dolopackstone lithofacies, showing variations in permeabilities associated with tan dolomites of categories I, II, and III.

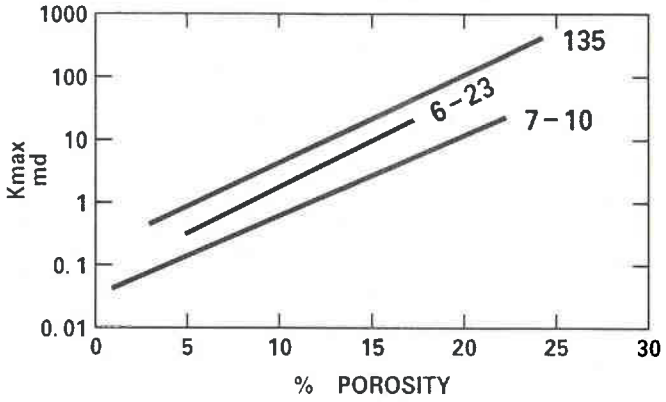

Figure 11. Cross-plot of whole-core-analysis porosity and permeability data from rocks of the burrow-mottled dolopackstone lithofacies, SCU 7-10, 6-23, and Fina Emmons Unit 135.

higher, 6.6 md, in the SCU 8-11. The average core-analysis porosity for this layer is 5–13.5%. Whereas petrographic and core-analysis studies suggest that this layer may in places act as a partial restriction to vertical flow, RFT data from the SCU 8-19 and 6-23 suggest that zones E and F are in pressure communication.

Low-porosity burrow-mottled dolopackstone layers dominated by gray dolomite should not form significant barriers to the vertical movement of reservoir fluids and gases. These layers—e.g., the low-porosity layer at the base of core unit 14C (Fig. 4, 4,730–4,733 ft)—contain a reduced but still significant amount (20–40%) of high-porosity and high-permeability tan dolomite typically occurring as vertically oriented burrow structures. These tan burrow structures should act as conduits for the vertical movement of fluids and gases. RFT data from zone E in the SCU 8-19 and 6-23 indicate this zone to be in vertical communication throughout, despite the presence of low-porosity gray-dolomite layers.

SUMMARY

The Grayburg reservoir interval at South Cowden Unit has a gross thickness of approximately 150 ft and is composed mainly of burrow-mottled dolopackstones that record subtidal mid-platform deposition. These dolomites are characterized by a distinctive vertically oriented gray/tan mottling. Tan oil-stained areas are carbonate-sand-filled burrows. These areas have core-analysis porosities generally ranging from 10% to 32% and permeabilities ranging from 2 to 500 md. Porosity in the tan-dolomite areas is mainly intergranular, intercrystalline, and moldic. Gray interburrow areas typically have porosities of 2–9% and permeabilities of 0.002–2 md.

Reservoir porosity is mainly a function of the degree of bioturbation—i.e., the relative amounts of gray and tan dolomite, and the extent of poikilotopic anhydrite cementation in tan-dolomite areas. An inverse relationship exists between anhydrite content and porosity. Limited core data suggest a general increase in anhydrite and a corresponding decrease in porosity in the northwestern (paleolandward) part of SCU. On a well-to-well scale, anhydrite distribution is variable, however, and can be difficult to predict. Anhydrite dissolution may have been an important porosity-forming process in some of the more coarsely textured tan dolomites, and the lower anhydrite content in the eastern and southeastern parts of SCU may reflect increased anhydrite dissolution by basin-derived fluids (Ruppel and Bebout, 1995) and/or decreased anhydrite precipitation from platform-interior-derived fluids.

Reservoir permeability is a function of bioturbation and anhydrite content, as described above, and pore size. Pore size in the tan-dolomite areas is largely related to the original depositional texture of the burrow-filling sediment and diagenesis. Very finely to finely crystalline tan dolopackstones, most likely reflecting dolomitization of muddy burrow-filling sediments, are characterized by very small intercrystalline pores and low permeabilities typically ranging from <1 to 16 md. Finely to medium-crystalline tan dolograinstones and washed dolopackstones are characterized by larger intergranular pores and significantly better permeabilities that vary from 100 to 500 md. Limited core data suggest that burrow-filling sediments may be muddier in the more western (landward) parts of SCU, resulting in more finely crystalline tan dolomites with smaller pore throats and lower permeabilities. Owing to differences in pore size, tan dolomites with similar porosities may have markedly different permeabilities. As a result, more than one porosity/permeability transform is needed to represent the SCU reservoir interval.

In general, the vertically oriented, permeable tan-dolomite burrow structures in the SCU reservoir interval provide favorable conditions for the application of a CO_2 flood, using horizontal injection wells. Rare, areally extensive, relatively thin sandy-dolomite/dolomitic-sandstone layers may, however, act as partial barriers to the vertical migration of reservoir fluids and gases. Thus, it is critical to understand the stratigraphic positions of these rare low-permeability layers relative to those of the horizontal CO_2 injection wells.

ACKNOWLEDGMENTS

The authors would like to thank Phillips Petroleum Co. for permission to publish this paper. This work was supported in part by a grant from the U.S. Department of Energy, Class II Oil Program, for the study of shallow-shelf carbonate reservoirs. Special thanks go to Kelly Curtis and Kathy Smith, Phillips Petroleum Co., for preparing the figures and plates. X-ray-diffraction analyses were conducted by Dave Cowan, PPCo., and mercury-injection data were analyzed by James Howard, PPCo. The Unocal Moss Unit 16-14 core was viewed through courtesy of the Texas Bureau of Economic Geology, Austin.

REFERENCES CITED

Bebout, D. G.; Lucia, F. J.; Hocott, C. R.; Fogg, G. E.; and Vander Stoep, G. W., 1987, Characterization of the Grayburg reservoir, University Lands Dune field, Crane County, Texas: Texas Bureau of Economic Geology Report of Investigations 168, 98 p.

Fischer, A. G.; and Sarntheim, M., 1988, Airborne silts and dune-derived sands in the Permian of the Delaware basin: Journal of Sedimentary Petrology, v. 58, p. 637–643.

Fogg, G. E.; and Lucia, F. J., 1990, Reservoir modeling of restricted platform carbonates: geologic/geostatistical characterization of interwell-scale reservoir heterogeneity, Dune field, Crane County, Texas: Texas Bureau of Economic Geology Report of Investigations 190, 66 p.

Galloway, W. E.; Ewing, T. E.; Garrett, C. M.; Tyler, N.; and Bebout, D. G., 1983, Atlas of major Texas oil reservoirs: Texas Bureau of Economic Geology, Austin, 139 p.

Garber, R. A.; and Harris, P. M., 1990, Depositional facies of Grayburg/San Andres dolostone reservoirs, Central Basin platform, Permian basin, *in* Bebout, D. G.; and Harris P. M. (eds.), Geologic and engineering approaches in evaluation of San Andres/Grayburg: Texas Bureau of Economic Geology, Austin, p. 1–20.

Harpole, K. J.; Gerard, M. G.; Snow, S. C.; and Caldwell, C. D., 1996, Use of production and well test data with predictive history matching to improve reservoir characterization for CO_2 flooding at the South Cowden Unit: Society of Petroleum Engineers Paper 35226, presented at 1996 Permian Basin Oil and Gas Recovery Conference, p. 633–641.

Kerans, C.; Lucia, F. J.; and Senger, R. K., 1994, Integrated characterization of carbonate ramp reservoirs using Permian San Andres Formation outcrop analogs: American Association of Petroleum Geologists Bulletin, v. 78, p. 181–216.

_____ 1995, Use of one- and two-dimensional cycle analysis in establishing high-frequency sequence frameworks, *in* Read, J. F.; Kerans, C.; and Weber, L. J. (eds.), Milankovitch sea-level changes, cycles, and reservoirs on carbonate platforms in greenhouse and ice-house worlds: Society for Sedimentary Geology (SEPM), Short Course 35, pt. 2, p. 1–20.

Leary, D. A.; and Vogt, J. N., 1986, Diagenesis of the Permian (Guadalupian) San Andres Formation, Central Basin platform, West Texas, *in* Bebout, D. G.; and Harris, P. M. (eds.), Hydrocarbon reservoir studies, San Andres/Grayburg Formations, Permian basin: Society of Economic Paleontologists and Mineralogists, Permian Basin Section, Publication 86-26, p. 67–68.

_____ 1990, Diagenesis of the San Andres Formation (Guadalupian), Central Basin platform, *in* Bebout, D. G.; and Harris, P. M. (eds.), Geologic and engineering approaches in evaluation of San Andres/Grayburg hydrocarbon reservoirs—Permian Basin: Texas Bureau of Economic Geology, Austin, p. 21–48.

Longacre, S. A., 1980, Dolomite reservoirs from Permian biomicrites, *in* Halley, R. B.; and Loucks, R. G. (eds.), Carbonate reservoir rocks: Society of Economic Paleontologists and Mineralogists, Core Workshop 1, p. 105–117.

Major, R. P.; Vander Stoep, G. W.; and Holtz, M. H., 1990, Delineation of unrecovered mobile oil in a mature dolomite reservoir: East Penwell San Andres Unit, University Lands, West Texas: Texas Bureau of Economic Geology Report of Investigations 194, 51 p.

Mitchum, R. M., Jr.; and Van Wagoner, J. C., 1991, High-frequency sequences and their stacking patterns: sequence-stratigraphic evidence of high-frequency eustatic cycles, *in* Biddle, K. T.; and Schlager, W. (eds.), The record of sea-level fluctuations: Sedimentary Geology, v. 70, p. 131–160.

Ruppel, S. C.; and Bebout, D. G., 1995, Effects of stratal architecture and diagenesis on reservoir development in the Grayburg Formation, South Cowden field, Ector County, Texas: Texas Bureau of Economic Geology Technical Report, Reservoir Characterization Research Laboratory, Carbonate Reservoirs, 81 p.

Ruppel, S. C.; and Cander, H. S., 1988, Effects of facies and diagenesis on reservoir heterogeneity: Emma San Andres field, West Texas: Texas Bureau of Economic Geology Report of Investigations 178, 67 p.

Siemers, W. T.; Prezbindowski, D. R.; Skinnider, V. L.; Maple, L. C.; Gerard, M. G.; Nagaty, M. E.; and Howard, J. J., 1995, Multidisciplinary study to optimize reservoir management of the North Penwell (San Andres) Unit, Ector County, Texas: American Association of Petroleum Geologists Bulletin, v. 79, p. 1407.

Sonnenfeld, M. D., 1991, High frequency cyclicity within shelf margin and slope strata of the upper San Andres sequence, Last Chance Canyon, *in* Meader-Roberts, S.; Candelaria, M. P.; and Moore, G. E. (eds.), Sequence stratigraphy, facies, and reservoir geometries of the San Andres, Grayburg, and Queen Formations, Guadalupe Mountains, New Mexico and Texas: Society of Economic Paleontologists and Mineralogists, Permian Basin Section, Publication 91-32, p. 11–51.

Tyler, N.; Galloway, W. E.; Garrett, C. M.; and Ewing, T. E., 1984, Oil accumulation, production characteristics, and targets for additional recovery in major oil reservoirs of Texas: Texas Bureau of Economic Geology Geological Circular 84-2, 31 p.

Tyler, N.; Bebout, D. G.; Garrett, C. M., Jr.; Guevara, E. H.; Hocott, C. R.; Holtz, M. H.; Hovorka, S. D.; Kerans, C.; Lucia, F. J.; Major, R. P.; Ruppel, S. C.; and Vander Stoep, G. W., 1991, Integrated characterization of Permian basin reservoirs, University Lands, West Texas: targeting the remaining resource for advanced oil recovery: Texas Bureau of Economic Geology Report of Investigations 203, 136 p.

Vail, P. R., 1987, Seismic stratigraphy interpretation procedure, *in* Bally, A. W. (ed.), Atlas of seismic stratigraphy, v. 1: American Association of Petroleum Geologists Studies in Geology, no. 27, p. 1–10.

Van Wagoner, J. C.; Posamentier, H. W.; Mitchum, R. M., Jr.; Vail, P. R.; Sarg, J. F.; Loutit, T. S.; and Hardenbol, J., 1988, An overview of the fundamentals of sequence stratigraphy and key definitions, *in* Wilgus, C. K.; Hastings, B. S.; Kendall, C. G. St. C.; Posamentier, H. W.; Ross, C. A.; and Van Wagoner, J. C. (eds.), Sea-level changes—an integrated approach: Society of Economic Paleontologists and Mineralogists Special Publication 42, p. 39–46.

Walker, D. A.; Golonka, J.; Reid, A.; and Reid, S., 1995, The effects of paleolatitude and paleogeography on Late Paleozoic carbonate sedimentation in West Texas; part II, Permian: West Texas Geological Society, v. 34, no. 6, p. 5–15.

Ward, R. F.; Kendall, C. G. St. C.; and Harris, P. M., 1986, Upper Permian (Guadalupian) facies and their association with hydrocarbons—Permian basin, West Texas and New Mexico: American Association of Petroleum Geologists Bulletin, v. 70, p. 239–262.

Carbonate Development and Potential Petroleum Productivity in the Southern Fort Worth Basin, Texas

Deborah K. Sacrey
Auburn Energy
Houston, Texas

A. H. Wadsworth
Wadsworth and Associates
Houston, Texas

ABSTRACT.—The Fort Worth basin is a peripheral wedge-shaped foreland basin, with as much as 12,000 ft of sediments in the deepest part. The basin is geographically and tectonically defined as south of the Muenster arch, west of the Ouachita thrust belt, north of the Llano uplift, and east of the Bend arch.

The northern counties of Montague, Jack, Wise, Denton, and Parker have long been prolific oil and gas producers. Pennsylvanian clastics and Mississippian and Cambrian–Ordovician carbonates have been the main productive targets. The stratigraphic column is basically the same over the whole basin, so why have the counties of Erath, Hamilton, Bosque, Somervell, and Coryell been underdeveloped?

During the Cambrian–Ordovician and through the Mississippian, the shelf edge of the eastern and southern North American continent was a stable carbonate bank. As much as 10,000 ft of sediments, ranging from wackestones and carbonate muds to algal mounds and reef buildups, was deposited. The advancing Ouachita thrust belt created foreland basins, such as the Black Warrior, Arkoma, Fort Worth, Val Verde, and Marfa basins. This deformation caused tilted and horsted fault blocks of limestones and dolomites to be juxtaposed against Mississippian and Pennsylvanian source shales.

A series of carbonate-bank buildups and tilted fault blocks has been mapped by the authors throughout the lower part of the Fort Worth basin. These anomalous areas, in conjunction with the use of satellite data, have helped identify potential hydrocarbon traps. The proximity to known productive areas and the availability of low lease costs, reasonable royalties, and shallow drilling could cause the southern part of the basin to become as prolific as the northern part.

Sacrey, D. K.; and Wadsworth, A. H., 2000, Carbonate development and potential petroleum productivity in the southern Fort Worth basin, Texas, *in* Johnson, K. S. (ed.), Platform carbonates in the southern Midcontinent, 1996 symposium: Oklahoma Geological Survey Circular 101, p. 355.

Sequence Stratigraphy and Reservoir Development, Marble Falls Limestone (Pennsylvanian), Central Texas

Walter L. Manger
University of Arkansas
Fayetteville, Arkansas

Patrick K. Sutherland
University of Oklahoma
Norman, Oklahoma

ABSTRACT.—The Marble Falls Limestone of central Texas is a Pennsylvanian carbonate interval packaged between black shales of Mississippian (Barnett) and Pennsylvanian (Smithwick) age. Exposures are limited to the Llano region, but the unit is extensively developed in the subsurface between the Llano uplift and north Texas. The Marble Falls reflects a complicated history of sea-level rise and fall related to compressional events associated with the development of the Fort Worth basin and the rising Ouachita fold belt and Electra and Muenster arches.

The lower carbonate member of the Marble Falls was deposited on a broad, elongate platform occupying much of central Texas. It is of Morrowan age in its entirety, but it has no equivalents elsewhere in the Llano region. The lower Marble Falls member changes facies to dark shale eastward toward the Ouachita fold belt and into coarser clastics northward toward the Muenster arch. Preservation of the lower member along the eastern Llano uplift is related to normal faulting that initiated the development of the Fort Worth basin. Significant hydrocarbons have been produced from this interval, called *Comyn* in the subsurface, from grain-dominated shelf facies below the Morrowan–Atokan unconformity.

The upper carbonate member of the Marble Falls rests unconformably on the lower member and is extensively developed throughout central Texas. It was deposited as a transgressive pulse that followed further compression of the Fort Worth basin. Mud-dominated carbonates exposed in the Llano region are equivalent to alluvial sediments and granite wash derived from the rising arches that bound the Fort Worth basin to the north and the Ouachita fold belt on the east side of the basin. In the subsurface north of the Llano exposures, carbonate mounds in the upper member provide reservoir-quality intervals that have produced hydrocarbons in Lampasas and Hamilton Counties.

The Smithwick black shale is the basinal equivalent of the Marble Falls Limestone. Deposition of this shale drowned carbonate deposition as the Atokan transgression progressed across the Llano region and Bend arch with continued downwarping of the Fort Worth basin. Reservoir-quality lithologies are developed in the Caddo Pool Member to the north and east of the Llano uplift.

Manger, W. L.; and Sutherland, P. K., 2000, Sequence stratigraphy and reservoir development, Marble Falls Limestone (Pennsylvanian), central Texas, *in* Johnson, K. S. (ed.), Platform carbonates in the southern Midcontinent, 1996 symposium: Oklahoma Geological Survey Circular 101, p. 356.

Depositional Environments and Sequence-Stratigraphic Framework of the Subsurface Council Grove Group (Permian) of the Hugoton Embayment, Kansas

Nicholas J. Pieracacos
Baylor University
Waco, Texas

ABSTRACT.—An integrated study of cores, well logs, thin sections, and conodont biostratigraphy has been used to establish a sequence-stratigraphic framework for the subsurface Council Grove Group in the Hugoton embayment of southwestern Kansas. Mixed carbonate–clastic deposits of the middle to upper parts of the Council Grove Group consist of progradationally stacked sequences including facies deposited within open-marine, high-energy-shoal, peritidal, and nonmarine environments.

From base to top, Council Grove Group sequences typically consist of lowstand calichified clastic mud/siltstone abruptly overlain by a trangressive and highstand shallow-marine limestone. Highstand deposits are in turn punctuated by a surface of abnormal subaerial exposure. Facies are systematically stacked into parasequence sets. The inflection between progradational and retrogradational parasequence sets, and non-Waltherian juxtaposition of terrestrial and marine facies, allowed delineation of sequence boundaries.

Lowstand deposits consist of nonmarine clastic mudstone and siltstone with variable pedogenic development. Red to variegated color, caliche, root traces, and subangular blocky-soil structure indicate paleosols and subaerial exposure. Transgressive deposits abruptly overlie lowstand clastics and are separated from the underlying paleosols by an abrupt flooding surface. A transgressive lag commonly overlies this flooding surface and consists of clastic intraclasts from the underlying paleosol. Transgressive deposits consist of thin, upward-deepening, shallow-subtidal, fossiliferous wacke/packstone to a maximum-flooding-surface fusulinid wacke/packstone containing moderately abundant conodont faunas of the normal-marine *Idiognathodus–Streptognathodus* plexus. Highstand deposits consist of thicker, upward-shoaling parasequences terminated by subaerial exposure. Exposure surfaces are characterized by microkarsting, brecciation, root mottling, and calichification.

Pieracacos, N. J., 2000, Depositional environments and sequence-stratigraphic framework of the subsurface Council Grove Group (Permian) of the Hugoton embayment, Kansas, *in* Johnson, K. S. (ed.), Platform carbonates in the southern Midcontinent, 1996 symposium: Oklahoma Geological Survey Circular 101, p. 357.

Characteristics of Cyclical, Mixed Carbonate/Siliciclastic Reservoirs: Early Permian Chase Group, Northern Oklahoma

James R. Chaplin
Oklahoma Geological Survey
Norman, Oklahoma

ABSTRACT.—The Early Permian Chase Group contains the reservoir system of the Hugoton field in Kansas and adjacent Oklahoma. The Chase Group outcrop belt in northern Oklahoma is a depositional sequence (340 ft) characterized by clastic-dominated units in recurring carbonate/clastic cycles. These cyclical carbonates and clastics are correlatable to both transgressive and regressive surfaces, respectively.

Transgressive parts (highstand phase) consist of a thinner (3–60 ft), more carbonate-rich marine/marginal-marine facies dominantly composed of shallowing-upward units of coated-grain, fossiliferous wackestones, packstones, and grainstones. Regressive parts (lowstand phase) of the cycles are characterized by a thicker (40–125 ft), more clastic-rich marginal-marine/continental facies consisting of reddish-brown, greenish-gray, and maroon mudstones/shales locally capped by exposure surfaces and weakly developed paleosols. The bulk of each major depositional cycle represents a single transgressive–regressive cycle. However, minor limited transgressions resulted in periodic renewed carbonate deposition locally within some siliciclastic-rich intervals. Each depositional cycle contains a vertical alternation of laterally continuous, successively shallower reservoir-prone marginal-marine/marine carbonates and siliciclastics capped by seal-prone marginal-marine/continental red beds and paleosols.

The overall cyclicity of these deposits suggests climate-influenced changes in sea-level oscillations. In this geographic setting, the Chase Group is interpreted to represent nearshore to offshore deposition on a gently dipping, low-relief surface (ramp-type depositional setting) rather than on an epeiric platform that terminated abruptly at a raised shelf margin that dropped rapidly into a relatively deep basinal setting.

The development of criteria to recognize transgressive–regressive surfaces in mixed carbonate/siliciclastic cycles, both at the surface and in the subsurface, may assist in correlating individual depositional sequences. In addition, the application of these criteria will aid in understanding the sequence-stratigraphic mechanisms that control reservoir distribution, quality, and development in shallow-marine/marginal-marine Midcontinent reservoirs.

Chaplin, J. R., 2000, Characteristics of cyclical, mixed carbonate/siliciclastic reservoirs: Early Permian Chase Group, northern Oklahoma, *in* Johnson, K. S. (ed.), Platform carbonates in the southern Midcontinent, 1996 symposium: Oklahoma Geological Survey Circular 101, p. 358.

Sonic Velocity in Carbonates—A Product of Original Composition and Post-Depositional Porosity Evolution

Flavio S. Anselmetti and Gregor P. Eberli
University of Miami
Miami, Florida

ABSTRACT.—Pure carbonate rocks, unlike siliciclastic sediments, show no direct correlation between acoustic properties (*P*- and *S*-wave velocity) and age or burial depth of the sediment, so that velocity inversions with increasing depth are common. Sonic velocity in carbonates rather is controlled by the combined effect of depositional lithology and several post-depositional processes, such as cementation or dissolution, that create carbonate-specific rock fabrics. Our study correlates these diagenetic fabrics to the sonic velocity of the rocks.

Measurements of ultrasonic velocities on unconsolidated carbonate muds under different stages of experimental compaction show that compaction, which is a function of burial depth, increases velocity where the sediment has not undergone intense diagenetic alteration after deposition. The susceptibility of carbonates to diagenetic changes, which occur much more quickly than compaction, causes a special velocity distribution in carbonates and complicates downhole velocity estimations.

The importance of these diagenetic alterations to ultrasonic velocity in carbonates is documented by a data set of 200 samples from different areas and ages that were measured under variable confining and pore-fluid pressures. Despite the almost monomineralic composition of the carbonates, V_p ranges from 1,500 to 6,500 m/s, and V_s ranges from 600 to 3,500 m/s. This range is caused mainly by variations in the amount and type of porosity. In general, the measured velocities show a positive correlation with density and an inverse correlation with porosity, but departures from the general trends of correlation can be as high as 1,500 m/s. These deviations can be explained by the occurrence of different pore types that form during specific diagenetic phases. Thus we are able to link sonic velocity to the diagenetic stage of the rock. Our data set further suggests that commonly used correlations like "Gardner's Law" (V_p – density) or the "time-average equation" (V_p – porosity) should be significantly modified toward higher velocities before being applied to carbonates.

Anselmetti, F. S.; and Eberli, G. P., 2000, Sonic velocity in carbonates—a product of original composition and post-depositional porosity evolution, *in* Johnson, K. S. (ed.), Platform carbonates in the southern Midcontinent, 1996 symposium: Oklahoma Geological Survey Circular 101, p. 359.